Robert Carachi
Editor

Atlas of Paediatric Surgical Imaging

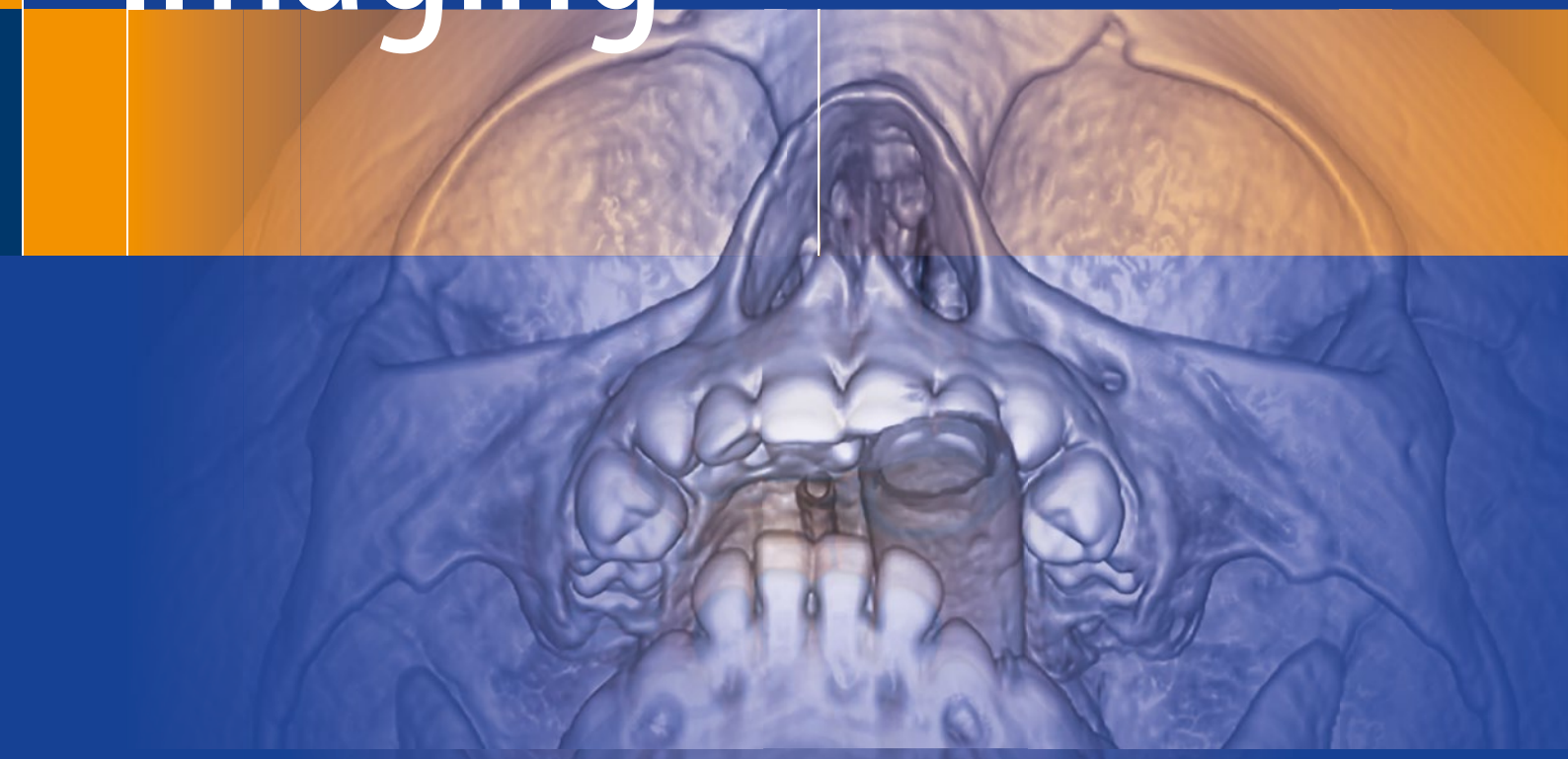

A Clinical and Diagnostic Approach

Springer

Atlas of Paediatric Surgical Imaging

Robert Carachi
Editor

Atlas of Paediatric Surgical Imaging

A Clinical and Diagnostic Approach

Springer

Editor
Robert Carachi
Surgical Paediatrics
University of Glasgow
Glasgow
UK

ISBN 978-3-030-32383-7 ISBN 978-3-030-32384-4 (eBook)
https://doi.org/10.1007/978-3-030-32384-4

This Springer imprint is published by the registered company Springer Nature Switzerland AG
The registered company address is: Gewerbestrasse 11, 6330 Cham, Switzerland

Preface

This radiology atlas is a comprehensive compendium of paediatric surgical conditions encountered in a busy children's teaching hospital. The expertise is drawn from a collection of current and archival images spanning three generations of paediatric surgeons and radiologists. This book deals with conditions that are encountered by the doctors who are in training for hospital practice or general practice and acts as a reference manual for most conditions encountered in childhood. I am grateful to late Professor Dan Young for passing his entire collection of images to me.

The book is organized in seven sections that are each dedicated to an anatomical region. Each section lists conditions under the categories of congenital, infection/inflammation, trauma, tumour, and acquired. It is hoped that this layout will make it simple to access and acquire knowledge of the conditions. As this book is on the use of radiological images in the development of a diagnosis, the text is based on a definition of the condition, clinical symptoms and signs, and the best imaging, with a detailed description of the radiological signs that indicate the conditions.

Line illustrations are used to illustrate some sections, and clinical photographs and pathological specimens are used to explain some radiological signs.

Glasgow, UK — Robert Carachi

A Tribute to Professor Daniel G. Young (1932–2013)

Dan Young, who died aged 80, was a man of boundless compassion whose reputation for always striving to do the best for each of "his children" stretched around the globe. Both a skilful, ground-breaking surgeon and an admired academic, he became Glasgow University's First Professor of Surgical Paediatrics. Yet he never forgot, or was forgotten by, his patients, many of whom remained in touch for years.

Just weeks before he died, one of his visitors was a mother who had lost her son 14 years earlier. She still remembered him caring for her boy as though he was his own.

A further mark of the esteem in which he was held was the renaming of the Glasgow Unit, where he worked for more than 20 years, as the Dan Young Neonatal Surgical Unit. A support centre run by the Scottish Spina Bifida Association (SSBA), which he had served as Honorary President, also bears his name.

"In the real sense of the word Dan had that unique, and sadly now rarely seen, vocation to his profession", said SSBA Chief Executive Andrew Wynd. "For him, long hours and hard graft were not something to be challenged, but something to be celebrated because in that commitment grew greater understanding and knowledge, greater experience and wisdom—although he would never have acknowledged any of these qualities in himself".

Born in Skipness, Argyll, Dan grew up on Lower Carbarns Farm, Netherton, outside Wishaw, and was educated at Netherton Public School, Wishaw Academy Primary School, and Wishaw High School.

In 1950, he began his medical studies at Glasgow University and during that time filled in as a Locum Resident on both the medical and surgical sides at the city's Royal Hospital for Sick Children. This was when he first became aware of the multiple health problems and high mortality rate of babies born with congenital defects, an experience that inspired him to specialise in this field.

Following his graduation in 1956, he completed his national service on a special short service commission to the Ghanaian government, where he was in charge of the medical reception station at a recruiting centre in Kumasi. From there, he went to the Liverpool School of Tropical Medicine, gaining a diploma in tropical medicine and hygiene, before returning to Glasgow to become an Assistant Lecturer in the University's Physiology Department. From 1961 to 1964, he was a Registrar in Surgery, during which time he became a Fellow of the Royal College of Surgeons in Edinburgh. There then followed a spell at the world-famous The Hospital for Sick Children at Great Ormond Street in London, where he was a Senior Registrar and Resident Assistant Surgeon. In the late 1960s, he was a Senior Lecturer in Paediatric Surgery at London's Institute of Child Health and Honorary Consultant Surgeon at Great Ormond Street and the Queen Elizabeth Hospital for Children in Hackney.

Dan returned north in 1969 to become Head of the Department of Surgical Paediatrics at Glasgow University, based at the Royal Hospital for Sick Children. In 1971, the hospital's state-of-the-art Neonatal Surgical Unit was established at Yorkhill, and the following year, he became a Fellow of the Royal College of Surgeons in Glasgow. His career spanned an era of many advances in his speciality, and in the 1960s and 1970s, he was involved in the introduction of the first shunts to control hydrocephalus in new-borns, a procedure that hugely enhanced the life expectancy of significant numbers of babies born with spina bifida and hydrocephalus.

He also treated a wide range of other conditions, including deformities such as cleft lip and cleft palate.

Whilst developing a fine paediatric surgery department, he had also cemented his reputation as an excellent Educator, training surgeons from all over the world and helping to establish the specialty of paediatric surgery in various countries. He was an Honorary Member of the associations of paediatric surgeons in Hungary, Egypt, South Africa, and America, as well as a Visiting Lecturer to Japanese and Australasian organisations, and was awarded a Doctorate from the University of Wrocław for his contribution in Poland and internationally.

During the 1980s, he chaired the committee that oversaw the establishment of the Intercollegiate FRCS in Paediatric Surgery and was an Examiner in all the Fellowship and Membership Examination of the British Royal Colleges of Surgeons for more than 30 years.

He was the British Editor of the *Journal of Pediatric Surgery* for 17 years and also contributed to and wrote numerous papers and books, including *A History of Surgical Paediatrics*, *Baby Surgery*, and *Children's Medicine and Surgery*.

In 1992, he was appointed Glasgow University's First Professor of Surgical Paediatrics, a role he held for 6 years. He retired from clinical practice at the same time but remained an influential Emeritus Professor, regularly teaching students at the bedside for another decade and mentoring numerous young surgeons.

A Fellow of the Royal College of Paediatrics and Child Health, he was President of the British Association of Paediatric Surgeons and the British Society for the History of Paediatrics and Child Health, holding the latter post until shortly before his death.

He was also Honorary President of the Scottish Spina Bifida Association for 30 years but was somewhat bemused, said Andrew Wynd, when its National Family Support Centre in Cumbernauld was named after him as a lasting tribute to his dedication.

Predeceased by his wife, Nan, and grandson, Euan, he is survived by his daughter, Rhoda; his son, Kenneth; and five grandchildren.

Chronology

Daniel Greer Young (1932–2013)

1932 Born on a farm in Skipness, Scotland

1956 Graduated from the University of Glasgow

Special Short Service Commission in Ghana

Liverpool School of Tropical Medicine

Assistant Lecturer in Physiology Department, University of Glasgow

Senior Lecturer and Honorary Consultant at the Hospital for Sick Children, Great Ormond Street Hospital, London, and at the Queen Elizabeth Hospital, Hackney

1969 Head of the Department of Surgical Paediatrics, University of Glasgow, based in the Royal Hospital for Sick Children, Yorkhill

1971 The Neonatal Unit at the Royal Hospital for Sick Children was established and when refurbished in 1991 was renamed "Dan Young Neonatal Unit"

1980 Chaired the Committee to oversee the establishment of the Intercollegiate FRCS in Paediatric Surgery in Britain

1988–2005 Editor for the British Isles and Ireland for the *Journal of Pediatric Surgery*

1991–1992 President of the British Association of Paediatric Surgeons (BAPS)

1992–1998 Appointed the First Professor of Surgical Paediatrics in the University of Glasgow Retired from clinical practice but was still active and continued teaching medical students and mentoring trainees for a further 10 years

1999 Awarded the prestigious Denis Browne Gold Medal

2008–2010 President of the British Society for the History of Paediatrics and Child Health

1977–2013 Named Honorary President of the Scottish Spina Bifida Association (SSBA) and continued his work for the Association for over three decades. In 2007, the SSBA, in recognition of his service, named their new building The Dan Young Building

For 30 years, he was an Examiner of the British Royal Colleges for the FRCS and MRCS and for the Diploma in Child Health for the Royal College of Physicians and Surgeons

Awarded a Doctorate by the University of Wrocław in recognition of his contributions to Polish paediatric surgery

Having assisted in the establishment of the speciality of paediatric surgery, he was made Honorary Member of many national and international paediatric associations

Alison Shaw

Professor D.G. Young

A Tribute to Dr. Elizabeth Mary Sweet (1928–2014)

Dr. Elizabeth Mary Sweet (Betty) studied medicine at Edinburgh University and subsequently undertook several posts in paediatrics before training in radiology. In 1963, she was appointed as Consultant Paediatric Radiologist at the Royal Hospital for Sick Children in Glasgow. She was only the third woman to hold such a Consultant Radiologist post in Scotland and the first in paediatric radiology. She retired at the age of 60 in 1988 after 25 years at the hospital.

At the time of her appointment, X-rays were the only tool available in radiology and consisted of plain films and contrast studies. In 1958 in Glasgow, Donald, McVicar, and Brown published their seminal paper "Investigation of Abdominal Masses by Pulsed Ultrasound", and the first commercial B scanner—the Diasonograph—became available. Betty, realising its potential for children, undertook much of the early work in paediatric abdominal ultrasound, particularly of the renal tract. This was greatly helped by the later provision of a "real-time" machine. Prior to her retirement, the department also acquired a CT head scanner and a gamma camera.

Betty's expertise in paediatric radiology was recognised when she became President of the European Society of Paediatric Radiology in 1985. She organised and hosted the annual meeting in Glasgow that year. She was a Member of their study group who drew up recommendations for the safe practice of paediatric radiology. She was granted Honorary Membership of the society in 1989. In 1993, along with Herbert Kaufmann (Berlin) and Hans Ringertz (Stockholm), she was a Coauthor of the book *The First 30 Years of the ESPR: The History of Pediatric Radiology in Europe* and wrote the chapter "Paediatric Radiology in Great Britain and Ireland", which outlined the development of the specialty.

Like many female consultants of her generation, she never married and, whilst working in Glasgow, undertook the care of her elderly mother, which involved a daily round-trip of over 80 miles. She was a private person who set extremely high standards for herself and for the department, and, perhaps, because of this, she was reluctant to delegate or to ask for help and could appear intimidating. In retirement, she enjoyed travelling and regularly attended ESPR

annual meetings. Sadly, she developed dementia in her 80s, ultimately spending her last few years in a home.

A former member of the hospital said, on learning of her death, “Betty was unique”.

Royal Hospital for Sick Children
Yorkhill, Glasgow, UK

Ruth McKenzie

Dr. Elizabeth Sweet

Acknowledgements

This book would not have been possible without the immense legacy of clinical and radiological images that Professor Young collected over his lifetime in Paediatric Surgery. It is a tribute to him and his family who passed on all this to me. I am deeply grateful to this enormous legacy. His wish was to create a book like this so that its information can be passed on to generations of trainees in Paediatrics and Paediatric Surgery.

I would like to thank especially my friend and past secretary, Mrs. Kay Byrne, who has been so helpful in seeing this project to completion. A special thanks to my wife, Annette, who spent hours finding images and ensuring all the chapters were correct before going to the publishers.

A special thanks to Mr. Lee Klein who expedited this book's publication with Springer.

I would also like to acknowledge the help I got with the initial research of some of the material in this book. Dr. Stephanie Lip, Dr. Murchison and Dr. Anastasija Getman.

Contents

Contributors

Ruth Allen, MD, FRCR Royal Hospital for Children, Glasgow, UK

Sandra Butler, MD Queen Elizabeth University Hospital, Glasgow, UK

Robert Carachi Surgical Paediatrics, University of Glasgow, Glasgow, UK

Susie Goodwin Royal Hospital for Children, Glasgow, UK

Greg J. Irwin, MD The Royal Hospital for Children, Queen Elizabeth University Hospital, Glasgow, Scotland, UK

Rasem Keilani, MD Amman, Jordan

Andrew McLaughlin, FRANZCR, MBChB, BMedSc Radiology Department, Christchurch Hospital, Canterbury, Christchurch, New Zealand

Stephanie Potts Surgical Paediatrics, University of Glasgow, Glasgow, UK

Introduction: Paediatric Radiology

1

Greg J. Irwin

1.1 Introduction

Radiology as a specialty came into being due to a series of significant discoveries in the field of physics. A succession of innovators has taken novel scientific phenomena, and from them developed strategies to image the human body.

Paediatric radiology as a separate subspecialty is relatively new, although the first clinical X-ray taken in America, on 3 February 1896, was of a 14-year-old boy's wrist. The first book specifically concerned with paediatric radiology was published in 1910.

In the 1940s, John Caffey described the association of multiple long bone fractures and chronic subdural haematomas, creating the debate that first established the existence of physical child abuse. Radiology continues to have a prominent role in the investigation of this condition. Caffey published his landmark textbook *Pediatric X-Ray Diagnosis* in 1945, which now continues in 2018 in its thirteenth edition.

The Society for Pediatric Radiology (SPR) was founded in America in 1958, electing Edward Neuhauser as its president, and was followed by the establishment of the European Society of Paediatric Radiology (ESPR) in 1963. Paediatric neuroradiology emerged as the first formal subspecialty of paediatric radiology during the late 1960s.

1.2 Discovery of the X-Ray

X-rays were discovered on 8 November 1895 by Wilhelm Conrad Röntgen, working in Wurzburg, Germany. Perhaps appropriately for the father of radiology, the discovery was made in a darkened room. He was performing experiments with cathode ray tubes, where streams of electrons pass across a vacuum, colliding forcefully with the metal of the anode. The tubes were entirely covered so that no light could escape, but nonetheless Röntgen observed that a screen several feet from the tube began to fluoresce when the current was applied.

It was apparent that some sort of invisible ray was being emitted by the tube and shining upon the screen. These he termed X-rays; the designation "x" was intended to be a temporary name, indicating that the nature of the ray was unknown. He immediately began to investigate the properties of this new form of ray. His earliest experiments investigated the ability of the X-rays to cast a shadow from various objects interposed between the tube and the screen, and recorded the results upon a photographic plate. Rather than stopping all of the X-rays, objects were shown to be variably transparent. Paper, wood, and cloth were penetrated easily, as were, to differing degrees, various metals.

One of the first recorded X-rays of a living human was performed on the hand of Röntgen's wife Anna-Bertha. Due to the low output of the unmodified tube, the exposure time was in the region of 30 min. By contrast, a modern hand X-ray exposure time is in the region of milliseconds. These early X-rays immediately showed their potential in medical investigation, successfully localising glass and metallic foreign bodies in various patients and facilitating their removal.

Röntgen's paper entitled "On a New Kind of Rays" (Übereineneue Art von Strahlen) was immediately published in December 1895. News of his discovery quickly spread, and Röntgen became famous and bestowed with many honours, including the Nobel Prize for Physics in 1901.

What is believed to be the first medical X-ray department in the world was set up in Glasgow Royal Infirmary, Scotland, in March 1896, by Dr. John Macintyre. Röntgen had sent a copy of his paper to Lord Kelvin in Glasgow in early 1896, who passed it on to Macintyre's group, along with necessary apparatus. Some of the examinations attributed to this department include the first X-ray depictions of a bullet, and another of a coin in the oesophagus (Figs. 1.1, 1.2, and 1.3)

Due to the long exposure times, early radiographs were much more successful in imaging the peripheral skeleton than the chest or abdomen, where movement artefact and the

G. J. Irwin (✉)
The Royal Hospital for Children, Queen Elizabeth University Hospital, Glasgow, Scotland, UK
e-mail: Greg.irwin@ggc.scot.nhs.uk

R. Carachi (ed.), *Atlas of Paediatric Surgical Imaging*, https://doi.org/10.1007/978-3-030-32384-4_1

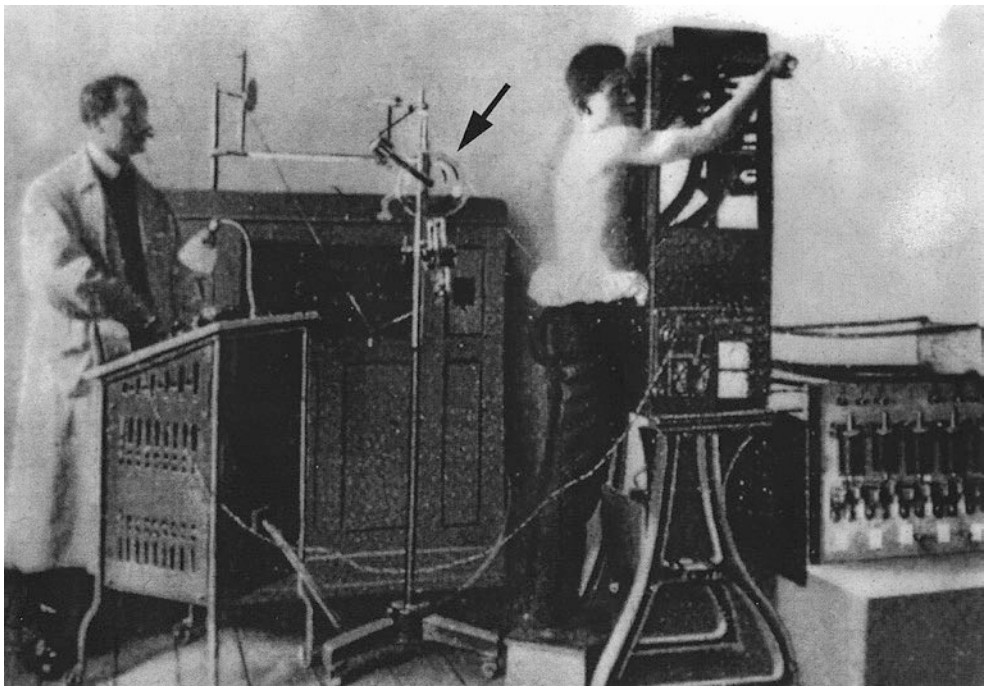

Fig. 1.1 An early photograph, probably late 1890s, of a chest X-ray being taken in Glasgow Royal Infirmary. Note the X-ray tube (arrow) is completely unshielded and is bathing the whole room in X-rays (Image courtesy of NHS Greater Glasgow and Clyde Archives)

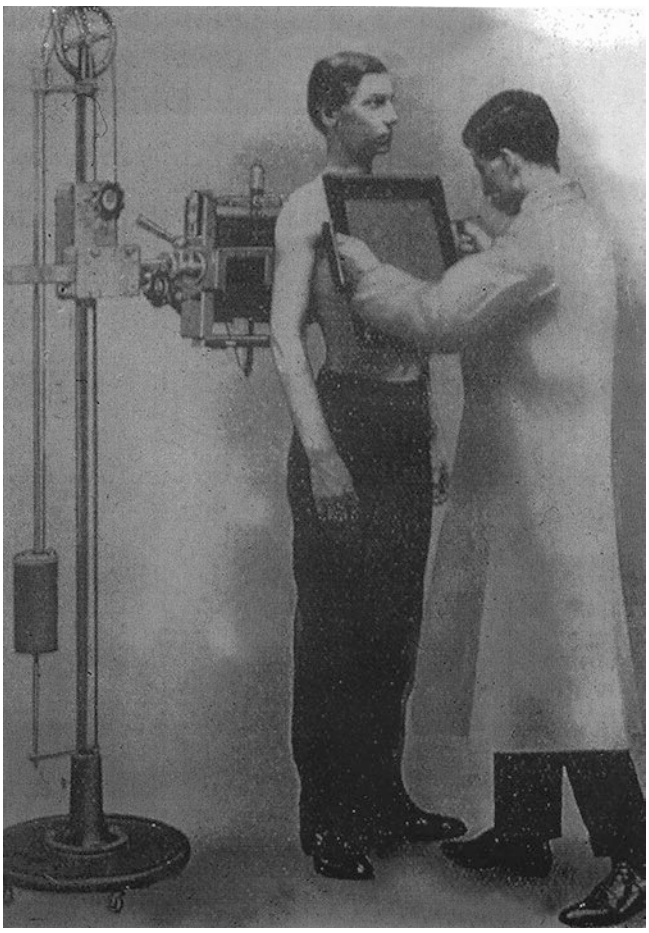

Fig. 1.2 A 1905 image of fluoroscopy. The X-ray tube is behind the patient. The examiner is standing directly in the primary X-ray beam, observing the movement of the heart and diaphragm on the fluorescent screen he is holding (Image courtesy of NHS Greater Glasgow and Clyde Archives)

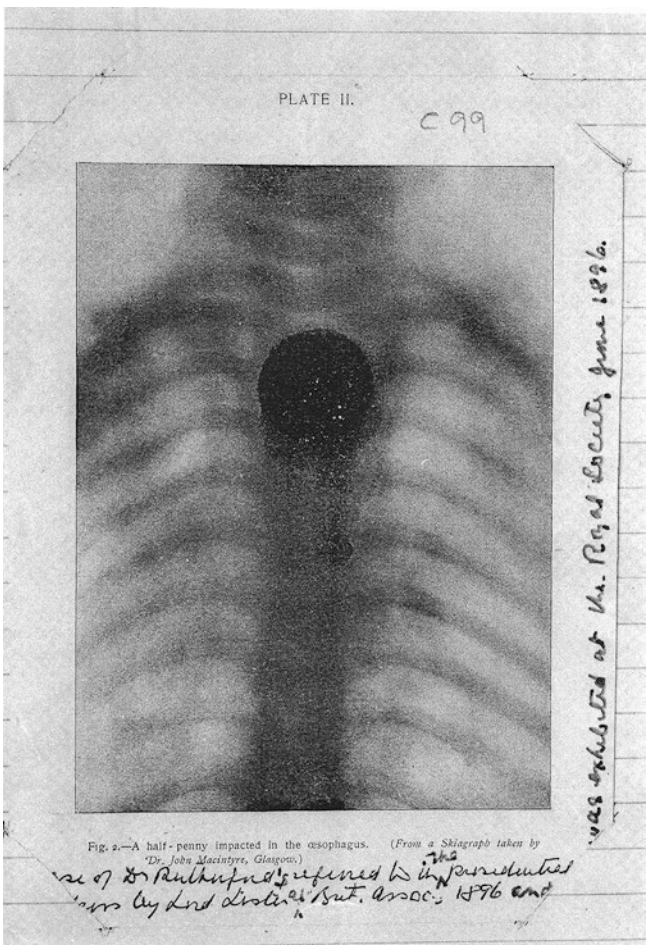

Fig. 1.3 An X-ray of a half penny impacted in a child's upper oesophagus, taken by Dr. John Macintyre. The image was exhibited at the Royal Society in June 1896 (Image copyright of Medical Illustration, Glasgow Royal Infirmary, used with permission)

thickness of the tissues spoiled the images. Improvements in X-ray tube design allowed for shorter exposures, as did advances in the construction of the film plates. Fluoroscopy was achieved by the examiner holding a fluorescent screen between his eyes and the patient, all the time directly in the path of the primary X-ray beam!

Although there were many early reports of skin damage, the harmful effects of radiation were not initially fully appreciated. Many early X-ray workers suffered burns, lost fingers, hands, or eyes, or succumbed to radiation-induced cancers. The Martyrs Memorial to 169 who lost their lives was dedicated in 1936 outside the Röntgen Institute of St. George's Hospital in Hamburg.

Modern X-ray set ups still use X-ray tubes based on the same design. They are, however, heavily shielded, and include collimators to enable the area irradiated to be minimized. Films have been replaced with digital sensors, and the processed images are sent electronically to picture archiving and communications systems (PACS). The images are then immediately available for reviewing at multiple geographically separate locations. Currently a National PACS system is installed and accessible across the whole of Scotland, on which all imaging modalities are stored.

1.3 Ultrasound

Medical ultrasound has its roots in the development of SONAR (Sound navigation and ranging). In the First World War, experiments were underway to develop sonar for submarines. It was known that bats could navigate by listening for the echoes of the high frequency sound waves they produced, and it was hoped to replicate this principle underwater. The sinking of the RMS Titanic after it struck an iceberg in 1912 had added impetus to the project.

An early system developed in 1914 by Fessenden was partially successful, but its direction-finding ability was limited owing to the low frequency of the sound waves it used. High-frequency sound waves (hence *ultra* sound) were produced with quartz crystals glued between steel plates by the French physicist Paul Langévin, using the piezoelectric effect. This is where crystals are caused to change size and vibrate by passing electrical currents through them and vice versa (the inverse piezoelectric effect). This produced a short "chirp" of high-frequency sound underwater. By timing how long it took the echo to return, and knowing the speed of sound in water, it was possible to determine the distance from the source of the sound to the source of the echo. In practice, this gave the distance from the ship to the submarine/seabed/iceberg. The pulse echo technique was developed using radio waves rather than sound waves in the development of RADAR (radio detection and ranging).

A parallel field of study was in the use of ultrasound to detect otherwise invisible flaws in metal. During the Second World War, several groups were investigating the technique at the same time in different countries. Wartime also proved the catalyst for further sonar development.

The application of ultrasound to medicine was initially confined to attempts at therapy, rather than diagnosis. High-frequency ultrasound generated heat, which was used in many conditions as symptomatic treatment. The destructive force of high-energy sound waves was also used as a neurosurgical tool for ablation of parts of the brain.

Working in America in the late 1940s, George Ludwig began animal experiments using metal flaw-detector equipment to identify foreign bodies, such as gallstones that had been surgically implanted into dogs. His work established many fundamental concepts of diagnostic ultrasonography.

Ian Donald, an obstetrician and gynaecologist working in Glasgow, Scotland, conducted experiments on tumours freshly removed from human patients. The ultrasound device was provided by a local boilermaker, where it was used to check the integrity of metal welds. It was immediately apparent that different traces were produced by different masses, and further experiments on *in vivo* tumours were planned. Difficulties were encountered in transferring the industrial equipment to clinical usage. Initially a small bucket of water with a latex bottom was placed on the patient's abdomen, which itself was smeared with lubricating jelly to exclude air. The ultrasound probe was then applied to the surface of the water. Subsequently, direct application of the probe to the skin, with olive oil as a coupling film, proved less hazardous. There was an early clinical success: a middle-aged woman thought to be dying of a gastric carcinoma with ascites, was instead shown to have an enormous ovarian cyst. This was removed, and the patient made a full recovery. Donald notes in his memoir, however, that after this success he was "inflicted with horrid specimens of [the patient's] grandchild's attempts at cooking by way of an expression of gratitude."

Donald went on to publish a landmark paper in the *Lancet* of 7 June 1958, "Investigation of abdominal masses by pulsed ultrasound." His co-worker James Willocks went on to establish the utility of biparietal measurement of the fetal skull to measure growth (Figs. 1.4 and 1.5).

From the mid-1960s there was a rapid increase in the use of diagnostic ultrasound, matched with great enhancements in the scanning machines. Early commercial machines were large and cumbersome, with either large fixed gantries or articulated probe arms. Original (A mode) scan displays were simply blips on an oscilloscope trace, although accurate measurements with these systems were possible. More advanced electronics needed to be developed before cross-sectional (B mode) images with grey scale could be produced. The next major innovation was that of real-time scanning, which relied upon mechanical rotating or oscillating transducers to quickly sweep back and forth across the area of interest, building up a moving picture. These in turn have been superseded by electronic phased array transducers. Doppler techniques have developed in parallel to grey scale imaging, and from the outset have allowed investigation of the movement of heart

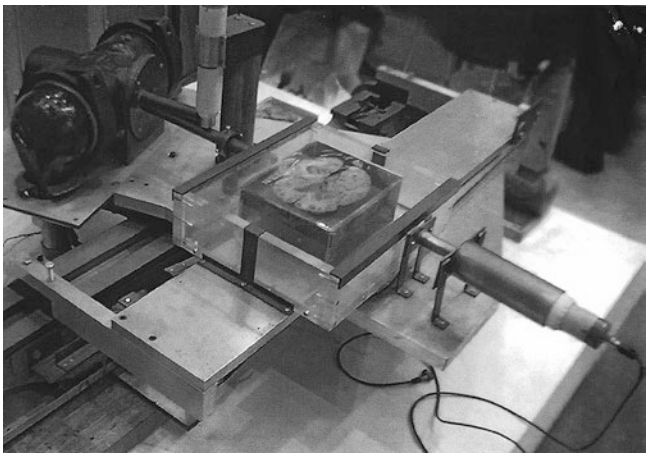

Fig. 1.4 Hounsfield's prototype for the CT scanner. Note the section of brain in the centre of the image

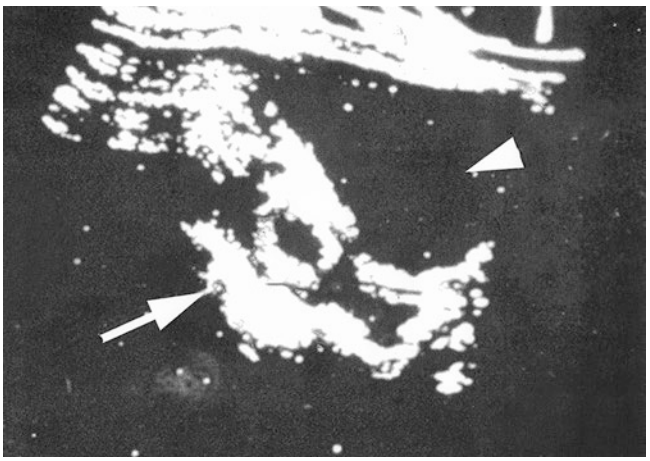

Fig. 1.5 1963 ultrasound performed by Prof. Ian Donald, showing a foetus in utero (arrow) using the urinary bladder (arrowhead) as an acoustic window

valves, and the flow of blood in peripheral vessels. The increasing processing power of newer computers has enabled the addition of 3D scanning, which uses advanced surface shading and volume rendering (Fig. 1.6). Further developments in ultrasound elastography, and contrast agent imaging are gaining widespread clinical use.

1.4 Computed Tomography

Sir Godfrey Hounsfield, an English engineer, invented the computed tomography (CT) scanner. During the Second World War he joined the Royal Air Force as a radar mechanic instructor. Joining EMI in 1951, he initially continued his work on radar and guided weapons. He subsequently led the design team building the first all-transistor computer to be built in Britain.

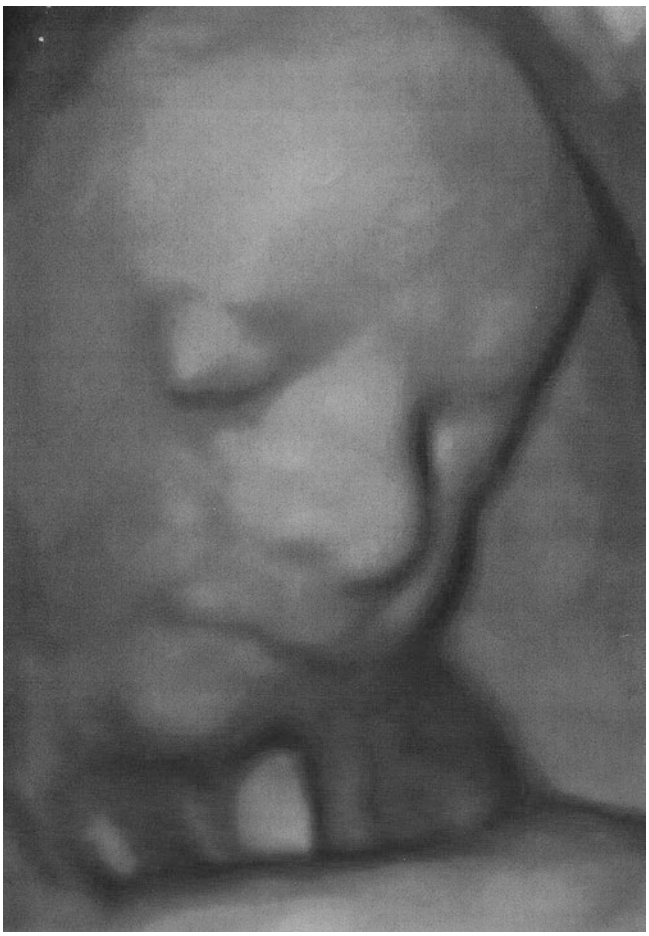

Fig. 1.6 Modern 3D ultrasound of a foetus of 20 weeks gestation

During a walk in the countryside in 1967, Hounsfield had the germ of the idea that was to become computerised tomography. He realized that "you could determine what was in a box simply by taking readings at all angles through it." In practice, this required a minicomputer to reconstruct a picture from X-ray measurements taken through the body at a multitude of different angles. The computer was essential because hundreds of thousands of calculations would need to be made.

Initial tests with gamma rays were too slow, but even switching to X-rays still required a scanning time of 9 h. The first scan of human tissue was performed on a preserved human brain from a local hospital museum, and successfully showed differentiation of grey and white matter. Fearing that the preservation process had enhanced the images, Hounsfield substituted fresh bullocks' brains. In scanning through the carcasses of pigs, problems were encountered as each picture took a day to acquire, during which gas bubbles formed and expanded within the tissues.

Faster prototypes were produced, and the first patient was scanned on 1 October 1971 at Atkinson Morley's Hospital in South London. The patient had a suspected brain lesion, and

the scan demonstrated a frontal cyst. The next step was a machine capable of scanning the body, and a larger and faster scanner was produced capable of taking a picture in 18 s. The first body images produced in the body prototype were of Hounsfield himself.

Hounsfield proposed a scale for measuring the relative absorption values in CT, from 1,000 for bone, 20–40 for tissue, 0 for water and −1000 for air. These Hounsfield units remain the standard unit for CT imaging density. He was awarded the Nobel Prize in Physiology or Medicine in 1979, sharing the honour with Allan Cormack, a South African physicist of Scottish descent.

1.5 Magnetic Resonance Imaging

Magnetic resonance imaging (MRI) is a complicated imaging technique, and the history of its development is no less complex. In many ways it is well suited to investigate children, giving fantastically detailed images with unparalleled soft-tissue contrast. However, the machine is expensive and apt to induce claustrophobia, and the long scan times may require sedation or general anaesthetic for younger patients. The use of strong magnetic fields precludes scanning of patients with certain metallic implants, but the absence of ionizing radiation secures it a place in the arsenal of the paediatric radiologist.

Expressed simply, placing the body in a strong magnetic field causes the hydrogen nuclei of the water molecules found throughout the body to line up. A brief radio wave is applied, which pushes these protons out of alignment. When the protons flick back into line, they release energy, which is detected and localised by the scanner. Areas with lots of water release relatively more energy, and the scanner builds up a cross-sectional picture of the body, depending upon the amount of water, and therefore the amounts of energy released.

MRI was initially termed Nuclear Magnetic Resonance (NMR). Working independently in the 1940s, Felix Bloch at Stanford University and Edward Purcell at Harvard University found that some nuclei in a magnetic field absorbed radiofrequency range energy and emitted this energy upon returning to their original state. Their discoveries in nuclear magnetic absorption earned them each a share of the Nobel Prize in Physics in 1952. NMR spectroscopy was used by physicists to investigate the properties of small samples in high-strength magnetic fields, not to produce anatomical images.

In the early 1970s, Raymond Damadian found that normal and cancerous tissue could be separated *in vitro* according to different physical parameters using NMR. This raised the possibility of non-invasive tumour characterisation, and in 1974 Damadian constructed a scanner with the intention of analysing the whole body.

In 1973 Paul Lauterbur, a professor of chemistry at the State University of New York, published a paper in *Nature* describing an imaging technique for the spatial localization of two capillary tubes of water inside a narrow tube of heavy water. The introduction of gradients allowed two-dimensional images to be produced. Reportedly, he was eating a hamburger at the time when the idea occurred, and he jotted it down on a napkin. The development of this idea resulted in the award of the 2003 Nobel Prize in Physiology or Medicine, shared with Sir Peter Mansfield. Mansfield is a British physicist who further developed the utilisation of gradients and showed how the signals could be mathematically analysed to develop a useful imaging technique. He discovered how fast imaging could be performed with the echo planar technique, and laid the basis for functional MRI.

By 1980, Edelstein and Hutchison at the University of Aberdeen in Scotland had developed a practical two-dimensional imaging technique, dubbed "spin-warp imaging," and the world's first clinical diagnostic MRI service was started at the Aberdeen Royal Infirmary in August of that year.

1.6 Nuclear Medicine

Nuclear medicine uses radioactive isotopes to image the body and to treat disease. As the isotopes can be attached to various pharmaceutical compounds, analysis of a wide range of physiological function and anatomy is possible. Two important applications of nuclear medicine in the field of paediatric radiology are imaging of the renal tract and oncology.

The 1903 Nobel Prize for Physics was shared by Henri Becquerel and Marie and Pierre Curie for their work in the discovery of radioactivity. Whilst investigating a possible connection between Röntgen's X-rays and natural phosphorescence in 1896, Bequerel discovered by chance that uranium emitted radiation that exposed photographic film. Marie and Pierre Curie continued his work, discovering polonium (named after Marie's native Poland) and radium.

Unfortunately, some early applications of radioactivity included the addition of radioactive compounds to water as a cure-all, and to toothpaste promising "radioactive brilliance."

The use of radioactivity in imaging required the use of tracers with a short half-life, to limit the potential for side effects. In 1937 iodine-131 was created, followed by the production of technetium-99m in 1938, which remains the most commonly used isotope in nuclear medicine. These and many other isotopes were created using a cyclotron, an apparatus that accelerates charged particles to great speed in a vacuum chamber and fires them at a target. The cyclotron

was invented and developed by Ernest Lawrence, later to receive the Nobel Prize in Physics for his work (and to have the element lawrencium named in his honour).

The use of isotopes in imaging was revolutionised in the1950s by the invention and development of the first clinically successful scintillation camera by Hal Anger at the University of California at Berkeley. The design principle of his gamma camera was so successful that it is still the basis of most of those used today. The technology has evolved to form the basis of single photon-emission computed tomography (SPECT) and positron emission tomography (PET), which permit cross-sectional imaging, analogous to CT. SPECT uses standard nuclear medicine tracers, but PET uses a different class of short-lived tracers that emit positrons, also produced in a cyclotron. The necessity of an accessible cyclotron has slowed the introduction of PET. As of 2008 there were approximately 1500 PET centres in the United States of America, while in the United Kingdom the modality was only emerging as a highly specialized regional service. The most widely used PET tracer is currently fluorine-18 fluoro-deoxy-glucose (FDG), which produces images of tissue metabolism.

The images produced in nuclear medicine are generally of low resolution, and these can now be enhanced by combining the images with high resolution CT techniques, hence SPECT/CT and PET/CT. The fused images produced by these complementary techniques combine functional information with anatomical detail, and these can be used to improve the localization of certain disease processes and enhance diagnostic accuracy. The primary application of PET in children is in oncology, where it particularly useful for the diagnosis and staging of disease, as well as for assessing the response of individual treatments.

1.7 Dose Considerations and ALARA

ALARA stands for "as low as reasonably achievable," and this is the guiding principle where ionising radiation is being used. The most effective way to reduce dose is to not perform the examination at all! X-rays, fluoroscopy, CT scans, nuclear medicine studies, and PET all use ionising radiation, and consideration should be given as to whether the information sought could be obtained using ultrasound or MRI scanning. If not, then the examination should be tailored to use the minimum radiation dose necessary to produce diagnostic images. To an extent, the risks of relatively low levels of radiation are unknown. Nonetheless, it is prudent and responsible to minimise any chance of potential iatrogenic injury to our patients. Children's tissues are inherently more radiosensitive than those of adults, and children also have longer to live and develop delayed (stochastic) effects of radiation.

Good communication between the surgeon and radiologist is vital to allow a collaborative approach to dose reduction. A close working relationship reduces errors and, particularly in emergency situations, the surgeon will often be present during the study.

Further Reading

Anger HO. A new instrument for mapping gamma-ray emitters. Biol Med Quart Rep. 1957;3653:38.

Burrows EH. Pioneers and early years: history of British radiology. Alderney: Colophon; 1986.

Coley BD. Caffey's Pediatric Diagnostic Imaging. 13th ed. Elsevier; 2018.

Donald I, MacVicar J, Brown TG. Investigation of abdominal masses by pulsed ultrasound. Lancet. 1958;271(7032):1188–95.

Griscom NT. History of pediatric radiology in the United States and Canada: images and trends. Radiographics. 1995;15(6):1399–422.

Hong J-Y, Han K, Jung J-H, Kim JS. Association of exposure to diagnostic low-dose ionizing radiation with risk of cancer among youths in South Korea. JAMA Network Open. 2019;2(9):e1910584.

Kirks DR. Eugene W. Caldwell lecture. Pediatric imaging: the oldest radiological subspecialty comes of age. Am J Roentgenol. 1999;172(2):291–9.

Rosenbusch G, Oudkerk M, Ammann E, Winter PF. Radiology in medical diagnostics: evolution of X-ray applications 1895–1995. Oxford: Blackwell Science; 1995.

Rotch TM. Living anatomy and pathology: the diagnosis of diseases in early life by the roentgen method. Philadelphia, PA: Lippincott; 1910.

Slovis I. Caffey's pediatric diagnostic imaging. 11th ed. Philadelphia, PA: Mosby; 2007.

The Nobel Prize. Wilhelm Conrad Röntgen. Biographical. https://www.nobelprize.org/prizes/physics/1901/rontgen/biographical/. Accessed 21 Oct 2018.

The Nobel Prize. Godfrey N. Hounsfield. Biographical. https://www.nobelprize.org/prizes/medicine/1979/hounsfield/auto-biography/. Accessed 21 Oct 2018.

Willocks J, Barr W. Ian Donald: a memoir. London: RCOG Press; 2004.

Head and Neck

2

Sandra Butler

This chapter is amply illustrated with both clinical and radiological imaging of a selection of conditions. Many congenital conditions are seen in the head and neck of infants and children. Also very common in all children are inflammatory conditions of the head and neck; only severe clinical conditions are described here. Also described in great detail are the wide range of head injuries from trauma, as well as tumours of the head and neck. Finally, a selection of acquired conditions is depicted.

2.1 Congenital Conditions

2.1.1 Craniosynostosis

Craniosynostosis is the premature fusion of one or more cranial sutures. It usually occurs as an isolated condition, but in 10–20% of cases, it may be part of a syndrome. Skull growth normally occurs perpendicular to the long axis of a suture. Premature closure, or synostosis, of a suture instead causes growth to occur parallel to the long axis, causing characteristic abnormalities of skull shape (Fig. 2.1).

Synostosis of the sagittal suture causes the skull to expand in its anteroposterior dimension, known as *scaphocephaly* (also called *dolichocephaly*) (Fig. 2.2). This is the most common type of synostosis. Standard skull X-rays are usually diagnostic, but CT scans with 3D reconstructions may be required if corrective surgery is being considered (Fig. 2.3).

If the synostosis affects the coronal or lambdoid suture bilaterally, the skull becomes abnormally short in the anteroposterior dimension, with commensurate increase in skull width, known as *brachycephaly*. Unilateral synostosis of the coronal or lambdoid suture causes anterior (frontal) or posterior (occipital) plagiocephaly respectively, giving the skull

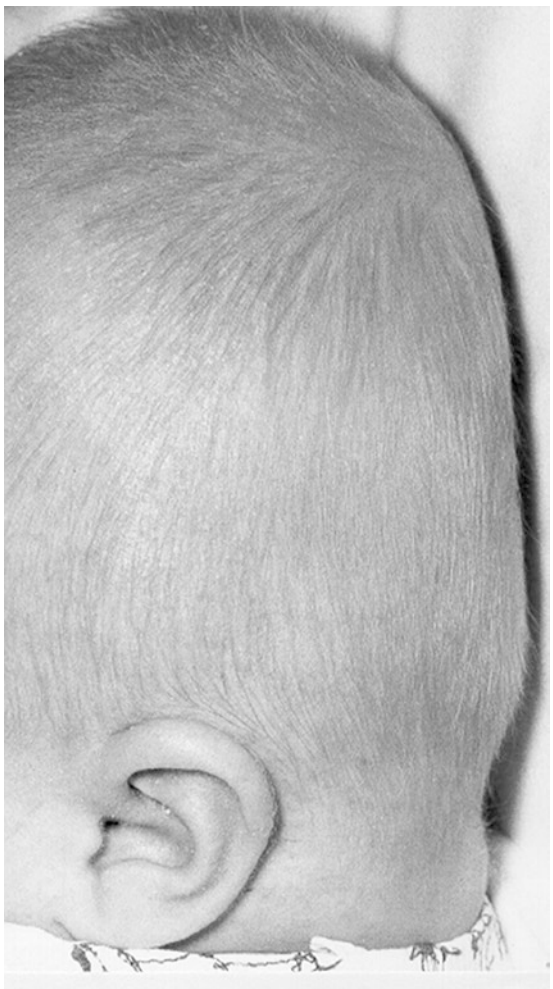

Fig. 2.1 Clinical photograph of flattened occiput in an infant due to premature fusion of the lambdoid sutures

an asymmetrical, skewed appearance. Posterior plagiocephaly due to synostosis may need to be differentiated from positional posterior plagiocephaly, increasingly seen due to babies being nursed exclusively in the supine position.

Synostosis of the metopic suture, the vertical suture in the centre of the frontal bone, leads to *trigonocephaly*. The child

S. Butler (✉)
Queen Elizabeth University Hospital, Glasgow, UK
e-mail: Sandra.Butler@ggc.scot.nhs.uk

R. Carachi (ed.), *Atlas of Paediatric Surgical Imaging*, https://doi.org/10.1007/978-3-030-32384-4_2

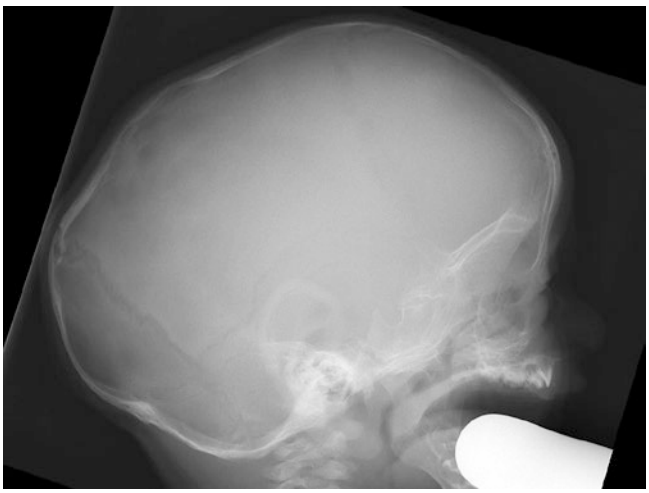

Fig. 2.2 Lateral skull radiograph demonstrating scaphocephaly due to premature closure of the sagittal suture

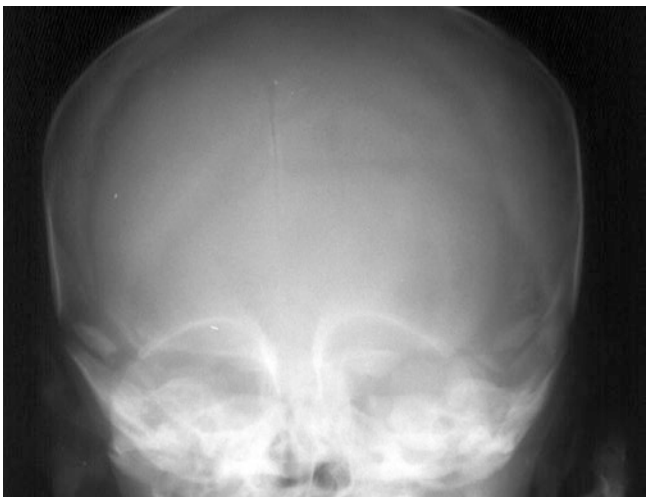

Fig. 2.4 Frontal skull radiograph demonstrating hypotelorism due to premature fusion of the metopic suture

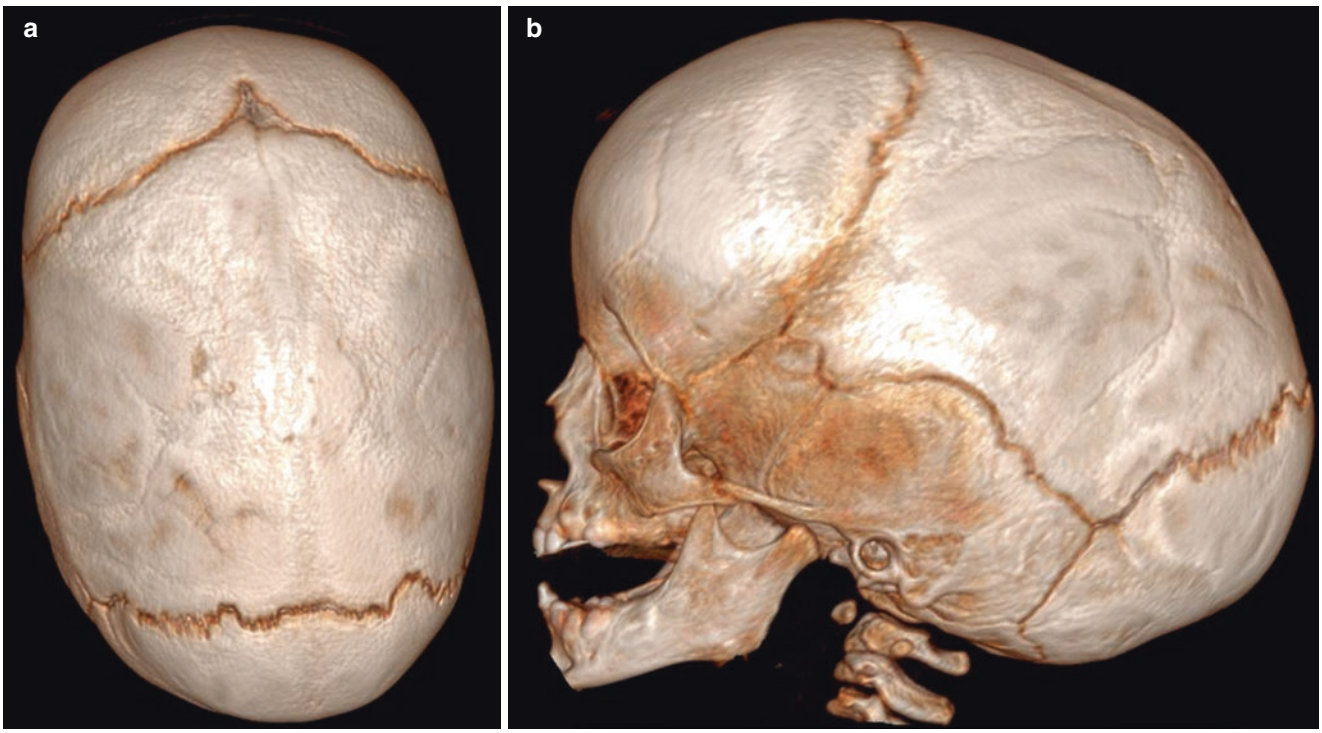

Fig. 2.3 3D reconstructed CT images of skull showing prematurely fused sagittal suture (**a**) and scaphocephaly (**b**)

has a triangular-shaped forehead that may be associated with hypotelorism (Figs. 2.4 and 2.5).

Intrauterine premature fusion of the coronal, sagittal, and lambdoid sutures results in a *cloverleaf skull* (in German, *kleeblattschädel*). In this severe type of craniosynostosis, bulging of the intracranial contents results in a characteristic trilobed appearance of the skull and thinning of the calvarial bones (Figs. 2.6 and 2.7). The condition is associated with a number of syndromes. Patients usually have intellectual impairment and proptosis.

A common secondary synostosis seen in surgical practice occurs after ventricular shunting. In these patients, treatment of hydrocephalus reduces the internal pressure within the skull vault, resulting in diminished growth stretch at the sutures and premature functional fusion of one or more cranial sutures (Fig. 2.8).

2.1.2 Encephalocele

An encephalocele, also known as *meningoencephalocele*, is a neural tube defect with sac-like herniation of brain tissue and meninges through a defect in the skull. Seventy-five percent of lesions are in the occipital region but other areas

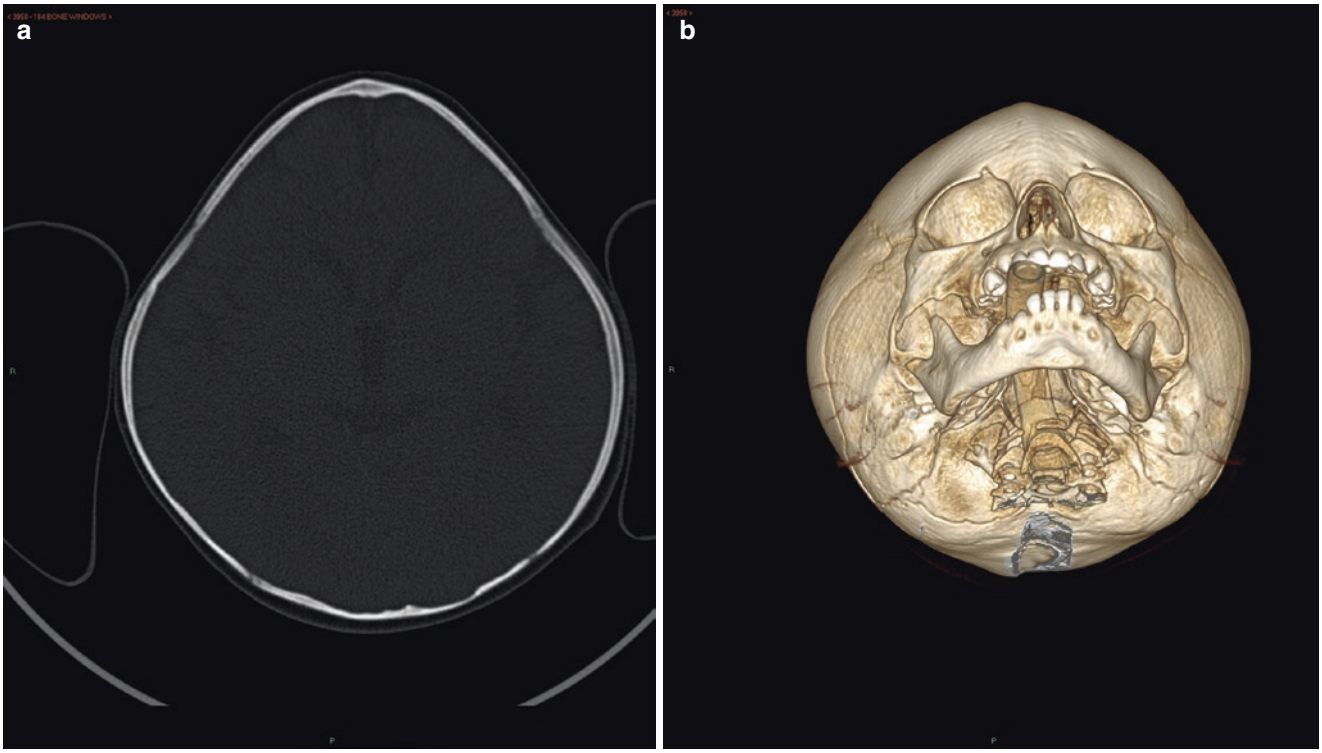

Fig. 2.5 Axial CT (**a**) and 3D reconstructed (**b**) images show trigonocephaly due to premature fusion of the metopic suture. Note the typical triangular appearance of the frontal bone, with a prominent midline ridge

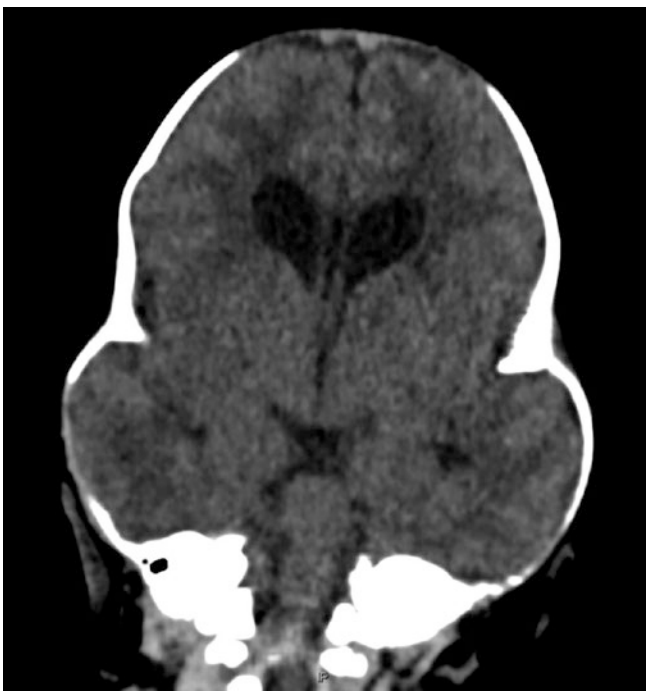

Fig. 2.6 Cloverleaf skull. Coronal reformatted CT image shows the trilobed shape of the skull due to bulging of membranous bone between the fused sutures

are affected (Fig. 2.9). There may be associated craniofacial abnormalities or other brain malformations. Hydrocephalus may also complicate this condition.

High-resolution CT may be used to delineate the anatomy of the bony defect, but MRI better defines the contents of the extracranial mass and its connection to the brain (Fig. 2.10). There may be associated Chiari or Dandy-Walker malformations, or migrational abnormalities of the brain. MR venography (MRV) is used to demonstrate any venous involvement in these lesions. Nasal encephaloceles may be difficult to assess clinically, and here CT is used in addition to MRI to investigate the bony anatomy. MRI is very helpful in differentiating a fronto-ethmoidal encephalocele from a nasal dermoid cyst or nasal glioma.

2.1.3 Anencephaly

Anencephaly is a neural tube defect that results in absence of a major part of the brain, cranial vault, and scalp. It is usually detected antenatally on fetal ultrasound scanning, which, in combination with elevated maternal alpha-fetoprotein measurement, allows for reliable diagnosis. Although the brain may appear normal initially, absence of the cranium is demonstrable from 11 weeks gestation. The

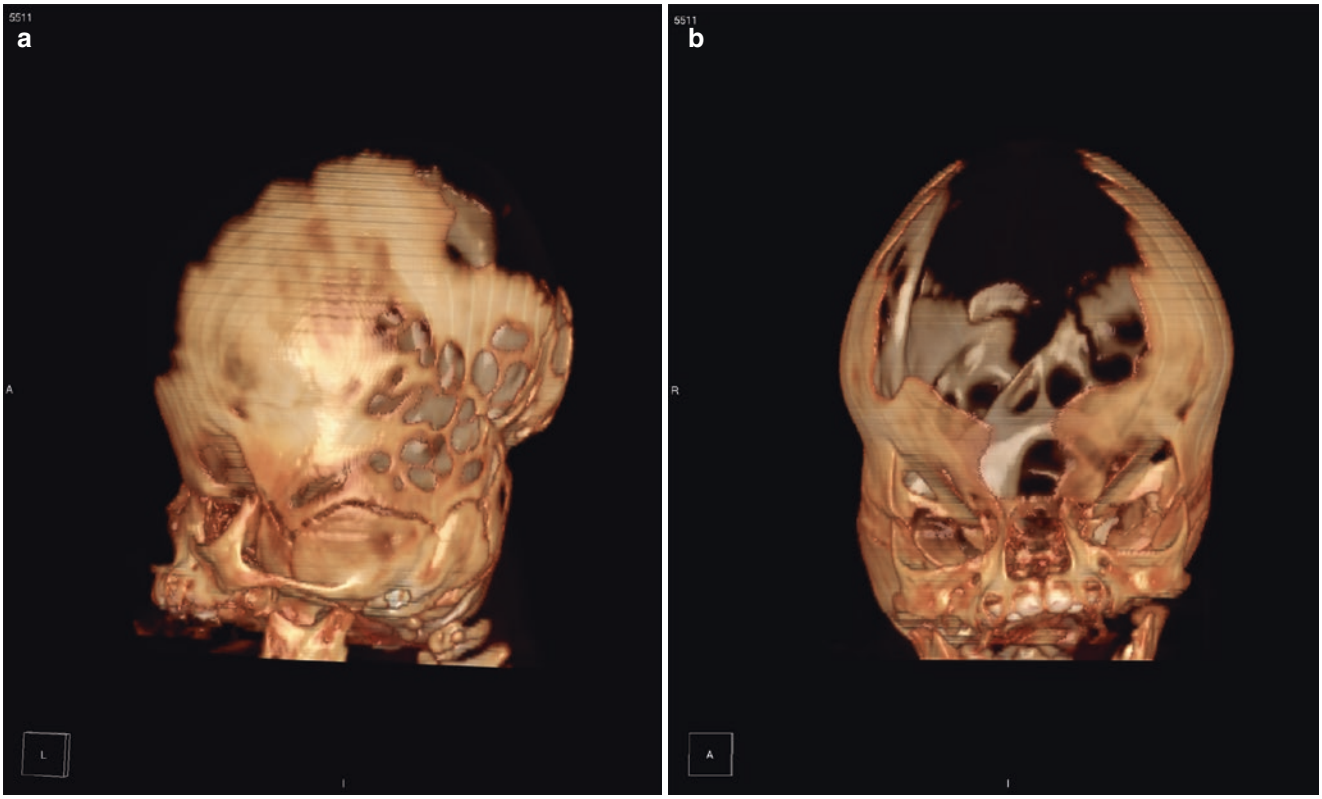

Fig. 2.7 Lateral (**a**) and frontal (**b**) 3D reformatted CT images of head demonstrating bulging and marked thinning of the calvarium in a child with cloverleaf skull

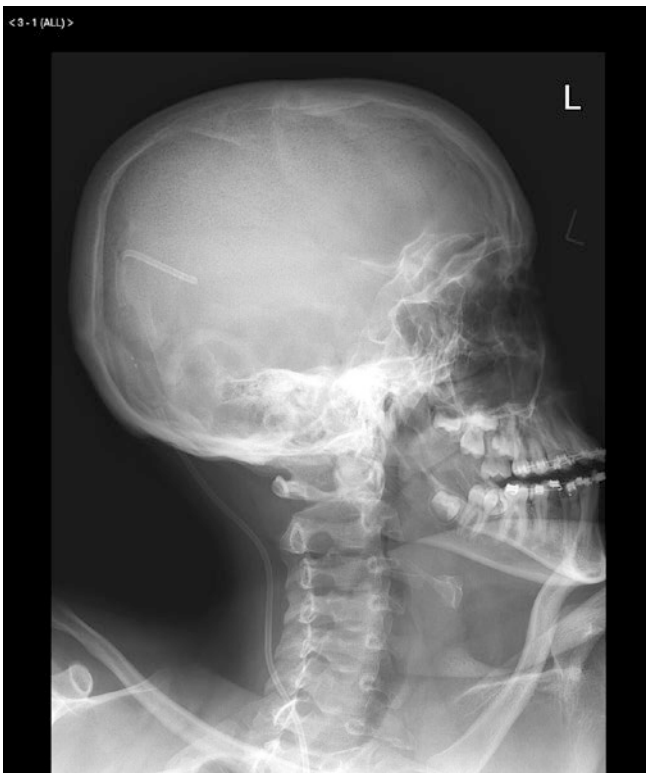

Fig. 2.8 Lateral skull radiograph showing secondary synostosis of cranial sutures as a result of ventriculoperitoneal shunt insertion

fetal brain becomes progressively more abnormal, appearing absent later in gestation. The condition is incompatible with life.

Post mortem radiographic assessment of an affected fetus is performed to look for other associated defects that may affect genetic counselling of the parents (Fig. 2.11).

2.1.4 Cutis Aplasia Congenita

In cutis aplasia congenita, a focal area of skin is absent at birth. It most commonly involves the scalp, but any part of the body can be affected. It typically presents as a solitary defect within the scalp, although multiple lesions can occur. The condition can be mistaken for iatrogenic injury caused by forceps delivery or application of a fetal scalp electrode during labour.

The majority of scalp lesions arise on the vertex, adjacent to the midline. The defect is usually seen as a well-defined, punched-out lesion within the scalp (Fig. 2.12). Some cases have an associated calvarial defect, which can be demonstrated on CT scanning (Fig. 2.13). Calvarial defects can lead to intracranial complications such as sagittal sinus bleeding or thrombosis and meningitis.

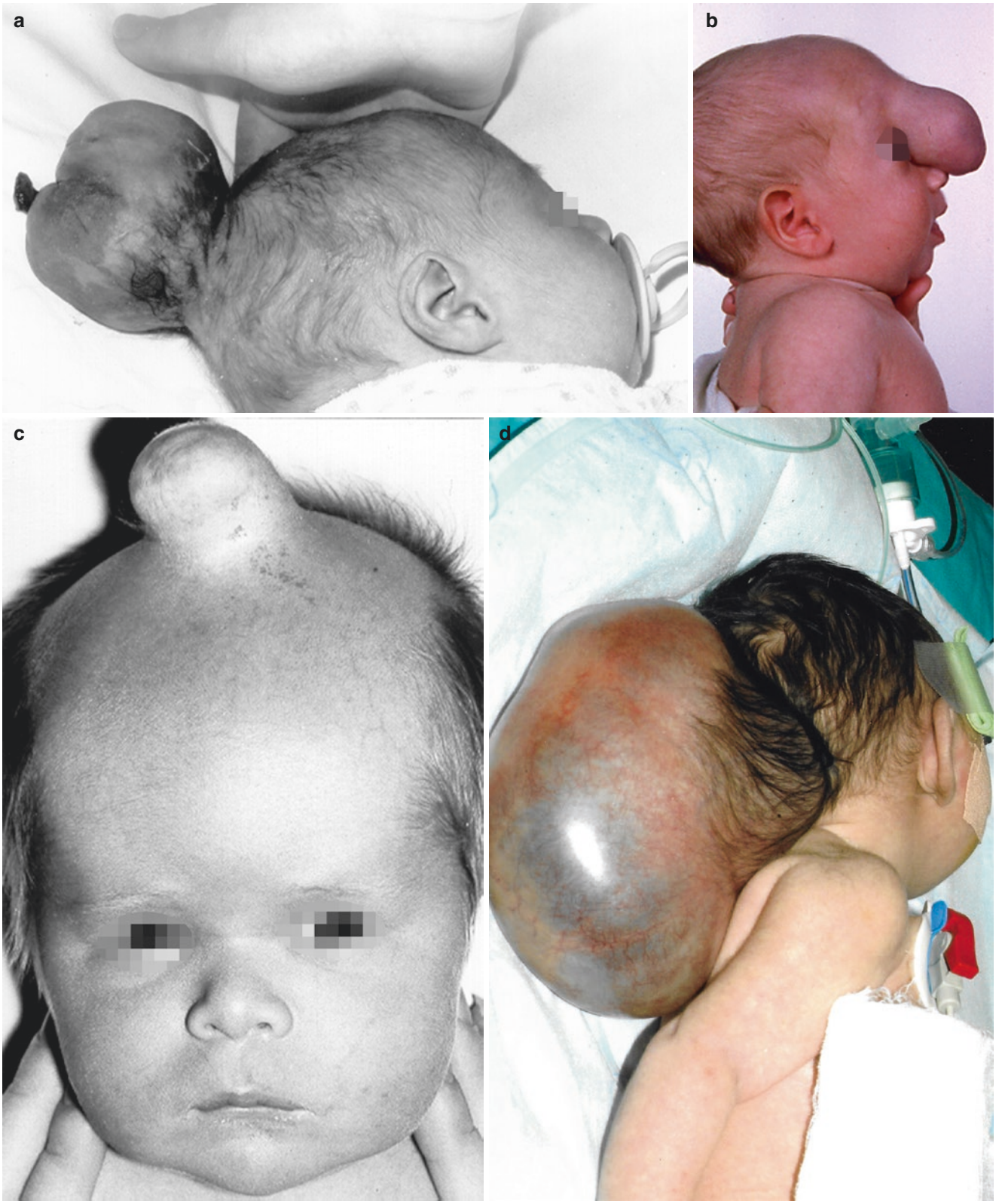

Fig. 2.9 (**a**) Clinical photograph of posterior encephalocele. (**b**) Clinical photograph of anterior encephalocele. (**c**) Clinical photograph of sagittal encephalocele. (**d**) Clinical photograph of occipital encephalocele

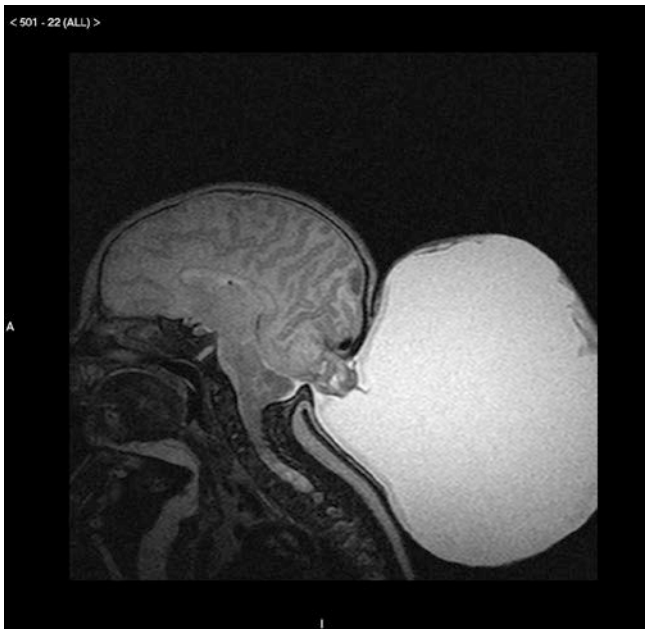

Fig. 2.10 Large occipital meningoencephalocele. T2-weighted sagittal MR image demonstrates a large CSF-filled sac extending from the occipital region of the skull. The cephalocele contains some brain tissue. There is associated distortion of the posterior cerebrum and cerebellum

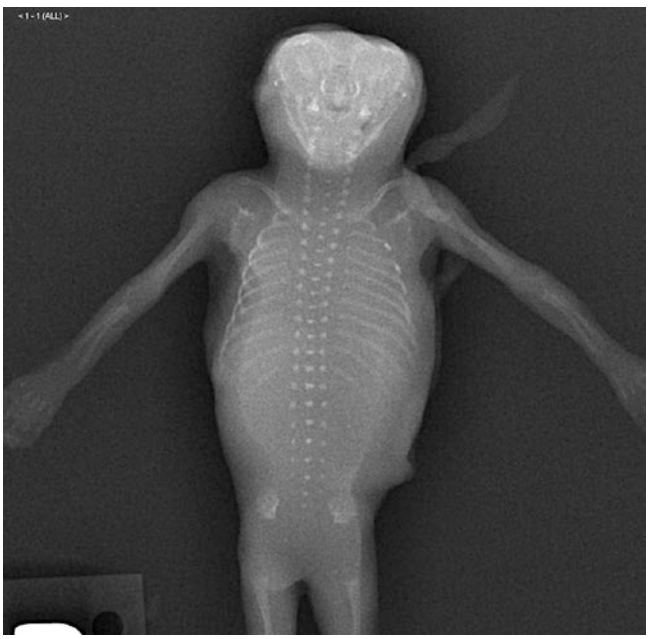

Fig. 2.11 Anencephaly. This AP fetal radiograph shows absence of the skull vault and brain tissue. The skull base and facial bones are present

2.1.5 Choanal Atresia

Choanal atresia is a condition characterised by anatomical closure of the posterior nasal passage. The closure may be unilateral or bilateral and may be bony, bony-membranous, or membranous. This condition is associated with a number of syndromes.

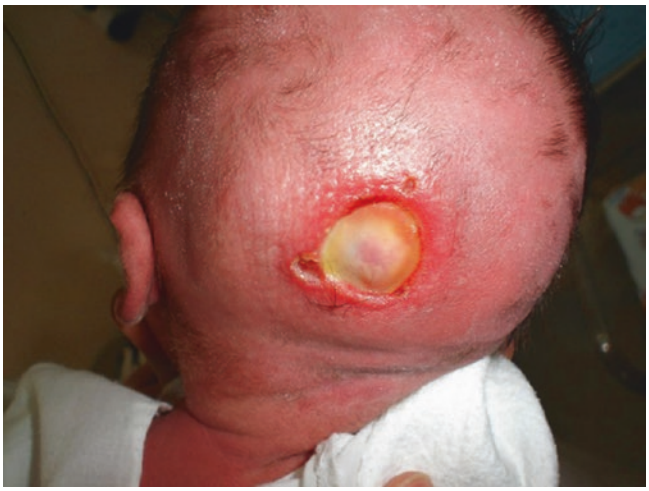

Fig. 2.12 Clinical photograph of cutis aplasia of scalp, showing a well-defined, punched-out lesion within the posterior scalp

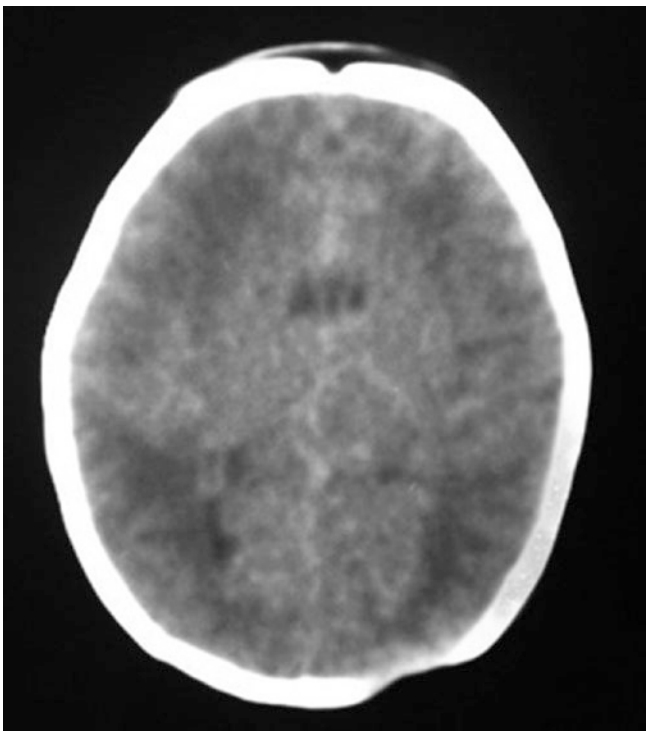

Fig. 2.13 Axial CT image demonstrates focal bony deficiency in the posterior left skull, subjacent to an area of cutis aplasia

A newborn baby breathes through the nose. In most infants, the technique of mouth breathing is acquired slowly during the first 3 months of life. Bilateral choanal atresia thus results in severe dyspnoea, or apnoea during feeds. When the condition is unilateral, the risk to life is much lower. Feeding difficulties are experienced because of the inability to suck and breathe at the same time.

Diagnosis can be confirmed by observing that the passage of a nasogastric catheter is arrested at the level of the choana, only a few centimetres into the nose. Historically, lateral radiographs of the skull were taken after the nasal cavities

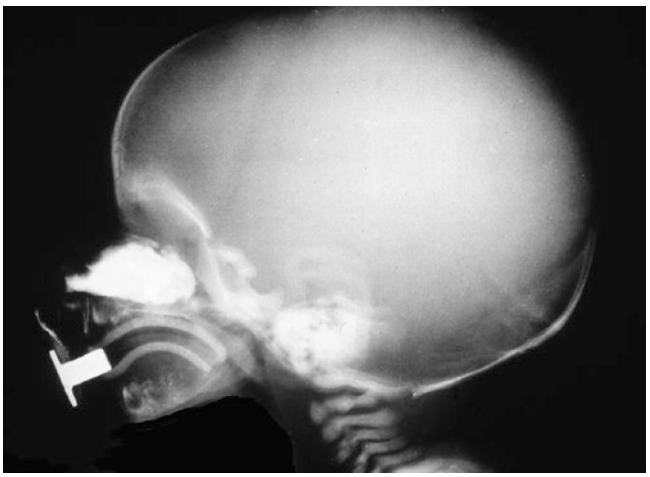

Fig. 2.14 Historical lateral radiograph demonstrating choanal atresia. Contrast fills the nasal passage with no evidence of drainage into the nasopharynx. Note the oropharyngeal tube maintaining patency of the airway

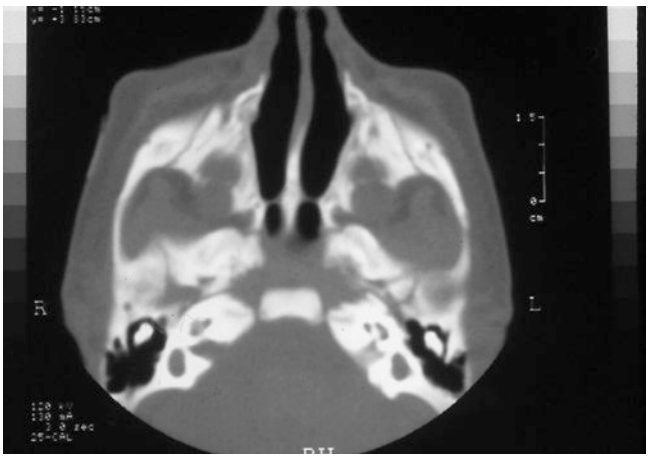

Fig. 2.15 Bilateral membranous choanal atresia. This historical axial CT image shows a thin membrane across the posterior nasal passage bilaterally

had been cleared of secretions and contrast medium inserted (Fig. 2.14). Today, CT is performed to demonstrate the anatomy of the nasal passage. To prevent false-positive diagnosis of membranous atresia, intranasal decongestants are administered before scanning, and gentle suction of each nostril is performed. The imaging features of choanal atresia include abnormal narrowing of the posterior choana on one or both sides due to medial bowing of the maxilla, thickening of the posterior vomer and the presence of a membranous or bony septum extending across the posterior choana, with an air-fluid level above the obstruction. Narrowing of either choana below 4 mm in transverse diameter is considered diagnostic of atresia (Figs. 2.15, 2.16, and 2.17).

2.1.6 Dermoid

Dermoids are developmental lesions that contain skin and skin appendages, arising from islands of ectodermal tissue.

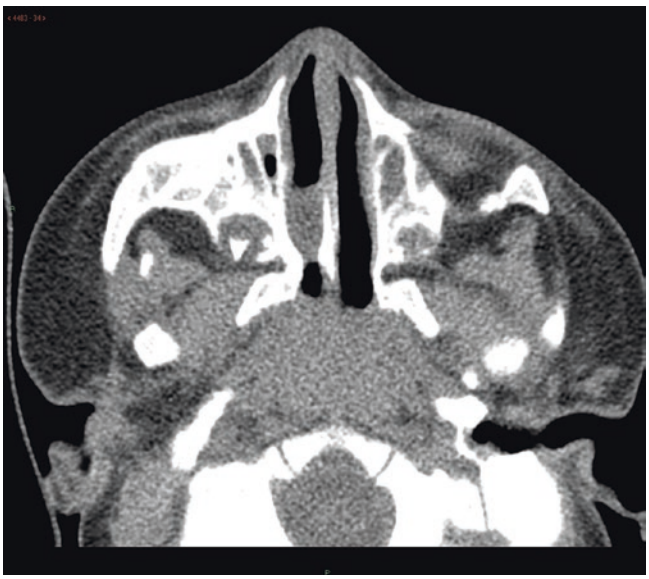

Fig. 2.16 Right-sided membranous choanal atresia. Axial CT image demonstrates a fluid level in the right posterior choana. Drainage of mucus is prevented by a thin membrane. There is thickening of the right side of the vomer and medial bowing of the right posterior maxilla

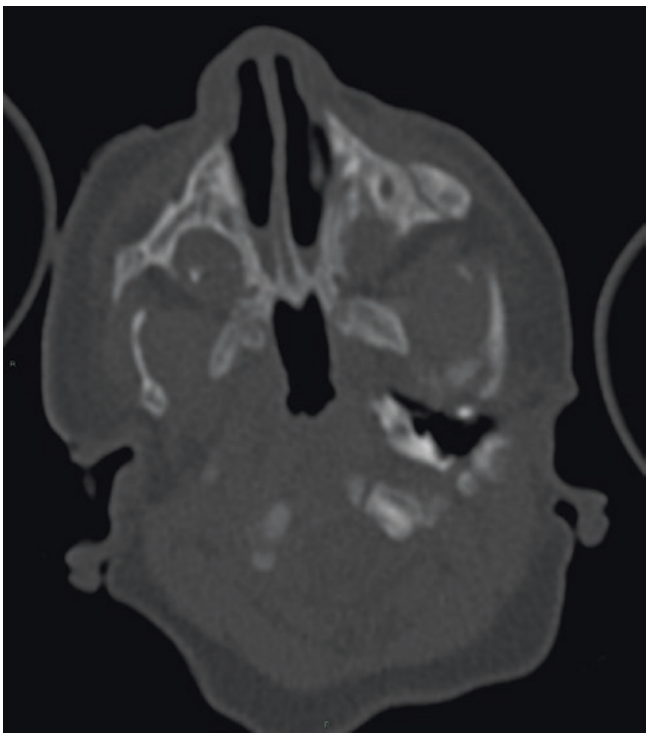

Fig. 2.17 Bilateral bony choanal atresia. Axial CT image shows obliteration of the posterior choana bilaterally due to a bony bar. The vomer is thickened and there is medial deviation of the posterior maxilla bilaterally. Bilateral fluid collections are present in the choanae

Although congenital, they may not be diagnosed at birth. They are slow-growing lesions and usually become apparent in the first decade of life, presenting as painless swellings. The commonest locations for dermoid cysts within the head are periorbital, nasal, submental, and along the cranial sutures.

2.1.6.1 Orbital Dermoid Cyst

Most orbital dermoid cysts are superficial and situated in the area of the lateral brow, adjacent to the frontozygomatic suture. Superficial lesions may also be identified along the medial canthus of the orbit. Deeper orbital lesions are rare and located within the eye. They can present with proptosis.

Imaging of superficial periorbital dermoid cysts is sometimes performed with MRI to determine if there is posterior extension into the orbit. The cysts appear as well-marginated lesions, which may cause scalloping of the adjacent bone. Internally, they have the signal characteristics of lipid because of sebaceous secretions. They therefore appear bright on T1 and T2-weighted sequences (Fig. 2.18). The internal lipid signal nulls out (becomes dark) on fat-suppressed sequences. The cyst contents usually do not enhance with contrast. There may be enhancement of the cyst wall.

2.1.6.2 Nasal Dermoid

In embryological development, a dural diverticulum that extends from the anterior cranial fossa to the nasal tip normally regresses and disappears. Incomplete separation of the dura from the skin can lead to dermal elements being pulled into the regressing dural tract. If this happens, a dermal sinus tract can form along the regression path. Dermoid and epidermoid cysts also can form along the path, either alone or in combination with a dermal sinus tract. Cysts can therefore occur anywhere along the course of the regressing dural tract, from the nasal tip to the anterior cranial fossa.

A nasal dermoid cyst presents as a swelling along the dorsum of the nose or the glabella. A sinus may be present with hairs and/or a sebaceous discharge emanating from its ostium. Intracranial extension cannot be determined clinically. Complications of nasal dermoid infection include meningitis, intracranial abscess, and venous sinus thrombosis.

Preoperative MR imaging is performed to confirm the diagnosis of a dermoid and exclude other causes of a midline nasal mass, such as a nasal glioma or nasal encephalocele. High-resolution MRI using very thin slices can help to identify an enhancing sinus tract. It is important to look for any intracranial extension (Fig. 2.19). High-resolution CT scanning is useful to assess for bony defects such as widening of the foramen cecum or a bifid crista galli if intracranial extension is suspected (Fig. 2.20). Dermoid cysts are identified as round lesions with high signal on T2-weighted MR imaging. They demonstrate variable signal intensity on T1-weighted imaging, depending on the cyst contents. If there is current or recent infection, the cyst may demonstrate contrast enhancement (Fig. 2.21).

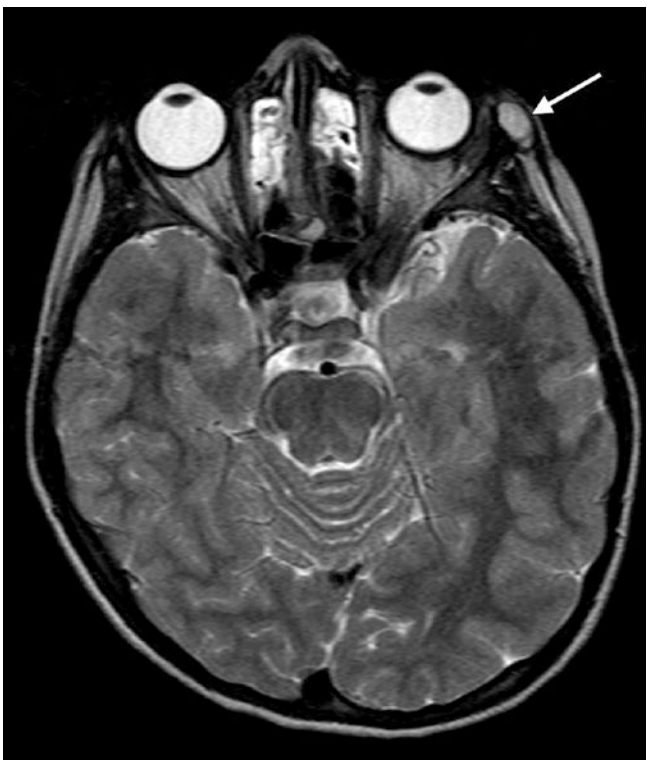

Fig. 2.18 Superficial dermoid cyst of left orbit (*arrow*). Axial T2-weighted MR image shows an ovoid structure with high signal contents along the lateral aspect of the left orbital wall

2.1.7 Haemangioma

The nomenclature and classification of vascular lesions have progressed from historical clinical descriptions such as "strawberry birthmark" and "salmon patch" to terminology based on the histopathological and blood flow patterns of these anomalies. A classification system, originally described by Mulliken and Glowacki in 1982, has been developed by the International Society for the Study of Vascular Anomalies (ISSVA) and is now considered the standard. The adapted system divides vascular anomalies into two broad categories: proliferating vascular tumours and vascular malformations. Vascular tumours demonstrate abnormal proliferation of endothelial cells, whereas vascular malformations are structural abnormalities of the capillary, venous, lymphatic, and arterial systems that grow in proportion to the child.

Haemangiomas, the most common tumour in infancy, with an incidence of 2–3%, represent the majority of proliferating vascular tumours. Infantile haemangiomas represent about 70% of all haemangiomas. They are found on the head and neck in approximately 60% of cases (Fig. 2.22). They typically appear within the first 6 weeks of life and proliferate in the first year. The tumours involute between 1 and 8 years of age, with complete involution occurring by puberty in most cases.

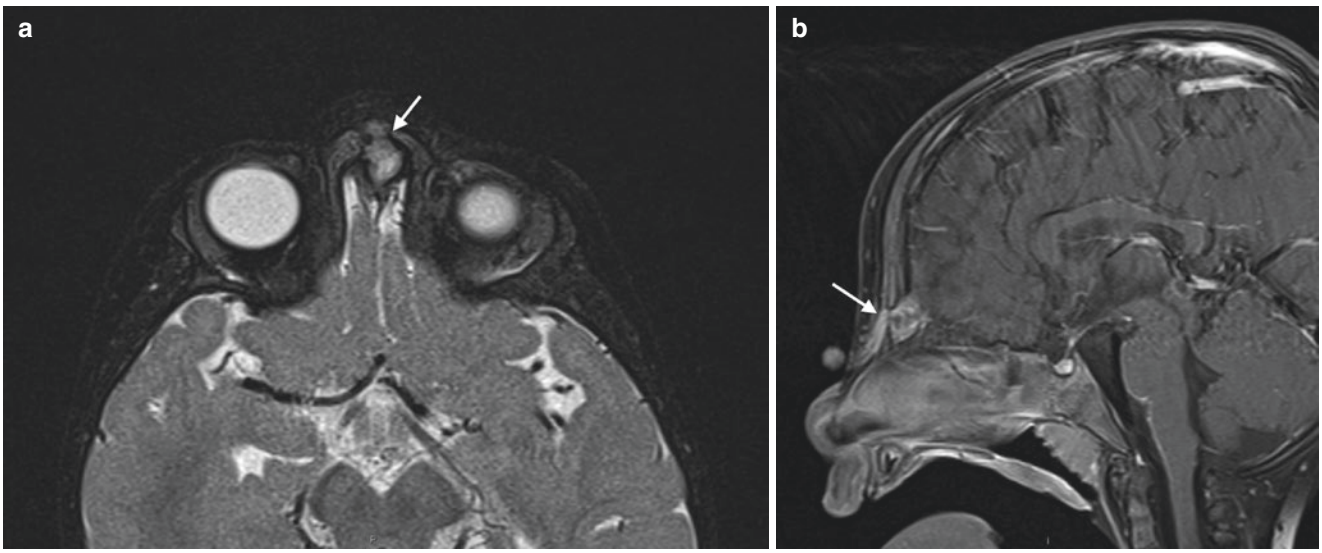

Fig. 2.19 Nasal dermoid tract with intracranial dermoid cyst. (**a**) Axial T2 short-TI inversion recovery (STIR) MR image shows a midline dermoid tract (*arrow*) extending from the glabella through the nasal bone, with a small dermoid cyst in the foramen cecum. (**b**) Sagittal post-contrast T1-weighted fat-saturated MR image demonstrates enhancement of the tract (*arrow*) and the intracranial dermoid cyst. The small ovoid structure anterior to the glabella is a skin marker denoting the position of the external punctum of the tract

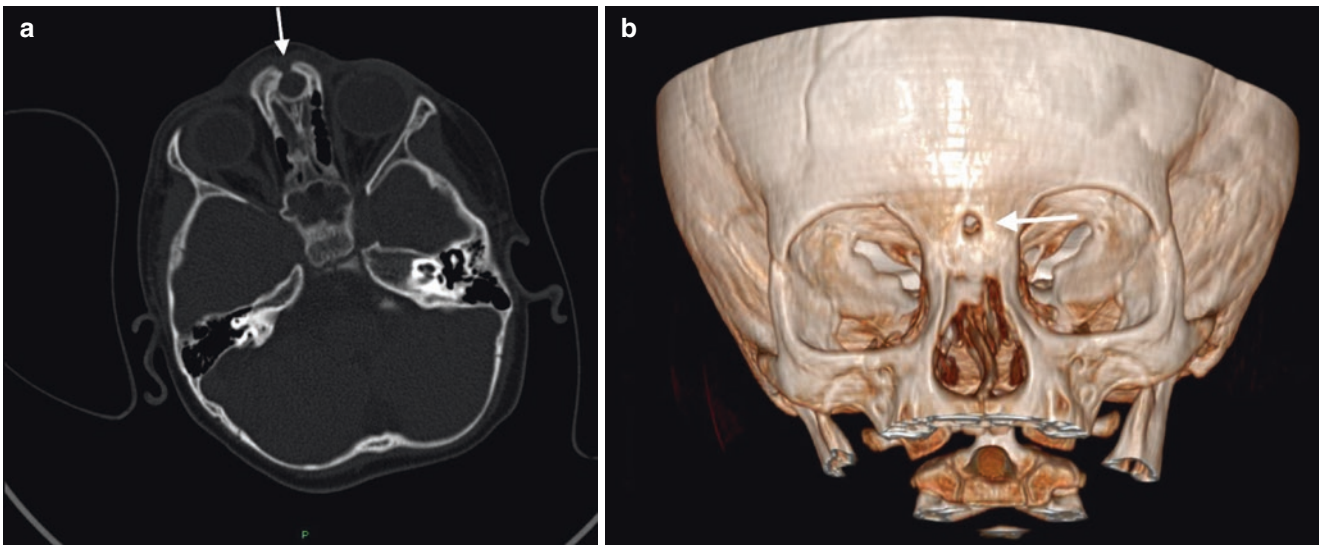

Fig. 2.20 Axial CT (**a**) and frontal view of 3D reformation (**b**) show a small, midline bony deficiency in the nasal bone (*arrow*) due to a nasal dermoid tract. An enlarged foramen cecum is seen posterior to the bony deficiency on the axial image

Nearly all infantile haemangiomas are managed clinically without imaging, but those that might affect the airway or disturb vision, and those that are associated with other anomalies, may be imaged in order to assess the extent of disease. Ultrasound and MRI are the most useful imaging techniques.

The orbit is a common site for infantile haemangioma, and MRI is the imaging modality of choice. MRI demonstrates a well-demarcated, lobulated mass with intralesional and perilesional flow voids, which represent ectatic vascular channels (Fig. 2.23). The lesions are high-signal on T2-weighted imaging, isointense to muscle on T1-weighted images, and typically demonstrate avid contrast enhancement, particularly in the proliferative phase (Fig. 2.24).

Orbital haemangiomas may be associated with cerebral and vascular anomalies in the PHACES syndrome (***P***osterior fossa anomalies, ***H***aemangiomas of the face, ***A***rterial abnormalities, ***C***erebral vascular anomalies, ***E***ye abnormalities, and **S**ternal or ventral developmental anomalies).

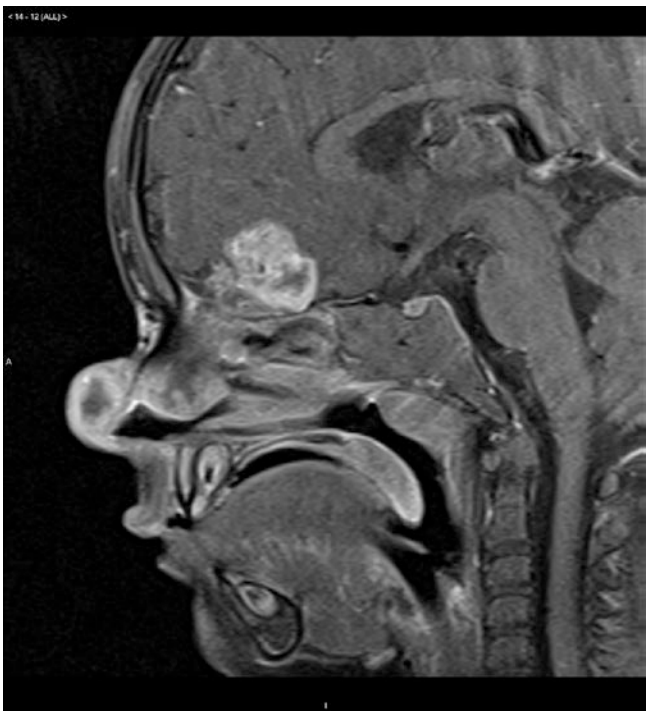

Fig. 2.21 Sagittal post-contrast T1-weighted, fat-saturated MR image shows an infected nasal dermoid with intracranial extension. Note the thick rim enhancement due to infection in both the extracranial and intracranial components

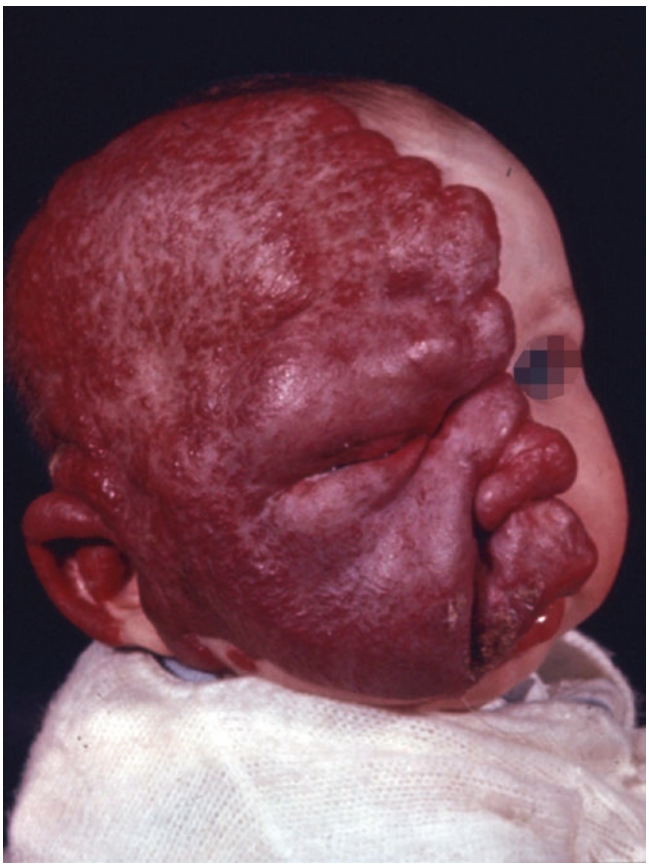

Fig. 2.22 Clinical photograph of an extensive infantile haemangioma affecting the right side of the face

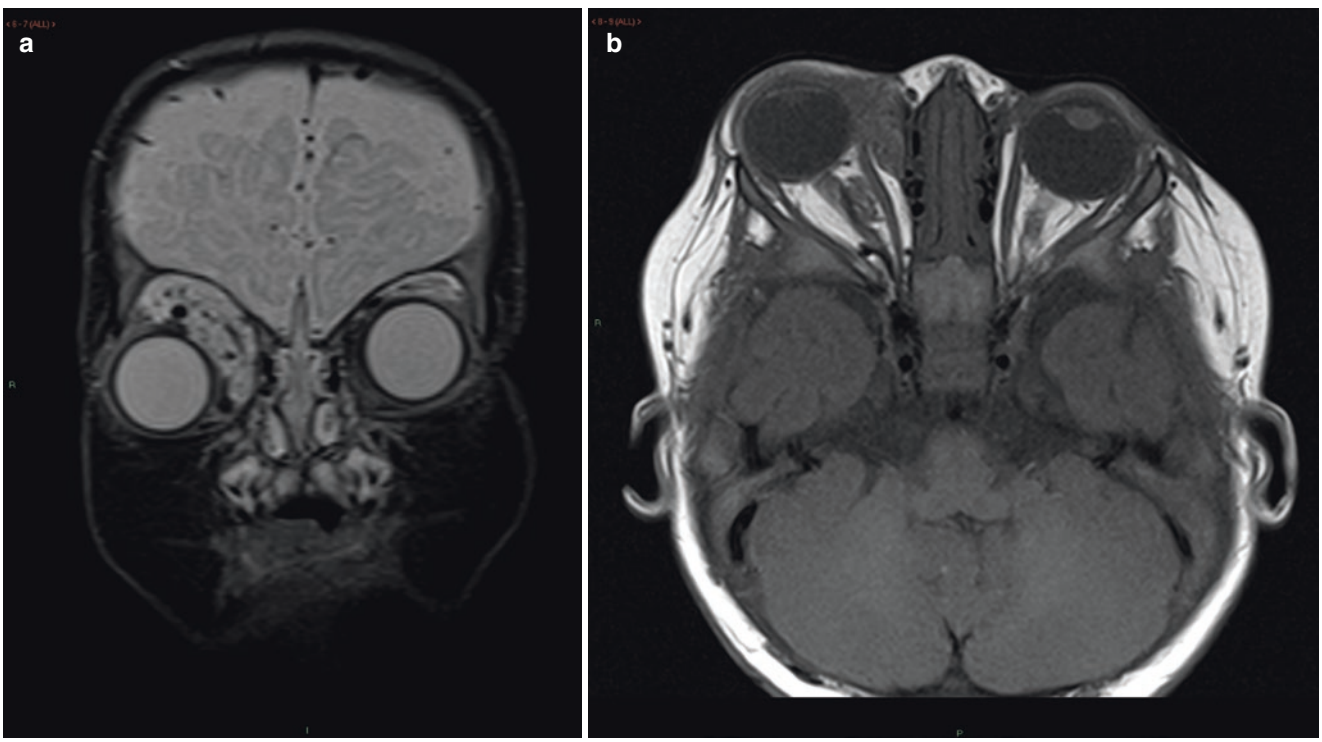

Fig. 2.23 Right intraorbital haemangioma. (**a**) Coronal T2 STIR MR image shows a high-signal, extraconal mass in the superior and nasal aspect of the right orbit. Note the low-signal flow voids within the lesion, representing vascular channels. (**b**) The lesion is of intermediate signal intensity on an axial T1-weighted MR image

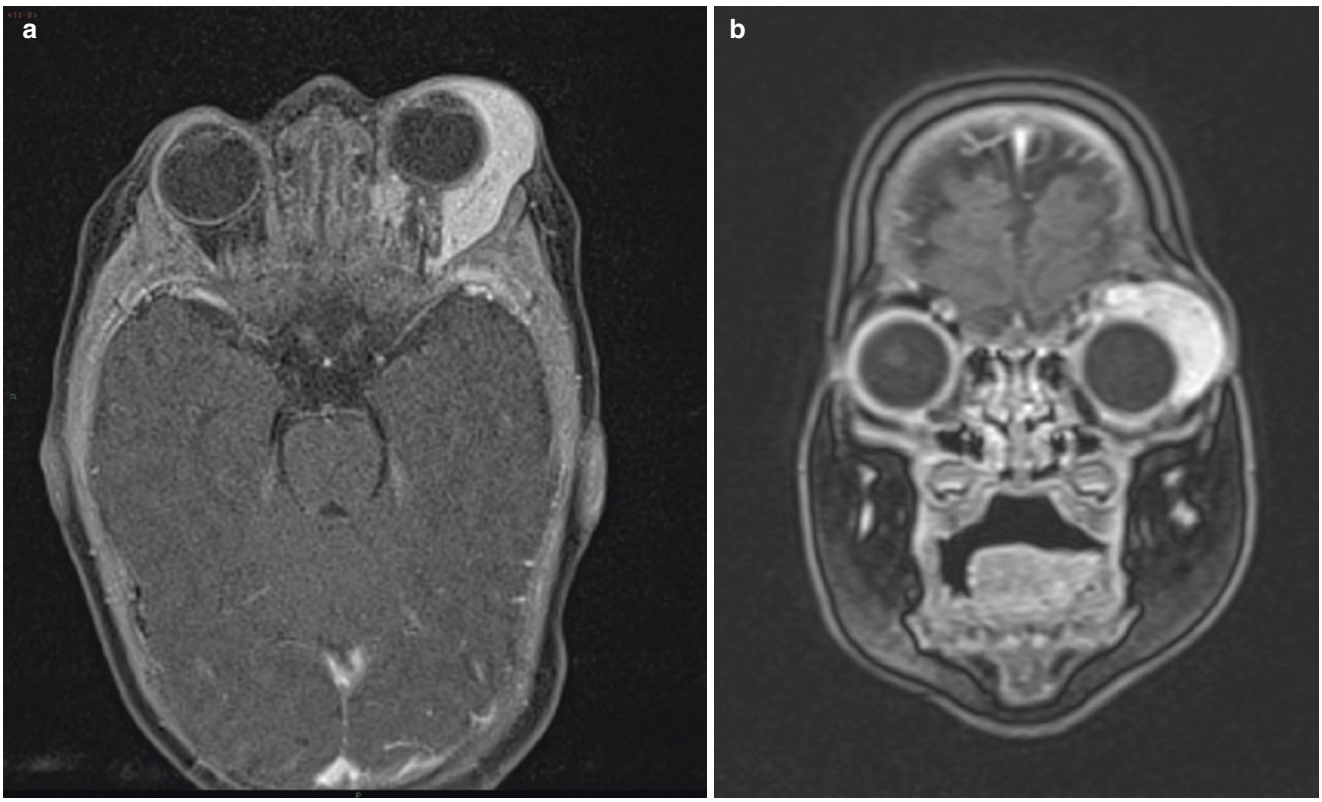

Fig. 2.24 Axial (**a**) and coronal (**b**) post-contrast T1-weighted fat-saturated MR images show avid enhancement of a left intraorbital haemangioma

2.1.8 Hydrocephalus

Hydrocephalus is a condition characterized by increased cerebrospinal fluid (CSF) within the ventricular system, causing dilatation of the ventricles (ventriculomegaly). ***Congenital hydrocephalus*** indicates that the condition is present at birth. It may have been diagnosed antenatally by ultrasound. Common causes of congenital hydrocephalus include myelomeningocele with Chiari II malformation, aqueductal stenosis, arachnoid cyst, and Dandy-Walker malformation. Genetic mutations are also associated with the condition. ***Acquired hydrocephalus***, on the other hand, develops after birth as a consequence of various neurological conditions. Common causes of acquired hydrocephalus include intraventricular haemorrhage (which most frequently affects premature infants), meningitis (usually bacterial), and tumours.

In infancy, hydrocephalus causes enlargement of the head. Clinical examination reveals enlarged fontanelles and separation of the cranial bones. Dilated scalp veins may be evident (Fig. 2.25). Eye signs include lid retraction, failure of upward gaze, and ultimately a picture of sunsetting of the eyes. Subsequently, there may be sixth nerve palsy with paralysis of the lateral rectus muscle, causing a convergent squint. The occipitofrontal circumference (OFC) should be measured and charted, taking account of the infant's gestational age. Serial measurements are necessary to establish

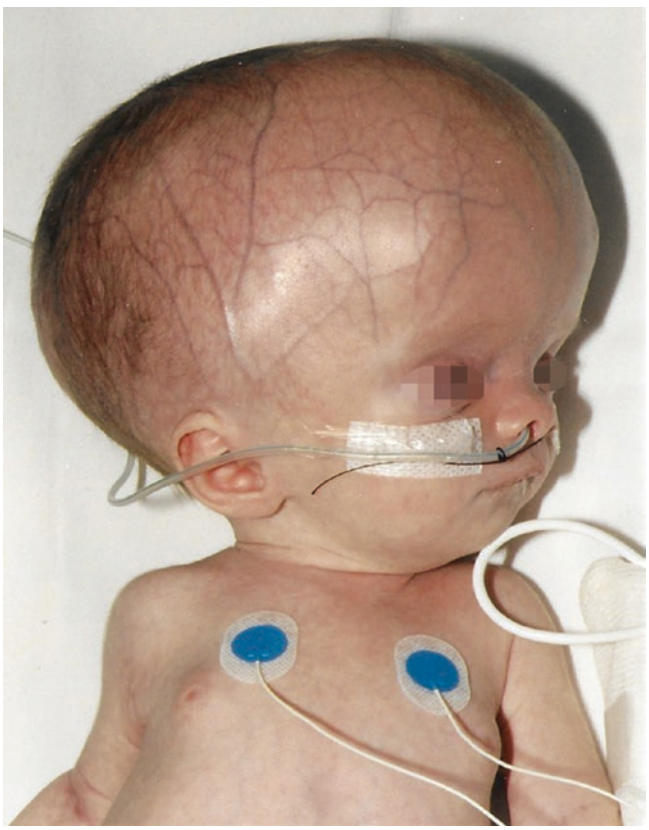

Fig. 2.25 Clinical photograph of severe hydrocephalus in a premature baby due to X-linked hydrocephalus. Note the dilated scalp veins

Fig. 2.26 Clinical photograph showing transillumination of an infant's head due to the increased volume of CSF owing to hydrocephalus

the diagnosis of progressive hydrocephalus. In the past, transillumination of the infant's head in a darkened room would demonstrate severe hydrocephalus (Fig. 2.26).

Over the age of 2 years, raised intracranial pressure in children with hydrocephalus tends to produce neurological symptoms before significant changes in head size become manifest. These symptoms may include headaches, nausea and vomiting, and visual problems.

Historically, the diagnosis of hydrocephalus was made with skull radiographs, which could show widening of the sutures (sutural diastasis) in children under the age of 2 years. In older children, the radiographs showed a copper-beaten appearance due to pressure from the brain on the inside of the skull. The pituitary sella may be widened and J-shaped. Today, cross-sectional imaging (CT and MRI) is used to diagnose and establish the cause of hydrocephalus. Cranial ultrasound can also be used in infants. Radiological characteristics of hydrocephalus include dilated ventricles (especially the temporal horns of the lateral ventricles), enlargement of the anterior and posterior recesses of the third ventricle, and effacement of the cerebral sulci (Fig. 2.27). Periventricular interstitial oedema resulting from transependymal flow of CSF can be seen in acute obstructive hydrocephalus and is manifest as hypodensity in the periventricular region (Fig. 2.28).

Hydrocephalus may be treated neurosurgically by endoscopic third ventriculostomy (ETV) or by diverting CSF using a ventriculoperitoneal (or occasionally ventriculoatrial) shunt (Fig. 2.29). CT scans are commonly requested to establish the position of the intracranial end of a shunt system (ideally within the ipsilateral ventricle) and to assess for the development of acute hydrocephalus if shunt malfunction is suspected. CT scanning is quick and relatively easy to perform, but the accumulated dose of ionising radiation from repeated exposure makes MRI a preferable modality when possible.

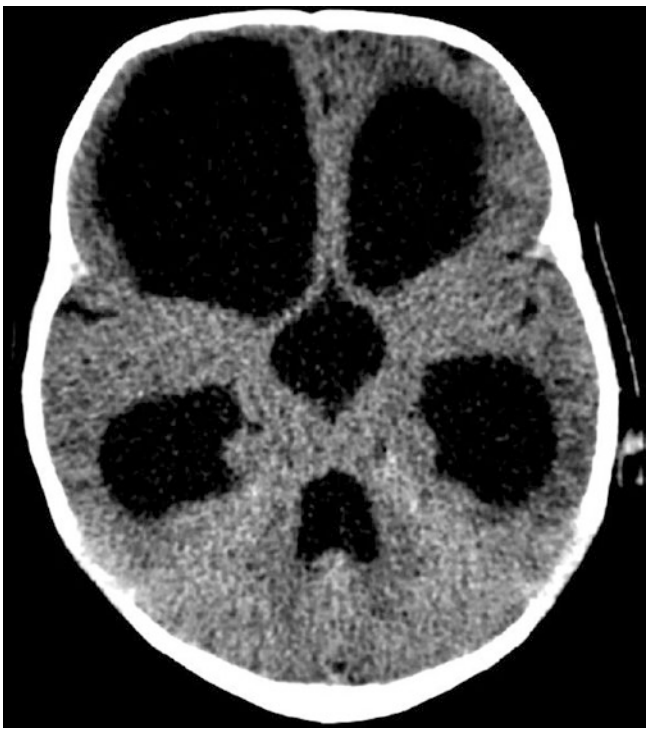

Fig. 2.27 Axial CT image demonstrates hydrocephalus causing dilatation of all four ventricles

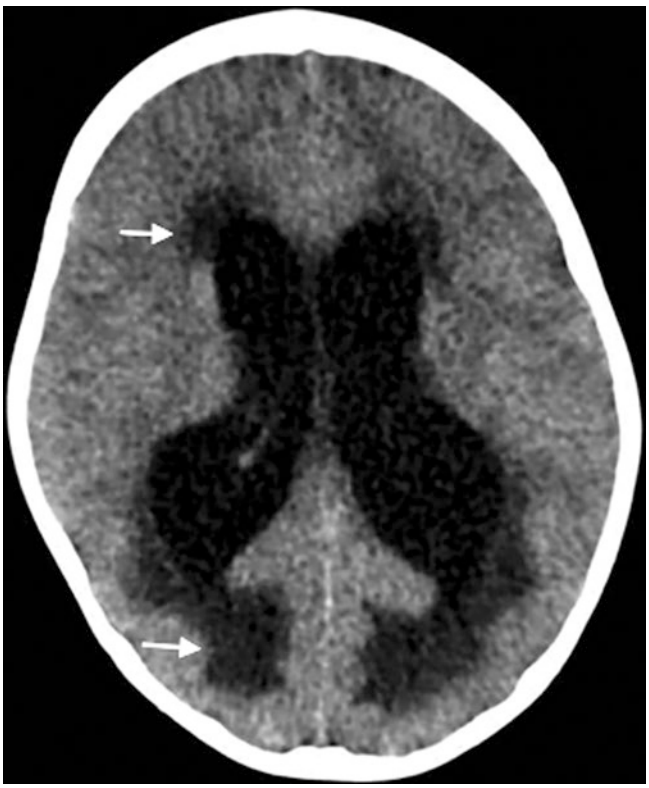

Fig. 2.28 Hydrocephalus. Axial CT image demonstrates low attenuation (low density) (*arrows*) in the periventricular white matter surrounding the dilated lateral ventricles, consistent with transependymal oedema

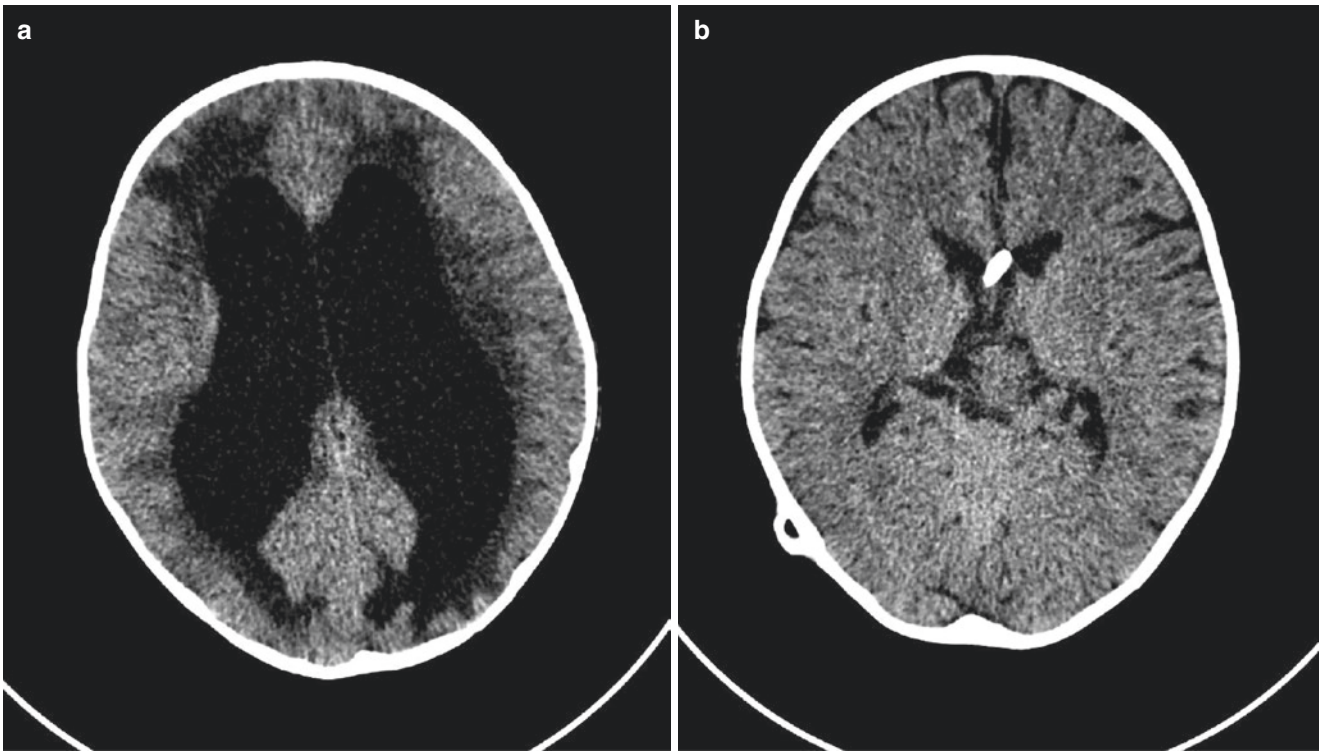

Fig. 2.29 Hydrocephalus. (**a**) Axial CT image shows dilated lateral ventricles with adjacent transependymal oedema. (**b**) Following insertion of a ventriculo-peritoneal shunt, the axial CT image demonstrates decompressed ventricles with the shunt catheter in situ

2.1.9 Chiari Malformations

The Chiari malformations are a heterogeneous group of congenital disorders that are characterised by anatomic anomalies of the cerebellum, brainstem, and craniocervical junction, with caudal displacement of the cerebellum (either alone or together with the lower medulla) into the spinal canal. There are at least four types of Chiari malformation; types I and II are the most common.

In the Chiari type I malformation, the cerebellar tonsils are caudally displaced below the foramen magnum. The condition may be asymptomatic in children. Symptoms, when present, include occipital headache (especially when straining or coughing) and symptoms associated with brain stem compression or syrinx. MRI is the imaging modality of choice. On sagittal MR imaging, the low-lying tonsils appear pointed or peg-like rather than rounded, and the tonsillar sulci are vertically oriented (Fig. 2.30). Cerebellar tonsils protruding more than 6 mm below a line that joins the anterior and posterior margins of the foramen magnum are considered abnormal in the first decade. Cerebellar tonsillar descent greater than 5 mm is abnormal in the second and third decades. Brain stem compression may occur, secondary to the displaced tonsils. A syrinx is seen within the spinal cord in approximately 25% of cases, most commonly within the cervical cord (Fig. 2.31). Craniovertebral malformations are commonly associated.

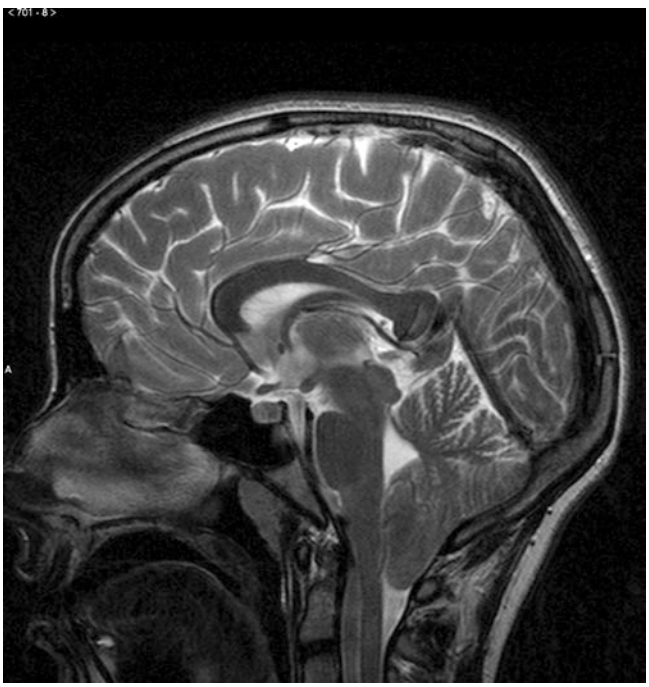

Fig. 2.30 Chiari I malformation. Sagittal T2-weighted MR image shows caudal descent of the cerebellar tonsils below the foramen magnum. The tonsils have a pointed appearance

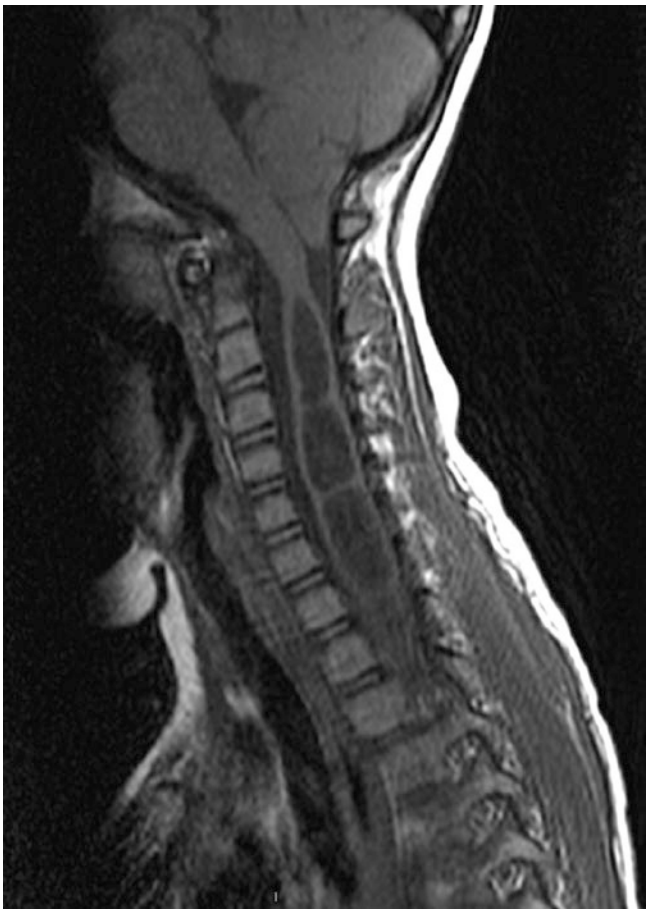

Fig. 2.31 Chiari I malformation with cervical cord syrinx. Sagittal T1-weighted MR image demonstrates CSF-intensity collections within an expanded cervical cord, consistent with a syrinx. The cerebellar tonsils lie below the foramen magnum and have a pointed configuration

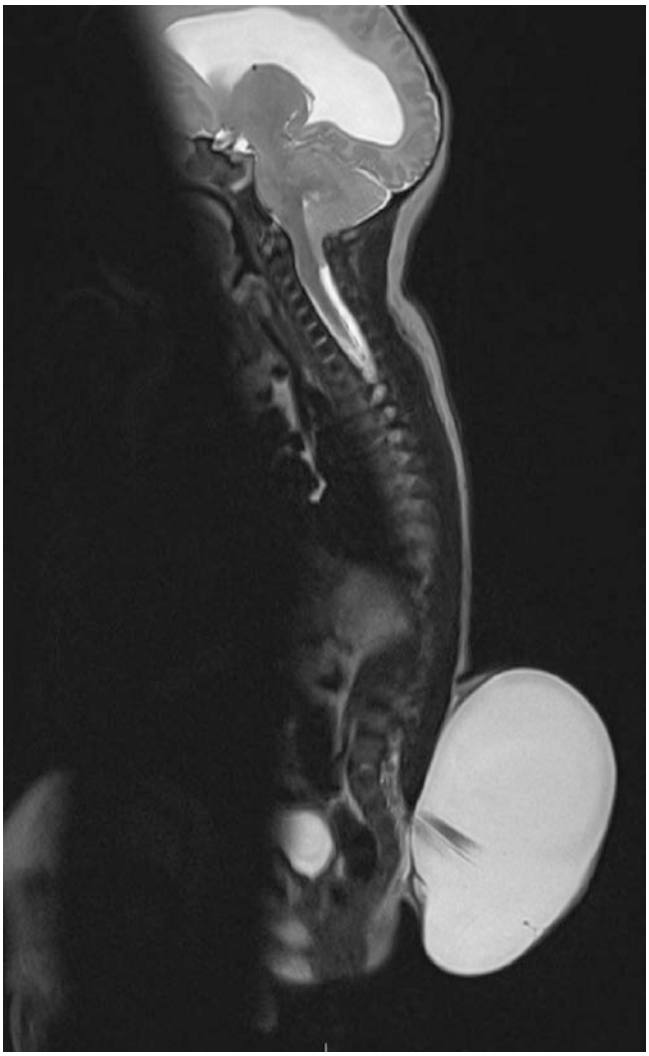

Fig. 2.32 Chiari II malformation and myelomeningocele. Sagittal T2-weighted MR image of the spine and posterior cranial fossa in a newborn infant shows a large lumbosacral CSF-filled sac containing neural tissue, consistent with myelomeningocele (spina bifida). The inferior cerebellum descends through the foramen magnum to lie posterior to the cervical spinal cord

The Chiari II malformation is characterized by a small posterior cranial fossa and descent of the cerebellar vermis and tonsils, fourth ventricle and medulla through the foramen magnum. It is almost always seen in association with myelomeningocele (Fig. 2.32). Sagittal MR imaging demonstrates a small posterior cranial fossa with caudal displacement of the inferior cerebellar structures and medulla into the spinal canal. The fourth ventricle is low lying. Cervicomedullary "kinking" is often evident. Other intracranial features include posterior and inferior stretching of the tectal plate (referred to as tectal "beaking"), callosal hypogenesis, and hydrocephalus (Fig. 2.33). Syrinx is present in 70–90% of cases (Fig. 2.34).

2.1.10 Dandy Walker Malformation

The Dandy-Walker malformation is a congenital abnormality of the posterior cranial fossa. The features that comprise the classic Dandy-Walker malformation are best appreciated on MR scanning. The cerebellar vermis is hypoplastic and rotated upwards (cephalad). There is cystic dilatation of the fourth ventricle, which extends posteriorly to fill the posterior cranial fossa. The posterior cranial fossa is enlarged, and there is elevation of the torcula, transverse sinuses and the tentorium cerebelli. The cerebellar hemispheres are usually displaced anterolaterally and the brain stem is compressed against the clivus (Fig. 2.35). There may be associated supratentorial abnormalities, such as dysgenesis of the corpus callosum, occipital encephalocele, polymicrogyria, and grey matter heterotopia. Hydrocephalus is a common association (90% of cases). Patients usually present in infancy with macrocephaly and symptoms related to hydrocephalus.

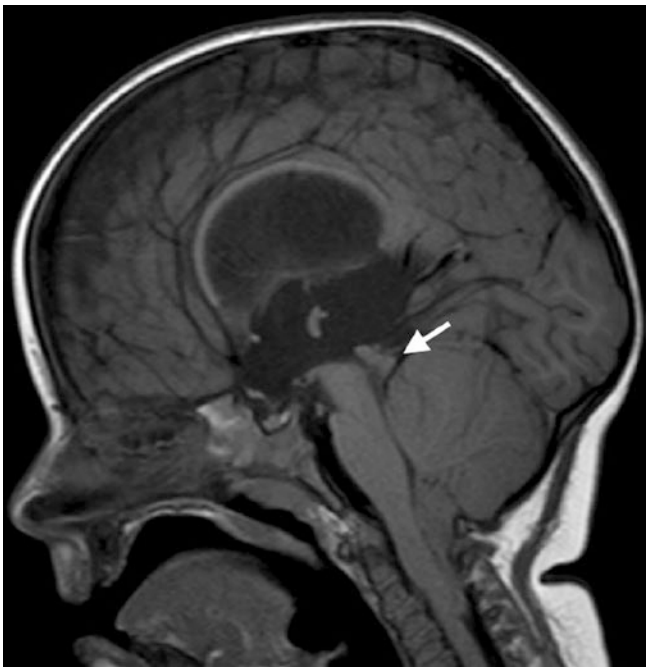

Fig. 2.33 Chiari II malformation. Sagittal T1-weighted MR image shows typical features of the malformation including a crowded posterior cranial fossa, caudal displacement of the inferior cerebellum and medulla into the spinal canal, and a low-lying fourth ventricle. There is beaking of the tectal plate (*arrow*). The third ventricle is dilated (due to hydrocephalus) and the corpus callosum is thin

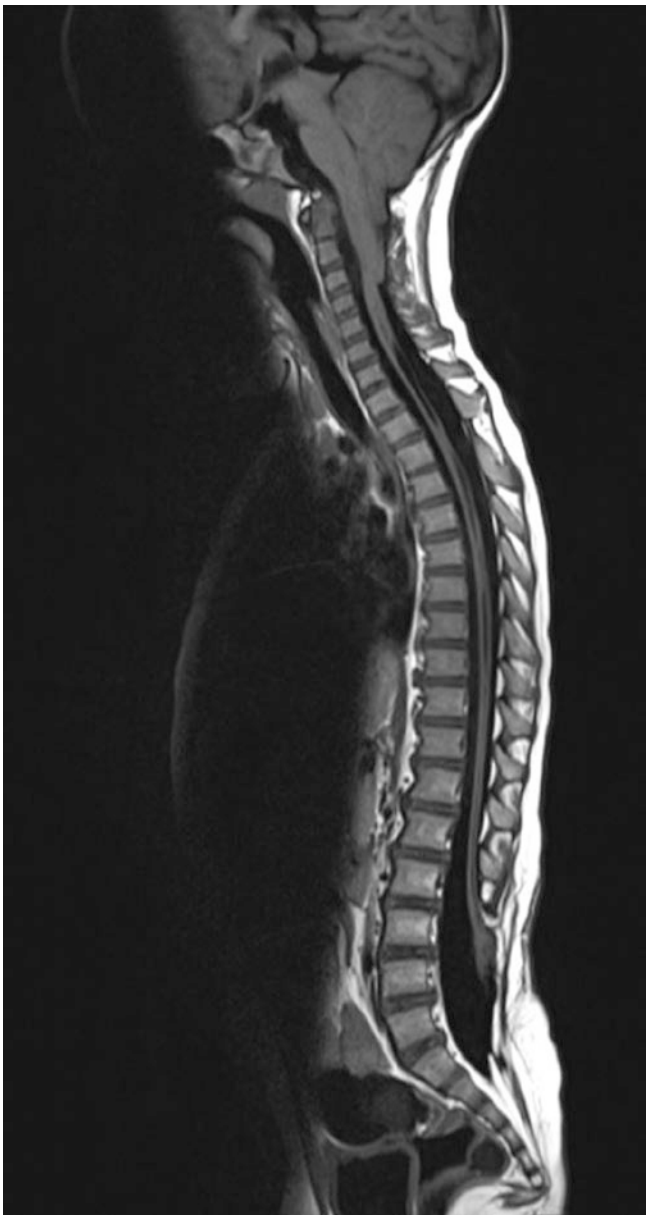

Fig. 2.34 Sagittal T1-weighted MR image of the spine and posterior cranial fossa in a child with previous repair of lumbosacral myelomeningocele. Features of Chiari II malformation are present at the craniocervical junction. Linear areas of T1-hypointense signal (similar to CSF) within the spinal cord are consistent with syrinx

2.1.11 Sturge-Weber

Sturge-Weber syndrome is a congenital disorder characterised by a port-wine stain (capillary malformation of the skin) of the upper face and scalp, usually involving the ophthalmic division of the trigeminal nerve (Fig. 2.36), and a vascular anomaly (angioma) of the underlying leptomeninges. Infants with the syndrome usually develop normally until they start to have focal or generalised seizures. In time, a spastic hemiparesis develops on the contralateral side and developmental delay becomes evident. Glaucoma may also develop and require surgical intervention.

Intracranially, the meningeal angioma affects the pia mater, the innermost layer of the meninges. Cortical calcification is found in the brain immediately below the angioma, commencing in the subcortical white matter and later involving the deep cortex. In childhood (usually after 2 years of age), radiographs of the skull show a characteristic double contour or "tram-track" sign of subcortical and cortical calcification (Fig. 2.37). Nowadays, skull X-rays no longer play a role in the diagnosis of Sturge-Weber syndrome.

The syndrome has classic features on CT imaging, including dense gyriform calcification, particularly in the parieto-occipital cortex. The cortical calcification is usually unilateral but can be bilateral in up to 20% of cases. Atrophy of the involved cerebral hemisphere ultimately occurs and is associated with thickening of the overlying calvarium (Fig. 2.38). MRI is the imaging modality of choice for showing the extent of the pial angioma. The angioma is identified as an area of prominent leptomeningeal enhancement on a post-contrast T1-weighted sequence. The ipsilateral choroid plexus is usually enlarged and enhances avidly with contrast (Fig. 2.39).

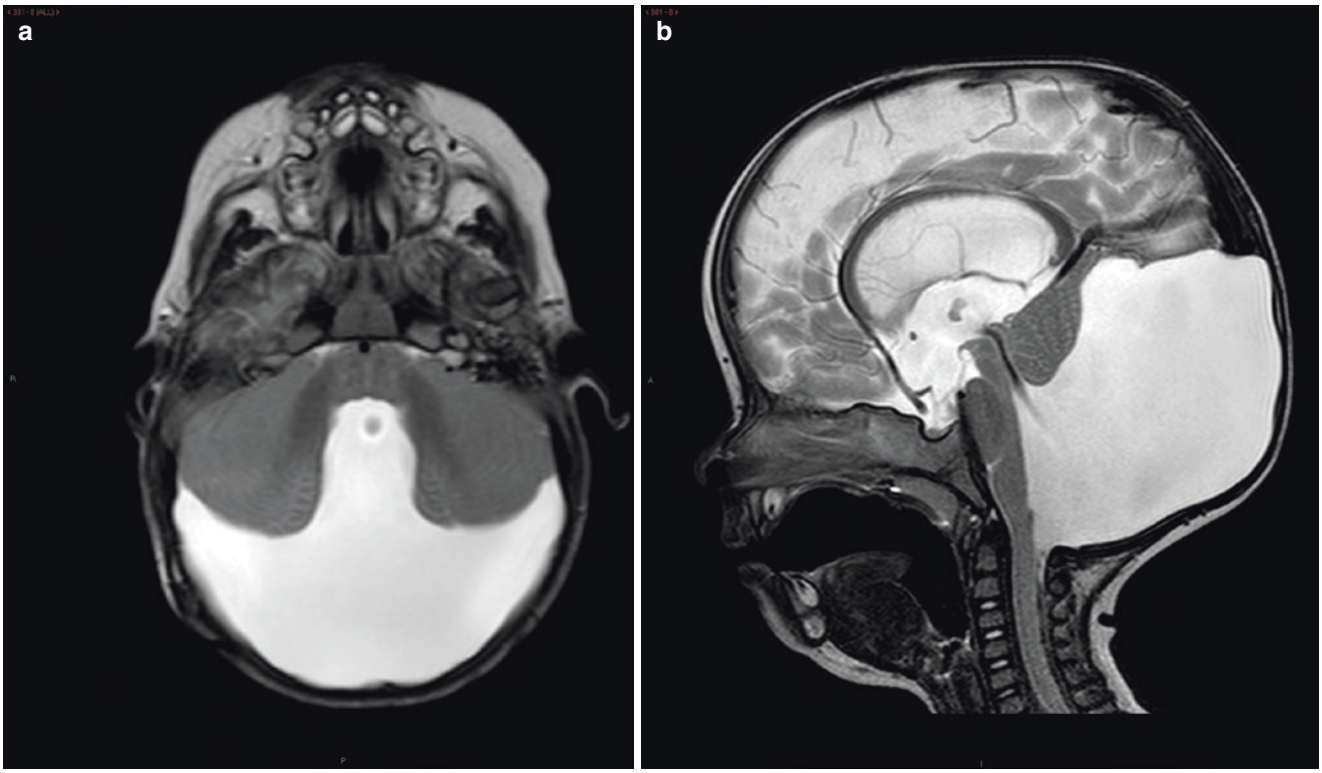

Fig. 2.35 Dandy-Walker malformation. Axial T2-weighted (**a**) and sagittal T2-weighted (**b**) MR images show a dilated fourth ventricle extending posteriorly to fill the posterior cranial fossa, which is enlarged. The cerebellar vermis is rotated upwards, the tentorium is elevated, and the brain stem is compressed anteriorly

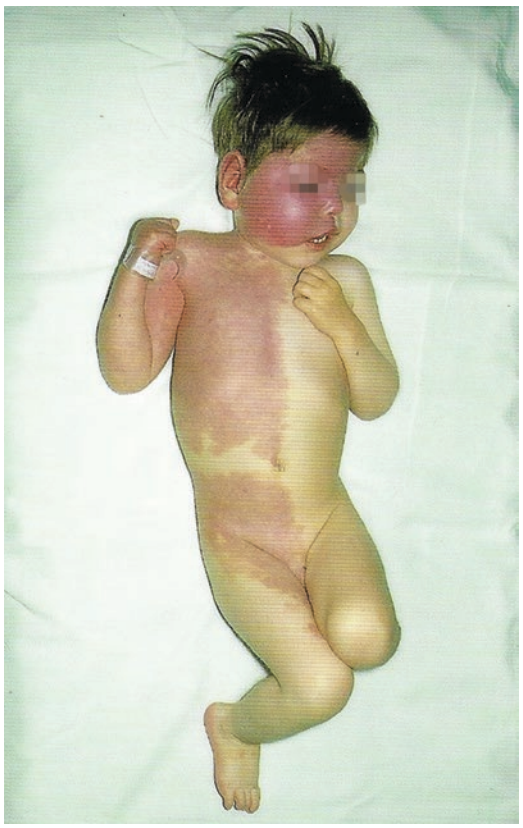

Fig. 2.36 Clinical photograph of Sturge-Weber syndrome, showing an extensive port-wine stain of the right side of the face and trunk

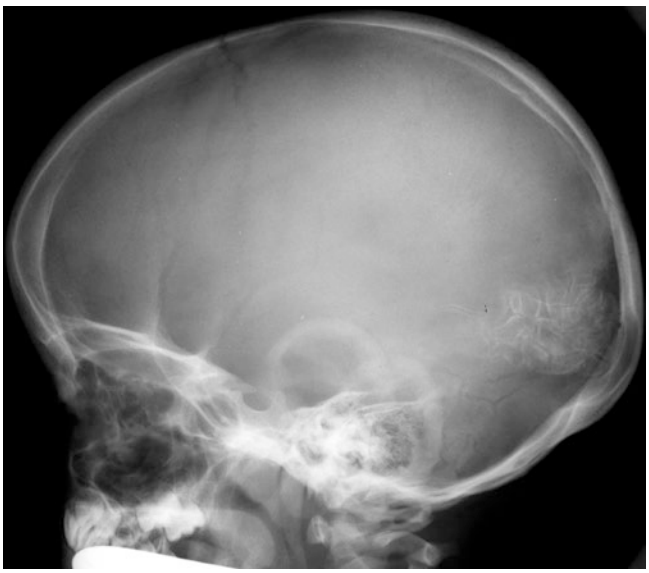

Fig. 2.37 Lateral skull radiograph shows the "tram-track" appearance of parieto-occipital subcortical calcification in a child with Sturge-Weber syndrome

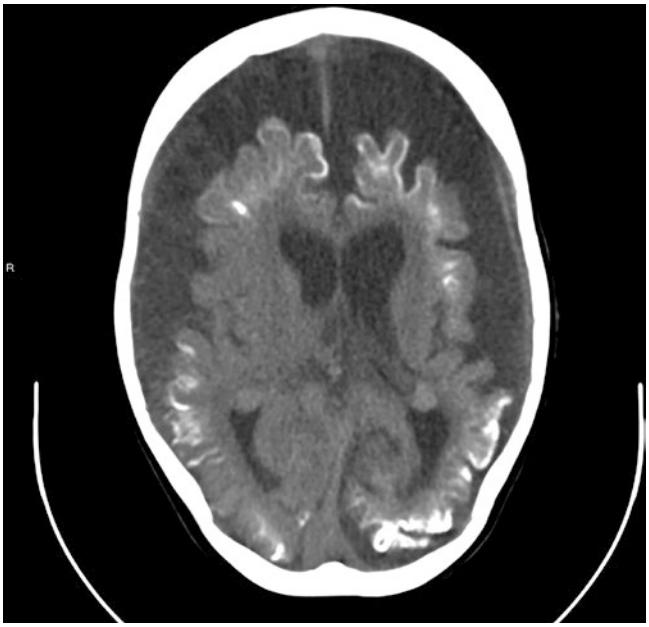

Fig. 2.38 Axial CT image of brain in a patient with Sturge-Weber syndrome, showing bilateral gyriform subcortical calcification. Both cerebral hemispheres are atrophic

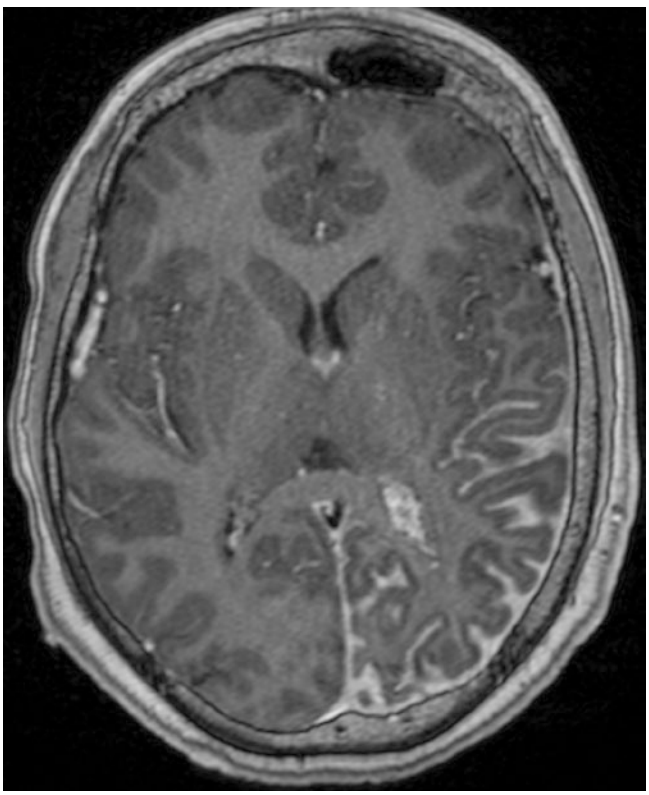

Fig. 2.39 Sturge-Weber syndrome. Axial post-contrast T1-weighted MR image demonstrates florid pial enhancement in the left parieto-occipital region. The left lateral ventricle choroid plexus is enlarged and enhances avidly

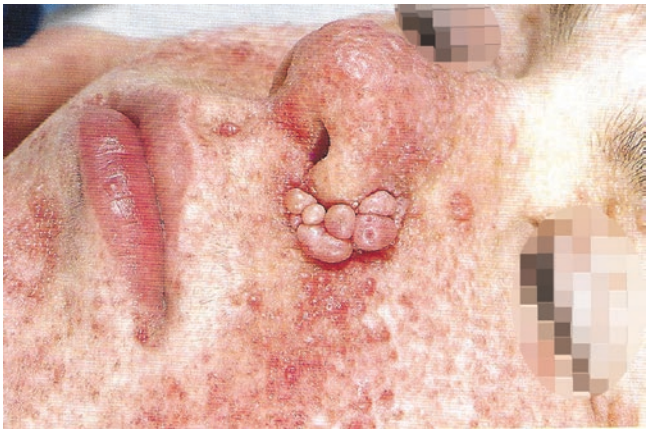

Fig. 2.40 Clinical photograph of facial angiofibromas (adenoma sebaceum) in a child with tuberous sclerosis

2.1.12 Tuberous Sclerosis

Tuberous sclerosis is a neurocutaneous disorder typified by the development of multiple benign tumours in various organs, including the skin, brain, kidneys, lungs, and bone. Facial manifestations visible on clinical examination include fibrous plaques of the forehead and facial angiofibromas (formerly known as *adenoma sebaceum*) (Fig. 2.40). The central nervous system lesions of tuberous sclerosis include cortical hamartomas or tubers, subependymal nodules, and white matter abnormalities. Patients may also develop subependymal giant cell astrocytomas, which can cause ventricular obstruction and hydrocephalus. Seizures occur in approximately 90% of patients. Infantile spasms or myoclonic seizures are often the presenting symptoms in infancy or early childhood.

MRI is the preferred imaging modality for detecting the intracranial manifestations of tuberous sclerosis. Cortical tubers are usually identified as areas of increased signal intensity in the cortical and subcortical regions of the brain on T2-weighted images. Subependymal nodules are found anywhere along the walls of the lateral ventricles, but are most commonly found in the region of the foramen of Monro. Subependymal nodules are usually high-signal on T1-weighted images and intermediate- to low-signal on T2-weighted images (Fig. 2.41). Calcified subependymal nodules are well demonstrated on CT (Fig. 2.42).

Subependymal giant cell astrocytoma (SEGA) is the term given to an enlarging subependymal nodule, usually situated near the foramen of Monro. The lesion demonstrates growth on serial studies and can cause hydrocephalus. It usually enhances with contrast (Fig. 2.43).

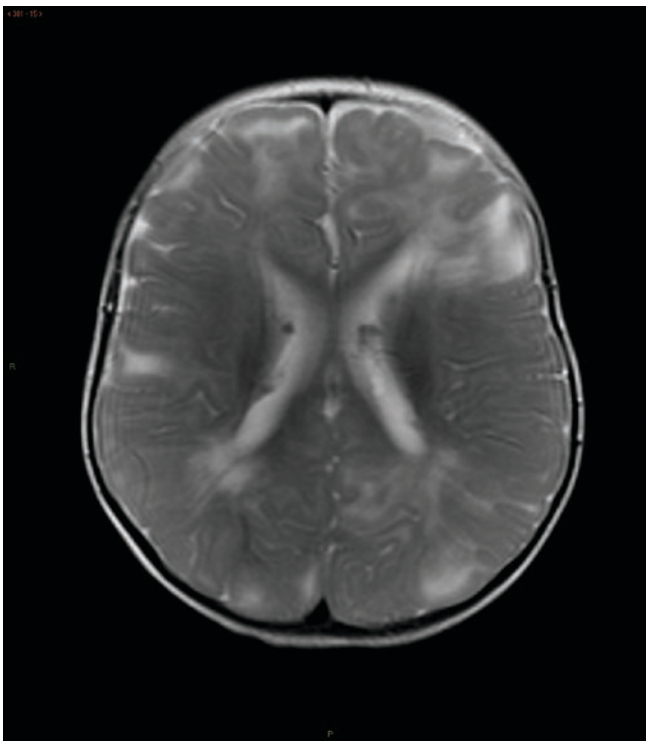

Fig. 2.41 Tuberous sclerosis. Axial T2-weighted MR image demonstrates high-signal lesions within the brain consistent with cortical tubers, with low-signal subependymal nodules along the lateral ventricles

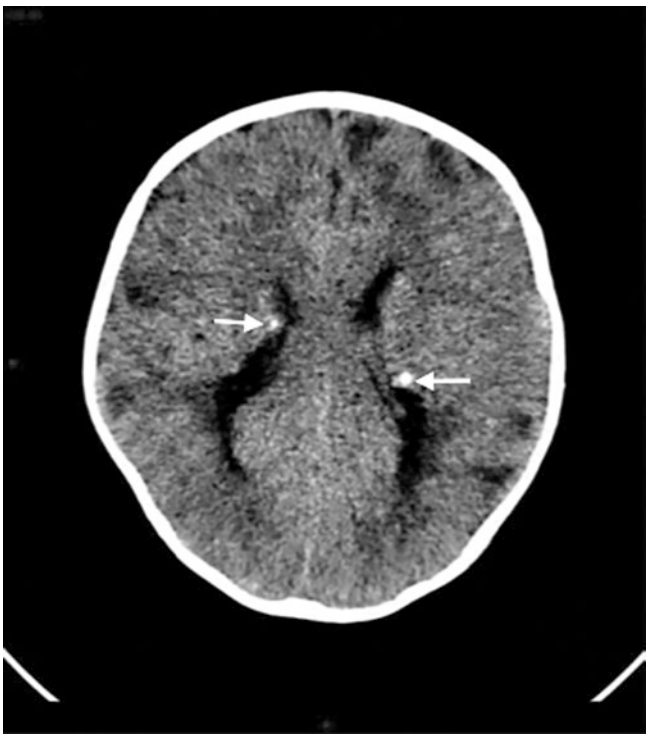

Fig. 2.42 Axial CT image shows calcified subependymal nodules (*arrows*) along the walls of the lateral ventricles in a patient with tuberous sclerosis. Cortical tubers are identified as areas of low attenuation within the brain parenchyma bilaterally

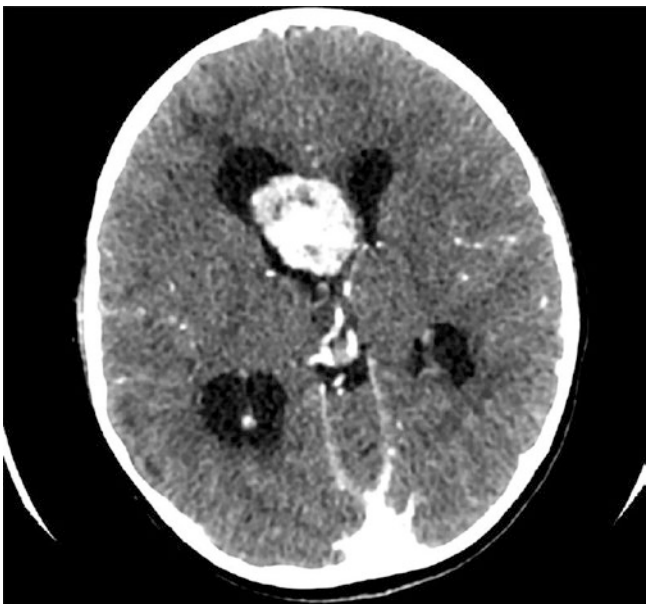

Fig. 2.43 Subependymal giant cell astrocytoma (SEGA) associated with tuberous sclerosis. Axial contrast-enhanced CT image shows a large, enhancing, soft-tissue mass at the foramen of Monro, causing hydrocephalus

2.1.13 Vein of Galen Aneurysmal Malformation

Vein of Galen aneurysmal malformation (VGAM) is a rare form of intracranial arteriovenous shunt where multiple feeding arteries drain directly into an enlarged median prosencephalic vein, which is the embryonic precursor of the vein of Galen. Although the condition is increasingly being diagnosed antenatally, it is more commonly detected postnatally as neonates develop progressive high-output cardiac failure.

Cranial ultrasound usually detects the malformation after cardiac investigations have failed to identify the cause of heart failure. Sonography reveals a hypoechoic or slightly echogenic posterior midline mass that exhibits turbulent blood flow on colour Doppler interrogation (Fig. 2.44). There may be ventricular dilatation due to mass effect on the third ventricle. A more detailed evaluation of the malformation is obtained with MRI. The dilated feeding and draining vessels appear as hypointense flow voids on T2-weighted imaging (Fig. 2.45). In addition to demonstrating the abnormality, MR imaging is used to assess ventricle size and establish whether any pre-existing brain insult has occurred. MR angiography is performed to delineate the vascular anatomy (Fig. 2.46). CT occasionally may be used to assess the malformation (Fig. 2.47).

Cerebral angiography fully characterises the lesion and is best performed at the time of embolisation, which is the treatment of choice (Fig. 2.48). Embolisation therapy is usually delayed until the infant is at least 6 months old. There is little role for surgery.

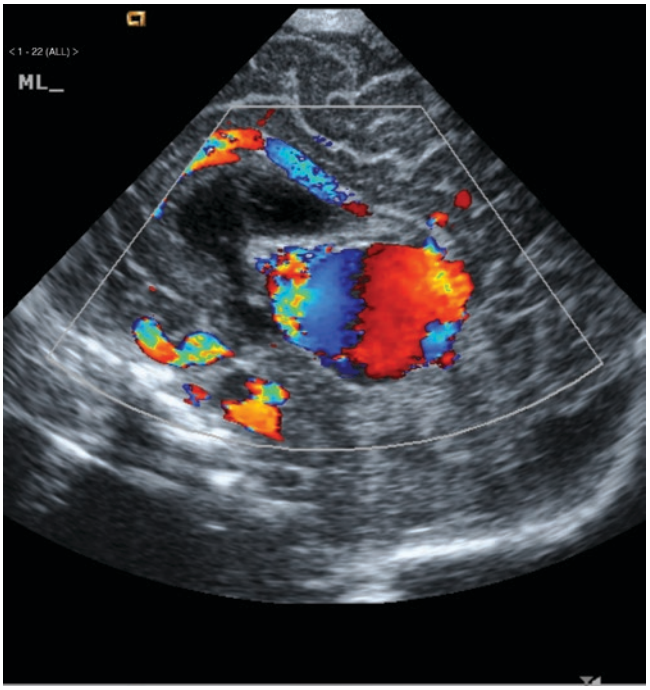

Fig. 2.44 Vein of Galen aneurysmal malformation (VGAM). Midline sagittal cranial ultrasound image with colour Doppler shows turbulent blood flow in a VGAM posterior to the third ventricle

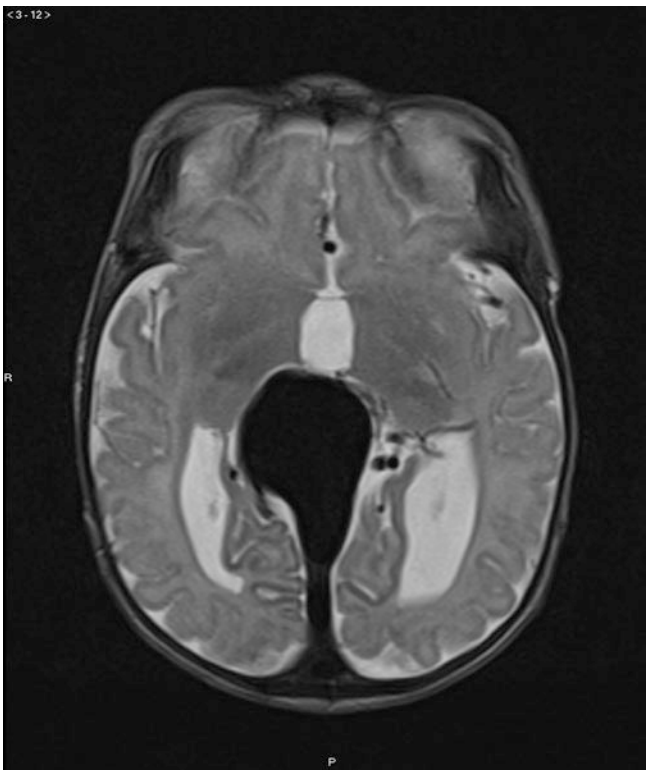

Fig. 2.45 VGAM. Axial T2-weighted MR image demonstrates a large, spherical, hypointense flow void posterior to the third ventricle, consistent with a VGAM. There is mild dilatation of the lateral and third ventricles

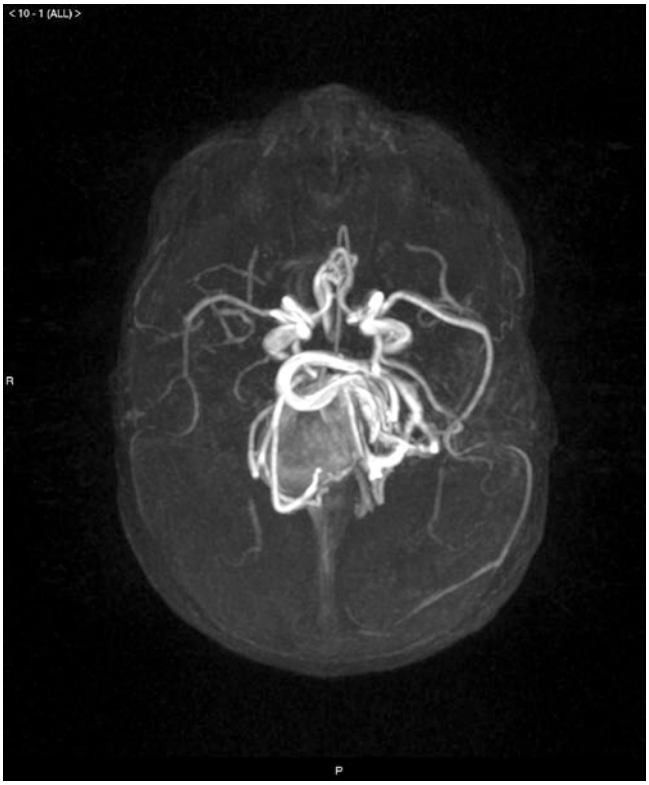

Fig. 2.46 VGAM. Reformatted image of an MR angiogram showing multiple dilated arterial vessels

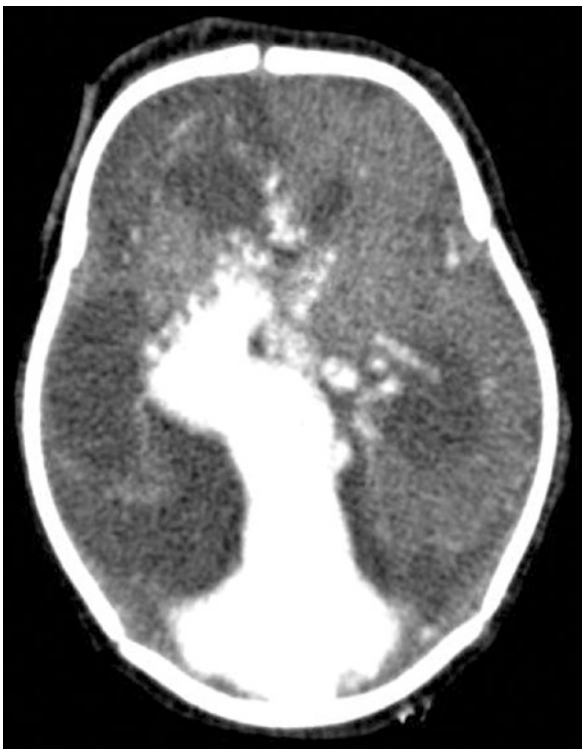

Fig. 2.47 VGAM. Axial contrast-enhanced CT image shows a large, enhancing, tortuous VGAM. Multiple arterial feeders are identified. There is hydrocephalus and parenchymal infarction within the right cerebral hemisphere

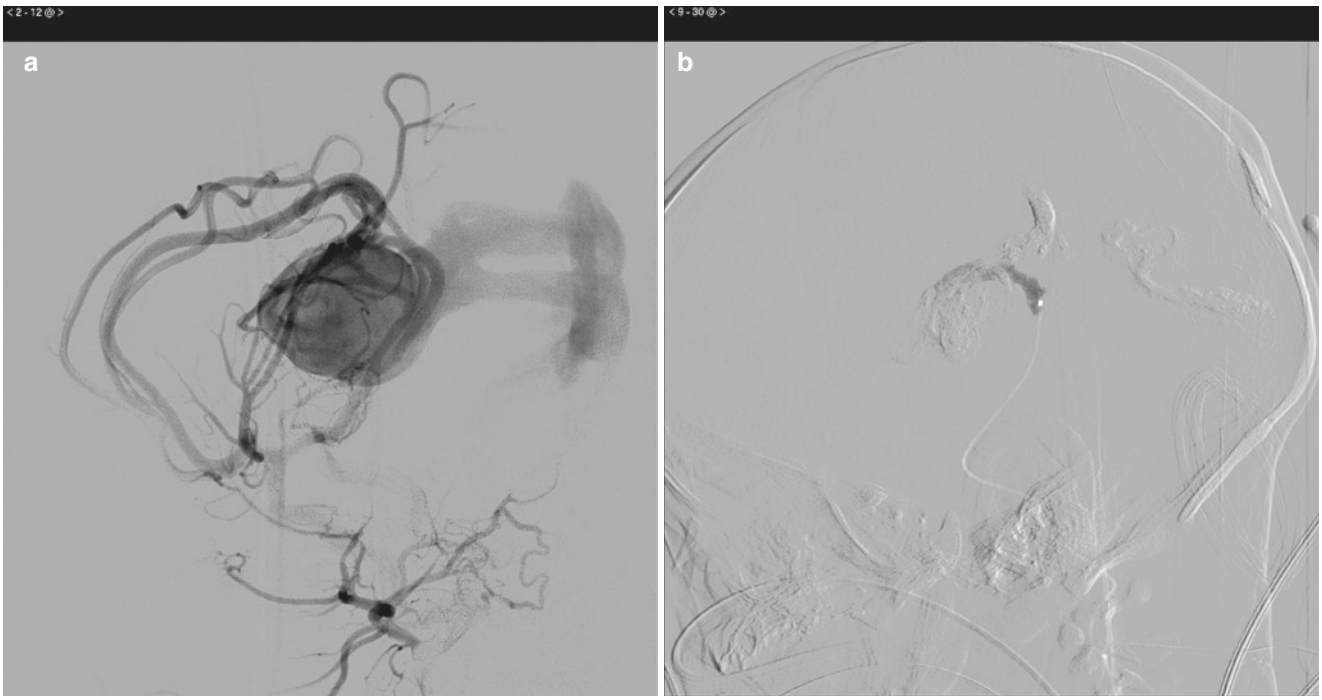

Fig. 2.48 (**a**) Intracerebral angiogram prior to embolisation shows a VGAM with dilated arterial feeders and dilated median prosencephalic vein. (**b**) Post-procedure image shows embolisation material within the malformation (*Courtesy of* Dr. J. Battacharya)

2.1.14 Lymphatic Malformation (Cystic Hygroma)

Lymphatic malformations are low-flow vascular malformations consisting of abnormally dilated lymphatic channels or cysts, lined with lymphatic endothelium. They can occur at any age but are more common in the paediatric population; 90% of cases occur before 2 years of age. Lymphatic malformations occur in lymphatic-rich regions, with 70–80% occurring in the head and neck. They are classified as macrocystic, microcystic, or mixed. Macrocystic lymphatic malformations are usually large, smooth, cystic superficial masses, which can involve deeper spaces and structures. Historically, these lesions were known as *cystic hygroma*.

The commonest location for a head and neck lymphatic malformation is the posterior triangle of the neck. Clinically, the malformation presents as a smooth soft-tissue mass with a rubbery consistency (Fig. 2.49). Macrocystic lesions can transilluminate. These malformations typically grow slowly, although they can expand rapidly during an upper respiratory tract infection or if intralesional haemorrhage or infection occurs. In these instances, the malformation can become life-threatening if it causes compression of vital structures such as the airway. Because of their infiltrative nature and disregard of fascial planes, lymphatic malformations of the head and neck can extend inferiorly into the axilla and mediastinum, or anteriorly into the floor of the mouth and tongue.

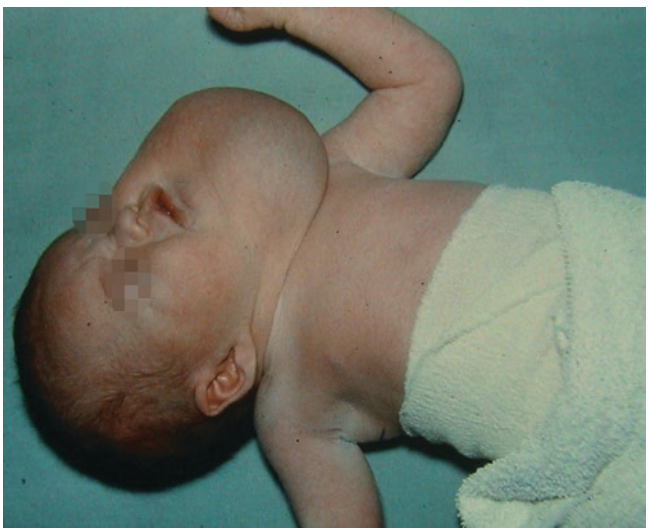

Fig. 2.49 Clinical photograph of a large lymphatic malformation (cystic hygroma) of the lower face and neck in a newborn infant

Lymphatic malformations of the head and neck are usually imaged using MRI, which can reveal the multicompartmental nature of the lesion and assess its relationship to important structures. The lesions usually appear as lobulated, septated masses which are intermediate to low signal intensity on T1-weighted images and high signal on T2-weighted images (Fig. 2.50). Internal fluid-fluid levels may be seen, particularly if haemorrhage has occurred within the lesion. This can be demonstrated with ultrasound

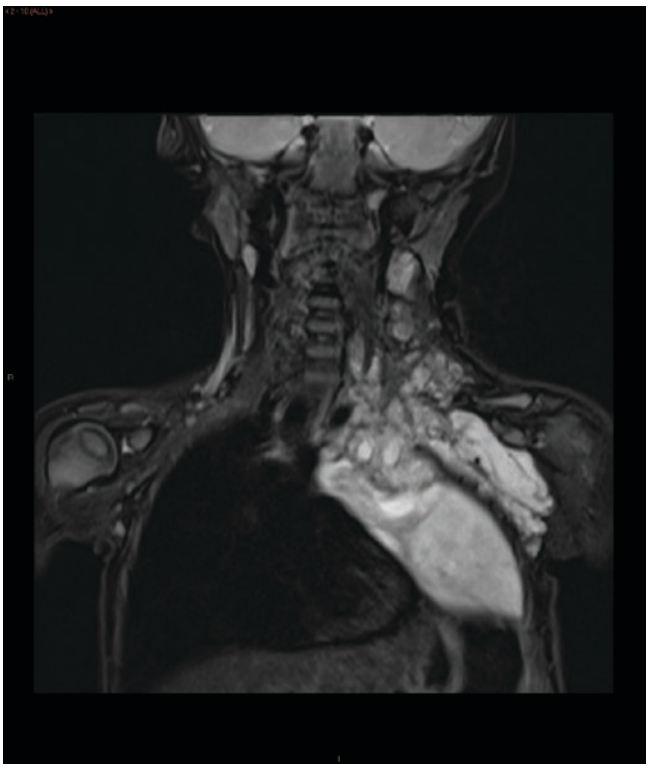

Fig. 2.50 Extensive lymphatic malformation. Coronal T2 STIR MR image of the neck and chest shows a large, infiltrative lymphatic malformation involving the left side of the neck, axilla, and left side of the thorax

in addition to MRI (Fig. 2.51). There is usually no significant enhancement of microcystic lymphatic malformations. Macrocystic malformations demonstrate only rim and septal enhancement following contrast administration, with no central filling of the cystic elements.

2.1.14.1 Antenatal Diagnosis of Cystic Hygroma

Cystic hygromas (macrocystic lymphatic malformations) may be detected in the antenatal period by ultrasound and assessed with fetal MR scanning (Fig. 2.52). If airway compromise is suspected, the baby may be delivered by an EXIT procedure (***Ex*** Utero ***I***ntrapartum ***T***reatment), in which the head is delivered by elective caesarean section with the baby still oxygenated via the placenta. This technique increases the time available to secure an airway, by tracheostomy if necessary.

2.1.15 Thyroid Disorders

Congenital hypothyroidism is usually detected on neonatal screening (heel prick test). The commonest cause of congenital hypothyroidism in the developed world is thyroid dysgenesis (aplasia, hypoplasia, or ectopia). Ultrasound and thyroid nuclear imaging are used in combination to establish whether any thyroid tissue is present and if it lies in a normal or ectopic location. The lingual location is the most

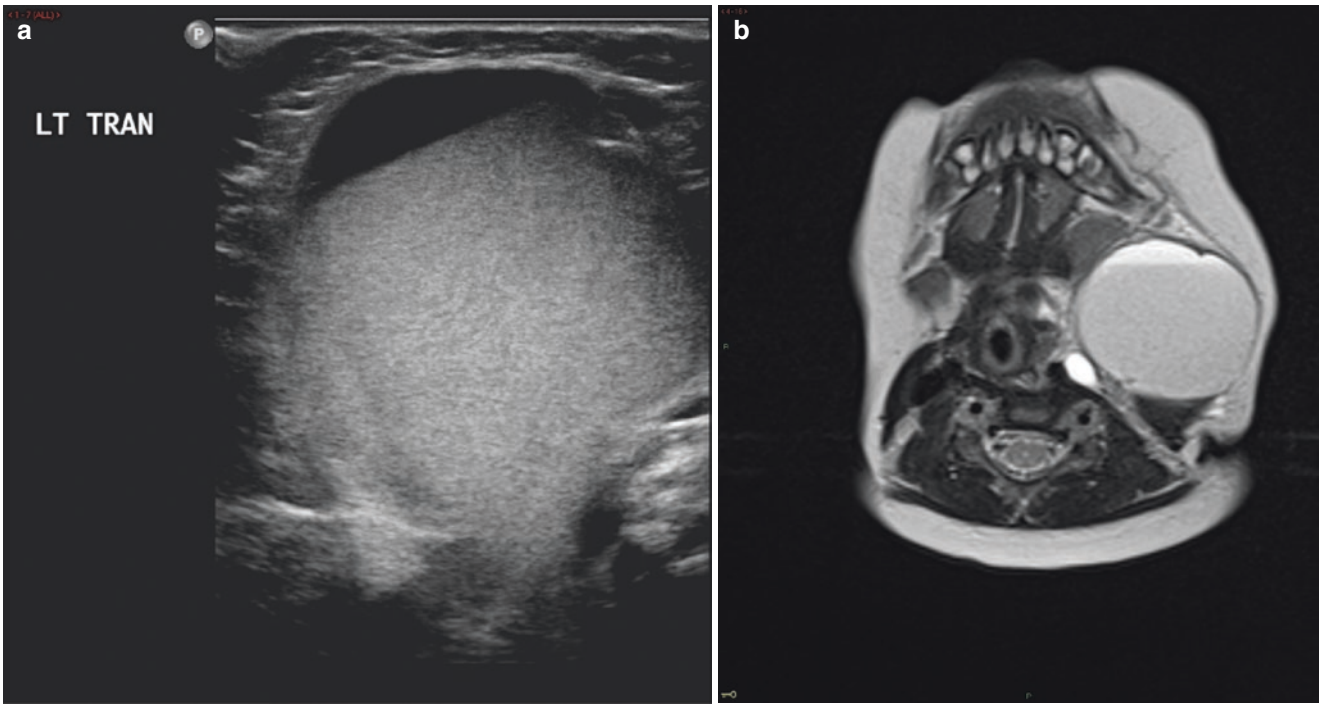

Fig. 2.51 Haemorrhage within a lymphatic malformation cyst. (**a**) Transverse ultrasound image of left side of neck shows a fluid-fluid level within a large cyst. Anechoic fluid lies superficial to more echogenic fluid. (**b**) Axial T2-weighted MR image in the same patient shows the fluid-fluid level within the cyst, which is due to haemorrhage. The airway is patent but displaced to the right

common site for ectopic thyroid tissue. On ultrasound, the ectopic thyroid gland is usually located near the hyoid bone and has normal echotexture (Fig. 2.53). Thyroid nuclear imaging demonstrates tracer uptake within the ectopic thyroid gland and no tracer uptake in the normal thyroid bed (Fig. 2.54).

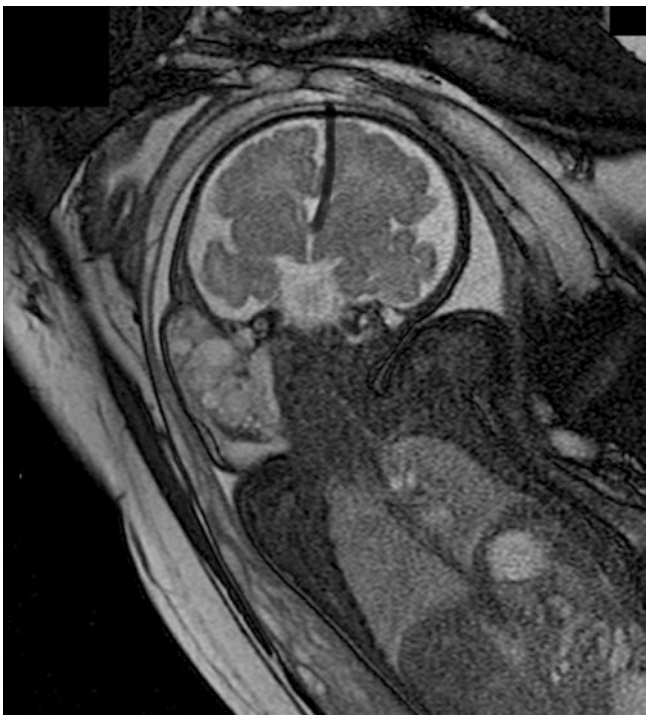

Fig. 2.52 Right-sided cervical lymphatic malformation in a 34-week-gestation fetus. Coronal T2-weighted image from a fetal MR study shows the multiloculated lesion on the right side of the fetal neck

Congenital goitre is a rare cause of neck swelling in newborns. It usually presents as diffuse enlargement of the thyroid gland at birth; nodular enlargement is less common. Infants are usually asymptomatic, although respiratory distress or stridor may occur if the enlarged gland exerts mass effect on the airway (Fig. 2.55). Thyroid hormone production may be increased, decreased, or normal. The condition may be caused by abnormal thyroid hormone production, transplacental passage of maternal antibodies, or maternal ingestion of antithyroid medication. Some cases are hereditary. Postnatal ultrasound reveals diffuse, homogeneous enlargement of the gland.

2.1.16 Thyroglossal Duct Cyst

Thyroglossal duct cysts are the most common type of congenital neck lesion, accounting for approximately 70% of all congenital neck anomalies. These midline neck swellings occur when there is incomplete obliteration of the thyroglossal duct during embryological development. The cysts can arise anywhere along the course of the duct, from the base of the tongue to the thyroid isthmus. They vary in size from a few millimetres to 3 cm. The cyst moves up and down on deglutition and especially on protruding the tongue. They are subject to recurrent infection and can present as a thyroglossal abscess, which may rupture to form a fistula. A thyroglossal cyst in the suprahyoid region may occasionally cause

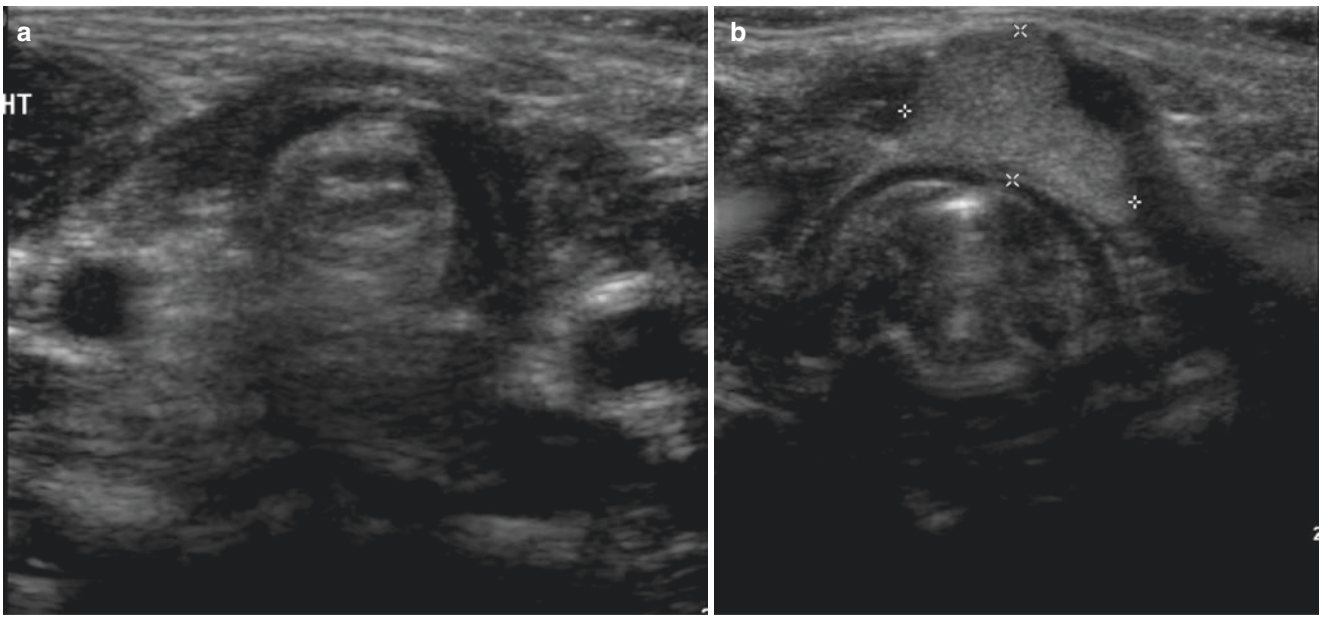

Fig. 2.53 Ectopic thyroid gland in a neonate. (**a**) Transverse ultrasound image shows absence of thyroid tissue in its expected position in the lower neck. (**b**) Transverse ultrasound image of the upper neck reveals lobulated ectopic thyroid tissue to the left of the midline at the level of the hyoid bone

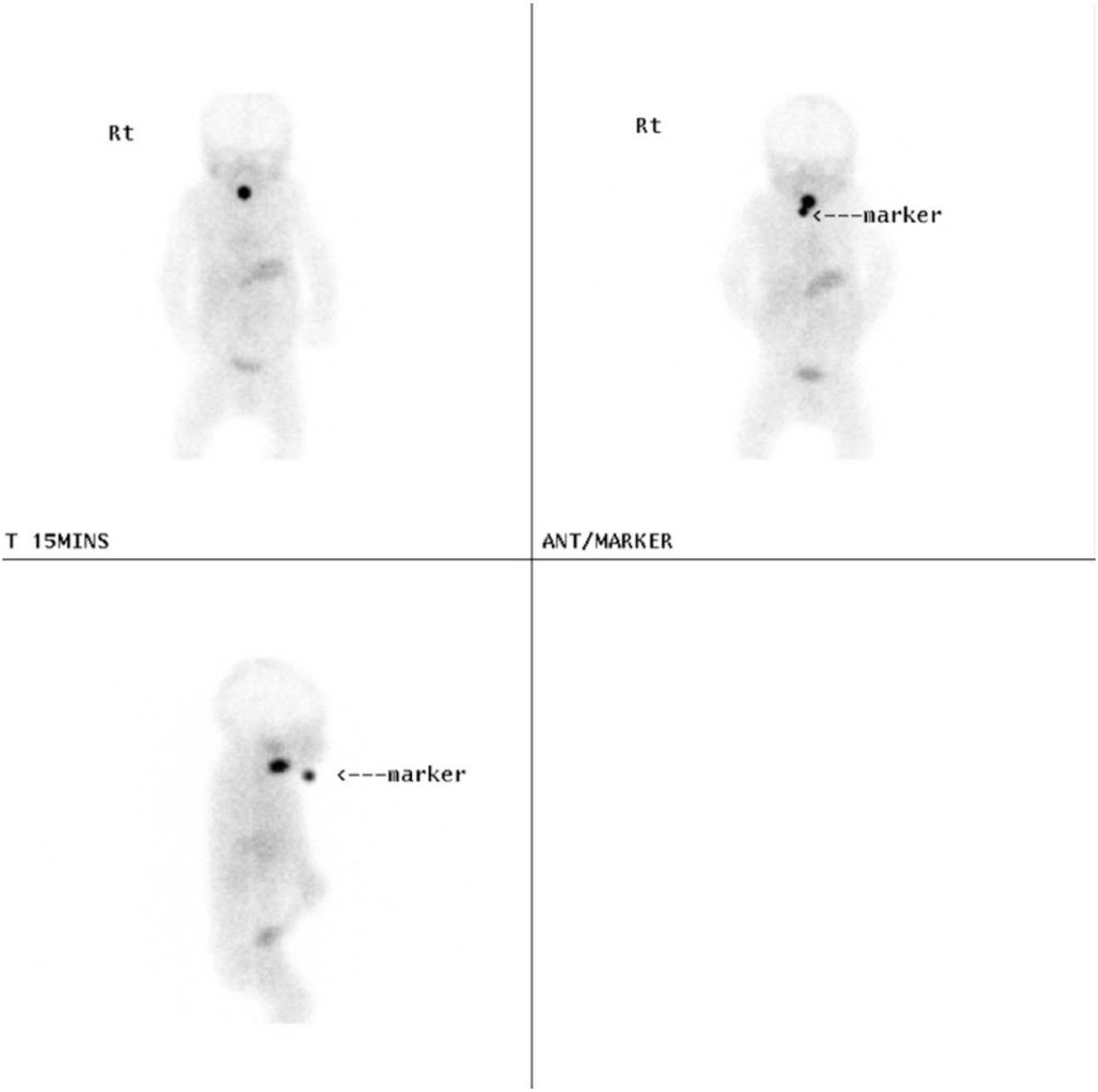

Fig. 2.54 Ectopic thyroid gland. Nuclear medicine thyroid scan using ^{99m}Tc-pertechnetate shows radioisotope uptake in the lingual region, posterior to a marker denoting the position of the chin. There is no radiotracer uptake in the normal thyroid bed

dysphagia, choking, or respiratory compromise, thus requiring early surgical intervention.

Thyroglossal duct cysts are usually diagnosed clinically (Fig. 2.56). Approximately 80% of cysts are situated at or below the level of the hyoid bone; 20% are above the hyoid. Ultrasound confirms the presence of a cyst and, more importantly, identifies the presence of normal thyroid tissue within the neck, thus preventing inadvertent surgical removal of an ectopic thyroid gland that could be mistaken for a thyroglossal duct cyst.

On ultrasound, a thyroglossal duct cyst is identified as a cystic structure in the anterior neck, either in the midline or just off-centre (within 2 cm of the midline). It can appear anechoic or hypoechoic, with a thin outer wall (Fig. 2.57). The cyst fluid may contain internal echoes from proteinaceous material. An uncomplicated thyroglossal duct cyst appears as a low-signal structure on T1-weighted MR imaging and is hyperintense on T2-weighted images (Fig. 2.58). The rim is non-enhancing unless inflammation is present. The cyst wall may be thick and irregular in the presence of haemorrhage or infection (Fig. 2.59).

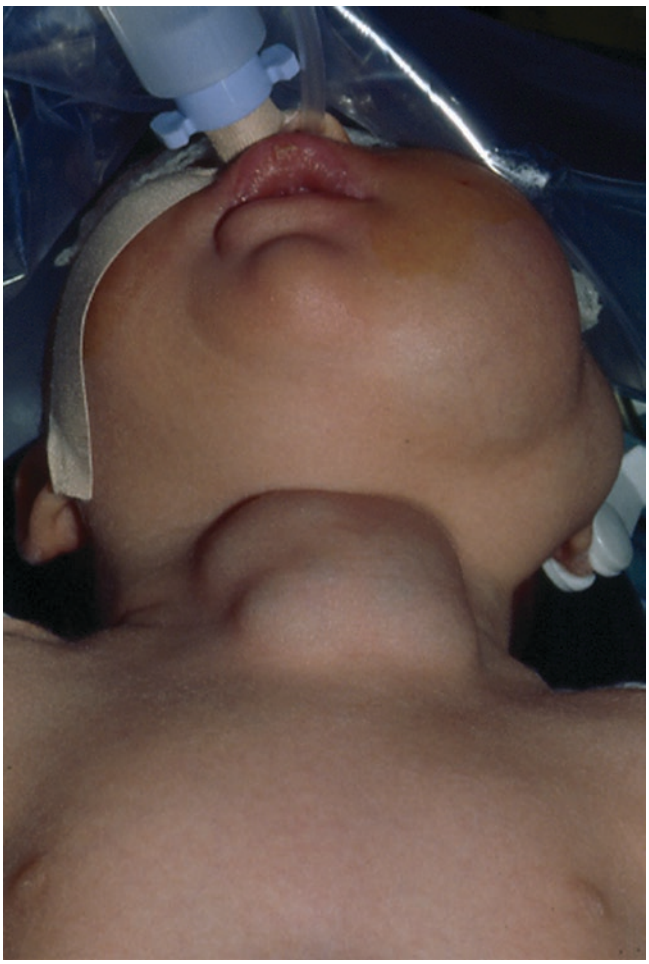

Fig. 2.55 Clinical photograph of thyroid goitre in a neonate. The infant is intubated (nasotracheal tube) to maintain the airway

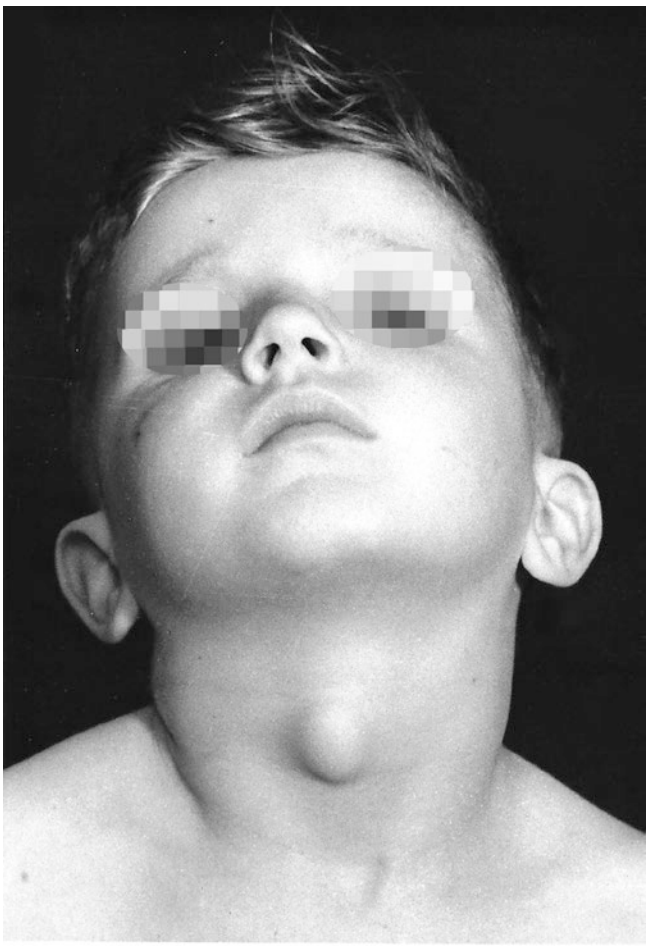

Fig. 2.56 Clinical photograph of a thyroglossal cyst within the neck

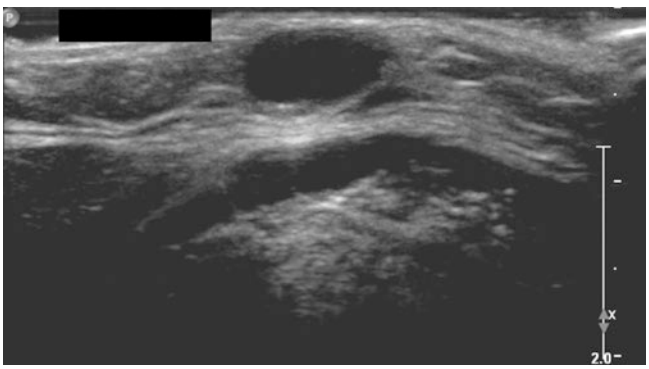

Fig. 2.57 Thyroglossal duct cyst. Transverse ultrasound image of the neck shows an ovoid anechoic structure to the right of the midline

2.1.17 Branchial Remnants

Branchial cleft anomalies are the second most common congenital lesion of the head and neck in children. They are believed to result from incomplete obliteration of the branchial apparatus, which forms the embryological precursors of the tissues within the head and neck. The anomalies manifest as cysts, fistulas, and sinus tracts. Branchial cysts are more common than fistulas or sinuses and tend to occur in older children or young adults. Fistulas usually occur in infants or younger children. Bilateral branchial cleft anomalies occur in 2–3% of cases and are usually familial. Second branchial cleft anomalies are most common, accounting for approximately 95% of cases. First branchial cleft anomalies account for about 1–4% of cases. Third and fourth cleft anomalies are very rare.

Approximately 75% of second branchial cleft anomalies are cysts. Most are located in the submandibular space, but they can occur anywhere along the course of the second branchial arch tract, from the tonsillar fossa to the supraclavicular region of the neck. Typically the cysts appear as painless, fluctuant swellings in the lateral aspect of the neck, adjacent to the anteromedial border of the sternocleidomastoid muscle at the mandibular angle. They may become painful and/or enlarge if infected. Fistulas or sinuses are usually diagnosed in infancy or early childhood with drainage of secretions or pus from an ostium at the anterior border of the sternocleidomastoid muscle within the lower third of the neck (Fig. 2.60).

First branchial cleft anomalies typically present as a cyst, sinus, or fistula between the external auditory canal and the submandibular area. There may be drainage of secretions from a tiny opening at the angle of the mandible or the external auditory canal.

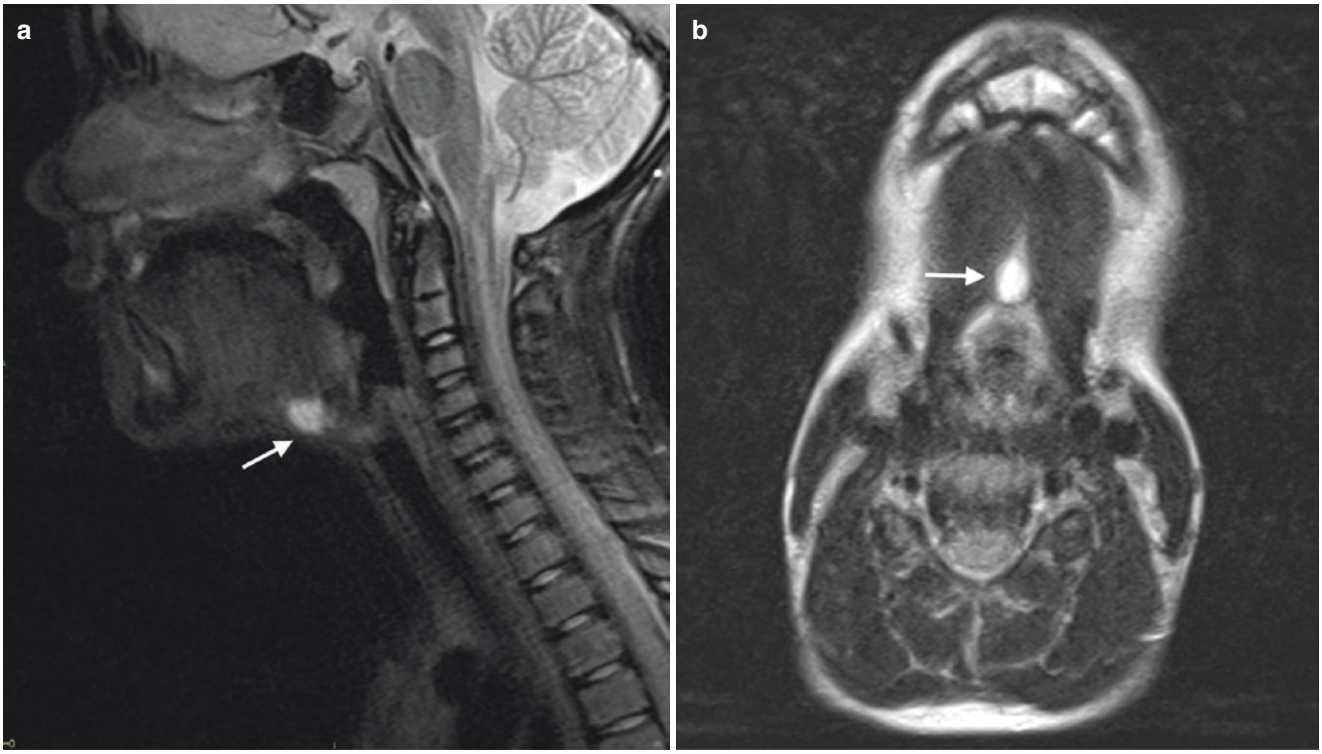

Fig. 2.58 Sublingual thyroglossal duct cyst on MRI. Sagittal T2 STIR (**a**) and axial T2-weighted (**b**) MR images show a small midline structure with hyperintense signal (*arrow*) in the sublingual region of the neck

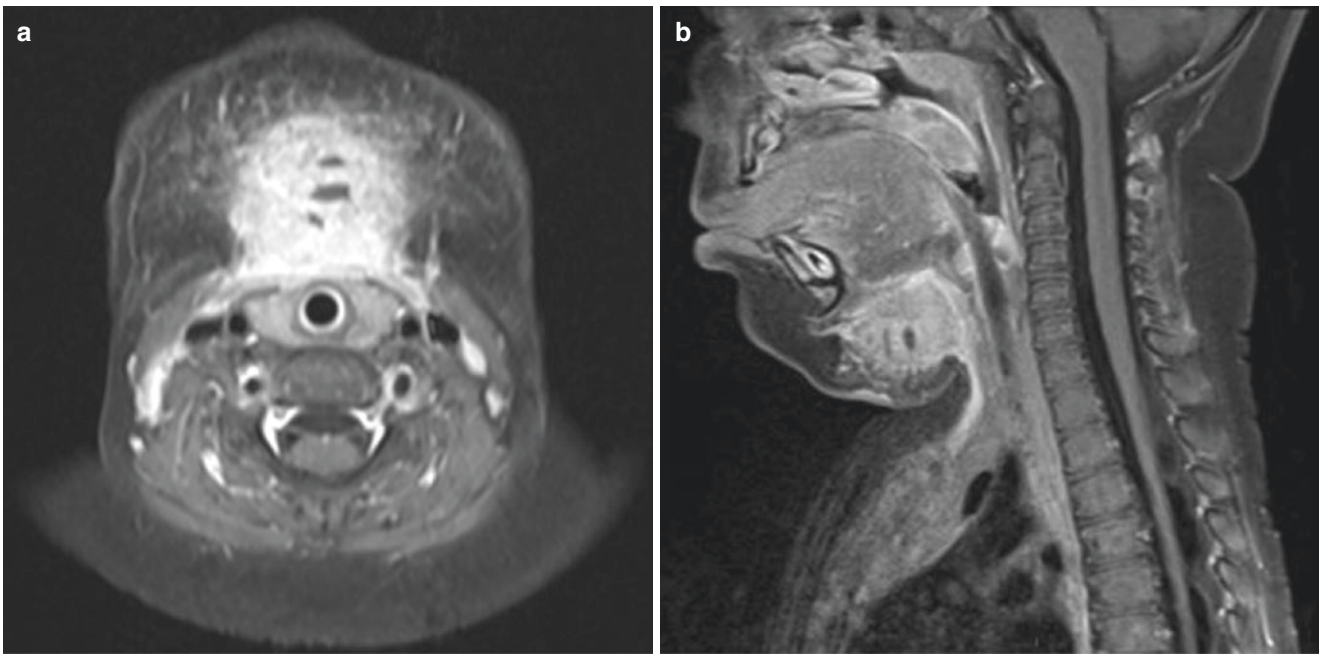

Fig. 2.59 Infected thyroglossal duct cyst. Axial (**a**) and sagittal (**b**) post-contrast T1-weighted fat-saturated MR images demonstrate an enhancing mass in the sublingual region, containing small, central, non-enhancing fluid collections

Ultrasound or MR imaging of branchial cleft lesions is most rewarding when cysts or tracts are distended, and it is worthwhile trying to perform imaging when the child's signs are most florid. Ultrasound shows non-infected cysts as anechoic, rounded structures with thin walls (Fig. 2.61). Internal echoes, consistent with debris, may be evident. The cysts are usually hyperintense on T2-weighted MR imaging. Their appearance on T1-weighted imaging is variable, depending on the proteinaceous content of the cyst. Uncomplicated cysts do not usually enhance with contrast. Cysts or tracts that have been complicated by an inflammatory process tend to enhance with contrast (Fig. 2.62).

Fistulography, a technique now very rarely used, was performed more frequently in the past. In this procedure, water-soluble contrast is injected into the ostium of a sinus or fistula via a thin catheter. Opacification of the tract is observed using fluoroscopy (Fig. 2.63).

2.1.18 Torticollis

Torticollis is a clinical finding of lateral head tilt with or without rotational spinal malalignment. Congenital torticollis, which is seen in neonates and infants, usually results from muscular causes (congenital absence of sternocleidomastoid muscle, congenital muscular torticollis) or craniocervical bony anomalies (occipitoatlantal fusion, cervical vertebral fusion, hemivertebrae). Congenital nystagmus and congenital paralytic squint are rarer causes. Secondary effects of torticollis in neonates and infants include rotation of the head to the opposite side and plagiocephaly.

Acquired torticollis is seen in older children and adolescents, often secondary to trauma, infection, inflammation, or tumours.

Congenital muscular torticollis collectively encompasses three types of congenital muscular disorder: *fibromatosis colli*, torticollis with a palpable mass in the sternocleidomastoid muscle; *muscular torticollis*, with tightness of the sternocleidomastoid muscle but no clinically palpable mass; and *postural torticollis*, with neither a mass nor tightness of the sternocleidomastoid muscle.

Unilateral contraction of the sternocleidomastoid muscle causes tilting of the infant's head towards the affected side and rotation of the chin to the opposite side. A non-tender mass may be evident within the muscle, which slowly increases in size for a few weeks before stabilising and eventually resolving. The right sternocleidomastoid muscle is more commonly affected. Birth trauma (e.g., forceps delivery) and intrauterine malpositioning (e.g., breech position) are potential causative factors for the condition.

Fibromatosis colli is usually diagnosed clinically (Fig. 2.64). If imaging is required to confirm the diagnosis, ultrasound is the modality of choice. Sonography typically reveals fusiform swelling of the sternocleidomastoid muscle, which may be hypoechoic, isoechoic, or hyperechoic relative to normal muscle (Figs. 2.65 and 2.66). The fusiform swelling can be seen to move synchronously with the muscle during scanning.

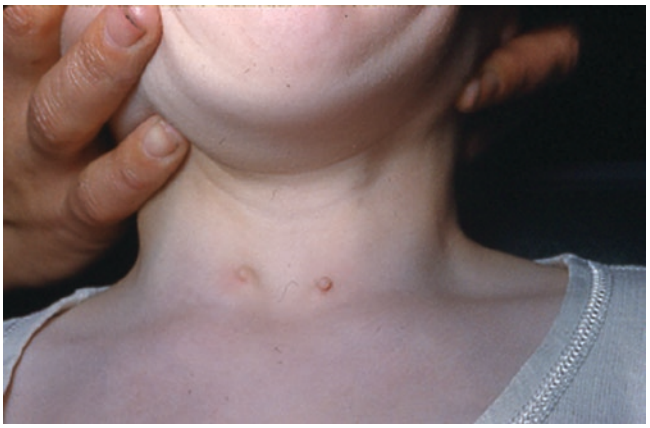

Fig. 2.60 Clinical photograph showing bilateral branchial sinus ostia in the lower neck of a child

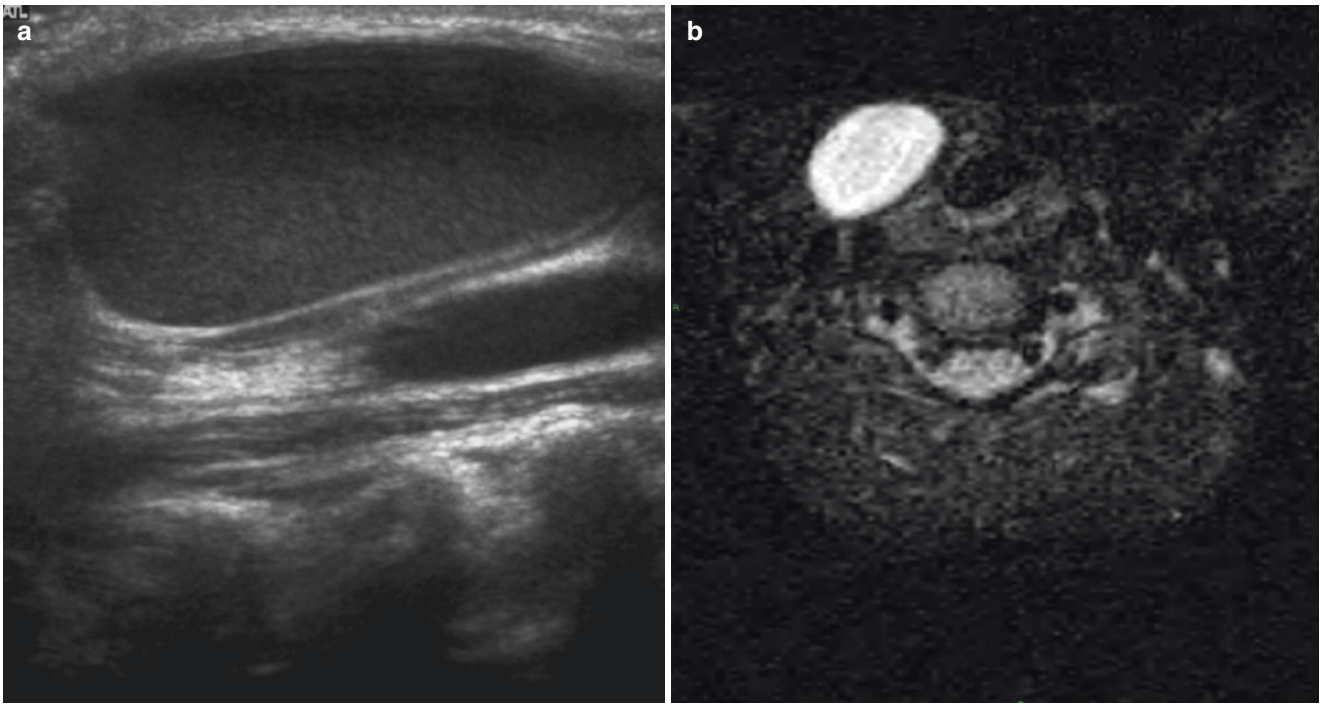

Fig. 2.61 Right-sided second branchial cleft cyst. (**a**) Longitudinal ultrasound image shows an ovoid cystic structure with hypoechoic contents within the right side of the neck. (**b**) The cyst is hyperintense (bright) on an axial T2 fat-saturated MR image

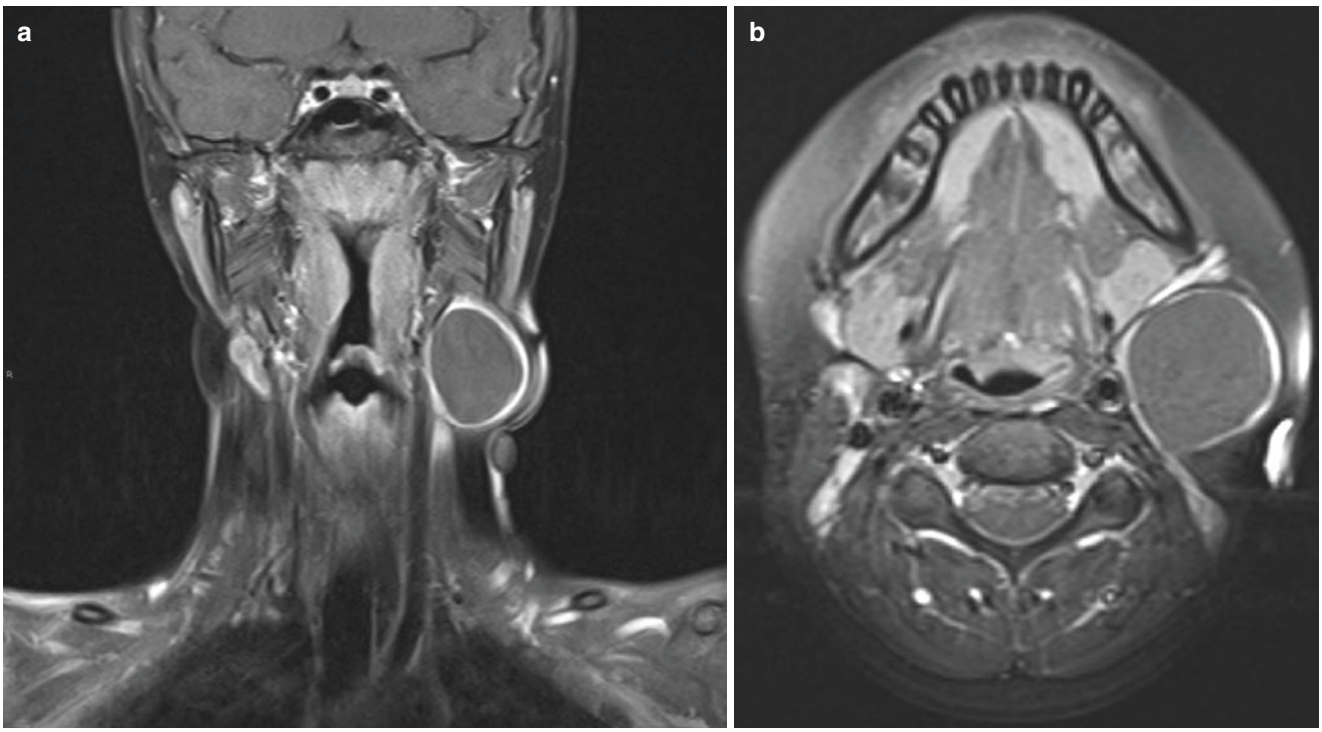

Fig. 2.62 Branchial cleft cyst. Coronal (**a**) and axial (**b**) post-contrast T1-weighted fat-saturated MR images show rim enhancement of a left-sided second branchial cleft cyst. The rim enhancement is most likely secondary to previous infection of the cyst

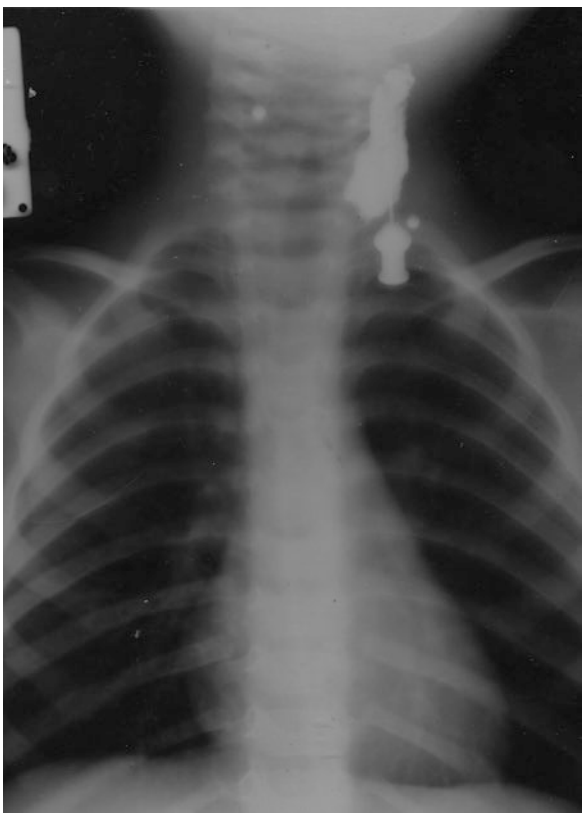

Fig. 2.63 Historical image of a branchial sinus fistulogram. Contrast media injected into the ostium of a left-sided branchial sinus opacifies the tract

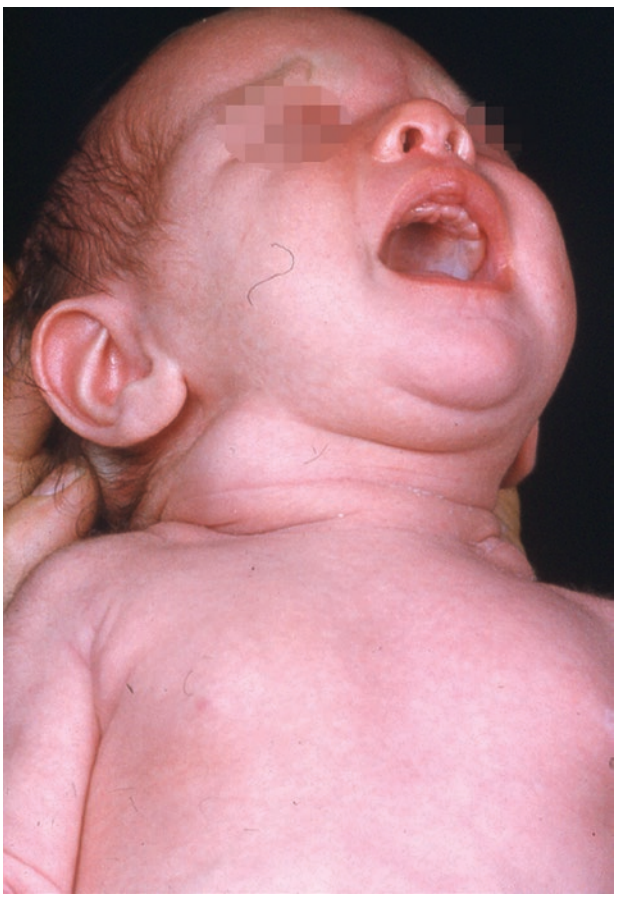

Fig. 2.64 Clinical photograph demonstrates swelling of the right sternocleidomastoid muscle, consistent with fibromatosis colli

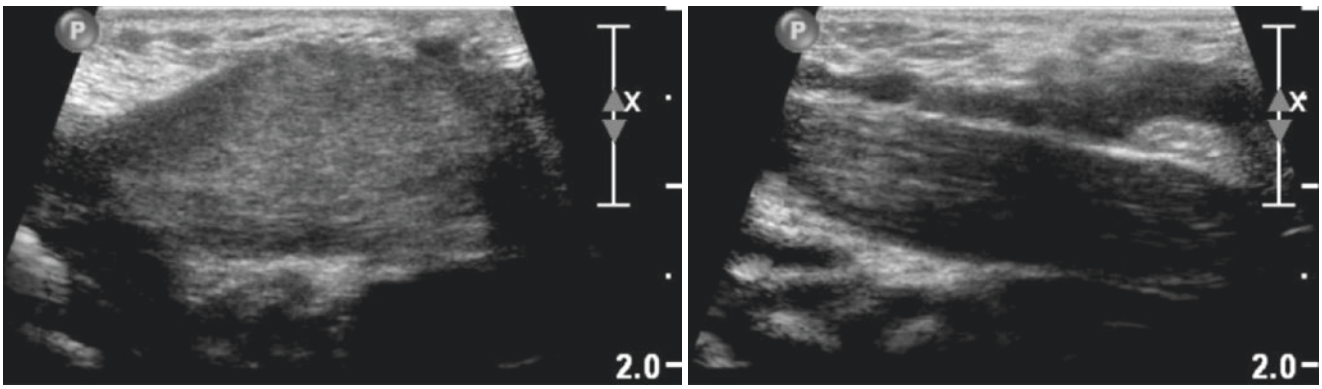

Fig. 2.65 Ultrasound appearance of right-sided fibromatosis colli in an infant. The longitudinal image of the right sternocleidomastoid muscle demonstrates fusiform swelling of the belly of the muscle. A longitudinal image of the normal left-sided sternocleidomastoid muscle is shown for comparison

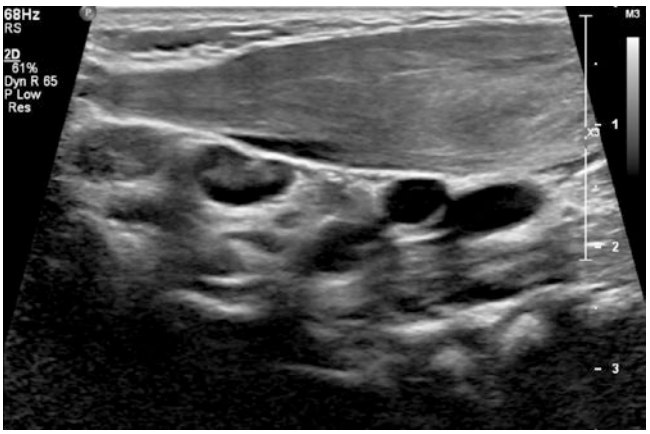

Fig. 2.66 Left-sided fibromatosis colli. Longitudinal ultrasound image shows the upper (cranial) end of the swelling in continuity with normal muscle

2.2 Infection/Inflammation

2.2.1 Toxoplasmosis

Toxoplasmosis is caused by the protozoan *Toxoplasma gondii*. It is a common parasitic infection in humans and is usually asymptomatic. The risk of developing symptoms is very low except for immunocompromised patients and a fetus infected in utero. The primary infection acquired in a pregnant woman is often asymptomatic, but it can cause severe and incapacitating disease in the developing fetus (congenital toxoplasmosis). *Toxoplasma* infection acquired by the mother prior to conception is usually of no threat to a developing fetus because of maternal immunity, unless the infection is reactivated during pregnancy by immunosuppression.

Congenital toxoplasmosis has a wide range of clinical manifestations and can be subclinical at birth. Fetal infection usually occurs in the third trimester, but more severe infection can occur if the fetus is infected earlier in the pregnancy. The presence of hydrocephalus, intracranial calcifications, and chorioretinitis is considered the classic triad of congenital toxoplasmosis. Other clinical manifestations include jaundice, rash, and hepatosplenomegaly. There may be microcephaly. Some infected infants, such as those infected in the third trimester, appear healthy at birth but are at high risk of developing seizures, developmental delay, chorioretinitis, and other symptoms months or years later.

The intracranial manifestations of congenital toxoplasmosis are the sequelae of a diffuse inflammatory process. Hydrocephalus occurs because of the presence of turbid proteinaceous CSF, ependymitis, and aqueductal obstruction. It can be demonstrated in neonates using ultrasound, CT, or MRI. Basal ganglia, periventricular, and cortical calcifications are common and best visualised on CT (Fig. 2.67). White matter abnormalities may be present and are identified as areas of low attenuation (hypodensity) on CT. The abnormal white matter is of increased signal intensity on T2-weighted MR images (Fig. 2.68).

Serological tests are usually performed to confirm *Toxoplasma* infection.

2.2.2 Sinusitis

A degree of sinusitis occurs in most viral upper respiratory tract infections in children, and recovery is usually spontaneous. Acute bacterial infection of a sinus may subsequently develop, however, and cause severe pain, the location of which depends on which sinus is affected. Forehead pain and tenderness occur when the frontal sinuses are affected. When the maxillary sinuses are involved, there is usually tenderness over the cheek area and some discomfort or aching in the upper teeth and jaw. Inflammation within the ethmoid sinuses can cause swelling of the periorbital soft tissues and pain between the eyes. Sphenoid sinusitis is less frequent but can cause earache, neck pain, and headache. More than one group of sinuses can be affected, so patients usually complain of pain or tenderness at various locations.

Acute paranasal sinus infection in children is often diagnosed clinically without the need for radiological investigation.

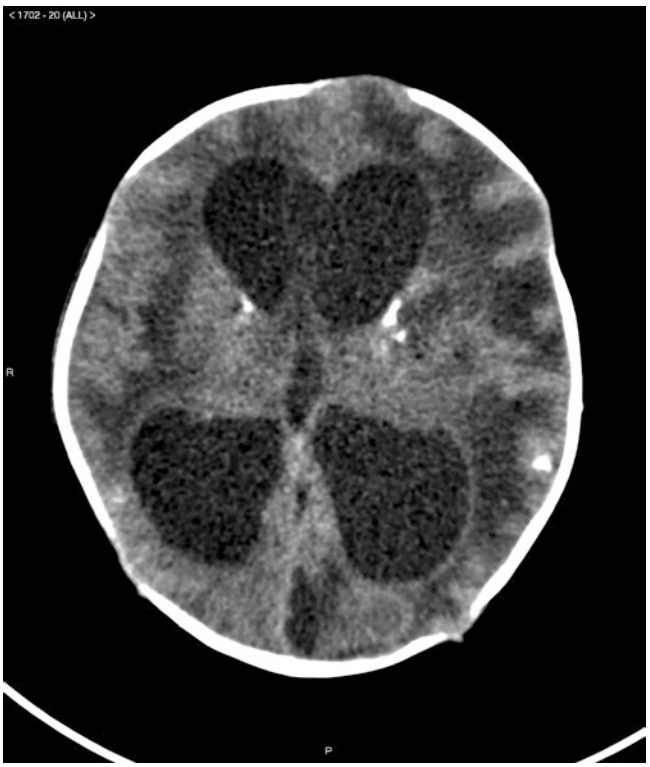

Fig. 2.67 Congenital toxoplasmosis of the brain. Axial CT image demonstrates ventriculomegaly, periventricular and peripheral calcification, and abnormal low attenuation (hypodensity) within the cerebral white matter

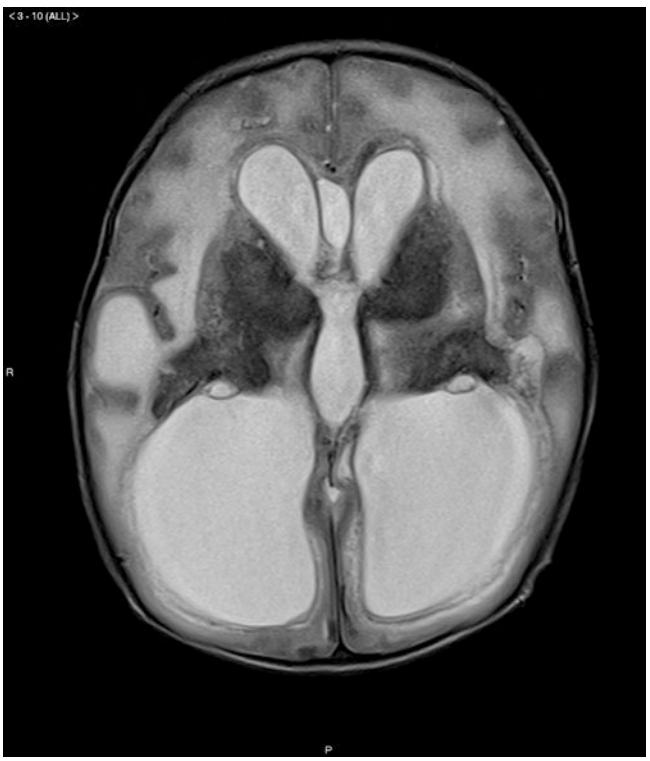

Fig. 2.68 Congenital toxoplasmosis of the brain. Axial T2-weighted MR image shows ventriculomegaly and abnormal increased signal within the cerebral white matter. Hypointense signal within the basal ganglia bilaterally is due to calcification

Purulent rhinorrhoea, nasal congestion, headache, and facial pain are common symptoms. Most cases will respond to appropriate antibiotic therapy. In a few cases, where the symptoms and signs are severe and progressive, it may be necessary to perform cross-sectional imaging to look for intraorbital or intracranial disease spread. There is no role for radiographs in the evaluation of complications of sinusitis in the paediatric patient.

Intracranial complications of sinus disease include epidural and subdural empyema, meningitis, encephalitis, parenchymal abscess, dural venous sinus thrombosis, and venous infarction. Intracranial spread of sinus infection is thought to occur via the valveless diploic veins of the skull, which penetrate the dura. The frontal skull seems to be particularly susceptible to the spread of infection because of its rich network of diploic veins and the occurrence of frontal and anterior ethmoid sinusitis in children.

On CT scanning, epidural and subdural empyemas are identified as low-attenuation extraparenchymal (extra-axial) collections, which demonstrate rim enhancement following contrast administration (Fig. 2.69). With MRI, the empyema

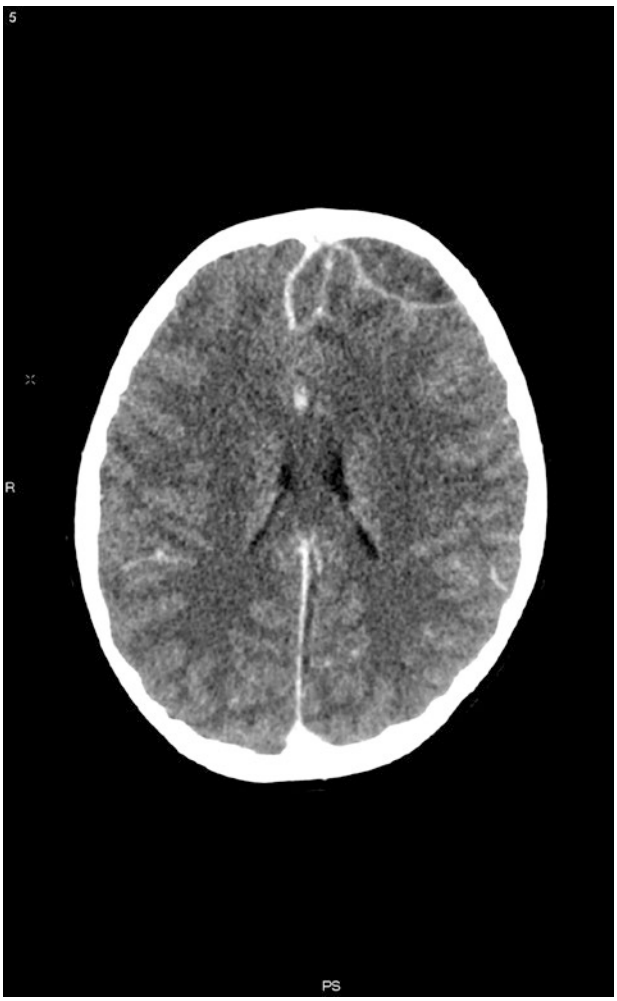

Fig. 2.69 Subdural empyema secondary to frontal sinusitis. Axial contrast-enhanced CT image demonstrates left frontal and left anterior parafalcine subdural empyemas with rim enhancement

is usually hyperintense (bright) on T2-weighted imaging and exhibits rim enhancement on post-contrast T1-weighted images (Fig. 2.70). Epidural abscesses form between the skull and dura and expand slowly because of the tight adherence of dura to the bone. Subdural empyemas develop in the space between the dura and arachnoid membrane. They can spread more rapidly and freely within this space.

Sometimes, intracranial spread of infection can occur from direct extension of osteomyelitis affecting the sinus walls. An extracranial subperiosteal collection can also arise secondary to frontal sinusitis and frontal bone osteomyelitis. This is known as Pott puffy tumour (Fig. 2.71).

Periorbital cellulitis, an inflammatory process confined to the preseptal soft tissues of the eye, usually results from contiguous spread of infection from adjacent facial structures. On CT scanning, there is diffuse soft-tissue thickening and areas of enhancement anterior to the orbital septum (Fig. 2.72). Orbital cellulitis, on the other hand, is a postseptal infection most commonly caused by paranasal sinusitis, which spreads to the orbit via the perivascular pathway. Development of an orbital subperiosteal abscess is usually associated with ethmoid sinusitis. A contrast-enhanced CT scan demonstrates a low-attenuation collection, usually with an enhancing rim, between the orbital wall and the adjacent medial rectus muscle (Fig. 2.73). There is often proptosis.

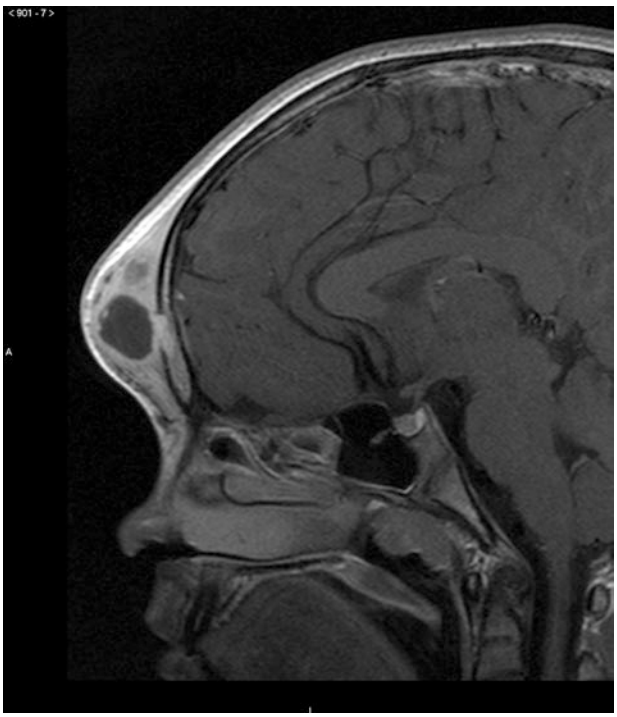

Fig. 2.71 Pott puffy tumour. Sagittal post-contrast T1-weighted fat-saturated MR image shows a large subperiosteal collection in the frontal region secondary to frontal sinusitis. Destruction of the outer table of the adjacent frontal bone is due to osteomyelitis

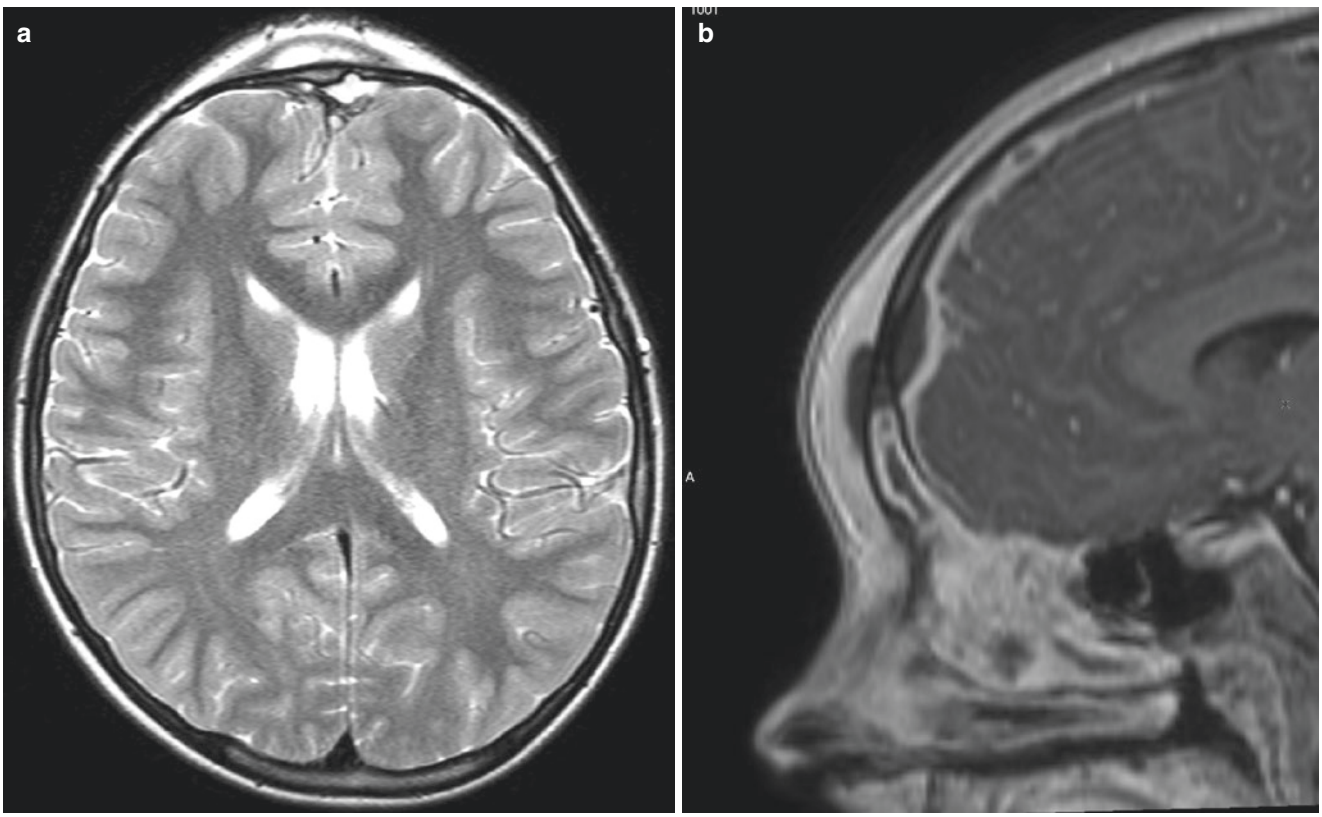

Fig. 2.70 Epidural abscess and subperiosteal collection secondary to frontal sinusitis and osteomyelitis. (**a**) Axial T2-weighted MR image shows a small, hyperintense left frontal epidural collection and a hyperintense subperiosteal collection. (**b**) Sagittal post-contrast T1-weighted fat-saturated MR image shows rim enhancement of the epidural empyema and enhancement of the soft tissues of the forehead around the subperiosteal collection. The frontal bone between the two collections is low-signal owing to osteomyelitis from frontal sinusitis

Complications of orbital cellulitis include thrombosis of the superior ophthalmic vein or cavernous sinus, meningitis, and intracranial abscess.

2.2.3 Root Abscess

A dental abscess occurs when there is bacterial invasion of the pulp space of a tooth. It is usually the result of advanced dental caries in children. The buildup of infection activates pain fibres within the pulp space, causing severe pain. The infection ultimately spreads down the root canal and into the periapical bone surrounding the root of the tooth, resulting in a periapical abscess.

On orthopantomography (OPT), a periapical abscess appears as a well-defined lucency adjacent or distal to the dental root tip, usually less than 1 cm in width (Fig. 2.74). There may or may not be surrounding sclerosis. It should be noted that an early dental abscess (within the first 10 days) might not demonstrate any radiographic findings. The abscess can spread to the adjacent soft tissues, causing cellulitis and facial swelling, and is usually associated with cervical lymphadenopathy (Fig. 2.75). Sometimes an abscess may perforate into the oral cavity or maxillary sinus, or extend into the adjacent bone, causing osteomyelitis (Fig. 2.76).

2.2.4 Mastoiditis

Acute mastoiditis, a disease of young children, is a complication of untreated otitis media. It is most frequently due to bacterial infection, with *Streptoccoccus pneumoniae* and *Haemophilus influenzae* accounting for most cases. Affected children typically present with retroauricular redness and swelling with concurrent (or recent) otitis media (Fig. 2.77).

A post-contrast CT scan of the petrous temporal bones and brain is performed to confirm the diagnosis and identify

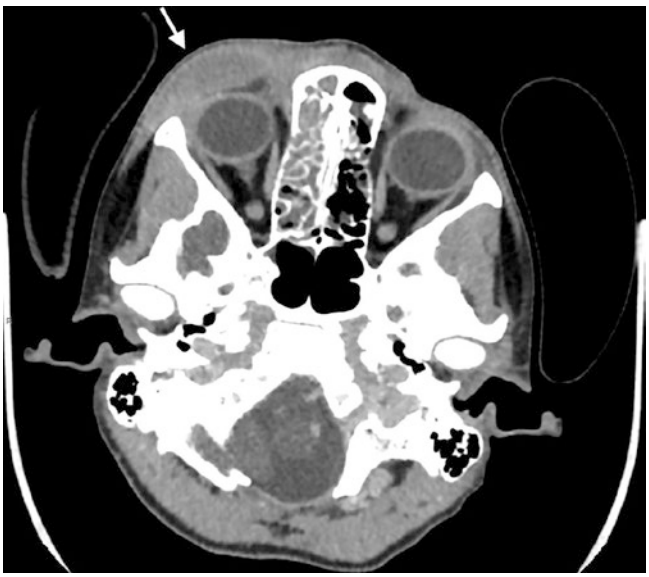

Fig. 2.72 Right periorbital cellulitis. Axial contrast-enhanced CT image demonstrates swelling of the right orbital preseptal soft tissues

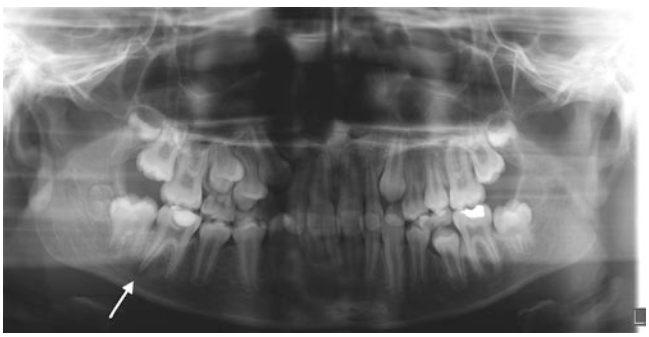

Fig. 2.74 Periapical dental abscess. Orthopantomogram (OPT) shows lucency around the root of the right lower first molar tooth (*arrow*), in keeping with a periapical dental abscess

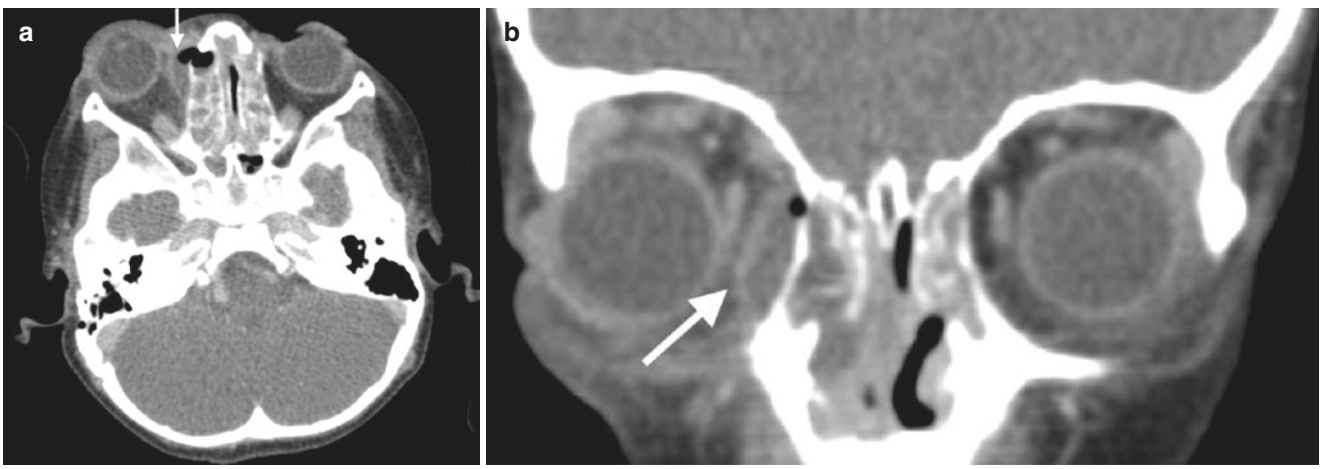

Fig. 2.73 Right orbital cellulitis with subperiosteal collection. Axial contrast-enhanced CT image (**a**) and coronal reconstruction (**b**) show a low-attenuation subperiosteal collection (*arrow*) containing a locule of gas within the medial aspect of the right orbit. The subperiosteal abscess demonstrates rim enhancement, and sinusitis is seen in the adjacent ethmoid sinus

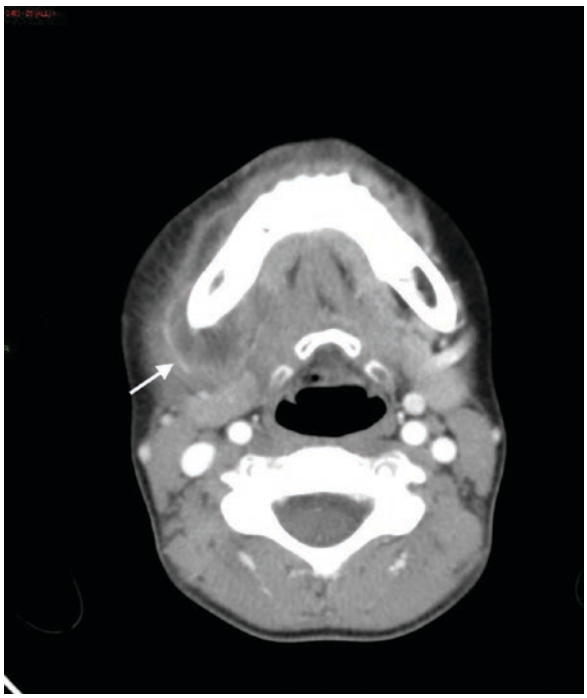

Fig. 2.75 Submandibular abscess secondary to dental abscess. Axial contrast-enhanced CT image demonstrates a rim-enhancing collection within the soft tissues below the right side of the mandible. The infection has spread from a dental abscess (same patient as Fig. 2.74)

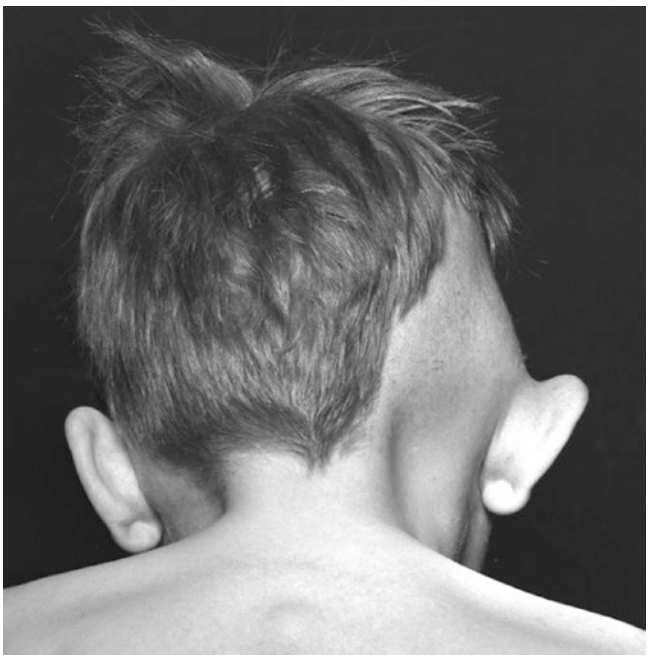

Fig. 2.77 Acute mastoiditis. Clinical photograph demonstrates swelling of the right post-auricular soft tissues

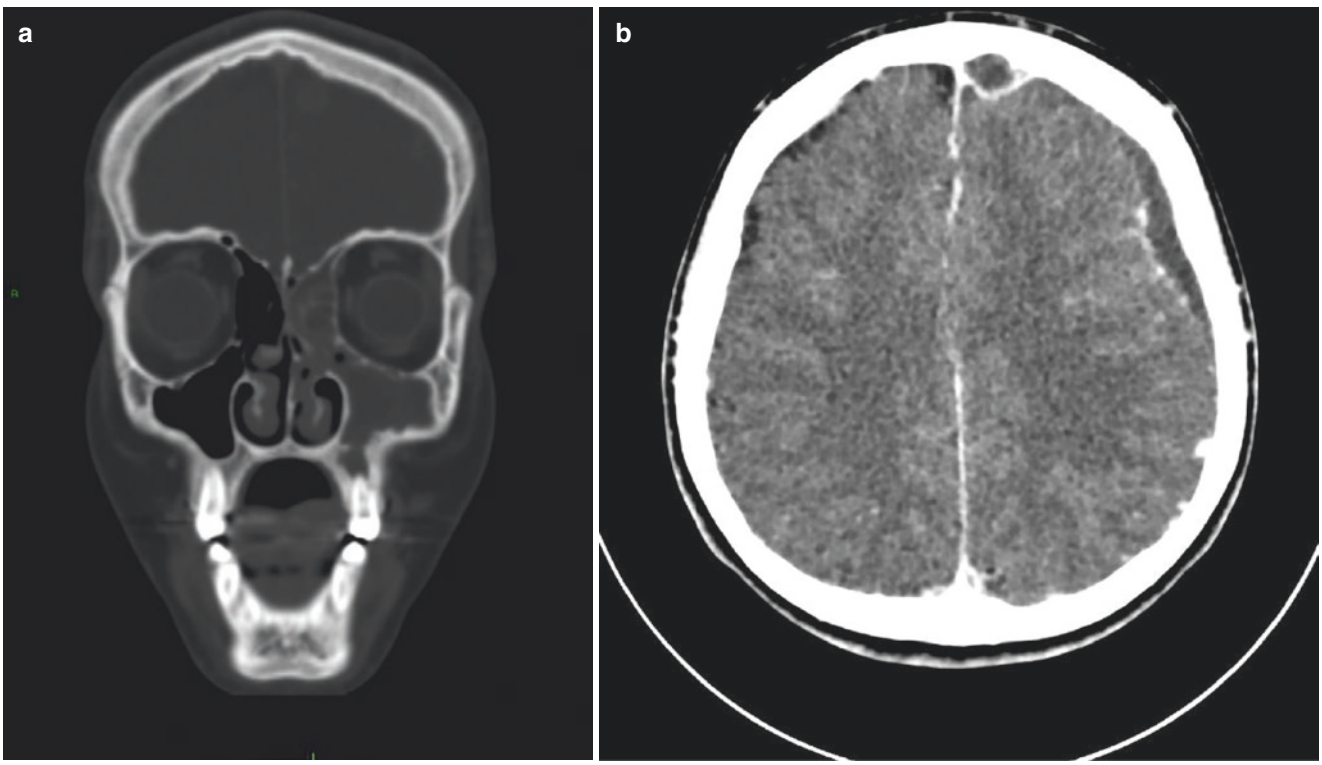

Fig. 2.76 Sinusitis and intracranial empyema secondary to dental abscess. (**a**) Coronal reconstructed CT image reveals bone destruction and a collection around the root of an upper left molar. This collection has spread into the left-sided paranasal sinuses. (**b**) Axial contrast-enhanced CT image of brain in the same patient reveals left-sided subdural empyemas from intracranial spread of the infection

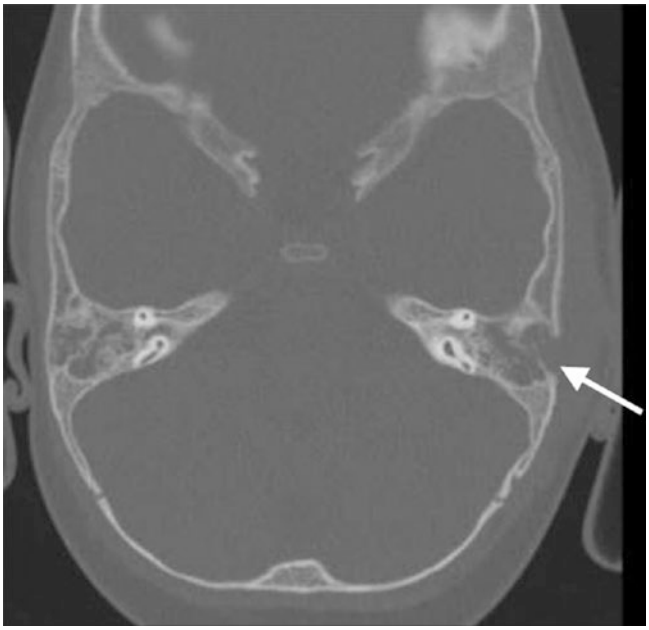

Fig. 2.78 Left coalescent mastoiditis. Axial CT image demonstrates destruction of the lateral wall and septa of the opacified left mastoid (*arrow*). There is associated retroauricular soft tissue swelling. The right mastoid air cells are also opacified

any intracranial complications. Middle ear and mastoid opacification on CT scanning with no evidence of bony resorption or destruction is classified as *incipient mastoiditis*. *Coalescent mastoiditis*, on the other hand, is the term used when imaging demonstrates erosion of the mastoid septa or mastoid walls (Fig. 2.78). Recognised complications of acute mastoiditis include bony destruction or osteomyelitis, subperiosteal abscess, and deep neck abscess (Fig. 2.79). Intracranial complications include epidural empyema, subdural empyema, brain abscess, meningitis, dural venous thrombophlebitis (sigmoid sinus thrombosis) and carotid artery spasm or arteritis (Fig. 2.80). MR imaging may be required to further evaluate any suspected intracranial complication (Figs. 2.81).

2.2.5 Parapharyngeal Abscess

A parapharyngeal abscess is a deep neck abscess that usually occurs following the spread of oropharyngeal infections such as tonsillitis, peritonsillar abscess, or dental infection. It also may be due to the spread of infection from one of the other neck spaces or following a penetrating injury to the neck (Fig. 2.82). It is exceedingly painful. Clinically, the abscess interferes with swallowing, and speech becomes "thick." In more severe cases, there may be dyspnoea, stridor, neck stiffness, drooling of secretions, and difficulty in opening the mouth. The tonsillar area is swollen and red, and the oedematous uvula is often displaced to the opposite side (Fig. 2.83).

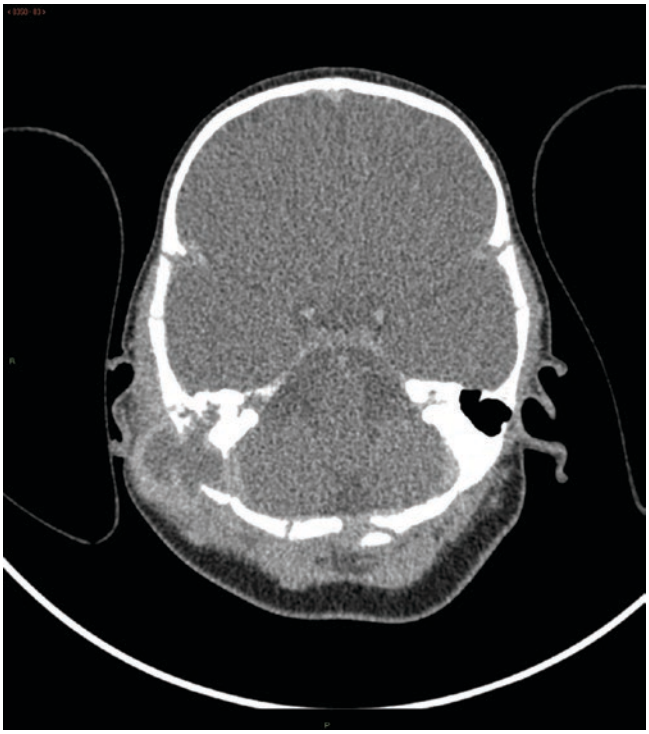

Fig. 2.79 Right mastoiditis with abscess formation. Axial contrast-enhanced CT image shows bony destruction and a collection within the right mastoid. The collection communicates with a subperiosteal abscess

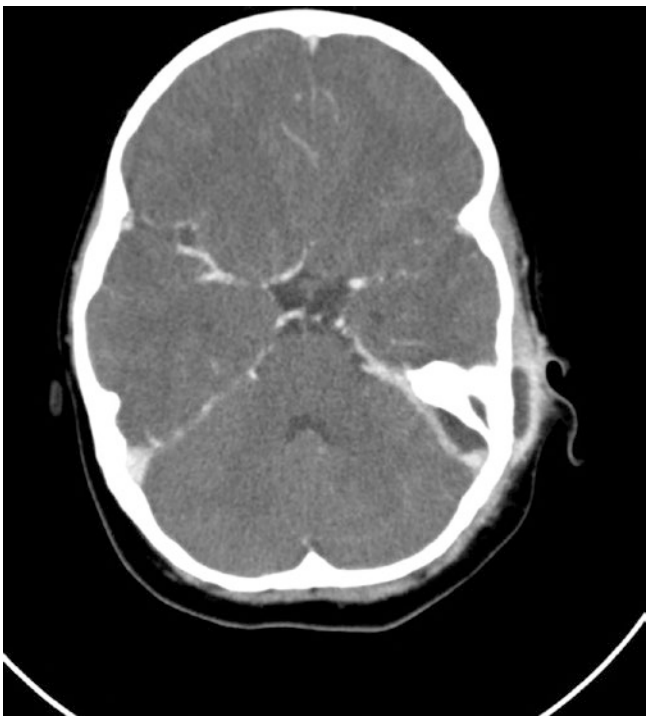

Fig. 2.80 Left mastoiditis complicated by adjacent subperiosteal and epidural abscesses. Axial contrast-enhanced CT image shows a rim-enhancing subperiosteal collection overlying the left mastoid. Intracranially, there is a rim-enhancing low-attenuation epidural empyema, which is displacing the adjacent sigmoid sinus

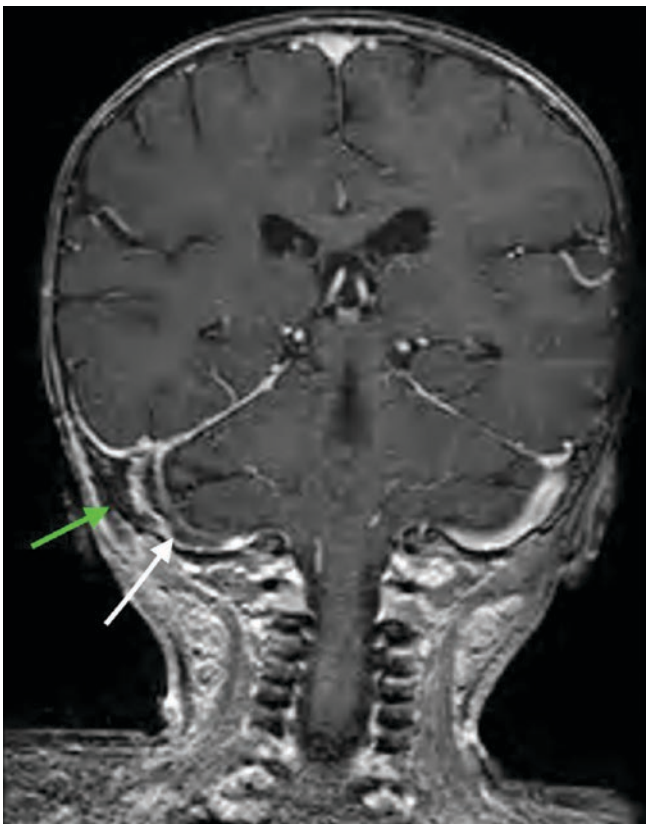

Fig. 2.81 Right mastoiditis complicated by thrombophlebitis. Coronal post-contrast T1-weighted fat-saturated MR image demonstrates thrombus within the right sigmoid sinus (*white arrow*) and an adjacent epidural abscess (*green arrow*)

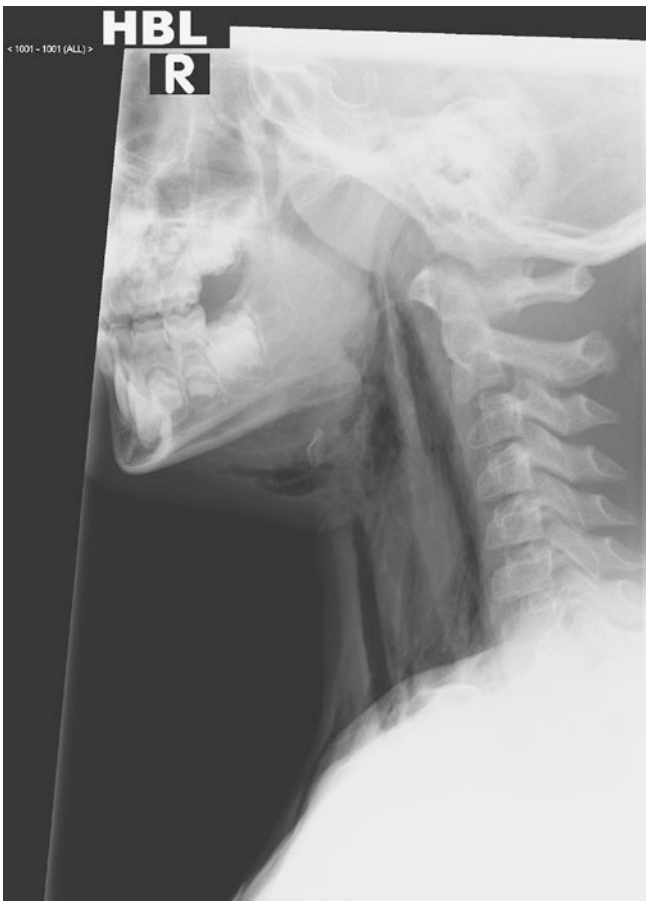

Fig. 2.82 Lateral radiograph of the neck demonstrating surgical emphysema and swelling of the prevertebral soft tissues following a penetrating neck injury

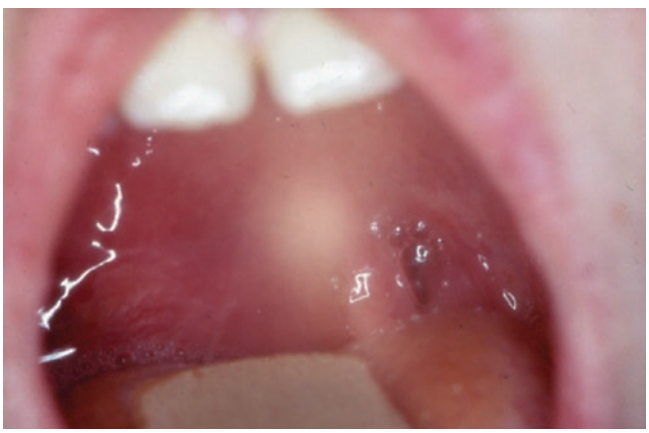

Fig. 2.83 Clinical photograph of a parapharyngeal abscess pointing in the fauces of the mouth

This condition requires urgent diagnosis and treatment, as compression of the airway can be fatal. Radiological confirmation of the diagnosis is usually performed with CT. On a contrast-enhanced CT study, a parapharyngeal abscess appears as a peripherally enhancing lesion with a low-attenuation centre (Fig. 2.84). Complications of parapharyngeal space infections include airway obstruction, spread of infection to other deep neck spaces or the mediastinum, thrombophlebitis of the internal jugular vein (Fig. 2.85), and mycotic aneurysm with possible rupture of the carotid artery.

2.2.6 Sialadenitis/Sialolithiasis/Sialectasis

Sialadenitis is inflammation of the salivary glands. It may be acute or chronic. In the acute form, the gland is swollen and painful to touch, and the overlying skin is red. A purulent exudate may be visible at the duct orifice. Acute sialadenitis is usually the result of bacterial infection; *Staphylococcus aureus* is a common causative organism. A calculus within the gland duct (sialolithiasis) is often a predisposing factor. The most common viral cause of acute sialadenitis is mumps, which frequently causes bilateral parotid swelling.

Ultrasound may be performed in cases of acute sialadenitis. The affected gland appears enlarged, with reduced parenchymal echogenicity (compared with the unaffected glands), and demonstrates increased vascularity.

Sialolithiasis is the development of a calculus within the salivary gland or duct. It is rare in children; when present, it usually affects the submandibular gland. It presents with recurrent swelling and pain in the submandibular region at

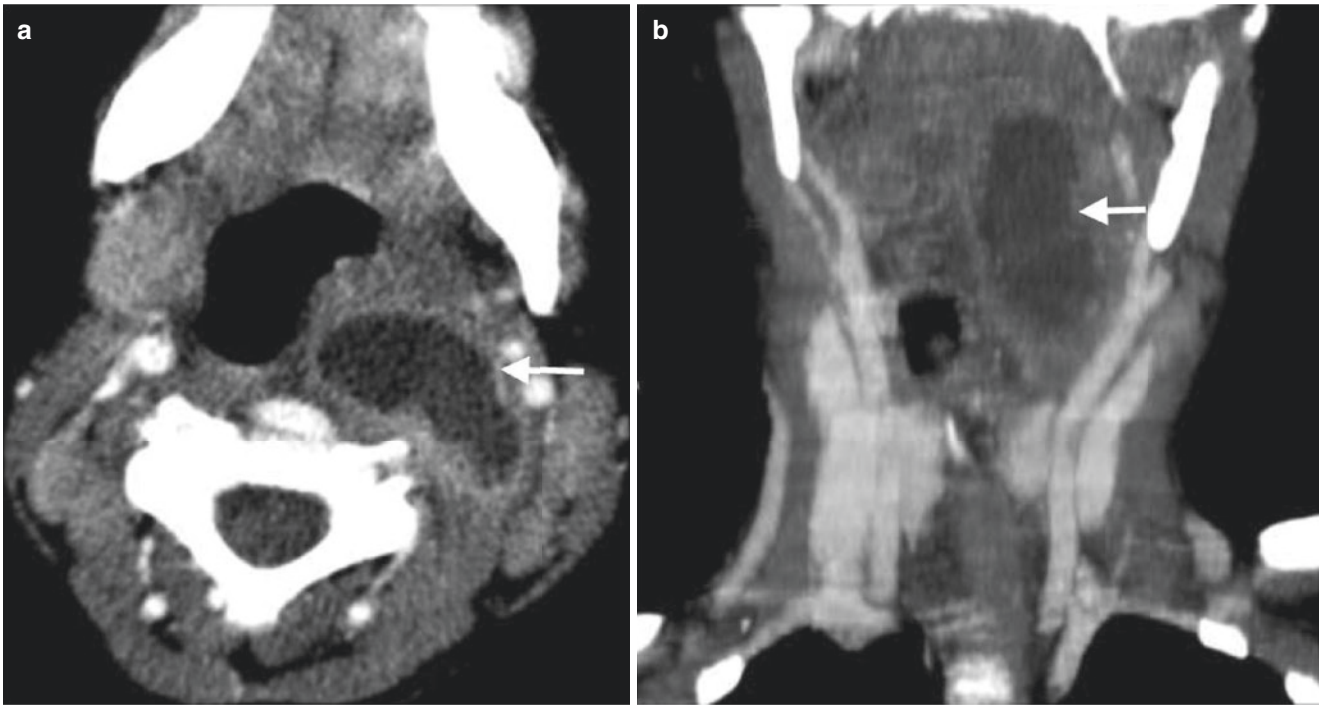

Fig. 2.84 Left parapharyngeal abscess. Axial contrast-enhanced CT image (**a**) and coronal reconstructed CT image (**b**) show a well-defined, rim-enhancing, low-attenuation fluid collection (*arrow*) in the left parapharyngeal space. The airway is patent but displaced to the right

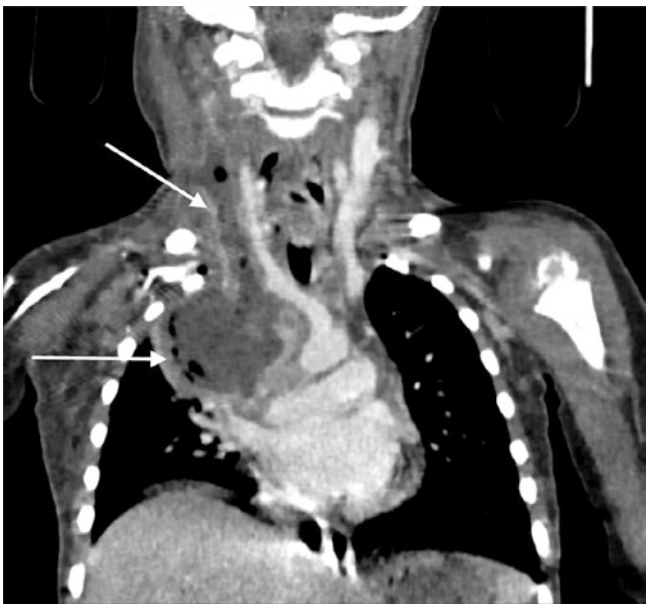

Fig. 2.85 Parapharyngeal abscess complicated by thrombophlebitis and mediastinal abscess. Coronal reformatted contrast-enhanced CT image demonstrates thrombus and gas within the right internal jugular vein, as well as a gas-containing collection in the right superior mediastinum

mealtimes because the calculus obstructs the submandibular duct and prevents saliva flow. The calculus may be palpable or even visible if it is near the duct orifice (Fig. 2.86). Not all stones are radiopaque. Conventional radiography can detect approximately 80–90% of submandibular stones. Oblique

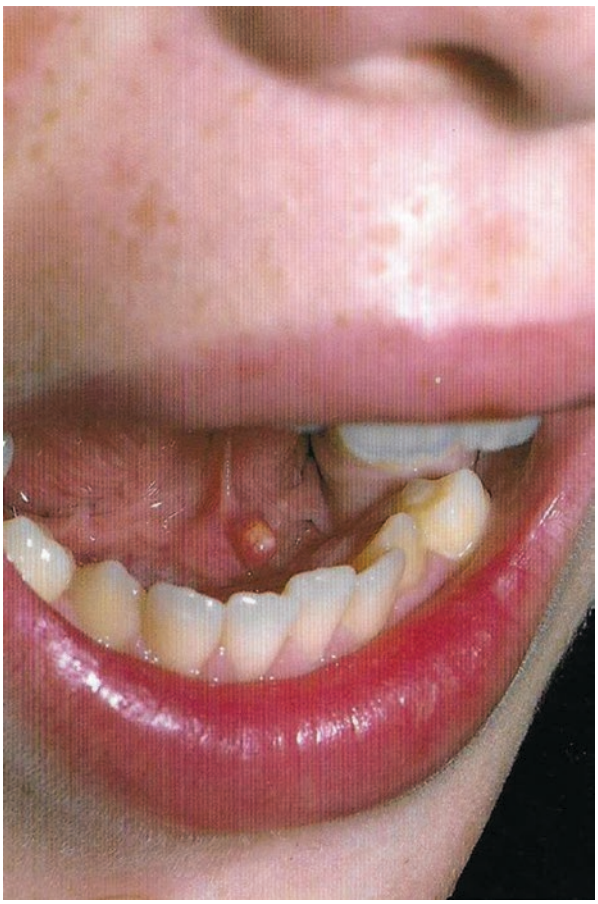

Fig. 2.86 Clinical photograph of calculus at the orifice of the left submandibular gland duct

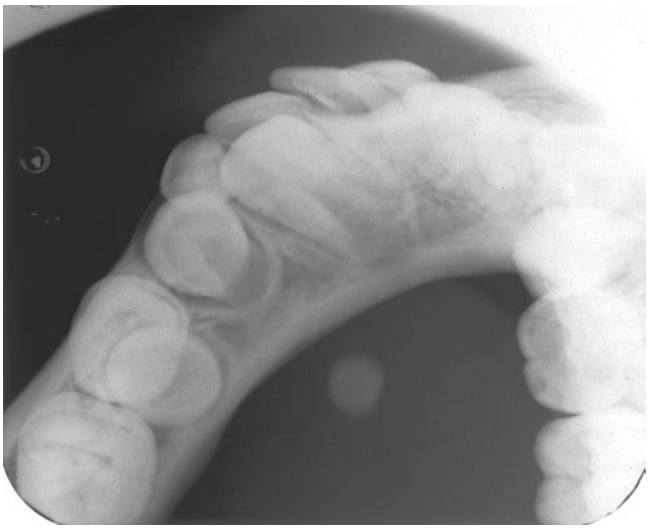

Fig. 2.87 Intraoral dental radiograph showing a radiopaque calculus in the submandibular area

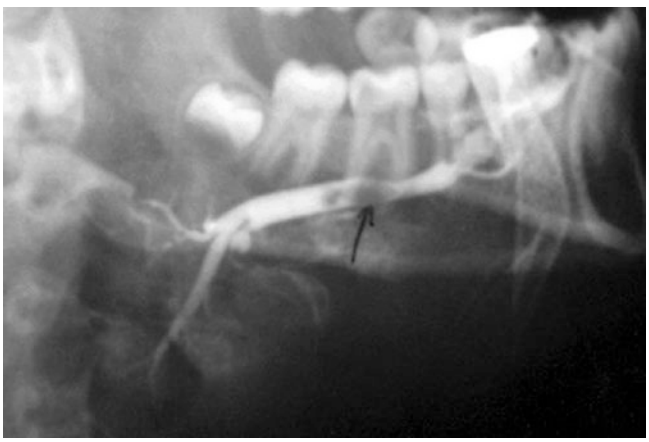

Fig. 2.88 Historical radiograph of submandibular sialogram. Contrast has been injected through a fine catheter inserted into the submandibular duct. The filling defect within the duct (*arrow*) is consistent with an intraductal calculus

views may be required to project the calculus away from the mandible and teeth (Fig. 2.87).

Sialography is a procedure in which a small amount of water-soluble contrast is injected directly into the gland duct and images are obtained with fluoroscopy. It can be used to demonstrate an intraductal calculus. The calculus is seen as a filling defect within the duct (Fig. 2.88). Sialography is contraindicated if there is associated acute sialadenitis, since it can make the infection worse.

Ultrasound can be used to diagnose sialolithiasis and can visualise non-radiopaque calculi. A calculus appears as a hyperechoic line with posterior shadowing, though very small stones may not demonstrate posterior acoustic shadowing. If the submandibular gland is acutely obstructed at the time of scanning, the gland will appear enlarged, and the ducts proximal to the stone will be dilated.

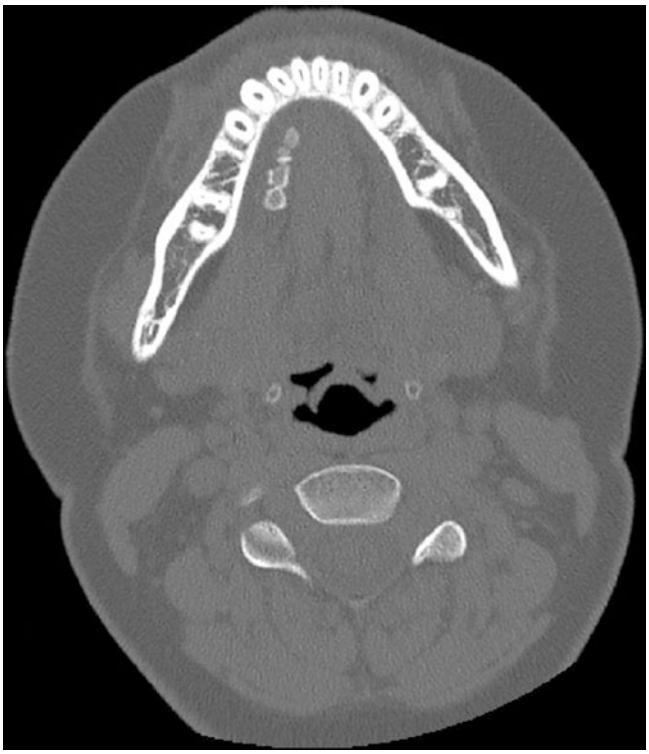

Fig. 2.89 Axial CT image shows a row of calculi within the right submandibular gland duct

CT or MRI can also be used to investigate suspected sialolithiasis (Fig. 2.89). These modalities (especially MRI) also give information about the gland itself.

Sialectasis refers to cystic dilatation of the salivary gland ducts. It can be seen in children who suffer from recurrent parotitis. In this condition, periodic parotid inflammation occurs over a period of years, usually associated with non-obstructive sialectasis. The aetiology of the condition is unknown. Recurrent parotitis is characterised by episodic painful swelling in the parotid region during mastication and/or swallowing. There is often associated fever and malaise.

Parotid sialography was the conventional radiographic technique for confirming sialectasis, typically showing multiple punctate and globular pools of contrast material within the gland, which persist on delayed radiographs (Fig. 2.90). Sialography has now been superseded by sonography, which is noninvasive and equally sensitive. In recurrent parotitis, the gland may or may not be enlarged. Multiple small, hypoechoic areas are seen within the gland parenchyma, probably reflecting both sialectasis of the peripheral ducts and surrounding lymphocytic infiltration, which is a recognised histological feature of the disease.

2.2.7 Cervical Lymphadenitis

Reactive cervical lymphadenitis is a condition characterised by inflammation of one or more lymph nodes in the neck. It

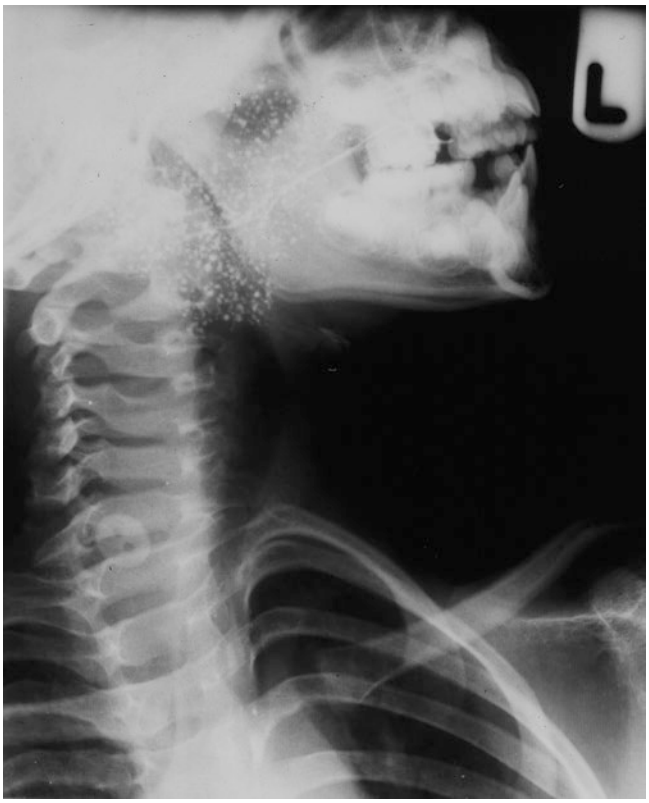

Fig. 2.90 Parotid gland sialectasis. Historical radiograph of parotid sialogram demonstrates multiple globular and punctate pools of contrast in dilated parotid ducts and ductules

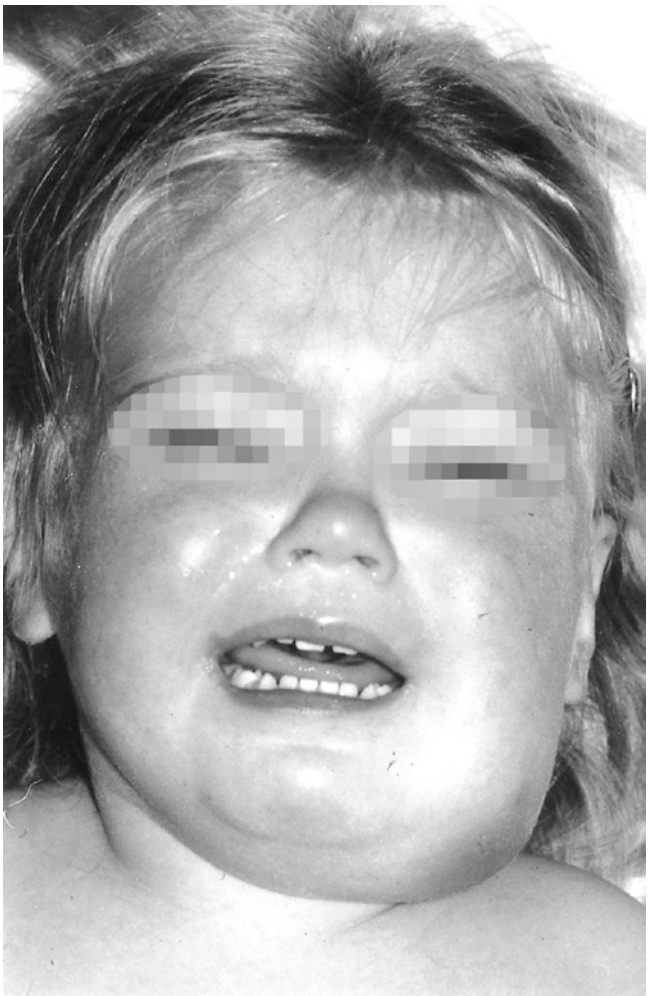

Fig. 2.91 Clinical photograph of left cervical lymphadenitis

is common in children and is usually seen in response to infection. Acute bilateral cervical lymphadenitis is usually caused by a viral upper respiratory tract infection (e.g., adenovirus, rhinovirus, enterovirus) or streptococcal pharyngitis. Acute unilateral cervical lymphadenitis is predominantly caused by *Staphylococcus aureus* or group A streptococcus infection of oropharyngeal origin.

A child with cervical lymphadenitis usually presents with a painful neck mass (Fig. 2.91).

Ultrasound is the imaging modality of choice. Reactive lymph nodes maintain their normal architecture, appearing as ovoid, hypoechoic structures with a preserved echogenic hilum; colour Doppler typically shows central vascularity (Fig. 2.92). The nodes may be matted together, appearing as a conglomerate mass.

The major complication of cervical lymphadenitis is abscess formation. As the inflamed lymph node undergoes suppuration, the centre of the node demonstrates heterogeneous decreased echogenicity with progressive necrosis and loss of the echogenic hilum. Nodal vascularity is decreased on colour Doppler assessment. Reactive oedema of the perinodal soft tissues is usually present. In the later stages of suppuration, the nodal abscess appears as a heterogeneous, hyperechoic or hypoechoic mass with a thick rim, which exhibits increased vascularity on colour Doppler (Figs. 2.93 and 2.94).

Tuberculosis and atypical mycobacterial infection are other causes of reactive cervical lymphadenitis. The posterior triangle and deep upper cervical lymph nodes are usually involved. Affected nodes are firm and usually non-tender (unlike other causes of lymphadenitis). Ultrasound reveals a matted, hypoechoic nodal mass, occasionally with calcification, and inflammatory changes in the adjacent soft tissues (Fig. 2.95).

2.2.8 Cerebral Abscess

Infections of the brain usually arise from haematogenously transmitted septic emboli. Less frequently, transdural spread may occur from adjacent sinus infection. Direct introduction of infection through trauma or surgical intervention occurs in a very small number of cases. If untreated, the initial period of parenchymal infection or cerebritis will progress to abscess formation; the affected area of the brain liquefies and

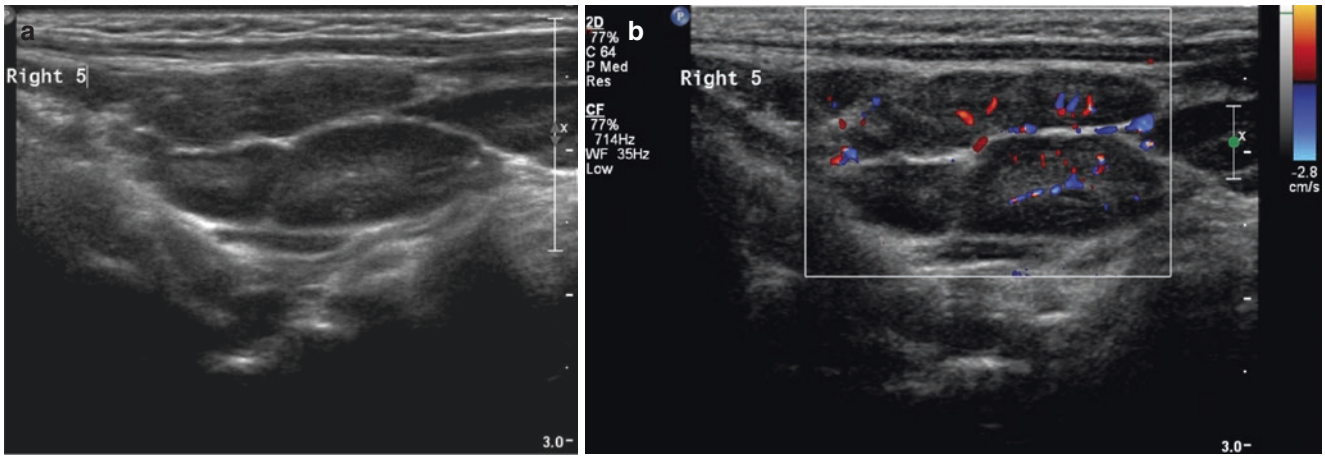

Fig. 2.92 Reactive cervical lymph nodes. (**a**) Longitudinal ultrasound image of a group of enlarged cervical lymph nodes. The nodes maintain their normal architecture and echogenic hila. (**b**) Colour Doppler image shows preserved vascularity within the centre of the nodes

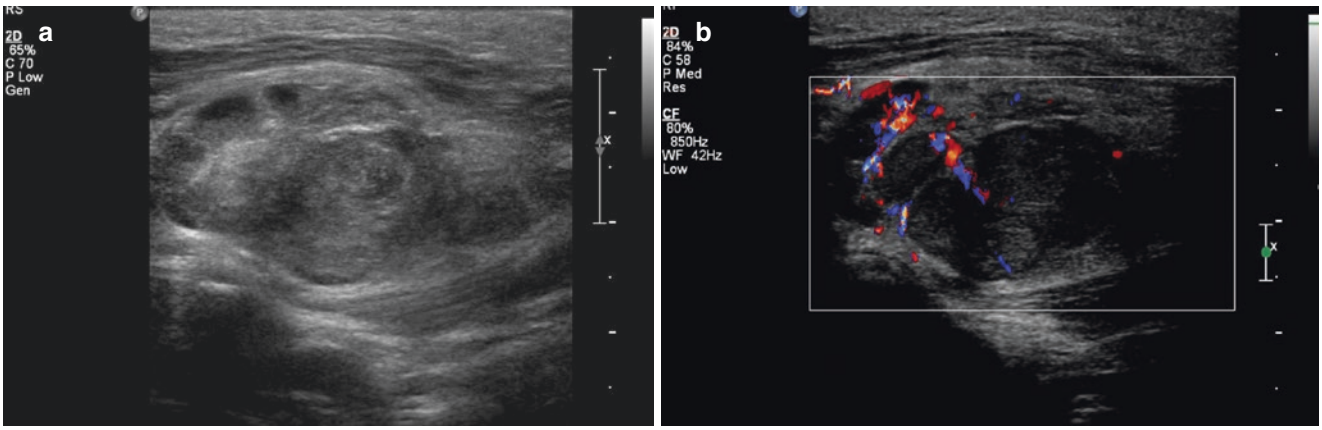

Fig. 2.93 Necrotic lymph node mass. (**a**) Ultrasound image demonstrates a heterogeneous, conglomerate lymph node mass with liquefaction. (**b**) Colour Doppler image shows peripheral vascularity

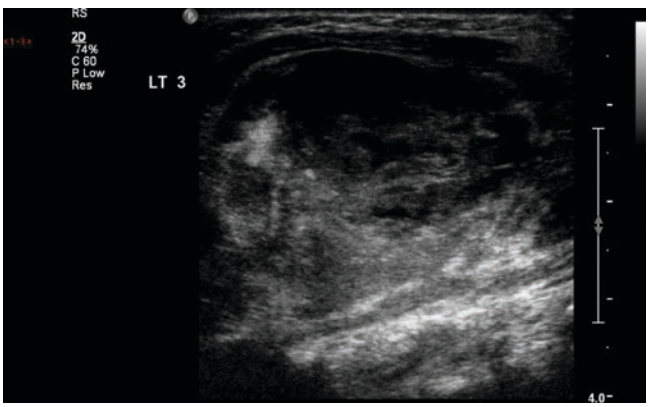

Fig. 2.94 Longitudinal ultrasound image shows an established lymph node abscess with echogenic and anechoic contents

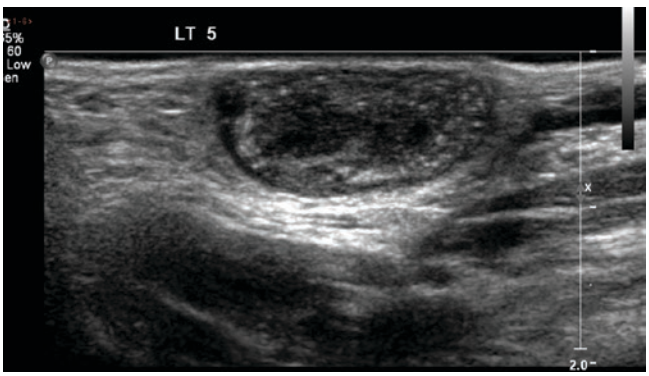

Fig. 2.95 Atypical mycobacterium infection of a posterior cervical lymph node. Longitudinal ultrasound image shows multiple tiny foci of increased echogenicity within the lymph node, consistent with intranodal calcification

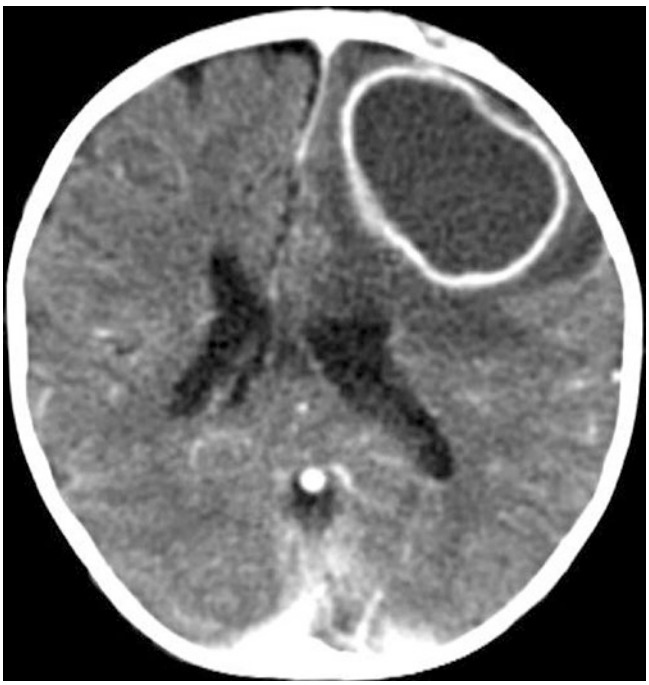

Fig. 2.96 Left frontal cerebral abscess. Axial contrast-enhanced CT image shows a large, low-attenuation fluid collection with a thin enhancing wall in the left frontal lobe of the brain. There is surrounding brain oedema and some distortion of the left lateral ventricle

becomes surrounded by a capsule of granulation tissue and collagen. Symptoms of cerebral abscess include headache, lethargy, reduced level of consciousness, vomiting, and seizures. Focal neurologic deficits may be evident.

CT or MRI can be used in the investigation of suspected brain abscess in children. In the emergency setting, CT is more likely to be performed. On CT scanning, a brain abscess appears as a round or oval-shaped area of low attenuation (low density), with a thin wall that enhances with intravenous contrast (Fig. 2.96). There is surrounding low-density brain oedema. An established brain abscess is of high signal intensity on T2-weighted MR imaging and has a hypointense wall, whereas on T1-weighted imaging, the abscess is of low signal intensity and the wall is of similar signal as the adjacent brain. The abscess wall enhances with contrast (Fig. 2.97).

2.3 Trauma

2.3.1 Head Injuries/Skull Fractures

Head injuries are the most common injuries in infants and young children. Injury severity is related to the mechanism of the trauma, which varies with the age of the patient. The vast majority of head trauma in children is mild, requires no

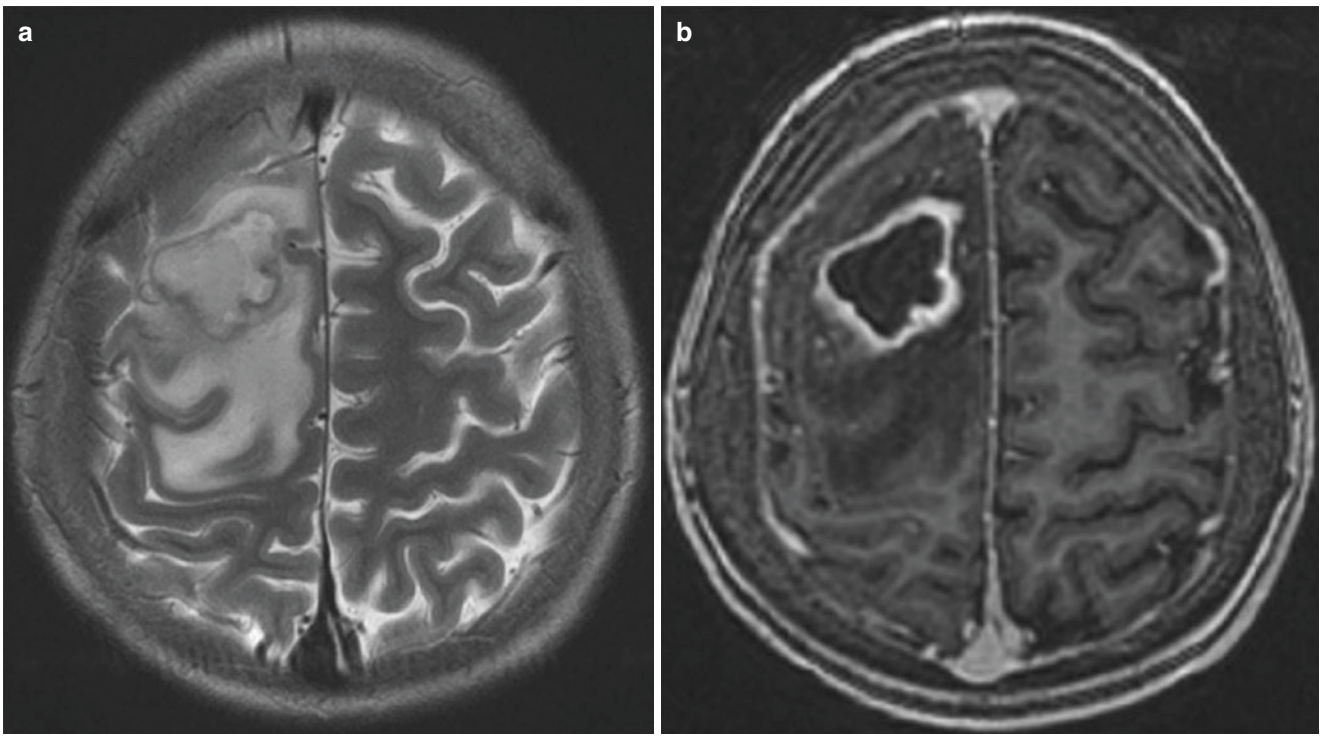

Fig. 2.97 Right frontal cerebral abscess. (**a**) Axial T2-weighted MR image shows a high-signal abscess with a low-signal wall in the superior right frontal lobe. There is marked surrounding brain oedema. (**b**) Axial post-contrast T1-weighted MR image demonstrates enhancement of the abscess wall

specific treatment, and has no sequelae. Only a small proportion of children with head trauma will have an intracranial injury. It is important to identify these individuals so that appropriate management occurs.

Radiology plays a vital role in the diagnosis and characterisation of head injuries in children. CT scanning is the imaging modality of choice because it can detect intracranial lesions that require urgent surgical intervention, such as extradural or subdural haematoma. For this reason, skull radiography is now rarely performed.

The most common type of skull fracture, linear fracture, is usually localised to the parietal or frontal region of the skull. These fractures are frequently the result of low-energy blunt trauma involving a wide area of the skull. The fracture extends through the entire thickness of the skull bone (Fig. 2.98). When the fracture is non-displaced, it heals spontaneously and no treatment is required. Complications may occur, however. For example, extradural haematoma (Fig. 2.99) can occur if the fracture involves a vascular channel; venous sinus thrombosis (Fig. 2.100) may follow a fracture in a venous sinus groove, or suture diastasis can follow a fracture involving a suture.

A depressed skull fracture occurs following a high-impact injury such as a blow from a golf club. The fracture is usually comminuted. Most depressed fractures occur in the frontoparietal region, where the skull is relatively thin. CT accurately defines the degree of bony displacement (Fig. 2.101). A fracture is clinically significant and requires elevation when the bone fragment is depressed deeper than the adjacent inner table of the skull. A depressed fracture may be compound if it is associated with a deep skin laceration or involves the paranasal sinuses.

2.3.2 Pond Fracture

The "pond" or "ping-pong" skull fracture is a depressed fracture of the infant skull caused by inner buckling of the skull. A fracture line is not visible radiologically. The fracture can occur following blunt trauma to the infant skull. The use of forceps during delivery has also been implicated in this type of fracture. Additionally, it may occur spontaneously owing to pressure on the fetal skull by a maternal bony prominence (sacral promontory or pubis), a uterine fibroid, or a fetal hand in utero. Clinical examination reveals a shallow depression of the infant skull contour (Fig. 2.102).

On a tangential skull radiograph, a pond-type fracture is visible as an inward depression of the skull; CT scanning demonstrates a smooth indentation of the calvarium with the absence of a distinct fracture line (Fig. 2.103). The periosteum and dura are usually intact.

2.3.3 Extradural Haemorrhage

Extradural haemorrhage, also known as epidural haematoma, is a haemorrhage into the space between the dura mater and the inner surface of the skull. It is usually caused by trauma and is often associated with a skull fracture. In young children, the haematoma is more commonly the result of a tear in the dural veins. In older children and adolescents, a middle meningeal artery tear is the most common cause. A diagnosis of extradural haemorrhage is usually suggested when a distinct lucid interval after injury is followed by a rapid reduction in the level of consciousness.

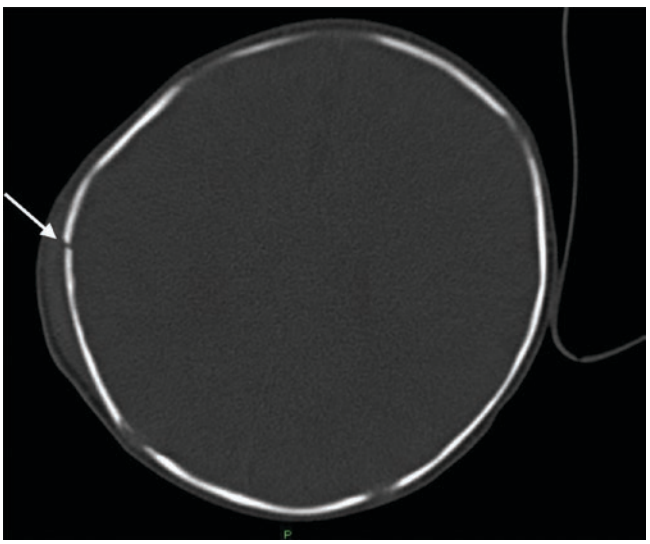

Fig. 2.98 Axial CT image demonstrates an undisplaced right parietal bone fracture (*arrow*) and adjacent scalp swelling

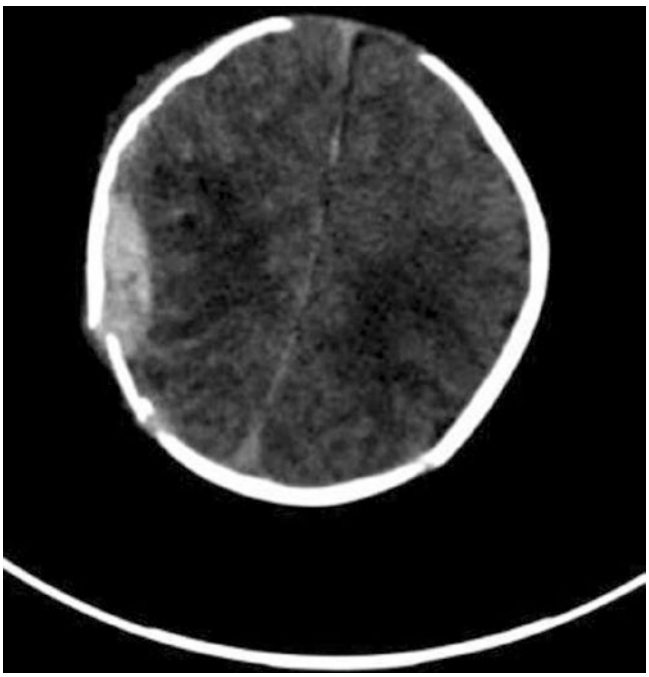

Fig. 2.99 Axial CT image shows an acute extradural haematoma complicating a right parietal bone fracture

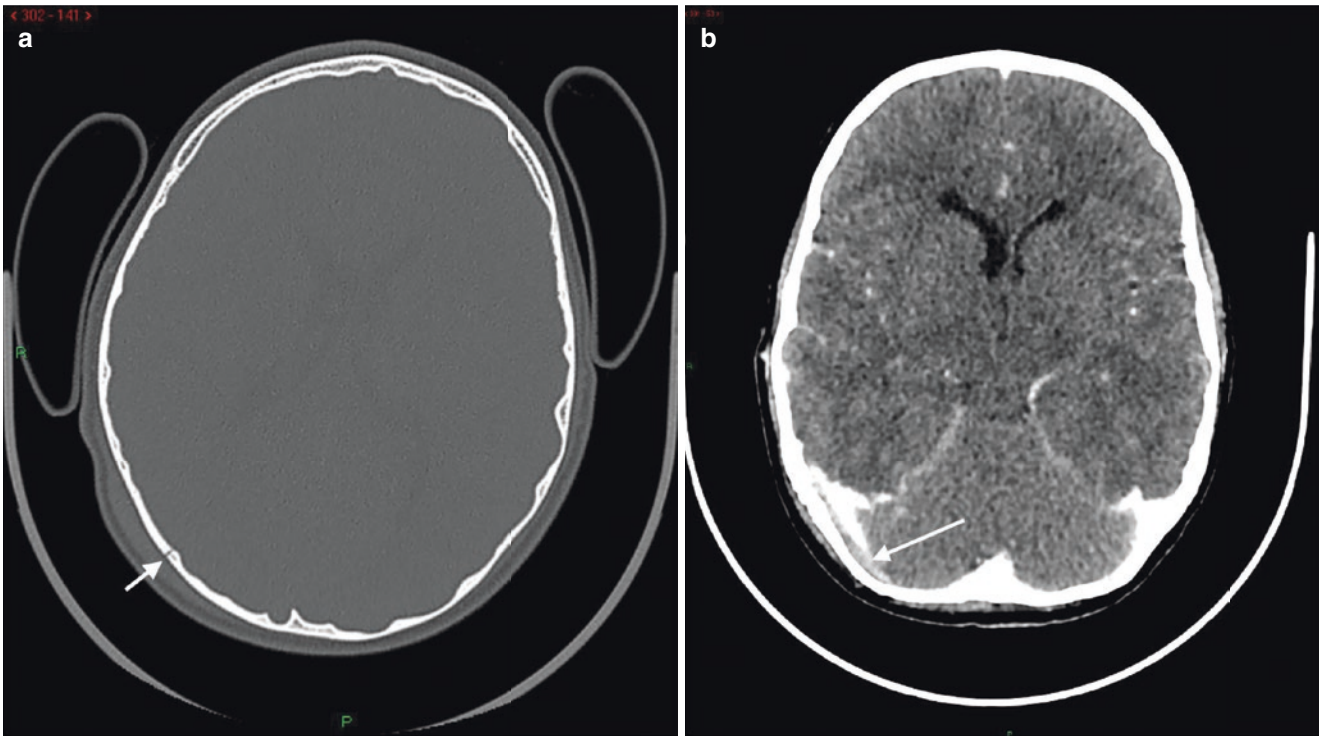

Fig. 2.100 Right occipital skull fracture complicated by thrombus in the adjacent transverse sinus. Axial CT image (**a**) shows an undisplaced fracture in the right occipital bone. Subsequent axial contrast-enhanced CT image (**b**) shows a filling defect in the adjacent right transverse sinus, consistent with thrombus

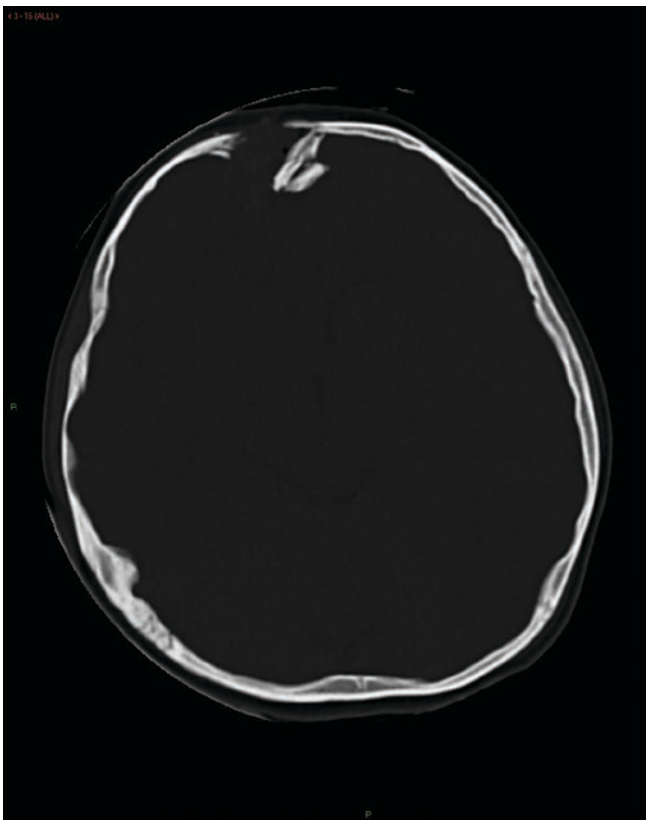

Fig. 2.101 Axial CT image shows a comminuted right frontal bone fracture with depressed bone fragments

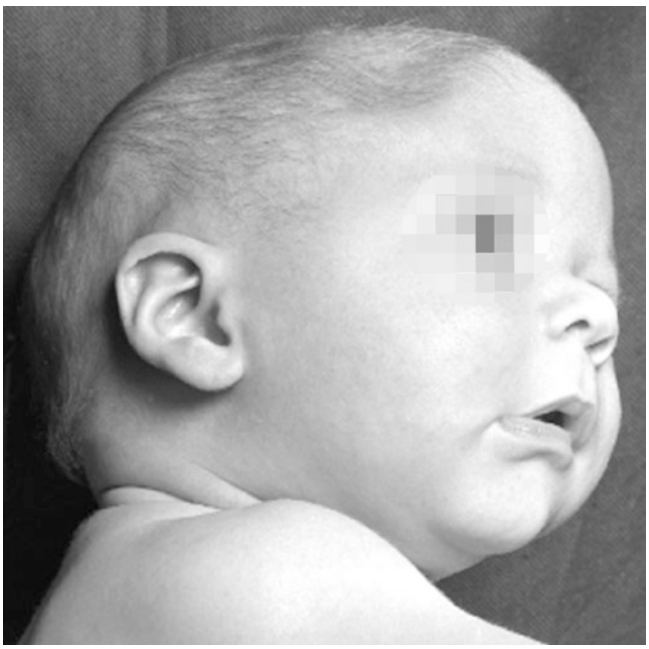

Fig. 2.102 Clinical photograph of a pond fracture on the right side of the head

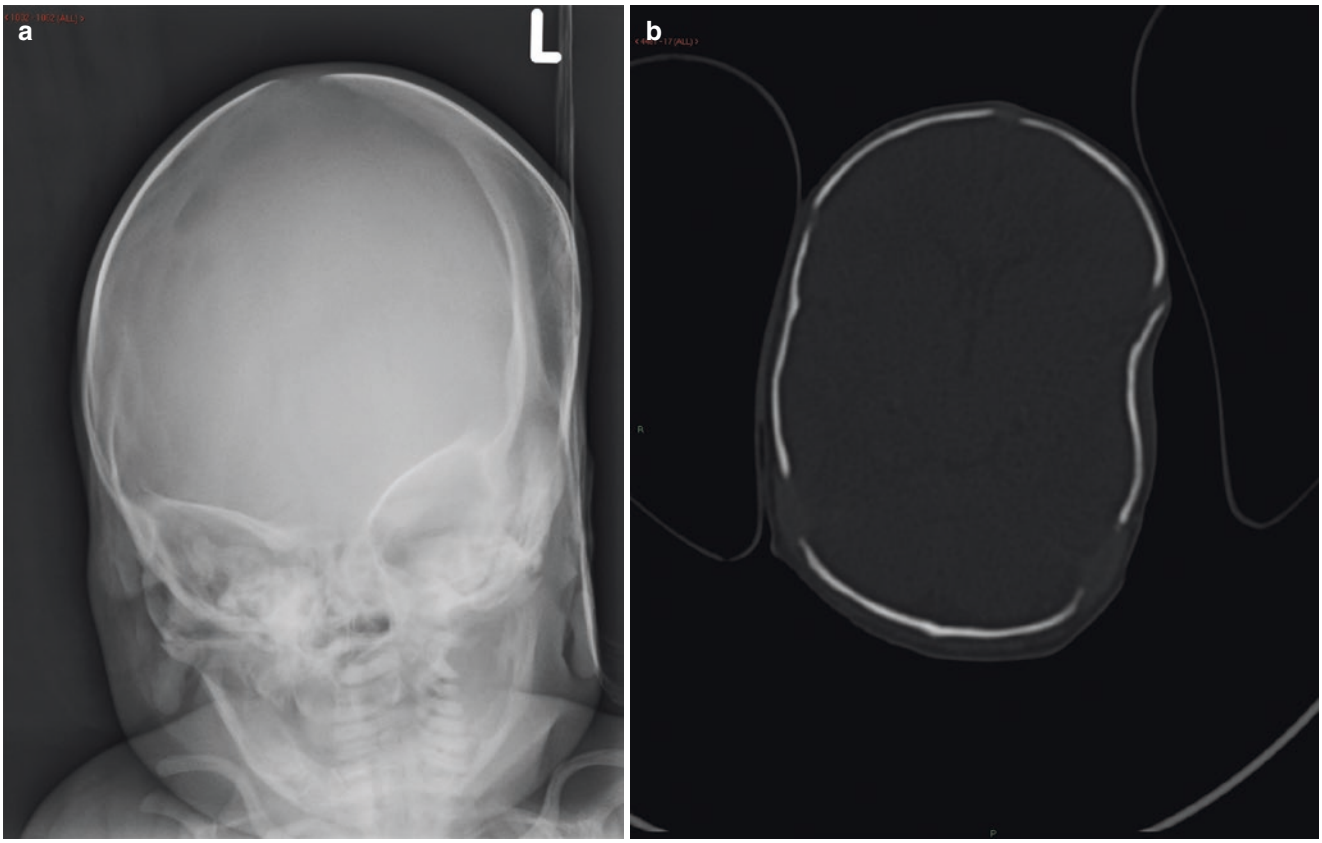

Fig. 2.103 Left-sided ping-pong (pond) skull fracture. (**a**) AP skull radiograph in a newborn infant demonstrates a shallow depression of the left skull contour. (**b**) Axial CT image shows a shallow depression in the left parietal bone. No fracture line is demonstrated

On CT, an extradural haemorrhage appears as a lentiform or biconvex-shaped area of increased attenuation (increased density) in the extraparenchymal (extra-axial) space between the brain and the skull. Because the dura is anchored at the sutures, extradural haematomas usually do not cross cranial sutures. A skull fracture and overlying scalp swelling are often present (Fig. 2.104). A large extradural haematoma can displace the adjacent brain and cause contralateral midline shift (Fig. 2.105).

2.3.4 Subdural Haemorrhage

Subdural haemorrhage, also known as subdural haematoma, is a collection of blood in the potential space between the dura and arachnoid mater of the meninges around the brain. The haemorrhage is believed to result from stretching and tearing of bridging cortical veins as they cross the subdural space to drain into an adjacent dural sinus. Subdural haemorrhage may occur following birth trauma, non-accidental injury, or accidental head injury. It may follow a relatively innocuous head injury in patients who have an underlying bleeding disorder (such as haemophilia) or who are on anticoagulant therapy. Infants with a subdural haemorrhage may present with seizures, irritability, or lethargy. Older children usually present with a reduced level of consciousness and pupillary abnormalities.

On CT scanning, an acute subdural haemorrhage appears as a crescent-shaped, high-attenuation (high-density) extraparenchymal (extra-axial) collection overlying the cerebral hemisphere (Fig. 2.106). Unlike extradural haematomas, subdural haemorrhages are not limited by sutures, but they are limited by dural reflections such as the falx cerebri and the tentorium. Within 1–3 weeks, the subdural haemorrhage becomes isodense to the adjacent brain cortex and is referred to as *a subacute haemorrhage* (Fig. 2.107). After approximately 3 weeks, the density of the haematoma becomes less than that of the brain and closer to that of CSF (Fig. 2.108). It is then known as *a chronic subdural haematoma*. A large subdural haematoma can displace adjacent brain structures, compress the ipsilateral lateral ventricle, and cause midline shift.

2.3.5 Cerebral Contusion and Diffuse Axonal Injury

Cerebral contusions—bruises of the brain—are usually the result of a rapid acceleration or deceleration injury in which the brain comes into forcible contact with the rougher edges of the inner table of the skull. Common locations for this type of injury are the antero-inferior temporal and orbitofrontal regions of the brain.

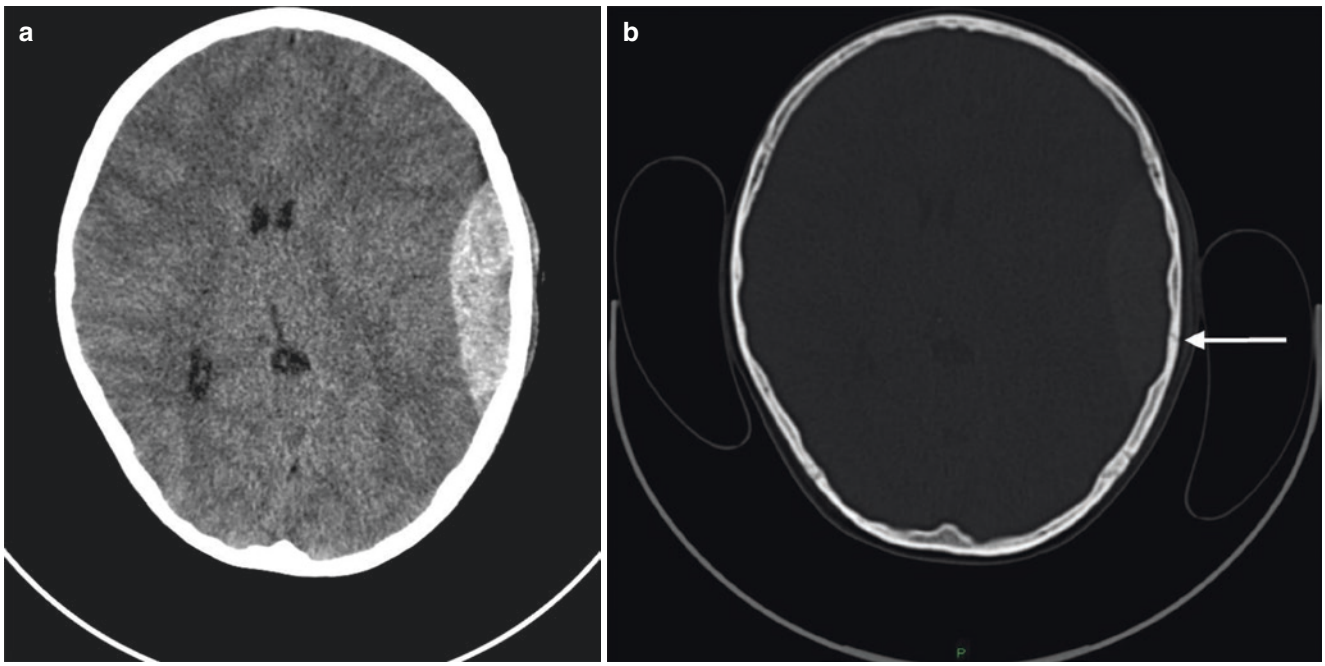

Fig. 2.104 Extradural haematoma associated with a parietal skull fracture. (**a**) Axial CT image shows a high-attenuation, biconvex haematoma overlying the left cerebral hemisphere. There is mass effect on the adjacent brain. (**b**) The same CT image viewed on bone window setting shows an undisplaced fracture (*arrow*) within the left parietal bone

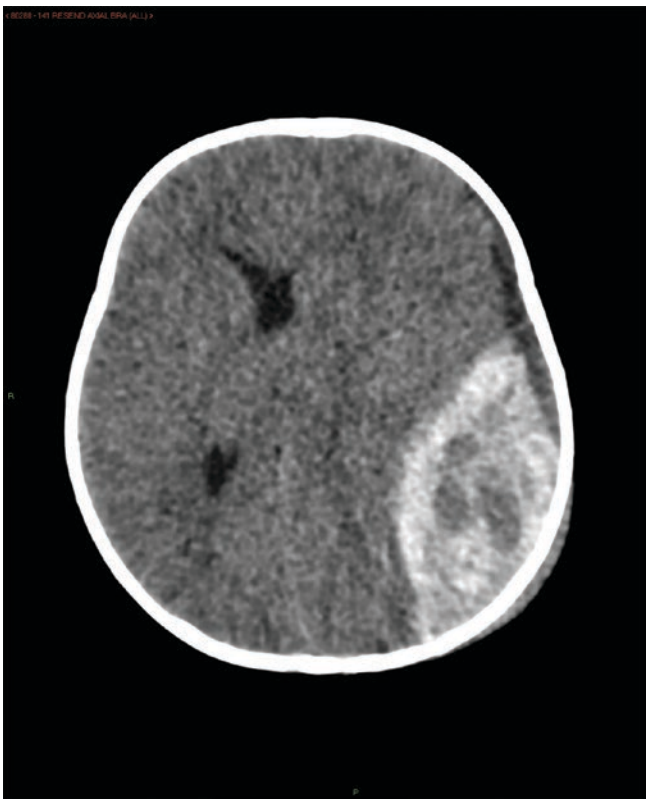

Fig. 2.105 Large extradural haematoma. Axial CT image shows a large, left-sided extradural haematoma, limited posteriorly by the left lambdoid suture. There is significant mass effect on the left cerebral hemisphere and left-to-right midline shift

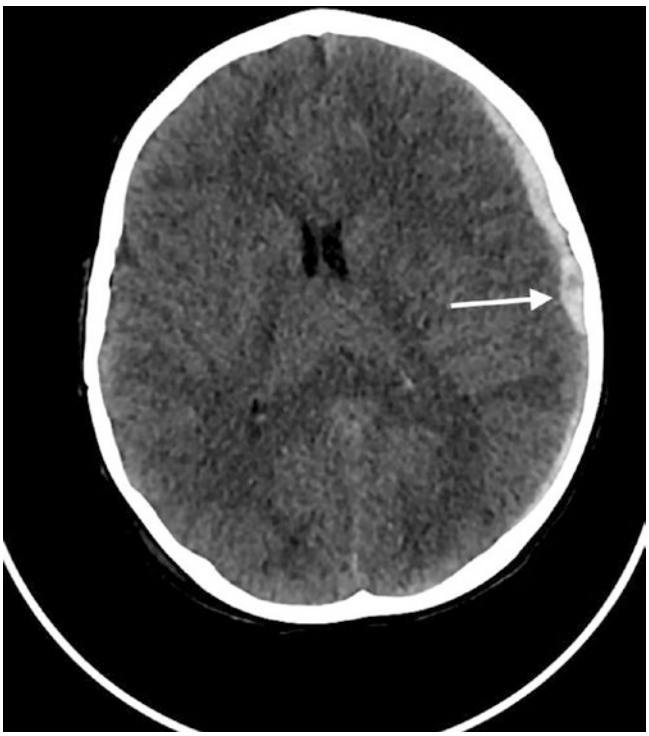

Fig. 2.106 Acute subdural haematoma. Axial CT image shows a crescent-shaped area of high-density haemorrhage overlying the left cerebral hemisphere

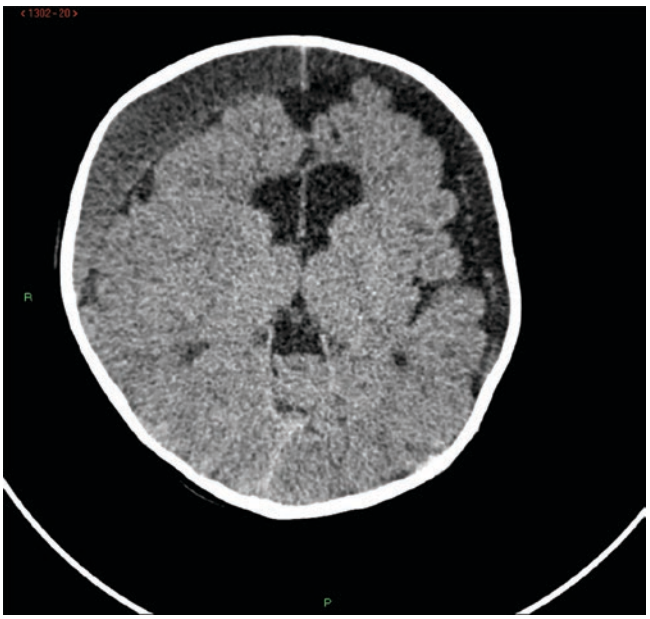

Fig. 2.107 Subacute subdural haematoma. Axial CT image shows an isodense (to brain) extra-axial collection overlying the right frontal lobe, causing localised mass effect on the adjacent brain. The haematoma is limited medially by the falx. A thinner, hypodense, chronic subdural haematoma is seen on the left side

CT is used to detect haemorrhagic cerebral contusions in the acute phase because it is very sensitive to the presence of acute blood within the brain. Acute intracerebral contusions are identified as areas of increased attenuation (high density) within the cortex or subcortical white matter, often with surrounding oedema. They can vary in size from tiny petechial foci to larger bleeds (Figs. 2.109 and 2.110).

Diffuse axonal injury (DAI) is a shearing injury resulting from rotational forces on the skull, causing stretching and disruption of nerve fibre tracts. This type of injury has a predilection for axons at the grey–white-matter junction. Shearing injuries can also be found in the deep white matter, corpus callosum, basal ganglia, and the brain stem.

CT is relatively insensitive for detecting diffuse axonal injury unless the lesions are overtly haemorrhagic (Fig. 2.111). MRI is the modality of choice in the assessment of DAI. By using sequences that are sensitive to blood products, microhaemorrhages can be identified as foci of hypointense signal (Fig. 2.112). Non-haemorrhagic lesions are visible as areas of increased signal on a fluid-attenuated inversion recovery (FLAIR) sequence (Fig. 2.113). Acute DAI lesions are bright on diffusion-weighted imaging and dark on the apparent diffusion coefficient (ADC) map because of restricted diffusion caused by acute cell death and cytotoxic oedema (Fig. 2.114).

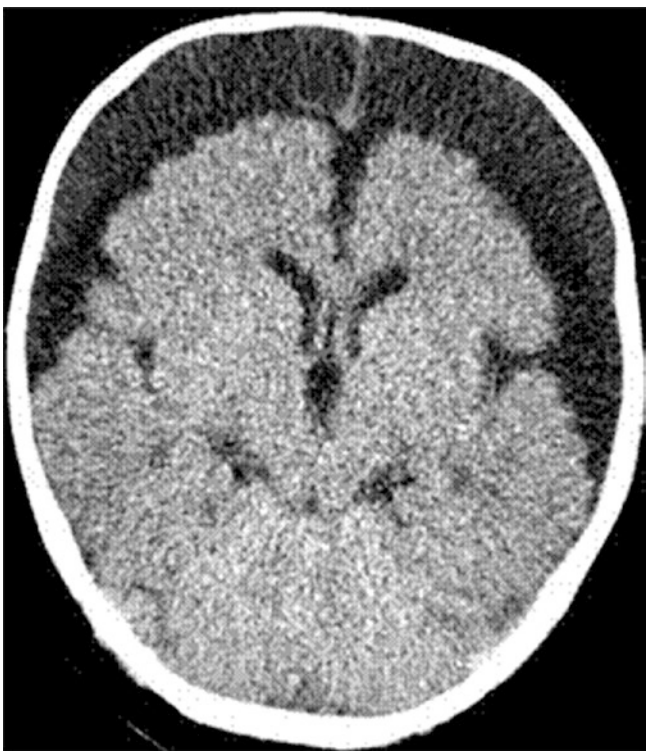

Fig. 2.108 Bilateral chronic subdural haematomas. Axial CT image shows hypodense extra-axial collections overlying both cerebral hemispheres

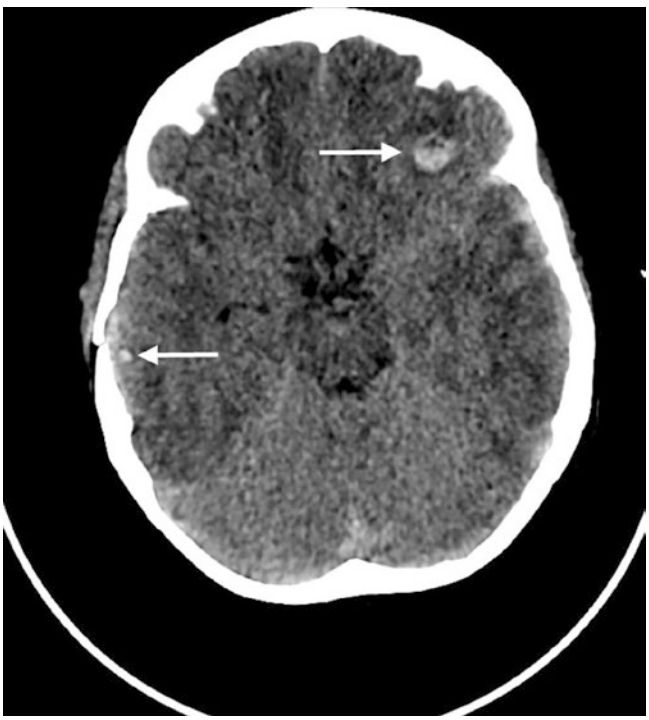

Fig. 2.109 Cerebral contusion. Axial CT image demonstrates a small, haemorrhagic cerebral contusion in the left frontal lobe. There is a smaller contusion peripherally in the right temporal lobe, adjacent to a skull fracture

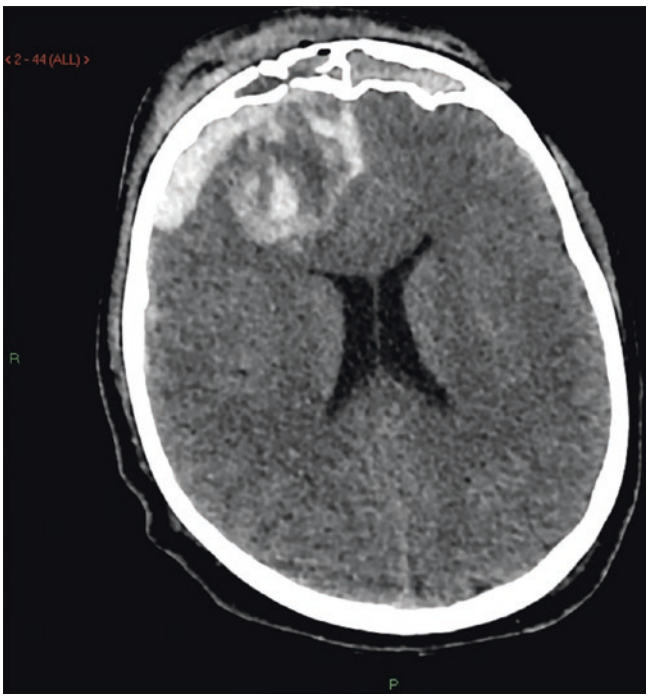

Fig. 2.110 Large frontal cerebral contusion. Axial CT image shows a large parenchymal haemorrhage in the right frontal lobe, adjacent to a compound fracture of the right frontal sinus. There is blood within the frontal sinuses and a right frontal subdural haematoma

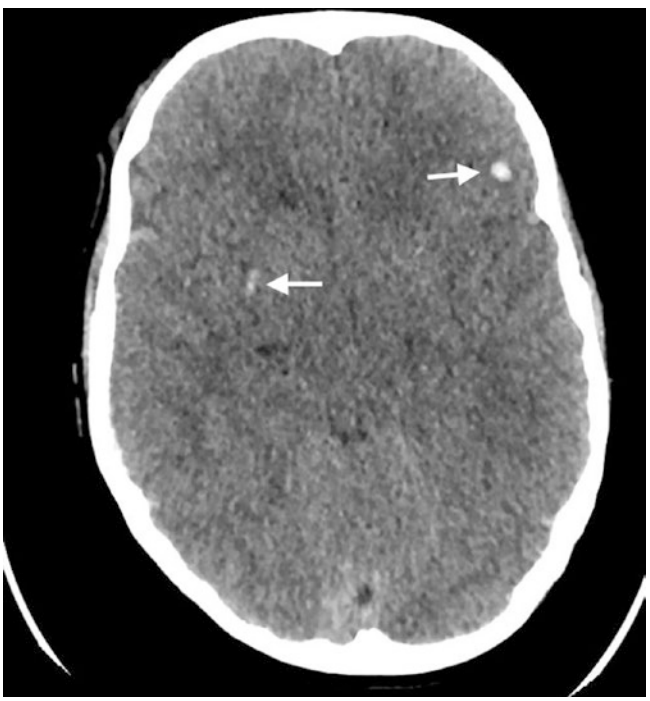

Fig. 2.111 Diffuse axonal injury (DAI). Axial CT image shows a tiny focus of haemorrhage in the right basal ganglia, most likely secondary to axonal shearing injury. There is also a small left frontal haemorrhage

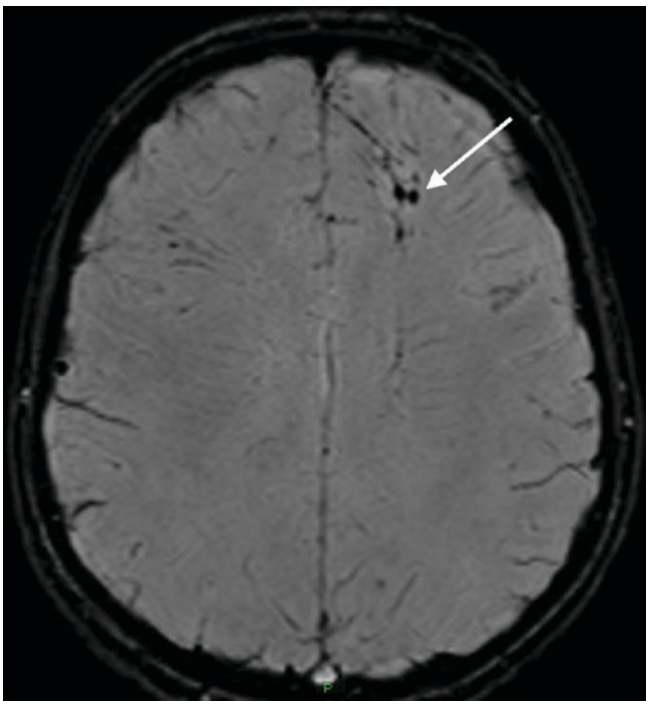

Fig. 2.112 DAI. Axial susceptibility-weighted MR image, which is sensitive for blood products, demonstrates tiny foci of low signal intensity (*arrow*) in the left frontal lobe, in keeping with tiny haemorrhages

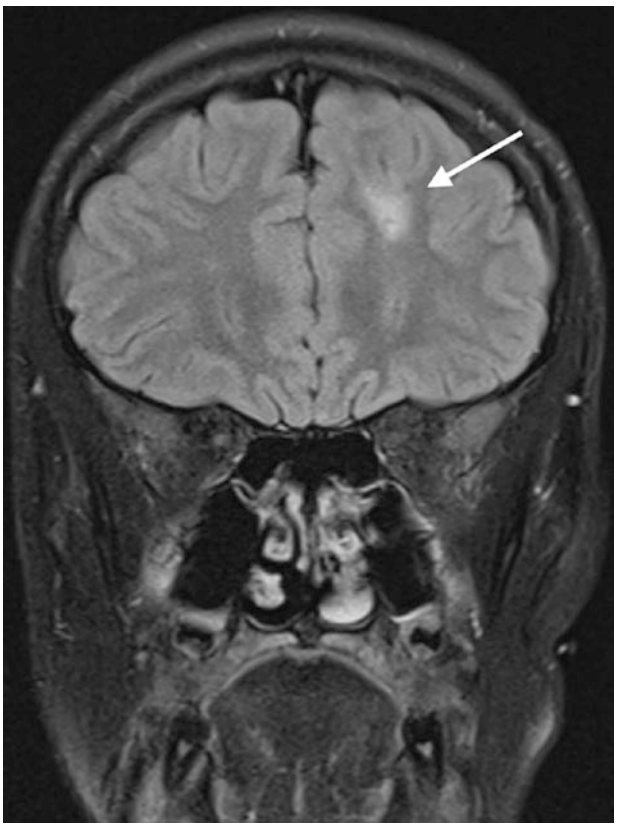

Fig. 2.113 Non-haemorrhagic DAI. Coronal T2 fluid-attenuated inversion recovery (FLAIR) sequence shows abnormal increased signal in the subcortical white matter of the left frontal lobe, consistent with axonal shearing injury

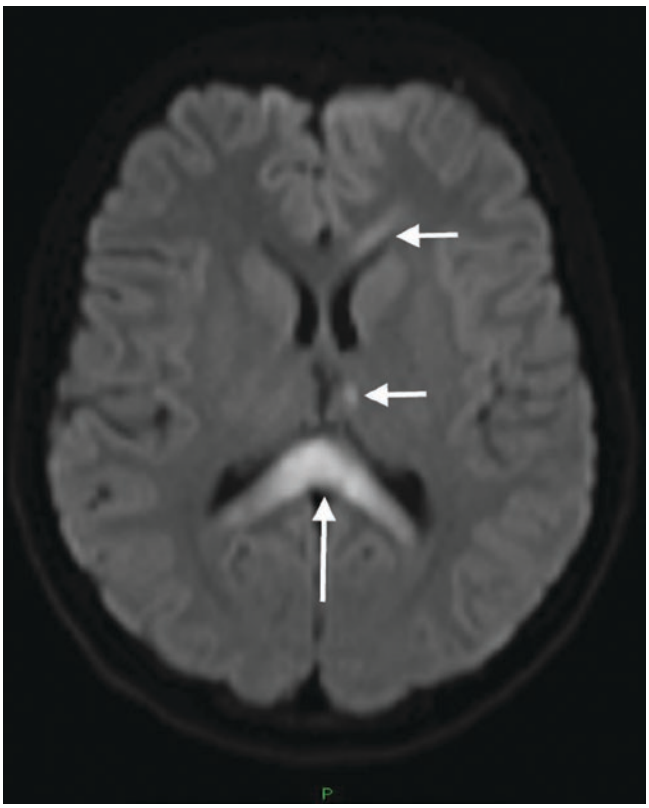

Fig. 2.114 Acute DAI. Axial diffusion-weighted image shows abnormal increased signal across the splenium of the corpus callosum. Smaller areas of abnormal signal are present in the medial left thalamus and the genu of the corpus callosum

2.3.6 Cervical Spine Injury

Cervical spine injuries are less common in children than in adults, but the anatomy of the developing cervical spine predisposes children to upper cervical spine injury. Younger children in particular tend to have more injuries in the area from the occiput to the C3 vertebra. The prevalence of upper cervical spine injury relates to physiological differences in the paediatric cervical spine. Younger children have a relatively higher fulcrum of motion at the C2–C3 level (compared to C5–C6 in adults) and a relatively large head. Developmental features such as ligamentous laxity, physiologic anterior wedging of vertebral bodies, shallow facet joint articulations, and weak neck muscles are other factors that contribute to injury in the immature cervical spine.

Initial imaging of the cervical spine may be performed with radiographs or CT scanning, depending on the clinical situation. An adequate cervical spine radiograph series must include two images: a lateral cervical spine X-ray incorporating the base of the skull and the junction of C7 and T1, and an anteroposterior cervical spine X-ray including C2 to T1. An open-mouth view of the odontoid process is advised if the child can cooperate, but this is often difficult in young children. If the radiographs obtained are suboptimal, CT scanning with multiplanar reformatting may be required (Fig. 2.115). CT scanning of the cervical spine should be considered in any child with a head injury who

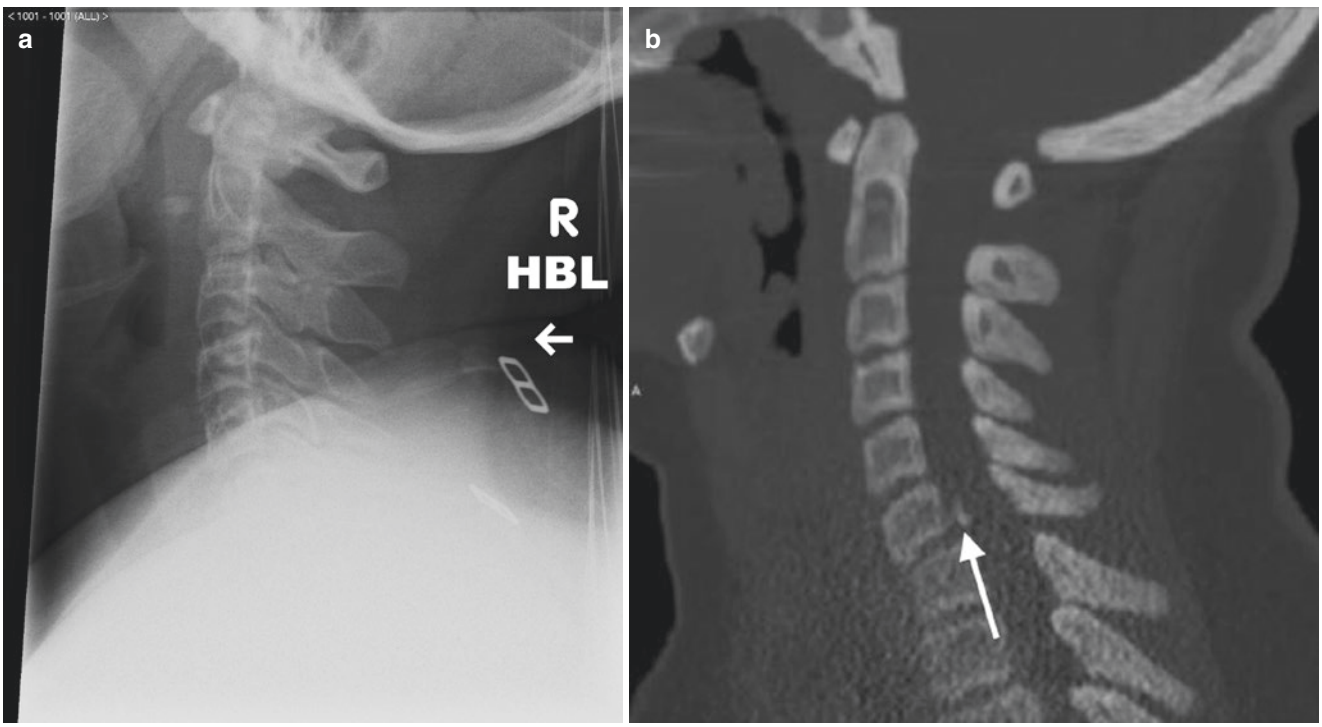

Fig. 2.115 (**a**) Inadequate lateral cervical spine radiograph, in which the cervical spine is visualised only down to the C5 vertebra. (**b**) Sagittal reformatted CT image in the same patient reveals a fracture through the posterior vertebral body of C6, with facet subluxation. This injury cannot be identified on the suboptimal lateral radiograph

has risk factors for a cervical spine injury, such as low Glasgow Coma Scale or focal peripheral neurology.

2.3.6.1 Atlanto-axial Ligamentous Injury

The atlantal transverse ligament extends between the tubercles of the lateral masses of C1 (atlas) and supports the posterior odontoid process of C2 (axis). Traumatic atlanto-axial subluxation or dislocation usually results from a hyperflexion neck injury, causing disruption of the ligament. The injury may be associated with a fracture of the odontoid process (also known as the dens) or a Jefferson burst fracture. Disruption of the ligament results in anterior displacement of C1 on C2. Posterior displacement is extremely rare.

On a lateral cervical spine radiograph, atlanto-axial subluxation or dislocation is diagnosed when there is widening of the atlantodental interval (ADI) of more than 5 mm. The ADI is measured between the anterior cortex of the odontoid (dens) and the posterior cortex of the anterior arch of C1. It measures 5 mm or less in normal healthy children. The injury also interrupts the smooth lordotic curve of the spinolaminar line, which is a line drawn along the anterior part of the spinous processes of the cervical spine and denotes the posterior margin of the spinal canal. Prevertebral soft tissue swelling may be evident (Fig. 2.116). The anterior movement of the C1 vertebra reduces the anterior-posterior (AP) diameter of the spinal canal. Spinal cord injury may occur if the cord is compressed between the odontoid process and the posterior arch of C1. This is appreciated on MR scanning (Fig. 2.117).

Conditions such as rheumatoid arthritis, Morquio syndrome, and Down syndrome may be associated with vertebral anomalies and ligamentous laxity. Consequently, affected patients may be predisposed to atlanto-axial subluxation and instability. Whilst these patients are usually asymptomatic, they are at increased risk of developing neurological injury with minor neck trauma. In Grisel syndrome, a non-traumatic cause of atlanto-axial subluxation, inflammation of the adjacent soft tissues of the neck causes laxity of the transverse ligament.

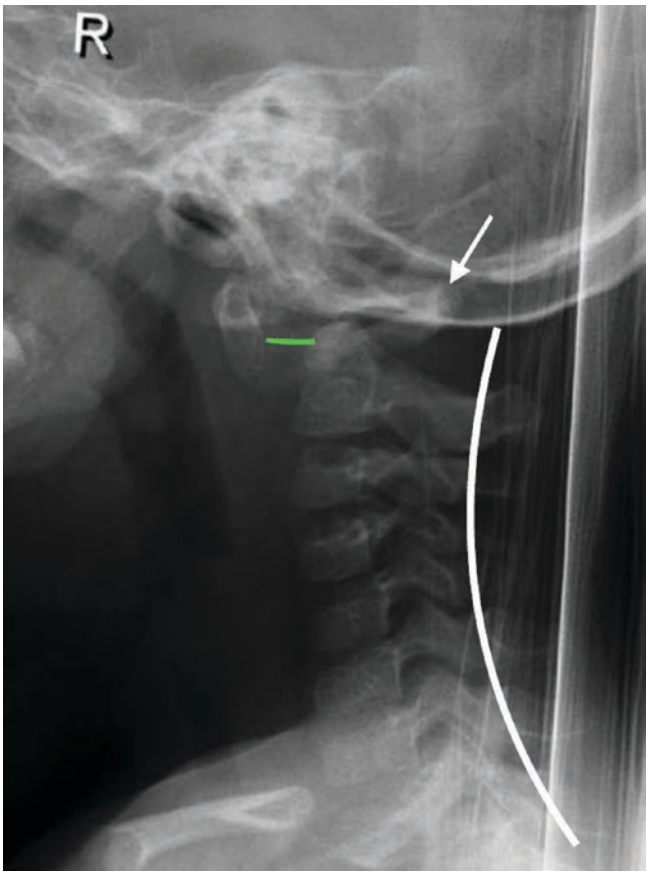

Fig. 2.116 Atlanto-axial dislocation. Lateral cervical spine radiograph demonstrates anterior movement of C1 relative to C2 and widening of the atlantodens interval (ADI, *green line*). There is interruption of the spinolaminar line (*white curve*), with the spinous process of C1 (*arrow*) lying anterior to the line. Prevertebral soft tissue swelling is present

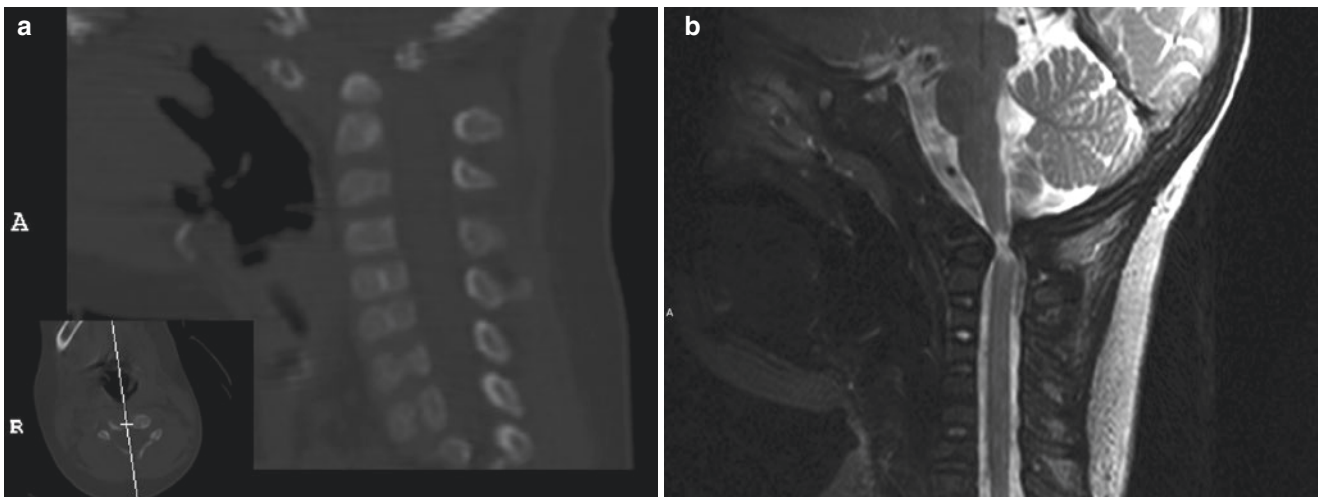

Fig. 2.117 Atlanto axial dislocation. (**a**) Sagittal reformatted image of cervical spine CT study demonstrates anterior displacement of the C1 arch with respect to the dens. The ADI is increased and the distance between the spinous processes of C1 and C2 is widened. The spinal canal diameter is compromised, owing to anterior displacement of the posterior arch of C1. (**b**) Spinal cord compression is confirmed on a T2-weighted sagittal MR image (area of increased signal within the proximal cervical cord)

2.3.6.2 Fractures of the Atlas

A Jefferson or burst fracture of the C1 ring is caused by an injury along the axis of the cervical spine, in which the occipital condyles are driven into the lateral masses of C1. Fractures usually occur through the anterior and posterior arches of C1. The fracture is manifest as asymmetry between the odontoid process and the lateral masses of C1 on the open-mouth odontoid view. These fractures are stable if the atlantal transverse ligament is intact. A distance of 6 mm or more between the lateral mass of C1 and the odontoid process is suggestive of ligamentous disruption. CT demonstrates the fracture line, which usually involves both the anterior and posterior arches. If there is injury to the atlantal transverse ligament, the ADI will be increased (>5 mm) on sagittal reconstructed images.

2.3.6.3 Odontoid Fractures

Odontoid fractures in children younger than 7 years of age occur most commonly through the cartilaginous synchondrosis (between the odontoid process and the body of C2). On lateral radiographs or sagittal reconstructions of CT images, this fracture is characterised by anterior displacement and anterior tilting of the odontoid process. There is associated prevertebral soft-tissue swelling.

2.3.6.4 Traumatic Spondylolisthesis of C2 (Hangman's Fracture)

A hangman's fracture is a fracture through both neural arches of the C2 vertebra, usually involving the pars interarticularis (the part of the lamina located between the superior and inferior articular facets). It is the result of a hyperextension injury of the cervical spine. The pars fractures may be visualised on a lateral cervical spine radiograph. Anterior subluxation of C2 on C3 due to horizontal tearing of the C2–C3 disc space, and increased distance between the spinous process tips of C1 and C2 are associated findings (Fig. 2.118). CT scanning provides more detailed evaluation of the injury (Fig. 2.119).

2.3.6.5 Subaxial Injuries (C3–C7)

Subaxial injuries are usually seen in older children and may be secondary to sports-related injuries or motor vehicle accidents. Wedge compression fractures occur with flexion and axial loading, resulting in loss of vertebral height. CT is performed to detect any retropulsed bone fragment. MRI may be required to define any associated ligamentous disruption or spinal cord contusion.

Bilateral facet dislocation is an unstable injury, often associated with spinal cord trauma. Radiographs show displacement of adjacent vertebrae and dislocation of facet

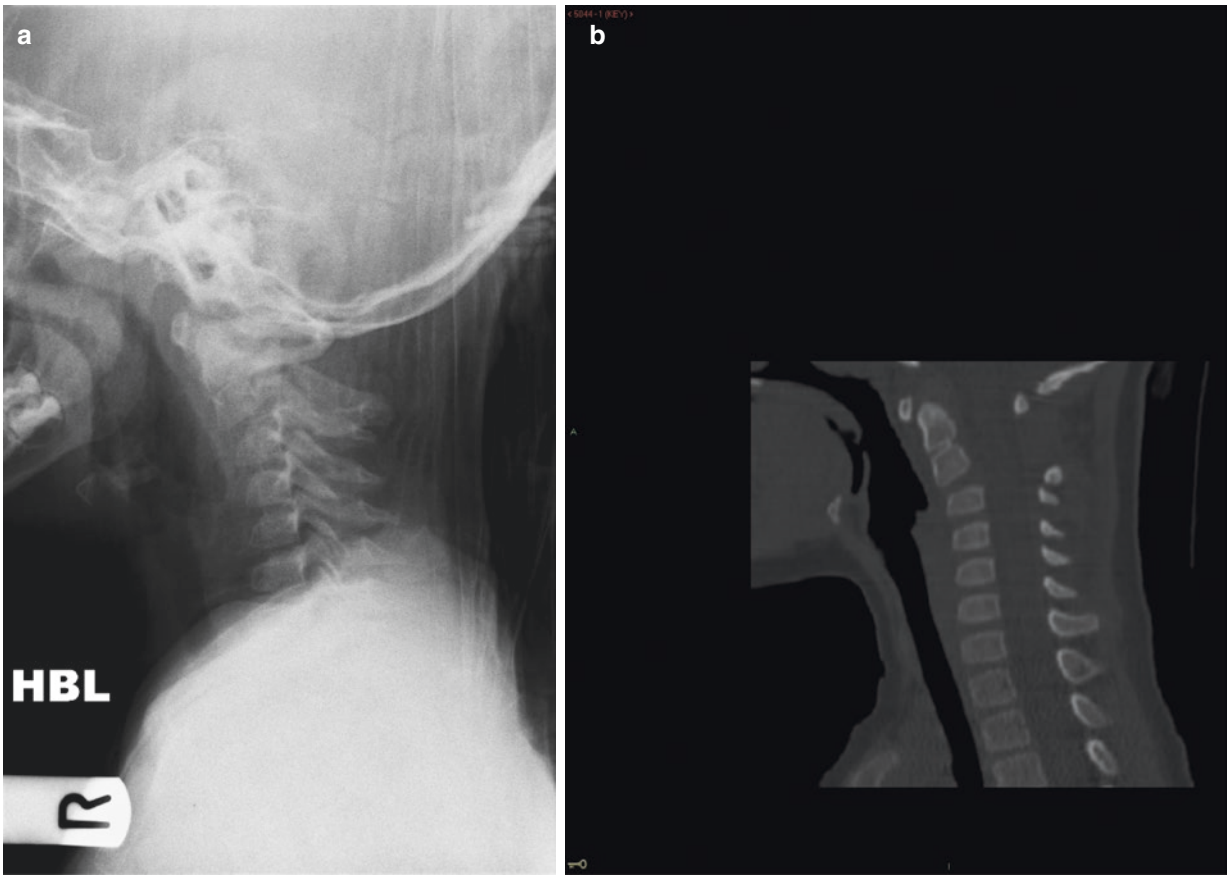

Fig. 2.118 Hangman's fracture. (**a**) Lateral cervical spine radiograph demonstrates anterior subluxation of C2 on C3, pars fracture and increased distance between the spinous processes of C1 and C2. (**b**) Sagittal reconstructed CT image shows widening of the C2–C3 intervertebral disc space due to horizontal tearing of the disc

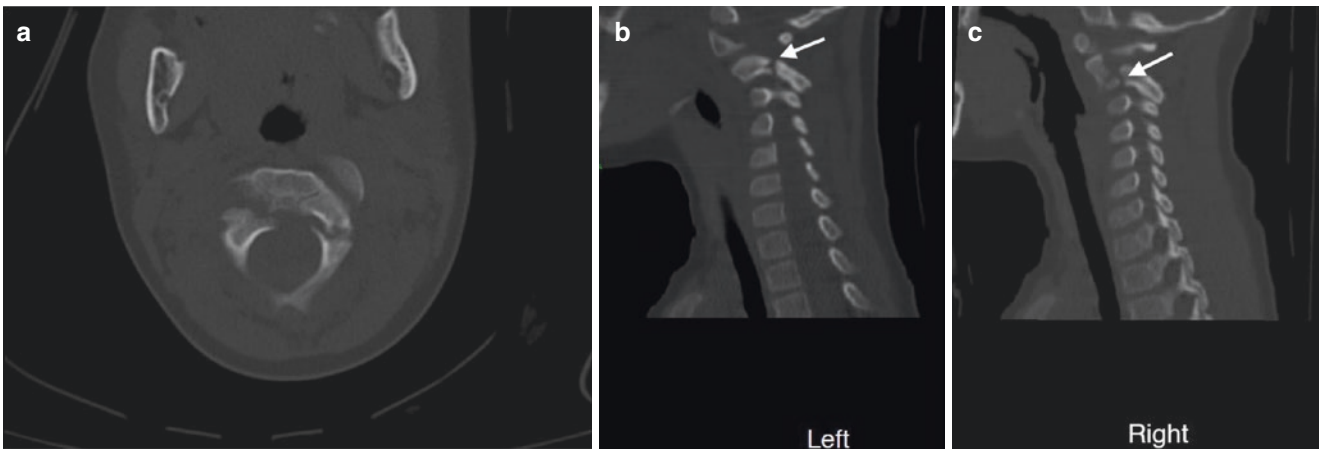

Fig. 2.119 Hangman's fracture. (**a**) Axial CT image shows a fracture through the left pars interarticularis and a fracture through the right pedicle of C2. (**b**) Left parasagittal reconstructed CT image shows the left-sided pars fracture of C2. (**c**) Right parasagittal reconstructed CT image shows the fracture of the right pedicle of C2, with the fracture line extending into the vertebral body

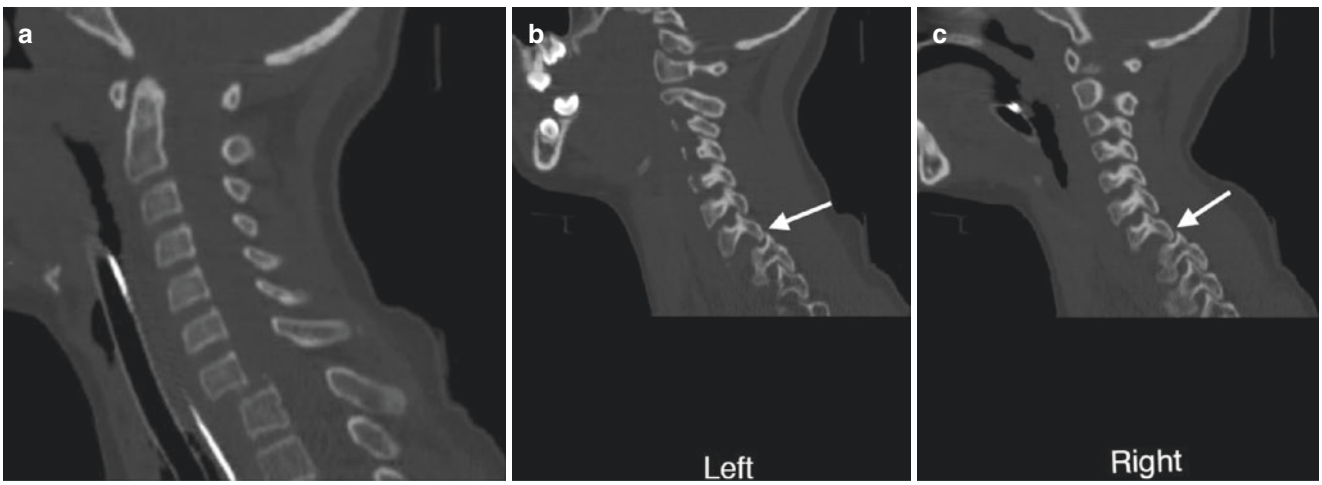

Fig. 2.120 Fracture dislocation at C7/T1. (**a**) Midline sagittal reformatted CT image of the cervical spine demonstrates a horizontal fracture through the inferior aspect of the C7 vertebral body and a further fracture through its spinous process. There is anterior displacement of C7 relative to T1. Left (**b**) and right (**c**) parasagittal reformatted CT images show that the inferior articular facets of C7 are dislocated anteriorly

joints. The facet dislocations and any associated facet fractures are well demonstrated on CT scanning (Fig. 2.120).

2.4 Tumour

2.4.1 Langerhans Cell Histiocytosis

Langerhans cell histiocytosis (LCH) is a disease characterised by idiopathic proliferation of histiocytes, producing local or systemic manifestations. The extent of the disease is variable both clinically and radiologically, ranging from self-healing lesions to life-threatening disseminated disease. The diagnosis is based on clinical and radiological findings, along with histopathological analysis of biopsy material.

LCH can affect any organ of the body. In children, those most frequently affected are the bones (80% of cases), skin (33%), and pituitary gland (25%), followed by the liver, spleen, haematopoietic system, lungs, lymph nodes, and central nervous system (excluding the pituitary). Any bone within the paediatric skeleton can be affected by LCH, but there is a predilection for flat bones, with the skull most frequently involved, followed by the mandible.

LCH lesions in the skull may present as painful areas of soft-tissue swelling. They may also be asymptomatic and noted incidentally by a parent. The lesions have a varied appearance on skull radiographs. They can be solitary or multiple and typically appear round or ovoid, with well-defined margins giving a "punched out" appearance (Figs. 2.121 and 2.122). A double-contour or bevelled-edge appearance may be seen when there is greater destruction of the inner than the outer table. Occasionally the bony lesions may enlarge, increase in number, and coalesce to form what is referred to as the "geographical skull." LCH skull lesions may be associated with an extracranial soft-tissue mass. The bony lesions and any associated scalp soft-tissue swelling are better demonstrated on

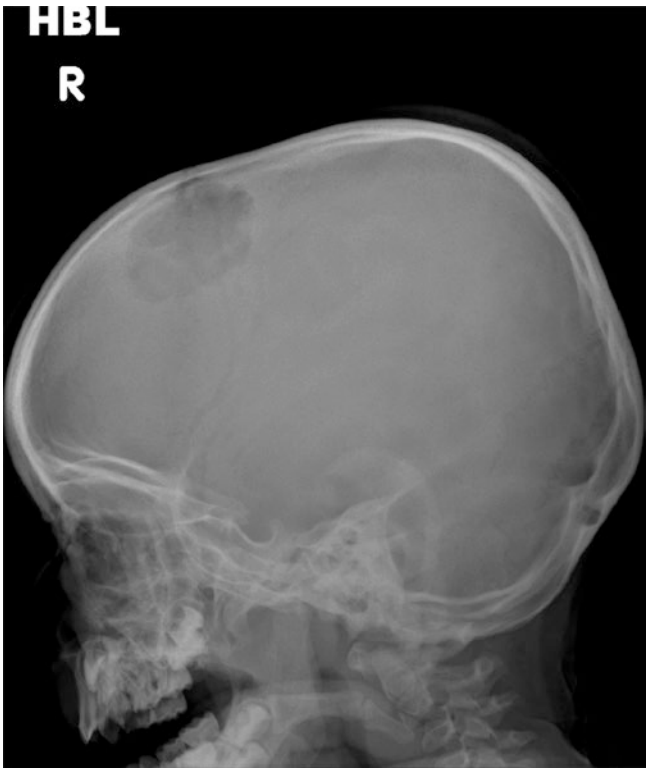

Fig. 2.121 Langerhans cell histiocytosis (LCH). Lateral skull radiograph shows a well-defined lytic lesion in the frontal region of the skull

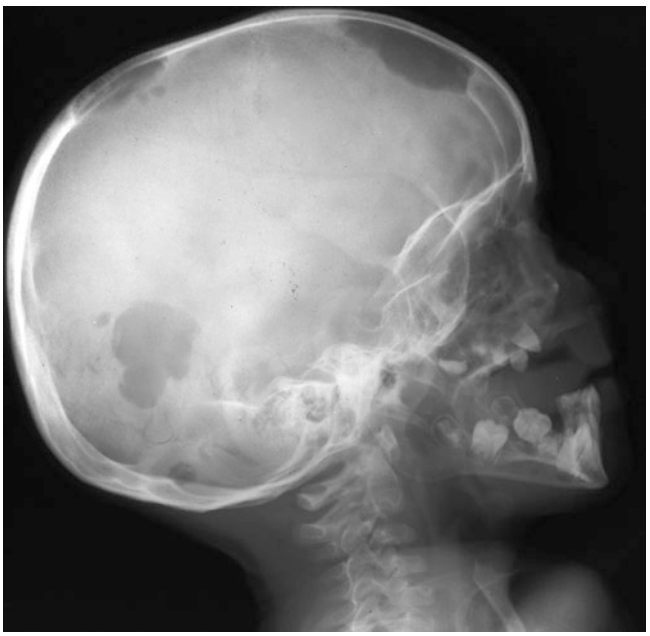

Fig. 2.122 LCH. Lateral skull radiograph shows multiple well-demarcated lytic skull lesions

CT scanning (Figs. 2.123 and 2.124). CT will also detect any associated epidural soft-tissue component (Fig. 2.125).

LCH also can affect the mandible or maxilla. Destruction of the alveolar bone around the teeth produces the radiological appearance of "floating teeth" (Fig. 2.126).

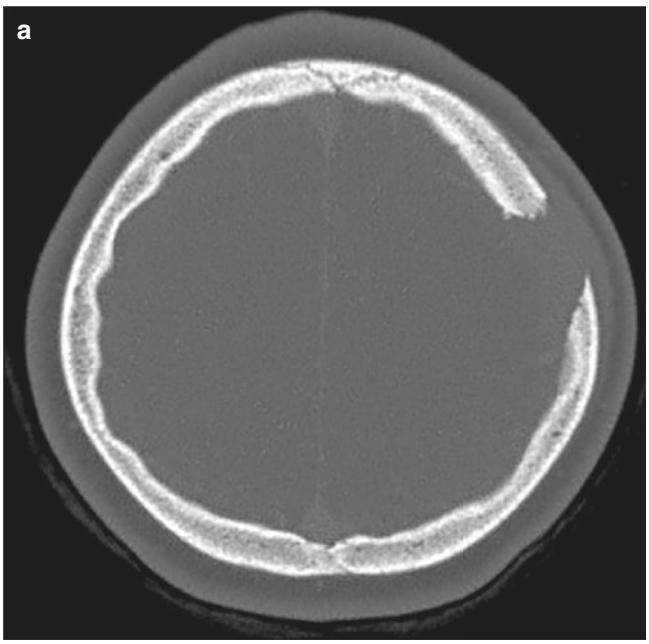

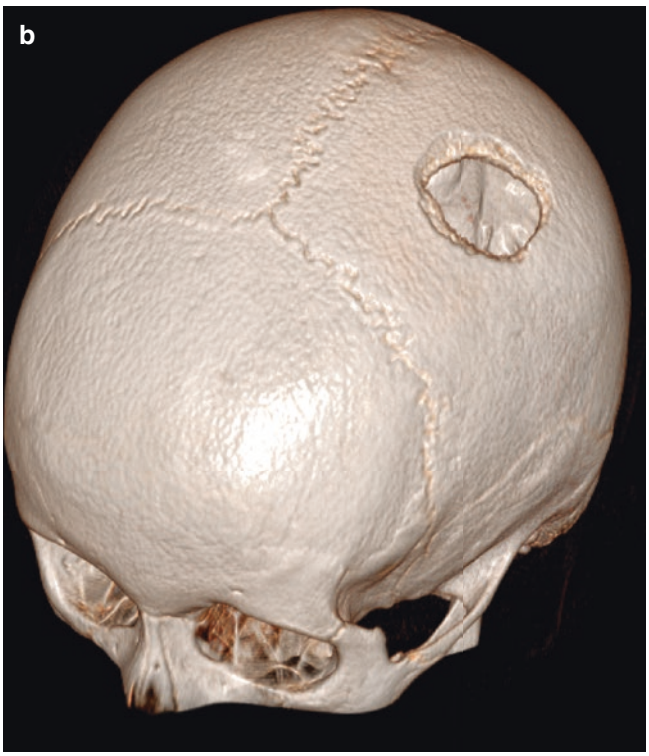

Fig. 2.123 LCH. (**a**) Axial CT image demonstrates a lytic lesion in the left parietal bone. (**b**) The greater destruction of the inner than the outer table results in the bevelled appearance of the lesion as seen on the 3D reformatted image

2.4.2 Congenital Cervical Teratoma

Teratomas are tumours containing all three germ layers (ectoderm, mesoderm, and endoderm). After the sacrum, the neck region is the second most common location for fetal and neonatal teratomas. Congenital cervical teratomas arising from the lateral neck region account for approximately

3% of teratomas in childhood and infancy. In the head and neck, teratomas also may arise from the nasopharynx and the brain.

Cervical teratomas usually develop during the second trimester of pregnancy. They are considered benign tumours and can be mature or immature. On antenatal ultrasound, a teratoma usually appears as a heterogeneous solid and cystic mass in the cervical region. It may be irregular and multiloculated. Calcification, which is present in approximately 50% of cases, is considered a pathognomonic feature. There may be associated polyhydramnios because of oesophageal obstruction.

Antenatal MRI allows better delineation of the complex tumour mass arising from the fetal neck. The tumour usually demonstrates heterogeneous signal on both T1- and T2-weighted sequences, depending on the amount of cystic,

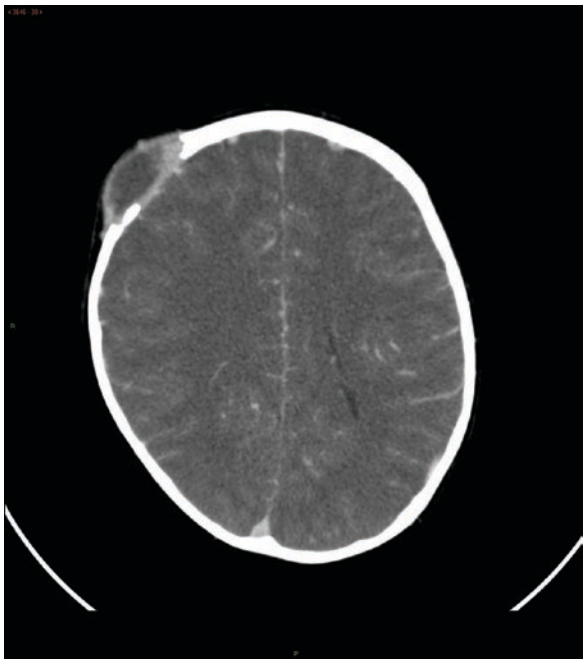

Fig. 2.124 Axial contrast-enhanced CT image demonstrates an extracranial soft-tissue mass in association with an LCH lytic bone lesion

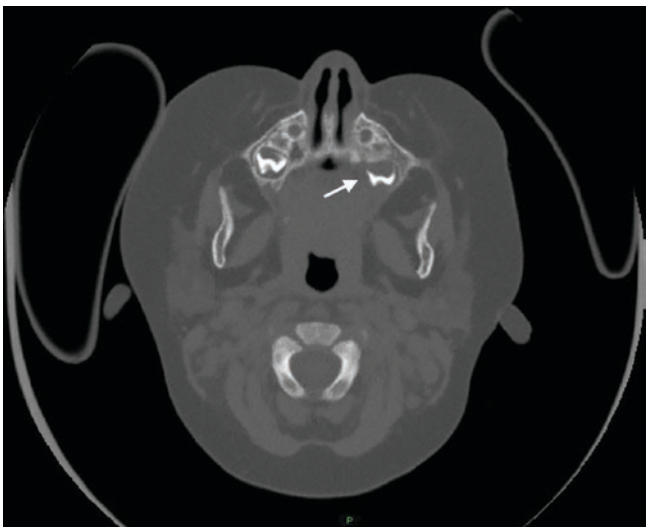

Fig. 2.126 "Floating tooth" appearance in association with LCH. Axial CT image demonstrates the loss of alveolar bone around an upper left deciduous molar tooth (*arrow*)

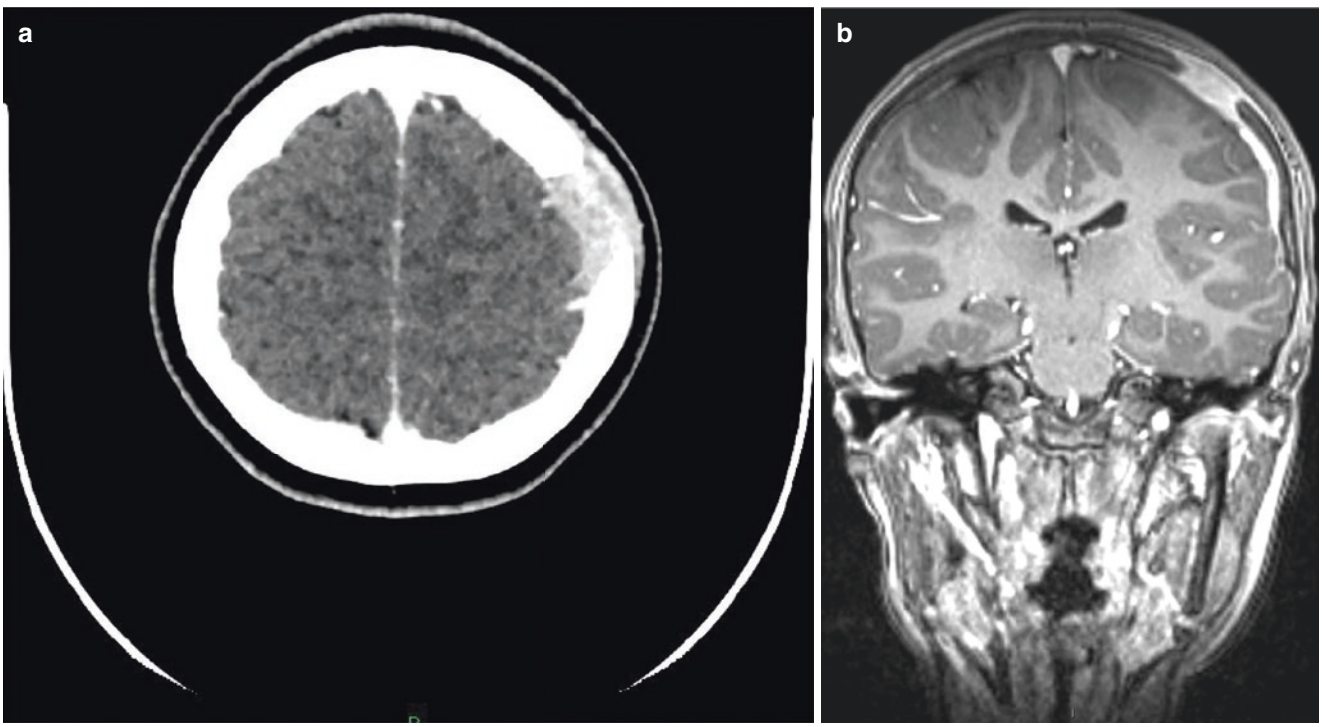

Fig. 2.125 (**a**) Axial contrast-enhanced CT image shows thickening and enhancement of the dura subjacent to an LCH bone lesion. (**b**) Coronal post-contrast T1-weighted MR image demonstrates the extent of the dural thickening and enhancement in association with the LCH lesion

solid, and fat components (Fig. 2.127). Calcification, if present, may be seen on particular sequences and is pathognomonic for teratoma. Because of their tendency to rapidly increase in size, neck teratomas can cause oesophageal and/or airway obstruction. Antenatal MR scanning is often performed to assess patency of the airway prior to delivery. Airway compromise may require the infant to be delivered by an EXIT procedure (Ex Utero Intrapartum Treatment), which preserves uteroplacental circulation whilst establishing a safe airway.

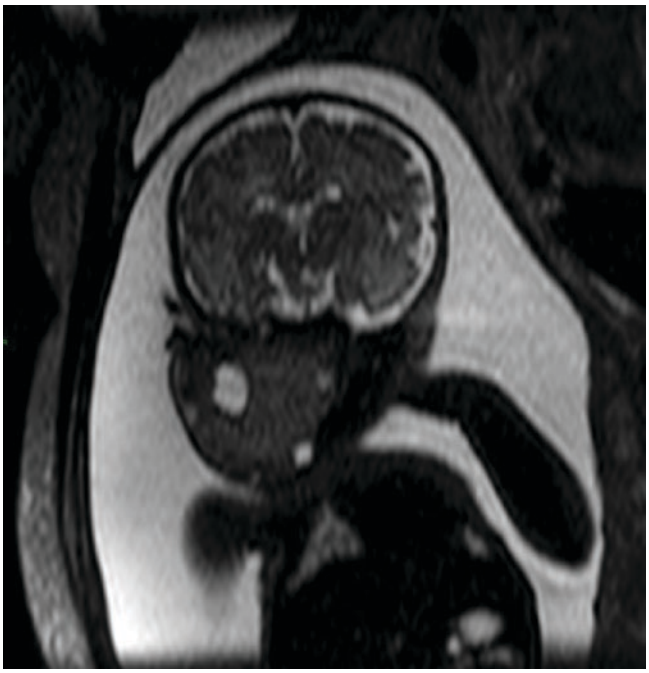

Fig. 2.127 Congenital cervical teratoma on antenatal MR study. The coronal T2-weighted image demonstrates a heterogeneous mass arising from the fetal neck

Postnatally, pre-operative delineation of the tumour extent and its relationship to neighbouring structures is important in order to achieve complete surgical resection of the mass. This is usually performed with MR imaging (Fig. 2.128).

2.4.3 Lymphoma

Lymphomas account for approximately 10–15% of all childhood cancers in developed countries and are the third most common malignancy after leukaemias and brain tumours. The aetiology of lymphoma is unknown, but potential risk factors include immunosuppression (e.g., post-transplantation) and previous chemotherapy.

Lymphomas may present as masses wherever lymph nodes are present in the body. In children and young adults, the cervical lymph nodes are the most common site of involvement in Hodgkin's lymphoma (Fig. 2.129). The cervical nodes may also be involved in non-Hodgkin's lymphoma. Enlarged cervical lymph nodes are a common manifestation of inflammatory disease in children, and at times it may be extremely difficult to decide whether enlarged cervical nodes are due to infection or to lymphoma. Clinically, reactive lymph nodes tend to be mobile, soft, and painful. Non-mobile, firm, and painless nodes are concerning for lymphoma.

Ultrasound is usually the first imaging procedure performed on a child presenting with enlarged neck lymph nodes. Various ultrasound features have been described for differentiating reactive lymphadenitis from lymphomatous nodes. Ultrasound features of lymphomatous nodes include nodal enlargement, round shape, absent or eccentric echogenic hilum, hypoechoic parenchyma, and a tendency for nodes to aggregate into a mass. Displacement of hilar vasculature and areas of absent nodal vascularity may be identified

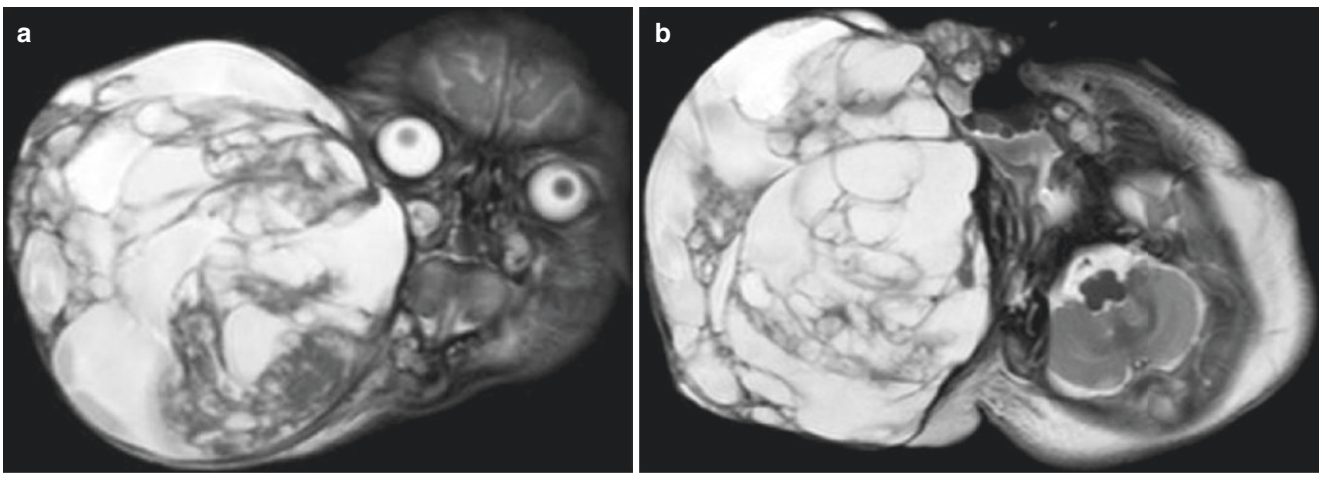

Fig. 2.128 Congenital cervicofacial teratoma on post-natal MR imaging. T2-weighted coronal (**a**) and axial (**b**) images show a complex lesion containing cystic and solid elements arising from the right side of the face and neck

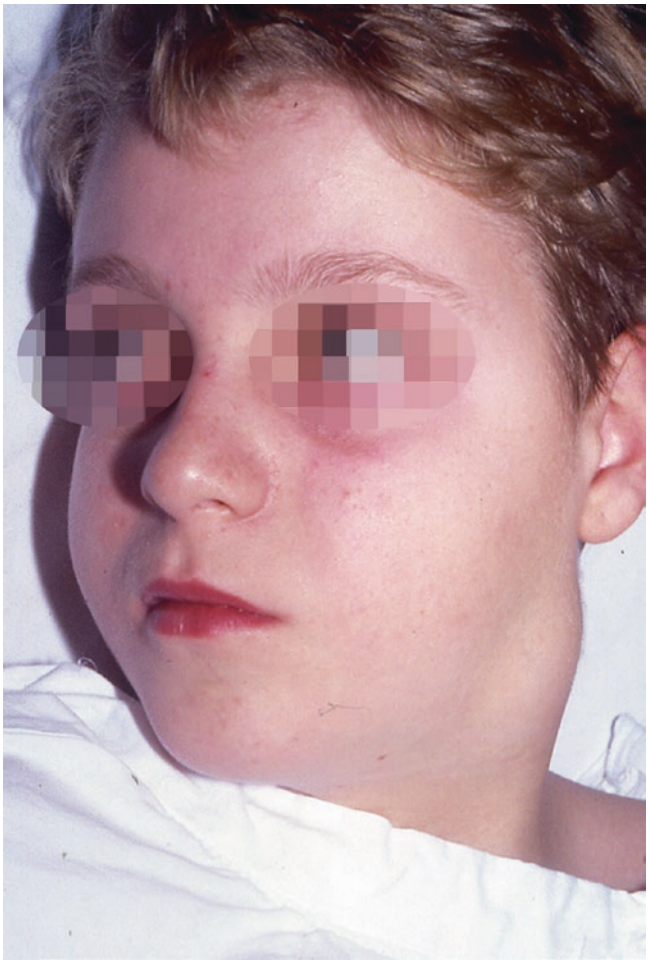

Fig. 2.129 Clinical photograph of enlarged left-sided cervical lymph nodes due to lymphoma

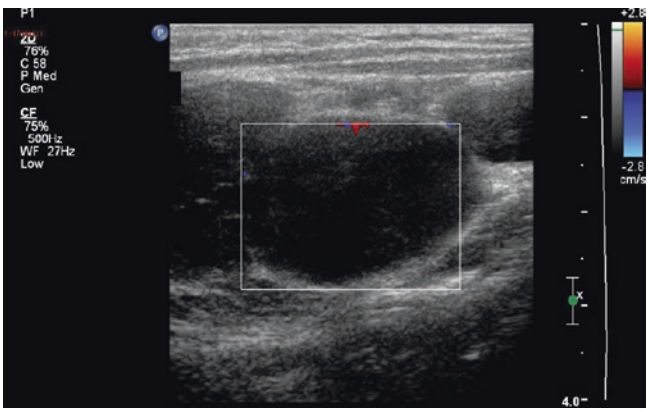

Fig. 2.130 Lymphomatous cervical node on ultrasound. The abnormal enlarged lymph node is round and hypoechoic, with loss of its central echogenic hilum and absence of normal vascularity on colour Doppler

on colour Doppler (Fig. 2.130). Some of these ultrasound features can be seen with reactive, benign lymph nodes, however, so lymph node biopsy is required to achieve a definitive histological diagnosis. Once the diagnosis of lymphoma is confirmed, the extent and sites of disease must be established to assess prognosis and plan treatment.

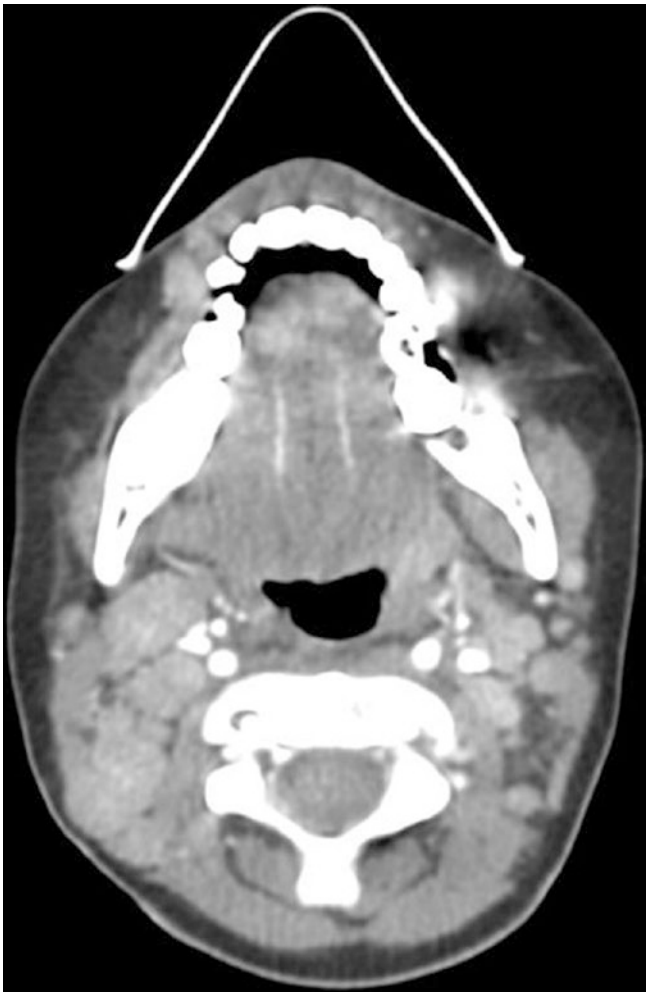

Fig. 2.131 Hodgkin's lymphoma. Axial contrast-enhanced CT image demonstrates a conglomerate lymph node mass within the right side of the neck

On CT scanning, lymphomatous neck nodes may be discretely enlarged or appear as a large soft-tissue mass due to nodal aggregation (Fig. 2.131). The nodes enhance with intravenous contrast. Central low attenuation (low density) within affected nodes implies intra-nodal necrosis. On MR imaging, affected lymph nodes show low to intermediate signal intensity on T1-weighted imaging and intermediate to high signal intensity on T2-weighted imaging (Fig. 2.132). Because of their high cellularity, lymphomatous lesions restrict water diffusion and appear hypointense (dark) on an apparent diffusion coefficient (ADC) map obtained with diffusion-weighted MR imaging (Fig. 2.133).

The use of positron emission tomography co-registered with CT (PET-CT) is now established in the assessment of paediatric Hodgkin's lymphoma. The tracer used is ^{18}F-labelled fluoro-2-deoxyglucose (^{18}F-FDG). Lymphomatous lesions demonstrate strong (avid) ^{18}F-FDG uptake (Fig. 2.134).

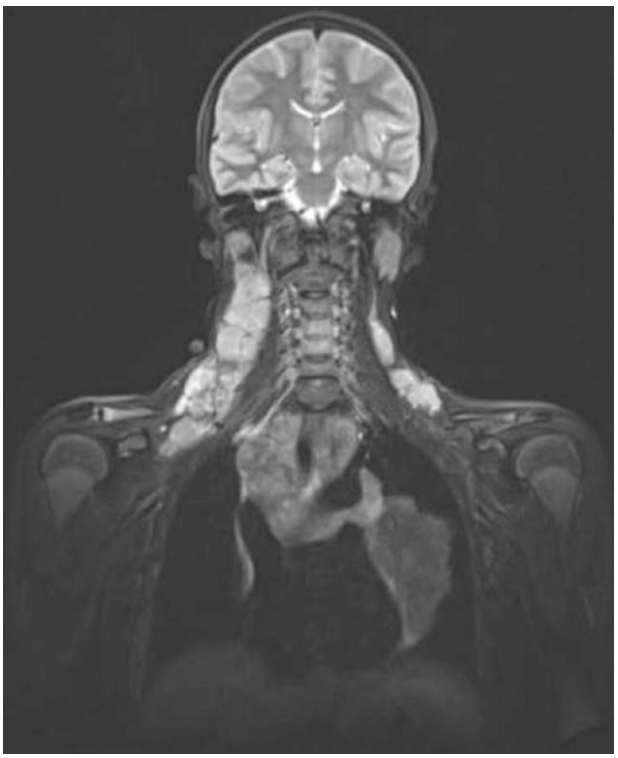

Fig. 2.132 Hodgkin's lymphoma. Coronal T2 STIR MR image shows enlarged intermediate- to high-signal cervical lymph nodes bilaterally, along with extensive mediastinal disease

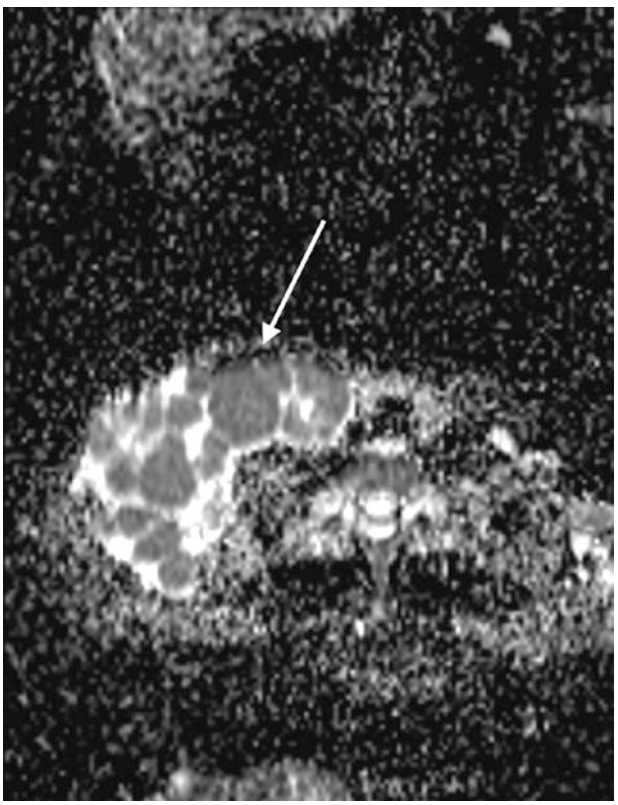

Fig. 2.133 Apparent diffusion coefficient (ADC) map from diffusion-weighted MR imaging shows hypointense (dark) signal in right-sided cervical lymphomatous nodes

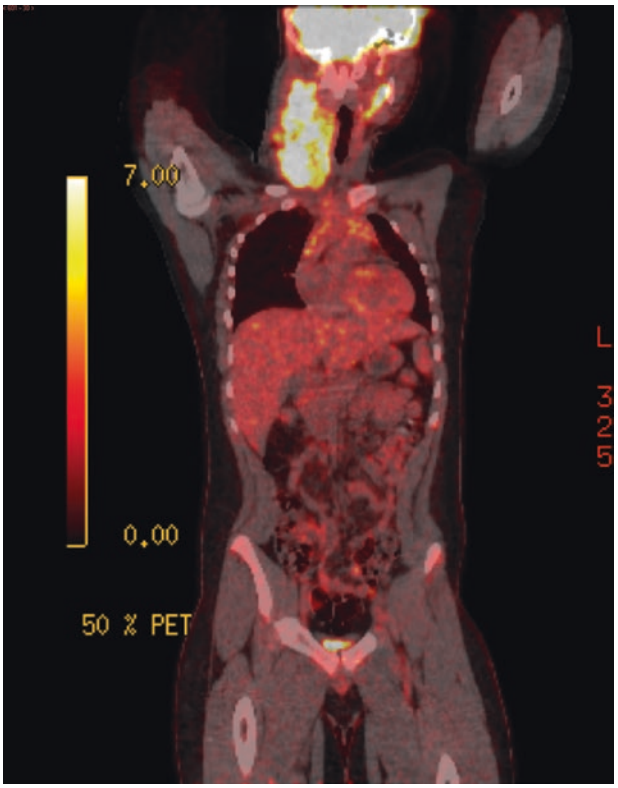

Fig. 2.134 Lymphoma. Coronal PET-CT image shows avid uptake of ^{18}F-FDG in the right cervical lymph nodes and a smaller area of uptake in the left cervical chain

2.4.4 Brain Tumours

Childhood brain tumours are the second most common paediatric malignancy after leukaemia. CT is the imaging modality most often used in the diagnosis of paediatric intracranial neoplasms, as patients often present acutely with concerning symptoms of raised intracranial pressure. MRI, with its multiplanar imaging capability, is the modality of choice for determining the exact extent of the tumour and its relationship to surrounding structures. It is therefore used in the staging of tumours. Spinal MR scanning is often performed at the same time to assess for disease spread ("drop metastases").

2.4.4.1 Infratentorial Tumours

The posterior cranial fossa is a common location for paediatric brain tumours. Posterior fossa tumours include medulloblastoma, astrocytoma, ependymoma, and brain stem glioma. Patients often present with clinical signs of hydrocephalus and raised intracranial pressure. The most common symptoms include headache, nausea, and vomiting.

2.4.4.1.1 Medulloblastoma

Medulloblastoma is the most common malignant posterior fossa tumour encountered in children in most series. Due to the rapid growth and malignant features of the tumour,

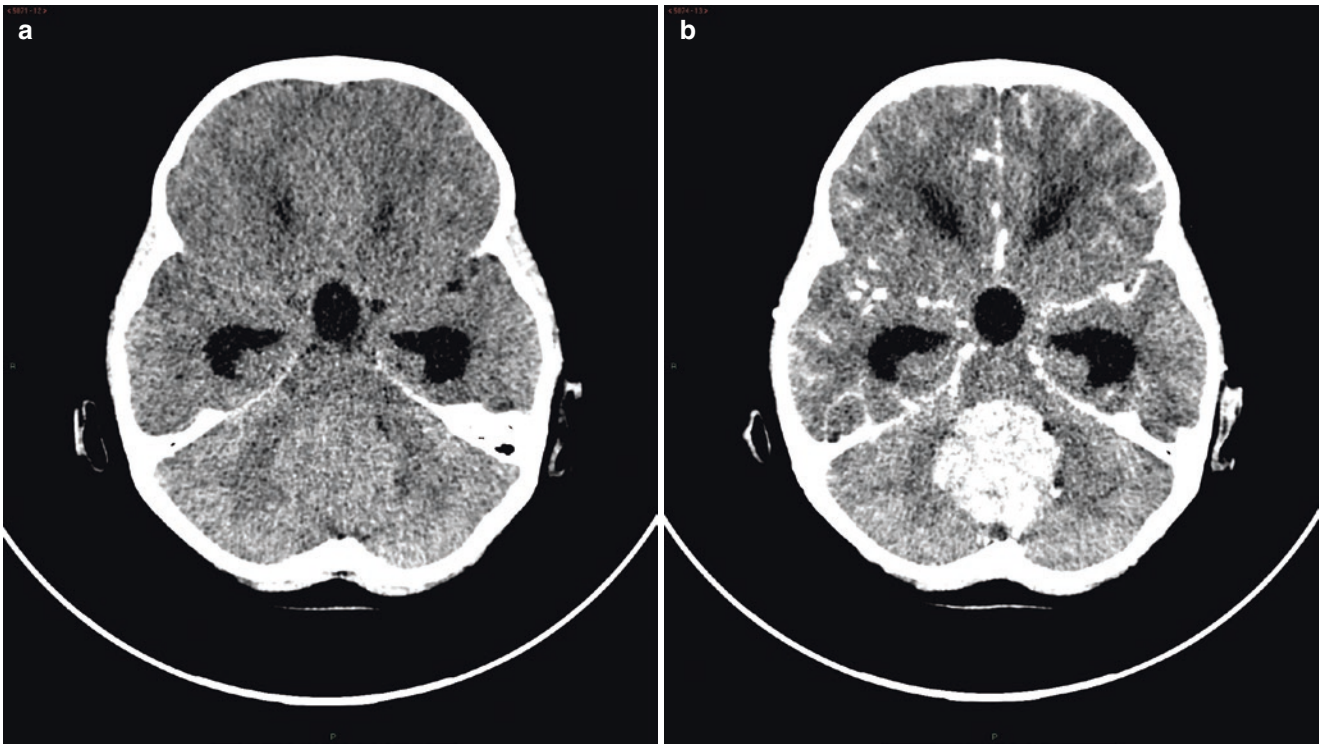

Fig. 2.135 Medulloblastoma. (**a**) Axial CT image reveals a dense midline mass within the cerebellar vermis, compressing the fourth ventricle and causing hydrocephalus. (**b**) The mass enhances diffusely following contrast administration

patients usually present with a short duration of rapidly developing symptoms, most commonly nausea, vomiting, and headache due to obstructive hydrocephalus. Truncal ataxia and papilloedema are common clinical signs.

The tumour is usually located in the cerebellar vermis. Anteriorly, it can impinge on the fourth ventricle, causing partial or complete obstruction of CSF flow. The tumour can extend posteriorly into the cisterna magna and down into the upper spinal canal. It may also extend laterally through the foramen of Luschka into the cerebellopontine angle cistern. Leptomeningeal spread via CSF pathways can result in intracranial tumour spread. Drop metastases to the spinal subarachnoid space and cauda equina are present in approximately 40% of cases at presentation, so spinal MR imaging is required.

On unenhanced CT, a typical medulloblastoma appears as a well-defined, hyperdense midline lesion within the cerebellar vermis (Fig. 2.135). Perilesional oedema is often present, as well as hydrocephalus due to mass effect on the fourth ventricle. With contrast administration, the tumour usually enhances diffusely, although patchy enhancement may occasionally occur.

The MRI appearance of medulloblastoma can vary. The most common appearance on T1-weighted imaging is that of a hypointense lesion (compared with the surrounding brain) within the cerebellar vermis. On T2-weighted images, the lesion can be hypointense or isointense and cystic components may be present, which are seen as hyperintense areas. Tumour enhancement may be uniform or patchy following gadolinium administration (Fig. 2.136). Leptomeningeal disease spread is identified as enhancing nodules on the surface of the brain. Spinal leptomeningeal spread or drop metastases appear as enhancing foci along the surface of the spinal cord and the cauda equina (Fig. 2.137).

2.4.4.1.2 Cerebellar Astrocytoma

Most cerebellar astrocytomas in children are of a specific histological type known as juvenile pilocytic astrocytoma, which is a low-grade tumour. The tumours can arise from the cerebellar vermis or the cerebellar hemisphere. Patients usually present with symptoms of raised intracranial pressure. Cerebellar signs may be present. Cerebellar astrocytomas can be cystic, solid, or solid with a necrotic centre. Approximately 50% of paediatric cerebellar astrocytomas are cystic with a mural nodule attached to the cyst wall.

The typical appearance of a cerebellar astrocytoma on CT is that of a large vermian or hemispheric tumour that is predominantly cystic. The solid part of the tumour is usually isodense to hypodense (compared with adjacent brain) on unenhanced scans. Contrast enhancement is often heterogeneous. When the tumour is cystic with a mural nodule, the cyst is round or oval and the nodule is round, ovoid, or plaque-like. The nodule demonstrates intense contrast enhancement (Fig. 2.138).

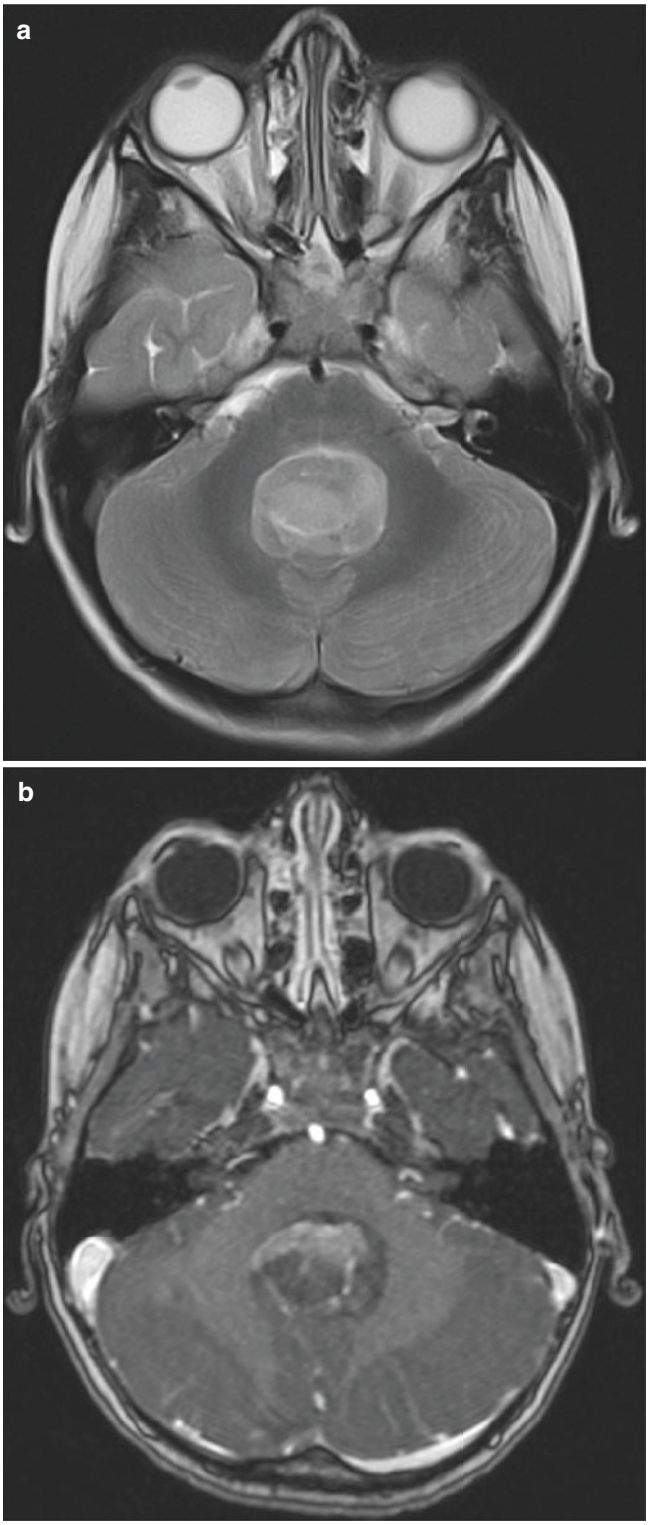

Fig. 2.136 Medulloblastoma. (**a**) Axial T2-weighted MR image shows a lesion of intermediate signal intensity in the cerebellar vermis, compressing the fourth ventricle. (**b**) Axial post-contrast T1-weighted image shows inhomogeneous contrast enhancement within the mass

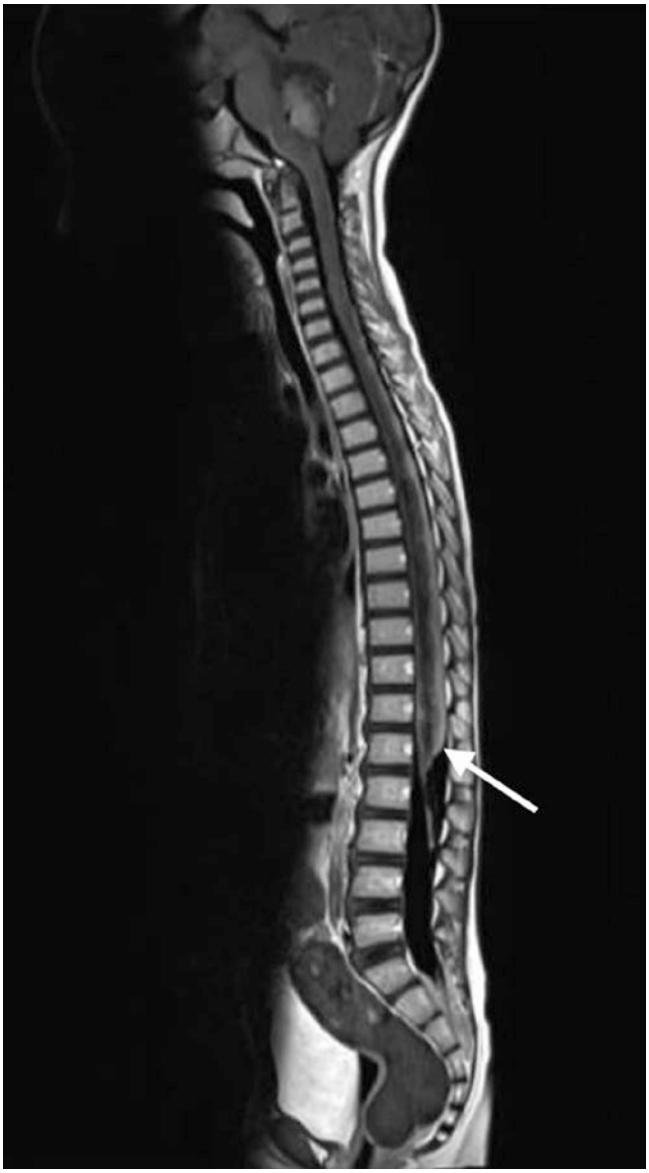

Fig. 2.137 Metastatic medulloblastoma. Sagittal post-contrast T1-weighted MR image demonstrates thick, irregular contrast enhancement along the surface of the spinal cord, consistent with spinal metastatic disease

The MR appearance of cerebellar astrocytomas is variable. Solid and cystic elements are identified, as on CT. In general, solid components appear as low signal intensity masses on T1-weighted images and as high signal intensity lesions on T2-weighted imaging. The cystic component is usually of higher signal intensity than the solid component on T2-weighted sequences. Any solid or mural components will enhance with gadolinium (Fig. 2.139).

2.4.4.1.3 Infratentorial Ependymoma

Infratentorial ependymomas develop from the floor or roof of the fourth ventricle and grow into the ventricular lumen. They tend to spread beyond the ventricle by extending through the foramina of Luschka and Magendie. Leptomeningeal spread is less common at presentation than

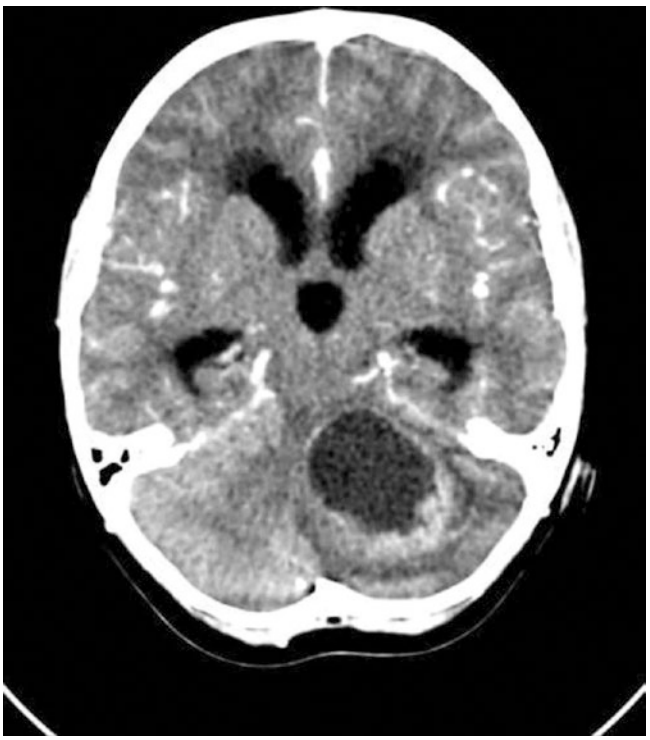

Fig. 2.138 Cerebellar pilocytic astrocytoma. Axial contrast-enhanced CT image shows a well-defined cystic lesion in the left cerebellar hemisphere with an enhancing mural plaque. The tumour compresses the fourth ventricle, causing hydrocephalus

with medulloblastoma. Patients usually present with symptoms of raised intracranial pressure and ataxia.

On CT scanning, an ependymoma appears as an isodense to hyperdense fourth ventricular mass. Punctate calcification is present in up to 50% of cases (Fig. 2.140). Small cysts may also be seen. The tumour enhances heterogeneously with intravenous contrast.

On MRI, ependymomas appear slightly hypointense relative to brain on T1-weighted imaging. T2-weighted images show a mass that is usually isointense to grey matter. Foci of T2 hyperintensity (due to cysts or necrosis) or hypointensity (due to calcification or haemorrhage) may be evident. The lesion enhances heterogeneously with gadolinium. The tumour may extend through the foramen of Magendie and the foramen magnum into the subarachnoid space behind the proximal cervical cord. Extension of the tumour through the foramen of Luschka into the cerebellopontine angle cistern is also a characteristic feature of ependymomas (Fig. 2.141). Drop metastases may be present on spinal MRI.

2.4.4.1.4 Brain Stem Gliomas

Brain stem gliomas classically present with cranial nerve palsies and ataxia. They are broadly categorised as either diffuse or focal. Diffuse pontine gliomas are poorly circumscribed, large lesions that have an extremely poor prognosis. Smaller, focal lesions have a better prognosis.

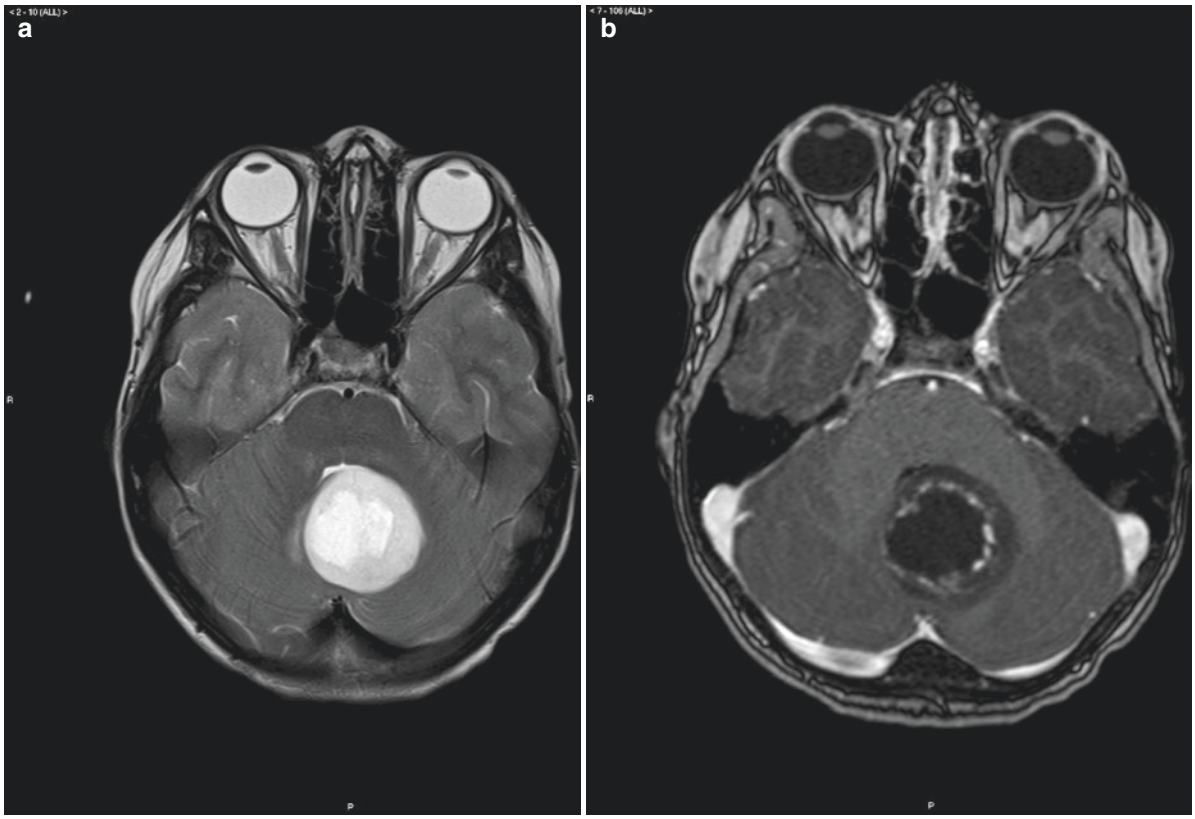

Fig. 2.139 Pilocytic astrocytoma of cerebellar vermis. (**a**) Axial T2-weighted MR image shows a well-defined high-signal mass in the cerebellar vermis, with a hyperintense cystic centre. The fourth ventricle is partially compressed. (**b**) Axial post-contrast T1-weighted MR image demonstrates contrast enhancement around the periphery of the cystic component

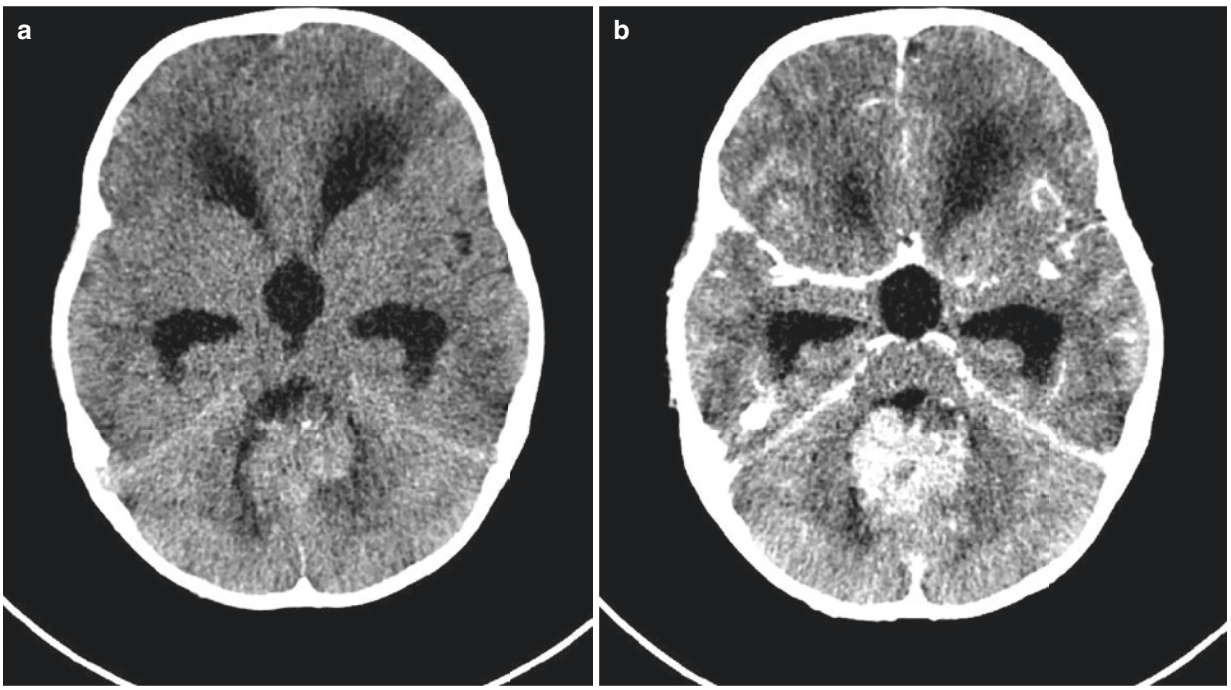

Fig. 2.140 Ependymoma. (**a**) Axial CT image shows a dense mass arising from the fourth ventricle, containing a tiny fleck of calcification. There is hydrocephalus involving the lateral and third ventricles. (**b**) The tumour enhances following contrast administration

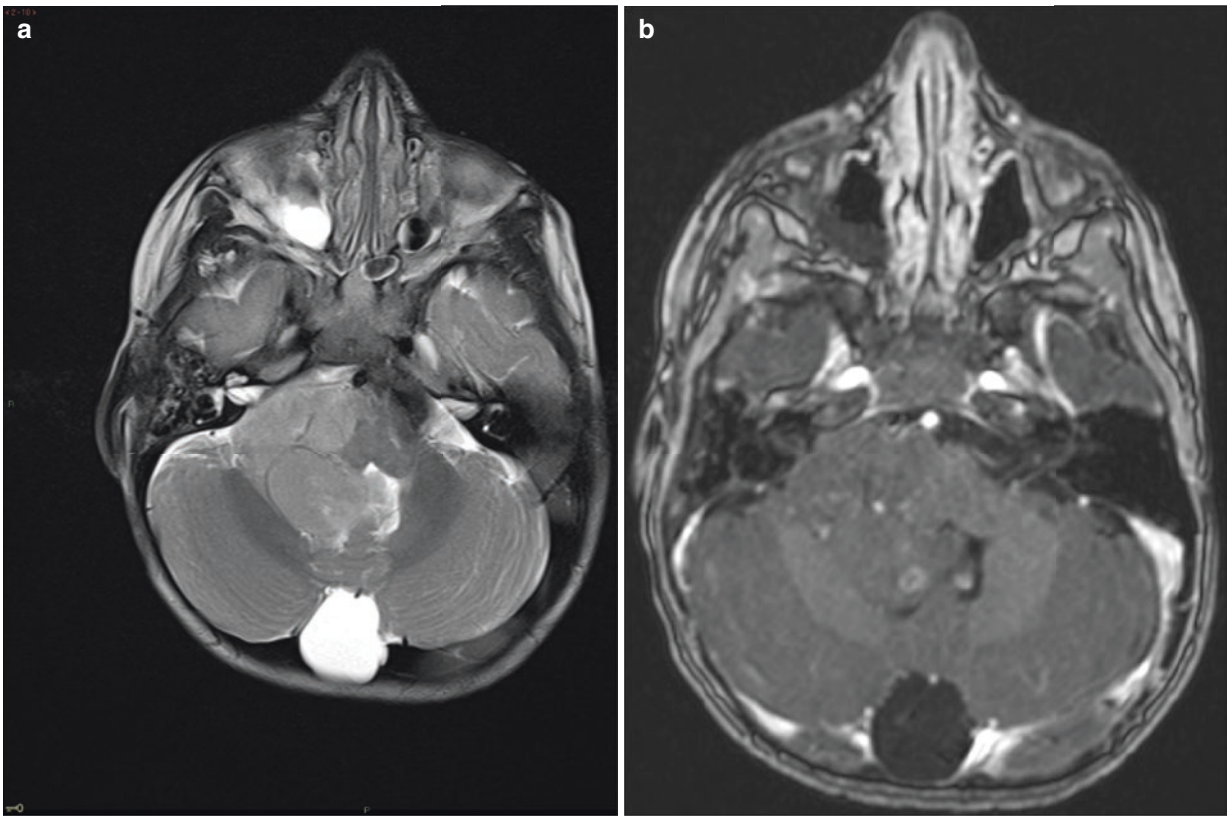

Fig. 2.141 Ependymoma with extension through the foramen of Luschka. (**a**) Axial T2-weighted MR image shows an isointense mass arising from the fourth ventricle and extending through the right foramen of Luschka to fill the right cerebellopontine angle. (**b**) Axial post-contrast T1-weighted MR image shows that the mass is poorly enhancing

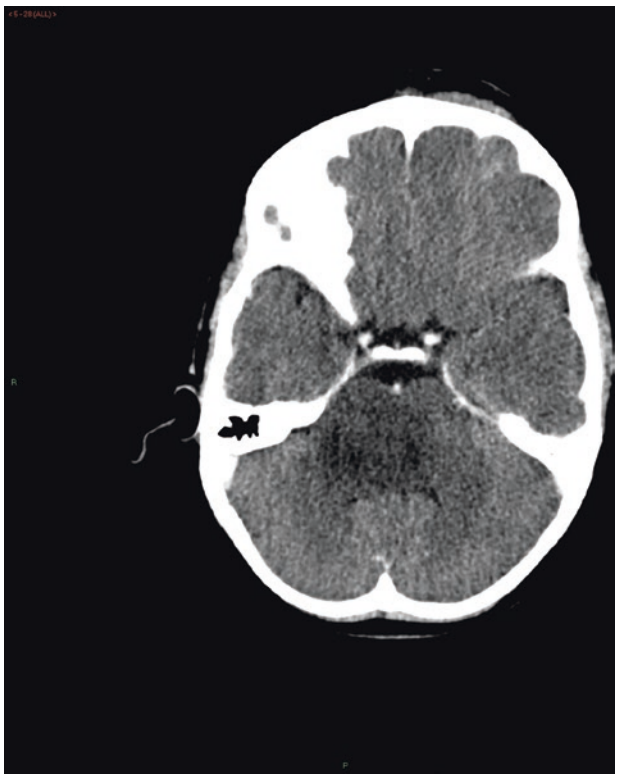

Fig. 2.142 Diffuse pontine glioma. Axial contrast-enhanced CT image shows a low-attenuation lesion expanding the pons. The enhancing basilar artery lies anterior to the swollen pons. The fourth ventricle is effaced

With its multiplanar capacity and the lack of artefact from the bony structures of the skull base, MRI is the study of choice when imaging brain stem tumours. If CT is performed, a diffuse pontine glioma will appear as a hypodense lesion that diffusely expands the pons (Fig. 2.142). On MR scanning, diffuse gliomas are seen as infiltrating masses, which are hypointense on T1-weighted imaging and hyperintense on T2-weighted images (Fig. 2.143). The lesion has ill-defined boundaries. Tumour expansion causes an increase in the AP diameter of the brainstem and posterior displacement of the fourth ventricle. Anterior growth of the lesion can encase the basilar artery. The tumours generally do not enhance with contrast.

Focal pontine gliomas occupy less than 50% of the transverse area of the pons. They may be poorly or sharply marginated. If peripheral in origin, they may grow exophytically into the fourth ventricle or the cerebellopontine angle cistern. Solid components of the lesion can enhance heterogeneously.

2.4.4.2 Supratentorial Tumours

Supratentorial tumours are more common than infratentorial tumours in children less than 2 years of age and older than 10 years. A comprehensive review of paediatric supratentorial tumours is beyond the scope of this chapter, which describes a selection of the more common tumours. Young

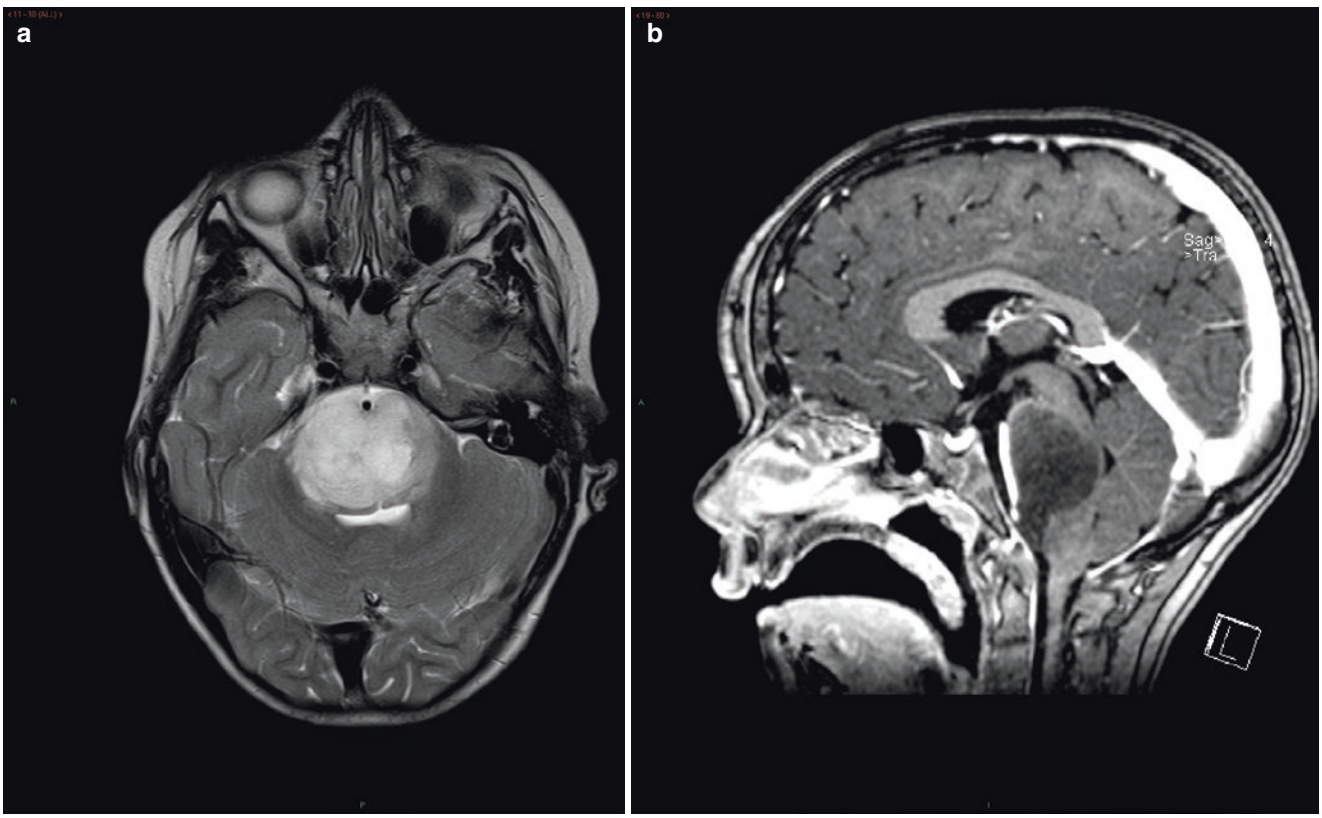

Fig. 2.143 Diffuse pontine glioma. (**a**) Axial T2-weighted MR image demonstrates a high-signal mass within the pons. (**b**) Sagittal post-contrast T1-weighted MR image shows that the tumour does not enhance with contrast

children with a supratentorial tumour may present with vomiting, lethargy, and macrocrania. Older children may present with seizures, visual disturbances, or endocrine dysfunction, depending on the site of origin of the tumour.

2.4.4.2.1 Astrocytomas

Astrocytomas, the most common cerebral hemisphere tumours of childhood, are a heterogeneous group that can vary from low-grade to high-grade. There is no characteristic location for the tumours, although they tend to develop deep within the hemispheres, usually involving the basal ganglia or thalamus. They are often large at the time of diagnosis. The presenting signs and symptoms depend on tumour location. Seizures, focal neurologic deficit, headache, and vomiting are common presenting symptoms.

Hemispheric astrocytomas have variable imaging appearances on CT and MRI. They can be solid, solid with a necrotic centre, or cystic. Although typically found deep within the hemisphere, they can occur in the central white matter or in the cortex. On unenhanced CT scans, the solid portion of the tumour tends to be isodense to hypodense relative to the adjacent brain parenchyma. Following contrast administration, the solid portion may enhance completely, partially, or not at all. On MRI, astrocytomas appear as large hemispheric lesions which are low signal compared with brain on T1-weighted imaging and high signal on T2-weighted images. Low-grade tumours tend to be homogeneous, well-circumscribed, free of haemorrhage, and associated with mild perilesional oedema. On the other hand, higher-grade tumours tend to be heterogeneous (owing to areas of necrosis or haemorrhage within the lesion), and they are associated with extensive perilesional oedema. Solid components may enhance completely, partially, or not at all (Fig. 2.144).

2.4.4.2.2 Craniopharyngioma

Craniopharyngiomas, which are relatively benign tumours, account for approximately half of tumours that arise in the sellar/suprasellar region in children. Presenting symptoms include headache, visual field defects, anterior pituitary dysfunction, and hypothalamic dysfunction. A craniopharyngioma is typically a lobulated lesion with single or multiple cysts that often encases the circle of Willis. Calcification is commonly present.

On CT scanning, a craniopharyngioma is identified as a suprasellar lesion that is usually cystic and at least partially calcified. Calcification can occur as a thin rim around a cystic component or as larger foci within the solid portion of the tumour. The solid component and cyst wall generally enhance with intravenous contrast (Fig. 2.145).

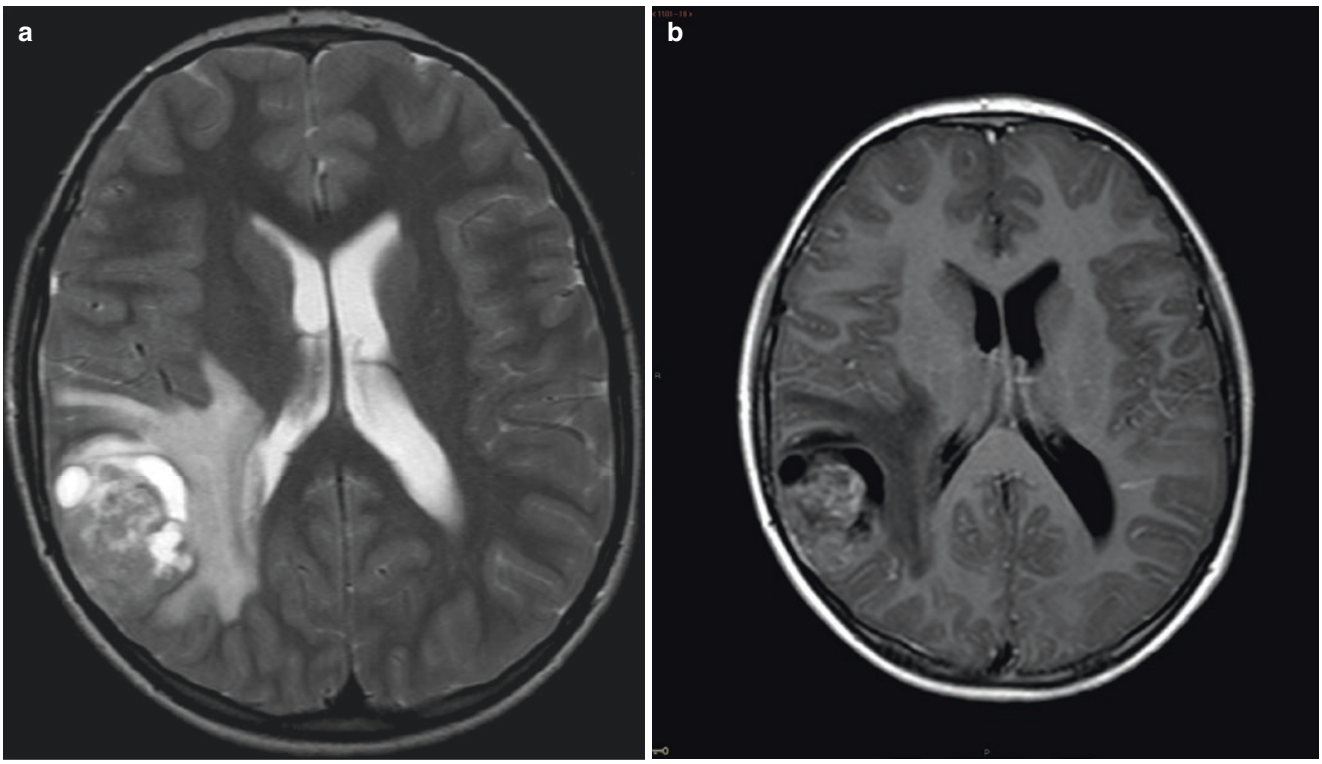

Fig. 2.144 Right parietal pleomorphic astrocytoma. (**a**) Axial T2-weighted MR image demonstrates a heterogeneous lesion in the right parietal lobe, containing solid and cystic areas. There is significant perilesional oedema. (**b**) Axial post-contrast T1-weighted MR image shows heterogeneous contrast enhancement within the solid portion of the mass

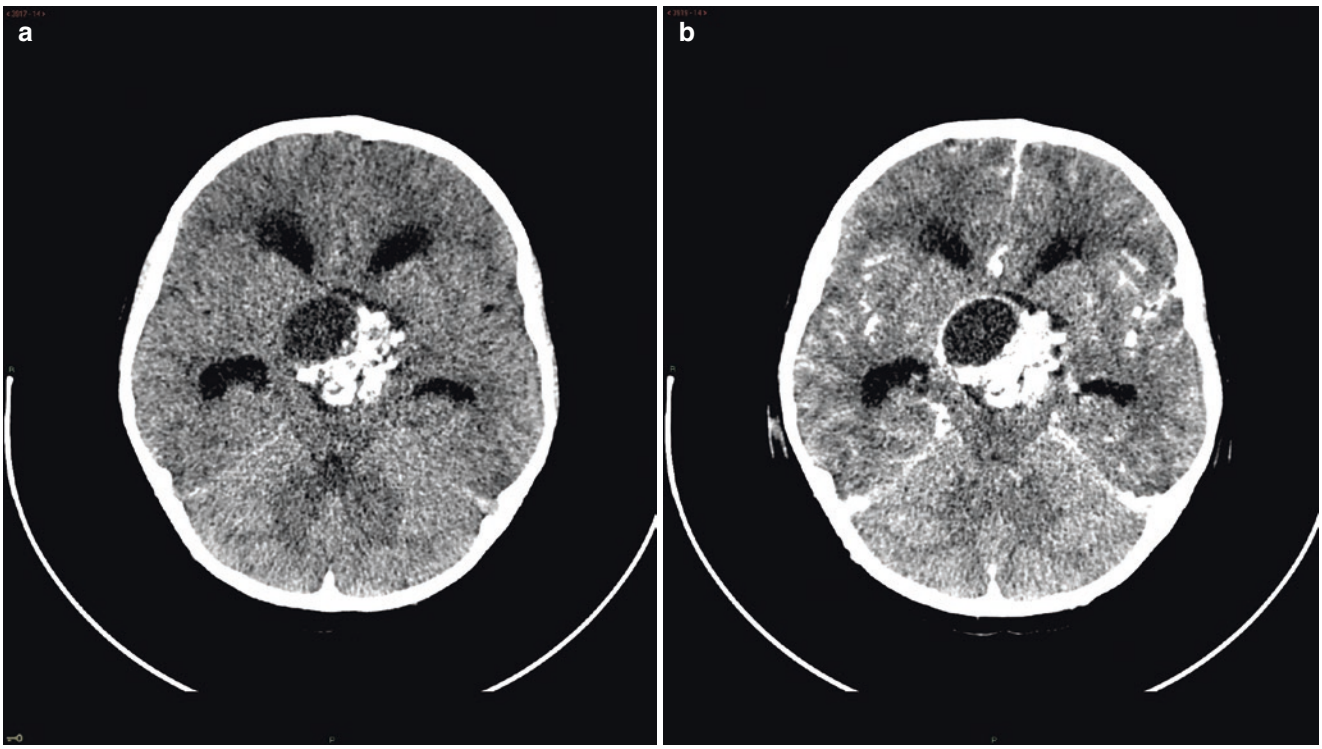

Fig. 2.145 Craniopharyngioma. (**a**) Axial CT image demonstrates a calcified and cystic lesion in the suprasellar region. There is hydrocephalus affecting the lateral ventricles. (**b**) Following contrast administration, there is rim enhancement of the cystic component

On MR imaging, craniopharyngiomas appear as multilobular, multicystic suprasellar masses. The cystic fluid signal can be variable on T1-weighted images, depending on the protein content of the fluid. The solid component can appear heterogeneous because of small cysts and calcification. The cystic and solid components are both high-signal on T2-weighted imaging, although the cystic elements tend to have higher signal intensity than the solid component. The solid portion of the tumour enhances heterogeneously with contrast. The thin cyst walls nearly always enhance (Fig. 2.146).

2.4.4.2.3 Pineal Region Tumours

Pineal region masses may compress the tectal plate and cause a defect in upward gaze known as Parinaud syndrome, or they may cause obstructive hydrocephalus if the cerebral aqueduct is compressed. Most tumours arising from the pineal gland are classified into germ cell and pineal parenchymal tumours. Germ cell tumours represent more than half of pineal tumours; of these, germinoma is the most common type. Pineal germinomas are ten times more common in males than in females.

On CT, a germinoma appears as an isodense to hyperdense, well-circumscribed mass in the pineal region that engulfs the physiological calcification within the pineal gland and enhances with contrast (Fig. 2.147). Hydrocephalus may be present. On MR imaging, the tumour is isointense to

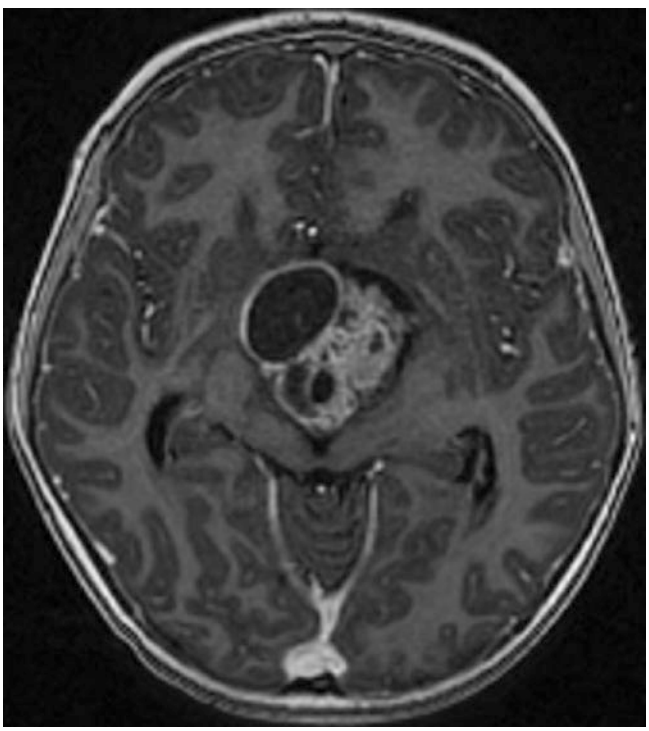

Fig. 2.146 Craniopharyngioma. Axial post-contrast T1-weighted MR image demonstrates enhancement of the solid part of the tumour and rim enhancement of the cystic components

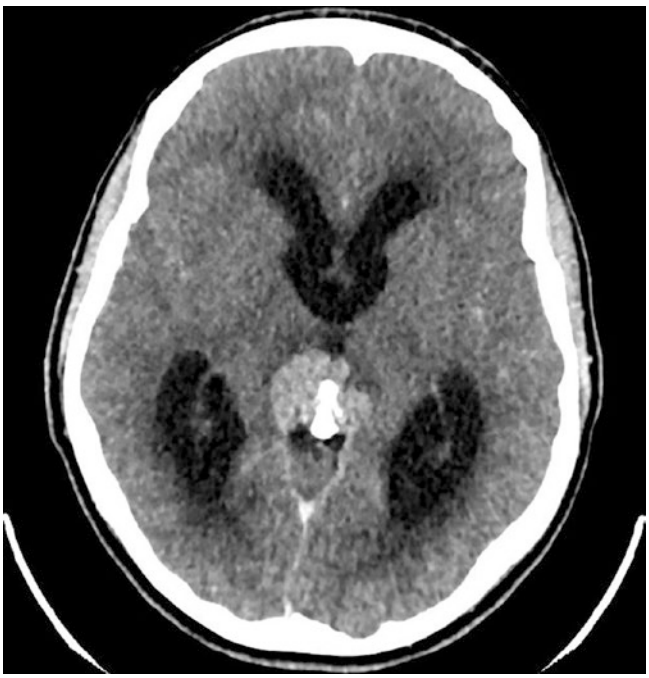

Fig. 2.147 Pineal germinoma. Axial contrast-enhanced CT image shows an enhancing lobulated mass engulfing the pineal calcification. There is hydrocephalus involving the lateral and third ventricles

hypointense relative to grey matter on T1- and T2-weighted imaging. Cystic elements may be visible. The tumour enhances intensely after contrast administration (Fig. 2.148). Spinal imaging is required because CSF seeding and spinal drop metastases can occur.

2.4.4.2.4 Choroid Plexus Tumours

Choroid plexus tumours (papillomas and carcinomas) are rare tumours arising from the epithelium of the choroid plexus. They are often found in infants and young children. The tumour cells produce CSF, resulting in hydrocephalus. The most common site of origin is the lateral ventricle.

A choroid plexus papilloma on CT scanning typically appears as a lobulated, isodense or mildly hyperdense intraventricular mass with occasional punctate foci of calcification. It is usually located in the trigone region of the lateral ventricle (Fig. 2.149). The tumour enhances homogeneously with contrast. On MRI, the tumour typically appears as a lobulated intraventricular mass that is isointense to brain on T1-weighted images and isointense to hyperintense on T2-weighted imaging. Small vascular flow voids may be seen within the tumour. Foci of haemorrhage or calcification are occasionally present. The lesion demonstrates uniform intense enhancement following contrast administration (Fig. 2.150).

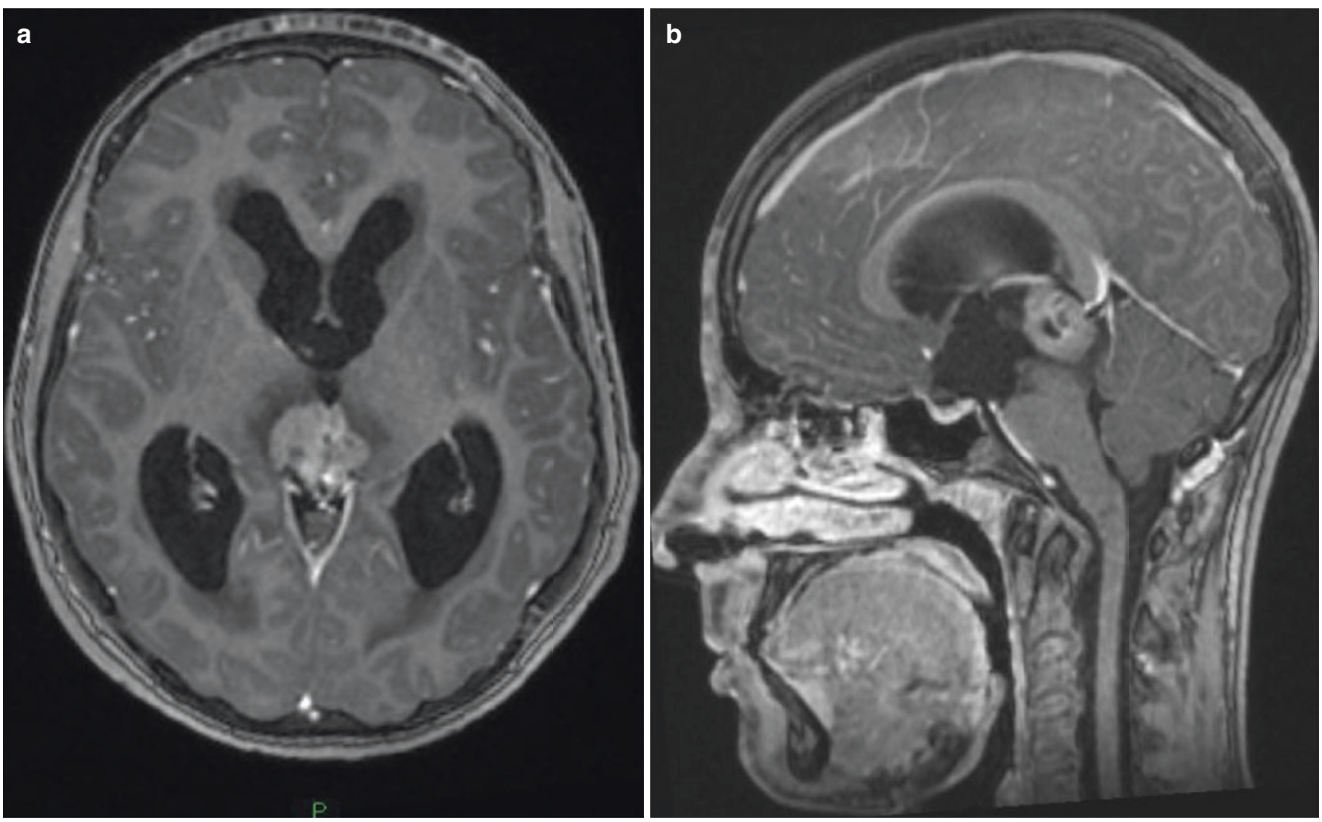

Fig. 2.148 Pineal germinoma. Axial (**a**) and sagittal (**b**) post-contrast T1-weighted MR images show an enhancing pineal gland tumour, which is compressing the cerebral aqueduct, causing hydrocephalus

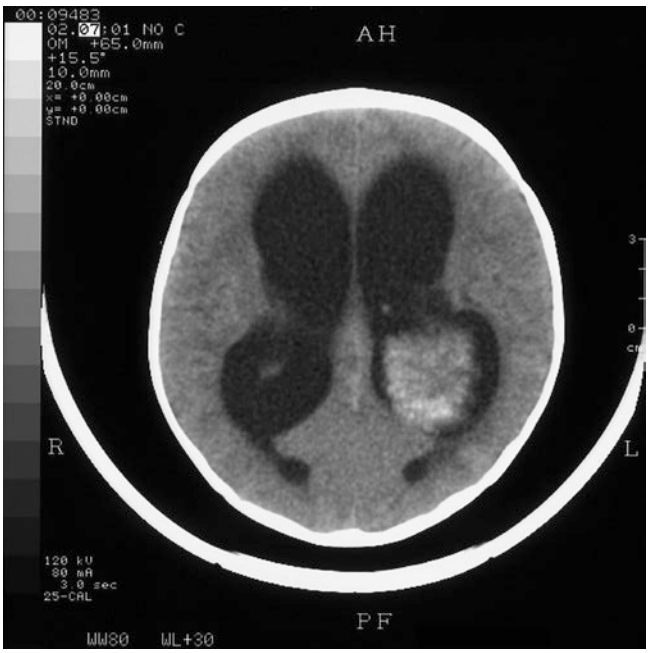

Fig. 2.149 Choroid plexus papilloma. Axial CT image shows a lobulated mass in the left lateral ventricle, with density similar to brain. Foci of calcification are present posteriorly within the mass. The ventricles are dilated

Choroid plexus carcinomas usually appear much more aggressive than papillomas on imaging studies. They are irregular in contour and heterogeneous in appearance, with a variable enhancement pattern. Cysts and haemorrhage are often present within the tumour. They nearly always grow through the ventricular wall into the adjacent brain and cause vasogenic oedema.

Choroid plexus tumours can spread via the CSF pathways, so spinal imaging is required because of the possibility of spinal metastases.

2.4.5 Orbital Sarcoma

Rhabdomyosarcomas are the most common soft tissue tumour in children. They are malignant tumours with skeletal cell morphology although they do not arise from muscle directly.

Primary orbital rhabdomyosarcomas account for approximately 25–35% of head and neck rhabdomyosarcomas and about 10% of all rhabdomyosarcomas in children. The orbit can also be involved secondarily by spread of rhabdomyosarcoma from other sites, such as the nasopharynx or infratemporal fossa. The most common histological type involving the orbit is the embryonal form. Primary orbital rhabdomyosar-

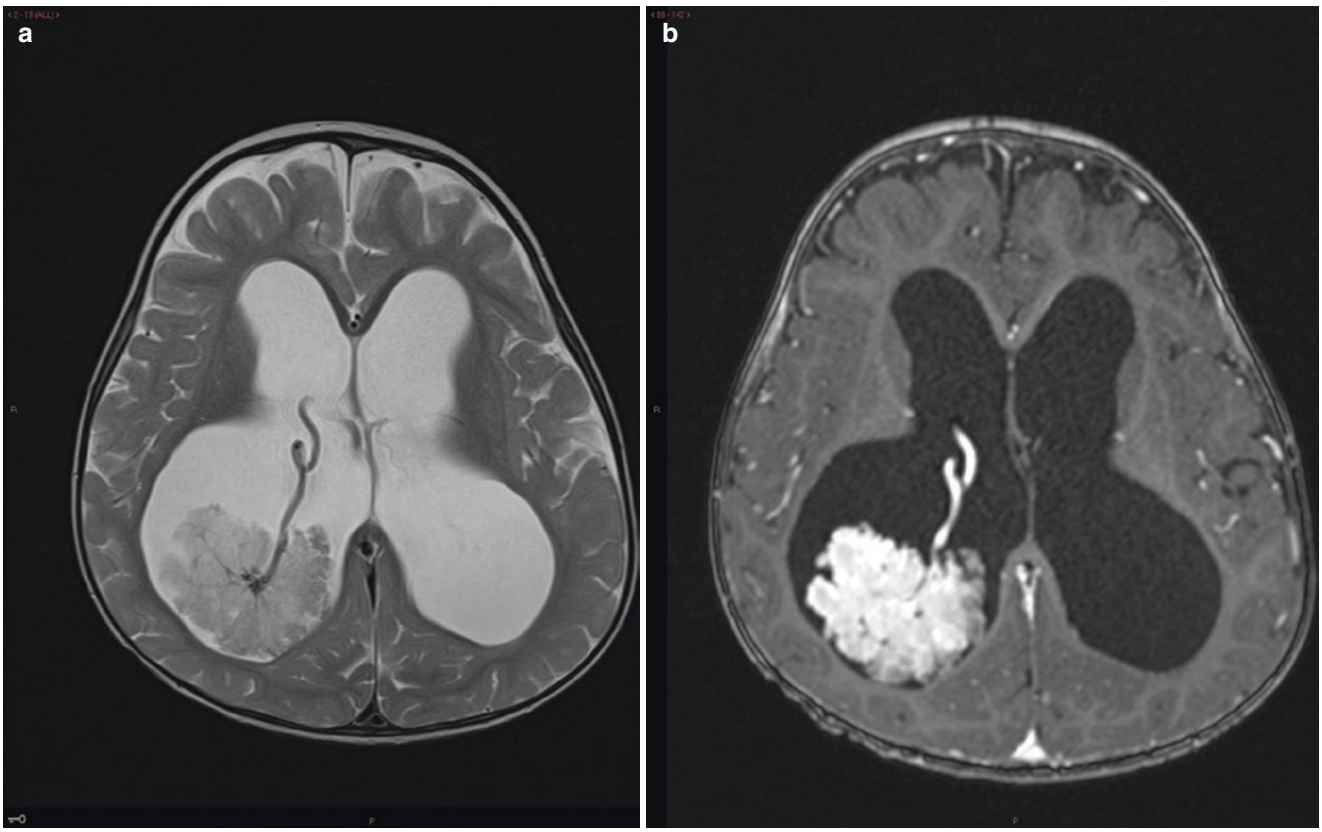

Fig. 2.150 Choroid plexus papilloma. (**a**) Axial T2-weighted MR image shows a lobulated mass within the right lateral ventricle. A large feeding vessel is visible. (**b**) Axial post-contrast T1-weighted image shows that the mass enhances intensely. There is dilatation of the ventricles due to hydrocephalus

coma most often occurs in the first decade of life. It is an aggressive, fast-growing tumour that presents with rapidly progressive proptosis or globe displacement. Conjunctival and palpebral swelling may also be present. Most tumours are extraconal or both intraconal and extraconal in location. The tumour frequently invades adjacent bones and soft tissues.

CT and MR imaging both have important roles in the staging and follow-up of orbital rhabdomyosarcomas, providing complementary information. CT is particularly valuable for demonstrating bone involvement, whereas MRI is sensitive for detecting intracranial extension of the tumour. On CT imaging, an orbital rhabdomyosarcoma usually appears as a well-defined, irregular, ovoid extraconal mass with density similar to muscle (Fig. 2.151). Eyelid thickening is frequently present. The tumour usually enhances with contrast. The tumour mass displaces or encases the extraocular muscles.

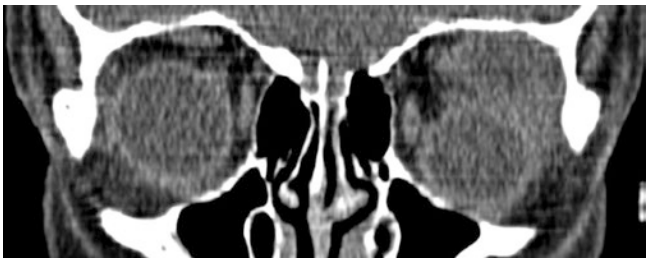

Fig. 2.151 Left orbital rhabdomyosarcoma. Coronal reconstructed CT image demonstrates a soft-tissue mass superiorly within the left orbit, displacing the left globe inferiorly. The density of the mass is similar to the adjacent extraconal muscles

Larger tumours tend to have less well-defined margins and are more likely to erode or destroy adjacent bone. On MR imaging, an orbital rhabdomyosarcoma is isointense relative to muscle on T1-weighted images, and usually hyperintense on T2-weighted images. The tumour enhances uniformly with contrast (Fig. 2.152). Intraorbital structures may be encased by the mass, and the globe is often distorted or displaced. Invasion into the paranasal sinuses or intracranial compartment may be seen with aggressive tumours.

2.4.6 Retinoblastoma

Retinoblastoma is the most common intraocular tumour in children. Most patients present before 4 years of age. Bilateral disease occurs in 30% of cases. Lesions may be unifocal or multifocal. Patients with a genetic form of retinoblastoma are at increased risk of developing intracranial tumours in the pineal or suprasellar region, a phenomenon known as "trilateral retinoblastoma."

Retinoblastoma is usually diagnosed by ophthalmologic examination, which reveals a white pupillary reflex (leukocoria) instead of the normal red reflex. The diagnosis can be confirmed with ultrasound. Solitary or multiple intraocular masses may be identified on ultrasound. Retinoblastoma is characterised as an echogenic soft-tissue mass within the globe (Fig. 2.153). Calcification may be seen within the lesion. The lesions are usually hypervascular on colour Doppler assessment (Fig. 2.154). Ultrasound can also dem-

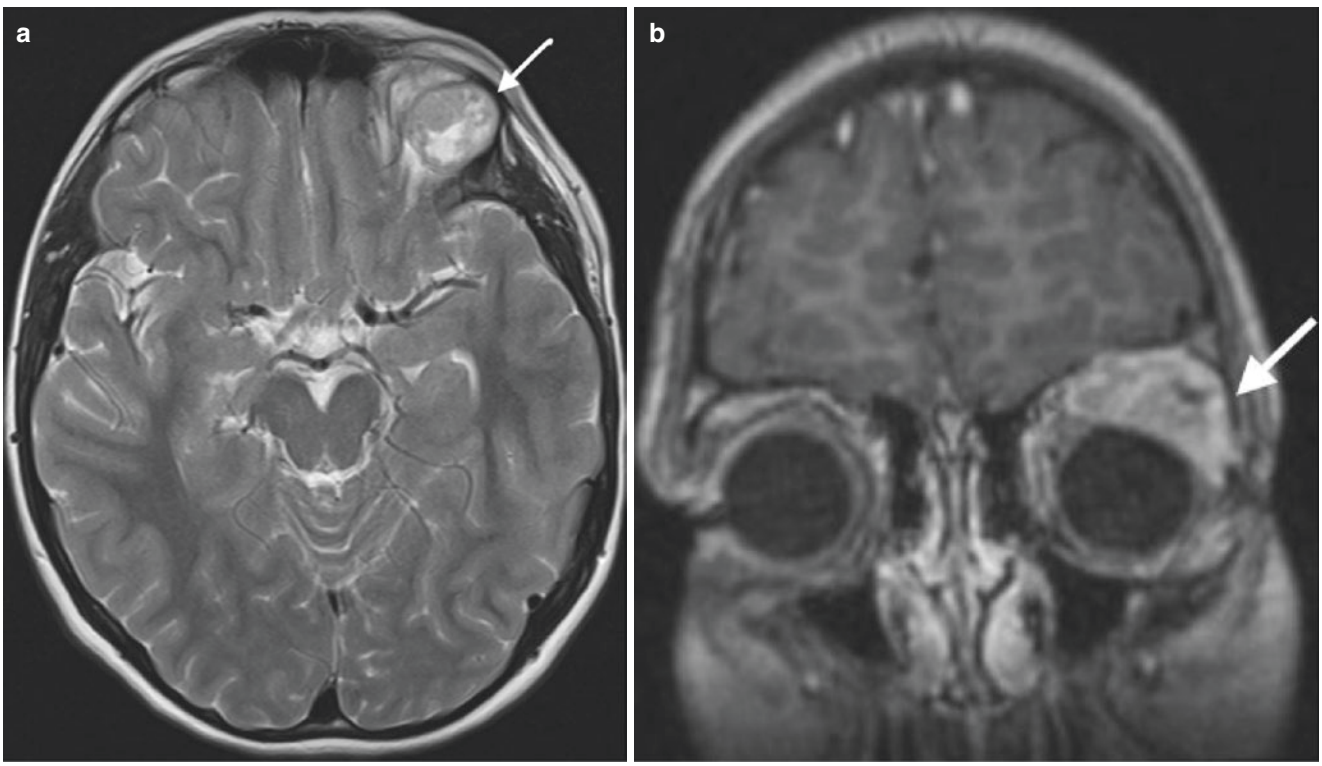

Fig. 2.152 Left orbital rhabdomyosarcoma. (**a**) Axial T2-weighted MR image shows an isointense to hyperintense lesion in the superior aspect of the left orbit. (**b**) Coronal post-contrast T1-weighted MR image demonstrates enhancement of the tumour

onstrate associated retinal detachment and vitreous spread. The vitreous may have echogenic debris from haemorrhage or tumour seeding. Tumour extension is poorly delineated with ultrasound.

MR imaging is used for staging because it can provide detailed information regarding the tumour, the retrobulbar structures, and the brain. Retinoblastoma lesions are usually hyperintense to vitreous on T1-weighted imaging and hypointense on T2-weighted images (Fig. 2.155). The lesions demonstrate moderate to marked enhancement with contrast. Calcification, if present, may be identified with certain sequences. Vitreous seeding may be identified as T1 hyperintense and T2 hypointense foci within the vitreous cavity. Retinal detachment with subretinal exudates also can be visualised. Staging of retinoblastoma should include evaluation of intraocular extension (to choroid or sclera), extraocular spread (optic nerve or orbital invasion), or intracranial extension (leptomeningeal or brain metastases).

CT is now seldom used for the diagnosis and staging of retinoblastoma. When performed, the tumour appears as an enhancing, intermediate-density soft-tissue mass or masses. CT readily depicts tumoral calcification (Fig. 2.155c).

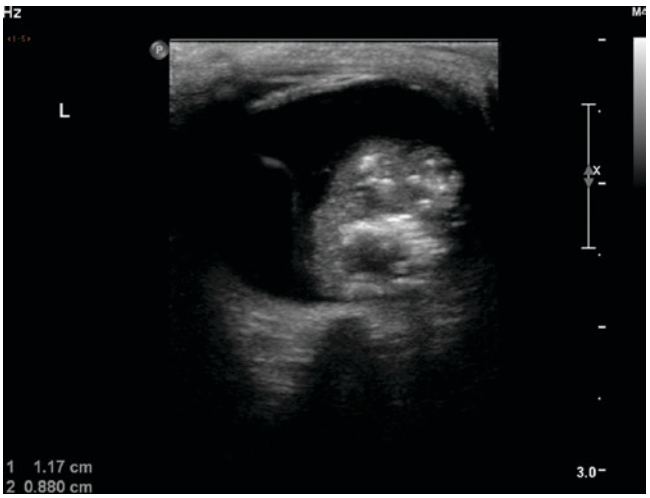

Fig. 2.153 Retinoblastoma. Transverse ultrasound image demonstrates an irregular, echogenic soft-tissue structure posteriorly in the left globe. Small foci of hyperechogenicity within the tumour represent calcification

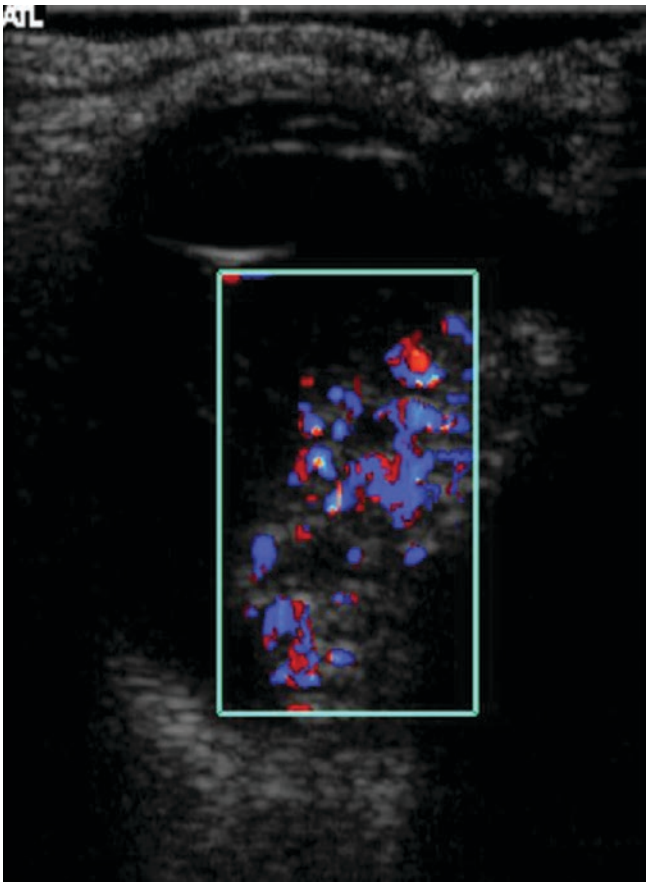

Fig. 2.154 Retinoblastoma. Colour Doppler ultrasound image demonstrates hypervascularity within the tumour

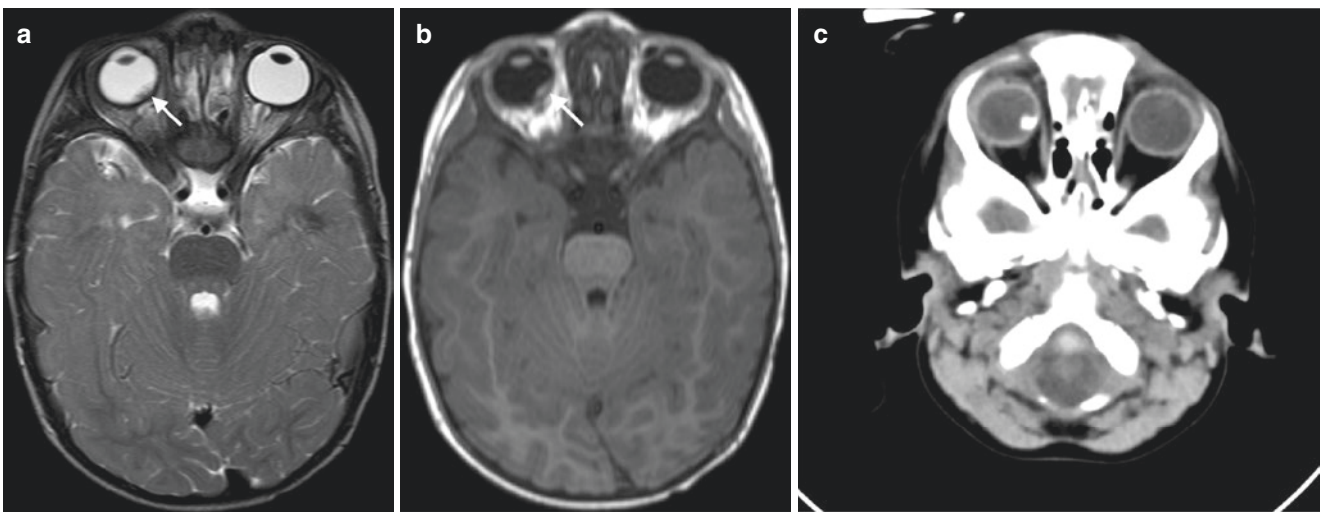

Fig. 2.155 Retinoblastoma lesion within the right globe. The lesion (*arrow*) is low-signal on an axial T2-weighted MR image (**a**) high-signal on an axial T1-weighted image (**b**) and calcified on an axial CT image (**c**)

2.5 Acquired Conditions

2.5.1 Intraventricular Haemorrhage

Intraventricular haemorrhage (IVH) is a complication seen more often in premature than term infants. The germinal matrix is a highly vascular structure, which is found in the caudothalamic groove between the thalamus and the head of caudate in premature infants. It is the classic site of haemorrhage in preterm infants. The haemorrhage is attributed to the intrinsic fragility of the germinal matrix vasculature and fluctuations in cerebral blood flow. Haemorrhage within the germinal matrix may rupture through the ependymal lining into the lateral ventricle. The germinal matrix begins to involute towards the end of the second trimester. As involution progresses, the risk of haemorrhage decreases.

Intracranial haemorrhage in preterm infants is usually diagnosed on cranial ultrasound. Papile and colleagues (1978) classified intraventricular and periventricular haemorrhage into four grades, depending on severity: *Grade 1* haemorrhage refers to subependymal (germinal matrix) haemorrhage only. *Grade 2* haemorrhage is extension of the subependymal haemorrhage into the lateral ventricle, without ventricular dilatation. *Grade 3* haemorrhage is intraventricular haemorrhage with ventricular dilatation. In *grade 4* haemorrhage, there is intraventricular haemorrhage within a dilated ventricle and periventricular haemorrhage due to periventricular venous infarction.

On cranial ultrasound, an acute grade 1 subependymal haemorrhage appears as a hyperechoic area along the inferior aspect of the frontal horn of the lateral ventricle and medial to the head of caudate in the coronal plane (Fig. 2.156). On parasagittal sections, the haemorrhage is identified as a hyperechoic area in the caudothalamic groove. In grade 2 haemorrhage, the intraventricular blood is seen as echogenic material filling part or all of a non-dilated ventricle (Fig. 2.157). In grade 3 haemorrhage, there is echogenic blood within the ventricle and ventricular dilatation (Fig. 2.158). The periventricular haemorrhage associated with grade 4 haemorrhage is identified as an irregular echogenic area in the brain parenchyma adjacent to the lateral ventricle. It is usually associated with intraventricular haemorrhage and ventricular dilatation (Fig. 2.159).

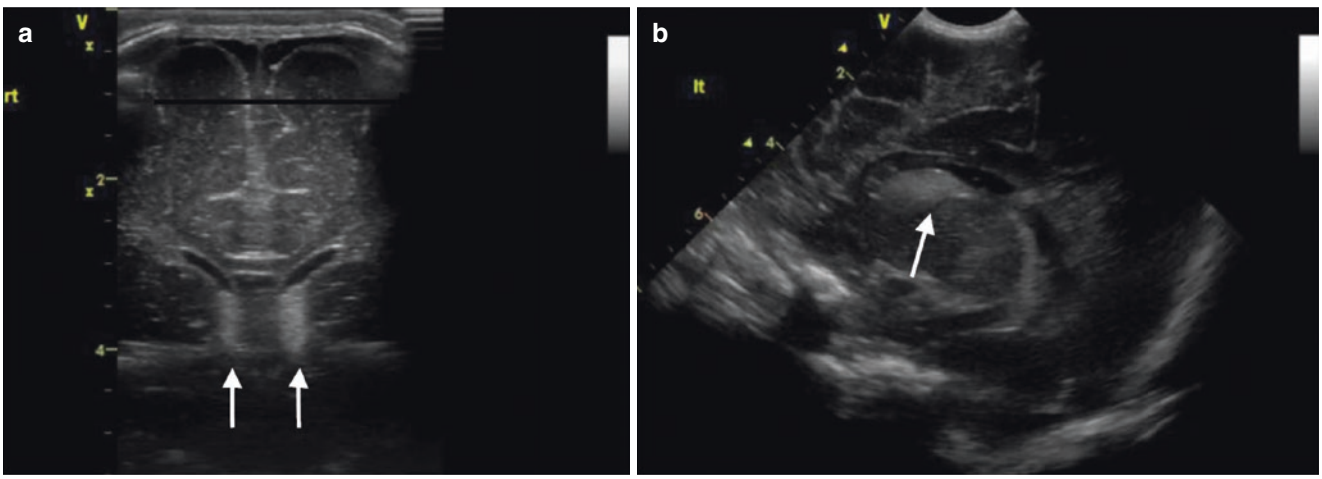

Fig. 2.156 Bilateral grade 1 subependymal haemorrhages. (**a**) Coronal ultrasound image shows bilateral hyperechoic foci along the inferior frontal horns of the lateral ventricles. (**b**) Left parasagittal ultrasound image shows the hyperechoic haemorrhage within the caudothalamic groove

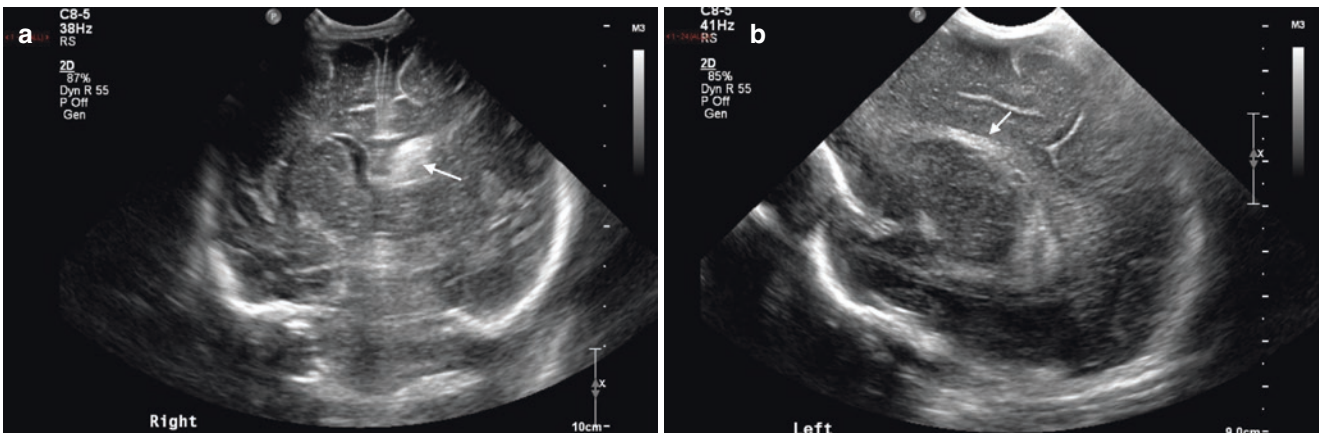

Fig. 2.157 Grade 2 intraventricular haemorrhage. Coronal (**a**) and parasagittal (**b**) ultrasound images show hyperechoic haemorrhage filling the left lateral ventricle. The ventricle is not dilated

In contrast to preterm infants, intraventricular haemorrhage is uncommon in term infants. Potential sources of intraventricular haemorrhage in term infants include choroid plexus haemorrhage, vascular malformation, tumour, extension of haemorrhagic venous infarction, coagulopathy, and extension of thalamic haemorrhage.

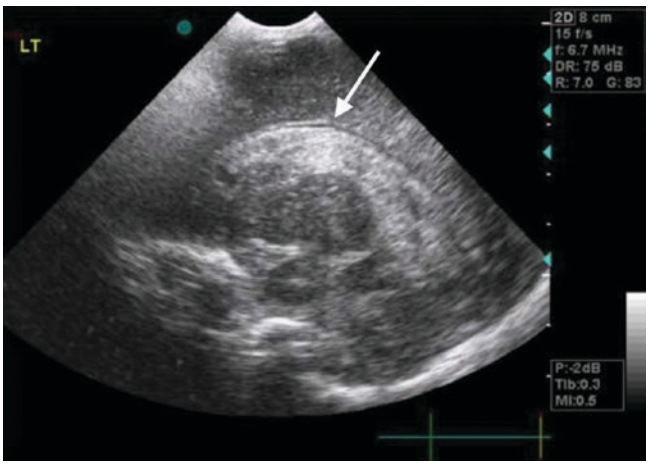

Fig. 2.158 Grade 3 intraventricular haemorrhage. Parasagittal ultrasound image demonstrates hyperechoic blood (*arrow*) within a dilated left lateral ventricle

2.5.2 Porencephalic Cyst

Porencephaly is a cystic area within the brain that communicates with the ventricle and/or subarachnoid space. Encephaloclastic porencephaly is the sequela of an insult that can occur in utero, in premature newborn infants, or in early infancy. Aetiologies include cerebral ischaemia, haemorrhage, trauma, and infection. The damaged area evolves over time into a fluid-filled cavity.

On ultrasound, a porencephalic cyst appears as a hypoechoic parenchymal cyst that communicates with a ventricle or the subarachnoid space. There is often ipsilateral ventricular dilatation (Fig. 2.160). MRI demonstrates a well-defined cyst that follows CSF signal intensity on all sequences. The cyst is lined by white matter and does not

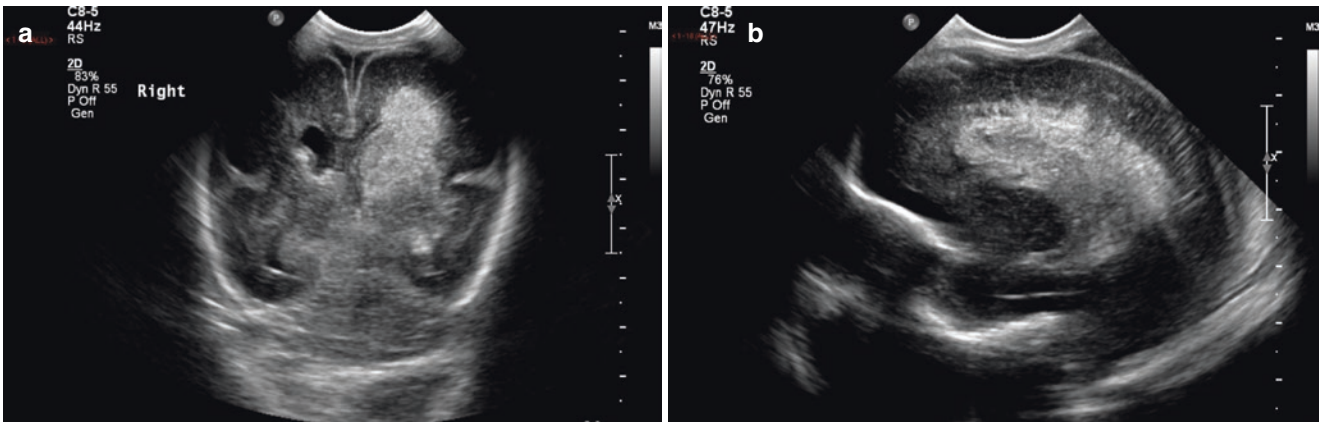

Fig. 2.159 Grade 4 haemorrhage. Coronal (**a**) and parasagittal (**b**) ultrasound images show a large intraventricular haemorrhage within a dilated left lateral ventricle. There is also echogenic haemorrhage in the surrounding parenchyma, due to periventricular venous infarction

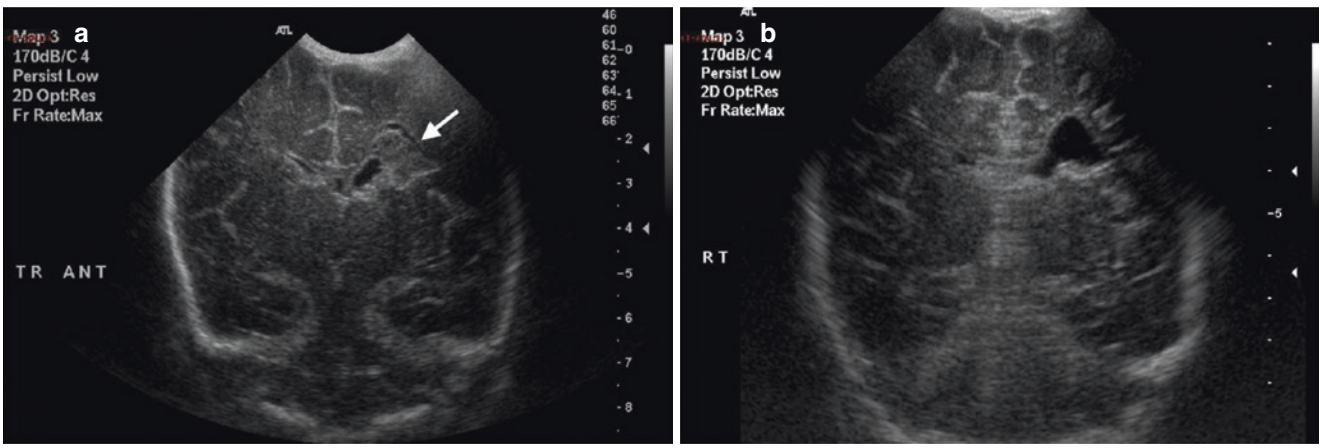

Fig. 2.160 Evolution of an encephaloclastic porencephalic cyst. (**a**) Coronal ultrasound image in a preterm infant demonstrates a resolving periventricular haemorrhage adjacent to the frontal horn of the left lateral ventricle. (**b**) Coronal ultrasound image obtained a few weeks later shows that the haemorrhage has been replaced by a CSF space, which communicates with the ventricle

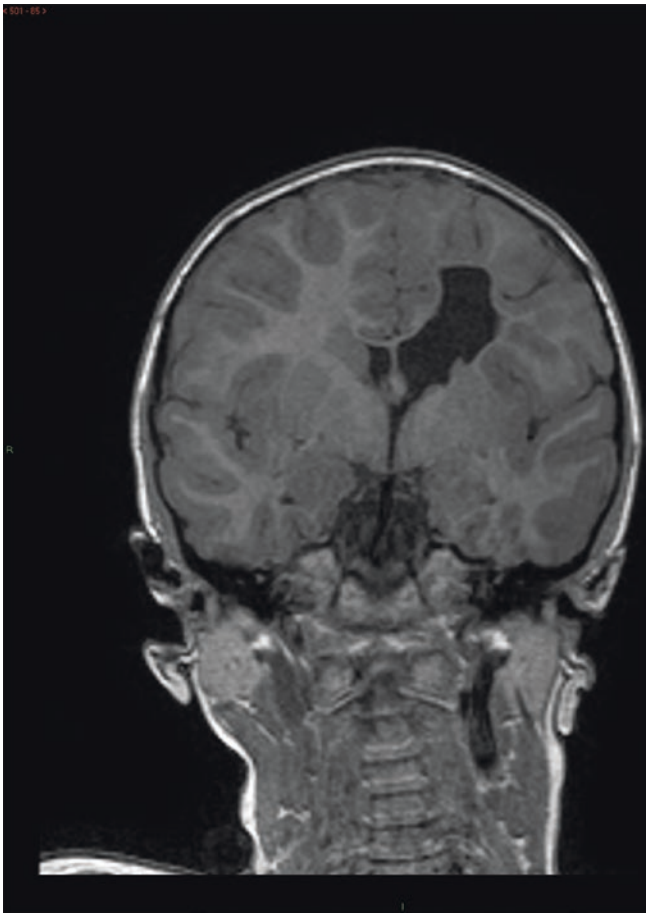

Fig. 2.161 Left frontal porencephalic cyst. Coronal T1-weighted MR image shows a CSF space communicating directly with the left lateral ventricle

enhance with contrast. Communication with the ventricle and/or subarachnoid space is typical (Fig. 2.161).

2.5.3 Paediatric Stroke

Although stroke is often thought of as an adult disease, it is unfortunately an important cause of morbidity and mortality in infants and children. By definition, perinatal stroke occurs before 29 days after birth, and childhood stroke occurs between ages 29 days and 18 years.

Stroke is a neurological injury caused by occlusion or rupture of cerebral blood vessels. It can be ischaemic, haemorrhagic, or both. Ischaemic stroke is usually caused by arterial occlusion, but it also can be caused by occlusion of cerebral veins or venous sinuses. Haemorrhagic stroke is the consequence of bleeding from a ruptured cerebral artery or bleeding into the site of an acute ischaemic stroke. Acute ischaemic stroke accounts for approximately 50% of all strokes in children. Recognised risk factors for acute ischaemic stroke in children include cerebral arteriopathy (e.g., moyamoya disease), congenital and acquired heart disease,

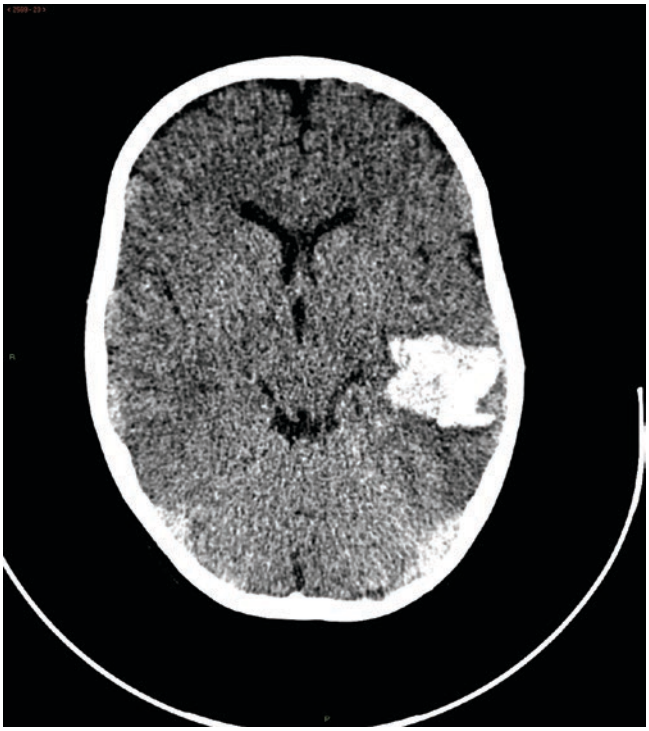

Fig. 2.162 Left temporal lobe haemorrhage secondary to a ruptured arteriovenous malformation (AVM). Unenhanced axial CT image shows acute haemorrhage within the left temporal lobe of the brain. A subsequent intracerebral angiogram revealed an underlying AVM

haematological disorders (e.g., sickle cell disease), and CNS infection (meningitis, encephalitis).

The clinical presentation of stroke depends on the age of the child and may not be specific. Infants with perinatal strokes usually present with focal seizures or lethargy in the first few days after birth. Infants and toddlers tend to present with nonspecific features such as lethargy, irritability, feeding difficulty, apnoeic spells, and hypotonia. Older children manifest more specific neurological signs similar to those in adults, including hemiparesis, gait disturbance, speech difficulties, and headache.

An unenhanced CT scan of the head should be performed in any child suspected of having stroke to exclude a haemorrhagic cause for the stroke and to assess for any neurosurgical emergency (Fig. 2.162). Cerebral venous sinus thrombosis may be evident as areas of increased attenuation (increased density) within the venous sinuses or within cortical veins. An acute ischaemic stroke may be detected on an unenhanced CT scan as a low-attenuation (low-density) area within a vascular territory, but the scan may show no abnormality if it is performed within the first few hours after the onset of symptoms. MRI is a more sensitive imaging modality for the early detection of stroke, as diffusion-weighted imaging can detect a hyperacute infarct before changes are visible on T2-weighted imaging. MR angiography and venography should also be performed to assess vessel patency and blood flow.

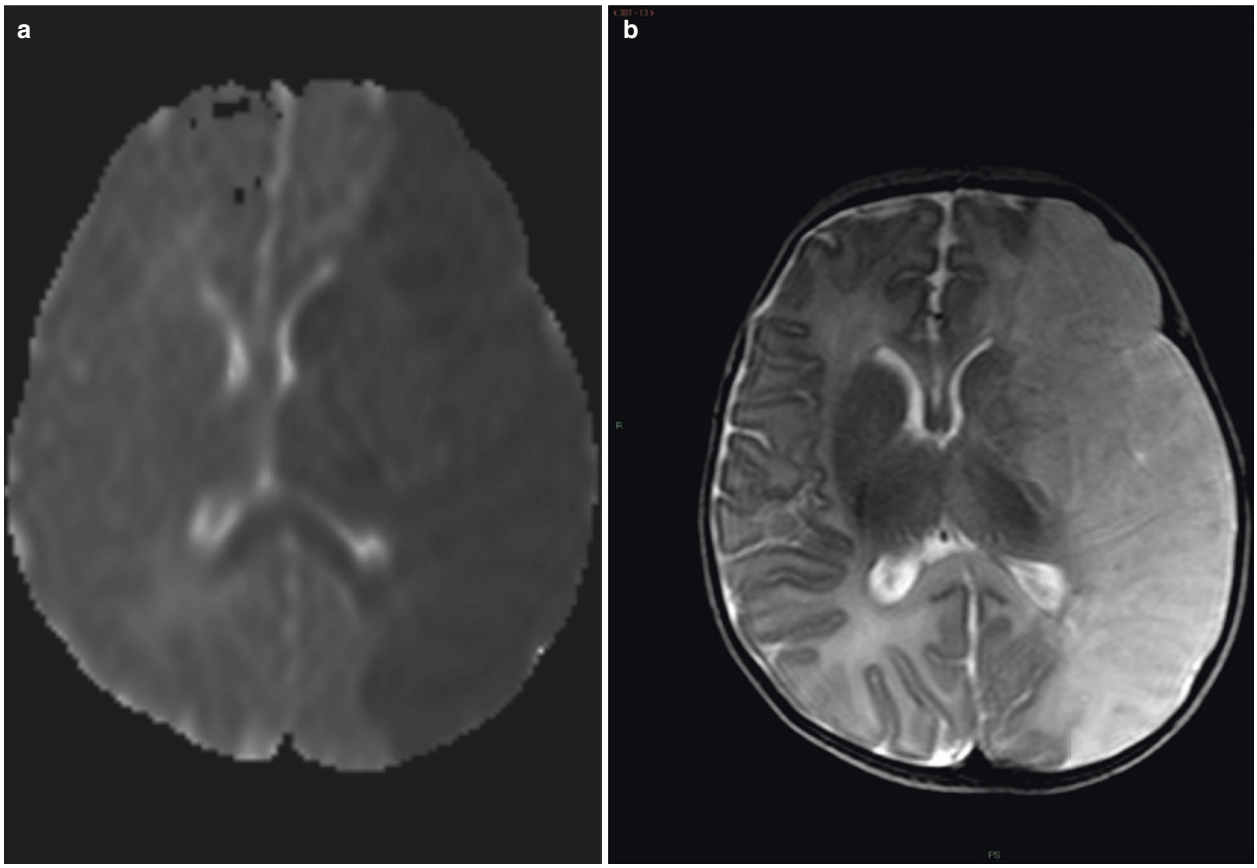

Fig. 2.163 Acute infarct in the left middle cerebral artery (MCA) territory. (**a**) Apparent diffusion coefficient (ADC) image from diffusion-weighted MRI shows hypointense signal in the left MCA territory, consistent with an acute infarct. (**b**) Axial T2-weighted MR image demonstrates increased signal within the infarcted territory, as well as localised brain swelling with effacement of cerebral sulci

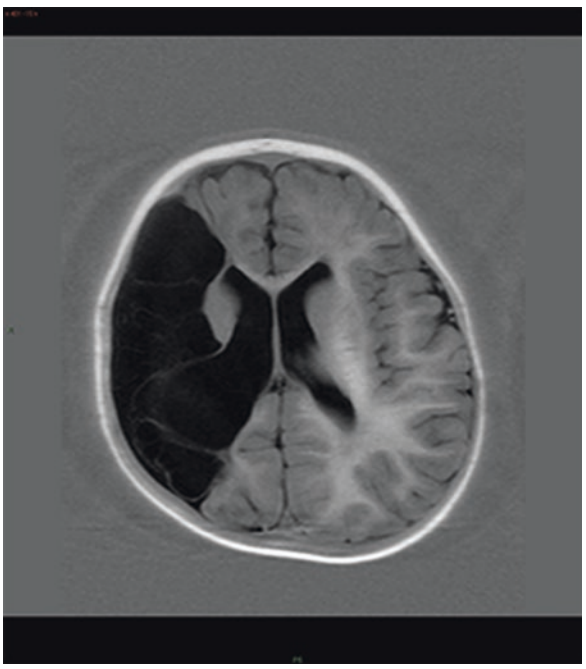

Fig. 2.164 Sequelae of right middle cerebral artery (MCA) territory infarct. Axial T1-weighted MR image shows cystic change in the right MCA territory after a previous infarct. Dilatation of the right lateral ventricle is secondary to the parenchymal loss

On MRI, an acute ischaemic infarct demonstrates restricted diffusion due to cytotoxic oedema and appears hypointense (dark) on the apparent diffusion coefficient (ADC) image (Fig. 2.163a). The infarct is of increased signal intensity on T2-weighted imaging and low signal on T1-weighted images. There is usually localised brain swelling (Fig. 2.163b). Over a period of weeks, the brain swelling settles and encephalomalacic cystic change appears in the infarcted area (Fig. 2.164). The parenchymal loss is associated with ipsilateral widening of adjacent subarachnoid and ventricle CSF spaces.

Further Reading

Adams A, Mankad K, Offiah C, Childs L. Branchial cleft anomalies: a pictorial review of embryological development and spectrum of imaging findings. Insights Imaging. 2016;7:69–76. https://doi.org/10.1007/s13244-015-0454-5.

Barkovich AJ, Raybaud C, editors. Pediatric neuroimaging. 5th ed. Philadelphia, PA: Lippincott Williams & Wilkins; 2012.

Bhattacharya JJ, Thammaroj J. Vein of galen malformations. J Neurol Neurosurg Psychiatry. 2003;74:i42–4.

Chung EM, Smirniotopoulos JG, Specht CS, Schroeder JW, Cube R. From the archives of the AFIP: pediatric orbit tumors and tumorlike lesions: nonosseous lesions of the extraocular orbit. Radiographics. 2007;27:1777–99.

Coley B, editor. Caffey's pediatric diagnostic imaging. 12th ed. Philadelphia, PA: Elsevier Saunders; 2013.

Dighe MK, Peterson SE, Dubinsky TJ, Perkins J, Cheng E. EXIT procedure: technique and indications with prenatal imaging parameters for assessment of airway patency. Radiographics. 2011;31:511–26.

Koeller KK, Alamo L, Adair CF, Smirniotopoulos JG. Congenital cystic masses of the neck: radiologic-pathologic correlation. Radiographics. 1999;19:121–46.

Kollipara R, Dinneen L, Rentas KE, Saettele MR, Patel SA, Rivard DC, Lowe LH. Current classification and terminology of pediatric vascular anomalies. AJR Am J Roentgenol. 2013;201:1124–35. https://doi.org/10.2214/AJR.12.10517.

Ludwig BJ, Wang J, Nadgir RN, Saito N, Castro-Aragon I, Sakai O. Imaging of cervical lymphadenopathy in children and young adults. AJR Am J Roentgenol. 2012;199:1105–13.

Lustrin ES, Karakas SP, Ortiz AO, Cinnamon J, Castillo M, Vaheesan K, et al. Pediatric cervical spine: normal anatomy, variants, and trauma. Radiographics. 2003;23:539–60.

Papile LA, Burstein J, Burstein R, Koffler H. Incidence and evolution of subependymal and intraventricular hemorrhage: a study of infants with birth weights less than 1,500 gm. J Pediatr. 1978;92(4):529–34.

Siegel MJ. Pediatric sonography. 5th ed. Philadelphia, PA: Wolters Kluwer; 2019.

Tsze DS, Valente JH. Pediatric stroke: a review. Emerg Med Int. 2011;2011:734506.

The Chest

3

Robert Carachi and Rasem Keilani

3.1 Introduction

This chapter deals with the congenital anomalies found in the chest and includes a large section on cardiac anomalies. It also has extensive sections on infection, trauma, and tumours of the chest wall and the mediastinum. The final section covers acquired conditions and problems encountered with shunts, central lines, and chest drains.

3.2 Congenital

3.2.1 Tracheomalacia (Fig. 3.1)

Tracheomalacia is the condition where the normal struts of cartilage that maintain the trachea patent are either malformed, as in the case in a number of infants with tracheaoesophageal fistula, or are compressed by vessels. This allows collapse of the trachea. The infant may suffer attacks of apnoea that require resuscitation. This is often associated with prematurity. It is also found in association with tracheooesophageal fistula, in which the cartilages are malformed. Once extubated post-operatively, the baby may get "sudden death-like attacks" due to a segment of tracheomalacia of the trachea and/or bronchus collapsing. Imaging can be difficult but flexible endoscopy can establish the diagnosis.

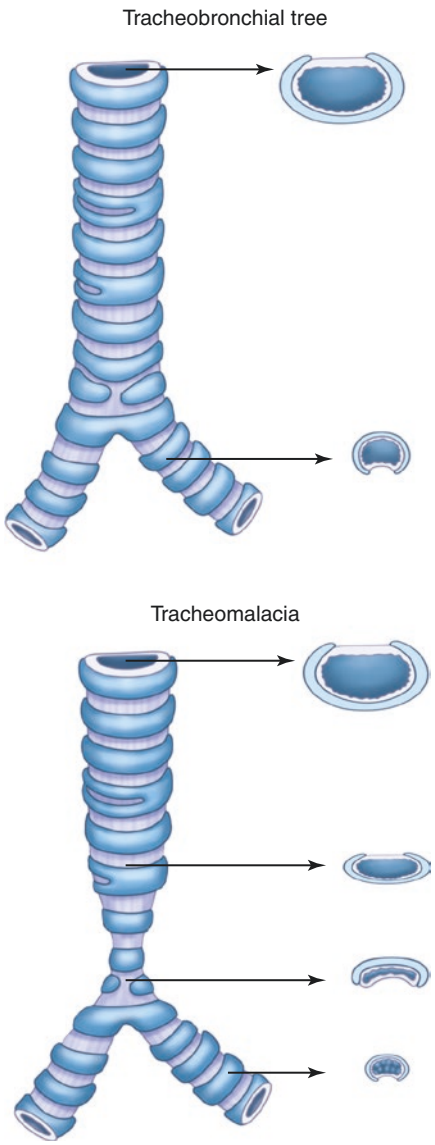

Fig. 3.1 Diagram of tracheomalacia

3.2.2 Chest Deformities (Pectus Excavatum/Carinatum)

3.2.2.1 Pectus Excavatum (Funnel Chest)

Pectus excavatum, or funnel chest, is depression of the lower sternum. No treatment is required in cases of minor depression, whereas severe deformity may be associated with kyphosis and may impair heart and lung function. Cosmetic correction is delayed until after the age of 4. The intercostal

R. Carachi (✉)
Surgical Paediatrics, University of Glasgow, Glasgow, UK

R. Keilani
Amman, Jordan

R. Carachi (ed.), *Atlas of Paediatric Surgical Imaging*, https://doi.org/10.1007/978-3-030-32384-4_3

cartilages are divided or resected, and the sternum is partially transected and elevated. The cause is not known, although some people have attributed the pectus excavatum to abnormal attachments of the diaphragm to the sternal ridge (Fig. 3.2a).

3.2.2.2 Pectus Carinatum

Pectus carinatum (pigeon chest) is a condition in which there is a marked sternal prominence that rarely causes aclinical upset but may rarely require surgery for cosmetic reasons (Fig. 3.2b).

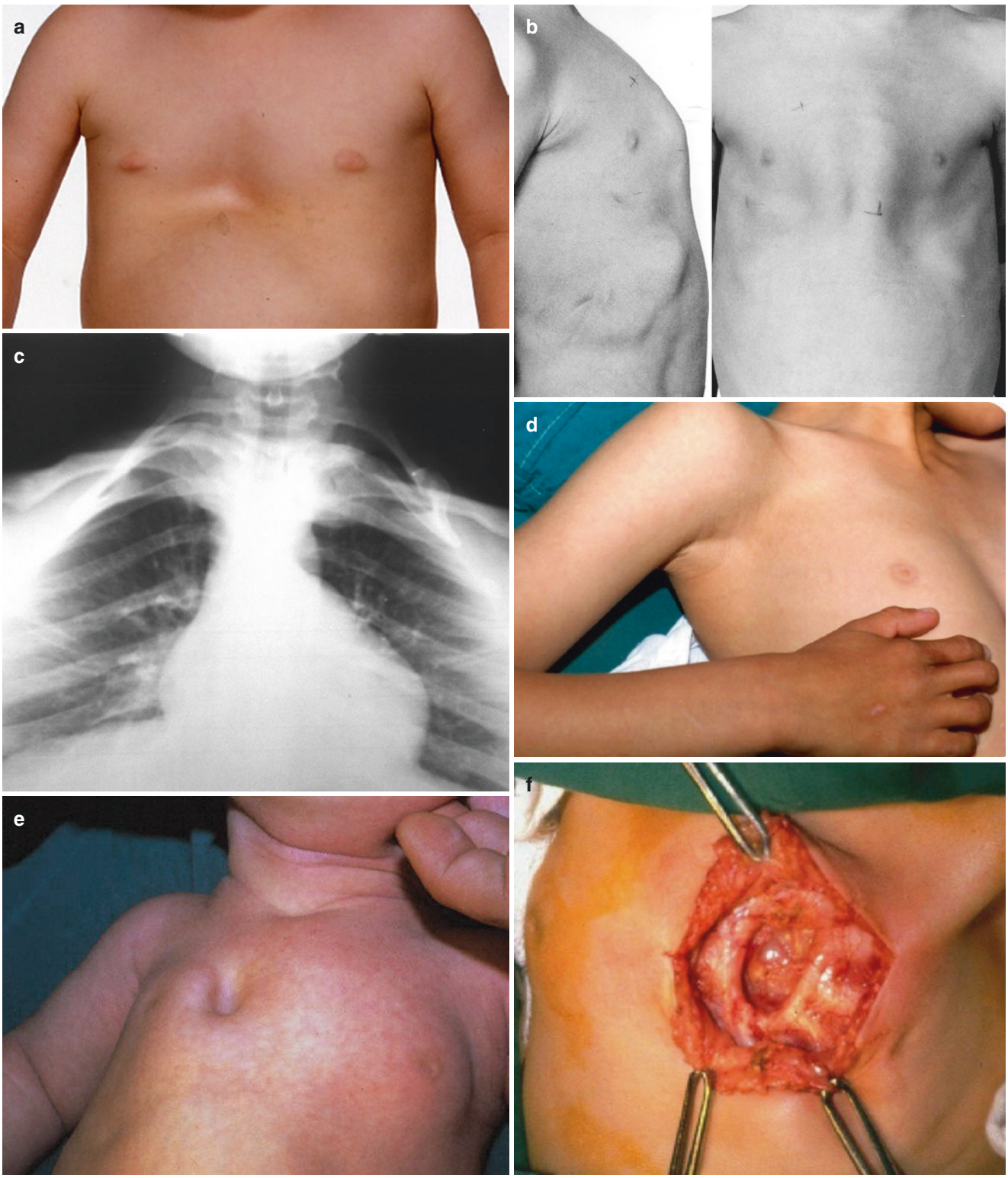

Fig. 3.2 (**a**) Pectus excavatum. (**b**) Pectus carinatum. (**c**) Cervical ribs. (**d**) Poland Syndrome. (**e**) Sternal cleft. (**f**) Sternal cleft operation. (**g**) Chest X-ray showing a bifid right rib

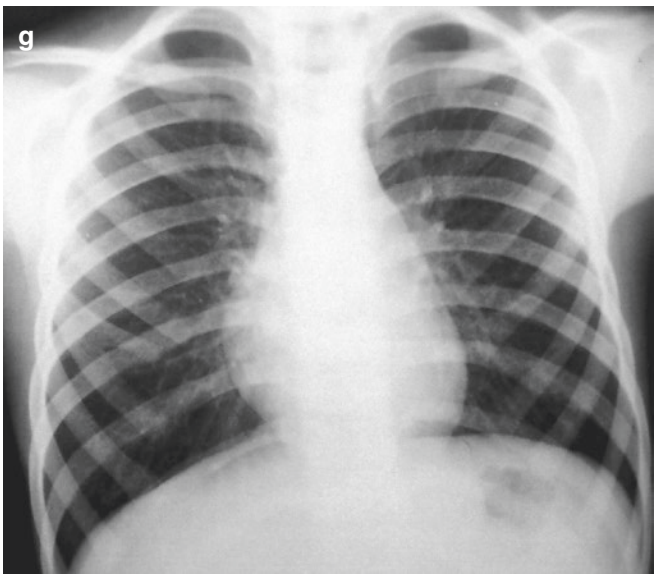

Fig. 3.2 (continued)

3.2.2.3 Harrison's Sulcus

Harrison's sulcus is a depression of the bony component of the chest wall that runs in a transverse fashion beneath both pectoral muscles. This is seen predominantly in children who have asthma or rickets but at times may be idiopathic. No treatment is necessary. This sulcus is most prominent in children under the age of 10, but as they grow older and develop more musculature and subcutaneous fat, it becomes less of a cosmetic problem.

3.2.2.4 Cervical Rib

Cervical rib is an extra rib seen as part of the association with Tracheo-oesophageal fistula (Fig. 3.2c). It can also occur independent of such associations. Symptoms include vascular and or nerve root compression from the rib or its fibrous attachments.

3.2.2.5 Poland Syndrome

Congenital absence of the breast, often seen in males, and absence of the sternal portion of pectoralis major, is known as Poland Syndrome (Fig. 3.2d).

3.2.2.6 Sternal Cleft

Absence of part of the sternum, or sternal cleft, is a rare condition and can be part of a spectrum of the pentalogy of Cantrell and Ectopia cordis (Fig. 3.2e, f).

3.2.2.7 Other Chest Wall Deformities

The 11th and 12th ribs are often designated as floating ribs. This is a variation of normal anatomy and may be confused with an abnormal abdominal wall mass. Reassurance is all that is necessary. The xiphoid process may assume a variety of shapes, some of which involve eversion of the process and produce a prominent lump beneath the skin in the midline. At times, this may be deviated to one side or another. This variation of the normal anatomy causes no problems and very rarely is surgery indicated. Reassurance of the parents is all that is necessary. In association with tracheo-oesophageal fistula and oesophageal atresia in the VACTERL (vertebral defects, anal atresia, cardiac defects, tracheo-esophageal fistula, renal anomalies, and limb abnormalities) group of anomalies, an extra set of ribs may be present. This is an interesting radiological finding but has little clinical significance. Chest wall deformities such as fused ribs or enchondromata may be due to previous thoracotomies. Very rarely is cosmetic surgery necessary to correct this. Another complication of thoracotomy is a "winged" scapula due to damage to the long thoracic nerve of Bell. Some children have a flattening of the lower portion of the chest wall after repair of a congenital diaphragmatic hernia. This is partly due to the congenital abnormality caused by the deficiency of the diaphragm on that side, and partly due to the repair, which creates considerable tension on the edges of the diaphragm and pulls the chest wall inward. This deformity becomes less of a problem as the child grows older (Fig. 3.2g).

3.2.3 Oesophageal Atresia, Stenosis, Tracheooesophageal Fistula

Oesophageal atresia has been known for centuries. Successful treatment of the condition has only been achieved—first by a staged procedure in 1939 and then by primary anastomosis in 1941 (Fig. 3.3a). Since then, major improvement in management of the condition has occurred and survival is expected unless the infant has other major anomalies. Oesophageal atresia has an incidence of approximately 1:3000 deliveries. The classical case, which accounts for practically 85% of infants with oesophageal atresia, is that the proximal oesophagus lies blindly in the upper part of the posterior mediastinum and the distal oesophagus communicates with the posterior wall of the trachea as a tracheooesophageal fistula (TOF). In 10% of infants there is no tracheooesophageal fistula, and in these infants the gap between the proximal and distal oesophagus is greater. The remaining infants have variations of this pattern, and there may be proximal and distal tracheooesophageal fistulae (Fig. 3.3b, c).

Oesophageal atresia may be diagnosed antenatally. It is looked for in ultrasound examination, particularly in patients who have polyhydramnios, which almost invariably accompanies the oesophageal atresia anomaly in the infant. Ultrasound examination can detect the dilated proximal blind end of the oesophagus. At birth the baby has attacks of choking, coughing and cyanosis, and "excess salivation": saliva dribbles from the mouth because there is no passage to the stomach. The swallowed secretions or feed regurgitate and are often aspirated into the respiratory tract. These signs,

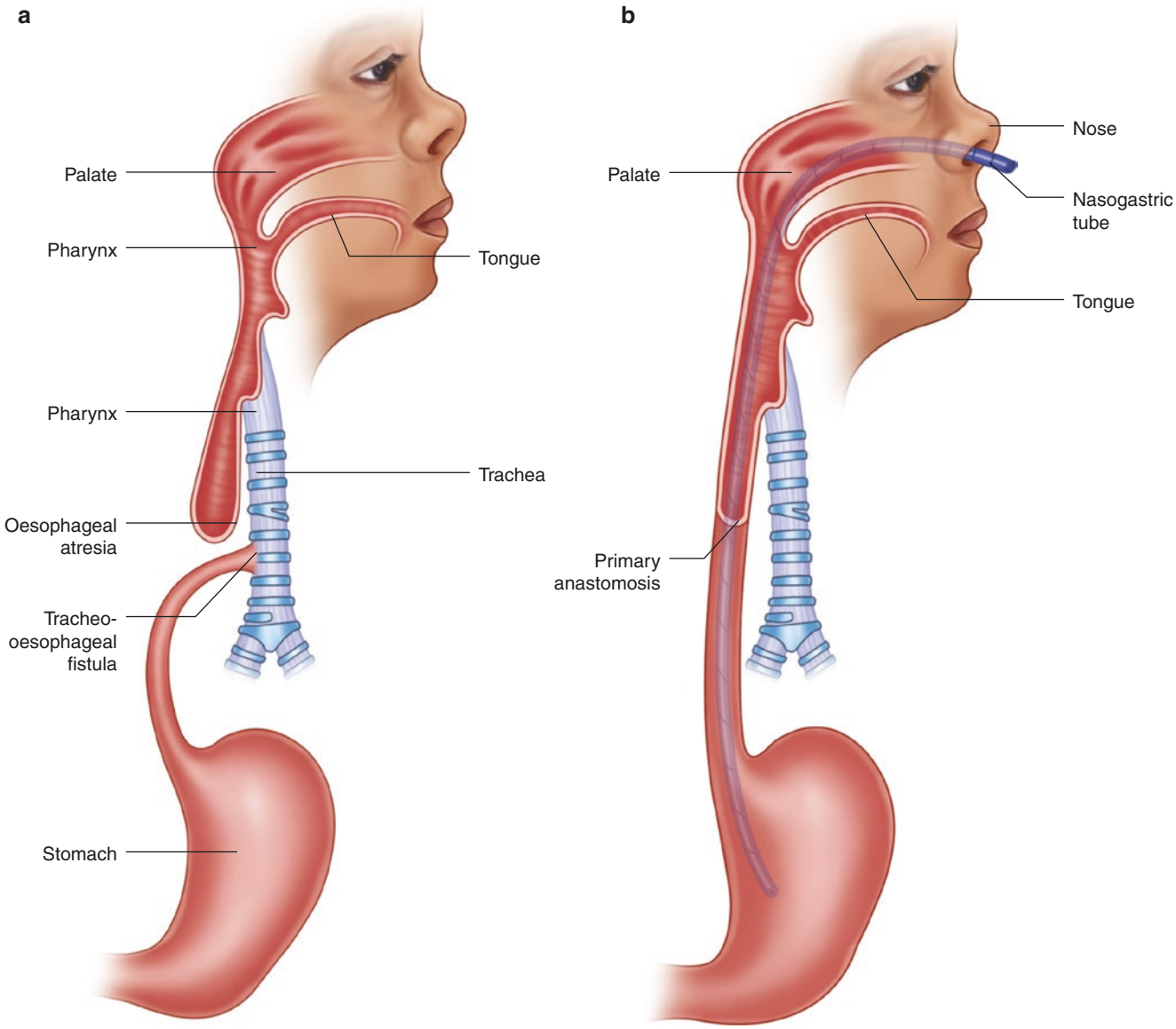

Fig. 3.3 (**a**) Diagram of oesophageal atresia and TOF. (**b**) Lateral view of oesophageal atresia and TOF. (**c**) Contrast showing oesophageal atresia and TOF with spillage into the trachobronchial tree leading to aspiration pneumonia. (**d**) Oesophageal atresia and TOF. Nasogastric tube coiled in pharynx. (**e**) Oesophageal atresia with TOF fistula. (**f**) Oesaphageal atresia with TOF. (**g**) Oesophageal atresia with no fistula, gasless abdomen and 13 pairs of ribs. (**h**) Tracheo oesophageal fistula diagram of oesophageal atresia and TOF. (**i**) Contrast showing tracheooesophageal fistula. TOF. (**j**) Colonic interposition for long gap oesophageal atresia

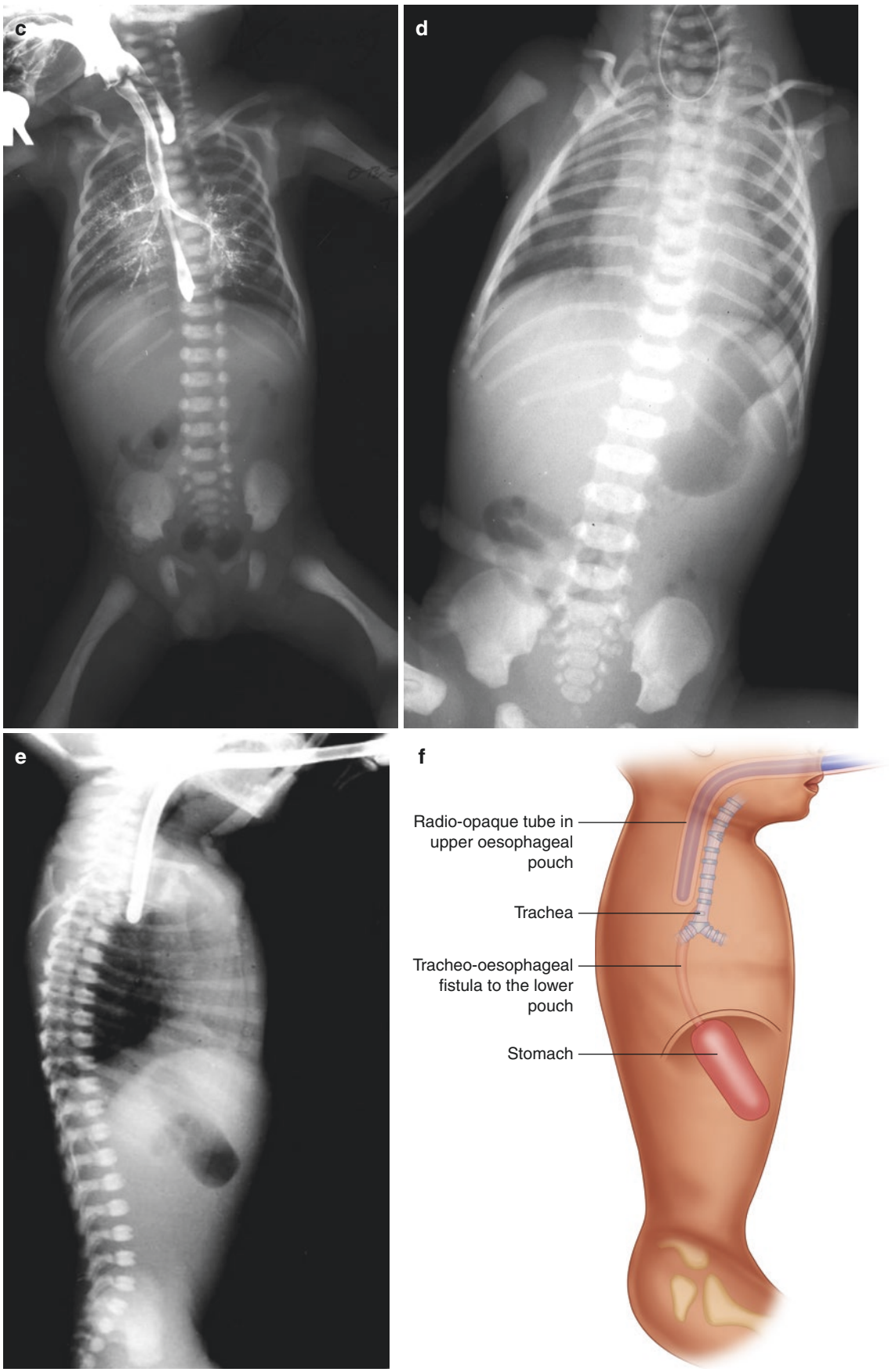

Fig. 3.3 (continued)

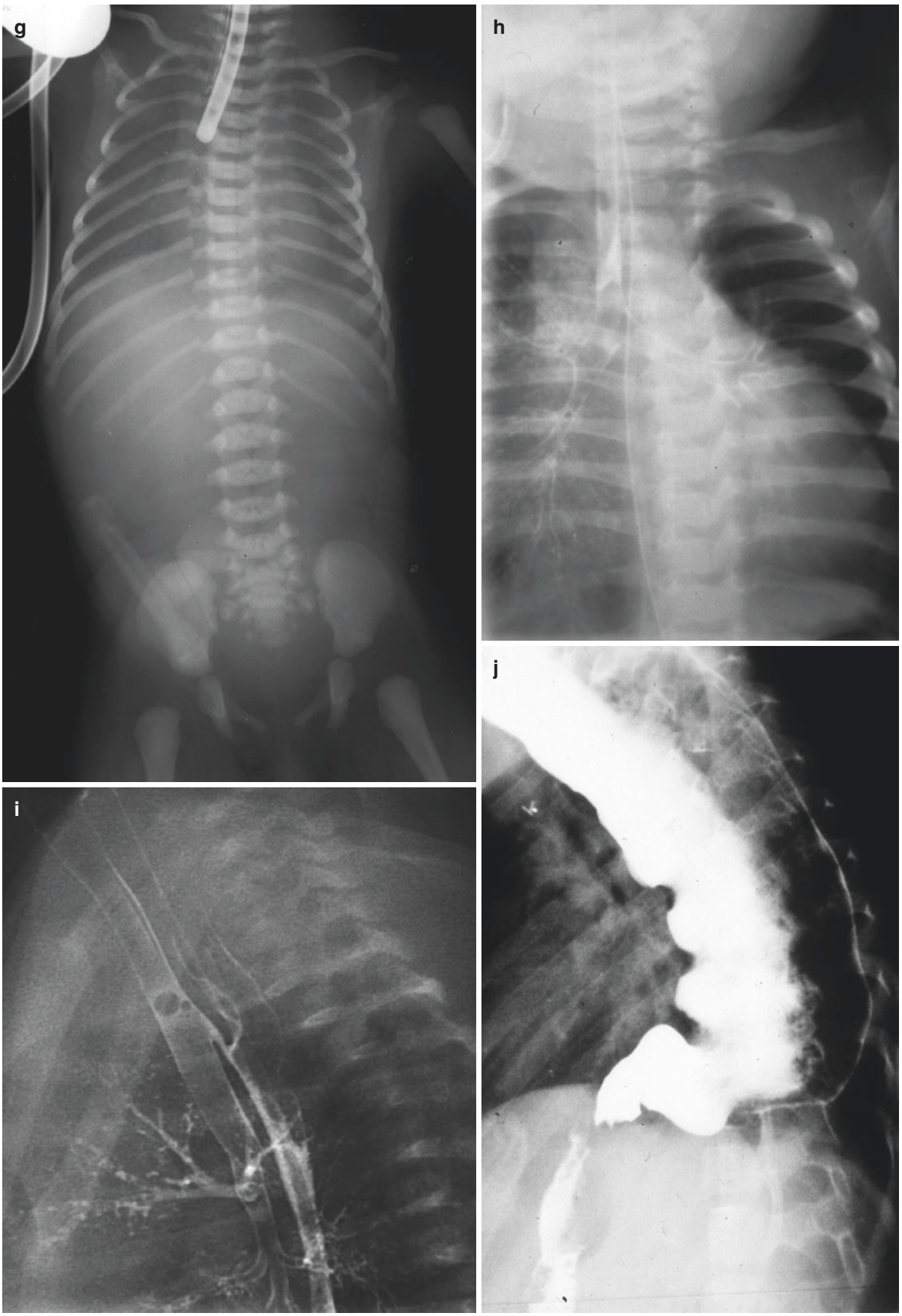

Fig. 3.3 (continued)

particularly in an infant of low birth weight, make one suspect the diagnosis. Many neonatal units routinely try to pass an orogastric tube into the stomach of all low-birth-weight babies, at birth, to aspirate the gastric contents. The tube is held up 10 cm beyond the lips in infants with oesophageal atresia (Fig. 3.3d–f).

Diagnosis is confirmed by passage of a radio-opaque tube as far as possible into the oesophagus and then taking a chest X-ray that includes the upper part of the abdomen with the field. This shows the hold-up of the radio-opaque tube at the level of the atresia. The inclusion of the upper abdomen shows if there is gas in the stomach, indicating that the infant must also have a tracheooesophageal fistula, the air having passed down the trachea through the tracheooesophageal fistula and onward to the stomach and bowel (Fig. 3.3g–i).

Infants with oesophageal atresia must be carefully examined. In addition to low birth weight, babies with oesophageal atresia frequently have other anomalies. These may be in the alimentary tract, such as duodenal atresia or imperforate anus, or in other systems such as the cardiovascular, urinary, or skeletal systems. A group of infants have the so-called VACTERL association (vertebral, anal, cardiac, tracheo-oesophageal, renal, and limb anomalies). The disease does not usually have a hereditary or familial aspect, but families occasionally have more than one child affected. The outcome of treatment of infants with oesophageal atresia is dependent on the number and severity of associated abnormalities. Infants without other anomalies have a very high survival rate but may have oesophageal dysmotility or problems with oesophageal stricture at the anastomotic level. Usually this is amenable to balloon dilatation, which sometimes has to be repeated on a number of occasions. Later, the child has more chance of having dysphagia with a food bolus obstructing the oesophagus, but this can be avoided by encouraging the child to masticate food fully before swallowing it (Fig. 3.3j).

3.2.4 Thymus

The thymus is a gland in the neck that is part of the lymphoreticular system. It is large at birth and can get bigger when stimulated. It occasionally causes airway obstruction because of its size. It eventually shrinks as the child grows older. At birth it can be seen as a prominent shadow and can be mistaken for a tumour. Thymic tumours may arise in it later in life and is associated with Myasthenia Gravis. Eighty percent of benign tumors can undergo calcification (Fig. 3.4).

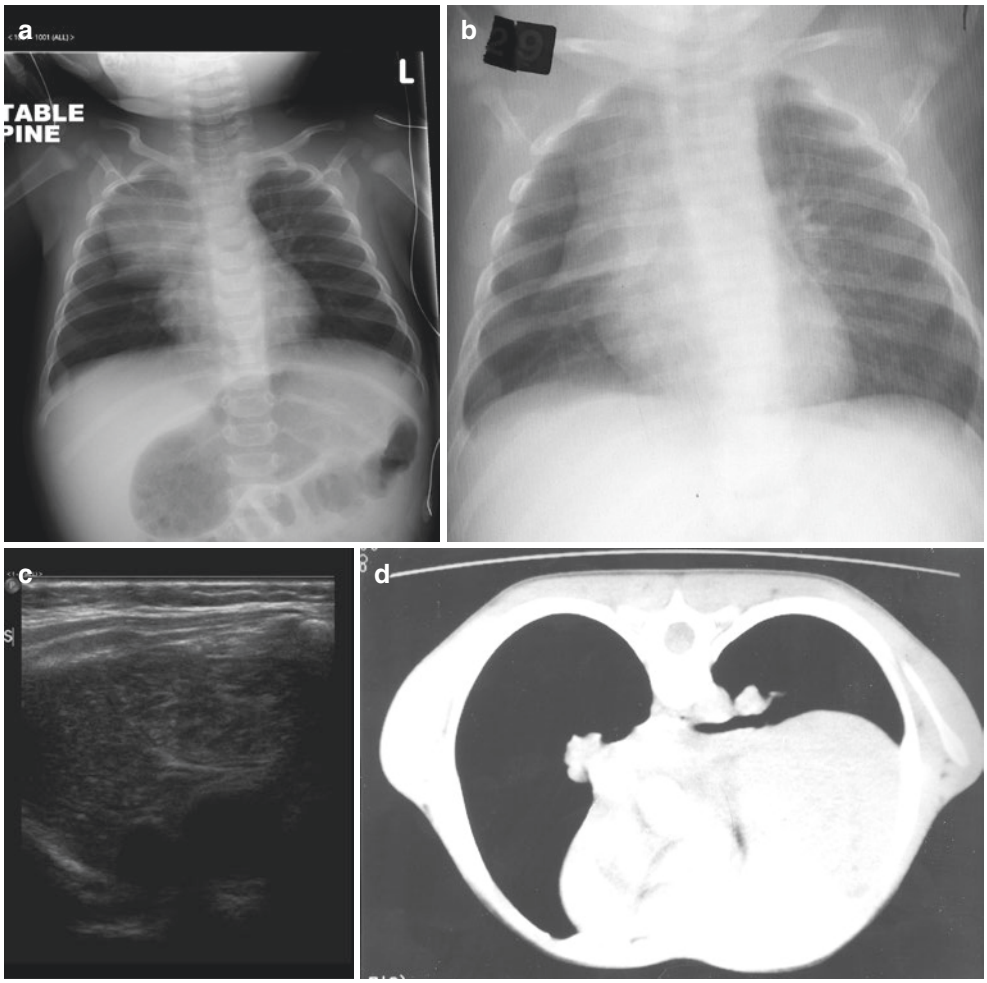

Fig. 3.4 (**a**) Enlarged thymic shadow. (**b**) Thymic shadow. (**c**) Ultrasound showing normal thymic tissue. (**d**) Thymolipoma

3.2.5 Vascular Ring (Fig. 3.5a, b)

Several aberrations can occur in the formation of the large arteries in the superior mediastinum. Among the most common are double aortic arch, right aortic arch with left ligamentum arteriosum, anomalous right subclavian artery, and anomalous innominate artery. In all these situations, the trachea and oesophagus may be compressed by vessels that run normally in front of them and abnormally behind them. The term "vascular ring" has been used to describe a variety of such vascular abnormalities. The clinical manifestations of aortic arch anomalies vary with the severity of encroachment of the abnormal vessel on the trachea, bronchus, or oesophagus (Fig. 3.5c, d). The features vary considerably in severity. The typical picture is of an underdeveloped infant with feeding difficulties and with constant laryngeal or tracheal stridor, wheezing, and cough. The child may find relief with extreme extension of the neck. When symptoms are delayed until later infancy, dysphagia may be obvious. There may be repeated severe respiratory infections. Patients with a double aortic arch tend to have signs at an earlier age than patients with other types of vascular rings. The diagnosis is confirmed by fluoroscopy visualising the tracheal compression, and during a barium swallow, when indentations of the oesophagus by the aberrant vessels can be visualised. It is frequently pos-

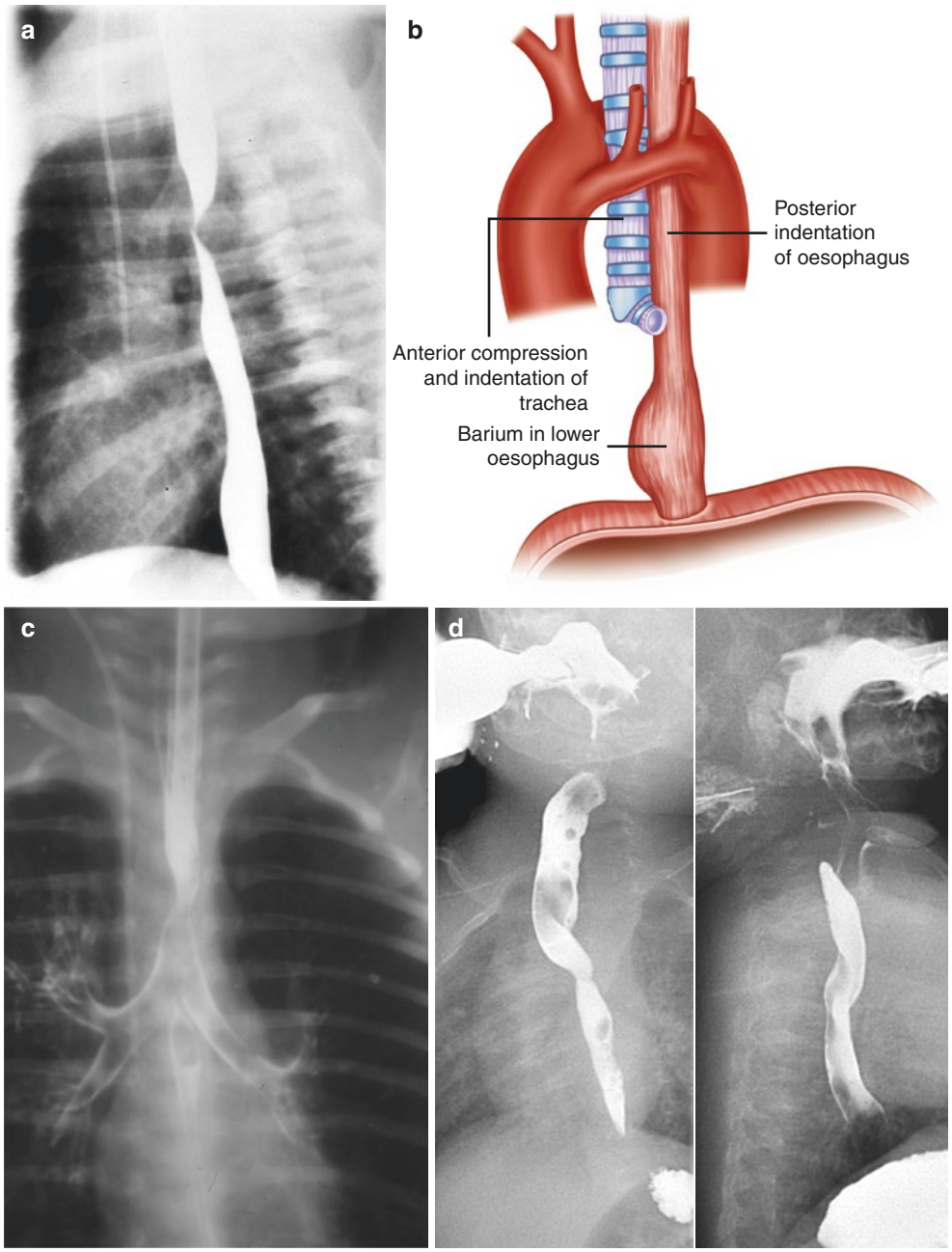

Fig. 3.5 (**a**) Vascular ring. (**b**) Diagram of vascular ring. (**c**) Vascular ring surrounding lower trachea. (**d**) Vascular ring with contrast

sible to identify the precise anomaly by this technique. Tracheobronchoscopy and further investigations by digital subtraction angiograph will better define the pathology.

3.2.6 Cystic Fibrosis (Fig. 3.6)

Cystic fibrosis of the pancreas is so named because it was first thought to be primarily a pancreatic disorder. It is now known that the primary defect is in a transmembrane protein of chloride ion channels of all body exocrine glands including sweat, intestinal, mucous and salivary glands, and liver. The gene that codes for this protein is located on chromosome 7, and the most common of the more than 400 so far described is at the ΔF 508 locus and accounts for about 74% of cases in Caucasians. Transmission of the autosomal recessive gene defects results in an incidence of 1 in 2000 in Caucasian and 1 in 90,000 in Oriental live births.

Although the gene defect is present in all nucleated body cells, it is only in those cells where the gene needs to be activated for normal cell function that abnormalities are recognised. It is not surprising, given the range of gene defects, that the disease has variable clinical manifestations. The pancreas is abnormal in more than 90% of the cases. A constant change is fibrosis with atrophy of the exocrine parenchyma. Cystic dilatation of acini and ducts is common but not invariable. Islet tissue, however, is rarely involved until later childhood or adolescence. Mucous glands throughout the body are grossly distended and they secrete an abnormal viscid mucus. Stagnation of mucus in the smaller bronchioles usually leads to infection, which in turn stimulates further mucus secretion. Infected sticky secretions spread throughout the bronchial tree leading to a chronic obstructive suppurative lung disease. The liver shows a focal type of biliary cirrhosis, most marked under the capsule, which may progress to produce portal hypertension.

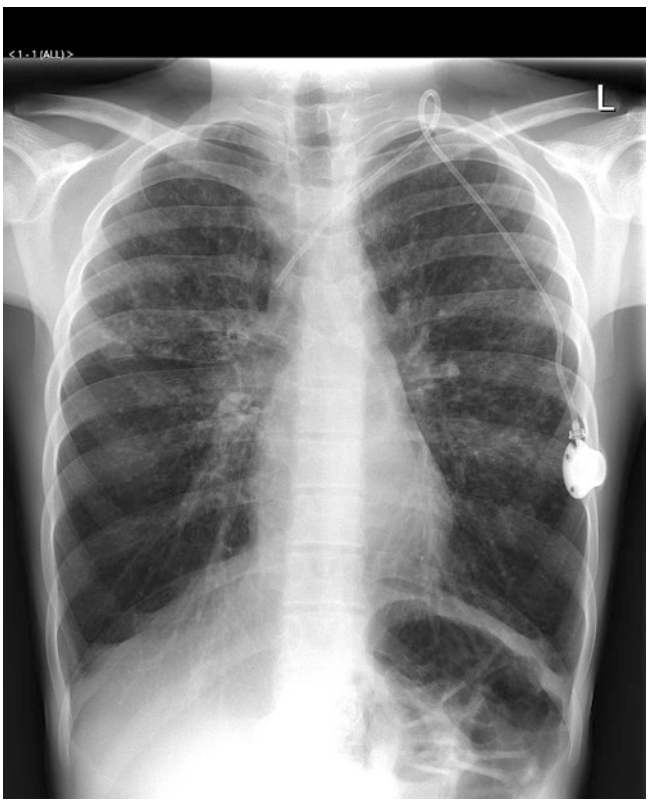

Fig. 3.6 Bronchiectasis in cystic fibrosis patient

The symptoms tend to occur in a more or less ordered fashion and the diagnosis is not often unduly difficult. In about 10% of patients the illness presents in the neonatal period in the form of meconium ileus in which inspissated meconium causes intestinal obstruction. The most common presentation, however, is in the form of an intractable respiratory infection dating from the early weeks or months of life. Indeed, cystic fibrosis of the pancreas should always be suspected when a respiratory infection in infancy fails to respond promptly to adequate antibiotic therapy. In the early stages of the disease, radiographs of the chest may show only increased translucency of the lung fields; later heavy interstitial markings appear; then multiple soft shadows representing small lung abscesses. In other cases, there may be lobar consolidation, empyema, or pyoneumothorax. In children who survive the early months of life, the respiratory picture may become that of bronchiectasis, increasing emphysema, and clubbing of the fingers. Sputum culture in such cases will most often show the predominant organism to be the staphylococcus aureus and pseudomonas aeruginosa. The frequency of pulmonary colonisation with Pseudomonas cepacia in adults with cystic fibrosis has recently increased and has been correlated with increased morbidity and mortality rates. Pulmonary colonisation by Pseudomonas cepacia is generally refractory to antibiotic treatment, and sensible precautions, such as avoiding contacts between Pseudomonas cepacia-colonised CF individuals and non-colonised children, should be taken.

In a minority of cases the respiratory infection is less prominent than the presence of semi-formed, greasy, bulky, and excessively foul-smelling stools. These features coincide with the introduction of mixed feeding. After the first year of life, the history of abnormal and frequent stools occurring in association with abdominal distension and generalised tissue-wasting may simulate coeliac disease. The differential diagnosis, however, can almost always be made on clinical grounds alone. In cystic fibrosis, a careful history will elicit that signs first appeared in the early weeks of life, whereas coeliac disease rarely presents before the age of 6 months. The excellent, often voracious appetite in a child with cystic fibrosis contrasts sharply with the unhappy anorexia of the coeliac child. Chronic respiratory infection of some degree, often severe, is an invariable accompaniment of cystic fibro-

sis, but it is not a feature of coeliac disease. Furthermore, the diagnosis of cystic fibrosis may be suggested by a history that previous siblings have the disease.

If the affected infant survives the first year, childhood often seems to bring a period of improvement in the chest condition. All too frequently, however, the approach to puberty is associated with corpulmonale. Less commonly, in about 10% during the second decade, biliary cirrhosis and portal hypertension develop, and may lead to massive gastrointestinal haemorrhage. In recent years, as an increasing proportion of sufferers from cystic fibrosis survive, insulin-dependent diabetes mellitus has been found in some as they approach puberty. A feature of these cases has been the absence of marked ketoacidosis. A further important manifestation, which seems to present in a majority of males who survive into adulthood, is aspermia and sterility. This has been shown to be due to absence of the vas deferens. Women have only slightly reduced fertility, associated with abnormal tubal ciliary movement and cervical mucus.

Some children with cystic fibrosis can develop distal small bowel obstruction. In this disorder, viscid mucofaeculent material obstructs the bowel and causes recurring episodes of abdominal pain, constipation, and acute or subacute intestinal obstruction. The cardinal sign is a soft, mobile, non-tender mass palpable in the right iliac fossa.

In the new-born infant destined to later develop the manifestations of cystic fibrosis, there is a markedly raised albumin content in the meconium. A simple test strip impregnated with a suitable reagent is available to detect an albumin level in meconium in excess of 20 mg/g (BM test Meconium: Boehringer). This method is not sufficiently reliable to serve as a screening test for cystic fibrosis. In neonates, there is a reliable method of screening, which is based on the serum concentration of immunoreactive trypsin (IRT). Serum IRT levels are abnormally high (>80 ng/ml) during the first few months of life, although in older children they fall to subnormal values. Screening for common gene defects using DNA probes for the more common gene defects can now be used for prenatal diagnosis, for carrier detection, and for help in diagnosis. Heterozygote identification from DNA analysis on buccal cells obtained by a mouth wash can help to determine whether a couple are at risk of having an affected fetus. Knowledge of the underlying gene defect in the affected child might help guide subsequent gene therapy. Prenatal diagnosis by chorionic villus biopsy obtained at 9–12 weeks post-conception will allow termination of an affected fetus.

3.2.7 Cystic Pulmonary Adenomatoid Malformation

Cystic pulmonary adenomatoid malformation (CPAM) may be a single or multicystic mass in pulmonary tissue in which there is a proliferation of bronchial structures at the expense of alveoli. The cysts are lined by cuboidal or columnar epithelium, which may appear to be of alimentary tract origin. The disease is considered a focal pulmonary dysplasia, or some prefer to designate it a hamartoma. In some cases, there is skeletal muscle in the cyst walls. The abnormality more often affects the lower lobes and is detected on X-ray of an infant with respiratory distress (Fig. 3.7).

3.2.8 Congenital Lobar Emphysema, Bronchogenic Cyst, Pulmonary Cyst

Congenital lobar emphysema (CLE), a postnatal overdistension of one or more lobes of a histologically normal lung, is thought to result from cartilaginous deficiency in the bronchial tree. The left upper lobe is the one usually affected; it expands across the superior mediastinum and compresses the left lower lobe, causing the infant increasing respiratory distress. Treatment of the disorder when the baby is severely compromised is lobectomy. Less severely affected infants may be helped by maintained positive airway pressure until the bronchi stabilise and gas exchange can occur freely (Fig. 3.8a–e).

3.2.8.1 Bronchogenic Cyst

Bronchogenic cyst is a discrete cyst of non-functioning pulmonary tissue, the cysts being lined by ciliated columnar epithelium and often including smooth muscle, glands, and cartilage. There is no communication with the tracheo-bronchial tree, and symptoms may be caused by pressure on the trachea or bronchi. X-ray shows a soft tissue swelling, which can be better visualised by CT scan. Treatment is excision and is usually a simple procedure (Fig. 3.8f–h).

3.2.8.2 Pulmonary Cyst

A pulmonary cyst occurs in the lung tissue parenchyma, and if it is infected or contains blood as a result of haemorrhage it can be a space-occupying lesion and cause pressure symptoms. A fluid level may be seen on a plain X-ray. This can be a solitary cyst or part of a cystic disease that can affect other parts of the lung, liver, pancreas, or kidney (Fig. 3.8i).

3.2.9 Sequestration of the Lung (Fig. 3.9)

Pulmonary sequestration of the lung may be intralobar, extralobar, or complete, depending upon whether the segment of lung tissue that has no communication with the main bronchial tree is within a lobe of the lung, is outside the lung although still attached to it, or is completely sep-

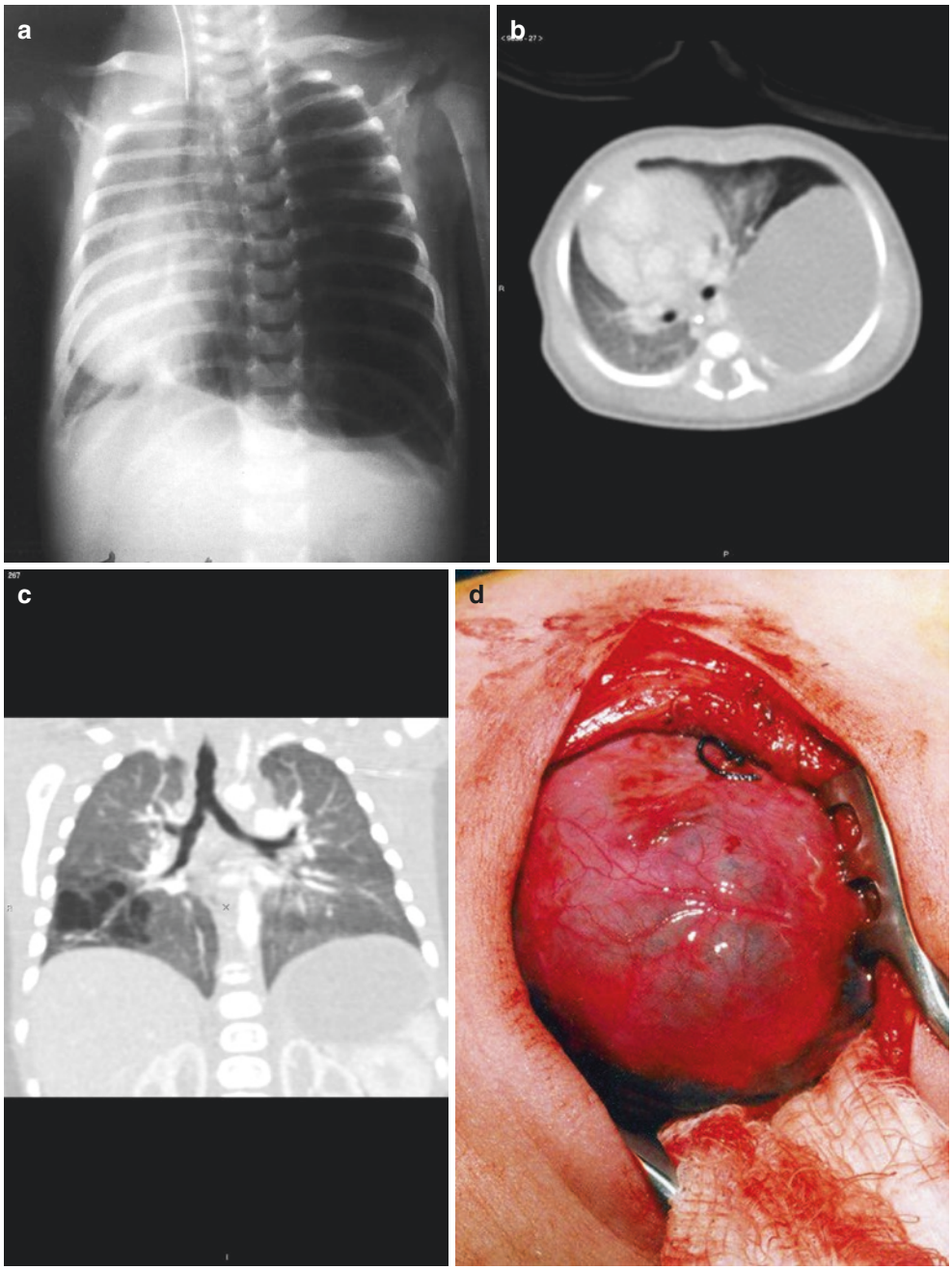

Fig. 3.7 (**a**) Operative photograph of CPAM. (**b**) CPAM type 3. (**c**) Cystic Pulmonary Adenomatoid Malformation CPAM CT scan. (**d**) Operative photograph of CPAM

arated from the lung. In the case of the extralobar and complete types of sequestration, the arterial blood supply is from the aorta and the venous return to the hemiazygous vein, whereas in the intralobar variety there may be a pulmonary artery supply with venous return by a pulmonary vein. The extralobar and complete sequestrations are most often on the left side, sometimes in association with a diaphragmatic hernia. Radiographic interpretation may be difficult without bronchography to demonstrate the absence of communication with the bronchial tree, and barium studies should demonstrate communication to the oesophagus or stomach. Symptoms occur only if infection is superimposed.

3.2.10 Congenital Diaphragmatic Hernia of Bochdalek (Fig. 3.10a, b)

The primitive, pleural, and peritoneal spaces communicate freely through the pleuro-peritoneal canal. Between the 8th and the 10th weeks these canals are obliterated by fusion of the dorsal pleuro-peritoneal membrane with the ventral septum transversum. Failure of closure of the pleuro-peritoneal can result in the congenital diaphragmatic hernia (CDH) of Bochdalek, commonly left-sided. During this process the bowel, returning to the abdomen, finds its way, together with the liver, into the chest and is partly responsible for the poor development of the lung, with consequent pulmonary hypoplasia.

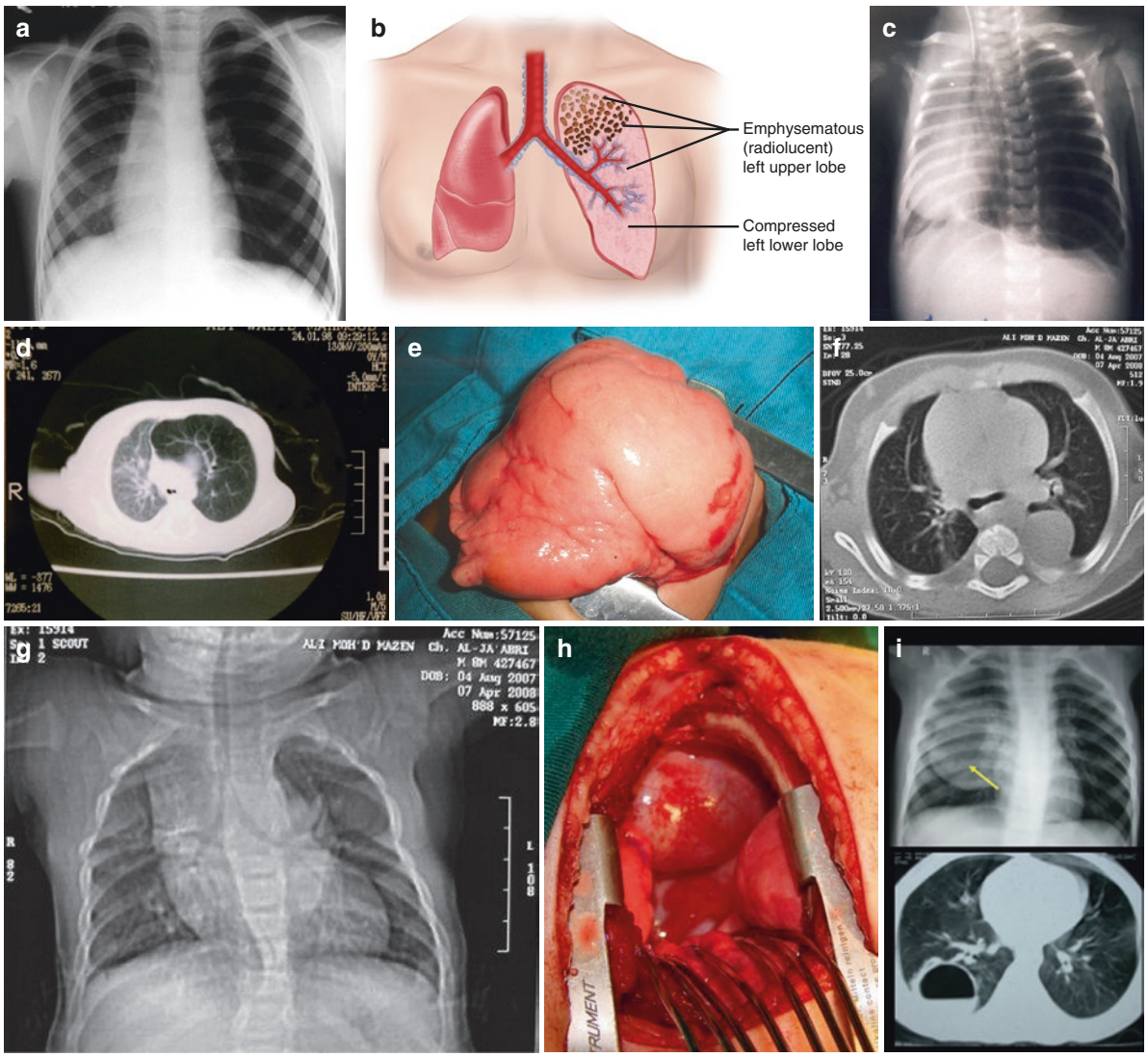

Fig. 3.8 (**a**) Congenital lobar emphysema. (**b**) Congenital lobar emphysema diagram. (**c**) Congenital lobar emphysema with mediastinal shift. (**d**) CT scan cross section of chest in congenital lobar emphysema. (**e**) Congenital lobar emphysema, operative view. (**f**) Bronchogenic cyst extrapulmonary. (**g**) Bronchogenic cyst extrapulmonary. (**h**) Bronchogenic cyst extrapulmonary. (**i**) Lung cyst

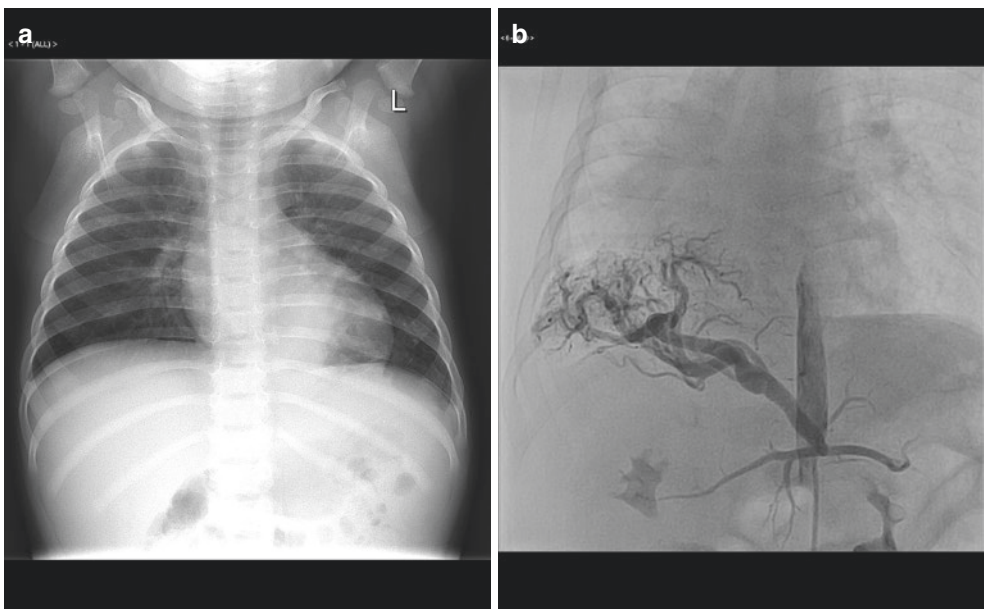

Fig. 3.9 (**a**) Sequestration of the lung. (**b**) Sequestration of the lung with vascular imaging arising from below the diaphragm

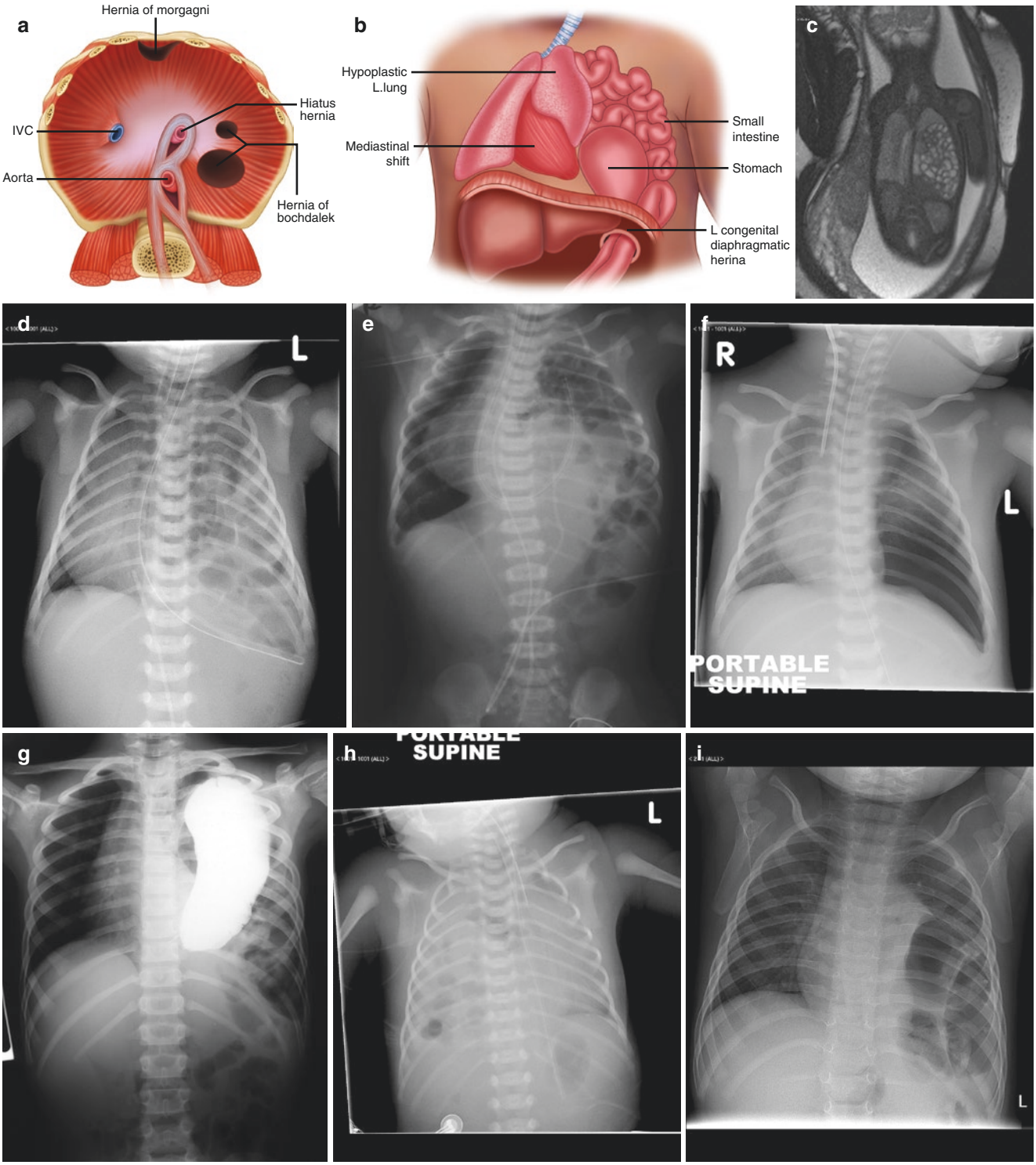

Fig. 3.10 (**a**) Diagram of the diaphragm with orifices for hernia formation. Types of hernia of the diaphragm. (**b**) Diaphragmatic hernia diagram. (**c**) Antenatal MRI scan showing congenital diaphragmatic hernia. (**d**) CDH with nasogastric tube in stomach in the abdomen. (**e**) CDH with stomach lying in the chest note position of NG tube. (**f**) CDH post repair showing hypoplastic left lung and pneumothorax beneath. (**g**) Diaphragmatic hernia barium contrast showing stomach in the chest. (**h**) Right sided CDH. (**i**) Recurrent CDH after a failed repair. Diaphragmatic hernia barium contrast showing stomach in the chest

In pulmonary hypoplasia, there is a low ratio of lung weight to body weight. The severity of pulmonary hypoplasia is a major factor inthe survival of neonates with congenital diaphragmatic hernia. In a series of 13 babies with congenital diaphragmatic hernia who died, the ipselateral lung weighed 3.7 g, while the contralateral lung weighed 13.3 g. A normal lung of the new-born should weigh 35 g. Histologically, the developmental arrest appears to occur between 10 and 12 weeks in a left-sided congenital hernia, whereas it is a little later, 12–14 weeks, in right-sided congenital diaphragmatic hernia.

Within hours of birth, the infant develops respiratory distress, which worsens as air enters the bowel lying in the chest. If left alone, this progresses to death from mediastinal compression and cardiac tamponade. Physical examination reveals a tachypnoeic, tachycardiac, cyanotic mottled baby with a bow-shaped chest and a scaphoid abdomen (Fig. 3.10c, d).

The trachea will be deviated to the side opposite the hernia and the apex beat will be displaced. The clinical findings may be confused with those of dextrocardia in a left sided hernia (Fig. 3.10e, f).

Investigation should include an X-ray comprising all the chest and abdomen. Gas-filled loops of bowel are seen in the chest (Fig. 3.10g–i).

3.2.11 Retrosternal Hernia (Morgagni)

Retrosternal hernia is an anteriorly placed hernia, with the defect between the sternal and costal attachments of the diaphragm (Fig. 3.11a, b). The transverse colon is the most commonly seen content of this hernia, which can be the cause of intestinal obstruction or even respiratory symptoms due to compression of the chest contents (Fig. 3.11c–e).

3.2.12 Hiatus Hernia (Gastro-oesophageal Reflux)

Vomiting in some infants becomes more troublesome than the mouthful of regurgitation, which is commonplace. This may be due to gastro-oesophageal reflux, which occurs more frequently and more easily in the infant who has a transverse oval abdominal cavity, as compared to the adult vertical oval abdominal cavity; a consequence is altered angulation between the oesophagus and stomach. Although apparently large amounts of vomit may be produced, if the infant continues to gain weight satisfactorily, there is no reason for major concern. When persistent, treatment with thickened feeds and the addition of Gaviscon therapy may help (Fig. 3.12a).

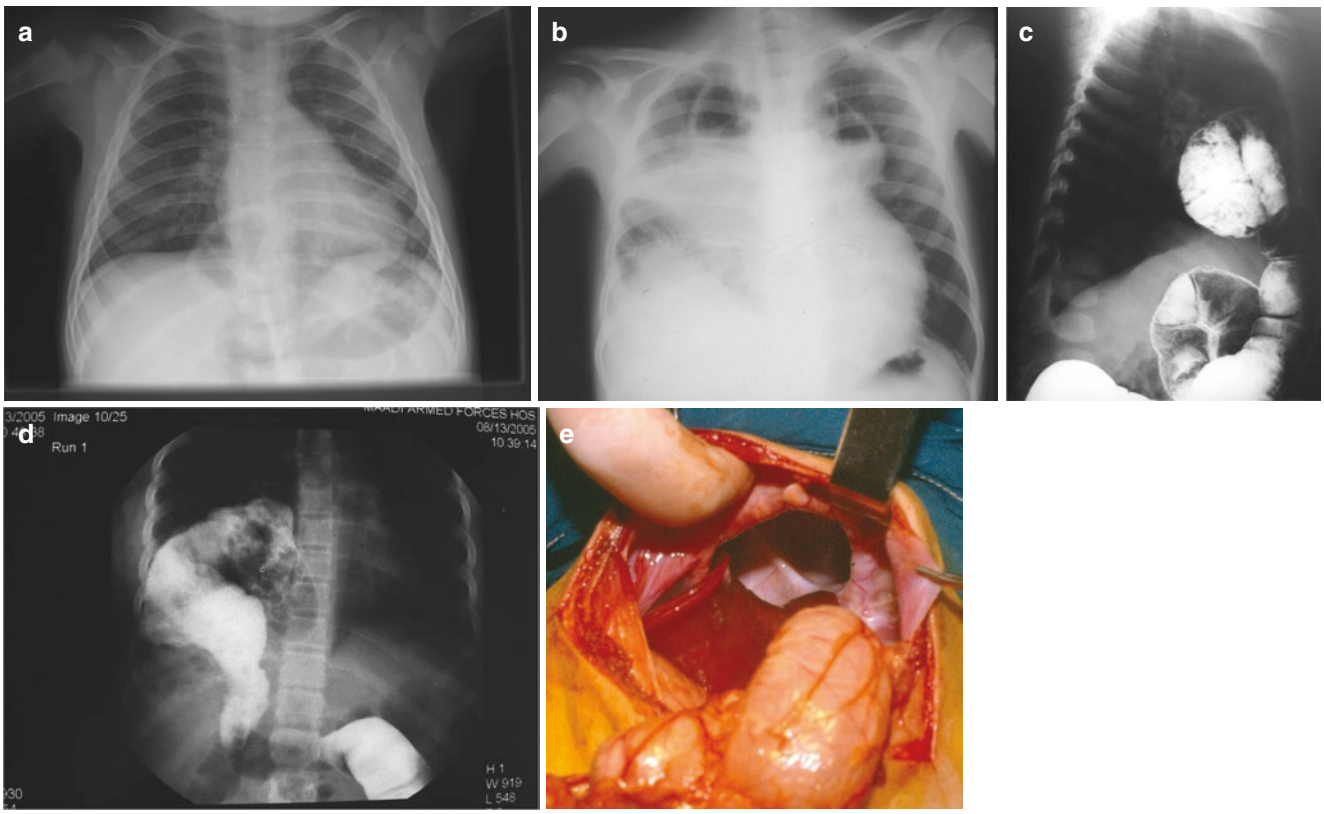

Fig. 3.11 (**a**, **b**) Morgagni. (**c**) Morgagni hernia Barium enema. (**d**) Morgagni. (**e**) Morgagni hernia reduced colon

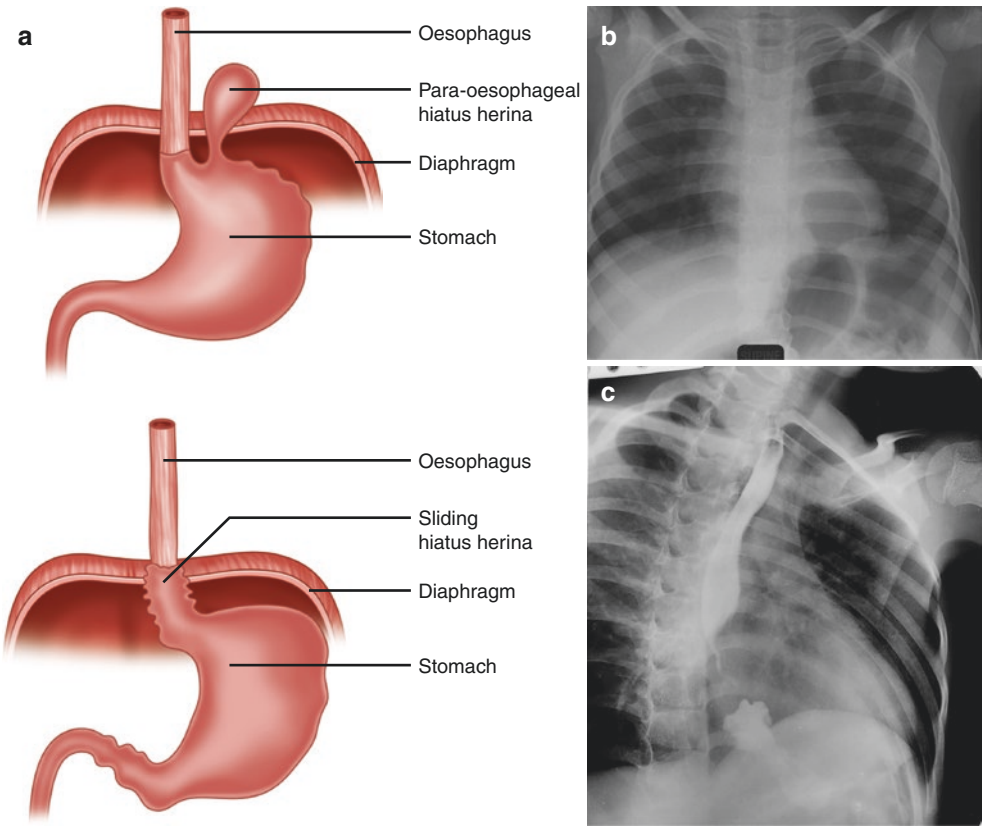

Fig. 3.12 (**a**) Para oesophageal hernia diagram. (**b**) Hiatus hernia with gas in the fundus of the stomach lying in the chest. (**c**) Hiatus hernia with GOR with an oesohagitis and a long oesophageal stricture

When X-ray demonstrates a para-oesophageal hernia, an earlier operation is indicated because spontaneous cure is unlikely. In contrast, 80% of cases of sliding hiatus hernia of infancy cure spontaneously. A small sliding hiatus hernia is a common phenomenon in infants. The majority of these infants do not have significant symptoms but continue to thrive satisfactorily. Sliding oesophageal hiatus hernia occurs when the cardia and the fundus of the stomach rise into the thorax through a loose hiatus, giving the illusion of a congenitally short oesophagus (Fig. 3.12b).

A para-oesophageal hernia is associated with an oesophagus of normal length. The cardia is still in the abdomen, but part of the fundus of the stomach prolapses alongside the oesophagus. Both types produce vomiting, which can predispose to "asthma" attacks, haematemesis, failure to thrive, regurgitation, rumination syndromes, and athetoid neck movements (Sandifer's syndrome), all of which are associated with severe gastro-oesophageal reflux. Where symptoms and signs persist, fundoplication is performed for the sliding hiatus hernia. The para-oesophageal hernia does not have the 80% spontaneous cure rate of the sliding hiatus hernia and requires an operation to reduce the hernial content to the abdominal cavity and repair the defect in the hiatus. Investigations should include a barium swallow and a meal specifically for reflux, flexible oesophagoscopy, and pH monitoring (Fig. 3.12c).

The Barret oesophagus, where there is a presence of ectopic gastric mucosa in the oesophagus, is a particularly difficult problem to treat in childhood. The use of antacids and other drugs such as Cimetidine, Cisapride, and Gaviscon all play a part in the symptomatic management of this condition. The long-term results of a Barret oesophagus are difficult to assess because of reports that have described areas of dysplasia in the ectopic mucosa, which could give rise to malignancy in long-term follow-up. These patients have to be kept under surveillance and have endoscopy and biopsies carried out on a regular basis.

3.2.13 Oesophageal Web (Fig. 3.13)

As a congenital anomaly, oesophageal web can present as an obstruction to swallowing and can be part of the spectrum of oesophageal atresia. If the web is incomplete, then it could present as a stenosis of the oesophagus. Occasionally Ectopic tissue, which may have pancreatic tissue or even respiratory and cartilaginous rings, is occasionally found upon excision.

3.2.14 Oesophageal Diverticulum (Fig. 3.14)

Oesophageal diverticulum can be congenital or can follow a repair of an oesophageal atresia. It can also be caused by ingestion of a foreign body, oesophagitis, or even traumatic instrumentation injury. If large, it can hold secretions and food and cause vomiting and obstruction.

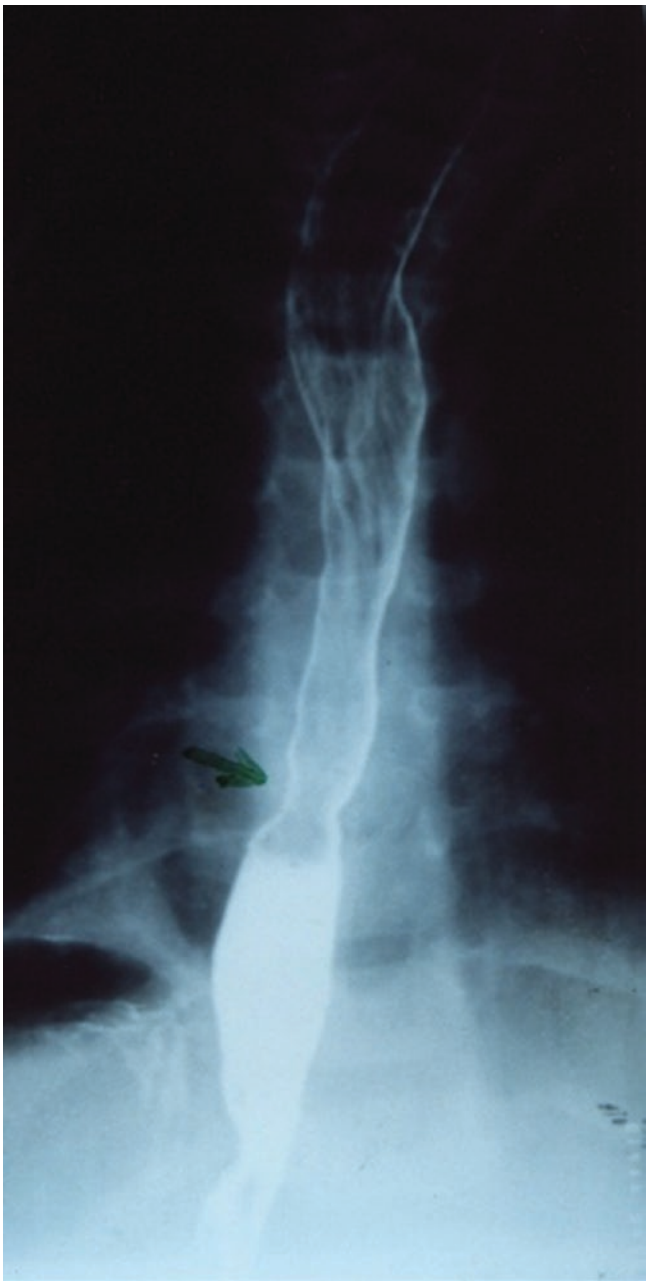

Fig. 3.13 Congenital oesophageal web

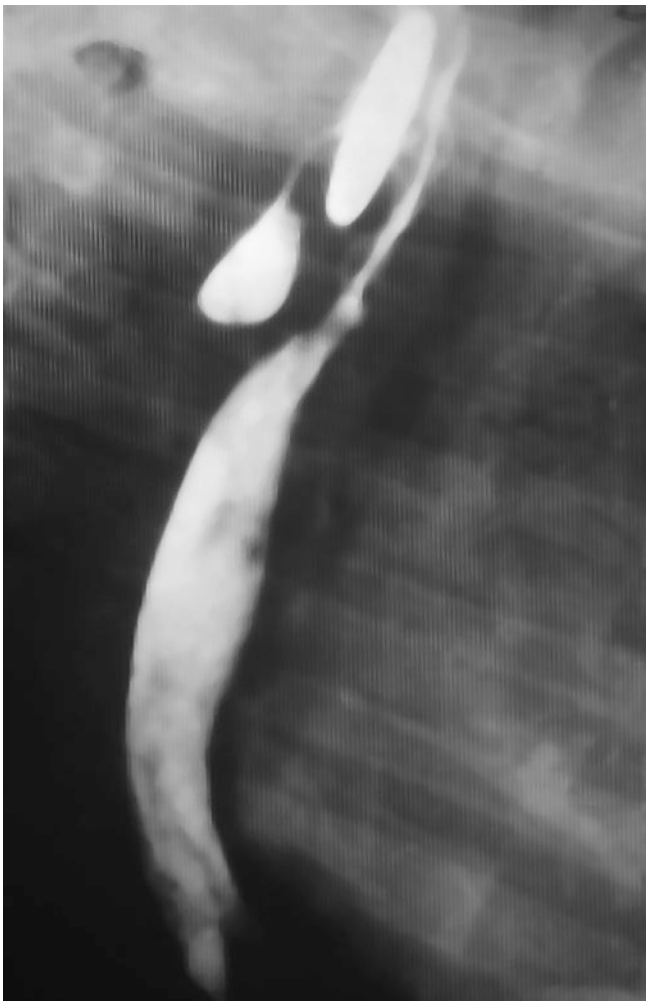

Fig. 3.14 Oesophageal/tracheal diverticulum after a leak from a TOF repair

3.2.15 Cardiac Anomalies

Developmental abnormalities of the cardiovascular system come a close second in terms of frequency to those of the nervous system. Remarkable though surgical advances in the correction of cardiac anomalies have been in recent years, it must be realised that some cases are still inoperable. The main efforts of the paediatric cardiologist and surgeon are now directed towards the malformations that so often cause death during early infancy. The marked fall in the incidence of rheumatic fever in the more prosperous countries has now resulted in congenital heart disease causing more morbidity than rheumatic heart disease.

The aetiological factors in congenital heart disease are only vaguely perceived at the present time. However, they may be divided into four causative categories: (1) environmental, (2) chromosomal, (3) genetic, and (4) multifactorial. It is known that certain environmental factors operating in early pregnancy can result in malformations, e.g., rubella embryopathy, heavy consumption of alcohol, maternal diabetes, phenylketonuria, and systemic lupus erythematosus. In most cases, however, no specific cause can be detected. Genetic influences seem not to be of great importance, although the relatives of affected children are more often similarly abnormal than would be expected to occur by chance. The risk that a sibling of an index patient also has congenital heart disease is of the order of 1 in 50, against a frequency of about 1 in 100 in the community at large. There are, however, single families in which the risk is much greater. In addition, cardiac malformations are

well recognised to frequently accompany several syndromes, e.g., trisomy 21 (atrioventricular septal defect, ventricular septal defect, atrial septal defect, tetralogy of Fallot), trisomy 18 (ventricular septal defect, patent ductus arteriosus, double outlet right ventricle, single umbilical artery), trisomy B (ventricular septal defect, atrial septal defect, dextrocardia, single umbilical artery), 45 XO Turner's syndrome (coarctation of the aorta, aortic stenosis), Noonan's syndrome (pulmonary stenosis, hypertrophic cardiomyopathy), Marfan's syndrome (defects of the aorta), polydactyly (ventricular septal defects), and triphalangeal thumbs (arterial septal defects in the Holt-Oram syndrome).

No classification of congenital heart disease is entirely satisfactory. It is convenient to subdivide the malformation into those that cause central cyanosis due to shunting of blood from the right to the left side of the heart, and those in which cyanosis is absent. The separation is not absolute. Less severe forms of anomalies such as Fallot's tetralogy may not cause cyanosis during the early months of life. Children with anomalies such as patent ductus arteriosus or ventricular septal defect, where there is a left to right shunt, may later develop cyanosis if pulmonary hypertension causes a reversal of the shunt through the defect. In every child with central cyanosis, care must be taken to avoid making a diagnosis of congenital heart disease in the rare case of congenital methaemoglobinaemia. The possible combinations and variations of cardiac malformations are so numerous that precise diagnosis frequently demands an extremely high standard of clinical expertise, plus skilled investigations.

Improvements in ultrasound techniques over the last decade have led to a steady increase in the use of these risk-free non-invasive methods and a decrease in the need for diagnostic cardiac catheterisation and angiocardiography which, being invasive, do carry some risk. With two-dimensional echocardiography providing detailed anatomical data and m-mode adding functional information, together with the addition of Doppler ultrasound to assess valvular function and colour-flow Doppler giving detail of flow direction and velocity, the cardiologist is in most cases able to make an accurate assessment of the nature and severity of complex lesions and plan management. The value of risk-free echocardiography in the sick new-born need not be emphasised.

Ultrasound techniques, however, have not rendered cardiac catheterisation and angiocardiography obsolete, and they are sometimes essential. Interestingly, as their need in diagnosis has lessened, they are acquiring an increasing role in the interventional manoeuvres that allow some lesions to be treated without recourse to conventional surgery. Balloon atrioseptostomy is long established in the palliation of certain cyanotic lesions, particularly transposition of the great arteries. Balloon dilatation of pulmonary valve stenosis is now the preferred treatment for that lesion, and the technique may be applied to aortic valve stenosis and coarctation of the aorta. Devices to occlude the ductus arteriosus at catheterisation are increasingly employed, and similar devices to close atrial and ventricular septal defects are being developed. Stenting of stenosed pulmonary and other vessels is now possible by catheter techniques.

3.2.15.1 Cyanotic Congenital Heart Disease

3.2.15.1.1 Transposition of the Great Arteries (Fig. 3.15a)

This is the most common type of cyanotic congenital heart disease presenting in the neonatal period. Boys are affected 2–3 times more than girls. No definite aetiological factors have been identified. Emergency palliative treatment is frequently required to save the infant's life.

The aorta arises from the right ventricle and the pulmonary artery from the left ventricle. The venae cavae and the pulmonary veins drain normally to the right and left atria respectively. Thus, the fundamental physiological derangement in complete transposition is that the systemic and pulmonary circulations are separate. This causes few if any problems in the fetus because the entire venous return is normally distributed through the right atrium and ductus venosus. After birth there is a major problem with functional closure of the ductus venosus and arteriosus so that oxygenated pulmonary venous blood is unable to reach the systemic circuit and the systemic venous return cannot reach the lungs for oxygenation. This results in severe systemic arterial desaturation. In transposition of the great arteries, unless there is a coexisting shunt at atrial or ventricular level or through the ductus arteriosus, life cannot be sustained.

Affected infants fail to thrive and are usually markedly cyanosed from birth. Dyspnoea may be present at rest with subcostal recession, and it is more obvious during feeds. Finger clubbing may develop early in life. The precordium is seen to be prominent and palpation reveals the notable left parasternal impulse of right ventricular hypertrophy. Thrills are absent. There may be no murmurs, but a loud systolic murmur may be heard best at the left lower sternal border. The pulmonary second sound is not remarkable. Cardiac enlargement of gross degree develops rapidly, and infants develop congestive cardiac failure. The characteristic cardiac silhouette in posterio-anterior radiographs shows an enlarged heart with a narrow supracardiac shadow, rather like an egg lying on its side. Lung vascularity may be increased. The crucial initial investigation in infants with cyanosis is the demonstration by arterial blood gas analysis of systemic

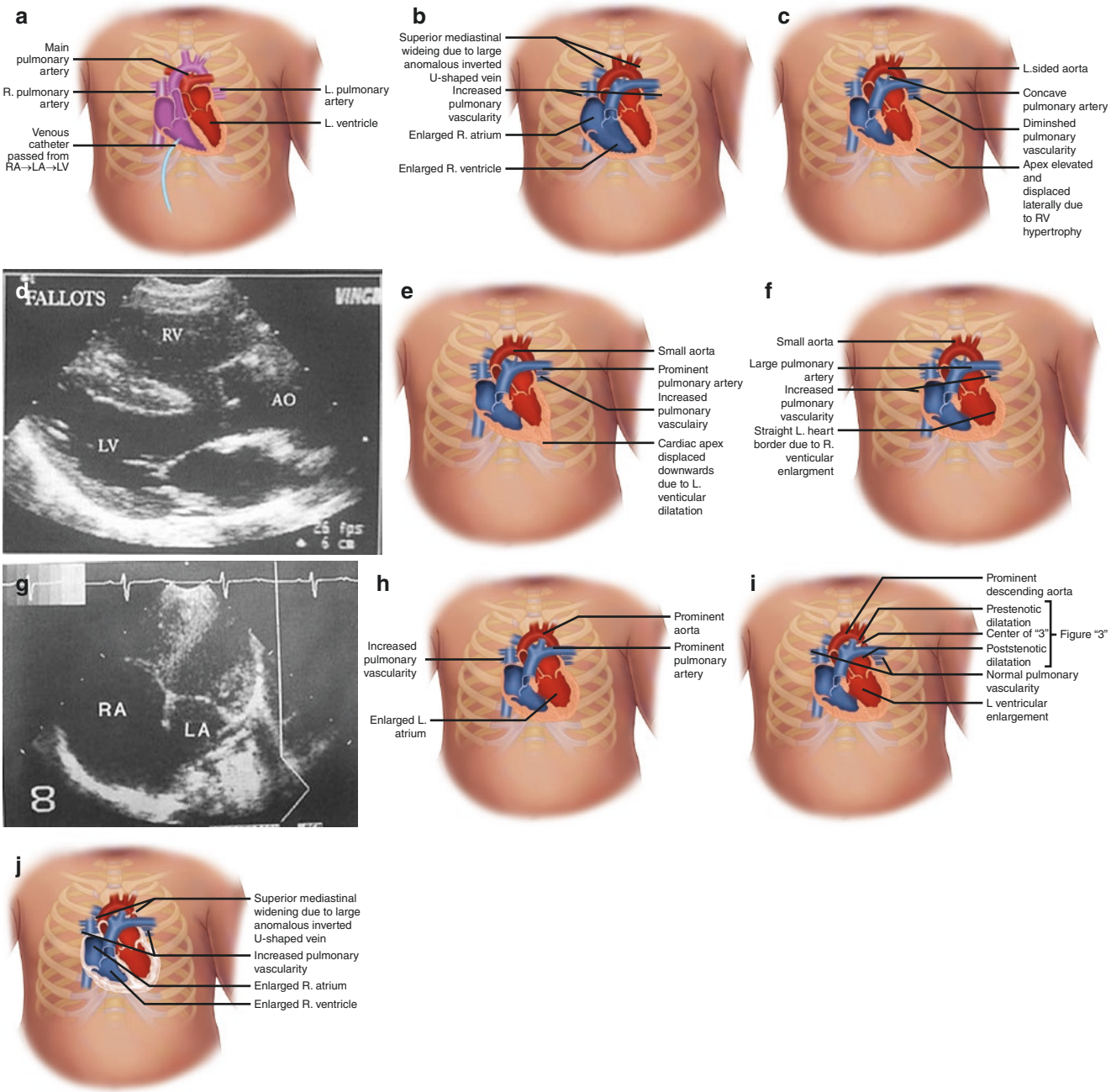

Fig. 3.15 (**a**) Transposition of the great arteries. (**b**) TAPVD 1. (**c**) Tetralogy of Fallot Chest X-ray. Transposition of the great arteries. (**d**) Two-dimensional echocardiogram of tetralogy of Fallot. The right and left ventricle are separated. (**e**) Chest X ray of ventricular septal defect. (**f**) ASD. (**g**) Two-dimensional echocardiogram of ASD. (**h**) Patent ductus arteriosus scan. (**i**) Coarctation of the aorta "Figure 3 sign". (**j**) Pericardial effusion

arterial hypoxaemia. In those infants without major intercirculatory mixing, the arterial PO_2 is in the range of 12–25 mmHg and even with associated ameliorating shunts the PO_2 rarely exceeds 40–50 mmHg.

The electrocardiogram shows right axis deviation with right ventricular or biventricular hypertrophy, and there may be a P pulmonale. Real-time echocardiography will reveal the aorta arising from the right ventricle and the pulmonary artery from the left. Cardiac catheterization will reveal that the catheter leaves the right ventricle by the aorta. The pulmonary artery blood has an oxygen concentration above that in the aorta. Various other shunts can be demonstrated according to their site.

Most infants go into cardiac failure in the early months of life with increasing dyspnoea, cyanosis, cardiomegaly, and hepatomegaly. This is frequently precipitated by intercurrent

respiratory infection. If untreated, 90% of children with complete transposition die by 1 year of age, and 95% by 5 years of age.

3.2.15.1.2 Total Anomalous Pulmonary Venous Drainage (Fig. 3.15b)

All the pulmonary veins, as well as the venae cavae, enter the right atrium. There must, of course, be an atrial septal defect for life to continue at all. There are several possible anatomical variations. Most commonly, the pulmonary veins form a common vessel that empties into a persisting left superior vena cava, less often into the right superior vena cava. The pulmonary veins may also unite to form a common trunk that drains directly into the right atrium or into the coronary sinus. Rarely, the pulmonary veins drain beneath the diaphragm into the inferior vena cava, or even into the portal vein.

These infants fail to thrive, are cyanotic, and become dyspnoeic on slight exertion. They are extremely prone to respiratory infections. Cardiac pulsation is forceful over the left parasternal area, that is, over the right ventricle and its outflow tract. The precordium may bulge. Auscultation often reveals triple or quadruple rhythm, and there is usually a blowing systolic murmur. The electrocardiograph shows right axis deviation, severe right ventricular hypertrophy, and a P pulmonale. Radiographs show right atrial and right ventricular enlargement with pleonaemic lungs. In the common type of anomaly with a persisting left superior vena cava, the supracardiac shadow is very broad, giving rise to the so-called "cottage-loaf," "Figure-of-eight," or "snowman" heart. Echocardiography will usually confirm the diagnosis. Cardiac catheterisation reveals the same oxygen concentration in the right atrium, right ventricle, pulmonary artery, and femoral artery; the pressures in the right ventricle and pulmonary artery are above normal. The diagnosis can also be confirmed by selective angiocardiography when opaque medium is injected into the pulmonary artery and pulmonary venous return to the right atrium is demonstrated.

Most affected infants develop right heart failure early with progressive dyspnoea, cardiomegaly, and hepatomegaly.

3.2.15.1.3 Fallot's Tetralogy (Fig. 3.15c, d)

Fallot's tetralogy is the most common type of cyanotic congenital heart disease in children over the age of 1 year. Males and females are equally affected. As with many congenital cardiac anomalies, precise aetiology is unknown.

The classical tetrad consists of pulmonary stenosis (rarely atresia), ventricular septal defect with right-to-left shunt, dextroposition (or rightward deviation) of the aorta, which receives blood from both ventricles, and right ventricular hypertrophy. There are many variations, depending upon the degree and type of pulmonary stenosis, the size of the ventricular septal defect, and the degree of overriding of the aorta. In most instances the pulmonary stenosis is infundibular, there being a long, narrow separate infundibular chamber; in others, it is a valvular stenosis. In some cases, there is a right-sided aortic arch, a matter of importance to the cardiac surgeon.

Clinical presentation is dominated by the degree of right ventricular outflow tract obstruction. Cyanosis may be marked from early childhood, although it is often absent in the first few months of life. It may be quite slight in less severely disabled children. Cyanosis is associated with stunting of growth, clubbing of the fingers, and polycythaemia. Affected children usually show marked breathlessness on exertion and take frequent rests in a very characteristic squatting position. The most severely affected infants with severe pulmonary stenosis have episodes of deep cyanosis, dyspnoea, unconsciousness, and convulsions. These hypercyanotic attacks occur typically on waking in the morning, but may be precipitated by crying, defaecation, eating, exercise, and hot weather. These are accompanied by marked metabolic and respiratory acidosis due to the severe degree of hypoxia. It has been postulated that these spells are due to infundibular spasm or shutdown. It has also been demonstrated that some of the haemodynamic consequences of an increase in infundibular stenosis can be alleviated by a beta-adrenergic blocking agent. The heart is not enlarged, and the apex beat may be difficult to locate. Right ventricular pulsation, however, can be readily felt over the left parasternal area, where there is often a systolic thrill. In most cases a loud systolic murmur is heard down the left sternal border, but this may be slight or absent when pulmonary stenosis is severe. The second pulmonary sound is often quiet and may be single. The characteristic radiographic appearances show a small heart with concavity in the region of the pulmonary artery and the apex raised above the left diaphragm (coeuren sabot). The lungs are oligaemic due to diminished pulmonary blood flow. The electrocardiogram shows marked right axis deviation and right ventricular hypertrophy.

Echocardiography will confirm the diagnosis. Cardiac catheterisation reveals a high right ventricular pressure, and the presence of an infundibular chamber or a valvar stenosis can be demonstrated. The catheter may leave the right ventricle through the overriding aorta. Angiocardiography shows simultaneous filling of the pulmonary artery and the aorta. It is also associated with other anomalies such as the VACTERL anomalies.

Fallot's tetralogy is not compatible with long life, and the child's exercise capacity gets progressively more limited. Indeed, only half of the children with this anomaly survive their third birthday without surgical intervention. Severely affected infants who have hypoxic episodes require early operation to ensure survival. There is a tendency to develop brain abscess in this disease, especially

after a Blalock-Taussig shunt. It often follows a respiratory infection, but the mechanism of its production is not understood. It should be suspected whenever an affected child develops neurological manifestations. These may also be due to severe anoxia or thrombosis, e.g., sudden hemiplegia. The investigation of these complications necessitates lumbar puncture, computed axial tomography (CAT scan), or investigation by nuclear magnetic resonance (NMR) in addition to electroencephalography.

3.2.15.1.4 Tricuspid Atresia

Tricuspid atresia is a relatively rare condition, but it must be considered in the differential diagnosis of every child with cyanotic congenital heart disease. There is little sex difference in the incidence of the condition.

The basic defect is the absence of communication between the right atrium and the right ventricle, so that all blood entering the right atrium from the venae cavae must cross an atrial septal defect to mix in the left atrium with blood from the pulmonary veins. There are several variations. Most often there is a patent ductus arteriosus, which diverts some of the blood entering the aorta from the left ventricle into the lungs. In some cases, there are ventricular septal defects allowing some blood from the left ventricle to enter the undeveloped right ventricle; in these cases, the great vessels are transposed, and there is then always a large ventricular septal defect. The pulmonary valve which, in such cases, forms the exit from the left ventricle, may or may not be narrowed. Thus, in all cases of tricuspid atresia there is complete systemic and pulmonary venous admixture. If there is substantial pulmonary blood flow, cyanosis may be slight.

As a rule, cyanosis is marked from birth with dyspnoea on feeding, failure to thrive, and early clubbing of the digits. Anoxic attacks of unconsciousness may occur. The heart is frequently but little enlarged, and the pulsation often felt in the left parasternal region arises from the left ventricle. There is a loud systolic murmur at the left sternal border. The second pulmonary sound may be quiet and single. The cardiac contour on radiographs may simulate that seen in Fallot's tetralogy, but oblique films will reveal underdevelopment of the right ventricle. An important diagnostic clue is to be found in the electrocardiogram, which shows left axis deviation and left ventricular hypertrophy. This may be associated with a P pulmonale due to high pressure in the right atrium. Echocardiography will confirm the diagnosis.

The overall prognosis without treatment for patients with tricuspid atresia is poor. Few affected infants survive for more than 1 year. Cardiac failure occurs with progressive dyspnoea, hepatomegaly, and oedema.

3.2.15.1.5 Other Types of Cyanotic Congenital Heart Disease

There are numerous other types of cyanotic congenital heart disease, but each occurs only infrequently. In **single ventricle**, the child is underdeveloped and unduly dyspnoeic. Cyanosis is variable in degree. Cardiomegaly is gross. A systolic thrill and murmur are found, sometimes also a mid-diastolic murmur. The electrocardiogram may show a left ventricular hypertrophy pattern. This difficult diagnosis has been rendered easier by echocardiography, which reveals only one A-V valve, one large ventricular chamber, and one diminutive one.

In **persistent truncus arteriosus**, a common arterial trunk drains both ventricles, thus giving origin to the systemic pulmonary and coronary circulations. Pulmonary arteries may arise from the common truncus or the blood flow to the lungs may depend entirely on the bronchial arteries, so that the degree of oxygen unsaturation is very variable. There may also be pulmonary hypertension in some patients. The presenting clinical features are therefore largely dependent on the volume of pulmonary blood flow and the presence or absence of associated significant truncal valve insufficiency. Thus, cyanosis may be severe or slight. Cardiomegaly is marked. A systolic or continuous murmur may be found. The second pulmonary sound is single. The chest X-ray may show absence of a pulmonary conus but a large aortic shadow, which can be seen by echocardiography. The electrocardiogram shows left ventricular or biventricular hypertrophy. Precise diagnosis in these anomalies is often possible without cardiac catheterisation or angiocardiography, although the use of cross-sectional sector echocardiography and colour Doppler has greatly increased the ability to make the diagnosis of truncus non-invasively.

In **Ebstein's malformation**, the posterior and septal cusps of the tricuspid valve arise from the wall of the right ventricle near the apex so that part of the right ventricle is, in fact, incorporated within the right atrium. There is, in addition, tricuspid incompetence. It is exceedingly rare. In severe cases, symptoms occur in the first months of life. The child is dyspnoeic on exertion, cyanosed to a variable degree, and poorly developed. Death ultimately takes place from right heart failure. On examination of the child, the neck veins are distended. Auscultation reveals triple or quadruple rhythm, and there may be both presystolic and soft systolic murmurs. The radiograph shows a huge atrium and the lung fields are often oligaemic. The electrocardiogram shows a large notched P wave and some degree of right bundle branch block. These patients are subject to atrial extrasystoles and to attacks of paroxysmal tachycardia. Cardiac catheterisation is dangerous, but echocardiography will establish the diagnosis. There is no effective medical treatment for the malformation, although patients suffering symptomatic arrhythmias should benefit from appropriate drug therapy. Surgery provides the only possibility of radically ameliorating the haemodynamic problems. As with other cyanotic malformations, the spectrum of severity varies and surgical intervention may not be required for many years.

3.2.15.1.6 Acyanotic Congenital Heart Disease with Left-to-Right Shunts

Defects in the interventricular septum can occur as isolated anomalies or in association with many other defects. Undoubtedly isolated ventricular septal defect is the most common form of congenital heart disease. The pathophysiology of ventricular septal defect is determined by the size of the defect and the state of the pulmonary vascular resistance. These two features govern the direction and magnitude of flow through the defect, and thus the clinical features and symptomatology. The site of the defect within the septum has little influence, but the size of the defect is dominant. The defect may be small and relatively benign, or large and associated with a reduction in life expectancy. When the ventricular defect is large, pressures in the systemic and pulmonary circuits remain equal (as in the normal fetus) or nearly equal. This results in a very high pulmonary blood flow (pleionaemic lungs), and in some cases in the development of pulmonary vascular obstruction. In babies with large ventricular septal defects, the sudden drop in pulmonary vascular resistance that follows the first few breaths of life in the normal new-born is less marked. Subsequently, in some infants, the normal involution of the muscular media of the fetal-type pulmonary arterioles fails to occur to any extent. As life goes on, the medial and intimal changes in these arterioles may increase progressively, with growing pulmonary vascular obstruction, until the left-to-right shunt is reversed due to severe pulmonary hypertension (Eisenmenger's syndrome). The other serious complication of large ventricular septal defects is congestive cardiac failure, which usually occurs within the first 6 months of life, but almost never in the early neonatal period. Infective endocarditis may affect small as well as large ventricular septal defects, but this is not a very common complication during childhood. Surgical closure of defects does not eliminate the chance of contracting the infection. The risk can be minimised by using antibiotic prophylaxis before dental extractions or tonsillectomy.

Ventricular septal defects are rarely clinically detectable at birth, since it takes a few weeks for the pulmonary vascular resistance to fall from the high intra-uterine levels. Thus, it is rare for a ventricular septal defect to be diagnosed at routine postnatal examination on the first day of life.

3.2.15.1.7 Small Ventricular Septal Defects (Fig. 3.15e)

This child is symptomless and normally developed. The heart is normal in size and minimally enlarged. A palpable systolic thrill in the left parasternal area is associated with a harsh systolic murmur maximal at the fourth left interspace. The electrocardiogram is normal or shows slight left ventricular preponderance. Most patients seem to remain trouble-free for many years.

3.2.15.1.8 Large Ventricular Septal Defects Without Pulmonary Hypertension

The child is often underdeveloped and sooner or later develops undue dyspnoea on exertion. There is often marked susceptibility to respiratory infections. The heart is enlarged with a forceful apex beat. A systolic thrill and loud pansystolic murmur are maximal at the left sternal border at the level of the fourth interspace. Radiographs show left or biventricular enlargement and pleionaemic lungs. The electrocardiogram shows left ventricular hypertrophy. Cardiac catheterisation reveals a higher concentration of oxygen in the blood in the right ventricle than in the right atrium, and the catheter may be induced to traverse the septal defect to enter the left ventricle. In some cases, the pressures in the right ventricle and pulmonary artery may be elevated due to the large volume of blood being shunted across the defect from the powerful left ventricle. However, in this "dynamic" type of pulmonary hypertension, there is no true pulmonary vascular obstruction. Until recently the definitive diagnosis of isolated ventricular septal defect depended upon cardiac catheterisation and angiocardiography. Now the diagnosis can be made with certainty, in the majority of cases, using cross-sectional echocardiography and colour Doppler. Therefore, echocardiography is invaluable in differentiating isolated defects from more complex anomalies, and should be performed in all symptomatic infants suspected to have ventricular septal defect.

3.2.15.1.9 Large Ventricular Septal Defects with Peripheral Pulmonary Hypertension (Eisenmenger's Syndrome)

In this type of case, symptoms are usually present from early infancy: failure to thrive, dyspnoea on exertion such as feeding, and repeated respiratory infections. When the pulmonary hypertension is severe, and especially if there is some overriding of the aorta, the right-to-left shunt so occasioned may cause constant or intermittent cyanosis to be present. Cardiomegaly may not be marked, but palpation reveals not only a powerful apical thrust but also excessive pulsation over the right ventricle and its outflow tract in the left parasternal area. There is no thrill and any systolic murmur is short. The second heart sound at the pulmonary area is loud and booming and usually single. Radiographs confirm the presence of enlargement of the main pulmonary artery and hilar branches with translucent peripheral lung fields. The electrocardiogram indicates biventricular hypertrophy or right ventricular hypertrophy, and there may be tall P waves due to enlargement of both atria. Cardiac catheter studies will show high pressures in the right ventricle and in the pulmonary arteries.

The natural history of ventricular septal defects has been considerably clarified in recent years and it is now clear

how variable may be the outcome of such lesions. The majority of children with isolated ventricular septal defects live normal lives both in terms of duration and quality. Approximately 50–60% of these defects close spontaneously. This usually happens during the first 5 years of life, but spontaneous closure can occur at any age. Infants with large defects and dynamic pulmonary hypertension may die during the first 6 months of life in congestive cardiac failure with hepatomegaly, pulmonary oedema, and crepitations, or from intercurrent bronchopneumonia. In other cases, the infant who was in congestive cardiac failure due to a large septal defect with torrential pulmonary blood flow survives only to develop later progressive pulmonary vascular obstruction. He may then become an adult with severe cyanosis, polycythaemia, and dyspnoea. Another outcome in some cases of large ventricular septal defects is the development, in time, of acquired infundibular stenosis due to narrowing of the right ventricular outflow tract by muscular hypertrophy. By the second or third decade, the left-to-right shunt is replaced by a right-to-left shunt due to severe subvalvular pulmonary stenosis, and the clinical picture becomes indistinguishable from that of Fallot's tetralogy. Rarely, the development of infundibular obstruction is associated with spontaneous closure of the ventricular septal defect, and the picture alters radically to that of an isolated pulmonary stenosis. Yet another unfavourable development, in some cases of ventricular septal defect, is prolapse of the right coronary aortic cusp into the left ventricle with consequent aortic regurgitation. This most commonly occurs toward the end of the first decade. At first a faint, high-frequency diastolic murmur appears in addition to the systolic murmur of the ventricular septal defect. Over time, the classical signs of aortic regurgitation replace those of the septal defect. This complication greatly worsens the prognosis, and death may ensue either from congestive cardiac failure or infective endocarditis. It is recommended that surgical treatment be offered as soon as significant aortic regurgitation is recognised.

3.2.15.1.10 Atrial Septal Defect (Fig. 3.15f)

Atrial septal defects are traditionally divided into "primum" and "secundum" types. The more common is a failure of closure of the ostium secundum, which is in the upper part of the interatrial septum. This defect is not uncommonly associated with partial anomalous pulmonary venous drainage in which one or both veins from the right lung enter the right atrium. Much less common, but more serious and arising at an earlier stage of embryogenesis, is failure of closure of the ostium primum in the lower part of the septum. The base of this defect commonly involves the mitral and tricuspid valves so that one or both maybe rendered incompetent. Furthermore, there is a high ventricular septal defect in many of these cases (atrioventricular septal defect).

3.2.15.1.11 Ostium Secundum Defect (Fig. 3.15g)

These children are usually symptomless save for undue susceptibility to respiratory infection. Girls are more often affected than boys, and they frequently have a somewhat characteristic slender asthenic body build. The sternum may be unduly prominent, with accompanying Harrison's grooves. The heart varies in size from normal to very large, but right ventricular pulsation is excessive over the left parasternal area. A soft systolic murmur is best heard at the second or third left interspace, and the second pulmonary heart sound is wide and persistently split. A mid-diastolic murmur may be heard at the tricuspid area when the atrial septal defect is large, with a greatly excessive pulmonary bloodflow. The X-ray shows a large pulmonary conus and pleionaemic lungs. Echocardiography is usually diagnostic.

The electrocardiogram shows partial right bundle-branch block (RsR pattern). There may be prolongation of the P-R interval or right ventricular hypertrophy. An increased oxygen concentration is demonstrable in the right atrium during cardiac catheterisation; a level about 95% suggests the presence of an anomalous pulmonary vein which has, in fact, been entered by the catheter from the right atrium. The catheter frequently crosses the atrial septal defect into the left atrium, but this can happen in a normal heart through the foramen ovale and is not by itself a significant occurrence. The precise site of the atrial septal defect can be determined by angiocardiography although this information is not essential before operation.

3.2.15.1.12 Ostium Primum Defect (Atrioventricular Septal Defect)

The child in this situation usually fails to grow normally from infancy. There may be episodes of cardiac failure, and respiratory infections are often severe. Cardiomegaly is associated not only with a powerful right ventricular thrust in the left parasternal area, but also with a displaced heaving apex beat due to left ventricular hypertrophy. When there is mitral regurgitation, a pansystolic murmur is heard at the apex and propagated into the axilla. A palpable systolic thrill is usually detected. There may be an apical mid-diastolic murmur. The pulmonary second sound is loud and widely split. The most characteristic electrocardiographic changes are left axis deviation, partial right bundle-branch block, and right ventricular hypertrophy. When mitral regurgitation is marked, there may be evidence of hypertrophy of the left or both ventricles. Heart block may be present when there is a complete atrioventricular septal defect. The diagnosis can be confirmed by echocardiography.

In ostium secundum defects of large size, increasing cardiomegaly is associated with a growing limitation of exercise tolerance. This can be aggravated by the late development of peripheral pulmonary vascular obstruction. An increased susceptibility to rheumatic fever may lead to superimposed

mitral stenosis (Lutembacher Syndrome). Patients with smaller defects may, however, live to a good age. In ostium primum defects, the expectation of life is considerably curtailed.

3.2.15.1.13 Patent Ductus Arteriosus (Fig. 3.15h)

Isolated patent ductus arteriosus results in shunting of blood from one side of the circulation to the other. The shunt volume depends on the length and internal diameter of the duct and on the systemic and pulmonary vascular resistances. As pulmonary resistance is usually much lower than systemic, the blood flow is from the aorta through the ductus to the pulmonary artery, and the lungs are pleonaemic. In a minority of cases where the ductus is very wide, the pulmonary and right ventricular systolic pressures may be so elevated as to approach systemic levels with the development of pulmonary vascular obstruction. This entirely alters the picture, and, indeed, in severe cases the blood flow may be right-to-left through the ductus with consequent cyanosis (Eisenmenger's syndrome). This type of peripheral pulmonary vascular obstruction must be distinguished from the "dynamic" pulmonary hypertension commonly found in the larger pulmonary arteries in cases of patent ductus arteriosus and due only to the torrential flow of blood reaching them from the aorta. The former situation is irreversible, whereas "dynamic" pulmonary hypertension can be completely relieved by simple closure of the ductus.

In the vast majority of cases, patent ductus arteriosus produces no cardiac symptoms during childhood. The special problems associated with patent ductus arteriosus in the preterm infant with the respiratory distress syndrome have already been considered in this chapter. However, even the child without symptoms is frequently rather underdeveloped for his age, and the dramatic growth spurt and increase in physical activity that is sometimes seen after successful closure of the ductus reveals, in retrospect, a degree of previous incapacity. The diagnostic physical sign is a continuous (machinery) murmur, loudest during systole but extending into diastole, maximal at the pulmonary area and well conducted under the left clavicle. It may be associated with a systolic thrill at the second left interspace. The murmur is caused by turbulent flow through the ductus itself. The pulses are collapsing in type due to a large pulse pressure. The heart may or may not be enlarged. X-ray will reveal prominence of the main pulmonary artery with increased lung vascularity. There may also be enlargement of the left ventricle. The electrocardiogram is often normal but may show some left ventricular preponderance. In young infants, the diastolic component of the murmur is not always audible.

When the patent ductus is complicated by peripheral pulmonary hypertension, a vastly different clinical picture presents itself. The child is markedly underdeveloped, highly susceptible to respiratory infections, and unduly breathless on exertion. Cardiomegaly is marked with a very large pulmonary artery, and the presence of combined ventricular hypertrophy can be demonstrated on radiographs, echocardiograms, and electrocardiograms. The lung roots show severe engorgement, but the periphery of the lung fields on radiographs are characteristically clear and translucent. The typical continuous murmur is no longer audible, being replaced by foreshortened systolic murmur. The second pulmonary sound, which tends to be obscured in a typical case of patent ductus, is now loud and booming. A systolic thrill is not always palpable. A large pulse pressure with collapsing pulses are still the rule. When the shunt is reversed from right to left, the presence of cyanosis makes differentiation from transposition of the great vessels with patent ductus a difficult matter without echocardiography.

Most cardiologists would not consider cardiac catheterisation a necessary investigation for patients with typical clinical findings of a patent ductus arteriosus. However, cross-sectional echocardiography will help rule out other structural malformations.

Other causes of continuous murmur may create confusion. A congenital aortopulmonary fenestration will be differentiated from patent ductus by ultrasound examination. More typically, the communication is large and does not cause a continuous murmur. A venous hum is usually best heard in the supraclavicular fossae. When it is loud, it may be transmitted below the clavicle. Hence it may be misdiagnosed as being from a patent ductus arteriosus. The murmur of a venous hum varies with position, whereas that of the patent ductus is constant.

Even a simple patent ductus arteriosus cardiac enlargement sooner or later develops. Death takes place from cardiac failure or infective endocarditis before middle age. When pulmonary hypertension complicates the picture, death is likely to occur in infancy or early childhood from cardiac failure or pneumonia.

3.2.15.2 Acyanotic Congenital Heart Disease Without Shunts

3.2.15.2.1 Pulmonary Stenosis

This defect occurring alone is usually due to fusion or malformation of the semilunar cusps. Infundibular stenosis in which there is a narrow infundibular chamber between the valve and the right ventricular cavity may also occur alone, but is more often associated with other anomalies (see Fallot's tetralogy). Fixed stenosis of the infundibulum coexisting with valvar stenosis is rare. Uncomplicated pulmonary stenosis is a common condition.

Most affected children are symptomless, and they are often well developed with somewhat highly coloured cheeks and lips. Slight cyanosis is seen only in a few very severe cases. Palpation reveals a powerful right ventricular thrust

over the left parasternal area and a systolic thrill at the second left interspace. At this area there is a harsh systolic murmur of ejection type that is conducted into the neck, under the left clavicle, and through to the back. The second pulmonary sound is quiet and usually single because the low pressure in the pulmonary artery makes the valve closure inaudible. Radiographs reveal post-stenotic dilatation of the pulmonary artery and translucent oligaemic lung fields. The electrocardiogram shows right ventricular hypertrophy; there may be a pulmonale and partial right bundle-branch block. Cardiac catheterisation demonstrates a high right ventricular pressure, with a steep pressure gradient between the ventricle and the pulmonary artery. Withdrawal tracings differentiate clearly between valvular and infundibular stenosis. Both cross-sectional and M-mode echocardiography techniques may appear normal in the presence of mild stenosis. If the valve is thickened, it should be detected on cross-sectional examination. Doppler studies will provide a satisfactory assessment of the gradient across the stenosed valve.

Mild degrees of pulmonary stenosis are compatible with long life, but the more severe cases end in cardiac failure before middle age. Apart from the risk of infective endocarditis, they do not die prematurely. Routine prophylaxis is therefore indicated throughout life in all patients, irrespective of the site or severity of stenosis.

3.2.15.2.2 Aortic Stenosis

Most cases of aortic stenosis include fusion of the cusps of the aortic valve. Less commonly there is a fibrous ring round the left ventricular outflow tract (subaortic stenosis). In rare instances the stenosis is supravalvar with a discrete ring of narrowing of the aorta. This defect has sometimes been associated with single or multiple constrictions along the major branches of the pulmonary artery. In some of the cases with supra-aortic stenosis, there have also been present characteristic facies, mental retardation, and an association with the severe form of idiopathic hypercalcaemia of infancy, and this syndrome is called William's syndrome. Isolated aortic valve stenosis is always congenital. When seen in association with a mitral lesion it may be either congenital or rheumatic. A chromosomal abnormality (deletion chromosome 7 for the elastin gene) has recently been identified in some instances of this syndrome.

This defect is more common in boys. Most are symptomless, but in a few, anginal pain develops on effort. The danger of sudden death during exertion is well known although it is, in fact, an uncommon event. Affected children are usually well grown. The maximal cardiac impulse is at the apex, although the heart is not commonly enlarged. A systolic thrill is palpable at the second right interspace and also along the carotid arteries and in the suprasternal notch. A harsh systolic murmur is best heard in the aortic area, and there may be a short, soft diastolic murmur. The pulse is anacrotic and of small volume. The pulse pressure is low. The heart may appear quite normal in radiographs. The electrocardiogram often shows left ventricular hypertrophy in these cases. The pressure gradient across the aortic valve can be assessed by Doppler ultrasound and confirmed by left heart catheterisation when operation is considered to be a possibility. The non-invasive technique is free of risk and may be repeated at intervals.

3.2.15.2.3 Coarctation of the Aorta (Fig. 3.15i, j)

Coarctation of the aorta is a relatively common anomaly, and one so amenable to surgical correction that palpation of the femoral arteries should form part of the physical examination of every patient of any age. The common site of narrowing of the aorta is just beyond the origin of the left subclavian artery and of the ligamentum arteriosum. The earlier classification into "adult" and "infantile" types should be abandoned. As most lesions are found in preductal position, and a small minority in postductal location, is has become fashionable to describe coarctation as preductal and postductal respectively: Those opposite the ductal mouth are described as "paraductal" coarctation. About 2% of coarctations are associated with Turner's (XO) syndrome, while around 15% of patients with Turner's syndrome have coarctation.

Isolated severe coarctation of the aorta may occasionally cause heart failure with pulmonary oedema in the young infant. The onset of cardiac failure is almost always within the first 3 months of life, but many infants present in the first week of life. Coarctation of the aorta is the most common structural anomaly causing heart failure in the first week of life in a cyanotic infant. In the vast majority of cases, however, the child is well developed and symptomless. The murmur, which maybe discovered during routine medical examination or during an intercurrent illness, is systolic in time. It is well heard at the aortic area, in the suprasternal notch, and in both interscapular areas. The apex beat is forceful due to left ventricular hypertrophy, but it may not be displaced for many years. The femoral pulses are absent or only weakly felt in comparison with the radial or branchial pulses. A marked blood-pressure difference can be shown between the arms and legs, and in time hypertension is established in the upper extremities, head, and neck. In adolescence, dilated and tortuous collateral vessels may be visible around the scapulae. Thus, the combination of weak or absent femoral pulses and an arm/leg pressure gradient is virtually diagnostic of aortic coarctation.

Radiographs may show no abnormality during childhood, but left ventricular enlargement ultimately develops. An over-penetrated film may reveal a notch in the aortic shadow at the site of the coarctation, and the narrow aortic arch above, with some dilatation of the aorta below this notch,

produces an outline somewhat like the shape of the numeral three (3). Notching of the inferior borders of the ribs by the enlarged intercostal arteries is seen in later childhood. The electrocardiogram may reveal left ventricular hypertrophy, but in the young infant with a severe degree of aortic obstruction, the ECG will show right ventricular hypertrophy because blood supply to the abdomen and lower limbs may be via the ductus arteriosus from the pulmonary artery. Cross-sectional echocardiography will usually demonstrate a coarctation and is invaluable in demonstrating any associated abnormality.

Coarctation presenting with heart failure in infancy is a lethal condition. Those who survive infancy may live into late middle age. Some die suddenly from a cerebrovascular accident. Most die in cardiac failure before the age of 40 years. A few develop rheumatic fever or infective endocarditis.

3.2.15.2.4 Hypoplastic Left Heart Syndrome

This syndrome comprises a wide variety of related anomalies associated with hypoplasia of the left ventricle and of the ascending aorta and aortic arch. Other constant findings include a large pulmonary artery, dilatation and hypertrophy of the right ventricle, and a patent ductus arteriosus. The hypoplastic aortic arch may show a preductal coarctation, or that part of the arch between the left subclavian artery and entrance of the ductus arteriosus may be atretic and represented only by a solid core of tissue. Other common anomalies include atresia (R hypoplasia) of the mitral and/or aortic valves. Severe endocardial fibro-elastosis may affect the left ventricle (only when the mitral valve is patent) or the left atrium. In cases where there is atresia of the aortic or mitral valve, it is obvious that the right side of the heart needs to maintain both the systemic and pulmonary circulations, and the pulmonary return to the left atrium has to be shunted across to the right side of the heart so that the right atrium becomes a mixing chamber for both oxygenated and venous blood. If the mitral valve is atretic and the aortic valve atretic or hypoplastic, and if there is no ventricular septal defect, the right ventricle alone is the propelling force for both pulmonary and systemic circuits. This explains the dilated pulmonary artery, while the patent ductus arteriosus, which appears to continue into the large descending aorta, permits a retrograde flow of blood into the arch of the aorta, thus supplying the brachiocephalic and coronary arteries. It will be readily understood that this syndrome is incompatible with life. Furthermore, there are frequently associated non-cardiac abnormalities.

The hypoplastic left heart syndrome is the most common cardiac cause of death in the neonatal period, and it ranks next only to transposition of the great arteries as a cause of death in all infants with congenital heart disease. The actual life span of affected infants depends on the severity of the obstructive valvar lesions. When the aortic or mitral valves are atretic, life is usually sustained for only a few days, whereas when the valves are hypoplastic, survival is longer and may extend for a few weeks. The clinical presentation is with the rapid development of severe dyspnoea, hepatomegaly, gross cardiomegaly, and oedema. Cyanosis is common, and in cases with a right-to-left flow through a patent ductus the lower half of the body may show a more severe degree than the head and arms. Some of those babies may initially be seen in severe cardiovascular collapse. Hypotension is common, as is the inability to maintain normothermia. Hypoglycaemia and a disseminated intravascular coagulopathy may occur in severely ill infants. Cardiac murmurs are inconstant, as are the electrocardiographic changes. Precise diagnosis is now established by echocardiography, which shows a very small left ventricle, a small or absent aortic root, and the mitral valve echo is absent or greatly reduced. In most cases cardiac catheterisation, which carries great risk, can be avoided.

3.2.15.2.5 Duct-Dependent Anomalies

In a number of congenital cardiac malformations, continued patency of the ductus arteriosus is essential for survival. In such life-threatening situations, the continuous infusion of prostaglandins PGE1 and PGE2 can prevent closure of the ductus until appropriate investigations, followed by surgical management, have been achieved.

In pulmonary atresia with intact ventricular septum, pulmonary atresia with ventricular septal defect, severe pulmonary stenosis, Fallot's tetralogy, and tricuspid atresia, where deepening cyanosis from birth is a common clinical feature, the continuous intravenous or intra-arterial infusion of prostaglandin can be life-saving.

3.2.16 Abnormal Vessels (Fig. 3.16)

Abnormalities of the great vessels in the neck and the chest can cause obstruction of the airway and the oesophagus by wrapping themselves around these structures as they exit from the root of the heart. Abnormalities of the subclavian vessels can cause severe airway obstruction in the neonate, especially if the trachea has a degree of tracheomalacia. This can be missed prior to a surgical procedure, such as thoracotomy for an oesophageal atresia; if missed, when it is time post-operatively to extubate the neonate, there is collapse of the airway due to the anomalous subclavian vessel passing in front of the trachea. Other abnormalities include the right sided aortic arch which can make surgery difficult and determine which side of the chest needs operated in anoesophageal atresia. This can be diagnosed preoperatively by taking a penetrated view of the neck in a chest X-ray.

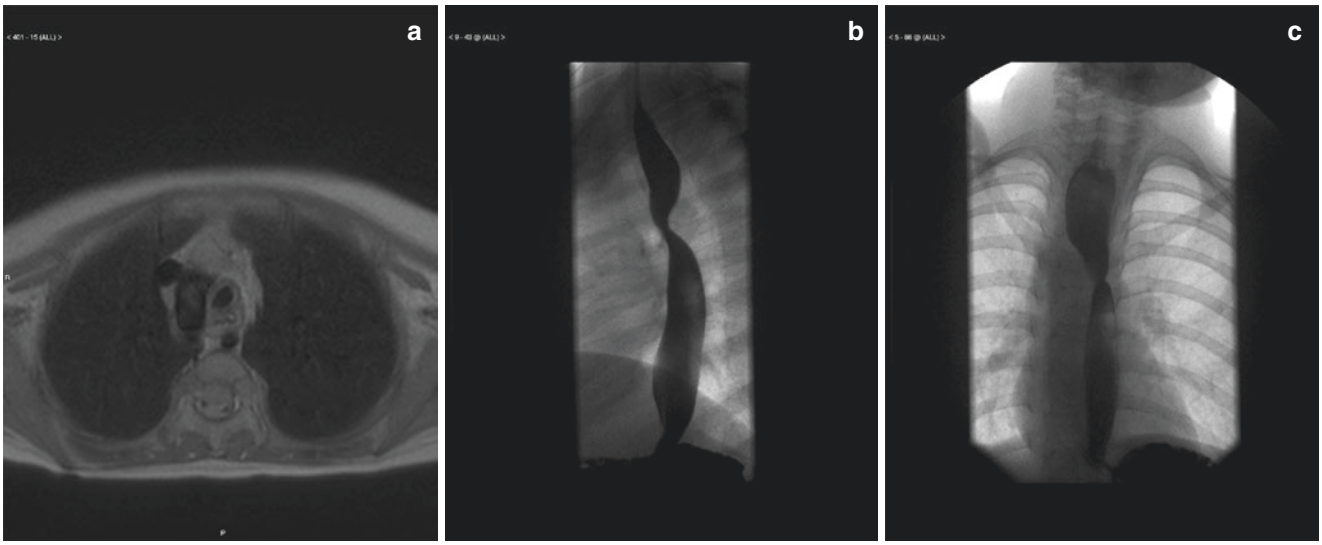

Fig. 3.16 (**a**) Aberrant left subclavian artery and right sided aortic arch. (**b**) Barium meal showing aberrant subclavian artery. (**c**) Aberrant subclavian artery

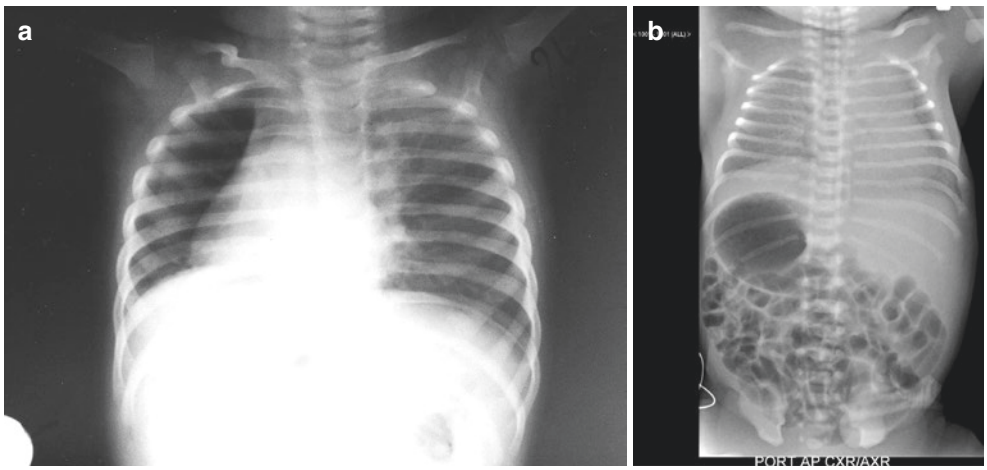

Fig. 3.17 (**a**) Dextrocardia. (**b**) Levocardia and situs inversus

3.2.17 Dextrocardia, Situs Inversus (Fig. 3.17)

Dextrocardia, situs inversus involves malpositioning of organs such that the organs appear as a mirror image of normal placement, and can be complete or incomplete. Situs inversus can cause confusion in acute appendicitis, and it also predisposes the patient to malrotation and volvulus. It can also be part of a spectrum where asplenia occurs.

3.2.18 Pulmonary Agenesis/Hypoplasia (Fig. 3.18a)

Agenesis of the lung is rare. Bilateral pulmonary agenesis is extremely rare and incompatible with life. When one lung or one lobe is absent, the patient is usually symptomless, although the heart is displaced into one hemithorax. In these cases, there may or may not be a bronchial bud present. The diagnosis is frequently made during a routine medical examination and can be confirmed radiologically. There is no specific treatment and the prognosis is good since the other lung is normal (Fig. 3.18b).

Bilateral pulmonary hypoplasia is often associated with oligohydramnios, which during prenatal life is commonly secondary to fetal urological abnormalities. Severe bilateral pulmonary hypoplasia is typically found in Potter's syndrome, where it is associated with renal agenesis and is frequent in babies with diaphragmatic hernia. The degree of pulmonary hypoplasia varies in this latter group from being severe with arrest of development estimated at 10–12 weeks in some infants with large left-sided diaphragmatic hernia, to minor degrees that do not interfere with function (Fig. 3.18c).

3.2.19 Haemangioma (Fig. 3.19)

In the neck or thoracic cavity, haemangioma can cause obstruction to the airways, especially with thrombocytopenia

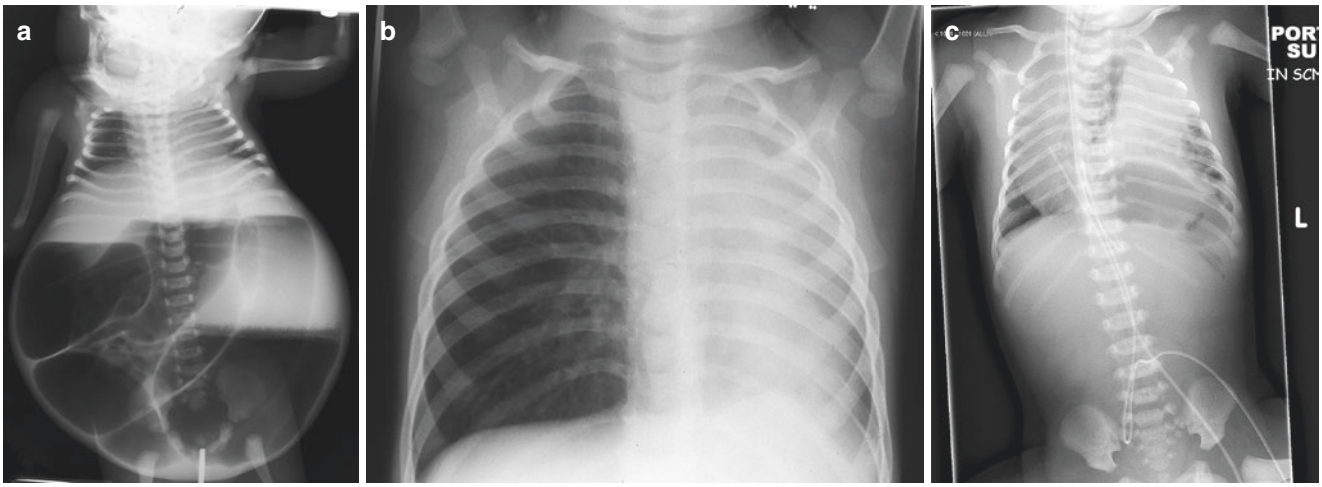

Fig. 3.18 (**a**) Bilateral pulmonary hypoplasia with gross distension of the abdomen. (**b**) Left pulmonary agenesis. (**c**) Bilateral Pulmonary Hypoplasia in a CDH

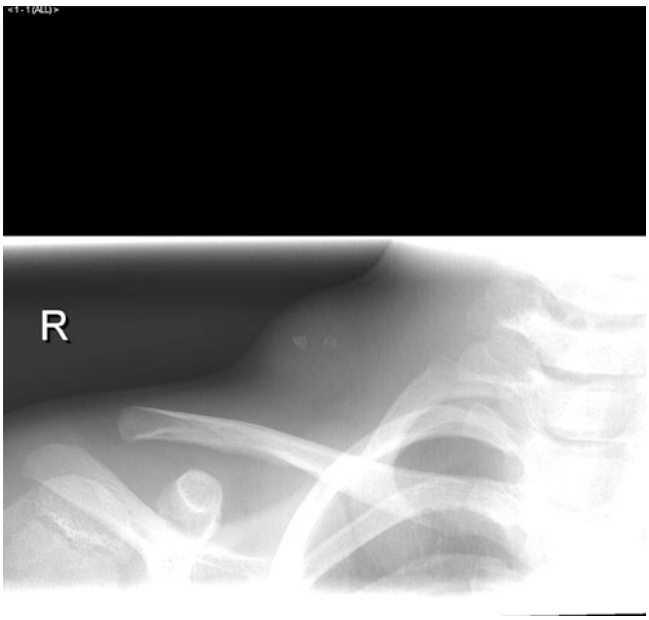

Fig. 3.19 Phleboliths

(KassebackMerritSyndrome). Bleeding into the tissues causes sudden enlargement and airway obstruction.

3.2.20 Lymphangioma (Fig. 3.20a, b)

Lymphangiomacan be infiltrative in all the tissues in the neck and cause superior mediastinal syndrome.

3.2.21 Eventration (Fig. 3.21)

Eventration results in a thinning of the diaphragm either due to congenital absence of the musculature or secondary to paralysis from surgical trauma with injury to the phrenic nerve. It is sometimes difficult to differentiate from congenital diaphragmatic hernia with a sac. Paradoxical movement is noted on screening.

3.2.22 Foregut Duplication (Fig. 3.22a)

Duplication of the foregut can arise anywhere from the mouth to the second part of the duodenum. It often presents as a cystic mass with or without a communication with the lumen of the foregut. In 30% of cases there is an association with abnormalities of the cervical spine. It can contain gastrointestinal or even respiratory epithelium (Fig. 3.22b–d).

3.2.23 Conjoined Twins

A rare conditionin which uniovular twins are still joined together. These twins are thoracopagus and omphalopagus, meaning joined at the thorax and abdomen, respectively (Fig. 3.23a–c). Imaging is important to determine which internal organs are shared, e.g., the heart, liver etc.

3.3 Infection/Inflammation

3.3.1 Oesophagitis (Fig. 3.24a, b)

Oesophagitis is often due to gastric reflux (GOR), especially associated with a Hiatus hernia. It causes heartburn, dysphagia, and occasionally vomiting and bleeding. It can be associated with a Barratts oesophagus, which could predispose to malignancy of the oesophagus later in life. The lining of the oesophagus is often inflamed, and contrast studies show an irregularity of the lining with fissures.

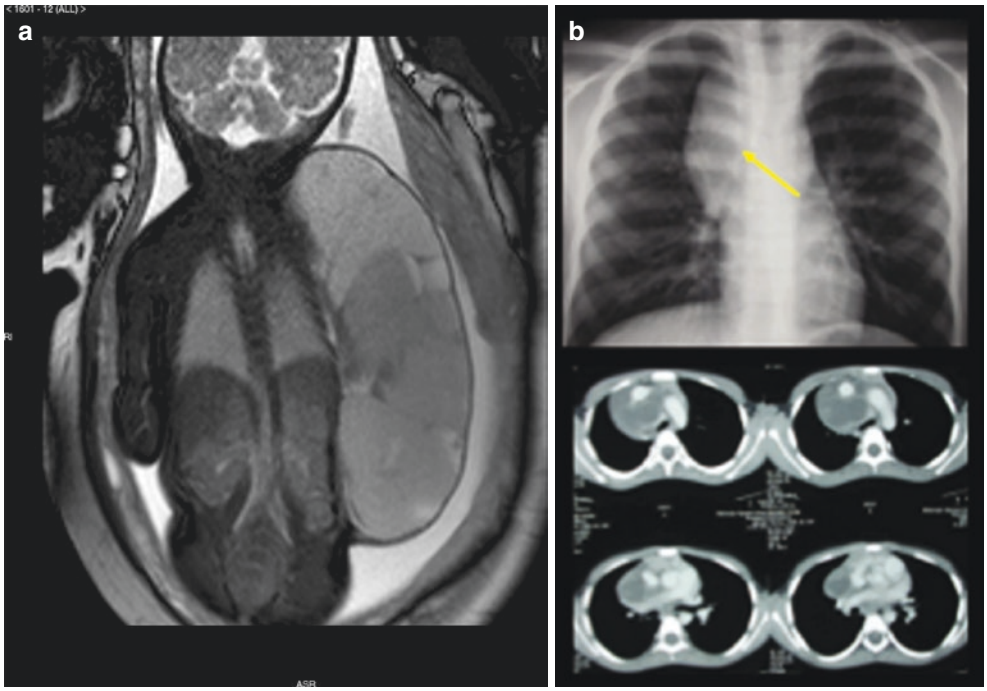

Fig. 3.20 (**a**) Antenatal MRI scan of a congenital lymphangioma affecting the chest wall. (**b**) Lymphangioma of the mediastinum

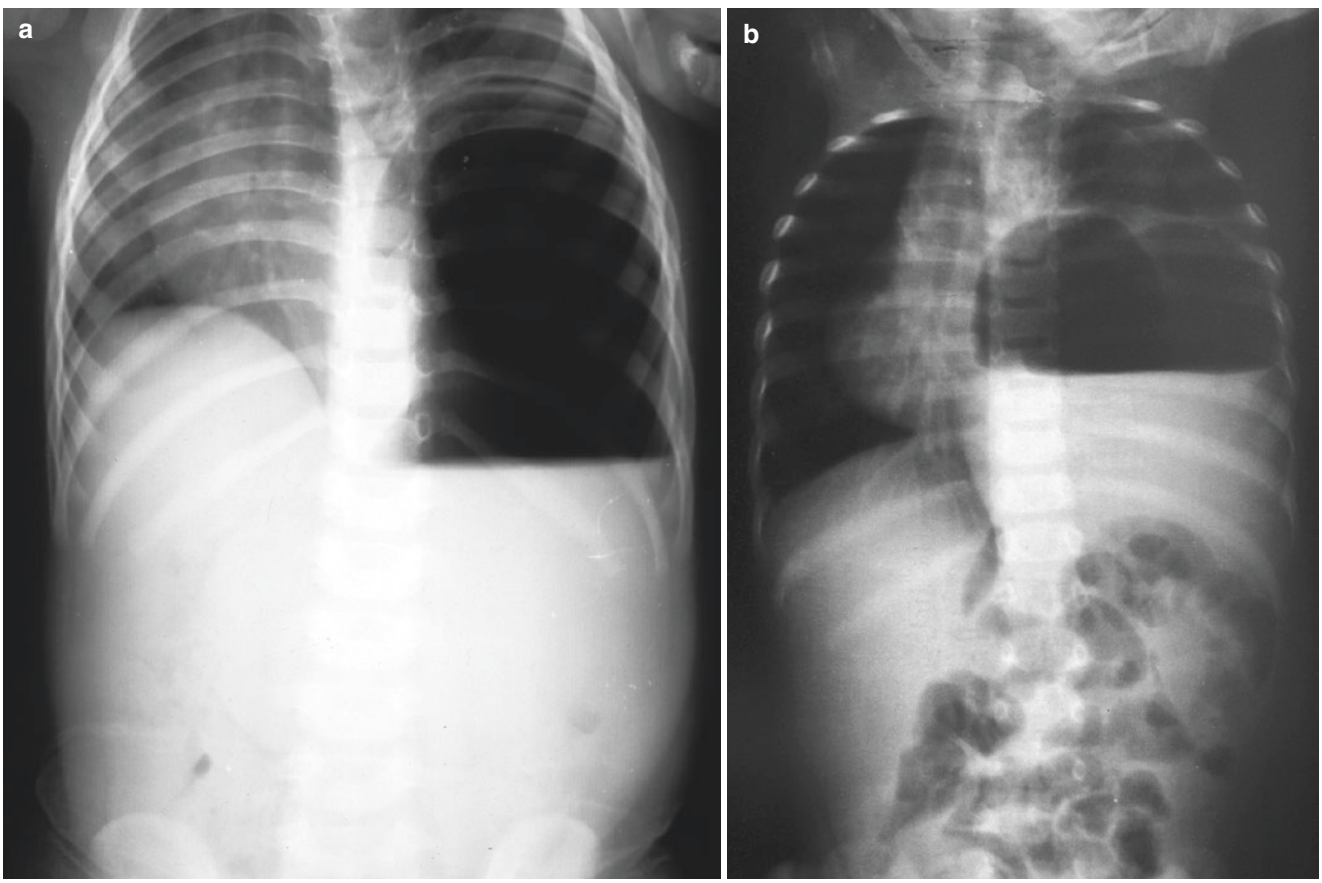

Fig. 3.21 (**a**) Eventration of the left side of the diaphragm. (**b**) Chest X-ray of left sided eventration

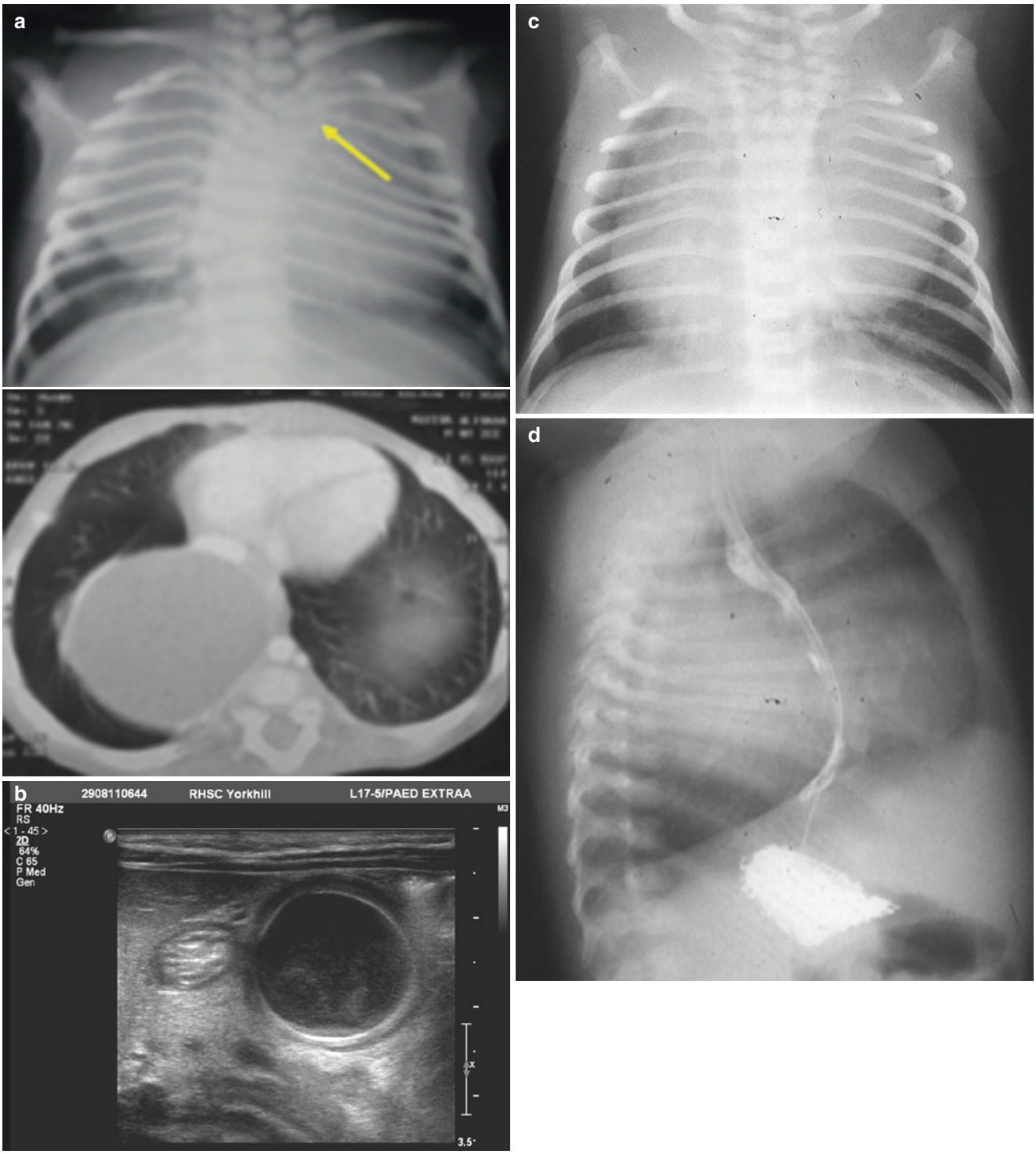

Fig. 3.22 (**a**) Foregut duplication cyst. (**b**) Foregut duplication cyst scan of the chest. (**c**) Foregut duplication cyst with cervical vertebral abnormalities. (**d**) Lateral chest X-ray Foregut duplication cyst with dye in the oesophagus showing it displaced

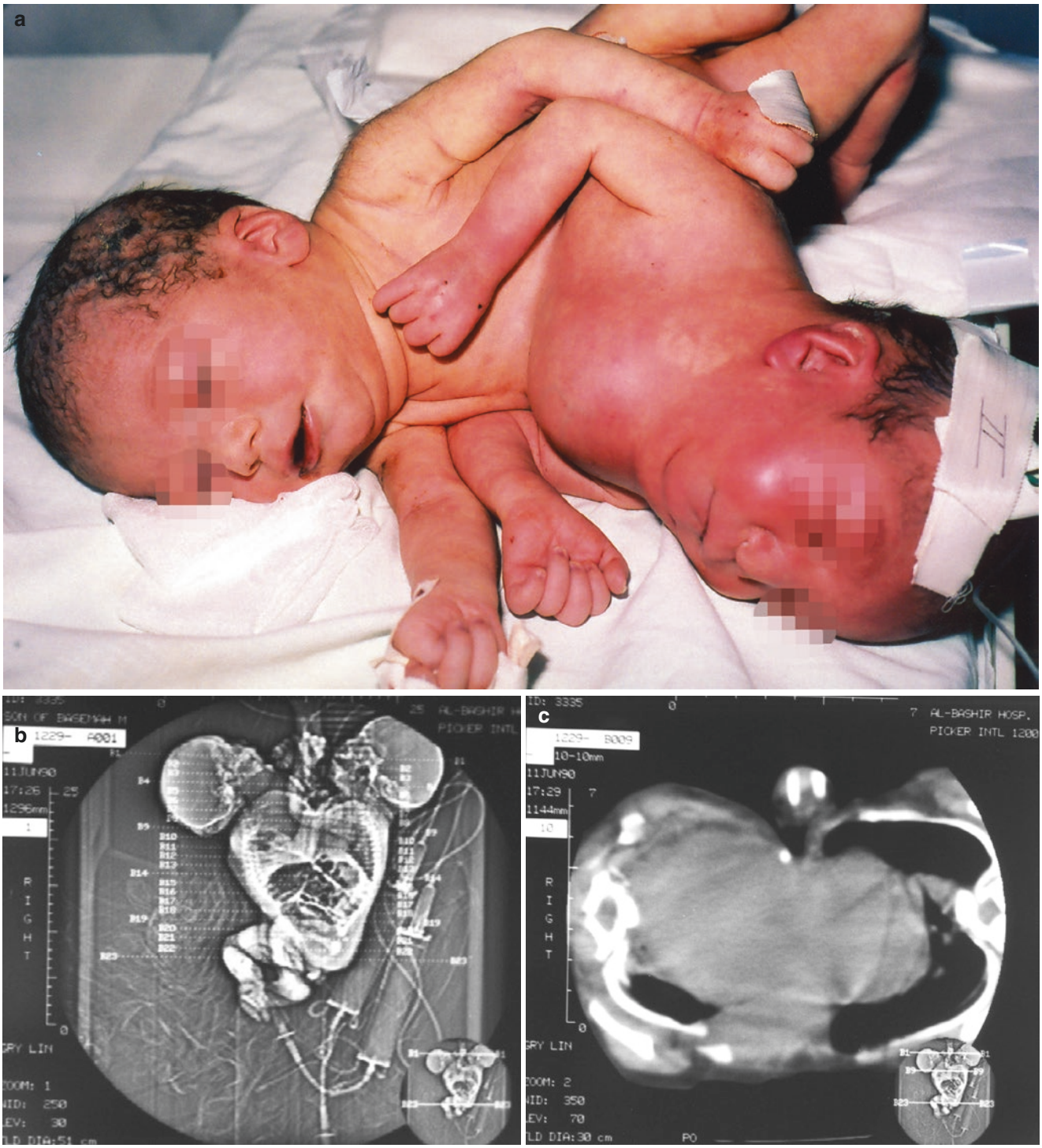

Fig. 3.23 (**a**) Conjoined twin. (**b**) Conjoined twin thoracoomphalopagus chest CT. (**c**) Conjoined twin chest CT

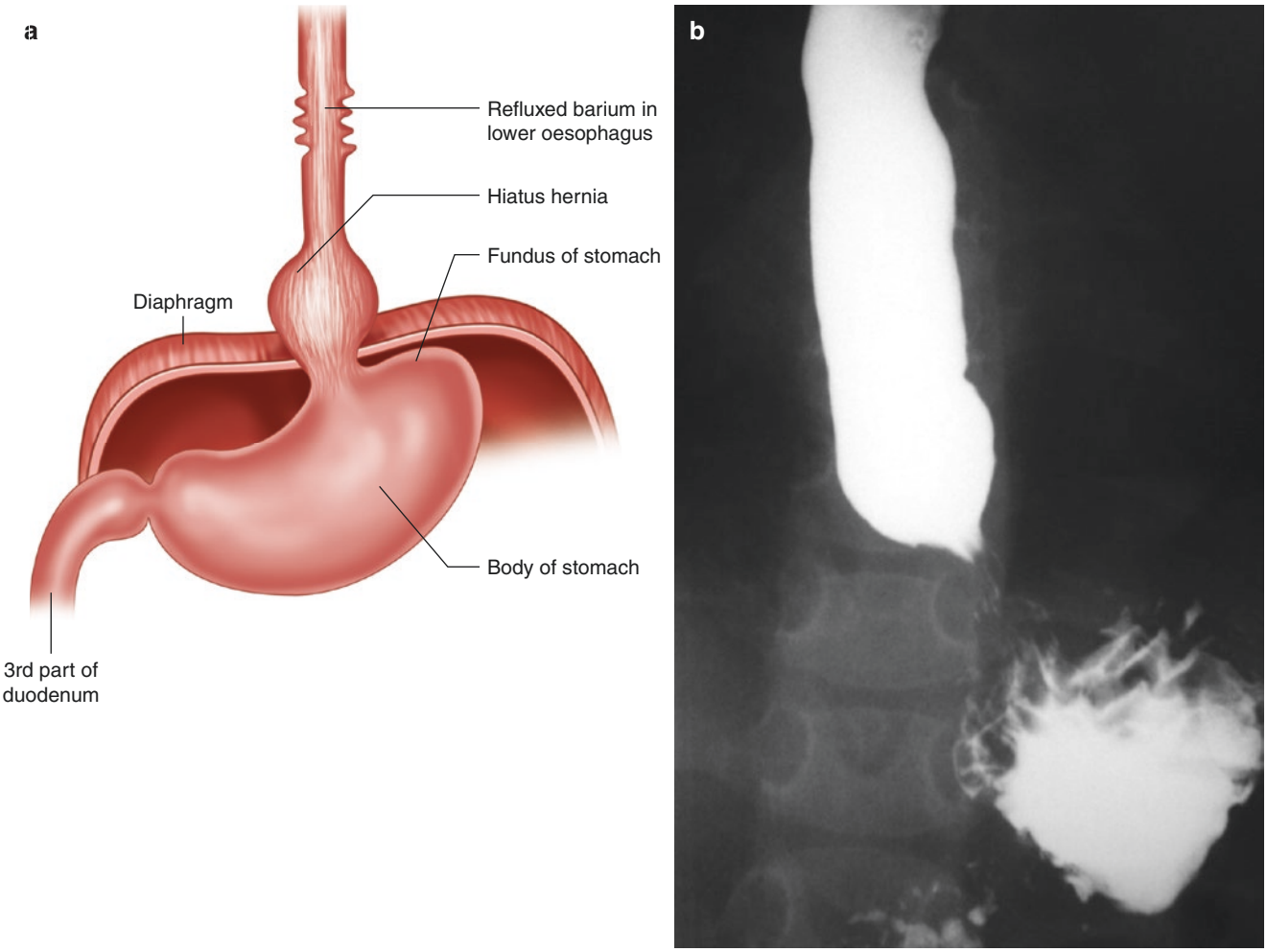

Fig. 3.24 (**a**) Oesophagitis (GOR). (**b**) Oesoghagitis in gastrooesophageal reflux

Oesophagitis can also be caused by caustic soda ingestion, other foreign bodies, batteries, fish bones, or trauma from endoscopes. The end result may be a very tight oesophageal stricture.

3.3.2 Tuberculosis (Fig. 3.25a–c)

The incidence of infection by human-type tubercle bacilli has fallen abruptly in Britain in the past 30 years. This has been due to (1) earlier diagnosis of phthisis in adults; (2) the detection by mass radiography of previously unknown sources of infection; and (3) the efficiency of modern antituberculous drugs in rendering patients non-infective within a relatively short period. The routine vaccination of tuberculin-negative children aged 11–13 years with BCG has also played a part. It would, however, be a grave error to regard the disease as having been defeated, and cases still occur too frequently to permit complacency. In some of the underdeveloped countries of the world, tuberculosis remains a major public health problem and is the most common cause of death. On the other hand, bovine tuberculosis, which until about 50 years ago was very common in the form of abdominal tuberculosis, cervical tuberculosis, and disease of bone and joints, has disappeared from Britain. Indeed, there is evidence to suggest that in indigenous British children, cervical adenitis is nowadays more often due to infection by atypical or "anonymous" mycobacteria than by the "typical" mycobacterium tuberculosis. However, intrathoracic tuberculosis is almost always caused by the human type of M. tuberculosis, and must be regarded as a major problem deserving close study and understanding by the physicians of all countries. Countries in which significant numbers of the population are affected by human immunodeficiency virus (HIV) have seen a marked resurgence of tuberculosis.

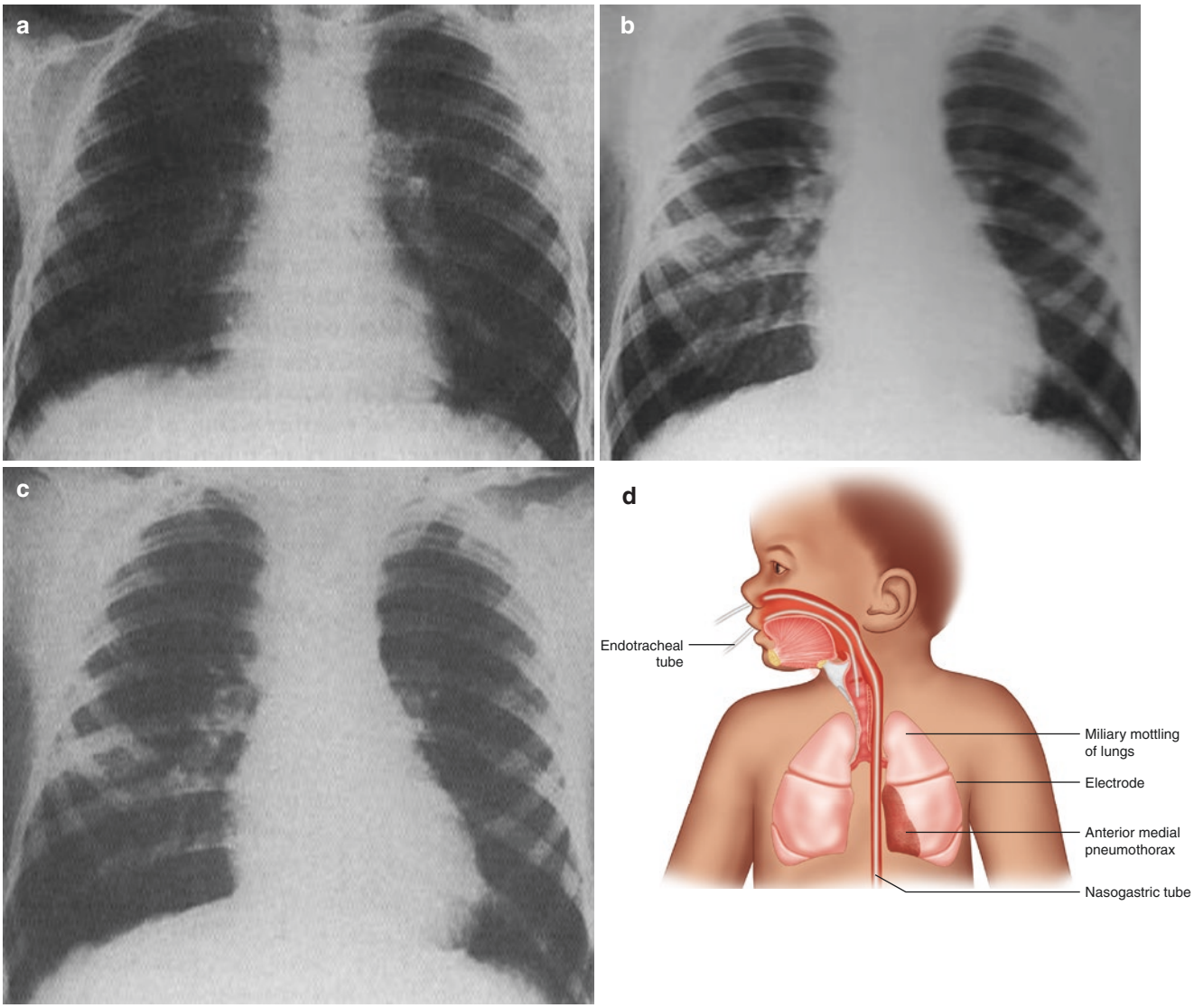

Fig. 3.25 (**a**) Radiograph of chest showing large primary tuberculous focus in upper left lobe. Early calcification is present. (**b**) Chest radiograph showing tuberculous cavity in right lower lobe. (**c**) Primary tuberculous complex showing a GHON's focus in right midzone with enlarged paratracheal glands. (**d**) Tuberculosis. (**e**) Tuberculosis old. (**f**) Tuberculosis with empyema of the left chest and calcified glands in the neck. (**g**) Tuberculosis

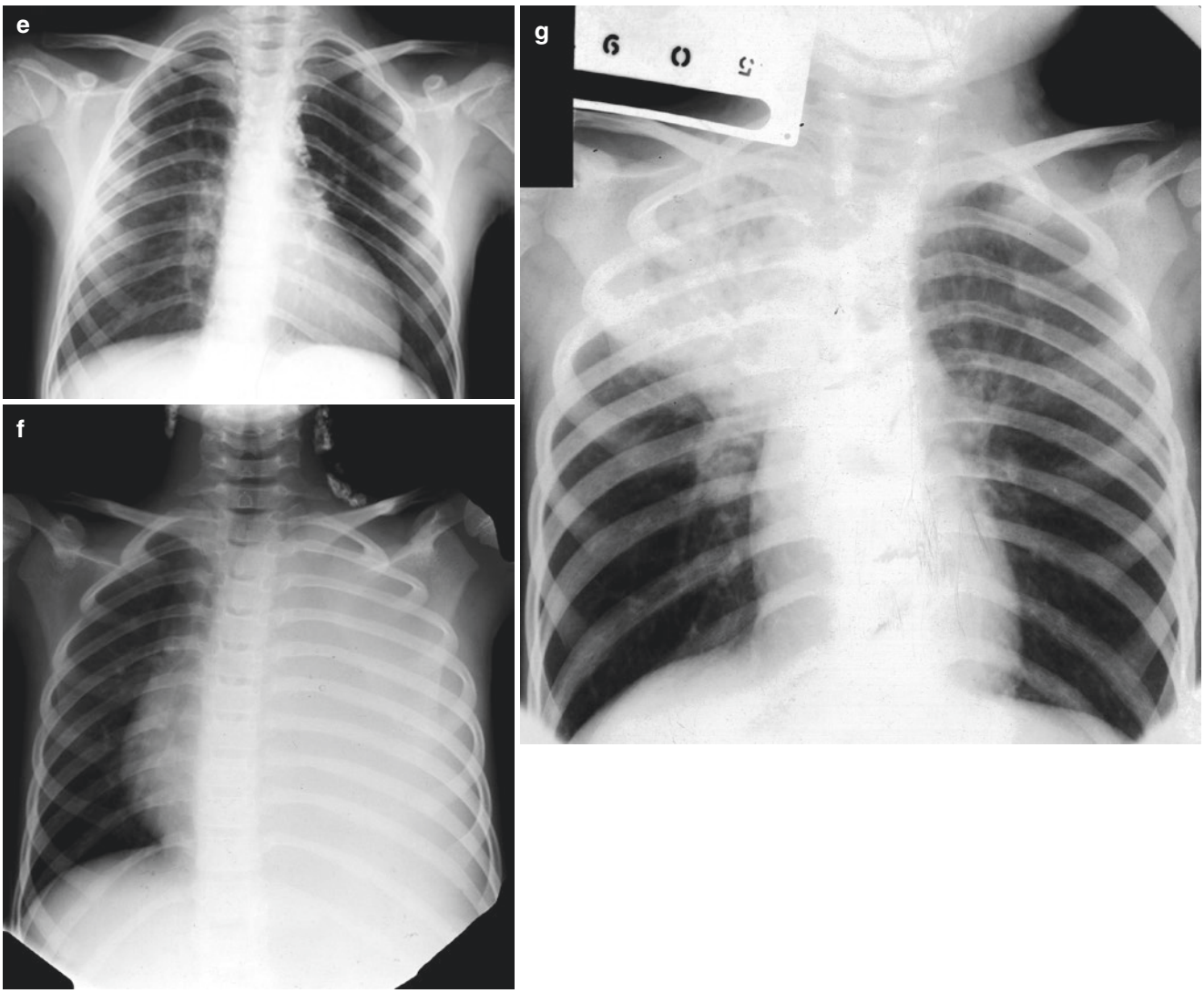

Fig. 3.25 (continued)

3.3.2.1 Intrathoracic Tuberculosis

3.3.2.1.1 Sources of Infection

By far the most usual source of tuberculous infection in infancy and childhood is the adult contact who suffers from "open" phthisis. In Britain, known cases of adult tuberculosis are quickly rendered non-infectious by appropriate drug treatment; the danger is undiagnosed or unsuspected adults. Infrequently, a child can be infected from a tuberculous animal such as a dog, and this possibility should not be overlooked (Fig. 3.25d, e).

3.3.2.1.2 Pathology

When patients of any age inhale tubercle bacilli for the first time, the bacilli produce a small caseous focus in the lung parenchyma. This is called "the primary focus," or Ghon's focus. It is usually single, occasionally multiple, and most often situated subpleurally, and in 45% of cases in the right upper lobe. From the primary focus, which is usually large enough to be visible to the naked eye, there is a peribronchial lymphangitis spreading toward the bronchopulmonary and tracheobronchial glands on the same side. These become enlarged and caseous, ultimately undergoing softening. Indeed, in primary tuberculosis the lung parenchyma lesion is small, almost trivial, while the regional lymph glands are heavily involved. This is in contrast to adult-type phthisis, in which the tissues have earlier been sensitised by primary tuberculosis, and where the lung parenchyma may show extensive infiltration, caseation, cavitation, and fibrosis, while the regional lymphadenitis is slight or absent. The primary focus, lymphangitis, and hilar adenitis constitute "the primary tuberculous complex." In more severe examples, the disease may spread upward, involving the paratracheal and the supraclavicular glands (Fig. 3.25f, g).

In the majority of cases, the primary complex heals by calcification in the primary focus and regional lymph nodes. These are visible on radiographs, but ultimately the calcium is absorbed so that no trace of the infection may remain. In others, especially infants and young children, the caseous hilar nodes exert local effects upon the adjoining bronchi, which are thin-walled and pliable. Most often the enlarged glands completely obstruct a primary or secondary bronchus, and the distal lobe or segment becomes airless. Histologically it shows resorption atelectasis and possibly low-grade tuberculous inflammation. Whereas in some cases the bronchial occlusion is brought about by extrinsic compression, in many cases the caseous glands erode their way through the bronchial wall, so that the mucous membrane is perforated and tuberculous granulation tissue can then be seen to fill the lumen. The right middle lobe is most often affected. This type of atelectasis or absorption collapse may completely resolve, but not infrequently it leaves behind bronchial narrowing and distortion, or a "dry" bronchiectasis that may become the seat of severe pyogenic infection many years later.

3.3.2.2 Acute Miliary Tuberculosis

This classical form of the disease arises from erosion of some part of the primary complex into a blood vessel and the discharge into the circulation of a large dose of tubercle bacilli. Like tuberculous meningitis, this is most likely to occur within the first 6 months after the primary infection. All the organs of the body are studded with small miliary tubercles that are usually visible to the naked eye. Erosion of a caseous gland into a branch of the pulmonary artery explains those uncommon cases where the miliary spread is confined to the lungs.

3.3.2.3 Acute Tuberculous Pneumonia

This rapidly progressive form of pulmonary tuberculosis may be lobar or lobular in distribution. Once common as "galloping consumption," it has become rare and is almost confined to young children. Cavitation, spontaneous pneumothorax, and tuberculous empyema were common complications, but they have virtually disappeared in Britain since the advent of the antituberculous drugs.

3.3.2.4 Clinical Aspects of the Primary Tuberculous Infection

The child with an intrathoracic primary infection may be symptomless or severely ill. When symptoms do appear, they coincide with the development, by the tissues, of an allergic sensitivity toward tuberculoprotein. This takes about 6–8 weeks to develop and may be demonstrated by means of a tuberculin skin test. In some patients, spontaneous manifestations of this allergic state appear in the form of phylctenular conjunctivitis or erythema nodosum, and these conditions should always be presumed to indicate tuberculous infection in children until they are proved to be otherwise caused. In some children, who are usually over the age of 5 years, the development of pleurisy with effusion makes the diagnosis easy.

In most cases, the symptomatology tends to be nonspecific and of a type common in other non-tuberculous ailments, including loss of energy, lethargy, undue irritability, anorexia, and a general loss of well-being. An irregular fever (37–38 °C) in the later afternoons is common. Less often there may be brisk sustained fever. Loss of weight or failure to gain are usual but not invariable. Local symptoms caused by the effect pressure from caseous mediastinal glands on surrounding structures are most severe in infants. Whereas in the school child cough may be relatively unimpressive, in the infant glandular pressure on the main bronchi frequently gives rise to spasmodic outbursts of coughing that closely simulate pertussis. In fact, the bronchi may be sufficiently narrowed by extrinsic pressure that a loud wheeze—"the asthmatoid wheeze"—may be heard. Physical examination of the chest is rarely helpful unless there is absorption collapse or obstructive emphysema. The diagnosis of primary intrathoracic tuberculosis must depend largely upon the ease with which the physician's suspicions are aroused. In some instances, of course, the child is brought to the doctor because of known recent contact with a tuberculous adult. The possibility of such contact, within or outside the family circle, should always be the subject of direct enquiry in the case of an unwell child in whom a satisfactory diagnosis has not been reached.

3.3.2.5 Diagnostic Tests

Tuberculin skin tests are, of all tests, the most useful in the diagnosis of primary tuberculosis. A positive reaction before the age of 3 years is evidence of active infection. After this age, a positive test may only indicate previous infection not now necessarily active, but in an ill child it obviously merits further investigation. The most reliable test is the Mantoux intradermal reaction using suitable dilutions of Old Tuberculin (OT) or purified protein derivative (PPD). The "tine" test is convenient in domiciliary practice, but less reliable. When large numbers of patients need to be tested, the Heaf test, which makes multiple punctures with a test-gun through undiluted OT or PPD, is useful. False negative results with all tests may be found in children who are overwhelmed by miliary tuberculosis and in those who are convalescent from measles. Apart from these exceptions, a negative tuberculin test, properly performed with active material, excludes tuberculosis. It must be remembered, however, that these tests lose some of their value in children who have been immunised with Bacille Calmette Guerin (BCG).

In the child with an active tuberculous infection, the standard Mantoux test is likely to give an area of induration exceeding 6 mm in diameter, with a larger area of erythema.

A chest radiograph may fail to reveal any abnormality in early primary tuberculosis. Most often, however, unilateral enlargement of the hilar glands is visible, but as this could be due to diseases other than tuberculosis, the chest radiograph by itself cannot justify a diagnosis of primary tuberculosis. Only very rarely is the primary focus in the lung parenchyma visible, although it can be large enough to be seen. It is quite exceptional for the primary focus to cavitate. When the primary complex heals by calcification it will become radiologically obvious, although no longer responsible for symptoms. It must be stressed that the diagnostic value of the radiograph is limited in primary tuberculosis, in marked contrast to adult-type phthisis where the lung parenchyma is heavily involved.

Gastric washings should be examined by direct staining, culture, and guinea-pig inoculation. They are of limited usefulness in diagnosis in view of the time-lag usually involved, but successful isolation of tubercle bacilli allows their sensitivities toward the anti-tuberculous drugs to be tested, and this information is valuable.

The erythrocyte sedimentation rate (ESR), preferably determined by the Westergren technique, is not of direct diagnostic value, but a raised ESR helps to confirm the presence of active disease, and serial estimations are valuable in assessing progress during treatment.

Enough has been said to make it clear that a diagnosis of active primary tuberculosis can rarely be established on the basis of a single test, and certainly not on the X-ray appearances. However, when all the findings are weighed together—clinical history, possible adult contact, results of tuberculin tests, radiographs, and ESR—it is almost always possible to arrive at a correct diagnosis.

3.3.2.6 Extrathoracic Tuberculosis

3.3.2.6.1 Sources of Infection

Cervical and abdominal tuberculosis were once common in Britain as a consequence of the ingestion of milk from tuberculous cows, but as we have already pointed out, bovine tuberculosis no longer exists in this country. However, bovine strains of tubercle bacilli are still isolated from immigrant patients of Asian and African origin, and it is, of course, not unknown for cervical tuberculosis to arise from the entry of human strain of tubercle bacilli. Primary infection of the skin, conjunctiva, or within the mouth following tooth extraction may also occur, and in such cases there is frequently a history of contact with an adult case of phthisis. The organisms presumably find entry through a minor break in the skin or mucous membrane.

3.3.2.6.2 Pathological Course

The primary tuberculous complex behaves in the same basic fashion regardless of its site. In cervical tuberculosis, the primary focus is in the tonsil, although it can only be seen under the microscope. There has often been preceding chronic sepsis in the tonsils. The affected cervical lymph nodes become caseous. They may later liquefy and coalesce, at the same time becoming adherent to the skin and surrounding tissues. If rupture occurs, the classical "collar stud" abscess extending through a fascial plane, or one or more sinuses discharging through the skin (scrofula), may develop. In abdominal tuberculosis the primary focus is in the small intestine. This is a solitary microscopic lesion, not to be confused with the secondary tuberculous enteritis, which may complicate advanced cases of adult type phthisis.

Mesenteric lymph nodes are massively involved, and rupture into the peritoneal cavity leads to the once common picture of tuberculous peritonitis. The possibility of cutaneous, conjunctival, or buccal primary tuberculosis should be considered when solitary but chronic enlargement of lymph nodes appears in unusual sites, e.g., pre-auricular, submandibular, or inguinal. In all types of extrathoracic tuberculosis, haematogenous spread may occur, although less acutely than in the intrathoracic disease. In the case of bovine infections, bone and joint lesions were at one time common complications that resulted in long periods of invalidism or crippling, and even in death.

3.3.2.6.3 Clinical Aspects of Extrathoracic Tuberculosis

The general symptoms tend to be common to all types of primary tuberculosis. They vary from none at all to listlessness, anorexia, undue fatiguability, low-grade fever, and loss of weight. When the cervical glands are involved, the first sign is a painless, firm, mobile mass at the angle of the jaw. Later, the glands become matted together, adherent to the skin, and no longer freely movable. Liquefaction is indicated by palpable fluctuation. Healingis by fibrosis and calcification, which become radiologically visible. The differential diagnosis from other causes of cervical adenitis can be made by tuberculin skin testing.

3.3.3 Acute Bronchitis (Fig. 3.26a–c)

Most cases of acute bronchitis are caused by an extension downwards of an upper respiratory viral infection, or they form part of the clinical spectrum of diseases such as measles, influenza, whooping cough, and typhoid fever. Secondary bacterial infection by pneumococci, H. influenzae, or staphylococci infrequently aggravates the damage to the bronchial tree.

The usual history is of a preceding upper respiratory illness with sudden worsening of a cough, malaise, and anorexia. Most children are not very ill, although infants may become dyspnoeic and toxic.

The cough is initially unproductive, but later sputum may be coughed up by the older child or vomited during spasms of coughing by the infant. Physical signs over the lungs consist of rhonchi and crepitations that vary considerably in severity and do not have a close correlation with the severity

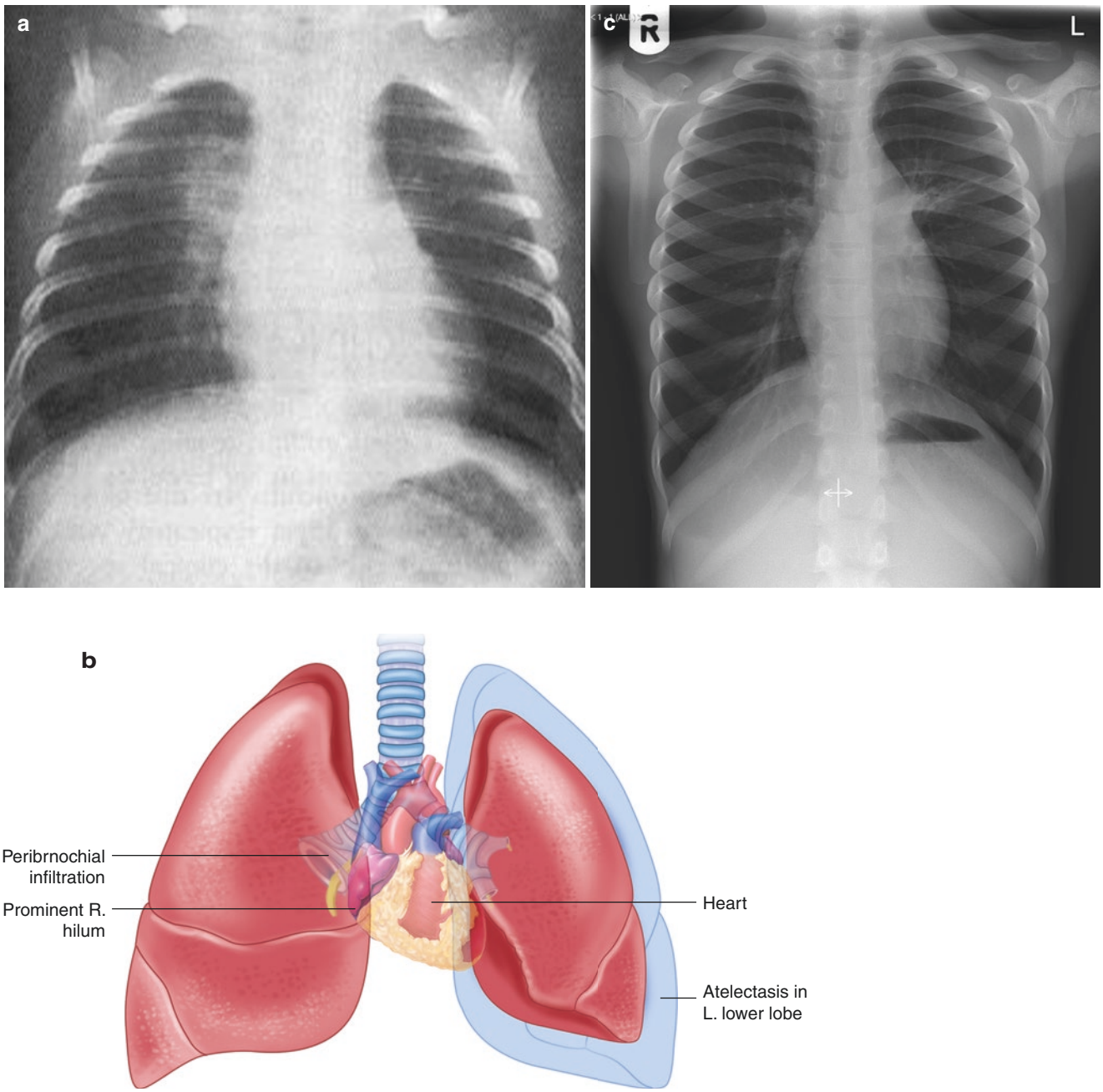

Fig. 3.26 (**a**) Acute bronchiolitis. (**b**) Diagram of acute bronchiolitis. (**c**) Acute bronchitis with air entrapment

of the illness. Recovery usually begins after a week, and serious sequelae such as bronchiectasis are rare.

3.3.3.1 Acute Bronchiolitis of Infancy

This is a disease that is seen only in infancy. It occurs in epidemic form every 2 or 3 years during the winter months. The great majority of cases are due to respiratory syncytial virus (RSV) which is, indeed, the most common cause of lower respiratory tract infections in infants and young children, although other viruses, including parainfluenza and adenovirus, can cause similar symptoms.

There is normally a preceding history of upper respiratory catarrh and slight cough. The infant then becomes acutely ill with inspiratory difficulty, resulting in visible subcostal and intercostal recession, but there is also marked expiratory difficulty and wheezing or grunting. Severe spasms of coughing may so interfere with feeding as to lead to dehydration. This is further aggravated by tachypnoea and increased insensible loss of water from the lungs. Hypoxia is reflected in agitation and restlessness, and there may be cyanosis. Tachycardia is marked, but the temperature rarely rises above 38 °C (101 °F) and may, in fact, be

normal. Bilateral obstructive emphysema causes the chest to be held in the inspiratory position and the percussion note is hyper-resonant. The breath sounds are diminished and there may be rhonchi or numerous crepitations. Radiographs of the chest show increased lung markings due to interstitial infiltrations and, often, over-inflation with increased translucency of the lungs. In the most distressed infants the PO_2 of arterial or arterialised capillary blood may be found to be dangerously low, and in these circumstances the PCO_2 is likely to be raised with a low blood pH. This respiratory acidosis and hypoxaemia may further be associated with a metabolic acidosis.

It is now possible for the virologist to rapidly confirm the presence of respiratory syncytial and other viruses in the nasopharyngeal secretions by means of immunofluorescent antibody techniques.

3.3.4 Lobar Pneumonia, Bronchopneumonia (Fig. 3.27a, b)

3.3.4.1 Acute Bacterial Pneumonia

An aetiological classification of the bacterial pneumonias would be of more practical value to the clinician, who is now

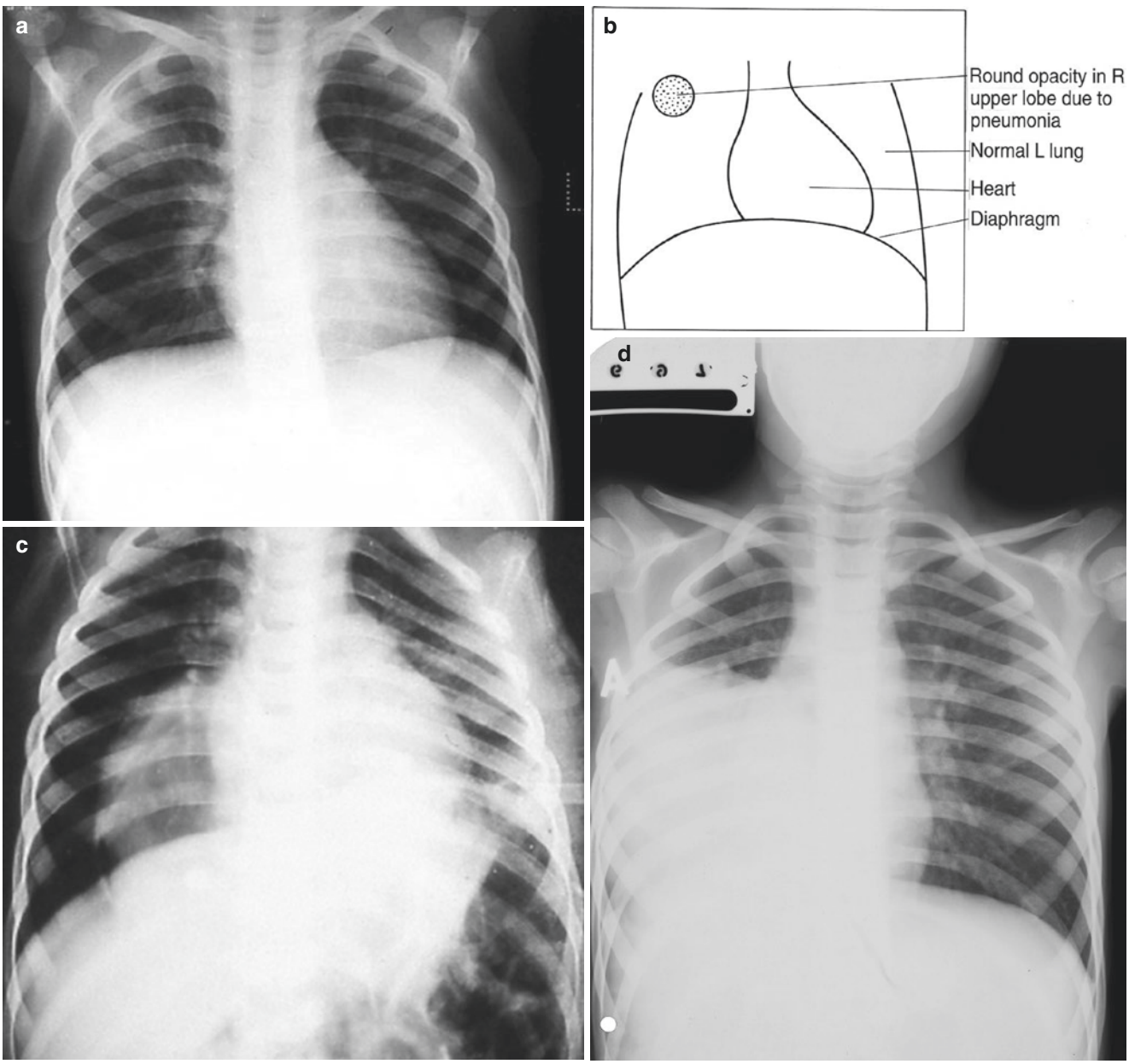

Fig. 3.27 (**a**) Upper lobe pneumonia (circular). (**b**) Upper lobe pneumonia diagram. (**c**) Lower lobe pneumonia. (**d**) Pneumonia

armed with effective antibacterial drugs, than the traditional subdivision into bronchopneumonia and lobar pneumonia.

Unfortunately, sputum is rarely obtainable from young children, and bacteria grown from the nose or throat are not necessarily those present in the lung. Nonetheless, it is often possible, from a knowledge of the epidemiology of the common pulmonary infections in a region, to hazard a shrewd guess as to the probable bacterial cause in the individual patient with pneumonia. This is also influenced by the age of the patient.

3.3.4.2 Bacterial Pneumonia in Infancy

In Britain today the most common bacterial causes of pneumonia during the first year of life are Staph aureus and haemophilus influenzae. Pneumonia is frequently preceded by a viral infection of the respiratory tract, which presumably damages the mucous membranes and permits its penetration by bacteria. Pneumococcal pneumonia, which was the common type in the pre-antibiotic era, has become relatively rare in the young infant. Occasional cases are caused by streptococci and coliforms.

The striking features in the staphylococcal cases are massive consolidation, destruction of tissue, abscess formation, and the frequent appearances of emphysematous bullae. When these rupture into the pleural cavity, the result is pyopneumothorax. In pneumococcal cases the lobular areas of consolidation rarely suppurate, and empyema has become a rare condition.

An upper respiratory infection frequently precedes pneumonia. The infant then becomes acutely ill, fevered, irritable, and restless. Feeds are taken reluctantly. Dyspnoea is associated with inspiratory dilatation of the alae nasi and expiratory grunting. There may be subcostal recession. Cough is severe and may precipitate vomiting. Diarrhoea may occur. Meningism is relatively uncommon. Early in the illness there may be only a few crepitations over the lungs. In staphylococcal cases, dullness on percussion over the affected areas, with bronchial or diminished breath sounds, becomes quickly obvious. The presence of consolidation can be confirmed radiologically. As the disease progresses, radiographs frequently reveal emphysematous bullae (pneumatoceles). Abscess formation may occasionally be demonstrable with fluid levels in the cavities.

3.3.4.3 Bacterial Pneumonia in the Older Child (Fig. 3.27c, d)

The great majority of cases of bacterial pneumonia in the older child are caused by pneumococci, which are invariably sensitive to benzylpenicillin. Although type-specific sera are available for many of the 32 types of pneumococci, they are now rarely used.

Post-mortem studies of pneumonia in older children are now fortunately exceedingly rare. The classical four stages—congestion, red hepatization, grey hepatization, and resolution—are well known. Complications such as empyema, pyopericardium, lung abscess, and bacterial endocarditis are also rarely seen today.

The onset is sudden, with high fever, malaise, and cough. Pain in the chest or abdomen on the affected side is common, but rarely as severe as in adults. Meningism is not infrequent, especially when the upper lobes are involved. A rigor is not common in the child, and a convulsion may herald the onset of the illness. Tachypnoea is the rule, but severe dyspnoea or cyanosis is uncommon. Circumoral pallor, inspiratory dilatation of the alae nasi, and an expiratory grunt frequently constitute a characteristic clinical picture. The movement of the affected side of the chest is diminished. Pleural friction is inconstant and usually transient. Dullness on percussion is the most definite sign, while bronchial breath sounds and fine crepitations are found in typical cases. In many children, the physical signs are remarkably slight in contrast to the segmental or lobar area of consolidation revealed by radiography. The white cell count is raised, but in childhood is of little prognostic significance.

3.3.4.4 Primary Atypical Pneumonia

Primary atypical pneumonia is relatively rare in children. Many cases so diagnosed are, in fact, examples of aspiration pneumonia secondary to upper respiratory catarrh, but there are undoubtedly cases of primary viral pneumonia.

Most cases are due to a virus-like agent that is a mycoplasma: Mycoplasma pneumoniae. Some cases are in fact examples of psittacosis or ornithosis due to contact with sick parrots or budgerigars. The causal organism in the case of psittacosis is Chlamydia psittaci. Another example of atypical pneumonia occurs secondary to Coxiella burnetii infection, the agent that causes Q fever.

There is infiltration of the bronchiolar walls, alveolar septa, and interstitial tissues by mononuclear cells. The alveoli are often free of exudate, but may be filled with a mixture of fibrin and mononuclear cells.

The incubation period is 10–21 days. The onset is characterised by headache, shivering, malaise, and fever. Cough develops subsequently, and blood staining of the sputum may be observed. There may be remarkably few physical signs over the lungs, often only a few localised crepitations, but the radiograph shows patchy consolidation confined to one or two lobes. Leucocytosis is absent. The somewhat delayed onset of cough contrasts with the situation in the much more common aspiration pneumonia, where cough has often preceded the constitutional upset. The nature of the causal organisms can be determined by sending a first specimen of blood to the virologist at the onset of the illness, and a second specimen 10–14 days later. A rising antibody titre will be found for the specific agent. In the case of mycoplasma infections, an early diagnosis is available from the

application of immunofluorescent antibody techniques to the sputum or nasopharyngeal secretions.

3.3.4.5 Interstitial Plasma Cell Pneumonia

This type of lung infection is a common cause of death in early infancy in some central and northern European countries. It is, however, rarely seen in Britain or the USA, except in association with such conditions as HIV infection, hypogammaglobulinaemia, cytomegalic inclusion body disease, and various malignant diseases when given immunosuppressive treatments such as radiotherapy, steroids, and cytotoxic drugs. The infective agent is a protozoan pneumocystis carinii.

The alveoli are filled with an apparently acellular exudate that shows a honeycomb appearance in sections. In the infant, the alveolar septa are infiltrated by plasma cells, but these are conspicuous by their absence in cases associated with hypogammaglobulinaemia. When special staining methods are used, the alveolar exudate is seen to be composed of parasites.

The predominant feature is progressively severe dyspnoea and cyanosis, which contrast with the paucity of physical signs over the lungs. Radiographs show a characteristic symmetrical ground glass opacity spreading outward from the lung roots. Areas of lobular collapse may give a finely mottled appearance, and emphysema is common. Interstitial emphysema or spontaneous pneumothorax may occur. The organism may be identified during life in material obtained by lung puncture or in tracheal and bronchial secretions obtained by intubation and bronchoscopy.

3.3.5 Pneumonia Staphylococcal/Candida Infection

See Sect. 3.3.4, Fig. 3.28.

3.3.6 Pleural Effusion/Chylothorax (Fig. 3.29)

In childhood, serious effusions into the pleural cavity are usually tuberculous, and they develop within 8–12 weeks of the primary infection. Rarely, the primary cause may be acute rheumatism, neoplasm, hydatid cyst, or chylous leakage. In tuberculosis cases, it is frequently possible to isolate tubercle bacilli from the fluid by culture or guinea-pig inoculation. Hydrothorax is seen in the nephrotic syndrome and cardiac failure; it is not, of course, inflammatory in origin.

The onset is often insidious with general loss of weight and slight fever. It may be more acute with pain in the chest, hypochondrium, or shoulder. Pleural friction may be audible but is usually transient and disappears as the effusion increases. When fluid has collected in the pleural space there is marked dullness to percussion, and the affected side of the chest shows diminished movement. In large effusions, the mediastinum is shifted toward the opposite side, and even the intercostal spaces may be filled in. In such cases there may be dyspnoea at rest. Above the fluid level the percussion note may have a "boxy" quality—skodaic resonance—due to compensatory emphysema of the un-collapsed portion of the lung. Auscultation over the effusion may reveal greatly diminished breath sounds and vocal resonance. In children, however, the breath sounds are sometimes well heard and bronchial in quality, so that consolidation is wrongly suspected. The posteroanterior radiograph shows a uniform opacity with a curved upper border. When air is also present, the fluid line is horizontal. Lateral and oblique films are necessary to define interlobar effusions. Thoracocentesis is necessary to confirm the diagnosis and to determine the nature of the fluid. In tuberculous cases the fluid is straw-coloured, and the cells are mostly lymphocytes, whereas in hydrothorax the cells are mostly of endothelial origin. The tuberculin skin test is of great diagnostic value.

3.3.7 Empyema/Hydatid Disease (Fig. 3.30a–c)

Over the past decade, the aetiology of empyema—a purulent collection with the pleural cavity—has vastly altered. Whereas empyema used to be either pneumococcal or streptococcal, the great majority of cases today are staphylococcal in origin and they are mostly encountered within the first year of life. Rarely, a pneumococcal empyema is seen in an older child in whom the diagnosis of lobar pneumonia has been delayed.

When an empyema complicates an acute staphylococcal pneumonia in an infant, or lung sepsis in cystic fibrosis, it is only part of the continuing septic process, so that the patient's temperature may show no significant alteration from its previous pattern. The physical signs in the chest are essentially those described in pleurisy with effusion, and the frequency with which bronchial breath sounds are heard in young infants can readily mislead the physician into thinking that they indicate consolidation alone. It is not always easy to detect the shift of the mediastinum that accompanies fluid in the pleural cavity in the case of a gravely ill dyspnoeic infant. Radiography and ultrasonography should be used to help in diagnosis, and if not responding to conservative treatment, aspiration should be performed. A neglected empyema can lead to alarmingly rapid deterioration and death, or it can become encysted.

Hydatid disease is highly infectious, often lodges in the liver and lungs, and presents as a cyst or multiple cysts of varying sizes (Fig. 3.30d–g).

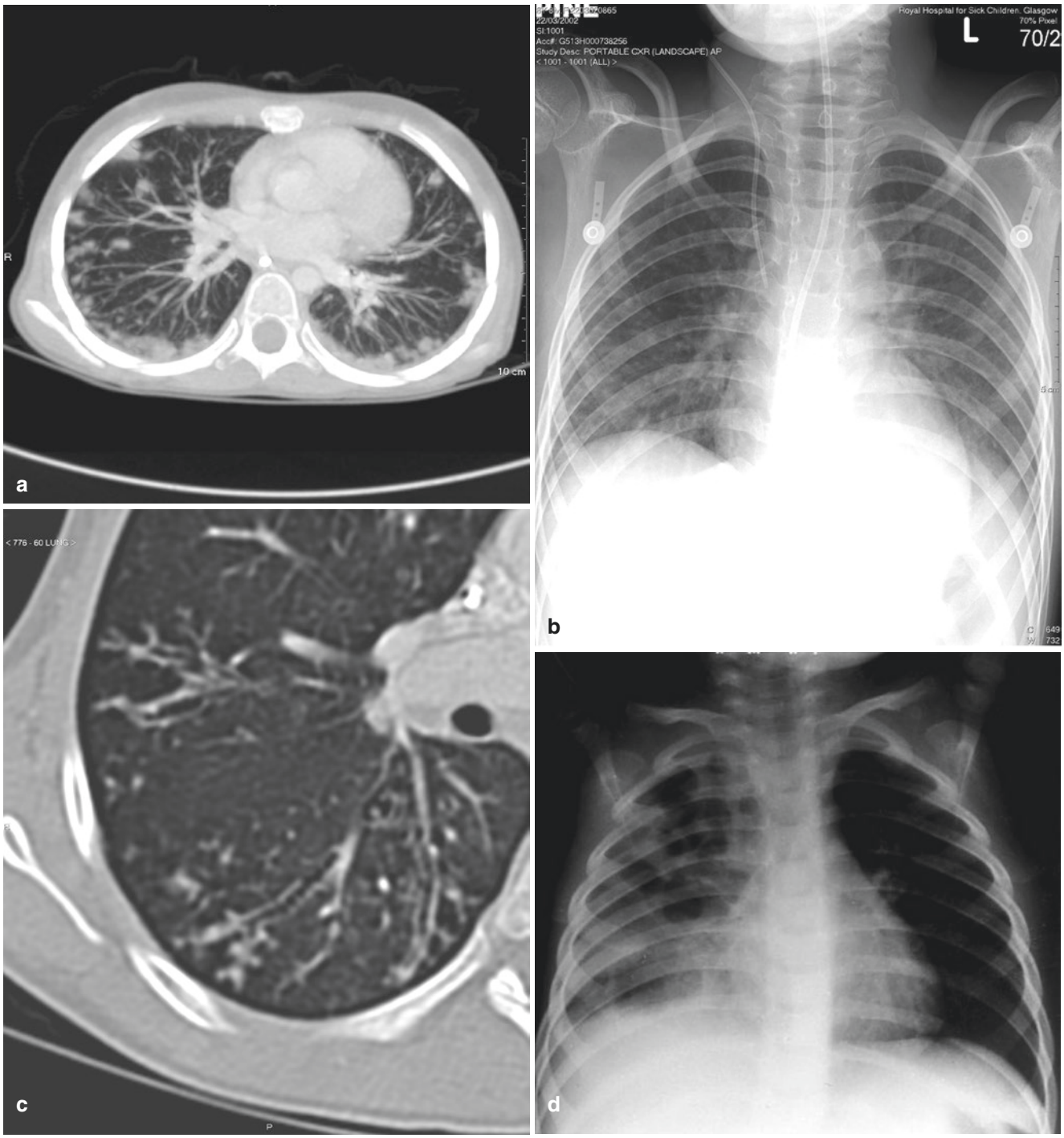

Fig. 3.28 (**a**) CT scan of candida pneumonia. (**b**) Candida pneumonia. (**c**) Mycobacterial pneumonia. (**d**) Staphylococcal pneumonia

3.3.8 Pericardial Effusion/Abscess

Pericardial effusion, if significant, produces low cardiac output and Tamponade. Diagnosis is made clinically: on auscultation the heart sounds are muffled and distant, and an echo quickly demonstrates the presence of fluid in the pericardial space with a constricted heart (Fig. 3.31).

3.3.9 Bullous Emphysema (Fig. 3.32)

The most common type of emphysema during infancy and childhood is obstructive emphysema. It may involve one lobe when a primary bronchus is partially obstructed to a degree that permits the entry of air into the alveoli but obstructs its egress during expiration (check valve). This is

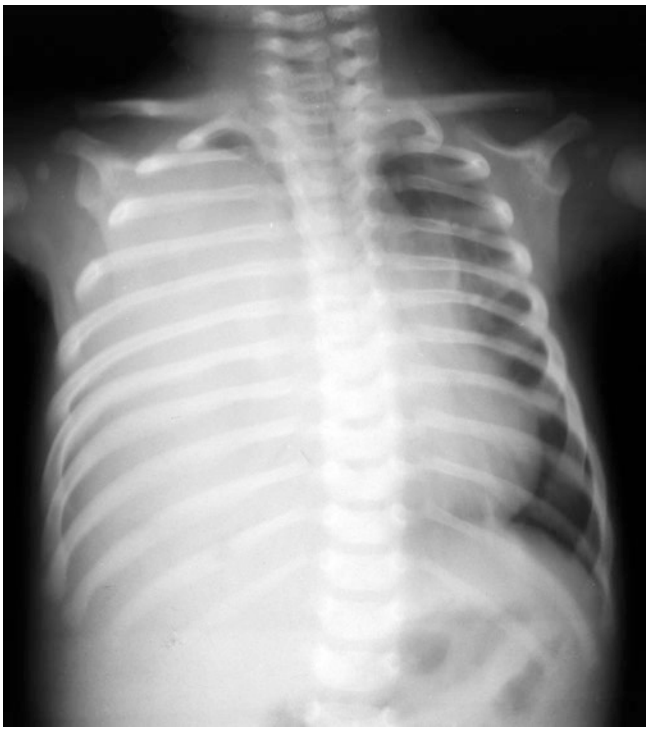

Fig. 3.29 Pleural effusion/Chylothorax

seen in primary tuberculosis but may also be caused by an inhaled foreign body. In lobar obstructive emphysema the lobe is over-distended with air. There is usually an "asthmatoid" wheeze at the open mouth, with hyperresonance and diminished breath sounds over the affected side of the chest. The mediastinum is displaced toward the opposite side and the ribs may even be separated. The radiograph confirms this, and shows increased translucency in the emphysematous lobe, which may in fact herniate across the mid-line.

Check-valve obstruction in the bronchioles results in generalised bilateral obstructive emphysema. This can occur temporarily in acute bronchiolitis, or in a chronic form that can lead to corpulmonale in cystic fibrosis. Generalised emphysema is uncommon in asthma during childhood. Radiographs reveal hypertranslucency in both lung fields, flattening and diminished excursions of the diaphragm, and the ribs tend to be horizontally placed instead of being "tiled."

Bullous emphysemais seen most often in staphylococcal pneumonia when multiple bullae or pneumatocoeles develop. If these rupture into the mediastinum, a rapidly fatal interstitial emphysema, without or with spontaneous

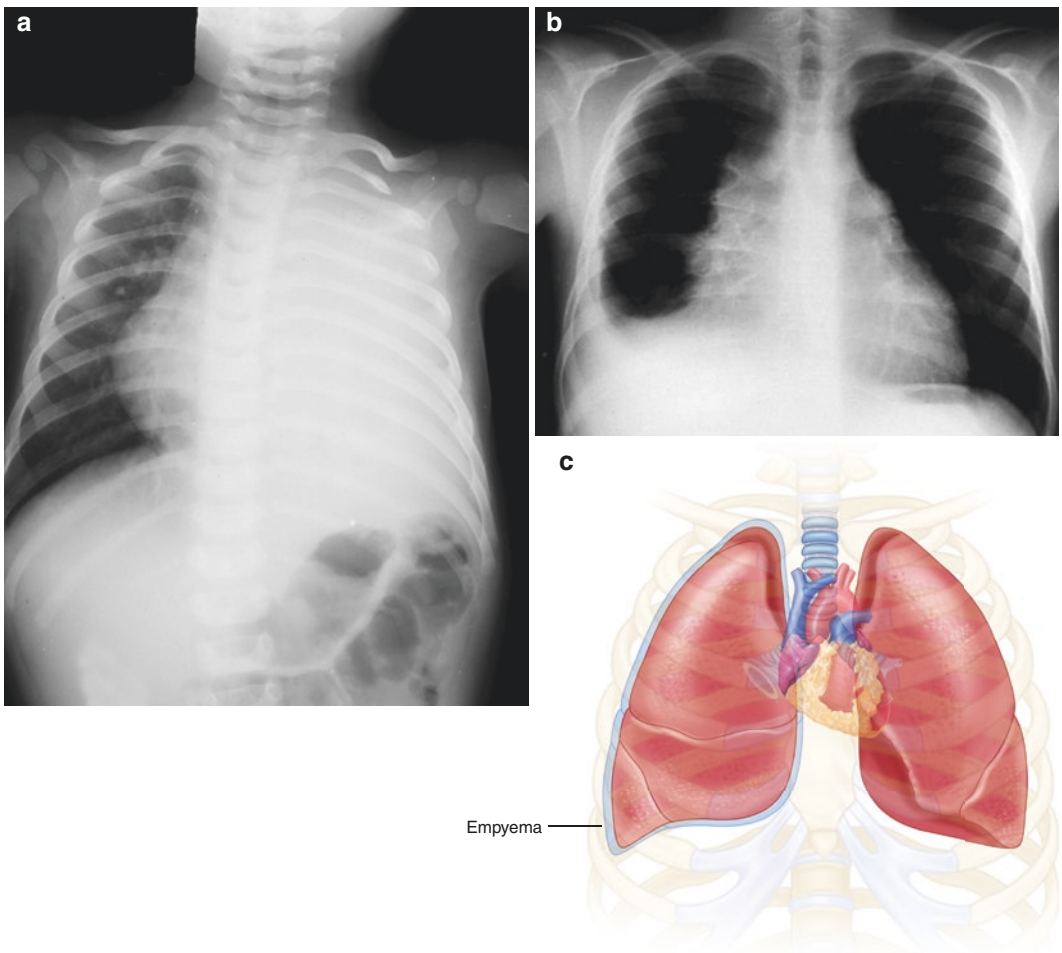

Fig. 3.30 (**a**, **b**) Empyema. (**c**) Diagram of empyema. (**d**, **e**) Hydatid cyst. (**f**) Multiple hydatid cysts in the liver. (**g**) Hydatid cyst (**d**–**g**: *Courtesy of* Dr. Nour)

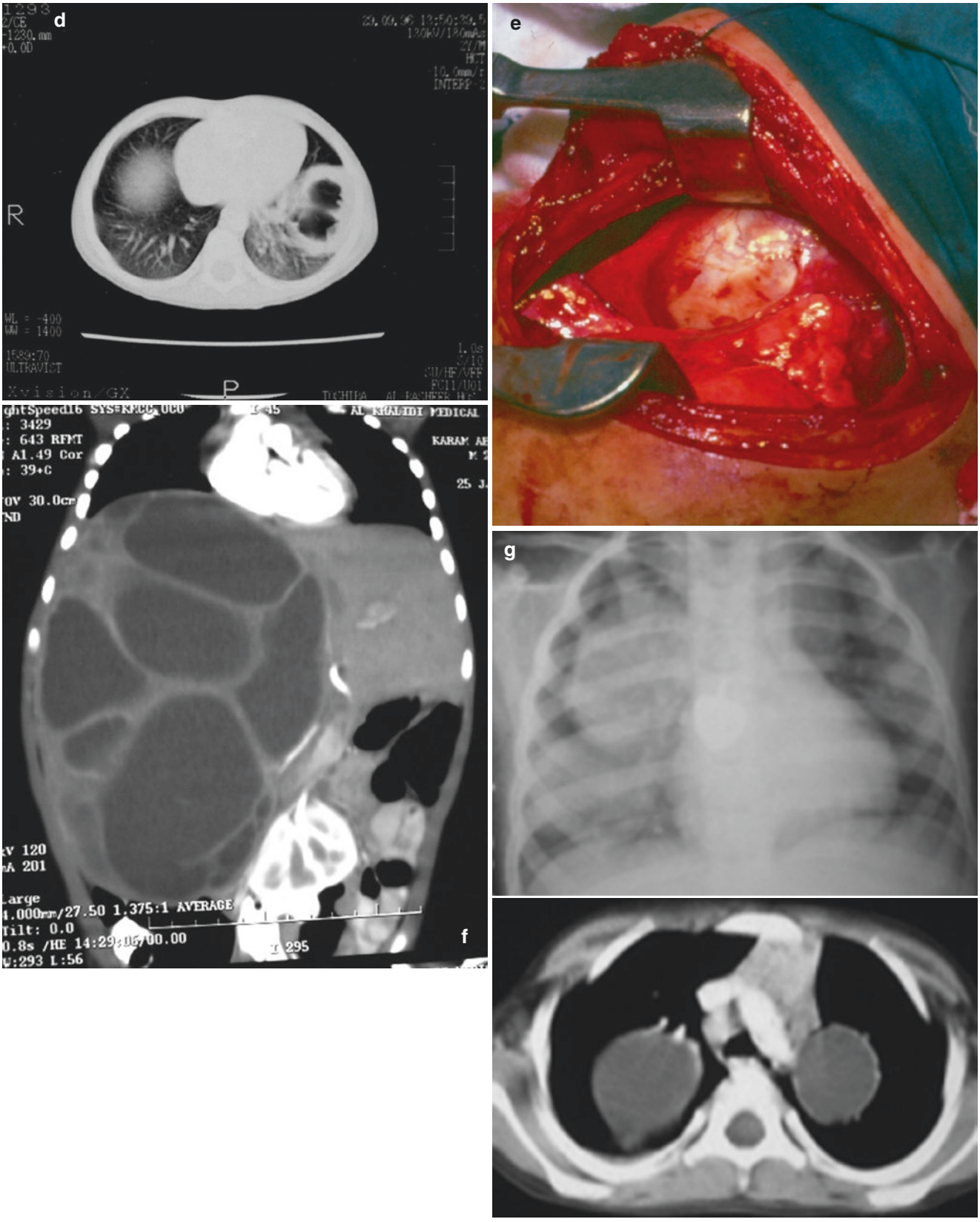

Fig. 3.30 (continued)

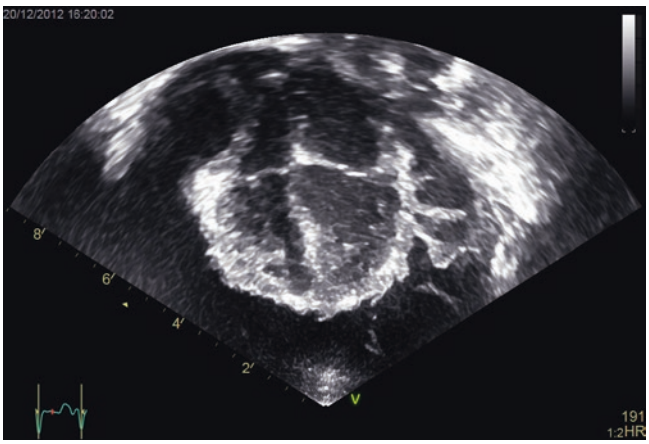

Fig. 3.31 Pericardial effusion

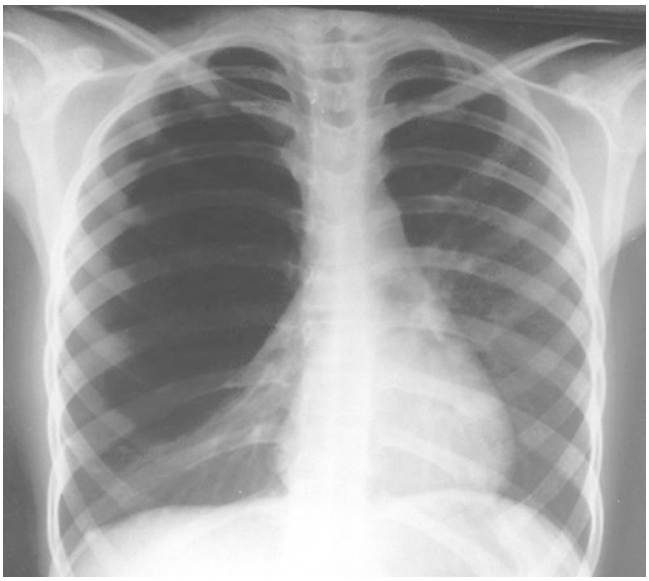

Fig. 3.32 Bullous emphysema of the right lung

pneumothorax, results. Subcutaneous emphysema with palpable crackling under the skin may arise from interstitial emphysema or from perforation of the trachea, pharynx, or oesophagus. It may also complicate thoracentesis. Interstitial emphysema and pneumothorax may also complicate attempts at resuscitation of the new-born by tracheal intubation and the administration of air or oxygen under pressure.

3.3.10 Lung Abscess (Fig. 3.33)

This is an infective process and often is a complication of a pneumonic process that has gone untreated. It may also be the result of an inhaled foreign body or a peanut aspiration. The lung parenchyma is destroyed and an abscess with pus in an air-filled cavity can be seen on X-ray with a fluid level. It can also be part of a clinical picture of bronchiectasis. Multiple abscesses of different sizes are usually the result of a septicaemia in an immunocompromised host.

3.3.11 AxillaryGland (BCG) (Fig. 3.34)

An enlargement of one or more axillary glands in the axilla may occur following a Bacillus Calmette–Guérin (BCG) vaccination.

3.3.12 Bronchiectasis (Fig. 3.35a, b)

Bronchiectasis is almost always an acquired disease. Two factors are commonly present: (1) bronchial occlusion with absorption atelectasis; and (2) infection that is usually due to pyogenic bacteria such as pneumococcus, haemophilus, and staphylococcus, but may sometimes be tuberculous. The diseases most commonly preceding bronchiectasis are bronchopneumonia, measles, pertussis, cystic fibrosis, inhaled foreign body, or primary tuberculosis. A very few cases may be related to some congenital weakness in the bronchial walls, structural abnormality of the lung such as sequestered lobe, or ciliary dyskinesis (Fig. 3.35c, d).

Bronchiectasis is nowadays much less common due to the use of antibiotics. It is mainly encountered in children from poorer sections of communities who live in overcrowded conditions that expose them to repeated respiratory infections, who have poorer nutrition, and, moreover, are less likely to receive an adequate convalescence after acute illnesses such as measles and pneumonia. The bronchiectatic patient of a bygone era reached a pitiful state in which putrid breath made him a burden to his fellows and himself. Sputum was abundant and malodorous. Exertion precipitated distressing outbursts of coughing and dyspnoea. The fingers and toes were grossly clubbed. Cachexia was marked. Death finally resulted from empyema, brain abscess, corpulmonale, or amyloid disease (Fig. 3.35e, f).

The clinical presentation today is very different. The child is usually brought to the physician because of persistent cough, dating often from an acute respiratory illness some months or years previously. In a few male cases, the bronchiectasis is a feature of congenital hypogammaglobulinaemia. In others it is part of the clinical

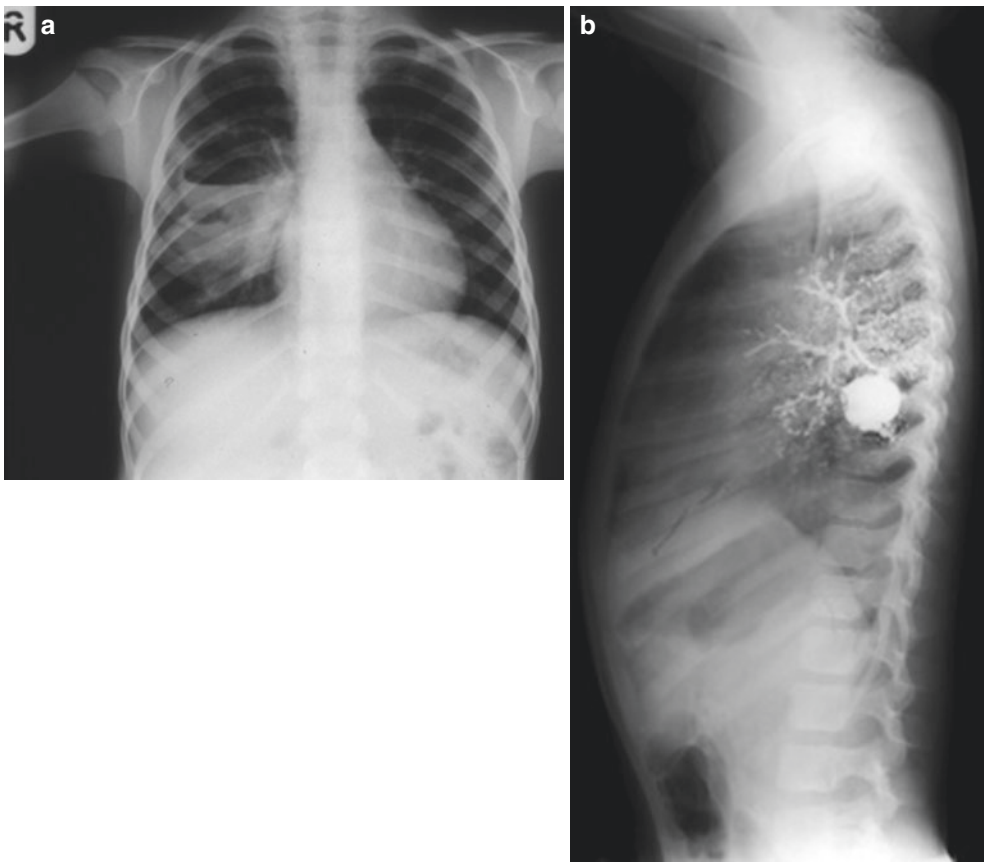

Fig. 3.33 (**a**, **b**) Lung abscess

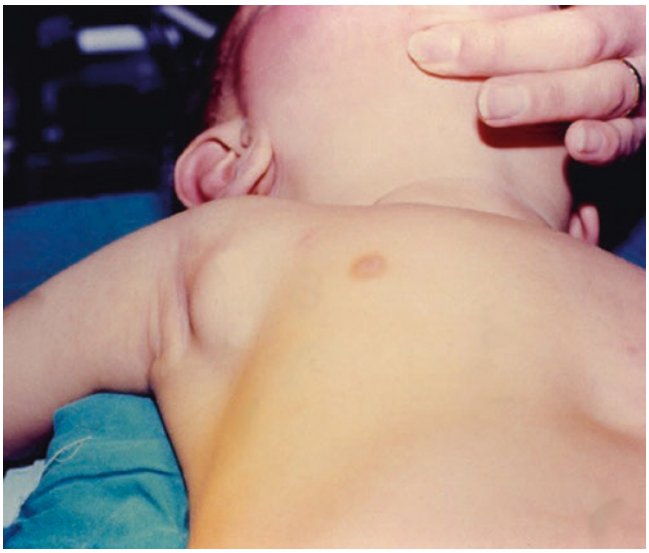

Fig. 3.34 Axillary mass

spectrum of cystic fibrosis. Purulent sputum is obtainable, but it is usually neither abundant nor malodorous. Haemoptysis, common in the adult, is a rare sign in the child. He is, however, likely to suffer from periodic episodes of fever and malaise, with aggravation of his cough, due to the retention of infected secretions within the bronchiectatic area of the lung. Nonetheless, his general condition is often remarkably good, and clubbing of the fingers is usually quite slight. Physical signs over the lungs are variable. There may be an impaired percussion note, diminished breath sounds, and mediastinal shift to the affected side. After the dilated bronchi have been emptied of pus by postural drainage, the breath sounds may become bronchial or amphoric with whispering pectoriloquy. In some cases, there are numerous crepitations over the diseased lobe. Chronic sinusitis is an almost invariable accompaniment, and although the causal relationship of one to the other is not clear, ciliary damage may be the common factor (Fig. 3.35g).

Radiographs may reveal cavities in the saccular type of bronchiectasis, whereas in the more common cylindrical type there are only heavy linear markings or, sometimes, no obvious abnormality. Confirmation of the diagnosis and estimation of the extent of the process can be obtained from well-planned bronchography. Bronchoscopy is frequently informative and imperative when there is suspicion of a foreign body. Sputum should be cultured from time to time to assist in the choice of suitable antibiotics. The most common predominating organism is H. influenzae. When staphylococci or pseudomonas are isolated, the probability of cystic fibrosis is high. In male children it is wise always to measure serum gamma globulin values.

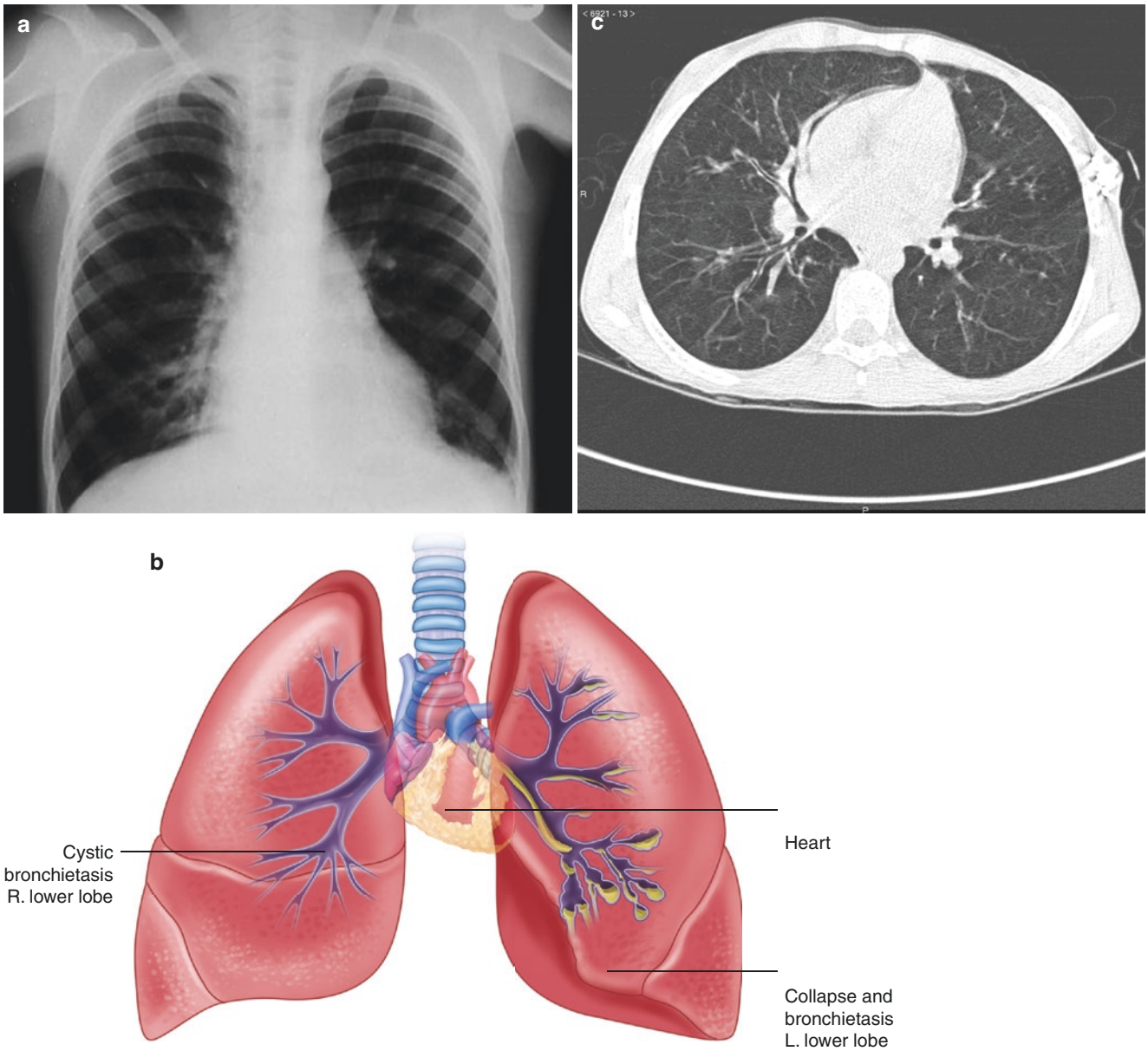

Fig. 3.35 (**a**) Bronchiectasis. (**b**) Bronchiectasis diagram. (**c**) Bronchiectasis CT. (**d**) Bronchiectasis signet ring formation. (**e**) Bronchiectasis with mucus plugging. (**f**) Bronchiectasis of the right upper lobe. (**g**) Bronchiectasis

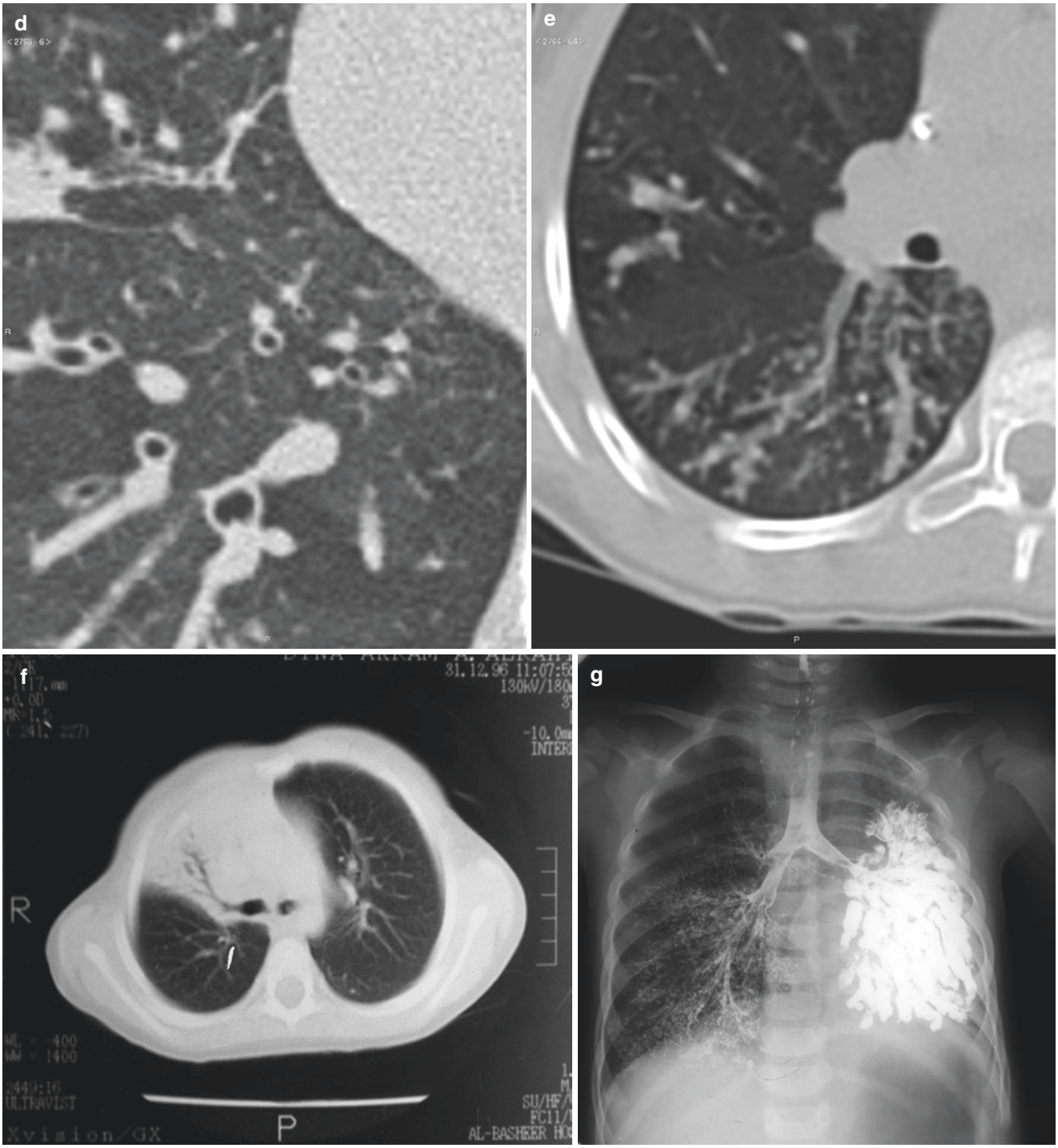

Fig. 3.35 (continued)

3.3.13 Aspiration Pneumonia/Meconium Aspiration (Fig. 3.36)

3.3.13.1 Aspiration Syndrome: Absorption Collapse (Atelectasis) of the Lungs

Resorption of air from a pulmonary segment or lobe is common in young children due to complete bronchial occlusion ("stop valve"). The thin-walled bronchi and bronchioles can be compressed by enlarged lymph nodes in tuberculosis, measles, pertussis, and malignant reticulosis. The narrow lumens can be blocked by mucopus, inhaled foreign bodies, or stomach contents, and by mucosal oedema due to allergy in asthmatic subjects.

The atelectatic portion of the lung occupies a smaller volume than normal. This causes compensatory emphysema of the other lobes of the lung, mediastinal shift to the affected side, a rise in the level of the diaphragm, and by some falling inwards of the chest wall.

The features will largely depend upon the primary disease. It is important to remember that while the inhalation of a foreign body produces immediate respiratory distress with coughing, choking, gagging, stridor, and cyanosis, it is possible for this short episode to pass unobserved in the case of a toddler. There may be quite a long "silent" interval before secondary bacterial infection in the obstructed bronchus produces symptoms. Foreign bodies composed of vegetable matter, e.g. peanuts, result in early severe bronchitis with fever, cough, and dyspnoea, whereas metallic or plastic substances may remain in situ for long periods without giving rise to obvious trouble. A segment of atelectasis may be obscured clinically by compensatory emphysema, and the condition becomes obvious only when posterio-anterior radiographs are examined. When a lobe or whole lung is collapsed there is diminished movement of the affected side of the chest with impaired resonance, diminished breath sounds, and tracheal or mediastinal shift toward the affected side. Collapse of an upper lobe can be differentiated from consolidation on the radiograph by the fact that in the former the lower border is convex, whereas in the latter it forms a straight line. A collapsed lower lobe is visualised as a jib-shaped shadow. The airless right middle lobe is seen in the lateral view as a triangular shadow.

3.3.14 Asthma (Fig. 3.37)

Asthma is a common disease and affects more than 10% of children. Yet it remains commonly under-diagnosed and under-treated.

The existence of an allergic basis to true bronchial asthma cannot be doubted. This disease is caused by hyperresponsiveness of the large and small airways of the tracheobronchial stress to various allergens. Rarely, attacks can be traced to exposure to one specific allergen, but in other cases there appears to be a plethora of possible anti-

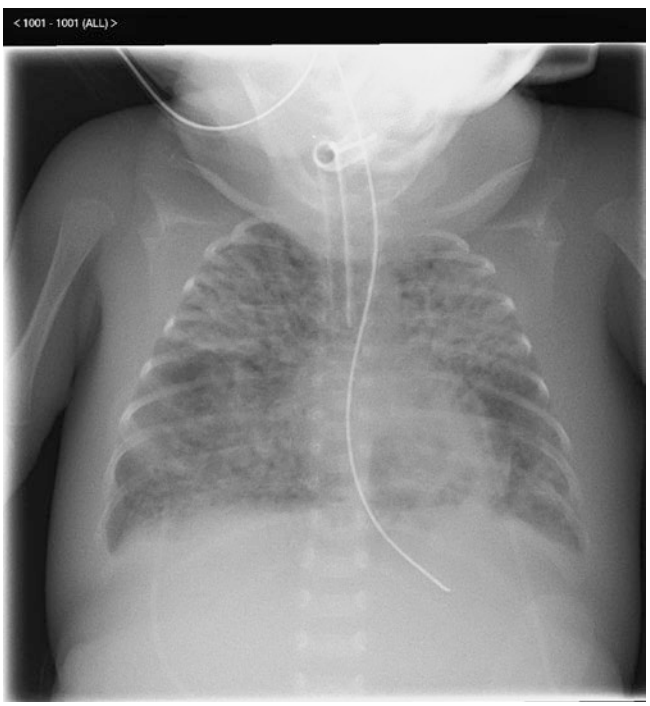

Fig. 3.36 Meconium aspiration

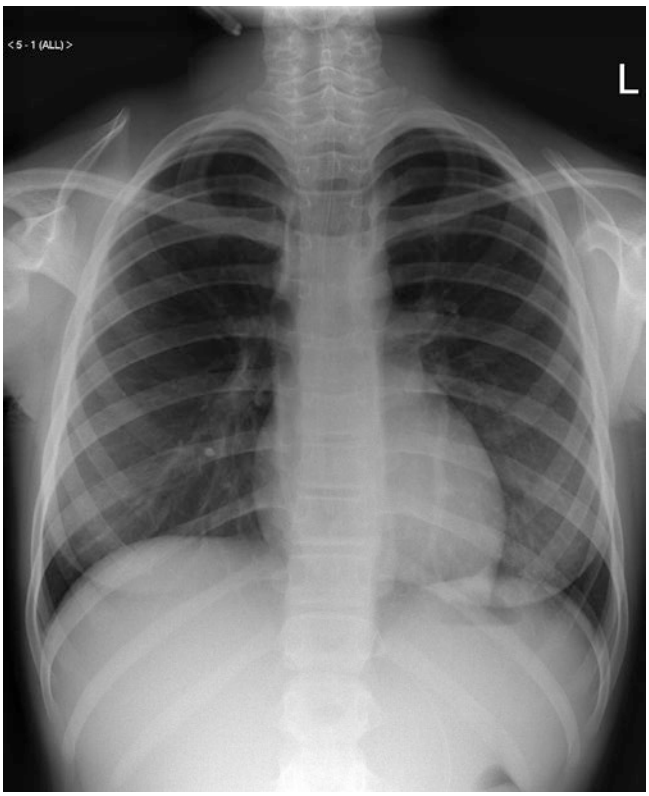

Fig. 3.37 Overinflated chest in acute asthma

gens. One of the difficulties in interpretation lies in the fact that symptomless and apparently normal individuals may quite commonly react to skin tests with a variety of foreign antigens. An important observation concerns the role of house-dust mites, Dermatophagoides pteronyssinus and farinae, as causes of allergic asthma. Several workers have now expressed the view that house-dust allergy promoted by these mites is the most common cause of allergic asthma in children in the United Kingdom. House dust from floors and even more from the surfaces of mattresses may contain 500 or more Dermatophagoides per gram. There is overwhelming evidence that smoking, and some evidence that passive smoking, produce a rapid reduction in lung function. Also, a child may show evidence of allergy to domestic pets and exposure to seasonal pollens. In children, asthma is rarely precipitated by food or drink, but if so, avoidance is indicated. The role of exercise-induced asthma is very important, especially in children who are expected to take part in regular games at school. It is also certain that emotional disturbances of a quite ordinary kind can precipitate attacks of asthma in some individuals, and psychotherapeutic approaches have been shown to be of value as an adjunct to standard drug treatment. That there is a genetic influence is also clear enough frequency with which obtained family history includes asthma or other allergic conditions such as eczema and hay fever. Many children with asthma have earlier suffered from atopic eczema, and they may continue to suffer from flexural eczema—the prurigo-asthma syndrome. They usually have raised total serum IgE concentrations and give positive reactions to skin tests of one or more of the common inhalant allergens. Asthmatic attacks are often precipitated by intercurrent respiratory viral infections. In some children this may be a manifestation of sensitisation to viral antigens, but the picture is confused by our not infrequent inability to distinguish true asthma from "wheezy" bronchitis, where the sole aetiological role may be played by virus and bacteria. This difficulty is particularly great in the young infant in whom a diagnosis of asthma is frequently impossible until time has elapsed. Although wheeze is not synonymous with asthma, asthma is common and alternative diagnoses are rare. Gastro-oesophageal reflux with aspiration may cause episodes of wheezing.

The typical acute asthmatic attack is rarely seen before the second birthday. It frequently starts during the night when the child is awakened by expiratory respiratory distress. He looks frightened as well as distressed. He can be heard to wheeze with each forced expiration and may show some cyanosis. The chest is held in the full inspiratory position and the prolonged expiratory phase can be seen to involve the use of the accessory muscles of respiration. The percussion note is hyper-resonant and there is diminution of the areas of cardiac and liver dullness. Air entry to both lungs is greatly reduced so that the breath sounds are almost inaudible in some patients. The expiratory phase is prolonged, and there may be many rhonchi. Coarse crepitations are more common in very young children. The sputum is composed of sticky mucus. Microscopic examination reveals many eosinophils and mucus in the shape of spirals. The blood may also show a mild eosinophilia.

Many asthmatic children become completely free from bronchospasm between attacks. In others, expiratory difficulty and wheezing become established as a more or less permanent disability. The sternum may become unduly prominent with the development of Harrison's sulci through the years. In some children, chronic respiratory infection still further aggravates the situation. Occasionally bronchial obstruction from tenacious mucus results in segmental or lobar atelectasis. This usually resolves spontaneously, and bronchiectasis is a rare complication. It should also be remembered that some children with asthma present only with a persistent nocturnal cough, which may respond to the appropriate anti-asthmatic therapy. Some children with severe asthma grow slowly, especially in middle childhood, and most of these have a delayed bone age. The vast majority, however, will eventually attain normal height. Asthma may endanger life during childhood, and it has been reported that in the United Kingdom approximately 1 in 21,000 asthmatic children die from the disease each year. Underrecognition and under-treatment of asthma contribute to these unnecessary deaths.

3.4 Trauma

Trauma is the most common cause of death in childhood. In the post-neonatal period to the age of 1 year, only 3% of deaths are due to injury or poisoning. From ages 1 to 4 years, however, 26% of deaths are caused by injury and poisoning, 35% from ages 5 to 9, and 44%, in boys, from ages 10 to 14 years. Many other children survive injuries, but go through life handicapped and often have severe physical and deep psychological scars. It is important that children are brought up in an environment in which it is safe and healthy for them to play and grow whilst allowing them to gain enough experience in living. Many injuries can be prevented, and it is the realisation of the dangers in the home and on the roads that has encouraged people, through bitter experience, to introduce legislation to prevent these hazards. The introduction of new toys using mercury/alkaline batteries has introduced a new hazard of severe burns and perforation of the oesophagus when these are accidentally swallowed.

The infant's mobility between the ages of one and two brings with it many falls and accidents. From the ages of 2 to 5, the child's world continues to expand rapidly, and the danger of accidents increases. More time is spent out of doors playing with other children, exploring and investigating their environment. A different set of dangers arises as the child begins school.

Trauma to the respiratory tract is uncommon because of the protection afforded by the compliant thoracic cavity. Infants and children are at risk from inhalation of foreign bodies. Children have a habit of putting objects in their mouth that may be inhaled inadvertently and cause, at worse, choking and death if prompt treatment is not instituted, or an episode of choking with subsequent persistent respiratory signs and symptoms. A misdiagnosis of asthma may be made, and the clue is the history of the acute choking episode. Inhalation of peanuts is dangerous; X-ray appearances vary from overdistension of the lung due to air-trapping, to collapse, where the foreign body obstructs the lumen and air is absorbed from the obstructed lobe or lung. Bronchoscopy and removal of the inhaled foreign body should be performed as an emergency. Intrapulmonary trauma occasionally occurs in infants who have suffered accidental trauma in falls or traffic accidents. Pulmonary contusion improves in most without active treatment. More severe injury to the lung is rare, but a torn bronchus or haemothorax may require urgent closure or drainage. The paediatric patient's thoracic cage is so much more resilient than the more rigid adult and can withstand remarkable trauma with relatively minimal damage.

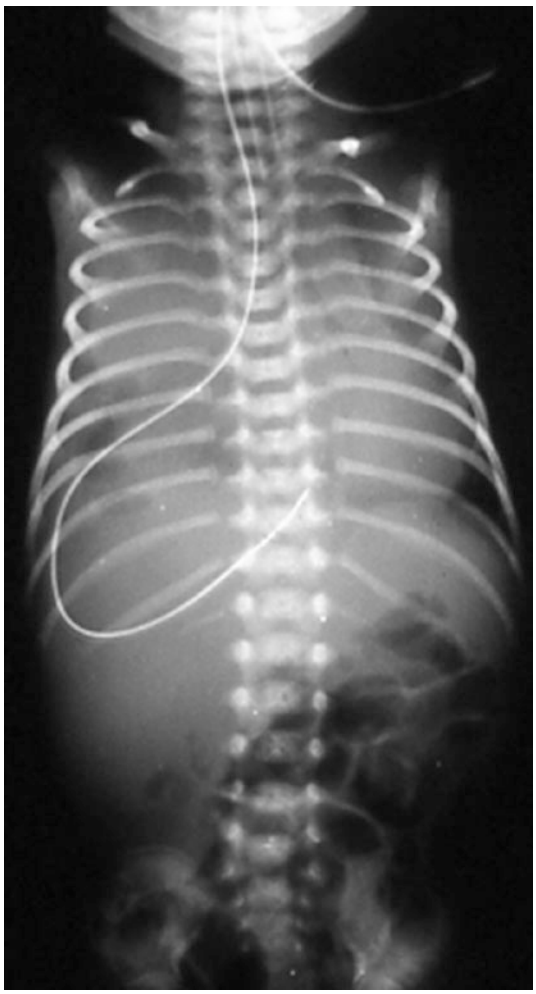

Fig. 3.38 Perforated oesophagus tube right pleural

3.4.1 Oesophageal Perforation/Stricture (Fig. 3.38)

This condition can be caused by (1) ingestion of caustic soda; (2) traumatic injury during rigid or flexible endoscopy, especially in a diseased oesophagus; or (3) complications following repair of a TOF. When it happens, there is an immediate chemical mediastinitis and the patient is pyrexial and goes rapidly into a shocked state. If the perforation is in the thoracic oesophagus, then a pneumothorax and pleural effusion results, whereas if it occurs in the abdominal oesophagus, one gets a pneumoperitoneum and peritonitis. Dye studies will confirm the site of perforation.

3.4.2 Pneumothorax (Fig. 3.39a–d)

Establishing respiration in the neonatal period is a major change that most infants successfully achieve with rapid uniform aeration of the lungs. In some infants, particularly the preterm who may have a surfactant deficiency, the lungs do not aerate evenly and the baby may generate patchy areas of high intra-alveolar pressures with resultant emphysematous ballooning of alveoli; this may rupture through the visceral pleura and result in a pneumothorax. This is a more common complication in infants and requires resuscitation and intermittent positive pressure ventilation. When air continues to leak into the pleural cavity, a tension pneumothorax ensues with displacement of the mediastinum and compression of the contralateral lung (Fig. 3.39e, f).

When the pneumothorax is small, the lung falls away from the chest wall ("relaxation collapse"), but there will be no signs directly referable to the pneumothorax. A tension pneumothorax with a strongly positive intrapleural pressure ("compression collapse") causes severe pain, dyspnoea, cyanosis, and circulatory collapse. There is hyperresonanceover the affected side and the breath sounds are distant or inaudi-

ble. The mediastinum and trachea may be displaced to the opposite side. When there is fluid as well as air in the pleural cavity, gurgling or splashing may be heard as the child's position is moved. Transillumination or a radiograph will confirm the diagnosis, although in the infant there may be difficulty in differentiating pneumothorax from a large diaphragmatic hernia or giant emphysematous bulla. Screening with a contrast swallow usually resolves the difficulty.

3.4.3 Pulmonary Haemorrhage/ Contusion/Pulmonary Interstitial Emphysema (Fig. 3.40)

When premature neonates are vitaminK-deficient they are susceptible to haemorrhage and can have a pulmonary haemorrhage. This is a very serious condition. The first indication is a change in the vital signs and blood in the endotracheal

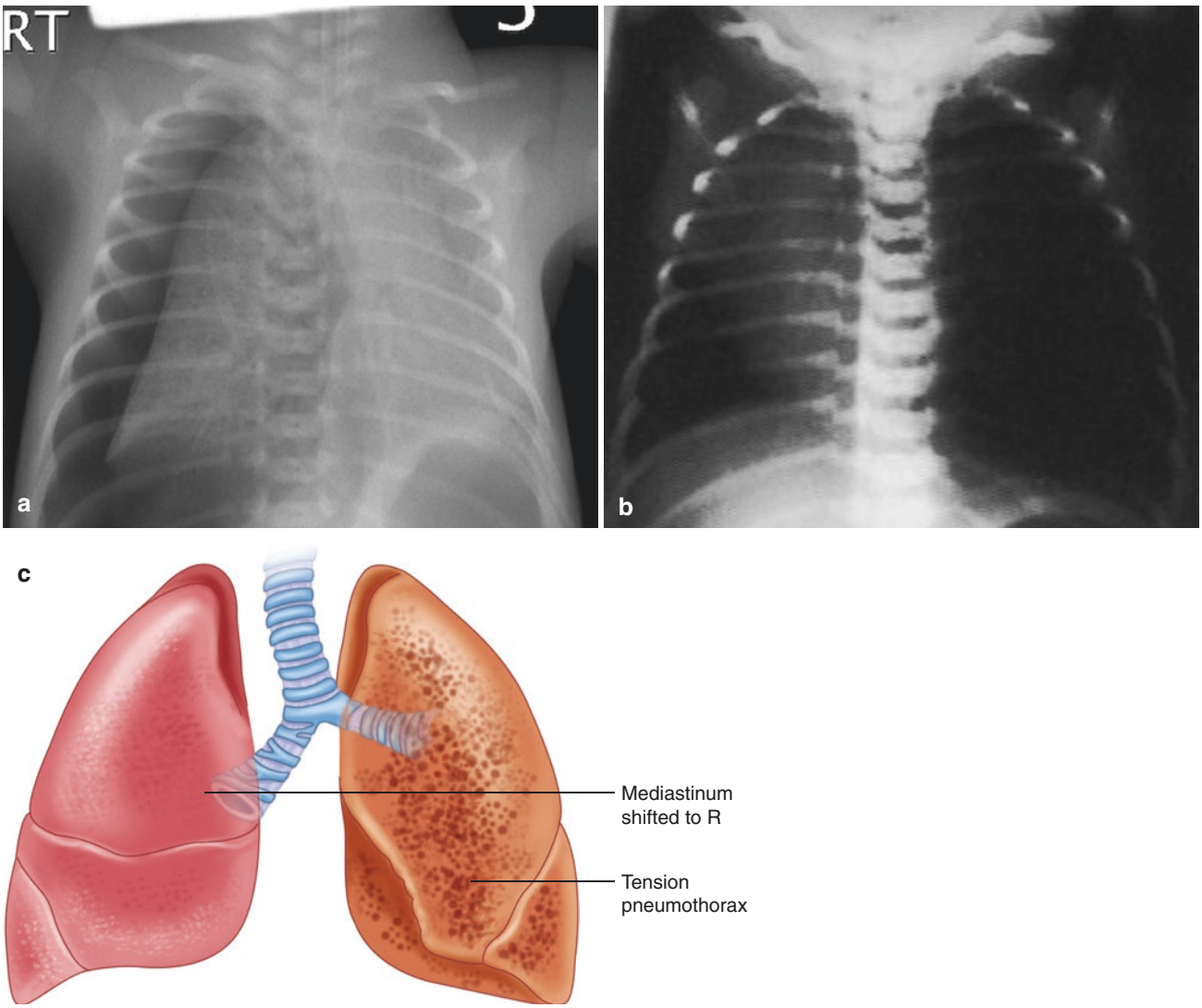

Fig. 3.39 (**a**, **b**) Pneumothorax. (**c**) Pneumothorax diagram. (**d**) Tension pneumothorax right side. (**e**) Pneumothorax in a post-op patient with Marfan's Syndrome. (**f**) Post-operative pneumothorax after sub-pulmonic CCAM removed

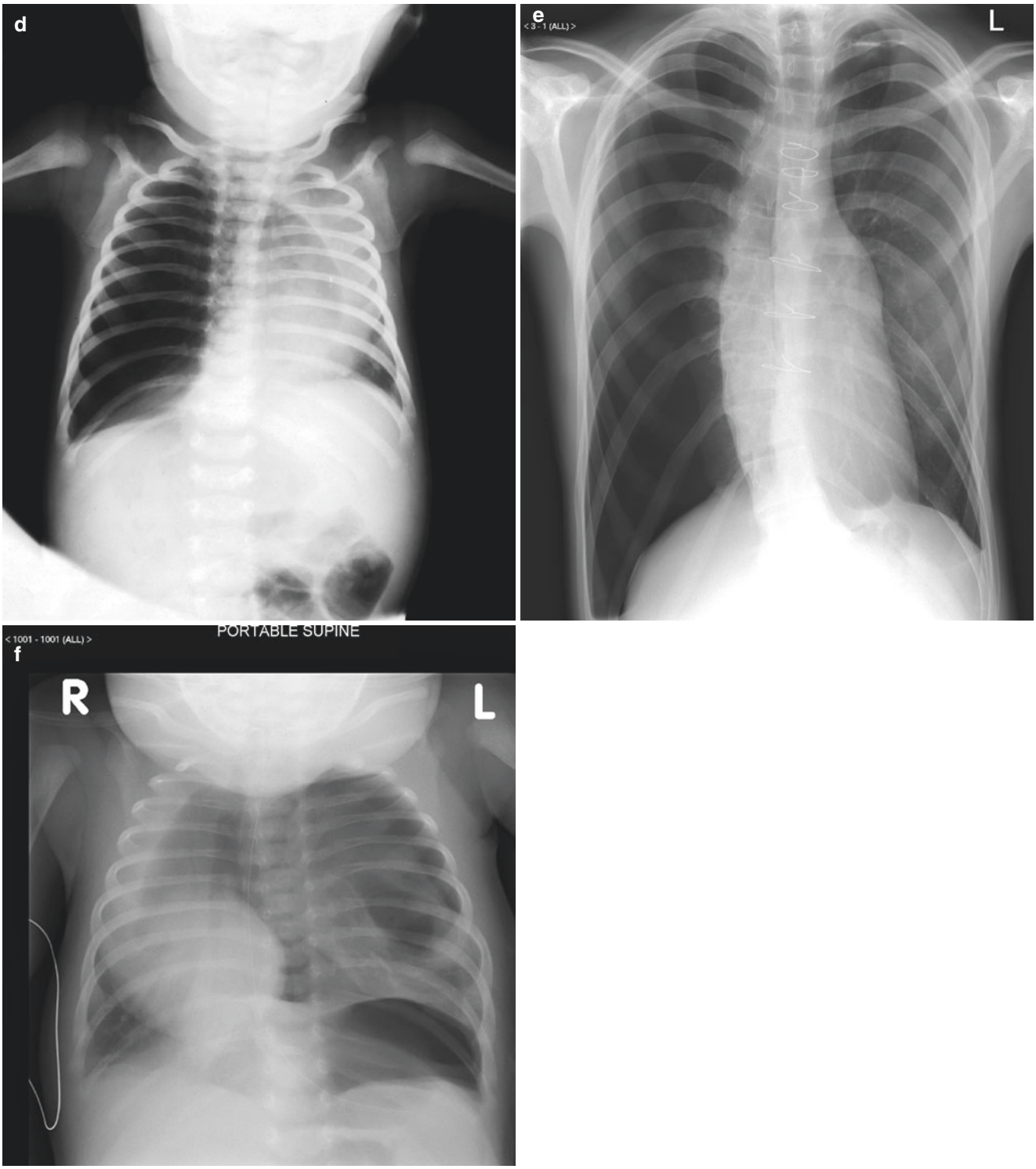

Fig. 3.39 (continued)

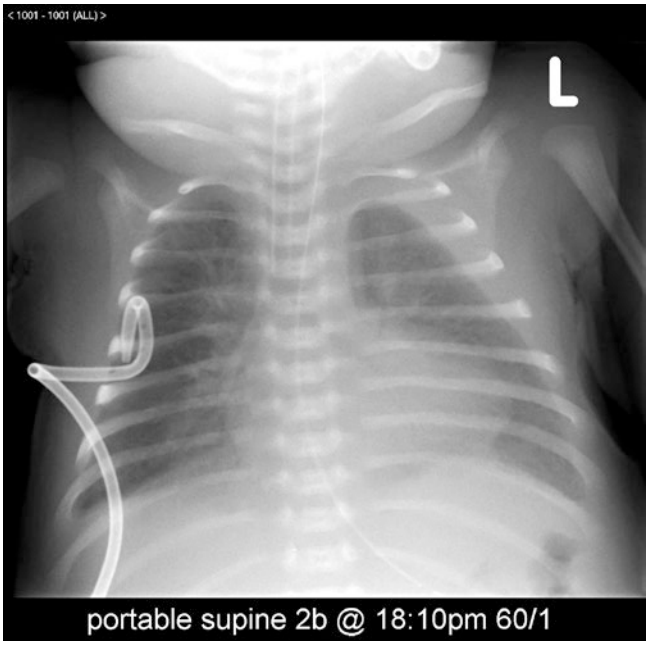

Fig. 3.40 Pulmonary interstitial emphysema

tube (ET) on suctioning. During routine toiletry of the ET tube, an X-ray shows opacity of the lung. Trauma can also be the cause of a pulmonary contusion from direct injury, like an excessive force applied to the rib cage.

Severe asphyxia can cause pulmonary interstitial emphysema (PIE), and there is an urgent need to ventilate and on occasion commencement of ECMO. Sometimes the cause can be a viral or microbial pathogen.

3.4.4 Chylothorax/Pleural Effusion/ Haemothorax (Fig. 3.41)

Sudden compression of the thorax can produce traumatic asphyxia. The mechanism by which this occurs is a retrograde pressure wave moving up to superior vena cava and valveless great veins to cause interstitial haemorrhage in the skin of the head, neck, and shoulders. Subconjunctival haemorrhage and submucous petechiae as well as a purple skin suffusion may be evident. This skin suffusion must be differentiated from cyanosis, which may result from additional intrathoracic damage. Post-traumatic flail chest is rarely seen in childhood.

3.4.5 Diaphragmatic Hernia (Fig. 3.42)

Traumatic diaphragmatic hernia is often caused by a polytrauma accident. The ruptured diaphragm can be missed in a patient with a severe head injury. The split diaphragm picked up on a routine X-ray allows the small and large intestines into the chest with compression of the lung and mediastinal displacement.

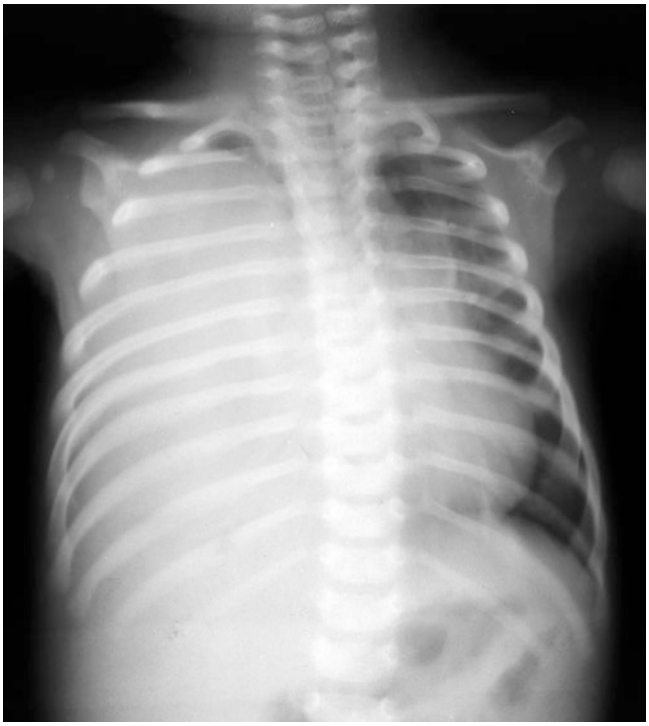

Fig. 3.41 Chylothorax, pleural effusion, haemothorax

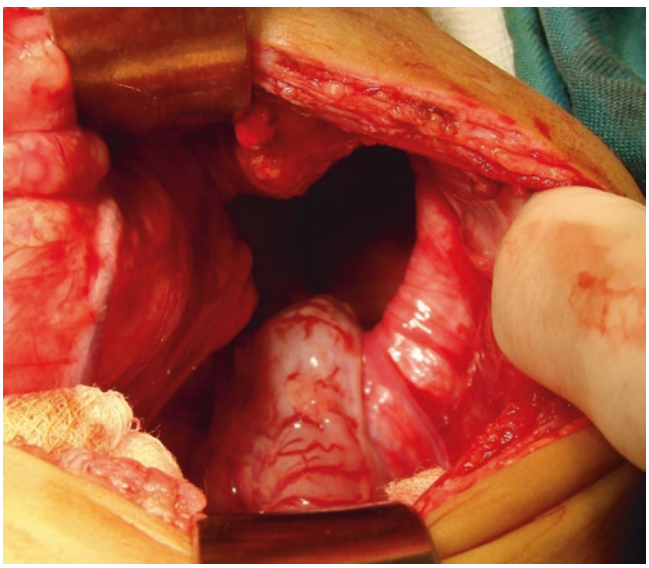

Fig. 3.42 Ruptured diaphragm post fundoplication, operative view

3.4.6 Foreign Bodies (Fig. 3.43a–c)

Children frequently place objects in their mouth and occasionally accidentally swallow them. Most pass down the alimentary tract and out of the anus in 24–48 h, but occasionally the coin, pin, or toy may stick in the oesophagus. This causes discomfort and inability to swallow freely. The offending foreign body may be removed by passing a catheter beyond the foreign body, inflating a balloon on the distal end of the

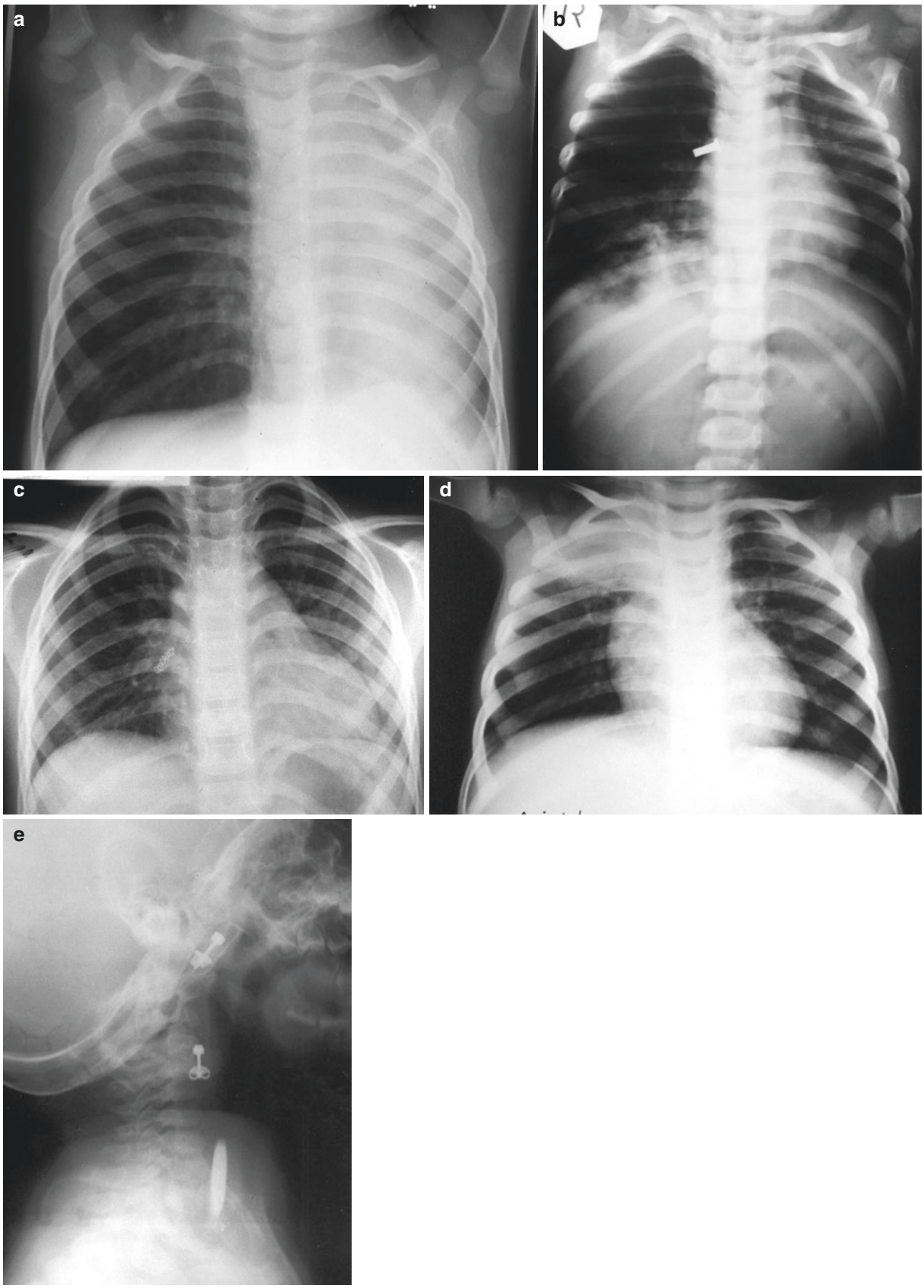

Fig. 3.43 (**a**) Peanut inhalation foreign body in right main bronchus. Note trapped air in right lung. (**b**) Foreign body aspiration in right bronchus. (**c**) Foreign body aspiration in right lower bronchus. (**d**) Foreign body aspiration in right upper bronchus with a collapsed lobe. (**e**) Foreign body in oesophagus—lateral chest X-ray

catheter, and then withdrawing the catheter and the object proximal to it. If this fails, removal is performed under direct vision through an endoscope while the child is under anaesthesia (Fig. 3.43d, e).

3.4.7 Fractured Ribs/Sternum (Fig. 3.44)

3.4.7.1 Penetrating Wounds of the Chest

These uncommon childhood injuries may follow impalement by a spike when falling off a fence or out of a tree. Life is threatened as soon as the pleural cavity is opened, and survival may be complicated by a haemothorax or an empyema. Wounds of the heart or great vessels are usually rapidly fatal, but prompt resuscitation and surgery may achieve a successful outcome.

3.4.7.2 Fracture of the Ribs

Broken ribs are usually caused by a crush injury or fall. They usually heal without any problems within 2–3 weeks. Early analgesia is necessary, but pain soon disappears. Liver damage with right-side injury or splenic damage with left should be excluded.

3.4.7.3 Fractures of the Sternum

This rare entity, if isolated, requires no treatment.

3.4.8 Surgical Emphysema (Fig. 3.45a, b)

Surgical emphysemas are caused by nonpenetrating injuries to the chest. They vary from simple contusions of the chest wall to gross damage to the lung, thoracic duct, heart, and aorta. Localised contusion, which resolves in 2–3 weeks, is the most common visceral injury. Children with flexible tho-

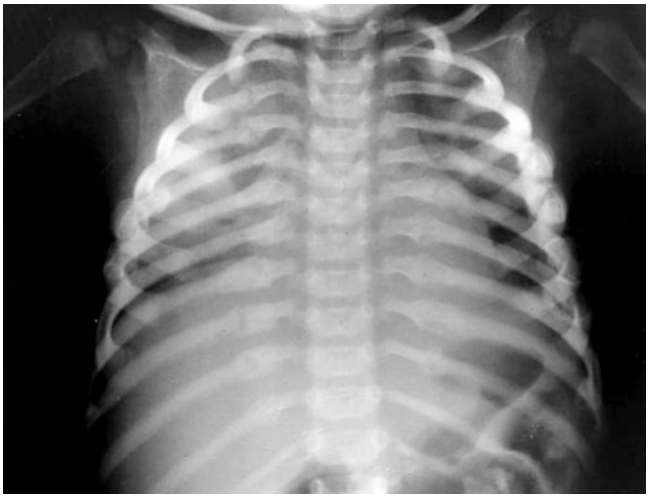

Fig. 3.44 Multiple fractured ribs. Evidence of healing old fractures posteriorly

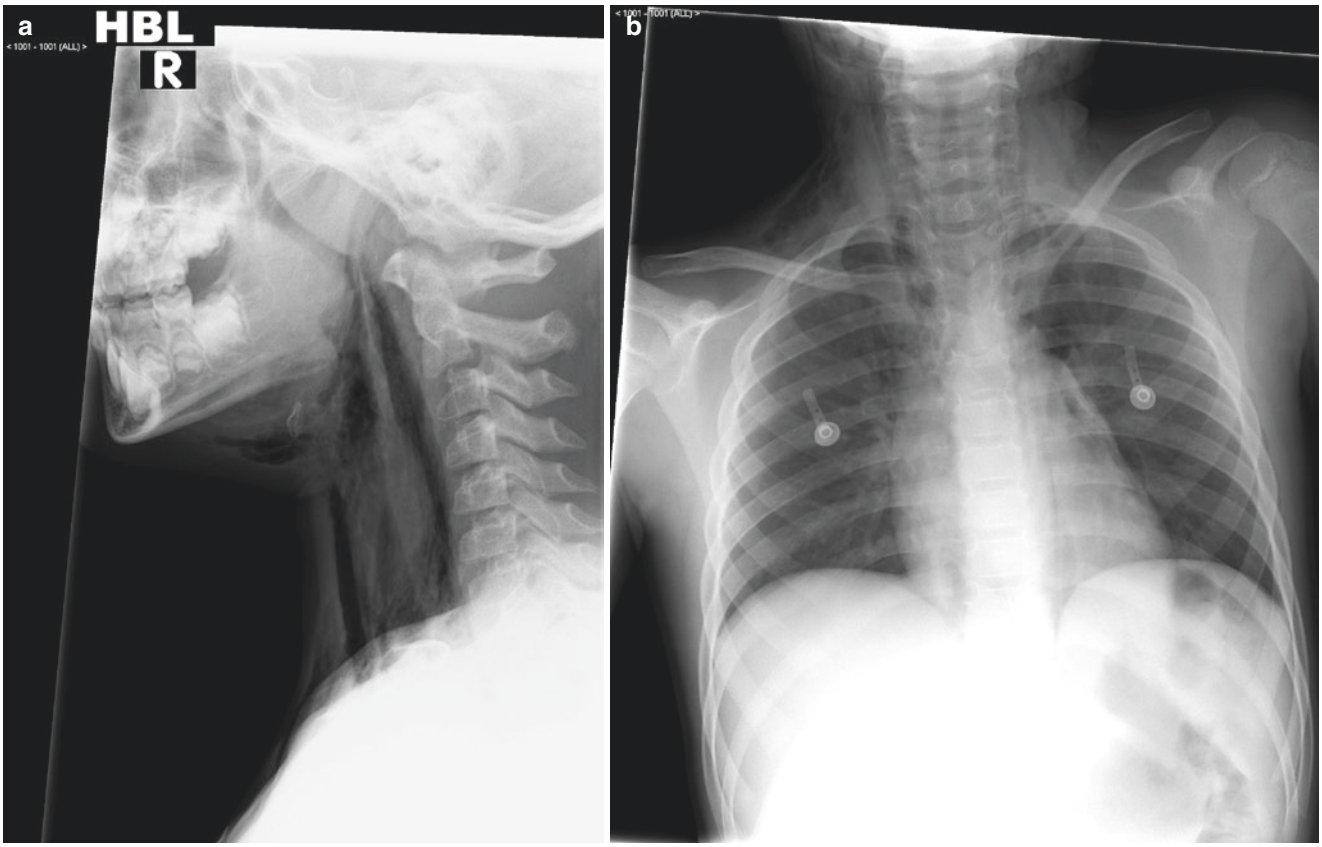

Fig. 3.45 (**a**) Surgical emphysema in the neck. Lateral view plain X-ray. (**b**) Surgical emphysema

racic cages may have severe visceral injuries without fracture, but ribs can be broken by crushing or direct blows. Such injuries can be complicated by subcutaneous surgical emphysema where the child may "blow up like a Michelin Man," and on palpation one can detect crepitus beneath the skin.

3.4.9 Pneumomediastinum (Fig. 3.46)

Air present in the mediastinum results from trauma external to the lung parenchyma or tracking of air from a ruptured bulla with air forced to the hilum and then into the neck. This causes swelling and the "Michelin man" appearance. In neonates on a ventilator, air can occasionally track retromediastinally and then retroperitoneally to rupture the peritoneal lining and create a pneumoperitoneum. This can be confusing as it can be mistaken for necrotizing enterocolitis (NEC) or a spontaneous perforation of the bowel.

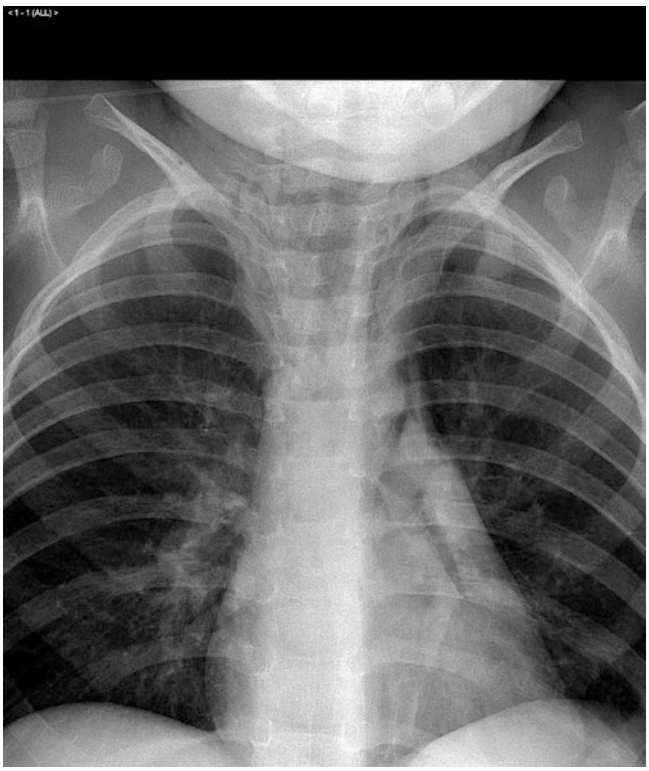

Fig. 3.46 Pneumomediastinum

3.4.10 ET Tube Problems (Fig. 3.47)

This section deals with the misplacement of Endotracheal tubes and the consequences.

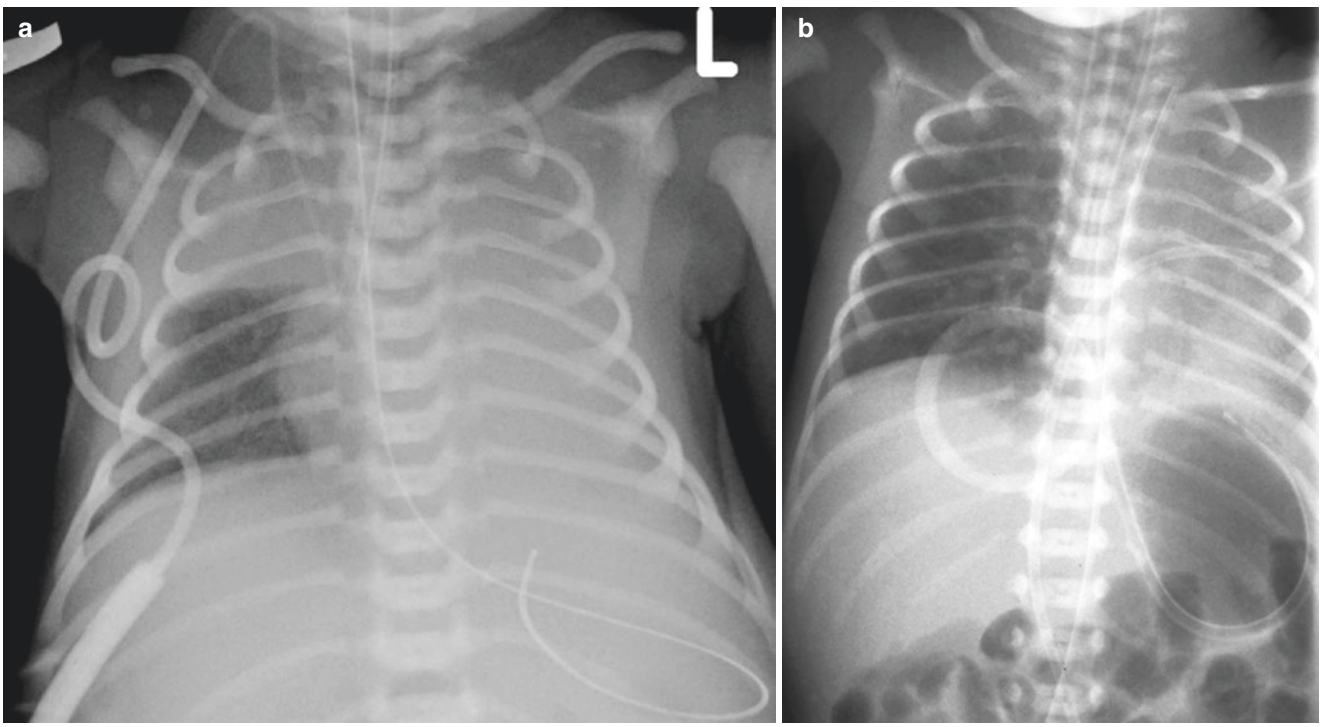

Fig. 3.47 (**a**) Et tube down right main bronchus causing collapse of upper lobe and over inflation of lower lobe. (**b**) Et tube down right main bronchus causing collapse of upper lobe and over inflation of lower lobe. ET down right main bronchus

3.4.11 Non-accidental Injury (NAI)/Battered Baby Syndrome

John Caffey, in 1956, published an article entitled "Some Traumatic Lesions in Growing Bones other than Fractures and Dislocations," in which he claimed that this was the least well-known and the most abused subject in the entire field of paediatrics and radiology. Since that time, more people have come to realise that many children are injured non-accidentally, and awareness of this condition has increased. An injury in a child that *does not fit in* with the explanation given should be suspect. Subdural and retinal haemorrhages produced by severe shaking, metaphyseal fractures of the long bones, and displacement of the epiphysis may occur with twisting of the arms and legs. An infant may be brought to hospital because of swelling of a limb or with a history of screaming when the limb is touched, or because of failure to move the limb. A history of trauma is usually unobtainable. Examination may reveal evidence of old bruising suggestive of previous child abuse. The typical lesion seen on X-ray is a small metaphyseal fracture that can easily be overlooked. Early recognition is of great importance because it may well prevent more serious injuries to these children. A full skeletal survey should be carried out in order to detect other injuries that have occurred in the past. Some infants and children present with head injuries, others with burns or scalds. Injury to internal organs can result from blows to the chest or abdomen. The first concern of the doctor is the safety of the child.

If there is suspicion of deliberate injury, admit the child to hospital. The accusation that parents or others have injured a small child is a very serious one, and may lead to prosecution. *Social Work and legal enquiries should be initiated only by senior members of the hospital staff and the situation requires delicate but firm handling.*

3.5 Tumours

This section can be divided into (1) Tumours of the chest wall; (2) Mediastinal tumours; (3) Pulmonary parenchymal tumours and pleural tumours; and (4) Hamartoma of the oesophagus.

3.5.1 Thoracic Wall Tumours (Fig. 3.48a–c)

Chest wall tumours are in the main malignant, but the benign conditions are a spectrum of thefollowingpathology: lipoma, neurofibroma, haemangioma, lymphangioma, mesenchymal hamartoma and others like fibrous dysplasia of the bone, chondroma, osteoma, fibromatosis, fibrous Dysplasia of the bone, aneurysmal bone cysts, and Langerhans cell histiocytosis are all interosseous lesions within the rib and cause cortical expansion with a lytic centre. The following benign conditions, on the other hand—chondroma, osteoma, and osteochondroma—are all well-defined lesions and expansile masses often with a diffuse stippling calcification within the tumour.

Mesenchymal hamartoma is an expansile mass occurring in the neonatal period. On a plain X-ray it shows sclerotic margins and cortical erosion and destruction. It has a soft tissue component and is a hard mass on palpation. It usually presents as a single mass in a rib, though multiple ribs on the same side may be involved, and it is positioned laterally or on the posterior aspect of the ribs. This is a benign, self-limiting condition that disappears with time and needs treatment only if the patient is symptomatic. Beware of large excisions, as long-term results can have a crippling effect on the patient (Fig. 3.48d–f).

Malignant chest wall tumours arise from the skeleton or the soft tissues. Ewings sarcoma and PNET tumours constitute about 50%, and rhabdomyosarcomas 20%. Other malignant rare conditions include fibrosarcoma, osteogenic sarcoma, synovial sarcoma, and neuroblastoma deposits from metastatic disease.

Ewings sarcoma is an aggressive, systemic disease often presenting late with spread. The most common site is the rib, then the clavicle, sternum, scapula, and other soft tissues around the chest. To plan treatment, utilize CT scans, MRI scans, and bone scans to determine the extent of the disease and whether pleural effusions, nodules, or metastases are present (Fig. 3.48g, h).

3.5.2 Mediastinal Tumours: Lymphoma, Leukaemia, Teratoma, Ganglioneuroma, Pneumoblastoma

Mediastinal tumours as shown in the figure arise at specific areas in the chest and the location can give one a rough idea about the pathology. Some 65–75% are malignant, and 40% occur in children under 2 years of age.

Anterior mediastinal tumours account for 44%, and 80% of these are malignant. These include lymphomas, germ cell tumours, and thymic tumours (Fig. 3.49a).

Middle mediastinal tumours account for 20%, and these are mainly of lymphatic origin: mainly leukaemia, non-Hodgkin's lymphoma, and Hodgkin's disease (Fig. 3.49b–i).

Posterior mediastinal tumours account for 36% and are mainly neurogenic and rarely germ cell tumours. Mediastinal neurogenic tumours arise from the sympathetic chain that runs from the thoracic inlet to the diaphragm. Intraspinal extension can occur and must be looked for in the MRI scan.

3.5.3 Pulmonary Parenchymal Tumours and Pleural Tumours

Pulmonary parenchymal tumours are rare in children and are mostly malignant. Primary benign conditions in the chest include pseudo tumours, which are inflammatory in nature, and pulmonary hamartoma.

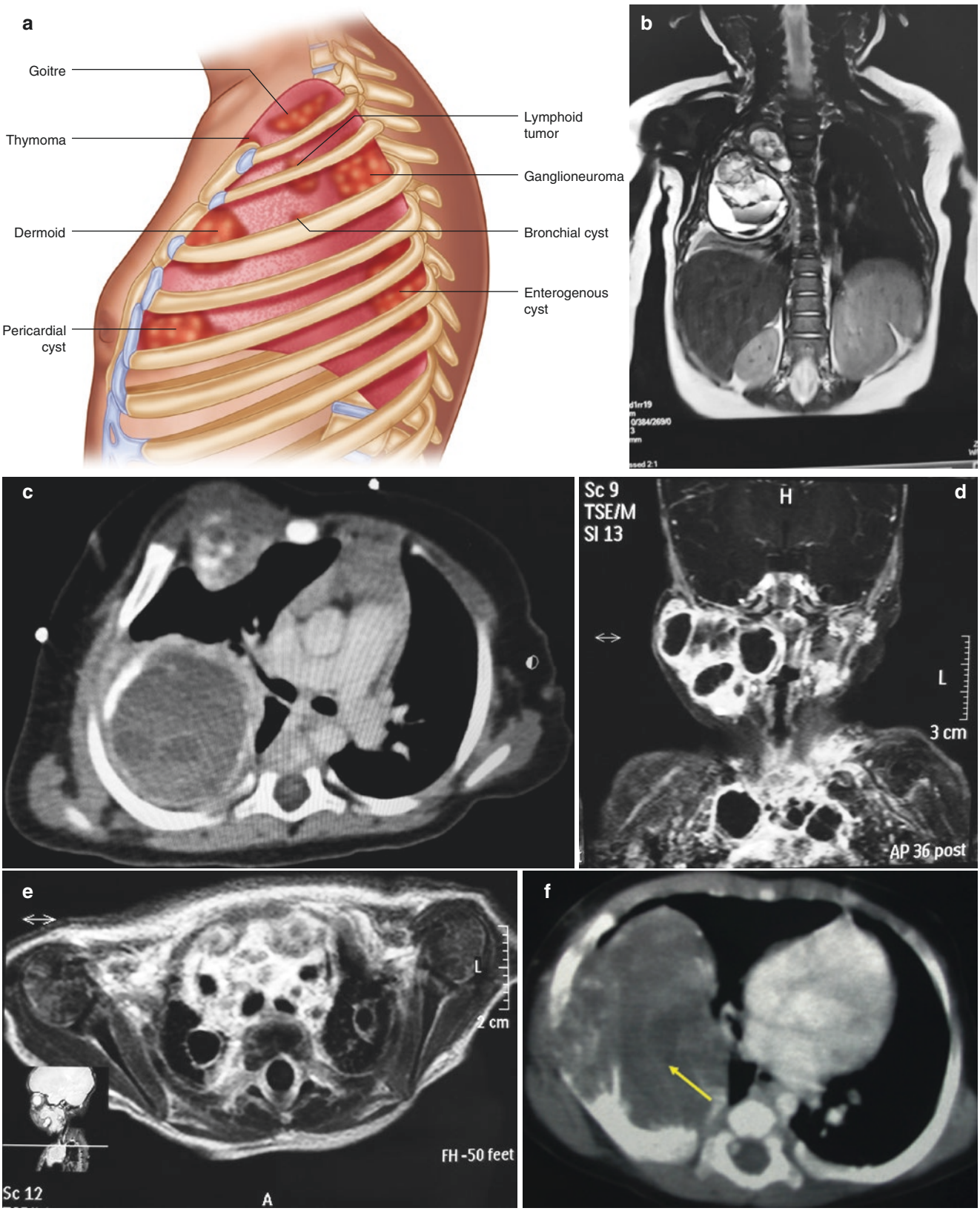

Fig. 3.48 (**a**) Diagram of tumour locations in the chest. (**b**) Chest mesenchymal hamartoma. (**c**) Chest mesenchymal hamartoma. (**d**) Mediastinal cystic hygroma. (**e**) Mediastinal cystic hygroma. (**f**) Hamartoma of the rib. (**g**) Ewing's Sarcoma: a homogenous mass with destruction of the posterior end of the third rib. There is a pleural effusion and pleural metastases. (**h**) Neuroblastoma metastases in the thoracic spine causing scoliosis and spinal cord damage

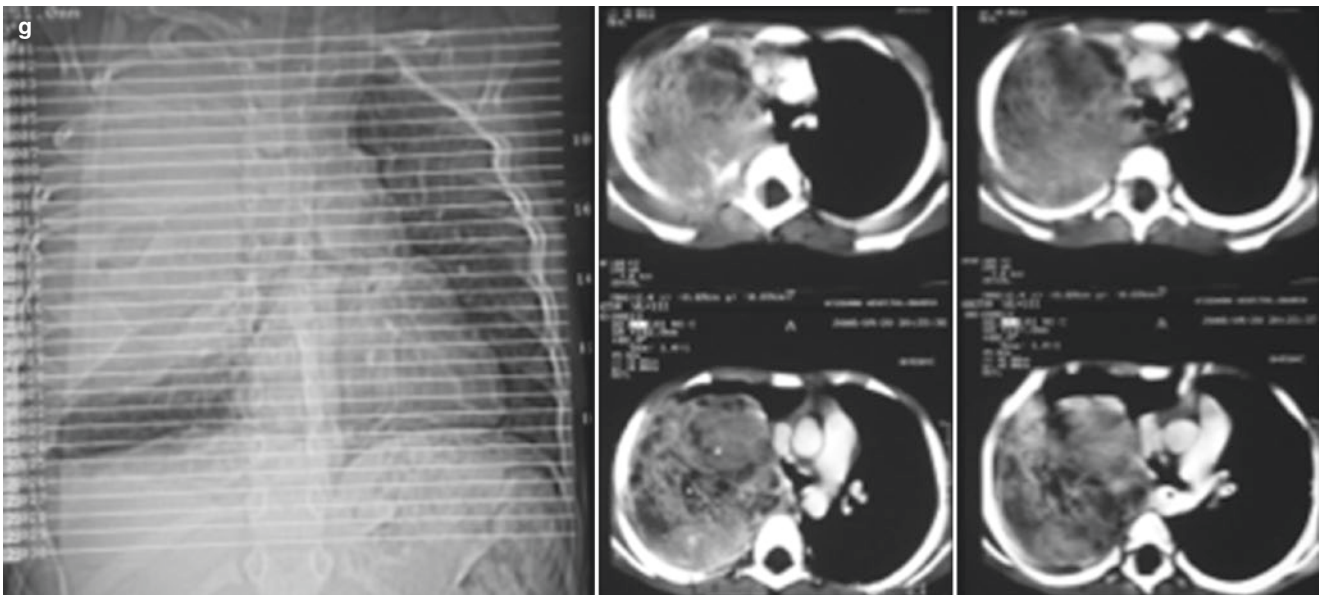

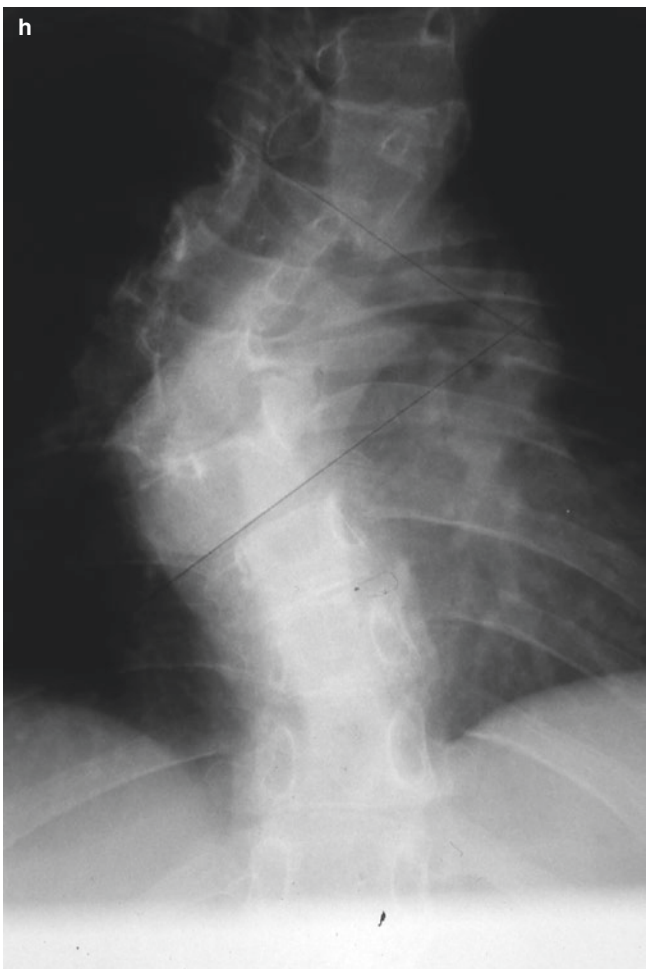

Fig. 3.48 (continued)

Endobronchial lesions include bronchial adenoma, and 80% of these are carcinoids that are slow-growing but can cause bleeding and over the years grow relentlessly, killing the patient.

Other conditions include papillomas that have a viral aetiology.

Other metastatic lesions include Wilmstumours, neuroblastoma, and osteogenic sarcomas. Pleuropulmonary blastoma, another rare tumour of the parenchyma of the lung, may present in childhood (Fig. 3.49j–o).

Pleural tumours are rare and are mostly metastatic from a Ewings sarcoma. Primary tumours are also rare and include pleuropulmonary blastoma, rhabdomyosarcoma, and mesothelioma.

Intrathoracic tumours are rarely primary in childhood. Lymphomas arising in the thymus compress surrounding

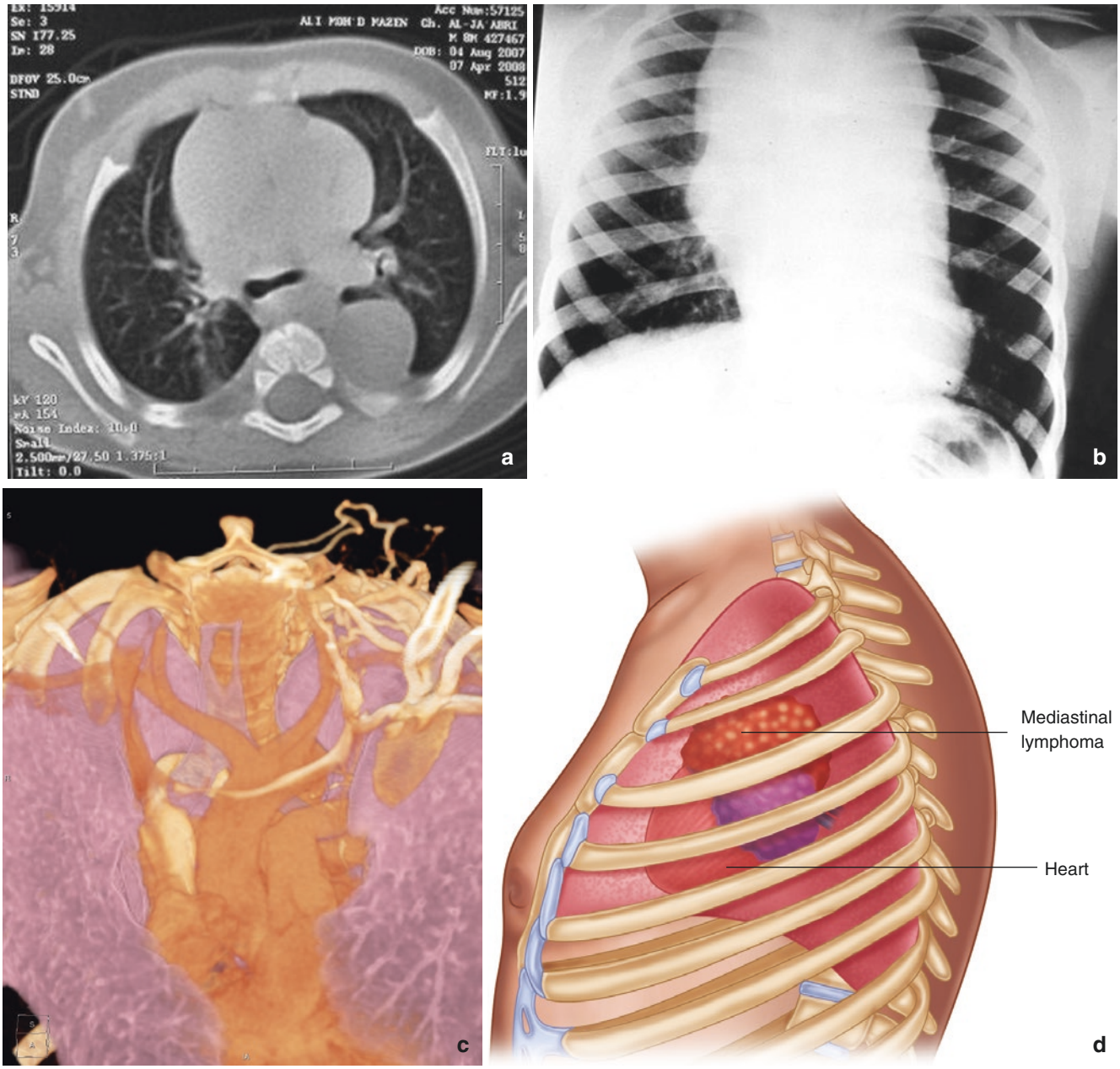

Fig. 3.49 (**a**) Ganglioneuroma in paravertebral area. (**b**) Mediastinal lymphoma. (**c**) Lymphoma with positive nodes on CT. (**d**) Mediastinal Lymphoma diagram. (**e**) Tracheal compression in ALL. (**f**) Lymphoma compressing the great veins. (**g**) Tracheal compression in acute leukaemia, lymphoma. (**h**) Chest X-ray of acute leukaemia. (**i**) Leukaemia/Lymphoma CT. (**j**) Neuroblastoma. (**k**) Multiple lung metastes from Wilms tumour. (**l**) Echocardiogram of the heart showing a Wilms tumour thrombus in right atrium prolapsing into right. (**m**) Canon ball metastatic deposit on left side of chest. (**n**) Mediastinal teratoma in a neonate. (**o**) Operative specimen of mediastinal teratoma

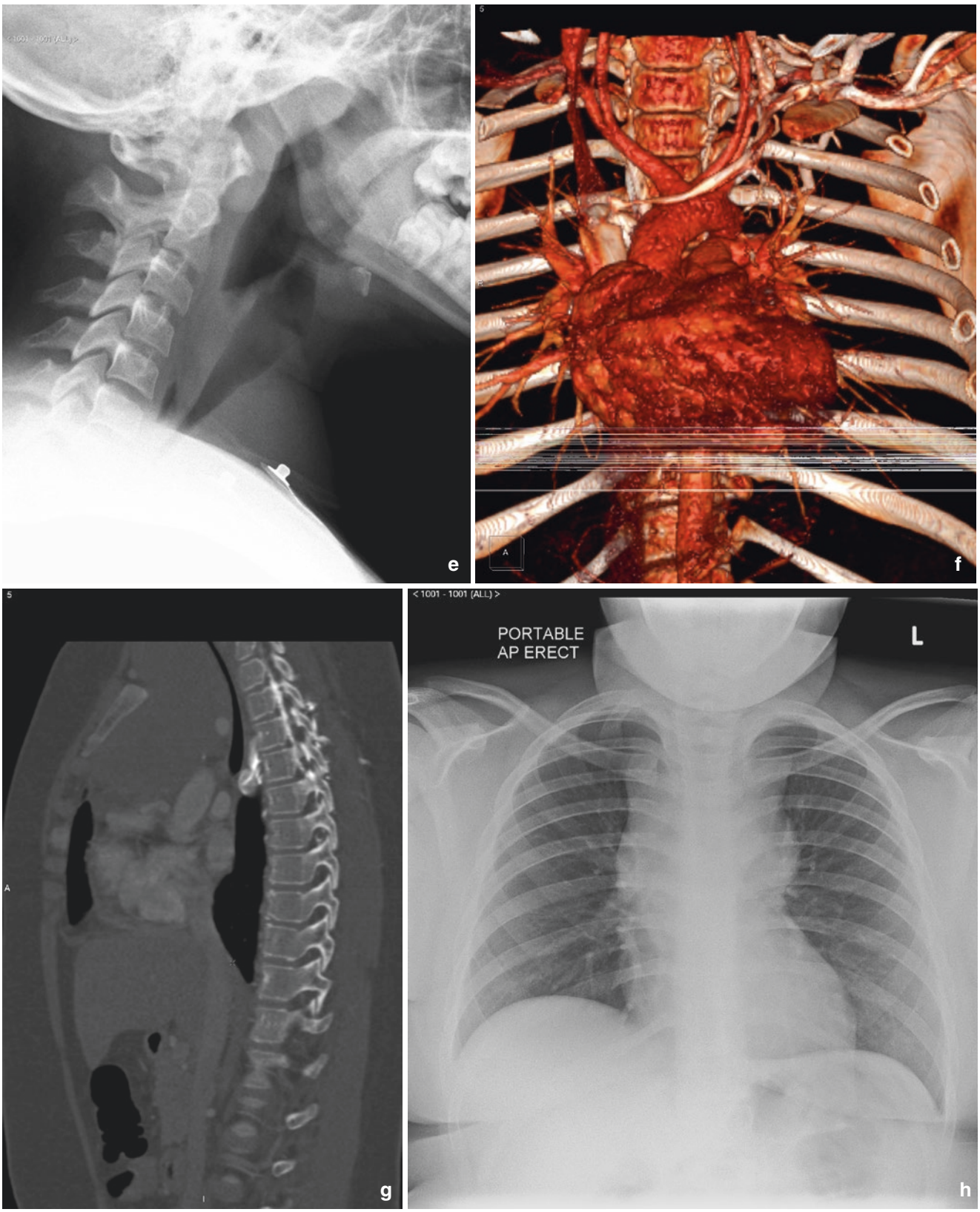

Fig. 3.49 (continued)

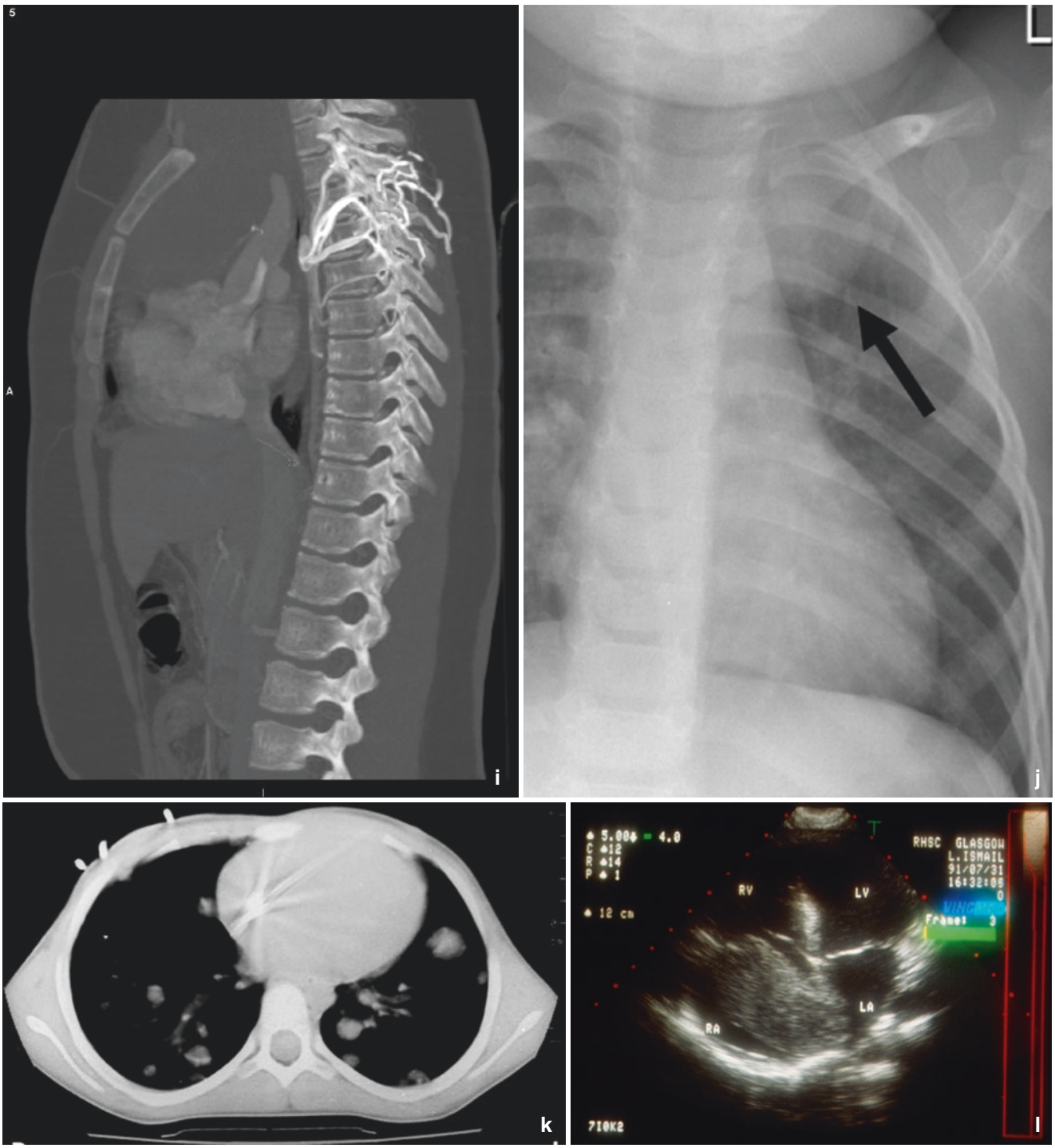

Fig. 3.49 (continued)

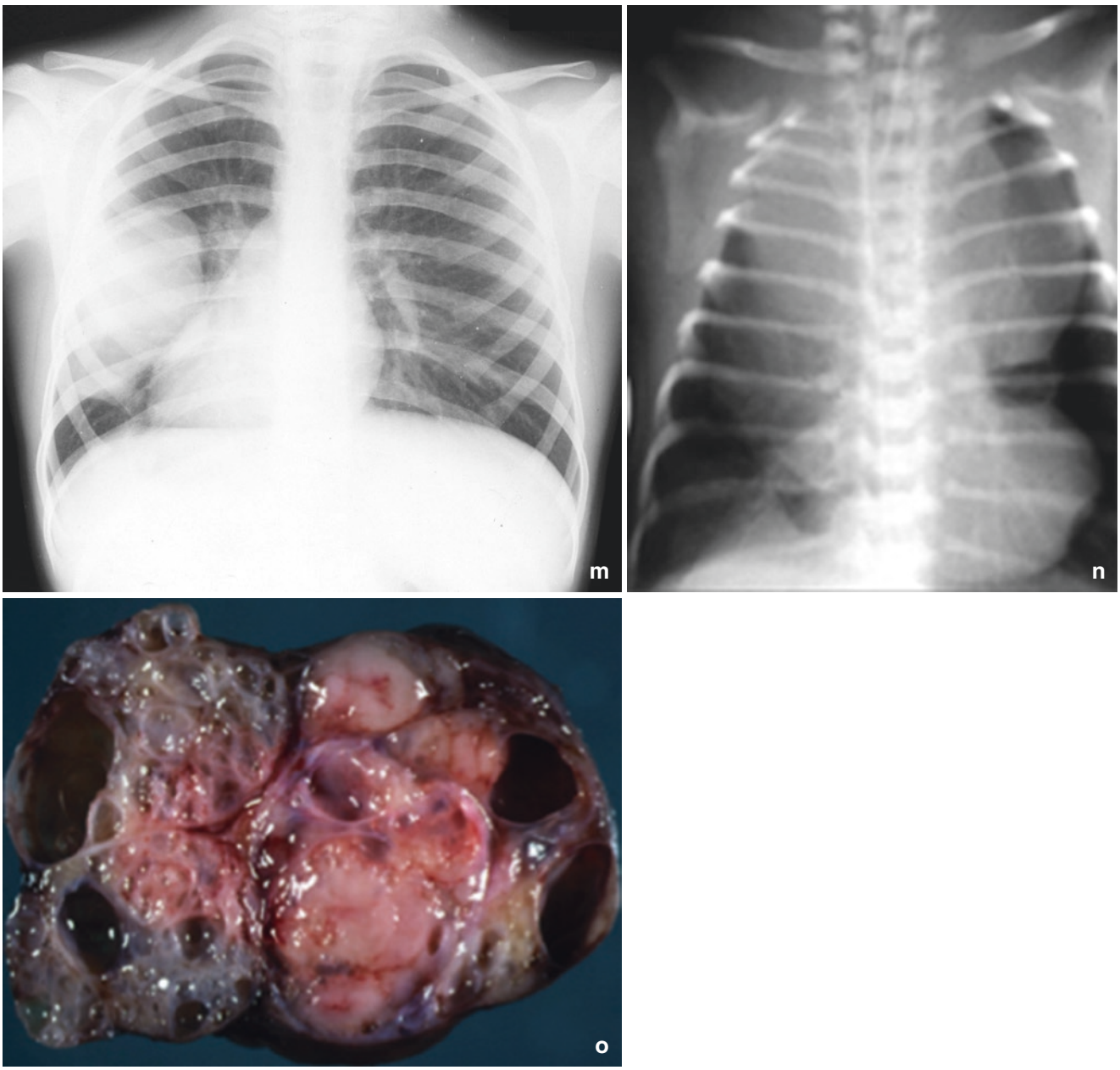

Fig. 3.49 (continued)

structures and cause cough, dyspnoea, stridor, venous distension, oedema of the face and arms, and dysphagia. Teratomata or dermoid cysts arise in the anterior mediastinum and can be demonstrated in lateral or oblique radiographs. Calcification is uncommon in these tumours, which are usually benign. The ganglioneuroma is a solid encapsulated benign tumour that may arise in the posterior mediastinum from one of the dorsal sympathetic ganglia. It may reach a large size before giving rise to symptoms, or may present with symptoms or signs due to noradrenalin secretion. Neuroblastoma may also develop in this situation. Radiographs in all these cases will reveal the paravertebral mass to be in the posterior mediastinum. Bronchogenic carcinoma is excessively rare in childhood, but bronchial adenoma sometimes causes bronchial obstruction with obstructive emphysema or absorption collapse. The diagnosis is suggested by haemoptysis, which is not otherwise common in children. It should be confirmed by CT scan. Ultrasound can differentiate cystic from solid lesions.

3.5.4 Hamartoma of the Oesophagus (Fig. 3.50)

This rare abnormality presents as a polyp in the upper oesophagus. It elongates and can even obstruct the airways if it finds itself into the pharynx.

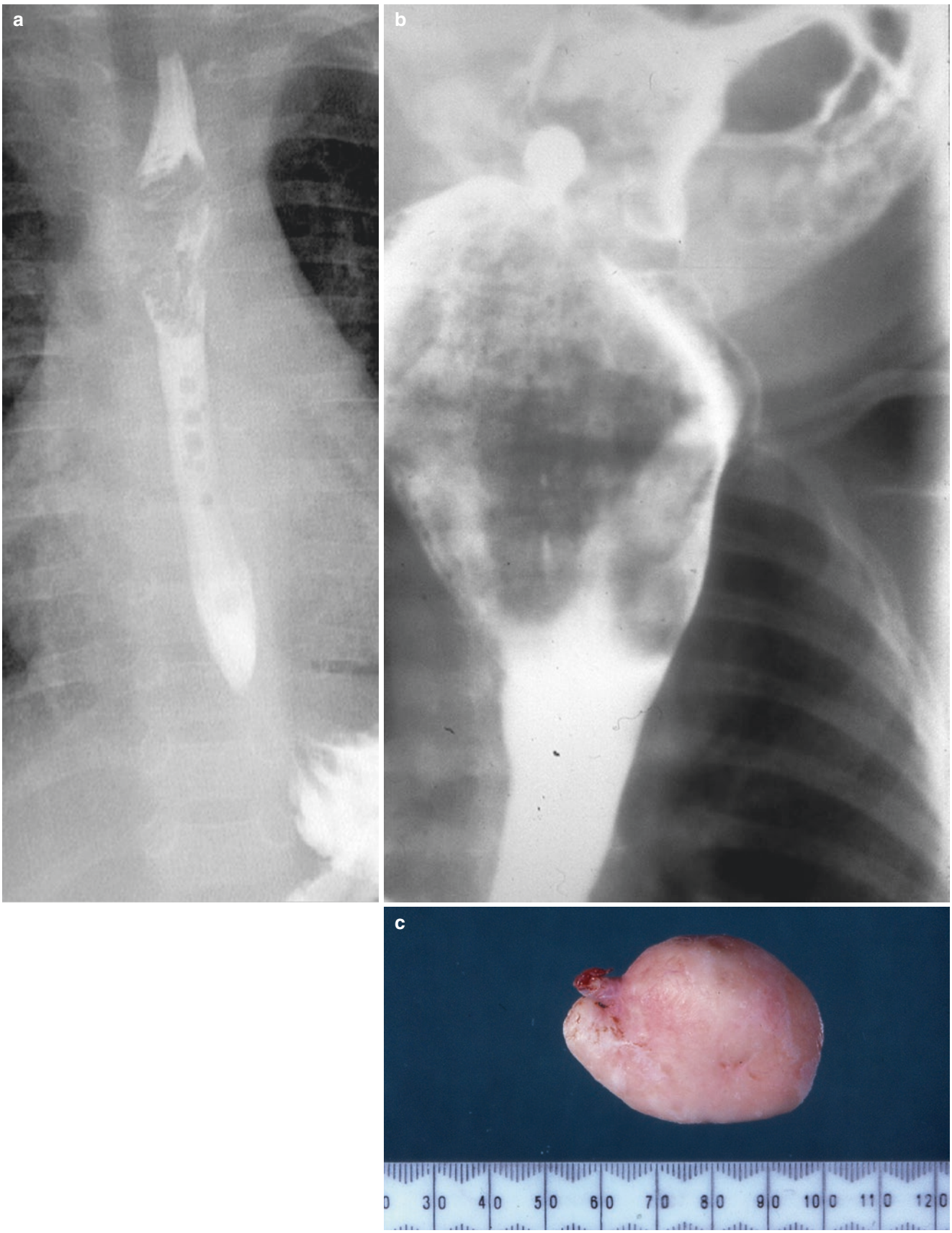

Fig. 3.50 (**a**, **b**) Oesophageal hamartoma. (**c**) Oesophageal hamartoma specimen

3.6 Acquired Conditions

3.6.1 Achalasia of the Cardia (Fig. 3.51)

This condition is caused by loss of ganglion cells in Auerbach's plexus. There is an incomplete or absent relaxation of the lower oesophageal sphincter with dilatation and absent peristalsis of the oesophagus, resulting in a megaoesophagus. Contrast studies demonstrate this condition with failure of the passage of food into the stomach.

3.6.2 Caustic Burns of the Oesophagus (Fig. 3.52a, b)

Ingestion of caustic soda causes an intense burn of the lining of the oesophagus, which is stratified squamous epithelium, as well as the whole wall of the oesophagus. This results in chemical damage and an inflammatory response with the development of a fibrous stricture. This can be localised, or it can extend from the mouth, through the oesophagus, and into the stomach (Fig. 3.52c–e).

3.6.3 Microcardia (Fig. 3.53)

A small heart seen on an X-ray is usually caused by constriction of the whole heart muscle in a shocked state, often from hypovolaemia. It may also be seen in extreme states of dehydration.

3.6.4 Cardiomegaly (Fig. 3.54)

This condition can be due to heart failure. The heart contour measures more than 50% of the width of the chest X-ray. The

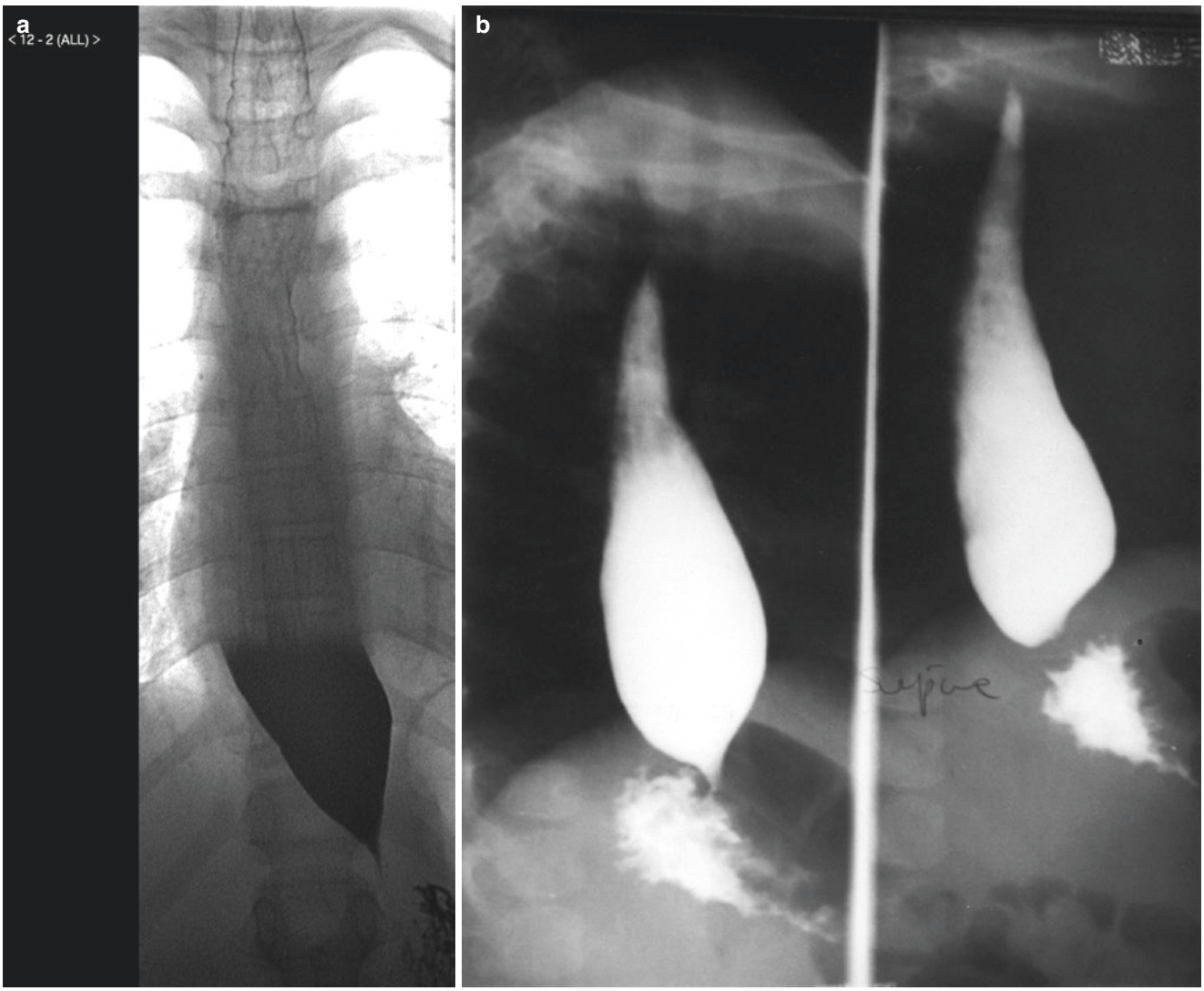

Fig. 3.51 (**a**) Achalasia of the cardia. (**b**) Achalasia

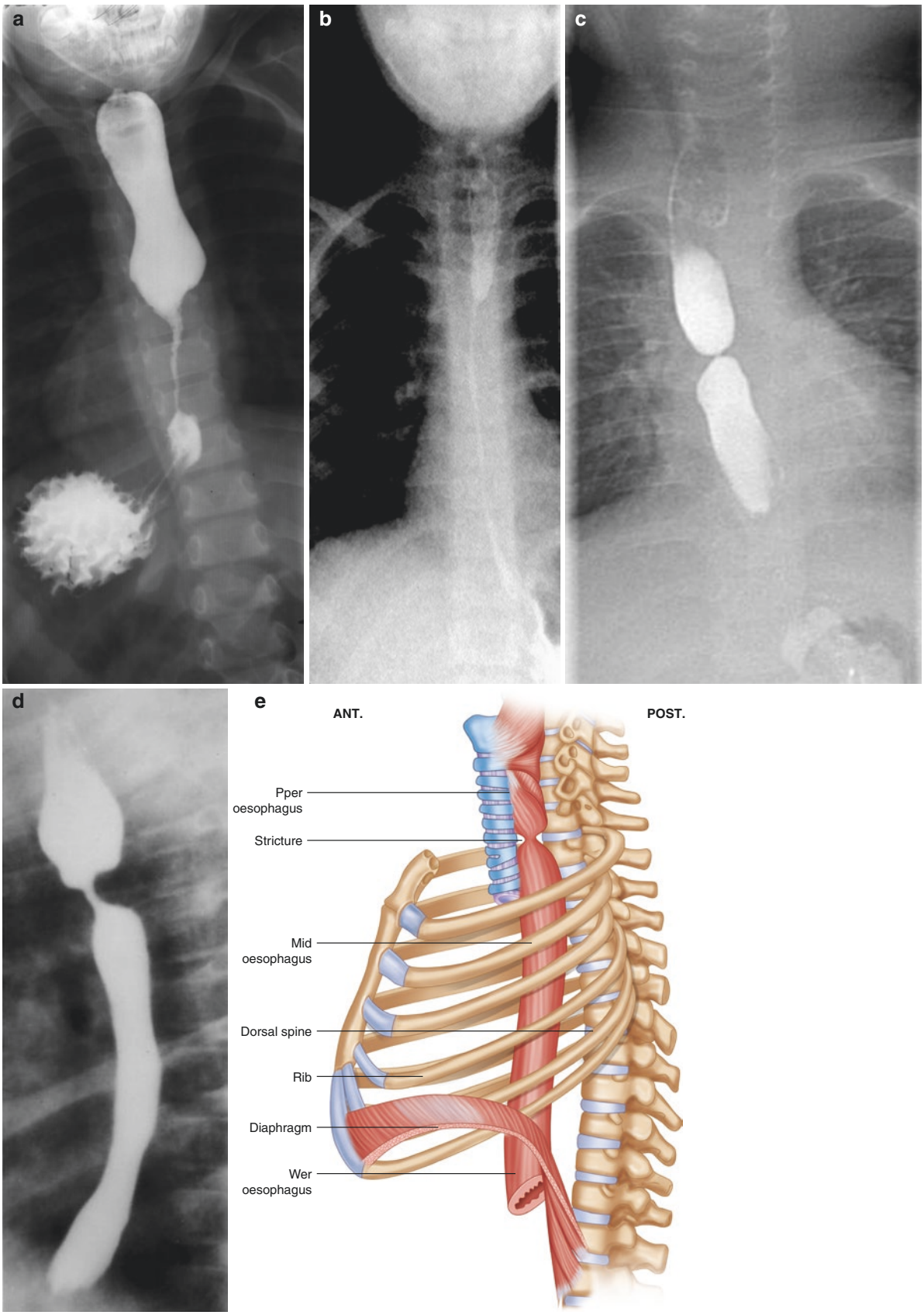

Fig. 3.52 (**a**) Oesophageal stricture with reflux and oesophagitis. (**b**) Long oesophageal stricture from caustic soda ingestion. (**c**) Mid oesophageal stricture. (**d**) Oesaphageal stricture secondary to ingestion of caustic soda. (**e**) Oesaphageal stricture

heart cannot cope with the fluid overload and becomes dilated and inefficient. It can be caused by septicaemia, viral myocarditis, or in the case of cardiomyopathies from hypertrophy of the hear and associated heart failure.

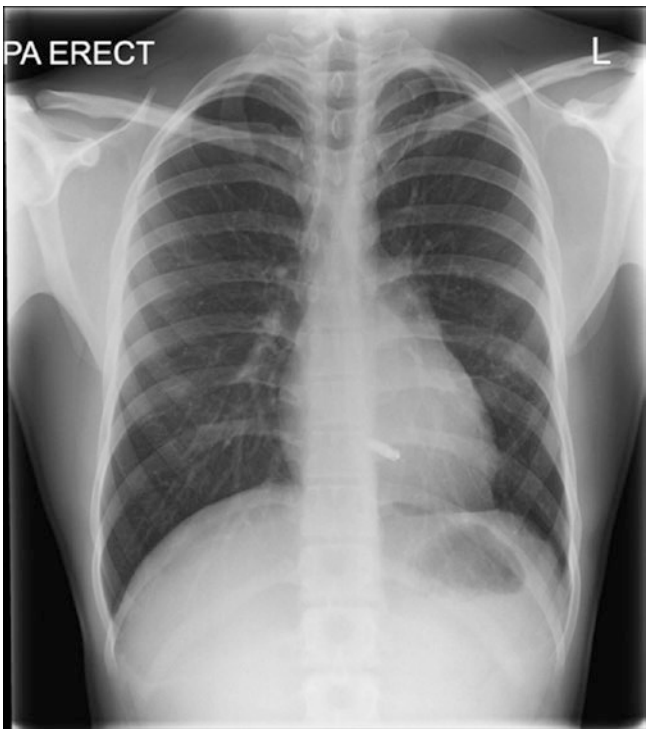

Fig. 3.53 Microcardia

3.6.5 Lung Collapse (Fig. 3.55)

Collapse of the lung may be due to extrinsic causes such aspneumothorax, pleural effusions, empyema, chylothorax, and congenital diaphragmatic hernia. It can also result from intrinsic causes such as a mucus plug or a foreign body obstructing the airway with reabsorption of the air in the lung parenchyma and collapse.

3.6.6 Surgical Complications: Shunts, Lines, Chest Drains

See Fig. 3.56a–f.

3.6.7 Extracorporeal Membrane Oxygenation/Liquid Ventilation

The extracorporeal membrane oxygenation (ECMO) procedure bypasses the lungs and provides support for the patient by oxygenating the blood extracorporeally through a membrane oxygenator. It is very helpful in neonates with meconium aspiration or pulmonary interstitial emphysema (PIE), and in pulmonary hypoplasia, especially in congenital diaphragmatic hernia, using a liquid ventilation to help expand and encourage the parenchyma to develop and grow (Fig. 3.57).

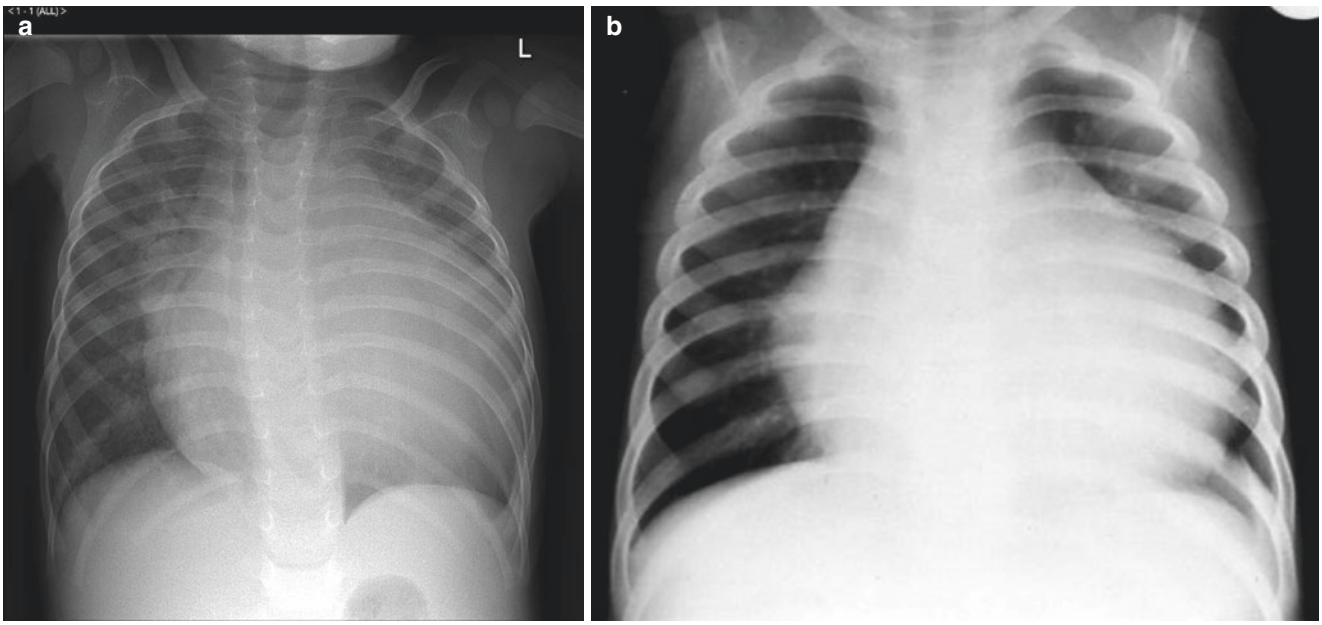

Fig. 3.54 (**a**) Dilated cardiomyopathy. (**b**) Cardiomegaly

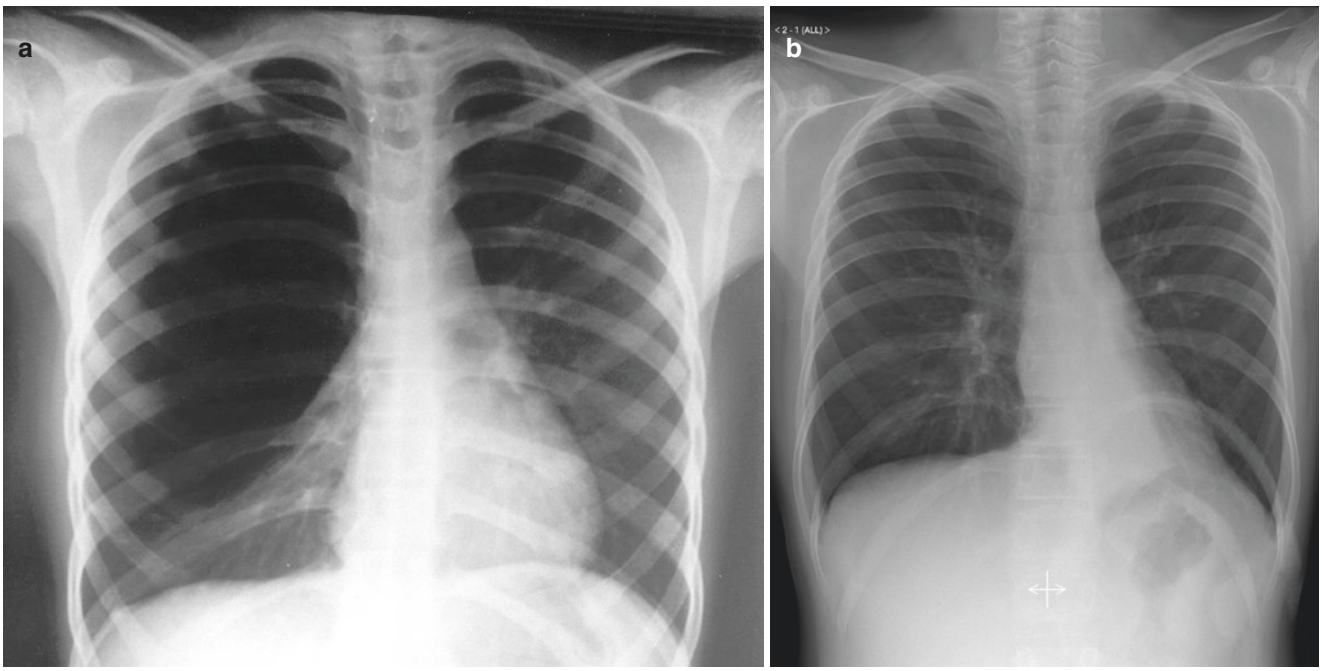

Fig. 3.55 (**a**) Collapse of right lower lobe. (**b**) Left lower lobe collapse

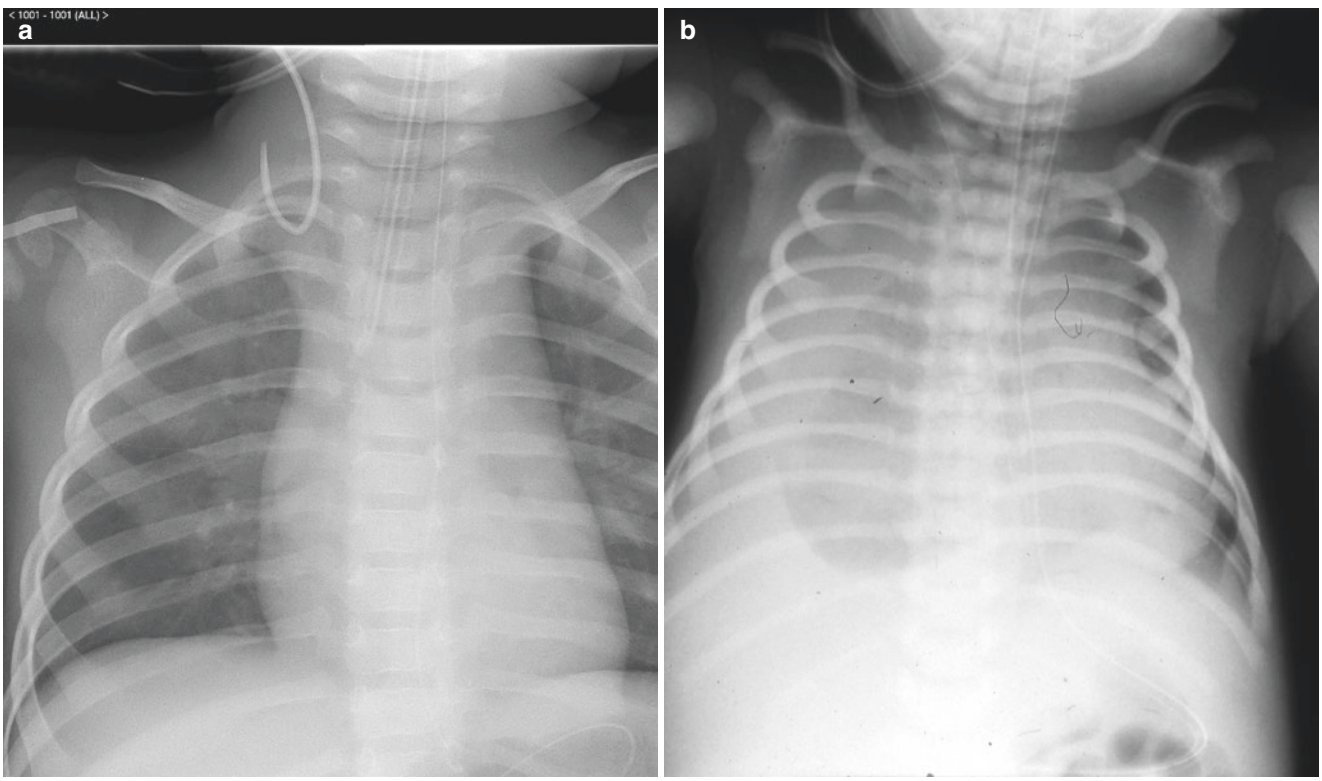

Fig. 3.56 (**a**) Misplaced internal jugular line. (**b**) Right pleural effusion. Complication of central line perforated internal jugular at base causing TPN to go into the pleural space. (**c**) UVC in the left atrium dislodged. (**d**) Central line removal with fracture of tubing and line floated into pulmonary trunk. Removal by interventional cardiologist. (**e**) Ventriculo atrial shunt for hydrocephalus misplaced. (**f**) Chest drain pulled out

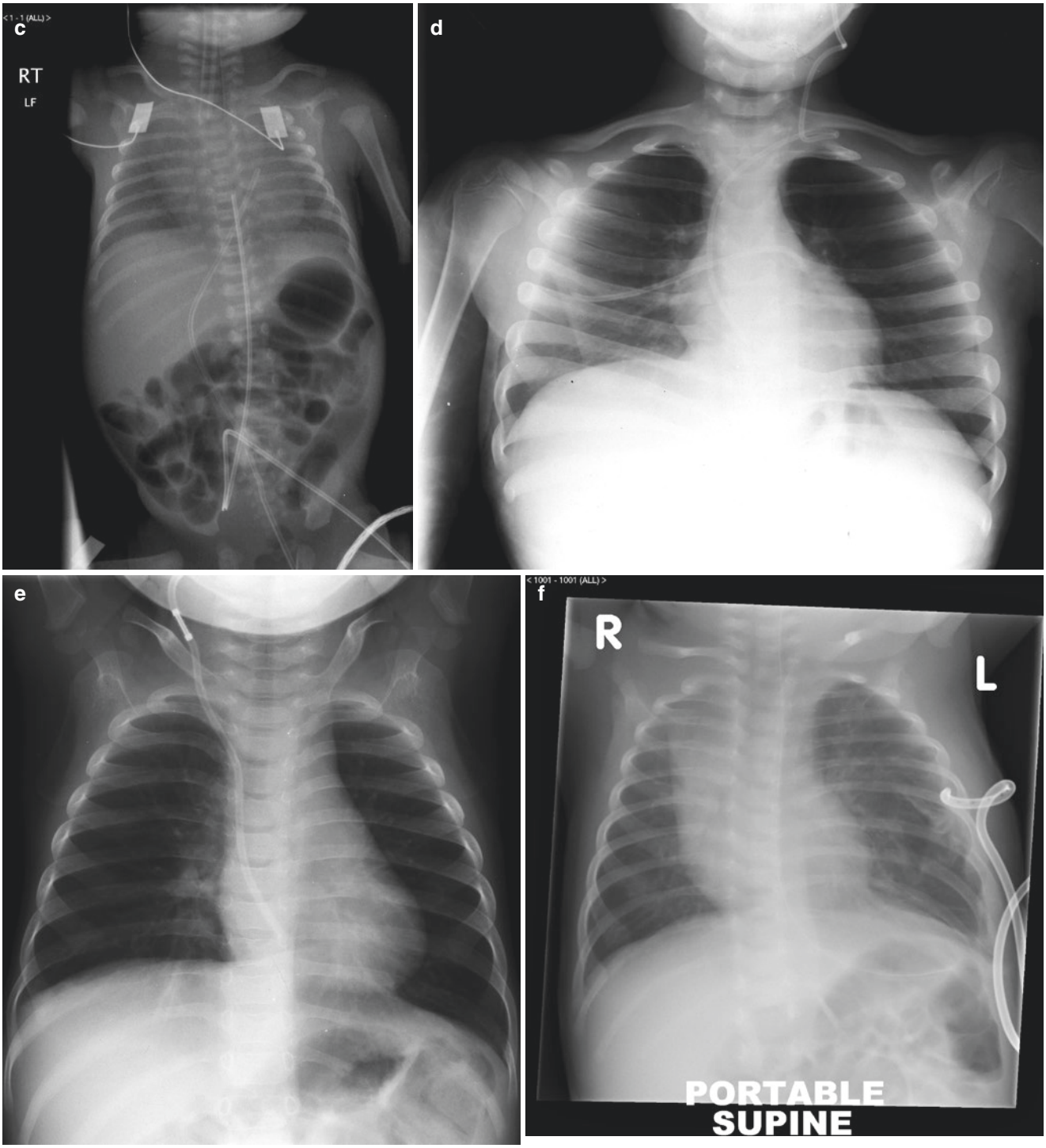

Fig. 3.56 (continued)

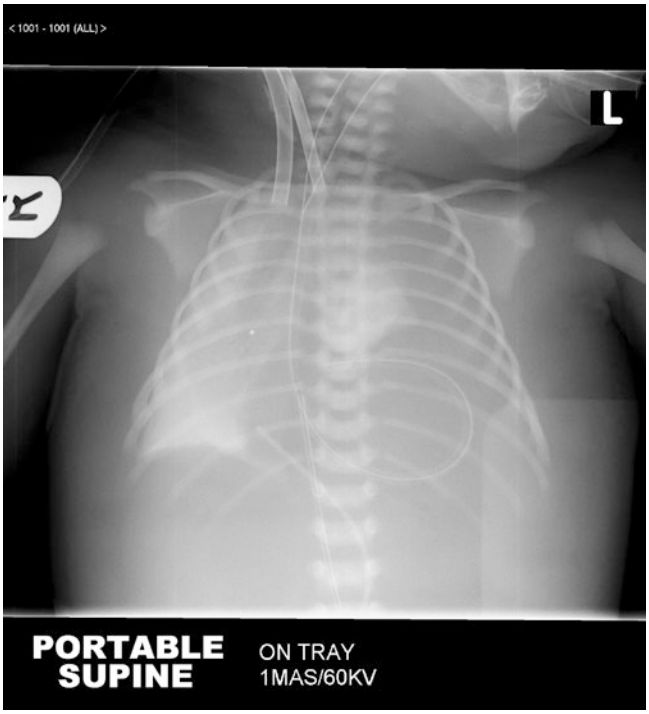

Fig. 3.57 ECMO patient on liquid ventilation dye in both lungs visible showing hypoplasia

3.6.8 Oesophageal Varices (Fig. 3.58)

Bleeding from oesophageal varices may be sudden and profuse and cause exsanguination of the patient. Rapid and adequate transfusion is necessary. Emergency endoscopy should be undertaken to establish this diagnosis, and injection of varices with sclerosant agents may be commenced. If this is impossible, then control of the bleeding may be achieved by giving intravenous infusions of vasopressin or somatostatin. Tamponading of the oesophageal and gastric varices may be possible with the Sengstaken tube. Insertion of this tube should be done by someone experienced in proper positioning of the balloons, and it should be done under imaging control. The oesophageal balloon is blown up to a pressure of 40 mmHg. This pressure will have to be released intermittently to prevent pressure necrosis. This measure should only be undertaken in an attempt to resuscitate the patient prior to more definitive treatment, which may include surgical transection of the oesophagus or hemitransection of the stomach (Tanner's operation). Emergency portocaval or splenorenal shunting is rarely necessary in children. Most patients with portal hypertension and variceal bleeding can be managed by repeated injections of sclerosants into the varices, thus allowing collaterals to develop and improve the drainage from the portal tract.

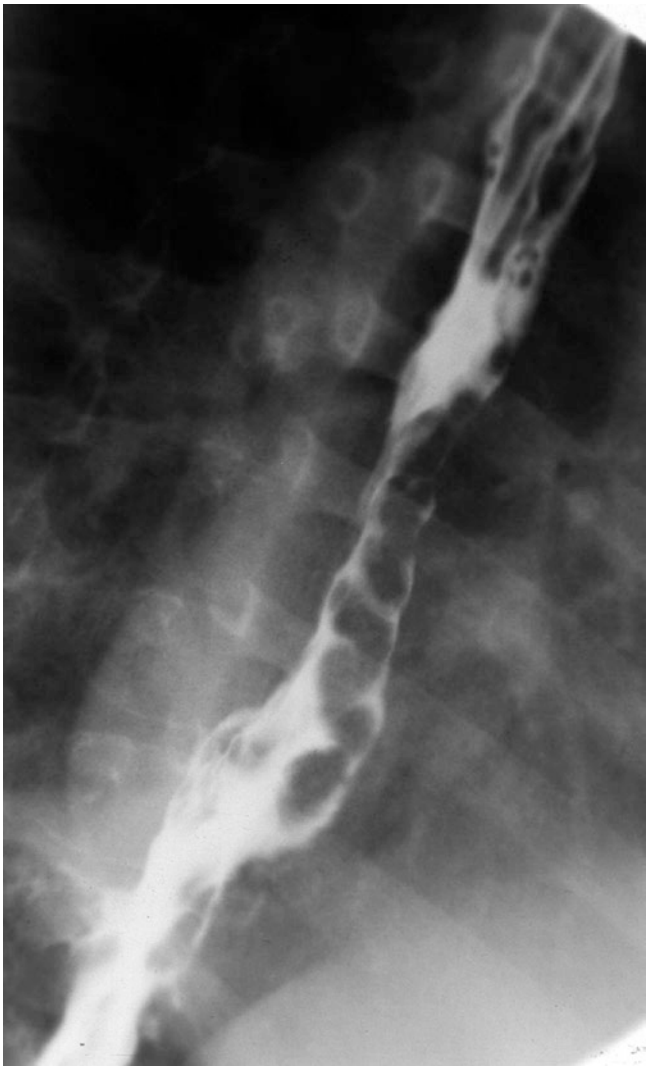

Fig. 3.58 Oesophageal varices

3.6.9 Tracheal Stenosis (Fig. 3.59)

This condition may be congenital and part of a tracheal agenesis, which is incompatible with life if it is extensive and the whole of the trachea is involved. Tracheal stenosis may result from traumatic intubation, and scarring from tracheostomy.

3.6.10 Chiladiti Syndrome (Fig. 3.60)

Chiladiti syndrome is characterised by abnormal anatomical interposition of the transverse colon between the liver and the diaphragm. Loops of bowl are visualised beneath the diaphragm on standard routine chest X-ray could be misinterpreted as air under the diaphragm from a perforated viscus.

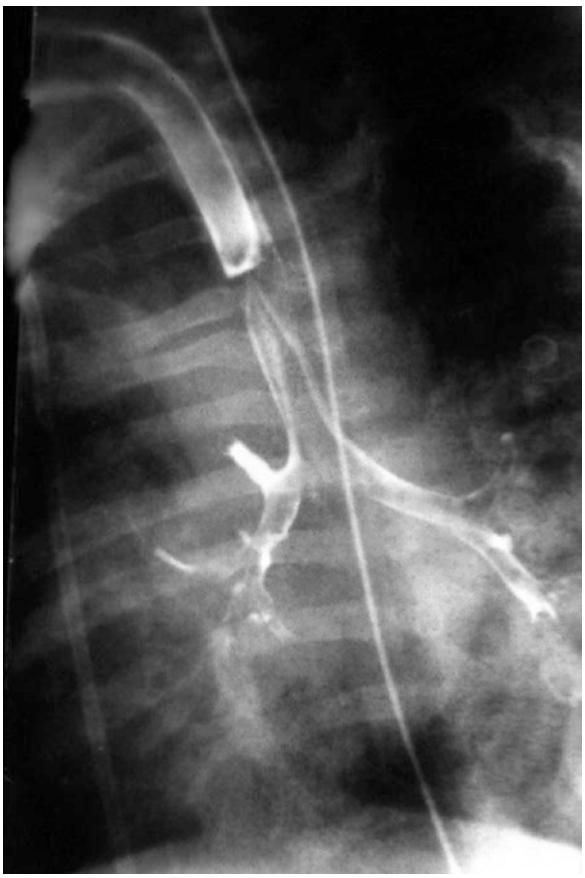

Fig. 3.59 Trachial stenosis bronchography

Further Reading

Caffey J. Some traumatic lesions in growing bones other than fractures and dislocations: clinical and radiological features: the Mackenzie Davidson Memorial lecture. Br J Radiol. 1957;30(353):225–38.

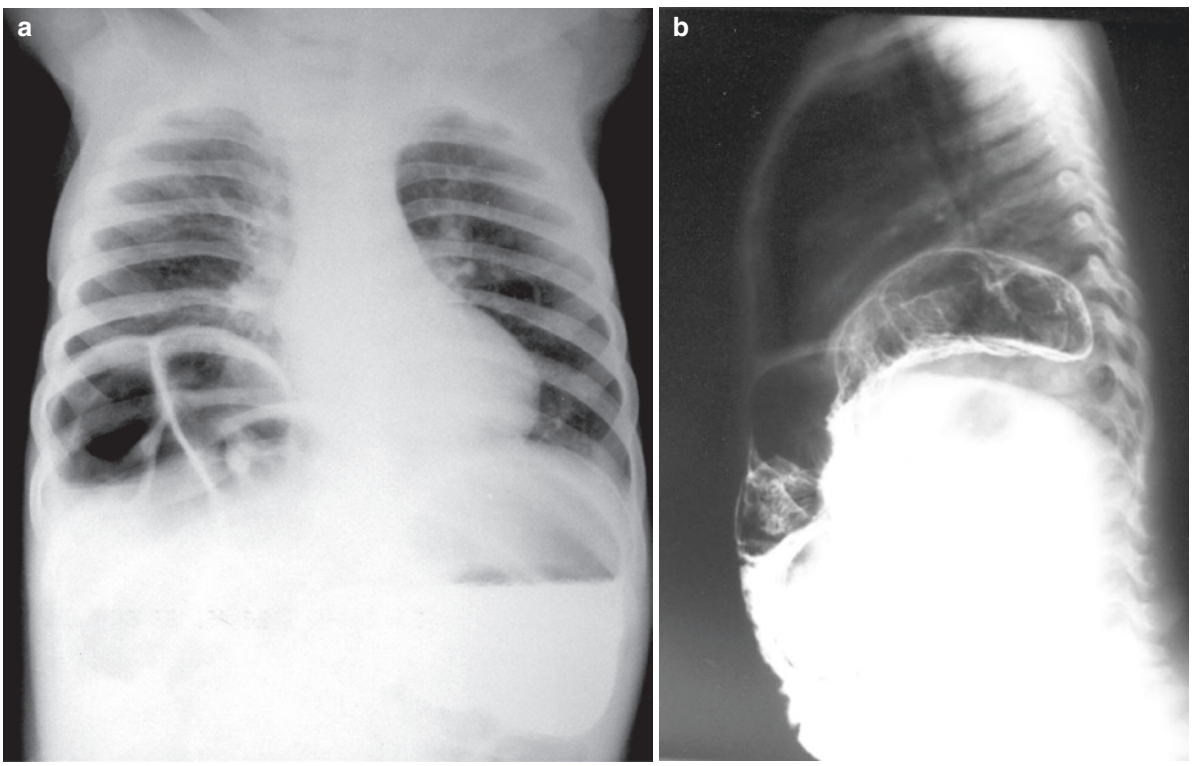

Fig. 3.60 (**a**, **b**) Chiladiti syndrome (Barium study)

Abdomen

4

Ruth Allen

4.1 Introduction

This chapter presents a lot of clinical detail of neonatal congenital causes of intestinal obstruction. In the older child, there are descriptions of acute appendicitis, intussusception, and trauma to abdominal viscera. The main abdominal tumours, abdominal lymphoma, teratoma, neuroblastoma, nephroblastoma, nephroblastoma and liver tumours are also discussed and illustrated. Some sections in this chapter are illustrated by only a figure and legend because they are rare.

4.2 Congenital

4.2.1 Gastroschisis (Fig. 4.1a, b)

This condition, which in the past was confused with exomphalos, has a very different clinical picture and should be regarded as a separate entity. The gastroschisis typically arises as a small punched-out lesion in the anterior abdominal wall lateral to the umbilicus, predominantly on the right. There is most commonly a bridge of skin between the defect and the umbilical cord which is usually intact. Through this defect protrudes intestinal contents, small bowel, large bowel, and at times even an ectopic testis or an ovary. After delivery there is a risk that the vascular pedicle of the prolapsed bowel will twist and compromise the intestinal blood supply. Babies with gastroschisis tend to be light for their gestational age and smaller than babies with exomphalos major. They very rarely have associated abnormalities that are life threatening. Malrotation of the intestines is not an uncommon complication with the bowel not properly positioned when it re-enters the abdominal cavity.

Postnatal plain radiography, ultrasound, and cross-sectional imaging have little place in the diagnosis of anterior abdominal wall defects, but they may play a part in the assessment of complications such as obstruction and pulmonary hypoplasia. Anterior abdominal wall defects are usually identified antenatally on ultrasound.

4.2.2 Exomphalos/Hernia into the Cord (Fig. 4.2a, b)

This defect involves the umbilical cord. There may be a thin walled sac covering the intestines, liver, or other abdominal organs that are visible. The defect varies from a few centimetres in diameter (exomphalos minor) to a swelling the size of a large grapefruit and may involve the whole of the anterior wall (exomphalos major). The latter may contain all or part of the liver. The umbilical cord arises from the apex of the cordal base of the sac. In most cases the sac is intact but in may be damaged during delivery and not clearly obvious. Introduction of maternal plasma α-fetoprotein screening and fetal ultrasound examinations has increased prenatal diagnosis. A detailed ultrasound examination can usually differentiate exomphalos from gastroschisis. Infants with exomphalos major are large at birth and 50% may have other underlying abnormalities including congenital defects of the heart, kidneys, or gastrointestinal tract. The mortality in this group is high because of the associated malformations.

Postnatal plain radiography, ultrasound, and cross-sectional imaging have little place in the diagnosis of anterior abdominal wall defects although they may play a part in the assessment of complications such as obstruction and pulmonary hypoplasia (Fig. 4.2c). Anterior abdominal wall defects are usually identified antenatally on ultrasound

4.2.3 Hiatus Hernia (Fig. 4.3)

Vomiting in some infants can be more troublesome than the mouthful of regurgitation, which is commonplace. This may be due to gastro-oesophageal reflux, occurring more

R. Allen (✉)
Royal Hospital for Children, Glasgow, UK
e-mail: ruth.allen@ggc.scot.nhs.uk

R. Carachi (ed.), *Atlas of Paediatric Surgical Imaging*, https://doi.org/10.1007/978-3-030-32384-4_4

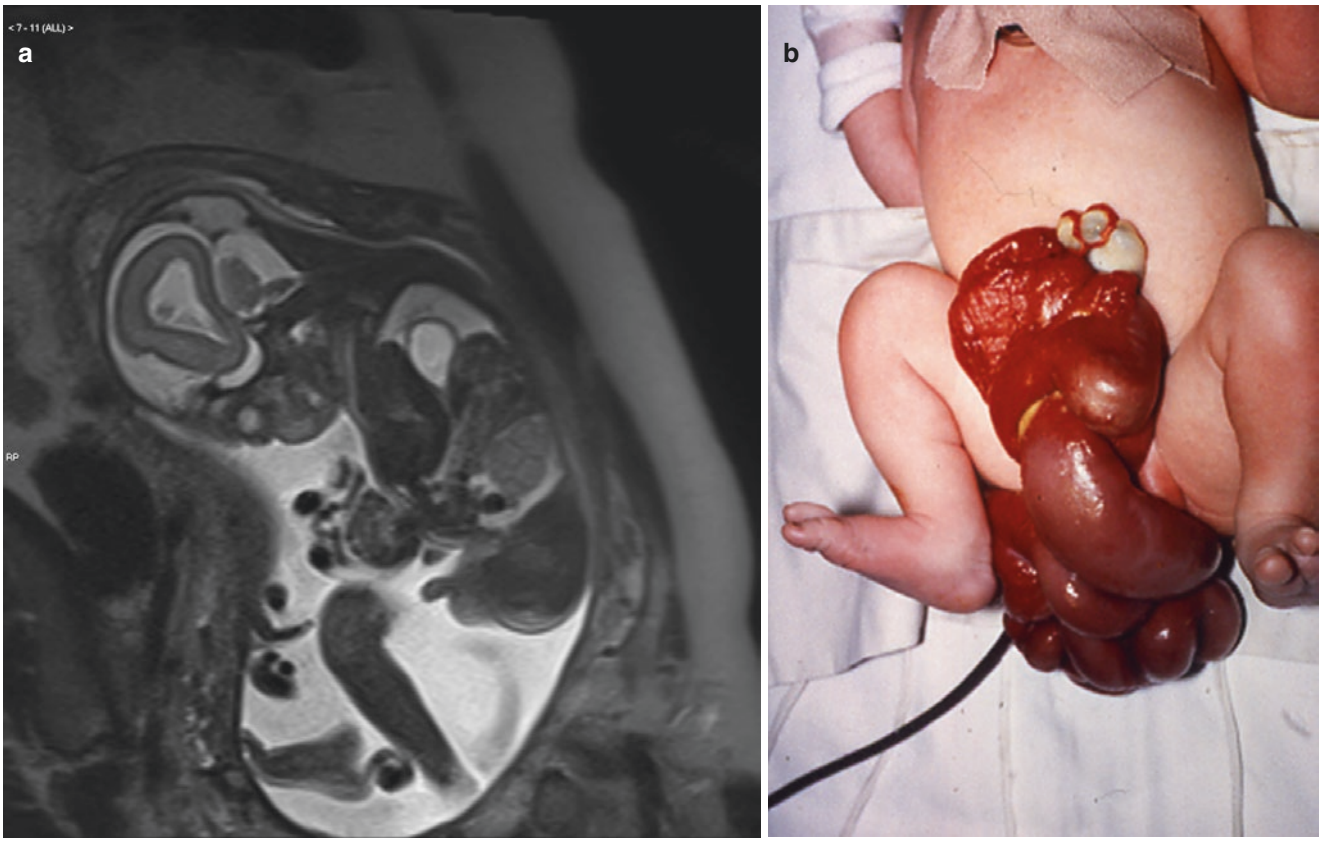

Fig. 4.1 (**a**) Gastroschisis—Fetal MRI with bowel herniation through anterior abdominal wall defect, very suggestive of a gastroschisis because the individual loops of bowel can be seen floating freely. (**b**) Gastroschisis soon after delivery. The bowel is thickened and matted and looks dry and dusky. The umbilical cord can be seen to the left of the abdomen

frequently and easily in the infant which has a transverse oval abdominal cavity (compared to the adult vertical oval abdominal cavity) that alters angulation between the oesophagus and the stomach. Vomiting may be of apparently large amounts, but if the infant is continuing to gain weight satisfactorily, there is no reason for major concern.

Where fluoroscopic studies demonstrate a para-oesophageal hernia, spontaneous resolution is unlikely, whereas with the sliding hiatus hernia of infancy, 80% resolve without treatment. Both types produce vomiting, which can predispose to "asthma" attacks, haematemesis, failure to thrive, regurgitation, rumination syndromes, and athetoid neck movements (Sandifer's syndrome), all of which are associated with severe gastroesophageal reflux. A para-oesophageal hernia is associated with an oesophagus of normal length. The cardia is still in the abdomen but part of the fundus of the stomach prolapses alongside the oesophagus. A small sliding hiatus hernia is common in infants and occurs when the cardia and the fundus of the stomach rise into the thorax through a loose hiatus, giving the illusion of a congenitally short oesophagus. The majority of these infants do not have significant symptoms but continue to thrive and will settle to have an oesophago-gastric junction below the diaphragm with no persistent hernia.

The Barret oesophagus, (the presence of ectopic gastric mucosa in the oesophagus), is a particularly difficult problem to treat in childhood. There are areas of dysplasia in the ectopic mucosa which could give rise to malignancy in long-term follow-up. These patients have to be kept under surveillance and have endoscopy and biopsies carried out on a regular basis to ensure that no malignancy supervenes.

A cystic mass, which may contain a fluid level and gaseous dilation of the oesophagus, may be appreciated on both plain radiography and cross-sectional imaging. Contrast fluoroscopy is used to assess the orientation and extent of the herniation and to provide information on oesophageal and gastric emptying.

4.2.4 Malrotation/Volvulus

Plain abdominal radiography is a nonspecific test in the assessment of children with suspected malrotation and should not be used to diagnose or exclude this entity. Radiographs may be completely normal in up to 20% of patients. The classical signs of proximal bowel obstruction are rarely present and, most often, findings are nonspecific.

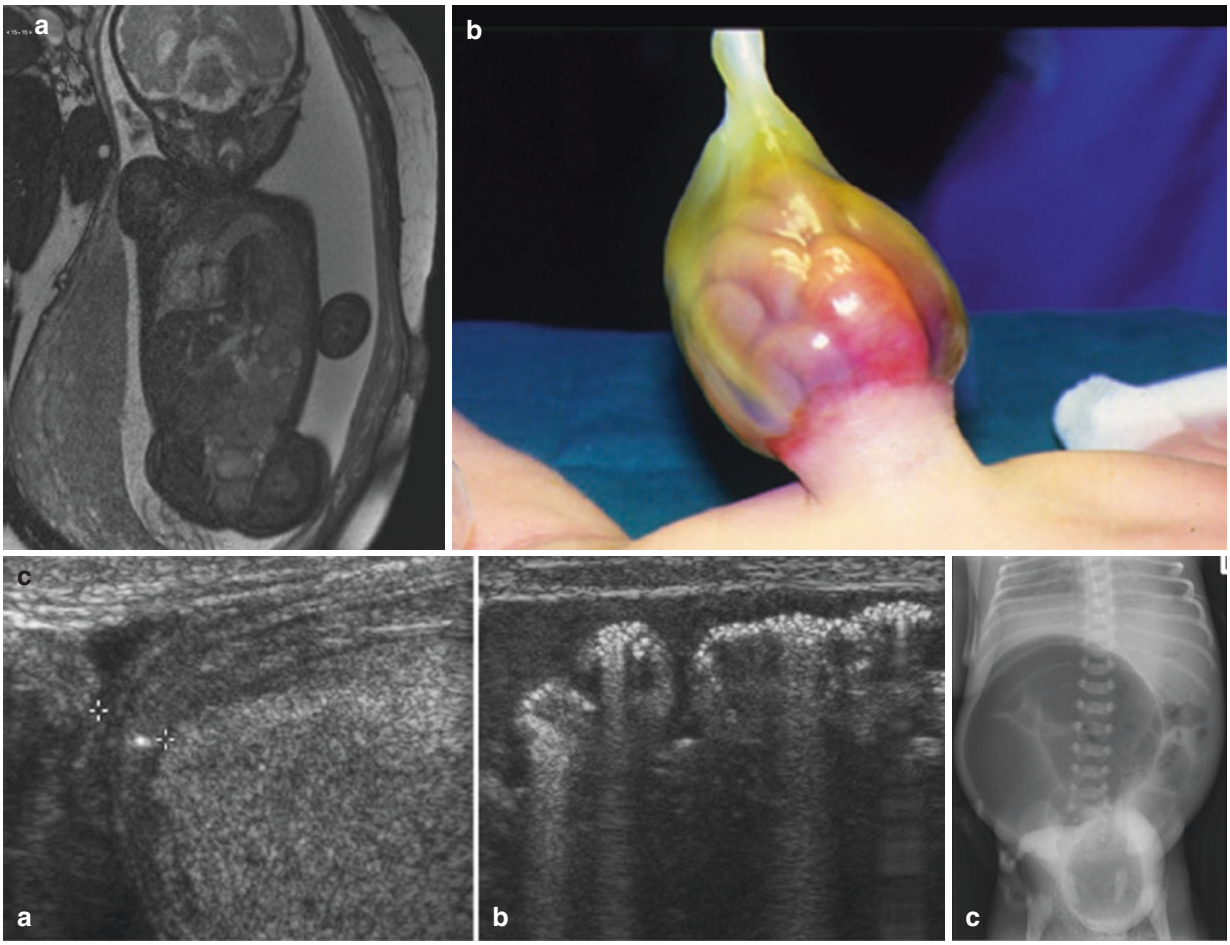

Fig. 4.2 (**a**) Exomphalos antenatal MRI scan showing a protuberance on the abdominal wall suggestive of an exomphalos minor as the liver is not herniated yet. (**b**) Exomphalos/hernia into the cord. (**c**) Plain abdominal X-ray in a neonate. An omphalocele is seen as a rounded soft tissue mass, with distended loops of bowel within the sac

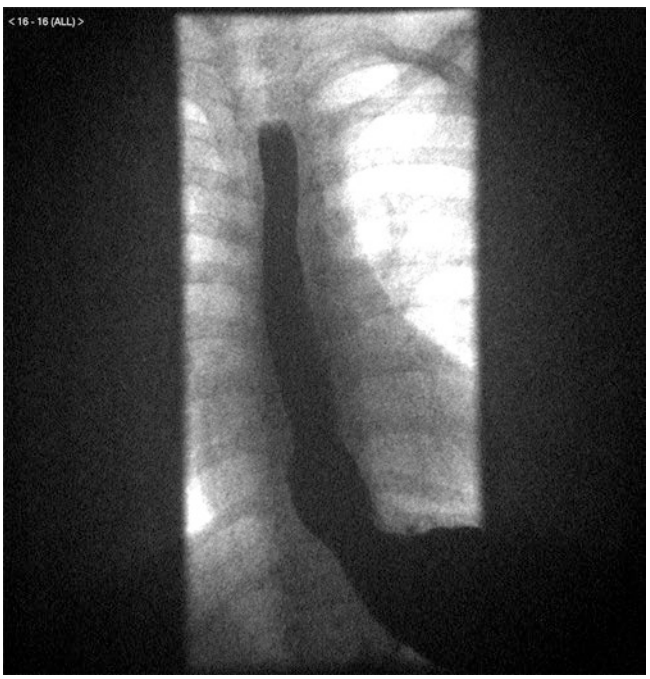

Fig. 4.3 Sliding hiatus hernia. See Chap. 3

They may be misleading, misinterpreted as the double bubble of duodenal atresia, or, if there is generalised gaseous distention (a nonspecific appearance particularly in sick acidotic neonates), as a more distal obstruction.

Upper gastrointestinal contrast examinations are currently the investigation of choice in the diagnosis and assessment of malrotation and volvulus (Fig. 4.4a, c). In the bilious vomiting infant, the vast majority of the studies (around 80%) will be normal, but this is accepted due to the morbidity and mortality of undiagnosed malrotation and volvulus. The rotation of the bowel and thus the mesenteric attachments are implied by orientation of the first and second parts of the duodenum and the duodenal loop and the position of the duodenal-jejunal flexure, which should be to the left of the spine at the same level as the pylorus. As with all investigations, contrast examinations are not 100% specific or sensitive. Problems may arise when the position of the DJ flexure either cannot be assessed or is not in a normal position due to gaseous distension of the surrounding bowel. The ligamentous attachments of the bowel are more mobile than is often appreciated.

No assumptions should be made from the position of the intra-peritoneal bowel on contrast follow-through, as this is mobile and cannot be used to imply the mesenteric attachments. The position of the caecum may also imply mesenteric attachments and can be assessed on either follow-through or enema examinations; however, when a contrast examination has been non-diagnostic the position of the caecum may be of limited value unless grossly abnormal, as the ligamentous attachments are more mobile than at the DJ flexure.

The classical appearance of volvulus is the corkscrew of unobstructed volved/twisted bowel; however, it should be recognised that volvulus can also present as complete obstruction, and this finding should be assumed secondary to volvulus until proven otherwise.

Ultrasonography may directly demonstrate volved bowel and mesentery—often beautifully defined on colour Doppler with the mesenteric vessels twisted in a "whirlpool." It can also be used to assess rotation by evaluating the relationship

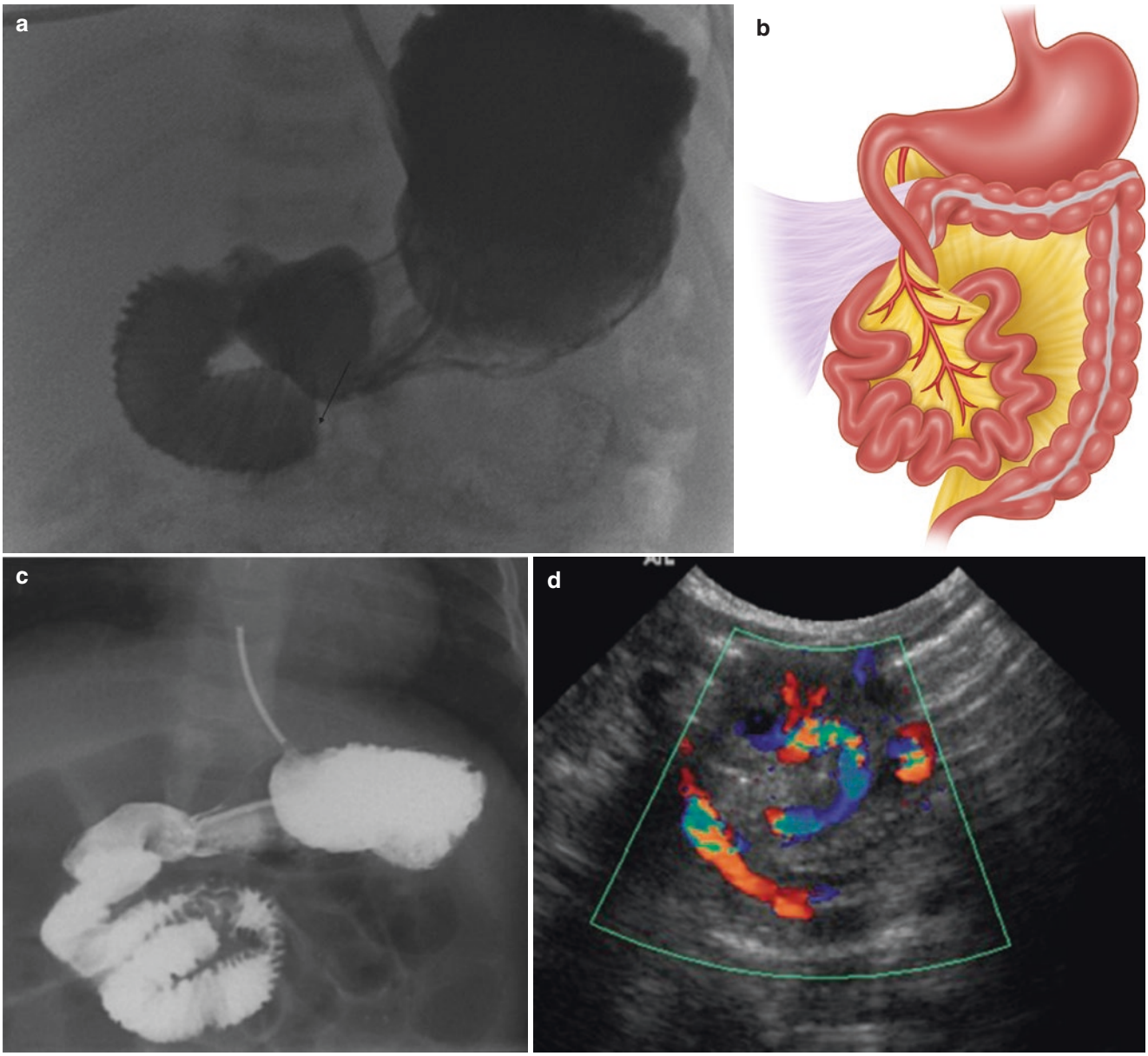

Fig. 4.4 (**a**) Volvulus with complete duodenal obstruction. (**b**) Diagram of a malrotation with a superimposed volvulus of the midgut, causing extrinsic duodenal obstruction. (**c**) Barium meal showing failure of rotation of the duodenum thus lying on the right side of the midline with an associated volvulus. (**d**) Volvulus seen on a colour Doppler ultrasound scan showing the whorled-like appearance of the base of the mesentery with the superior mesenteric vessels twisted. (**e**) Abnormal orientation of stomach in patient with organoaxial gastric volvulus. (**f**) Fluid level in a dilated stomach in a patient with gastric volvulus. (**g**) Volvulus of the sigmoid colon seen on a plain X-ray of the abdomen. Note the distension of the sigmoid colon in the centre of the abdominal cavity

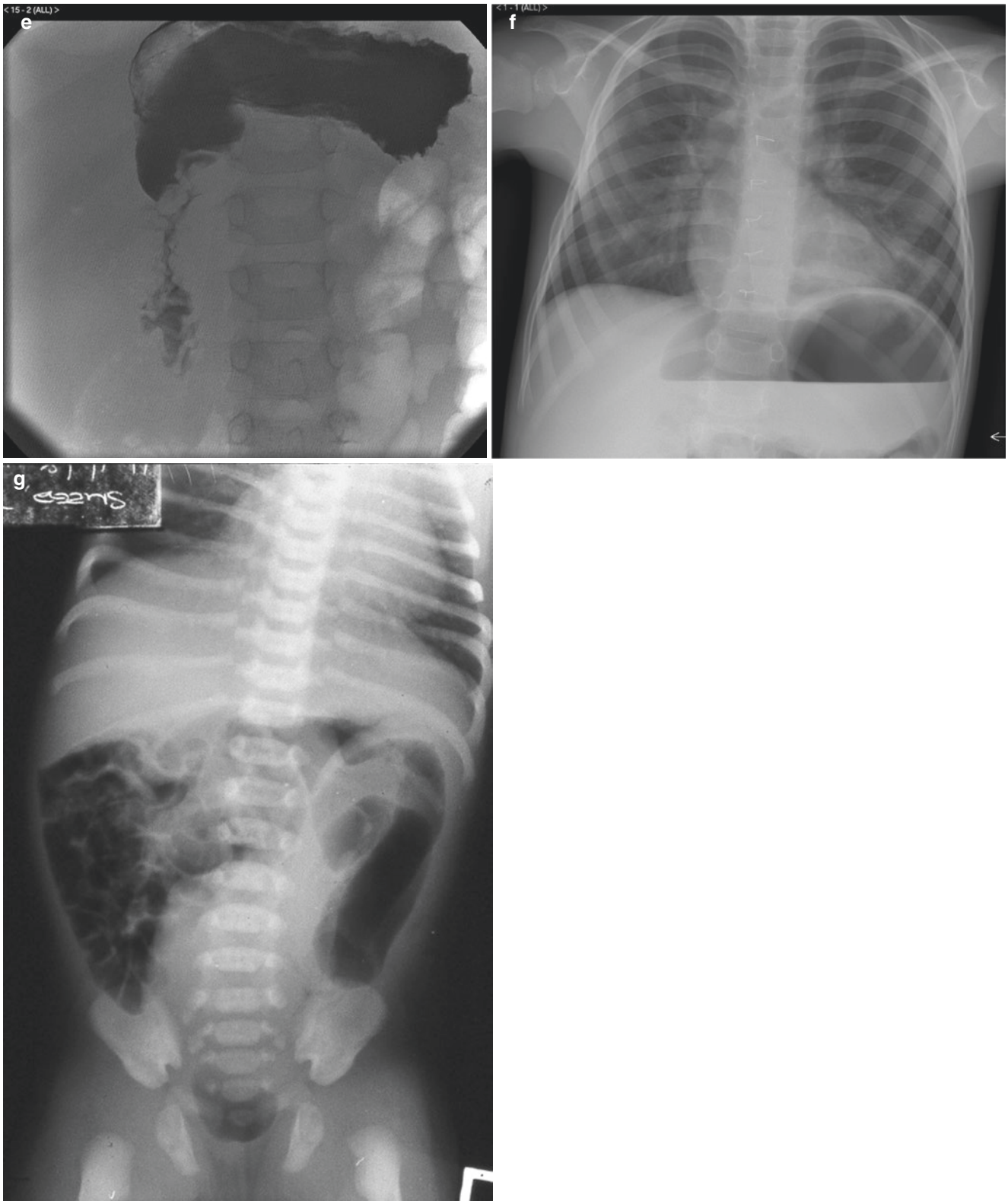

Fig. 4.4 (continued)

of the third part of the duodenum to the aorta and superior mesenteric artery (SMA), demonstrating its retroperitoneal course on compression ultrasound. The assessment of the relationship between the superior mesenteric vein and artery (at the junction of the superior mesenteric vein [SMV] with the portal vein) has also been quoted as a means of assessing rotation, although it is recognised that the position of these vessels is variable, and that rotation cannot be reliably assessed on this finding alone.

The stomach and sigmoid colon are two other areas of the gastrointestinal tract that can be affected. Imaging by plain X-ray or by contrast will demonstrate this abnormality (Fig. 4.4e–g).

4.2.5 Duodenal Atresia/Web/Stenosis

Abdominal plain films in duodenal atresia classically demonstrate a "double bubble" appearance with a dilated gas-filled stomach and first part of the duodenum (Fig. 4.5a, b). This has often been appreciated and diagnosed on antenatal ultrasound, with polyhydramnios and a fluid-filled "double bubble" appearance in the fetal abdomen. Contrast studies are of limited value and are rarely required (Fig. 4.5c). In the presence of non-complete obstruction there is a variable amount of distal gas, and barium/contrast studies may be indicated to delineate the site and anatomy of the obstruction and to assess rotation. Unexpected duodenal obstruction should be assumed to be secondary to malrotation and volvulus unless proven otherwise (Fig. 4.5d).

Ultrasound and cross-sectional imaging can be used to delineate extrinsic causes of an obstruction, including annular pancreas and a preduodenal portal vein.

4.2.6 Biliary Atresia

Investigation is necessary in infants with persistent jaundice. Biliary atresia is an uncommon disease, but is the most important cause of obstructive jaundice in infancy. The history is important with particular attention focused on the stools—have they been normally pigmented or pale acholic stools since birth? Investigations include: Haematological and liver function tests, screening for infection and metabolic causes, ultrasound examination, radionuclide studies, and in some cases percutaneous liver biopsy (Fig. 4.6a, b).

In addition, some centres perform endoscopic retrograde cholangio-pancreatography (ERCP), percutaneous transhepatic cholangiography, laparoscopy, duodenal intubation and aspiration. Despite all these tests, however, laparotomy and exploration may be necessary to establish the diagnosis. The aetiology of biliary atresia has been the subject of much research and speculation, but it is not simply a congenital malformation nor an obliterative ascending cholangitis, as the end result is obliteration of the bile ducts, progressive fibrosis of the liver, and death in the first 2 years of life unless surgical intervention is undertaken. The liver fibrosis results in portal hypertension and oesophageal varices, and ascites becomes a marked feature of the later stages. Biliary atresia is the primary pathology in about half of children developing end-stage liver disease.

An Ultrasound scan (USS) is the initial imaging technique employed in the assessment of neonates with obstructive cholestasis. Intrahepatic duct dilation is not a feature in these cases. An abnormal hyperechogenic triangular area >4 mm diameter the "triangular cord sign" may be demonstrated at the porta hepatis, cranial to the portal vein bifurcation and corresponding to the fibrous remnant of the duct. This has a 98% specificity for the diagnosis. The gallbladder may be absent, atretic, or abnormal on a fasted scan, but the presence of a gallbladder does not exclude the diagnosis. Other associated biliary abnormalities, including choledochal cysts, can also be demonstrated on ultrasound. Although MR cholangiography can be used, it is recognised as less accurate in this population and has not superseded USS.

Hepatobiliary scintigraphy (99mTc-DISIDA) or "HIDA" scanning with phenobarbital pre-treatment (to enhance hepatocellular function aiding differentiation from hepatitis) is used to demonstrate biliary obstruction with absence of excretion of the isotope into the intestine.

Transhepatic and percutaneous or intraoperative cholangiography may be required to assess the type and anatomy of the obstruction.

4.2.7 Choledochal Cyst

Idiopathic dilation of the common bile duct (Choledochal cyst) is rare in childhood. They often present with intermittent abdominal swelling, pain, and jaundice. Investigation reveals the cystic dilatation of the hepatic or common bile duct.

As with biliary atresia, ultrasonography is the initial imaging of choice. The anatomy and association of the lesions with the biliary tree and thus the type of cyst can be defined (Fig. 4.7a).

MR cholangiography has replaced more invasive cholangiography methods in the assessment of these lesions and can demonstrate their connections beautifully and assist surgical planning (Fig. 4.7b–d).

Hepatobiliary scintigraphy can be used to demonstrate accumulation of the radioisotope within the cyst and obstruction of passage into the intestine. In neonates with obstructive features and a choledochal cyst the presence of an associated biliary atresia should always be considered.

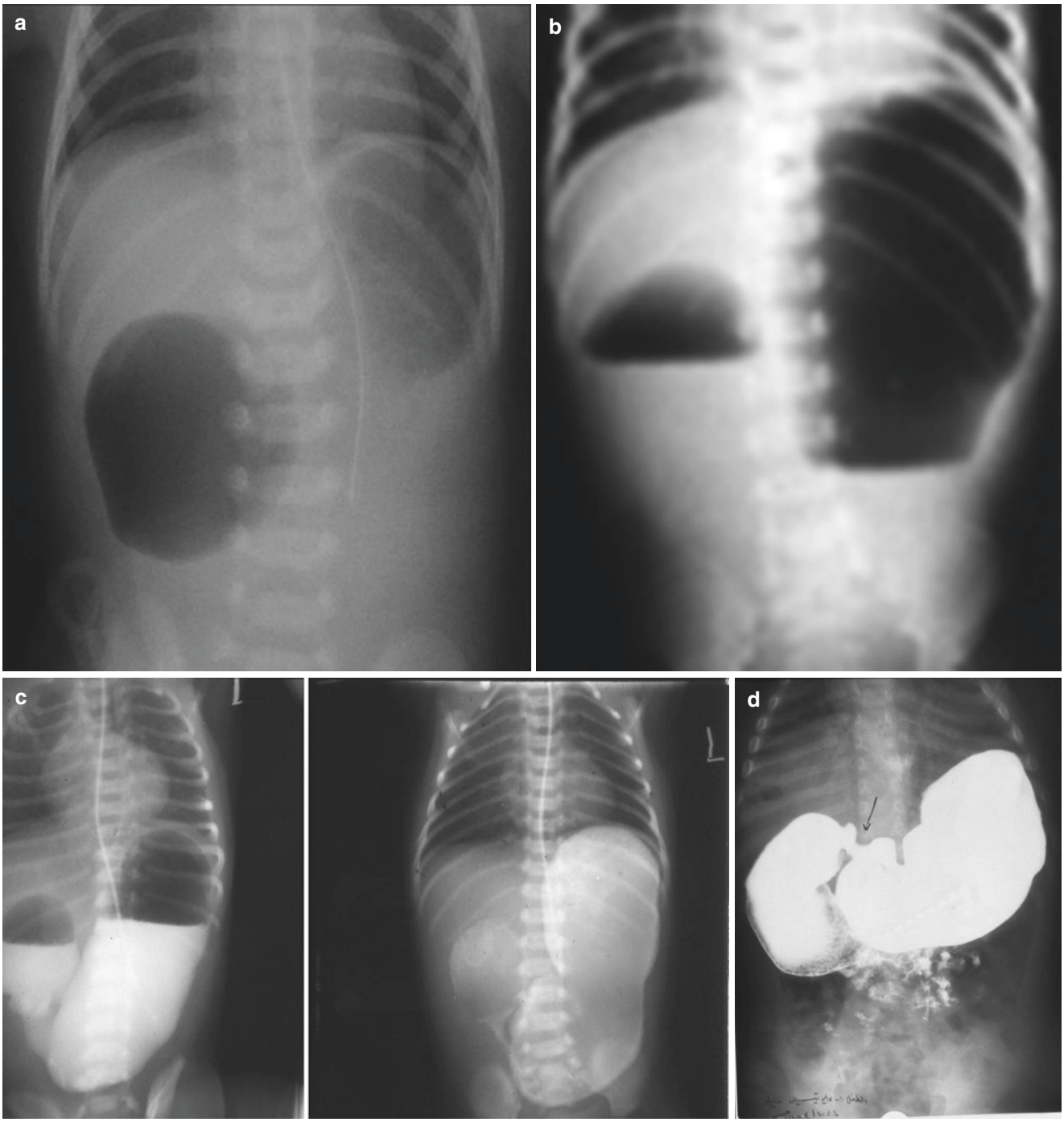

Fig. 4.5 (**a**) Plain X-ray of a neonate with duodenal atresia showing a double bubble: one bubble in the dilated stomach and the other in a dilated proximal duodenum at the level of the obstruction. There is a nasogastric tube in situ. The rest of the abdomen is gasless. (**b**) Duodenal atresia seen in an erect film showing the fluid air interface of the two bubbles of gas. (**c**) Duodenal atresia. This is a historic figure showing contrast in the stomach, which is grossly dilated, and in the duodenum. A nasogastric tube is in situ to aspirate the contrast. This study is no longer recommended. (**d**) A contrast study showing a duodenal stenosis/web with incomplete obstruction and contrast passing distally. The duodenum is large, as is the stomach, due to the obstruction. There is also an antral web seen, which is not causing obstruction. (**e**) Anatomical diagram of biliary atresia (**f**) Plain X-ray of the abdomen showing an incomplete duodenal web. Note the very distended stomach and duodenum with paucity of gas distally. At times the web, when incomplete, may have only a pinhole opening and be dragged on as a "windsock" effect. The ampulla of water may be caught up and even open on the surface of this membrane. (**f**, **g**) A plain X-ray of the abdomen showing a double bubble suggestive of duodenal stenosis because of gas passing distally. In an atresia this can sometimes happen due to the accessory duct of the pancreatic duct that can bypass the atresia. (**g**) Abdominal X-ray duodenal web

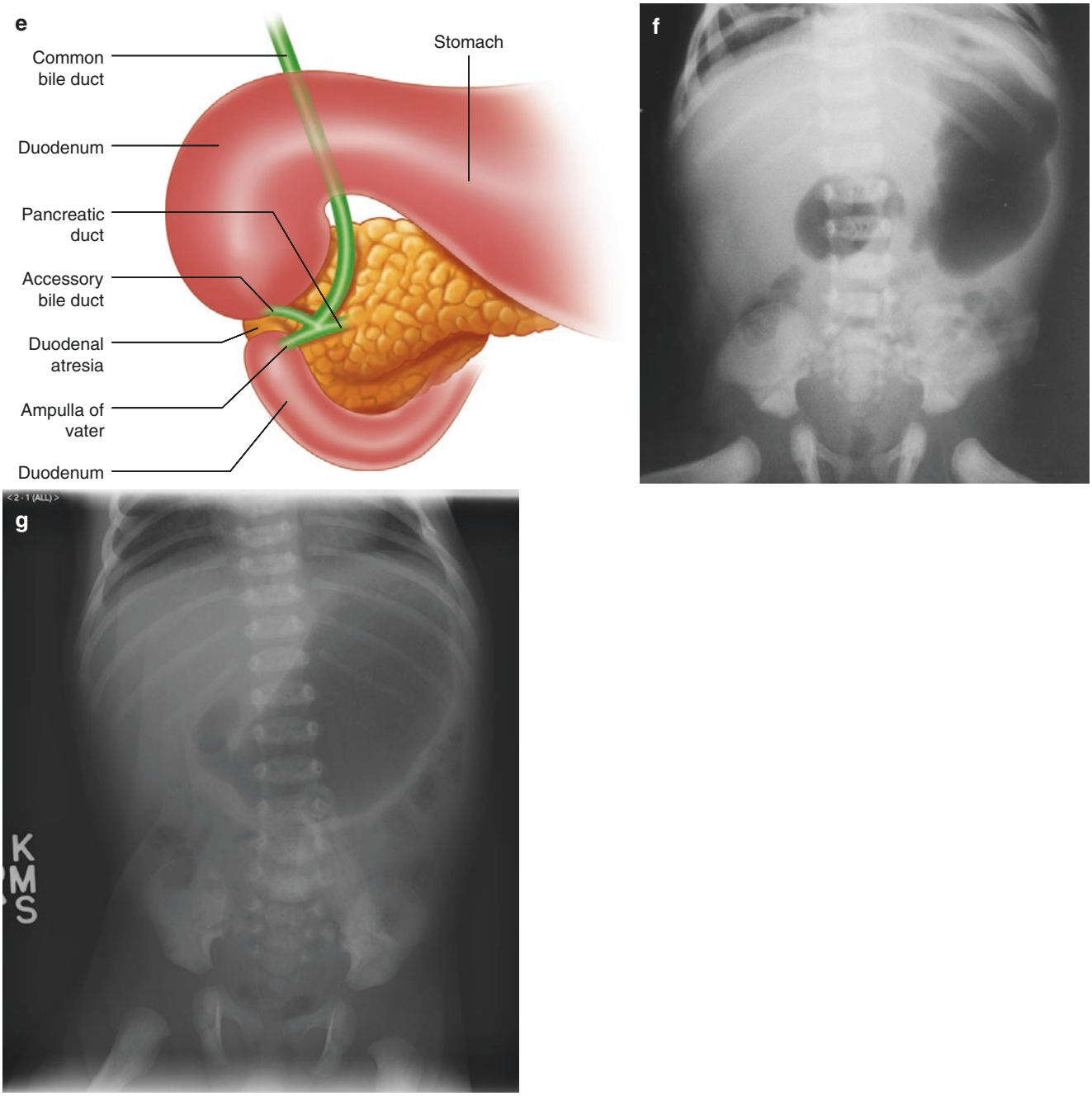

Fig. 4.5 (continued)

4.2.8 Small Bowel Atresia

If the obstruction is high in the small bowel, the infant starts vomiting, and the vomitus becomes bile-stained within 24 h of birth. If the obstruction is lower, abdominal distension occurs and the vomiting may not commence until the second or third day of life. The infant fails to pass any normal meconium. In small bowel atresia there is no sex preponderance. Diagnosis of atresia is sometimes made prenatally when ultrasound examination shows dilated loop(s) of bowel in the fetal abdomen. Postnatally, failure to pass meconium and vomiting suggest the obstruction. X-ray of the abdomen shows dilated bowel with fluid levels and a lack of gas in the distal bowel (Fig. 4.8b).

Plain abdominal radiography in proximal small bowel atresia/jejunal atresia may present as a "triple bubble" with a distended stomach, duodenum, and proximal jejunum (Fig. 4.8g). In more distal atresia the distended gas-filled bowel fills the abdomen, but with no gas demonstrated over the rectum (Fig. 4.8c, f).

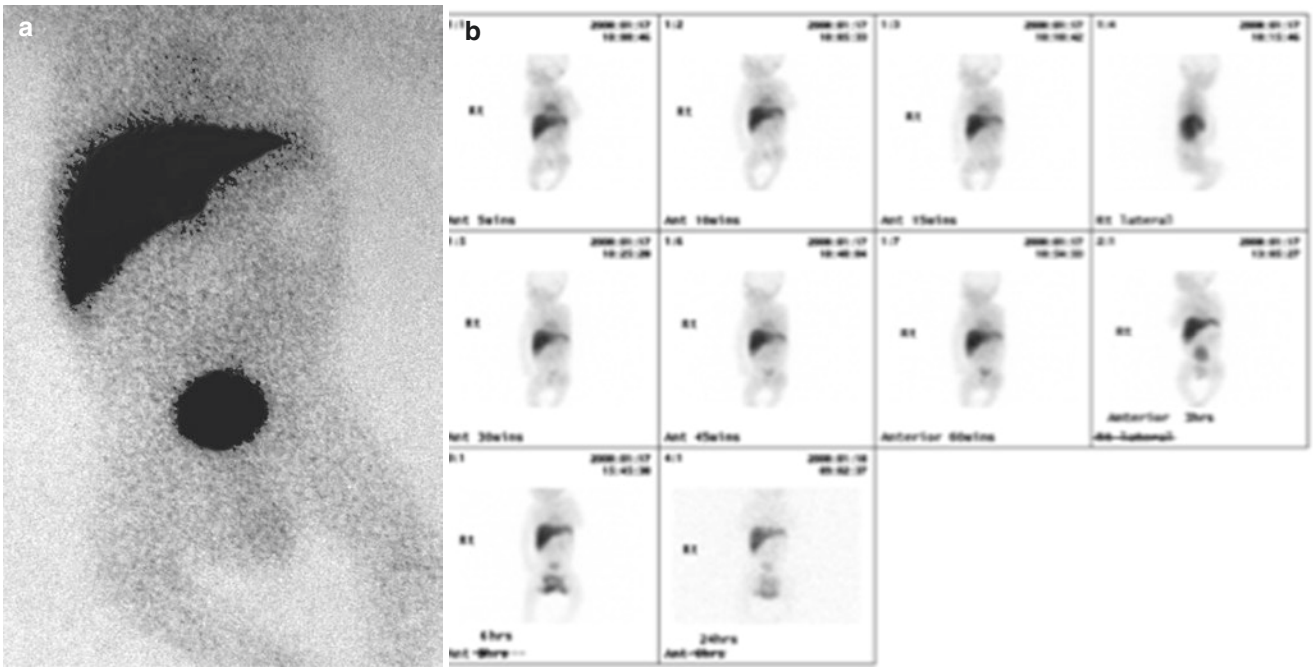

Fig. 4.6 (**a**) Biliary atresia. A HIDA scan showing concentration of isotope in the liver and no isotope in the small bowel. There is isotope in the bladder from renal excretion. (**b**) Nuclear medicine study—HIDA scan—indicates hepatic uptake and bladder uptake (urinary excretion of tracer). The study shows no excretion of isotope into gut and abnormal retention in the liver. There is artefact from isotope in the nappy

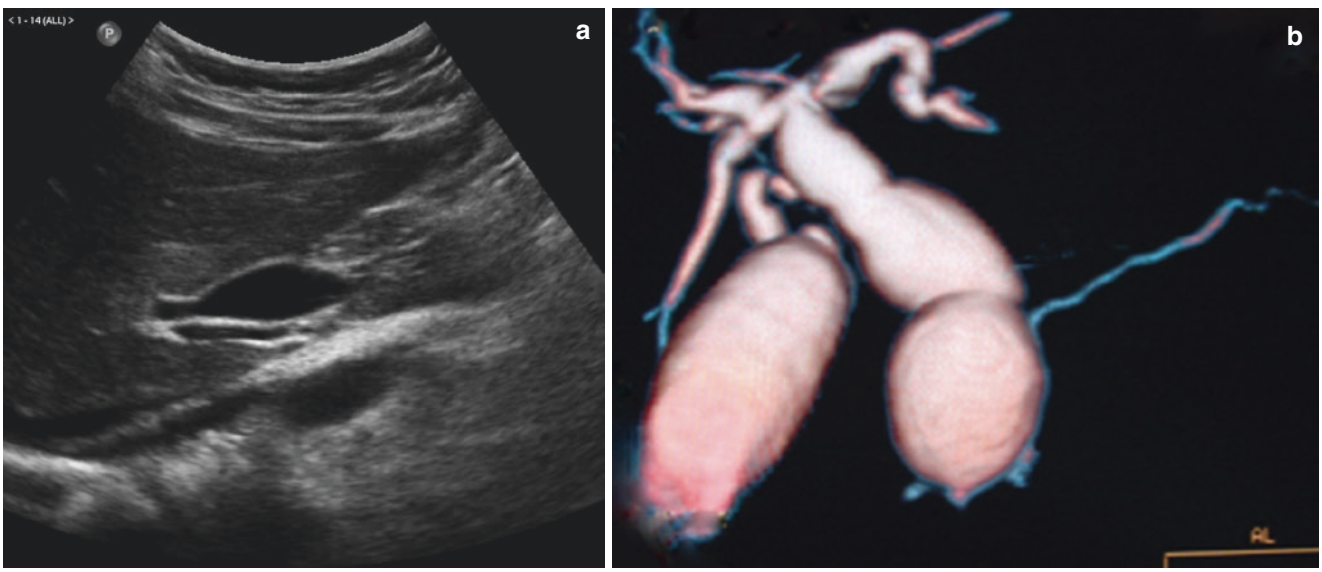

Fig. 4.7 (**a**) Ultrasound of the abdomen. A single sagittal view set obliquely demonstrating fusiform dilatation of the common bile duct, a type 1 choledochal cyst. (**b**) A coronal reconstruction of an MRCP demonstrating fusiform dilatation of a type 1 choledochal cyst. (**c**) Choledochal cyst; different view of **b**. (**d**) A preoperative study showing contrast injected through the gallbladder demonstrates an enlarged biliary system and a choledochal cyst causing obstruction and tapering to a fine stream in an attempt to enter into the duodenum

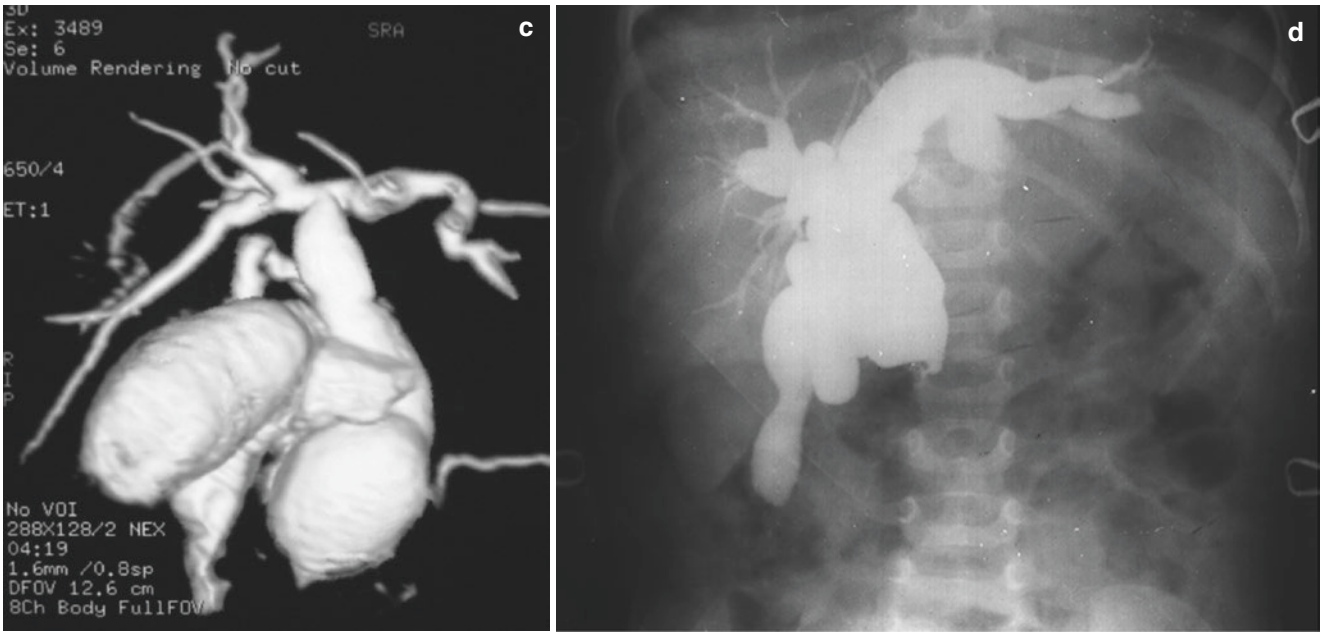

Fig. 4.7 (continued)

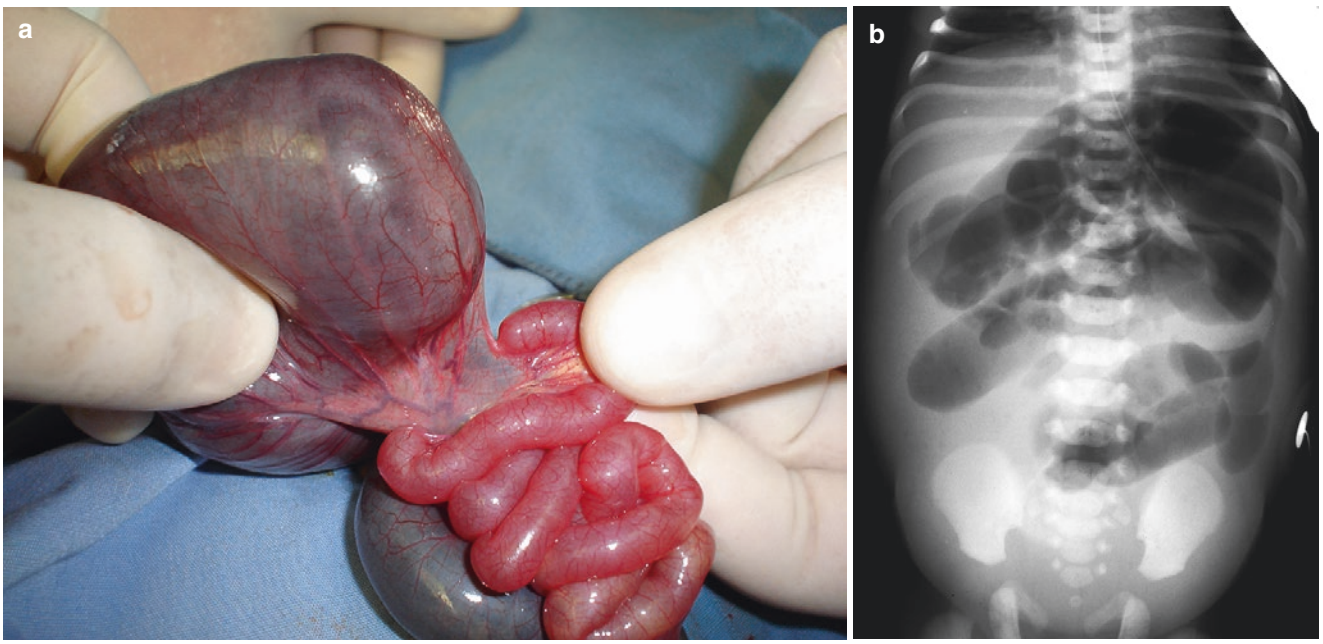

Fig. 4.8 (**a**) Clinical photograph—Atresia of small bowel. Note the discrepancy in size. There is a fine atretic fibre joining the two making this a type 1 atresia (**b**) Plain X-ray showing a jejunal atresia. Nasogastric tube in situ. (**c**) Plain X-ray of the abdomen showing gross neonatal abdominal distension. The distended loops make it difficult to tell if they are small or large bowel. (**d**) Plain radiograph showing a high jejunal atresia (**e**) Small bowel atresia proximal ileal type III. Water-soluble contrast enema, demonstrating a small unused colon also called a microcolon. (**f**) Plain X-ray showing a jejunal atresia. (**g**) Plain radiograph showing a triple bubble of a high Jejunal atresia

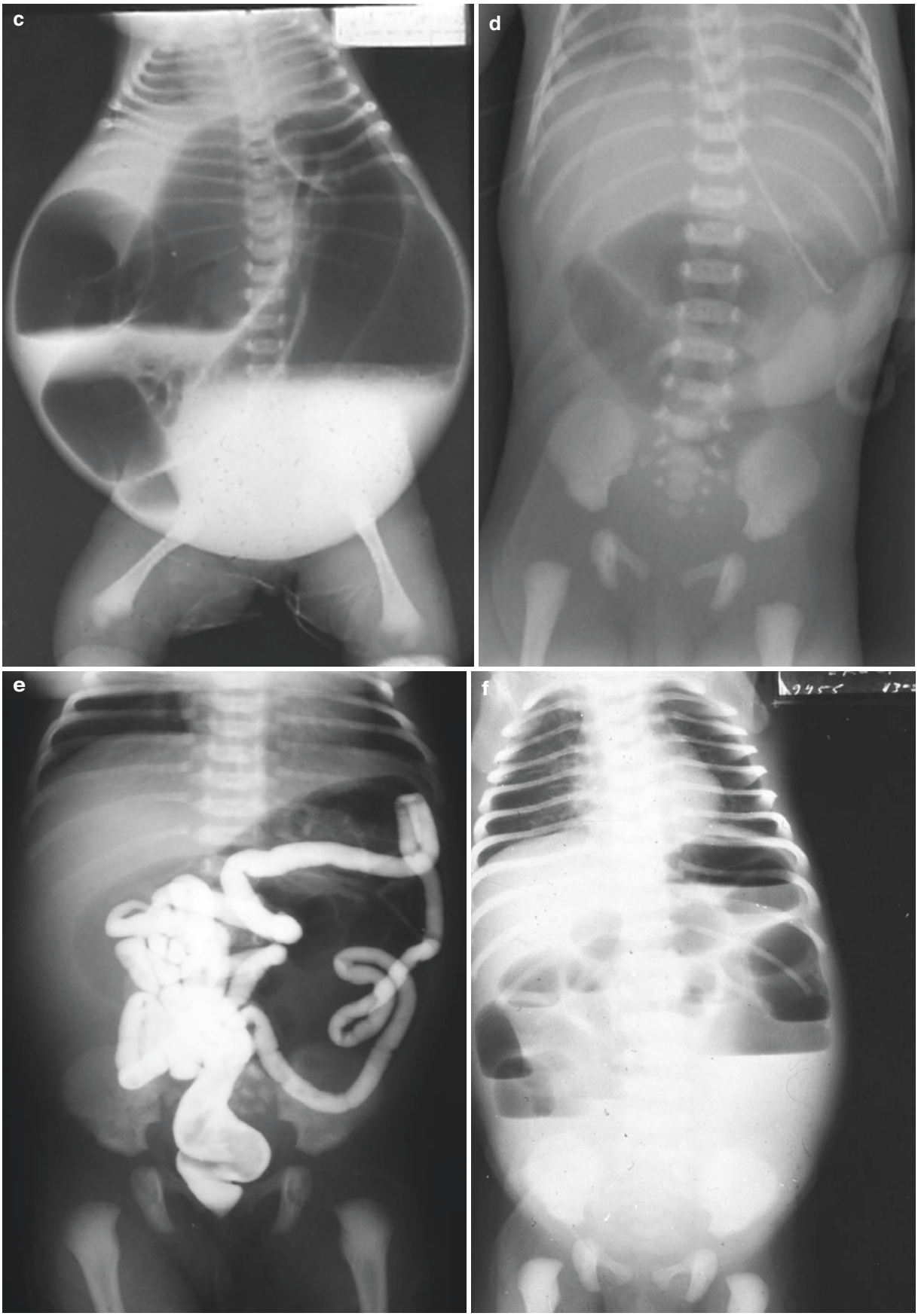

Fig. 4.8 (continued)

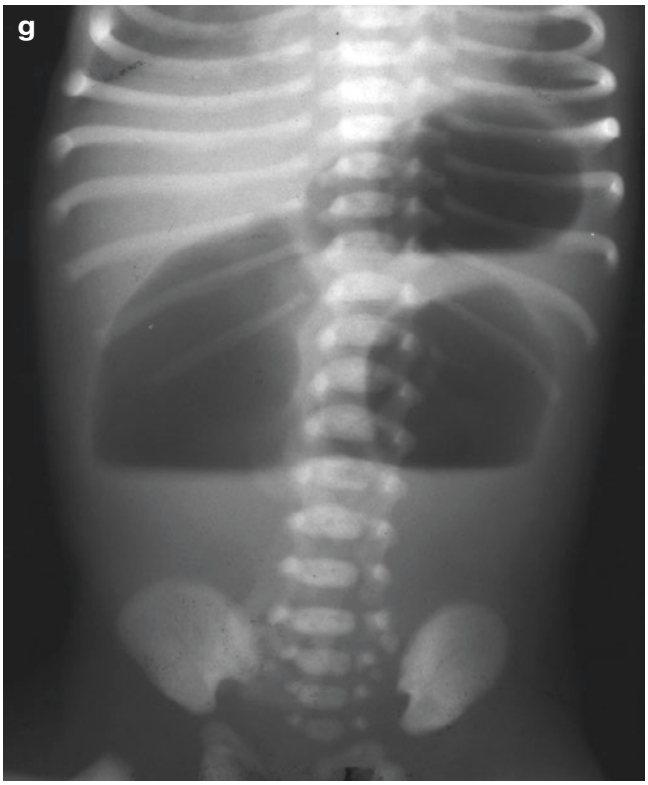

Fig. 4.8 (continued)

Contrast examinations may be of use if there is concern regarding malrotation/volvulus as a cause of small bowel obstruction, but otherwise add little to the assessment of proximal small bowel atresia.

In a distended gas-filled abdomen, a contrast enema is required to assess the position and appearance of the colon and identify the level of obstruction. In a distal atresia the colon is unused and small, a so-called "microcolon" (Fig. 4.8e).

4.2.9 Meconium Ileus/Meconium Plug Syndrome

Neonatal ileal obstruction occurs in one in ten infants with cystic fibrosis. The meconium in the lower ileum is dry green putty-like sticky material. Neonatal obstruction arising from impacted meconium presents a serious problem in early life. In meconium ileus, the middle or lower ileum above the obstruction is often distended and may be complicated by volvulus of this large obstructed loop. This can result in perforation; meconium peritonitis and secondary atresia of the small bowel may develop. This may occur antenatally and present as a complicated meconium ileus at birth with marked abdominal distension (Fig. 4.9a).

Abdominal distension and vomiting are early features and within a day or 2 a ladder pattern and visible peristalsis can be seen. The putty-like mass in the ileum may be palpated in the lower abdomen. Radiography reveals distended loops of small bowel without fluid levels due to the inspissated meconium which may give a mottled or granular or ground-glass appearance. Provided there is no associated atresia, gastrografin enemata can often be used to treat as well as diagnose meconium ileus (Fig. 4.9b, c).

4.2.9.1 Meconium Plug (Fig. 4.9d)

A firm plug may delay the passage of the first stools by hours or days and the infant may present with signs of intestinal obstruction. An underlying condition should always be considered in this situation, be it Hirschsprung's disease, septicaemia, dehydration, or cystic fibrosis. It is usually in the spectrum of small left colon syndrome.

Plain abdominal radiography will show dilated gas-filled loops of bowel in keeping with the distal obstruction.

Contrast enema in meconium ileus on the other hand, will demonstrate a microcolon, often with filling defects secondary to the viscid meconium. Contrast may be refluxed into the dilated plugged terminal ileum. Recognising whether meconium ileus is simple and may respond to the relatively hyperosmolar contrast and washouts and repeating the enema may be of use, or complicated by atresia and/or perforation, often with peritoneal calcification.

4.2.10 Colonic Atresia/Small Left Colon Syndrome (Fig. 4.10a)

Colonic atresia usually presents a few days later than an obstruction higher up, e.g., duodenal or ileal atresia. There is gross distension with bile-stained meconium. It can be confused with other conditions, such as Hirschsprung's disease and anorectal anomalies. Colonic atresia can occur anywhere along the colon and is not specifically related to so-called vulnerable ischaemia areas (water shed) seen in the region of the splenic flexure of the colon.

Small left colon syndrome can be confused with a long segment Hirschsprung's disease and can occur in small-for-dates babies and the infants of mothers who are diabetic. The diagnosis is made by a contrast enema showing a small calibre descending colon. The size ratio of rectum to sigmoid is normal. Biopsies may be necessary to exclude aganglionosis.

Plain abdominal radiography cannot distinguish distal small- from large-bowel obstruction and a contrast enema is required to assess the level of obstruction and appearance of the colon (Fig. 4.10b, c).

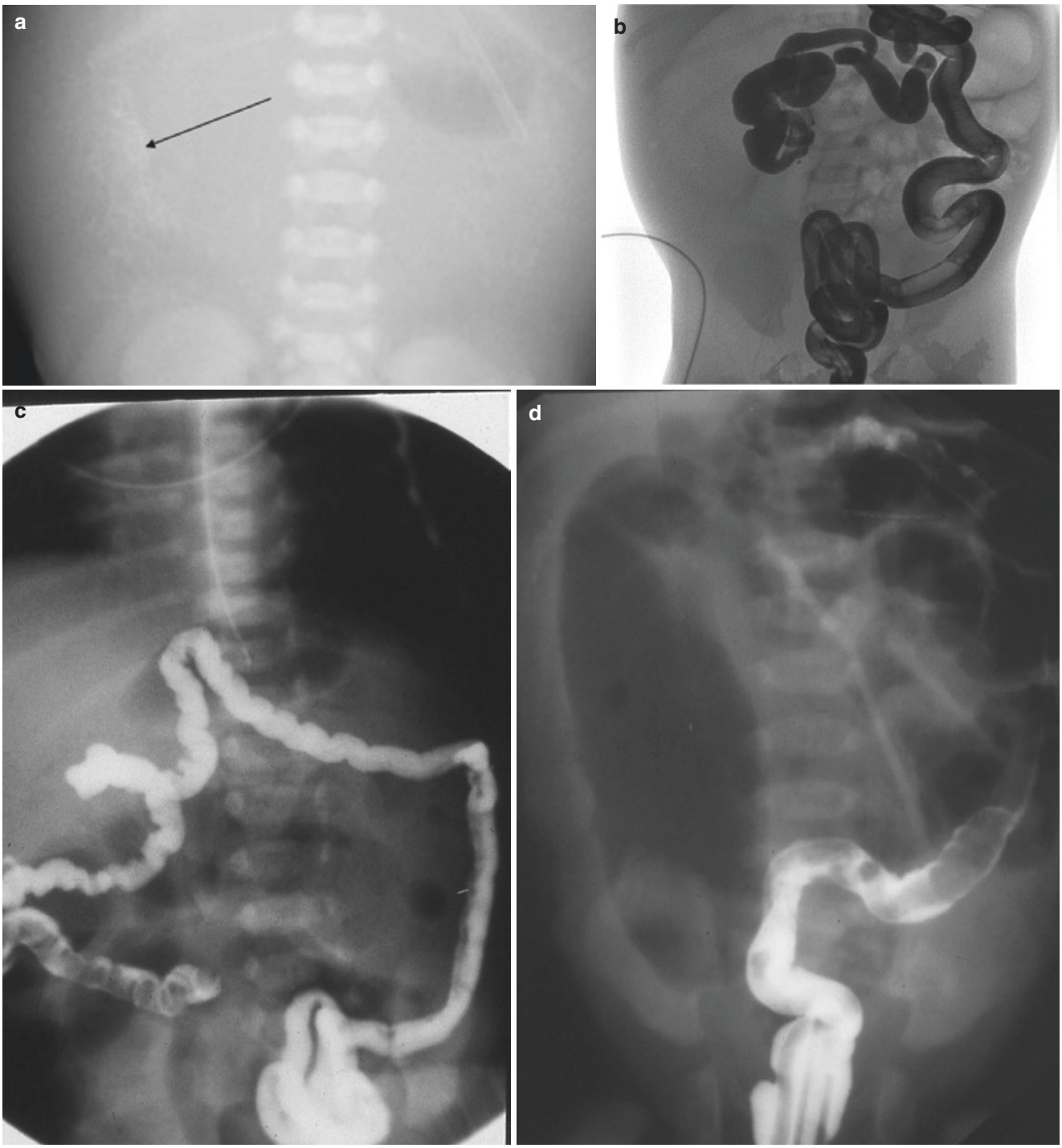

Fig. 4.9 (**a**) Plain X-ray of the abdomen with calcification. Complicated meconium ileus. (**b**) Contrast enema showing redundant loops of a disused microcolon with meconium plugs seen in the lumen. Proximal gaseous dilatation can be seen. Meconium ileus. (**c**) Contrast enema in a patient with meconium ileus. Note the small size of the colon. (**d**) Barium enema in meconium plug syndrome showing contrast in the unused colon and proximal dilatation from the obstruction

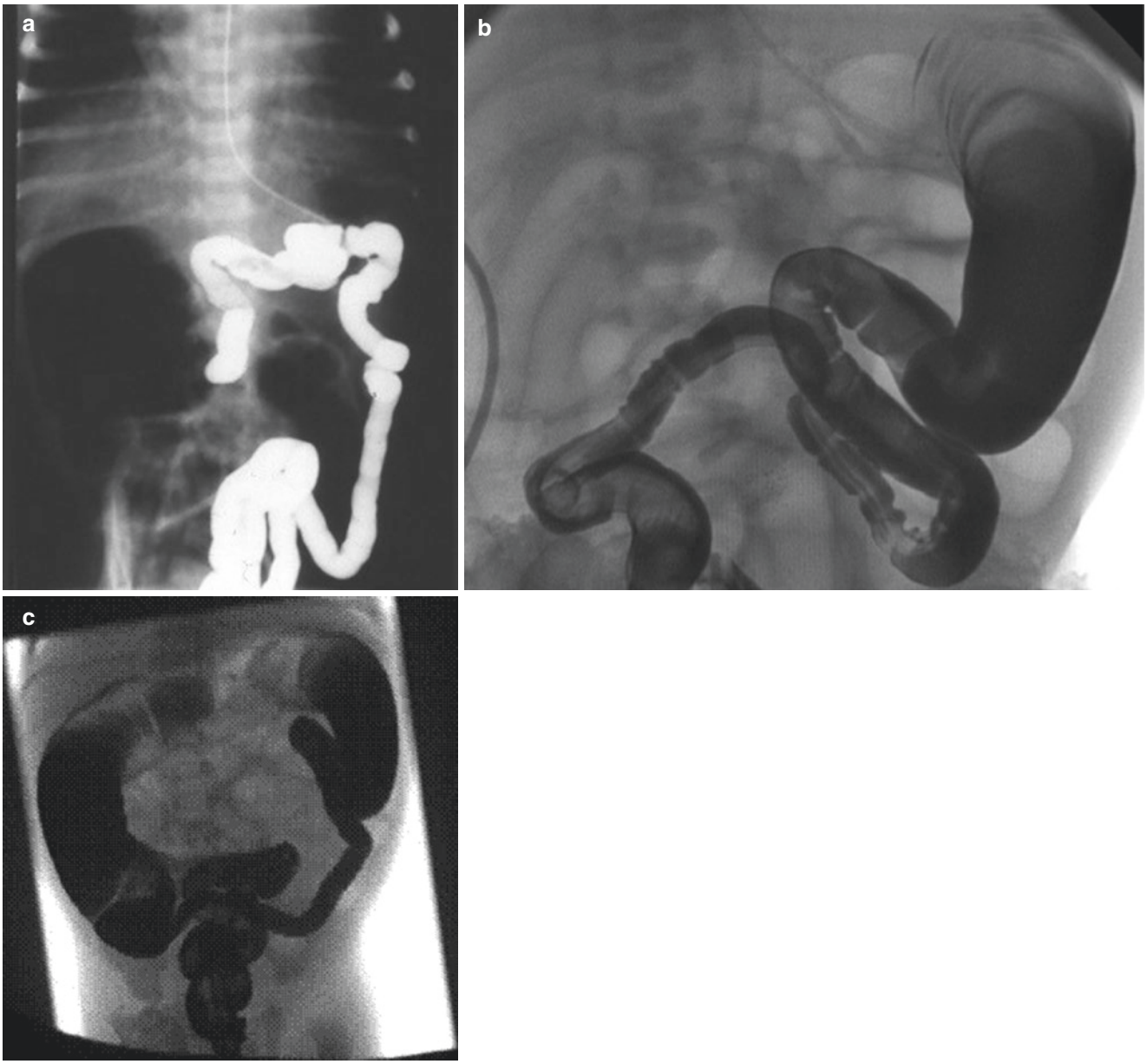

Fig. 4.10 (**a**) Barium enema showing a colonic atresia at the transverse colon. (**b**) Contrast enema in a small left colon syndrome. (**c**) Contrast study in small left colon syndrome. Note the proximal colonic dilatation and reflux into the small bowel

4.2.11 Meckel's Diverticulum

Meckel's diverticulum is found in about 2% of all post-mortem examinations in general hospitals. Most of these people have lived their allotted span without any symptoms and it is purely a chance finding. Remnants of the vitello-intestinal tract may, however, lead to dramatic surgical catastrophe in the first few years of life. In the early weeks of intrauterine life, the apex of the mid-gut loop has a wide communication with the yolk sac. This opening is narrowed to form the vitello-intestinal duct, and the duct and its accompanying artery and veins are normally obliterated. Vestiges of the duct or its vessels or cysts within it may persist. A vitello-intestinal fistula is rare and occurs when the vitello-intestinal duct fails to close. Small intestinal contents are discharged at the umbilicus. In Meckel's diverticulum the duct closes at the umbilical end but remains open at the intestinal end. The diverticulum, which may be half an inch to 2 in. long, arises from the antemesenteric border of the ileum one-to-three feet proximal to the ilecaecal valve, and generally has a small mesentery containing patent remains of the vitelline vessels. It may terminate in a thin cord attached to the umbilicus. The cord represents the fibrous remnants of the vitelline duct or its vessels, and may occasionally acquire a

new attachment elsewhere. The umbilical portion of the duct may remain to form a vitello-intestinal cyst. Although the vitelline duct is embryologically related to the ileum, its remnant is not necessarily lined throughout with ileal mucosa. In 25–30% of diverticulae there is heterotopic tissue—gastric, duodenal, colonic, or pancreatic. Complications from a Meckel's diverticulum can present in many ways, such as abdominal pain simulating appendicitis, intestinal obstruction, intestinal haemorrhage, intussusception, umbilical fistula, umbilical cysts or polyps, perforation, or as an incidental finding at operation. Plain radiography of the abdomen is rarely helpful. A Technetium (Tc) isotope scan can demonstrate around 30% of cases (Fig. 4.11a, b). Although most textbooks refer to Meckel's diverticulitis, this is a rare clinical condition, the signs and symptoms of which are usually indistinguishable from appendicitis and are diagnosed at operation. Perforation of a Meckel's diverticulum may result in peritonitis and haemorrhage. Intestinal obstruction is the most serious complication of Meckel's diverticulum. A volvulus may occur around the fibrous adhesion with loss of viability of the bowel. Intestinal haemorrhage arises from peptic ulceration from the heterotopic gastric mucosa. There may be a sudden passage of blood-stained stool in a young child without previous symptoms. Bleeding may be copious and while the first stool may be dark in colour, subsequent stools are usually bright red. The red cell count may fall to alarmingly low levels in a short space of time. Bleeding from a Meckel's diverticulum may be unaccompanied by pain, or there may be mild discomfort, in sharp contrast to the colic that accompanies bleeding in intussusception. There are usually scant abdominal signs. The ulcer may perforate soon after the onset of bleeding, and there may be evidence of peritonitis. There are no distinguishing features to intussusception where the lead point is a Meckel's diverticulum. As in idiopathic intussusception, the clinical picture is one of recurring abdominal colic with pallor, vomiting during paroxysms of pain, and the presence of blood and mucus in the stools.

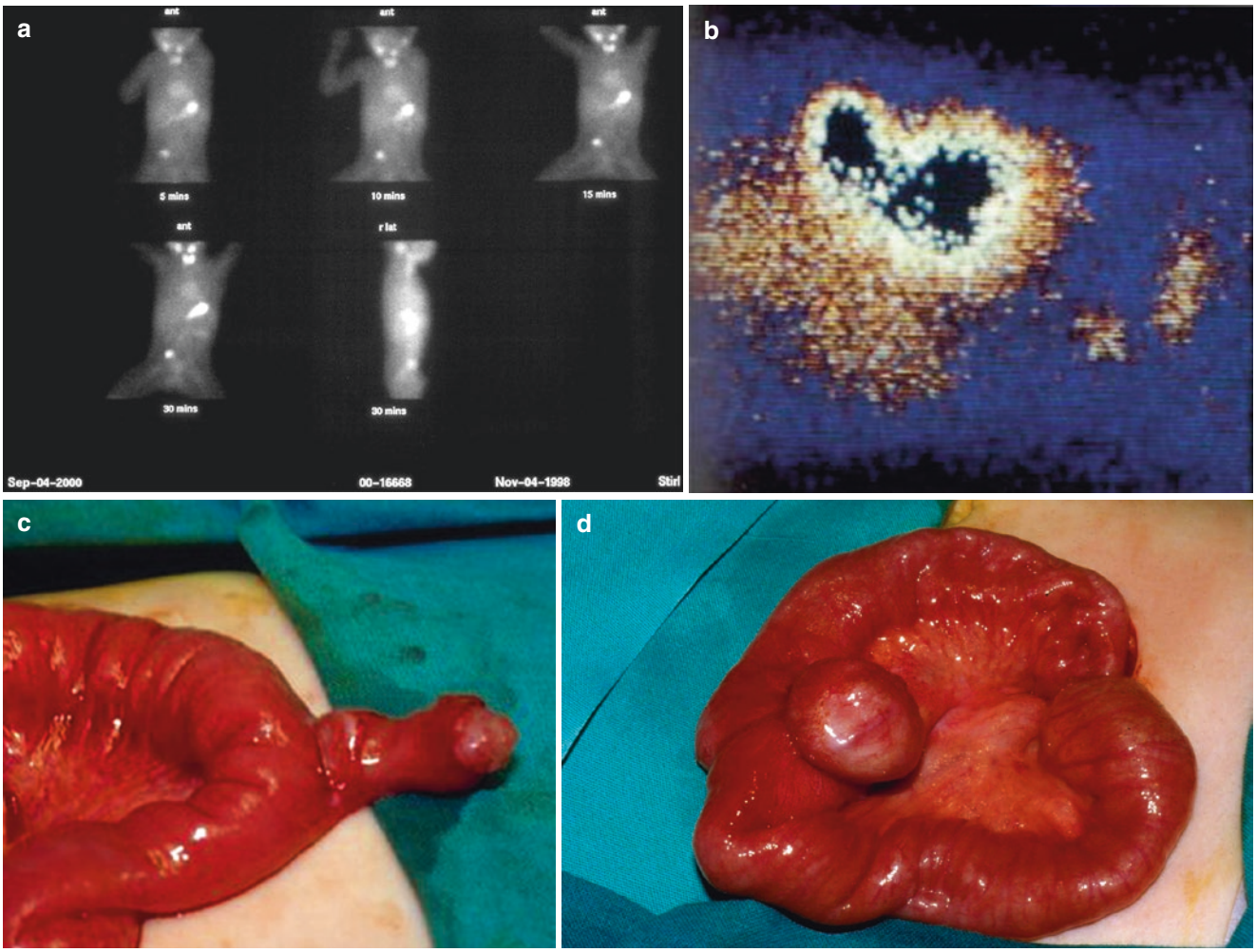

Fig. 4.11 (**a**) Meckel's diverticulum Tc Scan. (**b**) Meckel's diverticulum Tc scan. (**c**) Meckel's diverticulum operative photo. (**d**) Meckel's diverticulum operative photo

The diagnosis of Meckel's diverticulum by radiological methods is neither easy nor reliable. The diagnosis may be suggested by the presence of a calcified enterolith on plain radiography. While the diverticulum may be visualised as an outpouching of the ileum by bowel ultrasound, cross-sectional imaging, and contrast examinations, it cannot be reliably excluded by these methods, which do not replace laparoscopy. The diagnosis should be considered in atypical cases of intussusception where a pathological lead point is suspected (Fig. 4.11c).

When a Meckel's diverticulum is suspected as a cause of gastrointestinal haemorrhage and is therefore assumed to contain gastric mucosa, a Tc99pertechnate radio-isotope scan may indicate the diagnosis by demonstrating a focal "hotspot" in the mid-abdomen. Other methods of radiological diagnosis in the presence of ongoing severe haemorrhage include contrast and CT angiography and red cell scans.

4.2.12 Hirschsprung's Disease

In 1887 Harold Hirschsprung of Copenhagen described the clinical features of the condition that now bears his name. The primary pathology is lack of ganglion cells in the bowel for variable lengths from anus proximally. Aganglionosis is the alternative name for the condition. The proximal normally innervated colon is greatly hypertrophied and dilated as it tries to press the contents through the distal aganglionic bowel, which causes a functional obstruction. The rectum and rectosigmoid have a narrow calibre. The narrow segment may be short or long; short-segment aganglionosis is where the deficiency extends from the anus proximally into the rectum but not beyond the sigmoid colon; in long-segment aganglionosis, lack of ganglion cells extends more proximally and occasionally extends into small bowel (Fig. 4.12a).

Although the child appears to be healthy at birth, they are likely to have a delay in passage of meconium, develop abdominal distension and vomiting, and demonstrate failure to thrive. Constipation is usual, and in babies older than 1 month, constipation becomes an increasing problem; in early infancy, however, diarrhoea secondary to enterocolitis may supervene. Over 95% of term babies pass meconium within the first 24 h after birth and the remainder pass it within the next 24 h. Some patients show less well-defined clinical signs. There may be intermittent constipation and abdominal distension in the neonatal period, which is relieved by conservative measures. Gradually, constipation becomes more stubborn and there is marked enlargement of the abdomen. Peristaltic waves may be seen to pass along the dilated and hypertrophied transverse colon going from right to left. Faecal masses are usually palpable through the abdominal wall. Rectal examination may reveal an empty rectum with faeces at its upper limit, or there may be a palpable mass of faeces in the sigmoid colon, which can be palpated through the rectal wall. There may be faecal incontinence, soiling, or spurious diarrhoea. If untreated, growth in these patients is usually retarded and puberty may be delayed. The abdominal distension may be accentuated if enterocolitis becomes superimposed and may be relieved by the passage of quantities of foul-smelling faeces. Fluid loss may be an acute problem. Another common complication is ulceration of the mucosa and occasionally perforation. Rectal examination in the neonate by insertion of the little finger into the rectum may reveal meconium present and on removal an explosive evacuation of meconium or faeces and air results in a decrease in the abdominal girth. X-ray of the abdomen reveals dilated coils of bowel with lack of gas in the rectum. Clinically and radiologically the condition is a neonatal obstruction. A barium enema may show the narrow rectum and an expanded rectosigmoid with proximal dilation, but this appearance may not present until the infant is 2–3 weeks of age. Diagnosis is confirmed by a rectal suction biopsy. The rectal biopsy should be performed at least 2 cm above the anal margin because the terminal rectum and anal canal do not have ganglion cells even in the normal individual. A false diagnosis may be made if the biopsy is taken too low. The biopsies are usually given directly to the pathologist, who in addition to the above looks for the presence of increased nerve fibres using acetylcholinesterase staining as a useful adjunct in the histological diagnosis of Hirschsprung's disease.

Plain abdominal radiography may show gaseous distention of bowel, often with no gas in the rectum, but essentially non-specific for distal obstruction. In older children there may be faecal loading. Radiographs may demonstrate complications including the thumb printing of Hirschsprung's enterocolitis and perforation.

A contrast enema, if required, should be performed on unprepared bowel to assess the dimensions of the distal bowel and rectum and to assess for a transition zone, marking the transition of the un-innervated, contracted bowel to innervated bowel with normal diameter (Fig. 4.12d). Possible difficulties in interpretation include very-short-segment disease, where the un-innervated bowel is either bypassed by the catheter or the reduced diameter of the rectum, compared to the sigmoid, is not appreciated. In complete or total colonic Hirschsprung's, the contrast demonstrates microcolon with no focal transition point. Enterocolitis is a serious complication with a high mortality. It is diagnosed clinically. Enemas are not advised because of the risk of perforation (Fig. 4.12e–g).

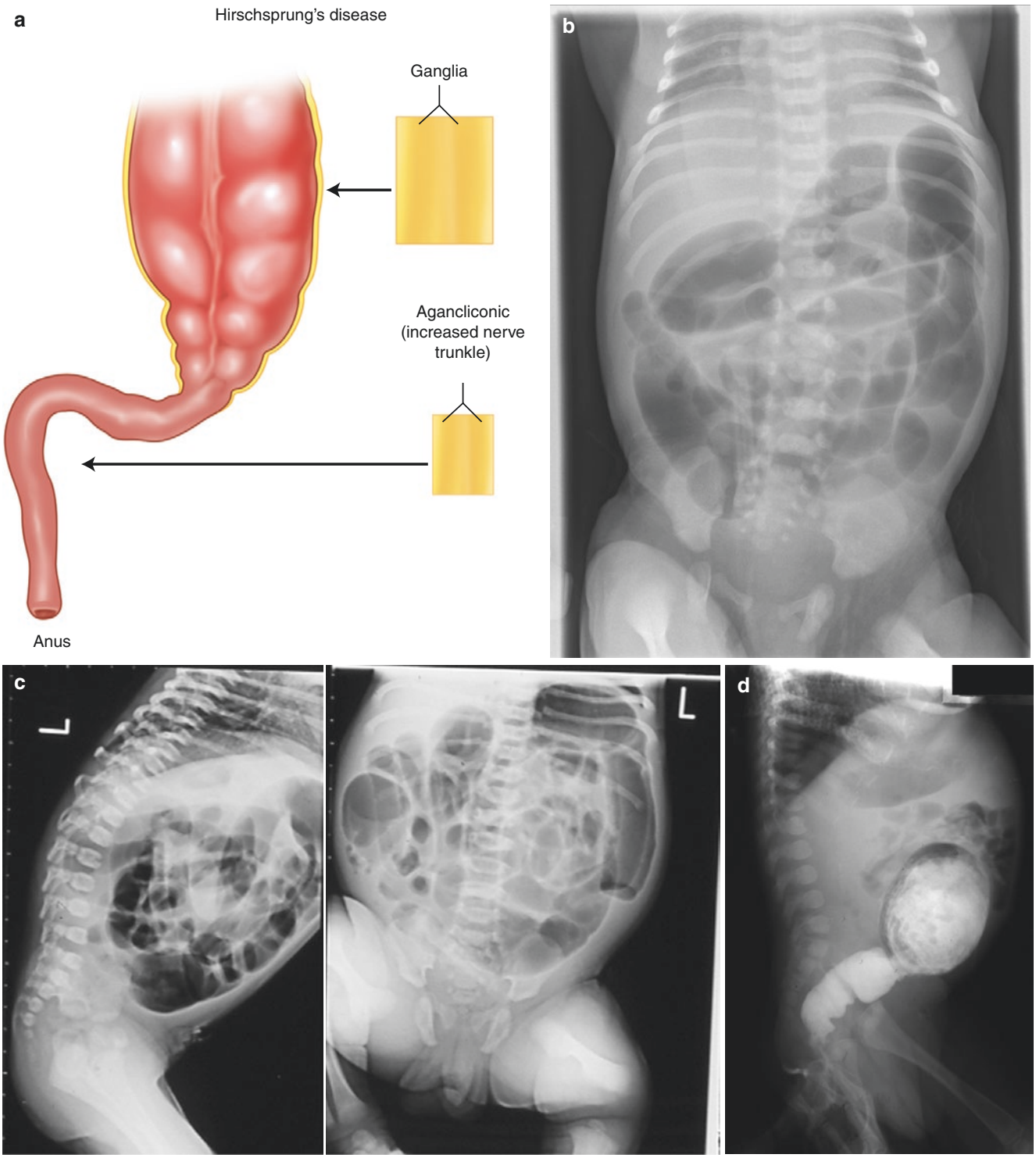

Fig. 4.12 (**a**) Diagram of Hirschsprung's disease (**b**) Plain X-ray of the abdomen showing distended loops of bowel and a gasless pelvis in Hirschsprung's disease. (**c**) Neonatal plain X-rays AP and lateral showing an obstructed bowel and a gasless pelvis in Hirschsprung's disease, (**d**) Contrast enema showing a transition zone in Hirschsprung's disease. The dilated loop has ganglion cells and the distal collapsed bowel is aganglionic. (**e**) Contrast enema showing transition zone in Hirschsprung's disease, (**f**) Contrast enema showing a low transition zone in short segment Hirschsprung's disease, (**g**) Contrast enema in Hirschsprung's disease demonstrating enterocolitis

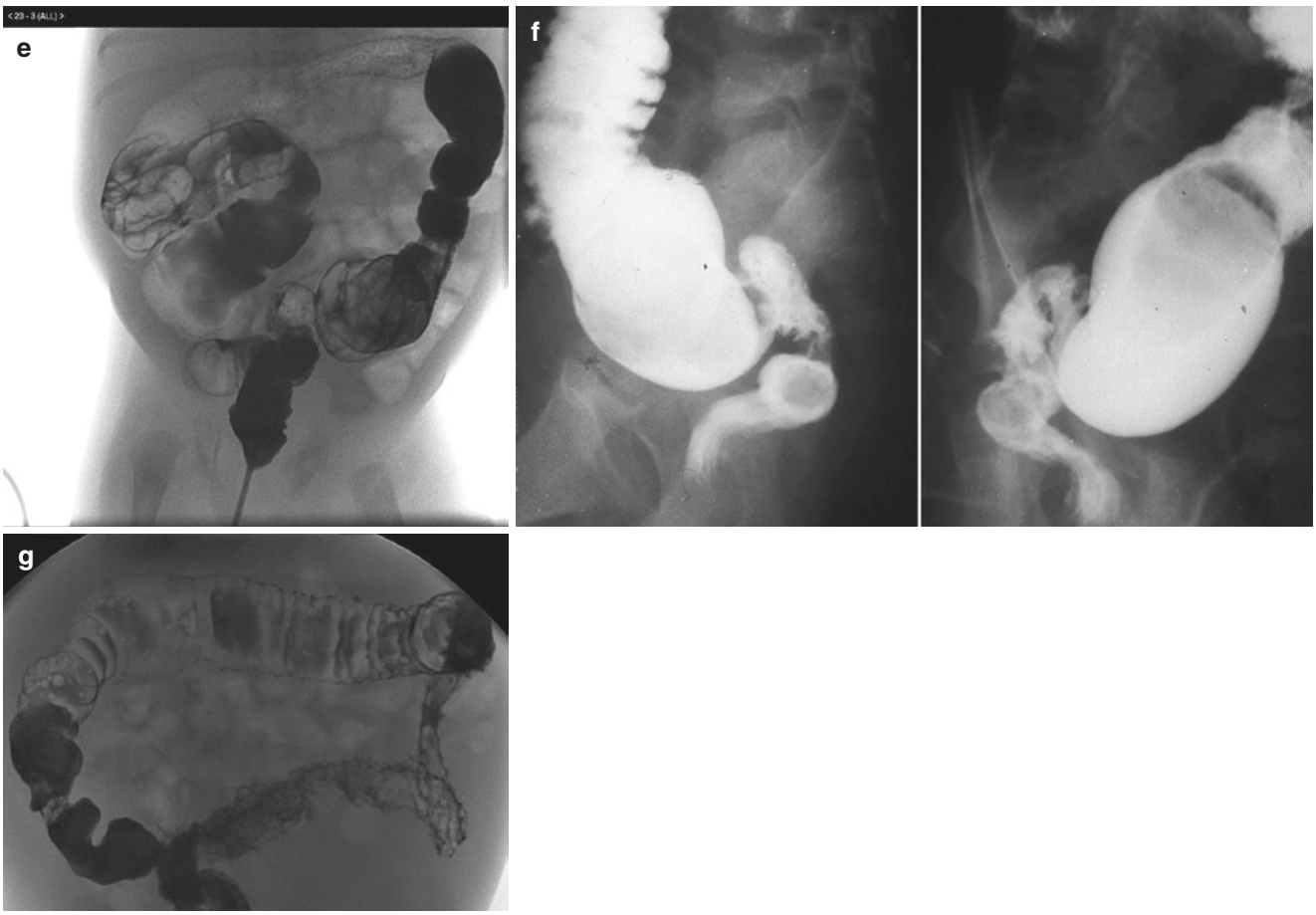

Fig. 4.12 (continued)

4.2.13 Anorectal Anomalies/Currarino Syndrome/Congenital Pouch Colon

In the 5-week embryo, the urogenital sinus and hind-gut empty into a common cavity—the cloaca—separated from the exterior by the cloacal membrane. By the downgrowth of a mesodermic fold (urorectal septum) the separation of the urogenital tract from the rectum is normally completed by the seventh week. For a time, there is a small opening between the rectum and the urogenital tract known as the cloacal duct. The urorectal septum also divides the cloacal membrane into the urogenital membrane anteriorly and the anal membrane posteriorly, and these become the external openings. A small invagination—the proctodeum—develops in the region of the future anus and the proctodeum and rectum join by rupture of the anal membrane during the eighth week. Rectal and anal anomalies and associated malformations are due to arrests in development in the seventh and eighth weeks of fetal life. A range of anomalies occur in the anorectal region, and some of these will be illustrated (Fig. 4.13a, b).

Anorectal anomalies are a spectrum of malformation from high to low lesions. In high anomalies the bowel terminates about the pelvic floor muscles, while in low lesions the bowel comes through the pelvic floor muscles normally and then terminates by a fistula to the perineum. Low lesions are more common. High lesions are frequently one of a number of anomalies in the baby, and there is an isolated defect of low anomalies in only one-third, while two-thirds are otherwise normal.

There are also less frequent intermediate anomalies in which the bowel comes into the pelvic floor muscles and terminates as a fistula to the bulbous urethra in the male and to the vulva in the female. All these lesions should be detected on the initial neonatal examination and the baby referred for investigation and diagnosis of the specific type at a specialist neonatal surgical unit. Because of the different pelvic anatomy of the male and female, the anomalies vary with sex in high lesions. Males have a fistula from the rectum to the urethra or bladder, and this may result in meconium being passed per urethra. In females the genital tract is interposed between the alimentary and urinary tracts so that the fistulous com-

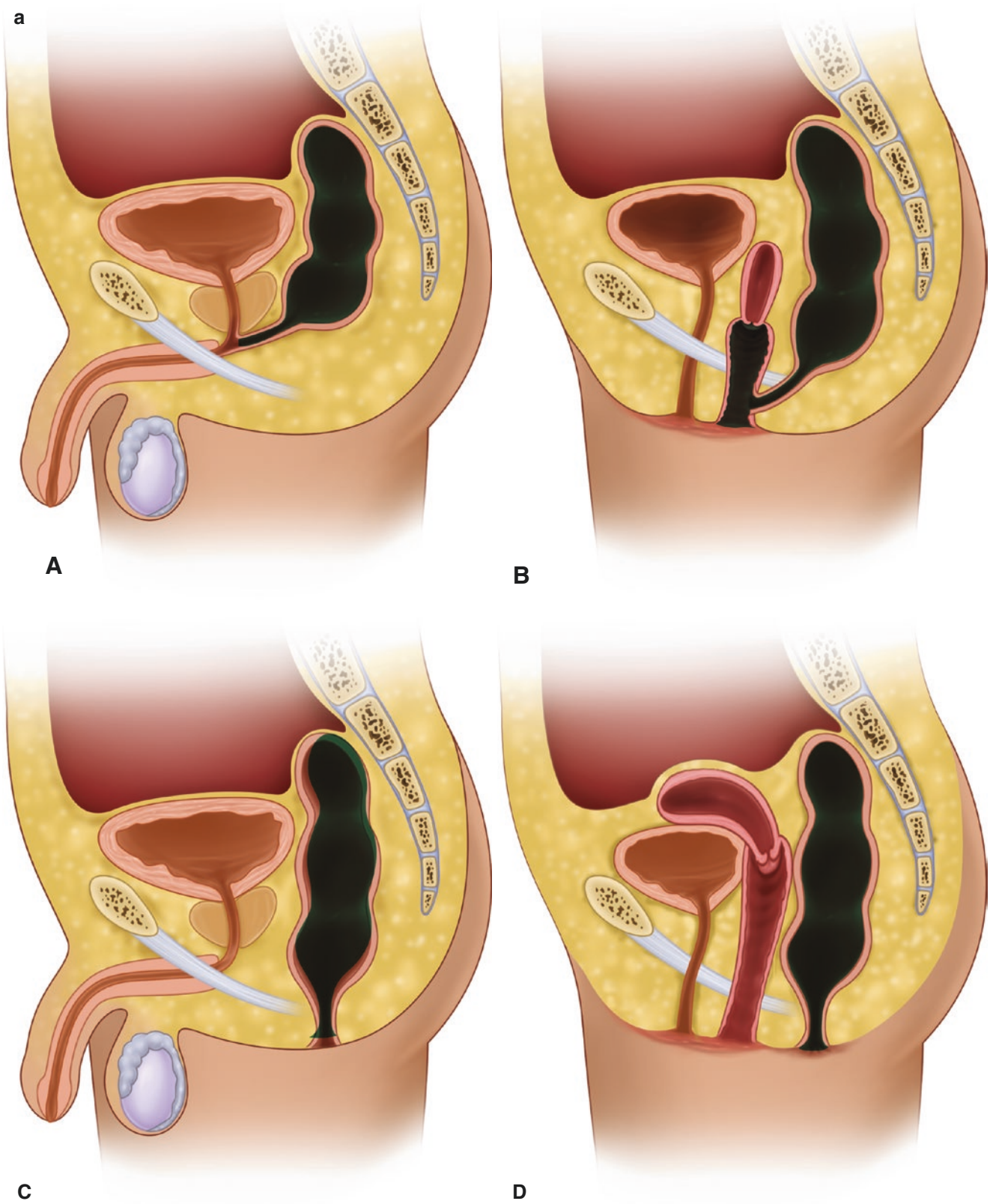

Fig. 4.13 (**a**) Anorectal anomaly - anatomical diagrams for high and low lesions in the male and female pelvis. (**b**) Sacral agenesis imperforate anus. (**c**) Anorectal anomaly showing distance from the atresia to the foreign body attached to the perineum suggestive of a low anomaly. (**d**) Imperforate anus – contrast examination outlines bladder and rectum. (**e**) Imperforate anus – clinical picture with anal membrane. (**f**) Currarino syndrome. Sacral abnormality (scimitar sacrum), anal stenosis, and a presacral mass

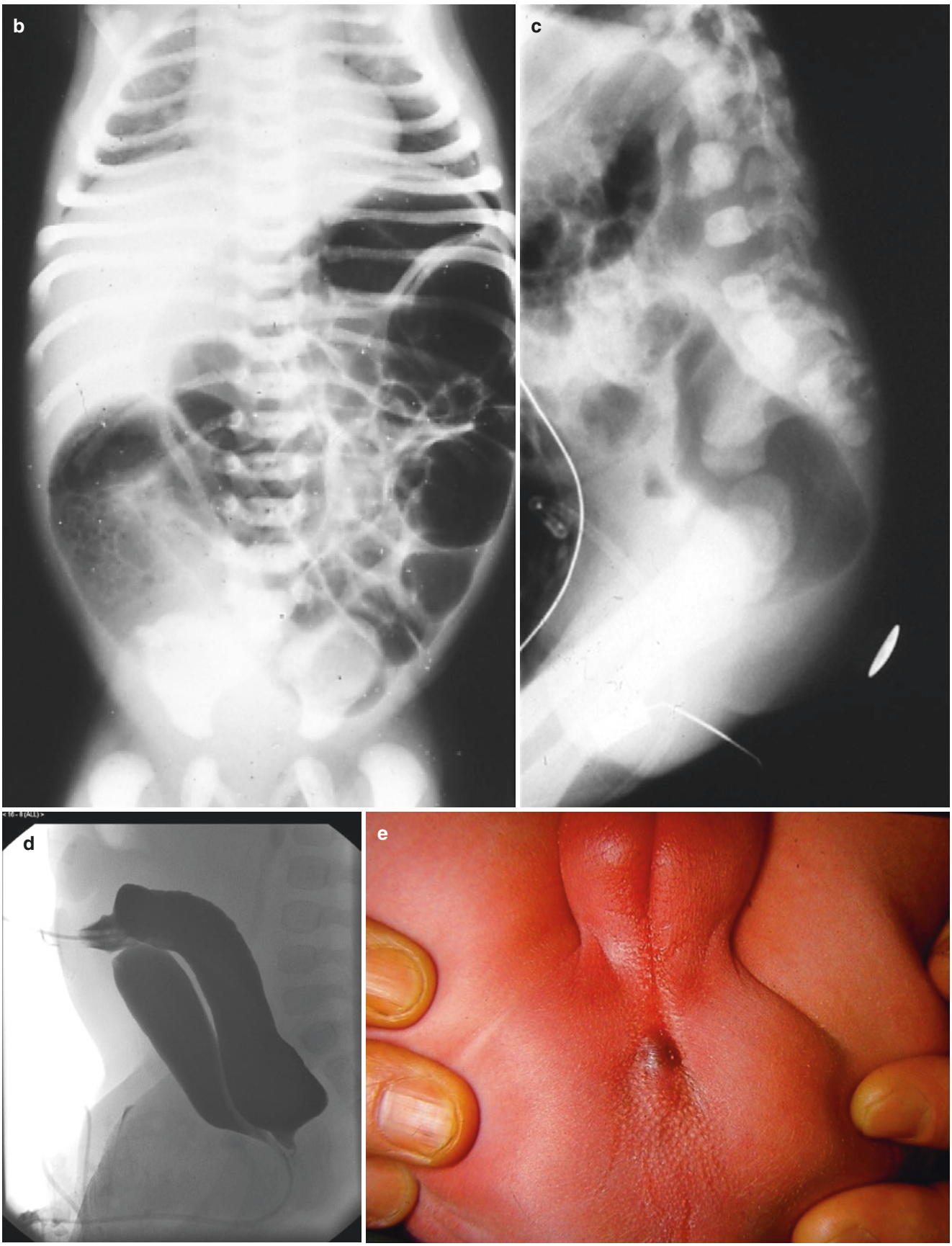

Fig. 4.13 (continued)

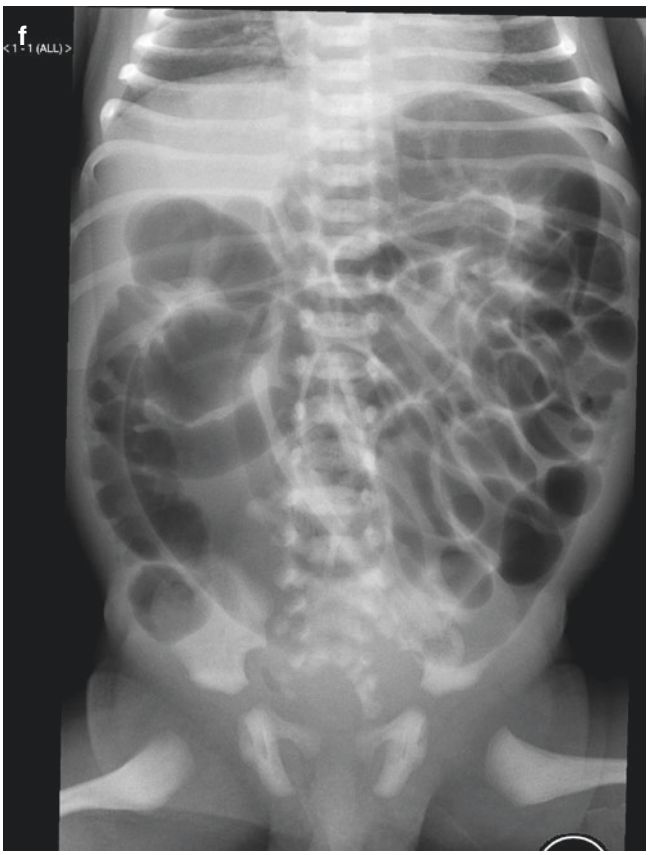

Fig. 4.13 (continued)

munication is from the rectum to the vagina. This may be high in the vagina and not visible but is more often low and may be seen. The low lesions usually have a fistula to the perineum. In the male this may be close to the scrotum or even onto the median raphe of the scrotum, whereas in the females it is to the perineum or entroitus. The uncommon intermediate types usually communicate with the bulbous urethra in the male and the vestibule in the female. Investigations of the infant with an imperforate anus should commence with a thorough general examination because of the frequency of other anomalies. Ultrasound examination of the urinary tract and to the perineum may help determine whether the infant has a high or a low lesion. At 24 h of age, once adequate time has allowed air to pass through the bowel to the rectum, X-rays of the abdomen and pelvis, in particular a lateral film with the baby inverted, are taken. If air is present below a line drawn from the pubis to the coccyx, the baby has a low lesion, and if above, a high lesion (Fig. 4.13b, c).

4.2.13.1 Anal Stenosis

The anus is in its normal position, but the anal canal shows a degree of stenosis and is less distensible than normal. This condition may be missed at birth and can present weeks, months, or even years later with chronic constipation and faecal soiling. There is delay in the passage of meconium and subsequently the infant has to press excessively to defaecate ribbon-like stools through the narrow canal. This condition will be missed completely if rectal examination is omitted. Repeated dilatation is necessary, the size of dilators being gradually increased until the little finger can be inserted. The infant may then be sent home and the mother given a supply of finger cots and instructed to continue dilatation for several months. Failure to continue dilatation may lead to retention of faeces and subsequently to rectal inertia, a secondary megarectum, and overflow incontinence.

4.2.13.2 Anal Membrane

A membrane occludes a normally situated anal canal. Meconium may be seen shining through the membrane, which bulges when the infant cries (Fig. 4.13e).

4.2.13.3 Covered Anus

This more common anomaly is often described as a low anorectal anomaly as the rectum comes down through the pelvic floor before coming to the malformed part. There is no evidence of the anus in the normal position. In a baby boy a raised ridge of skin or a narrow tract filled with meconium runs forward in the perineal raphe as far as the posterior aspect of the scrotum, where a speck of meconium may be seen at the abnormal orifice—the rectoperineal fistula.

4.2.13.4 Rectal Atresia

The anus looks apparently normal, but the rectal pouch ends blindly in the hollow of the sacrum. This is a rare anomaly that causes failure to pass meconium. The baby presents with low intestinal obstruction. Diagnosis is made on rectal examination.

4.2.13.5 Currarino Syndrome (Fig. 4.13f)

This syndrome is discussed fully in Chap. 8.

4.2.13.6 Congenital Pouch Colon

Congenital pouch colon (CPC) is a rare form of high anorectal malformation (ARM) in which part of or the entire colon is replaced by a pouch with a fistula to the genitourinary tract. According to the Saxena-Mathur classification, CPC is divided into five types. A single erect plain abdominal radiograph could be the most valuable single investigation to diagnose and classify CPC and to preoperatively plan the surgical strategy without the necessity of an invertogram [1].

Depending on the method of presentation, plain abdominal radiography may demonstrate distal bowel obstruction or associated vertebral anomalies. A prone horizontal beam "shoot through" film with a marker place on the perineum at the anal pit can help to identify the level of atresia in relation to the ischial bones.

Sonography is sometimes employed in this setting as it may demonstrate the distal pouch fistulae and associated abnormalities (including renal and spinal). It can be difficult to assess the exact level of the pouch in relation to other structures on ultrasound.

Prior to closure and repair, the anatomy of associated fistulae can be demonstrated by combined cystourethrography and distal contrast loopogram Fig. 4.13d. Cross-sectional imaging with MRI is less often performed, but can also demonstrate anatomy, fistulae, and associated anomalies.

4.2.14 Duplication of the Gastrointestinal Tract

Duplications are spherical or elongated hollow structures lined with some form of alimentary mucous membrane and intimately adherent to the alimentary tube. The duplication is always on the mesenteric border of the gut and the contents are clear, colourless, and mucoid in consistency. They may vary in size and shape, being saccular or tubular, and not infrequently communicate with the bowel.

Duplications below the diaphragm may present in four ways: (1) They may grow in size and cause intestinal obstruction; (2) an increase in tension within the cyst may cause abdominal pain; (3) the duplication may encroach on vessels in the mesentery and cause necrosis, sloughing, and bleeding in the adjacent bowel; and (4) a duplication lined with gastric mucosa may develop peptic ulceration and may perforate into the peritoneal cavity, into the adjoining bowel or into the pleural cavity.

Radiography may demonstrate a space-filling shadow and a barium series may show indentation of the lumen. Ultrasound and cross-sectional imaging may be required to delineate the lesion. It can be difficult to differentiate duplications from omental and mesenteric cysts (Fig. 4.14a).

Plain abdominal radiography may show a soft tissue mass or the sequelae of obstruction caused by the duplication. Contrast examinations most commonly demonstrate extrinsic compression but may identify direct communication to the duplicated lumen.

Ultrasonography demonstrates a mass, usually echolucent and fluid-filled, but occasionally containing haemorrhage, solid contents, or gas if there is direct communication to a gas-containing viscus such as colon or rectum. The sonographic appearance of the wall of the duplication cyst, with inner echogenic mucosa and outer hypoechoic muscle (so called "gut signature"), confirms the diagnosis.

CT and particularly MR imaging are alternative second-line modalities when ultrasonography is inconclusive or has not provided enough information for surgical planning. The duplication cyst contents are usually high-signal on T2-weighted sequences.

4.2.15 Lymphangioma/Lymphangiectasia

These arise from congenitally misplaced lymphatic tissue very similar to the cystic hygromas that occur in the neck. They vary greatly in size, are thin-walled, rounded or lobulated, and contain serous lymph fluid. The cysts may be small and lie in the substance of the omentum, or they may largely replace this structure. There is a slowly enlarging abdominal swelling with little associated discomfort. Cysts are usually mobile from side to side as they attach to the mesentery of the small bowel.

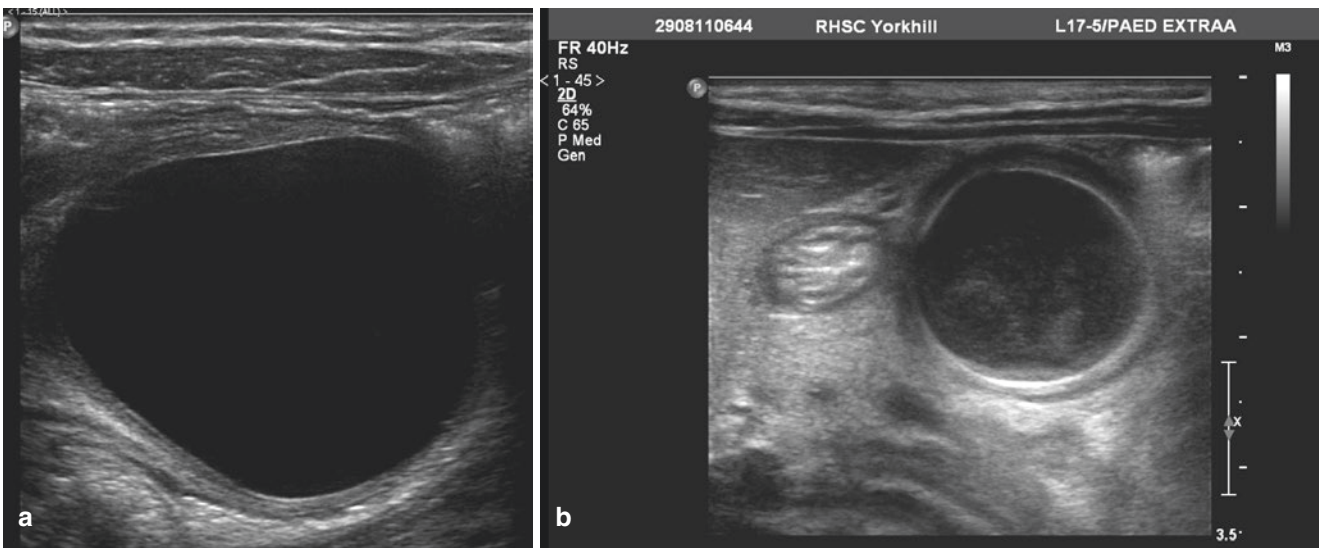

Fig. 4.14 (**a**) Ultrasound showing duplication of bowel. (**b**) Ultrasound showing gastric duplication

The imaging of lymphangioma/lymphangiomatous malformations is as variable as the range of lesions themselves.

Plain abdominal radiography is of varying use depending on the position of the lymphangioma. It may demonstrate a soft tissue mass or obstruction due to extrinsic compression.

Sonography is the modality of choice for simple lymphangioma cysts, demonstrating positions, relationships and a thin simple wall (unlike the "gut signature" of the wall of duplication cysts), usually containing echolucent fluid. They may be unilocular "simple" or multiloculated. The presence of haemangiomatous components, and of complications including haemorrhage, intussusception, and volvulus may also be appreciated.

For more complex lesions and retroperitoneal and disseminated disease, cross-sectional imaging, particularly MR imaging, is required. The signal of the cyst content can vary depending on whether it is serous chylous or haemorrhagic but is usually high-signal on T2-weighted sequences with low cellularity on diffusion-weighted imaging (Fig. 4.15).

4.2.16 Mesenteric Cysts/Omental Cyst

Mesenteric cysts may arise in any part of the mesentery or mesocolon. They are very often due to malformed lymphatic tissues and occur commonly at the jejunum or ileum. The cysts lie between the peritoneal leaves of the mesentery and may obstruct adjacent intestine.

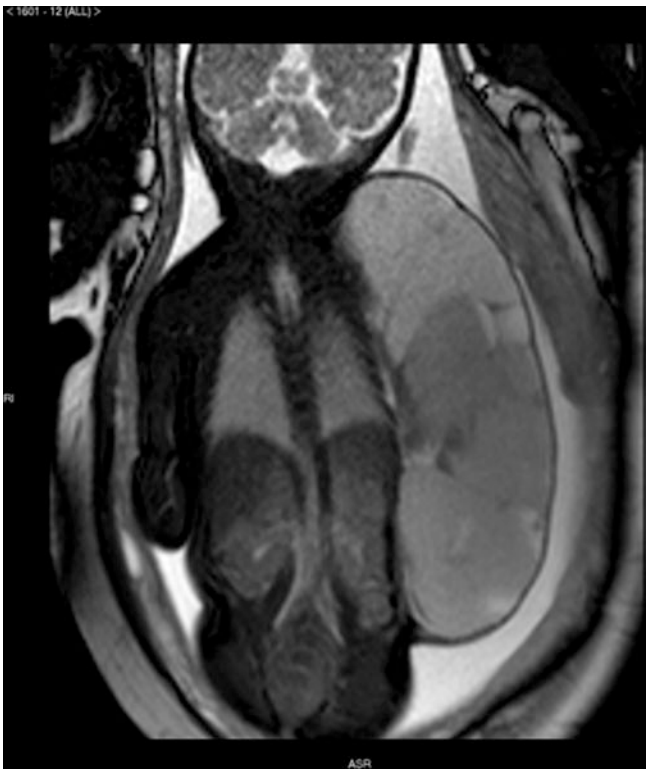

Fig. 4.15 Fetal MRI demonstrating a large lymphangioma

The imaging of lymphangioma/lymphangiomatous malformations is as variable as the range of lesions themselves.

Plain abdominal radiography is of varying use depending on the position of the lymphangioma. It may demonstrate a soft tissue mass or obstruction due to extrinsic compression (Fig. 4.16a, b).

Sonography is the modality of choice for simple lymphangioma cysts, demonstrating positions, relationships, and a thin simple wall (unlike the "gut signature" of the wall of duplication cysts), usually containing echolucent fluid. They may be unilocular ("simple") or multiloculated. The presence of haemangiomatous components, and of complications including haemorrhage, intussusception, and volvulus may also be appreciated.

For more complex lesions and retroperitoneal and disseminated disease, cross-sectional imaging, particularly MR imaging, is required. The signal of the cyst content can vary depending on whether it is serous chylous or haemorrhagic but is usually high-signal on T2-weighted sequences with low cellularity on diffusion-weighted imaging.

4.2.17 Inguinal Hernia

Plain abdominal radiography is not used in the initial diagnosis of suspected inguinal or femoral hernia; however, the hernia orifices must always be visualised and assessed on radiography, particularly in the assessment of an acute abdomen, as the presence of gas in herniated bowel loops may be diagnostic when the presentation is secondary to obstruction or herniation of bowel (Fig. 4.17a–d).

Ultrasound may be used to visualise herniated mesentery and gasless loops of bowel and differentiate from other structures such as thickened spermatic cord or hydrocele.

4.2.18 Femoral Hernia

Plain abdominal radiography is not used in the initial diagnosis of suspected inguinal or femoral hernia; however, the hernia orifices must always be visualised and assessed on radiography, particularly in the assessment of an acute abdomen, as the presence of gas in herniated bowel loops may be diagnostic when the presentation is secondary to obstruction or herniation of bowel.

Ultrasound may be used to visualise herniated mesentery and gasless loops of bowel and differentiate from other structures such as thickened spermatic cord or hydrocele.

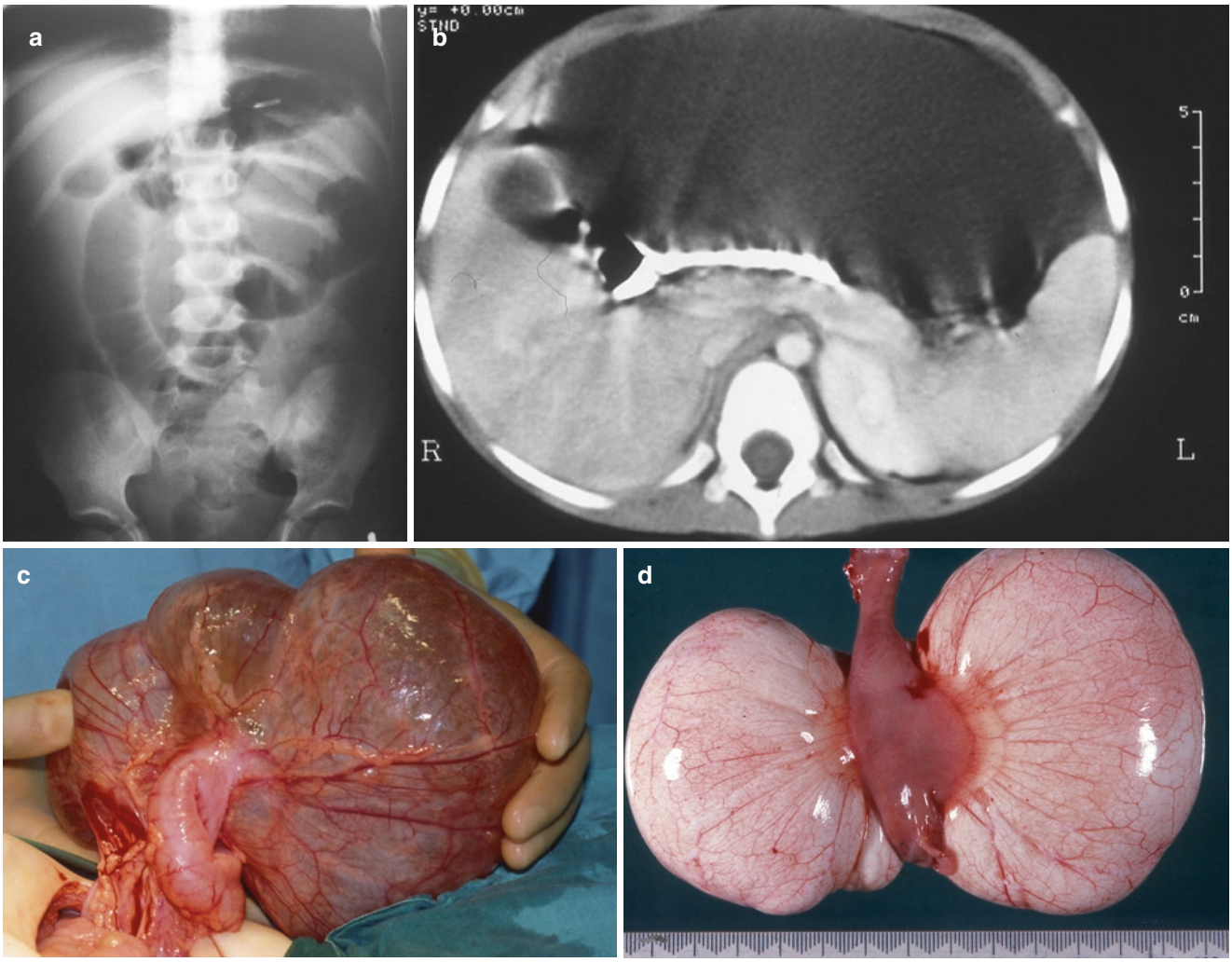

Fig. 4.16 (**a**) Plain X-ray of a chylous cyst in the mesentery causing intestinal obstruction. (**b**) Crossectional imaging of a mesenteric cyst. (**c**) Operative picture of a large clear mesenteric cyst. Intimately adherent to the small bowel. (**d**) Operative specimen of resected small bowel and a chylous mesenteric cyst

4.2.19 Hydrocele (Fig. 4.18)

Sonography is the imaging modality of choice for the assessment of scrotal pathology. A scrotal hydrocele or hydrocele of the spermatic cord will be demonstrated as an echolucent fluid collection. The main indication for imaging is to identify an underlying cause or other pathology particularly in the painful scrotum.

4.2.20 Situs Inversus (Fig. 4.19)

Plain abdominal radiography, as well as demonstrating integrity of the diaphragms and position of the cardiac shadow, will often determine the situs of the abdominal organs by the position of the stomach bubble (including the course of a nasogastric tube if in situ) and the outline of the stomach.

Sonography of the abdomen can demonstrate the position and presence of the upper abdominal solid organs and the abdominal systemic venous anatomy. It is important to determine the presence and normal appearance of the spleen and inferior vena cava (IVC), as abnormalities of these may indicate a heterotaxy.

Abdominal situs can also be demonstrated on cross-sectional imaging but this is rarely required to make the diagnosis. See Chap. 3.

4.2.21 Split Notochord Syndrome (Fig. 4.20a, b)

This condition is rare and can be mistaken for Spina Bifida because the lesion on the back involves a disrupted spine with herniation of bowel through the back. This condition is discussed fully in Chap. 6.

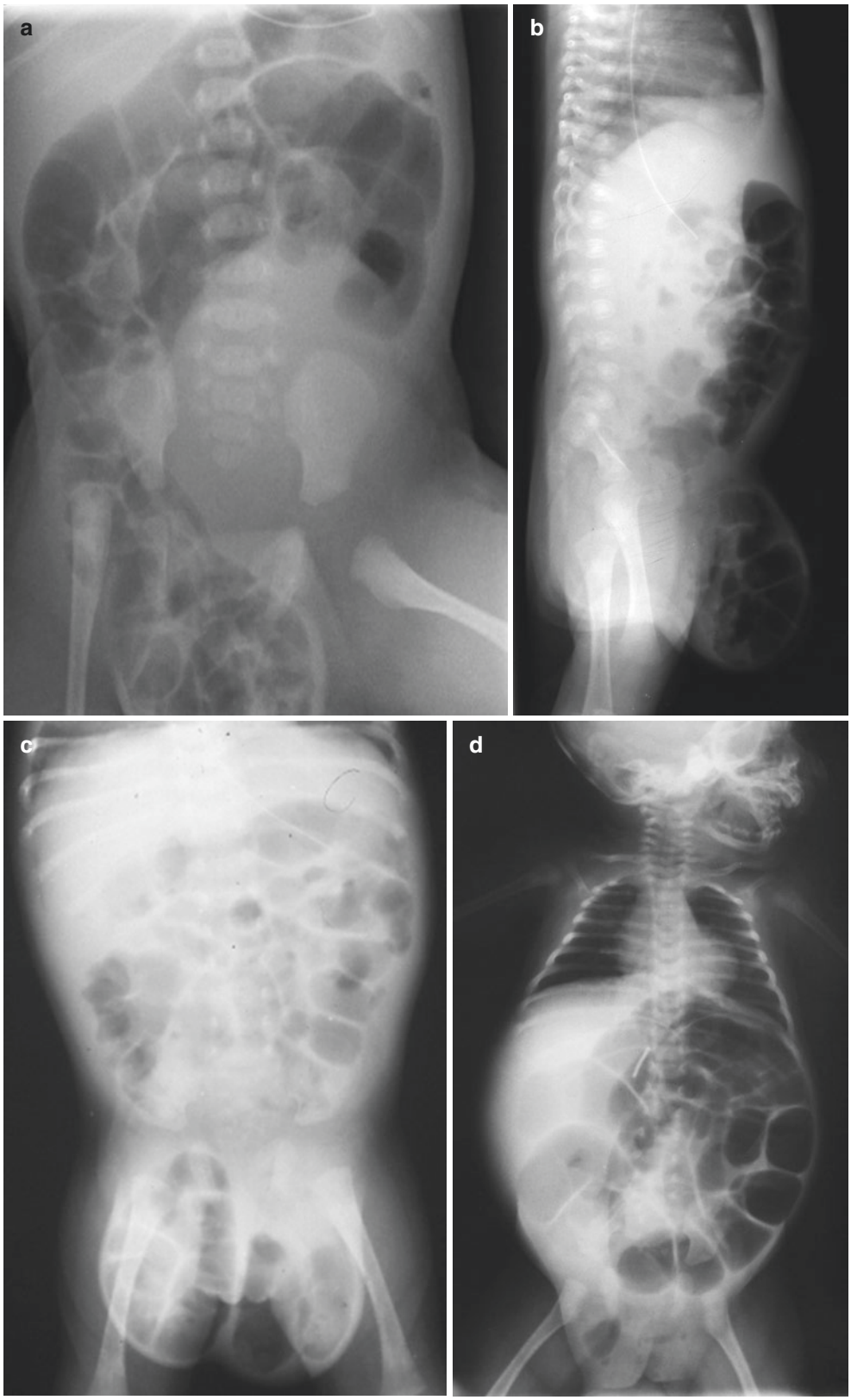

Fig. 4.17 (**a**) Plain X-ray AP showing bowel loops filled with air in the right groin. Obstructed inguinal hernia in a neonate. (**b**) Plain X-ray, lateral view of obstructed inguinal hernia. (**c**) Plain X-ray showing bilateral inguinal obstructed hernia in the Inguinal scrotal region. (**d**) Plain X-ray of a strangulated right inguinal hernia

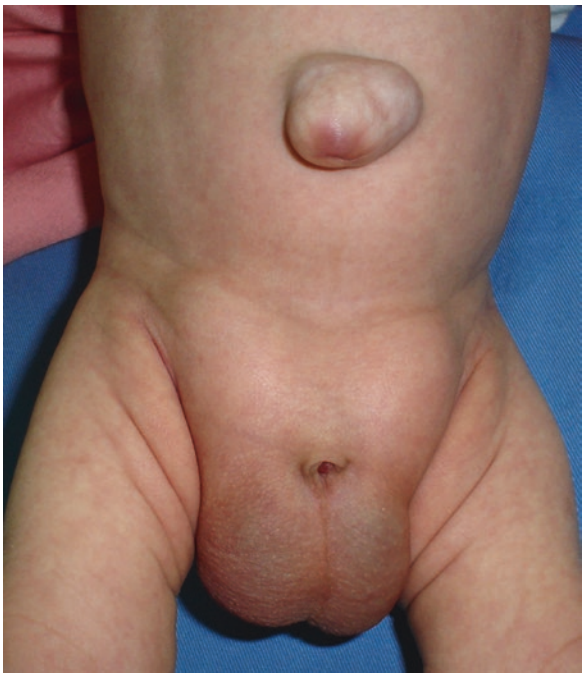

Fig. 4.18 Clinical picture of a neonate with bilateral hydrocoeles and an umbilical hernia. The bilateral hydroceles indicate a persistent patent processus vaginalis

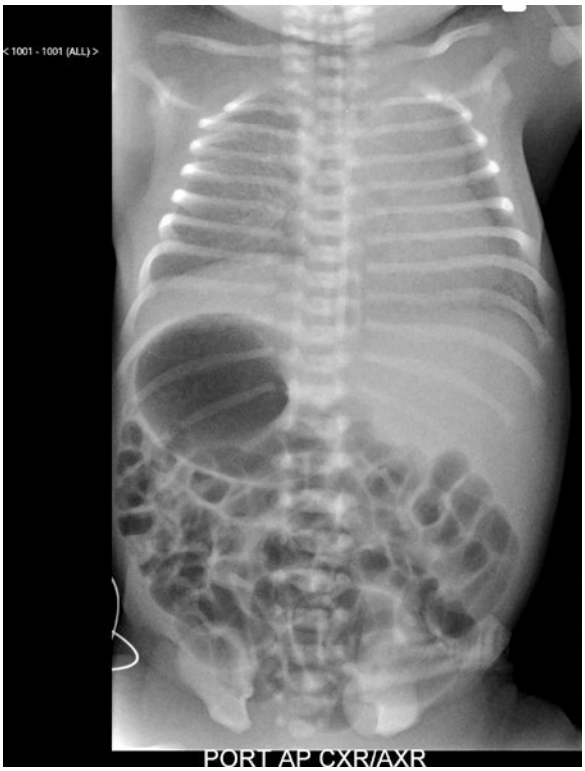

Fig. 4.19 Situs inversus. See Chap. 2

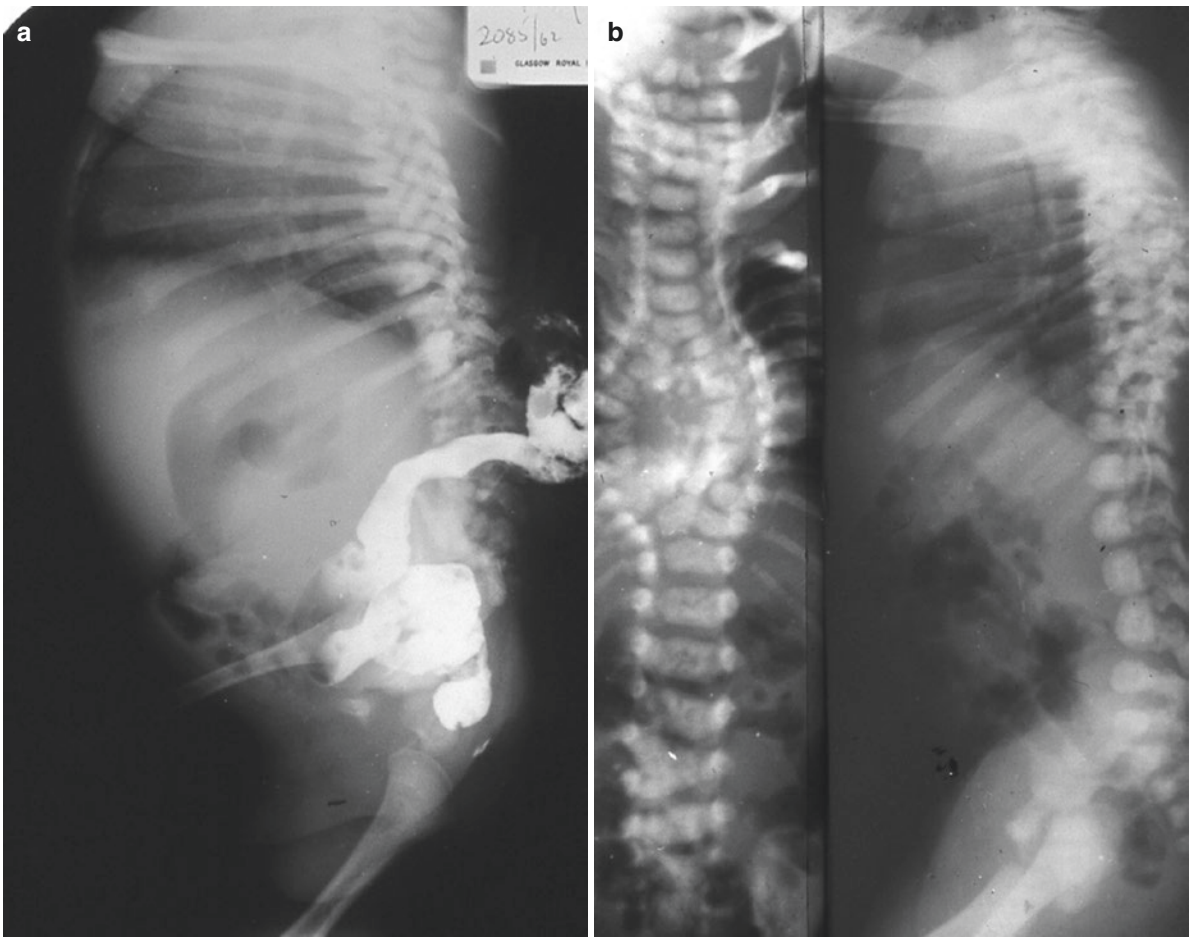

Fig. 4.20 (**a**) Split notochord syndrome. See Chap. 6. (**b**) Split notochord syndrome. See Chap. 6

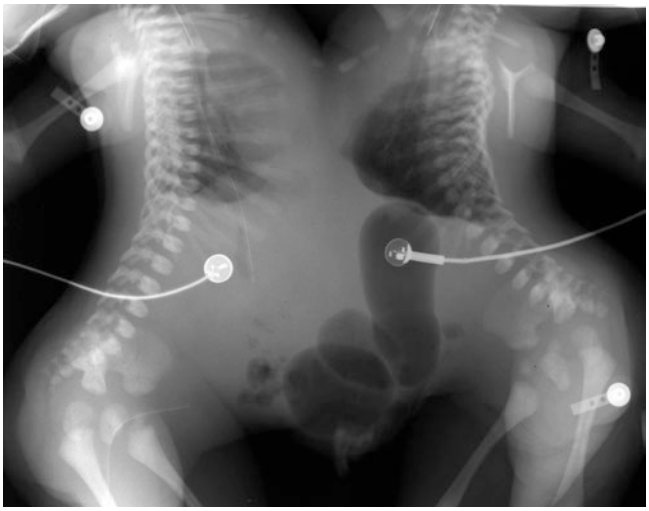

Fig. 4.21 Plain X-ray showing conjoined twins sharing abdominal contents

4.2.22 Conjoined Twins

The conjoined twins illustrated in Fig. 4.21 are attached through the abdomen and often share common organs, e.g., the liver. Separation can be difficult. The term used for this type of conjoined twins is omphalopagus and it occurs in about 34% of conjoined twins. Other conjoined twins are joined at the chest (thoracopagus or xiphopagus, in 40% of cases), the buttocks (pygopagus, in 18%), the ischium (ischiopagus, 6%), and the head (craniopagus, 2%).

4.2.23 Congenital Polycystic Kidneys (Fig. 4.22)

This condition is discussed fully in Chap. 5.

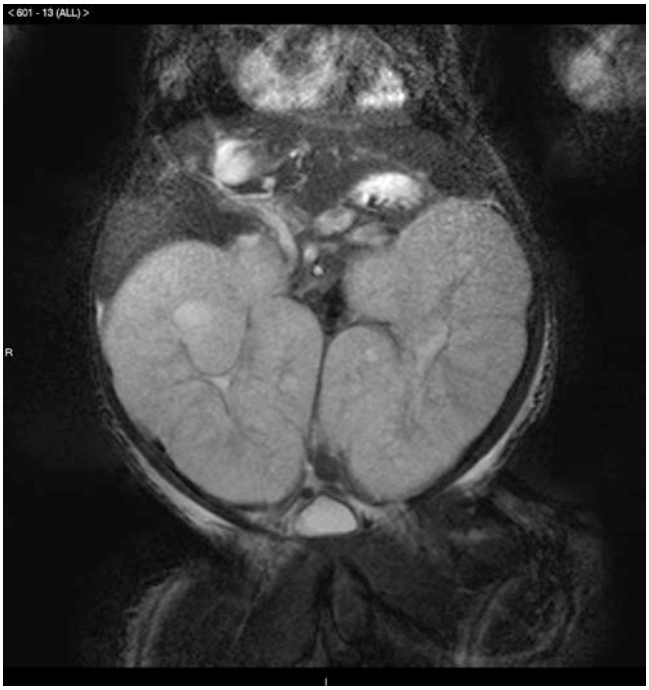

Fig. 4.22 Autosomal recessive polycystic kidneys. See Chap. 5

4.3 Infection/Inflammation

4.3.1 Necrotising Enterocolitis/Pneumatosis Intestinalis

Necrotising enterocolitis (NEC) is a severe disease of the gastrointestinal tract. Prematurity with low birth weight are the most commonly associated factors and occur in 90% of babies with this disease. Term infants are affected to a lesser extent and constitute about 10% of the affected group. Hypovolaemia and hypoxia result in damage within the mucosa cells initiating the NEC. It is multifactorial in origin, resulting in loss of integrity of the gut mucosal barrier with passage of bacteria into the wall of the bowel. Prematurity, respiratory distress syndrome (RDS), congenital cardiac malformations, umbilical vessel catheterisation, exchange transfusions, hypoglycaemia, polycythaemia, post-operative stress, and hyperosmolar feeds have all been implicated in the aetiology. Scholander in 1963 proposed the diving reflex as a mechanism which causes shutdown of visceral blood flow, especially in the superior mesentery artery resulting in ischaemic changes in the mucosa. Bacterial infection has been implicated in NEC and from time to time one sees some confirmation of this because of the clustering of the disease in neonatal units. There are protective antibodies in breast milk that decrease but do not completely protect babies at risk from NEC. The incidence of this disease varies from country to country. There is a very low incidence in Japan and a high incidence in the United States. The severity of the disease is variable, from a minor form that is managed entirely in the Neonatal Units, to a fulminating type of the disease with perforation, peritonitis, and death. Initially, one sees a preterm infant with signs of sepsis, vomiting of feeds, abdominal distension, and frequently the passage of blood or mucus in the stools. Clostridial infections have been associated with some outbreaks of NEC. If the disease continues to progress, peritonism develops and this is often appreciated first by observing abdominal distension. Examination of the abdomen may show signs of inflammation, redness, oedema of the abdominal wall with localised or generalised tenderness, and if the baby has a patent processus vaginalis, free fluid or even gas or meconium is occasionally seen in the scrotum. If a perforation has occurred, then one loses the area of superficial dullness of the liver on percussion of the abdomen. Palpation may reveal crepitus from the intramural gas, which can be palpated among the coils of distended loops of bowel, (intramural gas is an important sign of NEC). A plain X-ray

of the abdomen may show the pneumatosis intestinalis (gas within the bowel wall) and gas in the portal vein within the liver. This sign is often ominous and is associated with mortality. The extent of the NEC may be localised to an area of the bowel, very often the colon, but in extensive disease the whole of the gastrointestinal tract may be involved. The differential diagnosis early in this disease may be difficult, and one should consider diagnoses such as Septicaemia from other causes, volvulus neonatorum, Hirschsprung's enteritis, and infarction of the bowel.

Plain radiography remains the modality of choice in the radiological assessment and monitoring of necrotising enterocolitis (Fig. 4.23a). The assessment of these films includes:

- Bowel gas pattern—an abnormal pattern including dilation of bowel loops, which may be focal or generalised. These findings are nonspecific, but a persisting asymmetric pattern—"fixed abnormal loops"—is a concerning finding and may indicate focal necrosis or peritonitis.
- Intramural gas—the presence of intramural gas is highly associated with necrotising enterocolitis, but it is not present in all cases and therefore its absence does not exclude NEC. The amount of gas present does not relate directly to the severity of disease; intramural gas may present as linear gas outlining the bowel wall or a "mottled" appearance "enface," and can be generalise or localised. Any part of the bowel can be affected, but the most commonly affected is the distal small/proximal large bowel in the right iliac fossa.
- Portal venous gas—in the setting of NEC, this is intramural gas that has entered the veins of the bowel wall and passed into the portal venous system. It appears as branching radiolucencies (Fig. 4.23b, c).

Horizontal beam films (either decubitus or lateral shoot through, depending on the clinical status of the infant) may demonstrate free intraperitoneal gas and affect the timing of emergency intervention (Fig. 4.23d–f).

Ultrasonography provides complementary real-time assessment of the bowel, detailing bowel wall thickness, appearance, peristalsis, and vascularity. It may be more sensitive than plain radiography in assessing intramural, portal venous, and small amounts of free intraperitoneal gas. In addition, extraluminal findings and complications (peritoneal free fluid and collections) can be demonstrated (Fig. 4.23c).

Fluoroscopic contrast examinations are usually employed outside of the acute presentation of NEC to assess the bowel prior to reversal of bowel defunctioning or to assess chronic complications such as stricture (Fig. 4.23e).

4.3.2 Appendicitis

There is marked variation in the anatomy of the appendix. The appendix is attached to the posterior medial quadrant of the caecum. In childhood, the appendix lies in a retrocaecal position in 70% of patients. Obstructive appendicitis is common in childhood, the obstruction being caused by a kink, a faecolith, or the scar of a previous attack of inflammation. When inflammation occurs, there is an accumulation of purulent exudate within the lumen, and a closed loop obstruction is established. Blood supply to the organ is diminished by distension or by thrombosis of the vessels, and gangrene occurs early in children. Fluid is poured into the peritoneal cavity as a result of irritation, and within a few hours this fluid is invaded by bacteria from the perforated appendix or from organisms translocating the inflamed but still intact appendix. Peritoneal infection may remain localised by adhesions between loops of intestine, caecal wall, and parietal peritoneum. Appendicitis may present as uncomplicated acute appendicitis, appendicitis with local peritonitis, an appendix abscess, or diffuse peritonitis.

The onset of symptoms is vague and initially may be of a general nature. Only a third of younger patients are seen in hospital within 24 h of onset of abdominal symptoms, and the appendix has ruptured in a high percentage of these young patients before admission. The diagnosis is made late in many cases. One reason for delay in diagnosis is failure to suspect appendicitis in a child under 4 years of age, and another is the poor localisation of pain by the younger child. Although often not severe, the pain appears to come intermittently, and irritability, vomiting, and diarrhoea may result in the mistaken diagnosis of gastro-enteritis. Psoas spasm from irritation of the muscle by the inflamed appendix may cause flexion of the hip resulting in a limp, thus distracting attention from the abdomen and directing it to the hip joint. Vomiting occurs in most patients. The child is usually pyrexial, but the temperature is only moderately elevated to between 37 and 38.5 °C. Temperatures higher than this usually suggest upper respiratory tract infections or, occasionally, diffuse peritonitis from appendicitis. A history of constipation is uncommon, and in many patients, there is a history of diarrhoea. The clinical features in the older child are similar to those in the adult. Abdominal pain is usually followed by nausea and vomiting. The pain begins centrally and later shifts to the right iliac fossa. If the appendix is retrocaecal, abdominal pain and tenderness may be slight. If the child has a pelvic appendix, then tenderness may again be slight, or absent, or elicited only on rectal examination. Anorexia is a common accompanying sign.

The child with acute appendicitis is usually anorexic, listless, and does not wish to be disturbed. There is often a

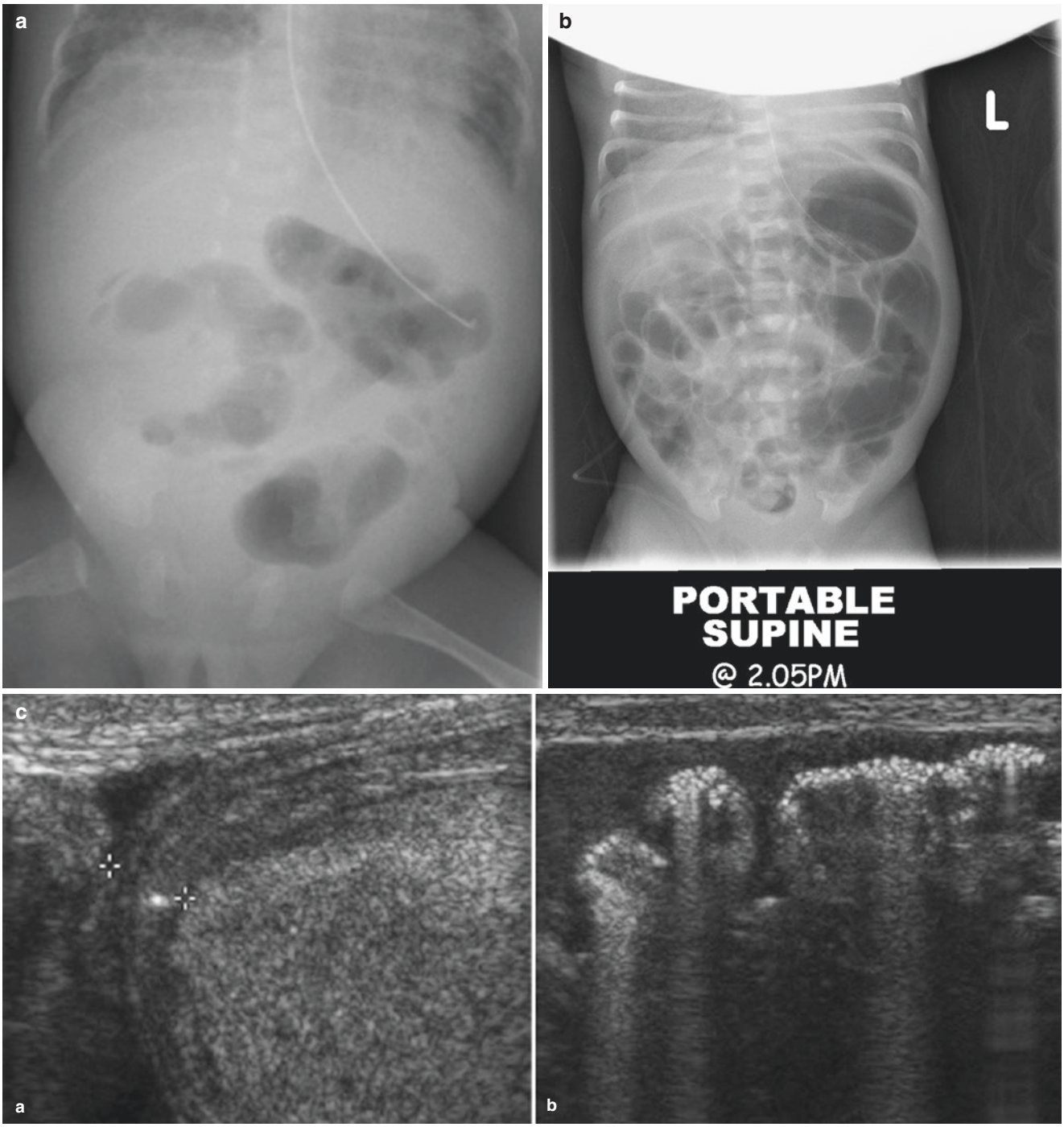

Fig. 4.23 (**a**) Plain X-ray of the abdomen of a premature baby with severe necrotizing enterocolitis. (**b**) Necrotising enterocolitis. Plain X-ray showing pneumatosis and perforation, free gas. (**c**) Ultrasound showing thickened loops of intestine with intramural gas and free fluid. (**d**) Plain X-ray of the abdomen in a premature baby with necrotizing enterocolitis and pneumatosis intestinalis. Note the gas in the area of the liver indicating portal venous gas. (**e**) Barium study in necrotizing enterocolitis showing a ragged colon, with early signs of spasm and stricture formation. Note how featureless the colon looks. (**f**) Plain X-ray with free gas and little evidence of gas in the abdomen intraluminally suggestive of necrotising enterocolitis, (**g**) Pneumatosis, (**h**) Pneumatosis intestinalis, (**i**) Pneumoperitoneum, (**j**) NEC with portal venous gas. (**k**) Post-operative pneumatosis with distended loops of bowel, free gas, and a nasogastric tube in situ

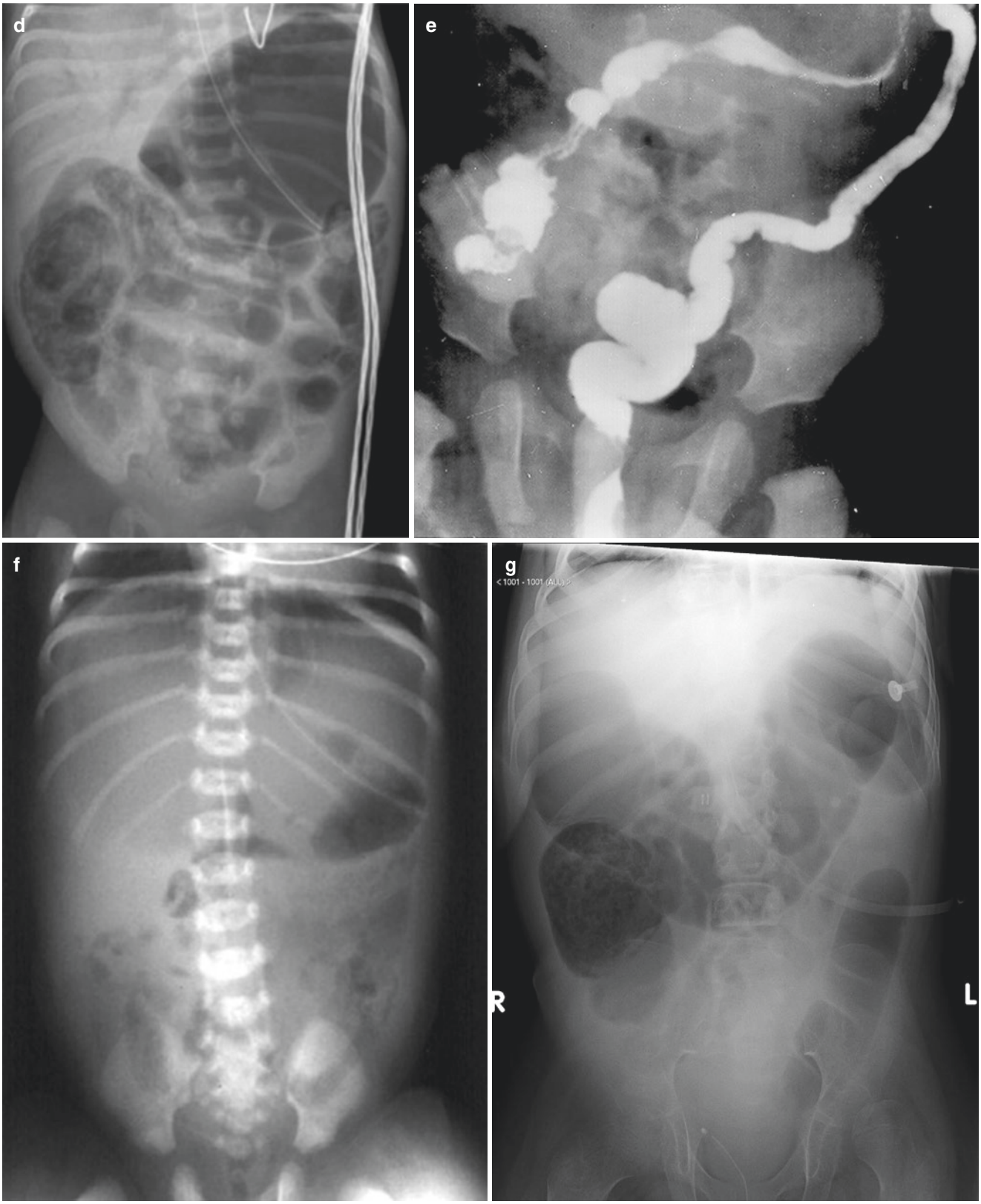

Fig. 4.23 (continued)

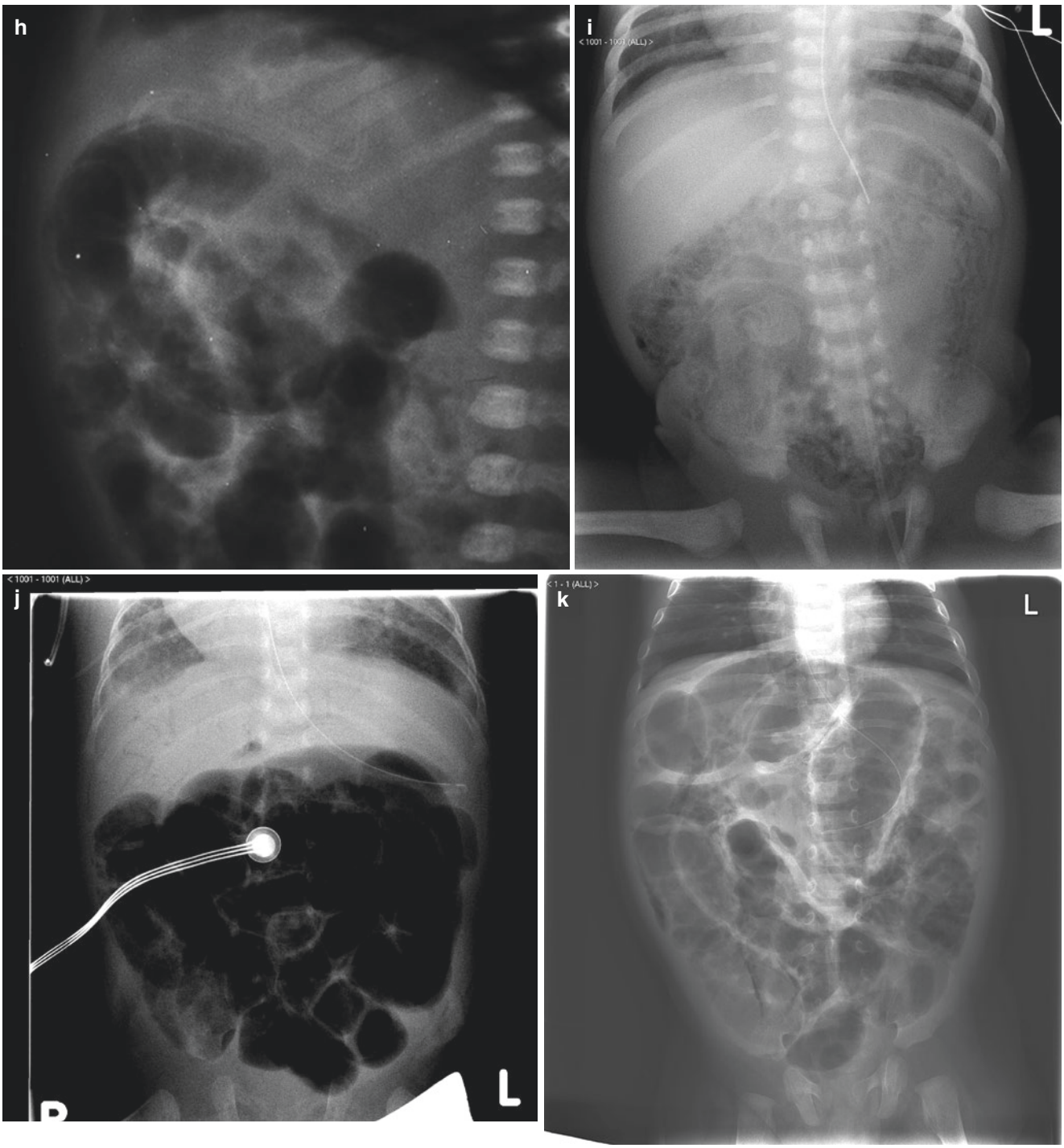

Fig. 4.23 (continued)

characteristic fetid odour from the tongue, which is furred. The child is usually irritable, crying, and uncooperative. A low-grade pyrexia is usual, but the temperature seldom exceeds 38.5 °C. Inspection alone, while attempting to gain the child's confidence, may be very informative. The most important physical sign on abdominal examination is the area of maximum tenderness located in the right iliac fossa and the presence of rebound tenderness. Plain X-ray of the abdomen may prove useful to exclude other pathology in suspected acute appendicitis. Differential diagnosis includes numerous other disorders, the most common of which is upper respiratory tract infection. Presence of a common cold, sinusitis, acute tonsillitis, or pharyngitis may all be associated with acute non-specific mesenteric lymphadenitis. This is the most common condition to be differentiated from acute appendicitis. The presence of enlarged glands elsewhere in the body accompanied with an upper respiratory tract infection may suggest this condition. Fever may be absent, but temperatures can be very high. The presence of abdominal tenderness is not as acute as that in appendicitis. It is usually more generalised and not localised to the right iliac fossa, and there is no rebound tenderness. The presence of a cough, an increased respiratory rate, and a runny nose may suggest a respiratory infection. Constipation can cause abdominal pain, nausea, and vomiting, with tenderness over the distended caecum. It can be easily mistaken for acute appendicitis. Faecal masses may be felt per abdomen or on digital rectal examination. Usually following a suppository, satisfactory evacuation of the colon and rectum will bring rapid relief in patients whose symptoms are caused by constipation.

Pyelonephritis and infection of the kidney and renal pelvis can usually be differentiated by a higher temperature, pus cells in the urine, and tenderness over one or the other kidney in the renal angle.

Intestinal obstruction may be due to incarceration of a hernia, secondary to anomalies, e.g., a volvulus around a vitello-intestinal remnant, or adhesions following previous abdominal operations. Vomiting, abdominal colic, abdominal distension, and constipation are the usual signs. After a thorough clinical examination, plain X-ray of the abdomen may be carried out to differentiate intestinal obstruction from appendicitis.

Primary peritonitis is an uncommon diagnosis and almost always affects the female. There is a diffuse infection of the visceral and parietal peritoneum, usually due to a pneumococcus. With the peritonitis there is exudation of fluid to the peritoneal cavity. Mesenteric lymph nodes are swollen. Diffuse abdominal pain, vomiting, dehydration, and a high fever are the main features, and diarrhoea may be present initially, but is usually followed by constipation.

Severe abdominal pain and vomiting may occur during passage of a renal calculus.

Hydronephrosis due to blockage of the pelviureteric junction by stricture, stone, or aberrant vessel may present with abdominal pain and nausea. The pain and tenderness are maximal in the flank. Red or white cells may be found in the urine.

Haemolytic Uraemic Syndrome may present with acute abdominal pain and may be confused with acute appendicitis. The presence of fragmented red blood cells on a blood film and the presence of oliguria are also suggestive of this disease.

Crohn's disease is an unusual diagnosis in childhood, but the incidence is increasing in Western countries. It can present with all the symptoms of acute appendicitis, and at operation the terminal ileum is found to be acutely inflamed and thickened. A biopsy reveals the diagnosis, and a barium meal and follow-through very often indicate the presence of other areas of the affected gut. In torsion of the right cord or testis confusion with acute appendicitis may occur whereas this is less likely with torsion of the left testis. Routine examination should always include the inguinal regions and the scrotum.

Inflammation of Meckel's diverticulum and intussusception in older children may simulate acute appendicitis. Other medical conditions that should be considered are diabetes mellitus, cyclical vomiting, and Addison's disease. The onset of menstruation may simulate appendicitis, and many girls have recurring attacks of lower abdominal pain, sometimes for a year before menstruation actually begins. Pain associated with torsion of an ovary or an ovarian cyst may also present with signs similar to those of acute appendicitis.

It is not uncommon for both adults and children to harbour threadworms (pinworms) without noticeable symptoms. Many symptoms and signs have been ascribed to the presence of threadworms, including weight loss, poor appetite, nausea, vomiting, and chronic abdominal pain.

Carcinoid tumour in the appendix is rare in childhood, but the tumour may obstruct the lumen of the appendix and lead to obstructive appendicitis. It is far more common to find this as an incidental finding on histopathology of the removed appendix. When it is present in the tip of the appendix, no further follow-up is necessary in these cases. In older children, if a carcinoid exists in the caecal region there is a chance of invasive disease with subsequent evidence of the carcinoid syndrome.

Plain abdominal radiography is rarely diagnostic in the assessment of suspected appendicitis and is usually normal. Subtle signs have been described, including blurring of the psoas shadow and of the properitoneal fat line; however; they are rarely diagnostic. A dilated loop of bowel in the right iliac fossa or developing small bowel obstruction may indicate appendicitis or the development of an associated inflammatory mass. The presence of a calcified appendicolith, which has been described in around 10–15% of cases, is diagnostic (Fig. 4.24a, b).

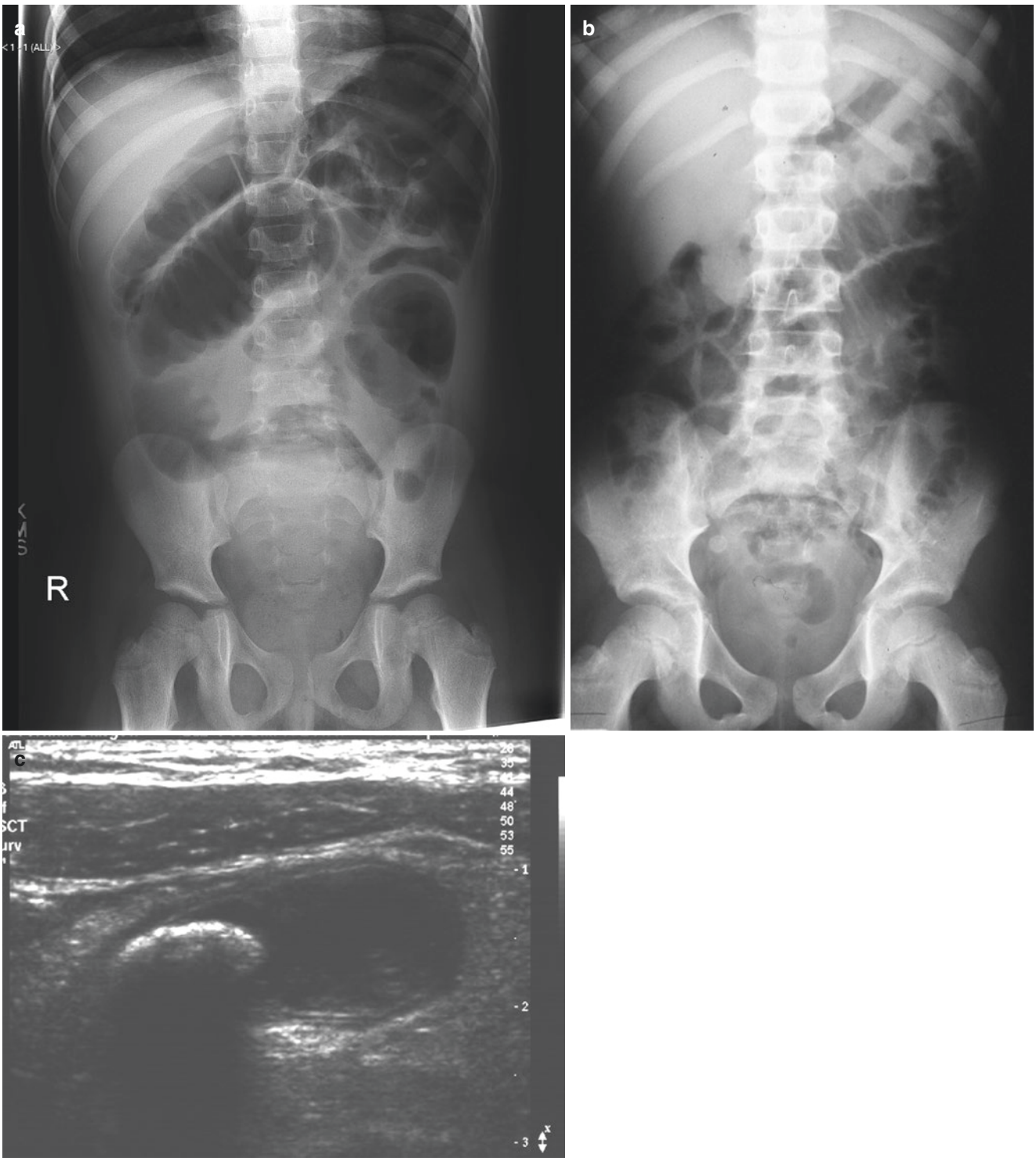

Fig. 4.24 (**a**) Acute appendicitis. Plain X-ray showing small bowel dilated loops. (**b**) Appendicitis. Plain X-ray showing faecolith in right iliac fossa. (**c**) Ultrasound in acute appendicitis

In the paediatric setting, ultrasound is the imaging modality of choice for the diagnosis and assessment of appendicitis and its complications. Graded compression of the right iliac fossa may demonstrate the inflamed appendix as a distended blind ending non-compressible structure, >6 mm in diameter, arising from the caecum. Associated inflammation of the mesenteric fat, localised ascites, mesenteric lymphadenopathy and the presence of an echogenic, calcified faecolith provide corroborating evidence. The appendix must be positively identified and may not be visualised due to a

retrocaecal position. Following perforation, ultrasound may be falsely reassuring. Complications of appendicitis, including an inflammatory mass and intraperitoneal and retroperitoneal abscess formation, may also be diagnosed on ultrasound.

Cross-sectional imaging by computerised tomography is usually reserved for the assessment of complications including abscess and collections when they have not been satisfactorily assessed by ultrasound.

4.3.3 Pancreatitis

Pancreatic disorders are uncommon in childhood, except that which is part of the generalised disease of cystic fibrosis (mucoviscidosis). Pancreatitis presents as an acute abdominal emergency, but the signs and symptoms are less dramatic than in adults. Abdominal pain and vomiting are the most consistent signs. Abdominal tenderness is more marked in the upper abdomen. A high index of suspicion is necessary by the clinician so that blood is taken for serum amylase estimation. In pancreatitis the level is considerably elevated, as is the urinary amylase. Ultrasound examination of the abdomen may show the swollen oedematous pancreas. The most common aetiology in Scotland is mumps, but many cases are idiopathic. Traumatic pancreatitis is infrequent but may be followed by development of a pancreatic pseudocyst. This can be followed by repeated ultrasound examination, and the majority will settle without the necessity of drainage into the stomach or bowel. Familial pancreatitis can affect succeeding generations or siblings.

Plain abdominal radiographs are not employed in the diagnosis or assessment of pancreatitis. The calcification of chronic pancreatitis is rarely demonstrated in the paediatric population.

Ultrasound is the initial modality of choice. It is used to identify possible causes of pancreatitis such as biliary abnormalities or calculi, and in the acute setting may demonstrate generalised or focal swelling and hypoechogenicity of the pancreatic gland in around 50% of cases. Prominence of the pancreatic duct and peripancreatic fluid can also point towards the diagnosis and can be appreciated particularly with high-resolution linear transducers. Contrast enhance ultrasound has been used to assess for pancreatic necrosis, and pancreatic pseudocysts may be demonstrated within or adjacent to the pancreas and are usually solitary, unilocular, and anechoic.

Cross-sectional imaging by CT and MRI can be used to assess complications of pancreatitis in the paediatric population. Magnetic resonance imaging using T2-weighted and T1 post contrast imaging can be very useful in the assessment of patients and can allow monitoring of patients with pseudocysts, particularly older patients who can cooperate without anaesthesia. This allows repeated follow up without the concern of repeated ionising radiation doses associated with CT scanning. MR cholangiography can provide assessment of morphology and dilation of the biliary and pancreatic ducts (Fig. 4.25).

4.3.4 Crohn's Disease

Crohn's disease may affect any part of the gastrointestinal tract but most commonly the terminal ileum and proximal colon. The lesions are basically chronic granulomatous and inflammatory with a tendency towards remissions and relapses. The histological changes are transmural, i.e., affecting all layers of the bowel wall with oedema and ulceration of the mucosa, fissures, submucosal fibrosis, and many inflammatory foci of mononuclear and giant cells. Perforation, haemorrhage, and fistula formation are uncommon complications in childhood (Fig. 4.26a).

In Crohn's disease the diarrhoea is much less severe than in ulcerative colitis; it is often intermittent and there may be little or no obvious blood or mucus in the stools. Crohn's disease presents with less specific signs and symptoms than ulcerative colitis, hence the delay in diagnosis often found in Crohn's disease.

General manifestations commonly include anaemia, loss of weight, growth failure, pubertal delay, erythematous rashes, and a low-grade fever. Other associated features are: erythema nodosum, pyoderma, iridocyclitis, arthralgia or arthritis, spondylitis, finger clubbing, anal skin tags, fissures, and fistulae. Quite frequently the disease presents with oral ulceration, and this may progress to extensive involvement of the buccal mucosa, which becomes oedematous and granulomatous sometimes years before there is evidence of intestinal involvement. Crohn's disease shows a segmental lesion, while ulcerative colitis is diffuse. The appearances vary from a "cobblestone appearance" due to thickened oedematous mucosa to narrowing of the lumen with the so-called "string sign." There may be fistulous tracts to adjacent loops of bowel. Biopsy of a perirectal lesion or even of the involved buccal mucosa may reveal diagnostic granulomatous changes. Colonoscopy and biopsy may provide an immediate diagnosis.

Plain abdominal radiographs are useful to assess for complications including obstruction, perforation, and toxic dilation, but have no routine role in the diagnosis or assessment of inflammatory bowel disease. Bowel wall thickening and "thumb printing" may be appreciated on plain films but are non-specific findings (Fig. 4.26b).

Assessment of the small bowel to determine extent of disease, bowel wall thickening, ulceration, and stricture formation can be challenging in the paediatric population. Ultrasound, including examination of the bowel wall with a high-resolution linear probe, can provide information about disease activity and

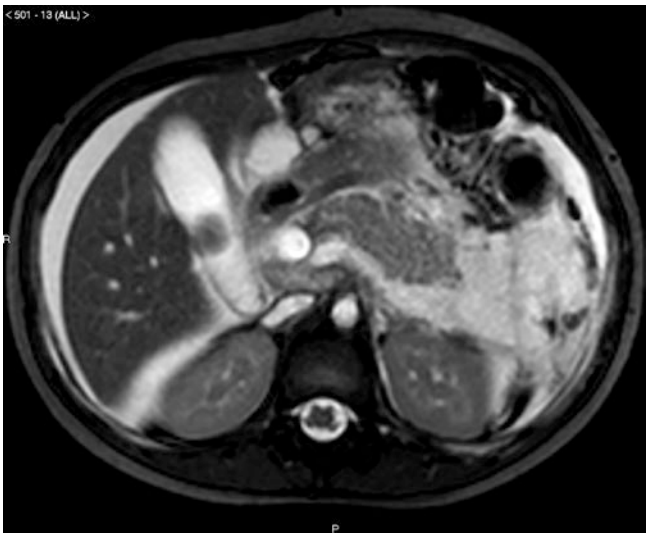

Fig. 4.25 T2 MRI scan in acute pancreatitis also showing a solitary gallstone in the gallbladder

complications, but can rarely assess the entire bowel. In younger children, barium follow-through examination, with screening and spot films of the terminal ileum, remains the most feasible examination, but is recognised to have significant intra-observer radiation, incurs a radiation burden, and does not provide extraluminal information (Fig. 4.26c).

Conventional cross-sectional imaging is of limited value, except in the assessment of extraluminal complications such as inflammatory mass or collections. In children who are able to cooperate, however, MR enterography has become the modality of choice for intra- and extraluminal assessment of the bowel, because of both the information obtained and the lack of ionizing radiation incurred. A variety of bowel preparation protocols exist, but they involve oral or nasogastric (NG) administration of contrast such as mannitol or polyethylene glycol. Protocols include the administration of an antispasmodic such as hyoscine and gadolinium contrast or diffusion weighted imaging. Enteroclysis is rarely performed in the paediatric population (Fig. 4.26d).

Imaging assessment of perianal and perirectal disease, abscess, and fistula formation is performed by MRI, utilising high-resolution multiplanar sequences with and without gadolinium contrast administration and requiring no preceding bowel preparation. The sequences can be angled to the pelvic floor and levator complex, allowing detailed information of the course and extent of fistula disease.

4.3.5 Ulcerative Colitis

Boys and girls are equally affected. The mean age of onset is about 10 years. There is no clear-cut inheritance pattern, but ulcerative colitis is more common in first-degree relatives than in the general population.

The mucous membrane of part or all of the colon, and sometimes of the terminal ileum, becomes hyperaemic, oedematous, and ulcerated. The lesion is continuous rather than patchy and usually involves only the mucosal and submucosal layers. The earliest lesion in many cases is a crypt abscess. Granuloma formation is rare. In some cases, oedema may give rise to pseudopolypoid nodules. Ulceration may extend through the muscularis, and perforation of the colon can occur. Usually perforation is preceded by toxic megacolon with dilatation of an ulcerated segment of the large bowel. Carcinoma is a common late complication. Hepatic complications such as sclerosing cholangitis and chronic active hepatitis can occur with ulcerative colitis in childhood.

The onset is sudden, with diarrhoea and the frequent passage of small stools containing blood and mucus. This tends to be most severe during the early morning but may also be nocturnal. There may be abdominal pain, anorexia, weight loss, or poor weight gain. Tenesmus is common.

Hypochromic anaemia due to chronic blood loss is almost invariably present. Hypoproteinaemic oedema may develop. Associated extraintestinal manifestations of the disease are more common in children than in adults. They may include erythema nodosum, aphthous stomatitis, conjunctivitis, iridocyclitis, haemolytic anaemia, arthralgia or arthritis, pyoderma gangrenosum, and finger clubbing. Colonoscopy may allow the examination of the whole colonic mucosa and thus the extent of the disease. Ulcerative colitis frequently runs an acute course in the child. The cumulative risk of carcinoma of the colon is 20% per decade after the first decade of the illness. Dysplastic changes in the colonic epithelium are considered to be pre-malignant.

Plain abdominal radiographs are useful to assess for complications including obstruction, perforation, and toxic dilation, but have no routine role in the diagnosis or assessment of inflammatory bowel disease. Bowel wall thickening and "thumb printing" may be appreciated on plain films but are non-specific findings.

Assessment of the small bowel to determine extent of disease, bowel wall thickening, ulceration, and stricture formation can be challenging in the paediatric population. Ultrasound, including examination of the bowel wall with a high-resolution linear probe, can provide information about disease activity and complications, but can rarely assess the entire bowel. In younger children, barium follow through examination, with screening and spot films of the terminal ileum, remains the most feasible, but is recognised to have significant intra-observer radiation, incurs a radiation burden, and does not provide extraluminal information (Fig. 4.27a).

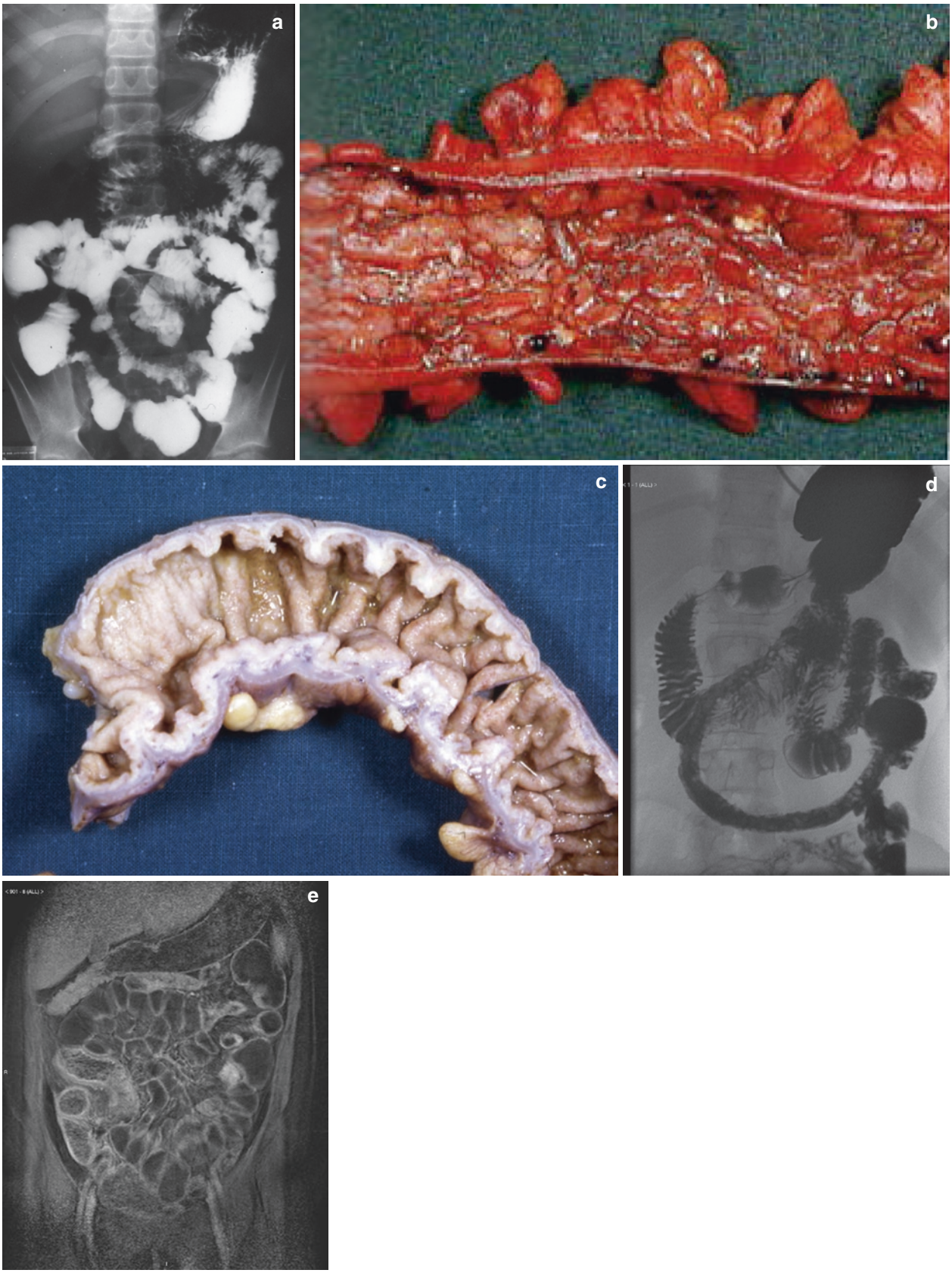

Fig. 4.26 (**a**) Barium meal and follow through showing multiple strictures and pseudocyst of the wall of the small intestine in Crohn's disease. (**b**) Crohn's disease. (**c**) Pathology specimen of resected ileum in Crohn's disease. The bowel is thickened. B1 resected operative specimen of Crohn's disease. (**d**) Long segment Crohn's disease seen on a contrast study of the intestine. (**e**) Crohn's disease. An MRI scan showing diseased bowel with stricture formation and spiculation of the wall of the bowel

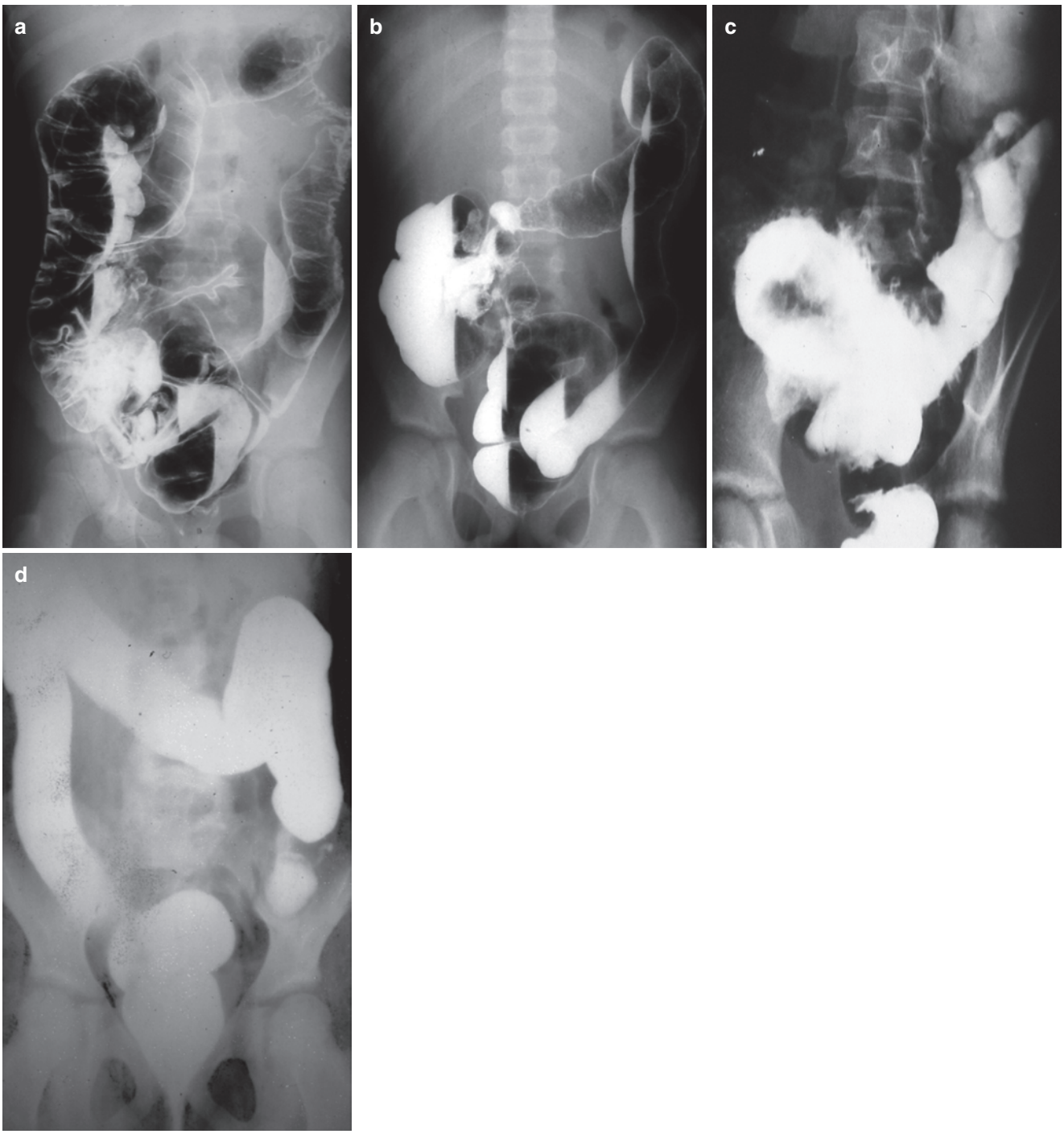

Fig. 4.27 (**a**) A contrast study showing features of a toxic megacolon in a patient with ulcerative colitis. (**b**) Ulcerative colitis. A contrast study showing a featureless colon with no haustrations. (**c**) Ulcerative colitis. Contrast showing spiculation of the wall of the colon suggestive of intense inflammation becoming transmural. (**d**) Lead pipe appearance of the whole of the colon in a patient with ulcerative colitis

Conventional cross-sectional imaging is of limited value, except in the assessment of extraluminal complications such as inflammatory mass or collections. In children able to cooperate, however, MR enterography has become the modality of choice for intra- and extraluminal assessment of the bowel, because of both the information obtained and the lack of ionizing radiation incurred. A variety of bowel preparation protocols exist but involve oral or NG administration of contrast such as mannitol or polyethylene glycol. Protocols include the administration of an antispasmodic such as hyoscine and gadolinium contrast. Enteroclysis is rarely performed in the paediatric population (Fig. 4.26e).

Imaging assessment of perianal and perirectal disease, abscess, and fistula formation is performed by MRI, utilising high-resolution multiplanar sequences with and without gadolinium contrast administration and requiring no preceding bowel preparation. The sequences can be angled to the pelvic floor and levator complex, allowing detailed information of the course and extent of fistula disease.

4.3.6 Lymphoid Hyperplasia of the Colon

This is uncommon in children but can present with recurrent abdominal pain and/or rectal bleeding. Radiologically the lymphoid hyperplasia is characterised by small uniform umbilicated polypoid lesions involving all or part of the colon. A fleck of barium in the centre of the polyp represents umbilication at the apex of the lymphoid nodule, and is unique for lymphoid hyperplasia. This benign lesion probably represents the normal response of lymphoid tissue in children to a variety of stimuli. Biopsy proof of the nature of the nodule may be required.

On fluoroscopic barium follow-through examination, the prominent lymph node follicles are seen as round, regular, smooth filling defects with no evidence of ulceration, and are particularly visible on screening of the terminal ileum. Normal small bowel features (valvulae conniventes) are maintained.

4.3.7 Psoas Abscess

Plain abdominal radiography is rarely useful in the diagnosis of psoas abscess. Plain films may show loss of psoas shadow and obscuring of the ipsilateral sacroiliac joint, although these findings may only be appreciated in retrospect. Only in the presence of a very large abscess is a mass, or mass effect appreciated.

In neonates and children, unlike adults, the retroperitoneum, including the iliopsoas muscle, can often be visualised on ultrasound. Depending on its composition, there may be swelling, hyperaemia on colour Doppler and echogenicity of the muscle with a fluid-containing abscess, of variable echogenicity (but usually hypoechoic). An echolucent ipsilateral joint effusion may be appreciated and does not necessarily indicate a concomitant septic arthritis but may be reactive.

Cross-sectional imaging, usually by contrast-enhanced CT in the acute phase, demonstrates a rim-enhancing lesion with a non-enhancing, low attenuation centre, and provides information on bony involvement, which is seldom appreciated on ultrasound.

Image-guided drainage (by ultrasound or CT) is now the mainstay of treatment.

4.3.8 Hydatid Disease

Tapeworms: Taenia saginata—beef tapeworm; Taenia solium—pork tapeworm; Hymenolepis species—dwarf tapeworm; taenia echinococcus (Hydatid cyst). Ingestion of raw or inadequately cooked beef or pork can result in human infection. Humans are the definitive host for both the beef (T. saginata) and pork (T. solium) tapeworms. Although the infections may be asymptomatic, epigastric discomfort, increased appetite, dizziness, and loss of weight sometimes occur. These features may be more marked in children and debilitated persons. Diagnosis is based on the passage of gravid segments through the anus. The differentiation can be made by a microscopical study of the number of lateral branches in the gravid uterus of each segment, the uterus of T. solium having about ten branches and that of T. saginata about 20. With T. solium infection a major danger is the ingestion of eggs from an infected person (heteroinfection) or self-ingestion of eggs (autoinfection). This can give rise to cysticercosis, where cysticerci develop almost anywhere including the brain, skin, muscle, and eye.

Taenia Echinococcus (Hydatid Cyst). The definitive host of Taenia echinococcus is the dog, wolf, fox, or jackal. Humans and sheep may become the intermediate host by swallowing the ova from the dog, which is especially likely in sheep-rearing countries such as Australia. The adult worm in the dog is very small (0.5 cm) but the ingested ovum when swallowed by humans liberates a six-hooked onchosphere into the small intestine. This penetrates to the tissues, usually the liver but sometimes lung, bones, kidneys, or brain to form a hydatid cyst. This has a three-layered wall—an outer layer of host fibrous tissue, a laminated middle layer, and an inner germinal layer that produces many daughter and granddaughter cysts.

These cysts present clinically with local pressure effects. The liver may be greatly enlarged and there may be a palpable rounded swelling over which the classical "hydatid thrill" can be elicited. Ultrasound and CT scanning can reveal the cystic nature of the lesions. Eosinophilia may be marked. The diagnosis may be confirmed by complement fixation, haemagglutination or latex-slide agglutination tests, but the hydatid ELISA test and improved immunoelectrophoresis tests are likely to prove more specific (Fig. 4.28).

Hymenolepis (Dwarf tapeworm). Mild infestations due to Hymenolepis (dwarf tapeworm) cause no symptoms, but heavy infestations can sometimes cause diarrhoea, irritability and fits. Diagnosis is made by finding the typical ova in the faeces.

A range of sonographic appearances are recognised. Type 1 cysts are simple and echolucent apart from fine internal debris (hydatid sand). In type II cysts, the inner membrane of the cyst separates with an "undulating" appearance. Type III refers to multiloculated lesions with "daughter" cysts. Type IV are complex heterogenous masses. Type V show evidence of calcification. Types I and III may not be distinguished from other causes of simple cyst or tumoral mass on imaging alone.

On CT the cystic components are low attenuation, comparable to water, and any calcification will be well demonstrated. On MRI the cyst wall is low signal on both T1- and T2-weighted imaging, with high signal contents on T2-weighted imaging.

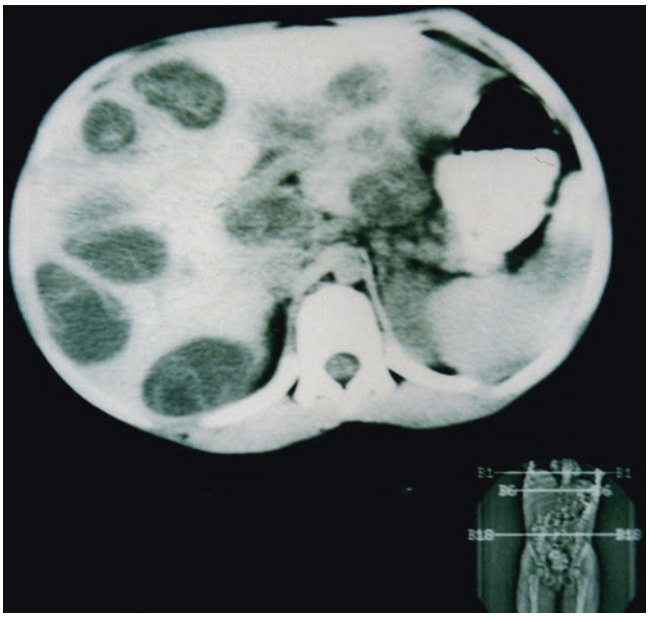

Fig. 4.28 CT of the liver showing multiple large Hydatid cysts in a patient on medical treatment

4.3.9 Ascaris

On sonography the gall bladder and biliary tree initially appear like cholangitis, with a thick-walled dilated gallbladder and dilated echogenic intrahepatic biliary ducts. The ascaris flukes may be visualised within the biliary tree and gall bladder as echogenic structures and casts, and may be seen to move in real time. On CT and MR cholangiography the flukes are rarely visualised except in heavy infection, where filling defects in the biliary tree may be appreciated.

The figures shown here show ascaris in the intestine after presenting with an intestinal obstruction (Fig. 4.29a, b).

4.3.10 Polyps

Inflammatory polyps can be caused by infections like Schistosomiasis and pseudopolyps by non-specific inflammatory conditions. These may be demonstrated as incidental findings on contrast enemas and follow through as luminal filling defects, but imaging plays little part in their assessment or follow-up (Fig. 4.30a, b).

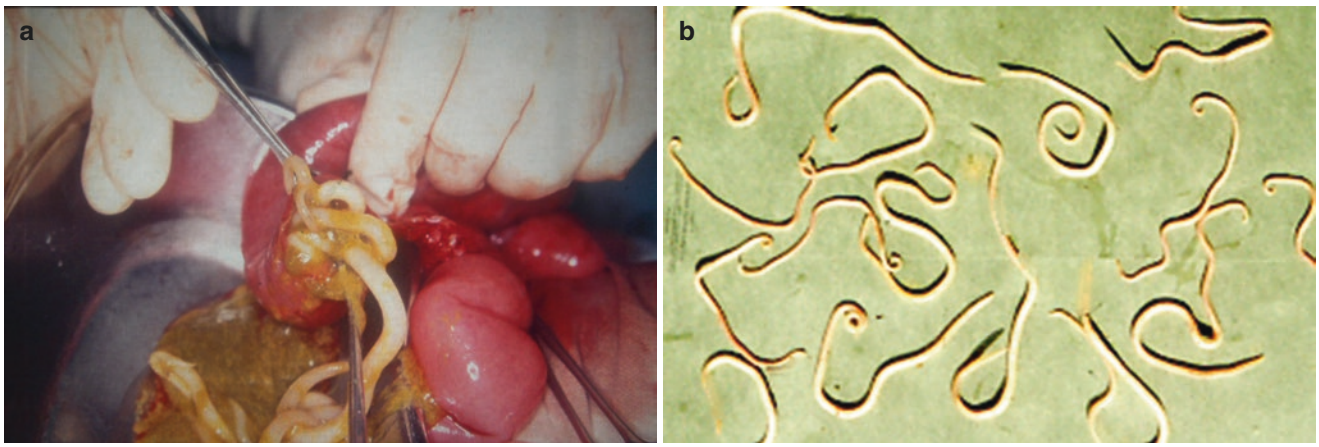

Fig. 4.29 (**a**) Ascaris. A preoperative picture of an enterotomy made for bowel obstruction due to a bolus of Ascaris infestation. (**b**) Ascaris worms

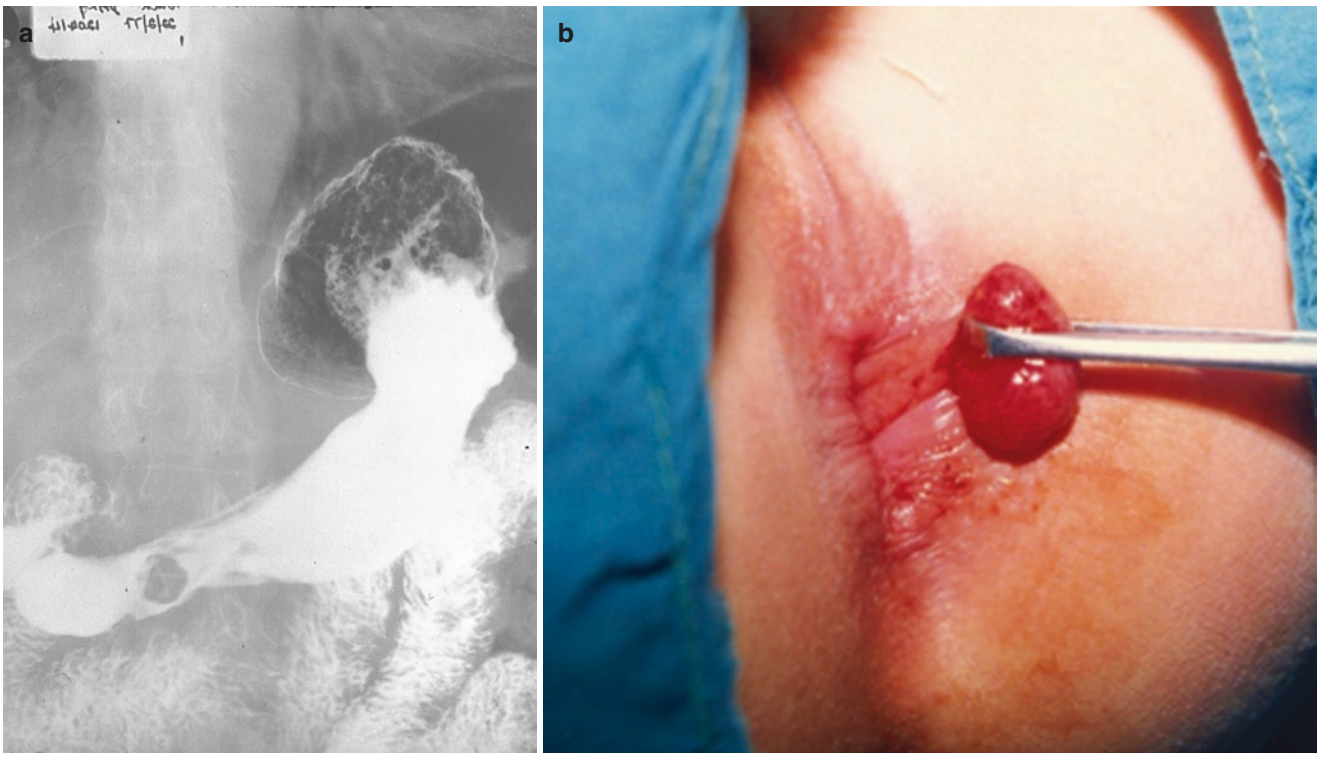

Fig. 4.30 (**a**) Gastric polyp in the antrum of the stomach seen on a barium meal. (**b**) Rectal polyp prolapsed outside the anus on a long pedicle. These polyps are called juvenile rectal polyps. They are solitary and are composed of inflammatory tissue, and can be also hamartomatous in nature but not malignant. They sometimes autoamputate themselves and are found in the nappy

4.3.11 Stomach

Although gastritis may be demonstrated as thickening and poor coating of the stomach, and duodenum and irregular ulceration may also be visualised, contrast examinations are no longer part of the assessment of these conditions.

4.4 Trauma

4.4.1 Foreign Bodies (Fig. 4.31a–j)

Abdominal radiography remains the mainstay of glass and metallic foreign-body assessment. It allows assessment of the position and consequences of ingestion, including obstruction and occasionally perforation. Cross-sectional imaging is rarely required, and MRI will be contraindicated in the presence of ingestion of a metallic body.

Particular care should be taken in the presence of battery ingestion and the ingestion of more than one magnet/magnetic toy, where mucosal damage and obstruction can be greater than first appreciated.

Occasionally foreign bodies may be inserted via the urethra into the bladder and are best imaged by sonography.

4.4.2 Liver (Fig. 4.32a–c)

Trauma to the liver after a severe impact injury following a fall, a car accident, or a non-accidental injury can be severe and life-threatening. A bruise may or may not be present externally as the abdominal wall in a child is very flexible. Liver injury may involve major tears with a hemoperitoneum or occasionally haemobilia with blood loss and shock. Imaging is best by CT scanning and follow-up by ultrasound.

4.4.3 Spleen (Fig. 4.33a–d)

Splenic injuries can occur following trauma, and if the spleen is pathologically enlarged, e.g., congenital hereditary splenocytosis or in malaria, minor injury can also cause severe disruption with blood loss. Bleeding can

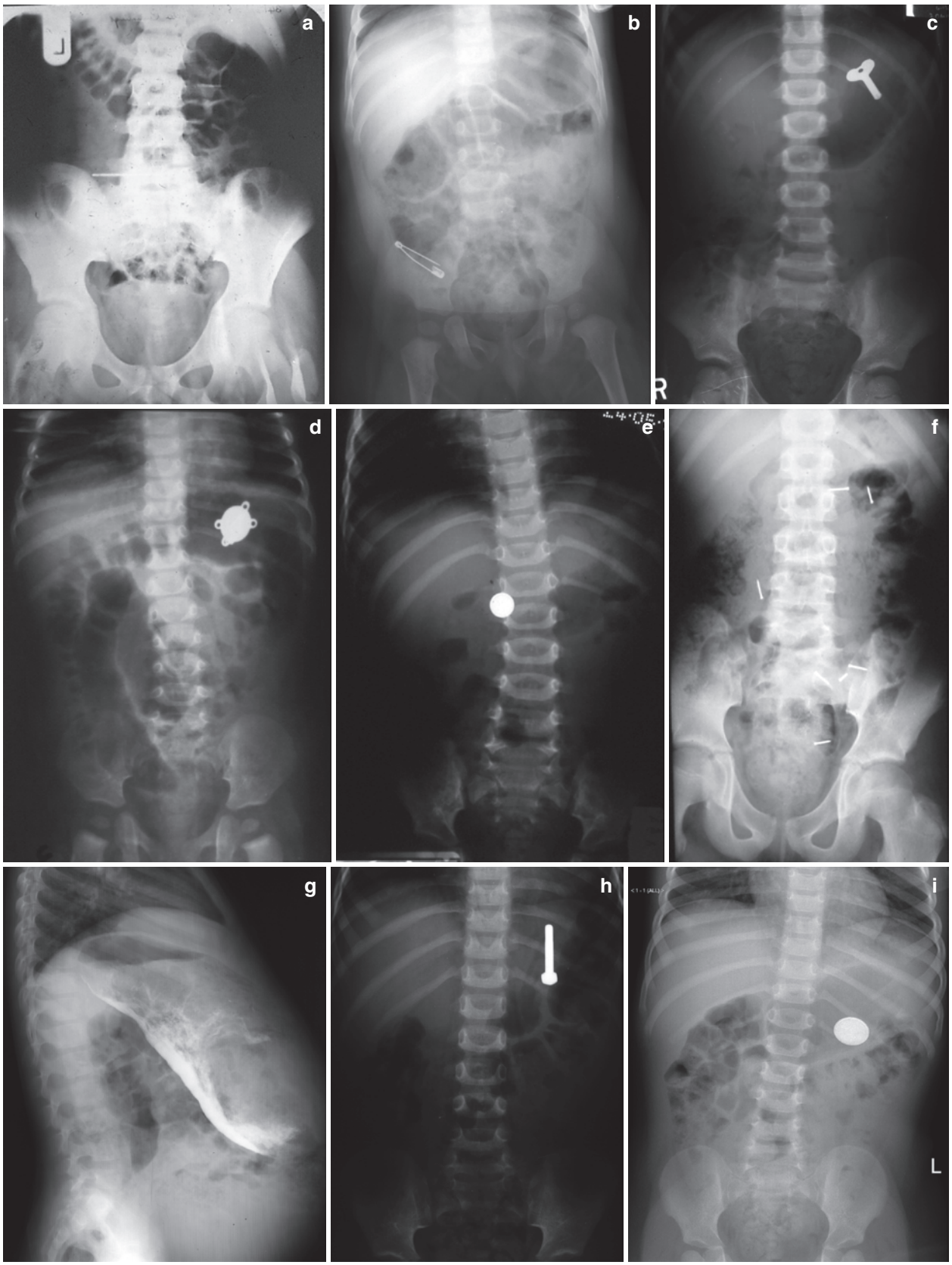

Fig. 4.31 (**a**) Foreign body in abdomen: needle. (**b**) Foreign body: safety pin. (**c**) Foreign body: key. (**d**) Foreign body in stomach. (**e**) Foreign body: button battery. (**f**) Foreign body: multiple small nails. (**g**) Foreign body. Hair bezoar in a patient who compulsively swallowed hair, causing intestinal obstruction. (**h**) Foreign body: screw. (**i**) Foreign body: button battery. (**j**) Foreign body: locket

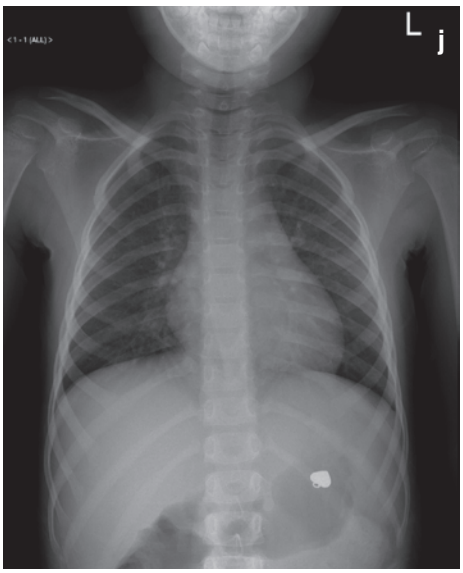

Fig. 4.31 (continued)

occur intracapsular, retroperitoneally, or intraperitoneally. CT is the best modality to identify the lesion and extent of severity. Follow up is by ultrasound to make sure healing has occurred. Isotope scans later on may be used to assess the function of the spleen to ensure it is still viable, as some cases of autosplenectomy caused by damage to the splenic vessels at the time of injury have been reported.

4.4.4 Renal (Fig. 4.34)

This is discussed fully in Chap. 5.

4.4.5 Pancreas/Pancreatic Pseudocyst

Ultrasound examination of the abdomen may show the swollen oedematous pancreas. Traumatic pancreatitis is

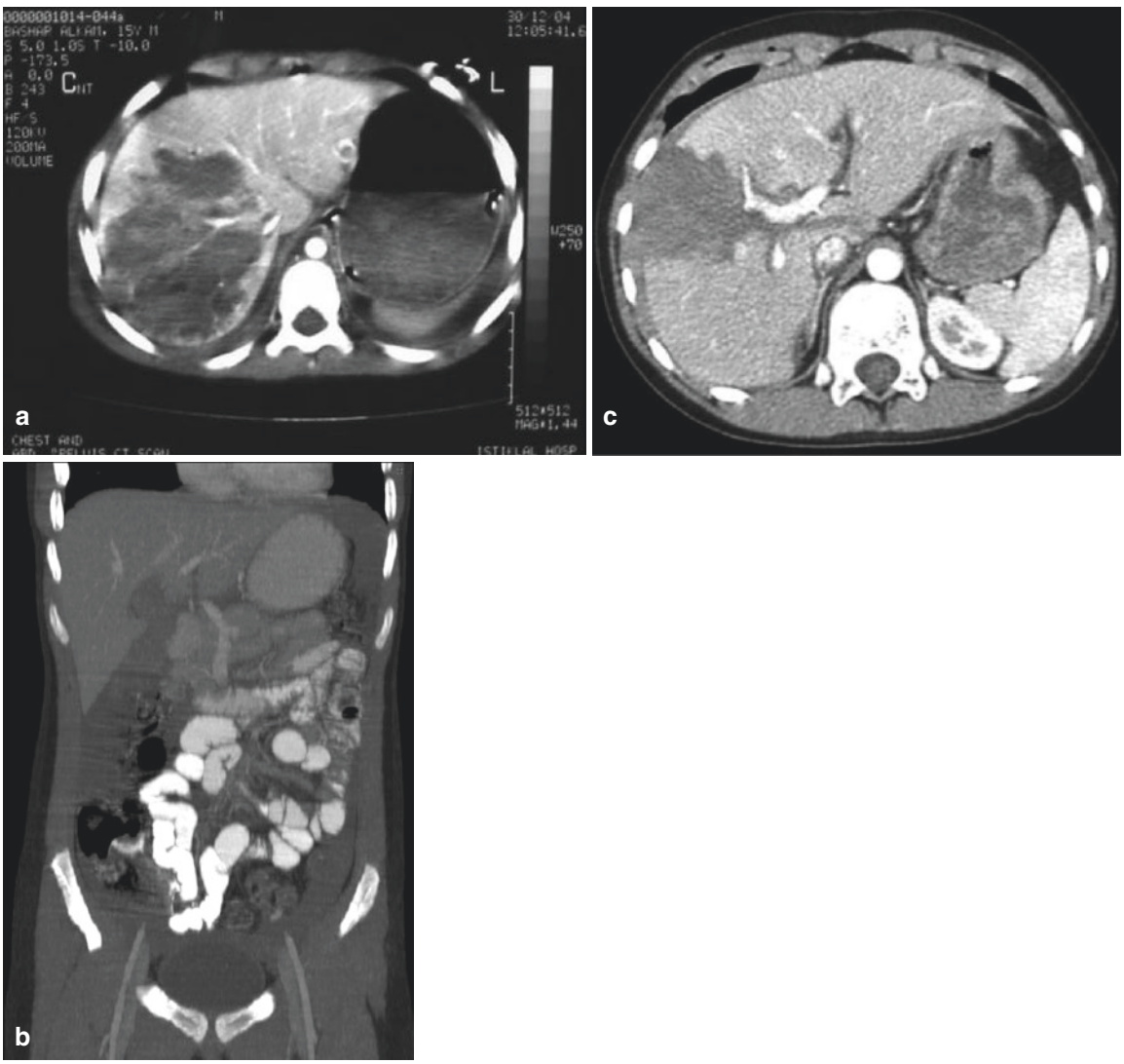

Fig. 4.32 (**a**) Major trauma. CT scan showing major disruption of the liver with a large haematoma in the right lobe of the liver and capsular tear. (**b**) Trauma with liver injury and hemoperitoneum. (**c**) CT scan showing a fracture of the liver with capsular tear and subcapsular haematoma

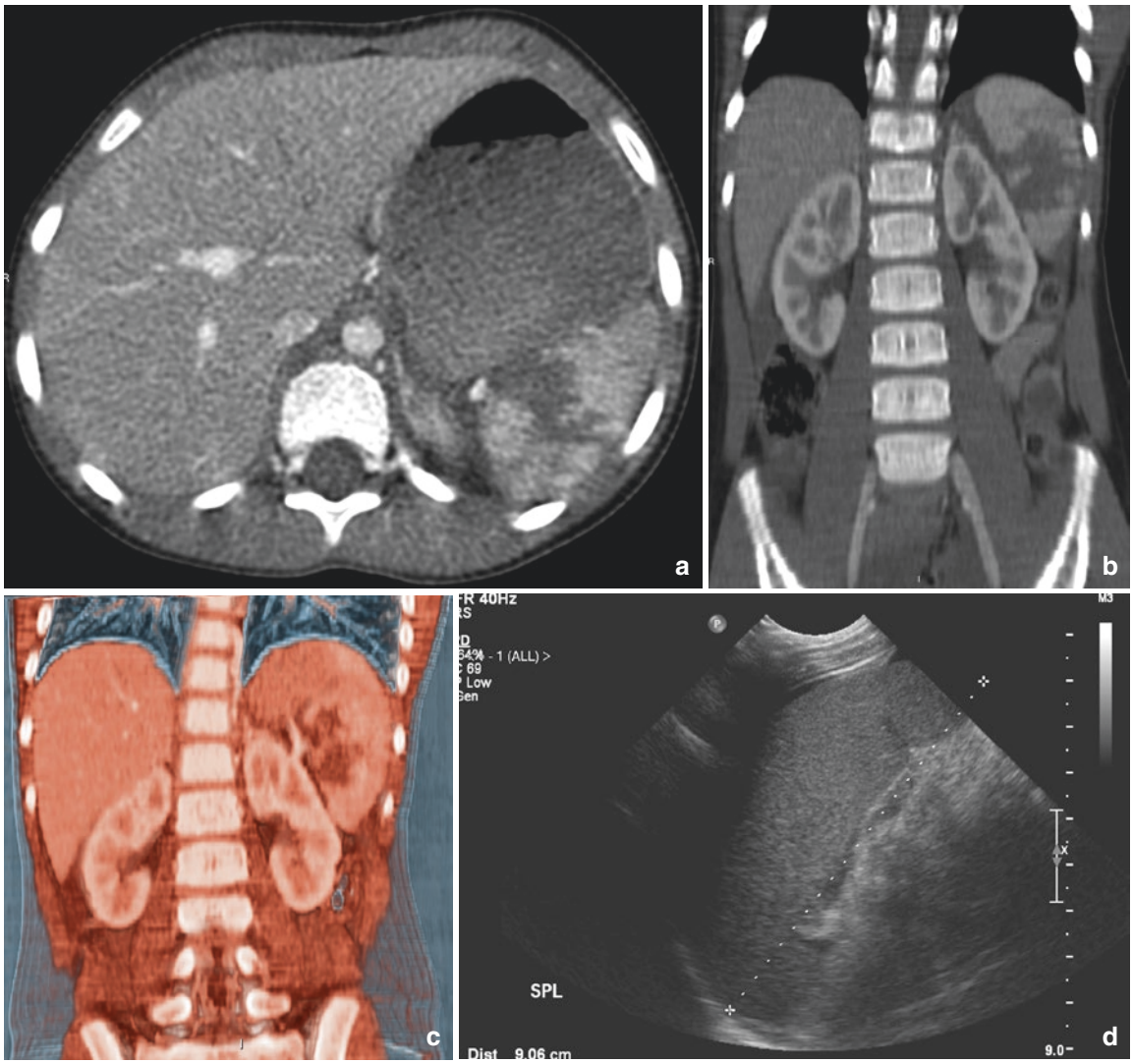

Fig. 4.33 (**a**) CT scan with contrast. Fall from a horse. The child sustained a shattered spleen. (**b**) Longitudinal MPR reconstruction showing shattered spleen. (**c**) MPR of shattered spleen. (**d**) Ultrasound follow up of shattered spleen. No free fluid. Almost normal scan

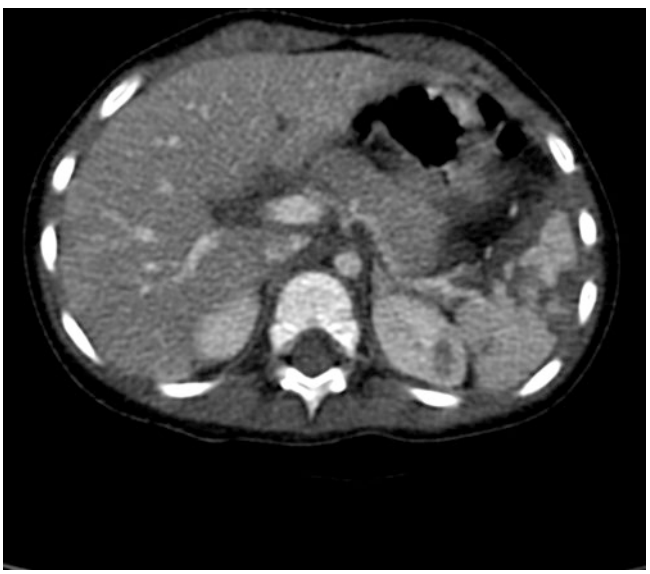

Fig. 4.34 CT scan demonstrating both fracture kidney and spleen following a road traffic accident

infrequent but may be followed by development of a pancreatic pseudocyst. This can be followed by repeated ultrasound examination, and the majority will settle without the necessity of drainage into the stomach or bowel. Familial pancreatitis can affect succeeding generations or sibs. It is a rare disorder of unknown aetiology (Fig. 4.35a–c).

4.4.6 Visceral

Abdominal trauma, accidental or non-accidental, may cause injury to the abdominal viscera. A plain X-ray of the abdomen and a serum amylase should be done to exclude the presence of traumatic or idiopathic pancreatitis and a pneumoperitoneum.

Computerised tomography is the imaging method of choice for the assessment of abdominal and pelvic trauma in the acutely injured child. It allows accurate and comprehen-

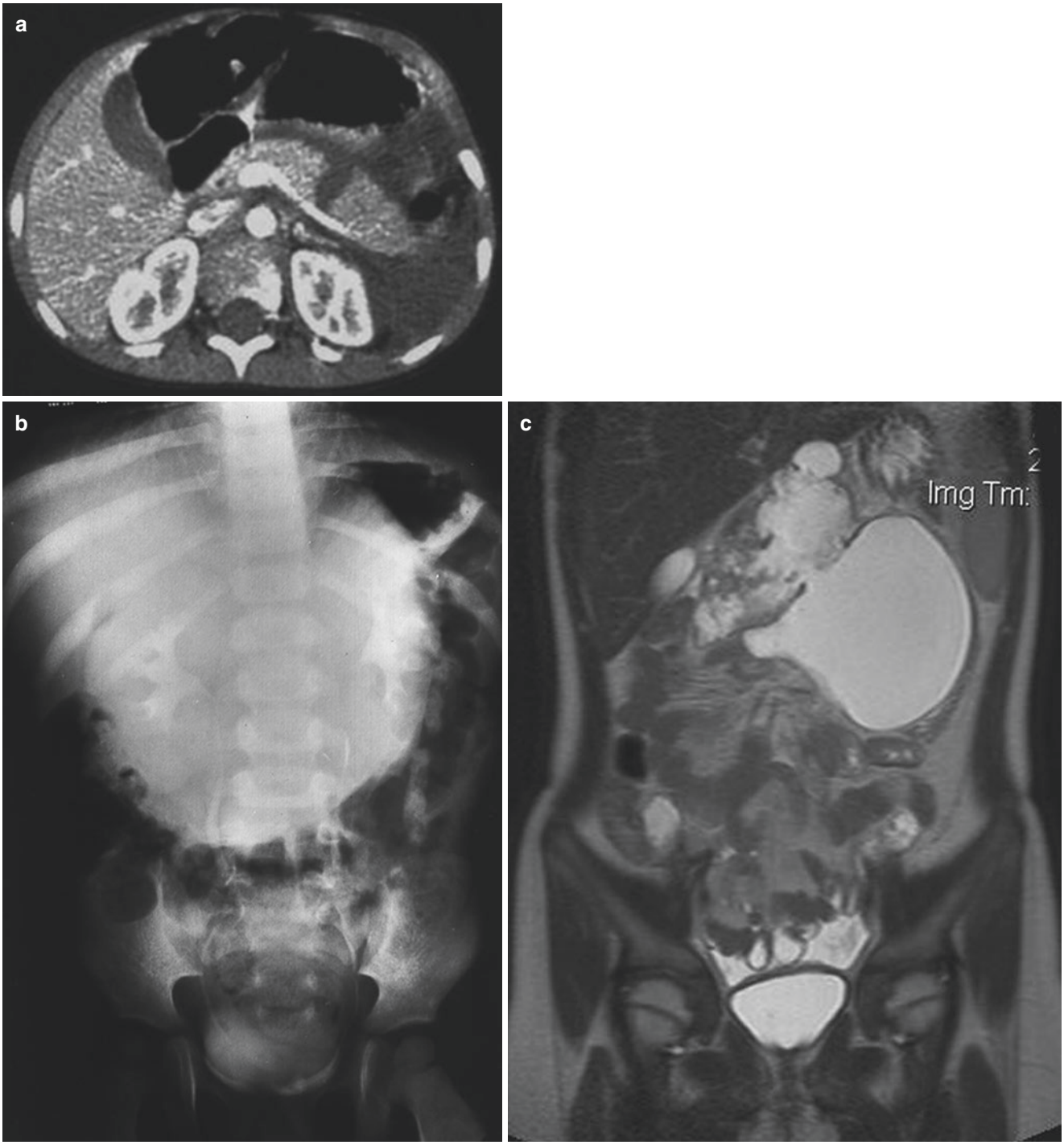

Fig. 4.35 (**a**) CT scan showing a hemoperitoneum and a fracture of the body of the pancreas. (**b**) Pancreatic pseudocyst is seen as a soft issue mass with the transverse colon spread around it and pushed downwards. (**c**) MRI showing a pancreatic pseudocyst

sive assessment and quantification of solid organ injury, intra-, and retroperitoneal haemorrhage, including vascular injury and hollow viscus injury/perforation. Associated bony and extra-abdominal injuries can also be assessed (Fig. 4.36).

Although haemodynamically unstable children may be examined with sonography, its value is limited as its sensitivity and specificity for both hemoperitoneum and solid organ injury are lower than CT and it does not provide information on hollow viscus injury or associated skeletal or thoracic injury.

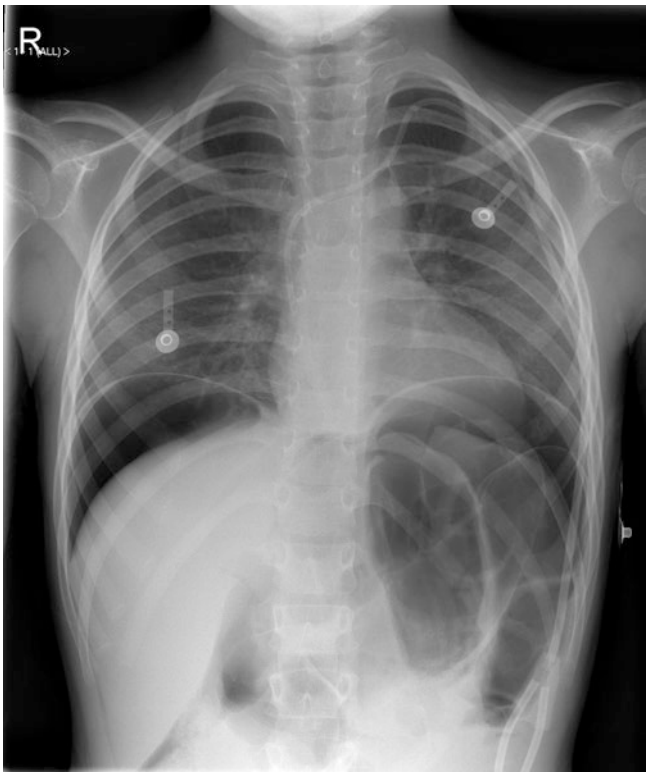

Fig. 4.36 Pneumoperitoneum

4.5 Tumour

4.5.1 Sacrococcygeal Teratoma

Sacrococcygeal teratoma may be diagnosed on antenatal sonography as a cystic or solid mass, usually at the distal portion of the spine. Most are diagnosed in the second trimester, although they have been described on ultrasound as early as 13.5 weeks. The earlier the mass is visualized in pregnancy, with the presence of fetal hydrops from arteriovenous shunting and cardiac failure, the worse the prognosis.

The classification of sacrococcygeal teratomas (American Academy of Pediatrics surgery section survey) is usually determined by imaging, whether pre- or post-natal. Type I are mainly external with little or no internal components, Type II are predominantly external but extend into the presacral space, Type III are external and internal with extension into the abdominal cavity. Type IV are entirely internal (Fig. 4.37a).

Antenatal MRI using fast T2-weighted sequences also demonstrates the lesions, with the cysts high signal and the solid elements of mixed or low T2 signal. The lesion may contain flow voids and calcification (Fig. 4.37d).

Postnatally, plain films may be useful to assess the integrity and appearance of the sacrum and the presence of calcification. Spina bifida and meningocele are the primary differential. Both sonography and magnetic resonance imaging can be used postnatally for assessment, typing, surgical planning, extension (including intraspinal extension) and follow-up before and after treatment. On sonography the mass is heterogeneous with cystic and solid elements and may be entirely cystic (in around 15%). The solid elements may be vascular. Intrapelvic and intraabdominal components are difficult to define fully on ultrasound and are better assessed on MRI. MRI may also help to differentiate a truly solid tumour from a microcystic one, both of which may appear echo-bright. Secondary findings due to mass effect (e.g., renal tract or bowel obstruction) may also be demonstrated on imaging (Fig. 4.37c–e).

4.5.2 Nephroblastoma (Wilms' Tumour)

Plain abdominal radiographs may demonstrate a large flank mass, obscuring the psoas outline with occasional calcification (in around 9%). Excretory urography is no longer part of tumour assessment (Fig. 4.38a).

Sonography demonstrates a heterogeneous solid mass which may contain anechoic haemorrhage, necrosis, or cyst formation, with echogenic areas of calcification and/or fat. The mass is often well circumscribed and tends to assume a spherical configuration with a surrounding claw of renal tissue. Tumour thrombus may be demonstrated extending into the renal vein and IVC (Fig. 4.38b).

Cross-sectional imaging using CT or MRI is used for further staging, including assessment of mass and adenopathy. On CT the mass is heterogeneous and may contain low attenuation fat, calcification, and haemorrhage (Fig. 4.38c). At MRI, the mass is low-signal intensity on T1 and high-signal on T2 imaging, enhancing heterogeneously with gadolinium, but with less intense enhancement than the surrounding renal parenchyma (Fig. 4.38e–f).

4.5.3 Neuroblastoma/Ganglioneuroma

Due to the multiple potential locations of both primary tumour and metastases, the imaging appearances can vary widely in position and appearance.

Radiographs may show a soft tissue mass containing calcification in around one-third, and may show destruction of associated bony structures and bony metastasis (Fig. 4.39a).

On sonography and cross-sectional imaging, tumour mass and associated lymphadenopathy engulfs and invades surrounding structures. Sonographically, neuroblastoma is heterogeneous and echogenic. Focal echogenic calcification is common (Fig. 4.39b).

Chest, abdominal, and pelvic imaging is required as part of staging. CT imaging is most commonly performed for

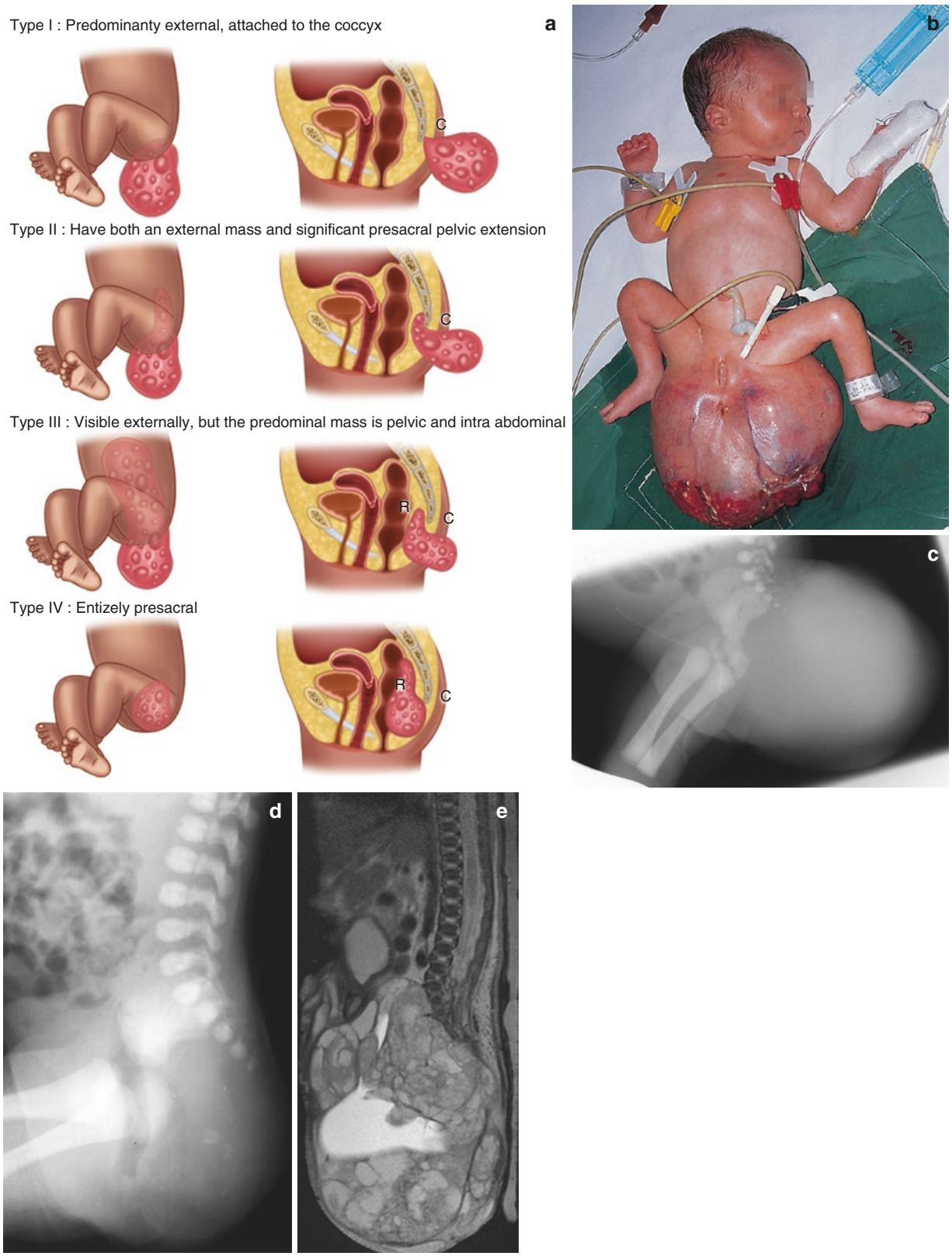

Fig. 4.37 (**a**) Diagram showing Classification of Sacrococcygeal Teratoma Type 1, Type 2, Type 3, Type 4. (**b**) Clinical Photograph of Type 2 Sacrococcygeal Teratoma soon after delivery showing ulceration and bleeding of the teratoma. Note the large veins on the surface. (**c**) Plain X-ray lateral view showing the soft tissue mass with deformity of the sacrum and coccyx. Note a catheter in the bladder. Sacrococcygeal teratoma. (**d**) Sacrococcygeal teratoma. Lateral view of another teratoma with calcification in the mass. (**e**) MRI scan showing large sacrococcygeal teratoma with cystic spaces. The tumour extends into the pelvis, making it a type 3 tumour

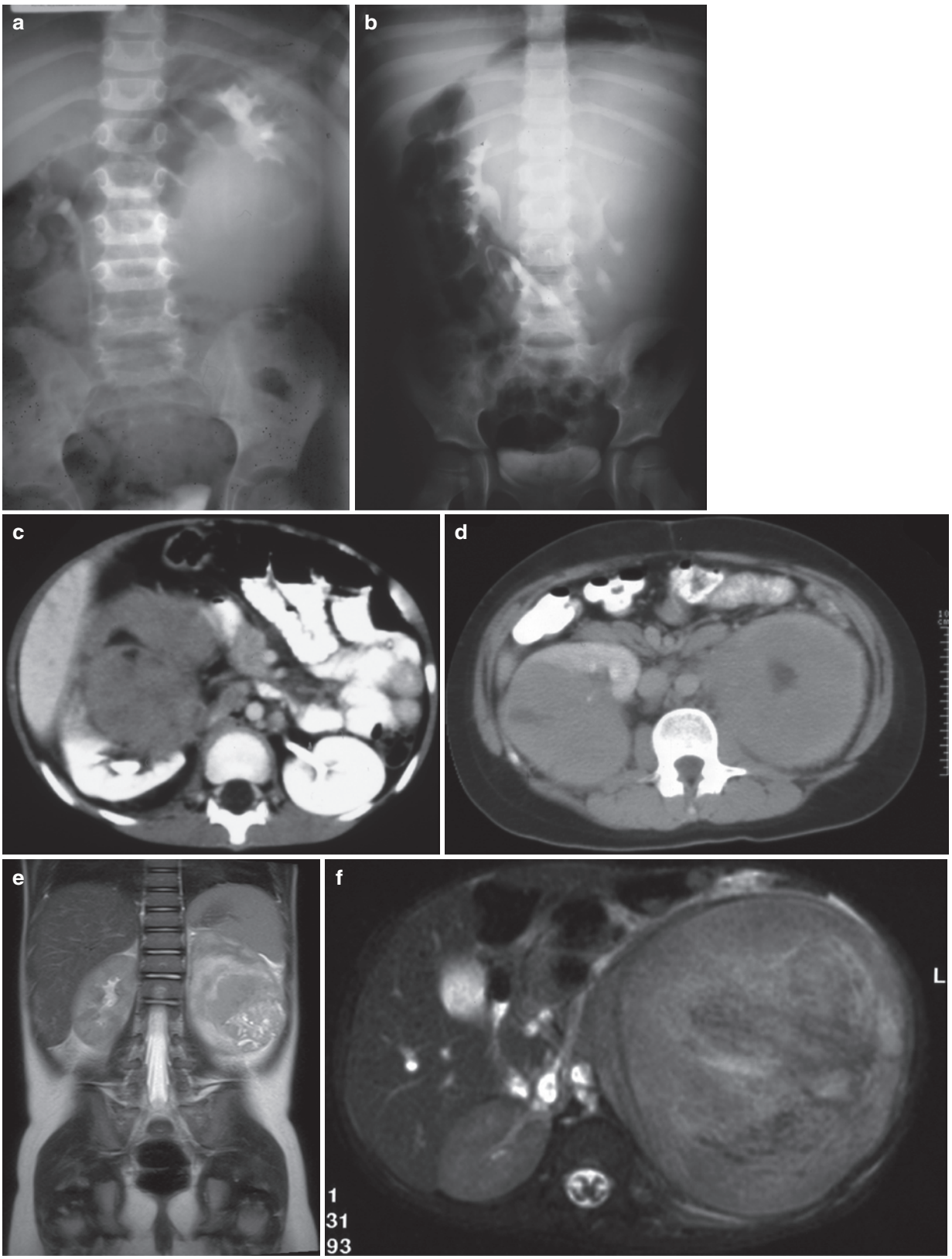

Fig. 4.38 (**a**) Intravenous urogram showing a nephroblastoma (Wilms') arising from the upper pole of left kidney. (**b**) Intravenous urogram showing deformity of the pelvicalyceal system. A large nephroblastoma arising from the left kidney crossing the midline. (**c**) CT scan showing nephroblastoma in cross section with extrarenal extension, (**d**) CT scan showing a bilateral nephroblastoma, (**e**) MRI scan in coronal plane of a left-sided nephroblastoma. (**f**) MRI axial plane showing a nephroblastoma in the left kidney. The central portion looks necrotic

assessment of thoracic and lung metastasis, and either modality may be used for abdominal and pelvic imaging. Cross-sectional imaging is used to define extent of disease, invasion of surrounding structures, and vascular involvement. Most tumours are heterogeneous in appearance, enhancing with contrast. In some cases (particularly perinatal 4S disease), there may be diffuse infiltration of soft tissue and solid organs (Fig. 4.39c–f).

Bony metastasis may be widespread and can be demonstrated well on whole body fat saturated/T2-weighted (e.g., STIR) imaging.

Nuclear scintigraphy can be used to assess both tumour and metastasis. A catecholamine analogue (metaiodobenzylguanidine, or MIBG, labelled with iodine 123) shows uptake in both the primary tumour and metastasis in around 70% of cases. Technetium-99mMDP scintigraphy can also be used to assess bony metastases (Fig. 4.39g, h).

4.5.4 Hepatoblastoma

On plain abdominal radiography, hepatomegaly or a right upper quadrant mass may be appreciated, which may contain calcification. On sonography, the hepatoblastoma is usually well circumscribed and may be lobulated. The sonographic appearances may vary significantly depending on the pathological type of the tumour, although most commonly echogenic they may be homogenous or heterogeneous with calcification, necrosis, and haemorrhage (Fig. 4.40).

Cross-sectional imaging also demonstrates a well-circumscribed mass which, as on sonography, may vary in attenuation and MRI signal. On contrast CT and MRI the tumour enhances, less than the surrounding liver parenchyma. Demonstration of the hepatic vasculature is important for assessment and staging.

4.5.5 Haemangioma: Liver (Fig. 4.41)

A hypoechoic liver mass with or without hydrops may be demonstrated on antenatal sonography.

Plain radiographs of the abdomen may show hepatomegaly or a mass, and in some cases, evidence of fine calcifications. In the case of larger lesions, chest radiography may demonstrate evidence of secondary congestive cardiac failure.

On sonography, small multifocal lesions are uniform and hypoechoic. Larger lesions may be heterogeneous with

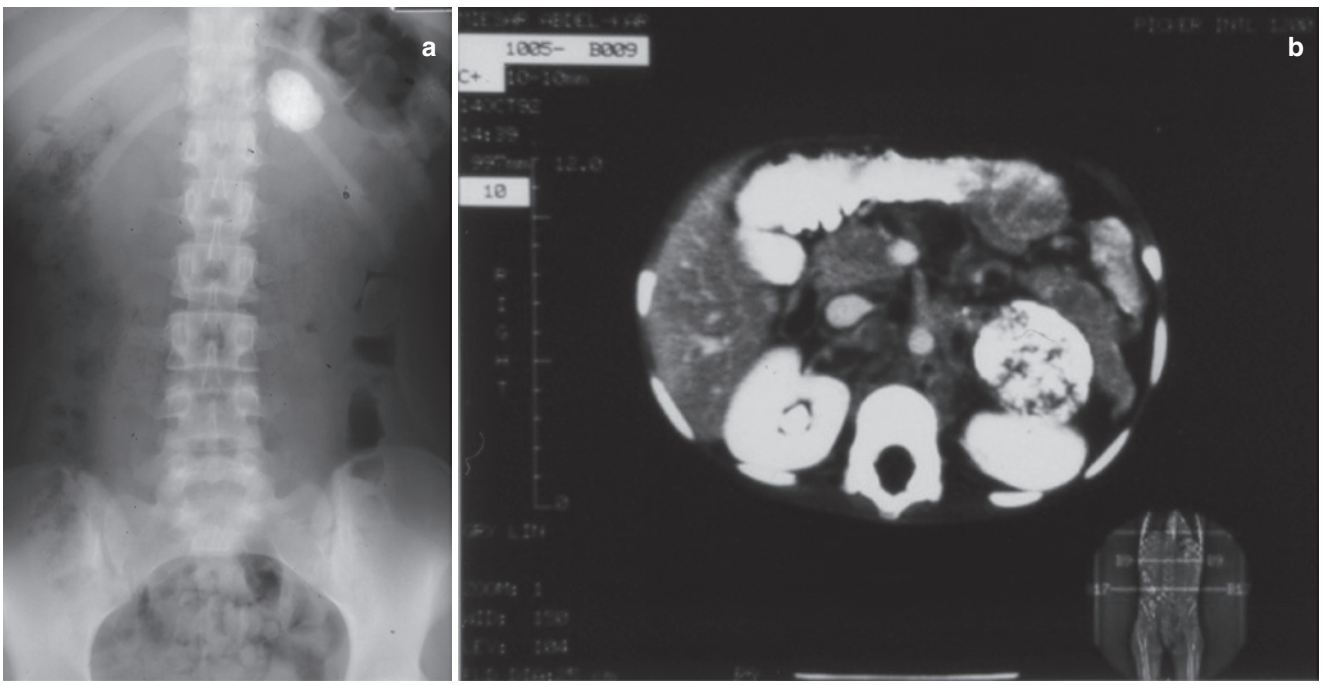

Fig. 4.39 (**a**) Plain X-ray showing calcification in the left adrenal in an older child, a ganglioneuroma. (**b**) Neuroblastoma CT scan. (**c**) A series of MRI images showing an extra adrenal neuroblastoma arising from the organ of Zukerkandl. (**d**) MRI scan showing a suprarenal neuroblastoma. (**e**) Scan showing vascular entrapment of the renal vessels. High-risk neuroblastoma. (**f**) Scan showing high-risk neuroblastoma. (**g**) I-MiBG scan Stage IV neuroblastoma. (**h**) I-MiBG scan Stage IV neuroblastoma

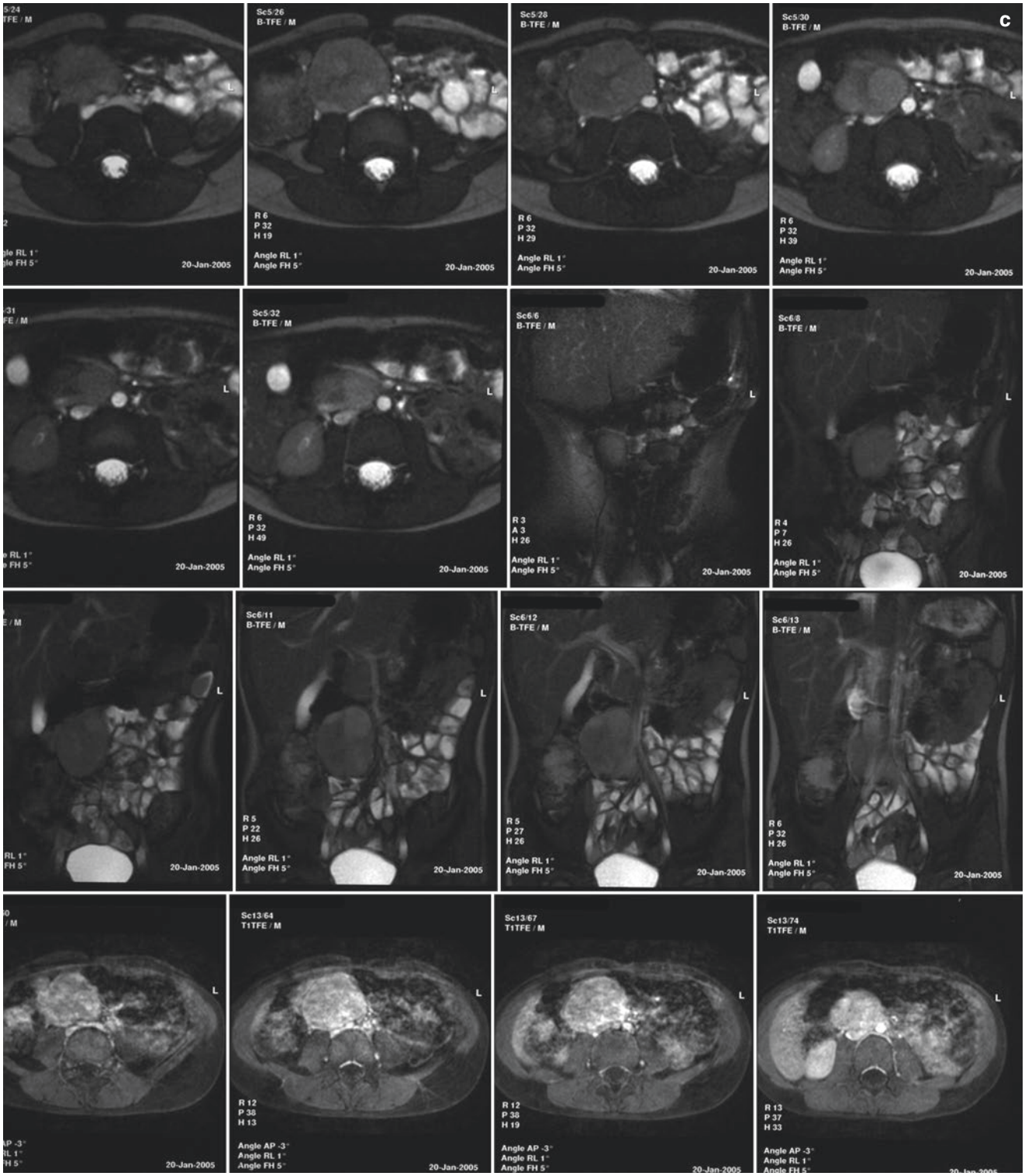

Fig. 4.39 (continued)

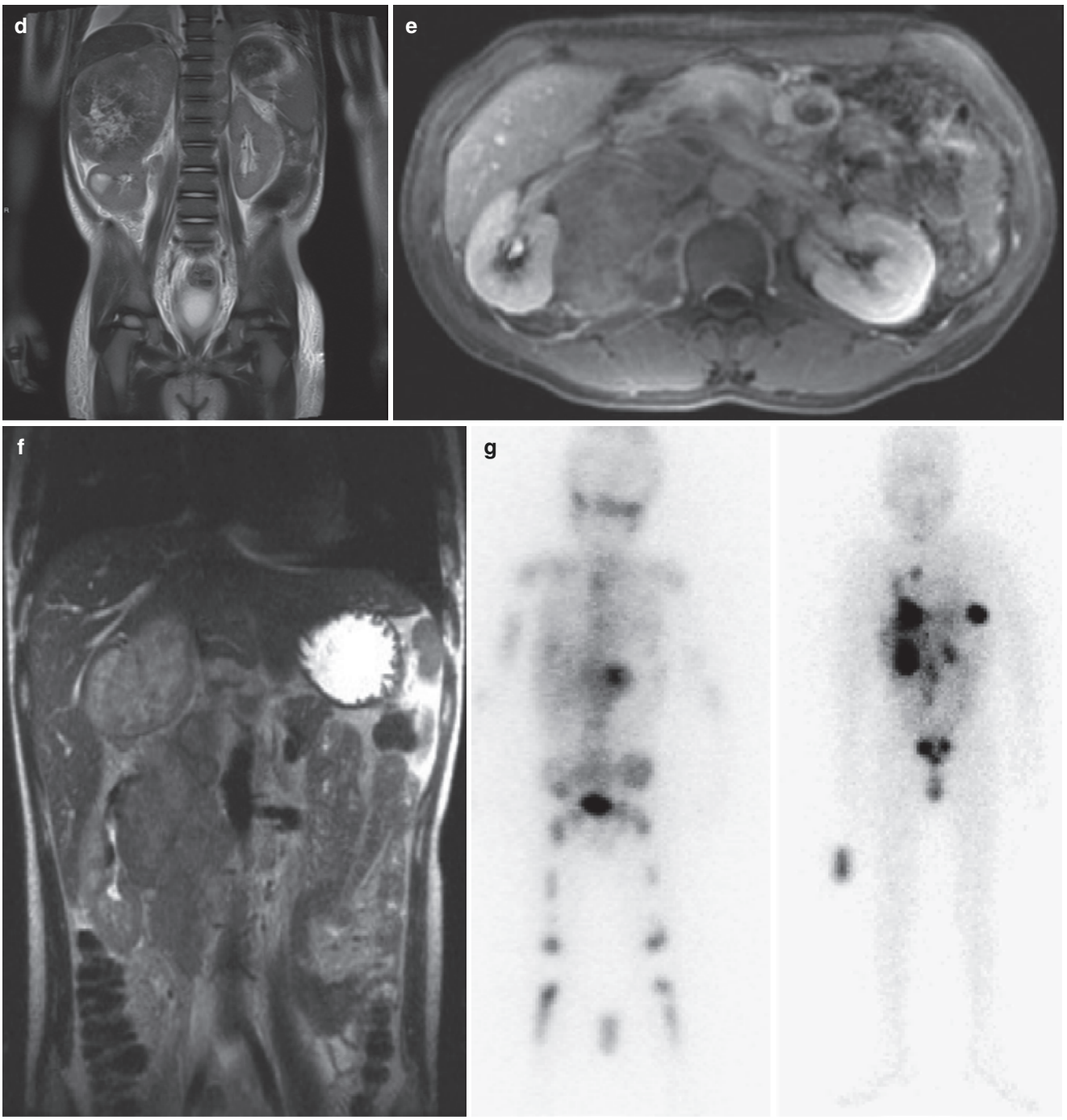

Fig. 4.39 (continued)

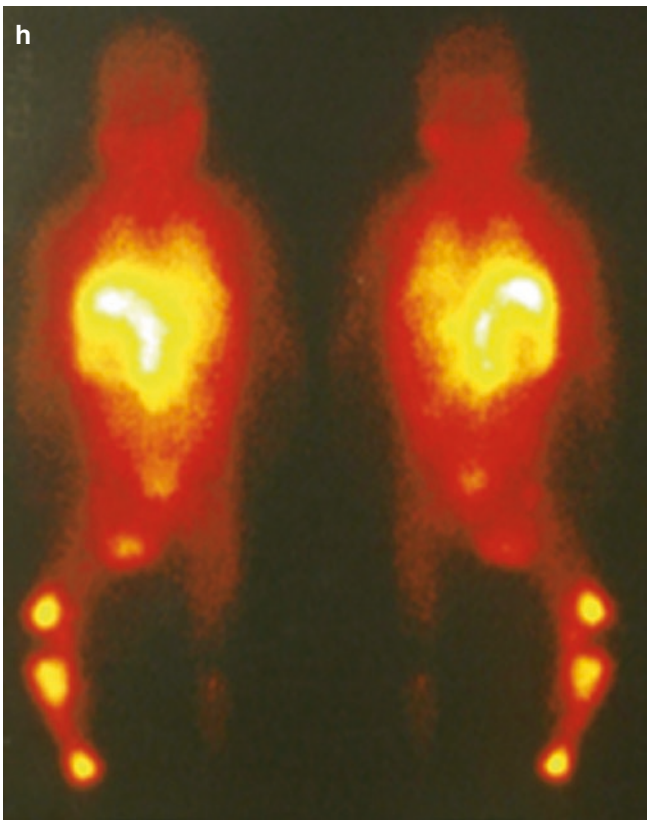

Fig. 4.39 (continued)

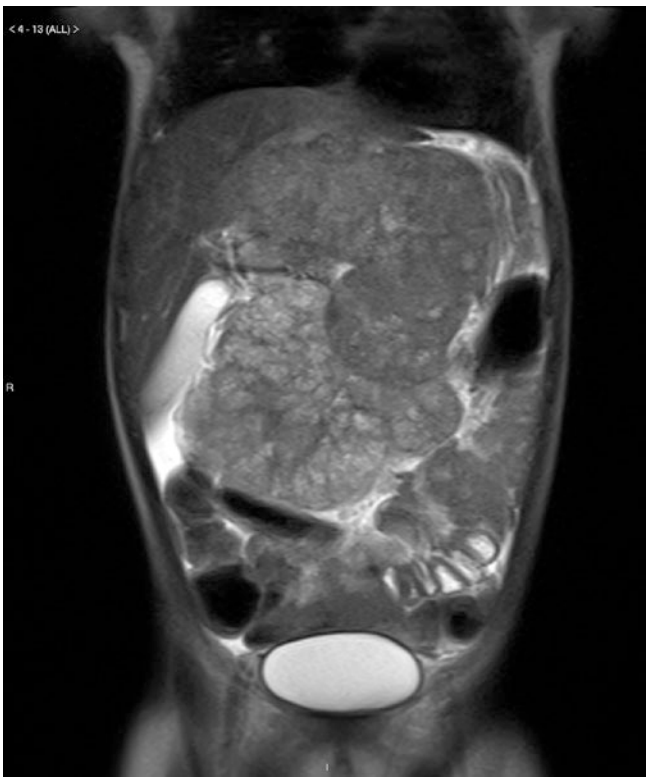

Fig. 4.40 MRI scan showing an extensive tumour arising from the liver. Hepatoblastoma

haemorrhage, necrosis, and calcification. In some cases, there may be diffuse infiltration of liver parenchyma. Larger lesions are highly vascular, with visible feeding vessels, enlarged hepatic artery and vein, and high flow on colour Doppler. Doppler flow can be variable with arterial and venous components, and in larger lesions there may be Doppler evidence of AV shunting.

On CT, enhancement patterns are similar to those seen in adult haemangiomata with centripetal "filling in" of the lesion. MRI is the more commonly used modality in the paediatric population, particularly the neonate. Lesions are low signal on T1 (with the exception of areas of haemorrhage) and markedly hyperintense on T2-weighted imaging. Vascular flow voids are demonstrated in or adjacent to the lesion. There is intense contrast enhancement with centripetal filling on dynamic imaging.

Angiography is now reserved for cases where embolic treatment is planned.

Liver haemangioma can also be imaged on scintigraphy, including red cells scans and sulphur colloid labelled technetium. These scans are no longer part of the routine diagnosis and assessment of lesions.

4.5.6 Haemangioendothelioma

A hypoechoic liver mass with or without hydrops may be demonstrated on antenatal sonography.

Plain radiographs of the abdomen may show hepatomegaly or a mass, and in some cases, evidence of fine calcifications. In the case of larger lesions, chest radiography may demonstrate evidence of secondary congestive cardiac failure (Fig. 4.42a).

On sonography, small multifocal lesions are uniform and hypoechoic. Larger lesions may be heterogeneous with haemorrhage, necrosis, and calcification. In some cases, there may be diffuse infiltration of liver parenchyma. Larger lesions are highly vascular, with visible feeding vessels, enlarged hepatic artery and vein, and high flow on colour Doppler. Doppler flow can be variable with arterial and venous components, and in larger lesions there may be Doppler evidence of AV shunting (Fig. 4.42b, c).

4.5.7 Polyposis Coli/Polyps (Fig. 4.43a)

Intestinal polyps: A solitary rectal polyp is a common cause of bleeding from the rectum. This low polyp is easily felt on digital rectal examination. The polyp is a granulomatous hamartoma of the mucous membrane, which becomes pedunculated by defaecation and may protrude at the anus like rectal mucosa prolapse. Polyps high in the rectum and lower colon require sigmoidoscopy under general anaesthesia and may be removed by snaring. Occasionally, juvenile

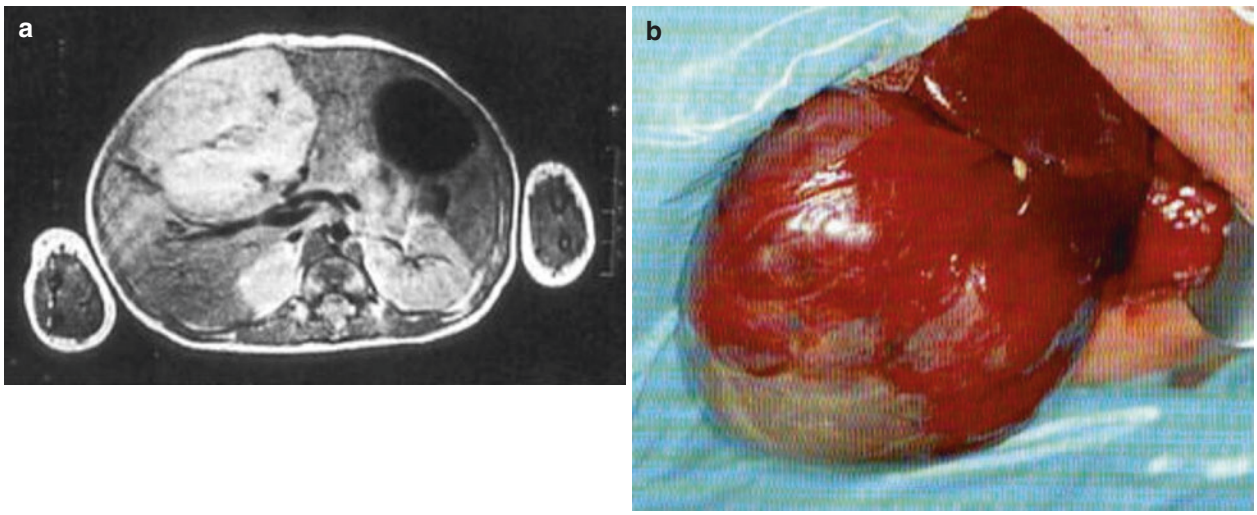

Fig. 4.41 (**a**, **b**) Haemangioma: liver

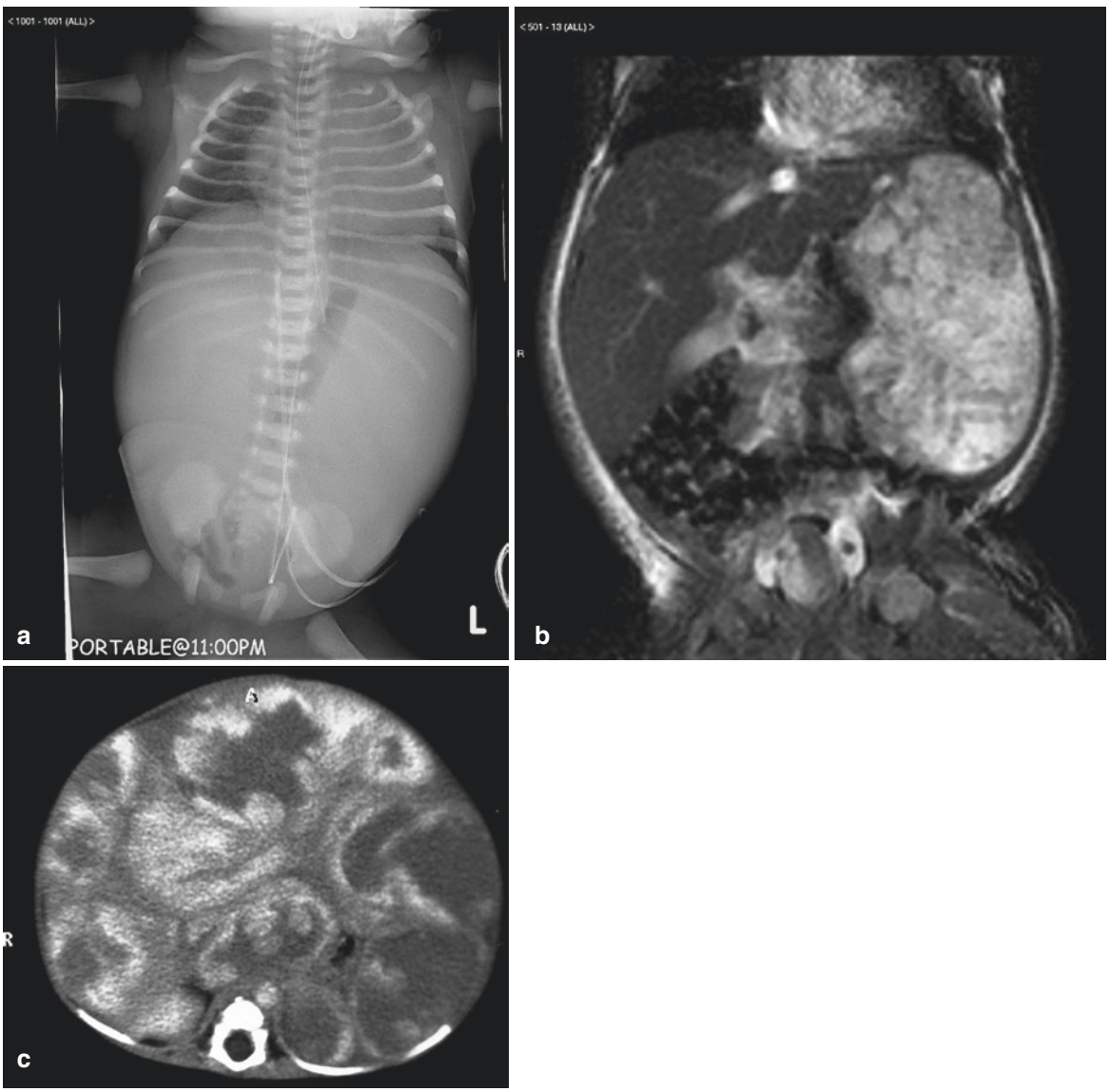

Fig. 4.42 (**a**) Plain X-ray with stomach displaced medially from haemangioendothelioma. (**b**) Haemangioendothelioma involving the left lobe of the liver (**c**) Scan showing the liver in cross-section with a typical uptake of contrast in the periphery of each tumour and poor uptake in the centre. Haemangioendothelioma

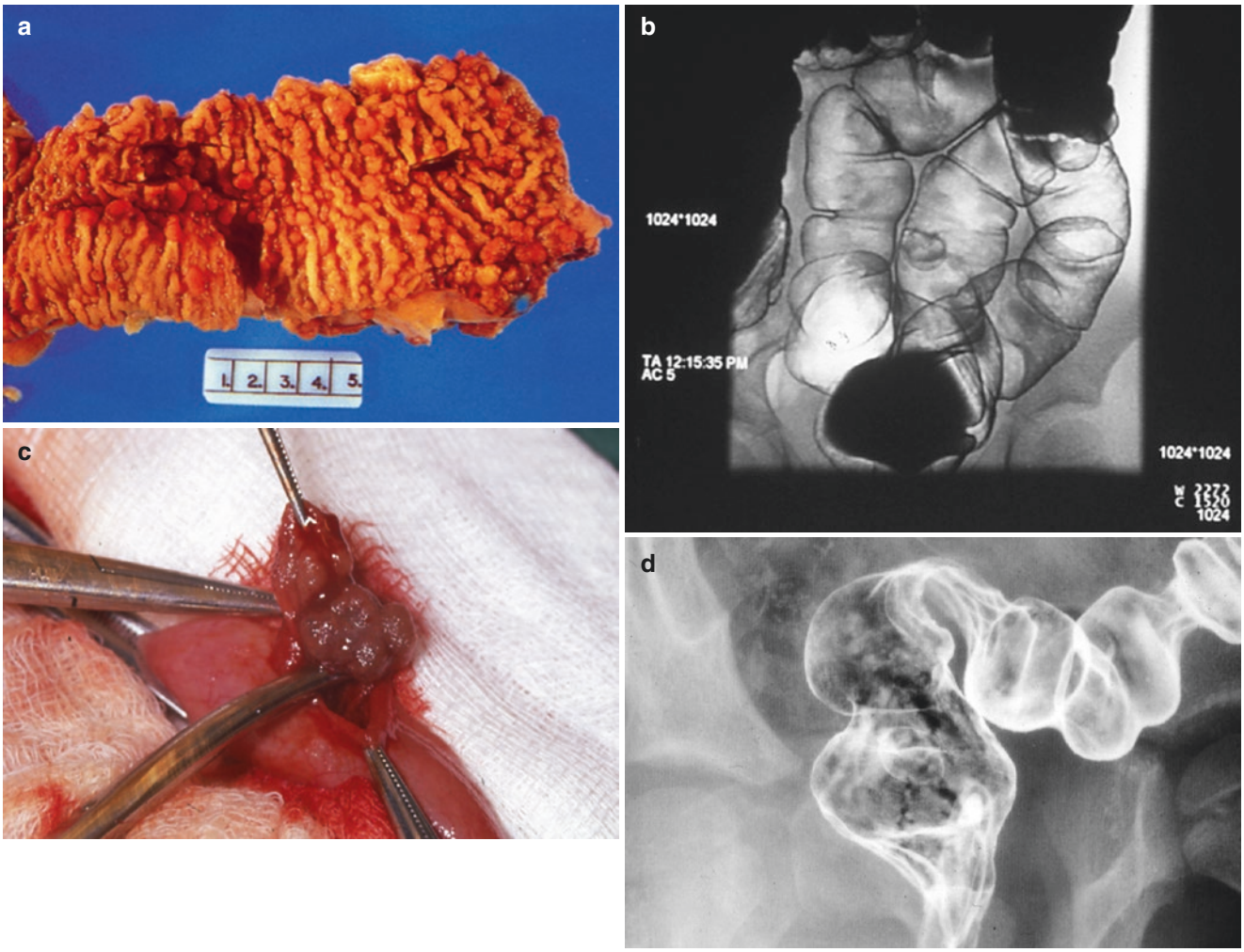

Fig. 4.43 (**a**) Polyposis coli. Operative specimen showing a carpet of polyps arising from the mucosal surface in the opened bowel. (**b**) Colonic polyp Solitary polyp seen on a double contrast examination. (**c**) Colonic polyp delivered on a long stalk after an enterotomy carried out. (**d**) Contrast inserted into the rectum demonstrating a solitary polyp

polyps are multiple and may be demonstrated by double contrast studies. True familial polyposis is very rare under the age of 12 years, but the rectum and colon can be carpeted with polyps that histologically are papillomas or adenomas of the adult type. This disease is usually carried as a Mendelian dominant and cancer of the colon develops in young adult life. Peutz-Jegher's syndrome is a familial condition in which polyps of the small intestine are accompanied by brown pigmentation of the lips and buccal mucosa. Symptoms and signs include repeated episodes of abdominal pain due to transient intussusceptions, blood loss from the intestinal tract, and anaemia. Polyps may be demonstrated incidentally on fluoroscopic contrast examinations as mural filling defects, but radiology is not used in the diagnosis or follow-up of lesions (Fig. 4.43b–d).

4.5.8 Teratoma/Sarcoma (Fig. 4.44a)/Germ Cell

On sonography, mature ovarian teratomas are complex and appearances reflect the pathological constituents of the individual lesion with echogenic, hypoechoic, and anechoic elements. The most characteristic appearance is of a hypoechoic "cystic" mass with an echogenic nodule. The presence of calcification and hair may cause posterior acoustic shadowing. There may be fat and fluid levels within the mass (Fig. 4.44b).

On CT, the presence of fat attenuation, hair, and calcium (occasionally with recognisable structures such as teeth) within the lesion is diagnostic. On MRI, fat signal and fat suppression can be demonstrated, and calcium-containing

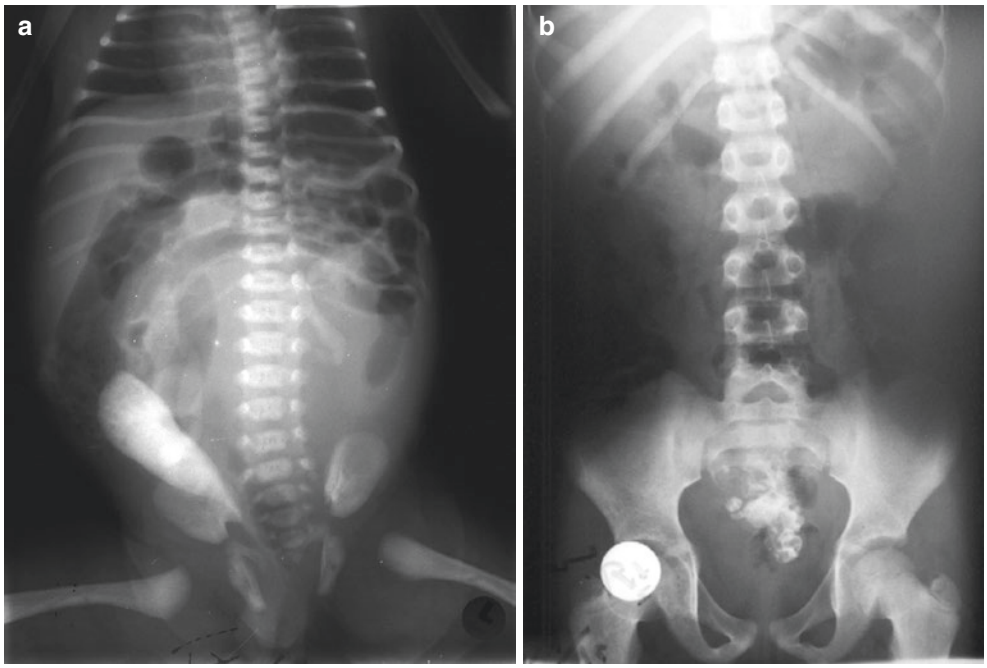

Fig. 4.44 (**a**) Plain X-ray of the abdomen showing a large pelvic sarcoma displacing all the pelvic contents by a pelvic sarcoma. There is contrast that has been inserted into the bladder to show how displaced it is. (**b**) Plain X-ray of the abdomen showing a well-defined pelvic calcified structure in an ovarian teratoma

structures appear low signal in T1- and T2-weighted sequences. Secondary features such as hydronephrosis from ureteric compression may be demonstrated on either modality.

Sarcomas of the genitourinary tract often present as abdominal masses, and plain X-rays show that a pelvic mass compresses the sigmoid colon and often causes intestinal obstruction. Imaging by CT scans and MRI scans demonstrate the origin of the tumour and its extent. Germ cell tumours arise from gonadal tissue but can also arise from extragonadal tissue and may be retroperitoneal or even extra pelvic. The malignant ones may produce a useful tumour marker, alpha-feto-protein (AFP). Screening by ultrasound, CT scans, and MRI scans demonstrate this mass, and histology confirms the tumour.

4.5.9 Hamartoma

Mesenchymal hamartoma of the liver may be visualised on plain radiography as a right upper quadrant mass/hepatomegaly.

Sonographic appearances are complex and variable, from a hypoechoic septated cystic mass to an echogenic solid mass containing a few cystic areas. Solid areas are relatively hypovascular. On CT the lesions are hypodense, with water attenuation and some enhancement of the septal and solid elements.

On MRI, the cystic components show high T2 water signal and the solid components are relatively low signal on both T1- and T2-weighted imaging, compared to the surrounding hepatic parenchyma. As on CT, the septae and stromal elements show some enhancement following contrast administration (Fig. 4.45a–c).

4.5.10 Lymphoma

Sonography is often the initial abdominal investigation in patients with suspected or histologically proven lymphoma. It allows assessment of nodes, including retroperitoneal lymphadenopathy, solid organ involvement, both focal and diffuse, including enlargement of the spleen. It also allows assessment of the mesentery, bowel wall, ascitic fluid, and peritoneal deposits present in T cell (Burkitt's) lymphoma. It is the best method to assess testicular involvement.

Abdominal CT can determine solid organ involvement and provide an assessment of lymphadenopathy. MRI imaging, both abdominal T2-weighted sequences and contrast enhanced T1-weighted imaging, demonstrates solid organ involvement and mesenteric peritoneal disease, but whole body T2-fat-saturated (e.g., STIR) imaging is increasingly used to assess lymphadenopathy burden, including skeletal lesions (Fig. 4.46).

Technetium 99m bone scintigraphy may be used to assess bony involvement in patients with bony pain or abnormal bone biochemistry.

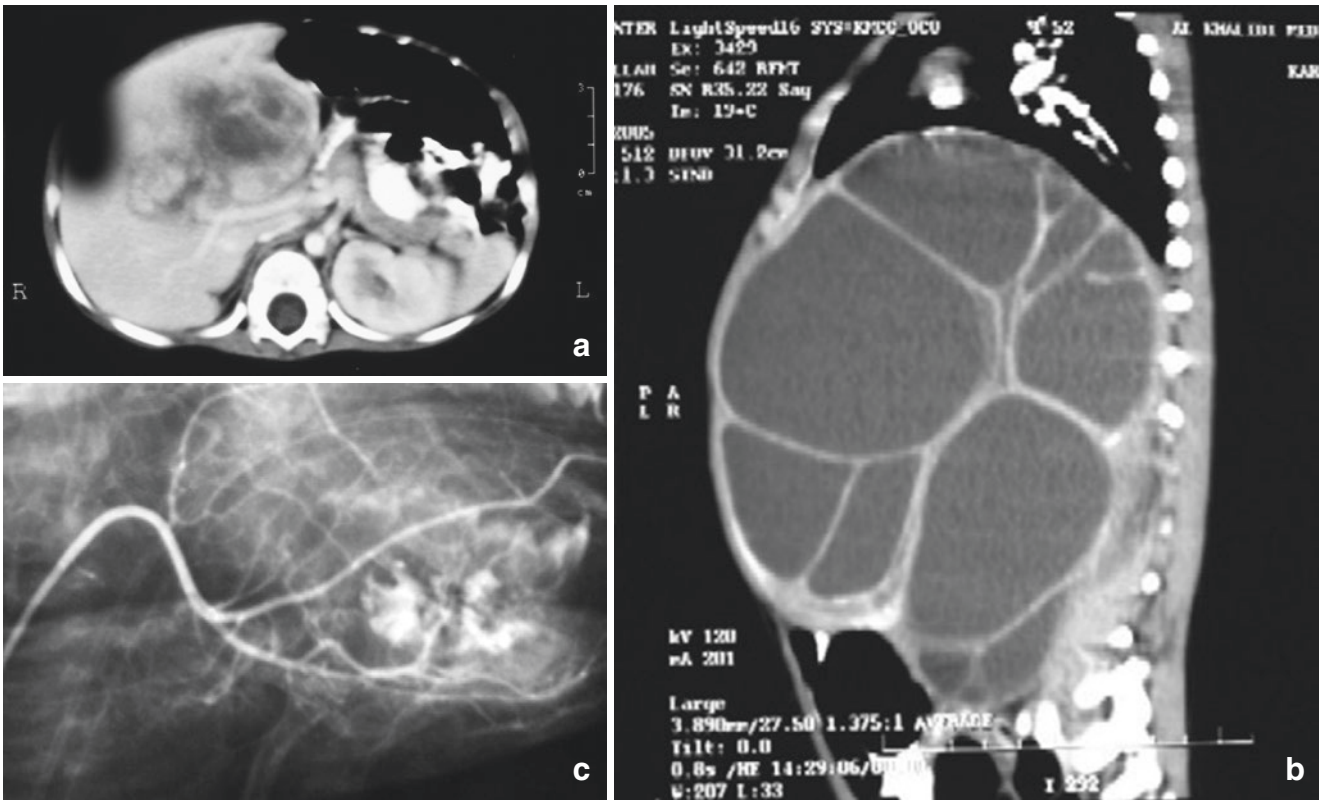

Fig. 4.45 (**a**) CT scan showing a hepatic hamartoma. (**b**) CT scan of a hepatic hamartoma with multiple cysts. (**c**) Hepatic hamartoma, multiple cysts, angiogram

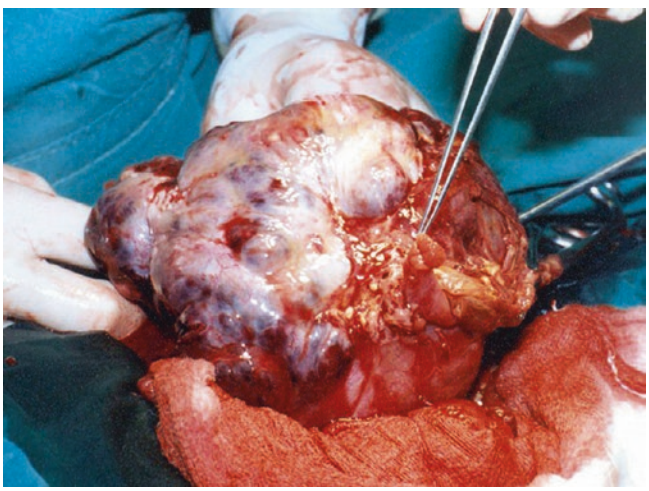

Fig. 4.46 Operative picture of an abdominal lymphoma

4.5.11 Burkitt's Tumour

Sonography is often the initial abdominal investigation in patients with suspected or histologically proven lymphoma. It allows assessment of nodes, including retroperitoneal lymphadenopathy, solid organ involvement, both focal and diffuse, including enlargement of the spleen. It also allows assessment of the mesentery, bowel wall, ascitic fluid, and peritoneal deposits present in T cell (Burkitt's) lymphoma. It is the best method to assess testicular involvement (Fig. 4.47a–c).

Abdominal CT can determine solid organ involvement and provide an assessment of lymphadenopathy. MRI imaging, both abdominal T2-weighted sequences and contrast enhanced T1-weighted imaging, demonstrates solid organ involvement and mesenteric peritoneal disease, but whole body T2-fat-saturated (e.g., STIR) imaging is increasingly used to assess lymphadenopathy burden, including skeletal lesions.

Technetium 99m bone scintigraphy is used to assess bony involvement in patients with bony pain or abnormal bone biochemistry.

4.5.12 Neurofibromatosis (Von-Recklinghausen's Disease)

Neurofibromatosis in the abdomen often presents with signs of obstruction from multiple ganglioneuromata affecting the intestine. These can grow to enormous size and even turn

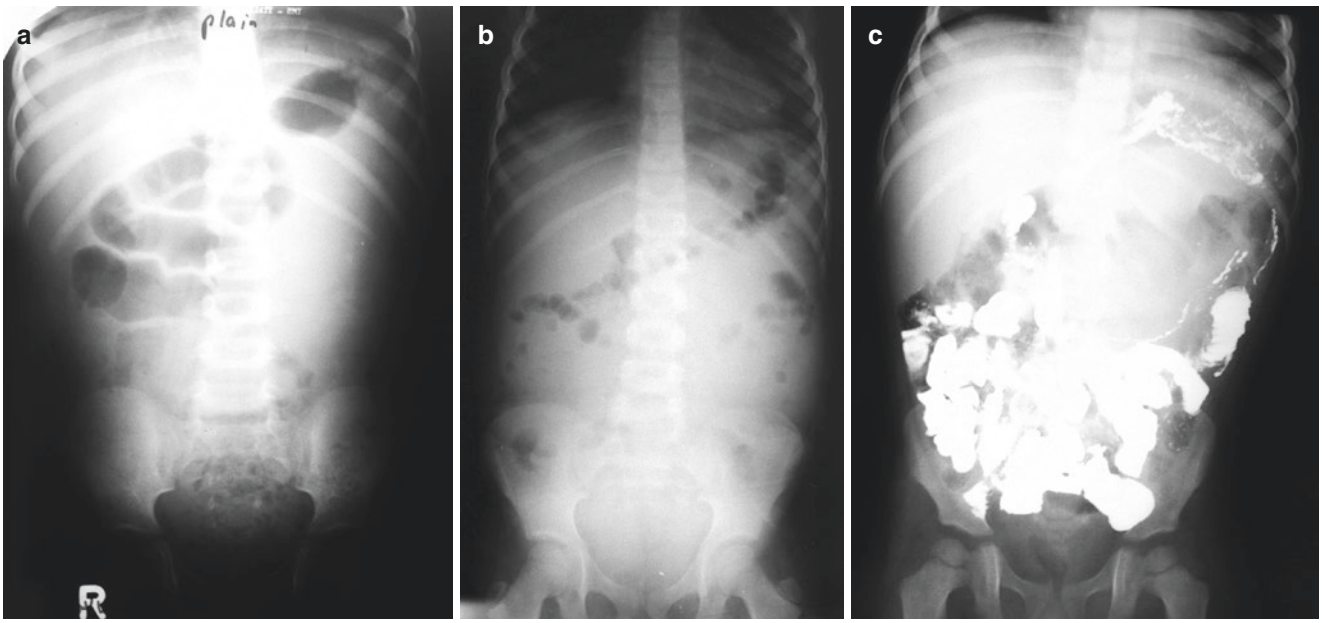

Fig. 4.47 (**a**) Plain X-ray showing a tumour mass in the abdomen. Burkitt's lymphoma. (**b**) Plain X-ray of Burkitt's lymphoma showing little gas in the bowel due to compression of the lymphoma. (**c**) Barium meal and follow through in Burkitt's lymphoma

malignant as neurofibrosarcoma. CT scans may demonstrate the multiple ganglioneuromata within the wall of the intestine growing relentlessly in all directions.

Neurofibromatosis is a phakomatosis with manifestations in the skin, eye, bone, soft tissues, and the central nervous system. As in tuberous sclerosis the earliest sign of neurofibromatosis is pigmentary change on the skin. Café au lait spots or patches are irregularly shaped macules and are often present at or shortly after birth and may increase in size and number with age. This cutaneous manifestation is virtually pathognomonic of neurofibromatosis. Therefore, a diagnosis of neurofibromatosis should be considered in children who have six or more café au lait spots greater than 0.5 cm in diameter. Other cutaneous manifestations are the presence of pedunculated neurofibromas.

This hereditary disease is also transmitted as a dominant characteristic. It is characterised by multiple tumours of the peripheral and central nervous system, café aulait spots, and various lesions of the vascular system and viscera. Two gene defects have been identified; the first, on chromosome 17, predisposes to the cutaneous features and peripheral nerve abnormalities, and the second, on chromosome 22, is associated with central nervous system tumours and acoustic neuromas. In childhood a progressive severe kyphoscoliosis in association with multiple caféaulait spots on the skin is a common mode of presentation. In some cases, palpable neurofibromata are to be detected along the course of subcutaneous nerves. The brain may be a site of focal pathology and various types of tumour (glioma, ependymoma, meningioma) may occur in the brain, spinal cord, or spinal nerve roots. Approximately 10–20% of patients manifest with seizures, intellectual deficit, and speech and motor delay.

4.5.13 Pheochromocytoma

This is very rare in childhood. The tumour may arise in the adrenal medulla (pheochromocytoma) or from chromaffin cells elsewhere such as the organ of Zuckerkandl (paraganglioma). In children both adrenals may be simultaneously affected. In some cases, the tumour is locally malignant. There is also an association in the adult with thyroid medullary carcinoma and multiple true neuromata.

In some cases, hypertension occurs in paroxysms that coincide with the liberation of the catecholamines by the tumour. These cause headaches, palpitations, and epigastric pain. Sweating may be profuse, and the child becomes prostrated. They may have a characteristically "startled" expression with wide palpebral fissures and dilated pupils. More often, however, the hypertension becomes chronic and produces retinal changes (papilloedema and exudates), cardiomegaly, and proteinuria. There may be hyperglycaemia and glycosuria. The intravenous pyelogram is usually normal unless the tumour itself is obstructing the ureter. Whenever recurrent or chronic hypertension is documented in the paediatric patient, pheochromocytoma should be considered in the diagnosis.

In every case it is essential to prove the diagnosis by demonstrating an excessive urinary excretion of VMA

(3-methoxy-4-hydroxymandelic acid) over 25 mmol/24 h; 5 mg/25 h. The site of the tumour can be defined by MRI computed tomography, or ultrasonography. The use of pharmacologic agents such as phentolamine (Rogitine) and histamine to aid in diagnosis of pheochromocytoma should be reserved for cases in which repeated measurements of catecholamines and their metabolites are normal and suspicion of pheochromocytoma is high.

Although the vast majority of pheochromocytomas (around 90%) are adrenal, they have the potential to arise anywhere within the sympathetic nervous system.

Appearances on sonography are heterogeneous with hypoechoic cystic areas, echogenic haemorrhage, and calcifications.

On CT, smaller tumours can be uniform in attenuation, but only rarely contain significant fat (and thus usually have Hounsfield units measured at >10). Larger tumours can be heterogeneous with cystic, necrotic, and haemorrhagic areas. Typically, enhancement of solid areas post contrast is avid, with lower washout rates than adenomas on dynamic studies, although care should be taken in the interpretation of findings if tumours are haemorrhagic or necrotic. Although risks with modern low osmolar contrast agents are low, in general if a pheochromocytoma is suspected clinically pre-imaging, contrast scans are avoided, and another modality used.

On MRI, pheochromocytomas are characteristically low signal on T1 and high signal on T2-weighted imaging (with higher signal on fat supressed T2 sequences) and enhance avidly with gadolinium contrast. In and out of phase imaging may help to differentiate from fat containing adenomas, but the technique is not infallible and overall MR appearances overlap significantly with other adrenal lesions. The presence of metastatic spread is the only reliable imaging criteria for malignancy.

As with neuroblastomas, I123MIBG scans may be used to identify adrenergic tumours. This is highly specific, but of limited sensitivity

4.6 Acquired

4.6.1 Portal Hypertension

On sonography the portal vein may be dilated and demonstrate abnormal flow in Doppler examination, with reversal of the normal hepatopetal flow a late and pathognomonic finding.

On sonography, CT, and MRI, the dilation of the portal vein may be accompanied by dilation of the mesenteric veins and abdominal wall veins, recanalization of the umbilical vein, and the formation of porto-systemic collaterals, including gastric and oesophageal varices. There may be splenomegaly and ascites (Fig. 4.48a–d).

Other findings depend on the aetiology of the portal hypertension, whether due to intrinsic liver disease, internal or external portal vein thrombosis, or obstruction. There may be changes of cirrhosis or fibrosis of the liver on ultrasound, with a shrunken irregular liver, other parenchymal disorders including polycystic disease, or cavernous transformation of the intrahepatic portal venous system following previous thrombus and occlusion.

Although rarely performed in children, radiological placement of a porto-systemic shunt may be a treatment option (trans-jugular intrahepatic porto-systemic shunts or TIPS).

4.6.2 Pyloric Stenosis (Fig. 4.49a, b)

Plain abdominal radiography may demonstrate a dilated gas-filled stomach, although this is a non-specific finding that can be replicated by air swallowing.

A contrast meal is now rarely employed in making the diagnosis of pyloric stenosis. Gastric dilation, marked peristalsis with delayed/obstructed pyloric opening, and a thin "string-like" pyloric canal are demonstrated.

Ultrasonography is now the modality of choice and is both sensitive and specific in making the diagnosis of pyloric stenosis. The length of the pyloric canal and the thickness of the pyloric muscle is assessed and should be <15 and <3 mm respectively. Pyloric opening can also be determined by gently filling the stomach with fluid. This may be useful in the presence of pylorospasm. In low-birth-weight and premature infants with pyloric stenosis, the length of the pyloric canal may not reach the 15 mm criteria (Fig. 4.49a, c).

4.6.3 Intussusception

Intussusception is a telescoping of one portion of the bowel into the adjacent segment. Most cases of intussusception (over 60%) occur during the first year of life, but the condition is rarely seen under the age of 1 month. The peak incidence is between the fourth and ninth months, and boys are more frequently affected than girls (3:2). In infants there is rarely any demonstrable cause, and a change from milk to a more solid diet may alter peristalsis in such a way as to initiate an intussusception. Infective causes have been sought but there is no clear pathogen that causes the intussusception. Enlarged mesenteric glands are almost always found at operation, and although the glands may be secondary to the intussusception, they may also be associated with a preceding lymphoid hyperplasia from infection. Only rarely is a definite mechanical factor found to be responsible for initiating the invagination. In older children, a Meckel's diverticulum or a polyp may be the apex and lead point of an intussusception,

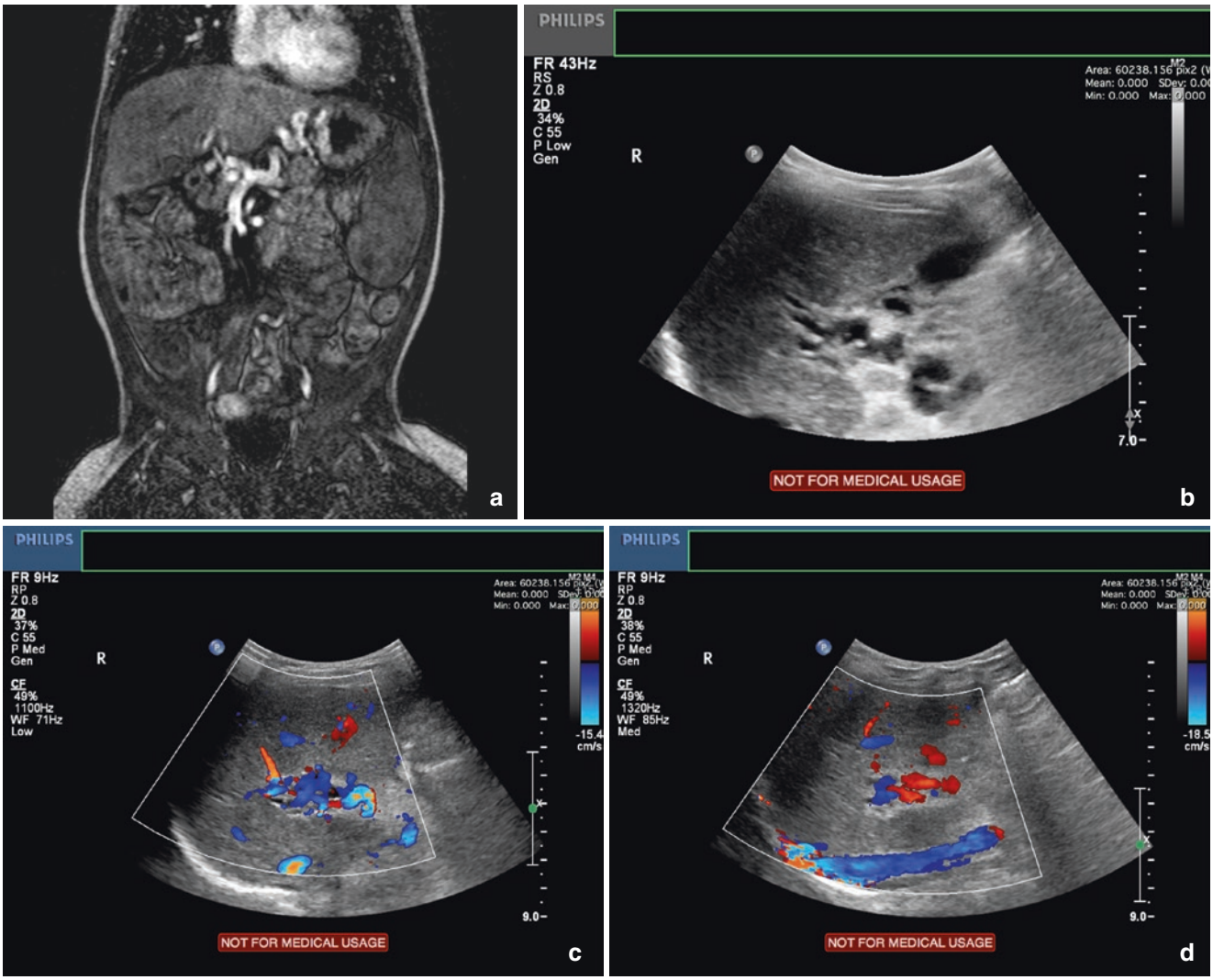

Fig. 4.48 (**a**) Portal hypertension-MRI showing dilated portal vessels and an enlarged spleen. (**b**) Ultrasound of portal hypertension showing dilated portal vessels. (**c**) Ultrasound of portal hypertension. Doppler scan showing dilated very prominent tortuous portal venous system following previous portal thrombosis. (**d**) Ultrasound of portal hypertension. Another view of Fig. 4.49c

but definite anomalies such as Meckel's diverticulum are found in only 2% of patients. Other underlying causes include angiomas, lymphoma, and intestinal haematoma. The peak incidence in the U.K. is in the winter months. There is no relationship between intussusception and seasonal diarrhoea, but upper respiratory infections commonly precede the onset of intussusception. The ileo-ileal and colo-colic type of intussusception are uncommon in childhood, and 90% are ileo-colic or ileo-caecal. Where the mesentery of the caecum and ascending colon has failed to become obliterated, the caecum is mobile and the apex of the intussusception may reach the sigmoid or even the rectum, where it may be felt by digital rectal examination. As the ileum advances through the ileo-caecal valve, its mesentery soon becomes constricted. As a consequence, the venous return is obstructed, causing oedema and congestion. The obstruction of blood supply may be followed by gangrene of the intussuscepiens. Obstruction of the lumen of the bowel is a consequence of intussusception, but symptoms and signs usually result in the infant or child presenting before intestinal obstruction is clearly established.

The patient is usually a healthy vigorous male infant of 3 months or older who was previously well. Onset is dramatic, as the child, without warning, screams, drawing up his knees as though in abdominal pain, and becomes pale. The attack ceases as suddenly as it began, and in a few minutes the child seems at peace and may even pass a stool and fall asleep. Parents are reassured by the apparent quick recovery and may postpone seeking medical advice. After a short lapse of time, varying from minutes to several hours, a further similar attack of colic occurs. This continues recurring at shorter and shorter intervals. A feature in these children is the pallor during spasms, probably due to a vaso-vagal reac-

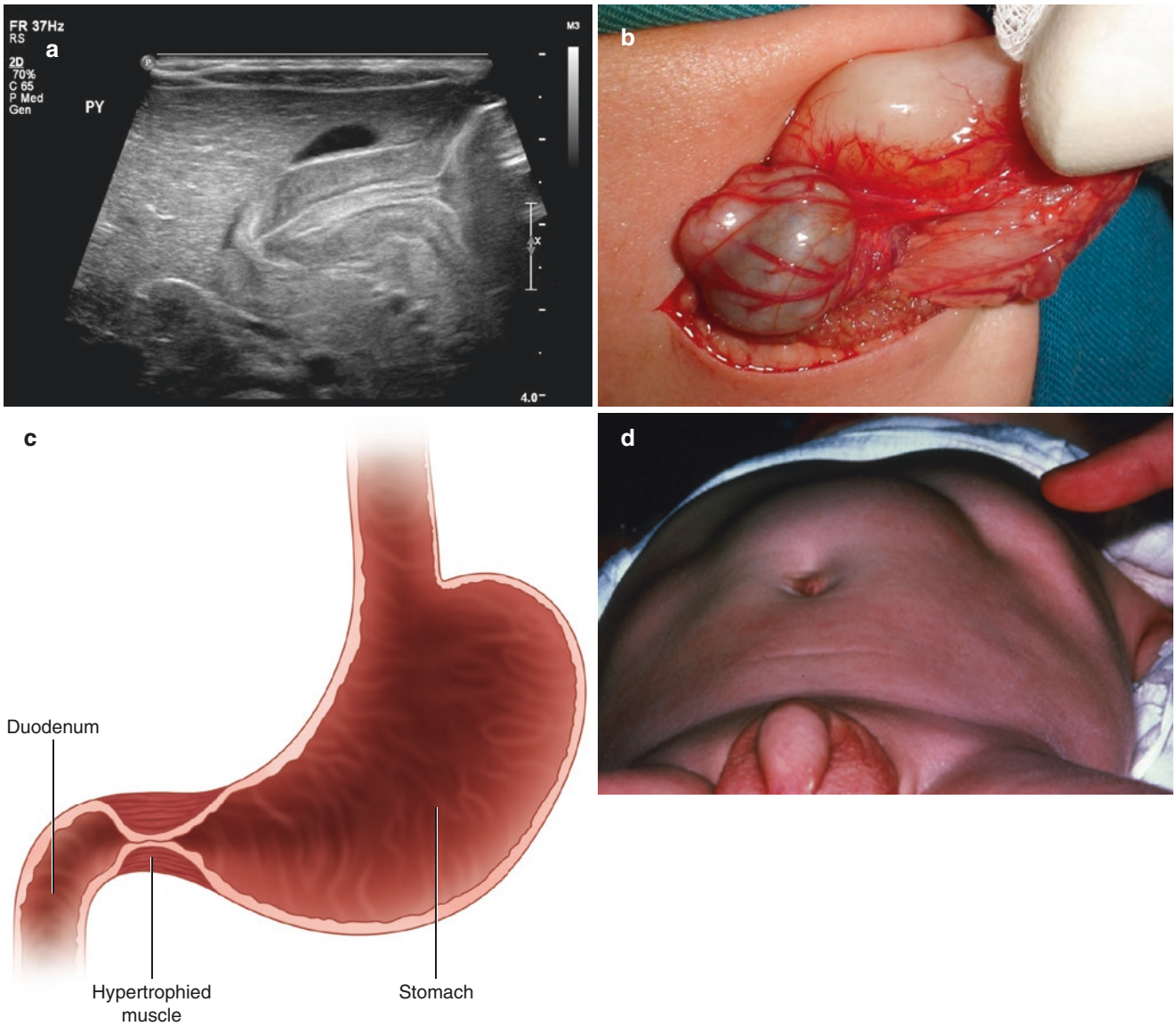

Fig. 4.49 (**a**) Pyloric stenosis. A longitudinal ultrasound examination showing elongation of the pylorus and thickening of the pyloric muscle. (**b**) Operative photograph of pyloric tumour in pyloric stenosis. (**c**) Pyloric stenosis. Diagrammatic representation. (**d**) Infant with hypertrophic pyloric stenosis showing visible peristalsis wave passing from left to right

tion. Vomiting is frequent in these episodes. Pain is not always a constant feature. The other common sign is the passage of mucus and blood per rectum. If the diagnosis is delayed, signs of intestinal obstruction supervene. Abdominal examination often reveals a sausage-shaped mass to the right of the umbilicus or in the right hypochondrium. There is no peritonism but tenderness or guarding directly over the mass may make its delineation difficult. Rectal examination demonstrates no faeces in the lumen, but blood and/or mucus is often present on the examining finger. The most important factor causing delay in diagnosis is the association of the idea of intestinal obstruction with intussusception. The triad of colic, vomiting, and abdominal distension are late signs. In the older child, the picture is less dramatic than in infants. Severe colic is not an outstanding feature and blood may not be passed per rectum for hours or even days after onset. The child usually experiences periodic attacks of colic and shows little interest in food. Between attacks the abdomen is soft, and no mass may be felt.

Diagnosis may be made on the history alone. Plain X-rays of the abdomen may reveal a soft tissue mass with signs of intestinal obstruction such as dilated loops and fluid levels. Ultrasound examination of the abdomen is now the modality of choice for diagnosis. An air or fluid enema will achieve reduction of the intussusception in 60–70% of patients. It is important when this procedure is carried out to ensure that

there is a backflow of air into the small bowel so that there is complete reduction of the intussusception. The differential diagnosis includes volvulus, which may present a similar picture, but there is seldom remission of pain. Palpation of the abdomen reveals an ill-defined swelling, usually in the central area. Ultrasound should differentiate this from intussusception. Gastroenteritis is perhaps the commonest cause of difficulty, but the onset is less dramatic and the colic rarely severe. The rectum in this case contains loose faeces or foul-smelling watery stools. Temperature is usually elevated, and vomiting may be a prominent feature. Palpation of the abdomen of a child with gastroenteritis reveals no tumour, but a generalised tenderness may be present. On auscultation there is increase in bowel sounds. In older children (aged 3 years or more), Henoch Schonlein Purpura may cause difficulty in the differential diagnosis. Blood in the rectum may be accompanied by loose motions, and there is evidence of haemorrhagic effusions elsewhere. A child with Henoch Schonlein Purpura may develop haemorrhage in the wall of the bowel and show signs of intussusception and indeed intestinal obstruction.

Recurrent intussusception occurs in 2% of patients with intussusception. The interval between the intussusceptions varies from 24 h to several years. Peutz-Jegher's Syndrome, which is the presence of small intestinal polyps associated with pigmentation of the buccal mucosa, may be a cause of recurrent intussusception.

Plain abdominal radiography may demonstrate a paucity of gas in the right iliac fossa, sometimes with a visible soft tissue mass and evidence of small bowel obstruction. Plain films, however, may be entirely normal or show non-specific gaseous dilation, and do not exclude intussusception. They can be useful to assess for the presence of perforation, although this is a rare complication at presentation (Fig. 4.50a–c).

Intussusception may be demonstrated on any cross-sectional imaging modality, but the modality of choice for the diagnosis and assessment of intussusception in a paediatric setting is ultrasound (Fig. 4.50d, e). The classical appearance of an intussusception is of a complex mass with a "doughnut" appearance containing layer of bowel wall and mesentery, often including lymph nodes. Most commonly an ileocolic intussusception is visualised in the right upper quadrant of the abdomen inferior to the liver; however, it may be demonstrated anywhere along the extent of the large bowel from the right iliac fossa to the left iliac fossa and pelvis.

4.6.4 Pneumoperitoneum/Calcification

Plain abdominal and chest radiographs may demonstrate a number of signs of pneumoperitoneum. The classic radiographic sign of "air under the diaphragm" is appreciated on the erect chest X-ray. On supine abdominal films, gas collects in the upper abdomen over the liver as a lucent "football sign" and under the diaphragm, making it appear continuous over the midline. Gas may also outline peritoneal ligaments (particularly the falciform ligament) and be seen on both sides of bowel wall as "Rigler's sign,"Small amounts of free gas can be difficult to appreciate on supine films; in neonates and critical care situations where an erect chest film is not an option, therefore, a left decubitus or lateral shoot through film may demonstrate small locules of intraperitoneal gas (Fig. 4.51a, b).

Sonography may demonstrate locules of intraperitoneal gas with echogenicity and posterior shadowing, but absence of such findings does not exclude perforation, and this modality should not be used to exclude perforation. Similarly, pneumoperitoneum cannot be easily appreciated on MRI (Fig. 4.51c, d).

CT is the cross-sectional modality of choice for assessing suspected pneumperitoneum and demonstrating underlying bowel pathology.

Intra-abdominal calcification in the neonate is often due to an antenatal perforation of the bowel or volvulus or from a complicated meconium ileus. A chemical reaction results in calcification in utero.

Other types of calcification can be seen with tumours that are teratomas and contain all three germ cell layers and therefore can contain bone and cartilage. Calcification may also occur following a haemorrhage into an adrenal gland after a crisis (sepsis, shock, etc.), and healing takes place by calcification of this. Other infections, e.g., tuberculosis of the abdomen, can heal up over time and leave their mark with calcified lymph nodes. Some tumours have a tendency to produce calcification especially neuroblastoma (with calcific stippling) and more rarely Wilms' tumour and renal carcinoma.

4.6.5 Intestinal Obstruction (Fig. 4.52a, b)

On plain radiography, the most common finding in cases of intestinal obstruction is gaseous dilation of bowel, with absence of gas distal to the obstruction. The presence of valvulaeconniventes or haustra can help to identify the level of obstruction, although it should be noted that these defining features are not visualised in neonates. Sites of obstruction such as herniae may be demonstrated. In acidotic patients, generalised distension of bowel may result and can be misleading. Soft tissue masses or areas of gas paucity can guide further imaging (Fig. 4.52c, d).

In children, if a focal pathology such as intussusception, appendix mass, or tumour is suspected, sonography is the initial modality of choice. Masses, collections or post-operative complications may be assessed further on CT or MRI.

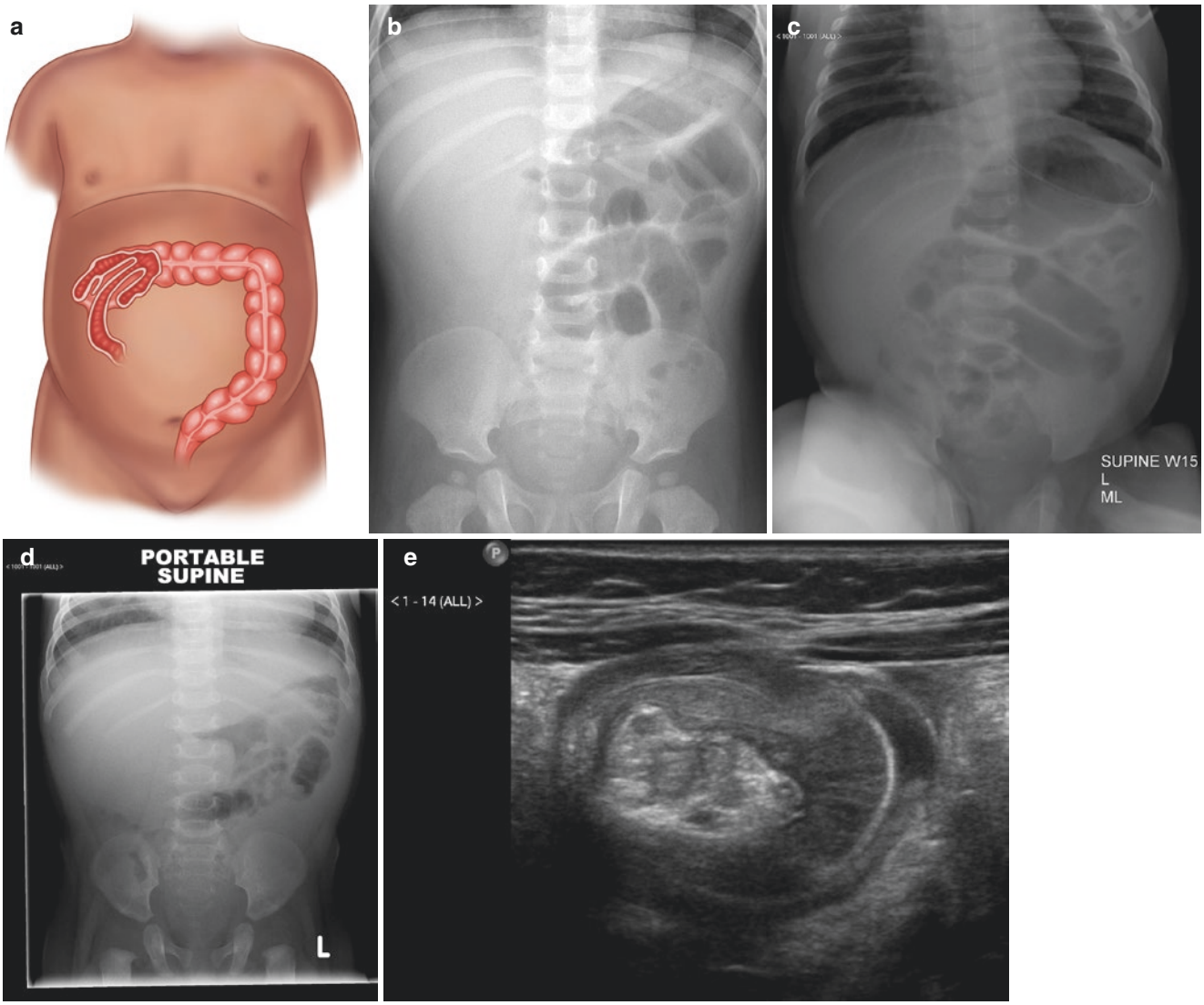

Fig. 4.50 (**a**) Intussusception. Diagram of ileo-colic intussusception showing the apex within the transverse colon in the right hypochondrium. (**b**) Intussusception. Plain X-ray showing a soft tissue mass in the right hypochondrium and an absence of gas in the right iliac fossa. Dilated loops of bowel seen on the left side of the abdomen suggesting obstruction. (**c**) Abdominal plain X-ray with paucity of gas in RIF intussusception. (**d**) Intussusception. Claw sign meniscus seen on air enema during an attempt to reduce an intussusception by insufflation. (**e**) Ultrasound of intussusception showing the target sign, doughnut sign or Mexican hat sign due to bowel lining the invaginated bowel in an intussusception

In neonates and patients with distal obstruction, fluoroscopic contrast examinations can determine site and sometimes cause of obstruction including malrotation, volvulus, bowel atresia, meconium ileus and plug syndromes, and Hirschsprung's disease.

4.6.6 Gallstones

Depending on their chemical composition, a proportion of biliary calculi may be detected/visible on radiography (Fig. 4.53a).

Sonography is the initial modality of choice. The morphology of the biliary tract and gallbladder, biliary tree dilation, and gallbladder wall thickening can be appreciated. Calculi are echogenic and mobile whilst in the gallbladder but may become impacted in the common bile duct. The duct cannot always be visualised adequately, particularly if the abdomen is gassy (Fig. 4.53b, c).

MR cholangiography, using highly T2-weighted, fat-saturated sequences that include three-dimensional datasets, has become the cross-sectional imaging modality of choice. Biliary tree anatomy and dilation are demonstrated. Calculi are demonstrated as filling defects within the biliary system (Fig. 4.53d–f).

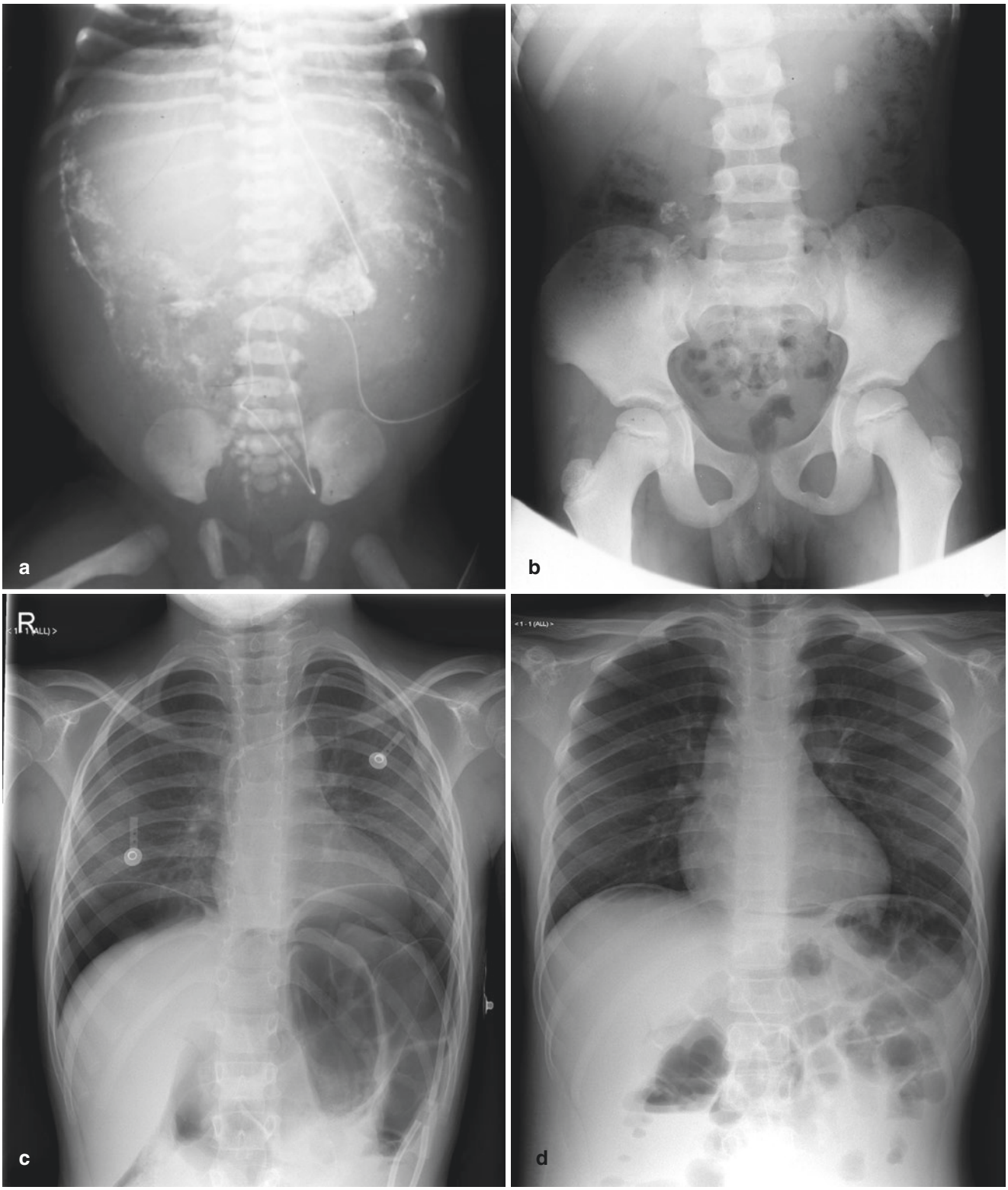

Fig. 4.51 (**a**) Intraperitoneal calcification. Plain X-ray showing extensive widespread intraperitoneal calcification from an intrauterine perforation. (**b**) Calcified mesenteric glands on a plain X-ray of the abdomen from tuberculosis. (**c**) Pneumoperitoneum. Free gas is seen on this plain X-ray with a lot of air under both diaphragms. A Hickman central line can also be seen. There are distended loops of bowel in the left hypochondrium. (**d**) Pneumoperitoneum post-laparotomy. It is normal to see some air in the abdomen up to 24 h after operative interventions in the abdomen

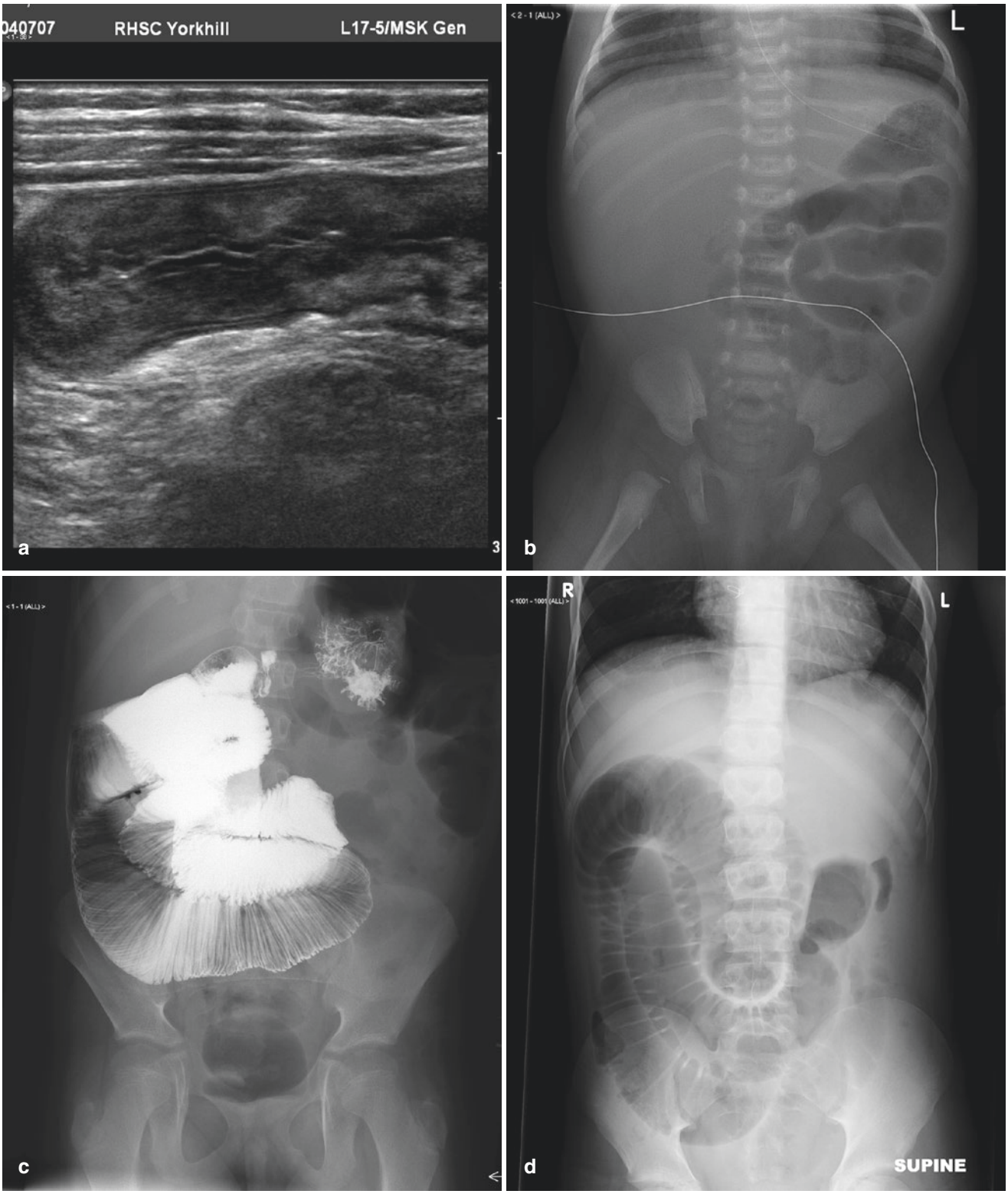

Fig. 4.52 (**a**) Ultrasound demonstrating loops of bowel below the surface of the abdominal wall. (**b**) Adhesion obstruction of the small bowel showing dilated isolated loops of bowel on the left side and no gas in the rest of the abdomen. (**c**) Small bowel obstruction, contrast seen within a closed loop of bowel in adhesion obstruction with volvulus. Note the dilated loops of small bowel with a pattern of circular valvulae conniventes as part of the wall of the small bowel. (**d**) Intestinal obstruction in a closed loop with a classical picture of a volvulus

4.6.7 Renal Stones (Fig. 4.54)

Renal stones and calculi are discussed fully in Chap. 5.

4.6.8 Constipation

Constipation may be defined as a difficulty or delay in defaecation that causes distress to the child and the parents. Encopresis, or faecal soiling, is the frequent passage of faecal matter at socially unacceptable times. Psychogenic causes are the most frequent. Faecal continence is the ability to retain faeces until delivery is convenient. Ingestion of fluid or food stimulates the gastrocolic reflex and result in two or three mass colonic propulsive activities per day. This process delivers faecal material to a normally empty rectum. On distension of the rectum, stretch receptors start a rectal contraction and a reflex inhibition is sent to the anal canal. This is mediated via the myenteric plexus of nerves in the submucosa and the plexus of nerves between the outer longitudinal and inner circular smooth muscle layers. The process produces sensation since the upper part of the anal canal has sensitive sensory receptors as well as stretch receptors. The motor element of the external sphincter and the puborectalis muscle make up the striated sphincter, together with the smooth muscle of the internal sphincter. The striated sphincter is able to contract strongly to prevent the passage of a stool at an inconvenient time. This, however, can only function for 30 s, i.e., long enough to contain a rectal contraction wave till it passes. The internal sphincter can maintain persistent tonic activity, thereby preventing leakage of stool between periods of rectal activity by maintaining closure of a resting anal canal. Clinical experience suggests that the external sphincters are of much less importance than the puborectalis sling and the internal sphincter. Defaecation occurs by inhibiting the activity of the puborectalis sling and

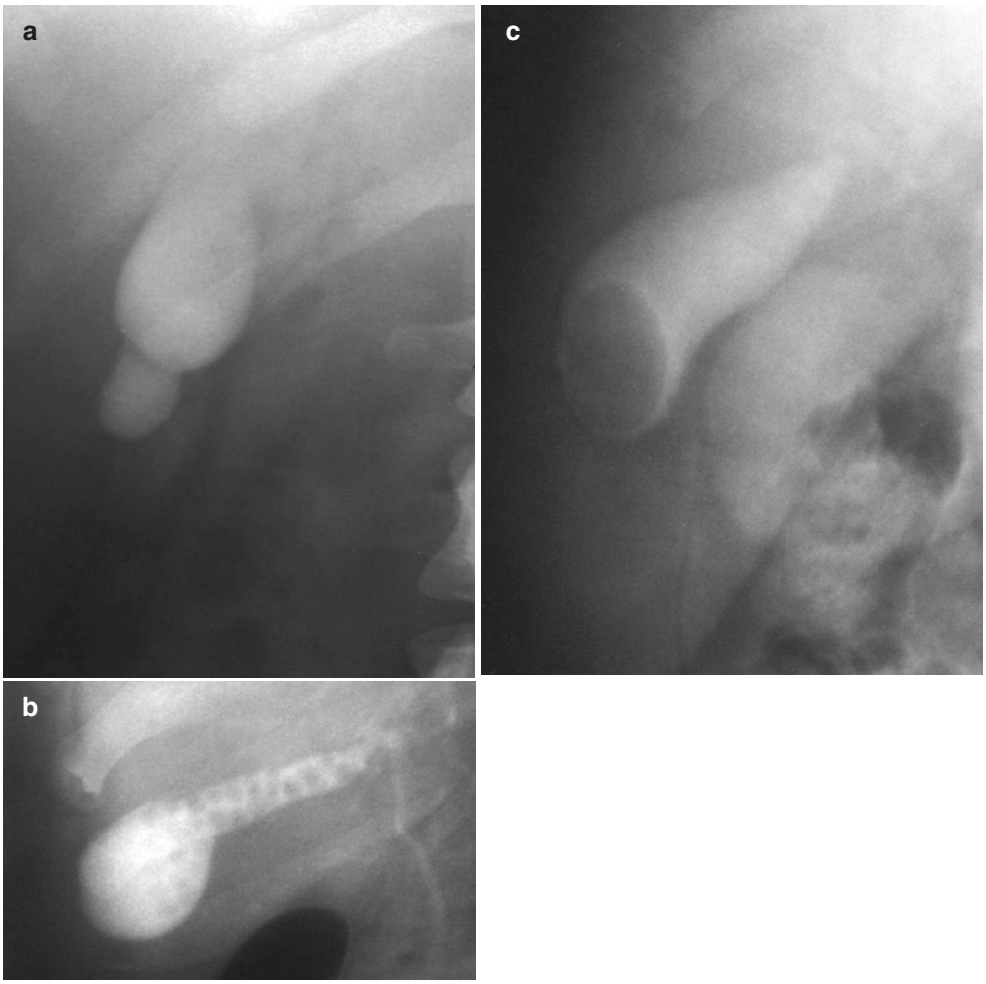

Fig. 4.53 (**a**) Large solitary gallstone seen on X-ray in gallbladder. (**b**) Multiple stones seen in gallbladder during cholecystography, (**c**) Preoperative cholecystogram outlining the normal anatomy of the gallbladder, cystic duct, hepatic ducts and the common bile duct with dye entering the duodenum. (**d**) Spherocytosis. Pigment gallstones in the gallbladder and splenomegaly on ultrasound examination. (**e**) Spherocytosis with gallstones in the gallbladder on ultrasound. (**f**) Ultrasound of gallbladder with gallstone

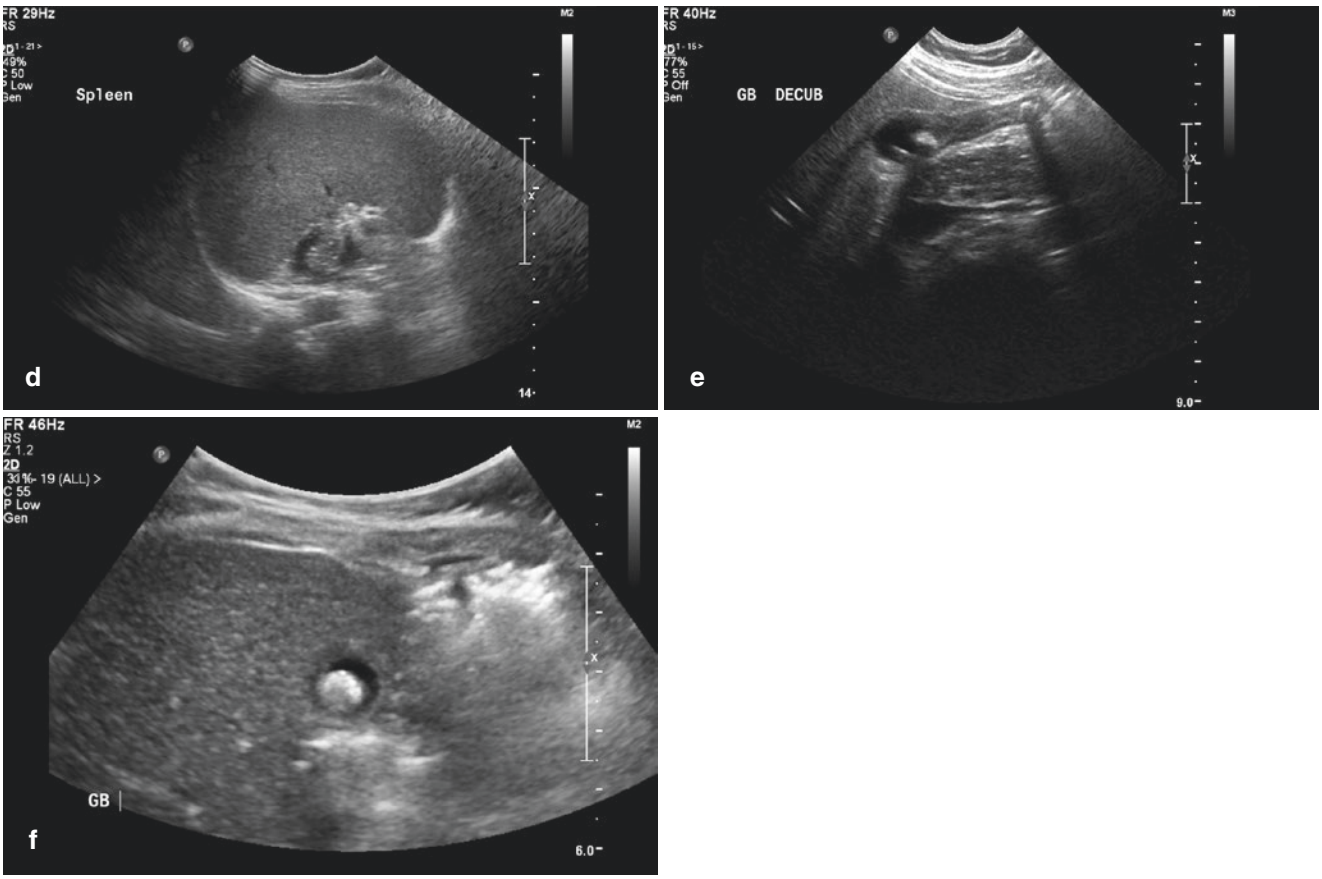

Fig. 4.53 (continued)

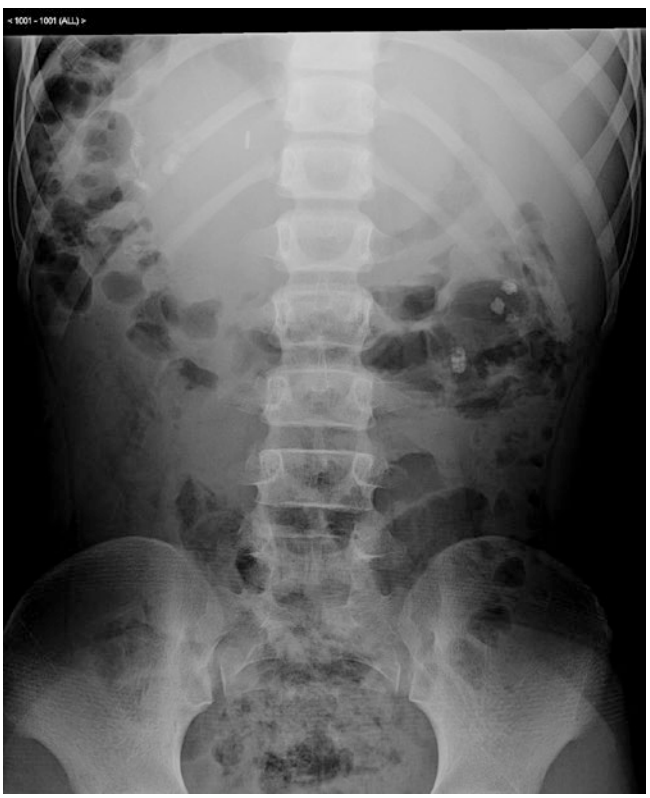

Fig. 4.54 Hyperoxalaemia liver: renal stones

the sphincter mechanism of the anus, thus allowing faeces to pass from the rectum into the anal canal. This is augmented by voluntarily increasing intra-abdominal pressure using the abdominal wall musculature as well as the diaphragm as accessory muscles for defaecation.

There are two main clinical states, the acute and the chronic state, which must be differentiated.

Acute constipation usually occurs in a child after a febrile illness with a reduced fluid intake. This situation arises when convalescing after an illness or in the immediate post-operative period. There is a danger that this acute state of constipation may progress to a chronic state if it is not identified early enough.

In chronic constipation, the rectum is overstretched and ballooned. The sensory receptors are inactive, and the bowel is flaccid and unable to contract effectively. A greater amount of water is absorbed from the faecal stream. The stool becomes harder, more solid, and more difficult and painful to pass. The faecal mass increases in size, and spurious diarrhoea can also occur from stercoral ulceration of the distended rectal mucosa.

History is important: failure of a normally born term infant to pass meconium within 24 h of birth makes it likely that there may be some underlying problem. Infants for whom childbirth has been abnormal take longer to establish

a normal defaecation pattern. The delay in establishing normal stooling may be a sign of other disorders, not only Hirschsprung's disease or anal stenosis, but systemic disorders such as hypothyroidism. Psychogenic causes are the most common origin of constipation in childhood.

In older infants and children, the distress caused by constipation may be related to pain. There may be abdominal discomfort, usually a dull ache, which may or may not be related to defaecation. Occasionally the pain may be localised to the right iliac fossa due to a distended caecum filled with stool. The pain may be in the anal region, particularly when an anal fissure has occurred, and bleeding may result from the mucosal tear.

There are occasions when there is no complaint of constipation, but the parents may notice a distended abdomen, and may even at times feel a mass arising out of the pelvis.

In a full examination of the child it is important to note the presence of any dysmorphic features, height and weight, as well as any signs of failure to thrive. Inspection of the abdomen should note any abdominal distension or the presence of local swelling. The abdomen is then palpated in routine fashion, feeling for any abdominal mass. A faecal mass can usually be indented through the abdomen, although at times the impacted mass may be so hard as to make it quite impossible to indent and may mislead one into thinking it is a malignant mass. A loaded, impacted colon with a megarectum can in turn cause retention of urine, resulting in a full bladder, which may or may not distress the child if this is a chronic situation.

Digital rectal examination must be carefully explained to the parents and the child before proceeding, explaining the importance of deciding whether constipation is a problem especially in the presence of diarrhoea, which may be spurious in nature. It is helpful to have a nurse in attendance to position the child in the left lateral position with knees bent in the fetal position. It is useful to carry on conversation during this investigation to relax an otherwise tense atmosphere, and also to explain to the parent and the child what is being done. While the child is in this position, it is important to examine the spine and the sacrum for any sign of spina bifida occulta. The position and size of the anus should be noted to exclude the possibility of an anterior ectopic anus or an anal stenosis. The skin around the anus should look normal. Erythema may indicate the presence of candida or streptococcal infection or may be due to topical applications by the parents. The presence of puckering of the anus, as well as the presence of a skin tag, may indicate an underlying anal fissure that could be the result of the vicious cycle of retention of stool, chronic constipation, and painful defaecation. The presence of soiling should be noted, and the consistency and volume of stool, if it is hard or soft or liquid in form, as well as whether there is any blood present.

Plain radiography has a limited role in the assessment and monitoring of constipation. Various scoring systems exist, but plain radiographs are largely recognised to have poor validity and reproducibility in the assessment of constipation. They may identify other pathology responsible for symptoms, but there is also the possibility that other pathology may be wrongly discounted due to the presence of faecal loading (Fig. 4.55a, b).

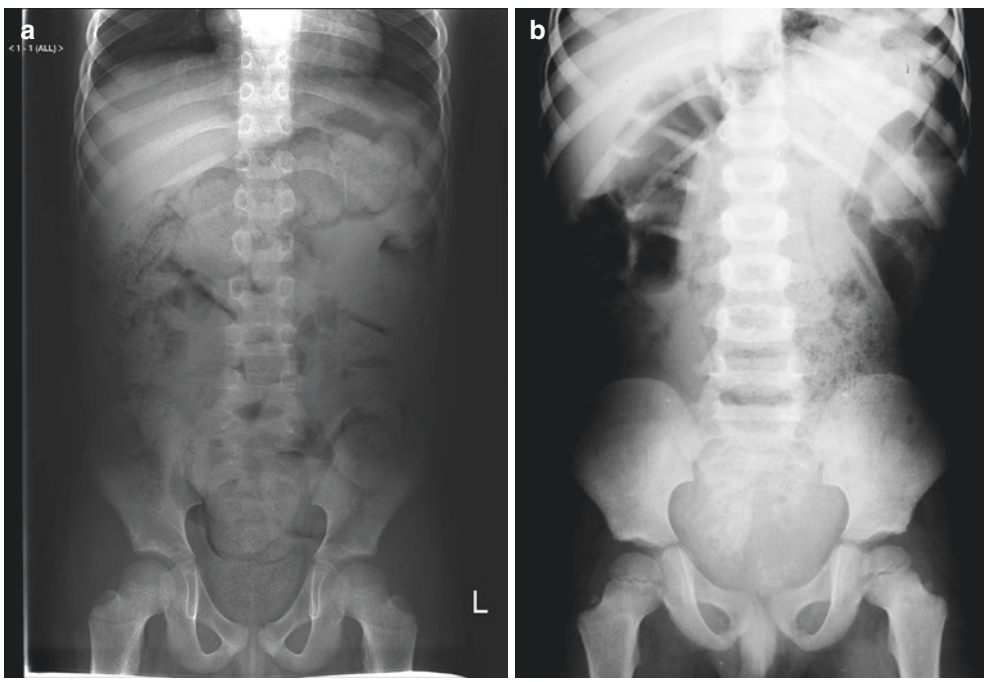

Fig. 4.55 (**a**) Constipation. Faecal masses seen on the plain X-ray in the pelvis and central abdomen. (**b**) Plain X-ray abdomen showing faecal loading in a patient with chronic constipation. (**c**) Constipation. Mega rectum with faecaloma seen on barium enema. Distended loops of bowel are seen proximally caused by the obstruction. (**d**) Barium enema in a child demonstrating gross rectal dilatation and obstruction with a mass of faeces. A faecaloma in a "terminal reservoir"

Fig. 4.55 (continued)

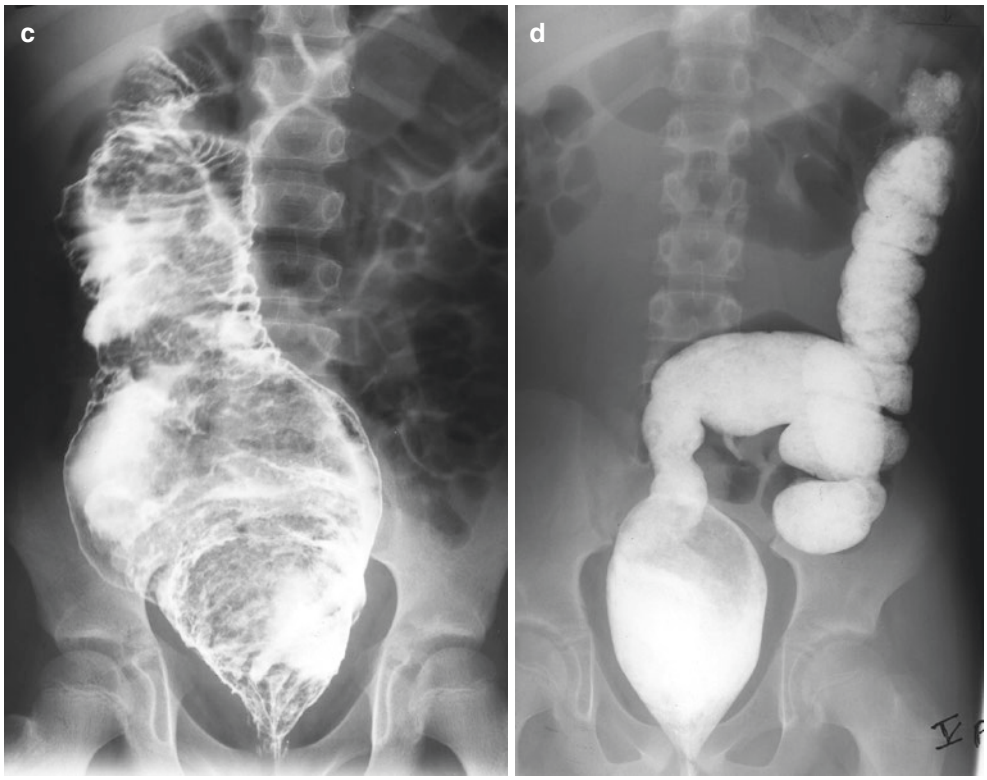

Formal total colonic transit studies can be performed by several methods and modalities. One recognised method is for markers to be ingested on days 1, 2, and 3 with a radiograph on day 6, providing maximum information on bowel transit with minimum radiation exposure.

Rectal diameter can be measured non-invasively at the time of urinary tract or abdominal ultrasound. It is recognised that a rectal diameter of 3 cm or greater is abnormal.

In neonates with difficulty stooling or older children who have never had normal stooling, it may be appropriate to examination the bowel with contrast fluoroscopy to assess bowel diameter and ascertain the presence of a transition zone. The presence of aganglionosis requires confirmation on biopsy.

4.6.9 Cardiospasm (Achalasia) (Fig. 4.56)

This is discussed fully in Chap. 3.

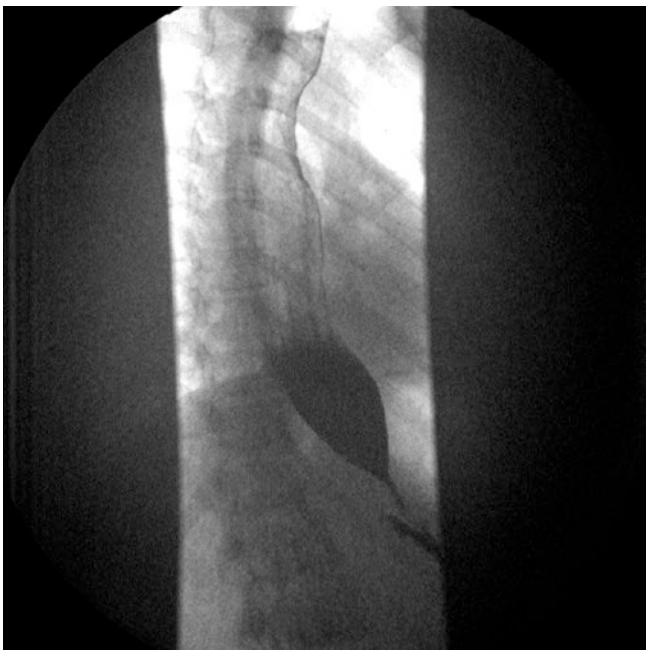

Fig. 4.56 Cardiospasm (achalasia). An oblique view of a contrast study showing the whole length of a dilated oesophagus with poor wave pattern. The abdominal oesophagus is seen with intense spasm allowing a fine stream of contrast through. A fluid level can be seen in the lower oesophagus

4.6.10 Colonic Stricture/Colonic Spasm

Colonic stricture presents as an intestinal obstruction and is due to an inflammatory process that has undergone fibrous

healing. This may cause luminal narrowing after necrotising enterocolitis, Crohn's disease, or a perforation (Fig. 4.57a–d).

Colonic spasm can be seen in the neonatal period and often, once the spasm goes, the lumen returns to normal. Imaging of the stricture or spasm is by retrograde contrast enema. The narrowing can be seen and can be in more than one area. The stricture may be narrow or long and if significant can cause proximal dilatation.

4.6.11 Perforation of the Bowel

Perforation of the bowel can be traumatic, from injury caused by endoscopic procedures or forceful passage of nasogastric tubes in an ill baby or child. Spontaneous perforation can occur in septic or embolic states as well as due to inflammatory conditions, appendicitis, volvulus, meconium ileus, Crohn's disease, toxic megacolon from ulcerative

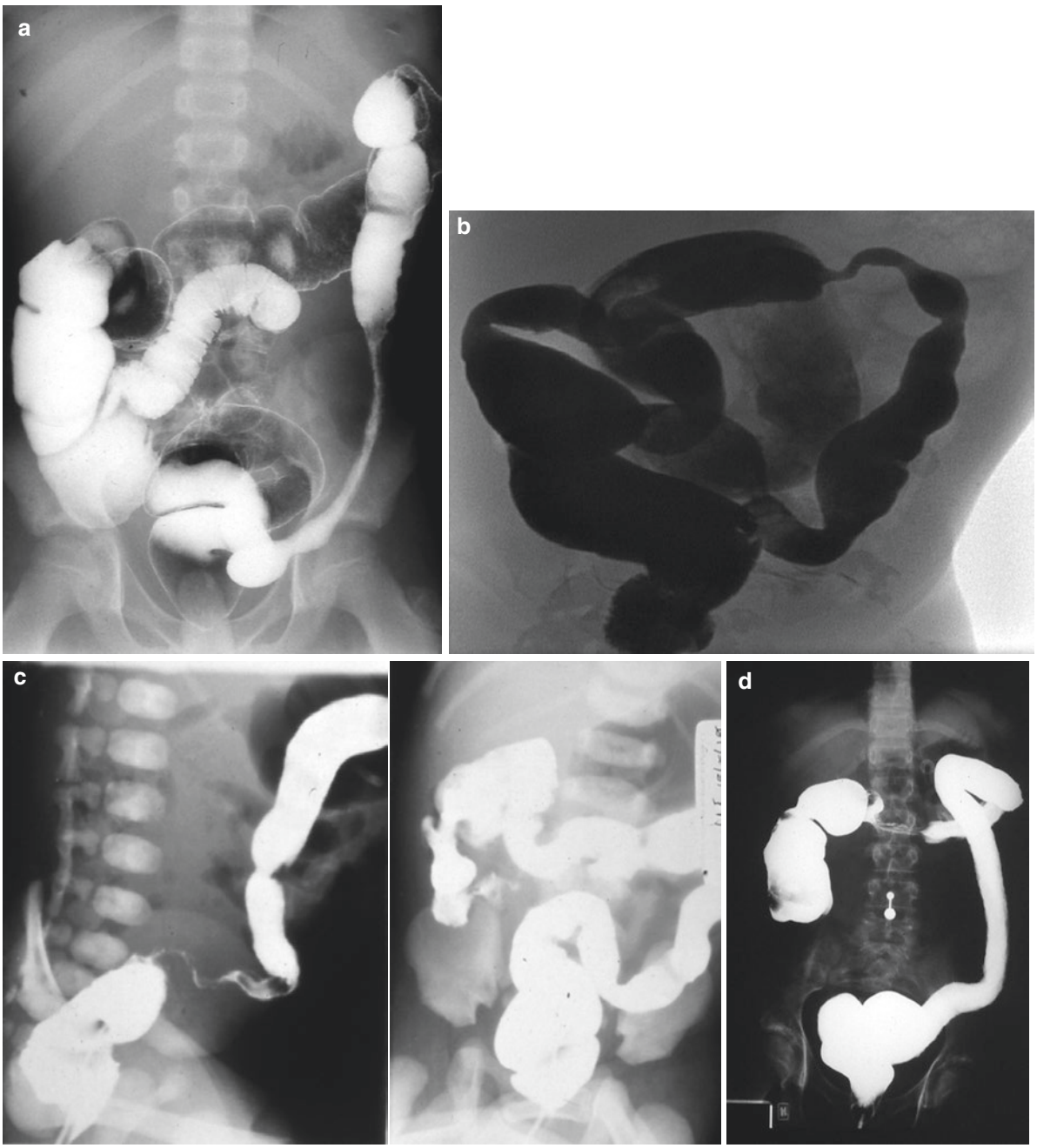

Fig. 4.57 (**a**) Colonic spasm/stricture. A contrast enema showing a long region in the descending colon with severe stricture and a dilated proximal transverse colon and caecum with reflux of contrast into the terminal ileum. (**b**) Colonic stricture in the transverse colon seen in this contrast study. (**c**) Colonic spasm/stricture. Multiple strictures seen in this contrast study done after recovery from necrotising enterocolitis. (**d**) Colonic spasm/stricture. Tight stricture in proximal transverse colon seen after a contrast study. The rest of the colon looks unhealthy with loss of haustrations

colitis, etc. The clinical presentation is of peritonism and plain X-rays will show free gas and air under the diaphragm. Occasionally in trauma with a ruptured viscus, a plain X-ray will not pick up the free gas, but a CT scan performed later will (Fig. 4.58a–d).

4.6.12 Ovarian Torsion

The most common mass in the abdomen of a neonate (female) is an ovarian cyst. Torsion of a pathologically enlarged ovary is often acute and presents with severe

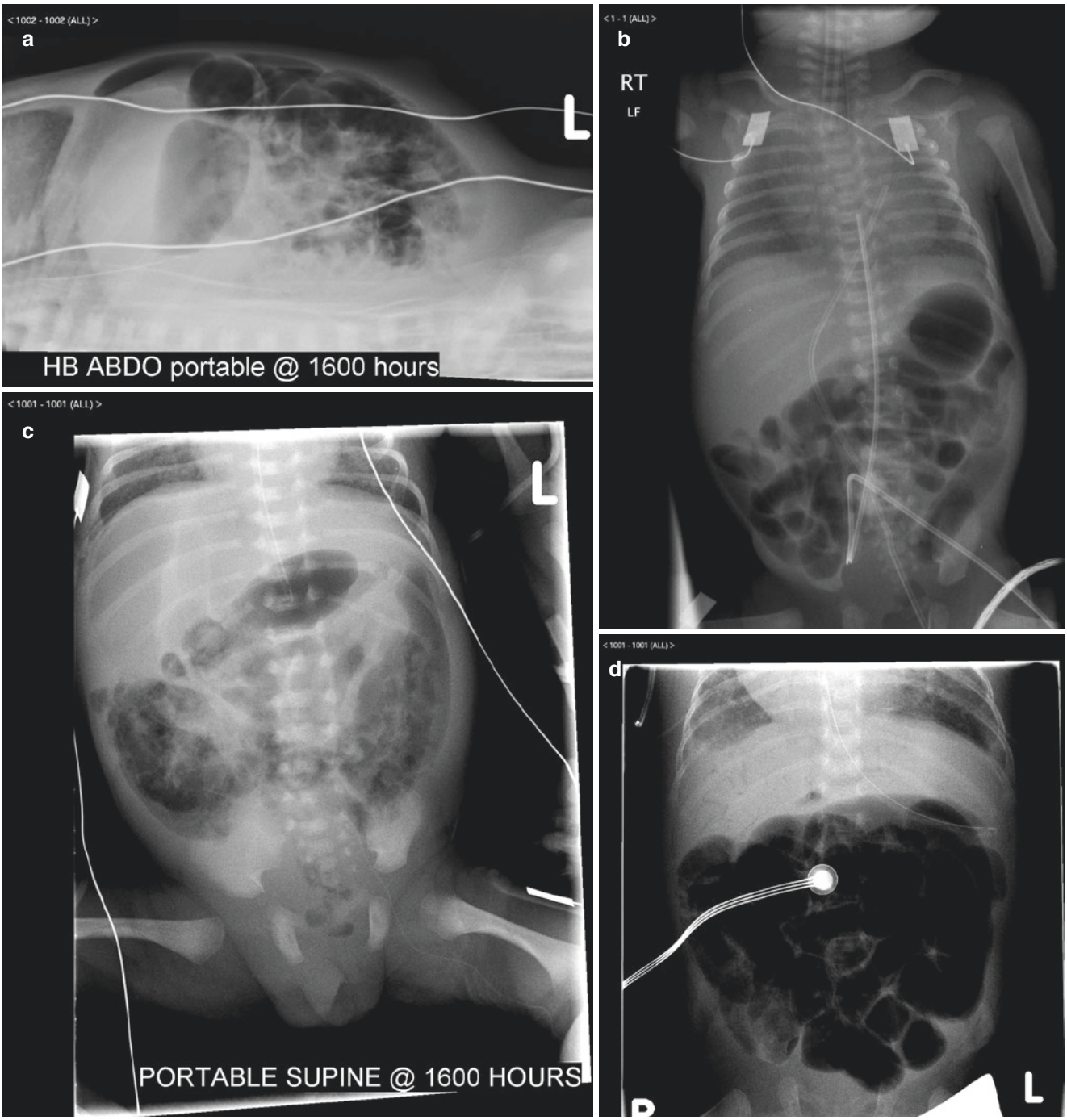

Fig. 4.58 (**a**) Perforation of the bowel. A plain X-ray lateral shoot through showing the presence of free gas following perforation in necrotising enterocolitis. (**b**) Umbilical line catheter and femoral line catheter in a premature neonate with distended loops of bowel, early signs of necrotising enterocolitis. (**c**) Necrotising enterocolitis with perforation. Plain X-ray of the abdomen including lower part of the chest. Pneumatosis seen extensively with evidence of free gas indicating perforation of the intestine. (**d**) NEC with portal venous gas

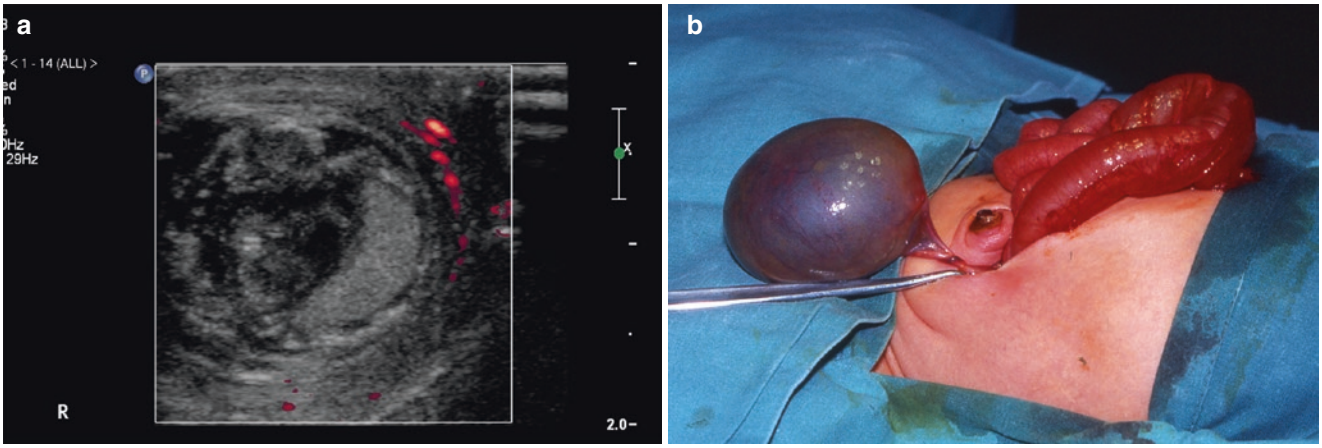

Fig. 4.59 (**a**) Antenatal torsion of the ovary. This scan shows disruption of the ovarian tissue indicating necrosis and the colour Doppler shows poor flow. (**b**) Ovarian torsion in a neonate. This is a preoperative view of the fallopian tube and a cyst probably due to an antenatal torsion

abdominal pain. Ultrasound is the investigation of choice to make the diagnosis. Ovarian tumours in older girls can be germ cells and may have raised tumour markers (AFP, HCG). Their size can initiate a torsion of the fallopian tube and bring them to light. Colour doppler ultrasound can demonstrate little flow of blood to the twisted ovary (Fig. 4.59a, b).

Reference

1. Mathur P, Saxena AK, Bajaj M, Chandra T, Sharma NC, Simlot A, et al. Role of plain abdominal radiographs in predicting type of congenital pouch colon. Pediatr Radiol. 2010;40(10):1603–8.

Further Reading

Al-Salem AH. Congenital paraesophageal hernia with intrathoracic gastric volvulus in two sisters. ISRN Surg. 2011;2011:Article ID 856568.

Kelly KB, Ponsky TA. Pediatric abdominal wall defects. Surg Clin N Am. 2013;93(5):1255–67.

Ledbetter DJ. Gastroschisis and omphalocele. Surg Clin N Am. 2006;86(2):249–60.

Rho JH, Kim JS, Kim SY, Kim SK, Choi YM, Kim SM, et al. Clinical features of symptomatic Meckel's diverticulum in children: comparison of scintigraphic and non-scintigraphic diagnosis. Pediatr Gastroenterol Hepatol Nutr. 2013;16(1):41–8.

Rozel C, Garel L, Rypens F, Viremouneix L, Lapierre C, Décarie JC, et al. Imaging of biliary disorders in children. Pediatr Radiol. 2011;41:208–20.

Genito-Urinary

5

Andrew McLaughlin and Robert Carachi

5.1 Introduction

Radiological investigation of congenital and acquired renal pathology constitutes a large part of paediatric radiology practice and makes use of every available imaging modality.

Ultrasound is the most frequently performed radiological examination. It carries the advantage of imparting no radiation dose and very rarely requires sedation. Improvements in sonographic technology allow an excellent view of the renal parenchyma and assessment of the renal collecting system, ureters, and bladder. It can confidently identify renal mass lesions, calculi, and perinephric collections. Serial ultrasound is the simplest means of monitoring renal growth.

Nuclear medicine scans such as ^{99m}Tc-dimercaptosuccinic acid (^{99m}Tc-DMSA) are the most sensitive modality for detecting renal scarring, and ^{99m}Tc-diethylenetriaminepentaacetic acid (^{99m}Tc-DTPA) or ^{99m}Tc-mercaptoacetyltriglycine (^{99m}Tc-MAG3) studies provide the best assessment of renal function and drainage.

Fluoroscopy is utilised in the micturating cystourethrogram to investigate for vesicoureteric reflux. Computed tomography (CT) is the mainstay in assessment of acute traumatic injury. A more recent development is that of magnetic resonance (MR) urography, which provides excellent detail of the renal parenchyma and collecting system and is particularly useful in the assessment of complex genitourinary malformations. Both CT and MR can be used in the investigation and staging of malignancy.

5.2 Congenital

5.2.1 Renal Agenesis

Renal agenesis may be bilateral and can be diagnosed prenatally by ultrasound in pregnancies complicated by oligohydramnios. The baby frequently has low-set ears, a flattened nose (Potter facies), spade-like hands, and may have club feet. After birth, respiratory distress due to pulmonary hypoplasia is very common, and intubation and intermittent positive pressure ventilation may be necessary. Abnormalities of the genitalia might be present. Unless the infant is maintained by dialysis and subsequent renal transplant, the outlook is fatal. Even with full support therapy, the respiratory aspect may prove fatal. Where renal agenesis is unilateral, the baby should survive normally (Fig. 5.1). Investigation usually shows the compensatory hypertrophy of the remaining kidney with some dilatation of the pelvis and the ureter (Figs. 5.2 and 5.3).

If this condition has not been identified on antenatal ultrasound, inability to identify any normal renal tissue on postnatal ultrasound will suggest the diagnosis. Because establishing this diagnosis is of critical importance, and may result in reorientation of care toward palliation, proving the complete absence of renal tissue with MRI or ^{99m}Tc-DMSA scan is prudent. Unilateral renal agenesis may be identified on antenatal ultrasound or be discovered incidentally on imaging in later life. In cases of renal agenesis or ectopia, the ipsilateral adrenal may attain a more vertical orientation than usual and is referred to as a "lying down adrenal."

5.2.2 Kidney: Polycystic

Autosomal recessive polycystic disease of the kidneys is a serious disorder that often has associated cystic disease of the liver. It may be diagnosed prenatally; the infants are often stillborn with massive abdominal distension or suffer early postnatal death. Uncommon in paediatrics is the adult,

A. McLaughlin
Radiology Department, Christchurch Hospital, Canterbury, Christchurch, New Zealand
e-mail: Andrew.McLaughlin@health.cdhb.nz

R. Carachi (✉)
Surgical Paediatrics, University of Glasgow, Glasgow, UK

R. Carachi (ed.), *Atlas of Paediatric Surgical Imaging*, https://doi.org/10.1007/978-3-030-32384-4_5

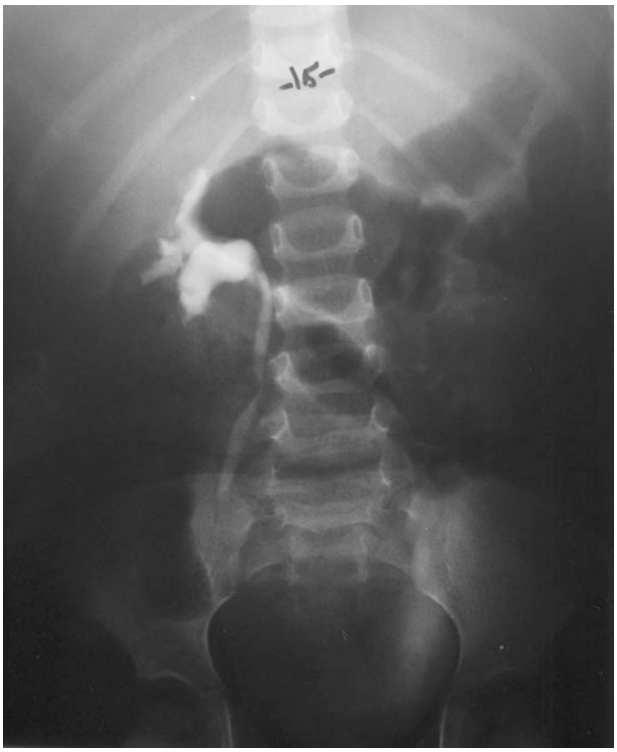

Fig. 5.1 Intravenous urogram showing an enlarged unilateral kidney and no sign of a contralateral one in agenesis of the kidney

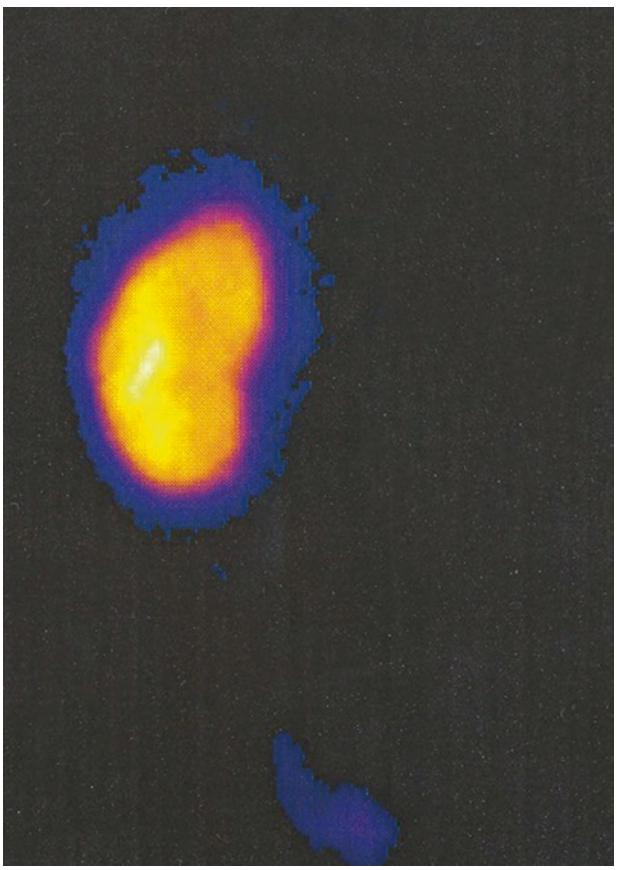

Fig. 5.2 Scanned nuclear medicine image of an enlarged kidney in agenesis of contralateral kidney

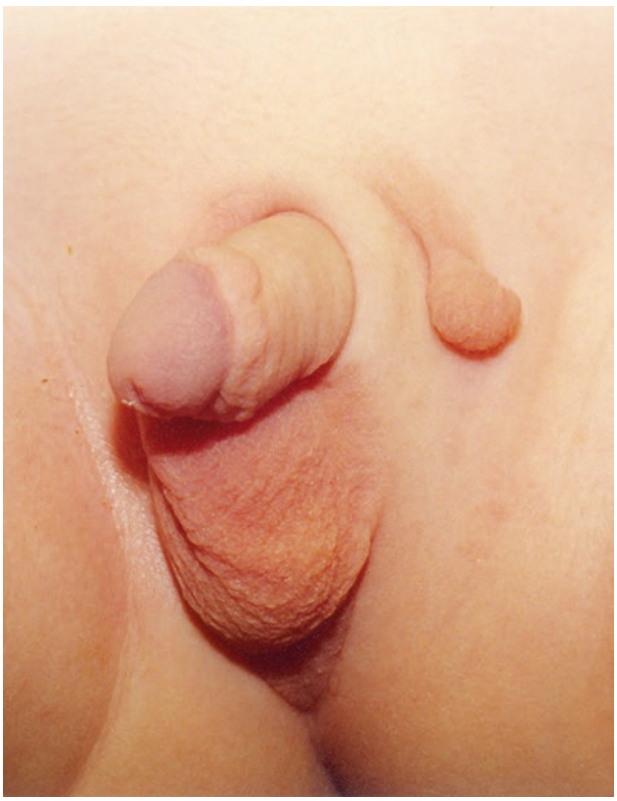

Fig. 5.3 Clinical picture of partial scrotal agenesis with penile anomalies in agenesis of the kidney

autosomal dominant type of polycystic disease with slowly progressive renal failure, which is more amenable to treatment by dialysis and transplantation as there is no liver involvement.

Autosomal Recessive Polycystic Kidney Disease: Plain X-rays may demonstrate symmetrical soft tissue density masses displacing bowel loops (Fig. 5.4a). Ultrasound will reveal the soft tissue masses are due to the markedly enlarged kidneys (Fig. 5.4b, c). The renal parenchyma appears abnormally echogenic, with loss of corticomedullary differentiation when scanned using a low-frequency transducer. Scanning with a high-frequency transducer may reveal a fine striated appearance to the renal parenchyma, which is caused by the presence of a multitude of tiny cysts. If the renal phenotype is at the less severe end of the spectrum, patients may survive to an age where transplant is possible, although these patients tend to develop periportal hepatic fibrosis.

Autosomal Dominant Polycystic Kidney Disease: This condition will sometimes result in the development of macroscopic renal cysts in later childhood. As simple renal cysts are uncommon in childhood, the presence of more than one cyst should suggest this diagnosis. Patients with Von Hippel-Lindauor tuberous sclerosis, both neurocutaneous syndromes, may also develop multiple renal cysts in childhood.

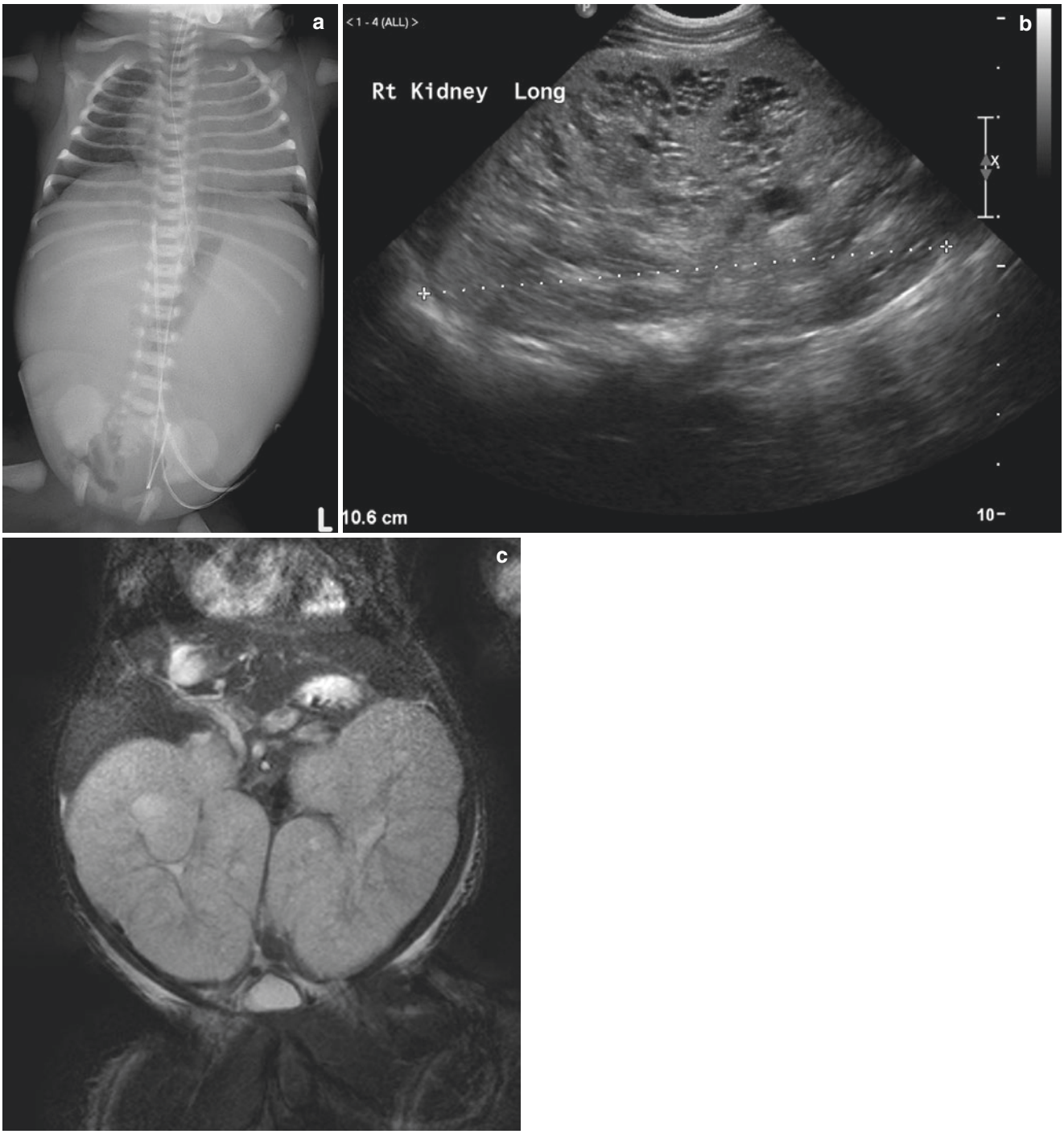

Fig. 5.4 (**a**) Plain X-ray of autosomal recessive polycystic kidney disease. The abdomen is distended by bilateral soft tissue densities, with medial displacement and distortion of the stomach bubble. The lungs are of low volume. (**b**) Longitudinal ultrasound image of an autosomal recessive polycystic kidney. The kidney is massively enlarged and echogenic with multiple tiny fluid spaces. (**c**) Coronal fat-saturated T2-weighted MR image of autosomal recessive polycystic kidney disease showing the enlarged kidneys largely filling the abdomen

5.2.3 Kidney: Multicystic Dysplastic

Multicystic dysplastic kidney (MCDK) is a condition in which one kidney is grossly enlarged, is non-functioning, and, as the name suggests, consists of multiple cysts. It is usually associated with ureteric atresia on that side (Fig. 5.5a, b). The disorder presents as a mass in the abdomen that may be detected by prenatal ultrasound or detected upon abdominal examination of the infant. The contralateral kidney is usually normal but must be checked. Nephrectomy

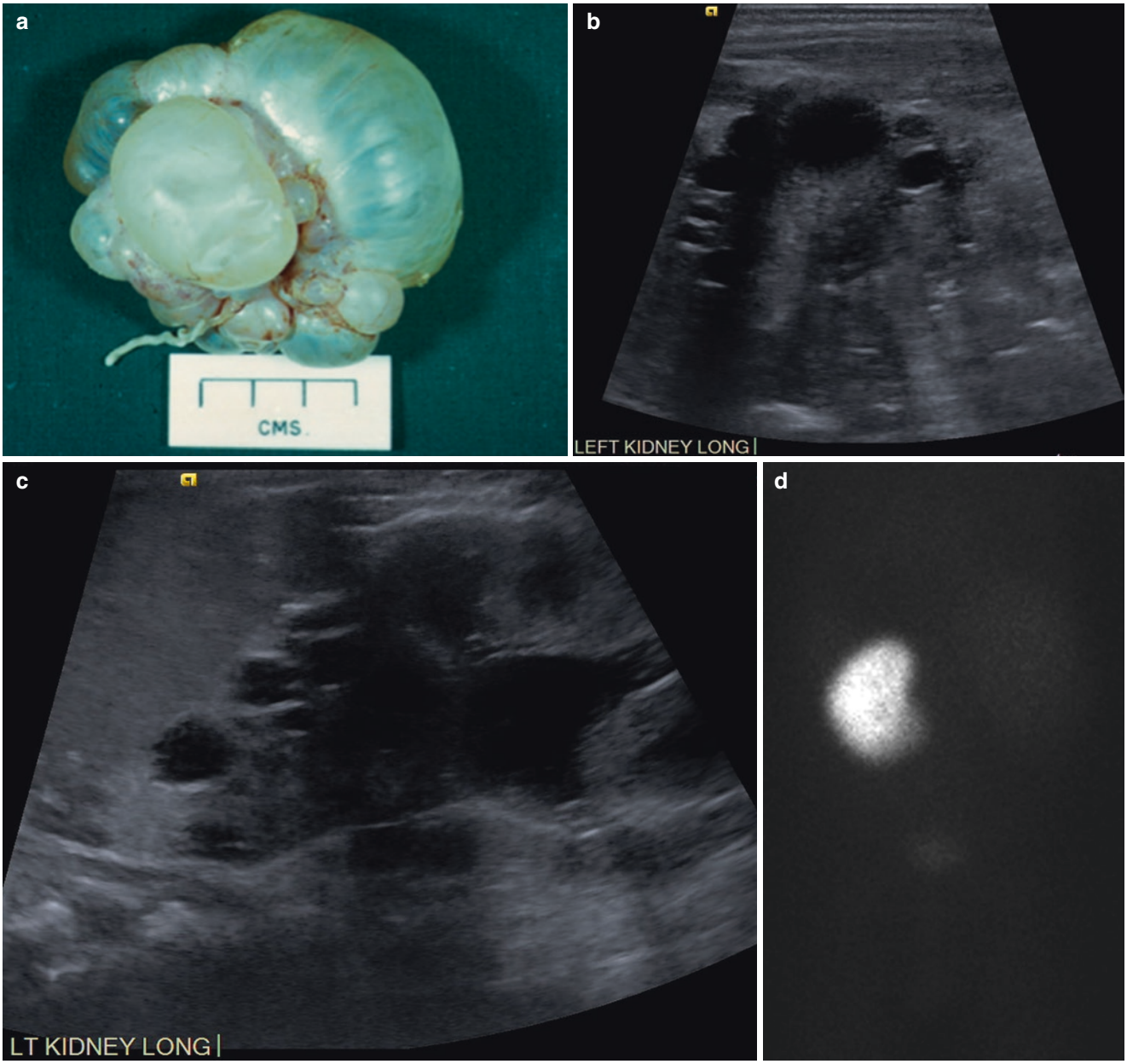

Fig. 5.5 (**a**) Pathological specimen of a multicystic kidney. (**b**) Longitudinal ultrasound image of a multicystic dysplastic kidney. Note the multiple non-communicating cysts of variable sizes with intervening echogenic stroma. (**c**) Longitudinal ultrasound images of a duplex kidney, with a multicystic dysplastic upper moiety. The lower moiety is normal. (**d**) DMSA image demonstrating complete absence of function in the left MCDK. There is normal uptake in the right kidney

of the multicystic kidney is usually recommended in case of subsequent enlargement of the cysts, infection within the cysts, or later development of hypertension. Some now advise continued supervision without active intervention unless a complication arises, and on occasion the kidney may atrophy and disappear.

Plain X-rays may demonstrate a soft-tissue density mass in one side of the abdomen, displacing bowel loops. Ultrasound will reveal that the renal parenchyma has been replaced by multiple non-communicating cysts (Fig. 5.5c). Often some abnormal echogenic stroma is visible between the cysts. The main purpose of imaging is to ensure the kidney is a multicystic dysplastic kidney, composed of multiple non-communicating cysts, rather than a markedly hydronephrotic kidney, in which the fluid-filled elements (which may be confused with cysts) represent the markedly dilated collecting system. ^{99m}Tc-DMSA will demonstrate complete absence of function in a multicystic dysplastic kidney (Fig. 5.5d).

Ultrasound may be used in follow-up to ensure the MCDK involutes and the contralateral kidney grows as expected.

5.2.4 Kidney: Duplex

Duplex kidney is the term given to the condition where the drainage system from the renal parenchyma is doubled in all or part of its length. This is often an anatomical finding of little functional significance. Urinary tract infection is frequently the reason for the investigation of the urinary tract during which the bifid system is found. A duplex kidney is more prone to have a ureterocele (intravesical cystic dilatation) on the distal end of the upper pole ureter which drains into the bladder lower than the normal site, or less commonly into the urethra or vagina (Fig. 5.6a). The latter can result in constant dampness of a child who also intermittently micturates normally. This wetting occurs more by day and is less troublesome at night when the child is asleep. The lower pole ureter always opens "above" the upper pole ureter—often into the normal site—but this ureter is more prone to have vesicoureteric reflux. Only the complications of duplex systems (which may be bilateral) require treatment. This also applies to horseshoe kidney, in which the lower poles of the kidneys are in continuity across the midline (see Sect. 5.2.5).

Duplex kidneys are often detected during antenatal ultrasound. A dilated collecting system limited to the upper or lower moiety or a parenchymal bar separating the collecting systems are indicative (Fig. 5.6b). A duplex kidney in which neither moiety is dilated may be very difficult to define as duplex using ultrasound, although a discrepancy in renal length may be a clue to the diagnosis. Such a non-dilated duplex kidney, however, is less likely to be clinically significant, although reflux is not excluded. In general, imaging of duplex kidneys is targeted at identifying potential complications (Fig. 5.6c). In the event of dilatation of a moiety, most often detected with ultrasound, further investigation is warranted to determine whether the moiety is refluxing or obstructed. A micturating cystourethrogram will demonstrate reflux (Fig. 5.6d), and once reflux is excluded, a ^{99m}Tc-MAG3 nuclear medicine scan can be used to assess for potential obstruction. A ureterocele may be visible in the posterolateral bladder as a cystic filling defect.

5.2.5 Kidney: Horseshoe

A horseshoe kidney may be nicely depicted on ultrasound, especially in the neonate, although the midline isthmus of connecting tissue may be missed if obscured by bowel gas or if the medial aspects of both lower poles are not carefully inspected. Ultrasound is also the best test for identifying dilatation of the collecting system and monitoring growth. Nuclear medicine (Fig. 5.7), CT, and MR can also demonstrate a horseshoe kidney, often as an incidental finding.

5.2.6 Kidney: Ectopic

The usual position of the kidneys is a high retroperitoneal one, the right kidney being about half a vertebra lower than the left. Kidneys are frequently palpable in the new-born and an assessment of their size can be made. Later the kidneys are not palpable unless they are abnormal or in an abnormal position. An ectopic kidney is usually paravertebral but lower in position than normal, and may present as a palpable mass in the iliac fossa. The kidney may develop even more caudal and be pelvic in position, being identified by ultrasound or an intravenous pyelogram (IVP) examination. Rarely the kidney may migrate across the midline and end with both kidneys on one side but with the ureter from the lower kidney (the ectopic one) crossing to enter bladder on the "normal" side. Sometimes the crossed ectopic kidney fuses with the other kidney, resulting in a cross-fused ectopic kidney, but usually with independent drainage systems and the ureters opening into either side of the bladder (Fig. 5.8a, b). These anatomical variations, which may never come to light in life, may be found by chance during an investigation of a patient for an unrelated reason, or upon investigation of a child with urinary tract infection or other urinary tract signs. The anatomical variation does not in itself require any treatment except in rare cases where there may be obstruction to drainage of urine at the pelviureteric junction or by extrinsic pressure where a ureter traverses behind the inferior vena cava.

Ectopic kidneys can usually be located using ultrasound in the neonate and young child. When a kidney does not lie in its expected position, examination of the lower abdomen and pelvis should be undertaken (Fig. 5.8c). In older children, bowel gas may make detection of an ectopic kidney difficult; if necessary a nuclear medicine ^{99m}Tc-DMSA examination can be used to determine the kidney position. A nuclear medicine ^{99m}Tc-MAG3 examination can be used to assess function in the presence of suspected obstruction.

5.2.7 Kidney: Hydronephrosis

Hydronephrosis results from obstruction to the free drainage of urine from the kidney. The hold-up may be at the pelviureteric junction due to either an intrinsic stenosis or malfunction at the pelviureteric junction, or extrinsic pressure from renal vessels passing to the lower pole of the kidney. If the obstruction is more distal at the ureterovesical junction or at the bladder neck, not only will the kidney pelvis be dilated, but the ureter will also show dilatation and often tortuosity. Hydronephrosis may present as a mass in one or the other

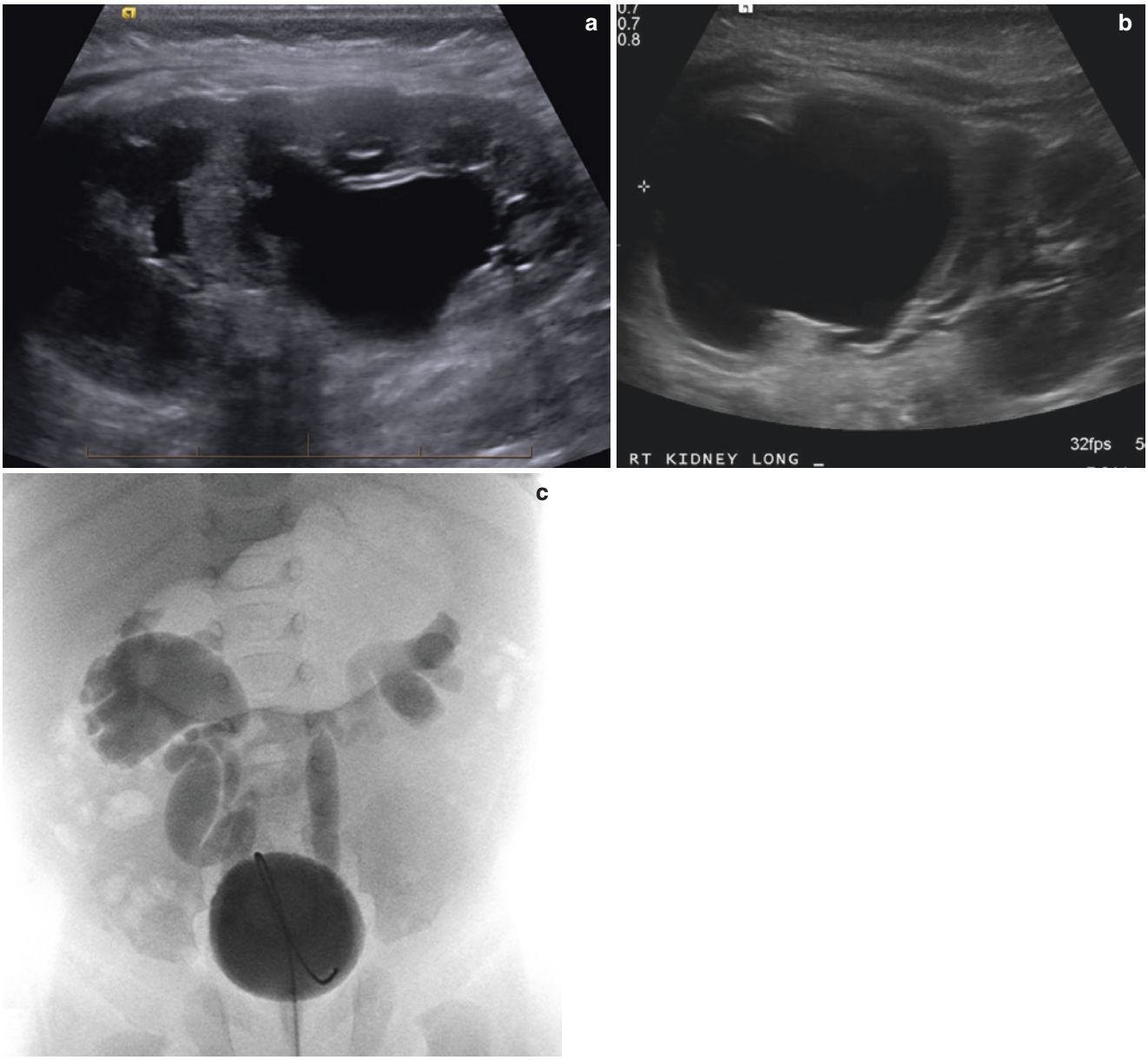

Fig. 5.6 (**a**) Diagram illustrating the ectopic insertion of an upper moiety ureter. (**b**) Longitudinal ultrasound image of a duplex kidney. The upper and lower moiety collecting systems are separated by a band of parenchymal tissue. (**c**) Longitudinal ultrasound image of a duplex kidney showing marked dilatation of the upper moiety due to obstruction at the vesicoureteric junction by a ureterocele. (**d**) Image from an MCU demonstrating bilateral duplex kidneys. There is reflux into both moieties on the right, with both ureters visible. On the left there is reflux into the lower moiety, which demonstrates a typical "wilting lily" configuration due to inferior displacement of the lower moiety collecting system by mass effect from the obstructed but non-refluxing upper moiety

side of the abdomen or may be detected during the investigation of a urinary tract infection or haematuria. Many infants have hydronephrosis detected inutero by ultrasound scanning, and in some this dilatation of the renal pelvis disappears by birth or in the postnatal period. In others, this obstruction and dilatation increases, and renal function is ultimately impaired. Before proceeding to operation, it is important to ensure that there is continuing and persistent obstruction at the pelviureteric junction. The hydronephrotic kidney of the young infant can undergo remarkable improvement after pyeloplasty, whereas the older child who has dilated pelvis and calyces will still have some residual dilatation of the calyces even after successful pyeloplasty.

The goal of radiological investigation of the dilated renal collecting system is to identify the cause of dilatation, and if potential obstruction is present, to identify the level of

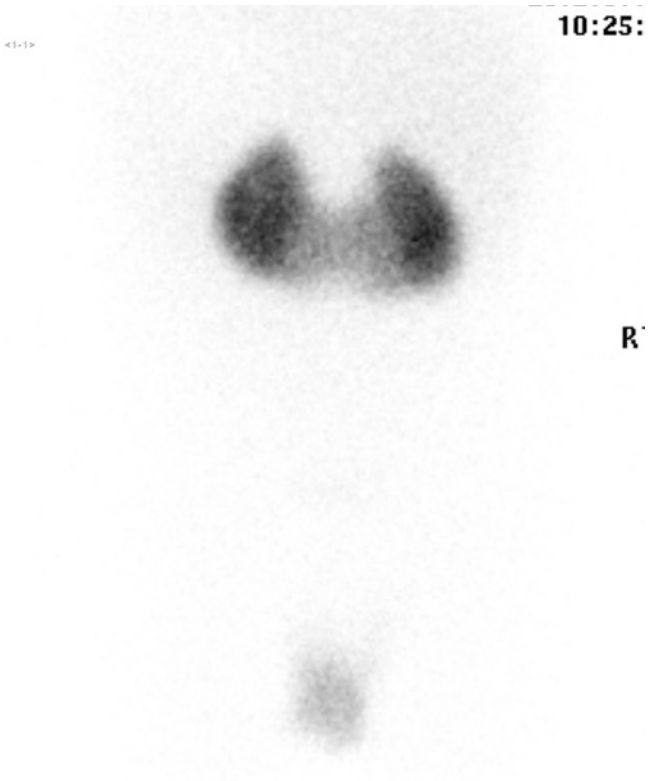

Fig. 5.7 ^{99m}Tc-DMSA image showing a horseshoe kidney. The lower poles of the left and right moieties are fused across the midline

obstruction and estimate the degree of functional impediment to urinary drainage. Once postnatal renal collecting system dilatation is confirmed or identified, usually by ultrasound, a micturating cystourethrogram can be performed to determine if vesicoureteric reflux is responsible (discussed in the next section). A micturating cystourethrogram can also evaluate the posterior urethra for the presence of valves in male infants with bilateral ureteric and renal pelvic dilatation. If reflux is not present, then the differential can be narrowed to pelviureteric junction obstruction, vesicoureteric junction obstruction (see Sects. 5.2.7.1 and 5.2.8.3), and a congenital megaureter. A functional nuclear medicine study such as a MAG3 can then be used to demonstrate drainage of radiotracer from the kidney to confirm any functionally significant obstruction.

5.2.7.1 Pelviureteric Junction Obstruction

Ultrasound of a pelviureteric junction (PUJ) obstruction will show a dilated renal pelvis without a dilated ureter. This results in a characteristic beaked appearance to the pelviureteric junction (Fig. 5.9a). Once reflux has been excluded, a MAG3 study will demonstrate failure of drainage of contrast at the level of the renal pelvis (Fig. 5.9b). Concomitantvesicoureteric reflux and PUJ obstruction (which could potentially result in a dilated renal pelvis and ureter) is very rare, but not completely unheard of.

5.2.8 Ureters: Anomalies

5.2.8.1 Hydroureter

Dilatation of the ureter (hydroureter) is often secondary to obstruction at the ureterovesical junction and less commonly secondary to more distal urinary tract obstruction at the bladder neck or in the urethra, e.g., urethral valves. There is frequent tortuosity of the ureter as well as dilatation. The hydroureter is usually found on investigation of a patient with urinary tract infection. Where there is ureterovesical obstruction, it is usually due to a stenotic segment of the distal part of the ureter, and this requires excision with reimplantation of the ureter in the bladder. Very dilated ureters should be tapered to reduce to a normal diameter prior to re-implanting the distal end into the bladder. Vesicoureteric reflux is more common in infancy than in childhood. Minor degrees of vesicoureteric reflux, usually found during investigation of the patient with urinary tract infection, are not of serious consequence. Patients with marked reflux, and particularly those with intrarenal reflux, are at risk of renal damage. It is probable that the majority who suffer renal damage have also had superimposed infection as well as reflux. The patient who has either gross reflux or who has "breakthrough" infections despite many courses of antibiotic therapy, should have reimplantation of ureters in the bladder. This is performed by reinserting the ureter through the bladder muscle at about 4 cm distant, and bringing the ureter along a submucosal tunnel to the old site in the bladder (Leadbetter Politano technique), or tunnelling the ureter across the trigone to the opposite side of the bladder (Cohen technique). Alternatively, the STING procedure of submucosal injection of teflon at the ureteric entrance to the bladder to prevent reflux has replaced many reimplantation operations. Rarely with single ureters, but occasionally with the upper pole ureter of a duplex kidney, the ureter may have an ectopic opening into the distal urethra, perineum, or vagina, resulting in continuous dribbling incontinence. The diagnosis is suspected in the child who appears to micturate normally but in addition is continuously damp or wet. Investigation reveals the duplex system and the upper pole ureter may have little function and is seldom worth preserving. Hence the upper pole is excised.

Ureteric calculi occur less commonly in childhood, but if they lodge in the ureter may result in proximal ureteric dilatation. Treatment is to perform cystoscopy and pass a dormier basket along the ureter to remove the stone. Treatment is rarely by open operation.

Dilated ureters may be readily identified with ultrasound, although the mid-ureter may be difficult to image due to overlying bowel gas. Distal ureteric dilatation is visible as a tubular fluid-filled structure behind the bladder (Fig. 5.10a, b). Proximal ureteric dilatation can usually be seen by using the kidney as a sonographic window (Fig. 5.10c, d).

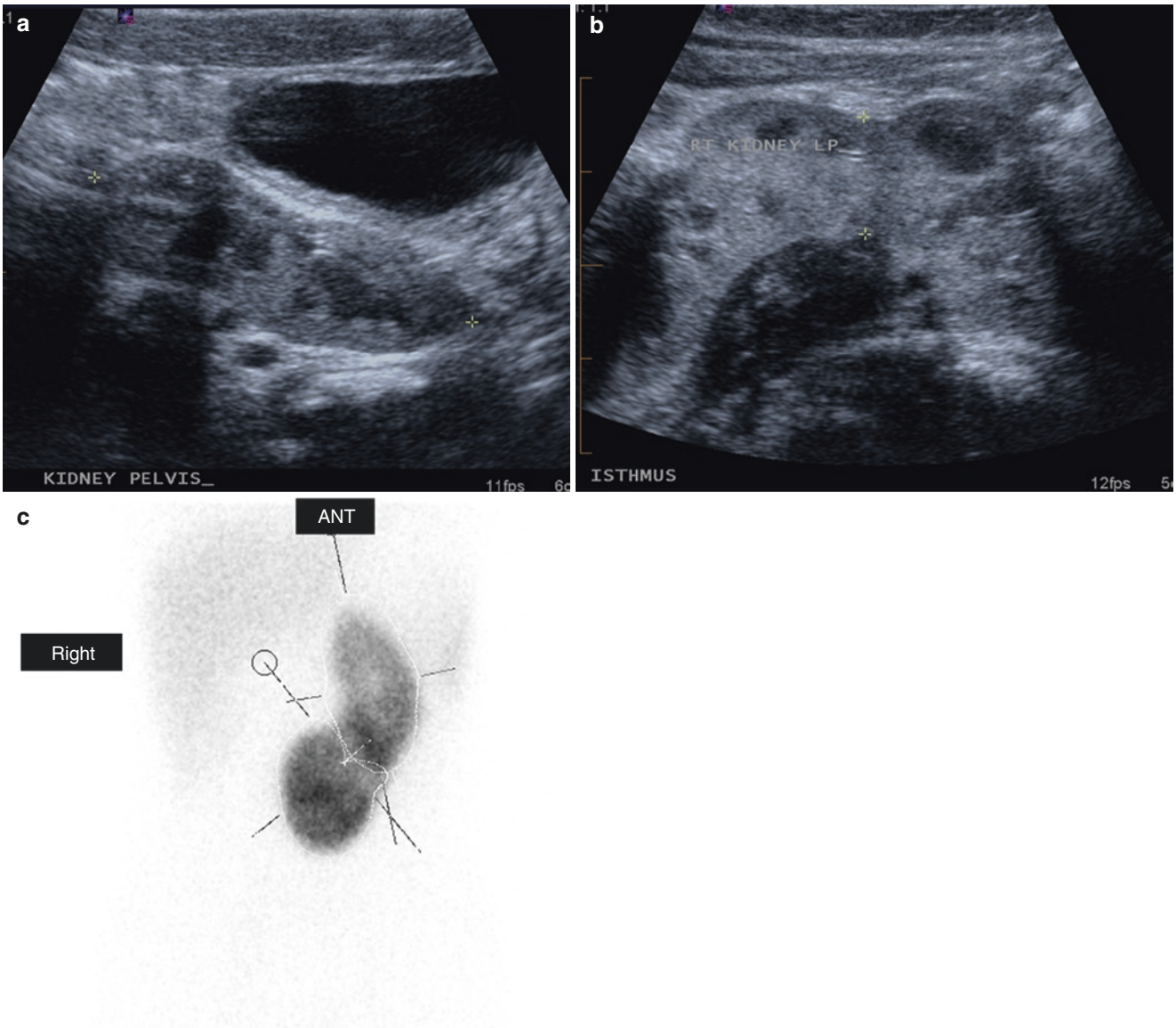

Fig. 5.8 (**a**) Longitudinal ultrasound image of an ectopic kidney in the right side of the pelvis, posterior to the bladder. (**b**) Longitudinal ultrasound image of a crossed fused ectopic kidney, showing the point of fusion overlying the right psoas muscle. (**c**) DMSA image of a crossed-fused ectopic kidney. The bilobed outline of the fused kidneys lies to the left of the midline

5.2.8.2 Vesicoureteric Reflux

The investigation of choice for potential vesicoureteric reflux (VUR) is the micturating cystourethrogram (MCU). A urethral catheter is inserted into the bladder using aseptic technique, and a water-soluble contrast agent is instilled via the catheter. Images taken during early filling of the bladder may demonstrate a ureterocele as a rounded filling defect. The patient is then screened during several episodes of voiding to determine if reflux occurs (Fig. 5.11a–c). Radiological grading is based on the extent of reflux and associated morphological changes to the collecting system: Grade I is reflux of contrast into a non-dilated distal ureter; Grade II is reflux of contrast into a non-dilated renal pelvis; Grade III is reflux into a mildly dilated ureter and renal pelvis; Grade IV is reflux into a dilated renal pelvis and tortuous dilated ureter; and Grade V is reflux into a grossly dilated renal pelvis with clubbed calyces and a markedly dilated and tortuous ureter.

5.2.8.3 Vesicoureteric Junction Obstruction

The typical ultrasound appearance of vesicoureteric junction (VUJ) obstruction is of a dilated renal pelvis and ureter.

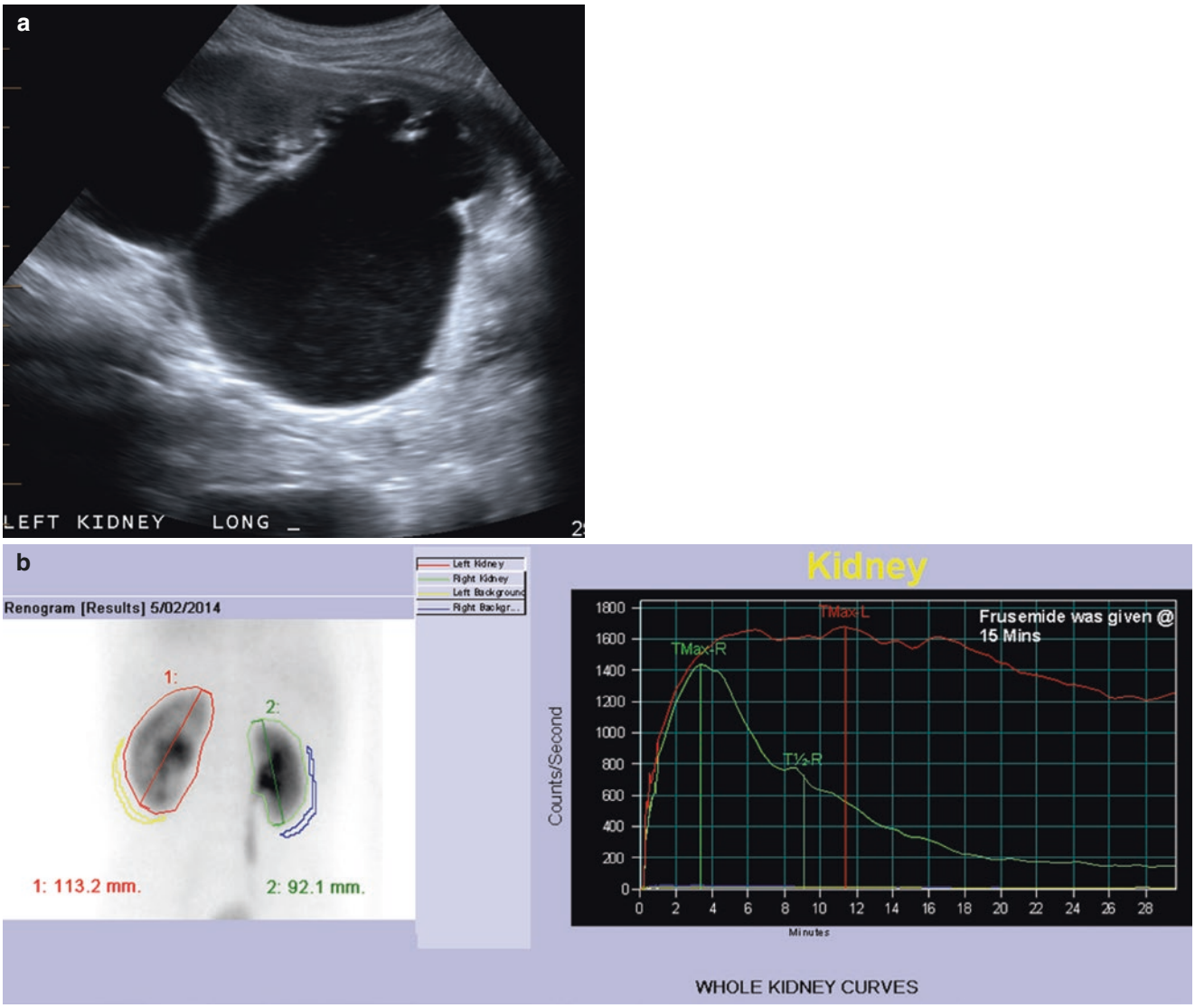

Fig. 5.9 (**a**) Longitudinal ultrasound image of the left kidney showing a typical pelviureteric junction obstruction configuration with a markedly dilated renal pelvis and no dilatation of the proximal ureter. (**b**) MAG3 study demonstrating left pelvicalyceal junction obstruction. The graphs of excretion of radiotracer against time are on the right side of the image. The right kidney drainage curve (green line) is normal, showing rapid washout of tracer. The left kidney (red line) shows prolonged accumulation of tracer with markedly delayed washout despite the application of frusemide, in keeping with obstruction

Once an MCU has excluded reflux as a potential cause, a functional nuclear medicine scan such as a ^{99m}Tc-MAG3 can be used to demonstrate obstruction of the drainage of radiotracer at the VUJ.

5.2.9 Ureterocele

Duplex kidney is the term given to the condition where the drainage system from the renal parenchyma is doubled in all or part its length. This is often an anatomical finding of little functional significance. Urinary tract infection is frequently the reason for the investigation of the urinary tract and the bifid system is found. A duplex kidney is more prone to have a ureterocele (intravesical cystic dilatation) on the distal end of the upper pole ureter, which drains into the bladder lower than the normal site or, less commonly, into the urethra or vagina. The latter can result in constant dampness of a child who also intermittently micturates normally. This wetting occurs more by day and is less troublesome at night when the child is asleep. The lower pole ureter always opens "above" the upper pole ureter—often into the normal site—but this

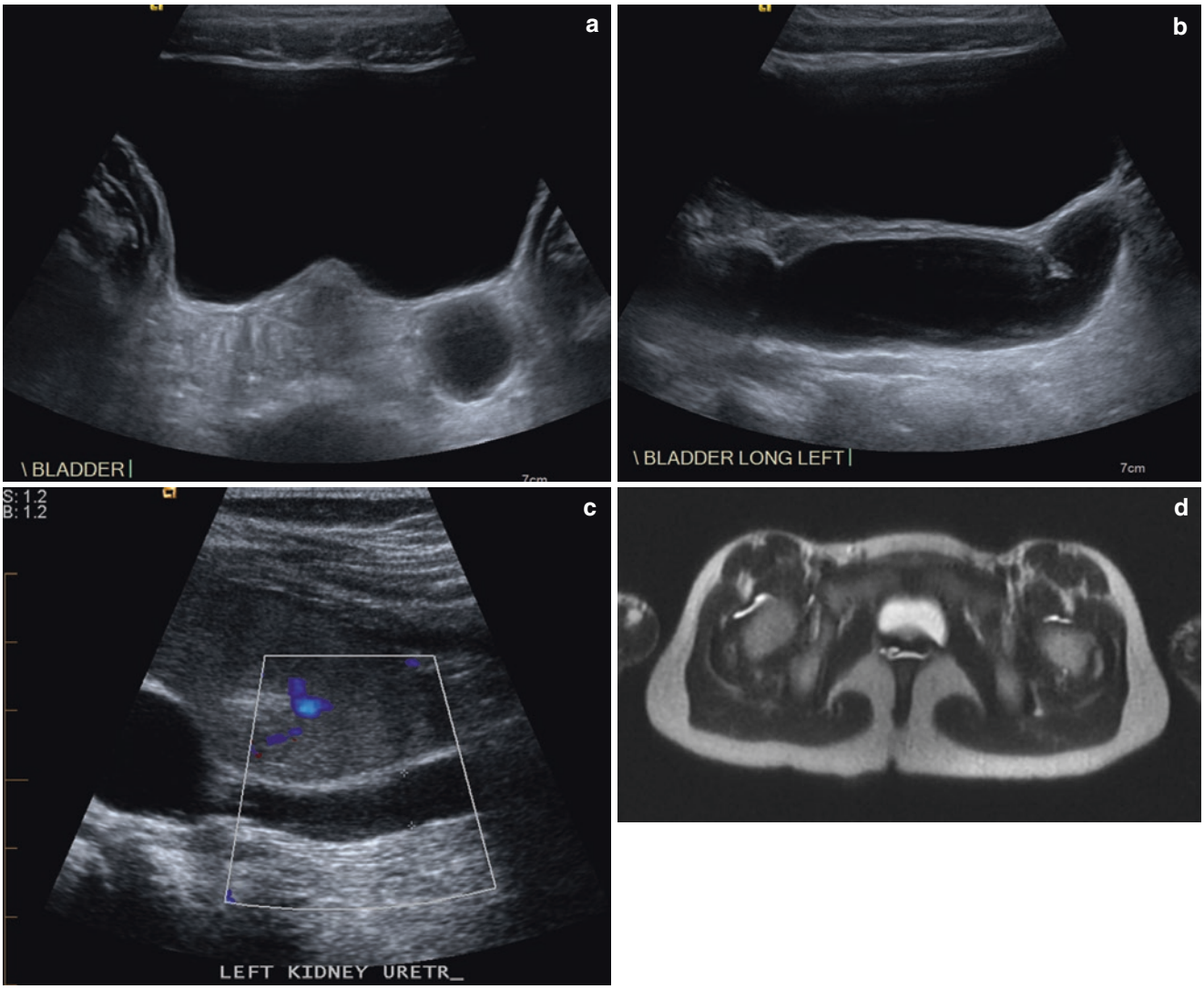

Fig. 5.10 (**a**) Transverse ultrasound image of the bladder with a dilated left distal ureter appearing as a rounded hypoechoic structure posterior to the bladder. (**b**) Longitudinal ultrasound image showing a dilated distal ureter as a tubular structure posterior to the left side of the bladder. (**c**) Longitudinal ultrasound image of a dilated proximal ureter. (**d**) Axial T2-weighted MR image showing an ectopic ureter inserting into the right side of the vagina. The vagina contains a small amount of T2 hyperintense fluid, with the ectopic ureteric insertion being visible as a tiny rounded T2 hyperintensity at the right side of the vagina. Image kindly provided by Dr Philippa Depree

ureter is more prone to have vesico-ureteric reflux. It is only the complications of duplex systems (which may be bilateral) that require treatment. This also applies to horseshoe kidney, in which the lower poles of the kidneys are in continuity across the midline (see Sect. 5.2.5).

On ultrasound, a ureterocele appears as a cystic filling defect arising from the posterior aspect of the bladder (Fig. 5.12a, b). The degree of dilatation of the associated renal pelvis and ureter can give an indication of the degree of obstruction. On MCU, a ureterocele appears as a unilateral filling defect in the bladder on early filling images (Fig. 5.12c). Later in the examination, a ureterocele may become invisible as the pressure of contrast in the bladder increases, or may even evert, and will then appear as an outpouching at the vesicoureteric junction (Fig. 5.12d). In the presence of a large ureterocele, a post-void image of the bladder should be obtained to demonstrate that the ureterocele is not blocking the bladder outlet.

Ectopic insertion of the ureter often results in a degree of obstruction and dilatation, which can occasionally allow identification of the ectopic point of insertion on ultrasound. In the older child, a T2-weighted MR of the abdomen with high-resolution sequences of the pelvis can be used to identify the ectopic insertion.

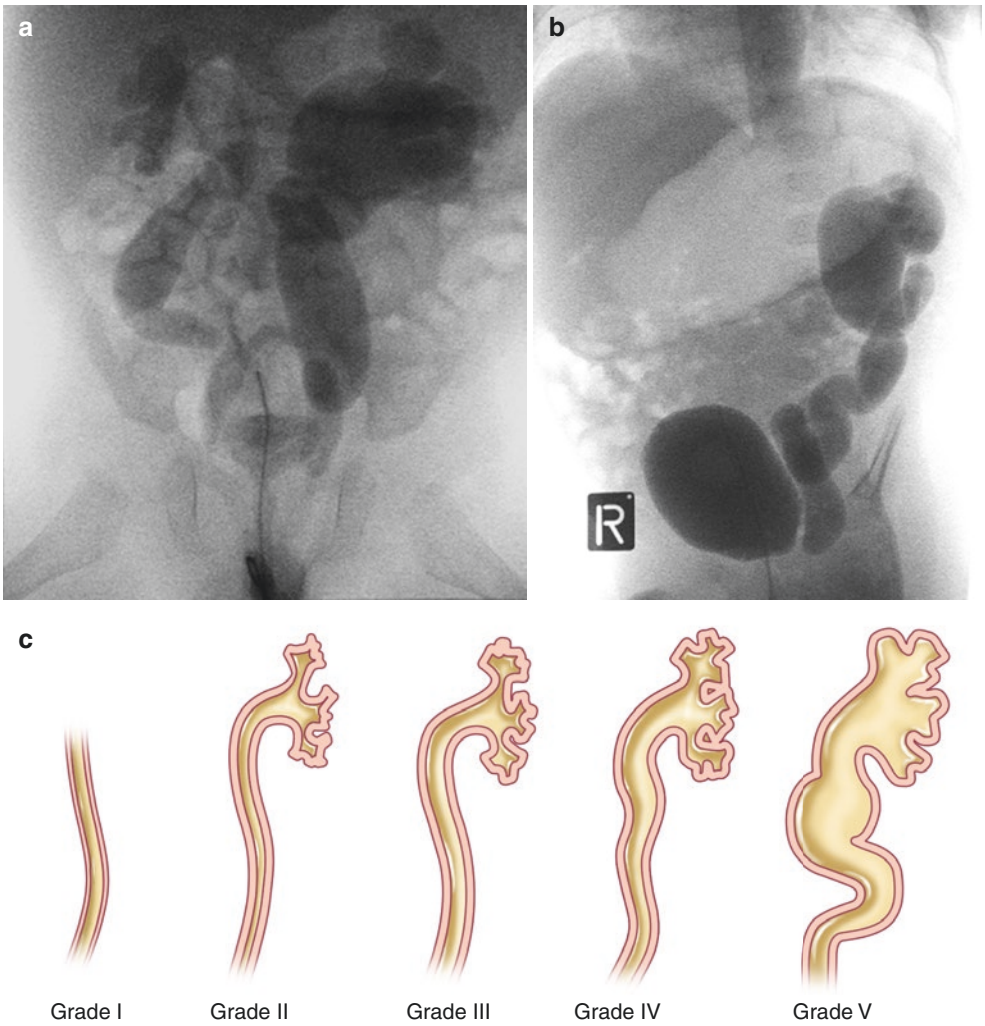

Fig. 5.11 (**a**) Image from an MCU demonstrating bilateral Grade V vesicoureteric reflux. Refluxed contrast outlines bilaterally dilated renal pelvis with clubbed calyces and dilated tortuous ureters. (**b**) Image from an MCU demonstrating left-sided Grade V reflux. (**c**) Grading of reflux

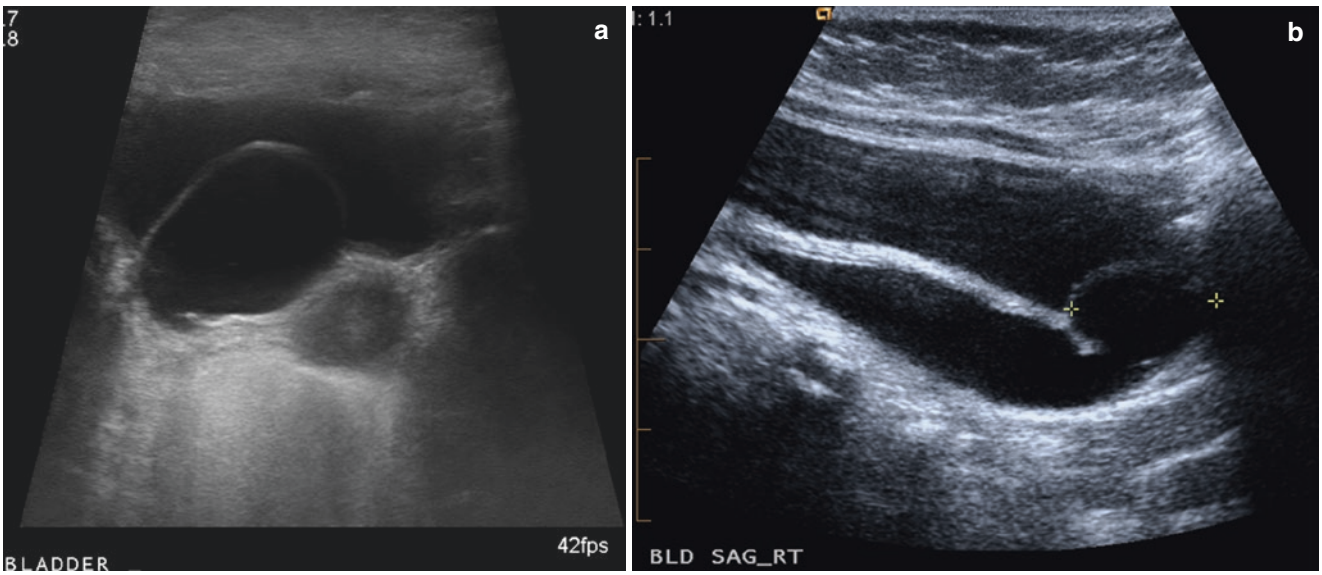

Fig. 5.12 (**a**) Transverse ultrasound image of the bladder showing a ureterocele as a rounded cystic structure at the posterior right aspect of the bladder. (**b**) Longitudinal ultrasound image of a dilated distal ureter due to an obstructing ureterocele projecting anteriorly into the bladder (right side of image). (**c**) Image from an MCU demonstrating a left-sided ureterocele as a rounded filling defect in the bladder. (**d**) Later image from the same MCU, demonstrating eversion of the left-sided ureterocele which now appears as an out-pouching at the vesicoureteric junction. A bladder diverticulum would appear similar to this image, but without the associated filling defect on the earlier image

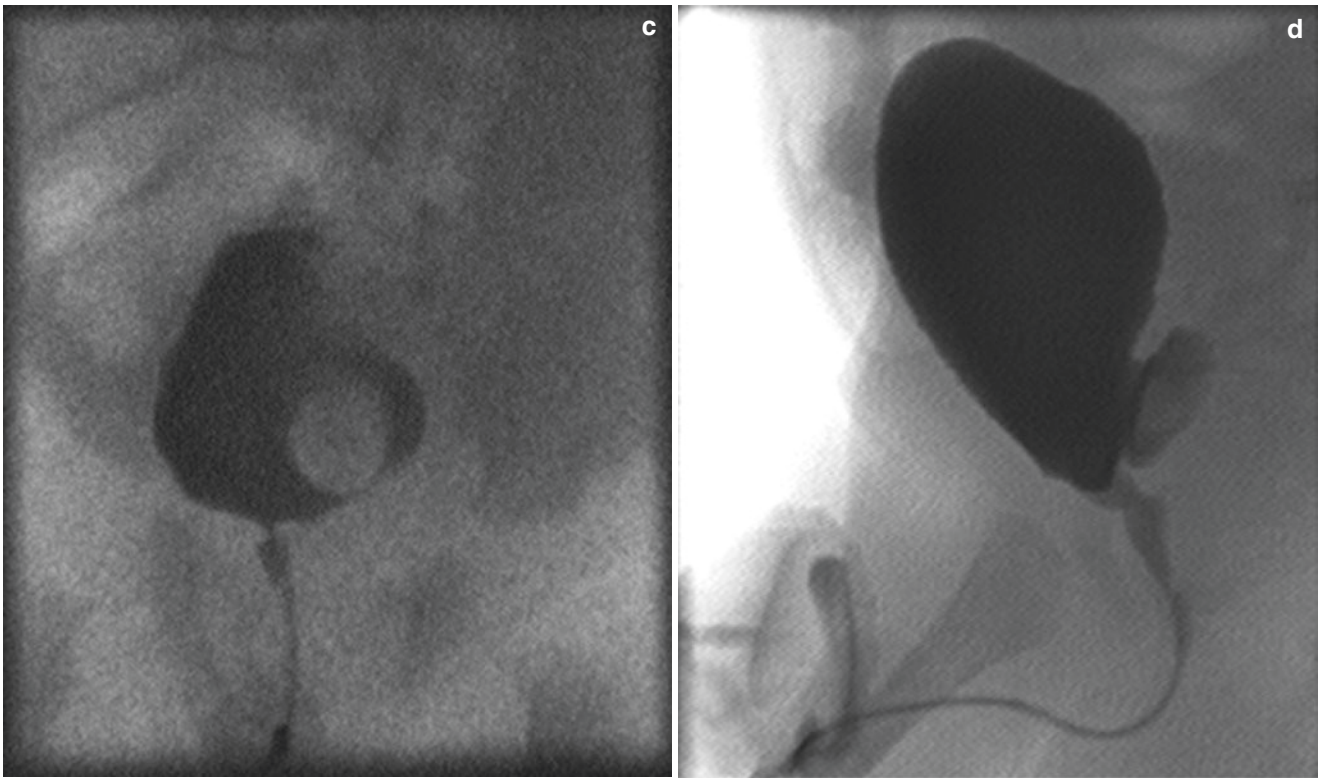

Fig. 5.12 (continued)

5.2.10 Bladder Diverticulum (Fig. 5.13)

A bladder diverticulum is visible on ultrasound or fluoroscopy as a variably sized out-pouching of the bladder wall.

5.2.11 Ectopia Vesicae and Vesicointestinal Fissure (Fig. 5.14a)

These anomalies, obvious at birth, present a frightening sight to the parents. Both deformities arise from midline deficiency of the infra-umbilical abdominal wall. The lower abdominal wall is usually reinforced by fusion of the genital tubercles. If these tubercles develop a little caudal to their normal position and then fuse in the midline, the lower abdominal wall will not be reinforced by mesoderm. The thin covering consisting of one layer of ectoderm and one layer of entoderm will break down and cause the deformity of ectopiavesicae (extroversion or extrophy of the bladder) with a dorsal urethral groove on the penis. If the genital tubercles develop even further caudally, the hypogastric area and the cloacal membrane break down to cause the rare deformity of vesico-intestinal fissure.

In ectopiavesicae the lower abdominal wall and the anterior bladder wall are absent, and the vesical mucosa prolapses through the defect. The umbilicus is usually lower than normal and represented by a scar at the apex of the bladder. There may be an associated exomphalos. The trigone and ureteric orifices lie exposed, and often urine can be seen spurting from the ureteric orifices. Pubic bones are widely separated, and the pubic symphysis is absent. In the male, the penis is short, thick set, and uptilted. The urethra forms a groove on the dorsal surface of the penis and the prepuce is split dorsally (epispadias). The scrotum is normally fused, but may be separated (bifid scrotum) and it may be empty. In the female, a vaginal orifice lies below the bladder and the clitoris is divided and lies below and posterior to the urethra. The exposed vesical mucosa is tender, and the urinary incontinence soon causes severe excoriation of the skin. Treatment of this condition has varied over the years and primary neonatal closure is now attempted in most cases. This may be with or without sacroiliac osteotomies prior to the procedure. If a functional bladder cannot be fashioned in the neonatal period, a free ileocolonic loop into which the ureters drain can form a urinary conduit. Many of these children have severe psychological problems in later life with suicidal tendencies because of the severe

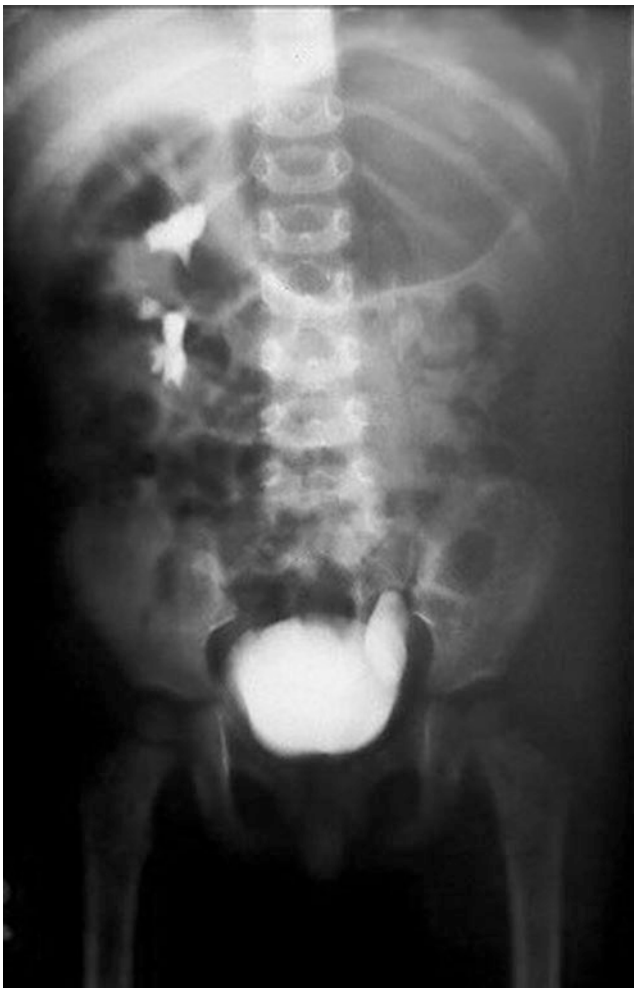

Fig. 5.13 IVU showing left-sided bladder diverticulum

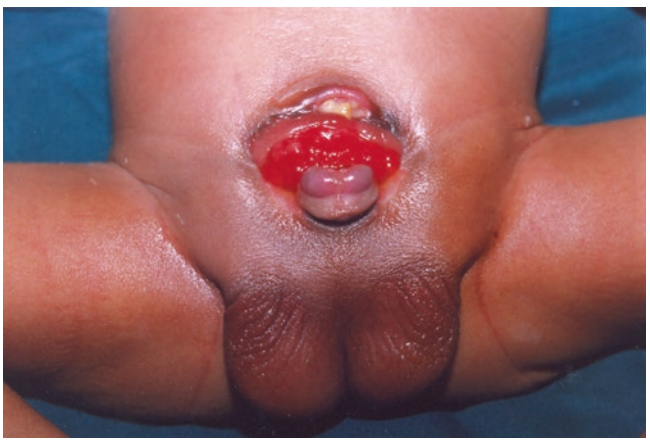

Fig. 5.14 Ectopiavesicae in a male with epispadias

deformity of the penis. All children with ectopiavesicae have wide separation of the pubic symphysis and have a waddling gait resembling that of a child with bilateral congenital dislocation of the hip.

Table 5.1 Classification of variants

1. Superior Vesical Fissure: A musculoskeletal defect is present but the bladder eventration is minimal and is limited to the apex
2. Pseudo-exstrophy: Musculoskeletal defects with no major defect except for subcutaneous location of the bladder
3. Duplicate exstrophy: Only a patch of exstrophic bladder mucosa in the infra-umbilical region is present but the urinary tract is intact
4. Superior vesical fistula: A tiny communication between the bladder and the exterior is present in addition to the musculoskeletal defect
5. Covered exstrophy with visceral sequestration wherein in addition to the musculoskeletal defect, an isolated ectopic bowel segment is present on the anterior abdominal wall near the genital area
6. Inferior vesical fissure

Table 5.1 illustrates a classification of the variants seen in clinical practice.

5.2.12 Neurogenic Bladder

A neurogenic bladder may present with incontinence and retention of urine, or more rarely as continuous dribbling or urine with retention. The neurogenic bladder is commonly associated with congenital deformities of the spine, myelomeningocele (spina bifida), tethering of the cord, sacral agenesis, trauma, tumours, anorectal anomalies, vascular disorder, and in some is idiopathic. In the more common partial sacral agenesis there is little external evidence of a spinal lesion but on X-ray sacral elements are found to be missing.

When secondary to spina bifida cystica or sacral agenesis, dribbling incontinence is usually a feature present from birth. Two types of presentation may occur. In the first, there is usually retention of urine with overflow incontinence. A large bladder is palpable and manual expression is possible, but if reflux is present damage may occur to the upper renal tract.

Urinary infection may occur with further deterioration in function and progressive damage to the renal parenchyma.

Secondary phenomena which develop in a neurogenic bladder include:

1. Thickening of the bladder wall with muscular hypertrophy and fibrosis.
2. Trabeculation of the bladder.
3. Diverticulae formation.
4. Ureterovesical obstruction secondary to pressure on the intramural part of the ureters with an obstructive hydronephrosis.

The typical ultrasound appearance of a neurogenic bladder is of a large volume, thick-walled bladder with trabeculations and potentially diverticula. It is important to obtain a

post-void volume to assess the completeness of bladder emptying if the patient is able to micturate on demand. The renal pelvicalyceal systems and parenchyma also need to be monitored to ensure upper tract obstruction is not developing due to muscular obstruction of the vesicoureteric junction or back-pressure from the abnormal bladder. Sometimes urinary retention or a neurogenic bladder can be the first indication of a spinal problem. Plain X-rays can demonstrate a vertebral abnormality such as spina bifida, which may herald an underlying spinal cord abnormality, but MR is the gold-standard investigation as it gives the best demonstration of the spinal cord, nerve roots, and thecal sac.

5.2.13 Urethral Anomalies, Posterior Urethral Valves

Posterior urethral valves are frequently diagnosed by antenatal ultrasound. The male foetal bladder will be of large volume, often with a characteristic "keyhole" appearance due to dilatation of the posterior urethra proximal to the valve (Fig. 5.15a). Upper renal tract dilatation and oligohydramnios are frequently seen in association. Very occasionally, rupture of the upper tracts due to severe obstruction may lead to urinary ascites (Fig. 5.15b). The bladder wall is usually grossly thickened secondary to the outlet obstruction, but this may be more easily appreciated after the bladder has been drained via a catheter (Fig. 5.15c). Postnatally, significant bilateral renal collecting system dilatation in a male infant should prompt evaluation for valves with a micturating cystourethrogram. The MCU will demonstrate a trabeculated bladder and a dilated posterior urethra (Fig. 5.15d). Occasionally the valve may be visible as a thin membrane traversing the urethral lumen at the site of calibre change (Fig. 5.15e), but frequently the valve itself is imperceptible on imaging. Bilateral vesicoureteric reflux is common, sometimes occurring spontaneously on bladder filling and before micturition is achieved (Fig. 5.15f). Careful ultrasound follow-up of the kidneys is required to ensure normal growth.

Urethral strictures are best demonstrated using urethrography, which will demonstrate a focal area of narrowing.

5.2.14 Ectopic Testis

In this condition the testes lie outside the normal line of descent into the scrotum and come to lie in some adjacent region. Undescended testes within the inguinal canal are difficult or impossible to palpate. A testis that is palpable over the inguinal canal, lateral to the external inguinal ring, is usually ectopic. By firmly pressing the testis medially along the line of the inguinal canal, the undescended testis will disappear into the abdomen, while an inguinal ectopic testis will become more prominent. The ectopic testis cannot be manipulated into the scrotum. Less common sites of an ectopic testis are in the perineum at the root of the penis or the upper thigh. The testis and epididymis may be atrophic and sometimes completely separate. Laparoscopy is used to identify an impalpable testis.

Ultrasound is a useful first investigation to locate a testis that is absent from the scrotum, as it can reliably assess the path of testicular descent through the inguinal canal. If this fails to identify the testis, then MR of the pelvis can be used.

5.2.15 Ovarian Cyst

Uncomplicated ovarian cysts are visible on ultrasound as anechoic thin-walled round or oval structures, intimately associated with ovarian tissue (Fig. 5.16a). In the event of haemorrhage into a cyst, the cyst content becomes complex but will not contain internal Doppler flow. If the haemorrhagic cyst ruptures, the escape of haemorrhagic fluid into the peritoneum will cause pain, and hypoechoic free fluid will be present in the pelvis. The presence of an ovarian mass such as a large cyst increases the risk of ovarian torsion. The typical ultrasound appearance of a torted ovaryis of an enlarged ovary with central echogenic stroma and peripheralized follicles (Fig. 5.16b, c). The presence of Doppler flow in an ovary does not exclude torsion, as some flow can still be present due to incomplete vascular occlusion and the dual blood supply of the ovary.

5.2.16 Persistent Mullerian Duct

In females the Mullerian ducts (paramesonephric ducts) develop into the uterine tubes, uterus, cervix, and upper part of the vagina. In males the Mullerian ducts should regress completely. Persistence of a portion of the Mullerian ducts in a male patient may result in a Mullerian duct cyst. On ultrasound or MRI, a Mullerian duct cyst appears as a midline cystic structure below the bladder base. Mullerian duct cysts do not communicate with the urethra. The main imaging differential is that of a prostatic utricle cyst, which will communicate with the urethra (Fig. 5.17).

Persistent Mullerian Duct Syndrome is a very rare condition that occurs when the derivatives of the Mullerian ducts (uterine tubes, uterus, cervix, and upper vagina) are present in a genetically and otherwise phenotypically male patient. In these cases there may be communication between the posterior urethra and the uterus (Fig. 5.18). Cryptorchidism is usually present.

5.2.17 Vagina

In the neonate, an obstructed vagina or uterus will be filled with debris due to maternal hormonal stimulation of the endometrium. If this condition is not identified on antenatal ultrasound or on physical examination of the neonate, it is unlikely to come to attention until menarche, when amenorrhoea and abdominal pain due to vaginal and uterine distension with blood prompt investigation. The distended vagina (haematocolpos) and uterus (haematometra) are visible on ultrasound as fluid-filled tubular structures, usually close to the midline. The findings can also be elegantly illustrated with MRI (Fig. 5.19), although this is not usually necessary.

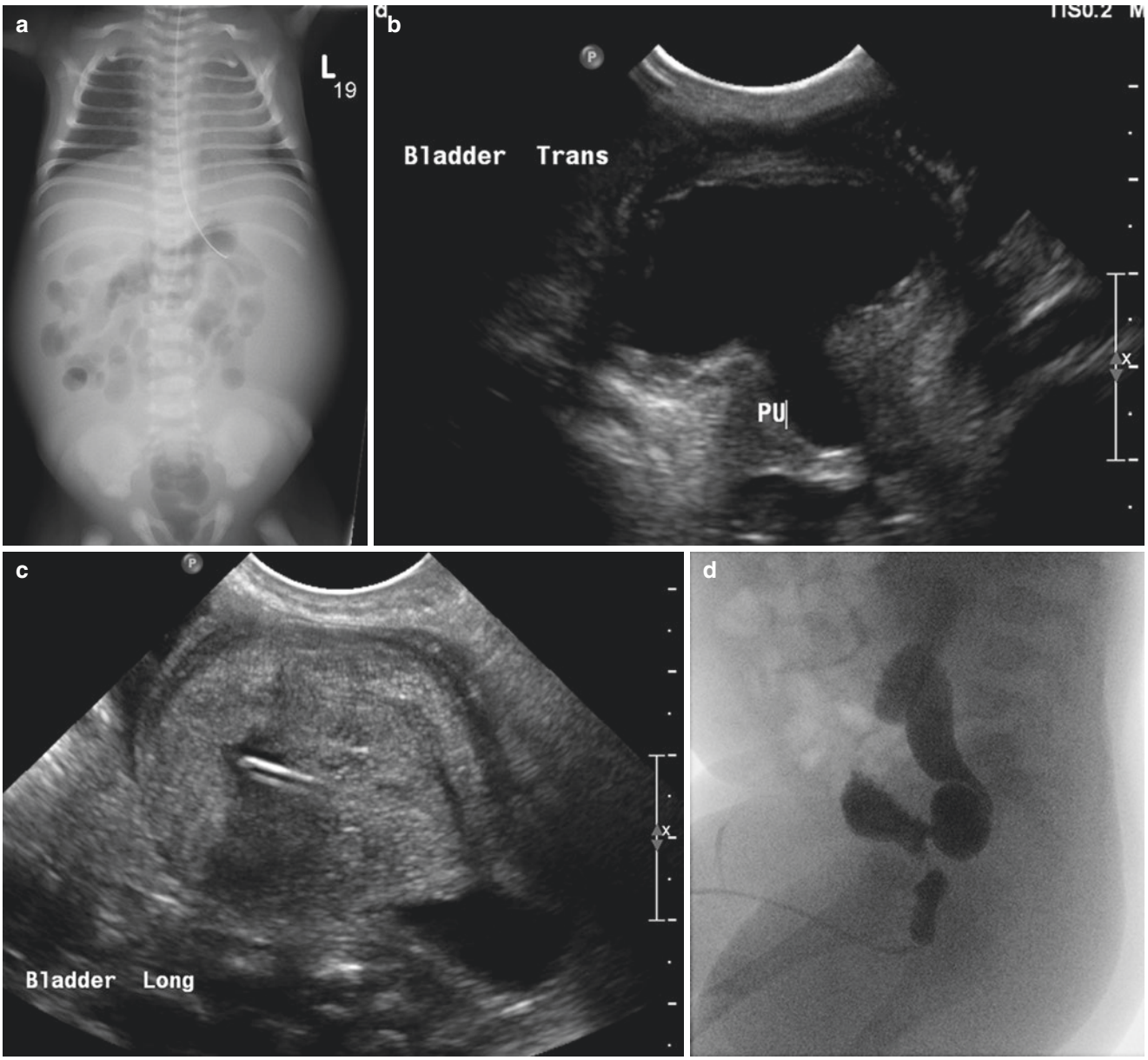

Fig. 5.15 (**a**) Transverse ultrasound image of the bladder in the presence of posterior urethral valves. The bladder shows the typical "keyhole" appearance due to the dilated posterior urethra (PU). (**b**) X-ray of a new-born with urinary ascites following rupture of the collecting system due to bladder outlet obstruction by posterior urethral valves. The abdomen is distended by fluid, which is displacing the gas-filled small bowel into the centre of the abdomen. (**c**) Longitudinal midline ultrasound image of the bladder, demonstrating gross bladder wall thickening. A urinary catheter is present in the collapsed lumen of the bladder, and anechoic urine is present in the dilated posterior urethra. (**d**) Image from an MCU demonstrating a dilated posterior urethra and trabeculated bladder typical of posterior urethral valves, and reflux into a left-sided ureterocele and ureter. (**e**) Image from an MCU demonstrating a dilated posterior urethra. The posterior urethral valve is clearly visible as a thin linear filling defect immediately distal to the dilated segment. (**f**) A post mortem specimen illustrating the position of the urethral valves in the posterior urethra causing obstruction

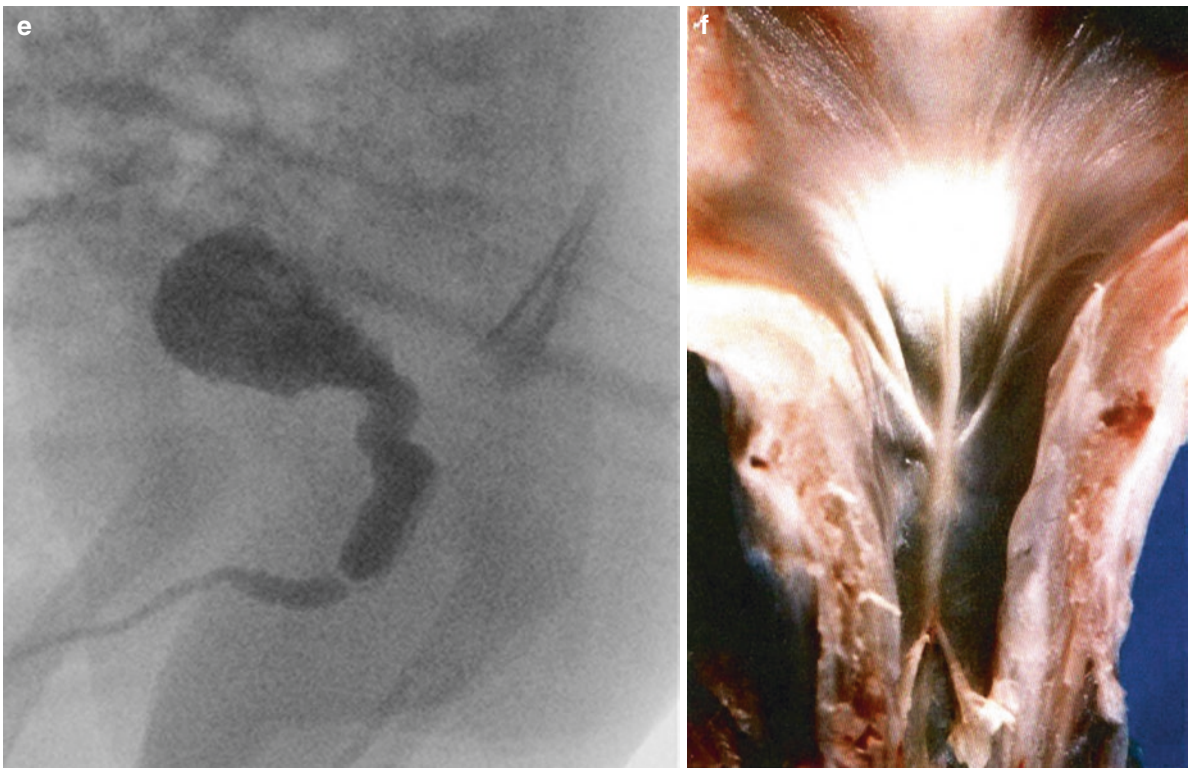

Fig. 5.15 (continued)

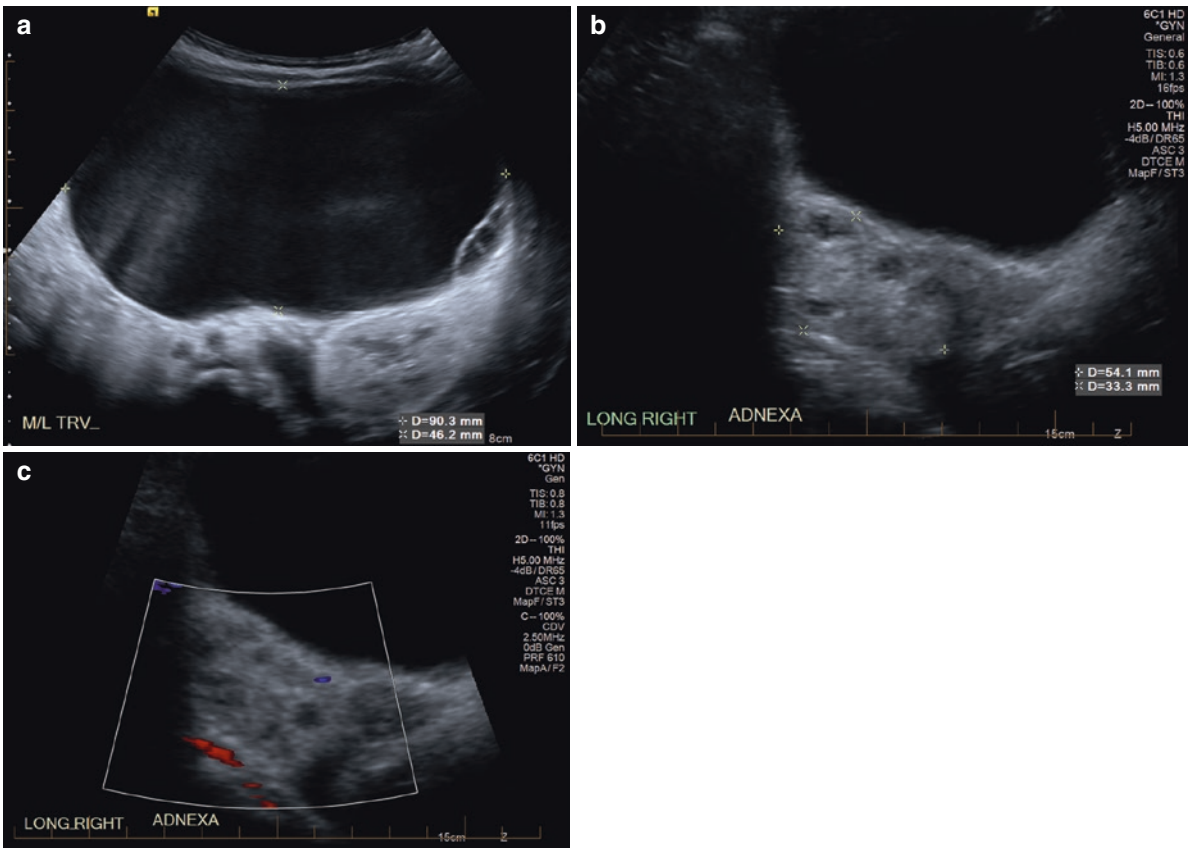

Fig. 5.16 (**a**) Image of a 9 cm ovarian cyst in an infant. The cyst contains a small number of daughter cysts at the periphery, suggesting it is of ovarian origin. (**b**) Longitudinal image of the right adnexa showing ovarian torsion. The ovary is enlarged and echogenic, with peripherally located follicles. (**c**) Longitudinal image of the same ovary as in (**b**). Note the paucity of vascular flow. Note that the presence of flow on Doppler does not exclude torsion

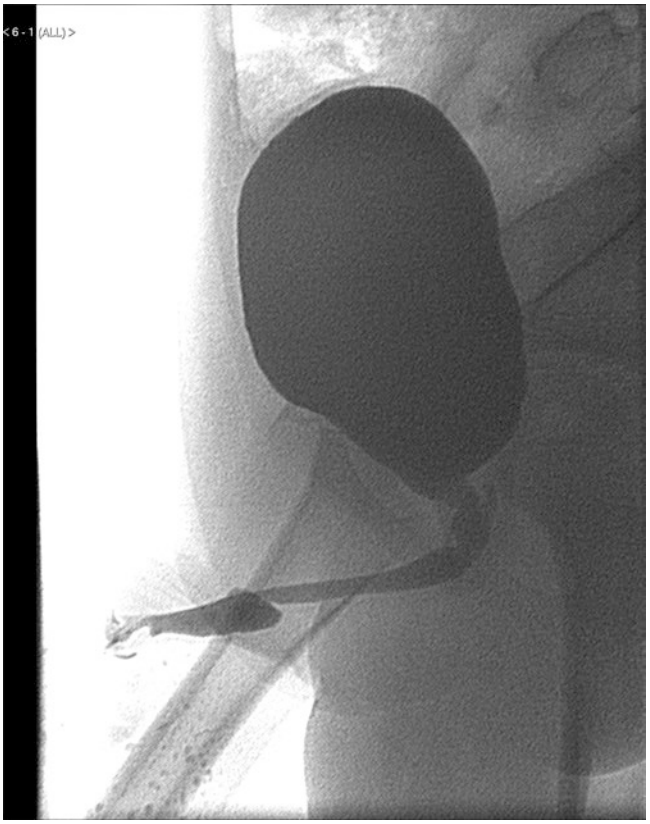

Fig. 5.17 Prostatic utricle. Image from an MCU demonstrating contrast filling a prostatic utricle, at the posterior aspect of the urethra

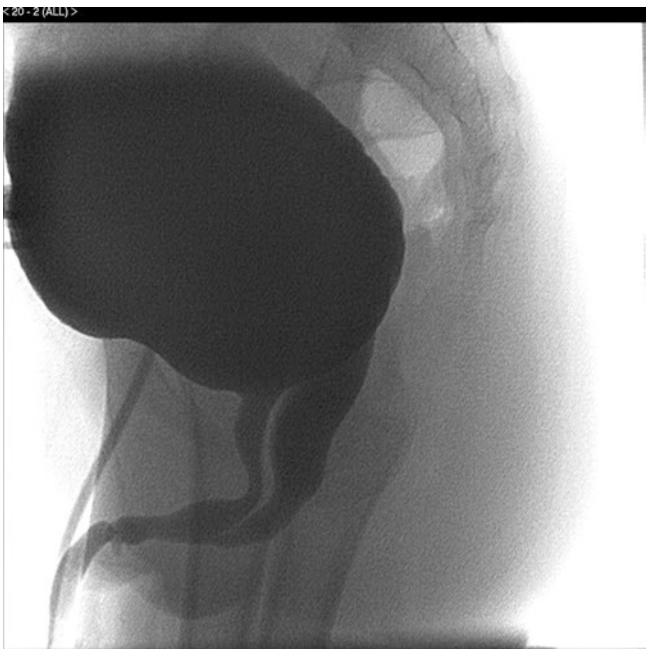

Fig. 5.18 Persistent Mullerian duct. Image from an MCU demonstrating filling of a uterine cavity at the posterior aspect of the male urethra

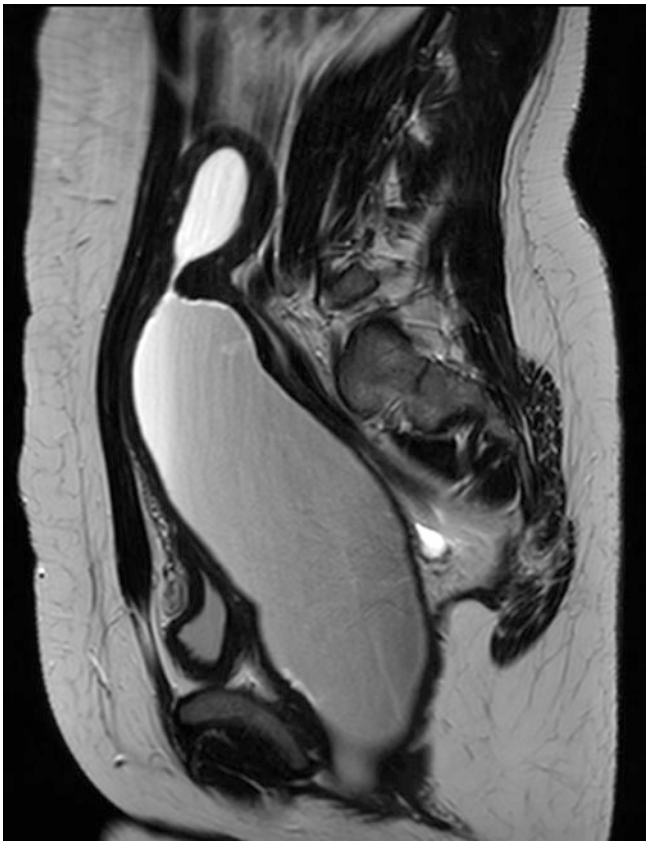

Fig. 5.19 Sagittal T2-weighted MRI image demonstrating haematometrocolpos. High signal fluid distends the obstructed vagina and uterus. The low-volume bladder lies anterior to the massively distended vagina

5.2.18 Hydrocalycosis

Hydrocalycosis is the term used to describe dilatation of an isolated major calyx due to an infundibular stenosis. The dilated calyx may retain its characteristic shape (Fig. 5.20a), or may become rounded, in which case it may be difficult to distinguish from a renal cyst. Imaging performed with contrast in the urographic phase will demonstrate communication between the calyx and the remainder of the collecting system, thereby excluding a simple cyst (Fig. 5.20b, c).

5.2.19 Retrograde Pyelogram

A retrograde pyelogram is performed by cannulating the ureteric orifice at the time of cystoscopy and injecting contrast material retrograde into the upper collecting system.

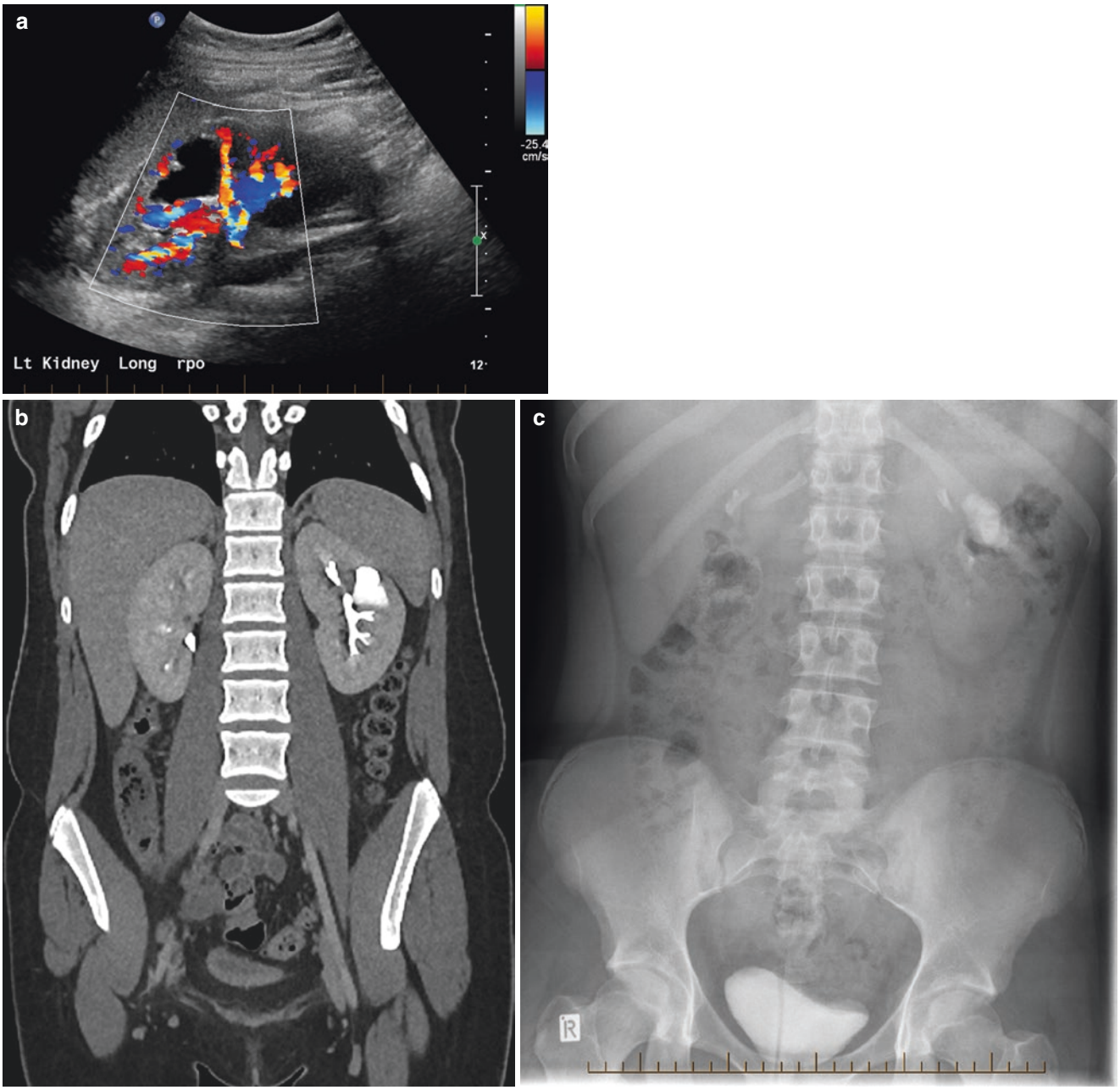

Fig. 5.20 (**a**) Longitudinal ultrasound image of a calyceal diverticulum. While the differential diagnosis of this anechoic structure would include a cyst, the morphology is suggestive of a dilated calyx. (**b**) Coronal contrast enhanced CT, urographic phase, demonstrating an isolated dilated calyx in the upper pole of the left kidney. Contrast within the calyx confirms continuity with the collecting system, thus differentiating it from a renal cyst. (**c**) Delayed plain film of the same patient as Fig. 5.19b, demonstrating persistence of contrast in the calyceal diverticulum. There is a trace of residual contrast within the renal collecting systems elsewhere, as well as in the bladder

5.2.20 Urachal Anomalies

The urachus is an embryological structure, tubular in shape, that connects the developing bladder to the umbilical cord. The urachus usually involutes to become a fibrous cord, the median umbilical ligament. Failure of complete involution of the urachus may result in one of several urachal anomalies. A patent urachus remains patent throughout its entire course, with leakage of urine from the umbilicus. When one end of the urachus fails to involute, the result is either a urachal sinus (failure of involution of the umbilical end of the urachus) or a vesicourachal diverticulum (failure of involution of the caudal end of the urachus). A urachal cyst may occur at any point along an otherwise obliterated urachus and may become infected.

A patent urachus can be elegantly demonstrated by MCU. A vesicourachal diverticulum can also be diagnosed on MCU or ultrasound as an outpouching of the midline anterior bladder wall. Urachal cysts are best shown with

ultrasound, as they lie at the deep aspect of the anterior abdominal wall between the bladder dome and umbilicus, very close to the midline (Fig. 5.21a, b). CT may be useful to clarify anatomy if extensive infective change distorts the usual anatomical relationships (Fig. 5.21c).

5.3 Infection/Inflammation

5.3.1 Calculi

Most paediatric renal calculi may be readily demonstrated with ultrasound. Calculi appear as echogenic foci in the collecting system, with posterior acoustic shadowing due to marked reflection of the sound waves at the surface of the stone (Fig. 5.22a). Colour Doppler interrogation may demonstrate "twinkle artefact," which is concentrated bright-speckled colour signal overlying the stone. Calculi within the ureters may be more difficult to identify with ultrasound due to overlying bowel gas, but calculi at the pelviureteric junction and in the distal ureter close to the vesicoureteric junction may be visualised by using the kidney or bladder as a sonographic window. While many renal calculi are visible on plain film (Fig. 5.22b), a reasonable proportion are not. CT can confidently identify all stones and assess their size and the degree of renal tract obstruction (Fig. 5.22c). While CT has the disadvantage of an increased radiation burden for the patient, modern CT scanners can produce diagnostic images at impressively low dose and can serve as a useful problem-solving modality when ultrasound and plain films

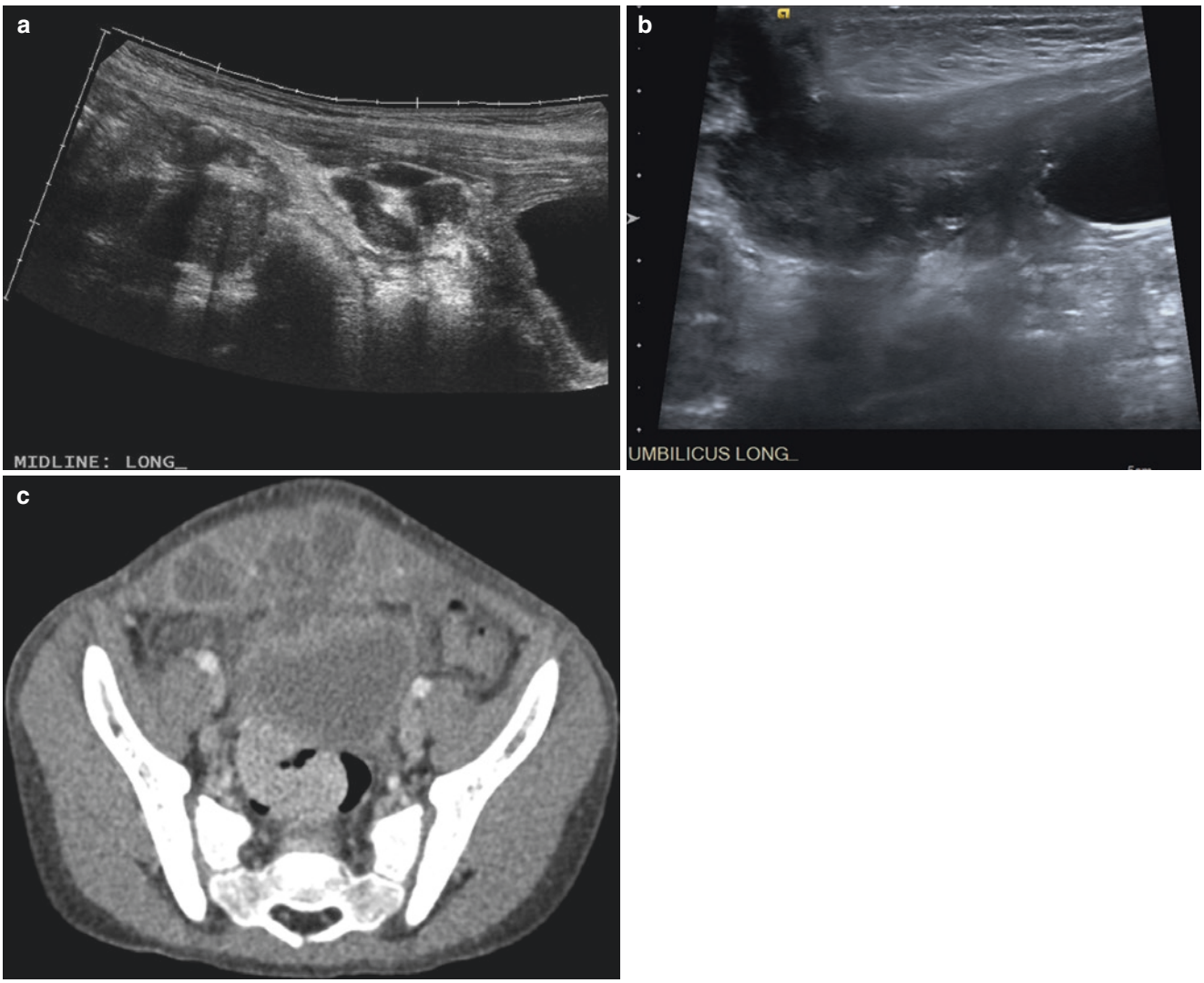

Fig. 5.21 (**a**) Longitudinal ultrasound image of a urachal cyst. The bladder is on the right side of the image and contains anechoic urine. Superior to the bladder there is a complex cystic structure which is predominantly hypoechoic. (**b**) Longitudinal ultrasound image of an inflamed urachal cyst. Hypoechoic material can be seen extending from the dome of the bladder (right side of image) to the umbilicus (left side of image). (**c**) Axial contrast-enhanced CT showing a multiloculated abscess of the anterior abdominal wall, arising from an infected urachal cyst. Note the thickened anterior wall of the bladder

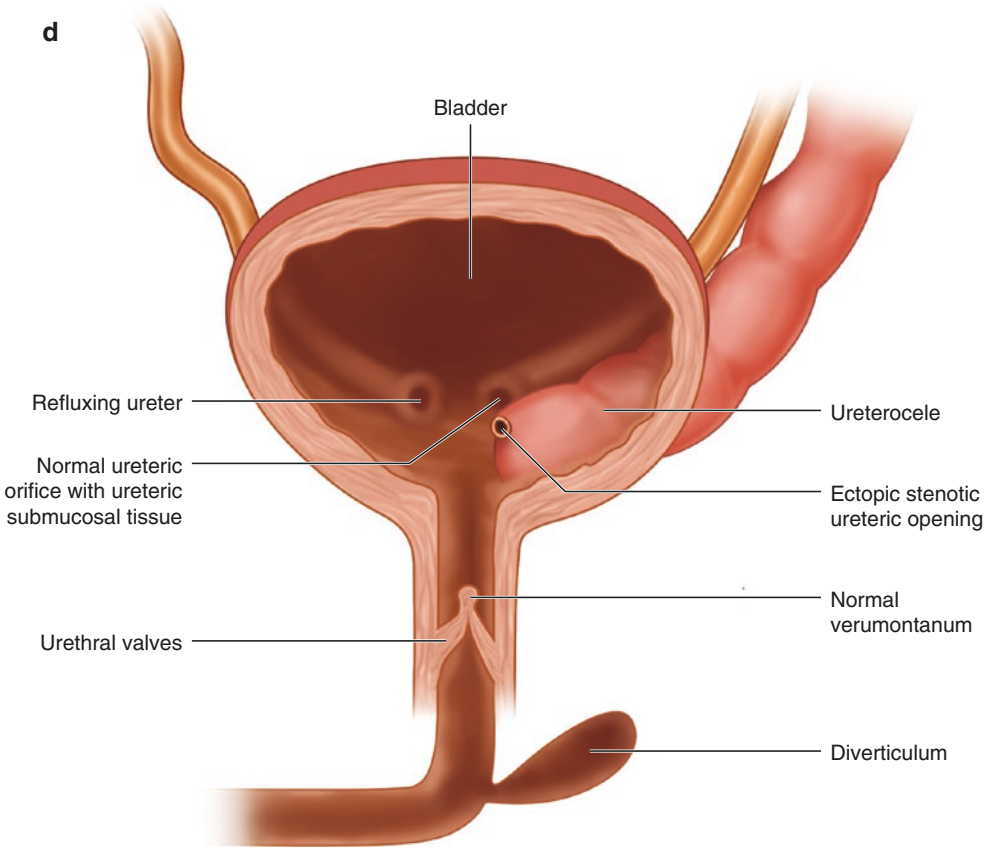

Fig. 5.21 (continued)

leave unanswered questions. Calculi in the bladder may similarly be diagnosed by the above modalities (Fig. 5.22d).

5.3.2 Xanthogranulomatous Pyelonephritis (Fig. 5.23)

Xanthogranulomatous pyelonephritis (XGP) is a form of chronic pyelonephritis, rare in children. It is often associated with renal calculi. On ultrasound the involved kidney is enlarged, and while it may be irregular, remains reniform. It may appear echogenic or heterogeneous if necrosis or focal abscess formation is present. Function is usually reduced or absent. Differentiation between XGP and renal neoplasia can be difficult, but the presence of calculi in the collecting system should sway the differential toward XGP. CT can help to confirm the diagnosis and can accurately depict extension of infection outside the kidney (Fig. 5.24a, b). The clinical presentation of this condition can sometimes be mistaken for a much more common condition called pyelonephritis (Fig. 5.24c).

5.3.3 Fungal Infection/Obstruction

Fungal infection of the renal tract usually occurs only in premature neonates and the immunocompromised. Ultrasound is usually the first imaging investigation. Fungal infection may produce many of the features seen in bacterial infection of the urinary system, with bladder wall thickening and debris. The kidneys may demonstrate focal or diffuse inflammatory change, which may be of variable echogenicity, usually with increased vascularity on colour Doppler unless focal abscess formation intervenes. Fungal infection of the kidneys may result in the formation of "fungal balls" (mycetomas), which appear on ultrasound as rounded, non-shadowing echogenic foci within the collecting system. They may cause obstruction (Fig. 5.25a).

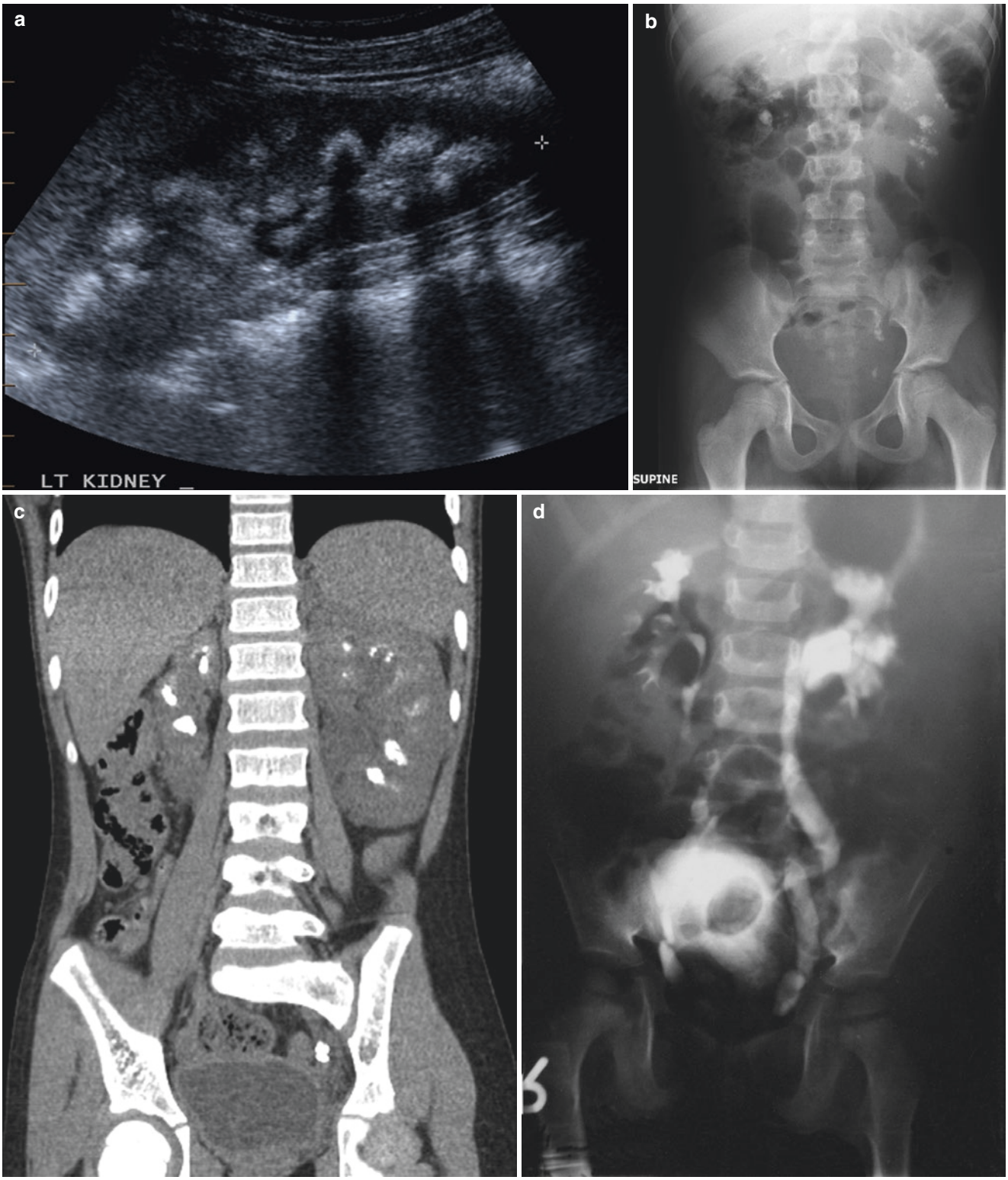

Fig. 5.22 (**a**) Longitudinal ultrasound image of the kidney in a patient with renal tubular acidosis, demonstrating multiple renal calcifications. The calcifications are echogenic and demonstrate posterior acoustic shadowing. (**b**) Plain X-ray of the same patient as in (**a**), demonstrating multiple calcifications overlying the renal shadows with calculi present in the left distal ureter. (**c**) Coronal non-contrast CT of the same patient as in (**a**), demonstrating multiple renal and ureteric calculi. There is dilatation of the left pelvicalyceal system indicating a degree of ureteric obstruction. (**d**) IV urogram demonstrating multiple bladder calculi, visible as filling defect within the bladder

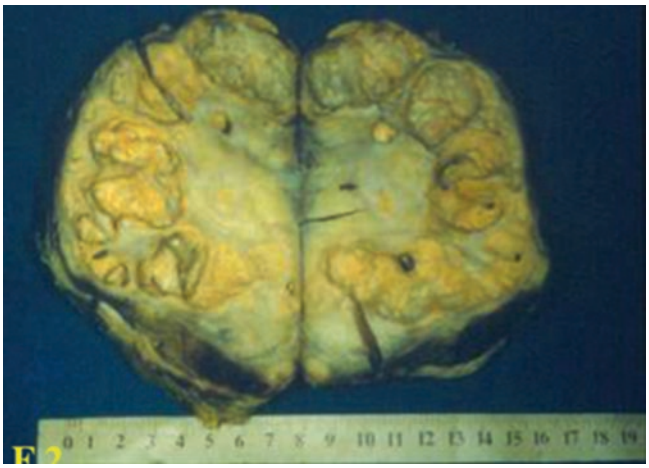

Fig. 5.23 Pathological specimen of xanthogranulomatous pyelonephritis (XGP)

5.3.4 Tuberculosis

Tuberculous infection of the renal parenchyma occurs via haematogenous spread of *Mycobacterium*. The radiological manifestations of acute infection are similar to other bacterial infections. On ultrasound, the kidneys may be swollen and echogenic, but may appear normal. Later, in the course of chronic infection, there will be parenchymal volume loss. Dystrophic calcification often occurs, and can be visible on plain X-ray, ultrasound, or CT. Infundibular stenoses within the collecting system may result in focal calyceal dilatation. End-stage renal tuberculosis typically results in a shrunken, heavily calcified kidney, the so-called "autonephrectomy" (Fig. 5.25b).

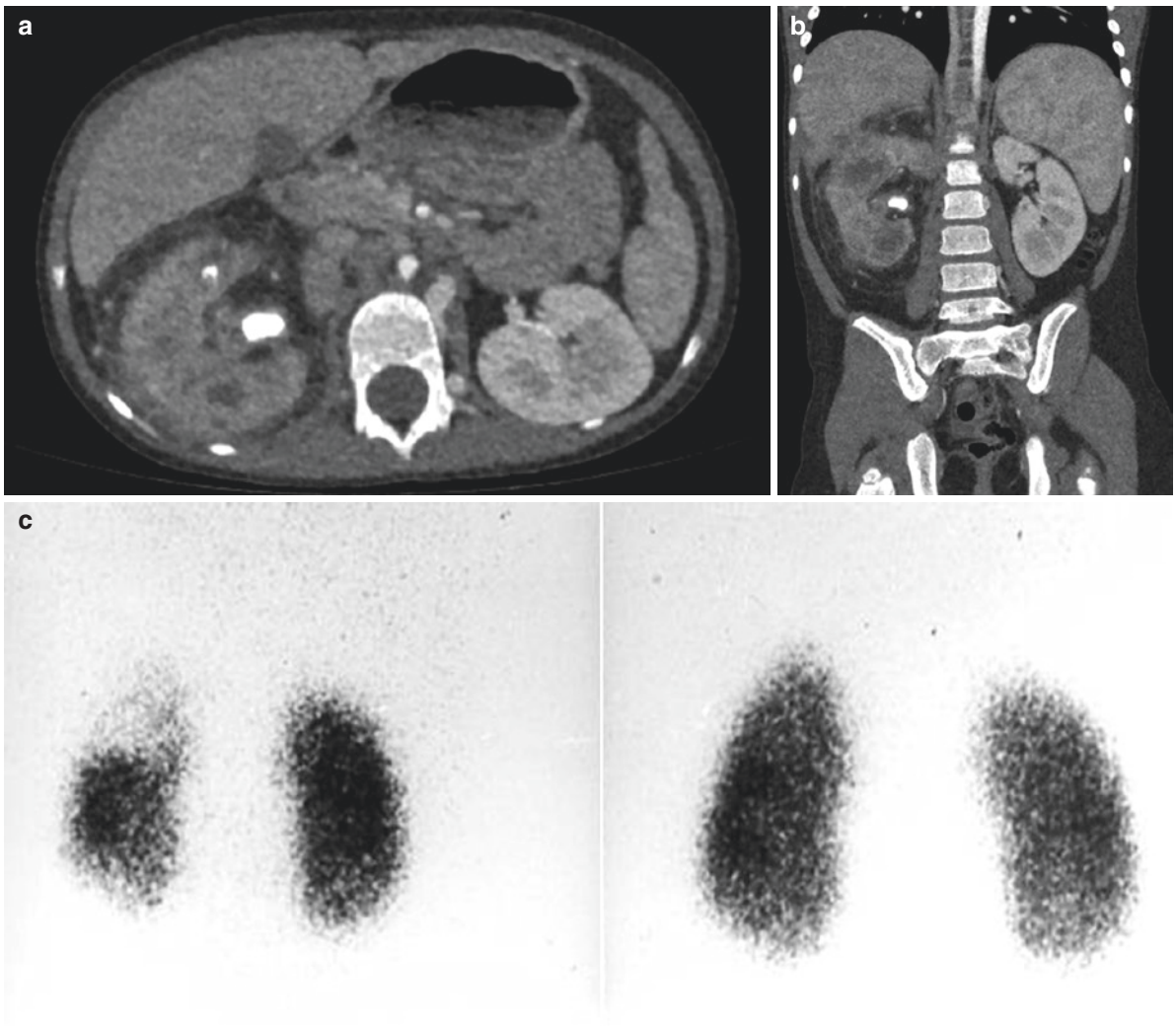

Fig. 5.24 (**a**) Axial contrast-enhanced CT of right-sided xanthogranulomatous pyelonephritis. A calculus is present in the renal pelvis with low attenuation change present throughout the swollen kidney. There is stranding of the perinephric fat. (**b**) Coronal contrast-enhanced CT of right-sided xanthogranulomatous pyelonephritis, the same patient as (**a**). There is focal fluid attenuation in the upper pole of the right kidney in keeping with an abscess with a further small perinephric abscess lying between the kidney and liver. (**c**) Figure shows ^{99m}Tc-DMSA scan of pyelonephritis in one kidney; note the flea-bitten appearance of the isotope scan in the upper pole

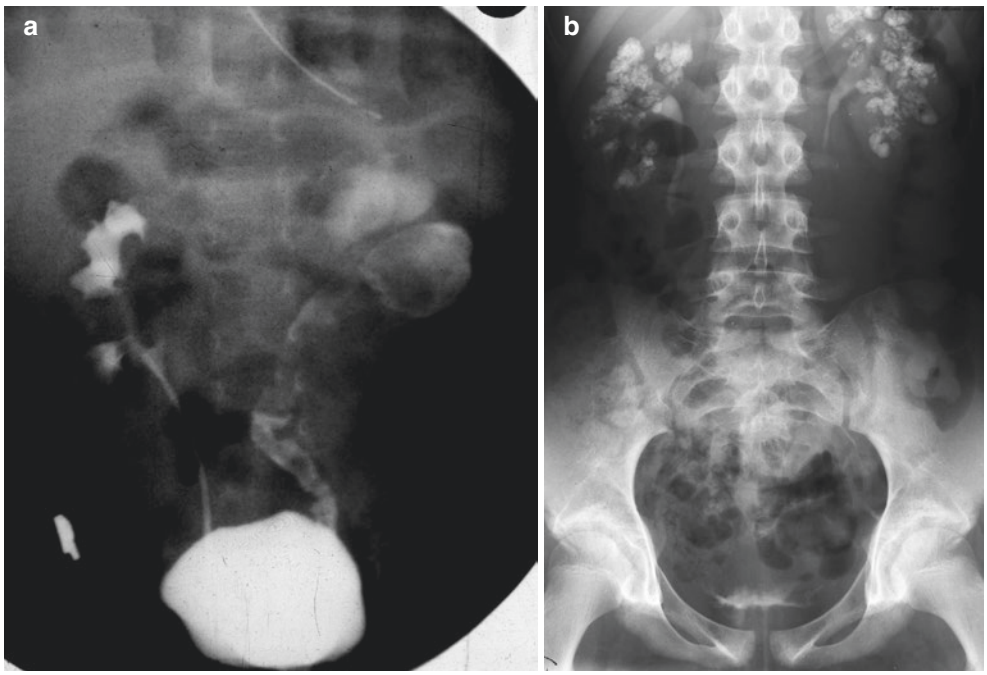

Fig. 5.25 (**a**) Fungal infection of the urinary tract shown on IVU. Multiple mycetomas, visible as filling defects within the dilated renal collecting systems. (**b**) Calcification of the kidneys in a case of renal tuberculosis

5.3.5 Cystitis Cystica

Cystitis is visible on ultrasound as bladder-wall thickening. In simple acute infective cystitis, the bladder-wall thickening is often diffuse and regular. Mobile debris within the bladder is often present in association, but when seen in isolation has low specificity for bladder infection. In haemorrhagic cystitis the bladder wall may be echogenic, thickened, and irregular (Fig. 5.26). Cystitis cystica is a result of chronic irritation of the bladder and causes irregular bladder-wall thickening, with small cystic foci bulging into the bladder lumen.

Emphysematous pyelonephritis, in which gas is present in or around the infected kidney, is very rare in children. In the adult population it usually occurs in the setting of uncontrolled diabetes or immunocompromise. Plain X-rays may show patchy lucency within the renal fossae. Ultrasound may show poorly defined or mobile echogenicity, which produces acoustic shadowing that is indicative of gas. CT can clearly show the gas and its relationship to the kidney, perinephric tissues, and collecting system.

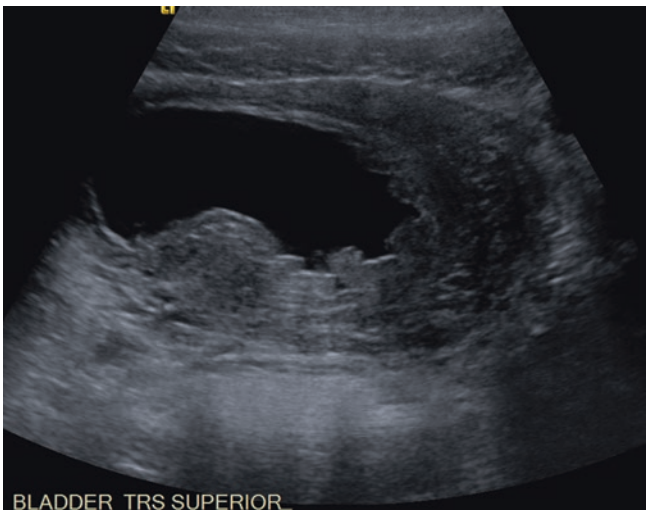

Fig. 5.26 Haemorrhagic cystitis. Axial ultrasound image of the bladder showing irregular thickening

5.4 Trauma

5.4.1 Kidney

Contrast-enhanced CT is the imaging method of choice in the investigation of acute renal trauma. On CT, lacerations of the kidney appear as non-enhancing linear areas, sometimes branching in configuration (Fig. 5.27a). CT also demonstrates perinephric haematoma and extravasation of contrast due to active bleeding (Fig. 5.27b, c). Delayed imaging may demonstrate extravasation of contrast from injury to the collecting system. While ultrasound can be used to image the kidney following trauma, it should be reserved for follow-up of injuries previously characterised with CT (Fig. 5.27d), delayed presentations of stable patients, or reassurance in the setting of a low pre-test probability of significant injury. A severity grading system of renal injury has been developed by the American Association for the Surgery of Trauma (AAST)

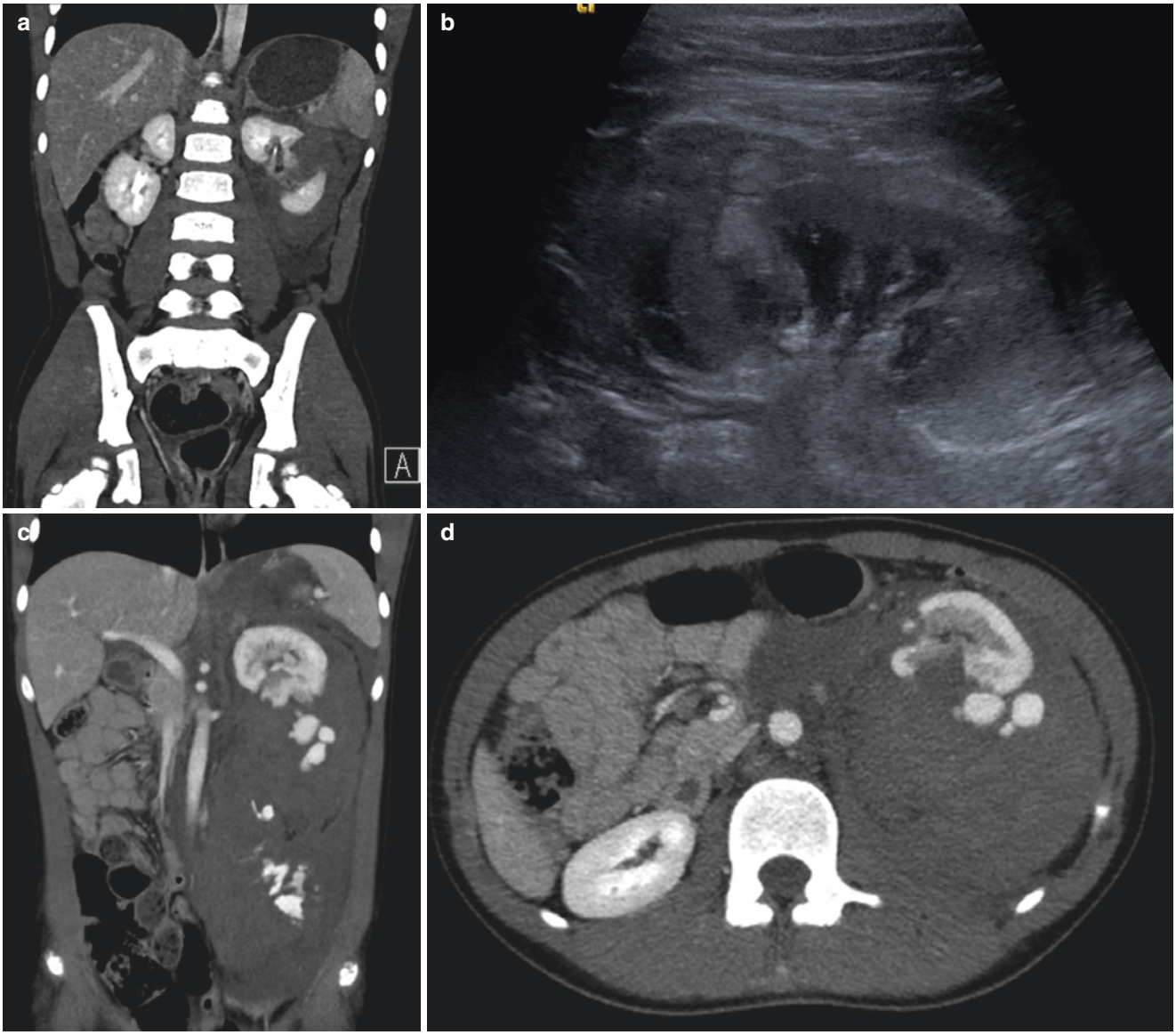

Fig. 5.27 (**a**) Coronal contrast-enhanced CT. There is a laceration through the mid interpolar left kidney with a large perinephric haematoma. (**b**) Longitudinal ultrasound image of left kidney of the same patient as in (**a**). The renal laceration is visible as an echogenic avascular defect in the mid interpolar kidney, communicating with echogenic perinephric haematoma. (**c**) Coronal contrast-enhanced CT. High-grade left renal injury with massive perinephric haematoma and active extravasation of contrast in keeping with active haemorrhage. (**d**) Axial contrast-enhanced CT in the same patient as in (**c**). Note the anterior displacement of the renal fragment by the large perinephric haematoma. The patient was successfully treated non-operatively

5.4.2 Collecting System

Delayed images from a contrast-enhanced trauma CT may demonstrate extravasation of contrast from a damaged renal collecting system. Demonstration of such a contrast leak can also be achieved using a plain film after a CT, and while the level of anatomical detail will be reduced compared to a CT, so will the radiation dose to the child. Ultrasound can be used to detect a urinoma, a focal collection of extravasated urine (Fig. 5.28).

5.4.3 Bladder

The suspicion of bladder injury may be raised by the presence of fluid and/or stranding adjacent to the bladder on ultrasound or CT. The most definitive imaging is by cystography, where contrast material is injected into the bladder via a urethral or suprapubic catheter under fluoroscopic screening. Contrast can be demonstrated leaking into the peritoneum or into the extraperitoneal space of Retzius (Fig. 5.29a, b).

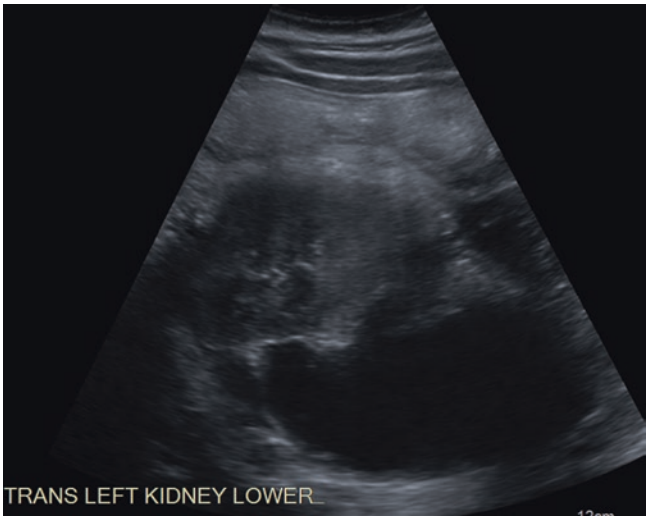

Fig. 5.28 Longitudinal ultrasound image of a kidney performed 5 days after a high-grade renal injury shows development of a well-defined anechoic fluid collection, in keeping with a urinoma and indicative of injury to the renal collecting system

5.4.4 Urethra

The male urethra is at risk of damage in straddle injuries. Ultrasound may demonstrate hypoechoic periurethral change in the region of injury (Fig. 5.30a), although retrograde urethrography is the definitive imaging. A thin catheter is inserted into the navicular fossa of the penile urethra and water-soluble contrast is injected from a syringe under fluoroscopic screening. Either a small balloon on the end of the catheter (the appropriate sizing of which can be difficult to estimate in the paediatric population) or manual pressure on the glans of the penis is required to prevent leakage of contrast. Imaging will demonstrate extravasation of contrast from the urethral lumen in the presence of a rupture (Fig. 5.30b) or truncation of the urethra in the setting of complete transection (Fig. 5.30c).

5.4.5 Testis

Testicular trauma is best assessed with ultrasound. Ultrasound will demonstrate intratesticular haematoma as a hypoechoic

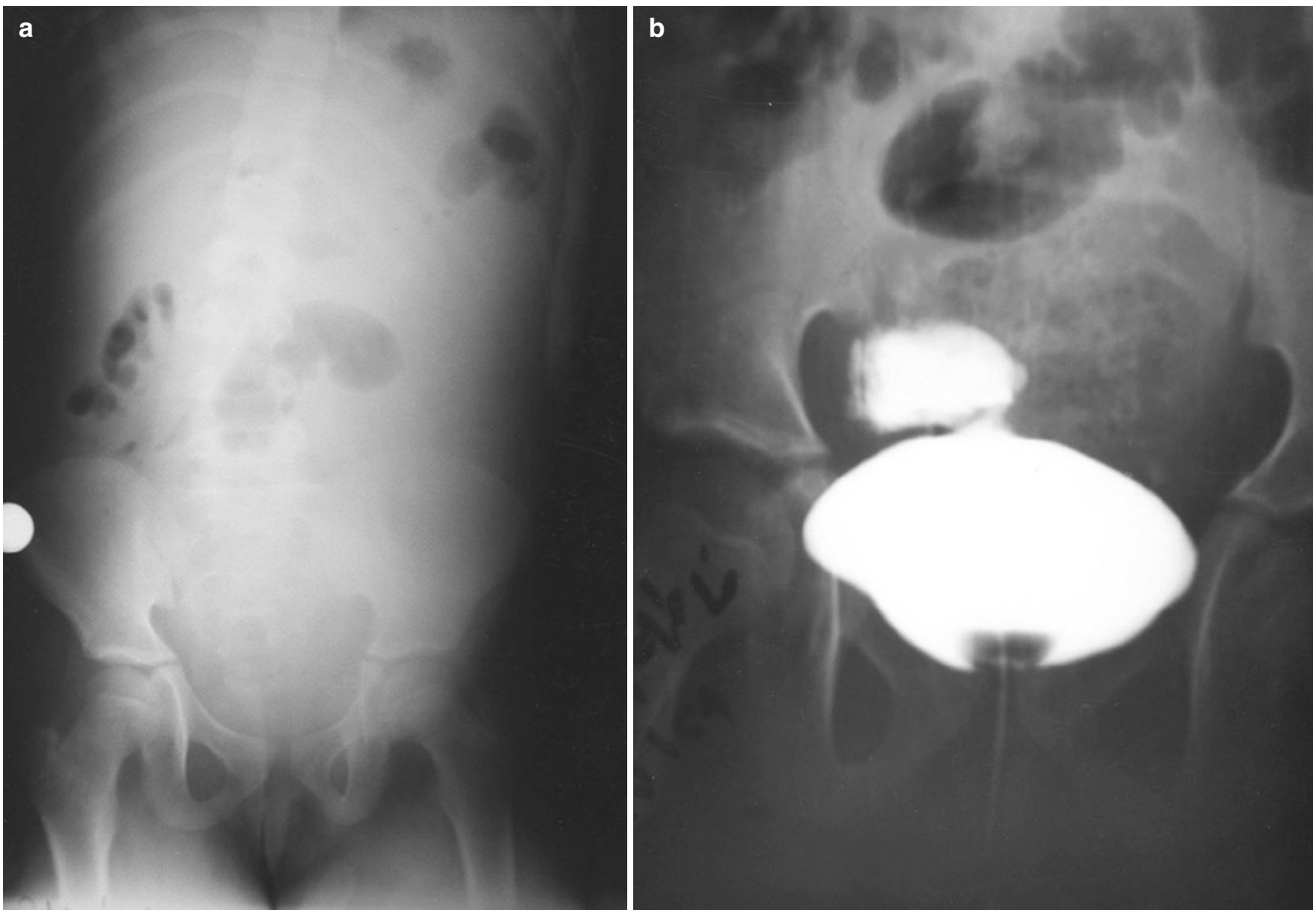

Fig. 5.29 (**a**) Bladder injury with urinary ascites. Note central displacement of gas-filled bowel loops. (**b**) Contrast leaking from the dome of the bladder after injury

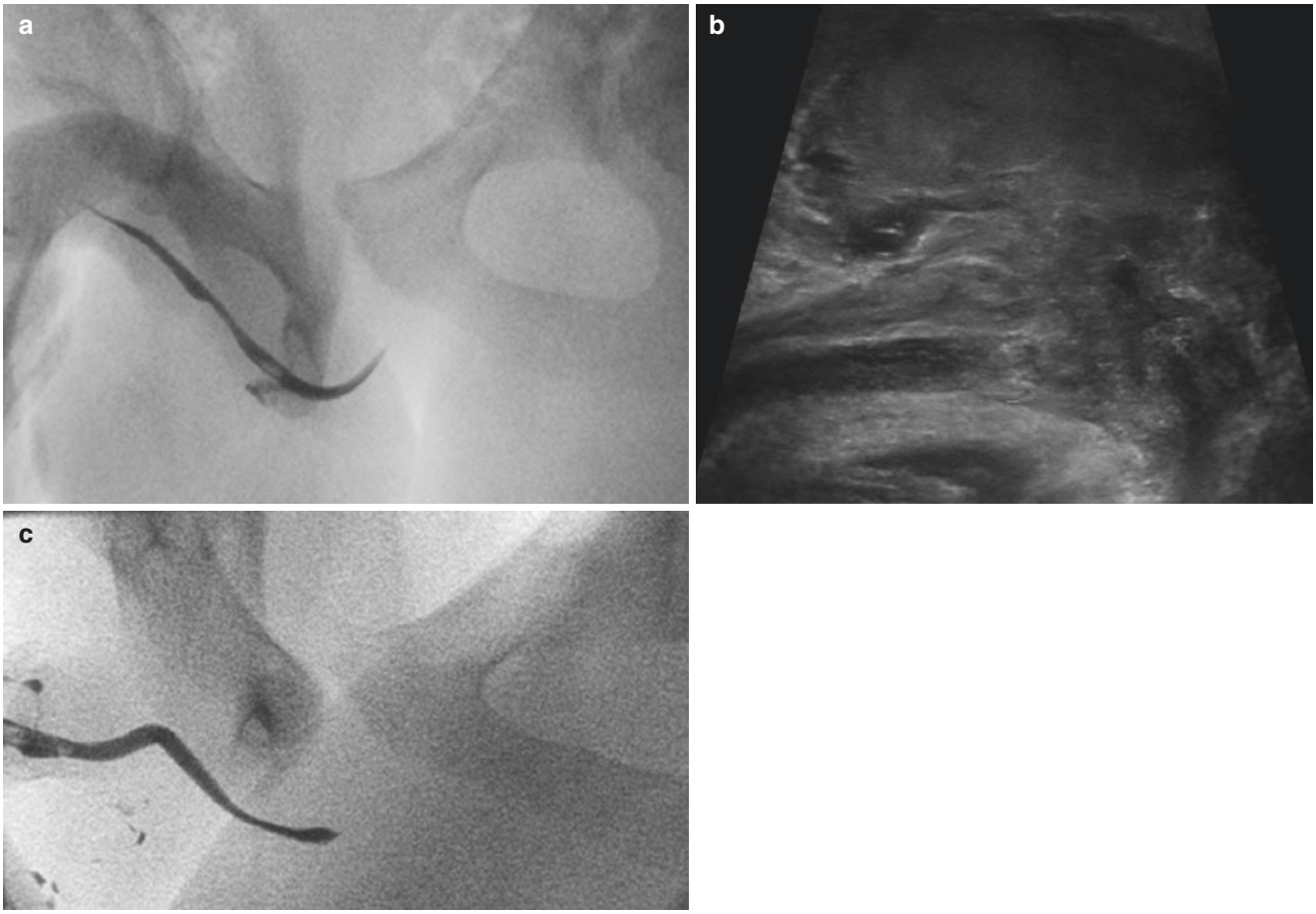

Fig. 5.30 (**a**) Urethrogram following straddle injury. There is leakage of contrast from the urethral lumen at the site of injury. (**b**) Transperineal ultrasound of the base of the penis. The corpus spongiosum and corpus cavernosa are visible as horizontal hypoechoic linear structure on the left of the image. In the near field there is a large echogenic haematoma that extends down to the root of the penis. (**c**) Retrograde urethrogram in the same patient as 5.30B. The urethra is truncated at the level of injury

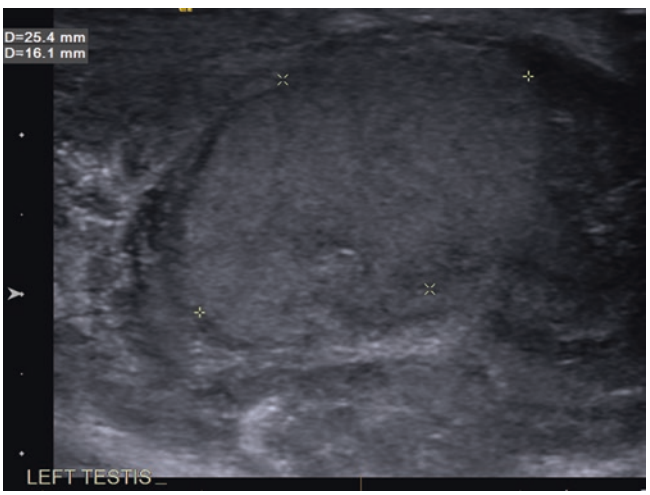

Fig. 5.31 Longitudinal ultrasound image of the left testis, showing a rounded hyperechoic collection in the testis, consistent with haematoma

region (Fig. 5.31). A laceration may have a more linear configuration. An ill-defined testis or intratesticular haematoma contiguous with an echogenic hydrocele is suggestive of testicular rupture.

5.5 Tumour

5.5.1 Kidney

5.5.1.1 Wilms Tumour (Nephroblastoma)

Wilms tumour is usually first imaged due to the presence of a palpable abdominal mass. Wilms tumours are typically large at presentation unless detected incidentally or as part of a screening programme (for example, in ultrasound screening of Beckwith Wiedemann syndrome). The tumours are usually solid and highly vascular, although large tumours may demonstrate heterogeneity or central fluid due to necrosis (Fig. 5.32a, b). They are bilateral in 10% of cases. Vascular invasion involving the renal vein and IVC is common, and can be identified with ultrasound, CT, or MR (Fig. 5.33a–f). Wilms tumour most frequently metastasizes to regional nodes, the lungs (Fig. 5.34), and liver. Local staging can be performed with contrast-enhanced MR or CT, with CT of the chest being also required. Other, rarer, paediatric tumours, such as clear cell sarcoma, may be indistinguishable from Wilms tumour on imaging, although clear cell sarcoma is more likely to metastasize to bone.

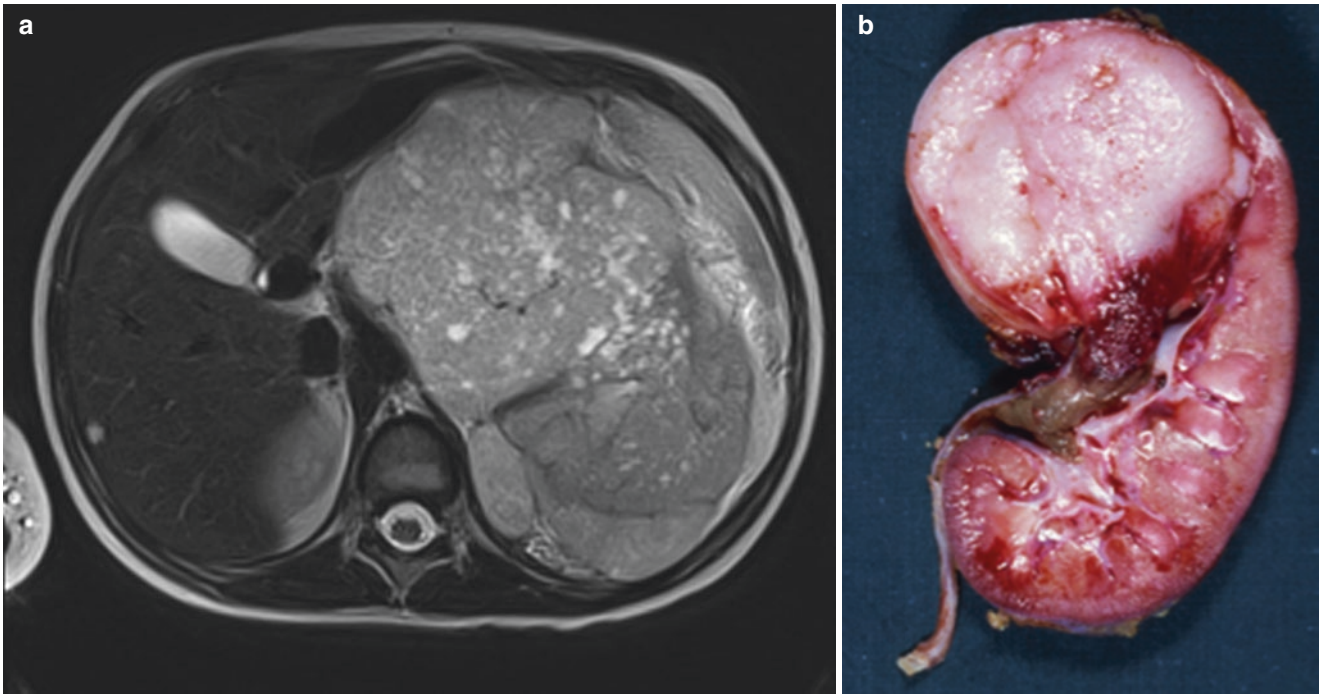

Fig. 5.32 (**a**) Axial T2-weighted MR image of a left-sided Wilms tumour. The heterogenous mass bulges across the midline. A single hepatic metastasis is visible. (**b**) Pathological specimen of Wilms tumour

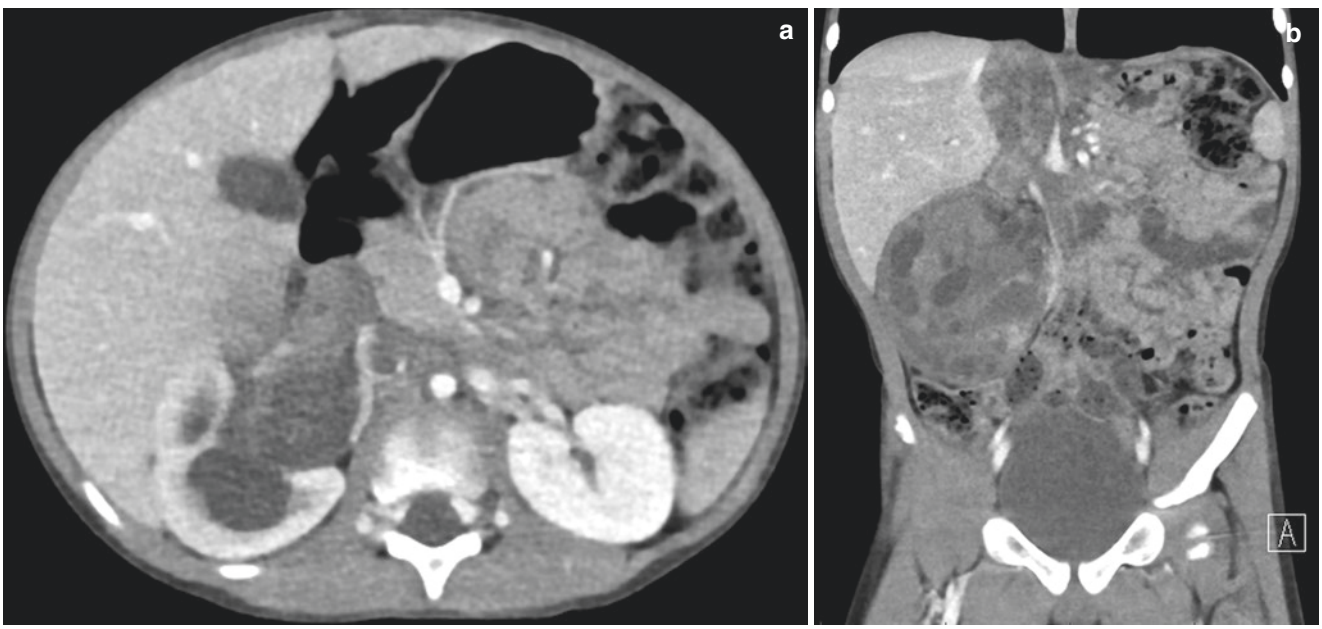

Fig. 5.33 (**a**) Axial contrast-enhanced CT of the abdomen showing a Wilm's tumour arising from the right kidney and extending into and distending the right renal vein and IVC. (**b**) Coronal contrast-enhanced CT of the abdomen showing a right-sided Wilm's tumour with extension of tumour-thrombus into the retrohepatic IVC. (**c**) Coronal contrast-enhanced CT of the chest showing tumour-thrombus extending above the level of the diaphragm, into the right atrium. (**d**) Transverse midline ultrasound images demonstrating intracaval extension of Wilm's tumour. The IVC is distended and contains echogenic tumour-thrombus. (**e**) Longitudinal ultrasound showing distension of the retrohepatic IVC which is filled with echogenic tumour thrombus. (**f**) Echocardiogram showing thrombus in right atrium. (**g**) Intraoperative view of Wilms tumour with intravascular thrombus. (**h**) Pathological specimen of Wilms tumour with intracaval tumour. (**i**) Intra-atrial Wilms tumour thrombus extracted from right atrium during bypass

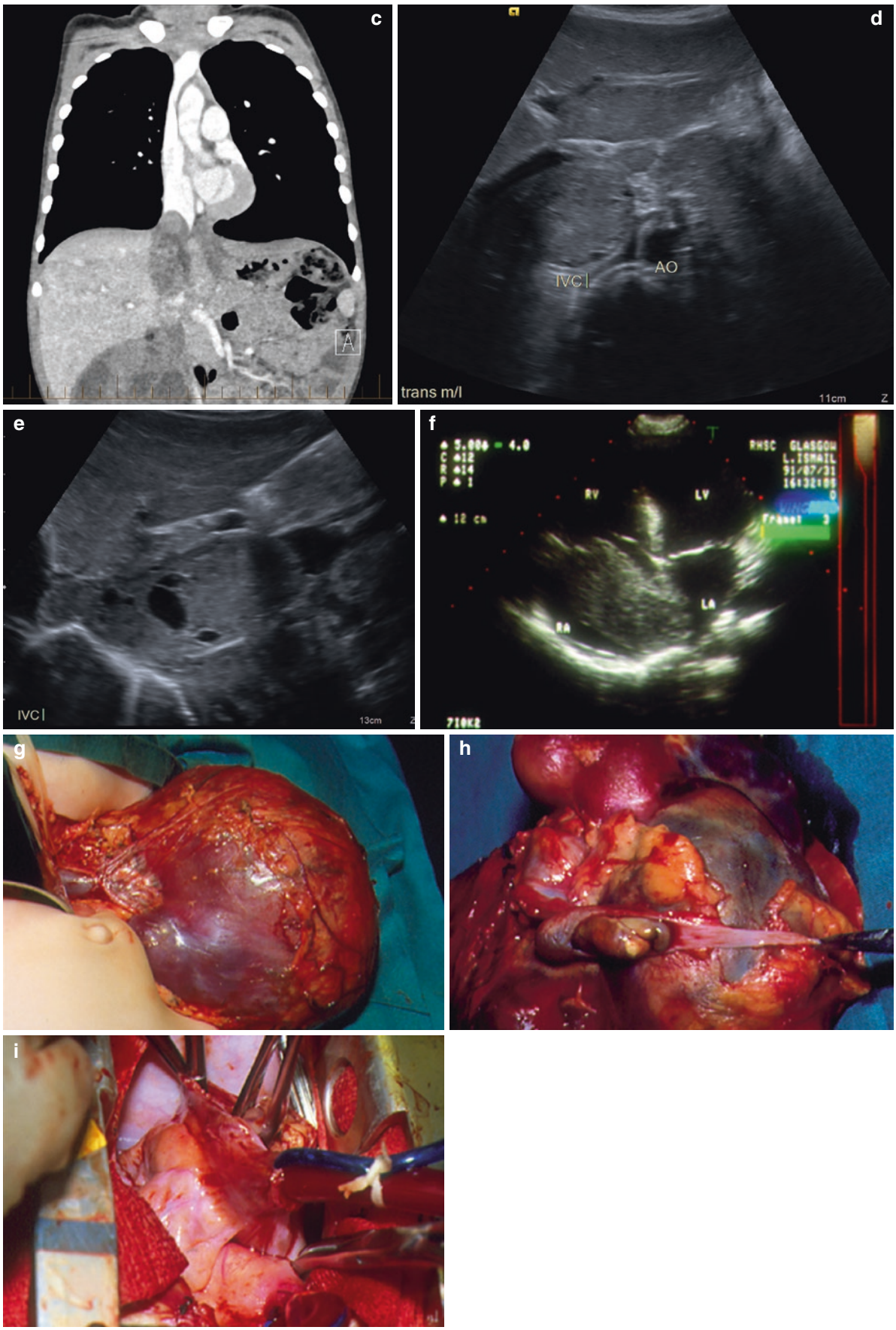

Fig. 5.33 (continued)

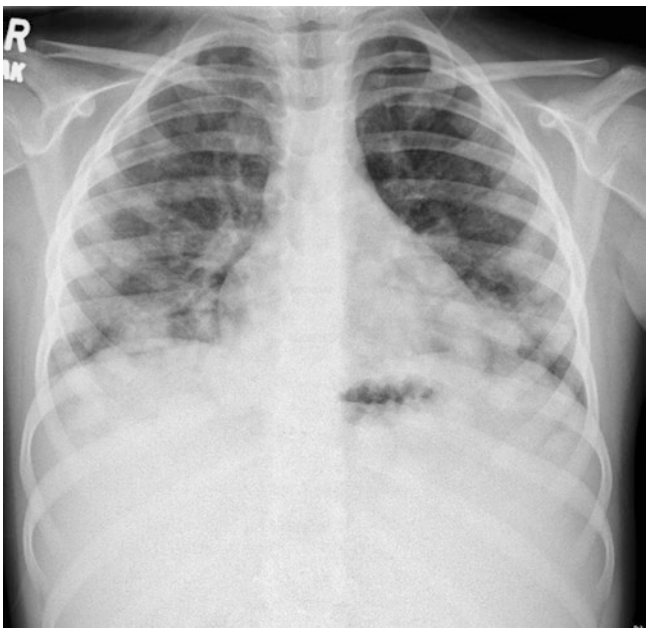

Fig. 5.34 Chest X-ray of a patient with metastatic Wilms tumour. Multiple pulmonary metastases are present

5.5.1.2 Nephroblastomatosis

Nephroblastomatosis is the term used to describe residual islands of metanephric blastema that fail to involute. Rests of nephroblastic tissue usually lie peripherally in the kidney, in a subcapsular location. They can be difficult to identify on ultrasound but tend to be hypoechoic relative to the cortex. They are of low attenuation on CT and are T1 and T2 hypointense on MR.

5.5.1.3 Congenital Mesoblastic Nephroma

Congenital mesoblastic nephroma (CMN) is the most common renal mass presenting in the new-born or young infant under 6 months of age (Fig. 5.35a–c). On imaging they are typically large, poorly defined infiltrating masses in which some of the normal architecture of the kidney may be preserved.

5.5.1.4 Angiomyolipoma

Angiomyolipomas (AMLs) are usually seen only in children with tuberous sclerosis (TS). On ultrasound, AMLs are echogenic due to fat content. The presence of fat content can be confirmed on CT or MR, provided the lesions are of reasonable size, although in the setting of TS and with typical echogenic ultrasound appearance, further characterisation is unlikely to be needed. Larger lesions carry a risk of haemorrhage.

5.5.1.5 Renal Cell Carcinoma

Renal cell carcinoma is rare in children but may present in older children with predisposing syndromes such as tuberous sclerosis and von Hippel Lindau Syndrome. They tend to appear as solid masses but may contain cysts, haemorrhage, calcification, and areas of necrosis.

5.5.2 Urogenital Rhabdomyosarcoma

Rhabdomyosarcoma may arise in the male or female lower genitourinary tract. In male patients this typically involves the prostate and bladder base (Fig. 5.36a, b). In female patients it typically involves the vagina (Fig. 5.36c–e). Male patients will often present due to obstruction of the urinary tract at the bladder outlet caused by a large solid mass, while female patients may present with vaginal bleeding or visible tumour. Initial radiological investigation is typically with ultrasound, which will demonstrate the tumour and potentially secondary signs of obstruction of the upper tracts (Fig. 5.36f). Local staging can be performed with MR or CT, with ^{99m}Tc-methyl diphosphonate (^{99m}Tc-MDP) bone scan and CT chest to investigate for skeletal and lung metastases respectively.

5.5.3 Testis (Fig. 5.37)

Paediatric intratesticular masses are rare. Malignant tumours are most likely to be of germ cell origin (yolk sac or teratomas), although sex-cord stromal tumours, haematological tumours and metastases can also occur. The first line of imaging is ultrasound. Appearances on ultrasound are not specific, as tumours may be solid, cystic, or mixed, and echotexture of any solid component may be variable relative to the normal testicular parenchyma. Tumours may also present as diffuse enlargement of the testis. Staging can be performed with MR or CT. Intratesticular epidermoid cysts are rare, but have a characteristic ultrasound appearance as well-defined round masses with concentric linear echoes due to multiple layers of desquamated keratin. Simple testicular cysts are rare, and a potential cystic neoplasm needs to be excluded. Other potential mimics of testicular tumours on imaging include focal infection/inflammation, haematoma, and infarct.

5.5.4 Ovary

Approximately two-thirds of paediatric ovarian tumours are mature teratomas, which are benign. They are bilateral in a quarter of cases. On ultrasound most appear as complex cystic masses with echogenic nodular components due to calcification or sebum content (Fig. 5.38a, b). Hair may be visible as tiny punctate or linear echoes. The minority may be completely uniform in echotexture. CT and MR can demonstrate

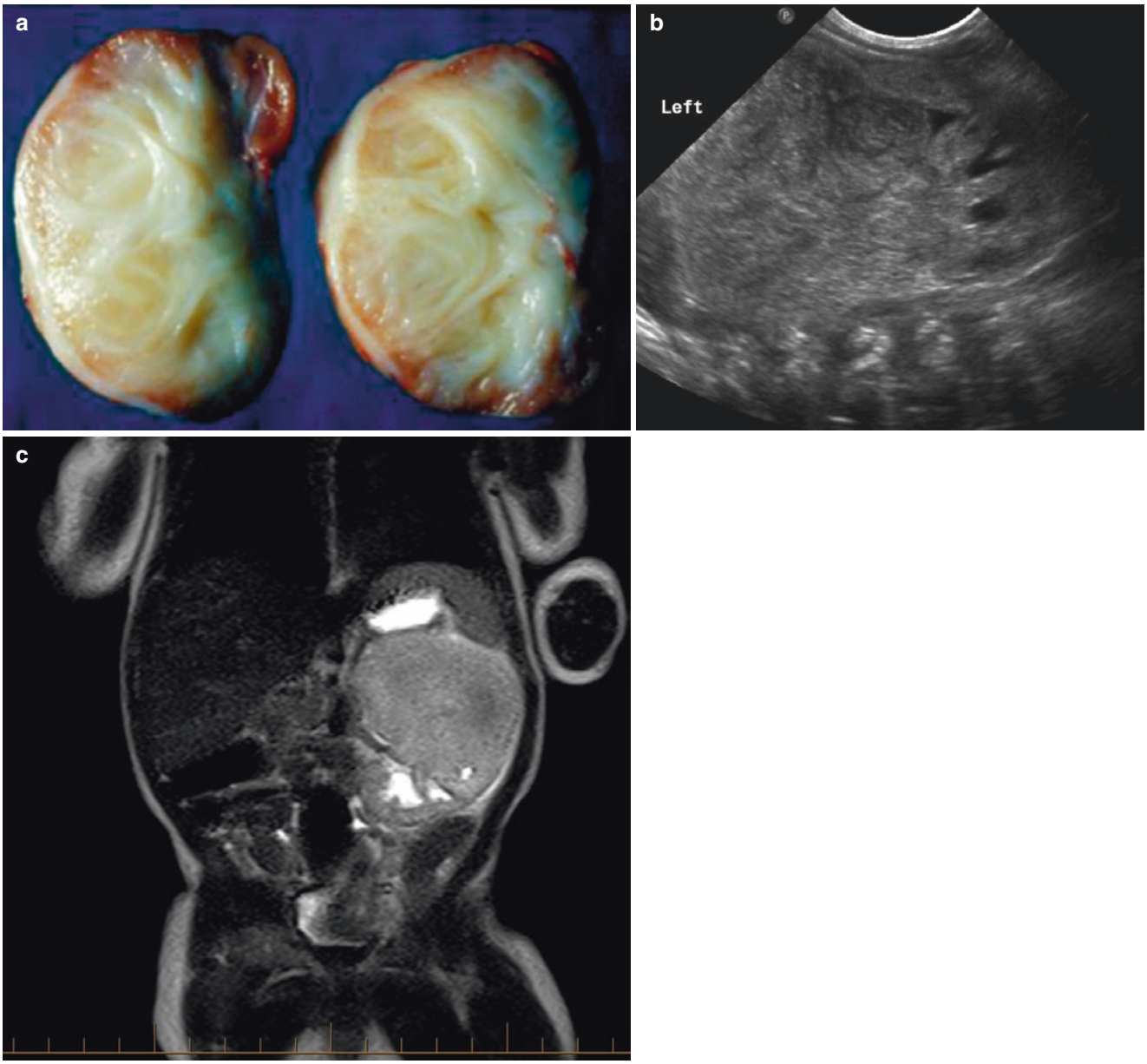

Fig. 5.35 (**a**) Pathological specimen of congenital mesoblastic nephroma. (**b**) Longitudinal ultrasound image of a mesoblastic nephroma in the left kidney of a new-born. The upper pole of the left kidney is replaced by an expansile echogenic mass. (**c**) Coronal T2-weighted MR image in a new-born demonstrating a mesoblastic nephroma at the upper pole of the left kidney

a fluid-filled cyst containing fat density, calcification, and other soft tissue (Fig. 5.38c).

The remaining one-third of ovarian tumours are mostly immature teratomas and dysgerminomas, which are malignant. These are usually large at presentation and predominantly solid, although they may contain areas of necrosis. Infrequent stromal tumours and epithelial carcinomas are usually more complex. Staging may be completed with MR or CT, with MR probably being superior at local staging in the pelvis. Common patterns of metastatic spread of malignant ovarian tumours include peritoneal and omental nodules with ascites, lymphadenopathy, and hepatic metastases.

5.5.5 Paratesticular Tumour

Patients with paratesticular rhabdomyosarcoma typically present with a painless enlarging scrotal mass. The tumour may arise from the spermatic cord, epididymis, or tunica. Ultrasound will demonstrate a solid mass with internal vascularity. A paratesticular mass will usually displace the testis, but if it is very large it may engulf the testis, making a paratesticular origin difficult to confirm (Fig. 5.39a, b). Local spread of disease is via lymphatics to the iliac and paraaortic nodes, with distant metastases to liver and lung also possible.

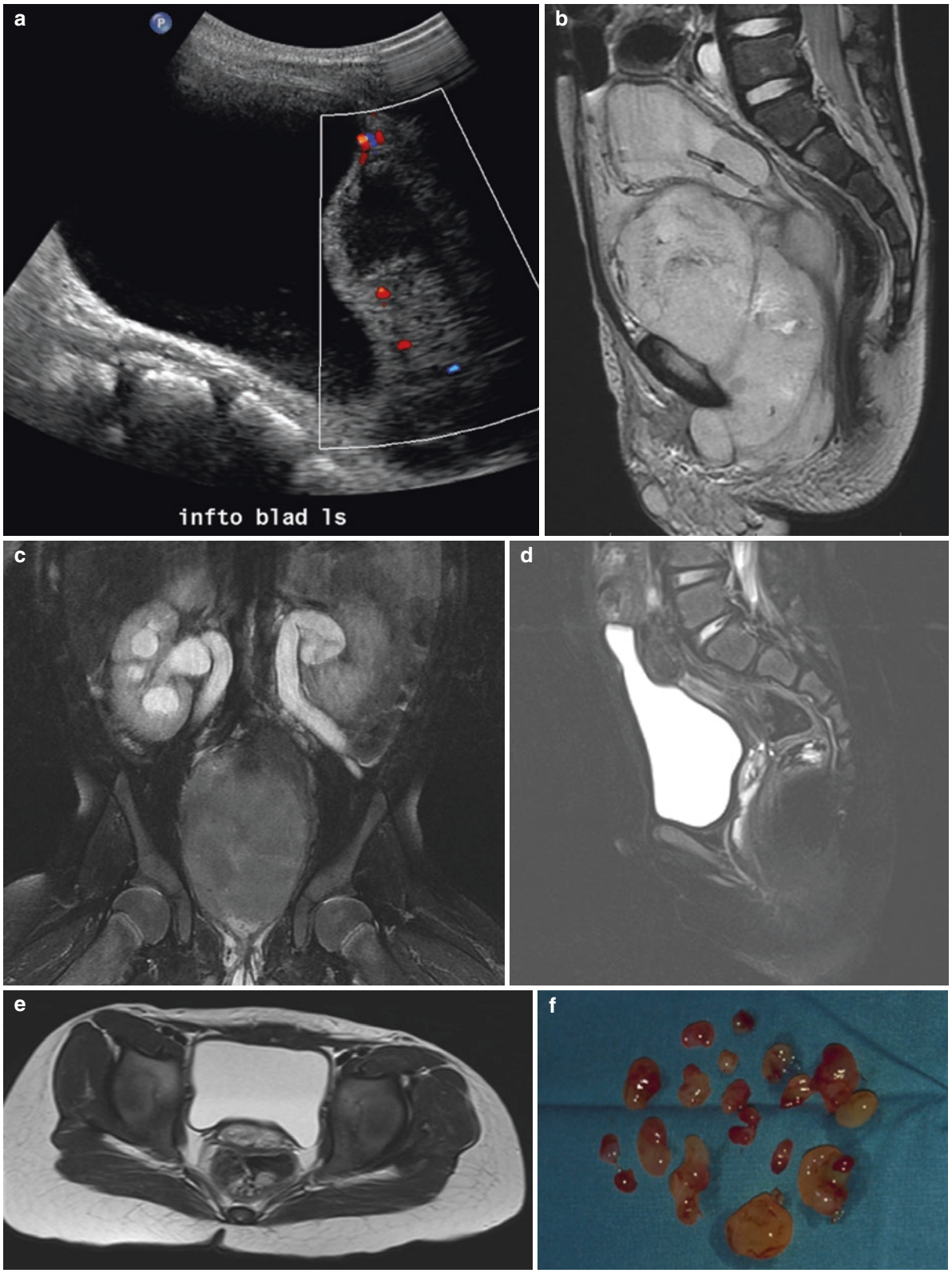

Fig. 5.36 (**a**) Midline longitudinal ultrasound image of a bladder-prostate rhabdomyosarcoma. A heterogeneous soft-tissue mass containing Doppler flow lies inferior to the bladder. (**b**) Sagittal T2-weighted MR image of a bladder-prostate rhabdomyosarcoma. The T2 hyperintense mass fills the anterior pelvis with superior displacement of the bladder (with contains a urinary catheter balloon) and posterior displacement of the rectum. (**c**) Coronal fat-saturated T2-weighted MR image of a bladder-prostate rhabdomyosarcoma. An intermediate signal mass lies in the pelvis. There is bilateral hydroureteronephrosis due to bladder outlet obstruction. (**d**) A sagittal fat-saturated T2-weighted MR image of vaginal rhabdomyosarcoma. The tumour is visible as heterogeneous elevated signal outlined by high signal fluid in the vagina, between the bladder and rectum and inferior to the uterine cervix. (**e**) Axial T2-weighted MR image of vaginal rhabdomyosarcoma. The T2 hyperintense tumour lies between the bladder and rectum. (**f**) Sarcoma Botroides

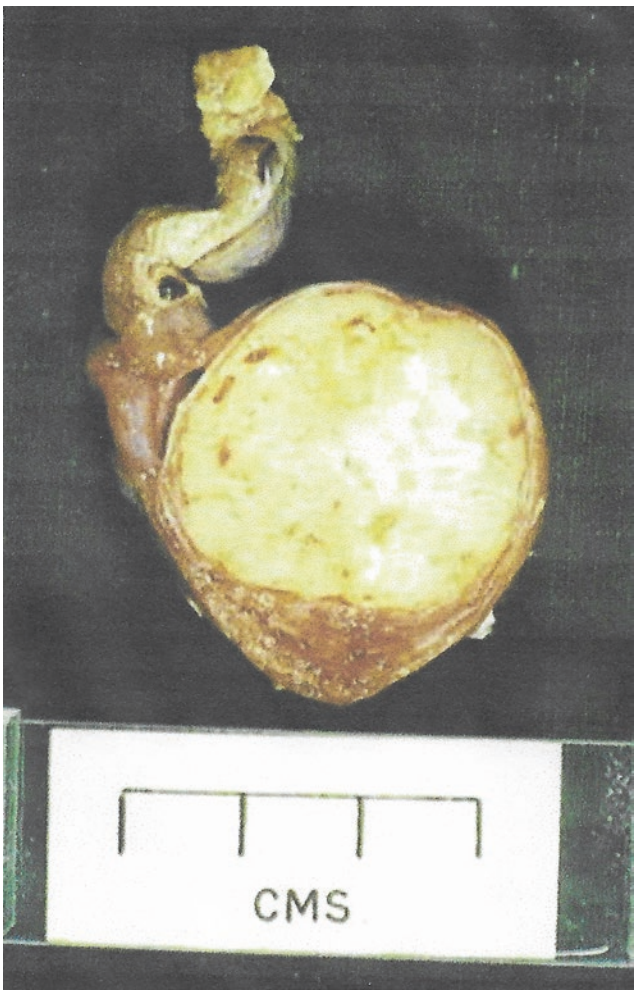

Fig. 5.37 Pathological specimen of testicular tumour

Staging can be performed with CT or MRI with ^{99m}Tc-MDPbone scan to examine for skeletal metastases.

5.6 Acquired

5.6.1 Bladder Neck Obstruction (Fig. 5.40)

The bladder responds by muscular hypertrophy and trabeculation, and sooner or later bladder distension occurs. Back pressure affects the upper urinary tract, the ureters become dilatated and tortuous, and hydronephrosis may develop. Some patients develop incompetence of their vesicoureteric junction resulting in vesicoureteric reflux. The onset of renal failure may be insidious. During fetal life, the kidneys produce urine from the fourth month and the effects of back pressure may therefore be present even before birth, the baby being born with distension of the bladder, ureters and renal pelvis. If the obstruction is complete, oligohydramnios results, with deleterious effects on fetal lung development, which cause severe postnatal respiratory problems that may be fatal. There may also be intrauterine postural deformities caused by the constrictive effect of the oligohydramnios. Occasionally no urine may be passed by the new-born infant in the first 24 h, but this should not cause alarm if the bladder is not markedly distended. The external genitalia should be carefully examined to exclude hypospadias with meatal stenosis. In the older infant or child, acute retention is usually due to minor causes such as meatal erosion. If warm baths and sedation do not give relief, catheterisation or suprapubic stab drainage will. Chronic retention may also create sufficient pain or distress to demand immediate drainage, but usually there is time for urological investigations and definitive treatment. Urethral valves, bladder neck obstruction, and urethral strictures may all be dealt with by a variety of surgical procedures, including diathermy of valves and dilatation or excision of bladder neck and urethral dilatation.

5.6.2 Urethra: Crohn's (Fig. 5.41)

Urethral involvement in Crohn's disease is rare. Rectourethral fistulae usually arise from uncontrolled perirectal and perianal disease. Once the urethra is involved, urethral strictures and urethrocutaneous fistulae may form.

Urethrography clearly demonstrates urethral strictures and can also outline urethral fistulae; however the most elegant depiction of the extent and three-dimensional configuration of the fistulae is provided by high-resolution MR, which can also demonstrate the relationship of the fistulae to the anal sphincter.

5.6.3 Epididymo-orchitis (Fig. 5.42)

Ultrasound is the imaging investigation of choice in suspected epididymo-orchitis. Typical features are an enlarged epididymis with increased vascular flow on Doppler imaging. If the testis is involved it may also be enlarged with increased flow. There is often a small associated hydrocele. Thickening of the overlying scrotal skin is also common. Potential mimickers of the ultrasound appearance of epididymo-orchitis include a recently detorted testis, torsion of the epididymal or testicular appendage, and vasculitis.

5.6.4 Neurogenic Bladder

See Sect. 5.2.12.

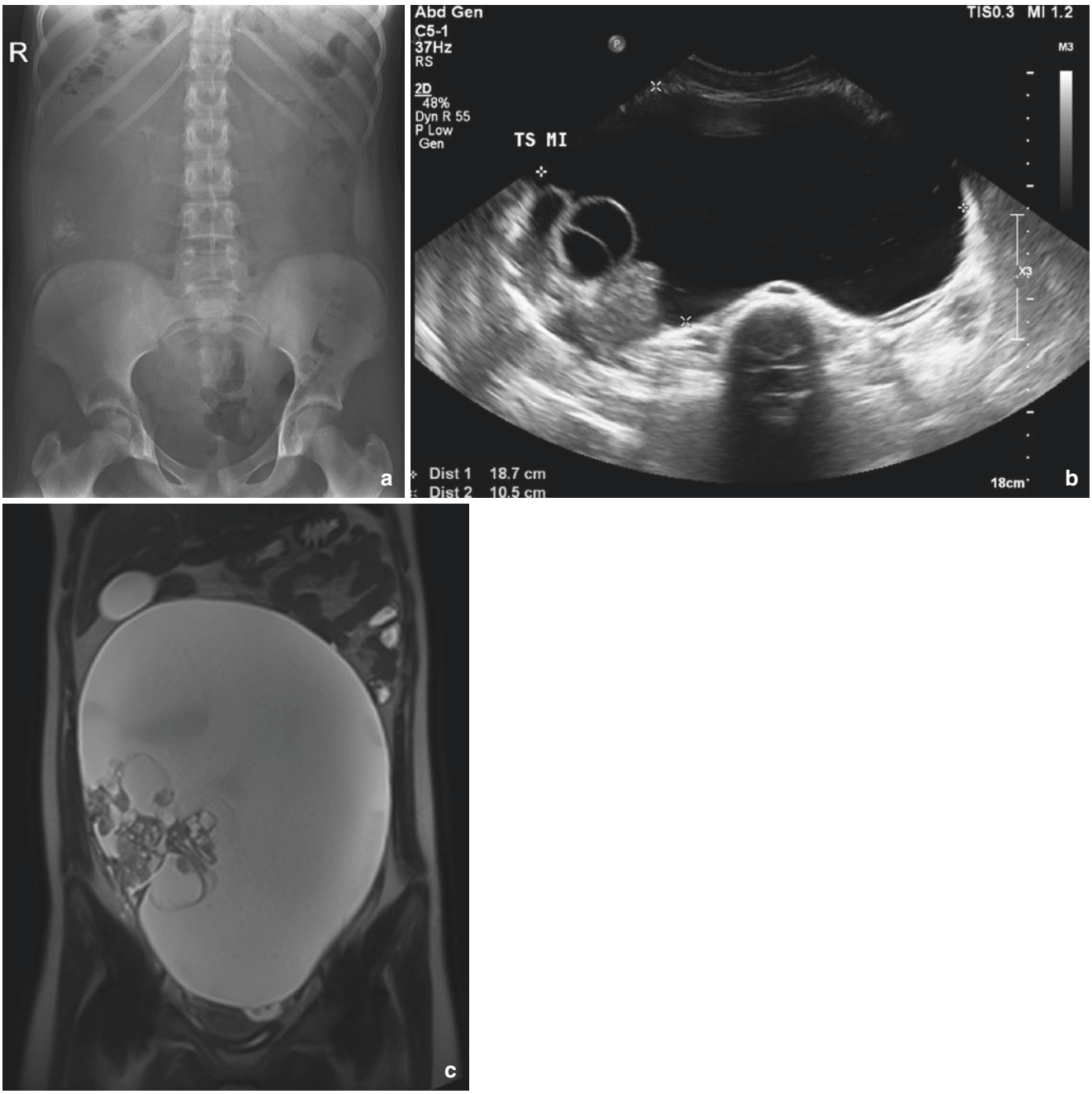

Fig. 5.38 (**a**) Abdominal X-ray demonstrating a large mature ovarian teratoma. Note displacement of bowel loops into the upper and left abdomen with calcification in the lateral right flank. (**b**) Transverse ultrasound image of the same patient as (**a**), demonstrating a large predominantly cystic abdominopelvic mass, with a lobulated solid/cystic component on the right. (**c**) Coronal T2-weighted MR of the same patient as (**a**) and (**b**), demonstrating the large, predominantly cystic ovarian teratoma

5.6.5 Torsion of the Testis

Torsion is usually of the spermatic cord, but in the infant, it may be of the testis within the tunica twisting on the epididymis. In the neonatal period, the presentation is with a large tender mass in the scrotum. Exploration usually shows an infarcted testis. In childhood, torsion may occur in the fully descended organ due to a sharp blow or to some sudden movement as in swimming. There is sudden severe pain, which may be in the lower abdomen, the groin, or the scrotum. Vomiting may occur. Examination reveals marked tenderness of the scrotum. The testis becomes swollen, hard, oedematous, and is often in a high position. A hydrocoele may develop in the tunica vaginalis. If mechanical relief is delayed, necrosis of the testis and epididymis supervenes, and the scrotum becomes discoloured and oedematous with

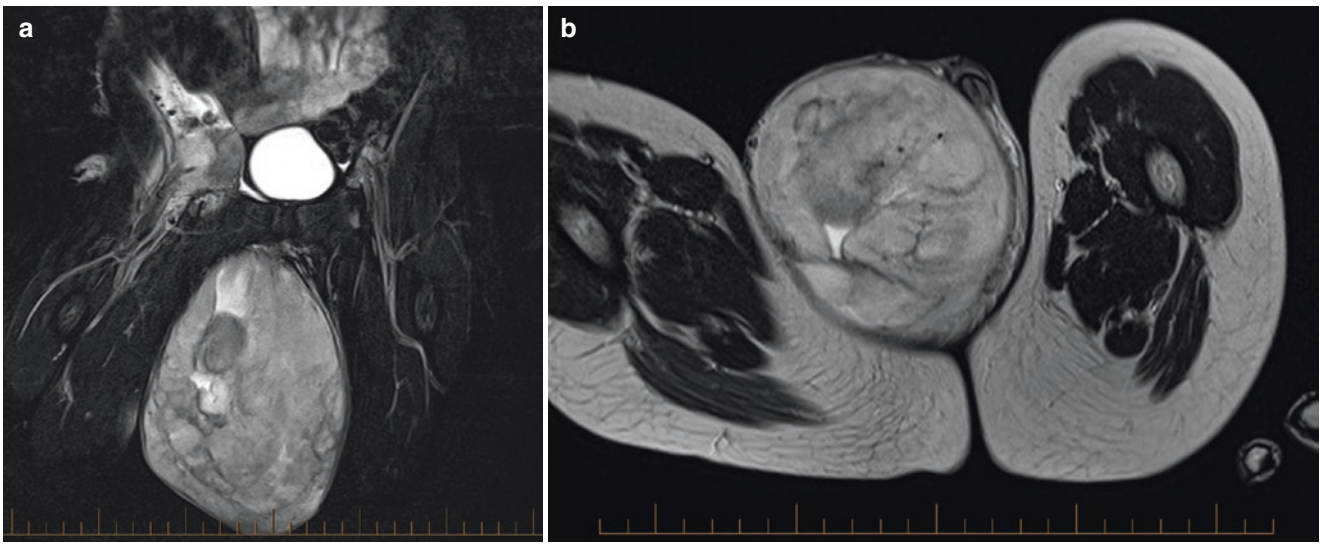

Fig. 5.39 (**a**) Coronal fat-saturated T2-weighted MR image of a large paratesticular rhabdomyosarcoma. Right external iliac lymphadenopathy is also visible. (**b**) Axial T2-weighted MR image of a right paratesticular rhabdomyosarcoma. The base of the penis is displaced to the left by the large tumour

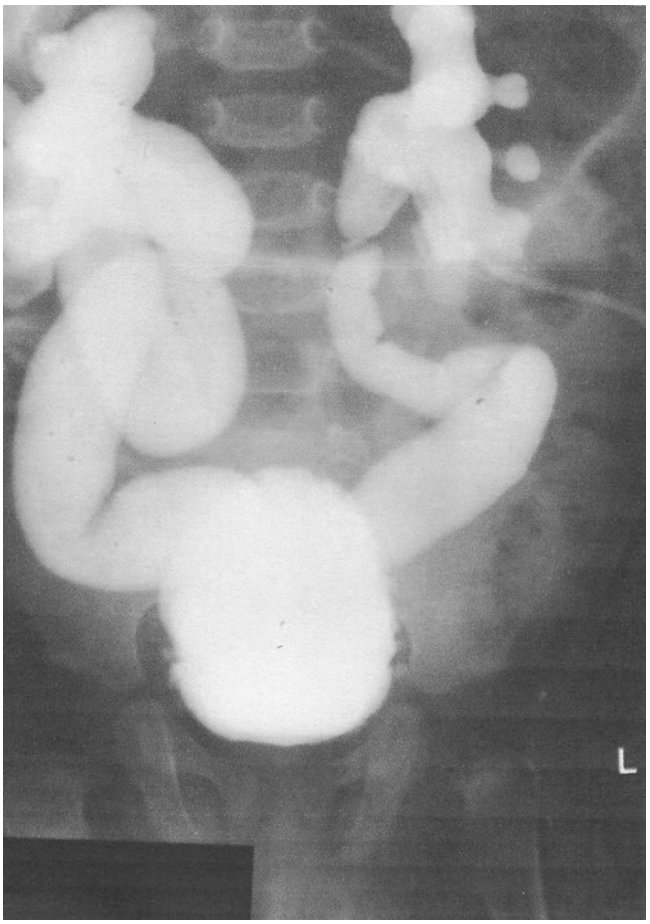

Fig. 5.40 Bladder neck obstruction

slow resolution and reabsorption of the infarcted testis over 2 or 3 months. Doppler ultrasound examination is very useful to determine whether there is blood flowing into the organ. In a torsion there is reduced blood going to the testis. Differential diagnosis between torsion and epididymo-orchitis, where there is increased blood flow to the organ, is usually clearly differentiated by ultrasonic examination.

This diagnosis may be difficult, and torsion may be confused with incarcerated hernia, acute epididymo-orchitis, idiopathic scrotal oedema, or even torsion of an appendage of the testis, or the vas or epididymis and acute appendicitis.

On ultrasound a torted testis is typically swollen and hypoechoic, but may be normal. The most important part of the examination is assessment of the blood flow with colour Doppler; absent or reduced flow in the symptomatic testis relative to the asymptomatic side is confirmatory (Fig. 5.43a). Direct comparison of blood flow is best achieved by a single transverse midline colour Doppler image showing both testes. A twist in the cord may be visible, but can be difficult to demonstrate.

5.6.6 Stents and Complications (Fig. 5.44a, b)

A plain X-ray may demonstrate appropriate location of a ureteric J-J stent, although correct placement is best demonstrated by an ultrasound showing the curled ends of the stent in the renal pelvis and bladder. The ends of a stent may

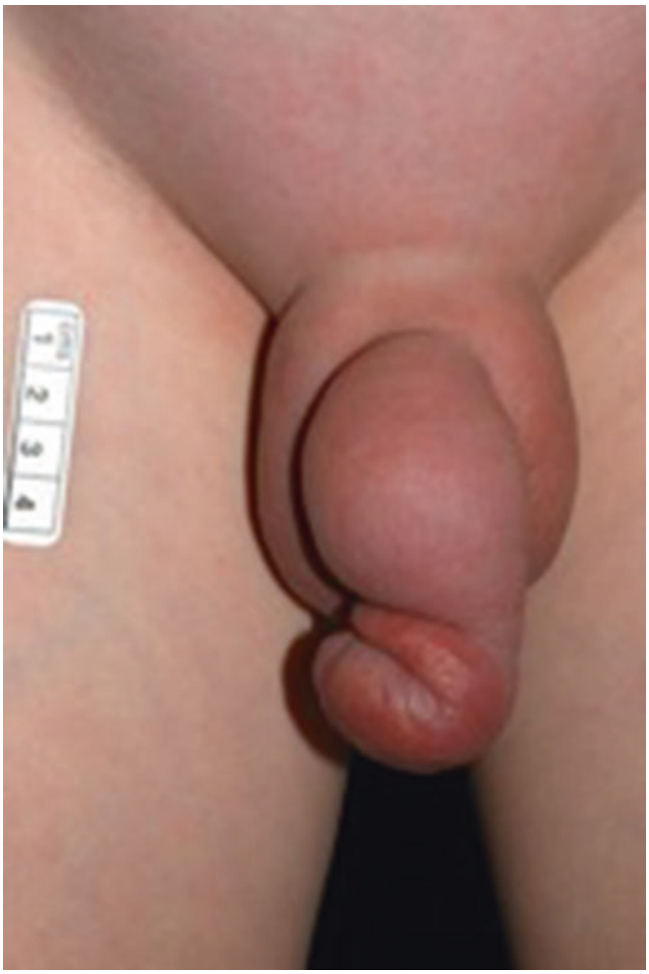

Fig. 5.41 Penile and scrotal oedema in a patient with Crohn's disease. The foreskin had a lump on the undersurface. A circumcision was carried out and a biopsy showed granulomas consistent with Crohn's disease. Further investigation of the gastrointestinal tract revealed more evidence of Crohn's disease. Image provided by Mr. S. O'Toole

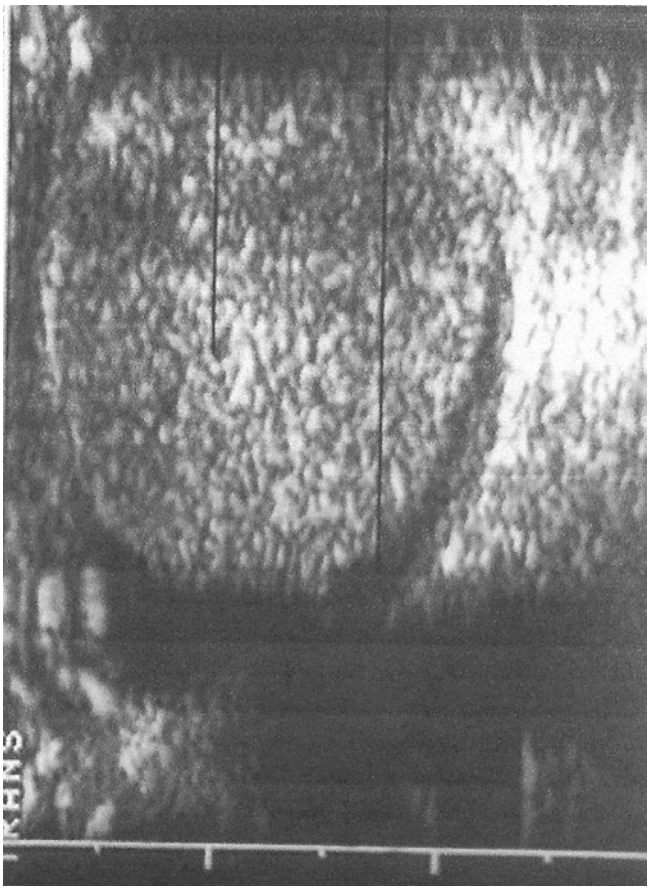

Fig. 5.42 Ultrasound scan of Epididymo-orchitis with increased blood flow

migrate proximally or distally. Failure of a stent due to obstruction can only be inferred on ultrasound by a failure of pelvicalyceal decompression or increasing dilatation.

5.6.7 Nephrocalcinosis

There are three main types of renal calculi in children: endemic, infective and rare metabolic disorders associated with nephrocalcinosis. The great majority of renal calculi found in children in the UK are secondary to infection of the renal tract, especially by Proteus vulgaris, which by maintaining a high urinary pH favours the deposition of phosphate in combination with calcium, ammonium, and magnesium. The typical "staghorn" calculus fills the renal pelvis and calyces. Calculus formation is especially likely when there is an obstruction in the renal tract, e.g., at the pelviureteric or vesicoureteric junction. Nephrocalcinosis is the deposition of calcium salts within the renal parenchyma, and it may be associated with urolithiasis. The calcification typically involves the pyramids, which appear echogenic on ultrasound (Fig. 5.45a). Very rarely, calcium phosphate or oxalate stones are a manifestation of primary hyperparathyroidism or hypervitaminosis D. They may also occur after prolonged immobilization for, e.g., chronic osteitis. Cystinuria, one of Garrod's original inborn errors of metabolism, is a rare cause of renal stone. In this condition there is a defect in the tubular reabsorption not only of cystine, but also of lysine, arginine, and ornithine. Despite the passage of the typical hexagonal crystals in the urine, only a minority of affected children develop calculi. The short stature of some children with cystinuria is related to the presence of similar absorptive defects in the mucosa of the small intestine. This condition must not be confused with the quite separate metabolic error called cystinosis, in which cystine is deposited in body tissues. Another exceedingly rare cause of renal lithiasis, also an inborn metabolic error, is primary hyperoxaluria. In addition to calcium oxalate calculi, extrarenal deposits

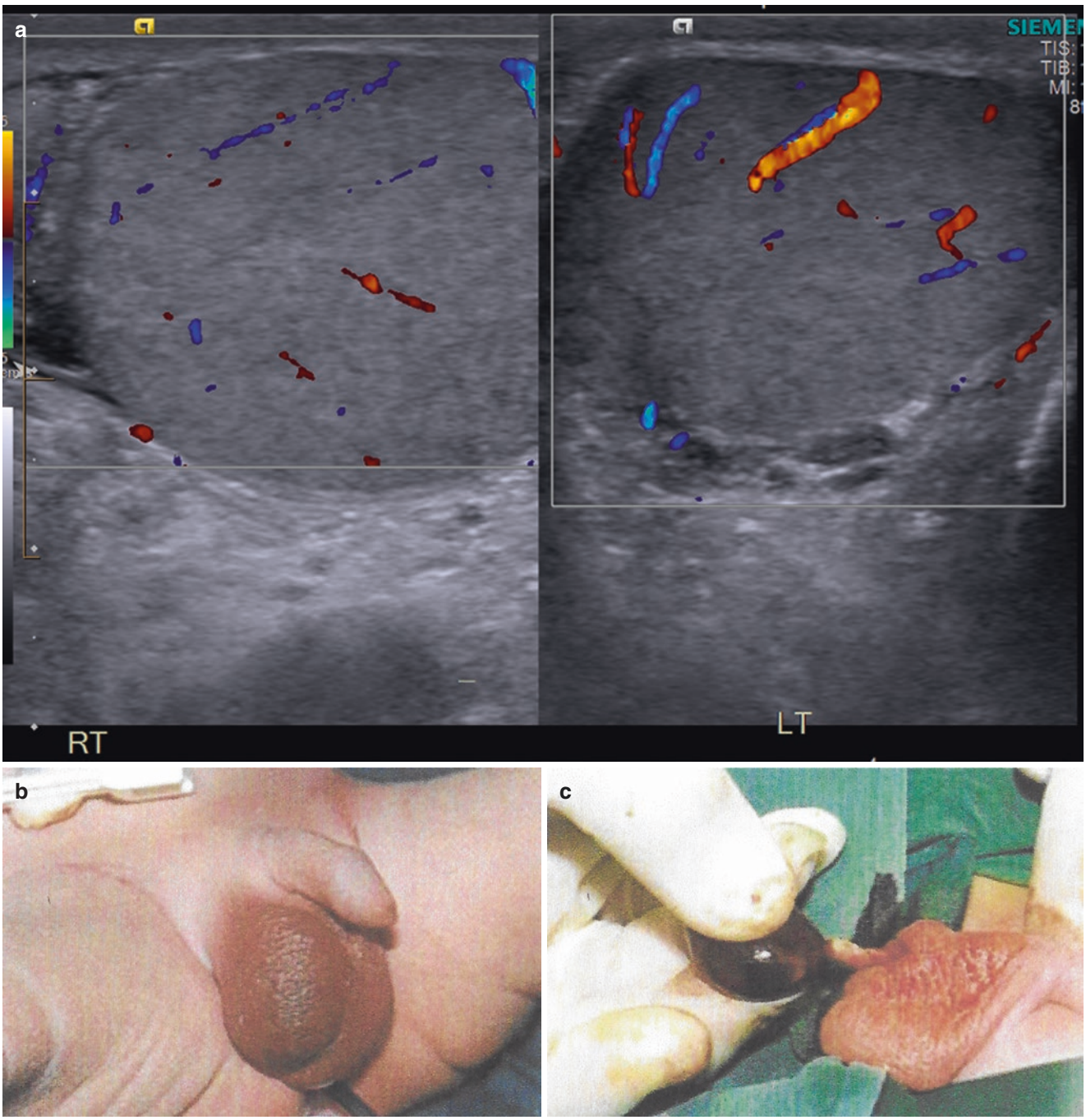

Fig. 5.43 (**a**) Axial ultrasound image of the testes. The symptomatic right testis shows reduced Doppler flow relative the left. Torsion was confirmed at surgery. (**b**) Clinical picture of acute torsion of the testis in a neonate. (**c**) Intra operative findings of torsion of the testis

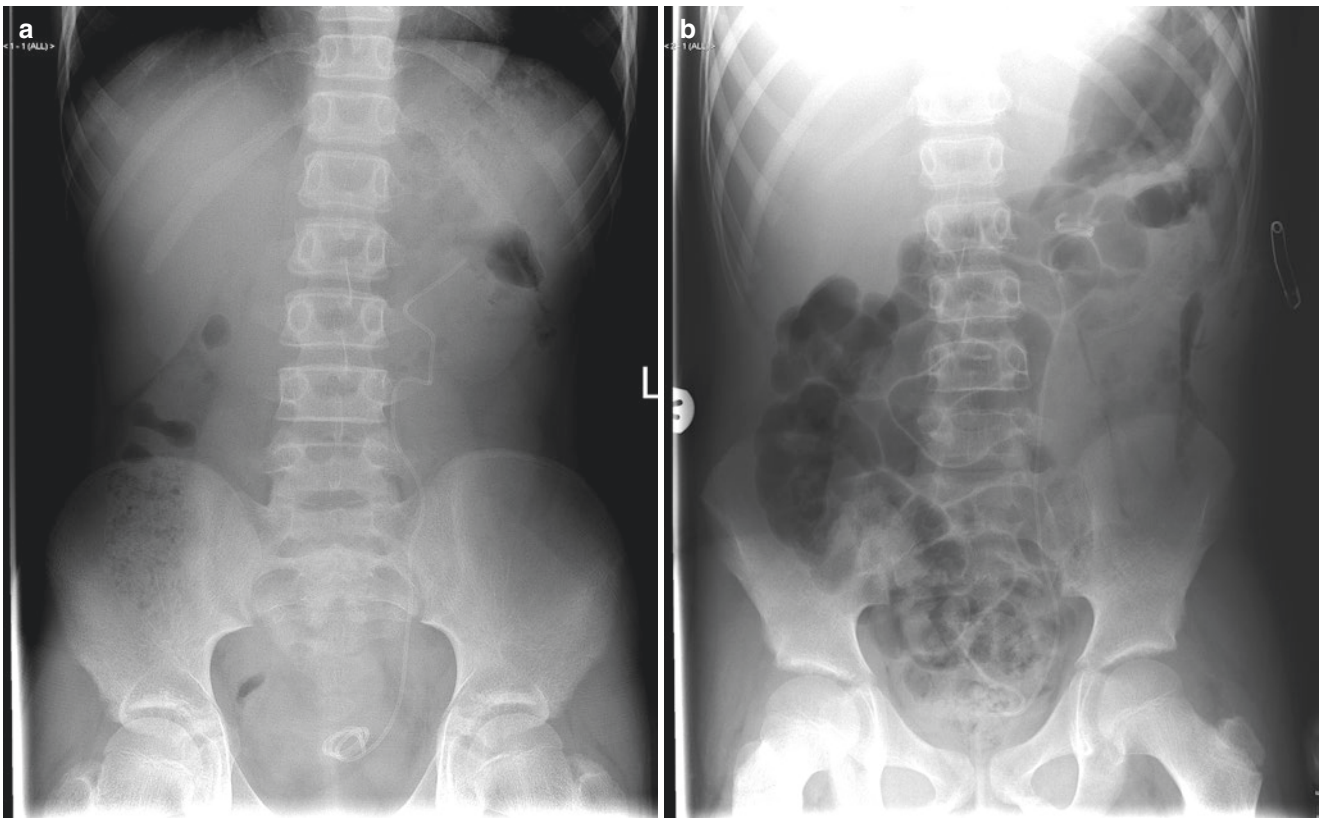

Fig. 5.44 (**a**) Complication of a left JJ stent, with the superior portion of the stent following an abnormal tortuous course. (**b**) Complication of a left JJ stent, with displacement of bowel loops from the left flank by a soft tissue density, consistent with a persistently dilated left kidney

may occur—oxalosis. This rare type of very dense nephrocalcinosis and nephrolithiasis is characterised by the continuous high urinary excretion of oxalate, which sufferers from primary hyperoxaluria always show. Other inherited metabolic diseases that increase the excretion of very insoluble substances and thus formation of renal stones are Lesch-Nyhan syndrome, 2,8-dihydroxyadeninuria, xanthinuria, and the orotic acidurias. In certain parts of the world, e.g., India and Thailand, endemic urolithiasis leads to the formation of vesical calculi that are composed of ammonium acid urate. There is evidence implicating dietary factors in their pathogenesis. This used to be seen in England, particularly in East Anglia, but declined in incidence in the early part of this century. Bladder calculi have similar imaging characteristics to calculi elsewhere within the renal tract, being dense on X-ray (Fig. 5.45b) and echogenic with shadowing on ultrasound (Fig. 5.45c).

The majority of children present as cases of urinary tract infection with pyuria. Classical renal colic with haematuria is relatively uncommon in childhood. In a few instances, and especially in primary hyperoxaluria, the infant or child has presented with chronic renal failure sometimes associated with renal osteodystrophy. The presence of a renal calculus can be confirmed by an abdominal X-ray. Calculi cause acoustic shadows and have a characteristic ultrasound appearance; therefore, nephrocalcinosis and renal calculi can be diagnosed by ultrasound examination. In confirmed cases it is wise to determine the urinary output of calcium, cystine, and oxalate so that metabolic disorders are not overlooked.

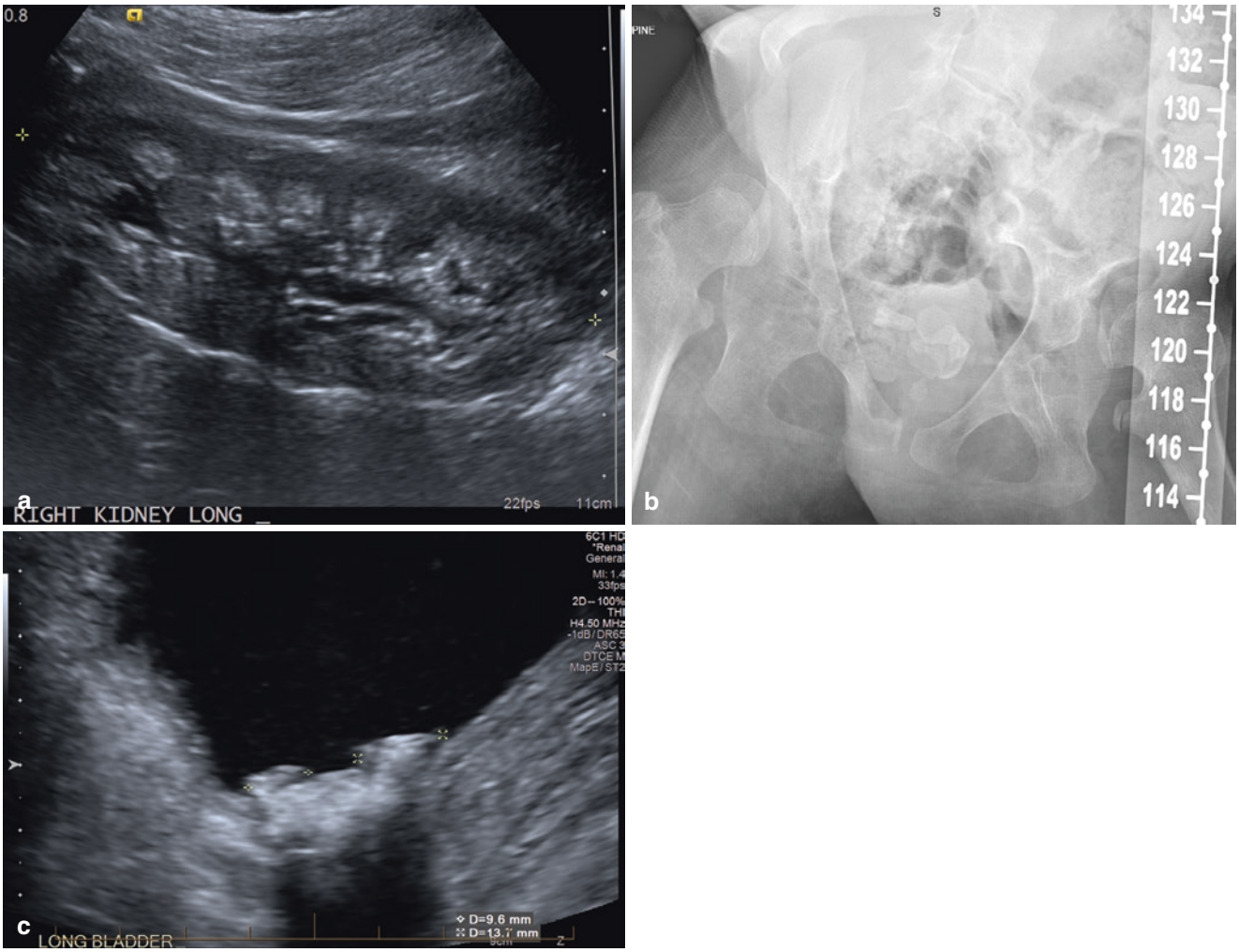

Fig. 5.45 (**a**) Longitudinal ultrasound image of the right kidney in a patient with nephrocalcinosis due to hypercalcaemia. The renal pyramids are markedly hyperechoic relative to the cortex. (**b**) X-ray of the pelvis in a patient with bladder calculi. The calculi are visible as large calcific densities projected over the lower pelvis. (**c**) Ultrasound of the bladder showing multiple dependent echogenic calculi with posterior acoustic shadowing

Further Readings

Aso C, Enriquez G, Fité M, Torán N, Piró C, Piqueras J, et al. Gray-Scale and Color Doppler Sonography of Scrotal Disorders in Children: An Update. Radiographics. 2005;25:1197–214.

Agrons GA, Wagner BJ, Lonergan GJ, Dickey GE, Kaufman MS. From the archives of the AFIP. Genitourinary Rhabdomyosarcoma in Children: Radiologic-Pathologic Correlation. Radiographics. 1997;17:919–37.

Bates DG. The bladder and urethra. In: Slovis TL, editor. Caffey's pediatric diagnostic imaging. 11th ed. Philadelphia, PA: Mosby Elsevier; 2008.

Fernbach SK, Feinstein KA. Normal renal anatomy, variants, and congenital anomalies. In: Slovis TL, editor. Caffey's pediatric diagnostic imaging. 11th ed. Philadelphia, PA: Mosby Elsevier; 2008.

Fernbach SK. Infections. In: Slovis TL, editor. Caffey's pediatric diagnostic imaging. 11th ed. Philadelphia, PA: Mosby Elsevier; 2008.

Frush DP, Sheldon CA. Diagnostic imaging for pediatric scrotal disorders. Radiographics. 1998;18:969–85.

Lowe LH, Isuani BH, Heller RM, Stein SM, Johnson JE, Navarro OM, et al. Pediatric renal masses: Wilms tumor and beyond. Radiographics. 2000;20:1585–603.

Riccabona M. The ureter and vesicoureteric refux. In: Slovis TL, editor. Caffey's pediatric diagnostic imaging. 11th ed. Philadelphia, PA: Mosby Elsevier; 2008.

Surratt JT, Siegel AJ. Imaging of pediatric ovarian masses. Radiographics. 1991;11:533–48.

Treves ST, Packard AB, Grant FD. Kidneys. In: Treves ST, editor. Pediatric nuclear medicine and molecular imaging. 4th ed. New York, NY: Springer; 2014.

Treves ST, Grant FD. Vesicoureteric reflux and radionuclide cystography. In: Treves ST, editor. Pediatric nuclear medicine and molecular imaging. 4th ed. New York, NY: Springer; 2014.

Spinal Conditions

6

Robert Carachi

6.1 Introduction

This chapter consists of conditions, many of which are already described in other chapters. Most of the conditions described include clinical figures.

6.2 Congenital

6.2.1 Neural Tube Defects

Dr. Tulp from Amsterdam recognised the deformity in children and coined the term Spina Bifida (Fig. 6.1a).

The complex neural tube system that develops from infolding of the dorsum of the fetus is the site of a number of different types of mal-development (Fig. 6.1b, c). The global term "neural tube defects" (NTD) is currently used to encompass infants who are born with spina bifida and meningocele or myelomeningocele defects and, at the cranial end of the neural tube, the meningoceles, encephaloceles, iniencephaly, and anencephaly. Hydrocephalus is often associated with NTD and is considered in Chap. 2, as it also occurs due to other causes. There is an interesting geographical variation in the incidence of the different types of NTD with the spinal anomaly of meningocele and myelomeningocele constituting 80% of NTD live-born infants in Europe, North America, Australia, and some communities in South Africa. Defects of the cranial end, particularly encephaloceles, are more common in South East Asia than in Europe and account for 40% of the NTD found there (Fig. 6.1d).

Scotland, particularly the West of Scotland, has been an area of high incidence of NTD. For every live-born child with NTD there has also been a stillbirth or early neonatal death of an infant with anencephaly. Previously, incidence of NTD was approximately 3 per 1000 live births, whereas over the last 15 years incidence has decreased to 1 per 1000 live births. A couple who have a fetus or child affected by a neural tube defect have an approximately a tenfold increased likelihood of subsequent siblings being affected, and if the couple have two siblings affected there is again a further increase by a factor of 3 for subsequent children. In 1992 an expert advisory group of the UK departments of health recommended that to prevent recurrence of a neural tube defect, women at risk should take a daily folic acid supplement until the twelfth week of pregnancy. To prevent a first occurrence of NTD, women who are planning a pregnancy should eat more folate rich foods and take 4 mg folic acid daily from the time they begin trying to conceive through the twelfth week of pregnancy. A Medical Research Council study published in 1991 suggested that folic acid offered a 72% decrease in the risk of a second affected child.

Detection of elevated maternal serum alpha fetoprotein levels and refinement in intra-uterine ultrasound diagnosis have resulted in intra-uterine diagnosis and pregnancy termination in many cases. A genetic predisposition to the development of neural tube defects may explain the higher incidence in those of Celtic (Irish, Welsh, and West of Scotland population) than in those of Anglo-Saxon or Norse origin in the British Isles, but folate deficiency is not uncommon in these populations (Fig. 6.1e).

6.2.2 Spina Bifida Occulta (Fig. 6.2a)

In spina bifida occulta there is failure of fusion of the spinous processus posteriorly. In most individuals this is a minor deviation from normal. A few children have an associated haemangiomatous or hairy patch over the site of the spina bifida occulta, and in these infants there may be some neurological deficit such as a foot drop or a sudden alteration in continence of urine or a problem deep to the lesion (Fig. 6.2b–d). Tethering of the cord is the most common problem, and if it produces neurological signs it merits exploration and freeing of the cord. Other variations of the

R. Carachi (✉)
Surgical Paediatrics, University of Glasgow, Glasgow, UK

R. Carachi (ed.), *Atlas of Paediatric Surgical Imaging*, https://doi.org/10.1007/978-3-030-32384-4_6

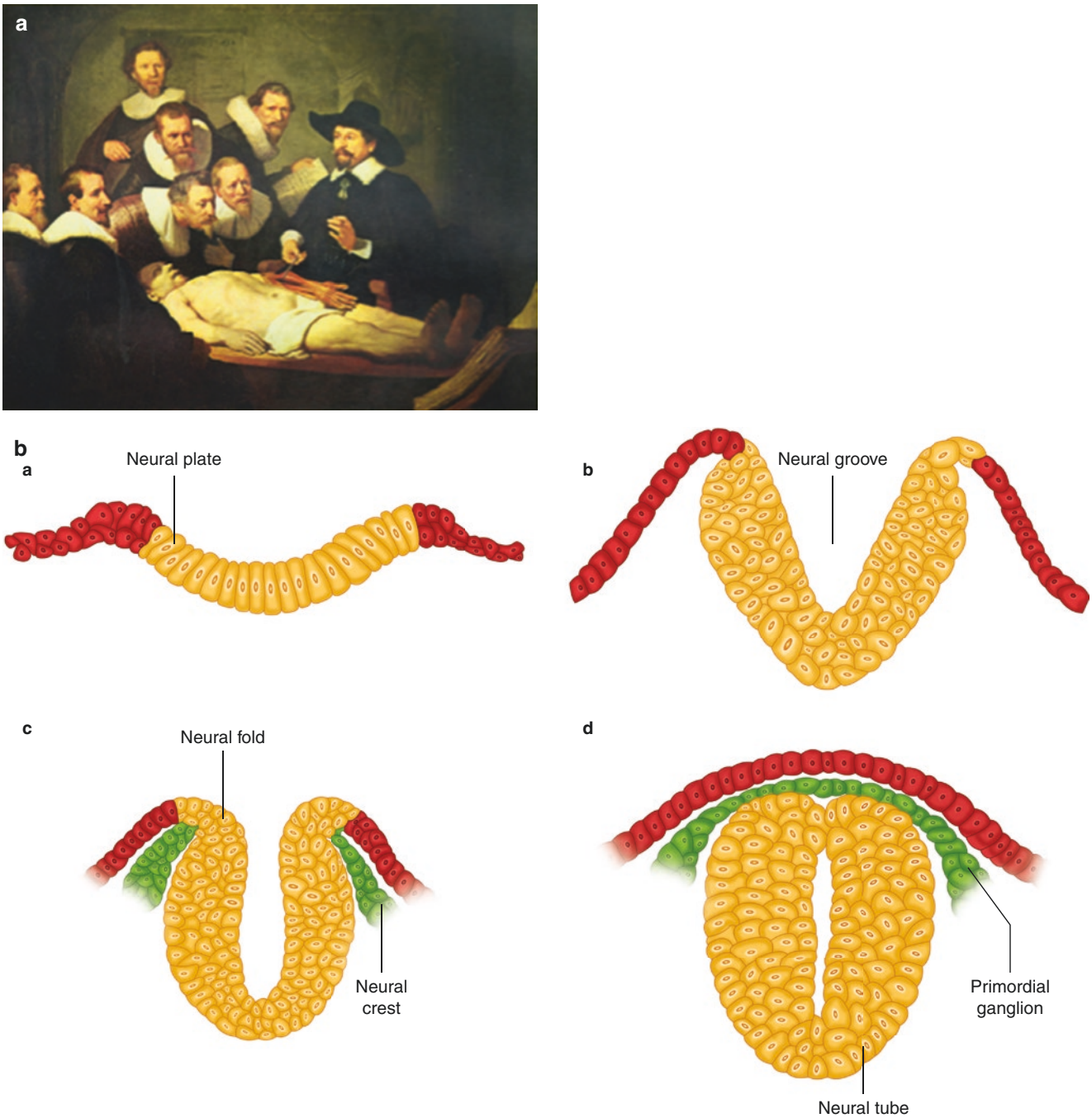

Fig. 6.1 (**a**) Dr. Tulp demonstrating an anatomy lesson. A painting by Rembrandt. Dr. Tulp coined the term Spina Bifida. (**b**) Neural Tube Development showing the neural plate folding to become the neural tube. (**c**) An experimental rat embryo showing the development of the neural canal. (**d**) Line drawing of spina bifida. (**a**) Normal spine; (**b**) Spina bifida occulta; (**c**) meningocoele; (**d**) myelomeningocoele. (**e**) A plain X-ray showing a severe form of spina bifida with total failure of development and fusion of the neural arches

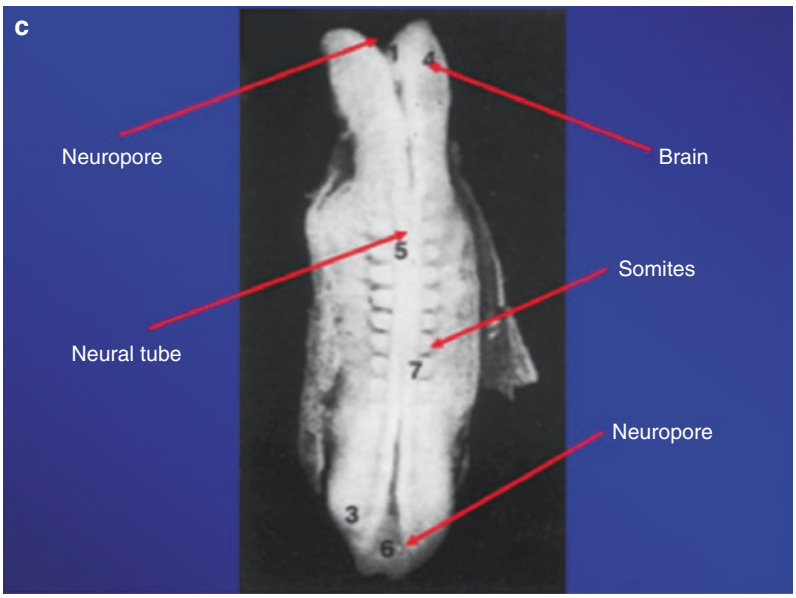

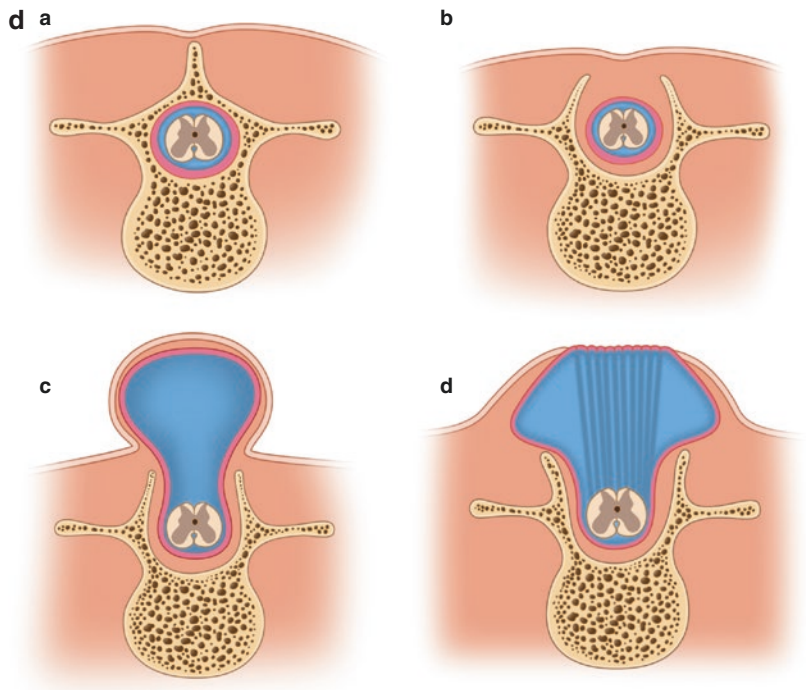

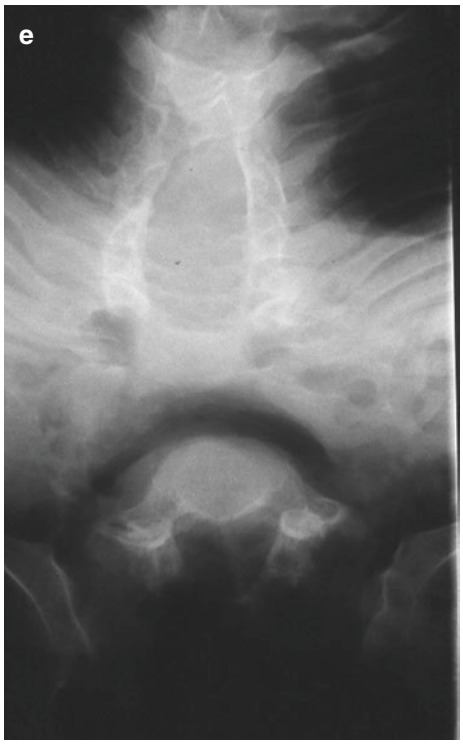

Fig. 6.1 (continued)

spine include an anomaly where a bony spur protrudes from the posterior aspect of the vertebral bodies and results in splitting of the cord (diastematomyelia). In a few patients this may merit exploration and removal of the bony spur. Visualisation of these has been greatly enhanced with the development of magnetic resonance imaging, which can give much better definition of the intra-spinal anatomy than was previously possible.

6.2.3 Spina Bifida Cystica/Meningocoele

The spina bifida defect may result in a *meningocele* in which there is simply a protrusion of the spinal cord coverings to form a sac that contains cerebrospinal fluid (CSF) (Fig. 6.3a). This defect accounts for less than 10% of infants born with spina bifida. There are no neurological sequelae from the meningocele itself, and treatment is excision of the sac and

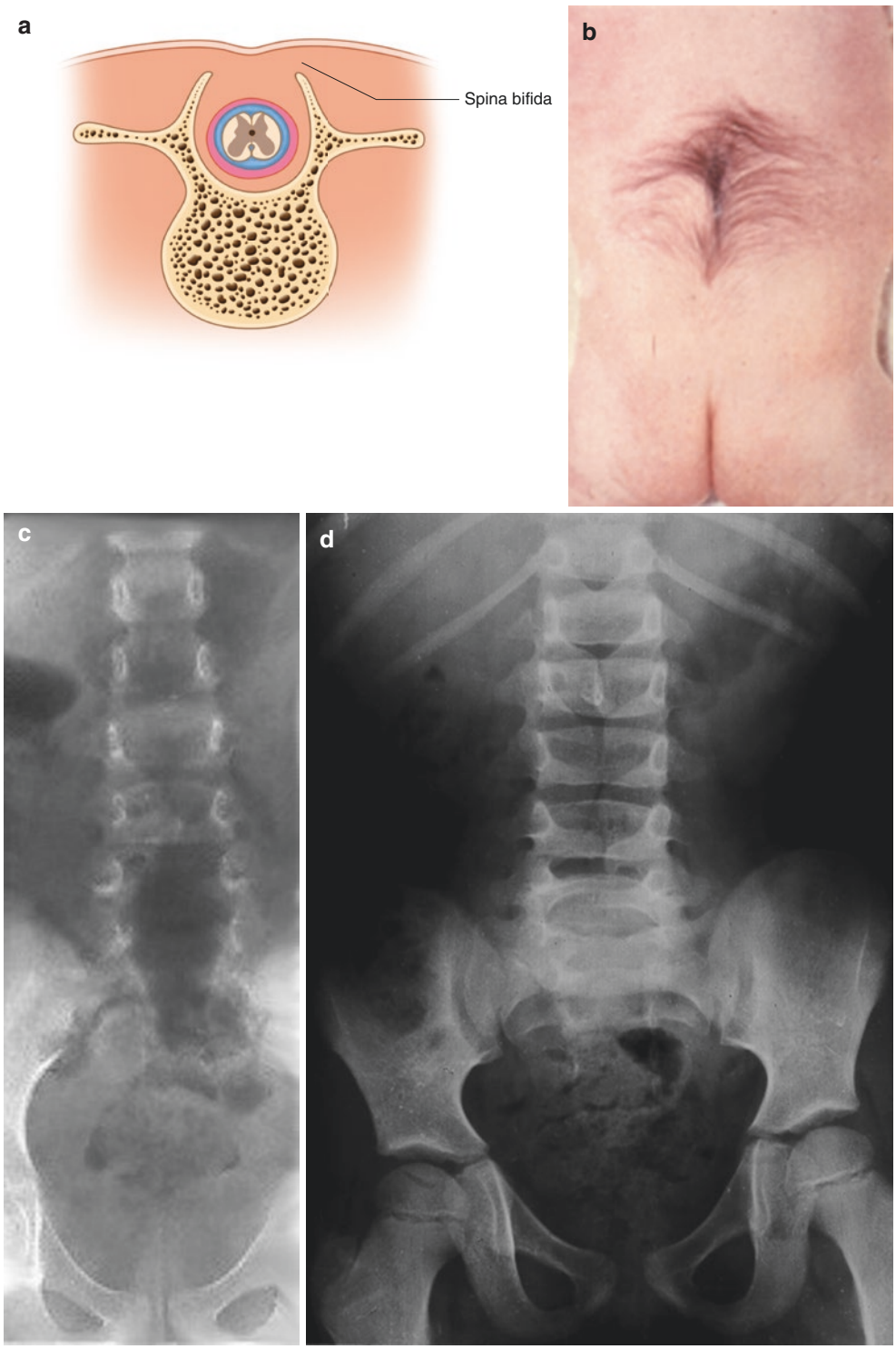

Fig. 6.2 (**a**) A diagram showing the least form of failure of development of the neural arch. (**b**) A clinical photograph of a hairy patch sometimes accompanied with a lipoma, but with intact skin and musculature indicating an underlying spina bifida occulta. (**c**) Nevus hairy back, X-ray showing spina bifida occulta. Note the failure of the laminae to meet in the midline. (**d**) Spina Bifida Occulta

closure of the dura and overlying structures. Fascial flaps can be brought across the spina bifida defect, and no attempt is made to alter the bony structure. The problem that may occur in these infants is the development of progressive hydrocephalus. Some infants already have hydrocephalus at birth and others develop it after excision of the meningocele (Fig. 6.3b).

6.2.4 Spina Bifida Cystica/Meningomyelocoele (Fig. 6.4a–c)

The more severe forms of spina bifida involve neural tissue and range from the *meningomyelocele* to the most severe end of the spectrum, *myelocele*, in which the cord lies exposed with no covering. The most common site of these lesions is

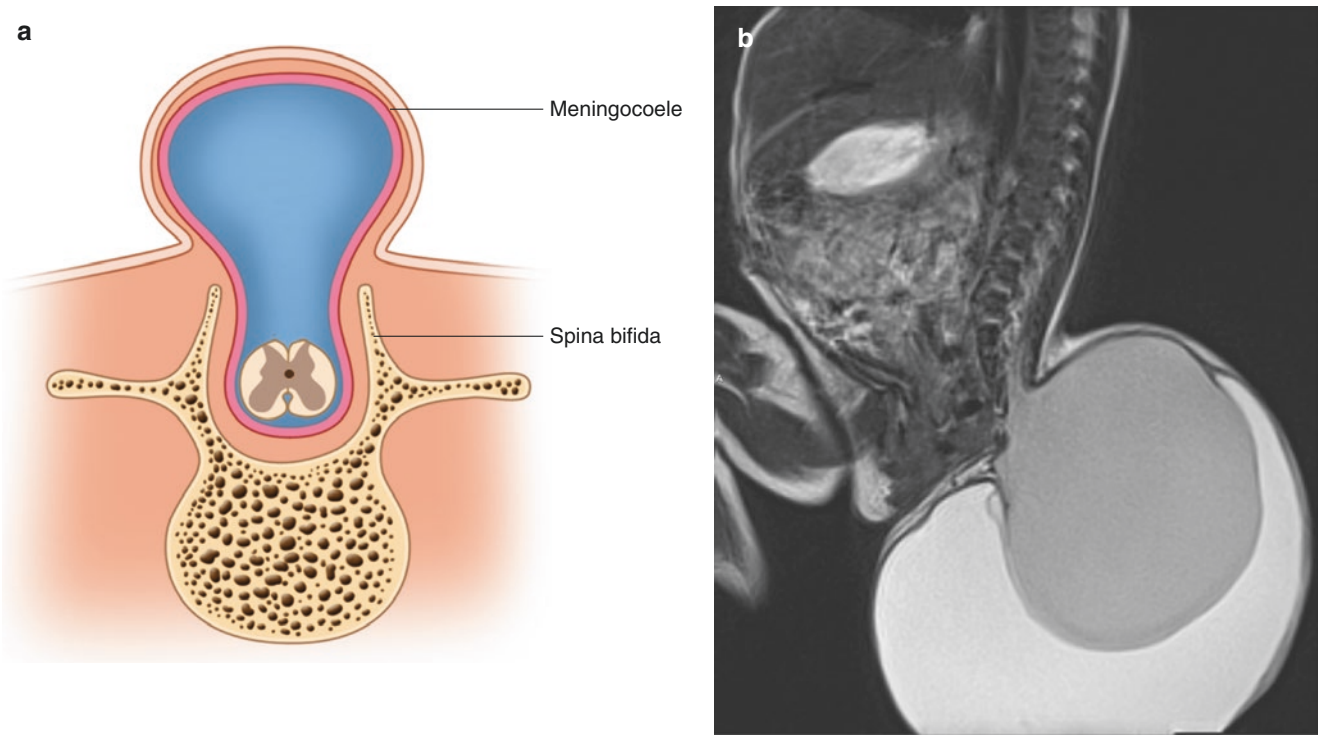

Fig. 6.3 (**a**) Diagram of a spina cystica meningocoele with no neural elements present. (**b**) Neonate born with a sacral meningocoele

the thoraco-lumbar area, in which case there is severe impairment of neural function in the lower half of the body. This affects both the motor and the sensory aspects to a level distal to the lesion. The next most common site is the sacral area, and affected infants may have much less severe affliction of the lower limbs, but defective neural supply to the bowel and bladder may give rise to serious problems of incontinence.

Effective management of the infant born with spina bifida depends on an initial detailed clinical examination and assessment of level of neurological impairment. Motor and sensory deficits are charted usually by physiotherapists who continue to help parents in managing the lower limb defects. The lack of muscle pull on the bones may leave them weaker than normal, and care in handling the infant is necessary to prevent fracture of their fragile bones. In consequence of the intrauterine paralysis that occurs in many of these children, there may be secondary structural problems and deformities, such as loss of the normal lumbar lordosis and kyphosis. These problems progress with time, as they are secondary to imbalance of muscular activity. Similar imbalanced muscle activity may result in dislocation of the hips, deformities of the knees, or severe feet deformities (talipes). On the initial examination it is also important to assess upper limb function, which is normal in the majority of infants; in a small number, however, due to further cord problems, upper limb problems become apparent as time goes by. A very common accompaniment of spina bifida is hydrocephalus, which will be progressive in many infants and require active treatment.

The goal of treatment of the infant with spina bifida is to maximise the potential of the child, rather than being in any way curative. The neurological problem has been in existence for 6 or 7 months before birth and the exposed neural tissue is irrevocably damaged. In some infants, however, early closure of the back defect may be indicated to prevent infection and fibrosis affecting parts of the spinal cord which were not previously damaged. Closure of the back also has an important cosmetic aspect in that it quickly allows the back to be covered by normal skin and is therefore much easier for the parents to manage. The one drawback of early closure of myelomeningocele is that progression of hydrocephalus requiring active treatment is almost invariable, and leaving the larger defects (in which paraplegia is complete) to epithelialise spontaneously can result in the production and reabsorption of CSF becoming balanced so that active intervention is unnecessary. This occurs in one-third of the patients. Decisions have to be made according to the circumstances of each individual child and family.

The neurological effect in the legs of Spina Bifida Cystica must be considered in the light of the patient as a whole—such a child has a 98% chance of urinary and faecal incontinence, may have hydrocephalus that has required drainage, and may have cerebral palsy and congenital anomalies.

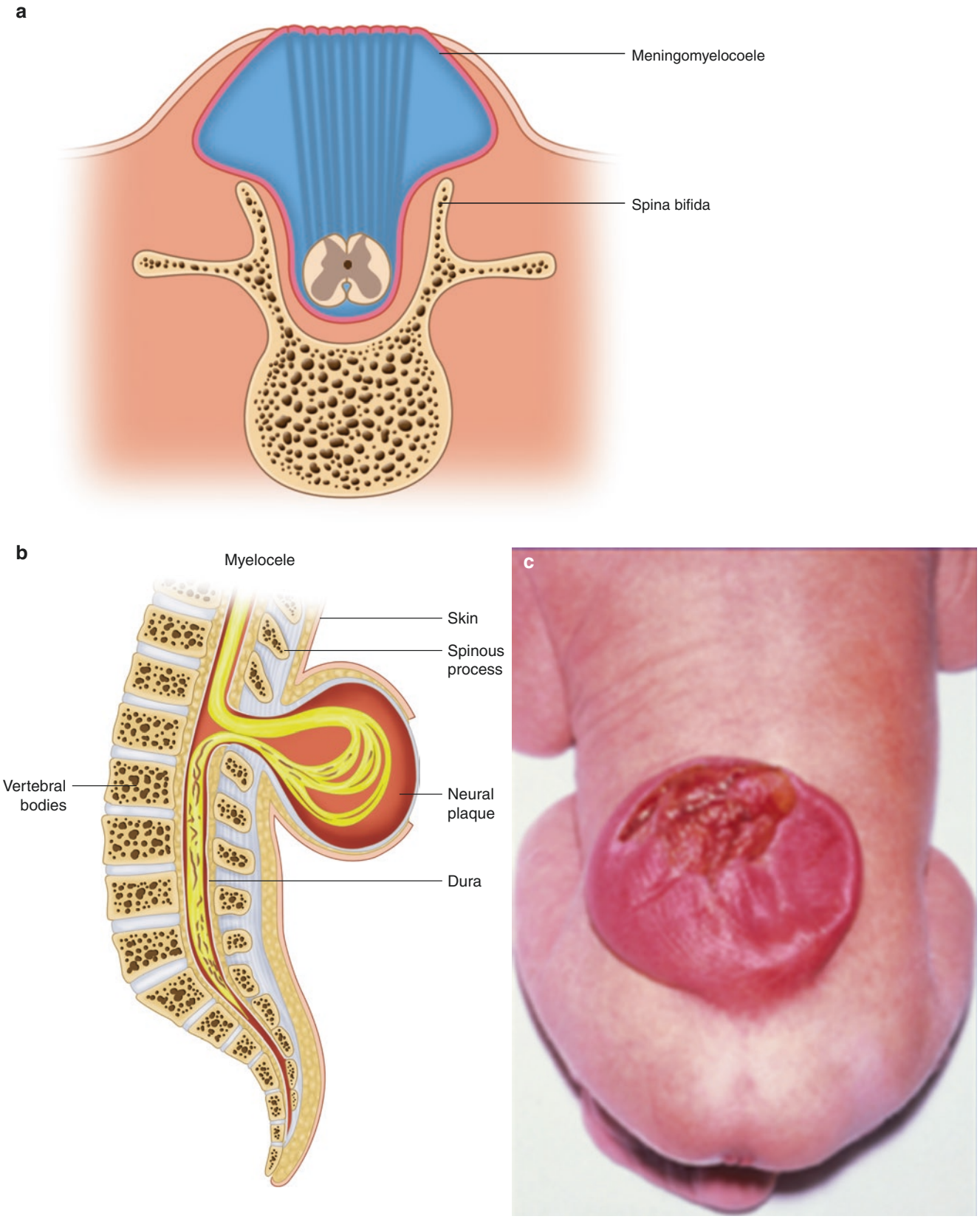

Fig. 6.4 (**a**) Diagram of a spina bifida cystica myelomeningocoele showing the disorganization of the neural placode and the neural plaque. (**b**) Lateral view of a diagram of the spine with a myelomeningocoele. (**c**) Clinical photograph of a lumbar myelomeningocoele

Sensory loss in the legs may be extensive, depending on the degree of nerve root or spinal cord damage. The motor dysfunction is largely due to root damage giving flaccid paralysis, but areas of spasticity may be present due to higher cord damage with intact lower cord segments and lower motor neuron function, together with a potential to develop severe deformity. Some problems are reasonably predictable—e.g., a common level of lesion about L4 will leave the roots of femoral and obturator nerves largely intact, while the sciatic nerve will be paralysed. As a result, the hip, subject to the pull of flexors and adductors but with no extensor or abductor muscle function, will dislocate. At a lower level, active quadriceps, unopposed by paralysed hamstrings, will produce recurvatum of the knee. The foot may be deformed in any direction, and loss of the normal weight distribution on the sole of the foot will readily lead to trophic ulceration in the anaesthetic foot.

Leg deformity may be controlled by a variety of procedures and function improved by calliper bracing. Any success in getting the child to stand or walk in some way with various aids will depend upon the child's intelligence, the degree of neurological damage, and the possible presence of spinal deformity, all of which are not under our control. One factor that may be controlled is obesity, which makes standing and walking more difficult. A wheelchair existence is the likely result in many children, and indeed later many may choose this as an easier way of life. The sensory loss gives rise to the problems of trophic ulceration. Any ill-fitting appliance or footwear may initiate this, and the ulcer can be very deep as well as slow and difficult to heal. Trophic ulceration is a much more common problem in the second decade of life than in the first.

6.2.5 Diastematomyelia

Diastematomyelia is a condition with a bony spur often splitting the neural tissue in two at the level of the spinal cord or lower down at the level of the cauda equina (Fig. 6.5).

6.2.6 Cervical/Thoracic Lesions

High lesions in the cervical spine may be confused with an occipital myelomeningocoele/meningocoele. Often on a plain X-ray this can be resolved by the obvious disruption of the cervical spine. The higher up the lesions occur, the more chance of a severe neurological disability with hydromyelia and syringomyelia (Fig. 6.6a, b).

6.2.7 Thoracic/Lumbar Lesions

Thoracic lesions are less common than lumbar lesions; however, the full spectrum can be also seen at this level (Fig. 6.7a, b).

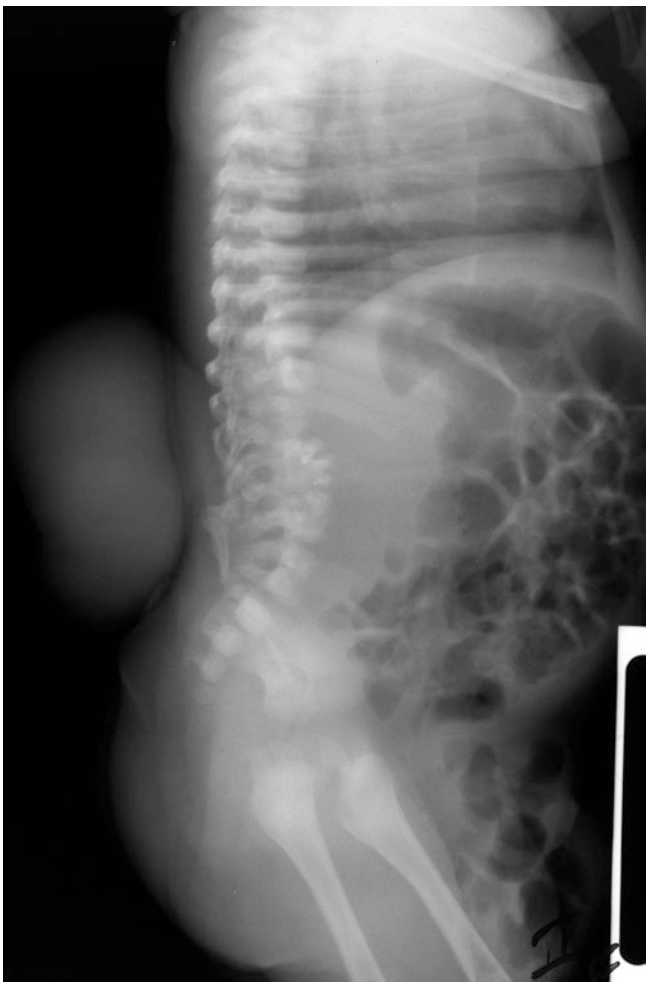

Fig. 6.5 Diastematomyelia with a bony spur often splitting the neural tissue in two at the level of the spinal cord or lower down at the level of the cauda equina

6.2.8 Lumbar/Sacral Lesions

Lumbar lesions are the most common abnormality in Spina Bifida, with resultant paralysis of the lower limbs, neurogenic bladder, and subsequent hydrocephalus (Fig. 6.8a–d).

6.2.9 Anterior Meningocoele

An anterior meningocoele may occur in the lumbar region. The lumbar spines are pushed back by the anterior mass which is fluid-filled (CSF) and is pushing loops of bowel away (Fig. 6.9).

6.2.10 Split Notochord Syndrome/Posterior Enteric Remnant

This condition is rare and can be mistaken for Spina Bifida because the lesion on the back involves a disrupted spine

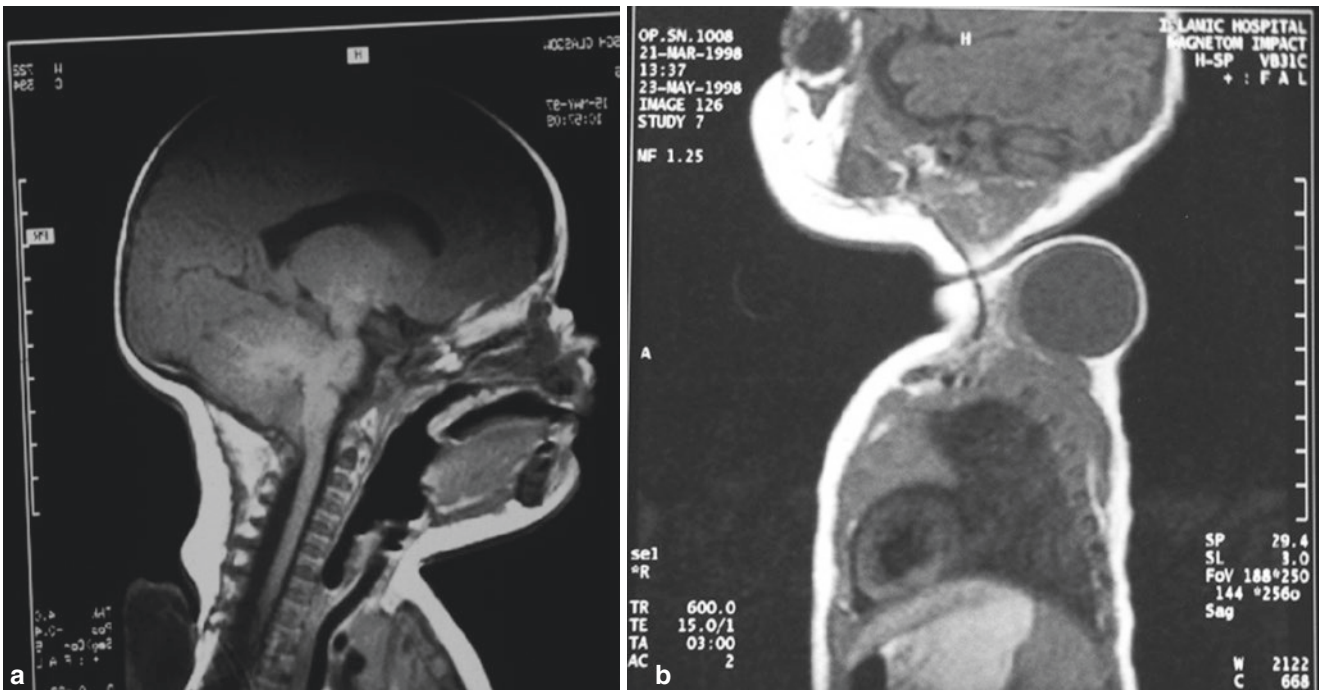

Fig. 6.6 (**a**) Scan showing lateral view of a high cervical meningomyelocele. (**b**) Scan showing a lateral view of a cervical meningocoele

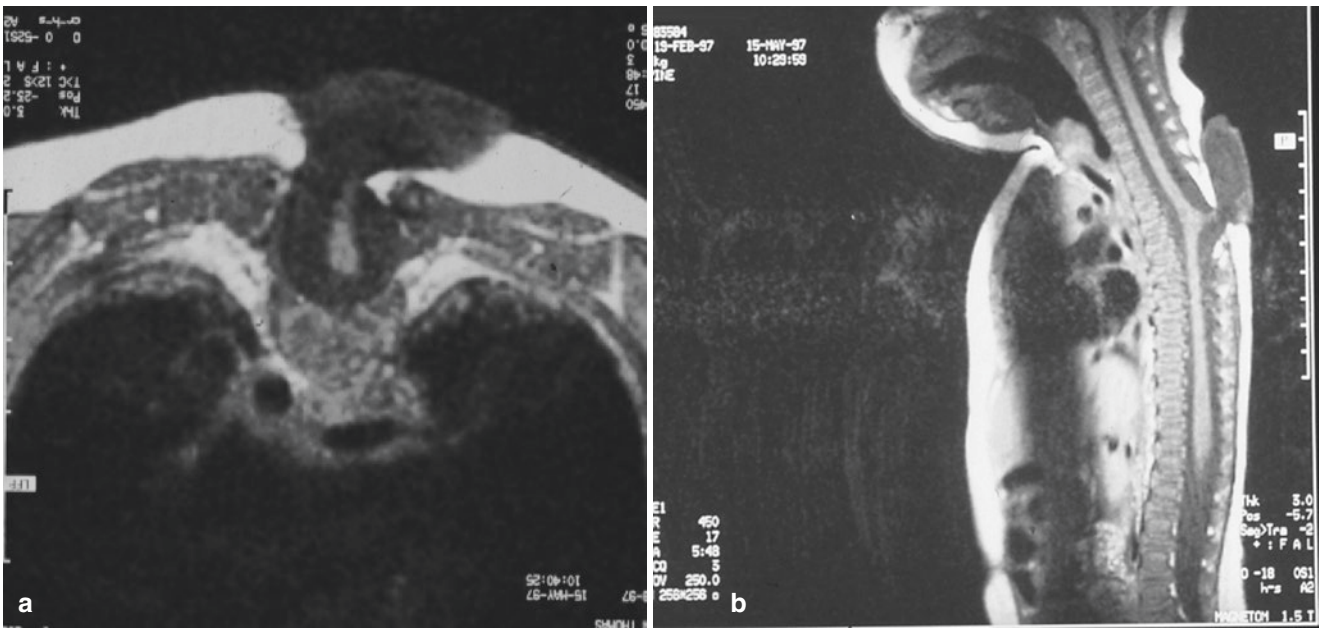

Fig. 6.7 (**a**) Cross-sectional view of a thoracic meningomyelocele showing the body of the vertebra and the laminae splayed out with the myelomeningocele protruding out of the back. (**b**) An MRI scan showing a lateral view of a thoracic myelomeningocele. Note how the spinal cord is tethered at the lesion

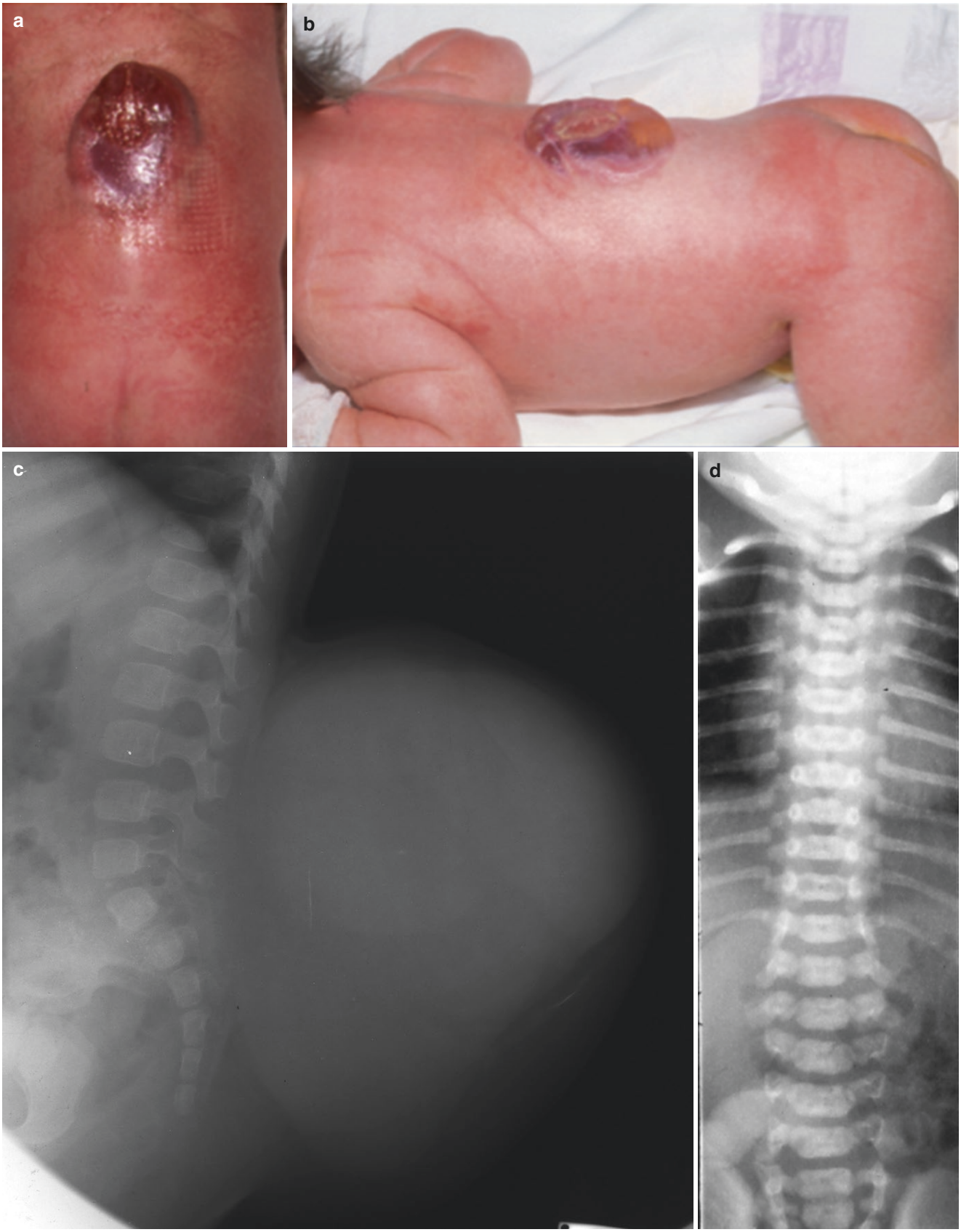

Fig. 6.8 (**a**) Clinical photo of a lumbar myelomeningocele. An open lesion leaking CSF. (**b**) Later view of the same patient with a lumbar myelomeningocele. Note how there is loss of the normal curvature of the spine. (**c**) Plain X-ray of a lateral view of the spinal column of a patient with a lumbo sacral myelomeningocoele. Note the soft tissue mass over the disrupted spine. (**d**) Plain X-ray anterior view of an extensive lumbosacral myelomeningocoele. Note the pedicles all everted in the lumbosacral region and loss of the laminae of the spine

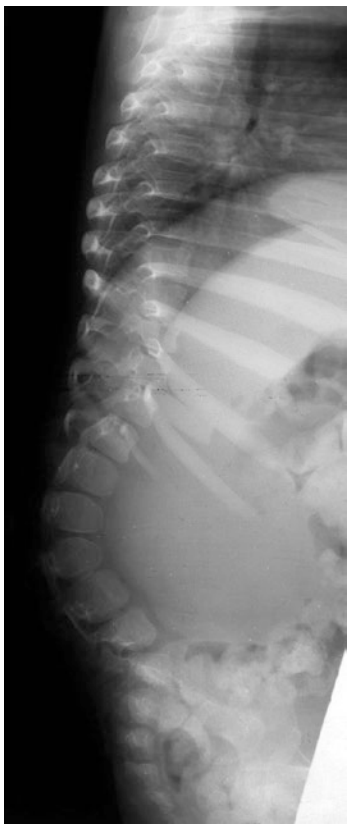

Fig. 6.9 Plain X-ray lateral view showing an anterior meningocoele in the lumbar region. The lumbar spines are pushed back by the anterior mass, which is fluid-filled (CSF) and is pushing loops of bowel away

with herniation of bowel through the back. This condition is discussed fully in Chap. 7 (Fig. 6.10a–d).

6.2.11 Scoliosis/Kyphosis (Fig. 6.11a, b)

Increased posterior curvature is seen in adolescent kyphosis or Schuermann's disease. This oesteochondritis of the epiphyseal plates of the vertebrae causes pain in the back and is treated by physiotherapy. Angular kyphosis may be congenital and due to hemivertebrae or due to infection such as tuberculosis. Kyphosis may occur in other situations such as achondroplasia or Von Recklinghausen's disease of bone as part of the general deformity of the skeleton.

6.2.11.1 Lordosis (Fig. 6.11c–e)

An exaggerated lumbar curvature is seen in bilateral congenital dislocation of the hips and rarely in older children with spondylolisthesis, as well as children and adults with neural tube defects. (Fig. 6.11f, g)

6.2.11.2 Fetus-in-Fetu: Extra Limb

A fetus-in-fetu is where a second fetus has been reabsorbed and tissue is left on the back of the baby that survived. An extra well-developed limb can be identified (Fig. 6.12).

6.2.11.3 Currarino Syndrome (Fig. 6.13)

This syndrome is discussed fully in Chap. 8.

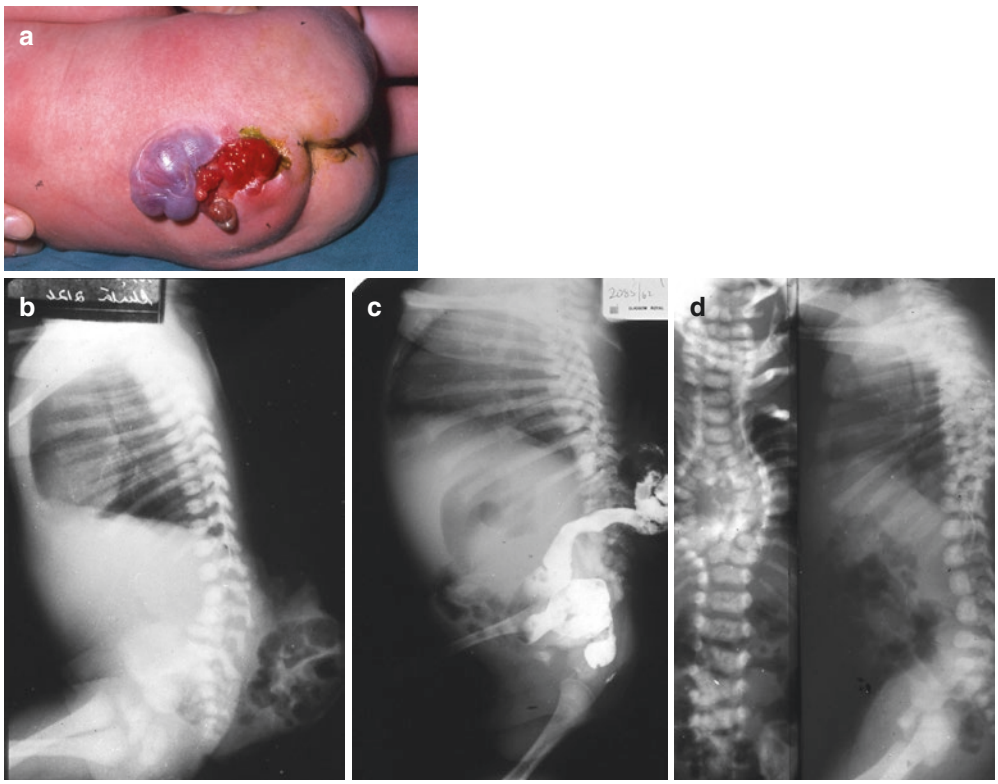

Fig. 6.10 (**a**) Clinical photograph of a split notochord syndrome showing a spina bifida myelomeningocoele and bowel herniating out from the back through the split notochord. (**b**) Lateral view plain X-ray of the patient showing loops of bowel herniating from the back lesion. (**c**) Split Notochord Syndrome. X-ray with contrast from below showing the herniated loops of bowel protruding from the back. (**d**) Split Notochord Syndrome. Plain X-ray pA and lateral view of the same patient showing an extensive lesion in the thorax with gross vertebral disruption. Some of the bodies of the thoracic vertebrae can be seen to be split in half where the notochord has divided

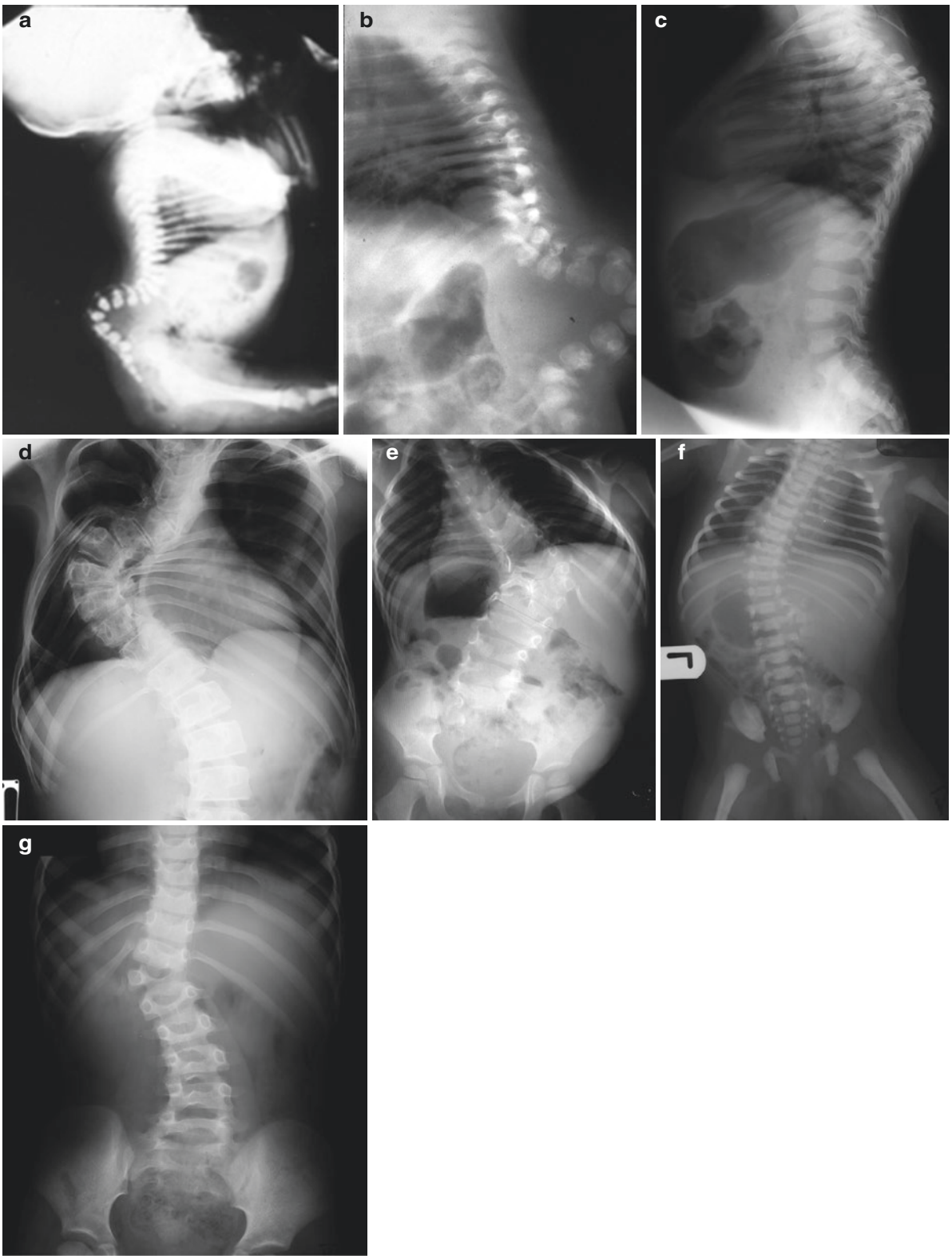

Fig. 6.11 (**a**) Babygram showing a lateral view of a severe gibbus, Kyphosis of the lumbar spine. (**b**) Severe Kyphosis of the lumbar spine with an acute angle, seen on this plain X-ray. (**c**) Plain X-ray lateral view showing a mid-thoracic kyphosis. (**d**) Plain X-ray showing a severe mid-thoracic scoliosis. (**e**) Plain X-ray of the spine showing severe disruption of the thoracolumbar spine resulting in a scoliosis. (**f**) Gentle scoliosis to the right. Plain X-ray posterior view. Some disruption of the upper lumbar vertebrae seen on the X-ray. (**g**) Plain X-ray of the spine showing loss of half of the first lumbar vertebra with resultant scoliosis

6.2.12 Sacral Agenesis (Fig. 6.14a, b)

See Chap. 4.

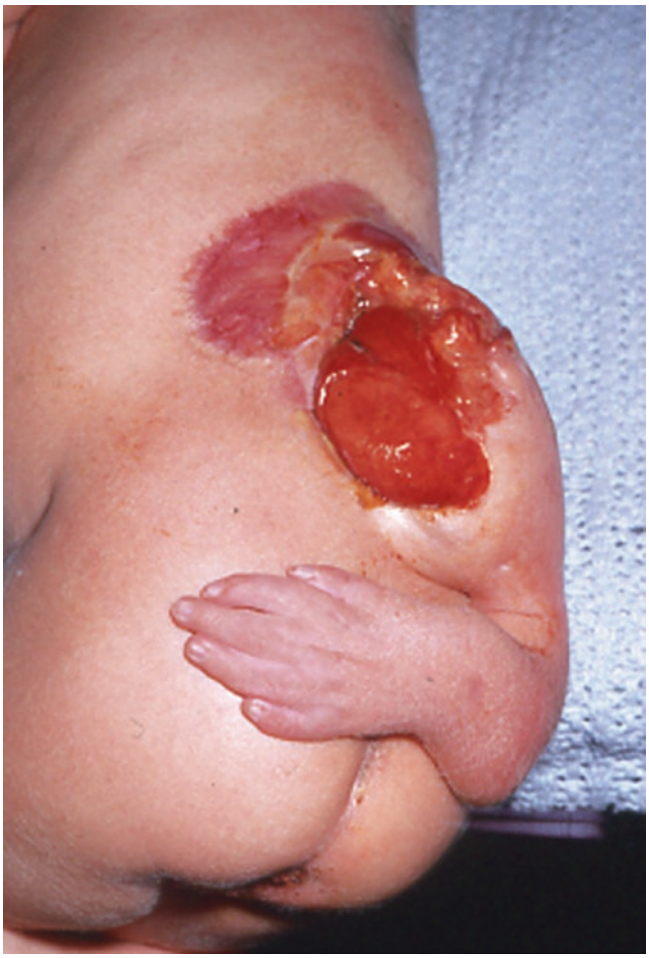

Fig. 6.12 Clinical photograph of a fetus-in-fetu where the second fetus has been reabsorbed and tissue is left on the back of the baby that survived. An extra well-developed limb can be identified

6.2.13 Hemi Vertebrae/Butterfly Vertebrae

These deformities can be single or multiple with absence of a section of a vertebra. Severe scoliosis can result from the abnormalities due to the instability of the spinal column (Fig. 6.15a–e).

6.2.14 Exstrophy (Fig. 6.16)

See Chap. 5.

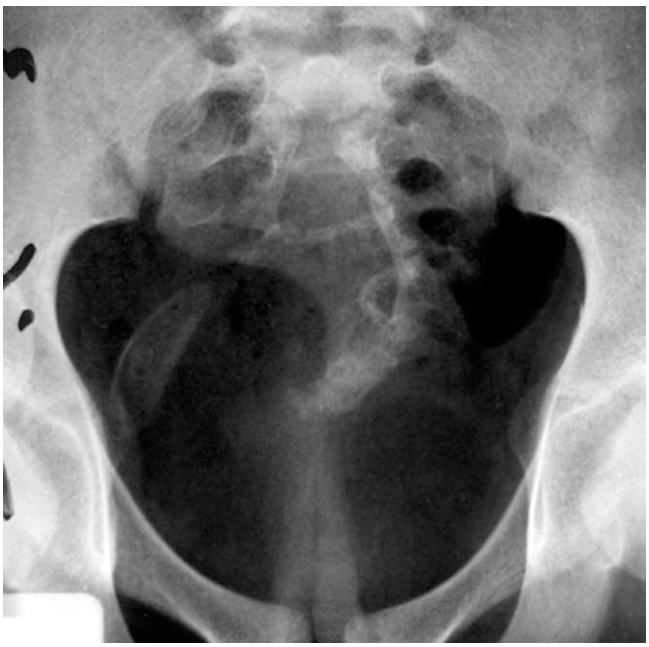

Fig. 6.13 Spina bifida with scimitar sacrum

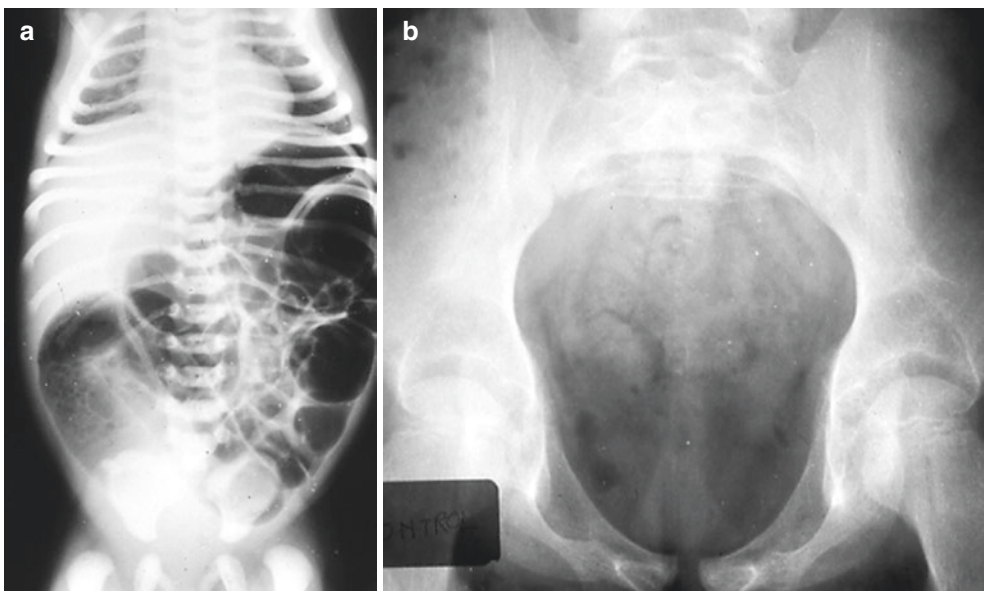

Fig. 6.14 (**a**) Sacral agenesis imperforate anus in a new-born. This X-ray shows a low intestinal obstruction as well as a sacral agenesis. (**b**) Sacral agenesis with total absence of the sacrum who presented at an older age with soiling

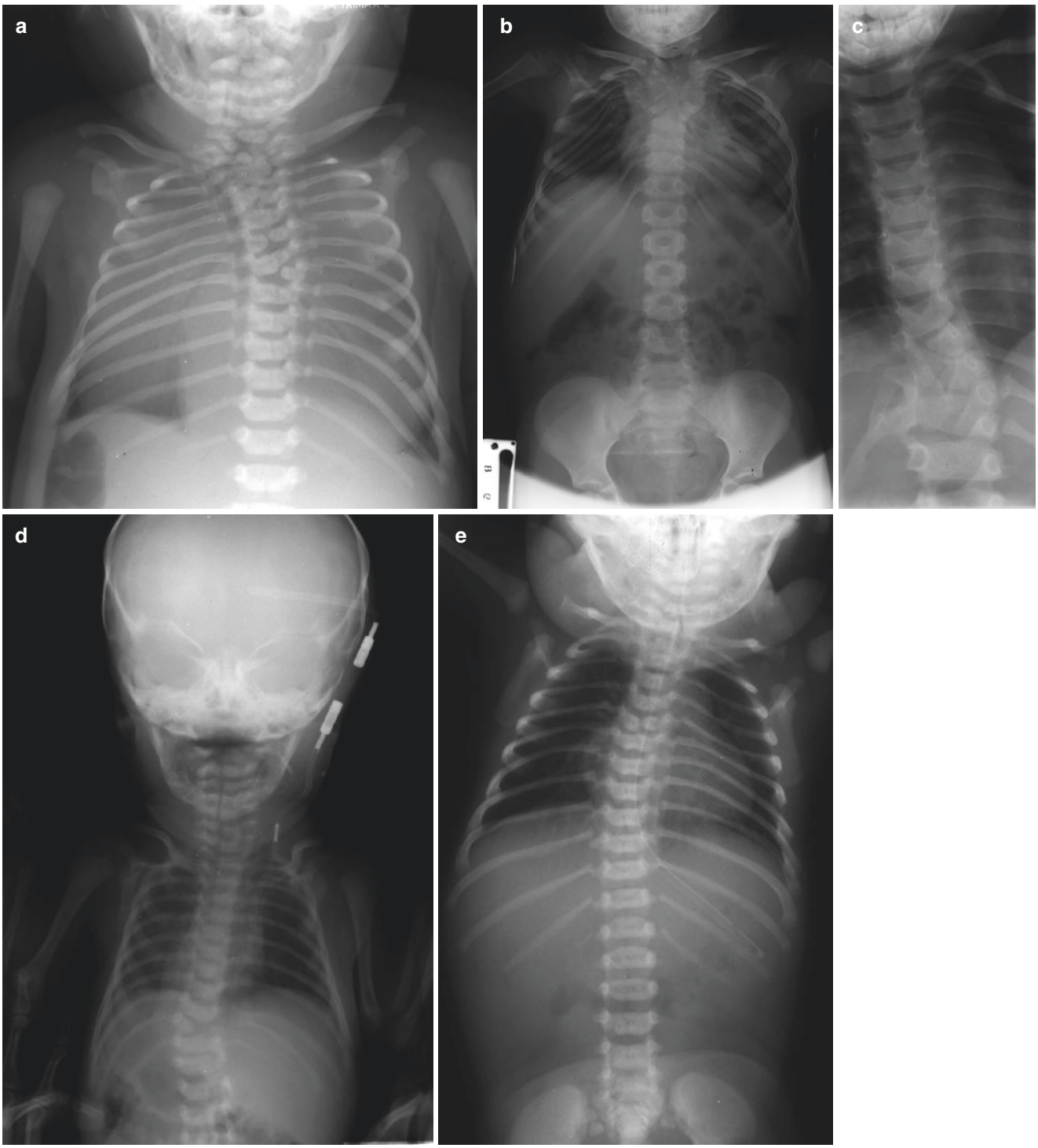

Fig. 6.15 (**a**) Plain X-ray of the spinal column showing severe disruption of the cervical and the upper thoracic spine with split vertebrae, hemivertebrae, and absence of vertebrae. (**b**) Severe deformity of the cervical and upper thoracic spine from poor development. (**c**) Plain X-ray showing lower thoracic hemivertebrae with resultant spinal deformity. (**d**) Plain X-ray in a neonate with a shunt in situ showing a single hemivertebra in the first vertebra. (**e**) Plain X-ray. Mid thoracic hemivertebra in a neonate with a nasogastric tube in situ

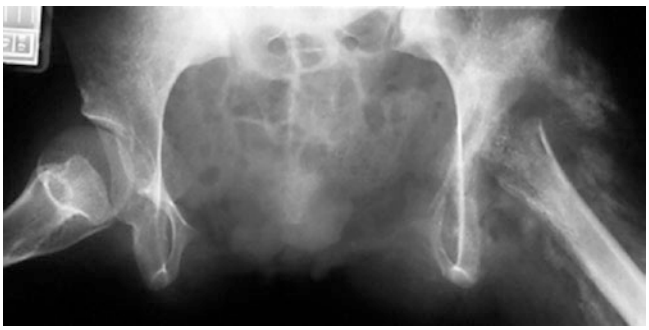

Fig. 6.16 Plain X-ray of the pelvis showing an absence of the pubic bones anteriorly in keeping with an exstrophy of the bladder

6.3 Infection and Inflammation

6.3.1 Paravertebral Abscess

A collection secondary to underlying disease of the spine, e.g., osteitis (Fig. 6.17a, b).

6.3.2 Discitis

Inflammation of the disc cushion protecting the vertebrae during movement. Diseases of the disc can be caused by trauma, natural wear and tear, and inflammation. Herniation of a disc can protrude dorsally and cause compression on the spinal cord (Fig. 6.18a, b).

6.3.3 Osteitis

The term *osteitis* is preferred to osteomyelitis as the bone marrow plays only a small part in this infection. The most common infecting organism is the staphylococcus pyogenase. Streptococcal osteitis is more common in infancy. The route of infection is blood-borne and may come from septic lesions such as boils, abrasions, and infected teeth and tonsils. In the neonatal period, infection probably enters through the respiratory or alimentary tract or umbilical cord and can be a consequence of a septicaemic episode (Fig. 6.19).

In childhood, infection can lie latent for long periods and the initial lesion is often healed and forgotten for 2–3 weeks before the onset of the disease. Acute osteitis is essentially a disease of childhood. Apart from neonatal osteitis, which is usually secondary to a septicaemia, the disease is relatively uncommon in the first 2 years of life. It is more common in boys, and trauma is a predisposing factor. The bones of the lower extremity are most liable to infection and the tibia and femur are by far the most common sites. The septicaemic phase may be of short duration, or it may last several days. Circulating organisms settle in the vascular metaphases of a long bone and lead to acute suppurative inflammation. This may progress to abscess formation where periosteal vessels are obliterated, and superficial portions of bone may undergo necrosis resulting in sequestrae at a later stage. Usually the diagnosis is made before this stage is reached, and antibiotic treatment arrests the progression of the disease. This condition is still prevalent in under-developed countries where there is a delay in the diagnosis and drugs for adequate treatment are unavailable.

The disease begins with acute pain affecting the limb, which may be preceded by a variable period of malaise. There may be a history of a recent injury or a primary focus of infection. The child is usually ill, flushed, restless, and the affected limb is kept still. There is resentment to any examination of the limb. There is usually a pyrexia and a rapid pulse. In the early stages there is no swelling of the limb, but by gentle palpation an area of maximum tenderness is found over the affected metaphasis. Swelling of the limb is associated with a sub-periosteal effusion, but cellulitis does not appear until the periosteum ruptures. There is a very high polymorphonuclear leucocytosis and an erythrocyte sedimentation rate (ESR) which is markedly raised. No radiographic changes are seen in the first week of the illness. Thus, radiography has nothing to offer in the early diagnosis of acute osteitis. Bone scans may prove helpful. Subsequently there is evidence of elevation of the periosteum and a translucent area of decalcification in the affected metaphasis. In more advanced cases, sequestra, areas of devascularised bone, may be seen.

6.3.4 TB Spine

Tuberculosis affects the spine because of its blood borne nature after entering the lungs. T.B. of the spine causes the so-called Potts deformity with severe Gibbus and Kyphosis (Fig. 6.20a–c).

6.3.5 Poliomyelitis

Although rare since the introduction of oral vaccination, poliomyelitis may occur and leave the child with a variable degree of flaccid paralysis, which is quite unpredictable in its pattern. Sensation remains normal. The problems are due to loss of function, the acquisition of

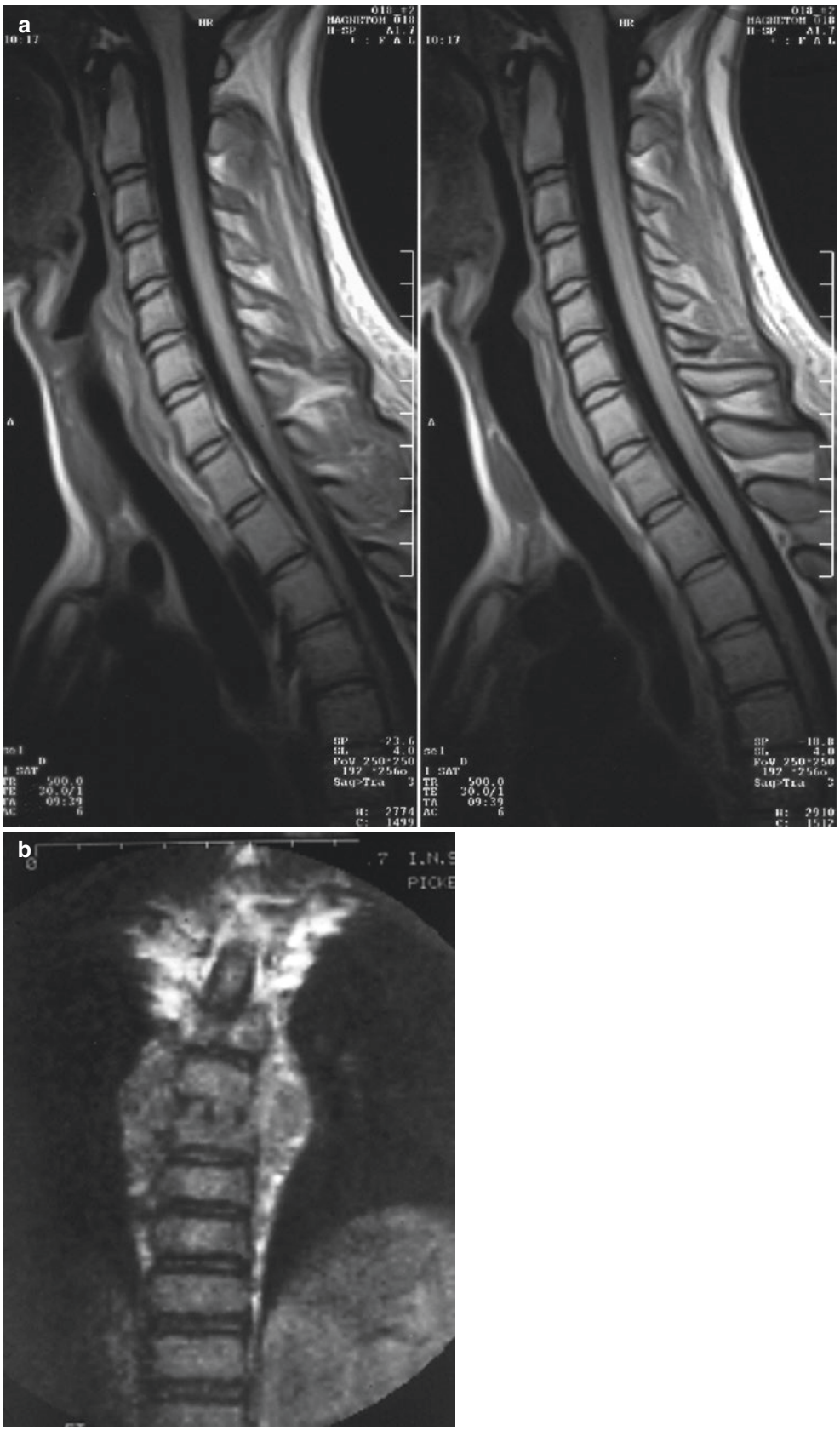

Fig. 6.17 (**a**) Paravertebral collection seen on MRI scan lateral view. (**b**) Paravertebral collection/abscess seen around the vertebral column

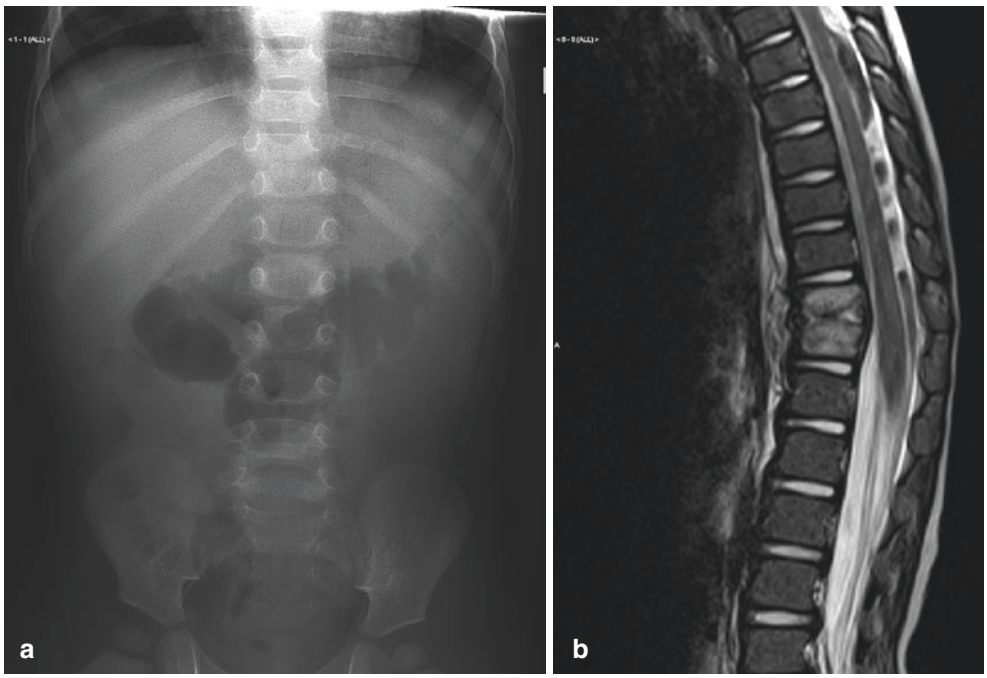

Fig. 6.18 (**a**) Plain X-ray showing discitis at level of spine t11/12. (**b**) MRI scan showing very localized discitis and paravertebral collection

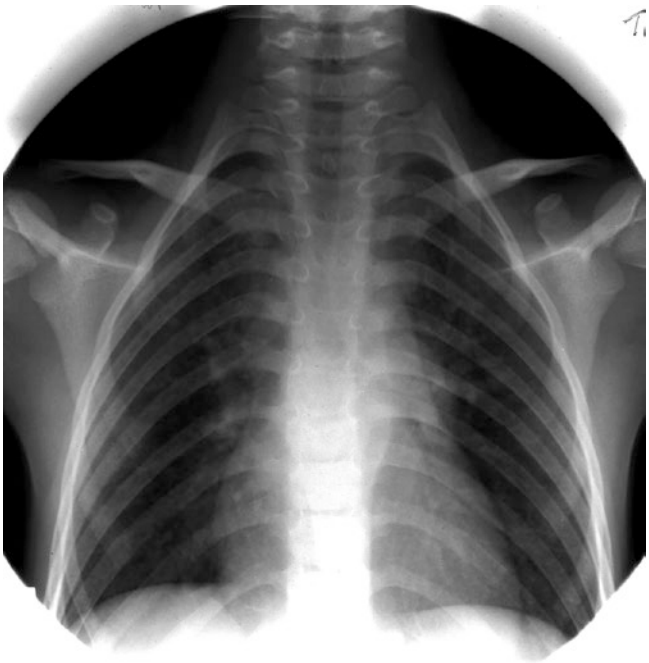

Fig. 6.19 Plain X-ray showing osteitis of the mid-thoracic vertebral column

deformity due to the unbalanced pull of muscles no longer opposed by paralysed muscles, and loss of growth potential due to lack of muscle pull and ability to bear weight. Each patient is an individual problem. Unstable legs may be supported by callipers, etc., and stiffening of joints or possible tendon transfers may control deformity and improve function. Leg length problems will have to be dealt with as outlined above.

6.4 Trauma

6.4.1 Injuries of the Spine (Fig. 6.21a)

The spine of a child is normally much more flexible than that of an adult, and consequently fractures of the spine are uncommon but may be missed when they do occur. Usually, injuries are in association with other, more extensive, injuries in the body. Although intrathecal fracture is rare, haemorrhage is less uncommon and may cause pressure on the cord with resulting paralysis that may be temporary or permanent. As with an adult at the scene of an injury, a child should not be lifted from the scene of an accident until some form of immobilisation of the neck is achieved, in order to avoid a cervical cord injury as a result of flexion of the child's spine. The diagnosis and treatment of injuries to the cord are along the same lines as those adopted in the adult.

6.4.2 Cervical Spine (Fig. 6.21b)

Fractures and dislocations of the cervical spine are uncommon in childhood and may cause transection of the cord. This is rare. Subluxation of the cervical spine can occur, but complete dislocation is rare. Head traction relieves pain and spasm and allows the facets to reset. Delay in recognition of cervical cord damage with consequent paraplegia may occur. See Chap. 2.

6.4.3 Dorsal Spine

Compression fracture may occur in an injury as a result of a car accident or falling from a height. Usually there is no per-

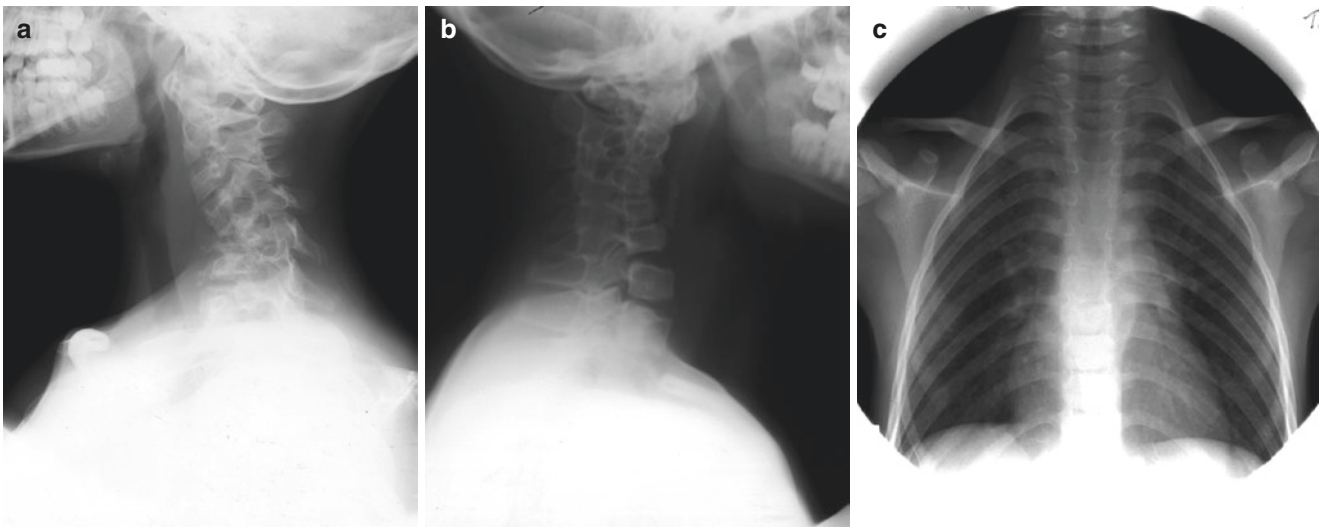

Fig. 6.20 (**a**) TB cervical spine. (**b**) TB cervical spine. (**c**) TB spine

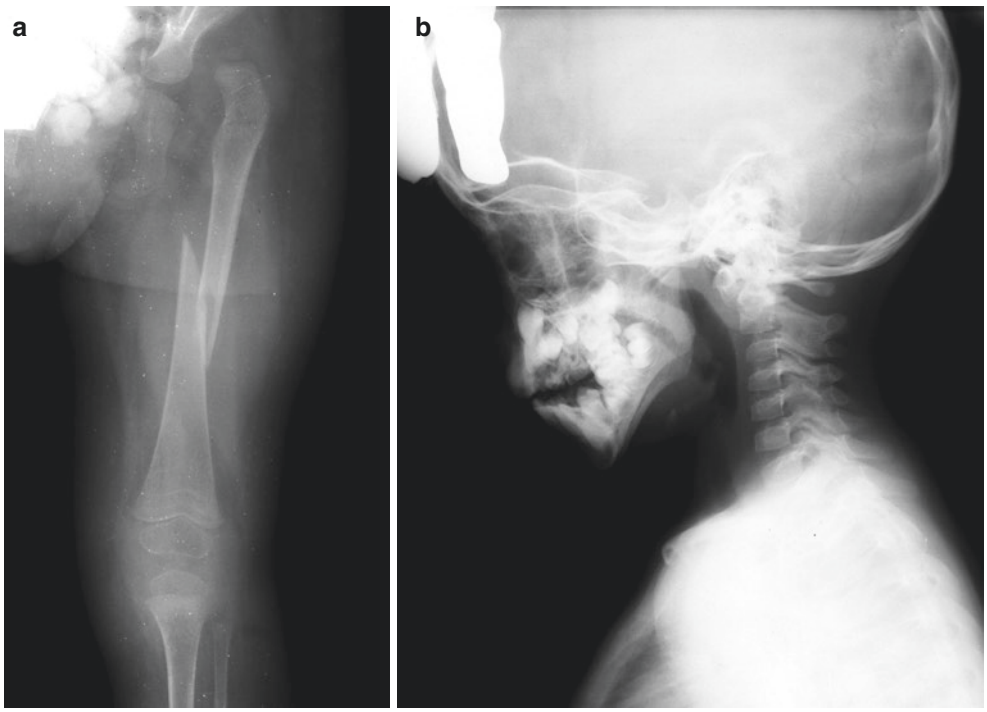

Fig. 6.21 (**a**) Plain X-ray of left hip and femur showing spiral fracture, as well as a dislocated hip. The bones are generally osteoporotic. (**b**) Atanto-axial dislocation

manent disability, and after a period of bed rest recovery is complete. See Chap. 3.

6.4.4 Lumbar Spine (Fig. 6.22a–c)

Fractures below the first lumbar spine are rare in children. Fractures of transverse processes or pedicles are rare, but may follow a torsion injury. Bed rest is all that is necessary and complete recovery is the rule.

6.5 Tumours

6.5.1 Tumours of the Spinal Cord

Tumours of the spinal cord are rare and can be benign or malignant. Here we have included an example of a lipoma of the cord causing compression symptoms (Fig. 6.23a), and an example of a neural sheath tumour in neurofibromatosis (Fig. 6.23b).

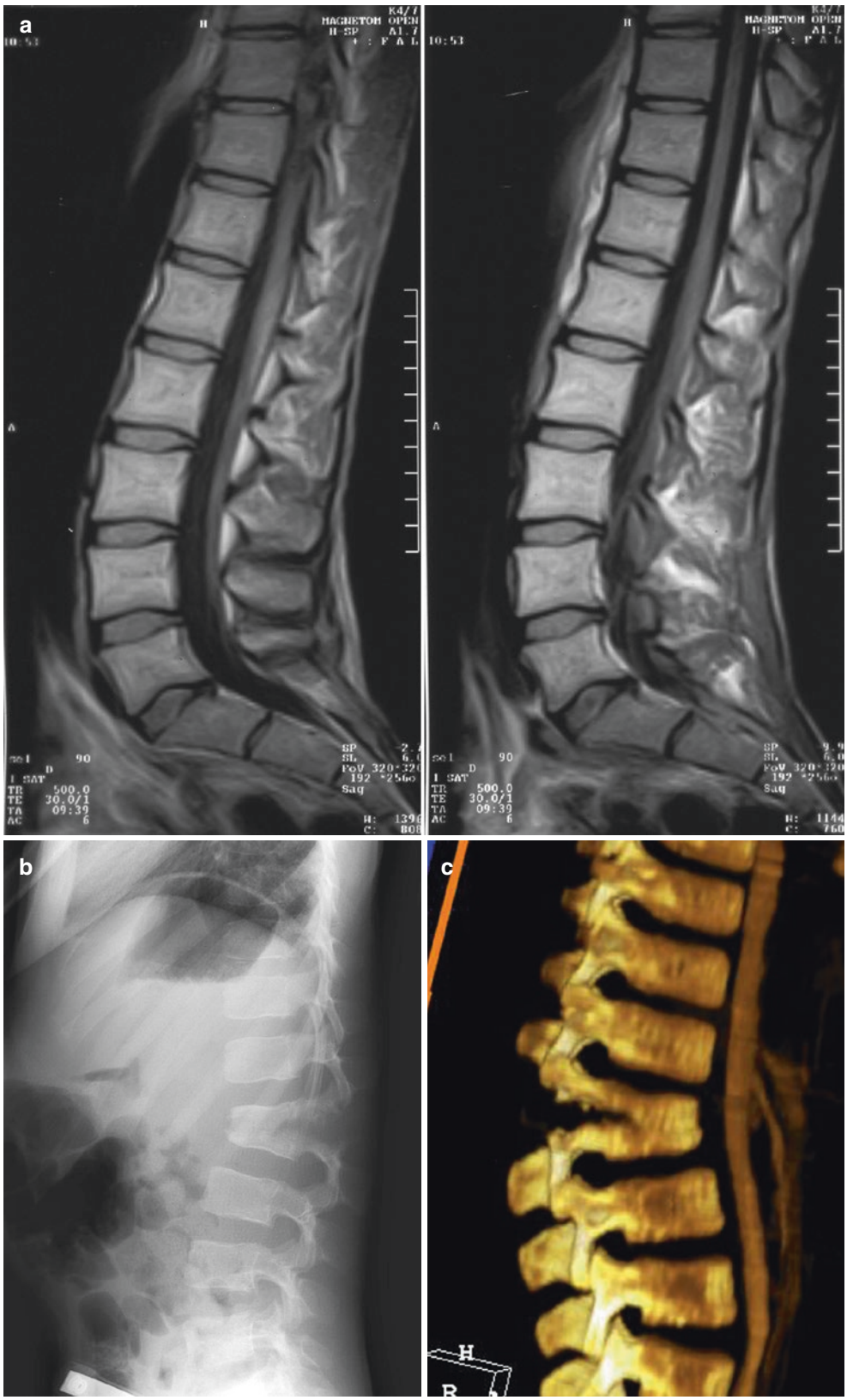

Fig. 6.22 (**a**) MRI scan showing vertebral injury. (**b**) Plain X-ray showing Chance fracture of lumbar vertebral body. (**c**) CT scan showing Chance fracture

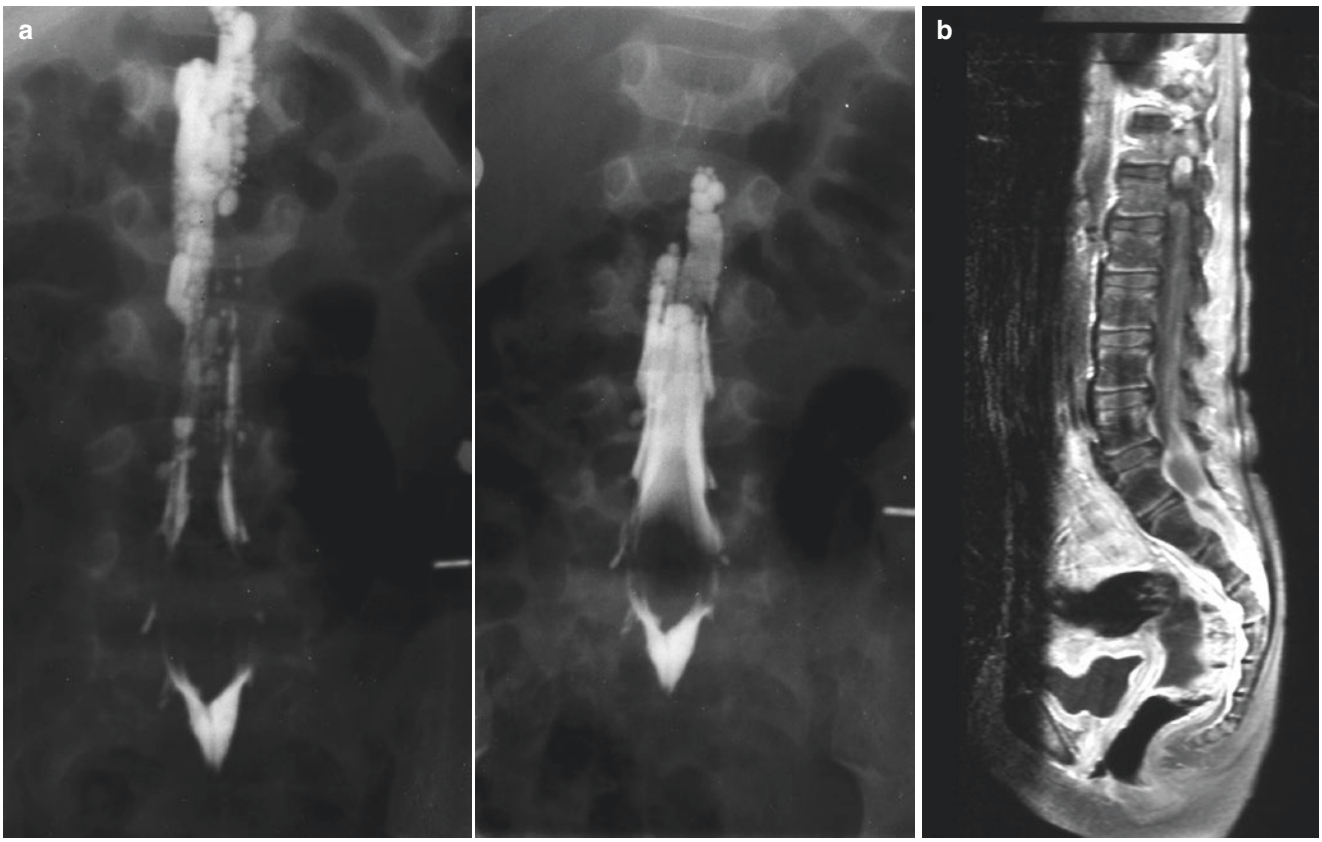

Fig. 6.23 (**a**) Myeloram spinal lipma. (**b**) MRI scan, lateral view of an intraspinal tumour

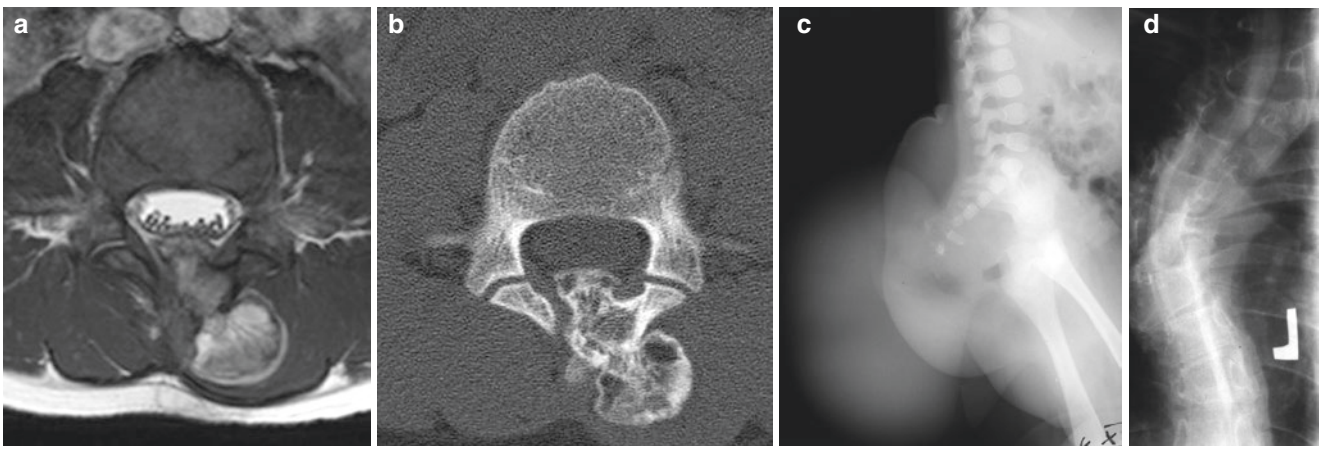

Fig. 6.24 (**a**) Scan showing osteochondroma of the vertebra. (**b**) Scan of vertebra showing an osteochondroma of the lamina of that vertebra with intraspinal extension. (**c**) Plain X-ray, lateral view of a sacrococygeal teratoma with distortion of the sacrum and coccyx. Note the soft tissue mass of the teratoma. D, Neurofibromatosis spine with scoliosis. A myelogram shows the deformity of the spinal canal

6.5.2 Tumours of the Vertebral Bones

Bone tumours can cause problems by encroaching on the spinal cord and can be primary as osteochondroma or osteosarcoma (Fig. 6.24a), or secondary from metastatic disease like neuroblastoma (Fig. 6.24b–d).

6.6 Acquired

6.6.1 Neurogenic Bladder (Fig. 6.25a–c)

See Chap. 5.

6.6.2 Scoliosis (Fig. 6.26a–c)

See Sect. 6.2.11.

6.6.3 Hydrocephalus

See Chap. 2.

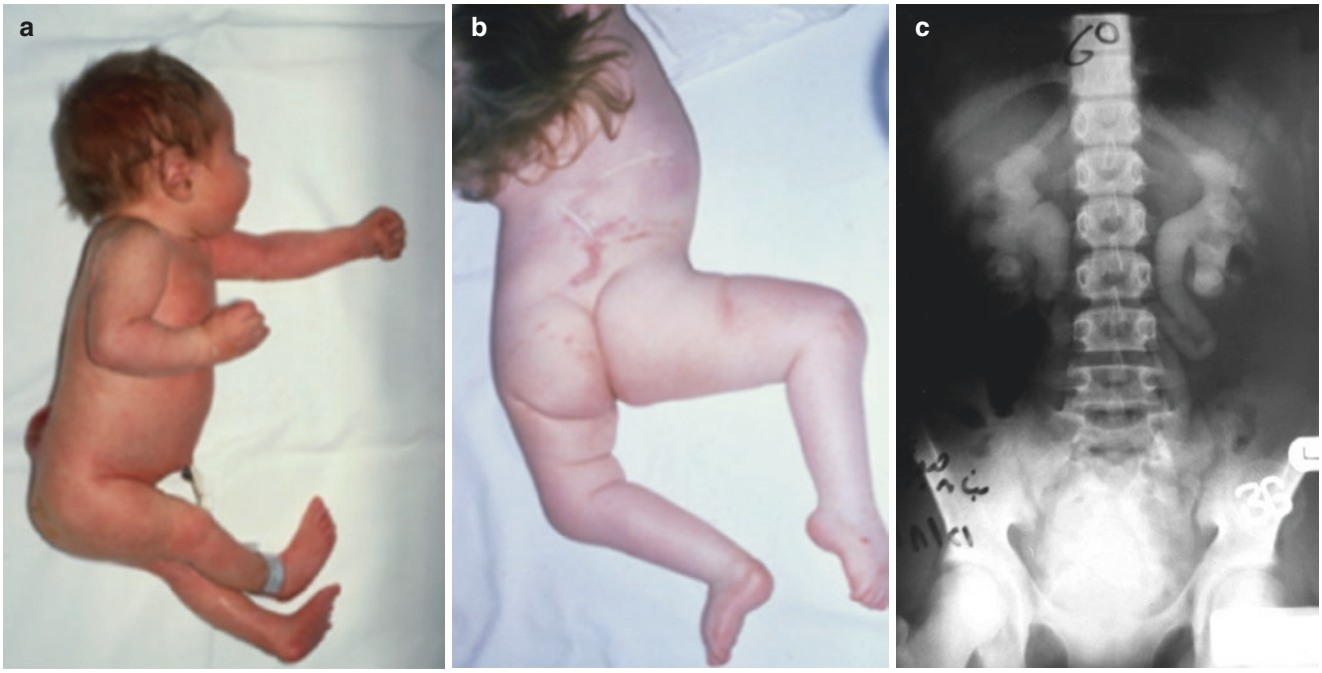

Fig. 6.25 (**a**) Spina Bifida with Myelomeningocoele that has ruptured during delivery. This baby has many of the acquired complications of this condition, namely, hydrocephalus, straight spine with loss of lumbar lordosis, Talipes Equinovarus, dislocated hips, neurogenic bladder, and a patulous anus with total paralysis from the level of the lesion down. (**b**) Clinical photograph showing deformity of the spine with increasing scoliosis as the child grows. (**c**) Intravenous urogram in a patient with spina bifida showing a neurogenic bladder, with bladder neck obstruction with vesicoureteric reflux and bilateral hydronephrosis

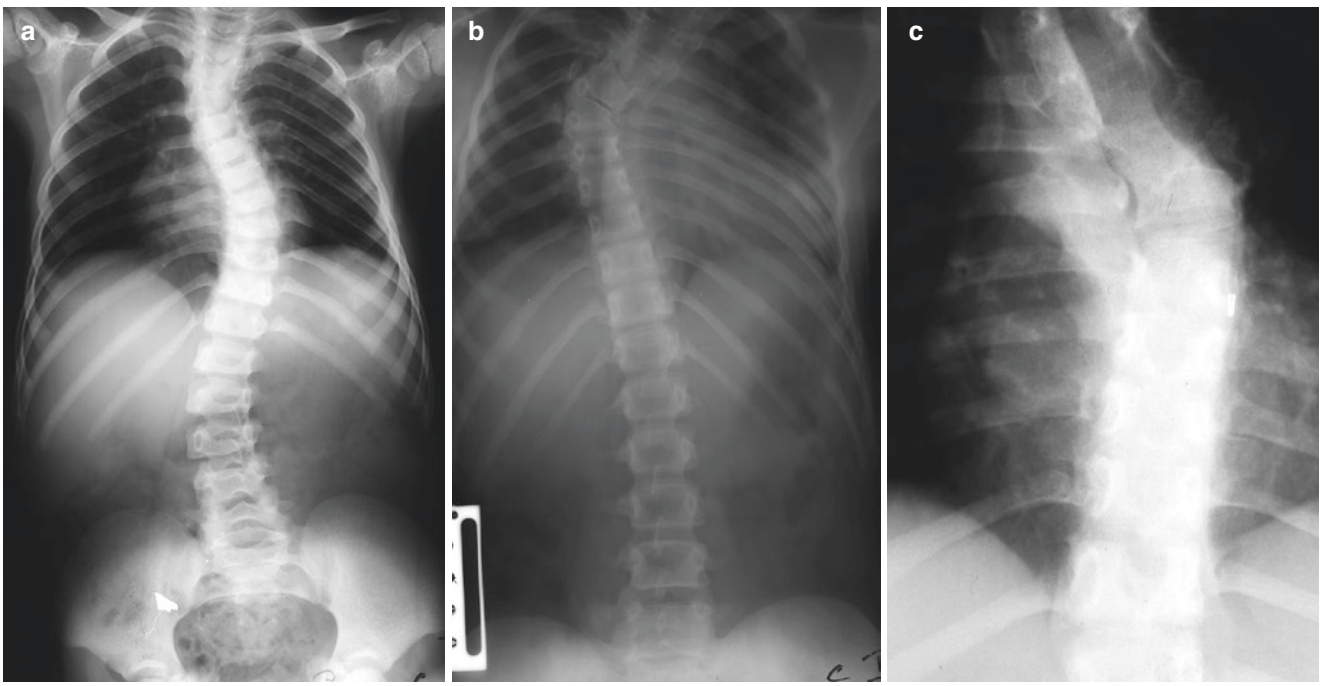

Fig. 6.26 (**a**) Acquired scoliosis of the spine. (**b**) Patient with a thoracic neuroblastoma excised and developed severe scoliosis after radiation therapy to the spine. (**c**) Thoracic neuroblastoma with intraspinal extension and paraplegia

Further Reading

Houtrow A. Spina bifida. In: McInery TK, Adam HM, Campbell DE, DeWitt TG, Foy JM, Kamat DM, editors. American academy of pediatrics textbook of pediatric care. 2nd ed. Itasca, IL: American Academy of Pediatrics; 2019.

O'Kane R, Begg T. The brain and central nervous system. In: Carachi R, Doss SHE, editors. Clinical embryology: an atlas of congenital malformation. Basel: Springer; 2019.

O'Kane R, Kommer M. Neurosurgical diseases of the nervous system. In: Goel KM, Carachi R, editors. Hutchison's atlas of paediatric physical diagnosis. 2nd ed. New Delhi: Jaypee Brothers Medical Publishers; 2014. p. 370–85.

Özek MM, Cinalli G, Maixner W, editors. Spina bifida: management and outcome. Milan: Springer-Verlag; 2008.

Musculoskeletal

7

Susie Goodwin and Robert Carachi

7.1 Introduction

This chapter discusses congenital malformations of the limbs and hands and provides extensive clinical/radiological information on management not discussed in other chapters. It is organised into Congenital, Infection and Inflammation, Trauma, Tumours and Acquired Conditions. Some of the conditions may be cross-referenced with other chapters where they are discussed in more detail

7.2 Congenital

7.2.1 Phocomelia

Congenital anomalies in the arm vary from almost complete absence (ectromelia), as it occurred in 1961/1962 following the use of thalidomide in pregnancy, to relative minor failure of differentiation of parts of the limbs in syndactyly. Gross failure of limb bud growth may leave the child with a small flipper-like limb (phocomelia) or a more substantial part to which an arm prosthesis may be attached (Fig. 7.1).

Increased sophistication of upper limb prostheses continues with steady improvement in the prognosis for those with arm reduction deformities. More subtle embryonic failure may leave the child with abnormalities such as congenital dislocation of the radial head with partial loss of elbow and forearm movement or with synostosis of radius and ulna with loss of forearm rotation. With these anomalies the forearm tends to be shorter. There is no effective treatment for these conditions although forearm osteotomy may be considered to put the hand in a more favourable position. In the distal part of the limb bud, developmental disorders may give rise to congenital absence of the radius in variable degree. The forearm is shorter, the thumb may be absent or hypoplastic, and the hand deviates to the radial side due to lack of support by the radius. This can occur as part of the VACTERL

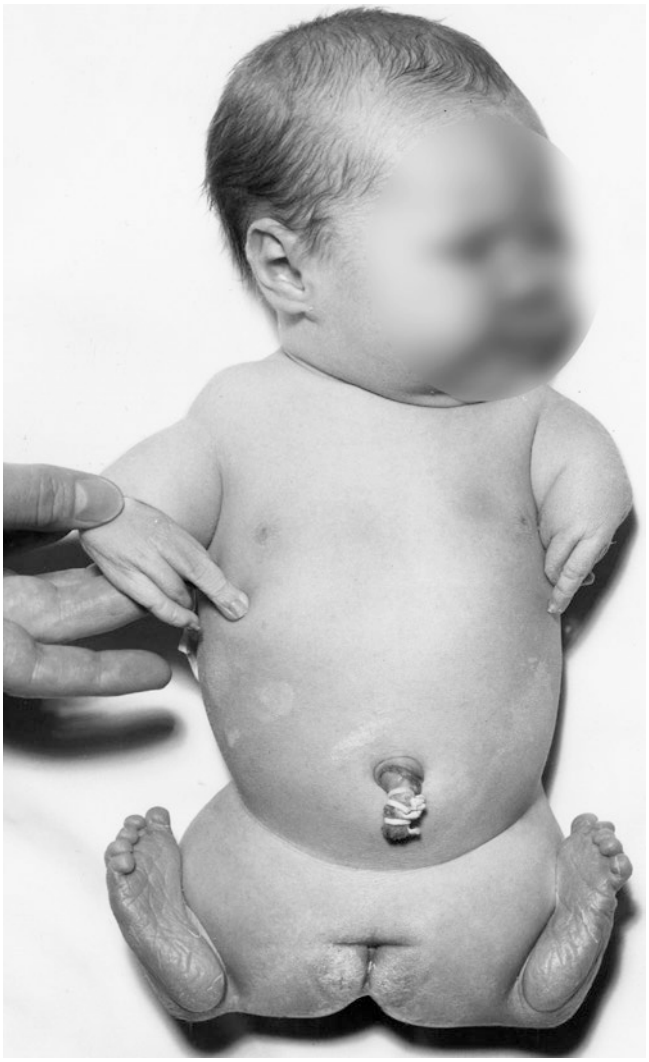

Fig. 7.1 Phocomelia

S. Goodwin (✉)
Royal Hospital for Children, Glasgow, UK
e-mail: susie.goodwin@ggc.scot.nhs.uk

R. Carachi
Surgical Paediatrics, University of Glasgow, Glasgow, UK

R. Carachi (ed.), *Atlas of Paediatric Surgical Imaging*, https://doi.org/10.1007/978-3-030-32384-4_7

(**v**ertebral defects, **a**nal atresia, **c**ardiac defects, **t**racheo-esophageal fistula, **r**enal anomalies, **l**imb abnormalities) association in oesophageal atresia. Some correction of hand position is possible to improve appearance and to a lesser extent function by surgical release of soft tissue deformity and repositioning of the carpus over the end of the ulna.

The term 'phocomelia' refers to upper limb bud malformation and is derived from the Greek *Phoke* (seal), and *melos* (limb). Syndromic associations include Cornelia de Lange syndrome, Holt-Oram syndrome and VACTERL association. Phocomelia is detected on antenatal ultrasound scanning, typically involving the upper limbs. Imaging demonstrates varying extremes of deficiency/foreshortening of the humerus, radius and/or ulna. Hands are present and may be normal or abnormal. While phocomelia tends to be diagnosed antenatally, postnatally it is best demonstrated radiographically [1].

7.2.2 Radial Deficiency

The radius is second only to the fibula in terms of congenital bone deficiencies. Absence of the radius (radial aplasia) lies on the extreme end of the spectrum of radial ray anomalies. On the less severe end, there may be radial hypoplasia, and there may be associated deficiency of the bones of the thumb (Fig. 7.2). It is bilateral in 50%. Radial dysplasia may be an isolated abnormality, or have syndromic association (for example Holt-Oram syndrome, Cornelia de Lange syndrome, VACTERL). Additional radiological investigations may therefore be indicated, such as renal tract ultrasound to look for associated abnormalities. On plain radiograph, there is often absence or deformity of the radius in addition to the trapezium, scaphoid and first ray. The ulna is often shortened and bowed, and may be fused proximally to the radial remnant where present.

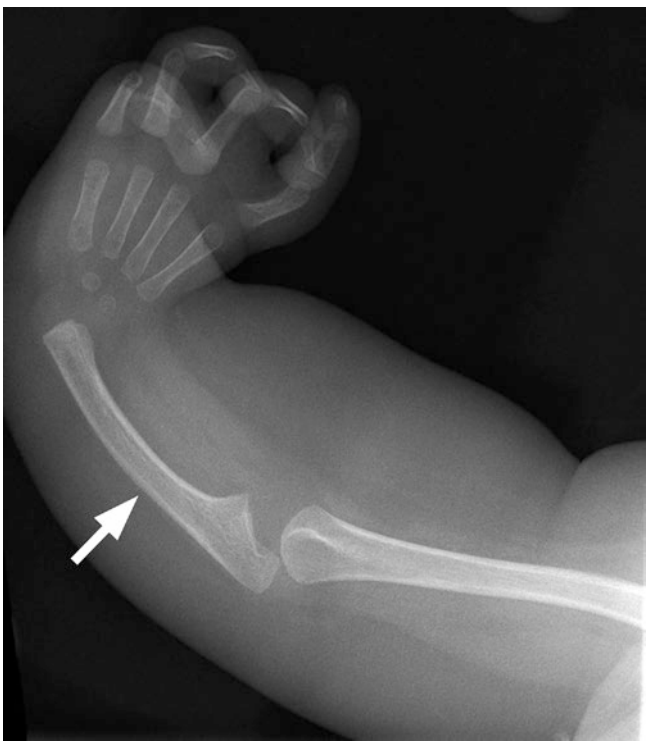

Fig. 7.2 Congenital absence of the radius, with radially deviated wrist, absent thumb, and shortened forearm (arrow)

7.2.3 Radio-Ulnar synostosis

Radio-ulnar synostosis is usually seen at the proximal third.

It is commonly congenital, but may also occur following trauma [2, 3].

7.2.4 Syndactyly ('Lobster Claw')

The term 'syndactyly' refers to congenital failure of separation of two or more digits, taking its name from the English *syn*, meaning 'united,' and Greek *daktulos* (finger) (Fig. 7.3). It is classified according to tissues involved, i.e. soft tissue (simple) syndactyly, or bony (complex) syndactyly. Complete syndactyly involves the entire length of the digit, and partial syndactyly involves only part of the length (Fig. 7.4). The condition may be isolated, however syndromic associations include Apert's and Poland syndromes (Fig. 7.5). The extent of soft tissue fusion will be evident clinically, and plain films are performed to assess bony involvement [2].

'Lobster claw,' otherwise known as 'cleft hand' deformity, is medically termed 'ecrodactyly,' derived from the Greek *ektroma* (abortion) and dactylos (finger), i.e. failure of formation of the central ray of the hand (Fig. 7.6). This is a longitudinal deficiency, and is divided into two types, typical and atypical, which have distinct clinical and anatomical features. Radiologically, the typical cleft hand is bilateral, commonly with syndactyly, with hypertrophy of the bone adjacent to the cleft. Atypical cleft hands on the other hand tend to be unilateral, rarely with syndactyly, and hypoplasia rather than hyperplasia, reflecting failure of formation [3].

7.2.5 Congenital Dislocation of the Hip (CDH)

This condition occurs more commonly in girls (five in every six will be female) and occurs in 1–2 babies in every thousand births. In 10% there will be a family history of a close relative with this condition. The causation is thought to depend on a number of factors such as high birth weight, full maturity, the presence of joint laxity and breech delivery—17% of babies with congenital hip dislocation are breech presentations compared with 4% of all deliveries

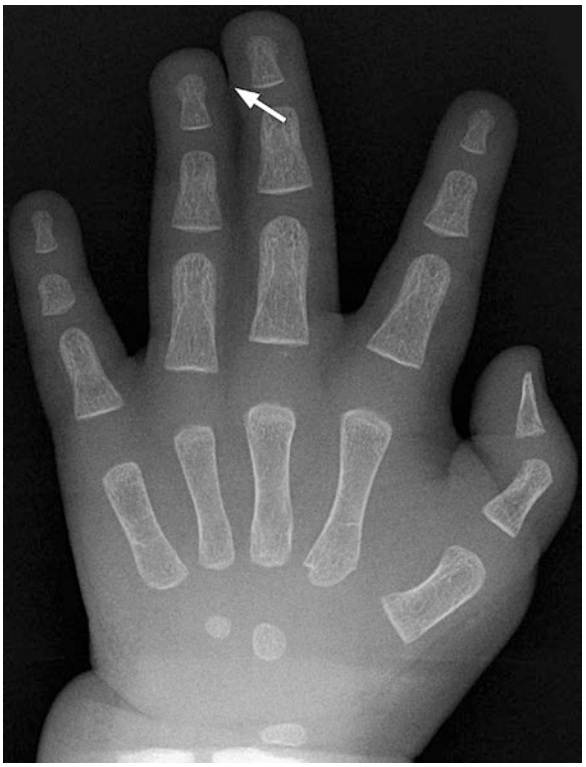

Fig. 7.3 Simple soft tissue syndactyly, with union of the distal digits (arrow)

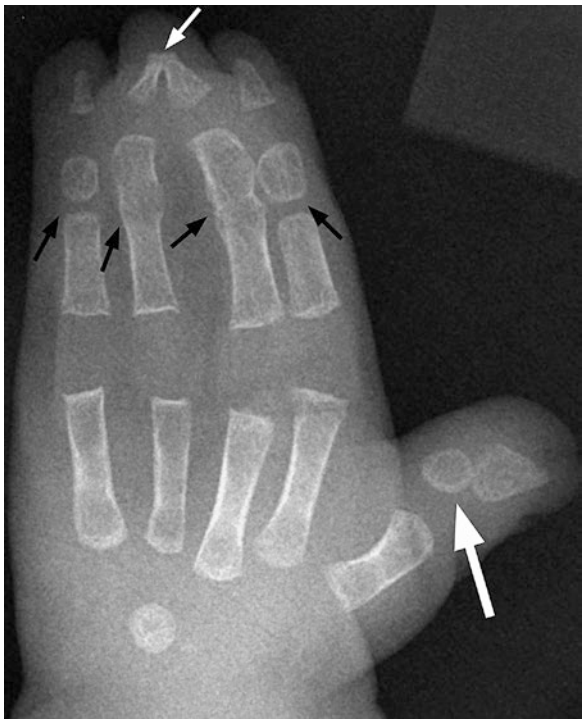

Fig. 7.5 Apert's hand with complex syndactyly (short white arrow), deficient interphalangeal joints ('symphalangism'; black arrows), and delta phalanx of thumb (long white arrow)

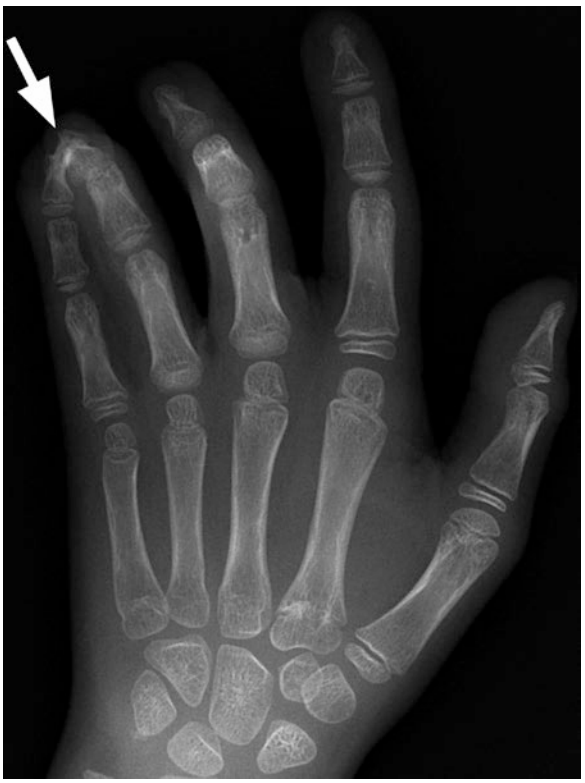

Fig. 7.4 Complex syndactyly with bony union of the distal phalanges (arrow)

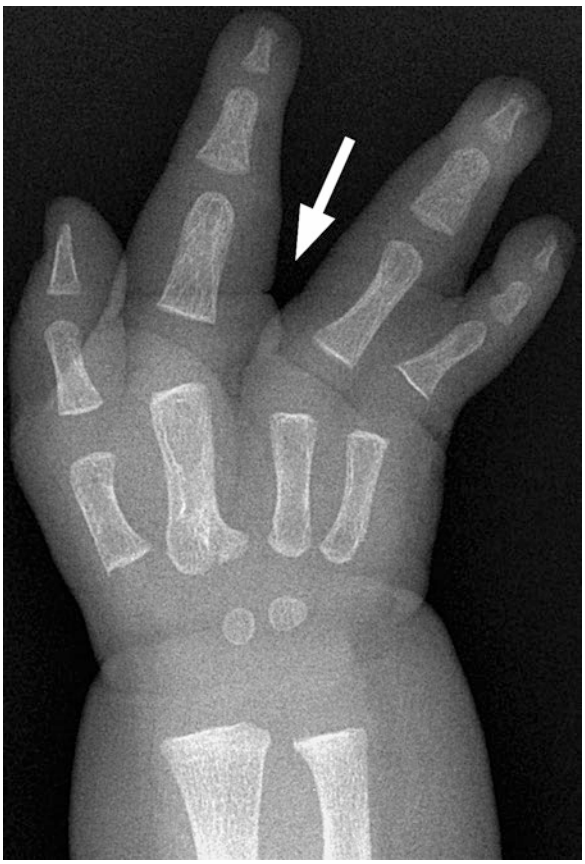

Fig. 7.6 'Lobster claw' (ecrodactyly, cleft hand; arrow)

being breech. It is thought that extreme flexion of the hip in the conduct of breech delivery levers the head of the femur out of the acetabulum. The joint capsule is stretched and the head of the femur comes to lie above the acetabulum with the hip extended and behind the acetabulum when flexed. The condition is commoner in North Italy and Brittany and rare in India and Africa. Excluding those with a neurological basis, e.g. myelomeningocele, in less than 5% the dislocation is prenatal and associated with other pathology such as arthrogryposis. In the vast majority the condition occurs during or shortly after birth and is detectable by the appropriate clinical tests. If undetected at birth, congenital dislocation of the hip may pass unnoticed. It is painless and there is no striking abnormality, apart from limitation of abduction of the hip which may be noted during routine infant examination or the "clicking" hip when the child is specifically tested when the child stands about 1 year to 18 months later when they may be noted to have a short leg and a limp.

In the newborn infant the diagnosis is clinical and depends upon the signs found when doing the Ortolani test. The technique is to examine the baby by grasping the flexed thigh and gently abducting the hip. In the normal hip full abduction occurs smoothly but if the hip is dislocated abduction is limited until, with a jerk, the upper thigh moves forward as the head reduces into the acetabulum. On allowing adduction, the femoral head and proximal thigh can be felt and seen to slip backwards. The Ortolani test usually ceases to be useful after the first 2–3 months. Radiographs are unhelpful in finding congenital dislocation of the hip (CDH) and a trial of the efficacy of ultrasound in the routine screening for CDH is currently being undertaken in the newborn. When performing the Ortolani test, sensitive hands may detect a faint clicking sensation but provided no displacement of the upper femur occurs these hips should be regarded as normal. In the older child, before walking, upward migration of the femur has not occurred and the only clinical sign is limited abduction—few children are detected at this age. Later the child has a short leg and extra skin creases due to bunching of the soft tissues. On walking, there is a characteristic dip when weight-bearing on the affected side— Trendelenburg's sign. With the femoral head no longer in joint to provide an eminence, there is a hollow in the groin at the mid-inguinal point. As seen in the affected hip socket is shallow and saucer-like and the femoral head lies above and outside this socket. The ossific nucleus is often small than the other side although the cartilaginous head is generally normal in size. There may even be a notch of a false acetabulum on the ilium above the true acetabulum due to pressure from the femoral head.

Ultrasound is the primary imaging modality in the assessment of CDH, also known as developmental dysplasia of the hip (DDH) (Fig. 7.7). This is performed in infants up to 6 months of age. Beyond this age, ossification of the femoral head means ultrasound will tend to be replaced by plain radiograph. Before 2 weeks of age, ultrasound does not tend to be performed as the ligaments remain lax. Several approaches to hip sonography are recognised, notably the Graf method, which focuses on static morphology (Fig. 7.8), and the Harcke method, which is more dynamic and focuses on femoral head position and stability. Different centres use variations and combinations of these techniques. Commonly, the Graf approach is used and supplemented by adding in stress views. Graf's technique

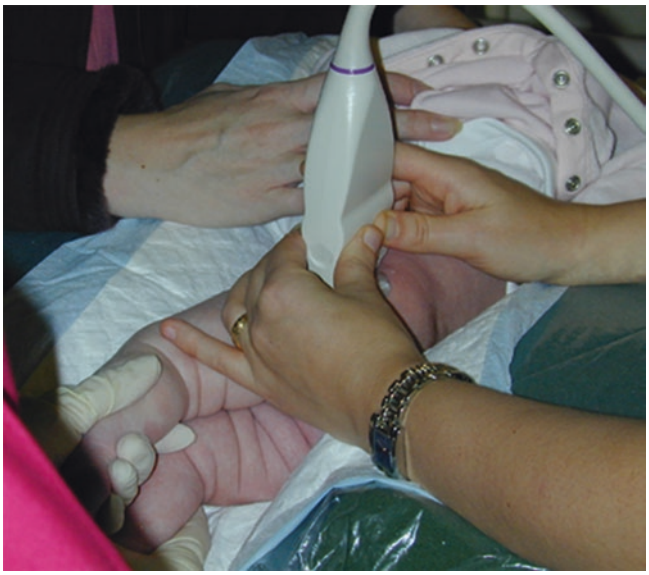

Fig. 7.7 Left hip ultrasound being performed in a baby using the Graf method

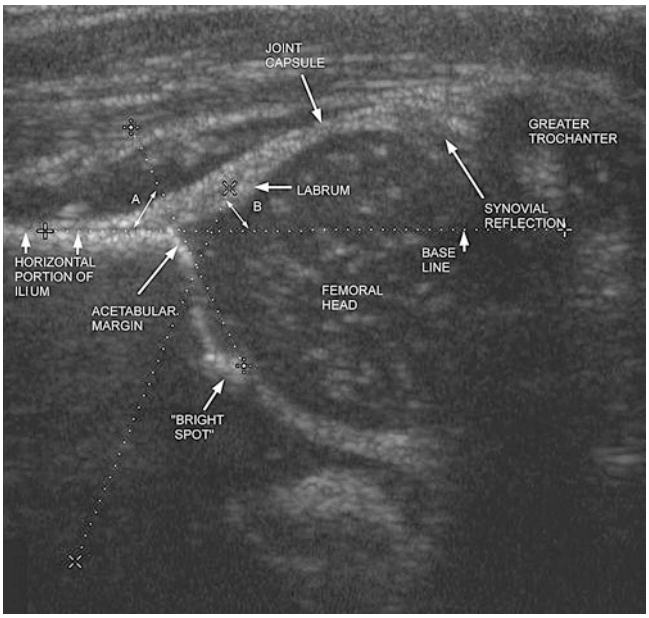

Fig. 7.8 Normal hip anatomy, landmarks and measurements evaluated in the Graf technique, including alpha and beta angles (A and B)

describes a standardised and reproducible method or assessing morphology. Three anatomical landmarks are identified using a linear transducer in the coronal plan:

1. Iliac line
2. Mid portion of the acetabular roof
3. Acetabular labrum

From these, two angles, alpha and beta, are measured. Alpha angle is the main value used, and is measured between the vertical iliac line and the acetabular roof. Normal value is 60° or above. Beta angle is measured between vertical iliac line and the acetabular labrum. Normal value is less than 77°, however the beta angle should always be considered along with alpha angle.

These measurements divide hips into types which have implications for management:

- Graf type I: Mature hip, good acetabular coverage, normal alpha angle 60+ (Fig. 7.9).
- Type IIa/b: Centred hip, but deficient acetabular roof, physiologically immature hip, alpha angle 50–59° (Fig. 7.10).
- Type IIc: Alpha angle 43–49° (Fig. 7.11).
- Type IId: Decentering hip, alpha angle 43–50.
- Type III: Decentred (dislocated) hip (Fig. 7.12). Poorly developed bony socket, deficient and upwardly displaced cartilaginous acetabular roof. Alpha angle less than 43°.
- Type IV: Decentred hip, downward displacement of the cartilaginous acetabular roof. Alpha angle less than 43° (Fig. 7.13).

Clinical follow-up is recommended for Type II hips regardless of subtype, and the majority will have matured and become Graf type I by 3 months of age. A minority of 1–2% will fail to mature and require treatment (Fig. 7.14).

Treatment is indicated in type III and IV hips.

Potential problems with hip ultrasound may be technical as it is operator-dependent. Scans in infants in harnesses or with deformities are also technically difficult.

Sonographic hip screening is performed in many countries, and is performed in our centre. A hip scan is performed in babies with abnormal findings on clinical examination, as

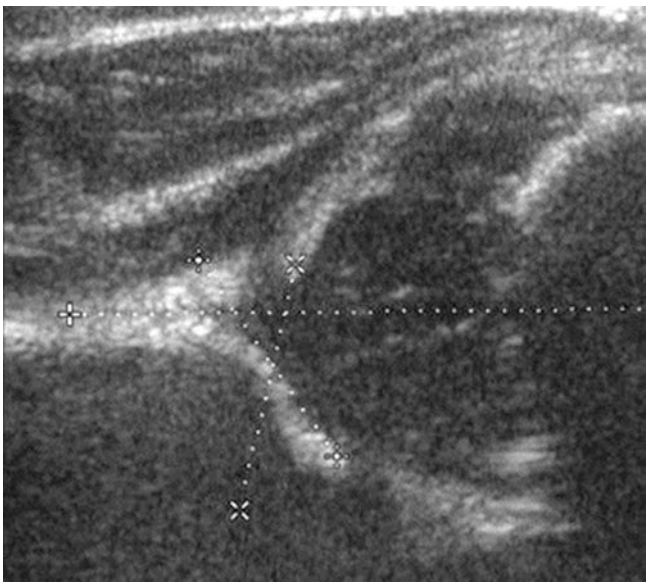

Fig. 7.10 Type II (A and B)

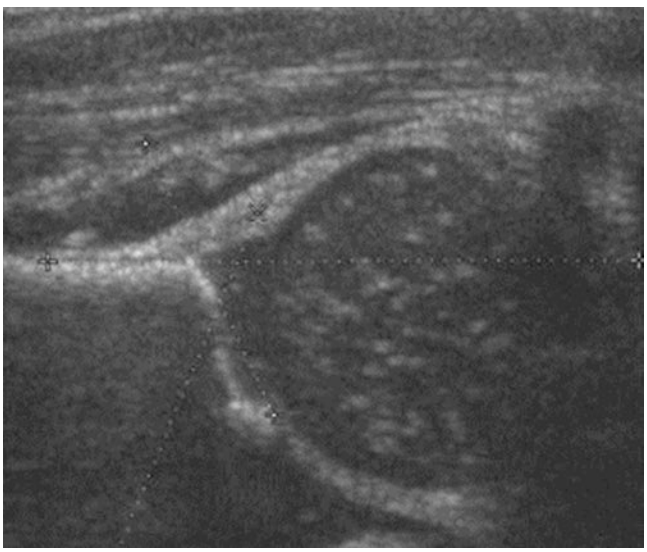

Fig. 7.9 Type I

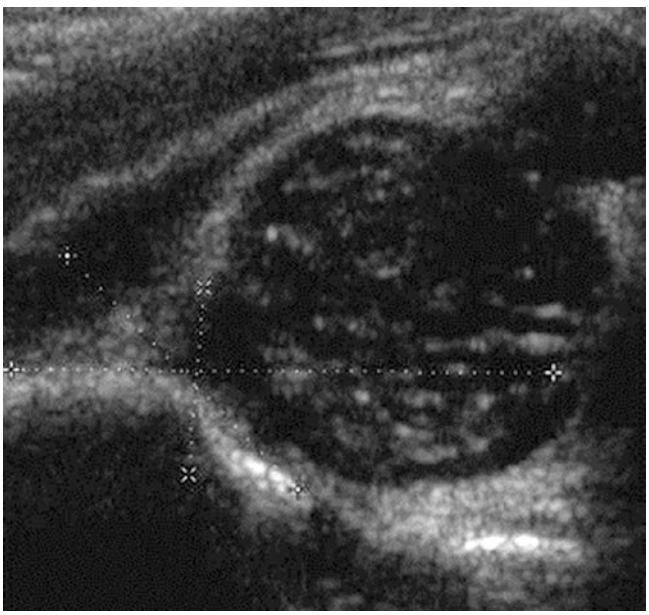

Fig. 7.11 Type IIC

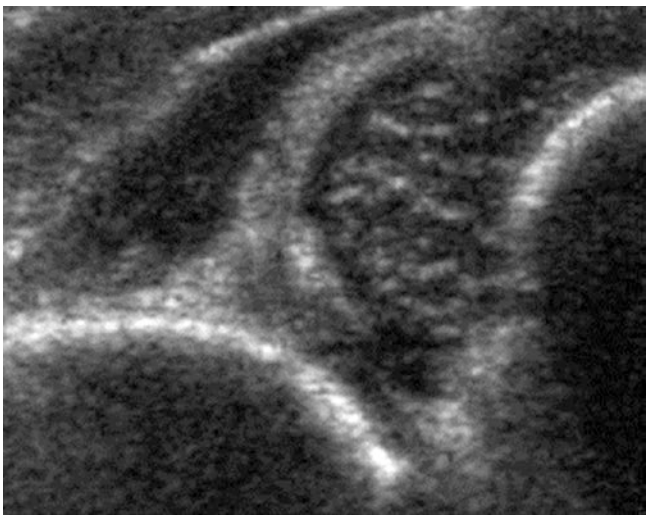

Fig. 7.12 Type III

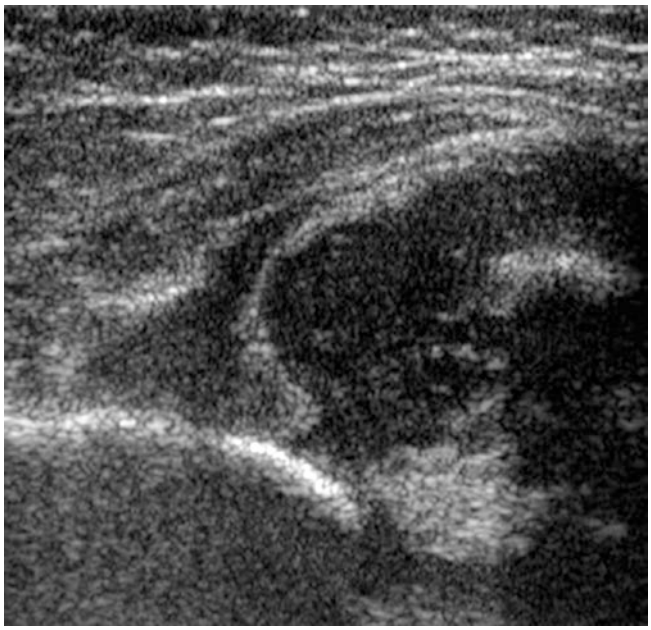

Fig. 7.13 Type IV

well as those with risk factors, including breech presentation and positive family history. The scan will usually be performed at around 4 weeks of age. Preterm infants should be scanned at a time allowing for correction of gestational age to avoid false positives. Ultrasound may be used in monitoring of infants in harnesses.

Plain film. AP pelvic radiographs may be used to assess the over 6 month age group for DDH. Frogleg views will often reduce a subluxed or dislocated hip, and therefore only tend to be performed along with the AP view. It is also important to remember that DDH may be picked up as an

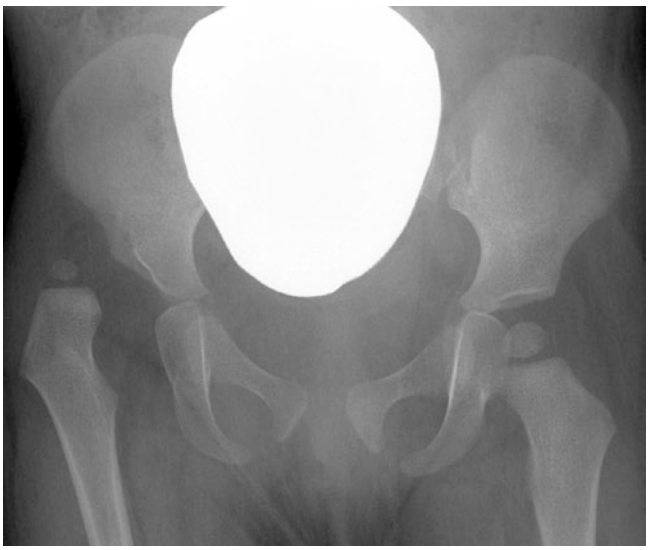

Fig. 7.14 Pelvic radiograph in right DDH. Shallow acetabulum, small right capital femoral epiphysis, superolateral displacement of the proximal femur

incidental finding on radiographs performed for other indications, for example spinal films. Radiographic features may include shallow acetabulum/increased acetabular angle (normal less than 30°), small capital femoral epiphysis, delayed femoral nucleus ossification, displacement of the proximal femur with respect to the acetabulum, usually in a superolateral direction. Femoral head coverage by the bony acetabulum may be measured in terms of percentage coverage or by the centre-edge angle. Serial measurements can be useful in follow-up of these children.

Cross-sectional imaging and arthrography. Cross-sectional imaging tends to be reserved for post-operative assessment following hip reduction. In our centre, targeted low-dose computed tomography (CT) is performed. This can be performed with cast in situ, and enables assessment of position of the femoral head within the acetabulum. Magnetic resonance imaging (MRI) is rarely used, however, DDH may be picked up incidentally on MR scans performed for other indications. Arthrography during manipulation under anaesthetic is often useful to orthopaedic surgeons, particularly as this is a dynamic form of imaging, and provides information regarding hip joint morphology and stability [2, 4].

7.2.6 Talipes Equino Varus

Talipes means "ankle and foot" i.e. the part of the body being described. Equinus means to be in a toe-down, plantar flexed position. Varus deformity involves medial deviation of the distal part of the limb while a valgus deformity is the opposite (Fig. 7.15).

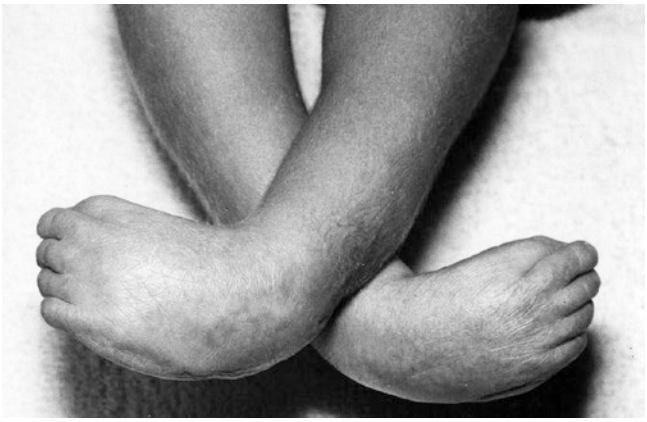

Fig. 7.15 Talipes equino varus

7.2.6.1 Talipes Equino-Varus: Club Foot

This common deformity occurs 2–4 times in every 1000 births, i.e. about twice as common as congenital dislocation of the hip. Boys are twice as often affected as girls, and in half of the affected children both feet are deformed. The diagnosis is obvious on inspection, the deformity being in three parts—the heel is drawn up, the foot inverted and the forefoot adducted—i.e. an equino-varus position. In a small minority the deformity is postural and can be corrected easily by manipulation to neutral and beyond. Repeated manipulation is sufficient treatment. The majority have rigidly deformed feet. In most this is the only problem but club foot deformities are also found in such conditions as arthrogryposis, Trisomy 18 and in spina bifida cystica. Initially the treatment is carried out as inpatient with daily manipulation of each element of the deformity—the correction obtained each day being maintained with the careful application of a Denis Browne splint to the foot (or feet) and as the deformity is overcome progressively the splint may be bent to hold a greater degree of correction and then connected to the other foot (normal or affected) by a connecting bar to hold the correction more effectively. Over a period of 7–14 days the foot will reach the over-corrected position and the baby can be sent home in the splints. It is necessary to continue to maintain an over-correction by remanipulation and reapplication of the splints as an outpatient every 2 weeks until the child starts to stand late in the first year. Alternative regimens to hold the correction obtained by manipulation involve the use of elastoplast strapping or plaster of Paris. To allow walking the splints are discarded and boots with an outer raise to the sole are supplied, with night boots and connective bar for night wear. The parents are instructed to manipulate the foot into the over-corrected position. Over the next few years these treatments can be abandoned gradually with a view to the child going to school at 5 years with normal footwear and a foot which is slightly small and stiffer than usual. If the foot is found to be inadequately corrected during the first year, or to be relapsing during the later years, a soft tissue release operation on the medical and posterior aspects of the foot and ankle is needed. About half of the affected feet will need this procedure and in a few with severe deformity, bony correction will be necessary.

7.2.6.2 Talipes Calcaneo-Valgus

As the name implies, this is exactly the opposite deformity from that of club-foot. This is usually the result of in-utero posture in that the foot has been caught in an upturned position with the sole against the uterine wall. Prognosis is excellent as natural improvement occurs with active movement on release from the uterus. All that is needed is for the parent to manipulate the foot into equino-varus frequently and the deformity resolves permanently within a few weeks.

7.2.6.3 Metatarsus Varus

In this less common deformity the forefoot is deviated inwardly in relation to the hind foot, as in club foot, but without equinus or inversion. This is best treated as early as possible with serial well-padded moulded plasters until the forefoot remains straight. In a small proportion surgical exploration is needed to release a tight medial tether.

This condition may be detected on antenatal ultrasound. Plain radiographs performed should include standing lateral and frontal views where possible. Where weight bearing is not possible, this may be simulated with a board.

Four radiographic features may be detectable [5]:

1. Hindfoot equinus: lateral talo-calcaneal angle <35°
2. Hindfoot varus: talocalcaneal angle <20°
3. Metatarsus adductus: talus/first metatarsal angle >15°
4. Talonavicular subluxation

7.2.7 Arthrogryposis

This name is used for a congenital condition affecting joints which may be localised or generalised. Differentiation of primitive mesoderm is impaired and the joints and soft tissues are deformed and almost completely rigid (Fig. 7.16). The muscles are atrophic and fibrous and the skin is tight so that the limbs resemble hose pipes. Arthroplasty has always failed to provide useful movement and the only treatment is to stabilise the affected joints in good position. On antenatal ultrasound, lack of foetal movement and evidence of contractures are features of this condition. Additional features in the case of syndromic arthrogryposis may also be detected antenatally. Radiographically, congenital limb anomalies tend to be symmetrical and most commonly affect the distal aspect of the limbs. The lower limbs are most commonly affected, and often the upper limbs also. Scoliosis will often

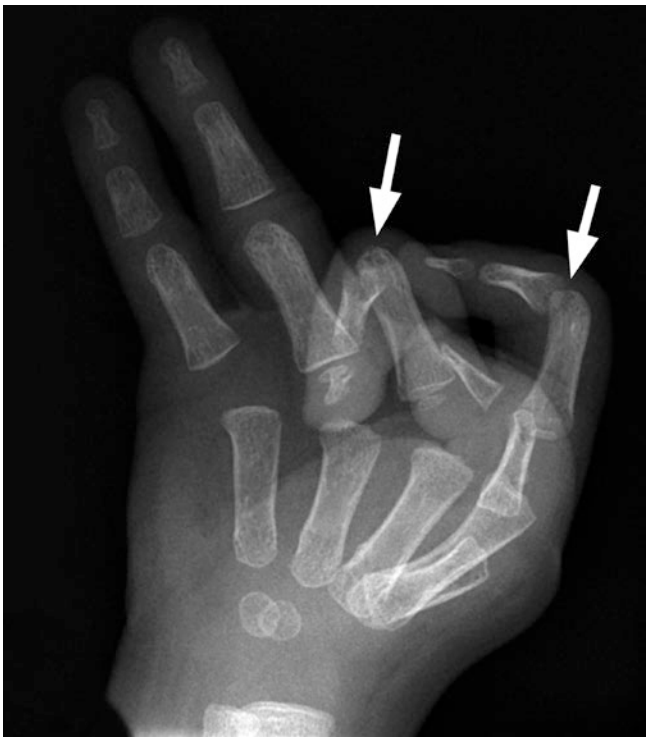

Fig. 7.16 Arthrogryposis. Multiple camptodactylies of the hand in a child with arthrygryposis (arrows)

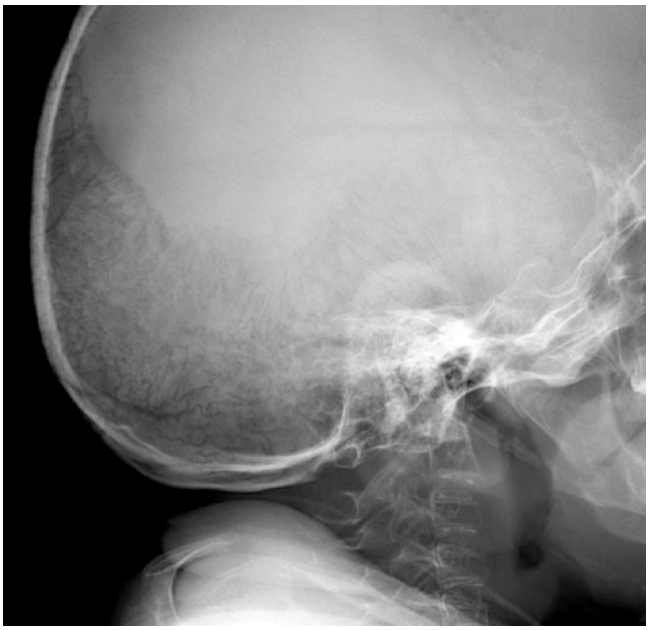

Fig. 7.17 Lateral view of the skull showing numerous wormian bones in osteogenesis imperfecta. The cervical vertebrae are osteopenic

develop as the child grows. Typically there will be reduced bone density, with reduced muscle bulk and there may be joint dislocation or subluxation. The bones will fracture more easily than normal, commonly in the perinatal period. MRI may help the surgeon evaluate joint integrity [2].

7.2.8 Osteogenesis Imperfecta

This condition is most often dominantly inherited and is characterised by excessive fragility of skeletal bone. Depending on the type, the sclera may be deep blue in colour and the infant may have prenatal fractures. This condition may progress to osteosclerosis if they live beyond a third decade. Three main types of osteogenesis are described:

1. The thick boned variety, where new-born babies have numerous fractures and stunted limbs, and may be mistaken clinically for other causes of dwarfism.
2. The slender fragile bone type, in which fractures occur postnatally.
3. Osteogenesis imperfecta cystica where the bones are honey-combed and the deformity progresses with advancing years. No treatment is available for this condition apart from protection from injuries and effective, prompt management of the fractures.

Pathologically, there is deficient synthesis of type I collagen, which results in reduced bone density, and therefore increased fracture risk. This also results in connective tissue abnormalities. Genetically, OI in most cases results from mutations in COL1A1 and COL1A2 genes. Inheritance may be autosomal dominant ± new mutations, or autosomal recessive. In terms on imaging, is helpful to consider whether the child has OI type II or one of the other types. Type II can be detected on antenatal ultrasound, and is one of the most lethal skeletal dysplasias. Radiological findings include poorly or unossified skull, small narrow thorax with beaded ribs, severely deossified spine with multiple vertebral body collapses, shortened wide bones of the extremities with reduced density and pathological fractures (Figs. 7.17, 7.18 and 7.19). Radiology is helpful in these children to suggest/support the diagnosis, and give severity indicators. Findings include variably ossified skull with abnormal wormian bones, reduced vertebral body heights, reduced bone density of the appendicular skeleton, and detection of pathological fractures. MRI may be helpful in assessment of basilar invagination [2].

7.2.9 Osteopetrosis/Chondroplasia

In this autosomal dominant (90% are new mutations) condition there is interference with endochondral ossification and is characterised by short limb dwarfism, a large head, and trident hands. Bones at the base of the skull which are cartilaginous

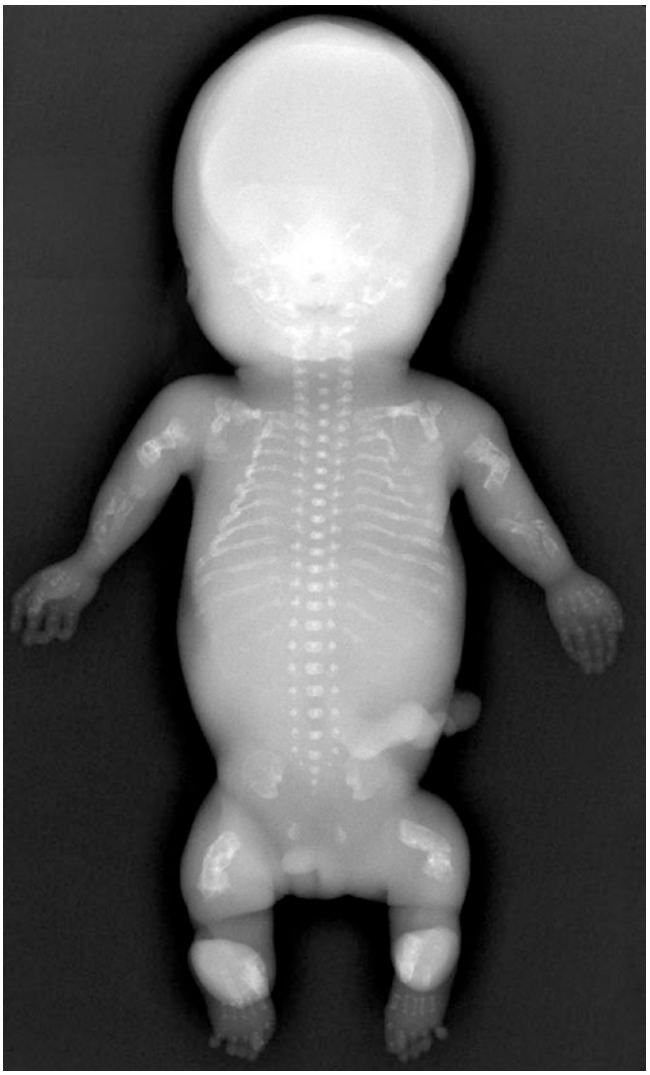

Fig. 7.18 Multiple rib and limb fractures in osteogenesis imperfecta

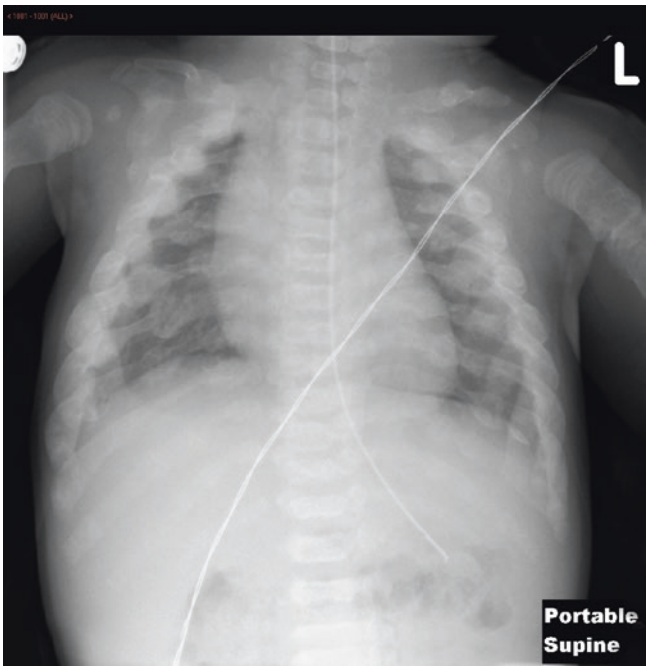

Fig. 7.19 Lethal osteogenesis imperfecta with numerous fractures

grow poorly, whereas skull vault which is formed from membranous bones grows normally. Hydrocephalus is a not uncommon complication of the poor basal skull growth which causes obstruction to CSF outflow. In osteopetrosis, chromosomal abnormalities result in defective osteoclast activity. The resulting bones are thickened and sclerotic, however structurally weakened and prone to fracture. Two types are described:

1. Infantile AR (precocious) type: poor prognosis. May result in stillbirth or infant death.
2. Benign adult (late onset) AD type: good prognosis. Normal life expectancy.

Radiographic features of infantile osteopetrosis are generalised sclerosis of the skeleton (Fig. 7.20) with metaphyseal splaying and evidence of pathological fracture. A 'hair on end' appearance of the calvarium may result from increased haematopoeisis. Skull base abnormalities are better demonstrated by cross sectional imaging which may identify cranial nerve compression from overgrowth of the foramina. The foramen magnum may also be narrowed, causing obstructive hydrocephalus [2, 6].

7.2.10 Achondroplasia

Achondroplasia is the most common form of non-lethal skeletal dysplasia, and features of this condition are detectable on antenatal ultrasound in the third trimester. While clinically proximal limb shortening is often most evident, on skeletal survey rhizomelia (proximal limb shortening), mesomelia (middle) and acromelia (distal) are demonstrated. Radiographic findings include large vault with small skull base, narrowed foramen magnum, small short thorax with anterior splaying of ribs, short pedicles with reduced interpedicular distance, posterior vertebral body scalloping, flattened acetabular roof, 'tombstone' iliac wings/trident pelvis/champagne glass pelvic inlet, metaphyseal flaring of the long bones with rhizomelic shortening of the femora and humeri, trident hand (Figs. 7.21 and 7.22). Apparent thickening of the long bones is an optical illusion caused by shortened length and the true thickness is in fact no different to normal. Cross-sectional imaging may demonstrate hydrocephalus secondary to narrowed foramen magnum. Achondroplasia is part of the 'achondroplasia group', which also includes thanatophoric dysplasia and hypochondroplasia [2].

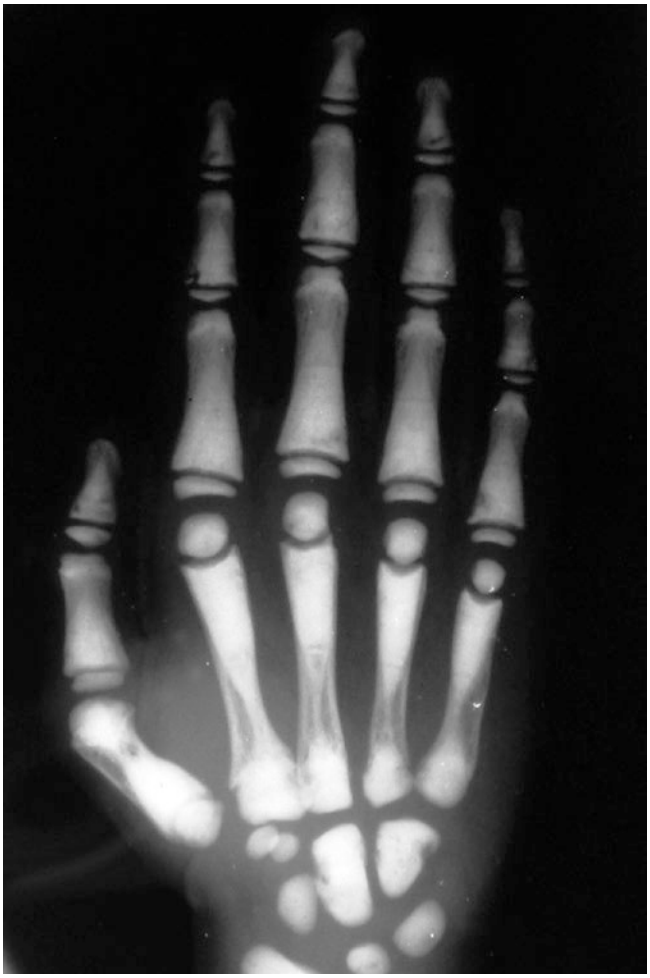

Fig. 7.20 Osteopetrosis with increased bone density, bone-within-bone appearance of the metacarpals, and fractures in the phalanges

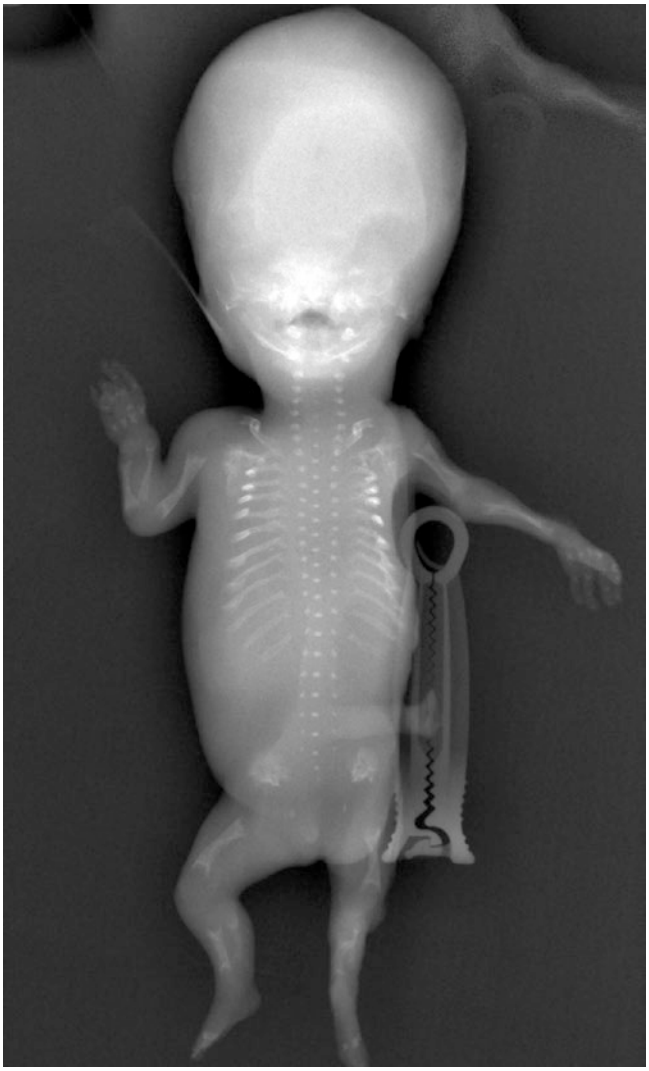

Fig. 7.21 Achondroplasia

7.2.11 Dyschondroplasia

In this condition there are rounded masses of unosified cartilage in the metaphysis and diaphysis of the long bones of the limbs, as well as in the metacarpals and phalangeas. The lesions are essentially endosteal rather than projections from the bone surface. Enchondromata in the hands may lead to gross deformity. Treatment is symptomatic.

Also known as enchondromatosis or Ollier's disease (named after the French surgeon of the late nineteenth century), this condition is most commonly seen in the hands and feet, affecting the short tubular bones (Fig. 7.23). Enchondromata may also occur in the metaphyses and diaphyses of the long bones.

Plain radiographs show lucent, expansile lesions of the medullary cavity with a narrow zone of transition, sclerotic margins, and may contain punctuate calcifications. Endosteal scalloping and cortical erosion may be present, but periosteal reaction is not a feature, unless there has been pathological fracture. Early onset enchondromatosis may result in disordered growth and shortened limbs.

CT shows the same features as plain film, but better shows the typical 'ring and arc' appearance. MRI shows a lesion of cartilage signal on all sequences, with variable contrast enhancement and typically absent marrow oedema (Fig. 7.24). Increased uptake is seen on isotope bone scan. When associated with vascular malformations, the condition is known as Maffucci's syndrome, named after the Italian pathologist, who described the condition prior to Ollier's syndrome. In these cases, there may be multiple calcified phleboliths seen on plain film secondary to the venous malformations. In both conditions, there is a 10–20% risk of malignant degeneration to chondrosarcoma, however this rarely occurs in childhood [2].

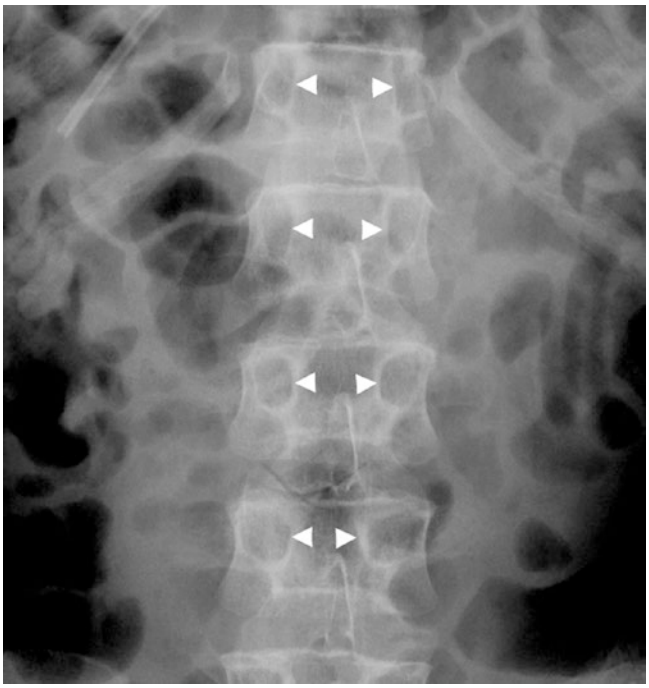

Fig. 7.22 AP view of the lumbar spine shows the interpedicular distance narrows on passing inferiorly. Note the tip of the ventriculoperitoneal shunt for obstructive hydrocephalus secondary to small skull base

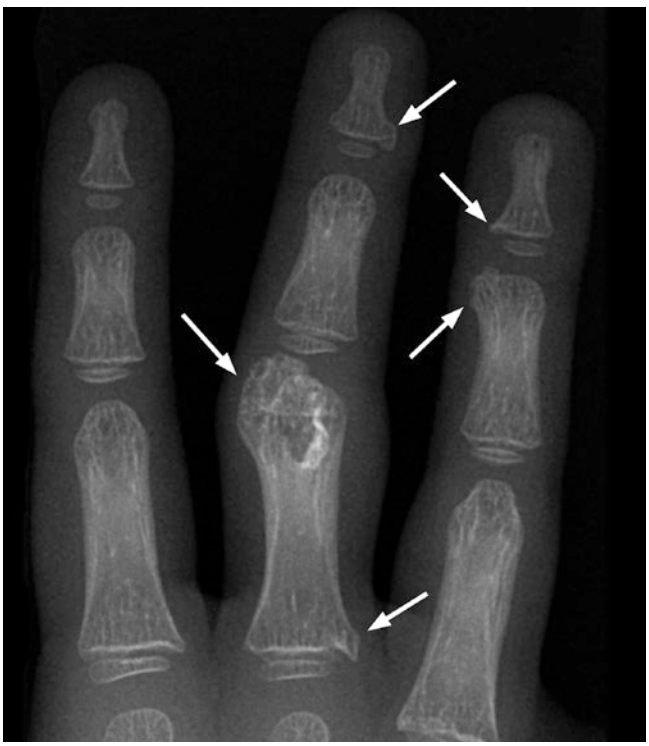

Fig. 7.23 Multiple exostoses (arrows) seen in Ollier's disease

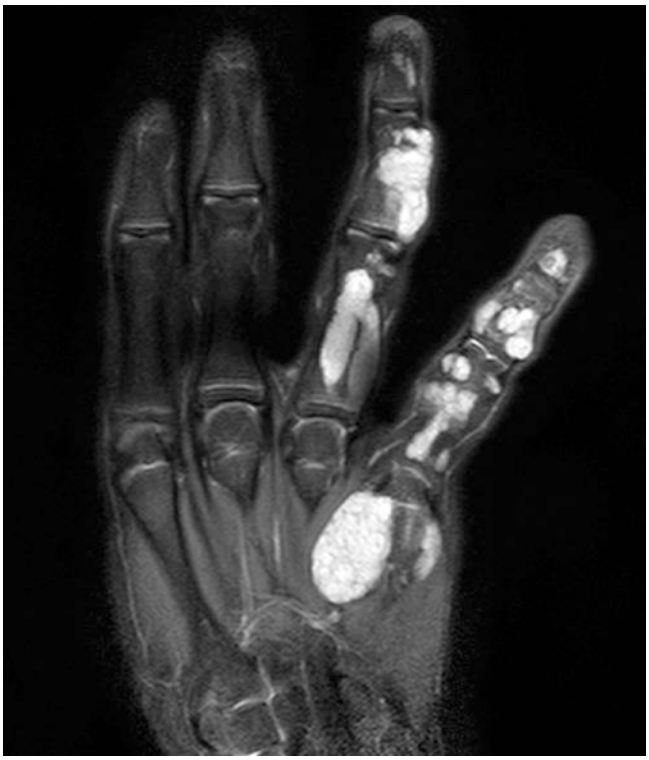

Fig. 7.24 Ollier's MRI T2W fat-saturated coronal image shows the distribution of the high-signal enchondromata

7.2.12 Hemihypertrophy

In hemihypertrophy, there is asymmetric overgrowth of one side of the body which involves bone, muscle and neurovascular structures. It may be an isolated (idiopathic) abnormality or associated with syndromes including Beckwith-Wiedemann syndrome and Sotos syndrome (Figs. 7.25 and 7.26). Asymmetric bone growth will be evident on plain film and there may be scoliosis. Idiopathic hemihypertrophy occurs without syndromic association. Associated abnormalities include organomegaly, medullary sponge kidney, hypospadias and genital enlargement. There is increased risk of malignancy in hemihypetrophy, both syndromic and isolated. Associated tumours include Wilms', hepatoblastoma and adrenal cortical adenoma. Children are therefore screened with abdominal ultrasound for these abnormalities.

7.2.13 Lymphoedema

In children, primary lymphoedema is commoner than secondary lymphoedema. There may be associated cardiac or gonadal abnormalities. In a child, unilateral leg swelling may lead to pelvic ultrasound to exclude pelvic mass, or

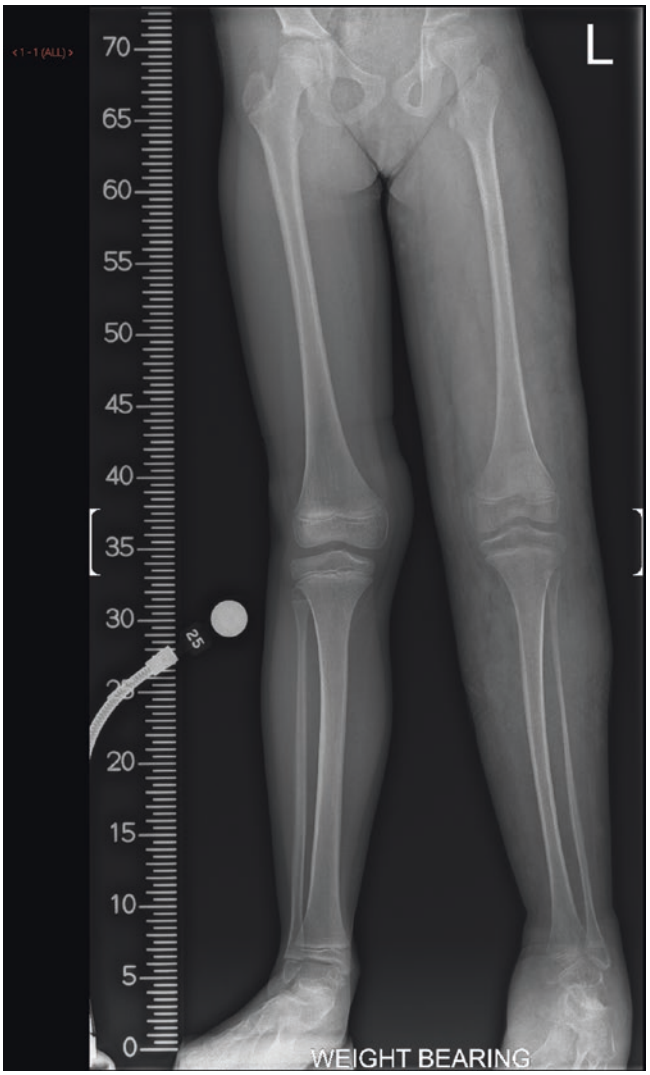

Fig. 7.25 Leg length film shows left hemihypertrophy in a child with Klippel-Trenaunay syndrome

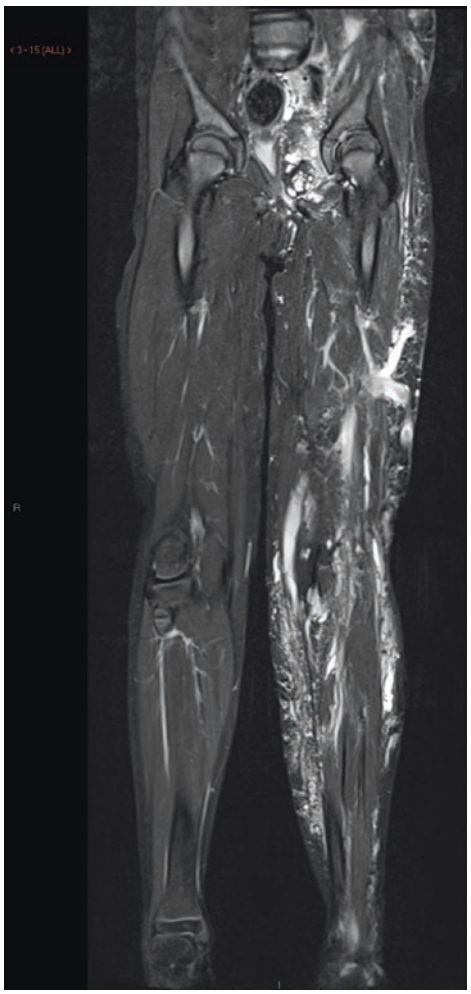

Fig. 7.26 MRI of the same child demonstrates widespread low-flow malformation of the left lower limb

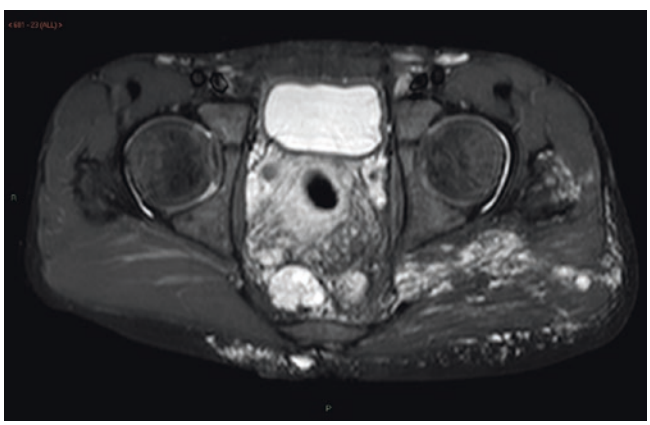

Fig. 7.27 MRI of a boy with extensive lymphatic malformation shows high T2W/fluid signal extending throughout the pelvis, gluteal muscles on the left, and buttock soft tissues

Doppler ultrasound being performed to look for deep venous thrombosis, however DVT is rare in children, and lymphoedema should also be considered. Often the diagnosis is made clinically, however in atypical cases, imaging such as MRI may be requested to evaluate extent and characteristics for example in lymphatic malformation (Fig. 7.27). Lymphangiography is now an outdated form of imaging, having been superseded by cross sectional imaging. In children with known associated conditions such as Turner's syndrome, further imaging will rarely be indicated [7].

7.2.14 Sprengel's Shoulder

Named after the German surgeon, Sprengel deformity of the shoulder describes the pectoral girdle abnormality in which there is congenital failure of the scapula to descend to normal position, resulting in abnormally high position, which is evident on plain radiograph. There may be associated omovertebral bone connecting the scapula to the cervical spine (Fig. 7.28). There are associations with Klippel-Feil syndrome and segmentation anomalies [2].

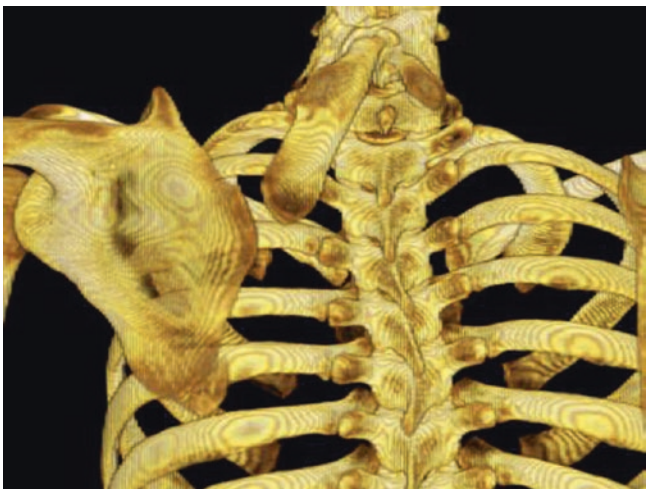

Fig. 7.28 Sprengel's shoulder. 3D CT reconstruction (posterior view) shows high-riding scapula on the left, and omovertebral bone extending from cervical spine

7.2.15 Proximal Femoral Focal Deficiency

PFFD encompasses a range of abnormalities from mildly shortened dysplastic femur to severely deficient femur with acetabular dysplasia. Many radiological classifications exist. Most commonly used is the Aitken classification which takes in the range of abnormalities from least severe type A to most severe type D. The femur is shortened in all the types. There are associated ipsilateral lower limb bone and soft tissue deformities.

- Type A: Femoral head present and attached to shaft with femoral neck. Cartilaginous connection between head and shaft which may later ossify or form subtrochanteric pseudarthrosis.
- Type B: Moderately dysplastic acetabulum containing femoral head; no osseous connection between femoral head and shaft at maturity.
- Type C: Severely dysplastic acetabulum; absent/very small femoral head not attached to femoral shaft. Tapered proximal end of proximal femoral segment.
- Type D: Absent acetabulum and proximal femur.

As the cartilaginous components will not be evident on plain film, MRI or ultrasound can add this information.

7.3 Infection/Inflammation

7.3.1 Pyomyositis

Localised primary infection of muscle, which may progress to abscess formation.

Ultrasound may demonstrate more superficial localised abscess collections within the muscles, and can provide

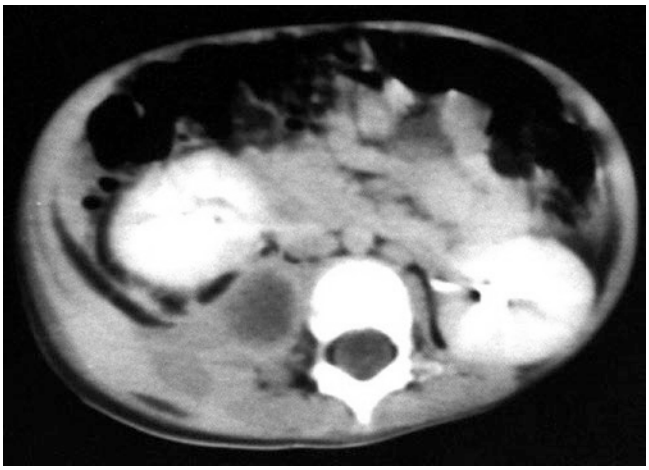

Fig. 7.29 Pyomyositis

image guidance for abscess drainage. MRI is the main imaging modality in children with pyomyositis. The following figure is a historic image in which a CT scan was performed (Fig. 7.29). MR will demonstrate enlargement and oedema of the affected muscle, and will accurately localised abscess collections which show rim enhancement on contrast enhanced sequences. There may be involvement of the adjacent soft tissues, with features of cellulitis, fascial oedema and there may be effusion of an adjacent joint. The underlying bone appears normal, allowing differentiation from osteomyelitis [2, 8].

7.3.2 Myositis Ossificans Progressiva

Swellings arise in association with connective tissue, fascia and tendons and progress to ossification. The muscles are only affected secondarily. There is characteristic shortening of the thumbs and great toes. The joints are stiffened and the neck becomes immobile. The child becomes bed-ridden and susceptible to recurrent chest infections. In localised traumatic ossification, where a muscle has been torn from its attachment a mass of bone may form within the muscle restricting its movement and limiting the range of movement of the joint and interference with the circulation. This is not a common complication of fractures in childhood but may follow injuries in the region of the elbow and the forearm (Fig. 7.30). The results of unrelieved arterial or venous obstruction are disastrous for the child. The mechanism of obstruction and the resulting changes in the tissues are varied. Inspection of the limb in all fractures is essential to make sure that the circulation of the limb is intact. If plaster of Paris is applied too tightly it may cause vascular compromise. The branchial artery may be occluded by pressure of bony fragments as a direct result of an accident. This may produce pallor of the limb and absence of the radial pulse. The vessel may be in spasm due to bruising or partial occlu-

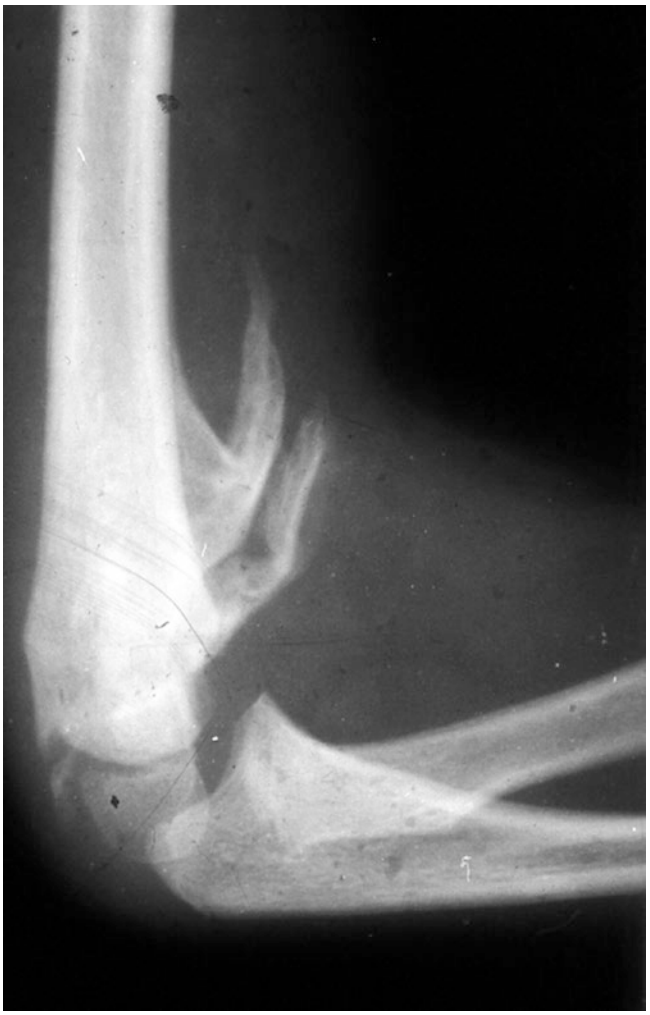

Fig. 7.30 Myositis ossificans (circumscripta). Lateral elbow radiograph shows new bone formation at the distal humerus secondary to previous trauma

sion by a bony fragment. Treatment of this clinical situation is immediate exploration of the fracture site. If not relieved the long-term results may be disastrous varying from losing the limb to severe ischaemia which affects not only the forearm muscles but also the median and ulnar nerves. The clinical picture of venous obstruction develops much more slowly than that of arterial obstruction. The pulse usually remains palpable but there are persisting signs of cyanosis of the hand and increasing pain. The presence of tissue oedema coupled with slow and continuous haemorrhage under a deep fascia may result in this clinical picture. Prophylactic elevation of the limb and removal of any tight plasters may be indicated to relieve the venous obstruction. Primary nerve injury as a complication of fractures in childhood is uncommon. The bruising of the radial and ulnar nerves may occur in supracondylar fractures of the humerus and of the perineal nerve in fractures of the upper end of the fibula. Separation of any epiphysis in a child is rarely accompanied by damage to the neighbouring growth area. A crush injury, however, may cause damage to this area resulting in very severe intractable deformity.

7.3.2.1 Mositis Ossificans Circumscripta (Fig. 7.30)

Imaging plays an important role in diagnosis, and is considered a 'Don't Touch' lesion, i.e. can be diagnosed from clinical and radiological findings alone and does not require biopsy. Plain radiographs are often diagnostic and demonstrate heterotopic new bone formation. Appearance on imaging evolves over time from the original trauma:

- 1–2 weeks: Early periosteal reaction, soft tissue mass
- 3–4 weeks: Peripheral calcification of mass, plane visible between mass and bone (often better seen on CT)
- Up to 6 months: New bone, well-defined cortex, reduction in size

Similar appearances will be demonstrated on CT. MRI may be performed in the earlier stages before calcification has evolved on the plain film, if there is diagnostic doubt clinically. MR at this stage may appear aggressive, with extensive soft tissue oedema and enhancement peripherally, and central heterogeneous signal. These appearances are non-specific and often cannot differentiate from other pathologies such as infection and soft tissue sarcoma however lack of invasion of surrounding structures is an indicator of benign pathology. CT performed at the 3–4 week stage shows diagnostic features of myositis ossificans, including lucent centre with calcified rim, and plane separating from underlying cortex. This allows differentiation from sarcoma, which tends to calcify centrally and progress peripherally. MRI at this stage is often not helpful. Ultrasound is sensitive in the early stage and can be useful for demonstrating the typical 'zone phenomenon' including early ossification [2, 9].

7.3.3 Osteitis/Osteomyelitis

The term osteitis is preferred by some to osteomyelitis as the bone marrow plays only a small part in this infection. The most common infecting organism is the staphylococcus pyogenase. Streptococcal osteitis is more common in infancy. The route of infection is blood borne and may come from septic lesions such as boils, abrasions, infected teeth and tonsils. In the neonatal period infection probably enters through the respiratory or alimentary tract or umbilical cord and be a consequence of a septicaemic episode. In childhood, infection can lie latent for long periods and the initial lesion is often healed and forgotten for 2–3 weeks

before the onset of the disease. Acute osteitis is essentially a disease of childhood. Apart from the neonatal osteitis which is usually secondary to a septicaemia, the disease is relatively uncommon in the first 2 years of life. It is commoner in boys and trauma is a predisposing factor. The bones of the lower extremity are most liable to infection and the tibia and femur are by far the most common sites. The septicaemic phase may be of short duration or last several days. Circulating organisms settle in the vascular metaphases of a long bone and lead to acute suppurative inflammation. This may progress to abscess formation where periosteal vessels are obliterated and superficial portions of bone may undergo necrosis resulting in sequestrae at a later stage. Usually the diagnosis is made before this stage is reached and antibiotic treatment arrests the progression of the disease. This condition is still prevalent in under-developed countries where there is a delay in the diagnosis and unavailability of drugs to treat is adequately.

The disease begins with acute pain affecting the limb which may be preceded by a variable period of malaise. There may be a history of a recent injury or a primary focus of infection. The child is usually ill, flushed, restless and the affected limb is kept still. There is resentment to any examination of the limb. There is usually a pyrexia and a rapid pulse. In the early stages there is no swelling of the limb but by gentle palpation an area of maximum tenderness is found over the affected metaphasis. Swelling of the limb is associated with a sub-periosteal effusion but cellulitis does not appear until the periosteum ruptures. There is a very high polymorphonuclear leucocytosis and an ESR which is markedly raised. No radiographic changes are seen in the first week of the illness. Subsequently there is evidence of elevation of the periosteum and a translucent area of decalcification in the affected metaphasis. In more advanced cases sequestrae, areas of devascularised bone may be seen. After cultures have been taken, treatment should be started promptly. The affected limb is immobilised and an intravenous infusion of flucloxacillin started. If an abscess has formed then operative intervention is necessary to allow the pus to discharge. Sequestrae may have to be resected if prompt effective treatment is not instituted rapidly enough to prevent devascularisation and necrosis of substantial areas of bone.

Plain films are performed in the first instance, but are often falsely negative particularly in the early stages (first 5–7 days weeks). The first sign will be soft tissue swelling and there may be effusion in the adjacent joint. Subsequently, changes include focal lucent lesion, periosteal rection, endosteal scalloping, and peripheral sclerosis (Fig. 7.31). Appearances on plain film are those of a lesion of high biological activity, similar to those seen with malignant pathologies, and cannot often distinguish the two. Triple phase bone scan is more sensitive than plain film, particularly in the early stages. Uptake is increased in the affected area on blood pool and delayed images, due to increased osteoblastic activity. MRI is the preferred imaging modality, offering similar sensitivity to triple phase bone scan, and providing additional information on anatomy and extent of involvement. Indications for MRI are spine/pelvic involvement, epiphyseal involvement and failure to respond to treatment (Fig. 7.32). Findings are fluid signal centre surrounded by marrow oedema, cortical destruction, periosteal reaction and abnormal enhancement. MR may also detect complications such as abscess formation and joint involvement (Figs. 7.33 and 7.34). CT is more useful for follow up and chronic osteomyelitis. It may also identify a sequestrum which may not be evident on MRI. PET-CT is also increasingly being used to investigate chronic osteomyelitis. Targeted ultrasound may be helpful in demonstrating joint effusion or abscess collection (Fig. 7.35) [2, 10].

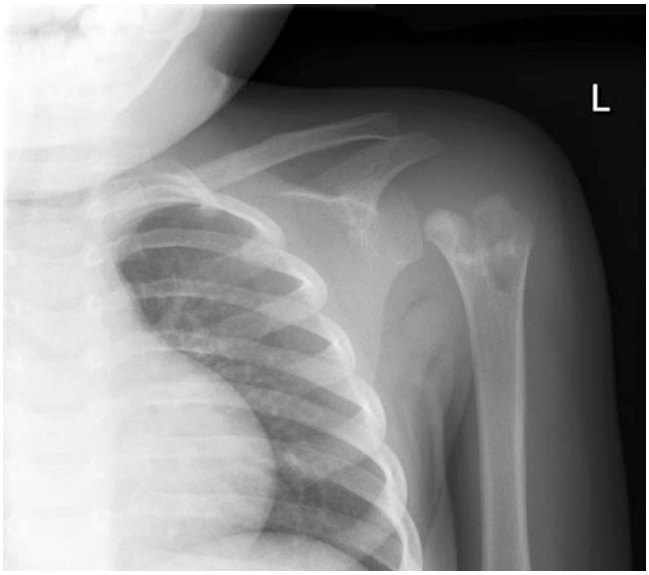

Fig. 7.31 Osteomyelitis of the shoulder in a 2-year-old infant. There is lucency and destruction of the left proximal humeral metaphysis and epiphysis

7.3.4 Arthritis (Figs. 7.36 and 7.37)

The well-known clinical picture of chronic polyarthritis with lymphadenopathy, splenomegaly, a rash and pericarditis was first described in Britain by George Frederic Still (1896) [11]. Since then the term "Still's disease" had been used to encompass the whole spectrum of rheumatoid arthritis in children. Recently the problem of nomenclature and classification was reviewed and the term juvenile chronic arthritis (JCA) has been accepted. It can present with a variety of clinical manifestations which will distinguish it from the clinical picture of rheumatoid arthritis in adults. We propose to recognise these clinical variations by separating juvenile chronic arthri-

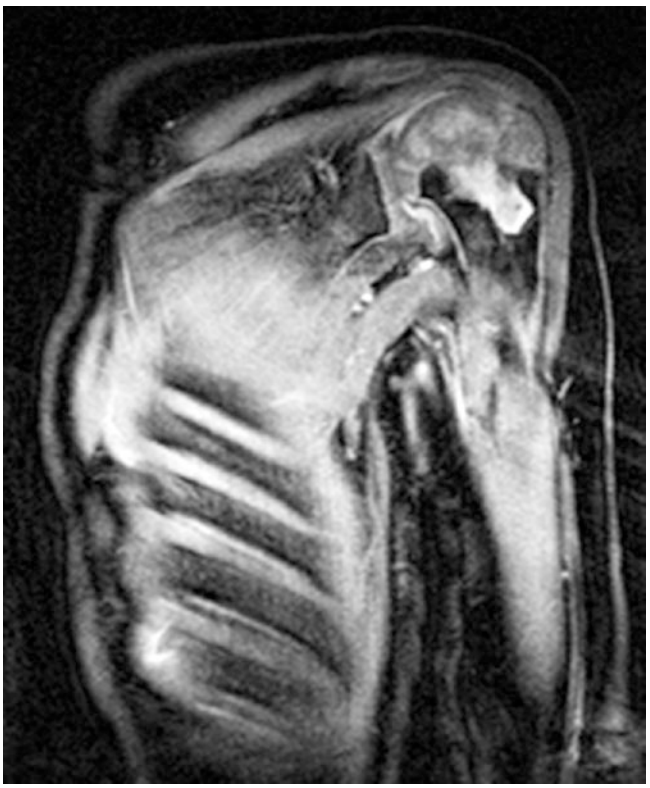

Fig. 7.32 MRI of the same child demonstrates abnormal signal in the proximal humeral epiphysis with high signal in the adjacent metaphysis

tis into three subtypes: (1) systemic onset JCA (Still's disease); (2) polyarticular onset JCA and (3) pauciarticular JCA.

7.3.4.1 Systemic-Onset JCA (Still's Disease)

The major signs and symptoms of this subtype of juvenile chronic arthritis are systemic. The most common age of onset of the disease is under 5 years but it can occur throughout childhood. Boys are affected as frequently as girls. Characteristic features are high remittent fever, generalised lymphadenopathy (including epitrochlear nodes), splenomegaly, polymorphonuclear leucocytosis and a rash. The rash has an irregular outline and is of coppery red colour. The best time to look for the rash is just after the child has had a hot bath or at the height of the temperature elevation. The fever shows diurnal swings as large as 2 or 3 °C which are rarely seen in acute rheumatic fever. Acute pericarditis is not very rare in this form of JCA but endocardial involvement is extremely rare. Joint manifestations are usually present at an early stage although they may initially amount to arthralgia without visible swelling. When the joints are involved they are frequently large ones, e.g. knees, hips, ankles, elbows and wrists. The cervical spine is another commonly affected site, presenting with pain, limitation of movement and torticollis. Also, peripheral joints may be involved. The surrounding

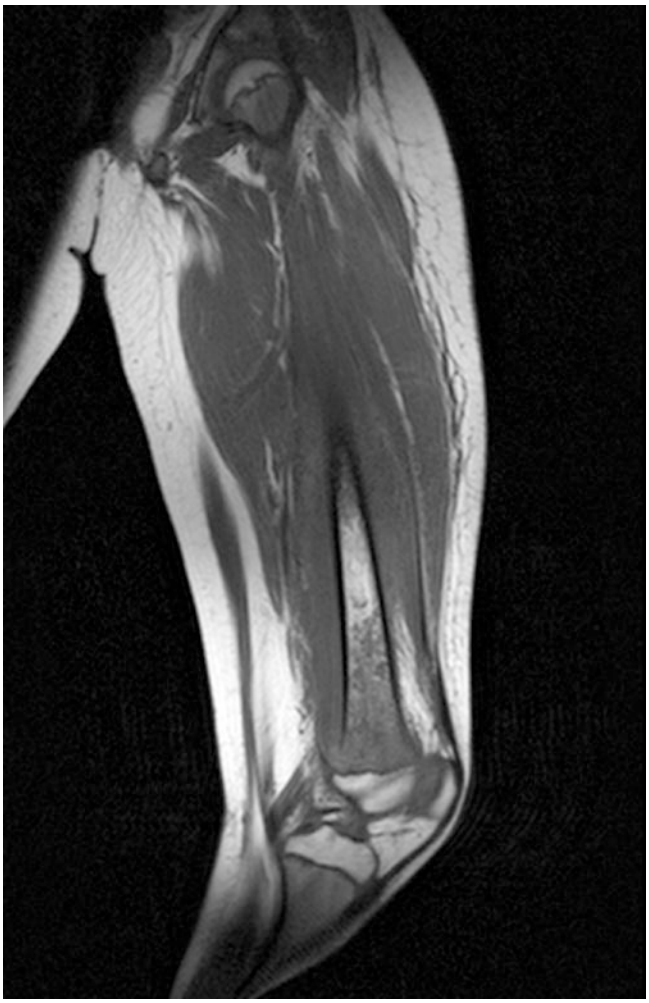

Fig. 7.33 T1W MRI of the distal femur shows bone marrow abnormality of the distal femoral metaphysis

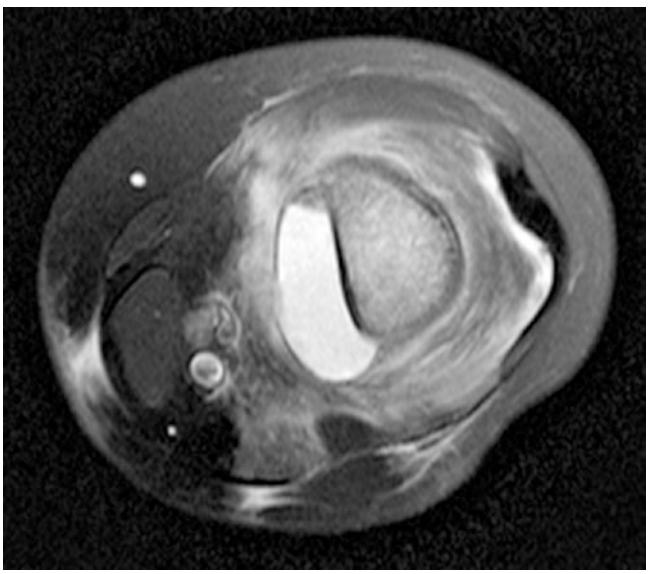

Fig. 7.34 Subperiosteal abscess formation on axial MRI surrounding soft tissue high signal

muscle atrophy and increasing limitation of movement and muscle weakness can lead to severe crippling. This subtype of JCA frequently runs a course of remission and relapses.

7.3.4.2 Polyarticular-Onset JCA

This type involves five or more joints but is not accompanied by the severe systemic disturbance such as high fever and rash of systemic onset type JCA. Girls are much more frequently affected than boys and although this type of JCA can occur at any age it is more often seen in children over the age of 5 years. The small joints of the hands and fingers may be severely affected. Children with polyarticular onset are divided into two groups: those with a negative blood rheumatoid factor present and a small group (10%) with a positive rheumatoid factor. Those with a positive rheumatoid factor are usually over 10 years of age and are more likely to develop destructive joint disease.

7.3.4.3 Pauciarticular-Onset JCA

In this group there is arthritis in 1–4 joints. Previously, a monoarticular type had been considered as a separate entity but now it is reasonable to include it within the pauciarticular onset sub group of JCA. It is essential to remember that children with pauciarticular type do not have symptoms and signs of a systemic or chronic illness. If the pauciarticular onset type is considered as a single entity, the knee and then

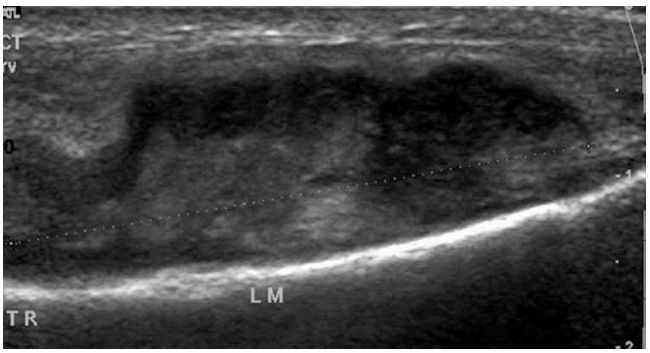

Fig. 7.35 Ultrasound of the distal femur allows real-time visualisation of abscess formation

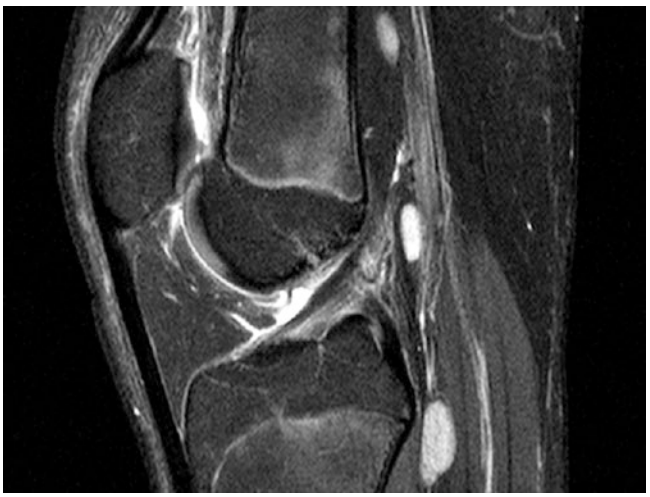

Fig. 7.37 Popliteal lymph node enlargement is a feature of JIA

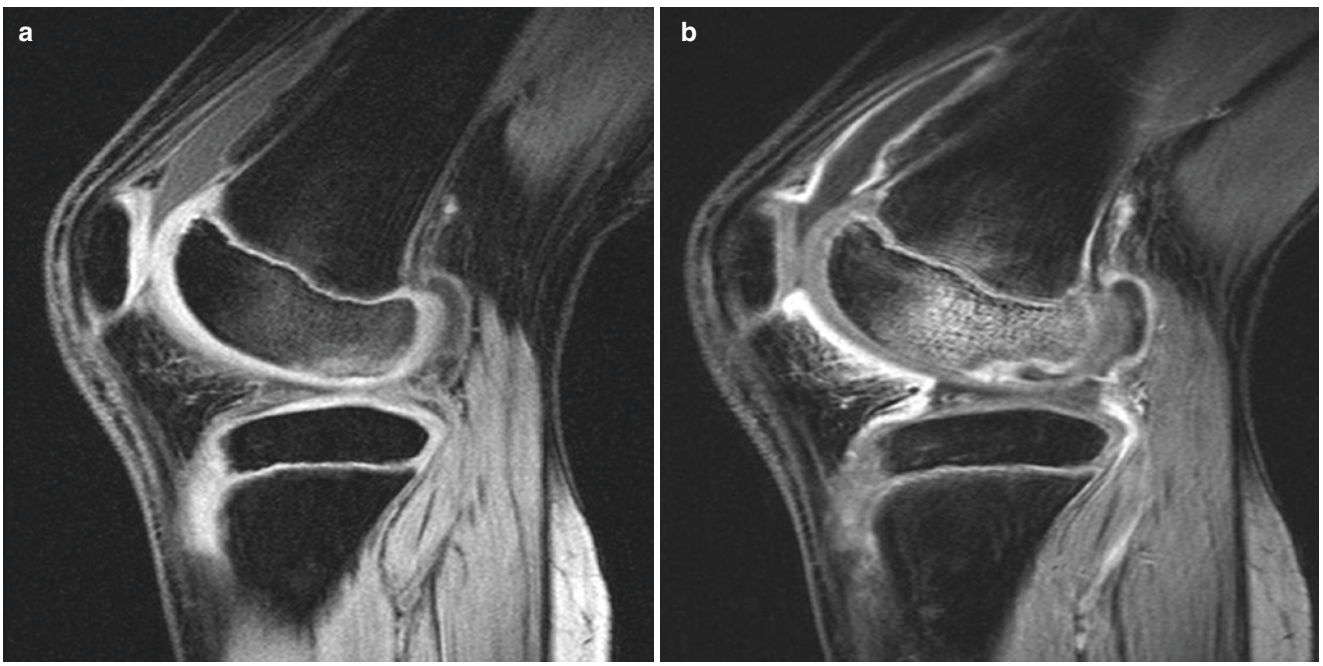

Fig. 7.36 JIA of the knee on (**a**) pre- and (**b**) post-contrast MRI sequences—knee joint effusion and abnormal enhancement of the synovium

the ankle are the most commonly involved joints but other large and small joints may be involved in this sub type of JCA. While the risk of chronic anterior iridocyclitis exists in all forms of JCA it is particularly common in the pauciarticular onset type especially in those with a positive antinuclear antibody (ANA) test. Iridocyclitis is often painless and thus it is important to arrange periodic slit lamp examination for children with pauciarticular onset JCA.

7.3.4.4 Course and Prognosis of JCA

Rheumatoid arthritis is a chronic systemic disease with a markedly fluctuating but ultimately self-limiting course. In some children remission may occur within a few months or years resulting in little or no deformity, in others the course is more prolonged and in these a greater degree of articular deformity, possibly permanent is likely.

The overall incidence of chronic iridocyclitis is 10% but in the pauciarticular type it is much higher. A routine slit lamp examination is mandatory in every child with juvenile chronic arthritis. Amyloid disease is a rare but potentially fatal complication and progressive enlargement of the liver and spleen and proteinuria are likely warning signs of this. The diagnosis of amyloidosis is confirmed by rectal or renal biopsy

7.3.4.5 Juvenile Idiopathic Arthritis (JIA)

Undertaking imaging in juvenile idiopathic arthritis is targeted clinically according to the individual child. Its uses include confirming diagnosis, evaluation of extent of disease, monitoring disease activity/progression and response to treatment. Findings vary depending on severity and duration of disease.

Plain films are performed in the first instance, largely to exclude alternative pathologies, and also to provide a baseline for follow-up. In the earlier stages, plain films are often normal as earlier disease affects the soft tissues such as synovium, with bone changes appearing later. Bone changes progress from osteopenia and periosteal reaction in the earlier stages, non-specific appearances. Progressive disease leads to later appearance of loss of joint space, joint subluxation and erosive arthropathy. Erosive changes appear later in children compared with adults due to predominantly cartilaginous composition of the paediatric skeleton. There may also be early physeal closure and ankylosis.

Ultrasound is better at visualising soft tissues particularly synovial thickening and joint effusion. High frequency linear transducers are well suited to visualising smaller joints such as the metacarpal-phalangeal joints and interphalangeal joints.

MRI, including post-contrast sequences, is the most sensitive modality for synovitis and bone marrow oedema. Thickened, enhancing synovium indicates active inflammation, while thickened non-enhancing synovium is in keeping with inactive pannus. Bone marrow oedema, joint effusion, erosions and lymph node enlargement are also features. MR changes may even appear before clinical symptoms and signs. It is also the best modality for visualising the TMJ and SIJ. MRI is usually targeted to the joint of concern where there is a specific clinical question which will influence management.

All the images modalities may pick up systemic features, such as pleural effusion and organomegaly [12].

7.3.5 Septic Arthritis (Figs. 7.38 and 7.39)

Young children commonly develop a benign, transient inflammation or effusion in the hip, probably as the result of minor injury. Pain in hip, thigh or knee develops with a limp or inability to stand on the leg and these symptoms frequently are found first on rising in the morning after a previous day's normal activity. Clinically the hip is found to have limitation of internal rotation and of abduction but other movements are usually free. There may be some muscle spasm on passively moving the hip but there is no wasting. Radiographs are normal except for soft tissue shadows which may indicate some hip joint distension. These findings exclude most other pathology but it is important to rule out the possibility of acute septic arthritis in its early stages, although in that condition all hip movements are affected. The term 'septic arthritis' is specifically used for proven bacterial joint infections. The more general term 'infectious arthritis' includes other pathogens in addition to bacteria, including

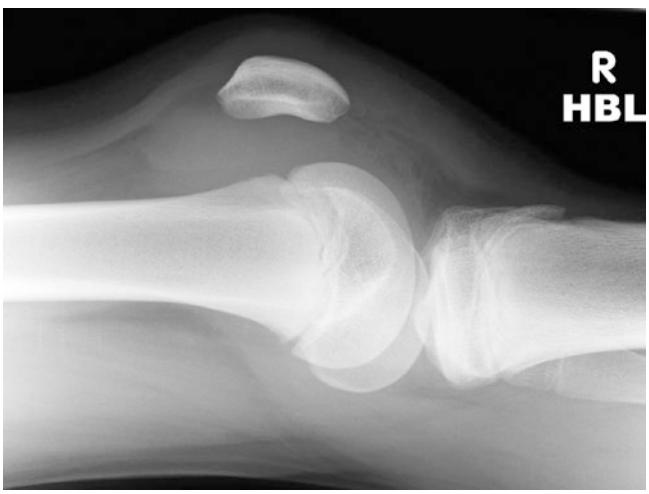

Fig. 7.38 Knee joint effusion in a child with septic arthritis

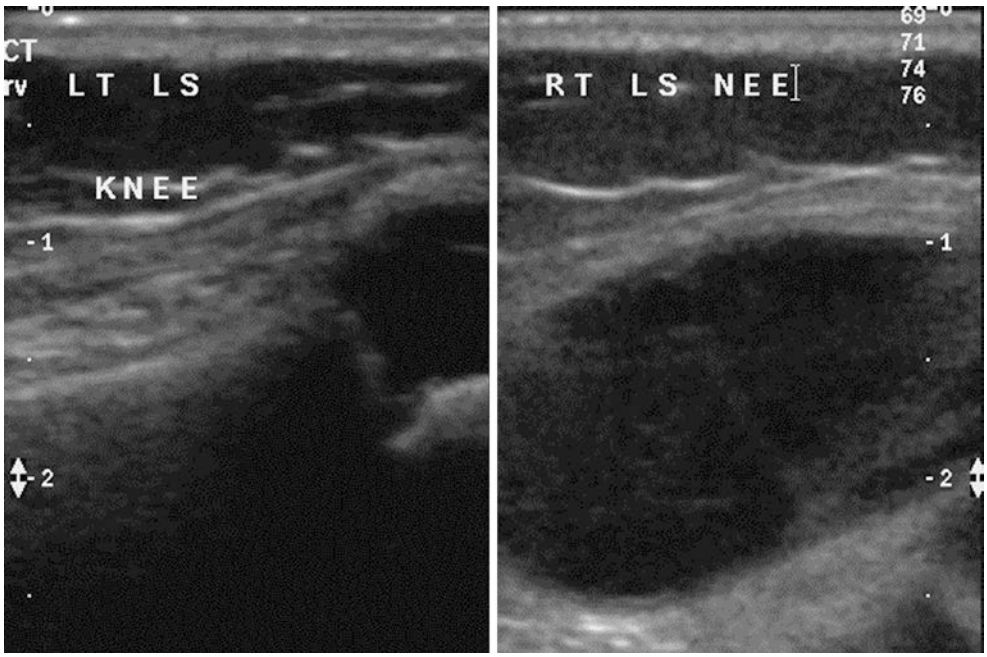

Fig. 7.39 US is sensitive for detecting joint effusion, however this is not specific to septic arthritis

viral and fungal agents. In children, the hip is a commonly affected joint, however imaging cannot differentiate septic arthritis from transient synovitis, and where there is clinical suspicion, arthrocentesis is indicated.

Plain radiographs are performed initially but are often normal in the earlier stages or show a non-specific joint effusion, particularly in the hip or knee. Joint effusions may be confirmed on US or cross-sectional imaging, however cannot distinguish infected from non-infected effusion. Ultrasound may characterise the effusion in terms of internal debris and septations, but again is non-specific. Additional findings on MRI include early cartilage destruction, erosion, synovitis, intra-articular debris and bone marrow oedema/associated osteomyelitis. Ultrasound and cross-sectional imaging may also be helpful to guide arthrocentesis. Unrecognised and untreated septic arthritis rapidly leads to joint destruction. On imaging, loss of joint space and erosive change will be evident, with relatively normal bone density [2, 13].

7.3.6 Osteochondrodysplasia: Others

7.3.6.1 Osteochondritis (Osteochondrosis)

This is a non-inflammatory derangement of the normal process of growth which occurs at various centres of ossification during the period of their greatest activity. Before puberty, the common sites are the femoral head (Perthes disease) and the tarsal scaphoid (Köhler's disease). Osteochondritis can also affect the tibial tubercle (Osgood Schlatter's disease) and calcaneum (Sever's disease) the second metatarsal (Freiberg's disease) and the vertebral epiphyses (Scheuermann's disease) but tend to occur at puberty

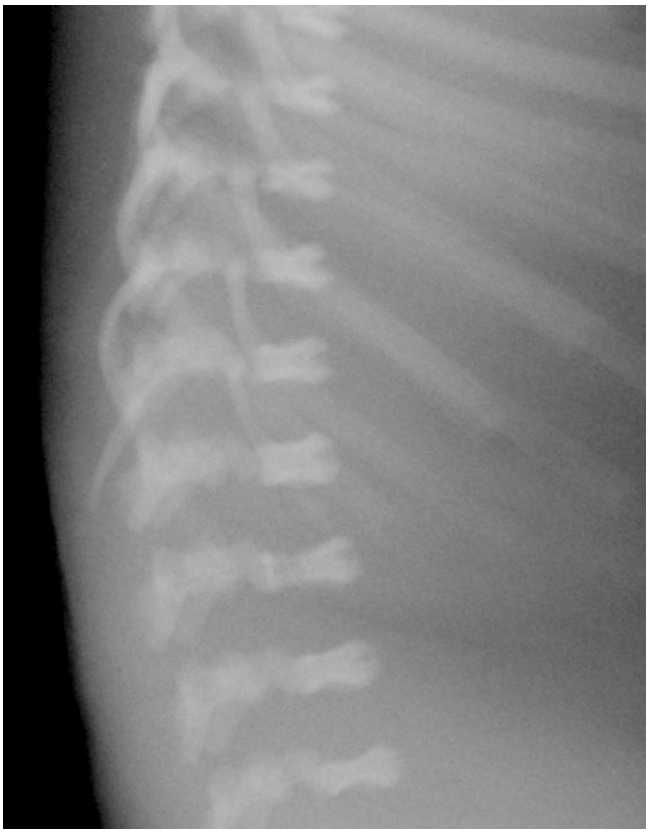

Fig. 7.40 Spondylometaphyseal dysplasia showing platyspondyly on lateral spinal radiograph

(Fig. 7.40). They are self-limiting diseases by may require immobilisation of the affected limb for periods of 6–8 weeks with physiotherapy to maintain muscle tone and power.

7.3.6.2 Osteochondritis of the Femoral Head (Perthes Disease)

This occurs largely in boys (five out of six will be boys, exactly the reverse of the sex ratio in congenital dislocation of the hip). Although it may occur between the ages of 2 and 10 years, the peak incidence is between 4 and 7 years. The condition occurs about once in every 2000 children. A small number have a family history of the condition and 10% will have both hips affected but not necessarily at the same time. Perthes disease is due to loss of blood supply, in part or in whole, to the femoral capital epiphysis which then undergoes avascular (aseptic) necrosis. The cause of the loss of blood supply is uncertain but children have a relatively tenuous blood supply to the femoral head under normal conditions. The articular cartilage is not primarily involved. Necrosis of the capital epiphysis usually causes synovitis of the joint giving rise to mild symptoms. The pathology and natural process of repair are paralleled by radiographic changes. In the very earliest stages, not often seen, the joint space may be enlarged by synovial effusion and thickening of the articular cartilage. The affected femoral head may seem relatively dense due to rarefaction in healthy, vascular bone of the pelvis and femur but this is followed by compression of the dead head, its reduction in height and the absolute increase in its density. At this time the natural process of repair involves an ingrowth of blood vessels with gradual revascularisation, the accompanying removal of dead bone and its replacement with living bone (creeping substitution). The dense bone mass appears to fragment radiologically and the portions of dead bone gradually become absorbed, being replaced with less dense living bone. This process takes 1–2 years and during this time the femoral head is softened and may also be partly subluxed from the acetabulum and is at risk of deformation due to weight-bearing forces so that the new live bone may be produced in a deformed shape leading to restriction of movement and possibly to osteoarthritic changes in later years.

The child usually presents with relatively mild complaints. Nearly all have a history of weeks or months of intermittent or continuous limp but only 50% admit to moderate pain at hip, thigh or knee. The child will be generally well. Examination will confirm the limp and some slight wasting of the thigh is usually seen. Hip movements are usually free except for limitation of internal rotation and abduction. The hip radiograph is usually diagnostic although occasionally the radiograph changes may lag some months behind the physical signs. It is usual to admit the child for a few weeks to allow bed-rest with traction during which time the irritability of the hip settles and full movements return. Orthodox treatment has been the relief from weight-bearing by bed-rest, the use of a weight relieving calliper, or most commonly by the use of crutches with a sling to suspend the affected leg. In the latter device a return to home and school is possible and the regimen would continue for about 1 year. In recent years carefully controlled studies have cast doubt on the value of this treatment and with grading of the degree of involvement of the femoral head, with the age of the child it may be possible to achieve a good result without such treatment. Hips showing lateral subluxation are best managed by containment of the femoral head in an abduction plaster-like a Batchelor plaster for congenital hip dislocation. See also Sects. 7.1.10 and 7.1.8.

7.3.7 Dysplasias

These conditions comprise a wide ranging group with different types of abnormalities of bone formation, and may affect any part of the skeleton. Many skeletal dysplasias present as short stature, which may be proportionate or disproportionate. Initial imaging is often a hand/wrist radiograph for bone age determination, allowing comparison with chronological age. Skeletal surveys are reserved for those children in whom a dysmorphology syndrome is suspected. This includes those with dysmorphic features or multiple congenital anomalies. Features of dysplasia may also be detected on antenatal ultrasonography. The dysplasias are a large group of conditions, made up of more than 350 distinct disorders, classified into around 32 different groups. This section will cover patterns of disordered bone formation and how radiology helps to classify these conditions. Achondroplasia is the commonest skeletal dysplasia and this group has been covered in Sect. 7.1.10. Covering all 350 individual conditions is beyond the scope of this chapter, and focus will rather be on radiological approach with a view to covering the main dysplasia groups. While certain features are specific to a condition, many features, when isolated, are non-specific, however groups of features together may indicate a diagnosis.

1. Disproportion

   The extremities are assessed for type of shortening, including rhizomelia (shortened humeri or femora), mesomelia (shortened radius/ulna or tibia/fibula) and acromelia (short hand and feet).

   Presence or absence of platyspondyly is assessed.
2. Epiphyseal ossification, metaphyses and diaphyses

   Small or irregular epiphyses indicate an epiphyseal dysplasia.

   Flared or irregular metaphyses indicate a metaphyseal dysplasia.

   Cortical thickening or marrow expansion of the diaphyses indicate diaphyseal dysplasia.

   Combinations of the above also give rise to additional groups such as spondyloepimetaphyseal dysplasias (Fig. 7.41).

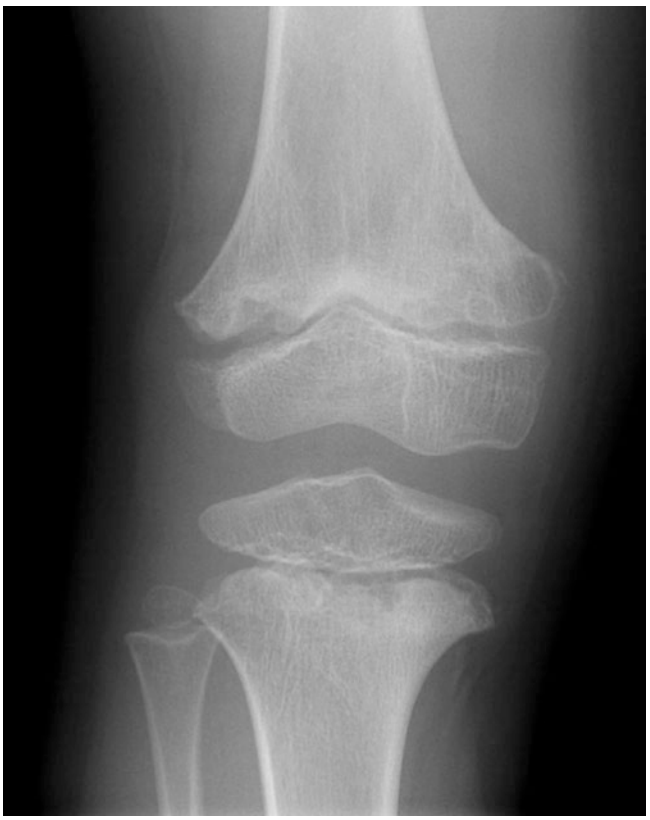

Fig. 7.41 Metaphyseal dysplasia. Radiograph of the knee shows metaphyseal widening and irregularity. This was a generalised finding and typical of metaphyseal dysplasia

3. Normal variant vs pathology

This part of the process is best performed by a radiologist with an interest in skeletal dysplasias, as recognising the difference between normal variation and pathology can be difficult and requires significant experience. This allows recognition of certain specific, sometimes pathognomonic, features, or aids categorisation into a broader group.

Dysplasias may be broadly classified into:

- Limb deficiencies: complete or partial limb absence (amelia or meromelia respectively)
- Limb shortening/dysplasia: subdivided into rhizomelic or non-rhizomelic dwarfism:
  - Rhizomelic conditions include achondroplasia, thanatophoric dysplasia, OI, rhizomelic chondrodysplasia punctata, asphyxiating thoracic dysplasia.
  - Non-rhizomelic conditions include diastrophic dysplasia, camptomelic dysplasia, chondroectodermal dysplasia, Kniest dysplasia, non-rhizomelic chondrondysplasia punctata, achondrogenesis, multiple epiphyseal dysplasia, metaphyseal condrodysplasia.
  - Non-limb-shortening conditions include metaphyseal dysplasia, progressive diaphyseal dysplasia.

7.4 Trauma

7.4.1 Cruciate Ligaments

Congenital deformity of the knee is rare, with the most common being congenital hyperextension that may be the result of an in-utero position in its simpler form, treated by gentle manipulation into flexion or fixation in progressively flexed plaster casts until a full range of movement is restored. Severe grades of this deformity are usually associated with fibrous contracture of the quadriceps muscle requiring surgical release.

7.4.1.1 Derangement Within the Knee Joint

(See also Sect. 7.3.5)

The lateral meniscus is occasionally congenitally deformed as a discoid lateral cartilage. This may give rise to no symptoms but can cause a loud clicking on flexion/extension movements possibly with mechanical disturbances of locking and instability. If the symptoms are persistently troublesome lateral menisectomy is needed. Tears of normal menisci, so common in the adult male, are rare in children but if symptoms of mechanical disturbance are troublesome menisectomy is indicated. The most common derangement within the knee is osteochondritis dissecans, usually found in boys over 10 years. An islet of bone, perhaps 1–2 cm in diameter, usually on the intercondylar aspect of the medial femoral condyle surface separates from the underlying bone. This may be the result of trauma or disturbance of the local blood supply. The button-like fragment of bone is avascular and, covered by the articular cartilage which holds it in place, lies in a bed of sclerosed bone. The articular cartilage may break down to allow the bone fragment to separate from its bed and become a loose body in the knee joint. The symptoms are usually of discomfort felt in the region, worse after activity, and often accompanied by a small joint effusion. There may be local tenderness but physical examination is usually unhelpful. Radiographs will demonstrate the lesion especially if an intercondylar view is requested. In the younger child, with restriction of weight-bearing and rotational strains as occur in football etc., the condition can be expected to heal over a period of 1–3 years. In the adolescent, the bone fragment may separate to become a loose body which should be removed. Although a defect in the articular surface is left, this tends to smooth off with cartilage growth.

In pre-adolescent children, ligamentous laxity along with relatively weak physis and bone means that tibial spine avulsion/osteochondral injury tends to occur instead of injuries

to the anterior cruciate ligament structure itself, as tends to be the pattern in adults. A more adult pattern of injury does tend to be seen in older children as skeletal maturity is approached.

Plain radiograph will show the avulsed tibial spine fragment in the intercondylar notch (Fig. 7.42).

MRI confirms osteochondral fracture and also visualises the ligament itself. In adolescents, MRI may show oedema and loss of continuity of the ligament where there has been partial or full tear. The knee joint can be fully assessed for additional injuries to other structures including bone oedema, meniscal tears and collateral ligament injury (Figs. 7.43 and 7.44) [14, 15].

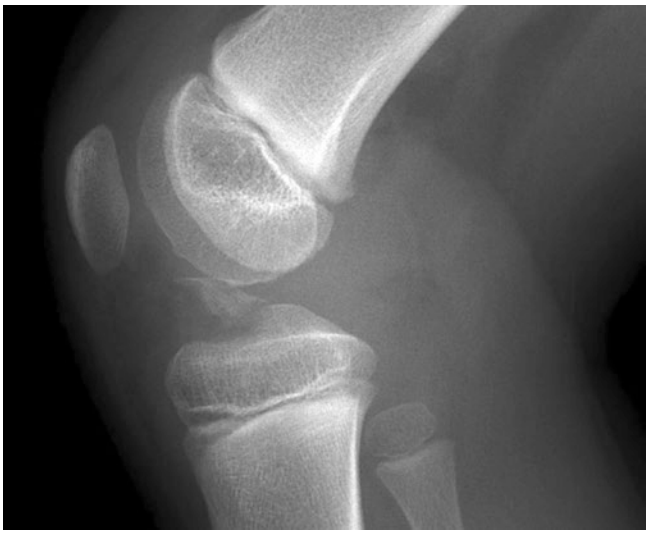

Fig. 7.42 Lateral knee radiograph shows avulsion of the tibial spine/ACL insertion site

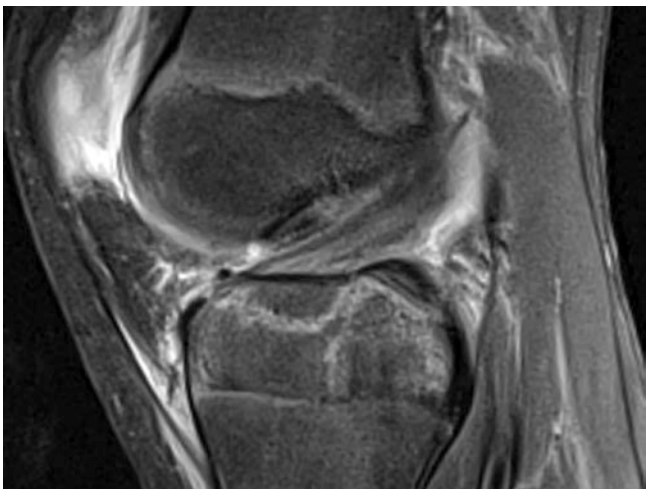

Fig. 7.43 Sagittal and coronal MRI knee demonstrates high signal outlining the avulsed tibial spine

7.4.2 Fractures (Figs. 7.45 and 7.46)

In children, healing of fractured bones is rapid and they do not suffer the consequence of stiff joints requiring physiotherapy or the added complication of deep vein thrombosis found in adults. A birth fracture is firmly united in 3 weeks, but as the child ages the speed of repair diminishes. If a

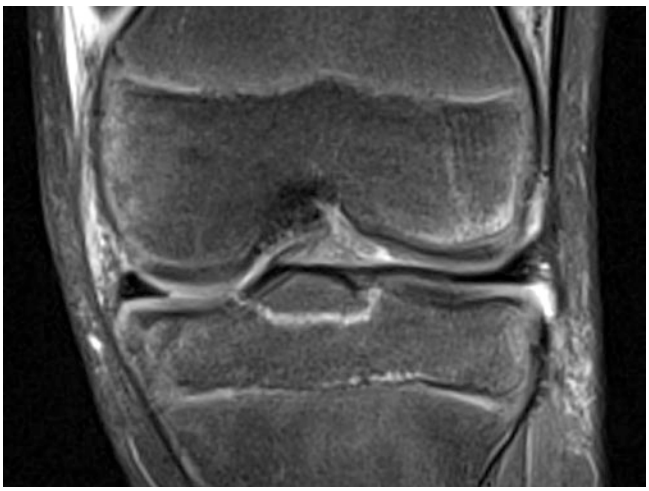

Fig. 7.44 Sagittal and coronal MRI knee demonstrates high signal outlining the avulsed tibial spine

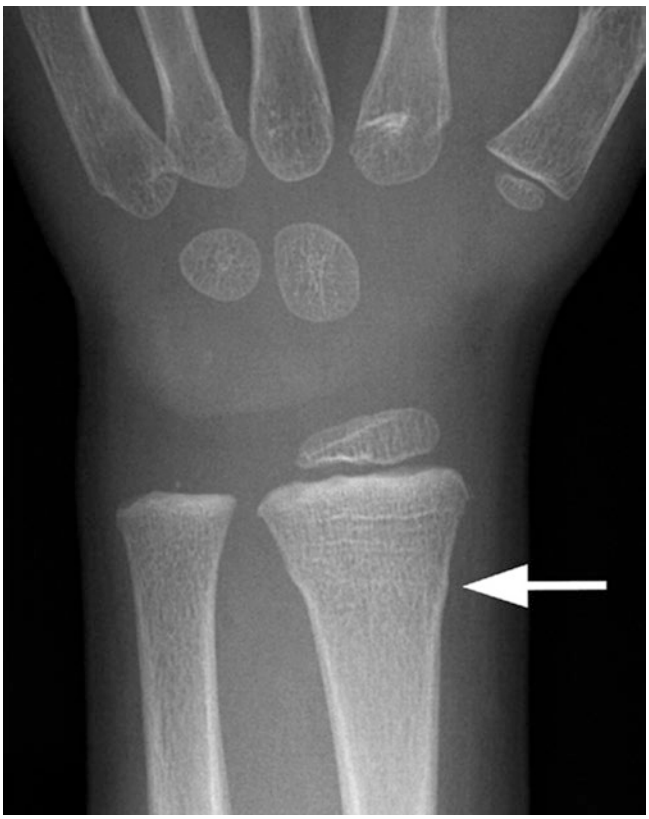

Fig. 7.45 Bulging of the distal radial cortex in buckle fracture

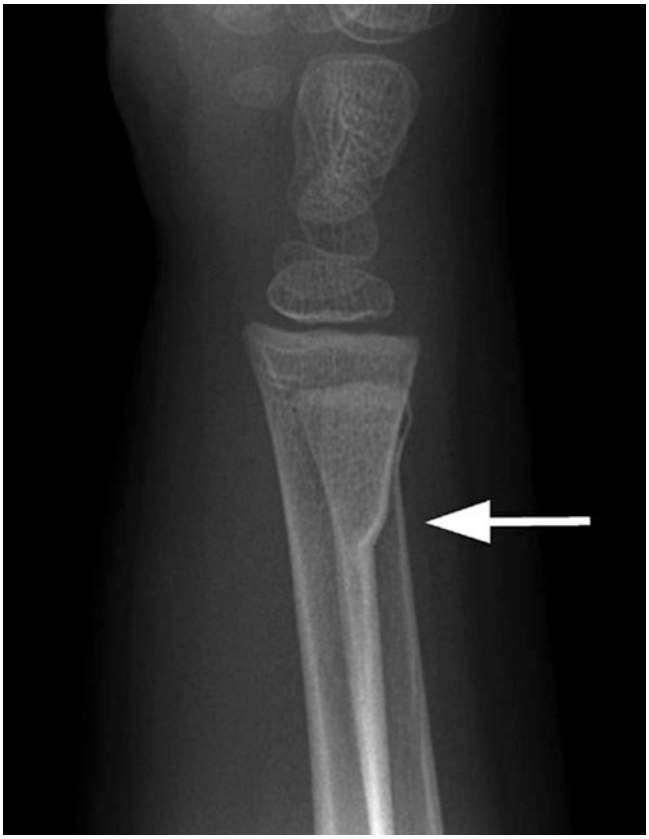

Fig. 7.46 Bulging of the distal radial cortex in buckle fracture

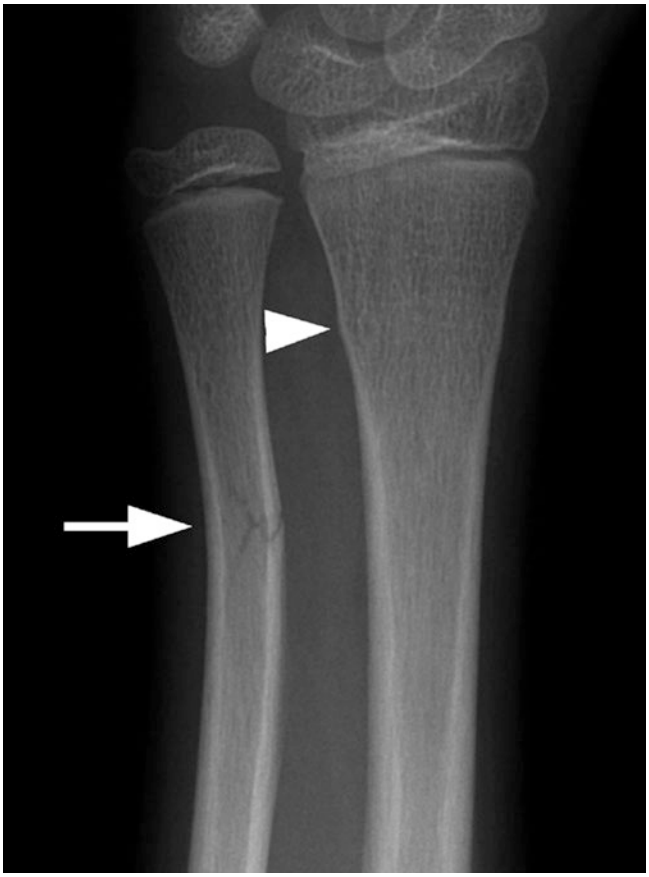

Fig. 7.47 Greenstick fractures of distal ulna (arrow)—break in the cortex on the convexity only. Buckle fracture of distal radius (arrowhead)

fracture unites with angulation of fragments, the resulting deformity usually corrects in an infant within a few months and the older child within a year or 2. Not only is angulation corrected, but if shortening results then the rate of growth of the fractured limb increased beyond its fellow until the limbs once more are equal in length. A good blood supply of a growing bone results in extensive haemorrhage at the site of a fracture, and may result in considerable blood loss, especially when the pelvis or femur is fractured. If the periosteum remains intact, a closed haematoma results and decalcification and absorption of the bone ends proceeds concurrently with the deposition of new bone and callus formation. Parents should be warned about a hard visible palpable swelling at the site of the fracture which will disappear with remoulding. When there is a tear of the periosteum blood extravasates into the adjacent tissues. Except in the bones of the skull and the clavicles which develop in membrane, primary and secondary centres of ossification appear in regular sequence. The radiologist or surgeon called upon to interpret the radiograph film of a suspected fracture must be familiar with the times of their appearance and of their fusion. Two centres of ossification are not uncommon in children and their appearance on a radiograph may be mistaken for a fracture. Different patterns of fractures tend to be seen in children compared with adults due to bone composition, and the presence of growth and growth plates. Growth also means faster fracture healing and more successful remodelling. The incomplete or greenstick fracture is common in childhood and may be found in three forms.

1. A hairline crack in the cortex resulting from torsional strain and presenting with slight local pain and tenderness. This may be overlooked on the immediate radiograph, and only after several days once there is a new bone formation present is the diagnosis obvious. This fracture may be accompanied by a slight pyrexia which suggests an inflammatory cause for the local pain and tenderness.
2. The compression fracture in which the radiograph shows a horizontal line of compressed cortex. Deformity is absent and local pain and tenderness subside quickly with rest and immobilisation in a plaster splint.
3. The common and typical greenstick fracture in which the cortex has broken through on one side and only bent or incompletely broken at the opposite side (Figs. 7.47 and 7.48). Deformity, local pain and tenderness are present, but there is no abnormal mobility or crepitus, the periosteum

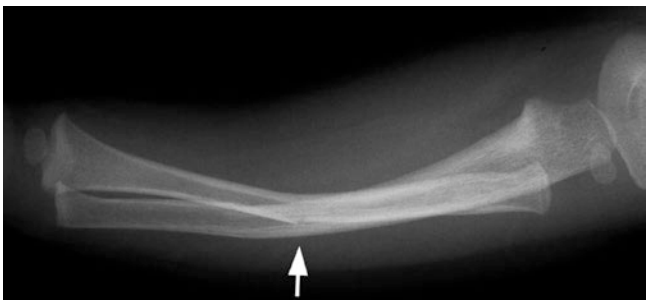

Fig. 7.48 Bending of the radius and ulna in plastic bowing injury (arrow)

frequently remaining intact. Where the force of an injury has been applied at the end of a long bone there may result not a fracture but a separation of the epiphyses. In minor degrees of this injury displacement is negligible and exact diagnosis is only evident on radiograph. In more severe forms the epiphyses may displace a triangular fragment of the metaphyses.

Complications of fractures:

- Non-union. Non-union in children is extremely rare. Delayed union is far commoner because of the inability of the child to keep still which results in inadequate immobilisation. This however, merely increases the amount of callus formation and never results in non-union. Re-fracturing a site in a child may result in prolonged non-union or a fibrous union.
- Localised traumatic ossification. Where a muscle has been torn from its attachment a mass of bone may form within the muscle restricting its movement and limiting the range of movement of the joint.
- Interference with the circulation. This is not a common complication of fractures in childhood but may follow injuries in the region of the elbow and the forearm. The results of unrelieved arterial or venous obstruction are disastrous for the child. The mechanism of obstruction and the resulting changes in the tissues are varied. Inspection of the limb in all fractures is essential to make sure that the circulation of the limb is intact. If plaster of Paris is applied too tightly it may cause vascular compromise. The branchial artery may be occluded by pressure of bony fragments as a direct result of an accident. This may produce pallor of the limb and absence of the radial pulse. The vessel may be in spasm due to bruising or partial occlusion by a bony fragment. Treatment of this clinical situation is immediate exploration of the fracture site. If not relieved the long-term results may be disastrous varying from losing the limb to severe ischaemia which affects not only the forearm muscles but also the median and ulnar nerves. The clinical picture of venous obstruction develops much more slowly than that of arterial obstruction. The pulse usually remains palpable but there are persisting signs of cyanosis of the hand and increasing pain. The presence of tissue oedema coupled with slow and continuous haemorrhage under a deep fascia may result in this clinical picture. Prophylactic elevation of the limb and removal of any tight plasters may be indicated to relieve the venous obstruction.

7.4.2.1 Nerve Injury

Primary nerve injury as a complication of fractures in childhood is uncommon. The bruising of the radial and ulnar nerves may occur in supracondylar fractures of the humerus and of the perineal nerve in fractures of the upper end of the fibula. Recovery is usually rapid. Damage to the growth area of a long bone. Separation of any epiphysis in a child is rarely accompanied by damage to the neighbouring growth area. A crush injury, however, may cause damage to this area resulting in very severe intractable deformity.

7.4.2.2 Pathological Fractures

Spontaneous and pathological fractures are not uncommon in childhood and are met in:

1. General affections of the skeleton such as osteogenesis imperfecta.
2. Neoplastic disease.
3. Generalised decalcification of bone.
4. Paralysed limbs or following prolonged recumbancy with immobilisation, there is decalcification of bones of the affected limbs.
5. Pseudoarthrosis is also rare, with persistent non-union of the clavicle. Similar appearances may occur in other bones in association with neurofibromatosis. The radiographic appearance is of bone sclerosis and expansion of the bone ends at the site of non-union. Improvement in appearance can be obtained by excision of the defect and the excessive bone with bone grafting and internal fixation.
6. Hyperaemic decalcification may result from a local focus of chronic bone infection and occurs quite early in acute haematogenous osteitis.

7.4.2.3 Dislocation of Traumatic Origin

The joint of a growing child is normally more flexible and is possessed of a greater range of movement than that of the adult. Actual dislocation is less common in children although minor sprains with or without an effusion of fluid in the joint can occur. Reduction of a dislocation under general anaesthesia is usually obtained without difficulty, and restoration of normal function is almost invariable. Physiotherapy is rarely necessary.

7.4.2.4 Injuries of the Spine

The spine of a child is normally much more flexible than that of an adult, and consequently fractures of the spine are uncommon but may be missed when they do occur. Usually, injuries are in association with other more extensive injuries in the body. Although intrathecal fracture is rare, haemorrhage is less uncommon and may cause pressure on the cord with resulting paralysis which may be temporary or permanent. As in an adult at the scene of injury, a child should not be lifted from the scene of the accident until some form of immobilisation of the neck is achieved, in order to avoid a cervical cord injury as a result of flexion of the child's spine. The diagnosis and treatment of injuries to the cord are along the same lines as those adopted in the adult.

Cervical spine. Fractures and dislocations of the cervical spine are uncommon in childhood and may cause transection of the cord. This is rare. Subluxation of the cervical spine can occur but complete dislocation is rare. Head traction relieves pain and spasm and allow the facets to reset. Delay in recognition of cervical cord damage with consequent paraplegia may occur.

Dorsal spine. Compression fracture may occur in an injury as a result of falling from a height or a car accident. Usually there is no permanent disability and after a period of bed rest recovery is complete.

Lumbar spine. Fractures below the first lumbar spine are rare in children. Fractures of transverse processes or pedicles are rare but may follow a torsion injury. Bed rest is all that is necessary and complete recovery is the rule.

7.4.2.5 Shoulder and Upper Limb

The Clavicle (Fig. 7.49). The clavicle forms the only bony connection between the shoulder girdle and the trunk. It is one of the most commonly fractured bones in the body. The clavicle is liable to break when force is applied to the outstretched hand, elbow or shoulder. Injuries to the clavicle may result from birth trauma. In infancy, fractures of the clavicle may present with a pseudoparalysis and pain when the arm is moved. It must be differentiated from Erb's palsy, osteitis of the clavicle, scapula or upper humerus. At times, children present with a swelling due to massive callus over the clavicle after the initial injury may have been missed. This usually disappears in a few months—no treatment is necessary. In children, reduction of a fractured clavicle is rarely necessary under the age of 6 years. The use of a figure of eight bandage or simple support in a sling may help relieve discomfort.

The Scapula. Most fractures of the scapula are due to direct trauma. Even if there is marked displacement treatment is conservative. Bed rest or a simple sling is the only treatment necessary. Winging of the scapula as the arm is held forward is normally the result of paralysis of muscles around the scapula as in poliomyelitis or after damaging the long thoracic nerve of Bell following thoracotomy e.g. after the repair of an oesophageal atresia. Winging may also be due to a benign exostosis on the deep surface of the scapula which can be removed surgically, or as a result of a condition known as fibromatosis.

7.4.2.6 Injuries at the Shoulder Joint

Dislocation of the shoulder is rare in childhood. Fractures of the surgical neck and upper third of the humerus are not uncommon. (Anterior, posterior, and rotational displacement may accompany both adduction and abduction types of injury.) Lateral as well as antero-posterior radiographs are essential in all cases. Impaction of the fracture is common and 10–20° of angulation is permissible without attempting correction. Moulding of the fracture takes place in 6 months to a year and what initially might appear unsatisfactory is usually passed as normal at the end of that period. If the fracture is not impacted it may be aligned by a hanging plaster cast as in the adult.

7.4.2.7 Injuries About the Elbow

The elbow joint is very vulnerable in the child and there is a wide range of degree of fracture displacement. Because of the lack of ossification in the epiphyses around the joint, experience is required to interpret the exact nature of the fractures on radiographs. Failure to correct displacement may result in deformity and loss of function in the joint.

7.4.2.8 Supracondylar and Intercondylar Fracture (Figs. 7.50 and 7.51)

There are two forms of these fractures: (1) extension type, 99%; (2) flexion type, 1%.

The extension type of fracture is caused by a fall on the outstretched hand. The fracture line runs transversely across the shaft immediately above the condyles and from below upwards and backwards. The deformity is threefold, the lower fragment being displaced backwards, tilted to the medial or lateral side, and rotated relative to the long axis of the humerus. Reduction is an emergency and effected as

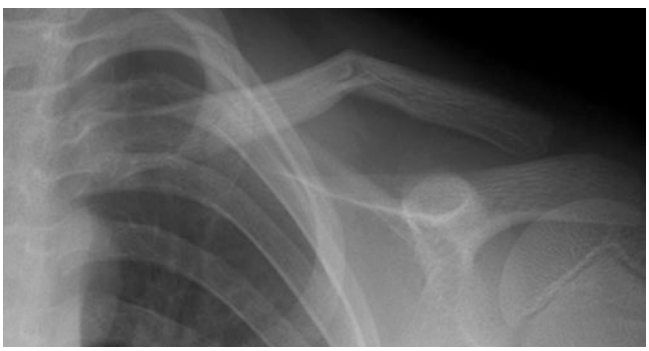

Fig. 7.49 Angulated fracture of midshaft left clavicle

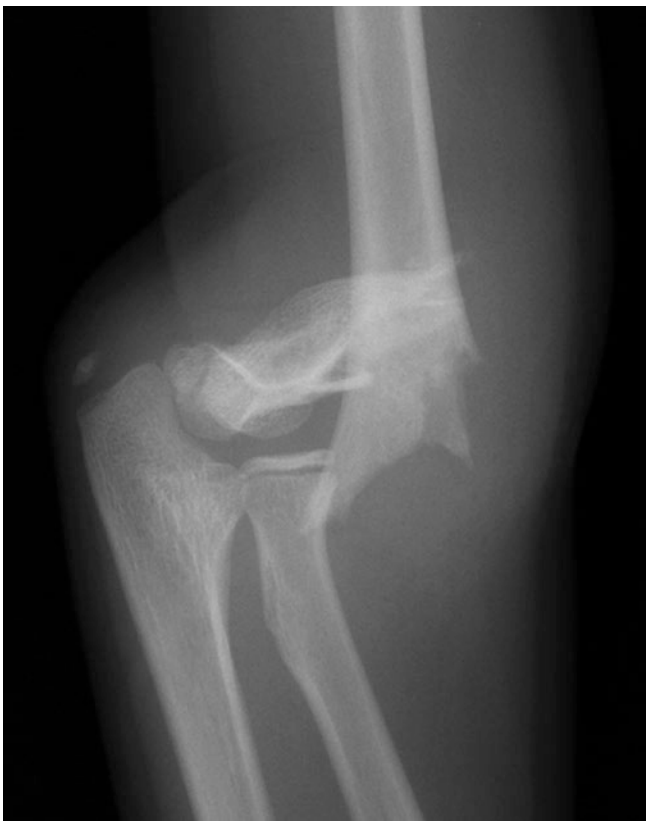

Fig. 7.50 Displaced supracondylar fracture

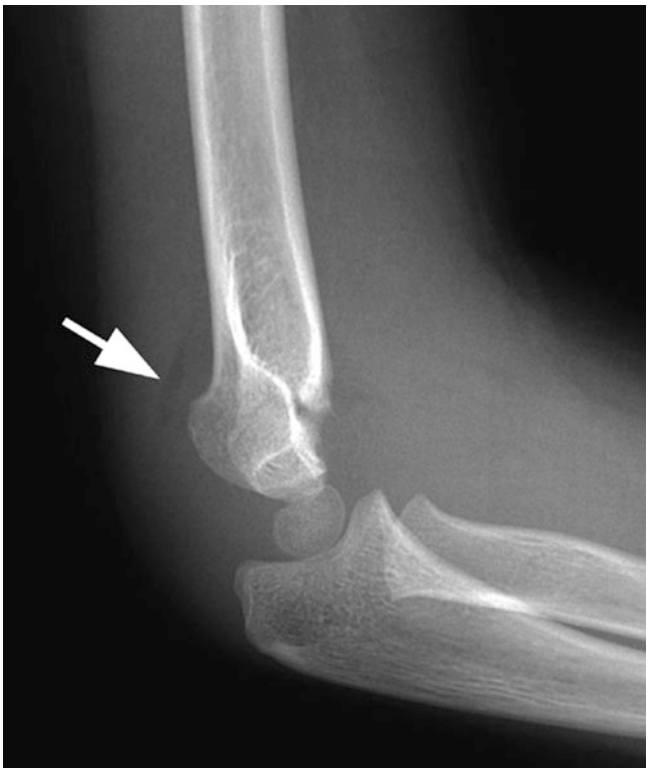

Fig. 7.51 Type II supracondylar fracture with joint effusion. Arrow indicates visible posterior fat pad

soon as possible after the injury. The patient is admitted to hospital and detained for 24 h after reduction to observe the peripheral circulation. Should there be any sign of circulatory impairment, treatment which involves exploration of the branchial artery should be instituted immediately. Failure to do so invites Volkman's paralysis. Reduction should be performed by an experienced surgeon. Traction is applied to the distal fragment with the elbow flexed to overcome the upward and backward displacement; the lateral or medial displacement is then corrected. Confirmation of reduction by radiograph is essential. Medial angulation must not be accepted since this will result in cubitus varus. Minor displacement is of little importance in the presence correct alignment. Mobilisation is by a plaster cast from shoulder to wrist with as much elbow flexion as possible. The radial pulse must not be obliterated by overzealous flexion. The plaster is usually removed in 3 weeks and replaced by a triangular sling. Active movements of the elbow are encouraged and the sling is removed in a further 2 weeks. On no account should massage or passive movement be permitted. Open reduction of this fracture is seldom necessary. However, this is necessary when the fracture is compound and when there is gross deformity of the fracture.

Flexion type occurs with a fall on the flexed forearm or on the elbow. The line of fracture runs upwards and forwards, the displacement is usually slight and there is no rotational deformity. The fracture is reduced and immobilised in extension for 10 days. The elbow is then brought to a 90° angle and immobilised for a further 10 days in a dorsal plaster slab.

Fracture of the lateral condyle may vary from an incomplete fracture or a flake injury, to a complete separation of the condyle. Displacement in the incomplete fracture is minimal and may only be shown as a thin flake of bone on a radiograph. This may appear following a severe jerk of the elbow. In older children the injury results from a fall on the outstretched hand causing the radial ligament to tear away. Treatment consists of a few weeks rest in a plaster slab with the elbow in flexion followed by active use. A complete fracture of the lateral condyle is more serious as permanent disability may result if treatment is inadequate. When displacement is gross and the fracture surface faces outwards open reduction and fixation with screws is the method of choice. Complications of this injury may result in an ulnar-neuritis or even osteoarthritis of the joint later in life.

Fracture of the medial condyle. Although a fracture of the medial condyle is rare in children, fracture of the epicondyle is not uncommon. The flexor muscles tear off their attachment following a severe strain. In the uncomplicated case, immobilisation of the elbow in flexion for 3 weeks in a plaster slab is all that is needed. The ulnar nerve is vulnerable because of its anatomical position and may be injured.

Fracture of the olecranon. This is uncommon and results from a fall on the point of the elbow. It may produce a simple

crack or a complete fracture with considerable separation of the fragments. Minor injury requires only symptomatic treatment with a sling. Open reduction may be necessary with internal fixation of the fragments when there is a wide separation in an extensive fracture.

Pulled elbow. This is a descriptive term for the injury at the upper end of the radius in an arm subjected to sudden traction i.e. snatching the arm to save a falling child. There is a subluxation of the radial head downwards through the annular ligament. This causes discomfort and the arm hangs by the side unused. There is no gross deformity and this with the ability to allow full flexion and extension adequately excludes more severe injury. Supination is limited and attempts to produce this cause pain. The diagnosis of a pulled elbow is a clinical one. Radiographs are usually normal and diagnosis rests upon the above physical findings together with the history of a traction injury. The condition wears off rapidly if a simple manipulation into full supination is carried out during which it is usual to feel a "click" as the radial head is reduced. In the minority in which a satisfactory outcome is not readily obtained, the child can be given a broad arm sling to rest the arm and spontaneous resolution will occur in 1–3 days.

Fracture of the neck of the radius. This is a comparatively rare type of fracture due to a fall on the outstretched hand with the forearm in supination. Manipulative reduction should be attempted but even if not completely successful, open reduction should seldom be undertaken. Excision of the head of the radius may ultimately be necessary.

Dislocation of the elbow joint. Posterior dislocation of the forearm bones behind the humerus is a common injury of childhood and is usually the result of a fall upon the outstretched hand. The loss of mobility and derangement of the normal relations of the olecranon and condyles enable the injury to be differentiated from a supracondular fracture. The diagnosis is confirmed by radiograph. Reduction by traction is usually easy but in children a general anaesthetic is needed. The joint is rested at 90° in a dorsal slab for 3 weeks. Active exercise is encouraged thereafter.

Fractures of the forearm occur in the following order of frequency. Distal third—75%, Middle third—20%, proximal—5%. Fractures of the upper third of the ulna is an uncommon injury in children and results from a fall on the outstretched hand with the forearm in pronation. When a fracture with angulation occurs in a single bone of the forearm, the radiograph must include both the elbow and wrist joints, lest dislocation is overlooked. In children it is possible to reduce both fracture and dislocation by fully supinating the forearm. The limb is immobilised in this position for 6 weeks.

Fractures of the middle third of both bones of the forearm. Though violence is indirect, the bones frequently break at the same level. The line of fracture is usually oblique, commonly the fracture is of a greenstick type either of both bones or of one only, the other being complete. Reduction of the displacement without rendering the fracture complete is not easy and deformity will usually recur within the cast. Immobilisation is by means of a padded plaster cast from axilla to the metacarpo-phalangeal joints, with a plaster strap across the palm. The elbow is held in the 90° position. In general, full supination is used for fractures in the upper third, mid-pronation for fractures of the middle third and full pronation for fractures of the lower third and immobilisation is maintained for about 6 weeks.

Fractures of the lower third of the forearm are of three common types:

1. Incomplete compression fracture of the lower third of the radius (buckle fracture). Local tenderness is the only sign of injury to the bone and a radiograph shows the transverse line of compressed cortex. Symptomatic treatment only is needed. A dorsal plaster slab from elbow to metacarpo-phalangeal joint immobilises the wrist and relieves pain which settles in 10 days.
2. Separation of the lower radial epiphysis. In the majority of injuries, the epiphysis carries with it a wedge of dorsum of the metaphysis and the injury is more accurately described as a fracture. This clinical picture resembles that of the Collé's fracture which is much less common in children. The typical dinner-fork deformity is present, the epiphysis being displaced and rotated dorsally. Correction of the deformity is usually obtained without difficulty. The method of reduction is similar to that employed in the treatment of Collé's fracture. It is wiser to place the wrist in a position of slight flexion before applying the plaster, as there is a greater risk in children of the epiphysis slipping back when the swelling has subsided.
3. Fractures of both bones about 2–5 cm above the epiphysis may be complete or incomplete and the common deformity is a backward displacement of the lower fragments. Reduction is usually easily achieved but the deformity is very liable to recur. This can be prevented by immobilising the forearm in full pronation.

The wrist and hand. Sprained wrist and fracture or dislocation of one of the carpal bones are extremely rare in young children, but from the age of 10–12 fracture of the scaphoid is not infrequent. Any child at this stage who is supposed to have a sprained wrist should be subjected to a careful radiograph examination. As in the adult, the line of fracture is easily missed unless oblique views of the wrist with the hand in radial deviation are taken. Fracture of the scaphoid tubercle is the more usual type of injury in children, but fracture of the waist of the scaphoid may occur. The former unites quickly whereas the latter requires prolonged immobilisation as in the adult. Ligamentous injuries of the carpus require 2 weeks of complete immobilisation.

Fractures of the metacarpals and phalanges follow the same pattern as in adults. Flexion fractures of the neck of the metacarpal bone of the index or little finger are not uncommon. Correction of the deformity can be effected by direct pressure on the head through the flexed proximal phalanx. The fingers are strapped over a rolled bandage in the palm for 2 weeks. In the common oblique fracture of the shaft of the metacarpal there is rarely any displacement and the application of a dorsal plaster of Paris slab for 3 weeks is all that is necessary. Local splinting of fingers is difficult in children because of their size. It is quite justifiable to include adjacent fingers as natural splints. Fractures of the metacarpals and the phalanges unite rapidly and immobilisation beyond 3 weeks is rarely required.

Open injuries of the hand are extremely common in children but fortunately most are of a minor nature which include abrasions and superficial skin wounds that require only first aid treatment. This is aimed at cleaning the wound and preventing infection. A sterile dressing is applied and the hand bandaged in the position of function. Examination of an injured hand is important in order to assess whether deeper damage has occurred to tendons or nerves. The posture of the hand results from a balance of the muscles controlling the fingers, both agonists and antagonists, and when this is impaired due to division of the tendons or paralysis of the nerves, there is an obvious deviation from the normal position. Damage to a flexor tendon results in greater extension whereas an extensor tendon cut will result in the finger being pulled into greater flexion. Immediate repair of divided tendons and nerves is important and should be done by a surgeon experienced in this type of work.

If the fingertip is crushed but the bone is not denuded the wound is gently but thoroughly cleansed. Damaged tissue is approximated and a firm dressing applied. Fractures of the distal phalanx require no further treatment. If the nail is partially avulsed it is trimmed off proximally leaving the distal part as a splint. If the tip of the finger is partially amputated it is stitched back on as the regenerative ability of the tissues of the child are indeed remarkable.

The pelvis. Fracture of the pelvis occur in children in consequence of falls, crushing injuries or by direct trauma in road traffic accidents. Of itself fracture of the pelvis is not serious although considerable blood loss into the tissues may occur. Bed rest with analgesia until the patient becomes comfortable is the only treatment necessary. Fractures of the pelvis do become very important when other soft tissues are damaged, in particular when the urethra suffers either partial damage as it passes through the pelvic floor or in more severe injury complete disruption of the urethra may occur. Extravasation of urine will occur if early recognition and treatment is not instituted. Passage of a catheter along the urethra to the bladder if possible and if not then exposure of the bladder and passage of a catheter, with control from above and below should be performed and urinary drainage continued for 10–14 days.

The hip and lower limb. All fractures in children except those in certain pathological bone disorders unite without difficulty provided the bone ends can be kept close together. Rigid fixation is not required unless one fragment is intra-articular when good position is impossible to maintain without operation and internal fixation. Open reduction plays some part in the wider displaced fractures of the upper third of the femur, but plating is not often advisable. Skeletal traction should not be used in children and repeated manipulation aimed at achieving anatomical reduction should be avoided.

A plaster of Paris splint should be used only if:

(a) It makes the child more comfortable.
(b) It prevents the fracture from displacing.

If a plaster cast is used a layer of cotton wool must separate it from the skin and instructions given for the child to be seen immediately if pain or discolouration of the limb ensues.

Femur. Fractures of the femoral neck follow major violence. They are treated by reduction and internal fixation. Fractures of the shaft are either transverse and caused by major violence or oblique caused by twisting injury which might be apparently trivial. Skin traction and a Thomas splint is preferred. The splint is fixed at the foot of the bed and the end of the bed raised on an elevator to avoid discomfort from pressure by the splint in the groin. These fractures heal readily and 1 week of splintage per year of age to a maximum of 6 weeks is sufficient to mobilisation. Foot movement is encouraged throughout this period and a close watch is kept for evidence of pressure on the lateral peroneal nerve in the region of the neck of the fibula. After the period of immobilisation a radiograph is taken and if the fracture is clinically and radiologically firmly united the splint is removed and knee movement commenced.

Fractures around the knee. The cruciate ligaments are firmly attached to the head of the tibia and their function is to prevent excessive gliding of the tibia on the femur. After a severe injury the entire articular facet of the tibia can be pulled out of the tibial head by these ligaments. There is always a severe haemathrosis. The fragment avulsed is often bigger than it appears on a radiograph. The fragment needs to be replaced under general anaesthesia during which procedure the femoral condyles thrust the displaced fragment of bone downwards into its proper position. A plaster cylinder is applied to the leg for 4 weeks.

Fractures of tibia and fibula. As in the femur, transverse fractures indicate severe direct violence and oblique fractures are due to twists. The latter are more common and may be overlooked unless radiographs in two planes are studied. Manipulation of transverse fractures is aimed at getting end-to-end apposition and angulations are corrected as a plaster

of Paris cast is applied. It is important to immobilise the knee with 25° of flexion and the ankle at right angles in order that quick recovery of muscle power and joint movement will occur after union of the fracture and removal of the plaster.

Fractures of the bones of the foot. The more severe types of fracture of os calcis are rare but cracks may occur and are not uncommon. Diagnosis is made on radiograph. A below-knee walking plaster cast is applied extending to the base of the phalanges and weight bearing is allowed. Plaster is removed after 3 weeks.

Fracture of the talus, although uncommon, may occur in association with severe crushing injuries, the bone being driven upwards between tibia and fibula. Avascular necrosis may result if the blood supply is damaged. Regeneration is slow and prolonged freedom from weight bearing is essential. Fracture of other small bones of the foot is uncommon. Union occurs readily if the foot is immobilised in a plaster cast for 4 weeks.

Fracture of the metatarsal bones and phalanges. Fractures of the base of the fifth metatarsal are not uncommon and require no treatment beyond rest for 2 weeks. Alternatively, a light walking plaster may be applied for the same period. Care must be taken not to mistake the common presence of an accessory bone the vesalianum for a fracture. A badly crushed foot is moulded back to its normal contours, held in a padded plaster cast and elevated on pillows. The metatarsals eventually remould themselves and function is excellent. Broken phalanges are splinted or bound to an adjacent toe.

Incomplete fractures are more common, as children's bones are more plastic and able to absorb more force prior to breaking.

Buckle fractures are evident on plain film as unilateral or bilateral bulging of the cortex (Fig. 7.47). These result from longitudinal force such as fall on outstretched hand. In green-stick fractures, the bone bends and there is cortical break in the convex side of the bone, without continuing to the other (concave) cortex. Plastic bowing injuries (Fig. 7.48) result from multiple radiologically occult microfractures along the bone, resulting in bending of the bone without a fracture line as such being demonstrated.

7.4.2.9 Physeal Injuries (Figs. 7.52, 7.53, 7.54, 7.55, and 7.56)

Multiple growth plates are seen in children, and may involve in fractures typically where a shearing or avulsion mechanism is applied. The Salter-Harris classification was described by two orthopaedic surgeons in 1963, which has five main types:

- Type I. Fracture completely through the growth plate with no bone fracture.
- Type II. Fracture through the physis continuing through part of the metaphysis. By far the commonest type (75%), usually seen in over tens.

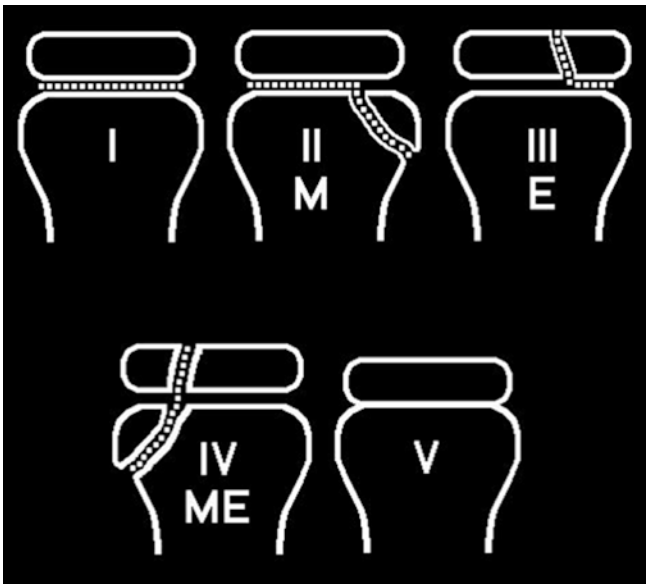

Fig. 7.52 Salter Harris classification

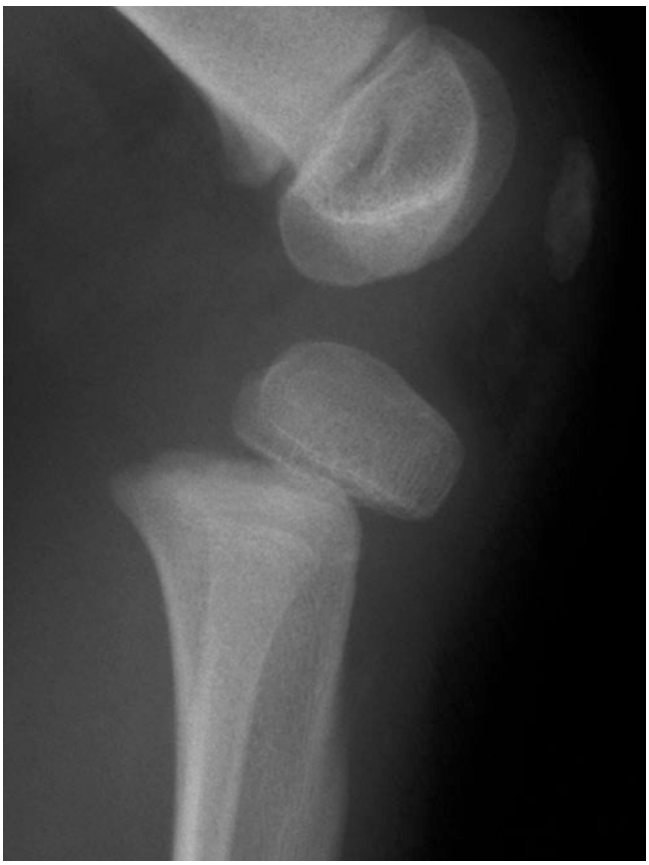

Fig. 7.53 Salter Harris types I-IV as described in text (Type I)

- Type III. Fracture through the physis continuing through part of the epiphysis.
- Type IV. Fracture through the metaphysis, growth plate and epiphysis.

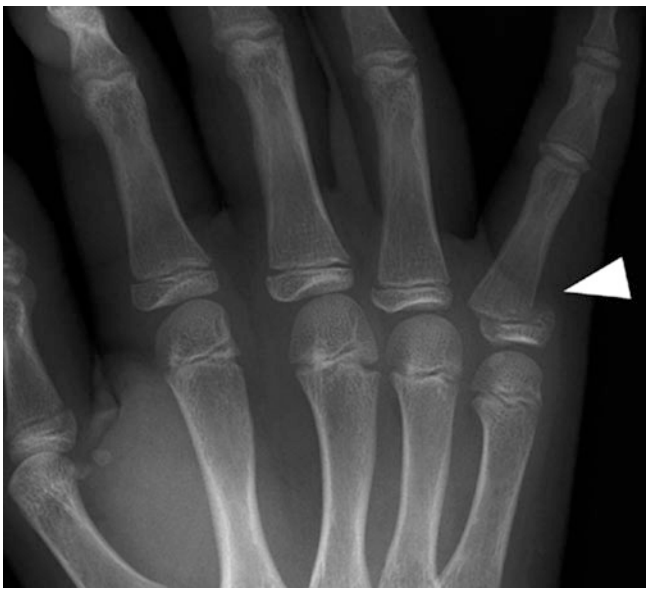

Fig. 7.54 Salter Harris types I-IV as described in text (Type II)

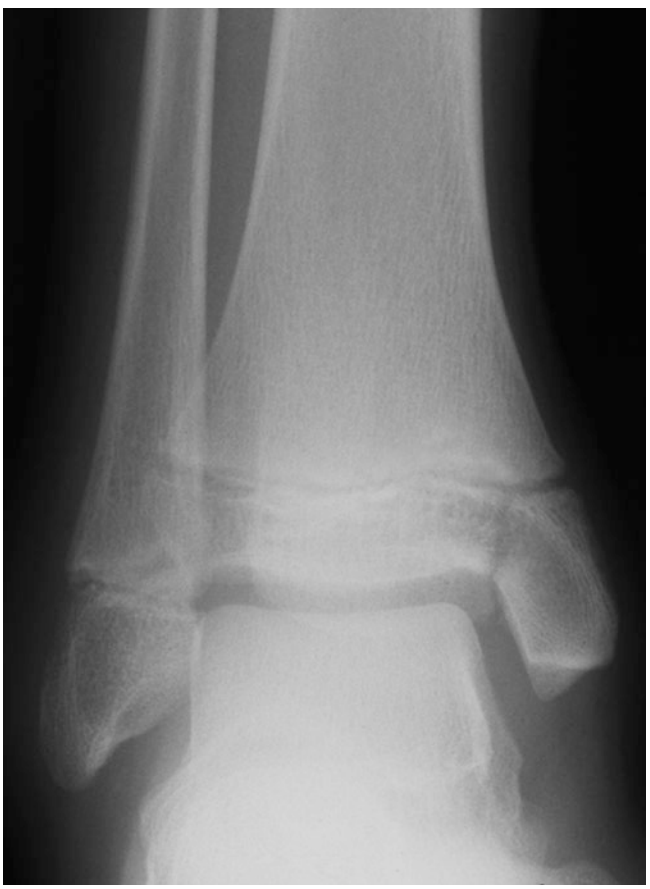

Fig. 7.55 Salter Harris types I-IV as described in text (Type III)

- Type V. Crush injury to the physis. Least common type (<1%) but with worst prognosis. This type is often difficult to pick up radiologically and is often diagnosed retrospectively.

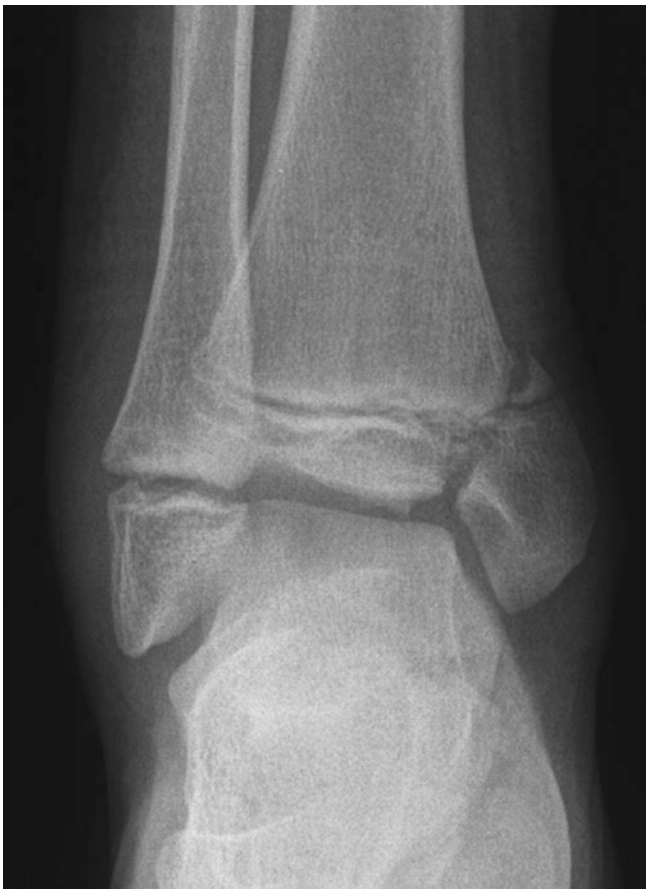

Fig. 7.56 Salter Harris types I-IV as described in text (Type IV)

The higher grades have a worse prognosis, with higher incidence of premature growth plate closure.

Clavicle. Middle third fractures are commonest and there is associated soft tissue swelling. Clavicle fractures are often seen on a single clavicle radiograph, but may be supplemented by a cranially angulated view if necessary.

Arm and elbow. Humeral fractures most commonly occur in the supracondylar region. Supracondylar fractures are classified into three types:

Type I: Undisplaced
Type II: Displaced with intact cortex
Type III: Completely displaced

On plain film, the fracture line may or may not be visible. Where the fracture line is not visible, secondary signs are crucial to raise suspicion of occult fracture. These are usually best seen on the lateral view. There may be evidence of a joint effusion, with elevation of the anterior fat pad and visible posterior fat pad (posterior fat pad is not normally visible). Loss of anterior humeral alignment is another indirect sign. The anterior humeral line should intersect the middle third of the capitellum on the lateral view. Where any of these signs are present without a definite fracture, re-imaging

7–10 days following injury is advised to look for evidence of healing fracture such as periosteal reaction.

Medial and lateral condylar fractures may have varying degrees of displacement seen on plain film. Condylar fractures may be misinterpreted as ossification centres. It is important to evaluate the elbow ossification centres in all elbow injuries to avoid this potential mistake. The mnemonic 'CRITOL' describes the order in which the ossification centres appear (Fig. 7.57).

- C—capitellum
- R—radial head
- I—internal epicondyle
- T—trochlea
- O—olecranon
- L—lateral epicondyle

Therefore if a bone fragment is seen at the lateral epicondyle in the absence of any of the preceding centres, this should be interpreted as a fracture.

CRITOL is also useful in interpreting epicondylar avulsion injuries. Medial injuries are more common and are also known as 'little league elbow' injuries, as often the mechanism is that of a throwing injury. An avulsed medial epicondyle may displace into the elbow joint and mimic an ossification centre (Fig. 7.58).

Steps for interpreting elbow radiographs:

- Evidence of joint effusion (elevated anterior fat pad, visible posterior fat pad)
- Alignment-anterior humeral and radiocapitellar alignment
- Ossification centres (CRITOL)
- Fracture line

Forearm, wrist and hand (Fig. 7.59). Torus, greenstick, bowing and complete fractures are seen in the forearm bones. Most occur in the distal forearm bones, however midshaft injuries are also common. Often both bones fracture. Where a single fracture is seen, the forearm should be scrutinised carefully for evidence of a second injury, which may be occult fracture or dislocation at the wrist of elbow. The Monteggia fracture dislocation is most commonly seen (Figs. 7.60 and 7.61). In this injury there is fracture of the midshaft ulna with radial head dislocation. In the Galeazzi type injury, there is radial fracture with dislocation of the distal ulna (Figs. 7.62 and 7.63).

In the hand, the phalanges are the most commonly fractured bones and may be Salter-Harris type injuries. It is important to remember that, while displacement and angulation of a phalangeal fracture can be assessed on plain film,

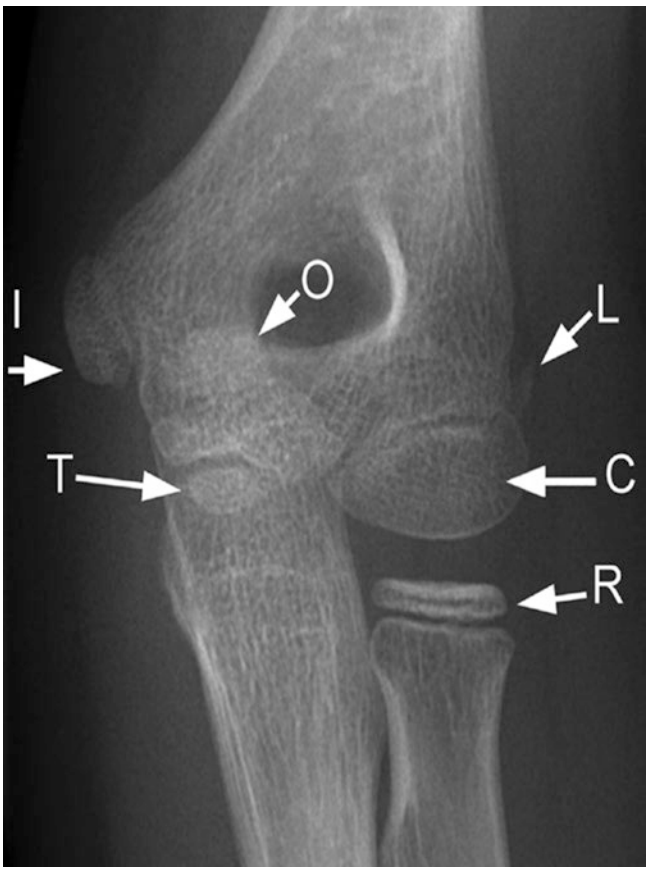

Fig. 7.57 The 'CRITOL' description of elbow ossification centres as described in the text

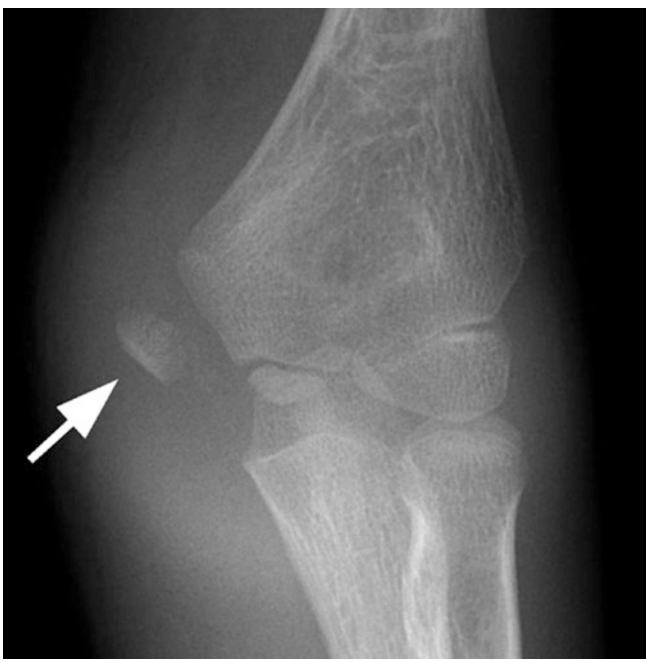

Fig. 7.58 Displaced medial epicondylar ossification centre (arrow) with soft tissue swelling

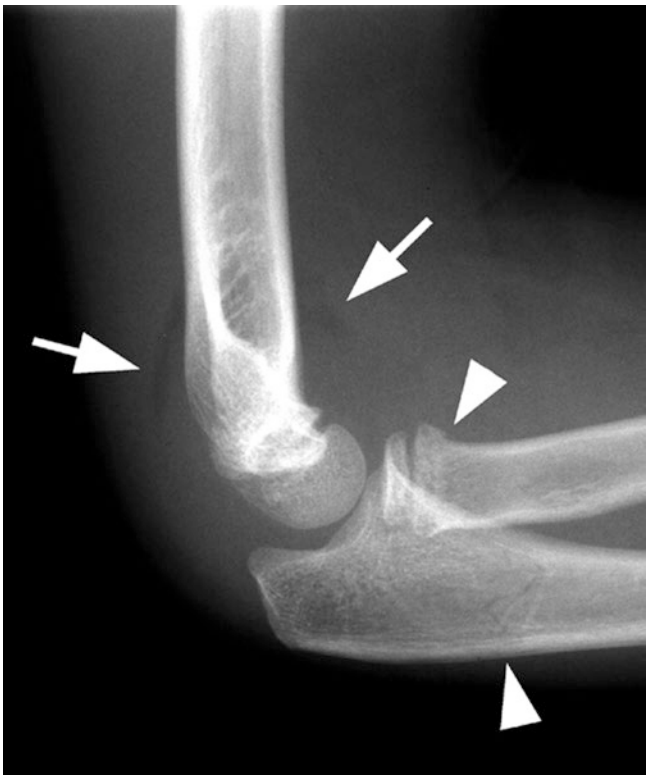

Fig. 7.59 Radial neck fracture and undisplaced proximal ulnar fractures (arrowheads) with elbow joint effusion indicated by elevated anterior and visible posterior fat pads (arrows)

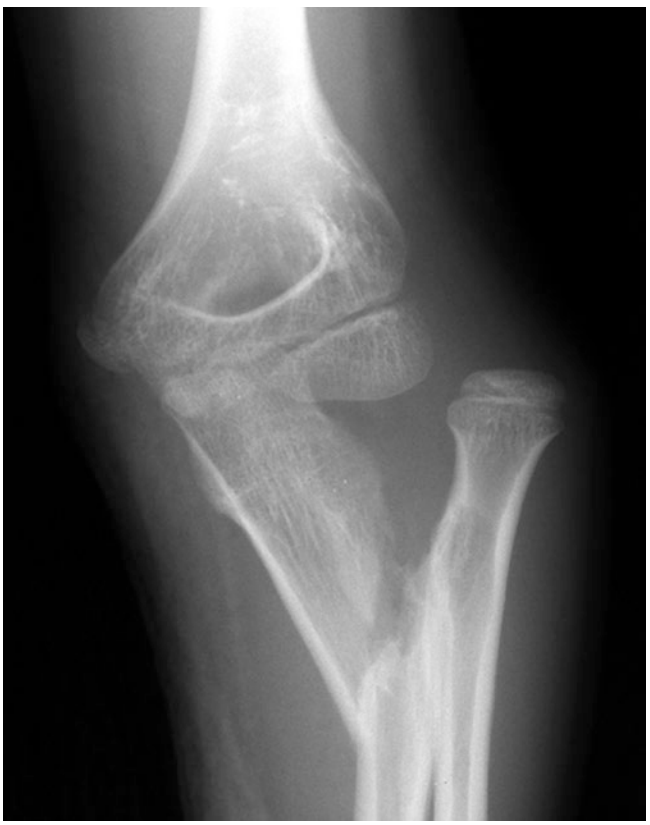

Fig. 7.60 Monteggia fracture dislocation injury. Dislocated radial head with fracture of proximal ulna

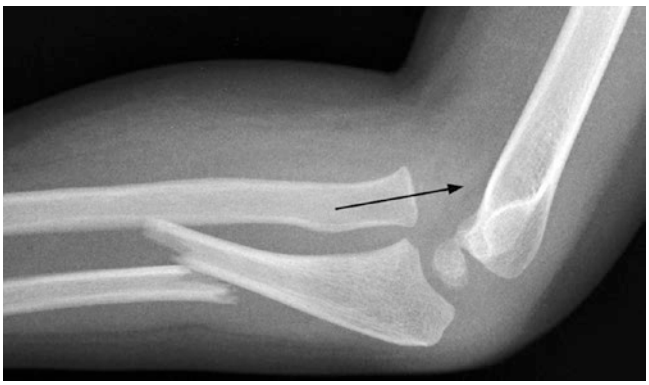

Fig. 7.61 Monteggia fracture dislocation injury. Dislocated radial head with fracture of proximal ulna. Black arrow on the lateral view indicates loss of radiocapitellar alignment, confirming radial head dislocation

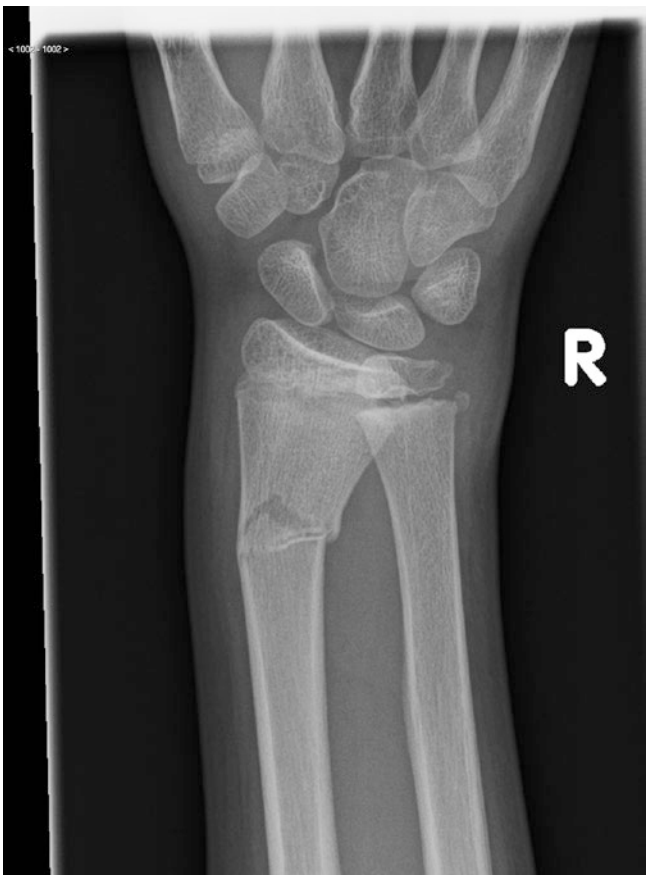

Fig. 7.62 Galeazzi fracture dislocation. Fracture of the radius with dislocation of the distal ulna (AP view)

rotational deformities cannot, and must be fully assessed clinically.

Pelvis, hip and femur. Trauma involving the pelvic ring may result in different patterns of injury depending upon the mechanism. Children may have incomplete fractures or, in younger children, single fractures to the pelvic ring due to more elastic bone composition. Most will be detected on plain film. CT is used to further assess unstable pelvic fractures.

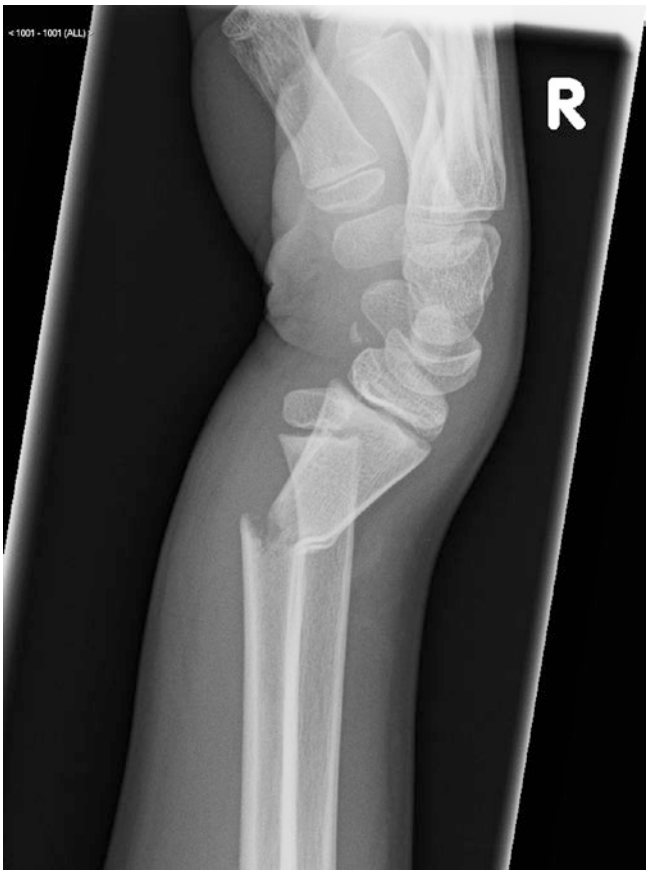

Fig. 7.63 Galeazzi fracture dislocation. Fracture of the radius with dislocation of the distal ulna (lateral view)

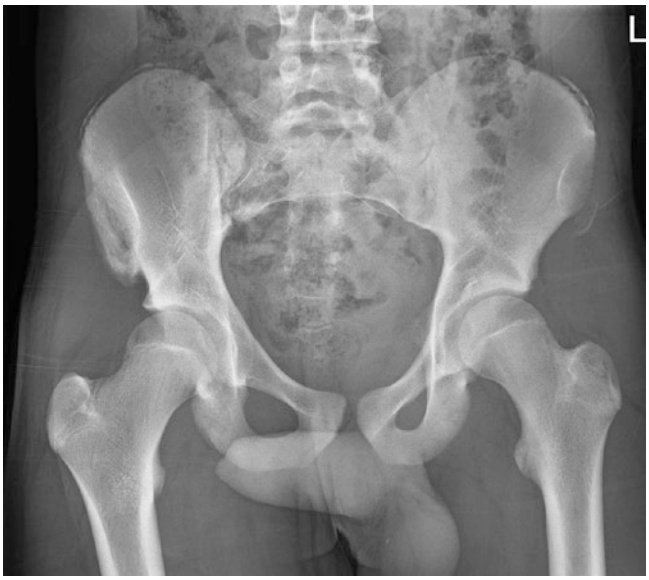

Fig. 7.64 Avulsion of the left anterior inferior iliac spine, at the rectus femoris insertion site. There is irregularity at the same site on the right due to previous similar injury

In the context of significant trauma, pelvic fractures may also be picked up where CT has been indicated for abdominal injuries.

The pelvic apophyses represent relatively weak points in the pelvic girdle, and may be avulsed by their muscular and tendinous attachments, typically in young athletes (Fig. 7.64). It is important not to mistake avulsed apophyses for secondary ossification centres.

Pain radiographs are used in imaging proximal femoral fractures, which may occur in significant trauma. Radiographs are useful in evaluating alignment, for example reduction in Thomas splint, and progress during healing. Femoral neck fractures are classified according to their relationship to the physis and trochanters.

Femoral diaphyseal fractures are usually complete fractures and evident on plain radiograph.

Slipped capital femoral epiphysis (SCFE) is a specific type of Salter-Harris type I fracture. Plain radiographs should include both a frontal and frog lateral view to increase sensitivity, as features are often more apparent on the lateral view. Initially there is widening of the physis and demineralisation of the metaphysis. The 'slip' itself involved posteromedial displacement of the capital femoral epiphysis. Plain films are useful in following up these children, remembering that this will be bilateral in around 20%. Both CT and MRI will detect early disease. MRI may show early marrow oedema.

Around the knee. This is an uncommon site for fracture. When fractures do occur around the knee, they tend to involve the epiphyses. Not all are evident on plain radiograph, and some require MRI for diagnosis. Salter-Harris type II are the commonest fracture type at the distal femur.

The anterior cruciate ligament inserts at the tibial spine, and this may be avulsed in a type of osteochondral fracture in children. This may be evident on plain film as a bone fragment in the tibial spine region, however these children will proceed to MRI which will confirm the origin of the bone fragment and also detect any concurrent injuries. See also Sects. 7.3.6, 7.3.1, 7.3.4, and 7.3.5.

Lower leg, ankle and foot. Fractures of the tibial diaphysis are usually apparent on radiograph. In toddler's fracture, the injury may be radiographically occult at first presentation. If suspected, repeat films in 7–10 days' time are advised, by which point there should be features of healing fracture such as periosteal reaction. Fibular fractures are less common, but with similar radiographic features.

Epiphyseal injuries of the distal tibia are usually Salter-Harris type II. Juvenile Tillaux fracture, named after the French surgical professor Paul Jules Tillaux, describes a Salter-Harris type III injury. It occurs in older children where the medial distal tibial growth plate has begun to fuse, and is distinguished from triplane fracture by lack of coronal component. In triplane fracture, there is additional coronal component in addition to sagittal fracture through the epiphysis and transverse fracture through the physis. CT is used to fully assess these injuries and for operative planning (Figs. 7.65, 7.66, and 7.67).

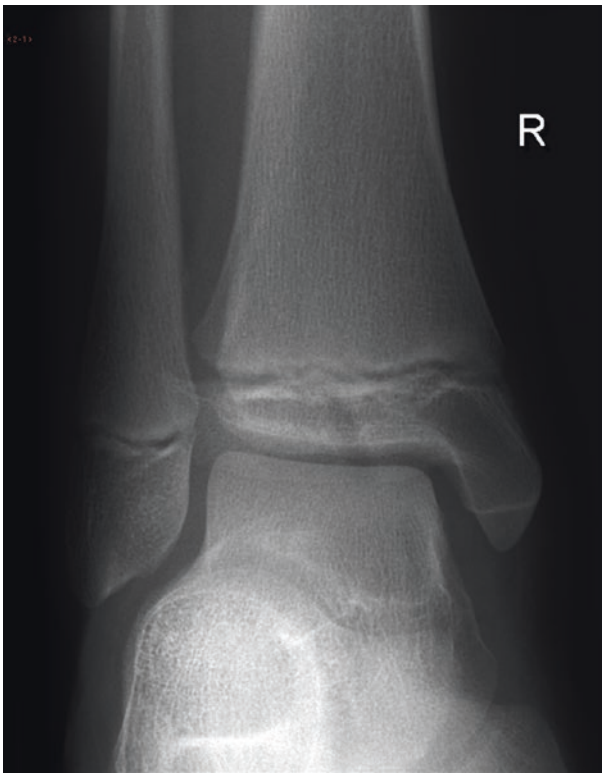

Fig. 7.65 Plain radiograph shows the sagittal component of triplane fracture through the distal tibial epiphysis on the AP view

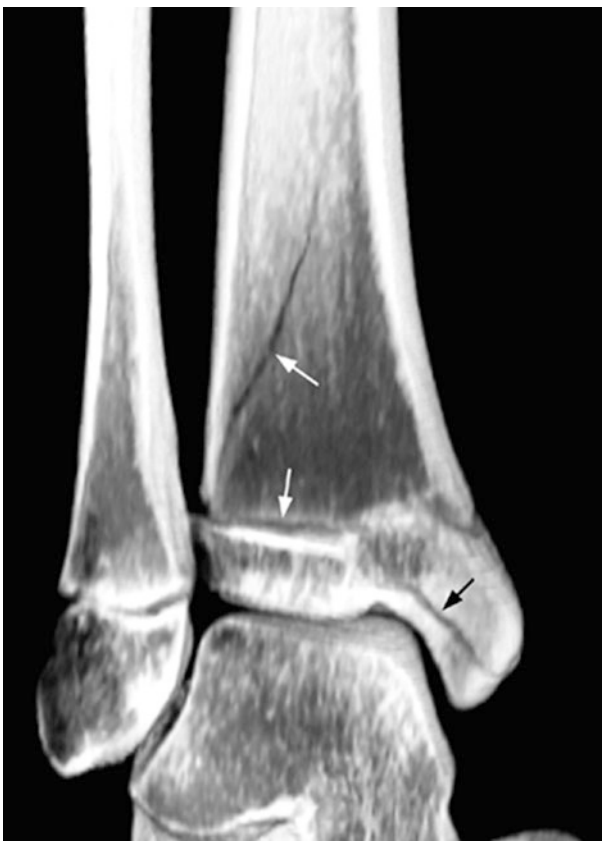

Fig. 7.66 CT demonstrated the three planes of fracture extension

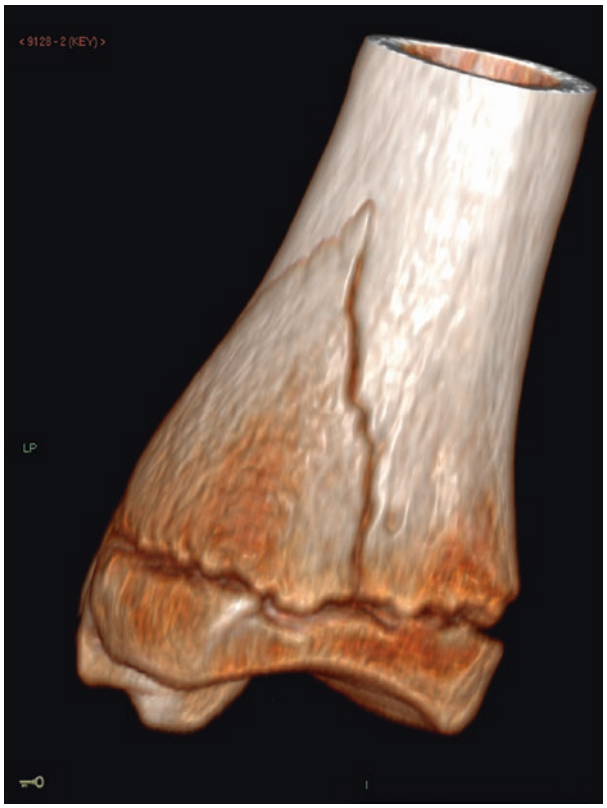

Fig. 7.67 CT reconstruction demonstrates the fracture in three dimensions

In plain films of os calcis fractures, features include sclerotic band through the bone, and loss of Bohler's angle which corresponds to depression of the os calcis due to fracture. Normal angle measures between 30° and 35°, and this angle is reduced in depressed fractures. Specific os calcis views improve sensitivity, however detail is often suboptimal and CT may be indicated for further information.

The most common fracture of the talar dome is ostechondral fracture.

Plain films are usually sufficient in assessment of fractures of the remaining bones of the foot. The fifth metatarsal is a common site of injury. Fracture at this site is most often transverse and therefore can be distinguished from the normal apophysis which is longitudinally orientated and appears at around 8 years. Avulsion of the apophysis may also occur.

Spinal fractures are rare in children. The cervical spine at C1/2 level is the commonest site in the under 8 age group. Technical difficulties and patient factors mean that obtaining adequate plain radiographs of the cervical spine is challenging. Where films are not adequate, for example where the cervical-thoracic junction or atlanto-axial junction is not visualised, cross-sectional imaging may be indicated. CT is often performed in the acute setting, and the child may proceed to MRI where soft tissue/ligamentous injury is suspected.

Cervical spine plain films may also be challenging to interpret due to a range of normal variants which can cause confusion.

These include multiple ossification centres, odontoid peg synchondrosis, apparent anterior vertebral body wedging (most commonly at C3), and pseudosubluxation of C2 on C3. A wider pre-odontoid space is seen in children compared with adults. A limit of 5 mm is used, compared with 3 mm in adults.

7.4.3 Non-accidental Injury (NAI)

The Royal College of Radiologists and Royal College of Paediatrics and Child Health publish guidelines on working in child protection. Good communication between all involved clinical teams and radiologists is crucial in all cases of suspected non-accidental injury, to ensure appropriate and safe investigation takes place. In terms of limb injuries, the question of non-accidental injury may arise from the clinical team or the radiologist. This may occur when an injury is not consistent with the stated history, and/or when specific patterns of injury are seen. Where NAI is included in the differential, skeletal survey may be undertaken. In children under 2 years old, skeletal survey forms part of the standard initial imaging. In older children this is performed selectively. Guidance recommends supervision of surveys by a radiologist, and that surveys are best performed during normal working hours. Skeletal surveys comprise a standard series of radiographs to image the entire skeleton. The limbs should ideally be straight and at least AP projections obtained of both sides. Standard limb views where possible are:

- AP of both upper arms
- AP of both forearms plus coned lateral elbow and wrist views
- AP both femora
- AP both lower legs plus coned lateral knee and ankle views
- PA hands
- DP of feet

Supplementary lateral or coned views may be added by the supervising radiologist, often to give additional detail of a metaphysis (Fig. 7.68). Follow-up views can improve sensitivity for metaphyseal fractures. CT may be indicated for additional information to characterise a limb fracture. Cross sectional imaging also provides information on associated soft tissue injuries where indicated. In limbs, metaphyseal fractures (also known as bucket handle or corner fractures) have a very high specificity for non-accidental injury (Fig. 7.68). They occur due to shearing forces on the growth plate. Diaphyseal fractures are non-specific, occurring in both accidental and non-accidental injury. Where the clinical history is not compatible with the pattern of injury or age of the child, the possibility of NAI is raised. A spiral fracture of the femur, for example, would not result from a fall, and would not be expected in a non-ambulant child. It can be difficult to accurately 'age' a fracture on plain film, particularly metaphyseal fractures, as these do not heal with callus formation. If a metaphyseal fracture is visible, this implies it is less than 4 weeks old. Diaphyseal fractures begin to heal at 1 week and complete by 12 weeks. It is important to look for radiological features of possible underlying conditions such as osteogenesis imperfecta, which predisposes to fracture.

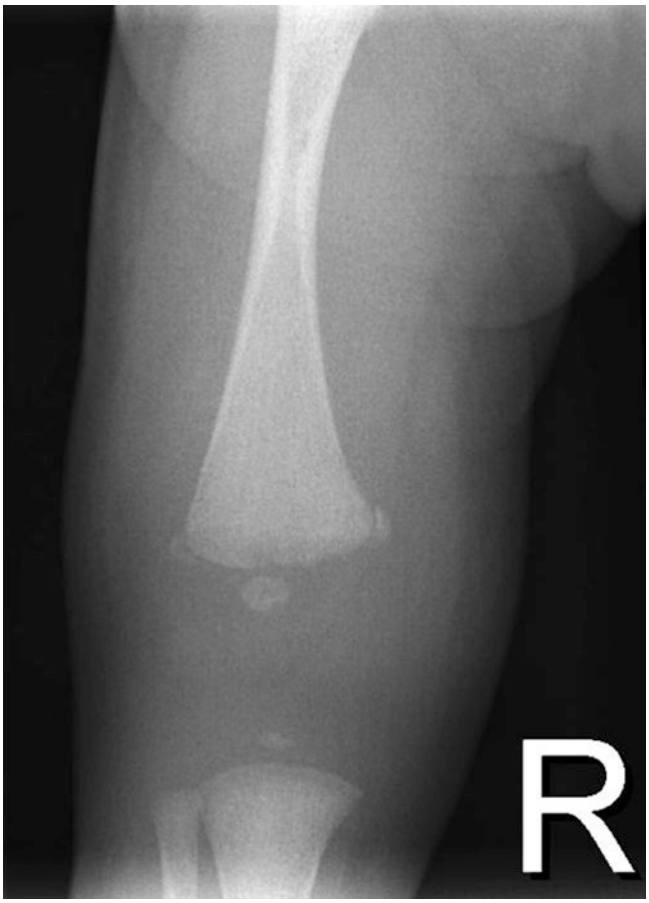

Fig. 7.68 Classic metaphyseal corner fractures, an injury with high specificity for non-accidental injury

7.4.4 Haemarthrosis

Blood within a joint is a type of effusion, with the commonest cause being trauma.

7.4.4.1 Lipohaemarthosis

Most commonly seen in the knee, haemarthrosis may be demonstrated on lateral plain film following intra-articular fracture. Fat and blood leak from the bone marrow into the joint, typically following tibial plateau fracture or distal femoral condylar fracture, and form a fat-fluid level, where the less dense fat layer is seen above more dense fluid layer. For this distribution to be seen, the film must be performed as a horizontal beam lateral. With undisplaced fractures, this may

be the only radiographic abnormality to imply the diagnosis (Figs. 7.69 and 7.70).

CT and MRI well demonstrate lipohaemarthrosis, and have superior tissue contrast, demonstrating three distinct layers—fat superiorly, lying above serous/synovial fluid, with blood cell layer lying dependently beneath. These layers may also be seen on ultrasound, although US is less likely to demonstrate the underlying bony injury (Figs. 7.71 and 7.72).

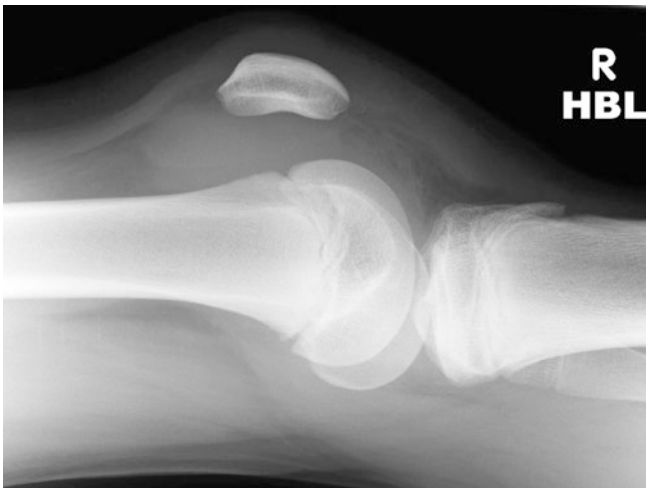

Fig. 7.69 Fracture of inferior pole of patella with well-defined homogeneous soft tissue density within the suprapatellar recess, in keeping with haemarthrosis

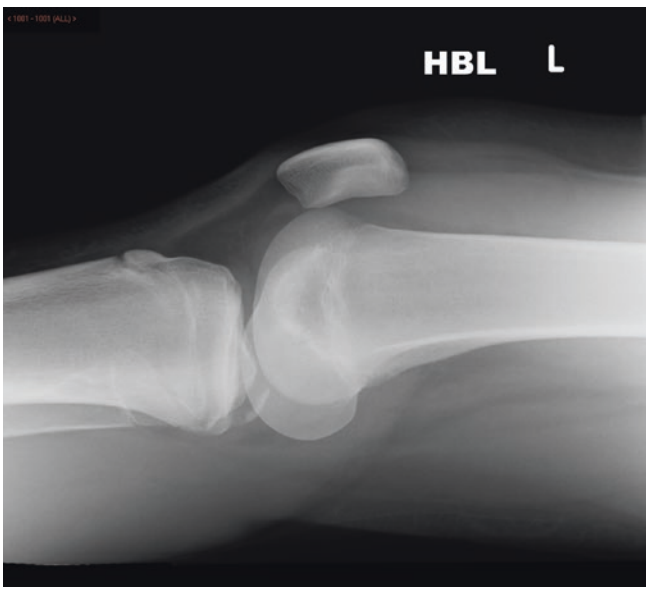

Fig. 7.70 Horizontal beam lateral view of the knee following trauma shows the typical fat-fluid level seen in lipohaemarthrosis, indicating intra-articular fracture

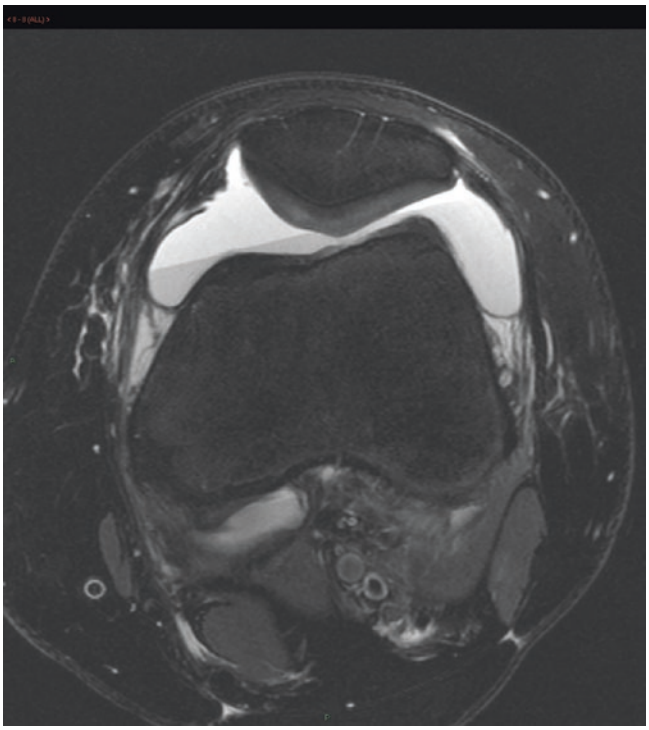

Fig. 7.71 Axial proton density MRI of the knee demonstrating fat-fluid level, with blood products lying dependently

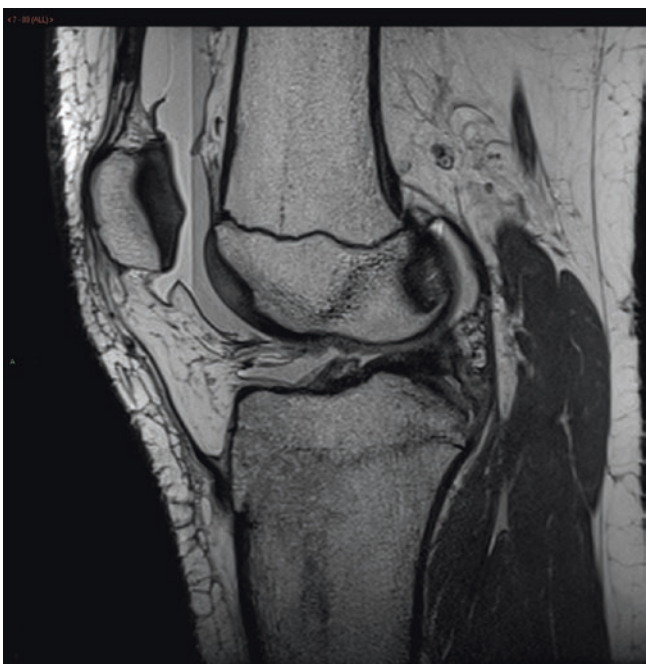

Fig. 7.72 Lipohaemarthosis on sagittal T1W MRI of the knee

7.4.5 Osteochondritis Dissecans

Plain films are performed initially, however the osteochondral defect may be radiographically occult. The femoral condyles are the commonest site, however other locations include the talar dome and capitellum. In the case of femoral injury, intercondylar views may be helpful. Early signs include poorly defined lucency or flattening at the site. This may progress to more conspicuous changes in density and irregularity of the bone. The bone fragment may be surrounded by a lucent rim. If displaced, the bone fragment may appear as an intra-articular body, particularly seen in the knee.

MRI is the preferred modality, confirming presence of an osteochondral defect and providing information regarding stability to guide management. The main MRI signs of an unstable injury include (Figs. 7.73 and 7.74):

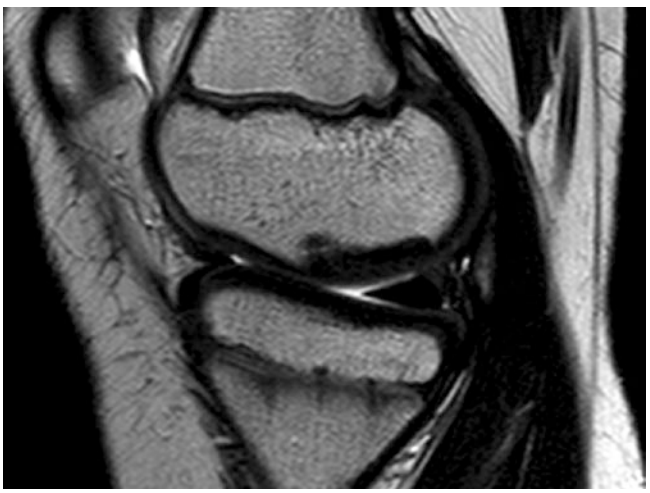

Fig. 7.73 Osteochondral fragment on MRI. There is a well-defined focal signal abnormality at the cortical surface of the medial femoral condyle, the commonest site

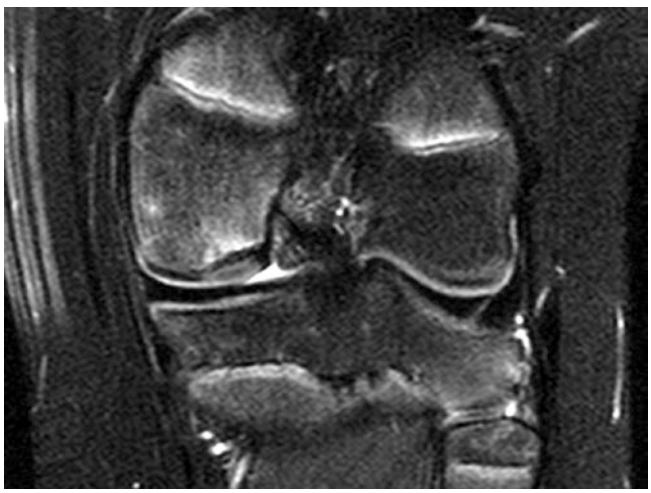

Fig. 7.74 Oedema surrounds the osteochondral fragment on this coronal T2 fat-saturated image

1. Linear fluid signal between fragment and donor site
2. Linear signal abnormality through the articular cartilage
3. Focal defect in cartilage
4. Cystic area beneath the fragment (measuring 5 mm or greater)

MRI is also useful in follow-up of conservatively managed children [2].

7.4.6 Patellar Region Conditions

7.4.6.1 Prepatellar Bursitis

The bursa directly overlying the superficial aspect of the patella may be acutely swollen with blood or serous fluid following a local injury. This usually subsides with protection of the part and chronic bursitis (housemaid's knee) is rare in children. Acute infection as a result of a penetrating injury or secondary to local soft tissue infection should be treated with antibiotics and possibly with surgical incision and drainage. Until positive bacteriological information is obtained, an antistaphylococcal antibiotic should be used on a "best guess" basis.

7.4.6.2 Semi-membranosus Bursa

This bursal swelling is relatively common—usually presenting as a painless, non-tender swelling in the medial part of the popliteal aspect of the knee just lateral to the tendon of semi-membranosus. The swelling is tense and most apparent with the knee extended, disappearing into the relaxed soft tissues as the knee bends. This bursa is deeply attached to but not in communication with the back of the knee joint. If large or persistently present the bursa can be excised but as may disappear spontaneously this treatment should be postponed for a year or more.

7.4.6.3 Patellar Dislocation

Typically occurring in athletic children as a result of direct medial blow or pivoting injury, subluxation or dislocation of the patella involves lateral displacement of the patella. It may occur repeatedly as a chronic condition. Both cause and effect may be demonstrated on imaging.

Plain films performed are AP, lateral and skyline view. The skyline view is most sensitive at demonstrating lateral displacement in relation to the femoral condyles, but may be normal in the case of transient dislocation.

MRI provides more information, particularly medial retinacular insertion avulsion, osteochondral defect, effusion/haemarthrosis, and bone oedema within the medial patella and lateral femoral condyle caused by impact of these surfaces during the injury. This pattern of findings indicates patellar dislocation. MRI may suggest this diagnosis in children scanned to look for other injuries such as

meniscal or cruciate injury, as it is not always suspected clinically.

MR or plain film may also reveal a shallow trochlear groove which predisposes to chronic patellar dislocation [16, 17].

7.4.6.4 Patellar Bursa

Diagnosis is often clinical. Ultrasound will easily confirm fluid collection in the pre-patellar bursa, and this will also be well seen on MRI, as will internal haemorrhage. Imaging can differentiate from soft tissue swelling. Plain film will demonstrate pre-patellar soft tissue swelling, and sometimes punctuate calcification if there has been internal haemorrhage [18].

7.5 Tumours

7.5.1 Sarcoma

Certain neoplastic conditions may present with bone or muscular pain, in particular these may be very misleading and result in delay of diagnosis. Bone lesions are common in leukaemia in children and may take the form of decalcification, osteoporosis, or subperiosteal shadows. Usually the presenting complaint is that of pain in the limbs, and bone changes may be mistaken for a low grade osteitis or even at times (growing pains). Another malignancy which presents with bony involvement is neuroblastoma which can be mistaken for an inflammatory condition of the bones or the joints. Langerhans cell histiocytosis used to be known as 'histiocytosis X'. Stage I, single lytic bone lesion and stage II multiple lytic bone lesions (both formerly known as eosinophilic granuloma of bone) can present with isolated bone pain.

Osteosarcoma and Ewing's sarcoma make up the majority of malignant bone tumours in children. Both have features of aggressive bone lesions, however differences in clinical and imaging features normally permit differentiation. Osteosarcoma tends to arise at the metaphyses (Figs. 7.75 and 7.76), while Ewing's occurs in the metaphyses and diaphyses, and occurs more frequently in flat bones. The matrix of an osteosarcomatous lesion tends to be 'cloud-like', compared with Ewing's which does not tend to be mineralised or sclerotic. The typical patterns of periosteal reaction also differ, with a 'sunburst' reaction or Codman triangle seen in osteosarcoma, and 'onion skin' pattern typically seen in Ewing's. Both tumours metastasise to lung, however bony metastases are seen in osteosarcoma but rarely in Ewing's. Plain film may also demonstrate pathological fracture. Cross sectional imag-

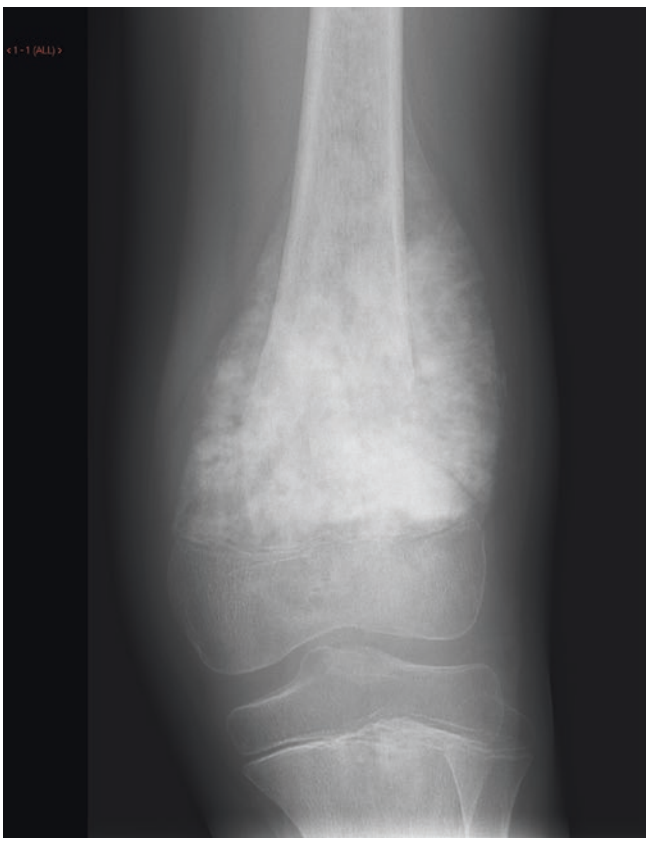

Fig. 7.75 Aggressive, bone-forming lesion of the distal femoral metaphysis on plain radiograph, proven osteosarcoma on biopsy

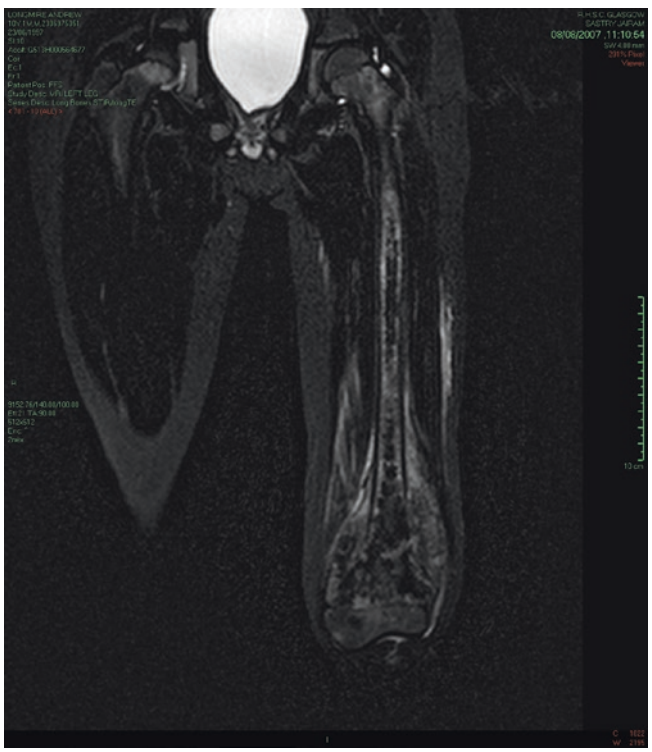

Fig. 7.76 Aggressive features of osteosarcoma on coronal STIR MRI, including cortical destruction periosteal reaction, and oedema in the surrounding musculature

ing is performed for biopsy/surgical planning purposes, staging, and to provide a baseline for follow-up purposes. CT chest is performed to identify pulmonary metastases, bone scan to image the primary lesion and look for bone metastases. Baseline chest radiograph is also performed. Pre- and post-contrast enhanced MRI is necessary for accurate local staging. Intraosseous tumour extension and soft tissue involvement are assessed, essential for surgical planning, particularly limb sparing surgery (Figs. 7.77, 7.78, and 7.79).

7.5.2 Eosinophilic Granuloma

The terms 'eosinophilic granuloma' (EG) and 'Langerhan's cell histiocytosis' (LCH) are often used interchangeably, however frequently EG refers to a single lesion whereas LCH refers to multiple and often multisystem lesions. The skeletal system is the most commonly affected body system. Lesions may be solitary or multiple. In asymptomatic children, lesions may be discovered on imaging incidentally, for example on a limb plain film performed following trauma to look for fracture. Almost half of lesions are found in the skull, almost a quarter in the pelvis, with the remaining seen in the femur, ribs, humerus, mandible and spine. The typical appearance of a skull vault lesion on plain film is a punched-out, lytic lesion with bevelled borders (Fig. 7.80). In the maxilla or mandible, a 'floating teeth' appearance is typical. Vertebral lesions may result in a vertebra plana appearance.

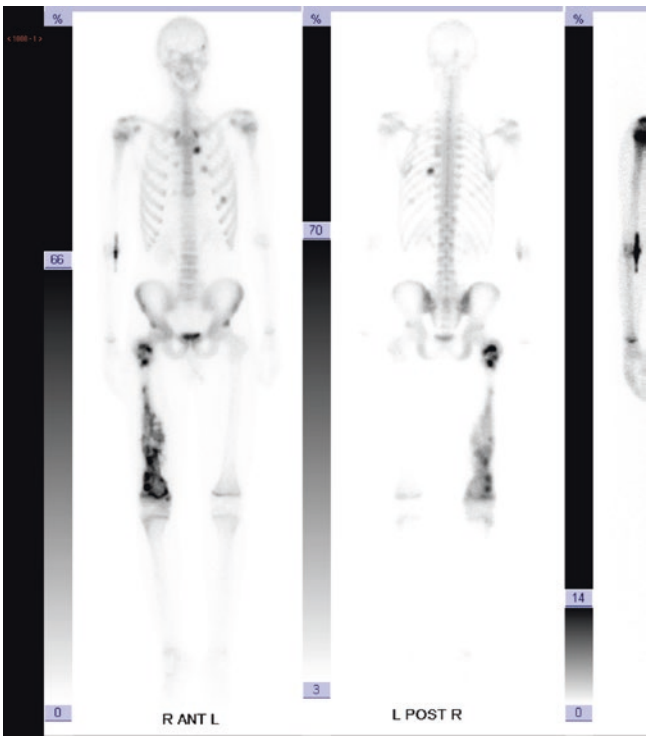

Fig. 7.78 Delayed phase bone scan shows intense uptake in the distal right femur, with additional uptake at the proximal femur

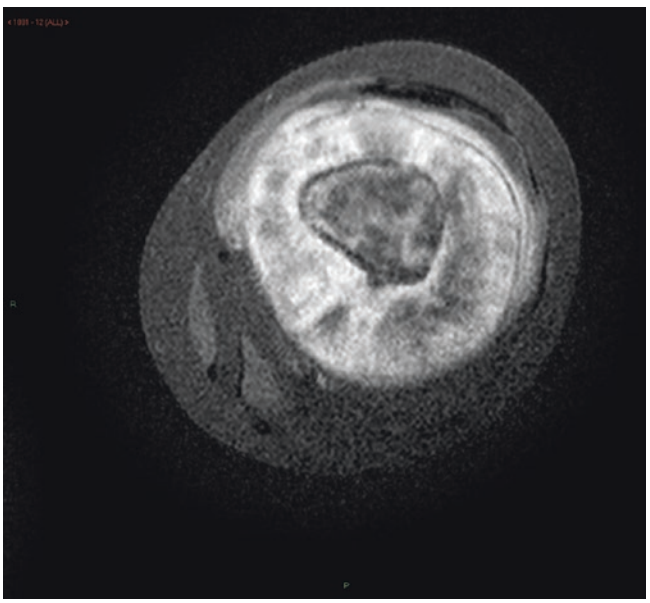

Fig. 7.77 Florid enhancement of the lesion on contrast enhanced axial MRI of the distal femur

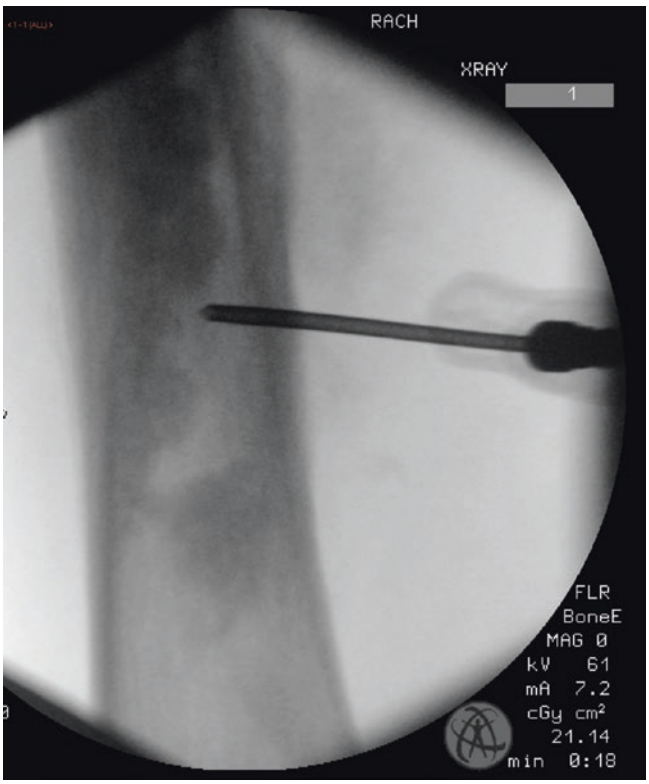

Fig. 7.79 Fluoroscopic-guided bone biopsy of distal femoral lesion, proven to be osteosarcoma

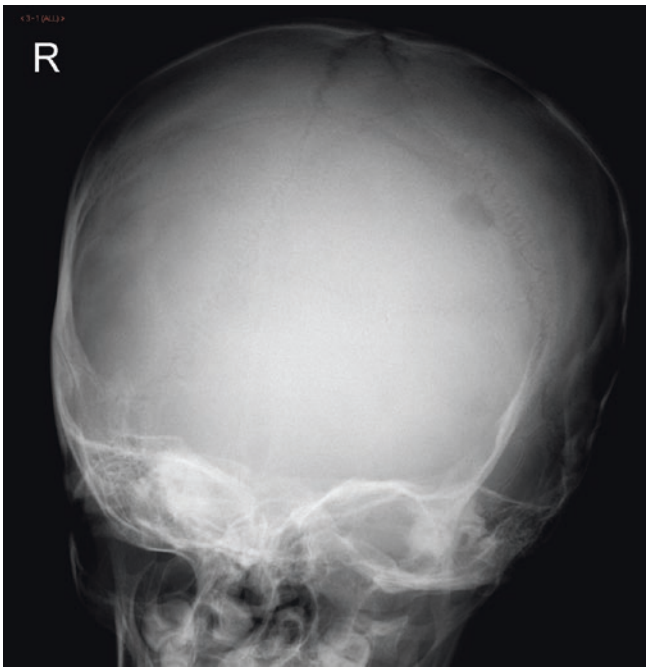

Fig. 7.80 Typical well-defined lytic lesion of the skull vault in LCH

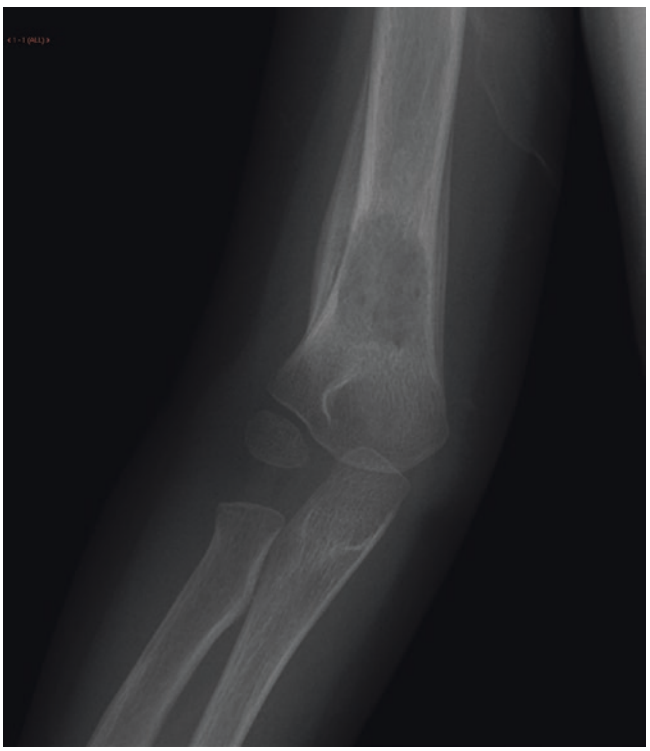

Fig. 7.81 Plain radiograph of the elbow shows lucent lesion of the distal humerus with lamellated periosteal reaction and endosteal scalloping. Non-specific mixed features, in this case of LCH

Radiographic appearances however are variable, and both aggressive and non-aggressive features may be present, depending on the phase of disease (Fig. 7.81) Aggressive features include periosteal reaction, cortical thinning, endosteal scalloping and soft tissue mass. With a solitary aggressive lesion, appearances are often non-specific and will be included in a differential diagnosis which will often include infection and bone tumour. Multiple rather than solitary lesions are more suggestive of LCH. Skeletal survey is often performed to identify quiescent lesions. This is useful for both diagnosis and follow-up. Additionally a survey may identify a lesion more amenable to biopsy than the initial lesion. Isotope bone scan is also performed at first assessment along with skeletal survey, as both modalities together provide an improved sensitivity. For follow-up, skeletal survey alone is normally performed. CT may be helpful in planning biopsy or surgery. Whole body MRI offers an alternative means of detecting and following additional lesions. MRI also demonstrates associated soft tissue components. Disease localised to the skeleton, particularly unifocal disease, has a good prognosis.

7.5.3 Ewing's Sarcoma

Sarcoma of bone is more common in the young adult while Ewing's sarcoma is more common in early childhood. In osteosarcoma the long bones are primarily affected and there is early spread of the disease to the lung. Children usually present with bone pains and diagnosis is made on radiograph. Improvement in survival has been dramatic since the introduction of chemotherapy plus surgery as compared with previous poor results with surgery alone. In Ewing's sarcoma the malignancy may be of primitive neural cells and presents with bone pain and tissue swelling and is radiosensitive as well as responsive to chemotherapy (Figs. 7.82 and 7.83).

7.5.4 Neurofibromatosis

MRI is the primary imaging modality. Lesions tend to be well defined and arise from nerves or neural plexus. Imaging cannot reliably differentiate benign neurofibroma or schwannoma from malignant peripheral nerve sheath tumour. Features associated with malignant peripheral nerve sheath tumour (MPNST) include larger size, irregular border, and rapid growth. Other features of NF1 may be present.

7.6 Acquired

7.6.1 Slipped Capital Femoral Epiphysis

Although much less common than congenital hip dislocation or Perthes disease, this condition is important and early diagnosis will avoid possible crippling deformity and complications.

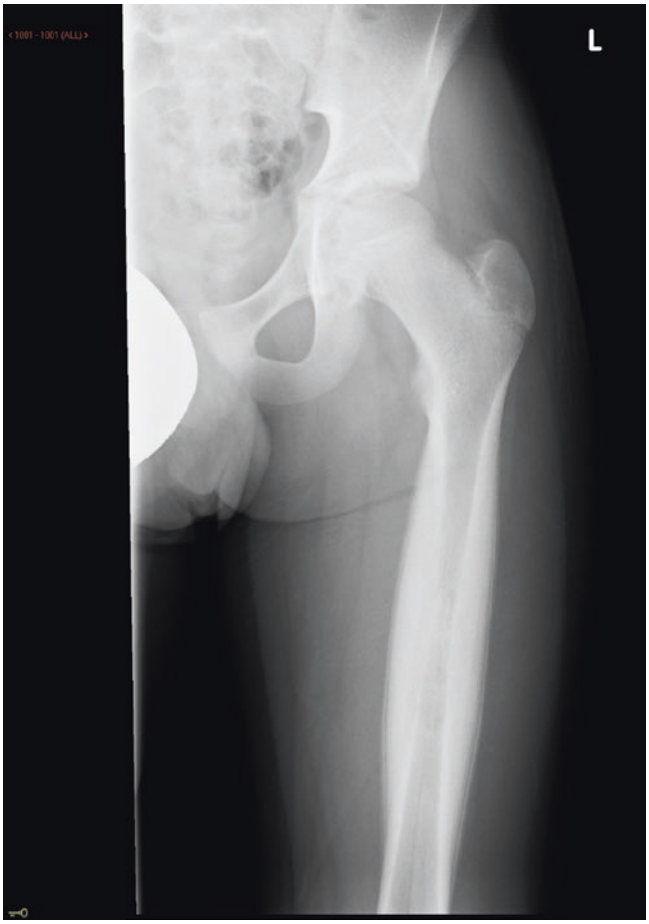

Fig. 7.82 Aggressive lesion of the femoral diaphysis with layered periosteal reaction in this case of Ewing's sarcoma

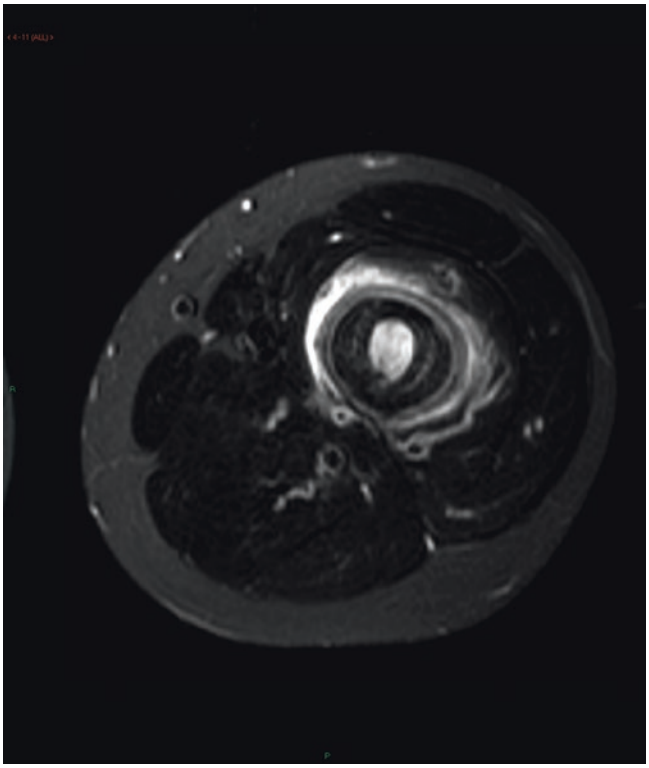

Fig. 7.83 Axial T2W MRI in Ewing's sarcoma. There is circumferential periosteal reaction of the femoral diaphysis with surrounding soft tissue oedema

The condition occurs in the pre-pubertal child usually within the age groups of 10–14 years in girls and 12–16 years in boys. Three-quarters of these children are obese or taller than average. The pathology is one of weakness at the upper femoral epiphyseal plate so that relative to the neck and shaft of the femur the femoral head epiphysis slips backwards. Although the alternative name of coxa vara would suggest a medial and downward slip the main direction of movement is backwards. The slip of the femoral head is insidious and initially the symptoms are slight, with limp and pain at the hip but such pain is often referred to thigh and knee. Depending on the severity of symptoms the adolescent may be detected early with a minimal slip of may proceed over months to a severe deformity and superimposed upon the gradual slip may be a sudden detachment of the femoral head so that symptoms are severe and the child resembles one with a femoral neck fracture. The child thus tends to present in one of three different ways—with minimal slip, massive chronic slip, or with an acute severe displacement. The diagnosis should be suspected in any adolescent particularly if heavily built or tall, who presents with a limp and pain. In the early minimal slip there may be little clinical abnormality except for slight restriction of flexion, abduction and internal rotation. As the degree of slip increased a frank external rotation deformity will develop. In advanced slips the condition will be obvious in antero-posterior radiographs but in minor degrees the AP view may appear normal and it is essential to have lateral view radiographs which are needed to demonstrate the backward slip (Figs. 7.84, 7.85, and 7.86). *See* Sect. 7.3.3.

7.6.2 Lead Poisoning

Lead is usually ingested in small quantities over long period and the manifestations of poisoning develop insidiously. There are various possible sources of lead such as lead-containing paint which may be used on a child's cot, flakes or paint from plasterwork or woodwork in old Victorian houses, burnt out lead batteries or swallowed pieces of yellow crayon. Pica is common in children suffering for lead poisoning and is a valuable clue to the diagnosis. It is more common in children from the poorest homes. Surma which contains lead sulphide is applied to the eyelids and conjunctivae of infants and children by Asian mothers, mainly for cosmetic reasons. It seems that an appreciable absorption of

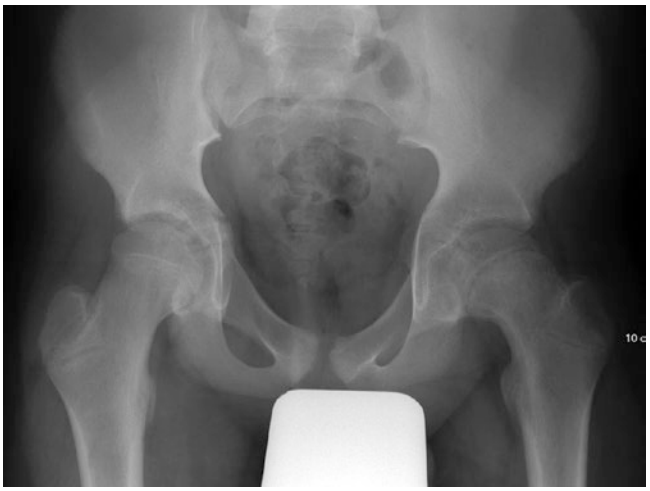

Fig. 7.84 Plain radiograph of left slipped femoral epiphysis

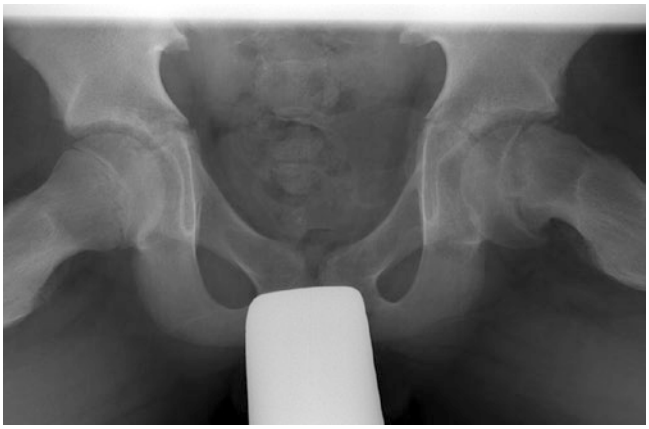

Fig. 7.86 Slipped epiphysis is often best seen on the frog lateral view. There is postero-medial displacement of the left capital femoral epiphysis. The right side is normal

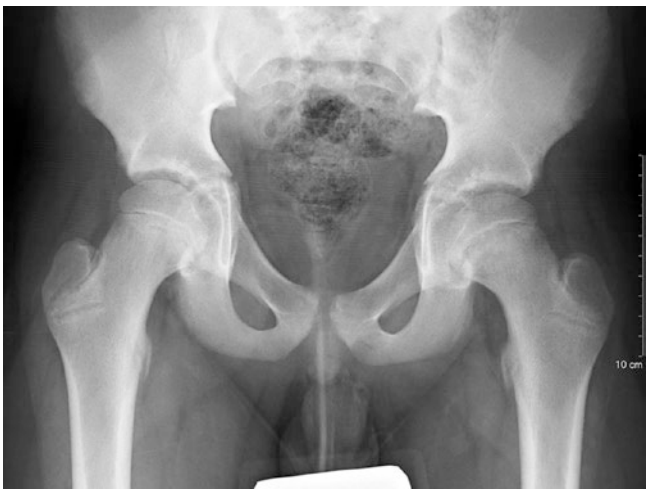

Fig. 7.85 Frontal view of the pelvis shows some demineralisation around the left proximal femoral physis, however the extent of the abnormality is much better appreciated on the frog lateral view

lead in these children occurs from drainage down the tear duct, or from rubbing the eyes and then licking the fingers. An early diagnosis is extremely important in lead poisoning because if it is left untreated lead encephalopathy may result in death or permanent brain damage.

The earliest signs such as lethargy, anorexia, vomiting and abdominal pain, are too common to arouse suspicion in themselves, but their persistence without other discoverable cause should do so. The pallor of anaemia is a frequent and characteristic sign. Insomnia and headache frequently precede the onset of lead encephalopathy with convulsions, papilloedema and a cracked-pot sound on percussion of the skull. Radiographs of the skull may then reveal separation of the sutures. Peripheral neuropathy is uncommon in the young child but may develop with paralysis of the dorsiflexors of the wrist or feet. Radiographs of the bones may show characteristic bands of increased density at the metaphyses but this is a relatively late sign and, therefore, of limited diagnostic value. Excess amino-aciduria is a common manifestation of renal tubular damage and glycosuria may also occur. Renal hypertension has also been reported. The most dangerous development, both in regard to life and future mental health, is lead encephalopathy. Depending upon the amount of lead ingested, this dreaded complication may develop quite quickly, or only following a long period of relatively mild ill-health.

The diagnosis of lead poisoning can be justified in the presence of two or more of the following findings:

1. Microcytic hypochromic anaemia with punctate basophilia.
2. Radio-opaque foreign bodies in the bowel lumen and lines of increased density at the growing ends of the long bones.
3. Coproporphyrinuria.
4. Renal glycosuria and amino-aciduria.
5. Raised intracranial pressure and protein in the cerebrospinal fluid.

However, the most sensitive test is a marked increase in the urinary excretion of lead after an oral dose of D-penicillamine, 20 mg/kg/day. Increased excretion of delta-aminolaevulinic acid is less commonly found in the child than in the adult with chronic lead poisoning. Interpretation of the blood lead concentration is, unfortunately, much more difficult. While levels below 1.9 μmol/L (40 μg/100 mL) exclude lead poisoning and levels in the region of 2.9 μmol/L (60 μg/100 mL) are associated with clinical signs it is possible that behaviour and learning difficulties occur at values between these levels.

Lead accumulates in the metaphyses, resulting in plain film appearance of dense metaphyseal bands. These appearances have a wide differential, including chronic anaemia, drugs, growth arrest lines, treated leukaemia, renal osteodystrophy, healing rickets and trauma. See Sects. 7.5.10 and 7.5.11.

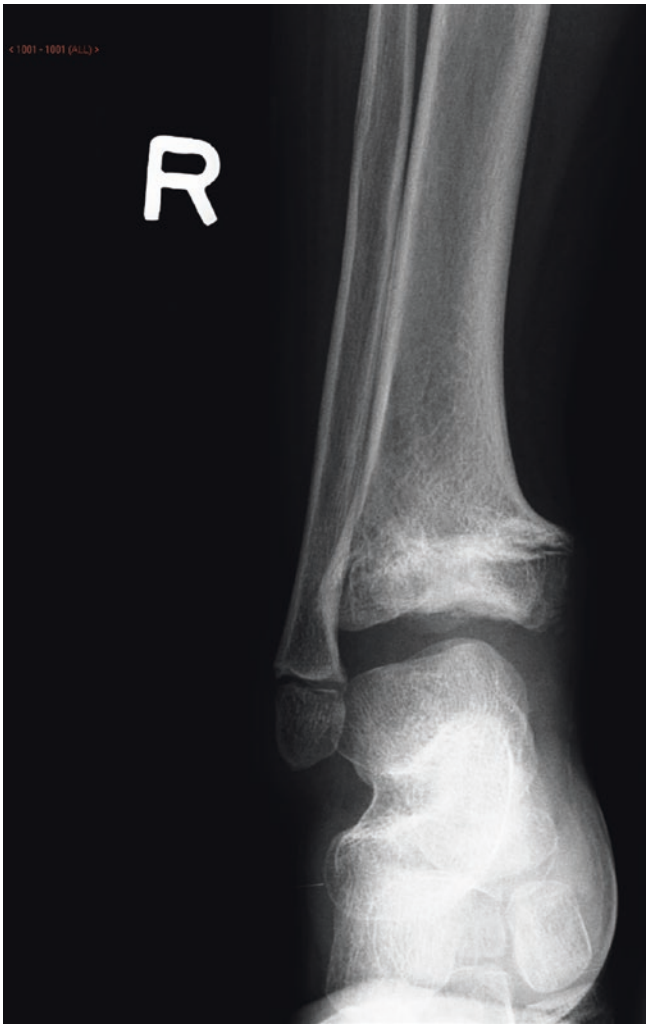

Fig. 7.87 Premature closure of the distal tibial physis and associated growth arrest secondary to meningeal sepsis

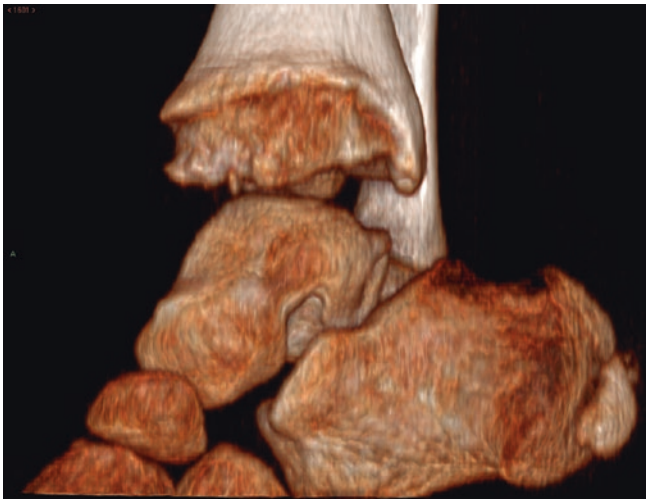

Fig. 7.88 3D CT reconstruction of the ankle joint in the same child showing abnormality of the distal tibial physis

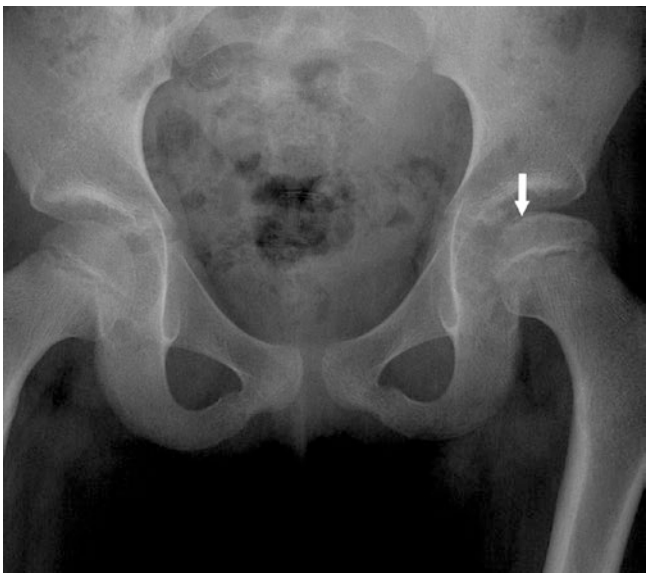

Fig. 7.89 Left-sided Perthes disease with reduction in height and sclerosis of the upper femoral epiphysis. A subtle subarticular lucent crescent can also be seen (arrow)

7.6.3 Impaired Growth (Vascular)

Premature epiphyseal closure may occur secondary to a variety of causes, resulting in shortened bone. Broadly speaking, any insult which disrupts blood supply to the physeal cartilage may result in premature closure and growth arrest (Figs. 7.87 and 7.88) This includes fracture, causes of local hyperaemia such as infection, arthritis, haemophilia and arteriovenous malformation, and rarer traumas including bone infarct, radiation or thermal injury, metabolic and congenital causes. Premature growth plate fusion is seen on plain radiograph.

7.6.4 Perthes Disease

Plain films are performed in the first instance and should include frontal and frog leg lateral views, as subtle findings, particularly subchondral lucency, may only be evident on the latter. Findings are as with any cause of avascular necrosis, and may be absent in the early stages (Figs. 7.89 and 7.90).

Early findings:

- Joint effusion: widened joint space
- Increased density of the capital femoral epiphysis
- Loss of clarity of the physis
- Lucency of the proximal metaphysic

Later findings:

- Fragmentation of the CFE
- Subchondral lucency (crescent sign)

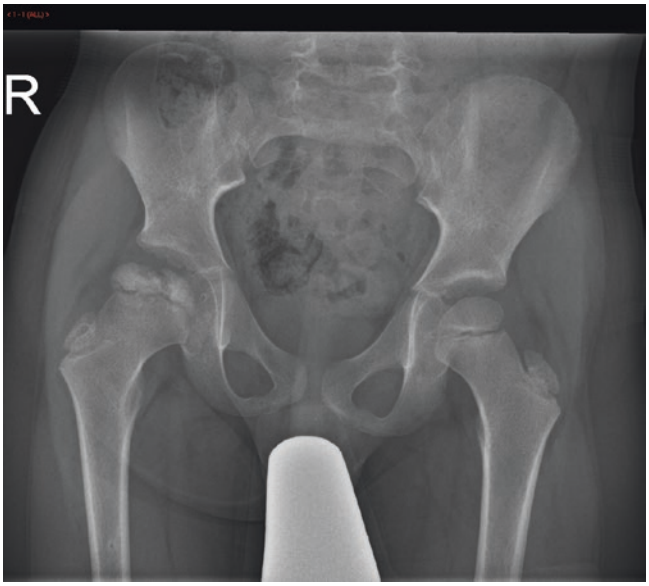

Fig. 7.90 Advanced Perthes disease of the right hip. Fragmentation and sclerosis of the CFE, with coxa magna deformity

Advanced findings:

- Widening and flattening of the femoral head
- Coxa magna deformity

MRI is more sensitive in the early stage, demonstrating epiphyseal oedema and reduced enhancement. In later-stage disease, MRI is useful for assessing femoral head deformity, congruency with the acetabulum, and containment within the acetabulum. Plain films are used in follow-up. It is important to examine the other hip for signs of avascular necrosis as this condition is bilateral in 10%, occurring asynchronously. Symmetric involvement suggests an alternative diagnosis [2, 19].

7.6.5 Femoral Aneurysm

Femoral artery pseudoaneurysm is usually iatrogenic, usually secondary to an endovascular procedure for which the femoral artery has been used for access. The diagnosis is usually confirmed on ultrasound, showing rounded vascular area adjacent to the puncture site. Colour Doppler demonstrates turbulent flow, typically resulting in a 'yin-yang' sign. Thrombus may have begun to form with the sac. Ultrasound is used to guide therapeutic thrombin injection where the neck is considered of small enough calibre. CT angiography shows contrast enhancement within the sac adjacent to the femoral artery puncture site. This may be performed in assessment for amenability to US guided thrombin injection (Figs. 7.91, 7.92, 7.93, and 7.94).

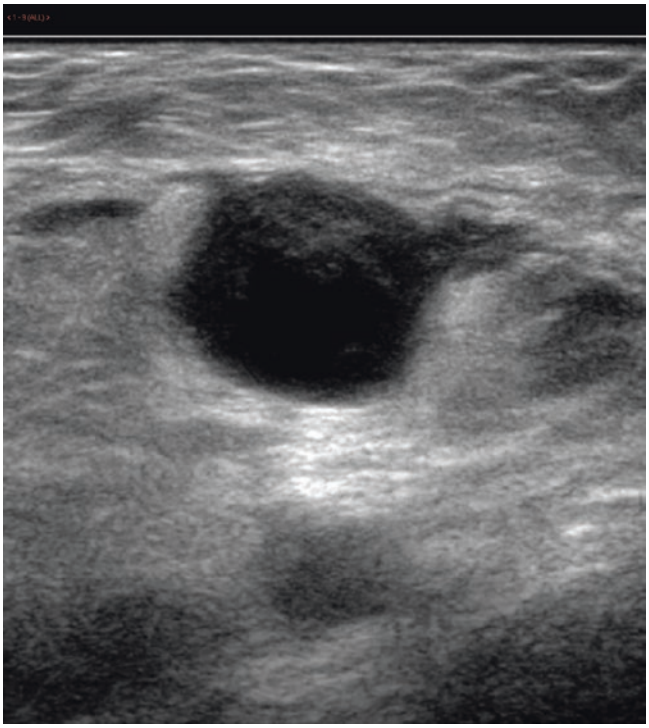

Fig. 7.91 Ultrasound of the left groin in a child with groin swelling following cardiac catheterisation. Greyscale image shows focal dilatation at the left common femoral arterial puncture site

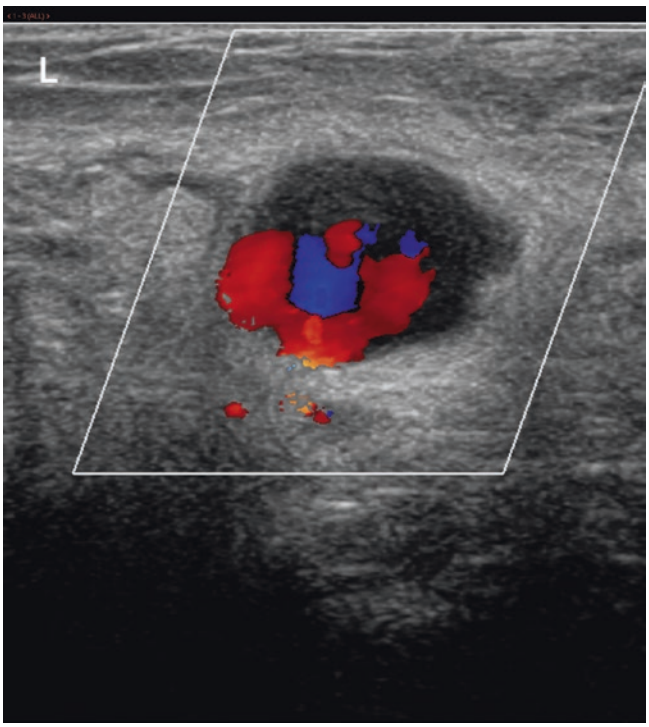

Fig. 7.92 Turbulent flow on colour Doppler with 'yin-yang' appearance typical of pseudoaneurysm

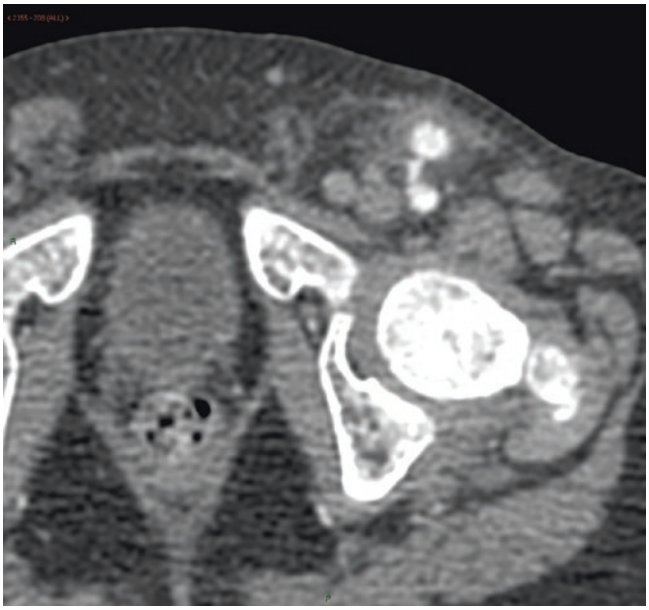

Fig. 7.93 Arterial phase CT scan confirmed focal pseudoaneurysm sac communicating with the left common femoral artery at the puncture site

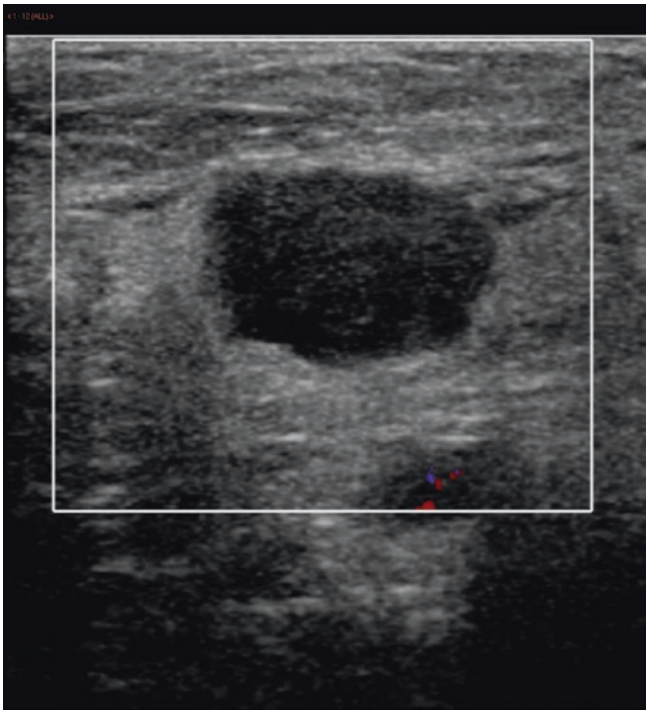

Fig. 7.94 Complete thrombosis of the pseudoaneurysm sac following ultrasound guided thrombin injection. No further treatment was required

7.6.6 Tumoral Calcinosis

Tumoral calcinosis (TC) is a rare condition, often with a familial basis, characterised by progressive, ectopic, periarticular deposits of calcium. These tumour-like growths which often infiltrate muscle and tendon, usually present as painless, solitary or multiple masses, typically found at large joints such as the shoulders, elbows or hips and less frequently the foot, leg, knee, and hand. The condition was first mentioned in the medical literature by Giard and Duret in 1898 and 1899, but the term 'tumoral calcinosis' did not become a defined clinical entity until it was described in the US literature by Inclan and colleagues in 1943. TC can manifest in three separate clinical settings: (1) as familial tumoral calcinosis; (2) in dialysis dependant patients with renal disease; and (3) in seemingly idiopathic sporadic cases without evidence of related abnormalities. An autosomal recessive metabolic disorder, generally observed in patients within the first two decades of life, who tend to have multiple areas of calcification. A positive family history is encountered in 30–40% of cases and there is a significantly higher incidence in those of sub-Saharan African descent.

Typical plain radiographic appearance is that of periarticular amorphous, lobulated calcification. CT helps to distinguish from other pathologies, as in this condition no destruction of the underlying bone is seen (Fig. 7.95).

7.6.7 Embolism

Peripheral arterial embolism in children is rare. Sometimes this is seen in infants who have had femoral arterial catheters, for example cardiac babies during PICU admission. Thrombus may accumulate secondary to catheterisation of the vessel and embolise distally resulting in an ischaemic limb. It is important not to allow imaging to unnecessarily delay treatment in this emergency situation.

Where imaging is indicated, Doppler ultrasound may be diagnostic. Greyscale imaging may visualise the thrombus itself, while colour Doppler provides information on vessel patency, speed and direction of flow. Spectral Doppler waveforms provide more detailed information, reflecting haemodynamic factors. In the normal lower limb, triphasic high-resistance waveforms are seen. This waveform is comprised of a systolic high resistance peak, followed by diastolic reversal, and a little forward diastolic flow. Where there is proximal occlusion, turbulent flow in the distal vessel occurs, there is loss of the steep systolic peak, and loss of normal diastolic reversal of flow.

CT, MR or catheter angiography provide additional means of imaging the vascular tree. Interventional radiologists can

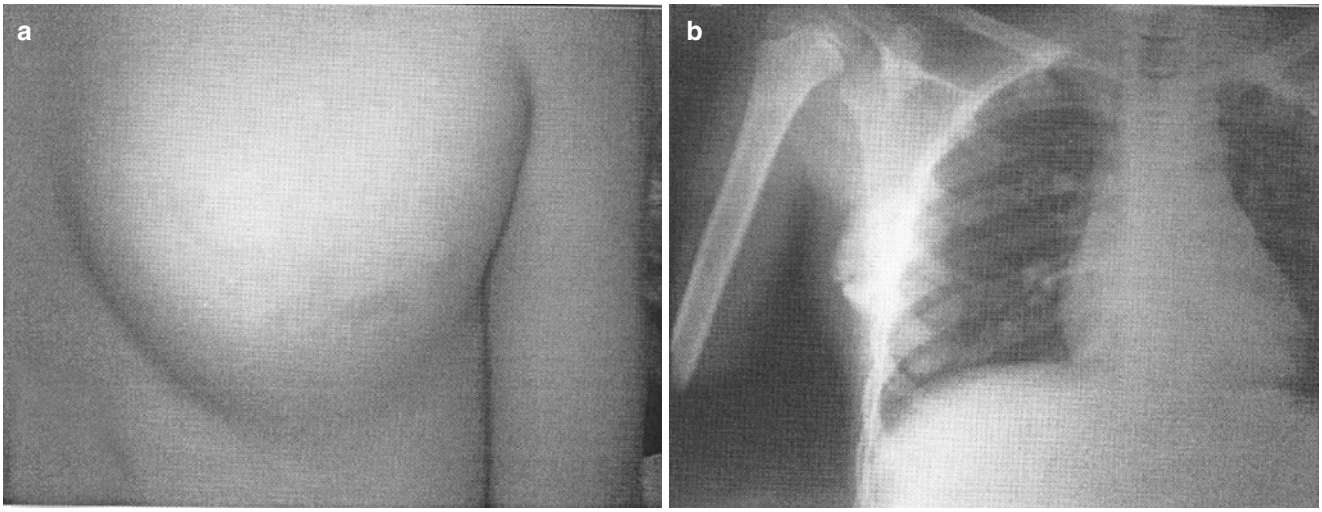

Fig. 7.95 Tumoral calcinosis of the chest wall. (**a**) Clinical picture. (**b**) Plain chest radiograph

offer catheter-directed thrombolysis or thrombectomy in appropriate cases.

7.6.8 Cavovarus

Weight-bearing plain films are performed. There is excessive plantar flexion of the metatarsals, elevation of the midfoot, varus hindfoot position, and dorsiflexion of the metatarsal-phalangeal joints. Plain films are useful in initial assessment and in follow-up (Figs. 7.96 and 7.97).

7.6.9 Planovalgus

Weight-bearing films are performed. There is loss of the normal alignment between the talus and great toe metatarsal on the lateral view. The AP is used to assess talo-calcaneal angle. Where this angle is greater than 35°, heel valgus is present. Plain films also allow assessment for concurrent tarsal coalition

7.6.10 Growth Arrest Lines

Growth arrest, for example during childhood illness, is followed by a phase of growth acceleration, resulting in transverse dense metaphyseal lines (Fig. 7.98) There is a wide differential to this appearance as described in Sect. 7.5.2, Lead poisoning.

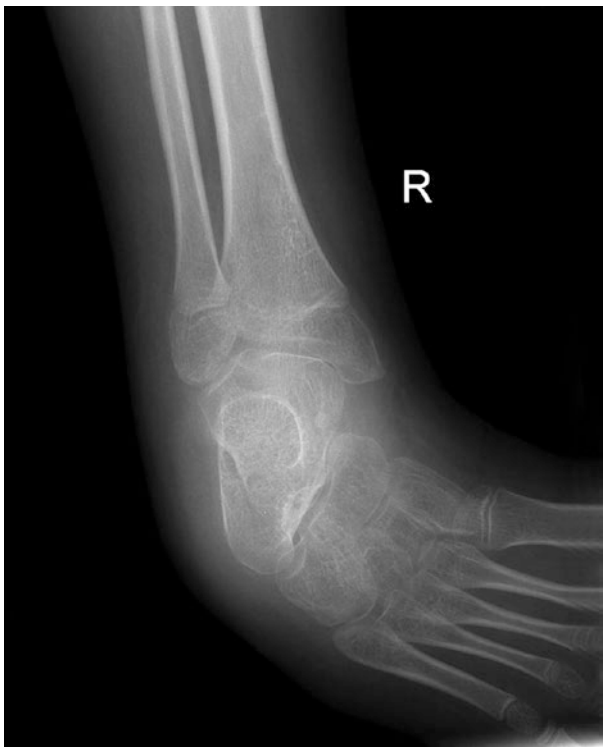

Fig. 7.96 Cavo-varus deformity on plain radiograph

7.6.11 Zebra Lines

The zebra stripe sign on plain film refers to dense metaphyseal bands in children with osteogenesis imperfect a who

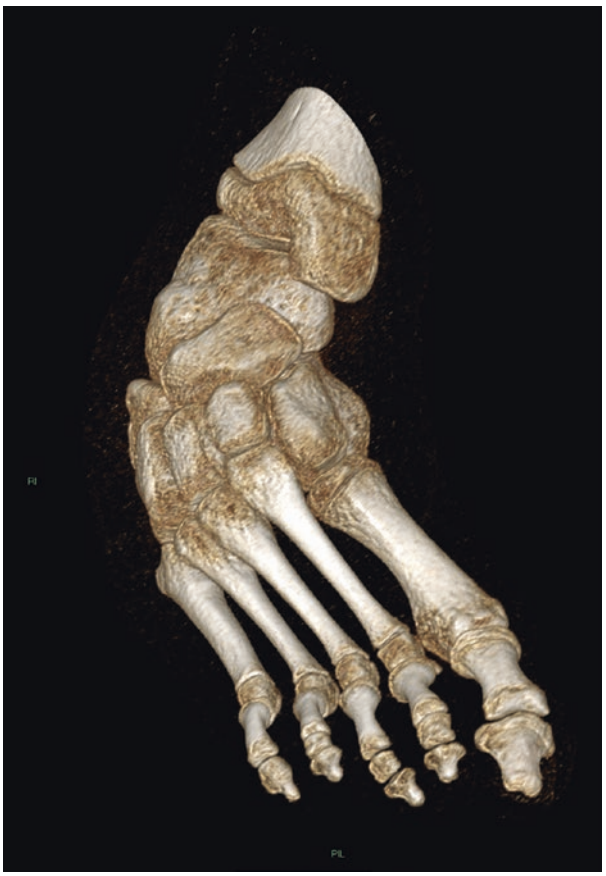

Fig. 7.97 3D CT reconstruction in the same child

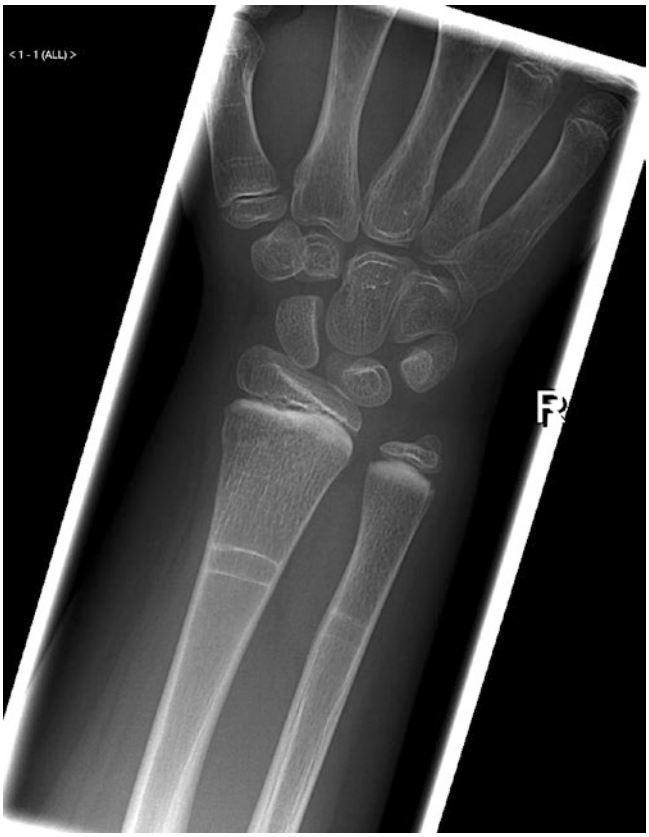

Fig. 7.98 Longitudinal and circumferential growth arrest lines on a plain film of the wrist

have been treated with bisphosphonates. Bisphosphonates are administered in cycles, resulting in multiple dense metaphyseal bands, hence comparison with zebra (Fig. 7.99). See also lead poisoning and growth arrest lines.

7.6.12 Rickets

Deformities such as genu varum and genu valgum may occur in neglected cases of infantile rickets, resistant rickets or renal rickets. Most bones show a remarkable return to normality with vitamin D supplementation. To prevent severe deformities occurring, splintage may be necessary. In renal rickets as in Fanconi syndrome (renal glycosuria with hypophosphatemic rickets), orthopaedic management is supportive.

Radiographic features include reduced bone density, fraying and splaying of the metaphyses, growth plate widening, and eventually bowing of the lower limb bones in ambulant children. Lack of normal mineralisation is most evident at the metaphyses which are most metabolically active. Changes are typically seen at the wrist, around the knee, and

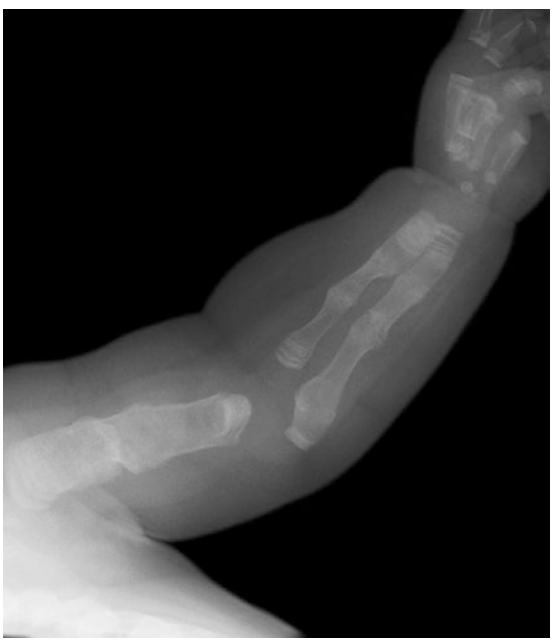

Fig. 7.99 Forearm of an infant with osteogenesis imperfecta on bisphosphonate therapy. 'Zebra lines' are present at the metaphyses. There are multiple healing fractures of the upper limb long bones

anterior ribs (known as rachitic rosary appearance). There may also be pathological fracture. Where rickets is suspected, an AP film of the wrist is initially performed (Figs. 7.100 and 7.101).

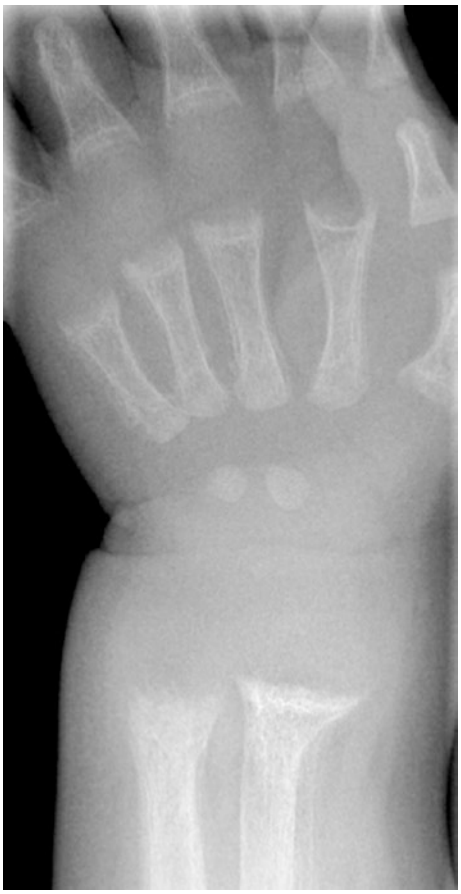

Fig. 7.100 Rickets affecting the wrist and hand. Typical cupping, splaying and fraying of the metaphyses

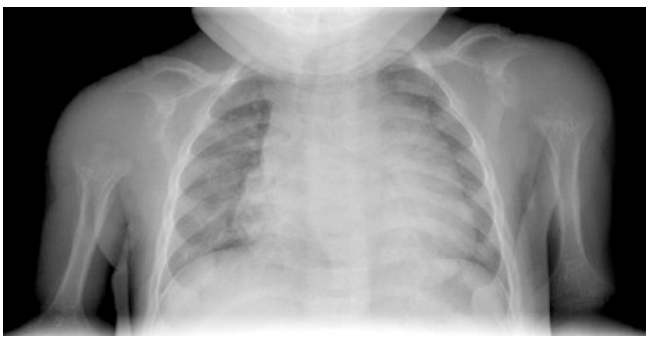

Fig. 7.101 Rickets affecting the chest. Expansion of the anterior rib ends producing a 'rachitic rosary' appearance

References

1. Rypens FR, Dubois J, Garel L, Fournet JC, Michaud JL, Grignon A. Obstetric US: watch the fetal hands. Radiographics. 2006;26:811–29.
2. Caffey J, Slovis TL. Caffey's pediatric diagnostic imaging. 1st ed. St. Louis, MO: Mosby Elsevier; 2008.
3. Kozin SH. Upper-extremity congenital abnormalities. JBJS. 2003;85:1564–76.
4. Graf R. Hip sonography: diagnosis and management of infant hip dysplasia. 2nd ed. Heidelberg: Springer; 2006.
5. Thapa MM, Pruthi S, Chew FS. Radiographic assessment of pediatric foot alignment: review. AJR Am J Roentgenol. 2010;194(6):S51–8.
6. Wilson CJ, Vellodi A. Autosomal recessive osteopetrosis: diagnosis, management, and outcome. Arch Dis Child. 2000;83(5):449–52.
7. Wright NB, Carty HM. The swollen leg and primary lymphoedema. Arch Dis Child. 1994;71:44–9.
8. Schulze M, Kötter I, Ernemann U, Fenchel M, Tzaribatchev N, Claussen CD, et al. MRI findings in inflammatory muscle diseases and their non-inflammatory mimics. AJR Am J Roentgenol. 2009;192:1708–16.
9. Lacout A, Jarraya M, Marcy PY, Thariat J, Carlier JY. Myositis ossificans imaging: keys to successful diagnosis. Indian J Radiol Imaging. 2012;22(1):35–9.
10. Gold RH, Hawkins RA, Katz RD. Bacterial osteomyelitis: findings on plain radiography, CT, MR, and scintigraphy. AJR Am J Roentgenol. 1991;157(2):365–70.
11. On a Form of Chronic Joint Disease in Children. Archives of Pediatrics & Adolescent Medicine. 132(2):195–200. https://doi.org/10.1001/archpedi.1978.02120270093020. ISSN 1072-4710.
12. Sheybani EF, Khanna G, White A, Demertzis JL. Imaging of juvenile idiopathic arthritis: a multimodality approach. Radiographics. 2013;33:1253–73.
13. Karchevsky M, Schweizer ME, Morrison WB, Parellada JA. MRI findings of septic arthritis and associated osteomyelitis in adults. AJR Am J Roentgenol. 2004;182:119–22.
14. Prince JS, Laor T, Bean JA. MRI of anterior cruciate ligament injuries and associated findings in the pediatric knee: changes with skeletal maturation. AJR Am J Roentgenol. 2005;185:756–62.
15. Lee K, Siegel MJ, Lau DM, Hildebolt CF, Matava MJ. Anterior cruciate ligament tears: MR imaging-based diagnosis in a pediatric population. Radiology. 1999;213:697–704.
16. Kirsch MD, Fitzgerald SW, Friedman H, Rogers LF. Transient lateral patellar dislocation: diagnosis with MR imaging. AJR Am J Roentgenol. 1993;161:109–13.
17. Diederichs G, Issever AS, Scheffler S. MR imaging of patellar instability: injury patterns and assessment of risk factors. Radiographics. 2010;30(4):961–81.
18. McCarthy CL, McNally EG. The MRI appearance of cystic lesions around the knee. Skeletal Radiol. 2004;33(4):187–209.
19. Dillman J, Hernandez RJ. MRI of Legg-Calve-Perthes disease. AJR Am J Roentgenol. 2009;193:1394–407.

Syndromes/Associations

8

Stephanie Potts and Robert Carachi

8.1 Introduction

This chapter consists of 30 conditions, many of which are already described in previous chapters. Its purpose is to highlight the syndromes and associations seen in congenital malformations. Each condition has a few references that allow for further reading. Most of the conditions described include clinical figures.

8.2 Beckwith-Wiedemann Syndrome

Beckwith–Wiedemann syndrome (BWS), also known as Exomphalos-Macroglossia-Gigantism syndrome, is the most common genetic syndrome characterized by overgrowth, tumour predisposition, and congenital malformations (Figs. 8.1 and 8.2). The majority of cases are sporadic, with 10–15% of cases being inherited in an autosomal dominant pattern [1]. The most common genetic mutation is hypomethylation of the maternal imprinting control region 2 (ICR2) in 11p15. The 11p15 imprinting region is also associated with Russell-Silver syndrome, which is a typical growth retardation syndrome. Opposite epigenetic alterations in 11p15 result in opposite clinical features shown in Beckwith-Wiedemann syndrome and Russell-Silver syndrome [2]. Neonates with BWS have a birth weight that exceeds the 90th centile, a large protruding tongue, and an abdominal wall defect or a hernia into the cord. Occasionally they may have eye proptosis with periorbital fullness, mid-glabellar capillary malformation (nevus flammeus), and earlobe creases and pits. These patients may have a history of hypoglycaemia and airway problems. Although intelligence is usually normal, mild-to-moderate developmental delay can be present. Pre-natal diagnosis involves the triad of visceromegaly, macroglossia, and exomphalos. The diagnosis of Beckwith-Wiedemann syndrome is typically made after birth on clinical examination. Clinical features are variable, and there are no absolute criteria for a clinical diagnosis. The main paediatric management issues are hypoglycaemia (hyperinsulinaemic hypoglycaemia), hypocalcaemia and the risk for embryonal tumours (primarily Wilms tumour), hepatoblastoma, neuroblastoma, and rhabdomyosarcoma. The hypoglycaemia can be persistent in infancy and sometimes hard to treat [3].

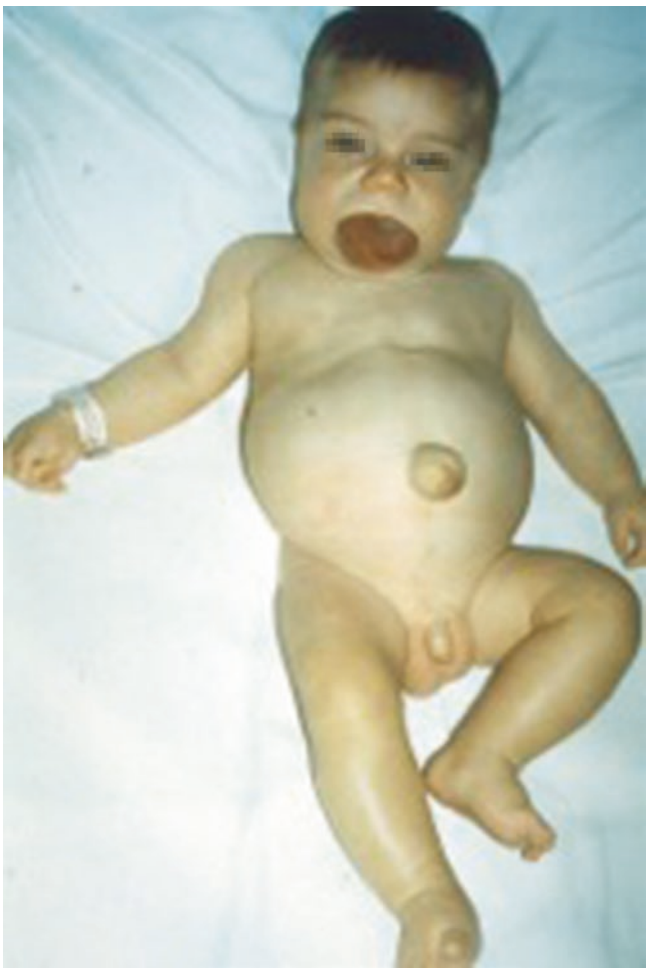

Fig. 8.1 Beckwith-Wiedemann syndrome

S. Potts · R. Carachi (✉)
Surgical Paediatrics, University of Glasgow, Glasgow, UK

R. Carachi (ed.), *Atlas of Paediatric Surgical Imaging*, https://doi.org/10.1007/978-3-030-32384-4_8

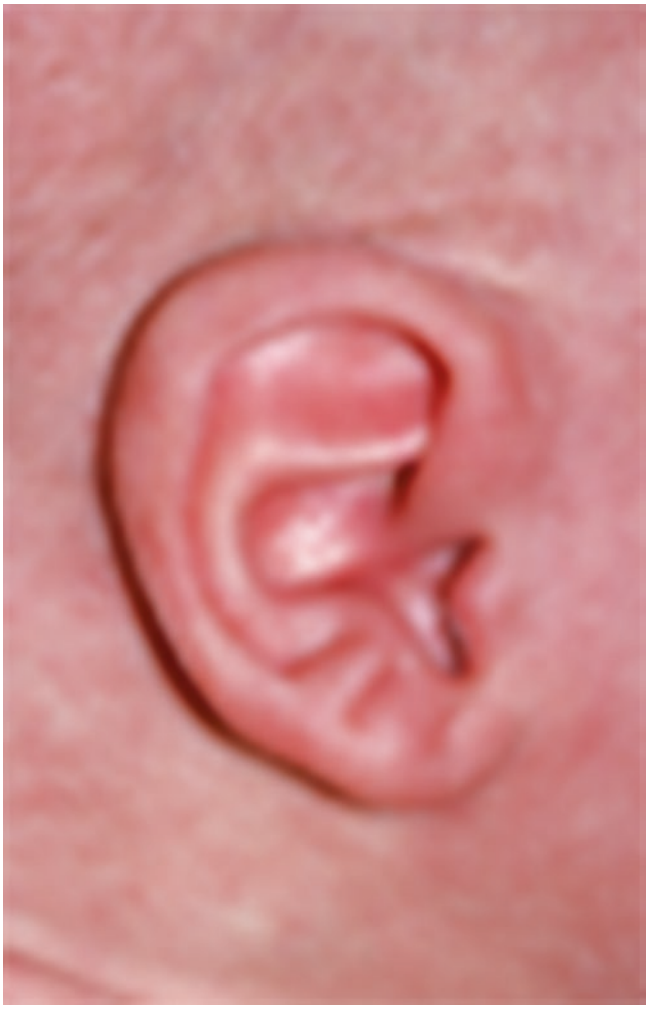

Fig. 8.2 Beckwith-Wiedemann syndrome

8.3 Conjoined Twins

Conjoined twins are identical twins joined in utero due to the incomplete anatomic separation between monozygotic twins (Figs. 8.3 and 8.4). Conjoined twins share a single common chorion, placenta, and amniotic sac. Approximately 75% of conjoined twins are female, and 70% are fused at the thorax (thoracopagus) or abdomen (omphalopagus). The diagnosis of conjoined twins can be made on routine fetal ultrasonography. Conjoined twins are typically classified by the point at which their bodies are joined:

- Thoraco-omphalopagus (joined at the chest, abdomen, or both)
- Thoracopagus or xiphopagus (joined at the chest)
- Omphalopagus (joined at the abdomen)
- Pygopagus (joined at the buttocks)
- Ischiopagus (joined at the ischium)
- Craniopagus (joined at the head)

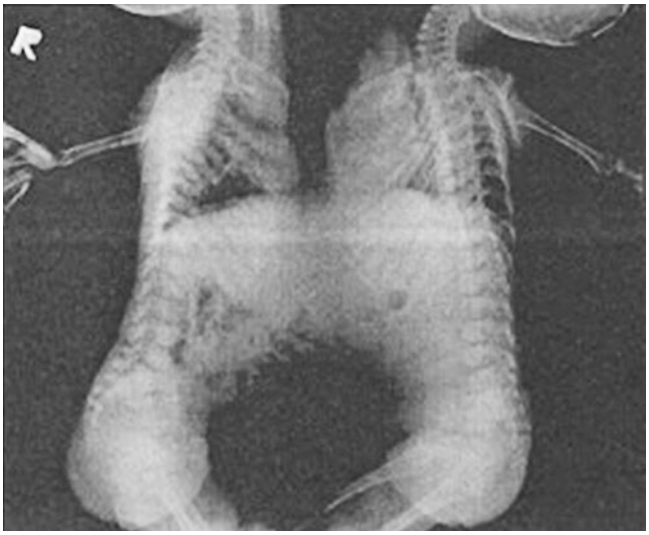

Fig. 8.3 Conjoined twins

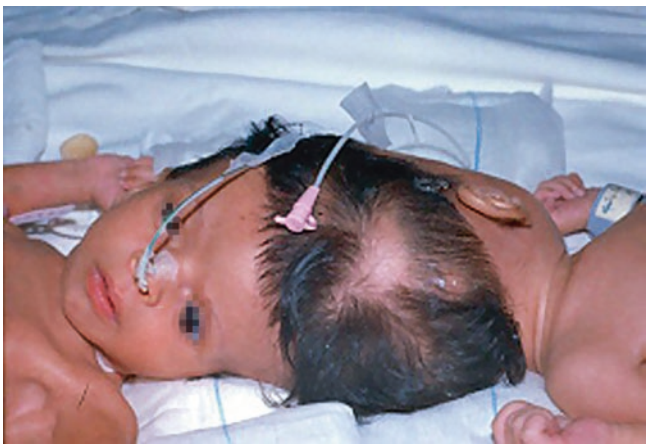

Fig. 8.4 Conjoined twins

8.4 Apert Syndrome

ApertSyndrome (Figs. 8.5, 8.6, and 8.7) is a genetic disorder characterized by craniosynostosis and complex hand and foot syndactyly [1]. This syndrome can be inherited in an autosomal dominant pattern; most cases, however, are sporadic and associated with increased paternal age. Mutations in fibroblast growth factor receptor 2 gene (FGFR2) on chromosome 10q25-10q26 (P253R&S252w mutations) cause Apert Syndrome. Different mutations in the same gene cause Crouzon and Pfeiffer Syndrome. Apert Syndrome is characterized by classical craniofacial abnormalities, including premature fusion of the coronal sutures resulting in skull and facial deformities with midface hypoplasia, a high forehead, beaked nose, and exorbitism, large fontanelles, flat faces, supraorbital horizontal groove, shallow orbits, hypertelorism, strabismus, downslanting of palpebral fissures, maxillary

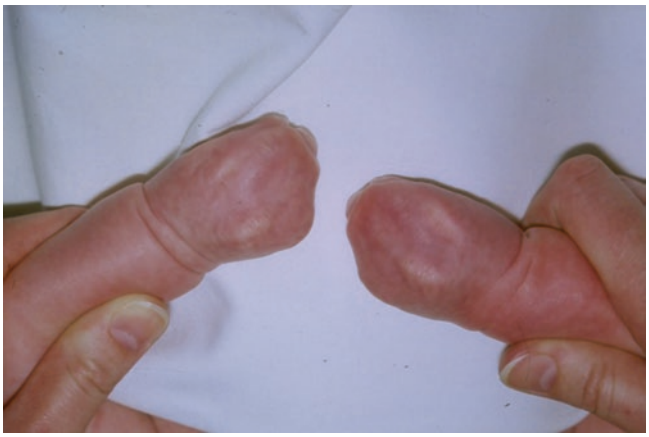

Fig. 8.5 Apert syndrome

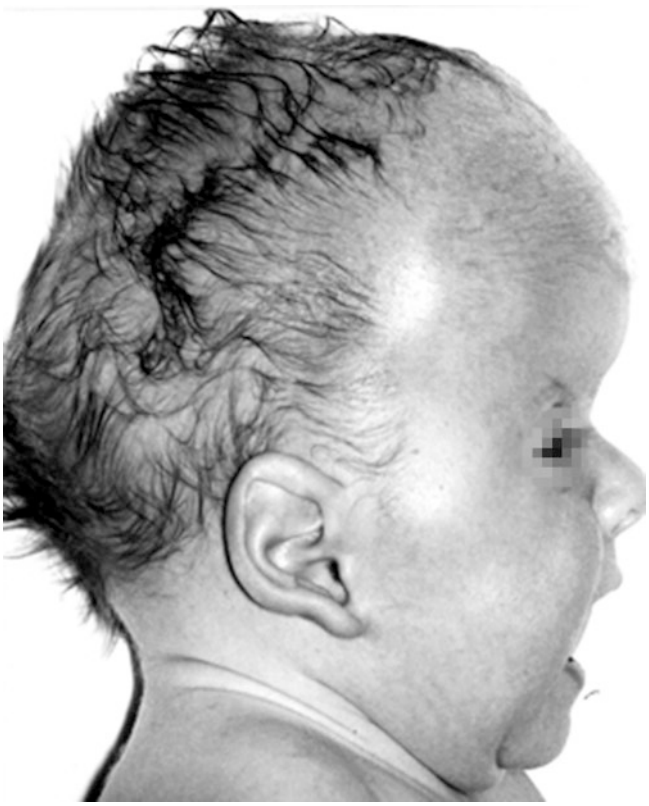

Fig. 8.6 Apert syndrome

hypoplasia, small nose, narrow palate with median groove, and cleft palate. It is differentiated from other craniosynostosis syndromes by the presence of complex cutaneous and bony syndactyly of the hands and feet, by the increased risk of structural malformations affecting the brain, palate, heart, and viscera, and by cognitive impairment. CNS abnormalities include: agenesis of corpus callosum, non-progressive ventriculomegaly, progressive hydrocephalus, absent or defective septum pellucidum, gyral abnormality, hippocampal abnormality, and megalencephaly. Limbs abnormalities include osseous or cutaneous syndactyly varying from partial fusion to total fusion (most commonly with complete fusion of the second, third, and fourth fingers), the distal hallux may be broad and in valgus position, and the fingers are often short. Other/occasional abnormalities include short humerus, synostosis of radius and humerus, limitation of joint mobility, genu valga, gastrointestinal abnormalities (pyloric stenosis, oesophageal atresia, ectopic anus), respiratory (pulmonary aplasia, anomalous cartilage), cardiac abnormalities (pulmonary stenosis, overriding aorta, ventricular septal defect, endocardial fibroelastosis), and genitourinary abnormalities (PCKD, hydronephrosis, bicornuate uterus, vaginal atresia, cryptorchidism, diaphragmatic hernia). The classic findings of craniosynostosis, causing skull deformity, and complex syndactyly are often readily identifiable on detailed ultrasound in the second trimester. The onset of craniosynostosis can be highly variable with a new-born infant. The diagnosis should be considered in fetuses with the typical hand and foot abnormalities but without obvious evidence of craniosynostosis on imaging [4].

8.5 Crouzon Syndrome (Craniofacial Dysostosis): Shallow Orbits, Premature Craniosynostosis, Maxillary Hypoplasia

Crouzon Syndrome (Fig. 8.8) is the most common craniosynostosis syndrome characterised by the premature fusion of the cranial sutures. It is inherited in an autosomal dominant fashion with a variable expression. Mutations in FGFR2 gene on chromosome 10q25-q26 account for over 90% of cases. In some cases, Crouzon Syndrome can be associated with acanthosis nigricans. In Crouzon Syndrome, the sutures fuse early, resulting in distorted bone growth and craniofacial abnormalities. The cranial, sagittal, and occasionally the lambdoidal sutures fuse early and are fully fused by 2–3 years of age, resulting in oxycephaly, plagiocephaly, dolichocephaly, brachycephaly and Kleeblattschaedel (clover leaf skull). In Crouzon Syndrome, the orbit and maxillary sutures also fuse early, leading also to frontal bossing, shallow orbits, ocular hypertelorism, ocular proptosis/exophthalmos, nasal septum deviation, narrowed or obliterated anterior nares, wide-beaked nose, low-set ears, severe maxillary hypoplasia, and cleft palate. Other clinical findings include pulmonary valve stenosis, tracheobronchial malacia, and subluxation of the radial heads [5].

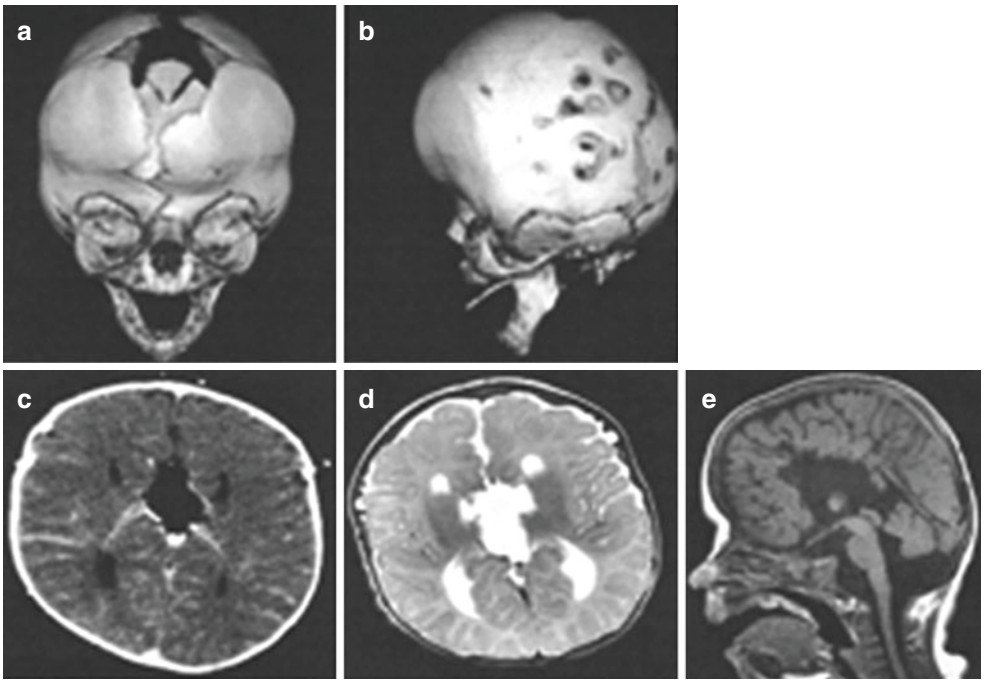

Fig. 8.7 Apert syndrome

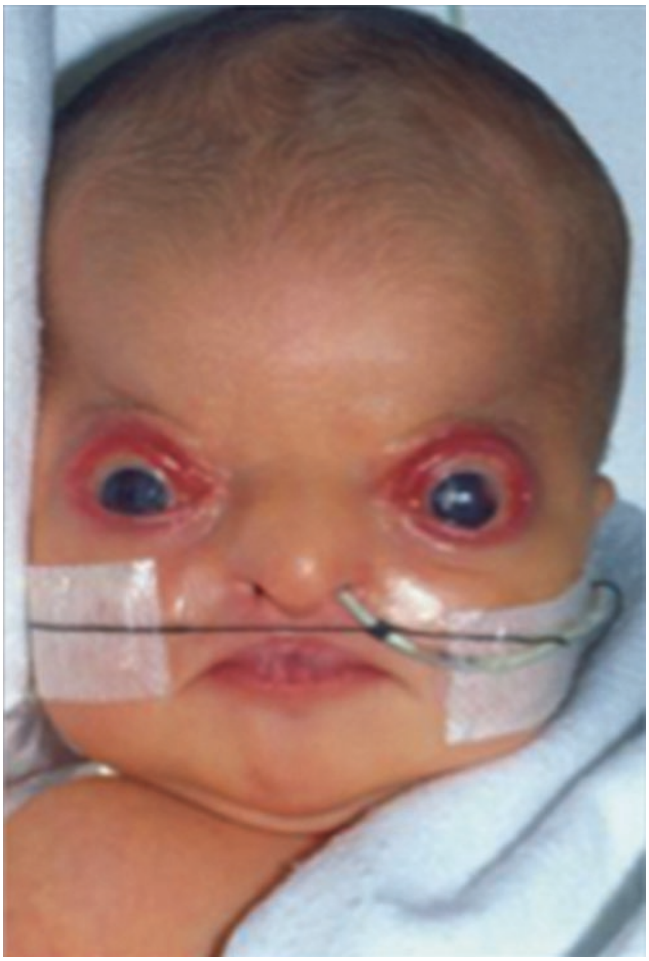

Fig. 8.8 Crouzon syndrome (craniofacial dysostosis)

8.6 Thalassaemia

The thalassaemias are haemoglobinopathies characterised by abnormalities in the production of the globin chains that make up haemoglobin, resulting in abnormal red blood cells more prone to haemolysis [6]. The Beta Thalassaemias are usually caused by point mutation in Beta globin genes on chromosome 11 that results in decreased production or absence of the Beta globin gene. Individuals with Beta thalassaemia minor/trait (heterozygous carrier state) are usually asymptomatic with a mild, well-tolerated anaemia with a haemoglobin>90 g/L that can often be confused with iron deficiency anaemia. Individuals with Beta thalassaemia intermedia exhibit a moderate anaemia without the requirement for blood transfusions. Splenomegaly may be palpated on examination. Beta thalassaemia major occurs when there are abnormalities in both globin genes. This presents within the first year of life with severe anaemia and failure to thrive. Extra-medullary haematopoiesis results in characteristic skull bossing and hepatosplenomegaly. Increased bone marrow activity can be visualised on skull X-ray, which can show the "hair-on-end sign." Iron overload occurs as a result of life-long blood transfusions and manifests as liver disease, endocrine failure, and cardiac toxicity.

The Alpha Thalassaemias are caused by deletions of the alpha globin genes on chromosome 16. There are two separate alpha genes on each chromosome. Deletion of all four alpha chains results in death in utero. HbH disease occurs if three alpha globin genes are deleted, resulting in moderate anaemia, haemolysis, hepatosplenomegaly, and jaundice.

Deletion of two alpha globin genes results in an asymptomatic carrier state, and deletion of one alpha gene results in a normal clinical state. Thalassemia is associated with reduced bone mineral density and fractures. Many causes are implicated, including hypogonadism, growth hormone deficiency, marrow expansion, and iron overload [7, 8].

8.7 Cranio-Cleido Dysostosis

Cranio-cleidodysostosis (Fig. 8.9) is a congenital polyostotic skeletal dysplasia that affects the orofacial, dental, and skeletal system, and is characterised by deficient formation of the clavicles with increased shoulder mobility with delayed and imperfect ossification of the cranium. Cranio-cleidodysostosis is a rare condition caused by a mutation in CBFA1 gene that arises in either an autosomal dominant inheritance pattern or sporadic mutation pattern (40%). There is failure of complete ossification of the membranous bones of the vault of the skull and the clavicle, as well as defective development of the pubic bones, vertebral column, and long bones [9].

Radiographic features: Skull—multiple wormian bones, widened sagittal sutures and/or fontanelles with delayed closure, resulting in brachycephaly, and enlarged biparietal diameter measurements, as well as abnormalities of the teeth and ear structures, broad mandible, over-retention of the deciduous teeth, supernumerary teeth, and high arched palate. **Chest**—hypoplasia/aplasia of lateral clavicle (may have two separate hypoplastic segments), supernumerary ribs, hemivertebrae with spondylosis, small and high scapulae/undergrowth of the shoulder blade. Neonatal distress can occur due to thorax being narrowed and bell-shaped. The pelvis may show delayed ossification and the limbs may have absent radius, fibula, and small terminal digits [9].

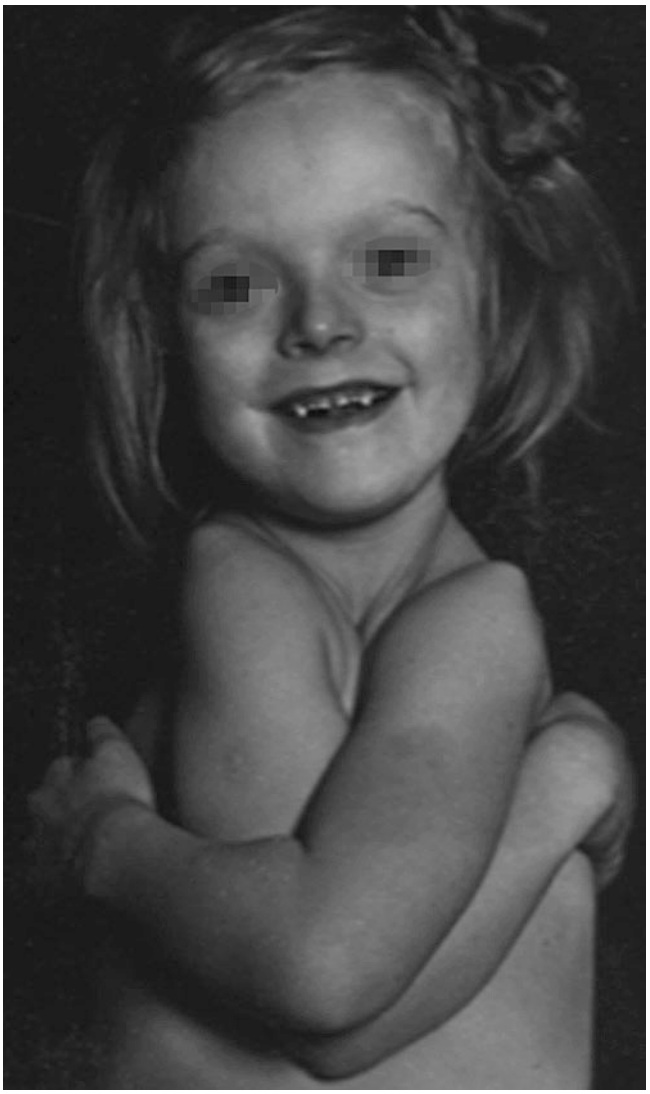

Fig. 8.9 Cranio-cleidodysostosis

8.8 Pierre Robin Sequence/Syndrome

Pierre Robin Sequence (PRS) (Fig. 8.10) is a craniofacial abnormality encompassing a triad of mandibular hypoplasia/micrognathia, glossoptosis, and airway obstruction. Micrognathia is identified at birth and is the defining feature of the diagnosis. Infants frequently present at birth with a hypoplastic mandible and breathing difficulties. The small mandible displaces the tongue posteriorly (glossoptosis), leading to airway obstruction resulting in low oxygen saturations, apnoea, and cyanosis. Feeding difficulties are common owing to trouble with breathing whilst eating. Gastroesophageal reflux and aspiration are common complications. Pierre Robin Sequence is also commonly associated with a wide U-shaped cleft palate. A wide range of chromosomal abnormalities are associated with PRS, suggesting there is a genetic influence that results in the PRS phenotype. The primary defect in PRS is an anatomical defect of mandibular outgrowth that impacts on oropharyngeal volume and patency of the palate, plus defects in cartilage growth, neuromuscular function, and fetal constraint. Pierre-Robin Sequence can occur in isolation (Isolated PRS), it can be associated with additional congenital malformations without a known syndrome diagnosis (PRS-plus), or it can be a phenotypic component of diverse conditions such as skeletal dysplasias, chromosomal abnormalities, teratogenic exposures, and neuromuscular disorders [10]. Stickler syndrome and 22q11 deletion syndrome are the two conditions most commonly associated with PRS. Eighty percent of infants diagnosed with PRS have other associated anomalies. Individuals affected by Pierre Robin Sequence are at risk of airway obstruction, hypoxia, corpulmonale, failure to thrive, and cerebral impairment.

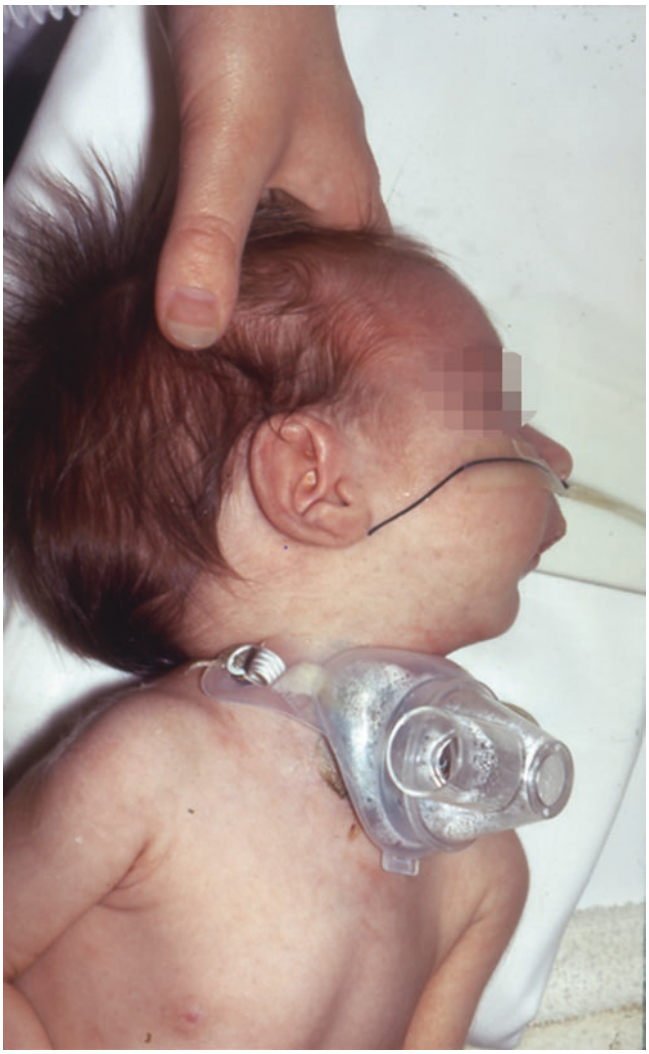

Fig. 8.10 Pierre Robin sequence/syndrome

8.9 Peutz-Jeghers Syndrome

Peutz-JeghersSyndrome (Fig. 8.11) is an autosomal dominant condition characterized by gastrointestinal hamartomatous polyps and epidermal pigmentation manifesting as blue/grey/brown spots on lips, buccal mucosa, and peri-oral areas. Mutations in serine/threonine kinase gene (LKB1/STK11) on chromosome 19p13.3, which usually acts as a tumour suppressor gene, result in the formation of the characteristic hamartomatous polyps. Hamartomatous polyps can be identified in the stomach, small bowel, colon, and sometimes in nasopharynx, bladder, biliary tract, and bronchial mucosa. Polyps are usually multiple, can be adenomatous, and undergo malignant changes in the gastrointestinal tract. Individuals with Peutz-Jeghers are at risk of developing a number of extra-intestinal tumours including bronchogenic carcinoma, benign/malignant thyroid cancers, gallbladder, biliary tract, breast (ductal), malignant tumours of the reproductive tract (malignant adenoma of cervix, unique ovarian

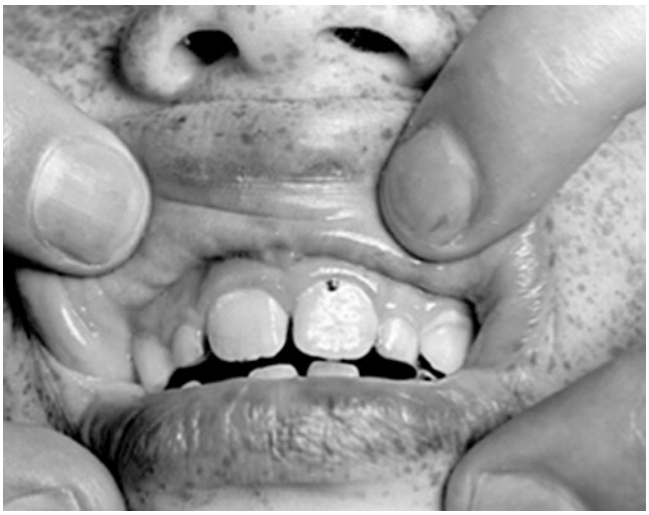

Fig. 8.11 Peutz-Jeghers syndrome

sex cord tumours causing sexual precocity, testicular sex cord and sertoli cell tumours leading to sexual precocity and gynaecomastia). Other complications of Peutz-Jeghers Syndrome include intussusception and gastrointestinal obstruction. Diagnosis is made via colonoscopy, upper GI series + small bowel follow-through, and pelvic ultrasound scan [1, 11].

8.10 Down Syndrome

Down Syndrome (Fig. 8.12) is a congenital genetic condition that arises as a result of Trisomy 21. The mechanisms involved are due to non-disjunction (>90%), translocation (5%), and mosaicism (1%). The risk of Down Syndrome increases with parental age. First trimester ultrasound scans at 11–14 weeks gestation can detect chromosomal abnormalities, including central nervous system, neck, gastrointestinal, and renal abnormalities. Part of the screening tests for Down Syndrome includes identification of a raised fetal nuchal translucency (fluid accumulation in the neck at 10–14 weeks gestation). The greater the extent of the fetal nuchal translucency, the greater the risk of abnormality. Many craniofacial abnormalities are characteristic of Down Syndrome including: prominent epicanthic folds, upward slanting palpebral fissures, Brushfield spots, protruding tongue, small mouth, small chin, small nose with low nasal bridge, brachycephaly, mild microcephaly with a round face flat occiput, late closure of fontanels, small low-set ears, high-arched palate, short neck with abundant neck skin. Up to half of children with Down Syndrome will have congenital heart defects, and all will undergo postnatal echocardiography. The most common cardiac malformation is an atrioventricular septal defect, followed ventricular septal defect. Tetralogy of Fallot is also relatively common in Down Syndrome. Individuals with Down Syndrome are of short

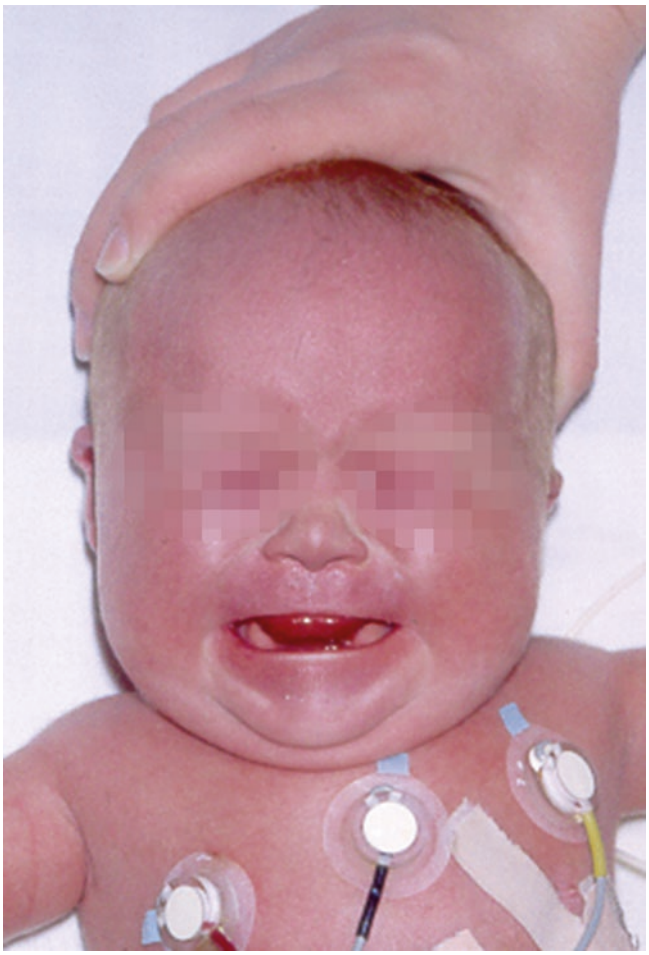

Fig. 8.12 Down syndrome

stature with growth restriction. Other skeletal abnormalities include pelvic dysplasia, relatively short metacarpals and phalanges, hypoplasia of middle phalanx of (incurving) fifth finger and short, broad hands, single palmar crease, simian palmar crease, and a wide gap between the first and second toes. There is an increased risk of gastrointestinal defects such as umbilical hernia, gastro-oesophageal reflux, Hirschsprung's disease, duodenal atresia, imperforate anus, and coeliac disease. Common neurological complications of Down Syndrome include learning difficulties, hearing impairment (recurrent otitis media), strabismus, cataract, increased incidence of epilepsy, and spinal cord compression secondary to atlanto-axial instability [1].

8.11 Poland Sequence

Poland Syndrome (PS) (Figs. 8.13 and 8.14) is acongenital anomaly characterized by the partial or complete absence of the pectoralis major muscle and thoracic wall abnormalities rib defects anomalies of the breast and nipple, a lack of subcutaneous tissue, the absence of pectoral and axillary hair,

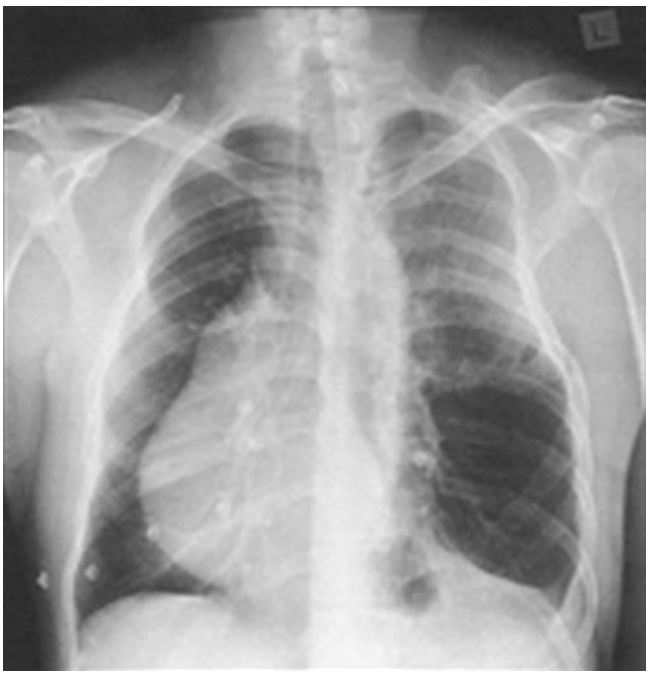

Fig. 8.13 Poland sequence

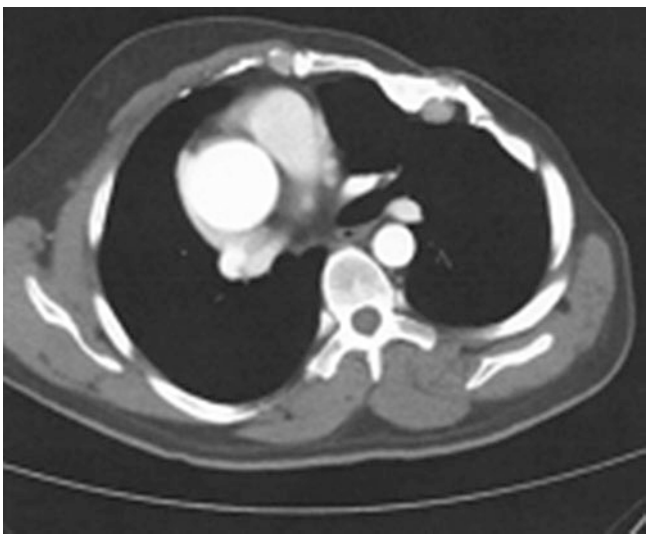

Fig. 8.14 Poland sequence

and an ipsilateral hypoplastic hand with varying degrees of syndactyly, brachydactyly, and oligodactyly. Individuals affected can also occasionally exhibit hemivertebrae, renal anomalies, and Sprengelanomalies. The combination of unilateral aplasia of the sternocostal head of the pectoralis major muscle, and an ipsilateral hypoplastic hand with simple syndactyly and short fingers, is typical for this condition. It occurs more frequently among males, and 75% of cases are situated on the right hemithorax in the unilateral form. In most cases, PS is sporadic. It is hypothesised that reduced blood flow to the affected side is caused by a primary defect in the development of the proximal subclavian artery with

early deficit of blood flow to the distal limb and the pectoral region resulting in the characteristic unilateral defect of pectoralis muscle and syndactyly of hand. Poland Syndrome is associated with dextrocardia. In left-sided Poland Sequence there is isolated dextrocardia without other cardiovascular defects associated with ipsilateral rib defects. Poland Syndrome is commonly associated with a Sprengel deformity (congenital elevated small scapula). Other accompanying deformities include: contralateral pectus carinatum, scoliosis, hepatomegaly, ectopic spleen, pectus excavatum, contralateral gynecomastia, and palmar hyperhidrosis. Prenatal diagnosis is possible by ultrasound identification of severe hypomelia, ipsilateral chest wall asymmetry, and thoracic hemivertebrae. The absence of congenital heart disease makes the diagnosis more certain, but does not entirely exclude other conditions, such as CHILD syndrome (congenital hemidysplasia with ichthyosiform erythroderma and limb defects). Chest X-rays identify absence of the anterior part of the rib, rib hypoplasia, contralateral pectus carinatum, pectus excavatum, scoliosis, and dextrocardia. Computed tomography (CT) scans highlight the absence of pectorals, rib, and chest wall deformities [12, 13].

8.12 Pentalogy of Cantrell

Pentalogy of Cantrell (Figs. 8.15 and 8.16) is a pentad of findings that include a defect of the lower sternum, a midline supraumbilical thoracoabdominal wall defect, a deficiency of the diaphragmatic pericardium, anterior diaphragmatic defect, and congenital cardiac anomalies. Pentalogy of Cantrell is an extremely rare phenomenon that can be fatal without surgical intervention. Because of various phenotypes of abdominal wall defect in Pentalogy of Cantrell, multiple factors are said to be responsible, including mechanical teratogens, major gene mutation, chromosomal abnormalities such as trisomy 13 and 18, and disrupted vessels defects. A developmental failure of the segmental mesoderm at approximately 14–18 days after conception (the time period for differentiation of somatic and splanchnic mesoderm) is believed to be responsible for these defects. Failure of the transverse septum (arising from the mesoderm) to partially or entirely complete the process of flexion or ventral folding is believed to cause the ventral diaphragmatic defects. Abdominal wall and sternal defects can also occur as a result of disrupted mesoderm development involving failure of ventral migration [14]. Because of the lower sternum and anterior diaphragmatic defects, this syndrome can be characterized by ectopia cordis, which is an anomaly in which the fetal heart lies outside the thoracic cavity. Cardiac anomalies can include ventricular septal defect, atrial septal defect, tetralogy of Fallot, and ventricular diverticulum. Various other associated anomalies have been reported and include cleft lip/palate, encephalocele, clubfoot, absence of tibia or radius, hypodactyly, gallbladder agenesis, and polysplenia. Pentalogy of Cantrell can be diagnosed by first-trimester antenatal sonogram, which can identify omphalocele and ectopia cordisas early as the twelfth week of gestation.

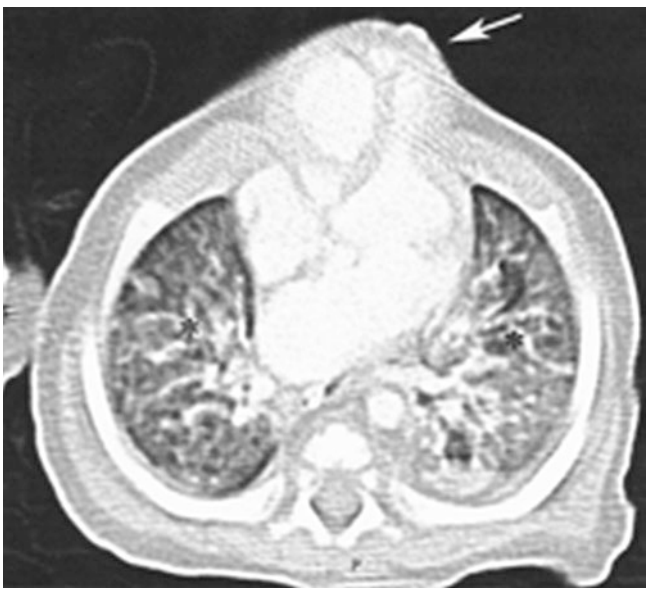

Fig. 8.15 Pentalogy of cantrell

8.13 Cushing's Syndrome/Congenital Adrenal Hyperplasia

Congenital Cushing's syndrome is due to bilateral nodular adrenal hyperplasia. Congenital adrenal hyperplasia (CAH) is one of the most common genetic disorders, characterised by impaired adrenal cortisol biosynthesis and androgen excess with or without salt wasting (Fig. 8.17). CAH is a potentially life-threatening disorder. 21-hydroxylase deficiency due to mutations in the CYP21A2 gene accounts for about 95% of cases of CAH. Neonatal screening of 17-hydroxyprogesterone is diagnostic [15]. Missed diagnosis can result in neonatal mortality in salt-wasting forms and incorrect sex of rearing in females with simple virilizing form. Preterm birth and neonatal illness can cause physiological elevation of 17OHP, thus complicating the diagnosis of CAH in the new-born period.

The imaging features of Cushing's Syndrome depend on the aetiology of the syndrome in the individual patient. If the source of the glucocorticoid is an adrenocortical tumour, then imaging may demonstrate an adrenal mass, but it should be recognised that adrenal tumours may be radiologically occult. Plain radiology may demonstrate calcification in some cases. On sonography, if there is a visible mass, this may be solid cystic or complex, containing hypoechoic areas

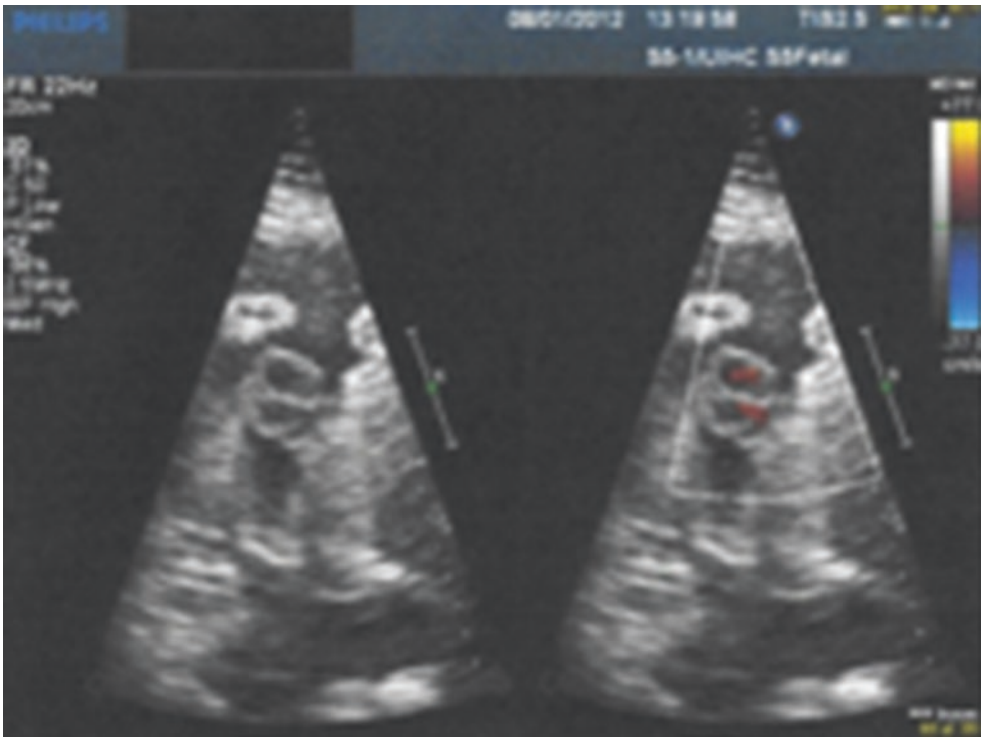

Fig. 8.16 Pentalogy of cantrell

Fig. 8.17 Cushing's syndrome/congenital adrenal hyperplasia

or necrosis and hyperechoic calcification, and there is usually a preserved tissue plane between the mass and surrounding organs. MR appearances are non-specific, intermediate signal on T1 imaging and high signal on T2 imaging with enhancement following gadolinium. In-and-out of phase imaging may be used to assess for the presence of fat. Imaging can demonstrate associated abnormalities such as tumour thrombosis and secondary features such as nephrocalcinosis and increased abdominal/retroperitoneal fat.

On CT, the lesions are typically well circumscribed, heterogeneous, and enhancing with no evidence of fat attenuation. They may contain high attenuation consistent with calcification. More often in the paediatric population there is adrenal hyperplasia, which may be primary (macronodular or micronodular) or more rarely, secondary to an ACTH secreting tumour, most commonly a pituitary microadenoma. Despite the hyperplasia, the adrenals may be normal in size on imaging. Nodules, if present, are small, often <6mm and may or may not be visible regardless of modality [16].

8.14 Klippel-Trenaunay Syndrome: Asymmetric Limb Hypertrophy, Vascular Malformations, Varicosities

Klippel-TrenaunaySyndrome (KTS) (Figs. 8.18 and 8.19) is a rare congenital angiodysplasia disorder characterised by a triad of port-wine stains, varicose veins, and bony and soft tissue hypertrophy, usually involving an extremity. Although it generally presents with grossly enlarged limbs, it can present with more serious features like haematuria, haematoche-

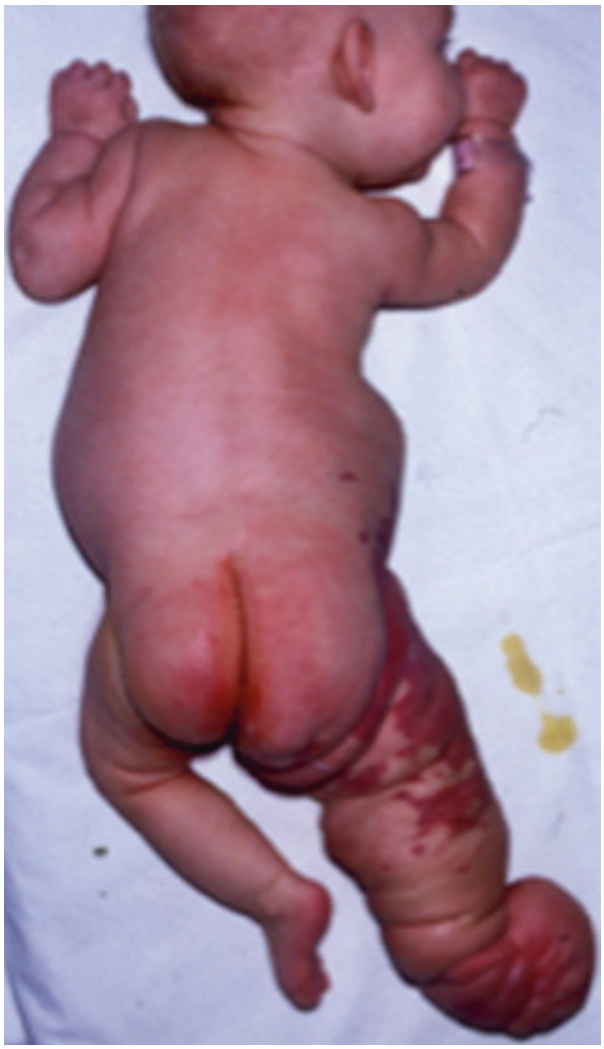

Fig. 8.18 Klippel Trenaunay syndrome

zia, and seizures [17]. Visceral involvement is rare, but has been described in the colon, small bowel, bladder, kidney, spleen, liver, mediastinum, and brain. KTS can manifest as congenital or early childhood hypertrophy of usually one limb: lower limb 95%, upper limb 5%, or both 15%. Limb abnormalities can include macrodactyly, disproportionate growth of digits, syndactyly, polydactyly, oligodactyly, and congenital hip dislocation. Craniofacial malformations include assymetric facial hypertrophy, microcephaly, and macrocephaly caused by a large brain. KTS can co-exist with Sturge-Weber syndrome, a triad of a port wine stain, varicose veins and hemangiomata, and bony or soft tissue hypertrophy of an extremity. Prenatal diagnosis is possible by ultrasound examination.

8.15 Marfan Syndrome

Marfan Syndrome (Fig. 8.20) [1] is a connective tissue disorder with skeletal, ligamentous, orooculofacial, pulmonary, abdominal, neurological, and cardiovascular manifestations. It has an autosomal dominant inheritance with mutations in the fibrillin (FBN1) gene on chromosome 15q15-21.3. Skeletal abnormalities include tall stature, long slim limbs, pectus carinatum, pectus excavatum, scoliosis, spondylolisthesis, pes planus, protrusion acetabuli (dislocation of acetabulum), hypermobile joints, high palate with dental crowding, dolichocephaly, malar hypoplasia, and enophthalmos. Individuals with Marfan Syndrome also have minimal subcutaneous fat and muscle hypotonia. Cardiovascular malformations include aortic root dilatation, aortic regurgitation, ascending aortic dissection, mitral valve prolapse, dilated pulmonary artery calcified mitral annulus, and dilatation or

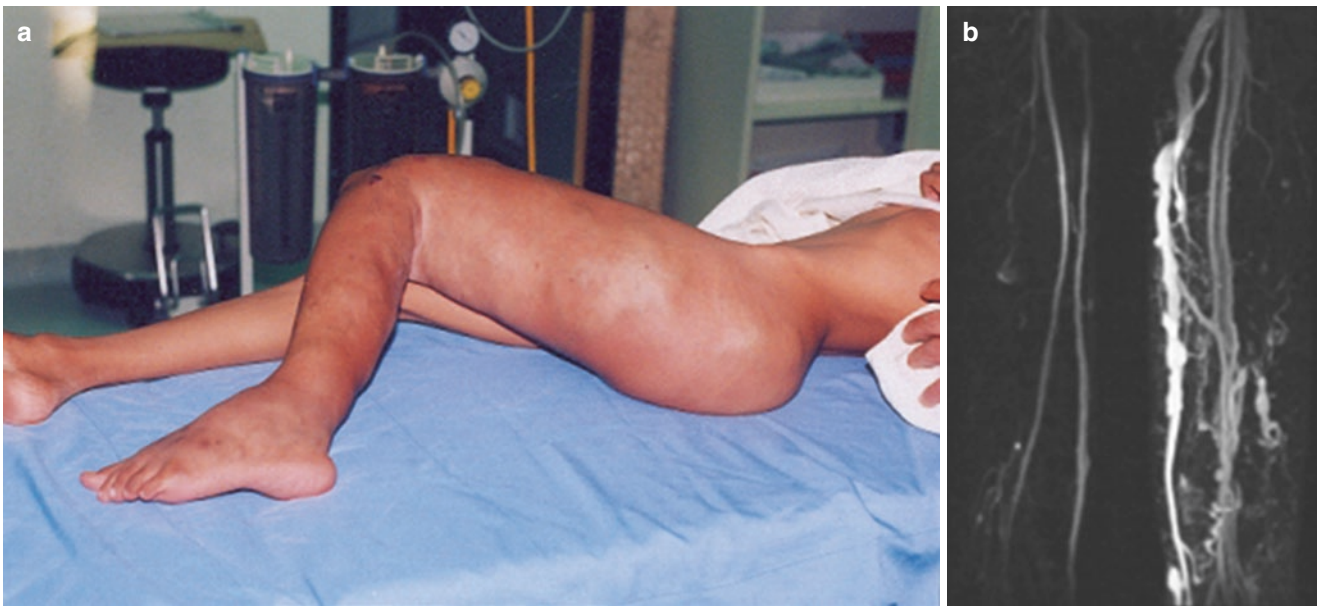

Fig. 8.19 Klippel Trenaunay syndrome

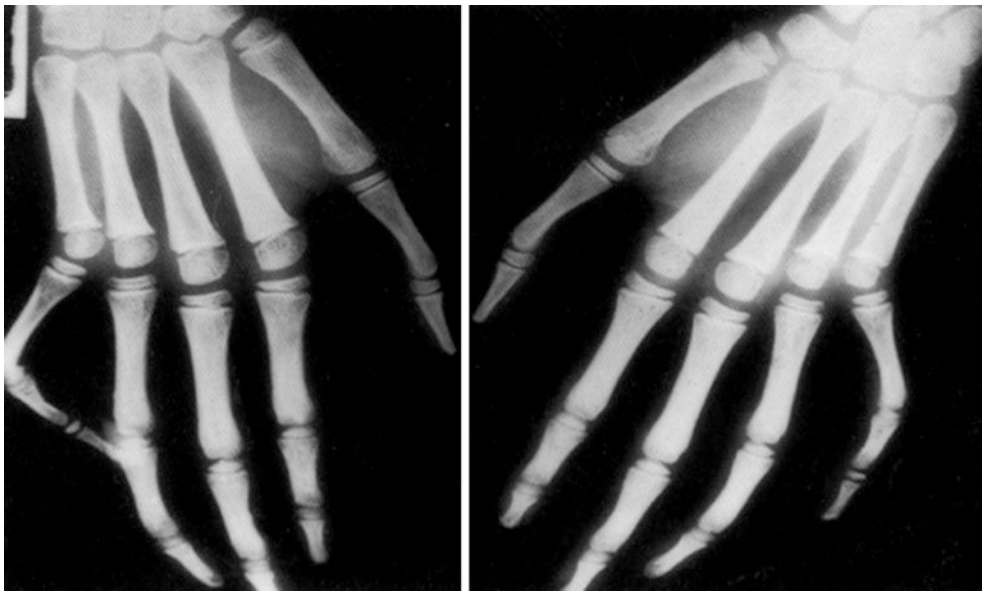

Fig. 8.20 Marfan syndrome

dissection of descending thoracic or abdominal aorta. Pulmonary complications manifest as spontaneous pneumothorax due to rupture of apical blebs [18].

8.16 Currarino Syndrome/Triad

The Currarino Triad (Fig. 8.21) is a multiple congenital anomalies syndrome consisting of an anorectal malformation (anal atresia), a sacral bony defect (sickle-shaped sacrum), and a presacral mass (meningocele and/or tumour [teratoma; hamartoma]). In most cases, autosomal dominant transmission is suggested [19]. The Currarino triad is a rare genetic anomaly resulting from abnormal separation of the neuroectoderm from the endoderm associated with mutations in HLXB9 gene on chromosome 7q36. The majority of patients present with intractable constipation in infancy. Other presentations are low backache, urinary tract infections, perianal sepsis, and meningitis (due to an anal/rectal fistula that communicates with the cord) [20]. Other malformations, such as renal (35%) and gynaecological (19%), are common. Hirschsprung's disease has also been recorded. Other rarer complications include pelvic abscess, malignant degeneration of a pre-sacral teratoma, E Coli ascending meningitis, and spinal cord tethering. Recurrence of a benign teratoma has been recorded. Urinary incontinence, dysmenorrhoea, dyspareunia, poor sphincter control, sacral anaesthesia, and headaches precipitated by coughing or straining have been reported. Prenatal diagnosis of Currarino Triad has been reported with ultrasound, although most cases are diagnosed postnatally in the first decade of life. Plain radiography shows the sacral anomaly as an asymmetrical, crescenteric, sickle- or scimitar-shaped sacrum with preservation of the first sacral vertebrae. Ultrasound can detect the sacral anomaly and presacral mass in Currarino Triad, as well as allow for assessment of the kidneys, which may be affected because of associated anomalies. Contrast studies are helpful in showing the anorectal malformation, proximal bowel dilatation, and presence of bowel fistulas and associated genital anomalies. MRI imaging is available to provide additional information on the presacral mass, including its size, composition, extent, and can also assess the involvement of adjacent structures and provide information on associated anomalies such as a tethered cord.

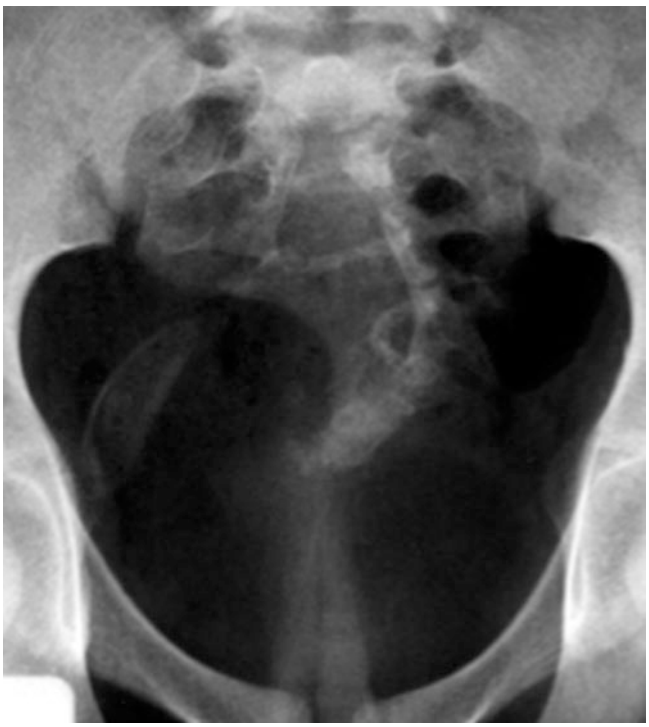

Fig. 8.21 Currarino syndrome/triad

8.17 Cornelia de Lange Syndrome

Cornelia de Lange Syndrome (Fig. 8.22) is a developmental disorder with widely variant features and severity among affected individuals. Cornelia de Lange Syndrome is characterized by prenatal and postnatal growth retardation and small stature, severe/profound intellectual disability, skeletal abnormalities involving the arms and hands, and distinctive facial features [1]. It is inherited in an autosomal dominant fashion with mutations in nipped-B homolog (NIPBL), SMC1A and SMC3 genes. Craniofacial abnormalities include microbrachycephaly, microcephaly, skull base dysplasia, synophrys, micrognathia, low-set ears, depressed nasal bridge, and small, widely spaced teeth. Skeletal abnormalities can include scoliosis, cervical malformations, pectus excavatum micromelia, phocomelia, oligodactyly, clinodactyly of fifth fingers, simian crease, proximal implantation of thumbs, flexion contracture of elbows, and syndactyly of the second and third toes. Affected individuals can also suffer from cardiac abnormalities including ventricular septal defects, atrial septal defect, pulmonic stenosis, tetralogy of Fallot, and hypoplastic left heart syndrome [21, 22]. Many affected individuals also have behavioural problems similar to those associated with autism. Additional clinical manifestations of Cornelia de Lange Syndrome can include excessive body hair (hypertrichosis), hearing loss, gut duplication/malrotation, volvulus, pyloric stenosis, diaphragmatic hernia, cleft palate, cryptorchidism, and hypospadias. Mandibular spurs can be identified radiologicallyup to 3 months of age. Dislocated/hypoplastic radial head, hypoplastic first metacarpal and fifth middle phalanx, short sternum, and 13 ribs can also be visualised. Neuroimaging can also be used to identify a variety of brain abnormalities.

8.18 Prune-Belly Syndrome

Prune-Belly Syndrome, also known as Eagle-Barrett Syndrome (Fig. 8.23), is a rare disorder characterised by partial or complete absence of the abdominal muscles, bilateral cryptorchidism, and/or urinary tract malformations. The urinary malformations may include dilatation of the ureters,

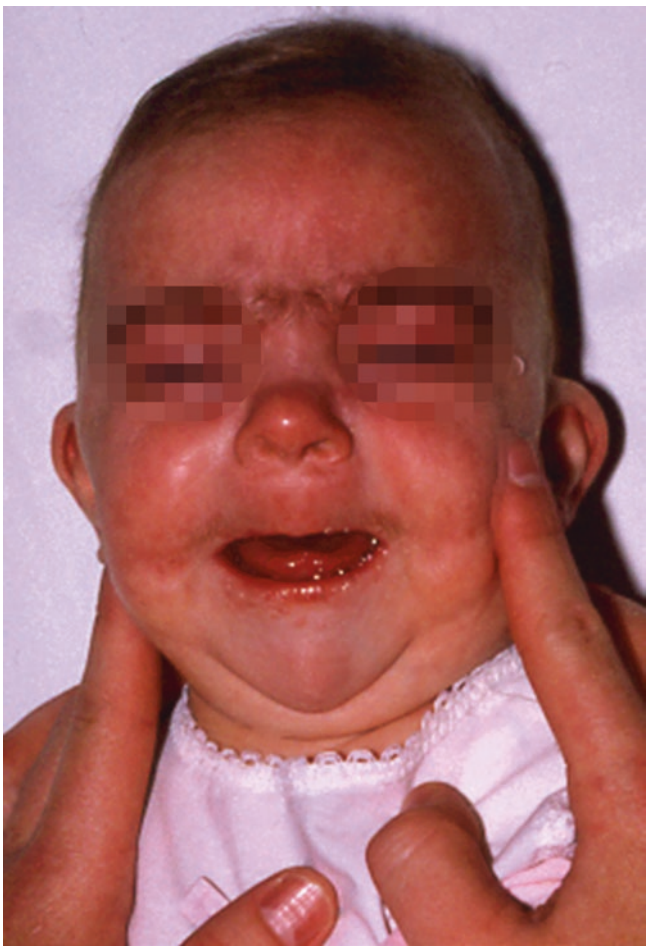

Fig. 8.22 Cornelia de Lange syndrome

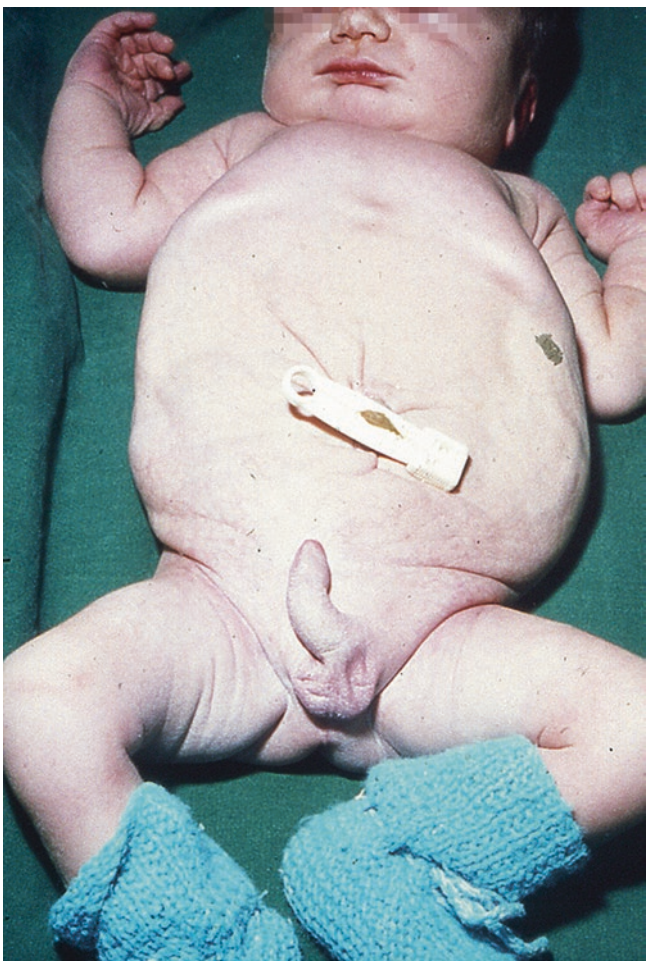

Fig. 8.23 Prune Belly syndrome

hydroureter, hydronephrosis, and/or vesicoureteric reflux. Complications associated with Prune-Belly Syndrome may include pulmonary hypoplasia as result of oligohydramnios and chronic renal failure. The exact cause of Prune-Belly Syndrome is unknown. There are two hypotheses. The first suggests that severe early gestational bladder outlet obstruction is secondary to an obstruction caused by urethral atresia and stenosis of the posterior urethral valves. If early urinary tract obstruction causes bladder distension and abdominal musculature deficiency, it will result in Prune-Belly Syndrome [23]. The second hypothesis suggests that abdominal muscle deficiency could be due to a defect in the migration of the lateral mesoblast between weeks 6 and 7 of pregnancy. This syndrome occurs most often in male infants, and rarely in females [24]. There is a high incidence of abnormalities associated with Prune-Belly Syndrome. Gastro-intestinal anomalies include malrotation, small intestinal stenosis, gastroschisis, and imperforate anus. Cardiac anomalies include tetralogy of Fallot and atrial and ventricular septal defects. Skeletal deformities include varus deformity of the feet, digital anomalies, and congenital dislocation of the hip. Pulmonary anomalies manifest as rib-cage narrowing and pulmonary hypoplasia. Antenatal sonography may detect megacyst (distended bladder) or enlarged hyperechogenic kidneys. Other cardiac, pulmonary, and skeletal abnormalities may also be picked up on antennal ultrasound scanning. Postnatal investigations such as intravenous pyelogram, ultrasound, voiding cystourethrogram, and X-ray may aid diagnosis and identify the extent of the condition.

8.19 Multiple Endocrine Neoplasia

Multiple endocrine neoplasia (MEN) syndromes are characterised by the combined occurrence of two or more endocrine tumours in a patient. Four types of MEN exist, all with autosomal-dominant inheritance patterns. MEN1 is caused by inactivating MEN1 mutations (MEN-1 is a tumour suppressor gene). MEN2A and MEN2B (MEN3) are caused by activating mutations of *RET*. MEN4 is caused by inactivating cyclin-dependent kinase inhibitor 1B (*CDKN1B*) mutations. Each MEN syndrome exhibits different combinations of pancreatic islet, anterior pituitary, parathyroid, medullary thyroid, and adrenal tumours [1]. MEN 1 encompasses parathyroid hyperplasia/adenoma, pancreatic endocrine tumours (gastrinoma, insulinoma, somatostatinomas), VIPoma, glucagonoma, and pituitary prolactinomaor GH-secreting tumour (adrenal and carcinoid tumours). MEN 2a includes medullary thyroid carcinoma, pheochromocytoma, and parathyroid hyperplasia, while MEN 2b includes medullary thyroid carcinoma, pheochromocytoma, mucosal neuromas, and Marfanoid appearance [25].

8.20 Tuberous Sclerosis Complex

Tuberous Sclerosis Complex [1] is a rare, multisystem genetic condition with autosomal dominant inheritance caused by mutations in TSC1, located at 9q34, and TSC2, on 16p13, which causes benign tumours that lead to organ dysfunction to develop in the brain, kidneys, lung, and heart. Tuberous sclerosis complex is highly variable in clinical presentation and findings. Disease manifestations continue to develop over the lifetime in an affected individual. A small number of children with tuberous sclerosis will develop multiple types of brain tumours during brain development up until the age of 5. Subependymal giant cell astrocytomas (SEGA) can develop at any age, but are most commonly identified after the teenage years. Other brain abnormalities include glioma-angioma lesions in the cortex and white matter resulting in seizures and intracranial mineralisation in the basal ganglia or periventricular region. These brain tumours results in complications such as epilepsy, intellectual impairment, learning disabilities, behavioural problems such as hyperactivity or autism, and hydrocephalus. Affected individuals develop multiple benign tumours known as angiomyolipomas, made up of blood vessels, muscle, and fat within the kidneys, usually by the age of 5. Further renal complications include polycystic kidney disease, renal cell carcinoma, tubular enlargement, and cyst formation with hyperplasia of tubular cells. Cardiac abnormalities include rhabdomyomas, which are the most common cardiac tumours in children, valve insufficiency, arrhythmias, including Wolf-Parkinson-White syndrome, ventricular septal defects, and other congenital cardiac anomalies. Lymphangioleiomyomatosis (LAM) is a condition in which tumours and cysts develop in the lungs, usually between ages 20 and 40. An estimated 40–60% of women with tuberous sclerosis will develop tumours and cysts inside their lungs. Cyst-like areas can be identified commonly in the phalanges and elsewhere with areas of periosteal thickening and radiological evidence of sclerosis. Cutaneous manifestations include patches of hypo-pigmented, thickened/fibrous skin, or red acne-like spots. Tuberous sclerosis can also affect the eyes, causing retinal hamartomas [26].

8.21 Potter's Syndrome

Potter's Syndrome (Fig. 8.24) is the phenotypic appearance caused by pressure in utero due to oligohydramnios. The pathophysiology of this condition can be explained by failure of renal bud development resulting in bilateral renal agenesis (BRA) but it can occur with other conditions, including infantile polycystic kidney disease, renal hypoplasia, and obstructive uropathy. Poor renal excretion of urine, or even absence, results in little amniotic fluid or oligohy-

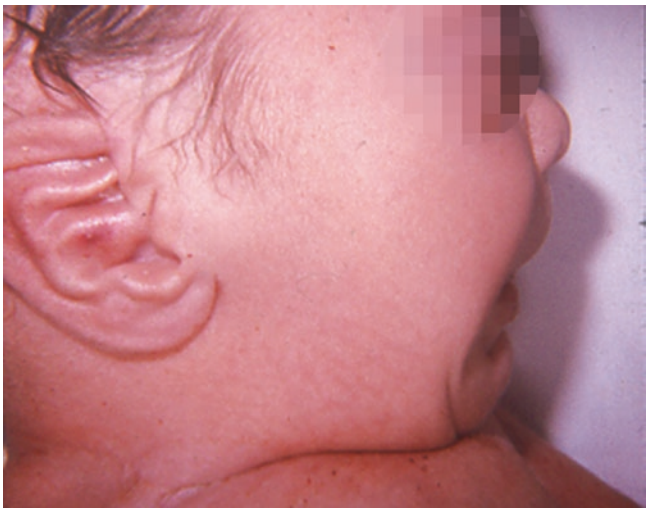

Fig. 8.24 Potter's syndrome

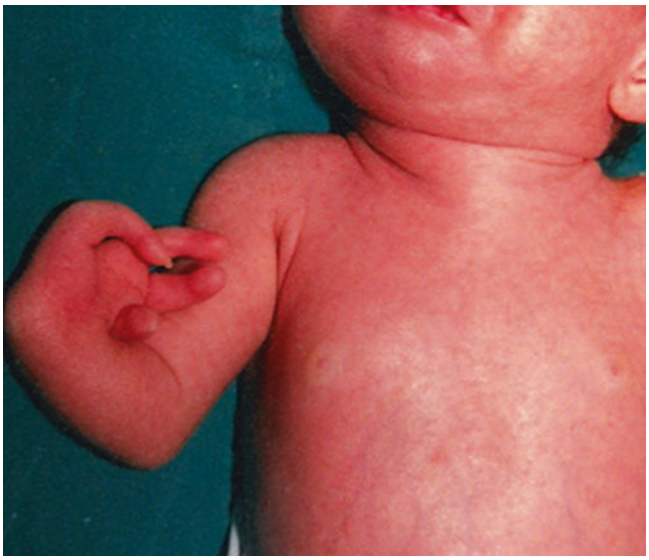

Fig. 8.25 VACTERL association

dramnios causing squashing of the fetus with the typical appearance of low set ears a narrow face and widely spaced eyes. Pulmonary hypoplasia is a common condition due to the absence of adequate amniotic fluid. A prenatal ultrasound may show oligohydramnios, absence of fetal kidneys, or severely abnormal kidneys in the unborn baby and failure to visualise the fetal bladder. Abdominal and chest X-rays can be useful in diagnosing the condition in a new-born [27, 28].

8.22 VACTERL Association

VACTERL association (Fig. 8.25) is a disorder that affects a variety of body systems. VACTERL is an acronym for Vertebral defects, Anorectal atresia, Cardiac defects, Tracheo-oesophageal fistula, Renal anomalies, and Limb abnormalities. At least three of these characteristic features must be present to qualify for this association. Defects in the vertebrae are present in 60–80% of people with VACTERL association. These defects may include hemi vertebrae, fused vertebrae, and absent or extra vertebrae. Anal atresia may be associated with genitourinary anomalies. Cardiac defects occur in 40–80% of individuals with VACTERL association. The most common cardiac defect is a ventricular septal defect. Severe defects include tetralogy of Fallot, double outlet right ventricle, atrioventricular canal defect, aorto-pulmonary window, and a vascular ring. Fifty to eighty percentage of people with VACTERL association have an oesophageal atresia and a tracheo-oesophageal fistula. Renal anomalies occur in a considerable number of individuals with VACTERL association. Affected individuals may be missing one or both kidneys or have abnormally developed or misshapen kidney. The most common renal manifestation is vesicoureteral reflux in addition to a structural defect followed by unilateral renal agenesis, and dysplastic/multicystic kidneys or duplicated collected system. Limb abnormalities are seen in around half of affected individuals. These abnormalities most commonly include poorly developed or missing thumbs or underdeveloped forearms and hands. Some of the features of VACTERL association can be subtle and are not identified until late in childhood or adulthood, making diagnosis of this condition difficult [29, 30].

8.23 CHARGE Syndrome

CHARGE Syndrome (Fig. 8.26) encompasses Coloboma, heart disease, atresia choanae, retarded growth and development/CNS abnormalities, genital anomalies and hypogonadism, ear anomalies, and deafness. Mutations in the gene CDH7 located on 8q12 is currently the only gene known to be associated with CHARGE syndrome. This encompasses a class of proteins important in early embryologic development by affecting chromatin structure and gene expression. CHARGE Syndrome usually occurs as a new autosomal dominant condition, with no family history; 97% of CHD7 mutations are de novo. The heart defects associated with CHARGE syndrome include tetralogy of Fallot, patent ductus arteriosus, double outlet right ventricle with an atrioventricular canal, Ventricular Septal Defect, Atrial Septal Defect, and right-sided aortic arch. Other associated abnormalities include micrognathism, cleft lip and palate, robin malformation sequence, DiGeorge sequence, renal anomalies, omphalocele, trachea-oesophageal fistula, rib abnormalities, scoliosis, hemivertebrae, hand anomalies including polydactyly, ectrodactyly, thumb hypoplasia, altered palmar creases, webbed neck, sloping shoulders, microcephaly, and growth hormone deficiency. CHARGE Syndrome remains a clinical diagnosis. Genetic confirmation

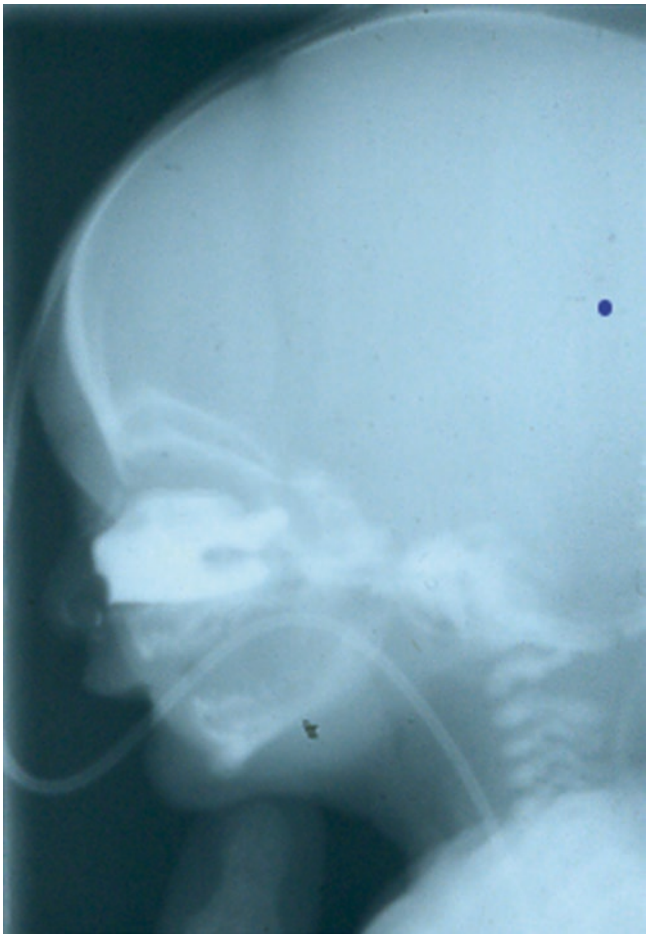

Fig. 8.26 CHARGE syndrome

can be made in the majority of patients by detection of heterozygous mutations in the CHD7 gene. Swallowing of saliva and food is a problem and has to be overcome by tube feeding. Gastro-oesophageal reflux is a complication of cranial nerve and autonomic dysfunction and results in aspiration pneumonia. Neurologic function in CHARGE syndrome may improve, however the early presence of gastro-oesophageal reflux and aspiration presents prolonged feeding problems for these babies. The loss of sense of smell is due to the absence or hypoplasia of the olfactory bulbs, evident on magnetic resonance imaging (MRI) scans [1, 31].

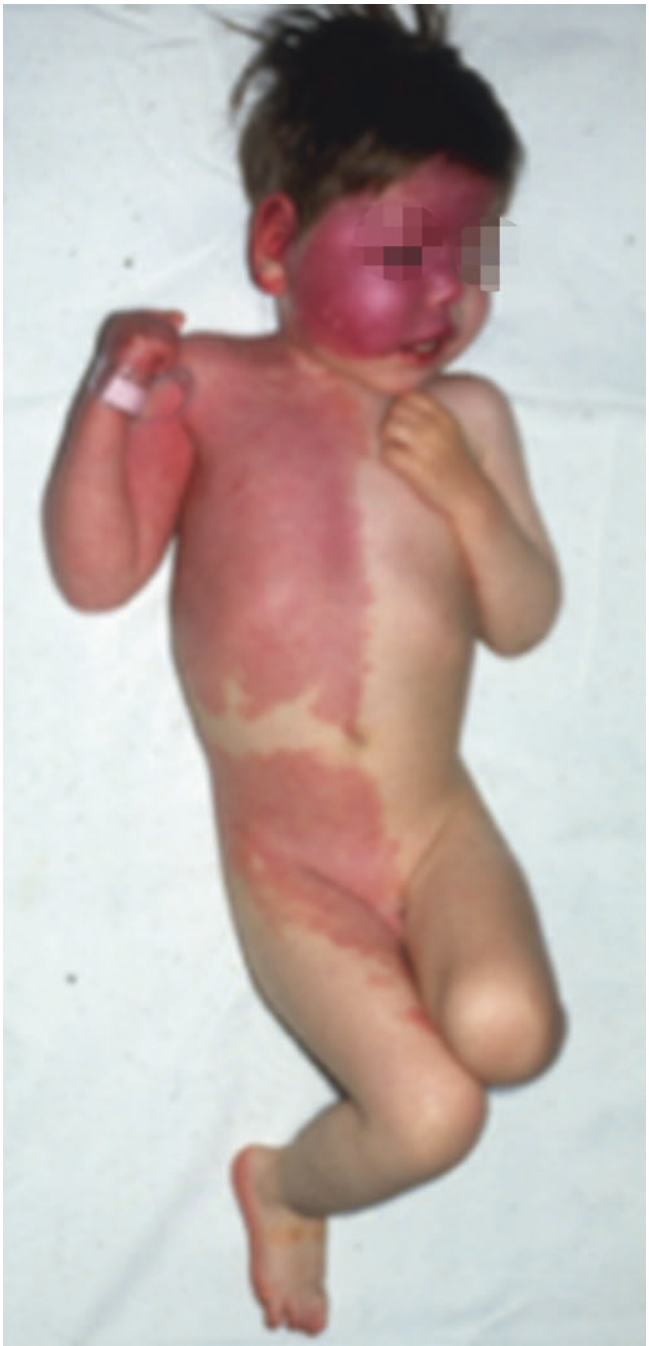

Fig. 8.27 Sturge-Weber syndrome

8.24 Sturge-Weber Sequence

Sturge-Weber Syndrome (SWS) (Figs. 8.27 and 8.28), also known as encephalofacial angiomatosis, is a sporadic congenital neurocutaneous disorder characterized by a port-wine stain (nevus flammeus) affecting the skin in the distribution of the ophthalmic branch of the trigeminal nerve and abnormal capillary venous vessels in the leptomeninges of the brain and choroid. Sturge-Weber syndrome may be complicated by seizures and these can be progressive and difficult to treat. Port-wine stains usually have underlying soft-tissue and bony-tissue overgrowth that may be mild or massive. Other clinical abnormalities include microgyria, macrocephaly, aortic coarctation, and macrodactyly. It is hypothesised to be a result of a somatic activating mutation in GNAQ. Capillary malformationsinvolve the arachnoid and pia mater, especially in occipital and temporal areas with secondary cerebral cortical atrophy and sclerosis resulting in

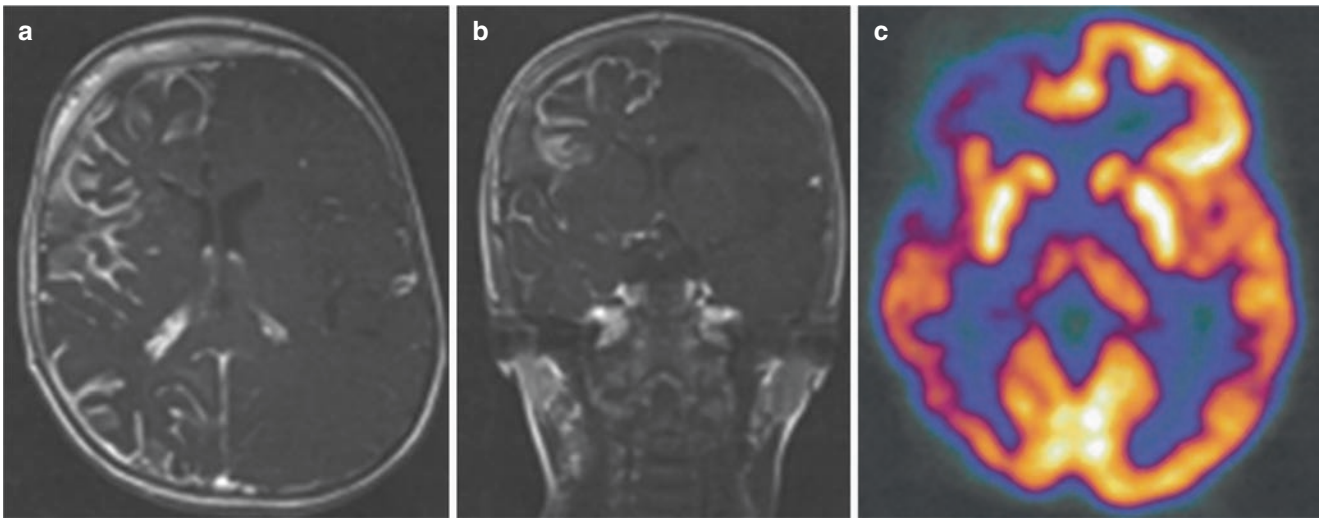

Fig. 8.28 Sturge-Weber syndrome

seizures. Radiologically, cerebral calcification can be seen earliest at 13 months, first noted in the occipital region. Plain skull X-rays show the classic "tram-line" calcifications in older children. T1-weighted magnetic resonance imaging (MRI) with gadolinium contrast is the recommended imaging technique for identifying SWS. Findings include leptomeningeal changes with enlargement of the transmedullary and periventricular veins. In infancy there may be little evidence of atrophy; however, during infancy atrophy and calcification can develop and can be visualised on computed tomography (CT) scans [1, 32].

8.25 Prader-Willi Syndrome

Prader-Willi syndrome (PWS) presents as neonatal hypotonia, intellectual impairment hypogonadism, dysmorphic facial features, and obesity. PWS occurs as a result of the absence of expression of paternal genes in the critical chromosome region 15q11.2-13. Paternal 15q11.2-q13 deletion is responsible for almost three-quarters of cases, around a quarter are caused by maternal uniparental disomy (UPD), and 1% of cases are sporadic or due to genomic imprinting centre defects. Babies are usually of a normal birth length, with deceleration in growth in the first few months. Other abnormalities include small penis, cryptochordism, hypoplastic labia minora and clitoris, hypogonadism, scoliosis, osteoporosis, microcephaly, clinodactyly, syndactyly, and kyphosis. Clinical diagnosis of PWS may be difficult during the neonatal period and infancy because many features do not appear till later [1, 33].

8.26 Silver-Russell Syndrome

Silver-Russell syndrome (SRS) is an imprinting defect disorder characterised by the five core clinical diagnostic criteria: (1) Intra uterine retardation; (2) Poor post-natal growth; (3) Relative macrocephaly with preservation of occipitofrontal circumference; (4) Classic facial phenotype; and (5) Asymmetry. The full aetiology of this syndrome remains unknown. Maternal uniparental disomy of chromosome 7 (mUPD3) and hypomethylation of imprinted control region 1 (ICR1) on chromosome 11p15 have been implicated in over 60% of cases. The most common skeletal abnormality is short stature. Without growth hormone (GH) therapy, the final height is about 151 cm in men and 140 cm in women. Other abnormalities that may be identified include immature osseous development in infancy and early childhood; late closure of anterior fontanel; limb asymmetry; a short/incurved fifth finger; and syndactyly of the second and third toes. Individuals with Silver-Russell display a classical facial phenotype characterised by a small triangular face, prominent forehead, relative macrocephaly, downturned corners of mouth and micrognathia. Other clinical manifestations can include hypoglycaemia, café au lait spots, renal anomaly, Sprengel deformity, inguinal hernia, cardiac defects, malignancy (craniopharyngioma, testicular seminoma, HCC, Wilms tumour), gastrointestinal abnormalities, and growth hormone deficiencies. Individuals with this condition are usually of normal intelligence. Diagnosis of Silver-Russell Syndrome remains clinical as there are currently no specific tests [1, 34, 35].

8.27 Kallmann Syndrome

Kallmann Syndrome is a very rare congenital condition characterised by gonadotropin-releasing hormone deficiency and hyposmia or anosmia and colour blindness. Mutations in KAL1, FGFR1, FGF8, CHD7, PROKR2, and PROK2 genes are responsible for Kallmann Syndrome. This disorder is a form of hypogonadotropic hypogonadism (HH). Clinical presentation with small genitalia, micropenis, and undescended testes, as well as delay in puberty. Characterized by low serum concentrations of testosterone. The features of Kallmann Syndrome vary, even among affected people in the same family Optic problems, such as colour blindness or optic atrophy, also can occur in KS patients. At puberty, such individuals fail to develop secondary sex characteristics. Affected females usually have delay in menarche and have poor breast development. Kallmann Syndrome is diagnosed clinically by the presence of arrested sexual maturation or hypogonadism as absence of secondary sexual characteristics, diminished libido, infertility, and amenorrhea in women. Tanner staging should be used during physical examination to assess the development of secondary sexual characteristics. Evaluation of breast development and pubic hair is necessary to diagnose KS. Diagnosis also includes hormonal analysis of gonadotropins (FSH, LH) and oestradiol. Serum levels of gonadotropins should be low and associated with low serum oestradiol concentrations. Magnetic resonance imaging (MRI) of pituitary and hypothalamus should be performed to diagnose KS. MRI imaging can identify abnormalities of the olfactory sulci and bulbs which can be hypoplastic or absent. Coronal T2-weighted MR image through the anterior fossa shows that the olfactory bulbs are absent and the left olfactory sulcus is hypoplastic.

8.28 Waardenburg-Shah Syndrome

Waardenburg-Shah Syndrome (Figs. 8.29 and 8.30) is a very rare congenital neurocristopathy and is characterized by Hirschsprung's disease, deafness, and depigmentation of hairs, skin, and iris with variable clinical expression. There are four types of Waardenburg-Shah Syndrome, all with autosomal dominant inheritance. Mutations in PAX3 gene located at 2q35 are responsible for types Type I and II. The MITF gene has also been implicated in Type II. EDNRP, EDN3, and SOX10 genes play a role in the development of type IV. There are five major and five minor diagnostic criteria for Waardenburg-Shah syndrome. Major criteria include sensorineural hearing loss, iris pigmentary abnormality with two eyes different colours/bicolor iris/characteristic brilliant blue iris, hair hypopigmentation (white forelock), dystopia canthorum (lateral displacement of inner canthi), and a first-degree relative previously diagnosed with Waardenburg-Shah Syndrome. Minor criteria include skin hypopigmentation, medial eyebrow flare (synophrys), broad and high nasal bridge with hypoplastic alae nasi, and premature greying of the hair. Hirschsprung's Disease is associated with type IV, and the diagnosis is made using the history, physical examination, plain abdominal X-ray, barium enema, anorectal manometry, and rectal biopsy [1, 36].

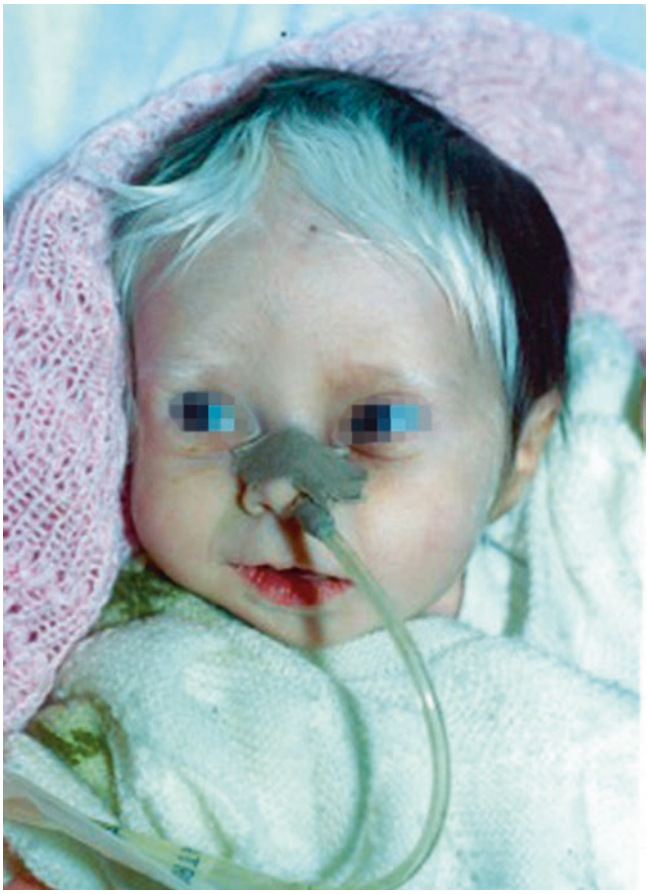

Fig. 8.29 Waardenburg-Shah syndrome

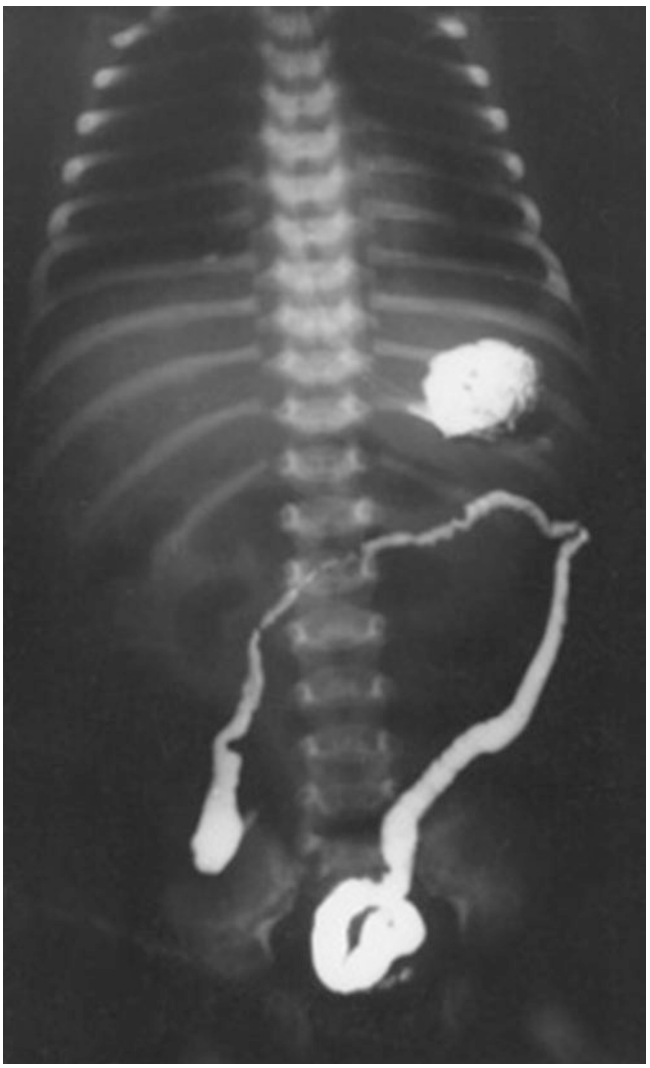

Fig. 8.30 Waardenburg-Shah syndrome

8.29 Ondine/Congenital Central Hypoventilation Syndrome

Ondine/Congenital Central Hypoventilation Syndrome (CCHS) is a manifestation of one of the neurocristopathies with poor respiratory control and dysautonomia. A heterozygous mutation of PHOX-2B gene is found in 90% of the patients. Symptoms of CCHS usually become apparent shortly after birth, and it is characteristically diagnosed in the new-born period. However, individuals can also be diagnosed in childhood or adulthood, depending on the severity of symptoms. Individuals with CCHS typically present with cyanosis, alveolar hypoventilation, and hypercarbia during sleep and, in more severely affected individuals, during wakefulness and sleep. These breathing complications occur despite the lungs and airways being anatomically and physiologically normal. Conditions associated with CCHS include Hirschsprung's Disease and tumours of neural crest origin, such as neuroblastomas, ganglioneuromas, and ganglioneuroblastomas. Postural hypotension due to poor regulatory function may also be present. Children with CCHS often have a characteristic appearance with a short, wide, flattened box-shaped face, decreased pupil responses to light, reduced pain perception, low body temperature, and occasional episodes of profuse sweating. Primary lung disease, muscle weakness, and cardiac disease should be ruled out by chest X-ray, CT, and echocardiogram. Brain and brainstem lesions need to be ruled out by MRI or CT.

8.30 Smith-Lemli-Opitz Syndrome

Smith-Lemli-Opitz Syndrome (SLOS) is a malformation and neurodevelopmental disorder characterised by typical dysmorphic facial features, multiple malformations, and cognitive impairment. Inheritance is autosomal-dominant with mutations in the gene encoding 7-dehydrocholesterolreductase (DHCR7) on chromosome 11q12-13. This mutation results in a metabolic defect in the conversion of 7-dehydrocholesterol to cholesterol, which leads to an accumulation of 7-dehydrocholesterol and a deficiency of cholesterol. Craniofacial abnormalities include: microcephaly with narrow frontal area, slanted or low-set auricles, ptosis, inner epicanthic folds, strabismus, broad nasal tip with anteverted nostrils, broad maxillary secondary alveolar ridges, micrognathia, ocular hypertelorism, absent lacrimal punta, cleft palate, macrostomia, bifid tongue, small larynx, and vocal cords. Skeletal abnormalities include Y-shaped syndactyly of the second and third toes, flexed fingers, asymmetrically short fingers, short proximally placed thumb, postaxial polydactyly of hand and less often feet, radial agenesis, clinodactyly, camptodactyly, ectrodactyly, metatarsus adductus, vertical talus, and dislocation of the hip. Genito-urinary abnormalities are common and found in up to 70%. Hypospadias, cryptochordism, micropenis, hypoplastic scrotum, bifid scrotum, microurethra, ureteropelvic junction obstruction, hydronephrosis, renal cystic dysplasia, renal duplication, renal agenesis, and reflux nephropathy have all been described. Cardiac abnormalities such as endocardial cushion defects, hypoplastic left heart, atrial septal defect, patent ductus arteriosus, and ventricular septal defect occur in 50% of individuals with Smith-Lemli-Opitz Syndrome. Neurological studies have demonstrated that individuals can have a variety of brain abnormalities, including microcephaly, holoprosencephaly, atelencephaly/aprosencephaly, abnormal gyri, aqueductal stenosis with hydrocephalus, incomplete separation of the mammillary bodies, agenesis of the corpus callosum, enlarged ventricles, cerebellar deformi-

ties, hippocampal hypoplasia, hypothalamic hamartoma, dorsal fusion of the dorsomedial nuclei and pulvinar of the thalamus, hypoplasia of the cerebral peduncles, and dysplasia of inferior olivary nuclei. Spinal cord abnormalities such as hydromyelia, holomyelia, and hypoplasia of the spinothalamic and spinocerebellar tracts have been described. Gastrointestinal anomalies can include adrenal enlargement, inguinal hernia, hepatic dysfunction, pancreatic islet cell hyperplasia, rectal atresia, cholestatic liver disease, pyloric stenosis, gallbladder aplasia, intestinal malrotataion, diaphragmatic hernia, anal stenosis and Hirschsprung's disease [1, 37, 38].

8.31 Shprintzen-Goldberg Syndrome: Marfanoid Habitus, Dolichocephaly, Ocular Proptosis

Shprintzen-Goldberg Syndrome is a connective tissue disorder characterized by craniosynostosis of the coronal, sagittal, or lambdoid sutures, dolichocephaly, distinctive craniofacial features, and skeletal changes. Neurological abnormalities include intellectual disability, hydrocephalus, dilatation of the lateral ventricles, and Chiari 1 malformation. Cardiovascular anomalies may include mitral valve prolapse, mitral regurgitation/incompetence, aortic regurgitation, and aortic root dilatation. Craniofacial anomalies include craniosynostosis, dolichocephaly, large anterior fontanel, high prominent forehead, ocular proptosis, strabismus, hypertelorism, downslanting palpebral fissures, maxillary hypoplasia, dental malocclusion, broad secondary alveolar ridge, and low-set posteriorly rotated ears. Skeletal abnormalities can include arachnodactyly, camptodactyly, genu recurvatum, pectus excavatum, pectus carinatum, hyperextensible joints, joint contractures, metatarsus adductus, talipes equinovarus, scoliosis dolichostenomelia, pes planus, scoliosis, joint hypermobility or contractures, and C1/C2 spine malformation. Other anomalies can include hypotonia, mental retardation, fine sparse hair, ptosis, bifid uvula, choanal stenosis/atresia, vocal cord paralysis, inguinal hernia, hyperelastic skin, hypospadias, and growth hormone deficiency. Minimal subcutaneous fat, abdominal wall defects, myopia, and cryptorchidism in males, are also characteristic findings. Plain X-rays can identify thin ribs, 13 pairs of ribs, box-like vertebral bodies, vertebral fusion, c1-2 abnormality, hypoplastic hooked clavicles, osteopenia, and bowing of the long bones (ribs/ulna/radius/tibia/fibula/femur) [1].

References

1. Jones KL, editor. Smith's recognizable patterns of human malformation. 6th ed. Philadelphia, PA: Elsevier Saunders; 2006.
2. Ko JM. Genetic syndromes associated with overgrowth in childhood. Ann Pediatr Endocrinol Metab. 2013;18(3):101–5.
3. Pappas JG. The clinical course of an overgrowth syndrome, from diagnosis in infancy through adulthood: the case of Beckwith-Wiedemann syndrome. Curr Probl Pediatr Adolesc Health Care. 2015;45(4):112–7.
4. Quintero-Rivera F, Robson CD, Reiss RE, Levine D, Benson C, Mulliken JB, et al. Apert syndrome: what prenatal radiographic findings should prompt its consideration? Prenat Diagn. 2006;26(10):966–72.
5. Scully C, Langdon J, Evans J. Marathon of eponyms: 3 Crouzon syndrome. Oral Dis. 2009;15(5):367–8.
6. Kusters E, Kerkhoffs JL, van Rossum AP. Thalassaemia diagnostics. Ned Tijdschr Geneeskd. 2014;158:A7988.
7. Wong P, Fuller PJ, Gillespie MT, Kartsogiannis V, Strauss BJ, Bowden D, et al. Thalassemia bone disease: the association between nephrolithiasis, bone mineral density and fractures. Osteoporos Int. 2013;24(7):1965–71.
8. Yee H, Mra R, Nyunt KM. Cardiac abnormalities in the thalassaemia syndromes. Southeast Asian J Trop Med Public Health. 1984;15(3):414–21.
9. Gonzalez GE, Caruso PA, Small JE, Jyung RW, Troulis MJ, Curtin HD. Craniofacial and temporal bone CT findings in cleidocranial dysplasia. Pediatr Radiol. 2008;38(8):892–7.
10. Tan TY, Kilpatrick N, Farlie PG. Developmental and genetic perspectives on Pierre Robin sequence. Am J Med Genet C Semin Med Genet. 2013;163C(4):295–305.
11. Tse JY, Wu S, Shinagare SA, Lauwers GY, Yilmaz O, Wu CL, et al. Peutz-Jeghers syndrome: a critical look at colonic Peutz-Jeghers polyps. Mod Pathol. 2013;26(9):1235–40.
12. Yiyit N, Işıtmangil T, Öksüz S. Clinical analysis of 113 patients with Poland syndrome. Ann Thorac Surg. 2015;99(3):999–1004.
13. Moir CR, Johnson CH. Poland's syndrome. Semin Pediatr Surg. 2008;17(3):161–6.
14. Pirasteh A, Carcano C, Kirsch J, T-LH M. Pentalogy of cantrell with ectopia cordis: CT findings. J Radiol Case Rep. 2014;8(12):29–34.
15. Sharma R, Seth A. Congenital adrenal hyperplasia: issues in diagnosis and treatment in children. Indian J Pediatr. 2014;81(2):178–85.
16. Marumudi E, Khadgawat R, Surana V, Shabir I, Joseph A, Ammini AC. Diagnosis and management of classical congenital adrenal hyperplasia. Steroids. 2013;78(8):741–6.
17. Sreekar H, Dawre S, Petkar KS, Shetty RB, Lamba S, Naik S, et al. Diverse manifestations and management options in Klippel-Trenaunay syndrome: a single centre 10-year experience. J Plast Surg Hand Surg. 2013;47(4):303–7.
18. Radke RM, Baumgartner H. Diagnosis and treatment of Marfan syndrome: an update. Heart. 2014;100(17):1382–91.
19. Köchling J, Pistor G, Märzhäuser Brands S, Nasir R, Lanksch WR. The Currarino syndrome—hereditary transmitted syndrome of anorectal, sacral and presacral anomalies. Case report and review of the literature. Eur J Pediatr Surg. 1996;6(2):114–9.
20. Low G, Irwin GJ, Haddock G, Maroo SV. Currarino triad: characteristic appearances on magnetic resonance imaging and plain radiography. Austr Radiol. 2006;50(3):249–51.
21. Whitehead MT, Nagaraj UD, Pearl PL. Neuroimaging features of Cornelia de Lange syndrome. Pediatr Radiol. 2015;45(8):1198–205.
22. Boyle MI, Jespersgaard C, Brøndum-Nielsen K, Bisgaard AM, Tümer Z. Cornelia de Lange syndrome. Clin Genet. 2015;88(1):1–12.

23. Byon M, Kim GJ. Prune-belly syndrome detected by ultrasound in the first trimester and the usefulness of vesicocentesis as a modality of treatment. Obstet Gynecol Sci. 2013;56(4):265–8.
24. Tonni G, Ida V, Alessandro V, Bonasoni MP. Prune-Belly syndrome: case series and review of the literature regarding early prenatal diagnosis, epidemiology, genetic factors, treatment, and prognosis. Fetal Pediatr Pathol. 2013;31(1):13–24.
25. Walls GV. Multiple endocrine neoplasia (MEN) syndromes. Semin Pediatr Surg. 2014;23(2):96–101.
26. Mettin RR, Merkenschlager A, Bernhard MK, Elix H, Hirsch W, Kiess W, et al. Wide spectrum of clinical manifestations in children with tuberous sclerosis complex—follow-up of 20 children. Brain Dev. 2014;36(4):306–14.
27. Dicker D, Samuel N, Feldberg D, Goldman JA. The antenatal diagnosis of Potter syndrome (Potter sequence). A lethal and not-so-rare malformation. Eur J Obstet Gynecol Reprod Biol. 1984;18(1–2):17–24.
28. Keirse MJ, Meerman RH. Antenatal diagnosis of Potter syndrome. Obstet Gynecol. 1978;52(1 Suppl):64S–7S.
29. Cunningham BK, Hadley DW, Hannoush H, Meltzer AC, Niforatos N, Pineda-Alvarez D, et al. Analysis of cardiac anomalies in VACTERL association. Birth Defects Res A Clin Mol Teratol. 2013;97(12):792–7.
30. Cunningham BK, Khromykh A, Martinez AF, Carney T, Hadley DW, Solomon BD. Analysis of renal anomalies in VACTERL association. Birth Defects Res A Clin Mol Teratol. 2014;100(10):801–5.
31. Hsu P, Ma A, Wilson M, Williams G, Curotta J, Munns CF, et al. CHARGE syndrome: a review. J Paediatr Child Health. 2014;50(7):504–11.
32. Sudarsanam A, Ardern-Holmes SL. Sturge-Weber syndrome: from the past to the present. Eur J Paediatr Neurol. 2014;18(3):257–66.
33. Tuysuz B, Kartal N, Erener-Ercan T, Guclu-Geyik F, Vural M, Perk Y, et al. Prevalence of Prader-Willi syndrome among infants with hypotonia. J Pediatr. 2014;164(5):1064–7.
34. Marsaud C, Rossignol S, Tounian P, Netchine I, Dubern B. Prevalence and management of gastrointestinal manifestations in Silver-Russell syndrome. Arch Dis Child. 2015;100(4):353–8.
35. SNK V, Balagopal RV. Clinical spectrum of Silver-Russell syndrome. Contemp Clin Dent. 2013;4(3):363–5.
36. Mahmoudi A, Rami M, Khattala K, Elmadi A, Afifi MA, Youssef B. Shah-Waardenburg syndrome. Pan Afr Med J. 2013;14:60.
37. Bianconi SE, Cross JL, Wassif CA, Porter FD. Pathogenesis, epidemiology, diagnosis and clinical aspects of Smith-Lemli-Opitz syndrome. Expert Opin Orphan Drugs. 2015;3(3):267–80.
38. Lee RW, Conley SK, Gropman A, Porter FD, Baker EH. Brain magnetic resonance imaging findings in Smith-Lemli-Opitz syndrome. Am J Med Genet A. 2013;161A(10):2407–19.

Index

R. Carachi (ed.), *Atlas of Paediatric Surgical Imaging*, https://doi.org/10.1007/978-3-030-32384-4